

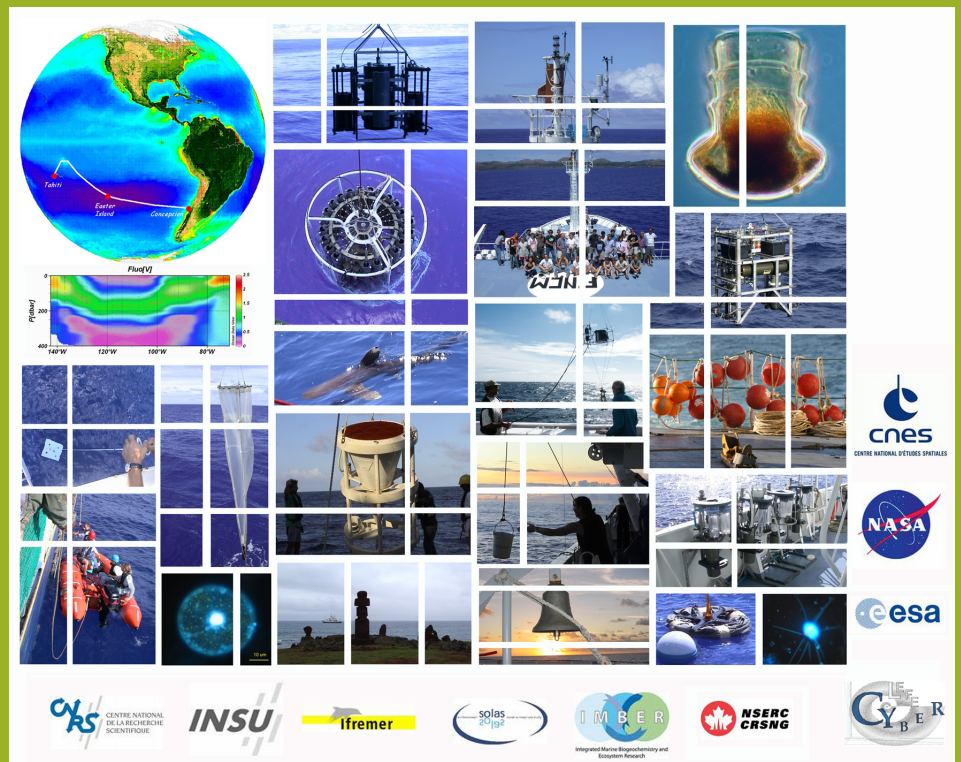
Biogeosciences

Special Issue:

Biogeochemistry and Optics

South Pacific Experiment (BIOSOPE)

Special Issue Editors: H. Claustre, A. Sciandra, and D. Vaultot



EUROPEAN
GEOSCIENCES
UNION

 Copernicus Publications
The Innovative Open Access Publisher

Obituary



This special issue is dedicated to the memory of our friend and colleague, Dominique Tailliez, who passed away on 26 March 2008. Responsible for the CTD-rosette deployment and data treatment during the numerous cruises organized by the French oceanographic community, Dominique had become a widely recognized pivotal contributor for more than 20 years. He was deeply appreciated not only for his professionalism and continuous availability but also for his involvement in many extraprofessional activities, most of them related to seafaring and to the maritime heritage. BIOSOPE was his last long-term cruise. He was a true and witty sailor who cherished the sea and who left behind extremely pleasant memories of the times we all shared with him both on land and at sea.

Biogeosciences

Special Issue:

Biogeochemistry and Optics South Pacific Experiment (BIOSOPE)

- H. Claustre et al.** Introduction to the special section bio-optical and biogeochemical conditions in the South East Pacific in late 2004: the BIOSOPE program

Biology and biodiversity

- J. Ras et al.** Spatial variability of phytoplankton pigment distributions in the Subtropical South Pacific Ocean: comparison between in situ and predicted data
- C. Grob et al.** Contribution of picoplankton to the total particulate organic carbon concentration in the eastern South Pacific
- S. Masquelier and D. Vaultot** Distribution of micro-organisms along a transect in the South-East Pacific Ocean (BIOSOPE cruise) using epifluorescence microscopy
- F. Le Gall et al.** Picoplankton diversity in the South-East Pacific Ocean from cultures
- L. Beaufort et al.** Calcite production by coccolithophores in the south east Pacific Ocean
- F. Gómez et al.** Two High-Nutrient Low-Chlorophyll phytoplankton assemblages: the tropical central Pacific and the offshore Perú-Chile Current
- F. Van Wambeke et al.** Factors limiting heterotrophic bacterial production in the southern Pacific Ocean
- R. Sempéré et al.** Distribution and bacterial availability of dissolved neutral sugars in the South East Pacific
- B. A. S. Van Mooy et al.** Phospholipid synthesis rates in the eastern subtropical South Pacific Ocean
- I. Obernosterer et al.** Biochemical characteristics and bacterial community structure of the sea surface microlayer in the South Pacific Ocean
- J. R. Dolan et al.** The "neutral" community structure of planktonic herbivores, tintinnid ciliates of the microzooplankton, across the SE Tropical Pacific Ocean

Biogeochemistry

- J. Charpentier et al.** Nitrous oxide distribution and its origin in the central and eastern South Pacific Subtropical Gyre
- P. Raimbault and N. Garcia** Evidence for efficient regenerated production and dinitrogen fixation in nitrogen-deficient waters of the South Pacific Ocean: impact on new and export production estimates
- S. Bonnet et al.** Nutrient limitation of primary productivity in the Southeast Pacific (BIOSOPE cruise)
- S. Blain et al.** Dissolved iron distribution in the tropical and sub tropical South Eastern Pacific
- P. Raimbault et al.** Distribution of inorganic and organic nutrients in the South Pacific Ocean – evidence for long-term accumulation of organic matter in nitrogen-depleted waters

continued on inside cover

Biogeosciences

continued from back cover

- T. Moutin et al.** Phosphate availability and the ultimate control of new nitrogen input by nitrogen fixation in the tropical Pacific Ocean
- S. Duhamel et al.** Growth and specific P-uptake rates of bacterial and phytoplanktonic communities in the Southeast Pacific (BIOSOPE cruise)
- F. Van Wambeke et al.** Heterotrophic bacterial production in the eastern South Pacific: longitudinal trends and coupling with primary production
- H. Claustre et al.** Gross community production and metabolic balance in the South Pacific Gyre, using a non intrusive bio-optical method
- L. Guidi et al.** Distribution and fluxes of aggregates $>100 \mu\text{m}$ in the upper kilometer of the South-Eastern Pacific
- L. Stemann et al.** Volume distribution for particles between 3.5 to 2000 μm in the upper 200 m region of the South Pacific Gyre
- I. Tolosa et al.** Distribution of lipid biomarkers and carbon isotope fractionation in contrasting trophic environments of the South East Pacific

Optics and bio-optics

- M. S. Twardowski et al.** Optical backscattering properties of the “clearest” natural waters
- A. Morel et al.** Natural variability of bio-optical properties in Case 1 waters: attenuation and reflectance within the visible and near-UV spectral domains, as observed in South Pacific and Mediterranean waters
- K. J. Voss et al.** Detailed validation of the bidirectional effect in various Case 1 waters for application to ocean color imagery
- D. Stramski et al.** Relationships between the surface concentration of particulate organic carbon and optical properties in the eastern South Pacific and eastern Atlantic Oceans
- D. Stramski** Corrigendum to “Relationships between the surface concentration of particulate organic carbon and optical properties in the eastern South Pacific and eastern Atlantic Oceans” published in Biogeosciences, 5, 171–201, 2008
- Y. Huot et al.** Particle optical backscattering along a chlorophyll gradient in the upper layer of the eastern South Pacific Ocean
- Y. Huot et al.** Relationship between photosynthetic parameters and different proxies of phytoplankton biomass in the subtropical ocean



EUROPEAN
GEOSCIENCES
UNION

Introduction to the special section bio-optical and biogeochemical conditions in the South East Pacific in late 2004: the BIOSOPE program

H. Claustre^{1,2}, A. Sciandra^{1,2}, and D. Vaultot³

¹CNRS, UMR 7093, Laboratoire d'océanographie de Villefranche, 06230 Villefranche-sur-Mer, France

²Université Pierre et Marie Curie-Paris 6, UMR 7093, Laboratoire d'océanographie de Villefranche, 06230 Villefranche-sur-Mer, France

³Station Biologique de Roscoff, UMR 7144 CNRS et Université Pierre et Marie Curie, BP 74, 29682 Roscoff Cx, France

Received: 28 November 2007 – Published in Biogeosciences Discuss.: 12 February 2008

Revised: 17 April 2008 – Accepted: 18 April 2008 – Published: 6 May 2008

Abstract. The objectives of the BIOSOPE (BIogeochemistry and Optics SOuth Pacific Experiment) project was to study, during the austral summer, the biological, biogeochemical and bio-optical properties of different trophic regimes in the South East Pacific: the eutrophic zone associated with the upwelling regime off the Chilean coast, the mesotrophic area associated with the plume of the Marquesas Islands in the HNLC (High Nutrient Low Chlorophyll) waters of this subequatorial area, and the extremely oligotrophic area associated with the central part of the South Pacific Gyre (SPG). At the end of 2004, a 55-day international cruise with 32 scientists on board took place between Tahiti and Chile, crossing the SPG along a North-West South-East transect. This paper describes in detail the objectives of the BIOSOPE project, the implementation plan of the cruise, the main hydrological entities encountered along the ~8000 km South East Pacific transect, and ends with a general overview of the 32 other papers published in this special issue.

Large scale investigations have been initially conducted as part of the transpacific SCORPIO sections performed along 43° S and 28° S (Reid, 1973) and the Hawaii-to-Tahiti shuttle experiment (Wyrтки and Kilonsky, 1984), following the EASTROPAC cruises carried out in 1967–1968. More recently, these observations have been supplemented with some WOCE sections (P6 lines, e.g. Wijffels et al. 2001; P19 line Tsuchiya and Talley, 1998) and with the rather intensive deployment of drifters and profiling floats as part of the ARGO program. The general patterns of the surface circulation in the South Equatorial Pacific region can be characterized by three main current regimes (Chaigneau and Pizarro, 2005a; Kessler 2006). On its equator side, the South Pacific Gyre (SPG) is delineated by the South Equatorial Current (SEC) flowing westwards and sometimes embedding the (weaker) South Equatorial Counter Current (SECC) (Wyrтки and Kilonsky, 1984; Eldin, 1983). On its polar side, the (weak) South Pacific Current (SPC), corresponding to the eastern extension of the West Wind Drift, flowing eastward near ~30° S, forms the southern closure of the subtropical gyre circulation (Stramma et al., 1995). Approaching South America, this current turns northwards and contributes to the diffuse surface flows of the broad Peru-Chile (Humboldt) Current (PCC); it can reach punctual velocities of 15–20 cm s⁻¹ (Chaigneau and Pizarro, 2005b) and sometimes presents complex motions near the coast, with important mesoscale activity (eddies and filaments) associated with the coastal upwelling regime (e.g. Shaffer et al., 1995). Below the PCC, the Peru Chile Undercurrent (PCUC), restricted to a narrow band near and above the shelf break, transports towards the pole the warm and salty subsurface equatorial waters (Silva and Neshyba, 1979).

1 Prior oceanographic knowledge of the South East Pacific

The South East Pacific (SEP 5° S–40° S, East of 150° W) makes the connection between tropical and high latitudes of the austral ocean. It remains the most sparsely-sampled oceanic region of the global ocean from both hydrodynamic (Leth et al., 2004) and biogeochemical (Daneri and Quinones, 2001) points of view.



Correspondence to: H. Claustre
(claustre@obs-vlfr.fr)

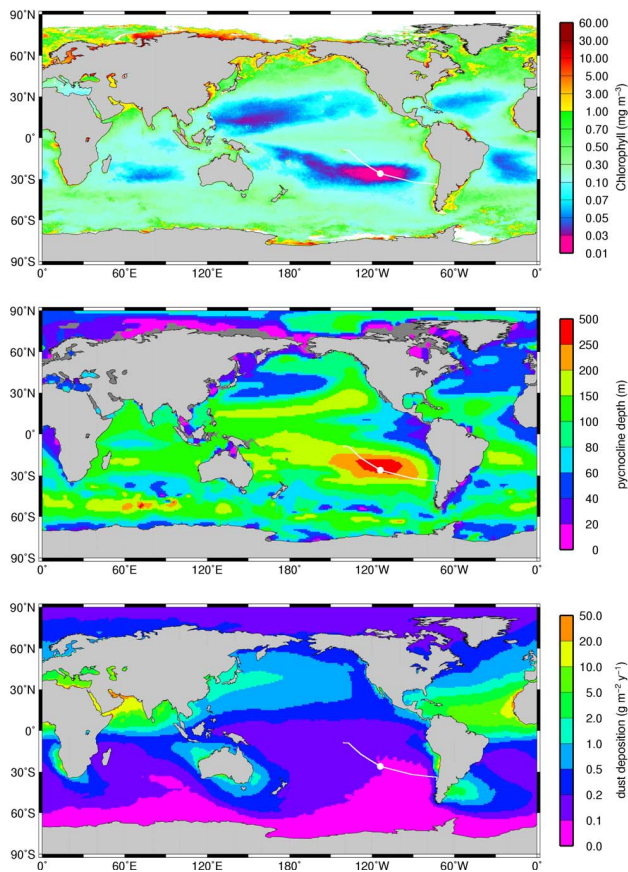


Fig. 1. Global context of the BIOSOPE cruise in the South East Pacific. (a) Annual composite image of SeaWiFS derived Chl-*a* for year 2000. (b) Distribution of the pycnocline depth (adapted from Fiedler and Talley, 2006). (c) Dust deposition flux at the ocean surface (adapted from Mahowald et al., 2005). The white line identifies the cruise track of the BIOSOPE cruise. The white circle corresponds to the GYR station located in the core of the SPG and investigated over a 5-day period.

Even fewer investigations have been dedicated to assess the biological and biogeochemical status of the SEP. Yet, this area, as a result of the hydrodynamical forcing described above presents a remarkable diversity of trophic conditions and even some singularities that do not have any counterpart in other areas of the world ocean. Basically three main biogeochemical regimes can be identified in this large water mass.

The SPG is the largest subtropical anticyclonic gyre and the least described region of the ocean (Longhurst, 1998; Claustre and Maritorena, 2003). Indeed, to our knowledge, the few biological observations reported to date concern phytoplankton production (Forsberg and Joseph 1963), some (very low) chlorophyll concentration along 105° W (Chavez et al., 1995), near surface phytoplankton determination along 110° W (Hardy et al., 1996) and a recent analysis on picophytoplankton distribution in the upper layer along 32° S

(Bouman et al., 2006; Grob et al., 2006). Thanks to satellite remote sensing of ocean color, some general surface properties of the SPG have emerged. The SPG is the most oligotrophic of all the sub-tropical gyres. In the vicinity of Easter Island (Rapa Nui), the surface chlorophyll-*a* concentration (Chl-*a*) is the lowest of the global open ocean with annual means as low as 0.019 mg Chl-*a* m⁻³ (Fig. 1a). These exceptionally low surface Chl-*a* correspond to very clear waters with deep penetration not only of visible but also of UV radiations (Vasilkov et al., 2001). Interestingly, these hyper-oligotrophic characteristics are also closely correlated with exceptional physical features (Fig. 1b). Actually, the pycnocline depth, derived from hydrological database, presents the largest values (>200 m) of the global ocean (Fig. 1b), precisely in the zone where the Chl-*a* concentration is the lowest (Fiedler and Talley, 2006). This apparently tight coupling between the physical and biological fields reveals an extremely deep nutrient source and a weak upward diffusion of nutrient fuelling the phototrophic production in the surface layer. Furthermore, due to the weak source of iron-rich desert dust in the southern hemisphere, atmospheric iron deposition is low, particularly in the SPG. Modelling results suggest that the deposition rate could be at least one order of magnitude lower than in the northern hemisphere (Mahowald et al., 2005) (Fig. 1c). Therefore, the upper waters of the SPG are expected to receive, in comparison to other oceanic regions, the lowest nutrients fluxes from deeper layers as well as the lowest iron flux from the atmosphere.

In contrast to the SPG, the equatorial and subequatorial Pacific waters have received considerable attention, particularly during the nineties in the context of the JGOFS program (Murray et al., 1995; Murray et al., 1997; Dandonneau, 1999). The impact of physical (e.g. upwelling strength), chemical (e.g. iron supply) and biological (e.g. grazing pressure) factors on the carbon cycle have been investigated and quantified in detail (Murray et al., 1994). Furthermore, the analysis of time series permitted to begin documenting the effect of ENSO on the inter-annual variability of some specific biogeochemical processes (Yoder and Kennelly, 2003). At the regional scale, these subequatorial waters are referred to as High Nutrient Low Chlorophyll waters because they present some moderate oligotrophic characteristics associated with significant amounts of nitrate. However, at a more local scale and in the vicinity of steep islands, these oligotrophic conditions might be temporarily or permanently relieved. The enhancement of water productivity has been reported in particular for waters west of the Galapagos Archipelago (Martin et al., 1994), Kiribati Islands (Messié et al., 2006) and Marquesas Archipelago (Signorini et al., 1999; Martinez and Maamaatuaiahutapu, 2004). The reasons behind this enhancement of productivity are still debated and are investigated mostly through modelling or remote sensing. In particular, no in situ investigation has been carried out to date for the remote Marquesas Islands.

The permanent upwelling associated with the PCC represents one of the most productive area of the global ocean (Carr, 2002) fuelling some of the largest fisheries. Despite this important biological and trophic impact, the PCC remains the least well known eastern boundary current system, both from their activity and phylogeny (Daneri and Quinones, 2001; Leth et al., 2004). As shown by Yuras et al. (2005), phytoplankton biomass covaries in phase with the upwelling-favorable winds along the Chilean coast while offshore phytoplankton biomass varies out of phase. This offshore biomass sometimes presents extreme westwards filamentous extension (200–300 km). These extensions are more important than what would be expected from the sole local dynamics of “wind driven” upwelling. The importance of mesoscale dynamics (meanders and gyres) and their interaction with the complex large scale circulation has therefore been proposed (Thomas et al., 1994; Leth and Shaffer, 2001) as regional specificities of SEP that might account for large offshore biomasses associated with these filaments.

2 Objectives of the BIOSOPE program

In 2001, after a whole decade of rather intensive field observations in various oceanic provinces as part of the JGOFS program, Daneri and Quinones wrote a contribution in the US JGOFS newsletter with a title clearly summarizing their concerns “Under sampled ocean systems: a plea for an international study of biogeochemical cycles in the Southern Pacific Gyre and its boundaries”. The BIOSOPE (BIogeochemistry and Optics South Pacific Experiment) program, jointly endorsed by the IMBER and SOLAS programs, was completely in line with this plea. Its overall goal was to explore and describe the biological, biogeochemical and optical characteristics of the South East Pacific. Using core measurements (in line with the former JGOFS core parameters) as well as new ones (e.g. based on the use of molecular biology and isotopic techniques, novel optical devices), two major goals were set.

1. Perform detailed studies in a certain number of oceanic provinces of the SEP in order to quantify the variables and processes that are essential to the understanding of trophic relationships, biogeochemical cycles of carbon and related elements as well as water optical signatures. The primary motivation of BIOSOPE was to study the South Pacific Gyre, expected to be the end member of oligotrophic conditions in the global ocean. But other SEP oceanic provinces were also of interest. The water masses west of Marquesas (local biomass enhancement visible from satellite) deserved to be investigated in the more general context of the HLNC conditions associated with the subequatorial area. Similarly, the upwelling zone extending offshore the Chilean coast was of great interest because of its particular filamentous patterns.

2. Understand in details the relationships linking optical properties of SEP waters to their biological and to biogeochemical characteristics. Besides surface Chl-*a*, an increasing number of biogeochemical or biological properties begin to be accessible from remote sensing (Ciotti and Bricaud, 2006; Uitz et al., 2006; Loisel et al., 2006; Siegel et al., 2002). The bio-optical models allowing the extraction of such “new products” still require validation and eventually refinement. A strong component of BIOSOPE was thus dedicated to optical and bio-optical studies. It was planned to elaborate a self consistent data base covering the complete range of trophic, biogeochemical and optical conditions that can be observable in open-ocean waters. Such a database would be invaluable to test and refine bio-optical models and eventually will allow identifying any peculiarity of the SEP with regard to other open ocean environments.

3 Implementation of the cruise

The BIOSOPE cruise took place during austral summer of 2004 (26 October–11 December), during a moderate phase of the El Nino Southern Oscillation ENSO¹. The ~8000 km transect, investigated with the French Research Vessel *I’Atalante*, started west of the Marquesas archipelago and ended off coastal waters of Chile (Fig. 2). Along this transect, two main types of stations (Table 1) were occupied, the so-called “short” and “long” stations.

The occupation of short stations, on a daily basis, had to cope with two main constraints. Sampling for biogeochemical flux measurements performed under simulated in situ conditions (e.g. production of the various biological stocks, nutrient assimilation) had to be performed two hours before sunrise while optical measurements had to be performed around noon in phase with satellite overpasses so that they could be used for ocean colour satellite validation. Consequently, the short stations generally consisted of two sub-stations, station StA (before sunrise) and StB (around noon), generally spaced by ~40 miles (~4 sailing hours apart). Certain measurements (CTD, other sensors, and some chemical measurements, e.g. nutrient and pigment concentrations) were systematically performed at both stations StA and StB. Their analyses confirm that, over the whole transect, the variability of StA vs StB remains extremely small (except for stations StA20 and StB20 in the vicinity of the Chilean coast) in comparison to the inter-station variability.

Six long stations were investigated for period longer than two days (Table 1), allowing the deployment of drifting moorings for sediment traps and production lines, and high frequency (3 h) repetitive sampling with the CTD-rosette. The position of four long stations was determined using real-time ocean colour data (SeaWiFS, MODIS, MERIS) looking

¹see: <http://www.ncdc.noaa.gov/oa/climate/research/2004/ann/enso-monitoring.html>

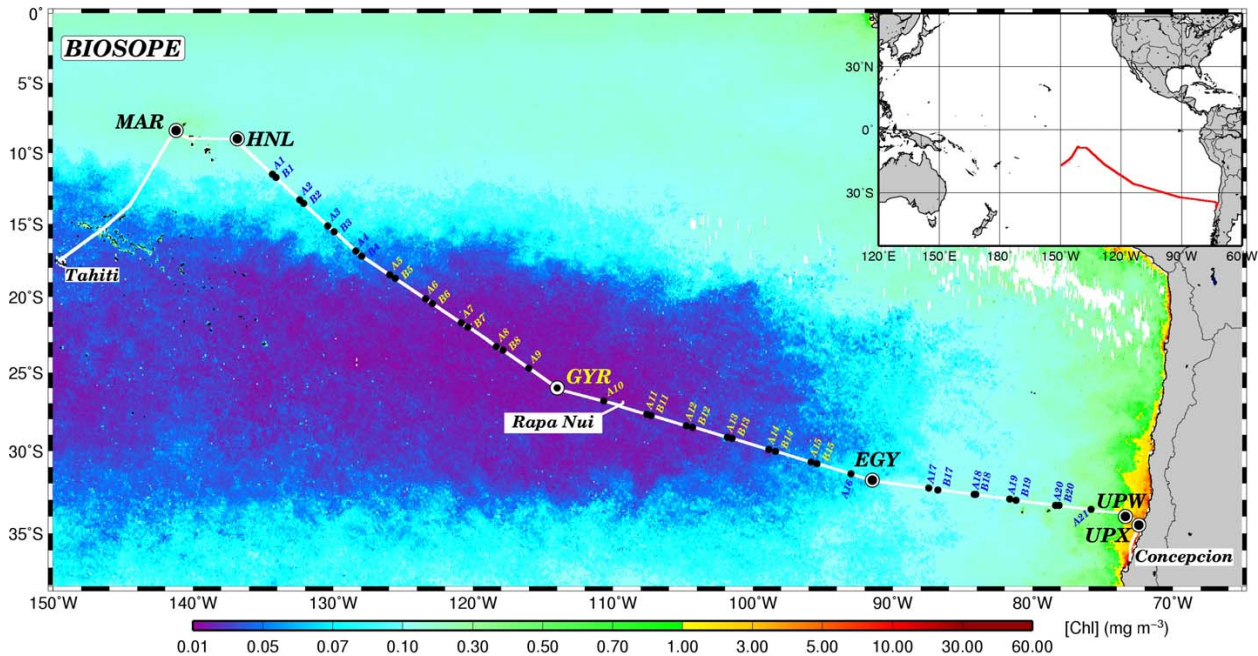


Fig. 2. Transect of the BIOSOPE cruise superimposed on a SeaWiFS composite image of Chl-*a* concentration in the upper layer for November–December 2004. The two main types of station, long and short, are indicated. The six long stations investigated for a period longer than 2 days are identified by a 3 letter code (see text). The 21 short stations are generally split into sub-stations A (early morning) and B (around noon). Four stations (referred as A9, A10, A16 and A21) did not follow this scheme. Note that the actual denomination for the short stations begins with St (Table 1), but the code has been simplified on this map to facilitate reading.

for the highest (MAR, west of Marquesas Island; UPW, UPX for the upwelling conditions off the Chile), and the lowest (GYR in the center of the South Pacific Gyre) surface Chl-*a* concentrations. It should be noted that the GYR station (114° W, 26° S) is extremely close to the location (115° W, 26° S) of the most oligotrophic area of the global ocean identified from an historical analysis of SeaWiFS ocean colour data². The reference station for High Nutrient Low Chl-*a* waters (HNL) in the subequatorial zone was set at the latitude of the Marquesas Archipelago, but east of it. Finally, the EGY station, located at the eastern border of the Gyre, was assumed to be representative of the transition zone between the South Pacific Gyre and the meridian branch of the anticyclonic circulation.

4 Water masses in the South East Pacific

4.1 The sub equatorial area: Marquesas to St2 (142° W–132° W)

North of 14° S, waters are under the influence of the equatorial regime. The eastward flowing South Equatorial Counter Current (SECC, ~141° W; 8° S) is embedded in the west-

wards flowing South Equatorial Current (SEC, ~138° W; 9° S) (Fig. 3). At 143° W, 11° S a vein of the SEC is also recorded in the subsurface water (data not shown). The post-cruise trajectories of 3 profiling floats deployed west of 132° W confirm that the area is clearly under the influence of the SEC (Table 2). Surface waters are warm (up to 27°C) and relatively fresh (~35.6) (Fig. 4). In the Marquesas area, a rather homothermous layer of 70–100 m develops, delineated by a steep thermocline, and associated with weak water column stability (Brunt-Vaisala frequency, Fig. 3). Nutrient concentrations [see also Raimbault et al. (2008) for further details on nutrient distribution along the transect] are significant (nitrates=1.88 μM) in surface around the Marquesas Islands (Fig. 5) and, in spite of a strong decreasing gradient, remain detectable until 132° W (nitrates >0.3 μM). The distribution of *in vivo* fluorescence, a proxy of Chl-*a*, and of particle attenuation coefficient (c_p), a proxy of particulate organic carbon (POC) are also uniform in this layer (Fig. 6). Moving eastwards, a sub-surface Chl-*a* maximum develops at ~70 m that lies on the pycnocline (station HLN- St1), while c_p remains homogenous in this layer. Oligotrophic conditions start at St2 with the presence of a deep chlorophyll maximum (DCM) located at ~120 m. Below (>300 m), a noticeable signal of Chl-*a* fluorescence higher than the other surface values observed during the transect is clearly associated with suboxic (<50 μmole kg⁻¹) conditions (Fig. 6b).

²see: http://earthobservatory.nasa.gov/Newsroom/NewImages/images.php3?img_id=16409

Table 1. Date and Location of the stations investigated along the BIOSOPE transect.

station	Date	Longitude	Latitude
MAR1	26 Oct. 2004	-141.23	-8.42
MAR2	27 Oct. 2004	-141.27	-8.39
MAR3	28 Oct. 2004	-141.26	-8.34
MAR4	29 Oct. 2004	-141.27	-8.32
HNL1	31 Oct. 2004	-136.86	-9.00
HNL2	1 Nov. 2004	-136.89	-9.01
HNL3	02 Nov. 2004	-136.98	-9.06
STA1	3 Nov. 2004	-134.35	-11.51
STB1	03 Nov. 2004	-134.10	-11.74
STA2	4 Nov. 2004	-132.39	-13.31
STB2	4 Nov. 2004	-132.11	-13.55
STA3	5 Nov. 2004	-130.38	-15.13
STB3	5 Nov. 2004	-129.93	-15.53
STA4	6 Nov. 2004	-128.38	-16.87
STB4	6 Nov. 2004	-127.97	-17.23
STA5	7 Nov. 2004	-125.95	-18.51
STB5	7 Nov. 2004	-125.55	-18.75
STA6	8 Nov. 2004	-123.41	-20.13
STB6	8 Nov. 2004	-122.89	-20.45
STA7	9 Nov. 2004	-120.86	-21.75
STB7	9 Nov. 2004	-120.38	-22.05
STA8	10 Nov. 2004	-118.33	-23.29
STB8	10 Nov. 2004	-117.89	-23.55
STA9	11 Nov. 2004	-116.02	-24.71
GYR1	12 Nov. 2004	-114.00	-26.00
GYR2	12 Nov. 2004	-113.99	-26.00
GYR3	13 Nov. 2004	-114.02	-26.02
GYR4	14 Nov. 2004	-114.02	-26.03
GYR5	15 Nov. 2004	-114.01	-26.06
GYR6	16 Nov. 2004	-113.99	-26.07
STA10	17 Nov. 2004	-110.67	-26.85
STA11	20 Nov. 2004	-107.59	-27.70
STB11	20 Nov. 2004	-107.29	-27.77
STA12	21 Nov. 2004	-104.75	-28.44
STB12	21 Nov. 2004	-104.31	-28.54
STA13	22 Nov. 2004	-101.83	-29.15
STB13	22 Nov. 2004	-101.48	-29.23
STA14	23 Nov. 2004	-98.87	-29.92
STB14	23 Nov. 2004	-98.39	-30.04
STA15	24 Nov. 2004	-95.83	-30.70
STB15	24 Nov. 2004	-95.43	-30.79
STA16	25 Nov. 2004	-93.00	-31.42
EGY1	25 Nov. 2004	-91.47	-31.82
EGY2	26 Nov. 2004	-91.47	-31.82
EGY3	27 Nov. 2004	-91.44	-31.85
EGY4	28 Nov. 2004	-91.41	-31.86
EGY5	29 Nov. 2004	-91.41	-31.90
EGY6	30 Nov. 2004	-91.41	-31.90
STA17	01 Dec. 2004	-87.43	-32.30
STB17	1 Dec. 2004	-86.78	-32.40
STA18	2 Dec. 2004	-84.21	-32.67
STB18	2 Dec. 2004	-84.07	-32.68
STA19	3 Dec. 2004	-81.64	-32.95
STB19	3 Dec. 2004	-81.20	-33.02
STA20	4 Dec. 2004	-78.37	-33.32
STB20	4 Dec. 2004	-78.12	-33.35
STA21	5 Dec. 2004	-75.84	-33.58
UPW1	6 Dec. 2004	-73.37	-34.00
UPW2	7 Dec. 2004	-73.39	-33.98
UPW3	8 Dec. 2004	-73.34	-33.86
UPX1	9 Dec. 2004	-72.42	-34.51
UPX2	10 Dec. 2004	-72.43	-34.58
UPX3	11 Dec. 2004	-72.49	-34.69

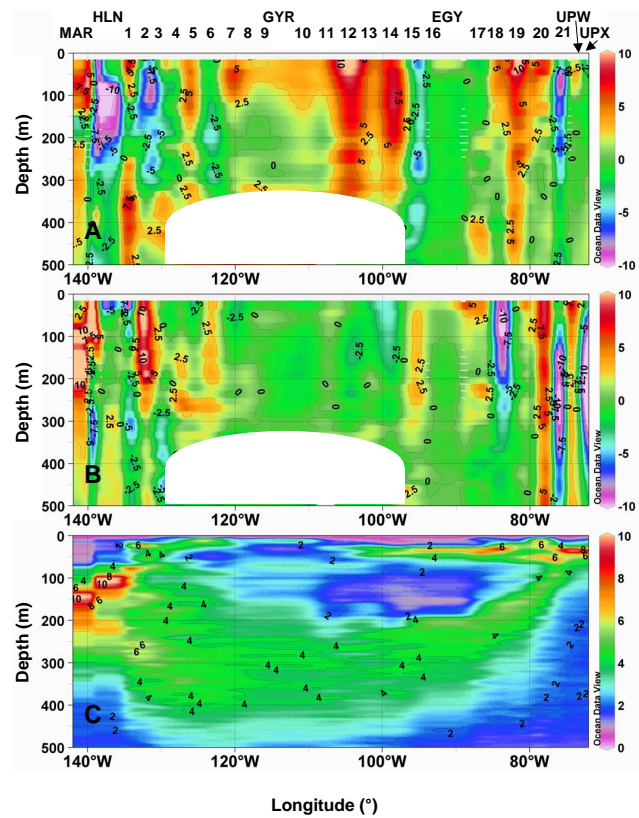


Fig. 3. Currents and Brunt-Väisälä frequency along the BIOSOPE transect. (a) Zonal component (cm s^{-1}): purple is westward and red is eastward. (b) Meridional component (cm s^{-1}): red is northward and purple is southward. (c) Brunt-Väisälä frequency (cyc h^{-1}). No current was monitored in the masked area (no echo for the 75 KHz RDI ADCP because of the very low level of particles in this layer).

This relative oxygen minimum likely reflects the signature of a north-westwards propagation of the oxygen minimum zone developing along South America (Fiedler and Talley, 2006). At this location, these suboxic conditions might also affect the degradation of particulate matter sinking from the upper layers.

4.1.1 The transition zone between the sub Equatorial area and the SPG (St2 to St6: 132° W–123° W).

In the surface/sub-surface layer of this area, the so-called South Tropical Surface Waters (STSW) (Fiedler and Talley, 2006) are clearly characterized by a very high salinity (Figs. 4b and 7), actually the highest of the Pacific (Tomczak and Godfrey, 2001), with the 36.5 isohaline being detected near the surface at 128° W, 15° S. These salty waters result from evaporation strongly exceeding precipitation (Tomczak and Godfrey, 2001). The area does not present any noticeable currents (Fig. 3), which is confirmed by the moderate displacement of the two profiling floats deployed

Table 2. ARGO floats deployed along the BIOSOPE transect. The left column refers to the 5 main zones defined in the paper.

	Float number/ http link	Date of deployment	Deployment location	
			Latitude	Longitude
Zone 1	2339/http://sio-argo.ucsd.edu/0049910c.html	5 Nov 2004	13.58	132.10
Zone 1	2338/http://sio-argo.ucsd.edu/0049909c.html	4 Nov 2004	12.00	134.09
Zone 1	2336/http://sio-argo.ucsd.edu/0045842c.html	26 Okt 2004	10.05	142.28
Zone 2	2342/http://sio-argo.ucsd.edu/0049913c.html	8 Nov 2004	18.82	125.45
Zone 2	2341/http://sio-argo.ucsd.edu/0049913c.html	7 Nov 2004	17.23	128.09
Zone 3	2348/http://sio-argo.ucsd.edu/0049919c.html	23 Nov 2004	29.30	101.50
Zone 3	2347/http://sio-argo.ucsd.edu/0049918c.html	21 Nov 2004	27.73	107.40
Zone 3	2346/http://sio-argo.ucsd.edu/0049917c.html	17 Nov 2004	26.14	113.93
Zone 3	2345/http://sio-argo.ucsd.edu/0049916c.html	11 Nov 2004	23.62	117.95
Zone 3	2344/http://sio-argo.ucsd.edu/0049915c.html	10 Nov 2004	22.11	120.36
Zone 3	2343/http://sio-argo.ucsd.edu/0049914c.html	9 Nov 2004	20.38	122.83
Zone 4	2356/http://sio-argo.ucsd.edu/0049927c.html	4 Dec 2004	33.06	81.18
Zone 4	2355/http://sio-argo.ucsd.edu/0049926c.html	3 Dec 2004	32.79	84.04
Zone 4	2354/http://sio-argo.ucsd.edu/0049925c.html	2 Dec 2004	32.30	86.79
Zone 4	2353/http://sio-argo.ucsd.edu/0049924c.html	1 Dec 2004	31.86	91.41
Zone 4	2352/http://sio-argo.ucsd.edu/0049923c.html	26 Nov 2004	31.43	92.88
Zone 4	2350/http://sio-argo.ucsd.edu/0049921c.html	25 Nov 2004	30.77	95.45
Zone 4	2349/http://sio-argo.ucsd.edu/0049920c.html	24 Nov 2004	30.09	98.32
Zone 5	2358/http://sio-argo.ucsd.edu/0049929c.html	6 Dec 2004	33.62	75.95

in this region (Table 2, floats #2341, #2342). This zone is also characterized by increasing oligotrophic conditions with the deepening of the nutricline. Nitrates are totally depleted (<3 nM) in the 0–100 m water column, while phosphates and silicates are still detectable (0.1 and $1 \mu\text{M}$, respectively). The DCM deepens very markedly eastward (~ 170 m at station 6). This is associated with a strengthening of the permanent thermocline, a consequence of the deepening of the sub-surface isotherm (e.g. the 15°C isotherms deepens from 240 to 320 m). In the deeper layer (>300 m) the fluorescence signal as well as the suboxic conditions observed north-westwards are clearly vanishing.

4.1.2 The central part of the SPG: (St6 to St13: 123°W – 101°W)

The central part of the gyre is characterized by the strongly stratified Eastern South Pacific Central Waters (ESPCW) (Emery and Meincke, 1986) that cover a wide range of temperature and salinity values (Fig. 7) and correspond to the water masses associated with the permanent thermocline (Tomczak and Godfrey, 2001). This area is delineated by extremely low levels of Chl-*a* fluorescence in the surface layer (~ 0.02 mg Chl-*a* m^{-3}) (Fig. 6) as well as by an extremely deep DCM which lies in the 160–200 m range over a distance of ~ 2500 km. The DCM position appears to be mainly driven by the density field (the base of the DCM follows the 26 kg m^{-3} isopycnal). The lowest levels of c_p in the 0–200 m layer are recorded in this region, especially at sta-

tion 6, 7 and 8. No inorganic nitrogen is a priori available for the biological production throughout the 0–150 m water column (nitrates <3 nM). In contrast, both phosphates and silicates are always present at significant concentrations (0.1 and $1 \mu\text{M}$, respectively). In the eastern part of the zone, on each side of 100°W , two eastward flowing current veins represent probably the signature of the South Pacific Current (west wind drift) which splits in two bands (Stramma et al., 1995) and delineates the northern limit of the Subtropical Front, also identified by the strong salinity gradient at $\sim 100^\circ\text{W}$. Mesoscale features related to Rossby waves (e.g. Wang et al., 1998) may also explain these current patterns. The six profiling floats deployed in this zone remained in a very restricted region (displacement of only a few degrees in latitude or longitude) over a three-year period (Table 2).

4.1.3 The transition zone between the SPG and the coastal upwelling area (St13 to St19: 100°W – 81°W)

East of 100°W , the transition zone between the salty ESPCW and the waters influenced by fresher Subantarctic Surface Waters (SASW) (Emery and Meincke, 1986; Tomczak and Godfrey, 2001) (Fig. 7) clearly delineates the core of the subtropical front (Chaigneau and Pizarro, 2005b). This zone also corresponds to a shoaling of the DCM which is located at 80 m at EGY station (91°W ; 32°S) and of the nutriclines (e.g. the $0.1 \mu\text{M}$ NO_3 isoline rises from 160 m at St 13 to 30 m at EGY). East of EGY (stations 17 to 19) HLNC conditions are observed with surface nitrates $>2.5 \mu\text{M}$ and

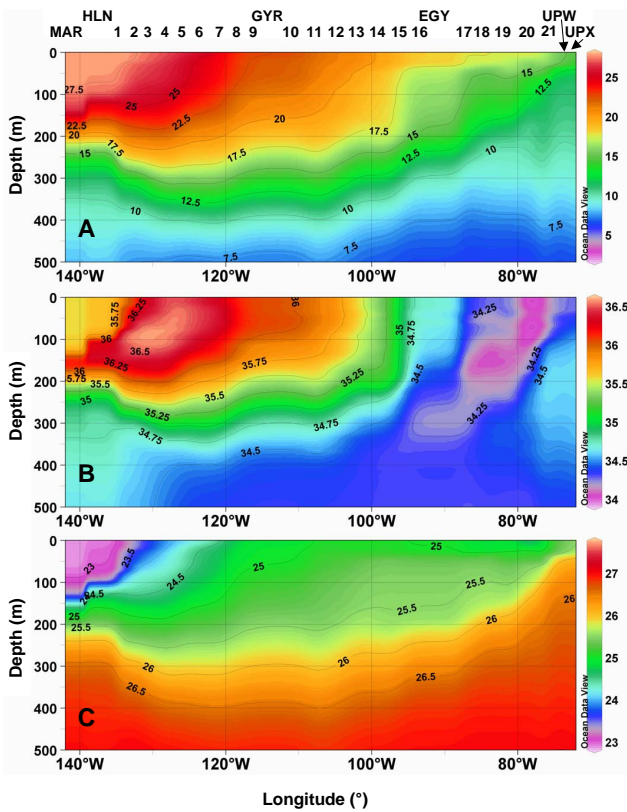


Fig. 4. Hydrological section along the BIOSOPE transect. (a) Potential temperature (°C). (b) Salinity. (c) Potential density (kg m^{-3}).

surface $\text{Chl-}a < 0.2 \text{ mg m}^{-3}$ (< 0.1 for St 19). At this location, a tongue of low salinity waters observed at a depth of 300 m progressively uplifts in an easterly direction and outcrops at the surface (salinity 34) at 78° W 33° S. Here, the waters present the highest oxygen saturation levels of the whole transect. This location, at the south-eastern edge of the SPG, corresponds to the source of the South Pacific Intermediate Water, ESPIW, (Emery and Meincke, 1986), which then spreads north-westwards into the intermediate layer of the SPG (Schneider et al., 2003) and transfers the surface water properties of the waters off central Chile to tropical latitudes.

4.1.4 The coastal upwelling area (St19 to UPX: east of 81° W)

East of 78° W, the ESPIW lies above the relatively saltier (> 34.5) Equatorial Subsurface Water (EESW) (Blanco et al., 2001) which extends in the 100–400 m range and is part, especially when approaching the Chilean coast, of the poleward Peru-Chile undercurrent (PCUC). The PCUC presents two veins at this location (Fig. 3) that have their velocity maximum at ~ 250 m. Two (0–500 m) veins of the equatorward PCC are also embedded with the PCUC illustrating the

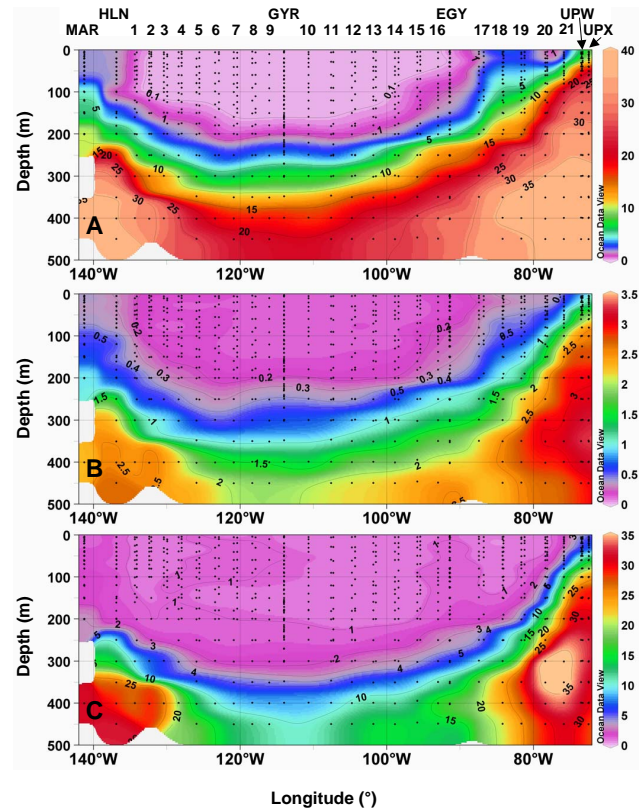


Fig. 5. Nutrient concentrations ($\mu\text{M l}^{-1}$) along the BIOSOPE transect. (a) Nitrate (NO_3). (b) Phosphates (PO_4). (c) Silicates (Si(OH)_4).

complexity of the circulation in the water off Chile (Shaffer et al., 1995). The only float deployed in this area ($\sim 76^\circ$ W; #2358, Table 2) presented a clear northern drift during the December 2004–December 2006 period. In the surface layer, the shoaling and the narrowing of the isotherms allow the delineation of a reduced mixed layer (~ 15 – 20 m) where the highest nutrient concentrations (nitrates up to $15 \mu\text{M}$ in surface) as well as the highest $\text{Chl-}a$ fluorescence (corresponding to $3 \text{ mg Chl-}a \text{ m}^{-3}$) and c_p signal are recorded. The intermediate layer where PCUC predominates is clearly associated with suboxic conditions and with a very significant signal of “deep” $\text{Chl-}a$ fluorescence.

5 Special issue presentation

The goal of this special issue is to present the knowledge gained concerning the South East Pacific based on the large dataset acquired during the BIOSOPE cruise. Although a disciplinary approach around three main topics (biology, biogeochemistry and optics) was adopted for data acquisition, many questions relevant to this project have benefited from multidisciplinary. The cruise strategy as well as on-board experimental design has been organized to promote

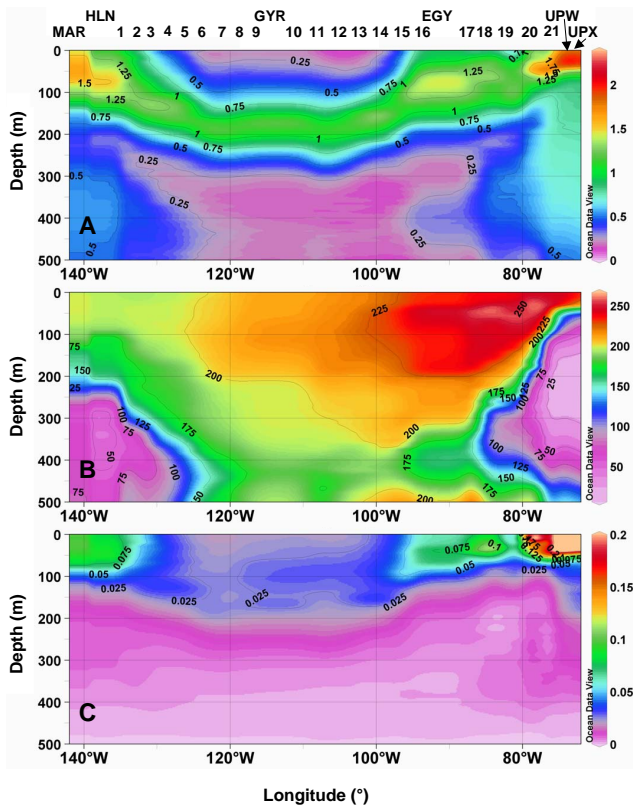


Fig. 6. Distribution of specific biogeochemical and optical properties along the BIOSOPE transect. (a) In vivo fluorescence of Chl-*a* (*V*). (b) Oxygen concentration ($\mu\text{M kg}^{-1}$). (c) attenuation coefficient, c_p (m^{-1}). The attenuation coefficient data have been processed as described in Claustre et al. (2007), by correcting for deep (450–500 m) values.

and favour such a synergic approach. Therefore, even if papers from this special issue (and for some others published elsewhere) are introduced below according to disciplines, most of the contributions have taken advantage of this collective effort so that paper scopes are often multidisciplinary too. Finally, it should be noted that some papers compare data acquired within the SEP with data acquired with similar techniques in other oceanic provinces. These papers represent a first step in revealing the existence (or the lack) of specificities of SEP waters with respect to other environments.

5.1 Biology and biodiversity

The very large trophic gradient that was extensively sampled during the BIOSOPE cruise offered a unique opportunity to better understand how the structure of biological communities in the open ocean adapts to varying nutrient conditions, with a specific focus on the extremely oligotrophic conditions of the central SPG. It is expected that under such conditions, the community structure shifts towards very small

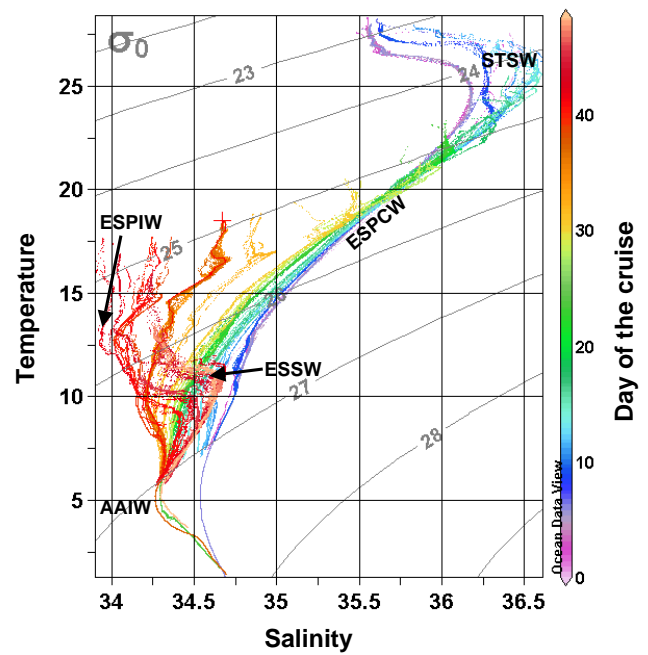


Fig. 7. Temperature-salinity diagram and identification of the main water masses encountered along the BIOSOPE transect. STSW : South Tropical Surface Waters ; ESPCW : Eastern South Pacific Central Waters; ESPIW: South Pacific Intermediate Water; EESW : Equatorial Subsurface Water; AAIW: Antarctic Intermediate Waters. The colour code refers to the day of the mission starting near Marquesas Archipelago (purple) and ending along the Chilean Coast (red). 224 CTD casts are used for this plot. Except for four deep casts (down to the sea floor), the other ones were performed down to 500 m.

cell sizes and that the microbial loop becomes dominant. However, whether the extreme conditions (e.g. depth of the DCM and relative isolation of the SPG waters) have favoured the establishment of yet unknown communities and micro-organisms is an intriguing possibility.

The autotrophic community was analysed in detail using different approaches, some of which are quite novel. The overall distribution of phytoplankton communities was assessed from HPLC pigment signatures and compared to distribution modelled from statistical relationships for the global ocean in order to highlight SEP peculiarities (Ras et al., 2008). Grob et al. (2007) relied on flow cytometry to determine the distribution of picoplankton and its impact on POC and on the particle attenuation coefficient. Masquelier and Vaulot (2008) used epifluorescence microscopy to look at picoplanktonic groups such as cyanobacteria (in particular those forming colonies), autotrophic picoeukaryotes, but also at larger protists such as ciliates and dinoflagellates (in particular some displaying intriguing green autofluorescence that are particularly abundant in this area). The diversity of picophytoplankton was assessed by novel culturing approaches (Le Gall et al., 2008). Beaufort et al. (2007)

investigated another important autotrophic group, the coccolithophorids, and in particular their impact on calcite production in the SEP.

With respect to larger autotrophs, the relation between the physico-chemical conditions and the composition of the diatom assemblage in two different HNLC conditions, the tropical central Pacific and the offshore Peru-Chile Current, was examined by Gómez et al. (2007). Numerous contributions to the knowledge of dinoflagellates, a group of special relevance in warm oligotrophic oceans have been presented in other journals (Gómez, 2006; Gómez, 2008a; Gómez, 2008b; Gómez, 2007a; Gómez and Furuya, 2007).

During BIOSOPE, heterotrophic bacteria have been studied in great details from the point of view of their production relative to primary production along the trophic gradient (Van Wambeke et al., 2008) and of the factor(s) regulating this production both spatially (Van Wambeke et al., 2007a) and temporally, with a special focus on the diel cycle and UV impact at long stations (Van Wambeke et al., 2007b). The relationship between bacteria and available sugars was investigated by Sempéré et al. (2008), while a new approach, based on the incorporation of labelled phosphorus into phospholipids, allowed showing that heterotrophic bacteria play a critical role in the phosphorus cycle, especially in the SPG (Van Mooy et al., 2008). The very specific bacterial community of the surface microlayer has been assessed both from the phylogenetic and activity points of view by Obernosterer et al. (2007).

Heterotrophic eukaryotes play a key role in recycling the organic matter from the microbial food web. The diversity of tintinnids was investigated with respect to the phytoplankton prey by Dolan et al. (2007) and follows on other recent descriptions of this microzooplankton group in the SEP (Dolan, 2006). The symbiotic association between the diatom *Chaetoceros* and the tintinnid *Eutintinnus* was investigated as an example of microplankton adaptation to the severe oligotrophic conditions (Gómez, 2007b). Microscope observations have also allowed elucidating the mysterious nature of the consortia between the protozoan *Solenicola* and the frustule of the diatom *Leptocylindrus mediterraneus* (Gómez, 2007c).

5.1.1 Biogeochemistry

Two “greenhouse” gases have been the subject of dedicated studies during BIOSOPE. Azouzi et al. (2007) provided an analysis of anthropogenic CO₂ penetration in the SEP and compared it with earlier estimates of anthropogenic tracers. Charpentier et al. (2007) focused on the processes of N₂O production and showed differences in the saturation level as well as in the source of this gas according to the hydrodynamic and associated trophic regimes considered. Nitrogen cycle was further addressed in Raimbault and Garcia (2008) who showed, in particular, that nitrogen fixation, while extremely low in the SPG, nevertheless sustained most

of new production in this area. This extremely weak nitrogen fixation was supported by extremely low abundance of the cyanobacterial *nifH* gene (Bonnet et al., 2008). Iron which is an essential element for life, in particular for nitrogen fixation, is vanishing low in the top 350 m (~0.1 nM) (Blain et al., 2008) which confirmed the extremely low atmospheric deposition recorded by Wagener et al. (2008). As a result of low iron concentration and low nitrogen fixation, phosphate concentration in surface layers was always above a threshold of 0.1 μM (Raimbault et al., 2008) and thus never constituted a limiting element for phytoplankton growth (Moutin et al., 2008), even in the hyperoligotrophic conditions of the SPG. A new method based on simultaneous spiking of water samples with ³³P and ¹⁴C allowed to measure autotrophic and bacterial contribution for various size fractions and suggested that the microbial community turns over very slowly (Duhamel et al., 2007). Primary production measurement using ¹³C labelling confirmed extremely low rates in the core of the SPG (100 mg C⁻² d⁻¹). These results were however partly contradictory with the bacterial carbon demand estimated by Van Wambeke et al. (2008). An optical technique based on the diel cycle in the attenuation coefficient (Claustre et al., 2008) suggested that rates of community production are much higher than expected and could result from exceptional DOC release during photosynthetic processes. This DOC release, unfortunately not measured during the cruise, might explain part of the discrepancies between bacterial carbon demand and production rates using various methods.

A new approach for particle flux determination, based on the optical quantification of particles forming the stock of large particulate matter (LPM >90 μm) was validated against the sediment trap fluxes at the six long stations and then applied along the whole BIOSOPE transect (Guidi et al., 2008). Significant diel variations in concentration and spectral slope of the particle size distribution were observed for particles smaller than 100 μm, but not for LPM (Stemmann et al., 2008). Finally, detailed characterization of the nature of the particle material was achieved using a combination of lipid biomarkers and carbon isotopic (δ¹³) composition (Tolosa et al., 2007).

5.2 Optics and bio-optics

The hyperoligotrophic conditions encountered in the centre of the gyre during BIOSOPE offered the opportunity to improve our knowledge of pure water optical properties by (1) setting upper limits to pure water absorption, especially in the UV range (Morel et al., 2007b) and (2) investigating in great detail backscattering properties by pure water (Twardowski et al., 2007) and permitting the evaluation of different values proposed for this coefficient. Furthermore (Morel et al., 2007a) highlighted optical singularities of Pacific waters when compared to Mediterranean waters, especially in the short wavelength domain including UV and for low Chl-*a*. The high penetration of UV radiation in the SPG was also

confirmed by (Tédetti et al., 2007). Additionally, previously published model of the so-called bi-directional effects in water upwelling radiances was validated for the first time in these extremely clear waters (Voss et al., 2007). Supplementing the BIOSOPE data-base with data from the eastern Atlantic Stramski et al. (2008) evaluate several approaches for quantifying particulate organic carbon concentration in surface waters from the determination of certain optical properties. Huot et al. (2008) built upon the unique optical measurements of Stramski et al. (2008) and Twardowski et al. (2007) to establish a relationship between the spectral backscattering coefficient and the Chl-*a* concentration and to examine the variations of the backscattering ratio with trophic status. Huot et al. (2007) evaluated the validity of various optical proxies of phytoplankton biomass, either derived from space or from in situ measurement, for the estimation of photo-physiological parameters used in bio-optical modelling of primary production. Finally, optical measurements made during BIOSOPE were also used by Uitz et al. (2008) to describe the photosynthetic characteristics of different phytoplankton groups and parameterize them for use in primary production models, and by Brown et al. (2008) to evaluate a new approach to estimate, from remotely sensed ocean colour, the concentration of substances other than Chl-*a*.

6 Final note: the evaluation process and the role of guest editors

All papers published in this special issue have been evaluated according to the normal procedure used for regular issues of Biogeosciences. In particular, none of the three BIOSOPE guest editors did intervene at any stage of manuscript evaluation. Their role was restricted to the revision of manuscripts prior to submission and to the coordination of the various submissions (ensuring consistency between the various manuscripts). For each manuscript, the BIOSOPE guest editors have provided a list of four to five potential referees which may or may not have been used by the regular Biogeosciences editors. Therefore, papers published in this BIOSOPE special issue comply with the general quality standards of Biogeosciences.

Acknowledgements. This BIOSOPE project was funded by the Centre National de la Recherche Scientifique (CNRS), the Institut des Sciences de l'Univers (INSU), the Centre National d'Etudes Spatiales (CNES), the European Space Agency (ESA), The National Aeronautics and Space Administration (NASA) and the Natural Sciences and Engineering Research Council of Canada (NSERC). This is a contribution to the BIOSOPE project of the LEFE-CYBER program. Dominique Tailliez and Claudie Bournot are warmly thanked for their efficient help in CTD management and data processing, Gérard Eldin for processing ADCP data. Drs Fiedler and Mahowald are warmly thanked for allowing getting access to their data used in Fig. 1 of this paper.

Edited by: S. Pantoja

References

- Azouzi, L., Ito, R. G., Touratier, F., and Goyet, C.: Anthropogenic carbon in the eastern south Pacific Ocean, *Biogeosciences Discuss.*, 4, 1815–1837, 2007, <http://www.biogeosciences-discuss.net/4/1815/2007/>.
- Beaufort, L., Couapel, M., Buchet, N., and Claustre, H.: Calcite production by coccolithophores in the south Pacific Ocean: from desert to jungle, *Biogeosciences Discuss.*, 4, 3267–3299, 2007, <http://www.biogeosciences-discuss.net/4/3267/2007/>.
- Blain, S., Bonnet, S., and Guieu, C.: Dissolved iron distribution in the tropical and sub tropical South Eastern Pacific, *Biogeosciences*, 5, 269–280, 2008, <http://www.biogeosciences.net/5/269/2008/>.
- Blanco, J. L., Thomas, A. C., Carr, M. E., and Strub, P. T.: Seasonal climatology of hydrographic conditions in the upwelling region off northern Chile, *J. Geophys. Res.*, 106, 11 451–411 468, 2001.
- Bonnet, S., Guieu, C., Bruyant, F., Prášil, O., Van Wambeke, F., Raimbault, P., Moutin, T., Grob, C., Gorbunov, M. Y., Zehr, J. P., Masquelier, S. M., Garczarek, L., and Claustre, H.: Nutrients limitation of primary productivity in the southeast Pacific (BIOSOPE cruise), *Biogeosciences*, 5, 215–225, 2008, <http://www.biogeosciences.net/5/215/2008/>.
- Bouman, H. A., Ulloa, O., Scanlan, D., Zwirgmaier, K., Li, W. K. W., Platt, T., Stuart, V., Barlow, R. G., Leth, O., Clementson, L. A., Lutz, V. A., Fukasawa, M., Watanabe, S., and Sathyendranath, S.: Oceanographic basis of the global surface distribution of prochlorococcus ecotypes., *Science*, 312, 918–921, 2006.
- Brown, C., Huot, Y., Werdell, P. J., Gentili, B., and Claustre, H.: The origin and global distribution of second order variability in satellite ocean color, *Remote Sensing of Environment*, in revision, 2008.
- Carr, M. E.: Estimation of potential productivity in eastern boundary currents using remote sensing, *Deep-Sea Res. II*, 49, 59–80, 2002.
- Chaigneau, A. and Pizarro, O.: Mean surface circulation and mesoscale turbulent flow characteristics in the eastern south Pacific from satellite tracked drifters, *J. Geophys. Res.-Oceans*, 110, C05014, doi:10.1029/2004JC002628, 2005a.
- Chaigneau, A. and Pizarro, O.: Surface circulation and fronts of the south Pacific Ocean, east of 120°W, *Geophys. Res. Lett.*, 32, L08605, doi:10.1029/2004GL022070, 2005b.
- Charpentier, J., Farias, L., Yoshida, N., Boontanon, N., and Raimbault, P.: Nitrous oxide distribution and its origin in the central and eastern South Pacific Subtropical Gyre, *Biogeosciences*, 4, 729–741, 2007, <http://www.biogeosciences.net/4/729/2007/>.
- Chavez, F. P., Buck, K. R., Bidigare, R. R., Karl, D. M., Hebel, D., Latasa, M., Campbell, L., and Newton, J.: On the chlorophyll *a* retention properties of glass-fiber gf/f filters, *Limnol. Oceanogr.*, 40, 428–433, 1995.
- Ciotti, A. M. and Bricaud, A.: Retrievals of a size parameter for phytoplankton and spectral light absorption by colored detrital matter from water-leaving radiances at seawifs channels in a continental shelf region off Brazil, *Limnology and Oceanography Methods*, 4, 237–253, 2006.
- Claustre, H., and Maritorena, S.: The many shades of ocean blue, *Science*, 302, 1514–1515, 2003.
- Claustre, H., Huot, Y., Obernosterer, I., Gentili, B., Tailliez, D., and Lewis, M. R.: Gross community production and metabolic bal-

- ance in the South Pacific Gyre, using a non intrusive bio-optical method, *Biogeosciences*, 5, 463–474, 2008, <http://www.biogeosciences.net/5/463/2008/>.
- Dandonneau, Y.: Introduction to the special section: Biogeochemical conditions in the equatorial Pacific in late 1994, *J. Geophys. Res.*, 104, 3291–3295, 1999.
- Daneri, G. and Quinones, R. A.: Undersampled ocean systems: A plea for an international study of biogeochemical cycles in the southern Pacific gyre and its boundaries, *US JGOFS Newsletter*, January 2001, 9, 2001.
- Dolan, J. R.: Re-discovered beauty - new images for old, descriptions - tropical tintinnids of the genus, *xystonellopsis* (ciliophora, tintinnia), *Protist*, 57, 251–253, 2006.
- Dolan, J. R., Ritchie, M. E., and Ras, J.: The “neutral” community structure of planktonic herbivores, tintinnid ciliates of the microzooplankton, across the se tropical Pacific Ocean, *Biogeosciences*, 4, 297–310, 2007, <http://www.biogeosciences.net/4/297/2007/>.
- Duhamel, S., Moutin, T., Van Wambeke, F., Van Mooy, B. A. S., Rimmelin, P., Raimbault, P., and Claustre, H.: Growth and specific p-uptake rates of bacterial and phytoplanktonic communities in the Southeast Pacific (BIOSOPE cruise), *Biogeosciences*, 4, 941–956, 2007, <http://www.biogeosciences.net/4/941/2007/>.
- Eldin, G.: Eastward flows of the South Equatorial Central Pacific, *Journal of Physical Oceanography*, 13, 1461–1467, 1983.
- Emery, W. J. and Meincke, J.: Global water masses: Summary and review, *Oceanologica Acta*, 9, 383–391, 1986.
- Fiedler, P. C. and Talley, L. D.: Hydrography of the Eastern Tropical Pacific: A review, *Progress In Oceanography*, 69, 143–180, 2006.
- Forgsbergh, E. D. and Joseph, J.: Phytoplankton production in the South-eastern Pacific, *Nature*, 200, 87–88, 1963.
- Gómez, F.: The dinoflagellate genera *Brachidinium*, *Asterodinium*, *Microceratium* and *Karenia* in the open SE Pacific Ocean, *Algae*, 21, 445–452, 2006.
- Gómez, F.: On the consortium of the tintinnid *Eutintinnus* and the diatom *Chaetoceros* in the Pacific Ocean, *Marine Biology*, 1899–1906, 2007b.
- Gómez, F.: Gymnodinioid, Dinoflagellates (gymnodiniales, dinophyceae) in the open Pacific Ocean, *Algae*, in press, 2008a.
- Gómez, F.: The consortium of the protozoan *Solenicola setigera* and the diatom *Leptocylindrus mediterraneus* in the Pacific Ocean, *Acta Protozoologica*, 46, 15–24, 2007c.
- Gómez, F.: New records of the dinoflagellate genus *Dicroerisma* (Actiniscales, Dinophyceae) in the Pacific Ocean *Chinese Journal of Oceanology and Limnology*, in press, 2008b.
- Gómez, F.: Nuevos registros del dinoflagelado *Craspedotella* kofoid, 1905 (Dinophyceae: Noctiluciales) en el Océano Pacífico., *Revista de Biología Marina y Oceanografía*, 42, 83–87, 2007a.
- Gómez, F., Claustre, H., Raimbault, P., and Souissi, S.: Two high-nutrient low chlorophyll phytoplankton assemblages: The tropical central pacific and the offshore Perú-Chile current, *Biogeosciences*, 4, 1101–1113, 2007, <http://www.biogeosciences.net/4/1101/2007/>.
- Gómez, F. and Furuya, K.: *Kofoidinium*, *Spatulodinium* and other Kofoidiniaceans (Noctiluciales, Dinophyceae) in the Pacific Ocean, *European Journal of Prostitology*, 43, 115–124, 2007.
- Grob, C., Ulloa, O., Li, W. K. W., Alarcon, G., Fukasawa, M., and Watanabe, S.: Picoplankton abundance and biomass across the eastern south Pacific Ocean along 32.5° S, *Marine Ecology Progress Series*, 332, 53–62, 2006.
- Grob, C., Ulloa, O., Claustre, H., Huot, Y., Alarcon, G., and Marie, D.: Contribution of picoplankton to the total particulate organic carbon concentration in the eastern South Pacific, *Biogeosciences*, 4, 837–852, 2007, <http://www.biogeosciences.net/4/837/2007/>.
- Guidi, L., Gorsky, G., Claustre, H., Picheral, M., and Stemmann, L.: Contrasting distribution of aggregates >100 μm in the upper kilometre of the South-Eastern Pacific, *Biogeosciences Discuss.*, 5, 871–901, 2008, <http://www.biogeosciences-discuss.net/5/871/2008/>.
- Hardy, J., Hanneman, A., Behrenfeld, M., and Horner, R.: Environmental biogeography of near-surface phytoplankton in the south-east Pacific Ocean, *Deep Sea Res. Part I*, 43, 1647–1-659, 1996.
- Huot, Y., Babin, M., Bruyant, F., Grob, C., Twardowski, M. S., and Claustre, H.: Does chlorophyll-*a* provide the best index of phytoplankton biomass for primary productivity studies?, *Biogeosciences*, 4, 853–868, 2007, <http://www.biogeosciences.net/4/853/2007/>.
- Huot, Y., Morel, A., Twardowski, M. S., Stramski, D., and Reynolds, R. A.: Particle optical backscattering along a chlorophyll gradient in the upper layer of the eastern South Pacific Ocean, *Biogeosciences*, 5, 495–507, 2008, <http://www.biogeosciences.net/5/495/2008/>.
- Kessler, W. S.: The circulation of the Eastern Tropical Pacific: A review, *Progress In Oceanography*, 69, 181, 2006.
- Le Gall, F., Rigaut-Jalabert, F., Marie, D., Garczarek, L., Viprey, M., Gobet, A., and Vaultot, D.: Picoplankton diversity in the South-East Pacific Ocean from cultures, *Biogeosciences*, 5, 203–214, 2008, <http://www.biogeosciences.net/5/203/2008/>.
- Leth, O. and Shaffer, G.: A numerical study of the seasonal variability in the circulation off central chile, *J. Geophys. Res.*, 106, 22 229–22 248, 2001.
- Leth, O., Shaffer, G., and Ulloa, O.: Hydrography of the eastern South Pacific Ocean: Results from the sonne 102 cruise, may-june 1995, *Deep-Sea Res. II*, 51, 2349–2369, 2004.
- Loisel, H., Nicolas, J. M., Sciandra, A., Stramski, D., and Poteau, A.: Spectral dependency of optical backscattering by marine particles from satellite remote sensing of the global ocean, *J. Geophys. Res.*, 111, C09024, doi:10.1029/2005JC003367, 2006.
- Longhurst, A.: *Ecological geography of the sea*, Academic Press, 398 pp., 1998.
- Mahowald, N. M., Baker, A. R., Bergametti, G., Brooks, N., Duce, R. A., Jickells, T. D., Kubilay, N., Prospero, J. M., and Tegen, I.: Atmospheric global dust cycle and iron inputs to the ocean, *Glob. Biogeochem. Cy.*, 19, GB4025, doi:10.1029/2004GB002402, 2005.
- Martin, J. H., Coale, K. H., Johnsson, K. S., et al.: Testing the iron hypothesis in ecosystems of the equatorial Pacific Ocean, *Nature*, 371, 123–129, 1994.
- Martinez, E. and Maamaatuaiahutapu, K.: Island mass effect in the marquesas islands: Time variation, *Geophys. Res. Lett.*, 31, L18307, doi:10.1029/2004GL020682, 2004.
- Masquelier, S. and Vaultot, D.: Distribution of micro-organisms along a transect in the South-East Pacific Ocean (BIOSOPE cruise) from epifluorescence microscopy, *Biogeosciences*, 5, 311–321, 2008,

- <http://www.biogeosciences.net/5/311/2008/>.
- Messié, M., Radenac, M.-H., Lefèvre, J., and Marchesiello, P.: Chlorophyll bloom in the western pacific at the end of the 1997–1998 el niño: The role of the Kiribati Islands., *Geophys. Res. Lett.*, 33, L14601, doi:10.1029/2006GL026033, 2006.
- Morel, A., Claustre, H., Antoine, D., and Gentili, B.: Natural variability of bio-optical properties in case 1 waters: Attenuation and reflectance within the visible and near-uv spectral domains, as observed in South pacific and mediterranean waters, *Biogeosciences*, 4, 913–925, 2007a, <http://www.biogeosciences.net/4/913/2007/>.
- Morel, A., Gentili, B., Claustre, H., Babin, M., Bricaud, A., Ras, J., and Tieche, F.: Optical properties of the “clearest” natural waters, *Limnol. Oceanogr.*, 52, 217–229, 2007b.
- Moutin, T., Karl, D. M., Duhamel, S., Rimmelin, P., Raimbault, P., Van Mooy, B. A. S., and Claustre, H.: Phosphate availability and ultimate control of new nitrogen input by nitrogen fixation in the tropical Pacific Ocean., *Biogeosciences*, 5, 95–109, 2008, <http://www.biogeosciences.net/5/95/2008/>.
- Murray, J. W., Barber, R. T., Roman, M. R., Bacon, M. P., and Feely, R. A.: Physical and biological controls on carbon cycling in the Equatorial Pacific, *Science*, 266, 58–65, 1994.
- Murray, J. W., Johnson, E., and Garside, C.: A U.S. JGOFS process study in the equatorial pacific (eqpac): Introduction, *Deep Sea Res. Part II*, 42, 275, 1995.
- Murray, J. W., Leborgne, R., and Dandonneau, Y.: JGOFS studies in the Equatorial Pacific (EQPAC), *Deep Sea Res. Part II*, 44, 1759, 1997.
- Obernosterer, I., Catala, P., Lami, R., Caparros, J., Ras, J., Bricaud, A., Dupuy, C., Van Wambeke, F., and Lebaron, P.: Biochemical characteristics and bacterial community structure of the sea surface microlayer in the South Pacific Ocean, *Biogeosciences Discuss.*, 4, 2809–2844, 2007, <http://www.biogeosciences-discuss.net/4/2809/2007/>.
- Raimbault, P., and Garcia, N.: Evidence for efficient regenerated production and dinitrogen fixation in nitrogen-deficient waters of the South Pacific Ocean: impact on new and export production estimates, *Biogeosciences*, 5, 323–338, 2008, <http://www.biogeosciences.net/5/323/2008/>.
- Raimbault, P., Garcia, N., and Cerrutti, F.: Distribution of inorganic and organic nutrients in the South Pacific Ocean -evidence for long-term accumulation of organic matter in nitrogen-depleted waters, *Biogeosciences*, 5, 281–298, 2008, <http://www.biogeosciences.net/5/281/2008/>.
- Ras, J., Uitz, J., and Claustre, H.: Spatial variability of phytoplankton pigment distribution in the South East Pacific, *Biogeosciences*, 5, 353–369, 2008, <http://www.biogeosciences.net/5/353/2008/>.
- Reid, J. L.: Transpacific hydrographic sections at lats. 43° S and 28° S: The scorpio expedition-iii. Upper water and a note on southward flow at mid-depth, *Deep-Sea Res.*, 20, 39–49, 1973.
- Schneider, W., Fuenzalida, R., Rodríguez-Rubio, E., Garcés-Vargas, J., and Bravo, L.: Characteristics and formation of eastern south pacific intermediate water, *Geophysical Research Letters*, 30(11), 1581, doi:1510.1029/2003GL017086, 2003.
- Sempéré, R., Tedetti, M., Panagiotopoulos, C., Charrière, B., and Van Wambeke, F.: Molecular distribution and bacterial availability of dissolved sugars in the South East Pacific Ocean in relation to photochemical oxidation reactions, *Biogeosciences Discuss.*, 725–750, 2008.
- Shaffer, G., Salinas, S., Pizarro, O., Vega, A., and Hormazabal, S.: Currents in the deep ocean off Chile (30° S), *Deep-Sea Res.*, 42, 425–436, 1995.
- Siegel, D. A., Maritorena, S., Nelson, N. B., Hansell, D. A., and Lorenzi-Kayser, M.: Global distribution and dynamics of colored dissolved and detrital organic materials, *J. Geophys. Res.*, 107, 3228, doi:3210.1029/2011JC000965, 2002.
- Signorini, S. R., McClain, C. R., and Dandonneau, Y.: Mixing and phytoplankton bloom in the wake of the Marquesas islands, *Geophys. Res. Lett.*, 26, 3121–3124, 1999.
- Silva, N. and Neshyba, S.: On the southernmost extension of the Peru-Chile undercurrent, *Deep-Sea Res.*, 26, 1387–1393, 1979.
- Stemann, L., Eloire, D., Sciandra, A., Jackson, G. A., Guidi, L., Picheral, M., and Gorsky, G.: Volume distribution for particles between 3.5 to 2000 μm in the upper 200 m region of the South Pacific Gyre, *Biogeosciences*, 5, 299–310, 2008, <http://www.biogeosciences.net/5/299/2008/>.
- Stramma, L., Peterson, R. G., and Tomczak, M.: The South Pacific current, *Journal of Physical Oceanography*, 25, 77–91, 1995.
- Stramski, D., Reynolds, R. A., Babin, M., Kaczmarek, S., Lewis, M. R., Rottgers, R., Sciandra, A., Stramska, M., Twardowski, M. S., Franz, B. A., and Claustre, H.: Relationships between the surface concentration of particulate organic carbon and optical properties in the eastern South Pacific and eastern Atlantic oceans, *Biogeosciences*, 5, 171–201, 2008, <http://www.biogeosciences.net/5/171/2008/>.
- Tédetti, M., Sempere, R., Vasilkov, A., Charriere, B., Nerini, D., Miller, W. L., Kawamura, K., and Raimbault, P.: High penetration of ultraviolet radiation in the South East Pacific waters, *Geophys. Res. Lett.*, 34, L12610, doi:12610.11029/12007GL029823, 2007.
- Thomas, A. C., Huang, F., Strub, P. T., and James, C.: A comparison of the seasonal and interannual variability of phytoplankton pigment concentrations in the Peru and California current systems, *J. Geophys. Res.*, 99, 7355–7370, 1994.
- Tolosa, I., Miquel, J. C., Gasser, B., Raimbault, P., Azousi, L., and Claustre, H.: Ecology and biogeochemistry of contrasting trophic environments in the South East Pacific by carbon isotope ratios on lipid biomarkers., *Biogeosciences Discussion*, 4, 4653–4696, 2007.
- Tomczak, M. and Godfrey, J. S.: Regional oceanography: An introduction., Pdf Version 1.2, available from: <http://www.es.flinders.edu.au/~mattom/regoc/>, 2001.
- Tsuchiya, M. and Talley, L. D.: A Pacific, 88° hydrographic section at 88°w: Water-property distribution, *J. Geophys. Res.*, 103, 12 899–12 918, 1998.
- Twardowski, M. S., Claustre, H., Freeman, S. A., Stramski, D., and Huot, Y.: Optical backscattering properties of the “clearest” natural waters, *Biogeosciences*, 4, 1041–1058, 2007, <http://www.biogeosciences.net/4/1041/2007/>.
- Uitz, J., Claustre, H., Morel, A., and Hooker, S.: Vertical distribution of phytoplankton communities in open ocean: An assessment based on surface chlorophyll, *J. Geophys. Res.*, 111, C08005, doi:10.1029/2005JC003207, 2006.
- Uitz, J., Huot, Y., Bruyant, F., Babin, M., and Claustre, H.: Relating phytoplankton photophysiological properties to community structure on large scale, *Limnol. Oceanogr.*, 53, 614–630, 2008.
- Van Mooy, B. A. S., Moutin, T., Duhamel, S., Rimmelin, P., and

- Van Wambeke, F.: Phospholipid synthesis rates in the eastern subtropical South Pacific Ocean, *Biogeosciences*, 5, 133–139, 2008, <http://www.biogeosciences.net/5/133/2008/>.
- Van Wambeke, F., Bonnet, S., Moutin, T., Raimbault, P., Alarçon, G., and Guieu, C.: Factors limiting heterotrophic prokaryotic production in the southern Pacific Ocean, *Biogeosciences Discuss.*, 4, 3799–3828, 2007a, <http://www.biogeosciences-discuss.net/4/3799/2007/>.
- Van Wambeke, F., Obernosterer, I., Moutin, T., Duhamel, S., Ulloa, O., and Claustre, H.: Heterotrophic bacterial production in the South East Pacific: Longitudinal trends and coupling with primary production, *Biogeosciences*, 5, 157–169, 2008, <http://www.biogeosciences.net/5/157/2008/>.
- Van Wambeke, F., Tedetti, M., Duhamel, S., and Sempéré, R.: Diel variability of heterotrophic prokaryotic production and UV doses in the South East Pacific, *Biogeosciences Discuss.*, 5, 435–462, 2007b, <http://www.biogeosciences-discuss.net/5/435/2007/>.
- Vasilkov, A. P., Krotkov, N., Herman, J., McClain, C., Arrigo, K. R., and Robinson, W.: Global mapping of underwater uv irradiances and DNA-weighted exposures using total ozone mapping spectrometer and sea-viewing wide field-of-view sensor data products, *J. Geophys. Res.*, 106, 27 205–27 219, 2001.
- Voss, K. J., Morel, A., and Antoine, D.: Detailed validation of the bidirectional effect in various case 1 waters for application to ocean color imagery, *Biogeosciences*, 4, 781–789, 2007, <http://www.biogeosciences.net/4/781/2007/>.
- Wagener, T., Guieu, C., Losno, R., Bonnet, S., and Mahowald, N.: Revisiting atmospheric dust export to the south hemisphere ocean, *Glob. Biogeochem. Cy.*, 22, GB2006, doi:10.1029/2007GB002984, 2008.
- Wang, L., Koblinsky, C. J., Howden, S. D., and Beckley, B.: Large-scale rossby wave in the mid-latitude south pacific from altimetric data, *Geophys. Res. Lett.*, 25, 179–182, 1998.
- Wijffels, S. E., Toole, J. M., and Davis, R.: Revisiting the south pacific subtropical circulation: A synthesis of world ocean circulation experiment observations along 32° S, *J. Geophys. Res.*, 106, 19 481–19 513, 2001.
- Wyrski, K., and Kilonsky, B.: Mean water and current structure during the hawaii-to-tahiti shuttle experiment, *Journal of Physical Oceanography*, 14, 242–254, 1984.
- Yoder, J. A. and Kennelly, M. A.: Seasonal and enso variability in global ocean: Phytoplankton chlorophyll derived from four years of seawifs measurements, *Glob. Biogeochem. Cy.*, 17, 1112, doi:1110.1029/2002GB001942, 2003.
- Yuras, G., Ulloa, O. and Hormazábal, S.: On the annual cycle of coastal and open ocean satellite chlorophyll off Chile (18°–40° S). *Geophys. Res. Lett.*, 32, 1029–1033, 2005.

Spatial variability of phytoplankton pigment distributions in the Subtropical South Pacific Ocean: comparison between in situ and predicted data

J. Ras^{1,2}, H. Claustre^{1,2}, and J. Uitz^{1,2,*}

¹UPMC Univ Paris 06, UMR 7093, Lab. d'Océanographie de Villefranche sur mer, 06238 Villefranche-sur-mer, France

²CNRS, UMR 7093, LOV, 06230 Villefranche-sur-Mer, France

* now at: Marine Physical Laboratory, Scripps Institution of Oceanography, University of California at San Diego, 95000 Gilman Drive, La Jolla, CA 92093-0238, USA

Received: 29 August 2007 – Published in Biogeosciences Discuss.: 2 October 2007

Revised: 17 January 2008 – Accepted: 25 January 2008 – Published: 12 March 2008

Abstract. In the frame of the BIOSOPE cruise in 2004, the spatial distribution and structure of phytoplankton pigments was investigated along a transect crossing the ultra-oligotrophic South Pacific Subtropical Gyre (SPSG) between the Marquesas Archipelago (141° W–8° S) and the Chilean upwelling (73° W–34° S). A High Performance Liquid Chromatography (HPLC) method was improved in order to be able to accurately quantify pigments over such a large range of trophic levels, and especially from strongly oligotrophic conditions. Seven diagnostic pigments were associated to three phytoplankton size classes (pico-, nano and microphytoplankton). The total chlorophyll-*a* concentrations [TChl*a*] in surface waters were the lowest measured in the centre of the gyre, reaching 0.017 mg m⁻³. Pigment concentrations at the Deep Chlorophyll Maximum (DCM) were generally 10 fold the surface values. Results were compared to predictions from a global parameterisation based on remotely sensed surface [TChl*a*]. The agreement between the in situ and predicted data for such contrasting phytoplankton assemblages was generally good: throughout the oligotrophic gyre system, picophytoplankton (prochlorophytes and cyanophytes) and nanophytoplankton were the dominant classes. Relative bacteriochlorophyll-*a* concentrations varied around 2%. The transition zone between the Marquesas and the SPSG was also well predicted by the model. However, some regional characteristics have been observed where measured and modelled data differ. Amongst these features is the extreme depth of the DCM (180 m) towards the centre of the gyre, the presence of a deep nanoflagellate population beneath the DCM or the presence of a prochlorophyte-enriched

population in the formation area of the high salinity South Pacific Tropical Water. A coastal site sampled in the eutrophic upwelling zone, characterised by recently upwelled water, was significantly and unusually enriched in picoeucaryotes, in contrast with an offshore upwelling site where a more typical senescent diatom population prevailed.

1 Introduction

East of Tahiti, the South East Pacific Ocean is characterised by very contrasting trophic environments, covering a large range of total chlorophyll-*a* concentrations [TChl*a*]. These environments comprise the “permanently” (Dandonneau et al., 2004) “hyper-oligotrophic” centre of the South Pacific Subtropical Gyre (SPSG; Longhurst, 1998; Claustre and Maritorena, 2003) where SeaWiFS imagery presents average surface TChl*a* concentrations of 0.02 mg m⁻³ (<http://oceancolor.gsfc.nasa.gov/SeaWiFS/>). This gyre is distinguished by its hydrodynamic stability, its unique magnitude, the transparency of its waters (Morel et al., 2007) and extremely weak sources of nutrients from deeper layers (Raimbault et al., 2007) as well as from the atmospheric flux (Mahowald, 2005; Wagener et al., 2008; Claustre et al., 2008). To the West, the mesotrophic environment of the Marquesas archipelago prevails in a predominantly HNLC (High Nutrient Low Chlorophyll) zone (Claustre et al., 2008 and references therein). To the East, the waters become strongly eutrophic as the Chilean coastline is subjected to an offshore transport of surface waters, thus inducing strong hydrodynamics and the upwelling of deep, cold and nutrient-rich waters at the coast (Longhurst, 1998; Claustre et al., 2008 and references therein).



Correspondence to: J. Ras
(josephine.ras@obs-vlfr.fr)

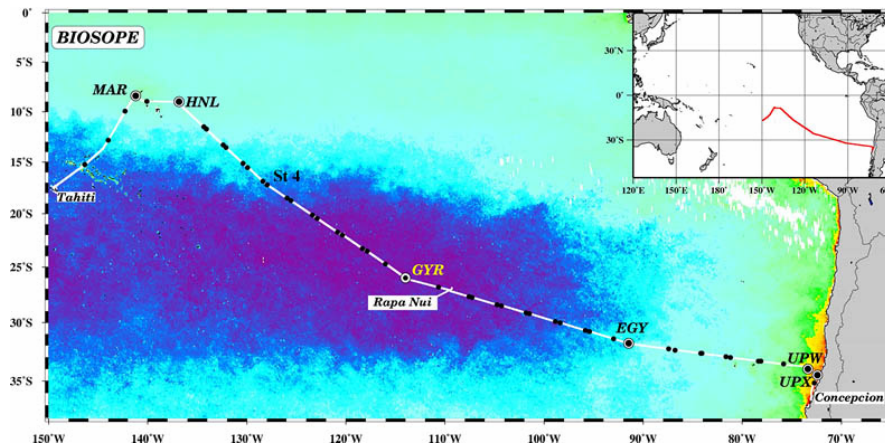


Fig. 1. Map of the BIOSOPE cruise track superimposed on a SeaWiFS ocean colour composite, the dark purple indicating the extremely low concentrations (0.017 mg m^{-3}) of TChla.

The BIOSOPE cruise (BIOgeochemistry and Optics South Pacific Experiment), carried out from October to December 2004, took place between Tahiti (French Polynesia) and Concepcion (Chile). It can be described as a voyage of exploration across unique and contrasting environments where oceanographic data are still scarce to this day (Claustre and Maritorena, 2003). Besides the aspects of oceanographic investigation aiming at the assessment of the biogeochemical and optical properties of the ocean as a function of surface water [TChla] the wide range of trophic conditions observed during this cruise was ideal for carrying out calibration and validation activities for ocean colour remote sensors.

During the past decades, high performance liquid chromatography (HPLC) techniques have rapidly evolved, allowing for phytoplankton biomass and composition in the oceans to be described in detail using algal pigment biomarkers. Indeed, the [TChla] has been a widely used biomarker for the phytoplankton biomass in the oceans (Yentch and Menzel, 1963; Parsons and Strickland, 1963; O'Reilly et al., 1998). Accessory pigments have either photosynthetic properties allowing the phytoplankton cells to increase their light-harvesting spectrum, or a role of photoprotection in dissipating the excess of light energy received and reducing the oxidation that takes place due to stress in conditions of strong irradiance. The major accessory pigments have also proven to be useful chemotaxonomic indicators (Goericke and Repeta, 1992; Wright and Jeffrey, 1987; Moore et al., 1995; Guillard et al., 1985). Hence, the chlorophyll-*a* and accessory pigment distributions have become important descriptors of the spatial and temporal variations of the autotrophic biomass and taxonomic composition. From the pigment composition of natural communities, Claustre (1994), Vidussi et al. (2001), and recently Uitz et al. (2006), have proposed to derive pigment-based size classes relevant to picophytoplankton (less than $2 \mu\text{m}$), nanophytoplankton (between 2

and $20 \mu\text{m}$) and microphytoplankton (greater than $20 \mu\text{m}$). Based on the statistical analysis of a global HPLC database, the proposed parameterisation allows these three pigment-based size classes and their vertical distribution to be retrieved from remotely sensed TChla concentrations (Uitz et al., 2006). Although the database was extensive (~ 2400 profiles), extremely few profiles were from the South East Pacific so that the “global” parameterisation might be somewhat biased not taking into consideration certain characteristics of this rather unknown and vast area.

Thus, in the context of the BIOSOPE cruise, the objectives related to the analysis of the distribution of phytoplankton pigments are double. The first aim of this study is essentially descriptive and explorative where the spatial (along transect and vertical) distribution of phytoplankton pigments is analysed in this “mare incognita” of the South-East Pacific Ocean. The second aim is to investigate whether the in situ distributions of pigment-based size classes conform with the predicted distributions derived from the application of the Uitz model to the remotely sensed (SeaWiFS) TChla concentrations. By doing so, it is expected that any difference between measured and predicted distributions could be scrutinized and further interpreted in terms of distinct regional features of the South-East Pacific relative to the mean (global ocean) trend.

2 Material and methods

2.1 Sampling area

Sampling was performed between the 26 October and the 11 December 2004 in the South Pacific along a transect starting in the vicinity of the Marquesas archipelago (141°W , 8°S) and ending in the upwelling of the Chilean coast (73°W , 35°S) (Fig. 1). Six sites along this transect were studied

over 2- to 5-day periods: MAR: Marquesas archipelago (141.3° W; 8.4° S); HNL: HNLC area east of the Marquesas islands (136.8° W; 9° S); GYR: centre of the South Pacific gyre (about 300 nautical miles west of the “navel of the world”, a native name for Easter Island; 114° W, 26° S); EGY: eastern border of the gyre (91.4° W, 31.8° S); UPW: upwelling site situated above the abyssal plain, about 70 nautical miles from the coast (73.3° E; 34° S); UPX: upwelling site situated above the continental shelf, about 18 nautical miles from the coast (72.4° E, 34.5° S). In addition, twenty one short-term (less than 5 h) stations were studied each day during the transit between the long stations.

2.2 Sample collection and storage

Seawater samples were collected using a CTD-rosette system equipped with 21 twelve litre Niskin bottles. The samples for pigment analysis were collected at about 10 depths, twice a day, from the 09:00 a.m. and noon CTD casts (local time).

The water samples were vacuum filtered through 25 mm diameter *Whatman* GF/F glass fibre filters (0.7 μm particle retention size). Filtered volumes varied between 5.6 L in the hyper-oligotrophic waters and 1 L in the upwelling zone. The filters were immediately stored in liquid nitrogen then at -80°C until analysis on land.

2.3 Chlorophyll and carotenoid pigment extraction and analysis

Extraction and analysis of the BIOSOPE samples were completed between the 7 March and the 27 April 2005. The filters were extracted at -20°C in 3 mL methanol (100%), disrupted by sonication and clarified one hour later by vacuum filtration through *Whatman* GF/F filters. The extracts were rapidly analysed (within 24 h) by HPLC with a complete *Agilent Technologies* system (comprising *LC Chemstation* software, a degasser, a binary pump, a refrigerated autosampler, a column thermostat and a diode array detector)

The pigments were separated and quantified following an adaptation of the method described by Van Heukelem and Thomas (2001). Modifications to this method allowed for increased sensitivity in the analysis of ultra-oligotrophic waters. As an example of the sensitivity and resolution of the method, Figs. 2a and b represent two typical chromatograms originating from the centre of the gyre (surface and Deep Chlorophyll Maximum respectively) where at least sixteen pigment peaks were identified.

The sample extracts (100% methanol), premixed (1:1) with a buffer solution (tetrabutylammonium acetate or TBAA 28 mM), were injected onto a narrow reversed-phase C8 Zorbax Eclipse XDB column (3 \times 150 mm; 3.5 μm particle size) which was maintained at 60°C . Separation was achieved within 28 min with a gradient between a solution (A) of TBAA 28 mM: methanol (30:70; v:v) and a solution (B) of 100% methanol according to the following program:

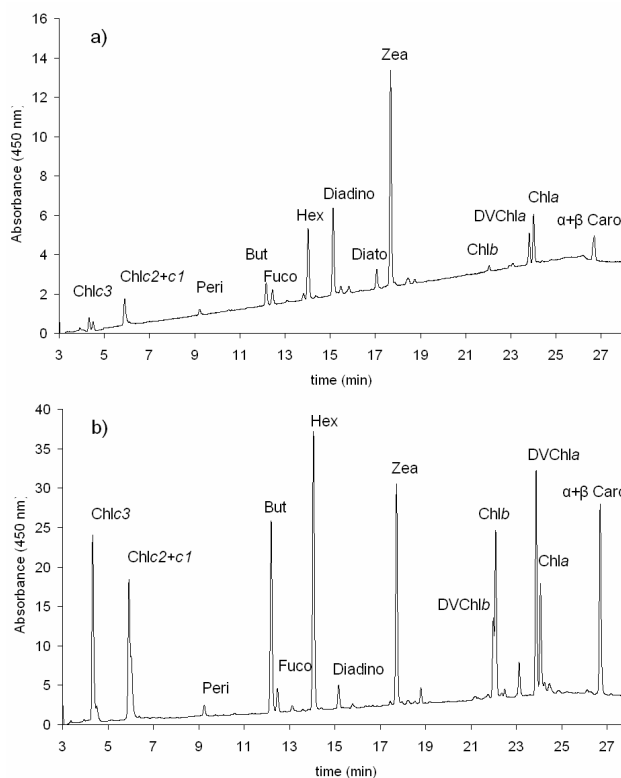


Fig. 2. HPLC chromatograms from (a) the surface and (b) the DCM at 180 m at the hyper-oligotrophic GYR station. Detection absorption wavelength is 450 nm.

(t(min);%B;%A), (0;10;90), (25;95;5), (28;95;5). A diode array detector allowed for the absorption of most pigments to be detected at 450 nm, while chlorophyll-*a* and its derivatives were detected at 667 nm and bacteriochlorophyll-*a* at 770 nm. The diode array absorption spectra of each peak were used for identification purposes.

Pigment concentrations (in mg m^{-3}) were calculated from the peak areas with an internal standard correction (Vitamin E acetate, Sigma) and external calibration standards which were provided by DHI Water and Environment (Denmark).

This method has proven to be satisfactory in terms of resolution, sensitivity, accuracy and precision (Hooker et al., 2005), with the detection of about 25 separate phytoplankton pigments (listed in Table 1), with a lower limit of detection (3 times Signal:Noise ratio) for chlorophyll-*a* of 0.0001 mg m^{-3} and with an injection precision of 0.4%.

2.4 Phytoplankton pigment-based size classes

While TChla is the universal proxy for phytoplankton organisms, accessory pigments (chlorophylls-*b* and *c*, and carotenoids) are specific to phytoplankton groups (Table 1), and their respective proportion to TChla is a proxy of the community composition (e.g. Gieskes et al., 1988; Jeffrey and Vesk, 1997; Mackey et al., 1996; Prézelin et al., 2000).

Table 1. List of the pigments used in this study, along with their abbreviations, calculation and their taxonomic significance (From Jeffrey and Vesk, 1997). The main algal groups used here to describe the phytoplankton community composition are indicated in bold.

Chlorophylls	Abbreviation	Sum	Taxonomic or biogeochemical significance
Chlorophyll- <i>a</i>	Chl <i>a</i>	Chl <i>a</i> + allomers + epimers	All – except Prochlorophytes
Divinyl Chlorophyll- <i>a</i>	DVChl <i>a</i>		Prochlorophytes
Total Chlorophyll- <i>a</i>	TChl <i>a</i>	Chl <i>a</i> + DVChl <i>a</i> + Chl <i>d</i> <i>a</i>	All
Chlorophyll- <i>b</i>	Chl <i>b</i>		Green algae
Divinyl Chlorophyll- <i>b</i>	DVChl <i>b</i>		Prochlorophytes
Total Chlorophyll- <i>b</i>	TChl <i>b</i>	Chl <i>b</i> + DVChl <i>b</i>	Green algae, Prochlorophytes
Chlorophyll- <i>c</i> 2	Chl <i>c</i> 2		Various
Chlorophyll- <i>c</i> 3	Chl <i>c</i> 3		Prymnesiophytes , Chrysophytes
Bacteriochlorophyll- <i>a</i>	BChl <i>a</i>		Photoheterotrophic bacteria
Peridinin	Peri		Dinoflagellates
19'-Butanoyloxyfucoxanthin	But		Pelagophytes , prymnesiophytes
Fucoxanthin	Fuco		Diatoms , prymnesiophytes, some Dinoflagellates
19'-Hexanoyloxyfucoxanthin	Hex		Prymnesiophytes
Zeaxanthin	Zea		Cyanobacteria, Prochlorophytes
Alloxanthin	Allo		Cryptophytes
Diatoxanthin	Diato		Various
Diadinoxanthin	Diadino		Various
Lutein	Lut		Chlorophytes
Neoxanthin	Neo		Green algae
Violaxanthin	Viola		Green algae
Prasinoloxanthin	Pras		Prasinophytes
Carotenes	Car	a-Car + b-Car	Various
Chlorophyllide- <i>a</i>	Chl <i>d</i> <i>a</i>	Chl <i>d</i> <i>a</i> + Chl <i>d</i> <i>a</i> -like	Senescent diatoms
Phaeophorbide <i>a</i>	Phd <i>a</i>	Phd <i>a</i> + Phd <i>a</i> -like	Grazor faecal pellets
Phaeophytin <i>a</i>	Pht <i>a</i>		Grazor faecal pellets

Here we used the pigment grouping method proposed by Claustre (1994) and Vidussi et al. (2001) and recently improved by Uitz et al. (2006). Seven pigments are used as biomarkers of several phytoplankton taxa: fucoxanthin, peridinin, alloxanthin, 19'-butanoyloxyfucoxanthin, 19'-hexanoyloxyfucoxanthin, zeaxanthin, total chlorophyll-*b* (for abbreviations see Table 1). These taxa are then gathered into three size classes (micro-, nano-, and picophytoplankton), according to the average size of the cells. The fraction of each pigment-based size class with respect to the total phytoplankton biomass is calculated as follows:

$$\text{Greater than } 20 \mu\text{m} : f_{\text{micro}} = (1.41[\text{Fuco}] + 1.41[\text{Peri}]) / \text{wDP} \quad (1a)$$

$$2 \text{ to } 20 \mu\text{m} : f_{\text{nano}} = (0.60[\text{Allo}] + 0.35[\text{But}] + 1.27[\text{Hex}]) / \text{wDP} \quad (1b)$$

$$\text{Less than } 2 \mu\text{m} : f_{\text{pico}} = (0.86[\text{Zea}] + 1.01[\text{TChl}b]) / \text{wDP} \quad (1c)$$

where wDP is the sum of the concentration of the seven weighted diagnostic pigments:

$$\text{wDP} = 1.41[\text{Fuco}] + 1.41[\text{Peri}] + 0.60[\text{Allo}] + 0.35[\text{But}] + 1.27[\text{Hex}] + 0.86[\text{Zea}] + 1.01[\text{TChl}b] \quad (2)$$

Each diagnostic pigment is associated to a coefficient which represents an estimate of the average ratio of the TChl*a* concentration to the diagnostic pigment concentration. These

coefficients have been obtained by multiple regression analysis, performed on a global pigment database (Uitz et al., 2006). Eventually the TChl*a* biomass associated with each class is derived according to:

$$[\text{TChl}a]_{\text{micro}} = f_{\text{micro}} \times [\text{TChl}a] \quad (3a)$$

$$[\text{TChl}a]_{\text{nano}} = f_{\text{nano}} \times [\text{TChl}a] \quad (3b)$$

$$[\text{TChl}a]_{\text{pico}} = f_{\text{pico}} \times [\text{TChl}a] \quad (3c)$$

2.5 Computation of the in situ derived euphotic depth

The depth of the euphotic zone (*Ze*), representing the depth where irradiance is reduced to 1% of its surface value, was computed using the in situ [TChl*a*] profiles according to the model developed by Morel and Maritorena (2001). The water column [TChl*a*] was progressively integrated with increasing depths and *Ze* was consequently determined through an iterative process which is described in Morel and Berthon (1989).

2.6 Remotely sensed surface chlorophyll-*a* used to derive the phytoplankton vertical community composition

The algorithm developed by Uitz et al. (2006) was applied, and the vertical profiles of [TChl*a*] associated with the three

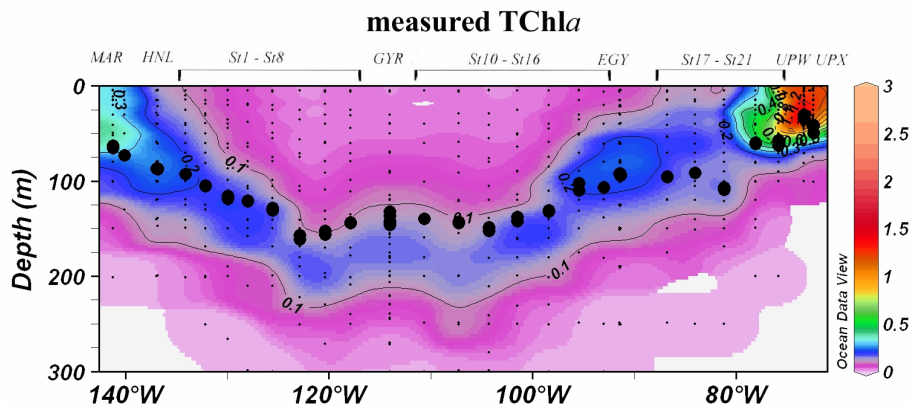


Fig. 3. Contour plot of the measured TChla concentrations (mg m^{-3}) for the Biosope cruise transect. Large black dots represent the depth of the euphotic layer, Z_e (m). Small black dots represent collected water samples at each sampling station. (Ocean Data View (ODV) software, version 3.0.1, R. Schlitzer, <http://odv.awi-bremerhaven.de/>, 2005).

afore-mentioned pigment-based size classes were derived. This implies the use of the near-surface TChla concentrations, which can be obtained from remotely sensed ocean colour.

For each station sampled during the BIOSOPE cruise, the corresponding near-surface [TChla] was extracted from SeaWiFS imagery ($[\text{TChla}]_{\text{sat}}$, mg m^{-3}), given the geographic location and date of sampling. When no $[\text{TChla}]_{\text{sat}}$ was available, values were extracted from the SeaWiFS images corresponding to ± 1 day, ± 2 days, or ± 3 days, with respect to the date of in situ sampling. For 39% of the stations, the date of SeaWiFS and in situ measurements coincided, for 42% they were 1-day shifted, for 10% they were 2-day shifted, and for 9% they were 3-day shifted. This strategy was chosen in order to keep all the data. A detail of the full procedure to derive vertical profiles is given in Uitz et al. (2006). Only a short summary is given below.

Firstly, the satellite derived euphotic depth was computed from the $[\text{TChla}]_{\text{sat}}$ value by using successively the statistical relationship linking $[\text{TChla}]_{\text{sat}}$ and the column-integrated content (Eq. 8 of Uitz et al., 2006), and that of Morel et Martorena (2001) relating the column-integrated content and $Z_{e,\text{sat}}$. The euphotic depth was then compared to the mixed layer depth (Z_m) to determine whether the water column was stratified (i.e. $Z_e \geq Z_m$) or mixed (i.e. $Z_e < Z_m$). For stratified waters, the $[\text{TChla}]_{\text{sat}}$ value was used to generate dimensionless profiles (with respect to depth and to biomass) of TChla associated with micro-, nano-, and picophytoplankton. Depth profiles were restored to physical units by multiplying the depths by $Z_{e,\text{sat}}$ and the concentrations by the mean TChla concentration within the euphotic layer. For mixed waters, the $[\text{TChla}]_{\text{sat}}$ value was used to determine the proportion of each pigment-based size class, eventually multiplied by the $[\text{TChla}]_{\text{sat}}$ value, and extended through the water column to generate uniform vertical profiles.

3 Results

3.1 General hydrographic conditions

General hydrographic conditions, including the distribution of temperature and salinity, are detailed in the introduction of this special issue (Claustre et al., 2008).

3.2 Pigment distribution

In terms of algal biomass (Fig. 3), the surface TChla concentrations were lowest at the hyper-oligotrophic centre of the SPSG (0.017 mg m^{-3} at station 6), while the highest surface values were found at both ends of the transect in the eutrophic upwelling area (up to 1.5 mg m^{-3}) and in the mesotrophic Marquesas area (0.200 to 0.400 mg m^{-3}). Furthermore, a progressive deepening of the DCM towards the centre of the gyre could be observed, varying from 50 m depth in the Marquesas area to 180 m in the centre of the gyre (reaching 190 m at Station 6). Pigment concentrations at the DCM in the SPSG were generally 10 fold those observed at the surface (Fig. 4a). Down to 50 m at the Chilean upwelling, the TChla profile is generally homogenous.

The mean clear sky daily PAR irradiance at the surface is $51.8 \text{ mol quanta m}^{-2} \text{ d}^{-1}$ (Huot et al., 2007). This covers the whole transect, the variability due to latitude being insignificant. Figure 3 illustrates how the Z_e , which therefore corresponds to the $0.5 \text{ mol quanta m}^{-2} \text{ d}^{-1}$ isolume, closely follows the position of the DCM except in the centre of the gyre where the DCM is clearly below the Z_e .

In contrast with TChla, the accessory pigments do not all exhibit the same East-West “symmetrical” distribution. Figure 5 illustrates the vertical distribution of 6 representative pigments.

Total chlorophyll-*b* or TChl-*b* (Fig. 5a), reflecting both chlorophytes, prasinophytes (chlorophyll-*b*) and prochlorophytes (divinyl chlorophyll-*b*), showed minimum

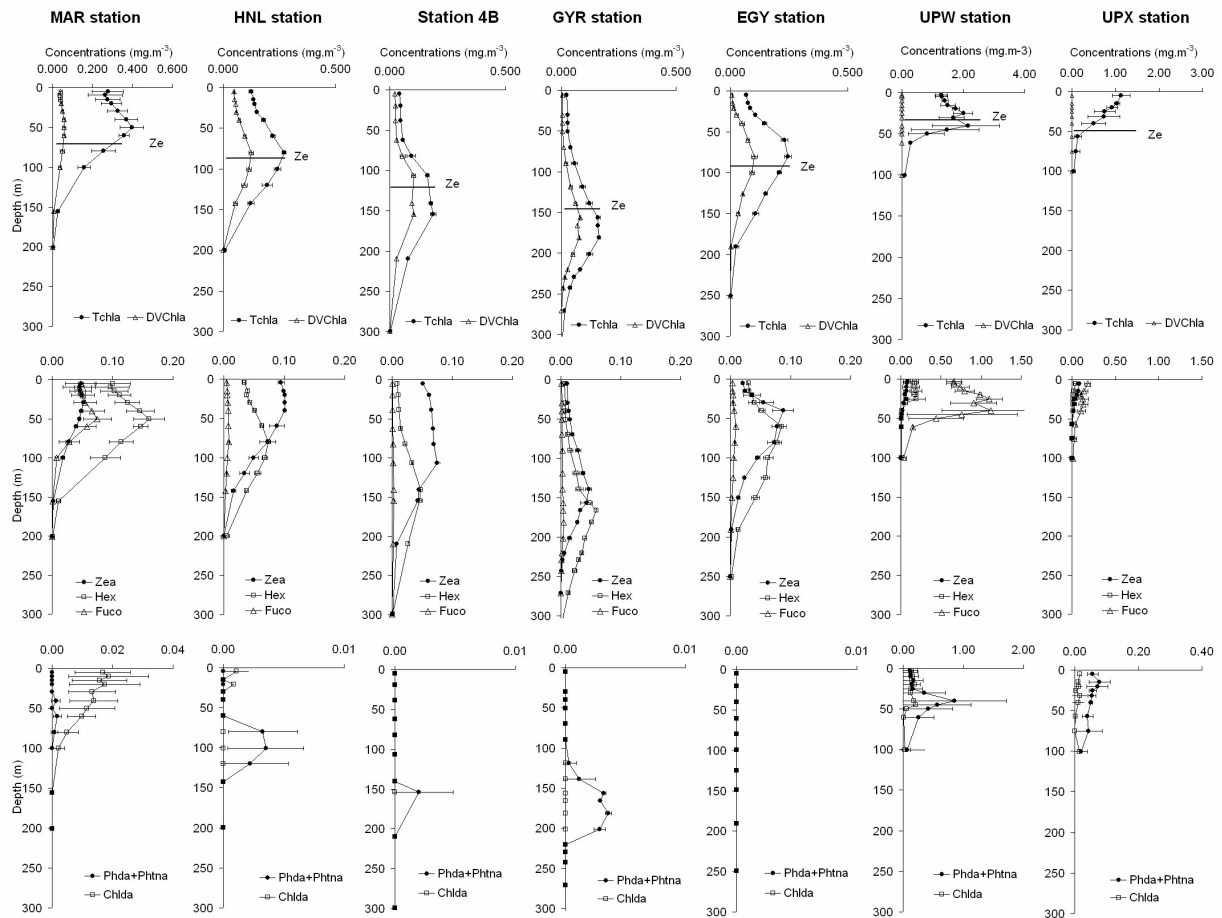


Fig. 4. Average vertical pigment profiles (mg m^{-3}) at the MAR, HNL, St4B, GYR, EGY, UPW and UPX sites: **(a)** Total chlorophyll-*a* and divinyl chlorophyll-*a*, the horizontal lines represent the depth of the euphotic layer (*Ze*); **(b)** zeaxanthin, 19'-hexanoyloxyfucoxanthin and fucoxanthin; **(c)** degradation products: phaeophorbide-*a*+phaeophytina and chlorophyllide-*a*. Horizontal bars represent the average value \pm SD.

concentrations at the surface of the gyre (less than 0.001 mg m^{-3}), while the deep maximum (down to 200 m) could reach more than 0.100 mg m^{-3} . Maximum concentrations were encountered at station 20 (0.245 mg m^{-3}) and station UPX (0.400 mg m^{-3}). Because divinyl chlorophyll-*b* is totally absent in the upwelling zone, this feature is likely the signature of green eukaryotes. A remarkable feature in the gyre system is the high TChl-*b* concentration below the DCM which is essentially composed of divinyl chlorophyll-*b* (reaching up to 100% of TChl-*b*).

Divinyl chlorophyll-*a* or DVChl-*a*, (Figs. 4a and 5b), representative of prochlorophytes, was detected over the whole studied area, except for the upwelling zone, with surface water concentrations varying around 0.040 mg m^{-3} at the MAR station, increasing to 0.050 at the HNL station then progressively decreasing to 0.003 mg m^{-3} in the centre of the gyre. East of the gyre, surface concentrations did not exceed 0.008 mg m^{-3} . At depth, the distribution of DVChl-*a* concentrations generally followed that of the DCM (Fig. 4a).

The photoprotecting zeaxanthin or Zea (Figs. 4b and 5c), found in cyanobacteria and prochlorophytes, showed very low surface values in the centre of the gyre (around 0.010 mg m^{-3} at the surface) and progressively increasing concentrations with depth, with a maximum (about 0.050 mg m^{-3}) above the DCM, around 150 m. A particular zone, coinciding with the South Pacific Tropical Water mass between HNL and station 4, was characterised by high and constant zeaxanthin concentrations between the surface and 100 m depth. In the upwelling area, zeaxanthin was detected in very low concentrations, while the photoprotecting diadinoxanthin and diatoxanthin, (essentially typical pigments of diatoms and prymnesiophytes) significantly increased (data not shown).

19'-Hexanoyloxyfucoxanthin or Hex (Figs. 4b and 5d), representative of chromophyte nanoflagellates, was detected throughout the whole studied area, with highest concentrations at the extremities of the transect: in the Marquesas archipelago (0.060 – 0.130 mg m^{-3} and 0.130 – 0.180 mg m^{-3}

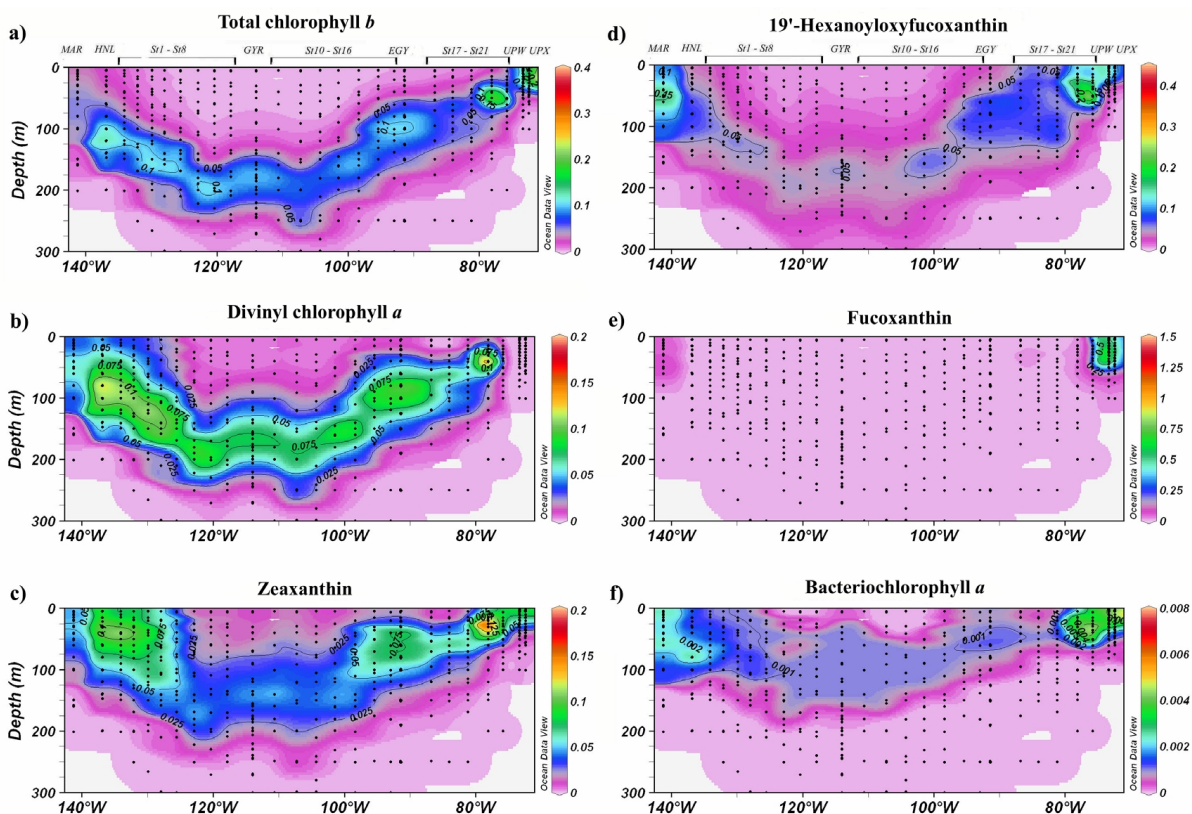


Fig. 5. Vertical cross sections for pigment concentrations (mg m^{-3}) across the BIOSOPE cruise transect. (a) Total chlorophyll-*b*; (b) divinyl chlorophyll-*a*; (c) zeaxanthin; (d) 19'-hexanoyloxyfucoxanthin; (e) fucoxanthin; (f) bacteriochlorophyll-*a*.

at the surface and 50 m depth respectively), around stations 20 and 21 (0.140 mg m^{-3} and 0.400 mg m^{-3} at the surface and 50 m depth respectively) and at station UPW ($0.140\text{--}0.230 \text{ mg m}^{-3}$ and 0.320 mg m^{-3} at the surface and 40 m depth respectively). The 19'-hexanoyloxyfucoxanthin concentrations at the UPX site were lower than 0.067 mg m^{-3} . Lowest concentrations were found at the centre of the gyre: 0.005 mg m^{-3} at the surface and 0.050 mg m^{-3} at the DCM. Interestingly, throughout the central gyre the Hex concentrations were twice higher around 270 m depth than at the surface (0.011 mg m^{-3}).

Fucoxanthin or Fuco (Figs. 4b and 5e), a tracer of diatoms, was found in very low amounts throughout the SPSG. Significant concentrations were only found in the Marquesas waters (0.020 to 0.080 mg m^{-3} at the surface and up to 0.100 mg m^{-3} at 50 m depth) and in the upwelling zone, particularly at station UPW (0.700 and 1.600 mg m^{-3} at the surface and at 40 m depth respectively). Fucoxanthin concentrations did not exceed 0.200 mg m^{-3} at station UPX.

At the MAR station, bacteriochlorophyll-*a* concentrations (BChl-*a*, Fig. 5f) in the first 100 m varied around 0.0015 and 0.0035 mg m^{-3} . At the HNL station, they were variable but lower than at MAR (between 0.0010 and 0.0016 mg m^{-3}), although a slight deep maximum was observed around 80m

depth (0.0015 to 0.0033 mg m^{-3}). The surface BChl-*a* concentrations within the gyre system remained extremely low and close to detection limits (0.0005 mg m^{-3}), while a BChl-*a* deep maximum was observed around 100 m (0.0010 mg m^{-3}). In the upwelling area, the BChl-*a* concentrations were the highest measured over the whole transect (between 0.0020 and 0.0090 mg m^{-3}).

Minor pigments such as prasinoxanthin and alloxanthin, respectively associated to prasinophytes and cryptophytes, were never detected in the Marquesas area and hardly in the SPSG (data not shown). However, prasinoxanthin, associated to chlorophyll-*b*, as well as neoxanthin, violaxanthin and lutein (typical indicators of chlorophytes and prasinophytes), were found in significant concentrations at the coastal upwelling UPX site, thus suggesting an important localised contribution of green picophytoplankton in these waters.

Chlorophyllide-*a* or Chlida and phaeopigments (Fig. 4c) were scarce in the gyre, sometimes detectable at the DCM. Chlida was present in significant and variable amounts at the MAR and UPW stations. The degradation products derived from the demetallation of chlorophyll-*a* associated to grazing activities (phaeophorbide-*a* and phaeophytin-*a*) were found in high concentrations essentially in the upwelling area, with

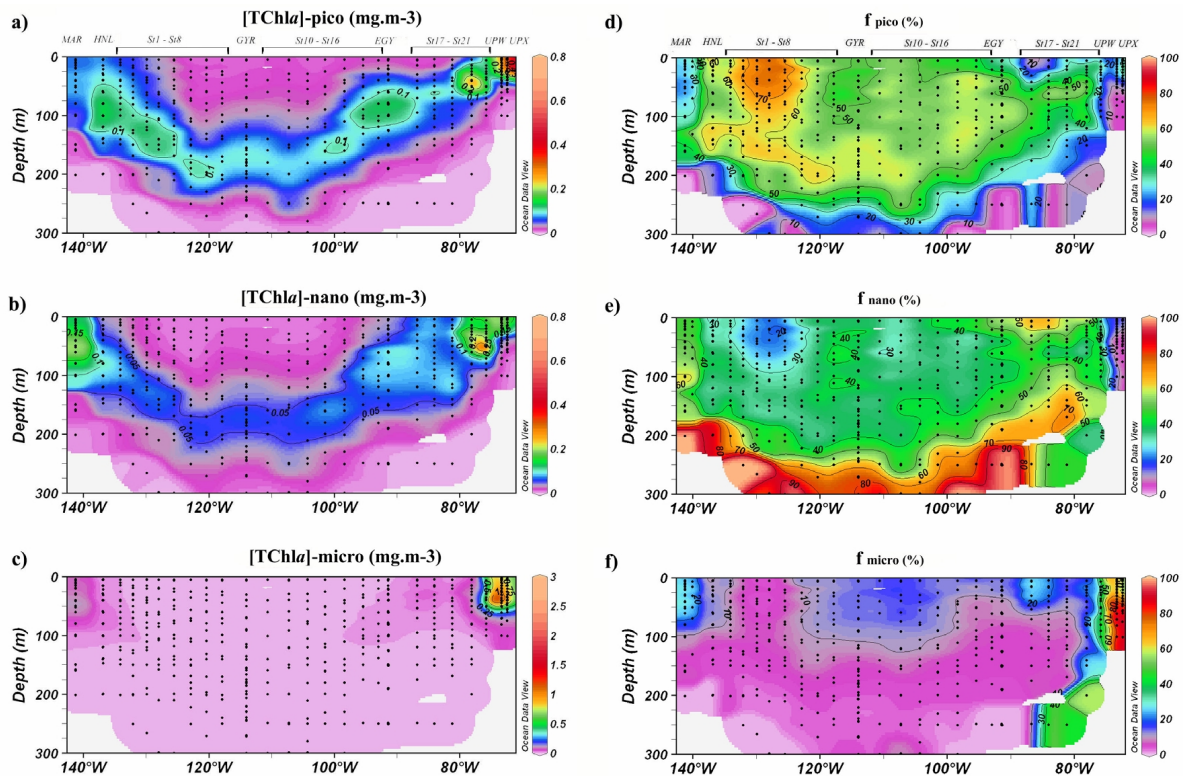


Fig. 6. Biosope cruise cross sections of in situ TChla concentrations in mg m^{-3} (a–c) and percentages (e–g) associated to the pico-, nano- and microphytoplankton size classes. Black dots represent sampling points.

the phaeopigment to TChla ratio increasing constantly with depth up to values of 1.500. Degradation pigment concentrations generally showed a good correlation with the fucoxanthin concentrations (data not shown).

3.3 Distribution of the phytoplankton pigment based size classes

Picophytoplankton, represented by cyanobacteria and prochlorophytes in this study, present similar variations to TChla (Fig. 6a), with a deep maximum coinciding with the DCM (around 180 m in the centre of the gyre). Picophytoplankton is unusually high at the UPX station. In terms of percentages of TChla, the highest values for picophytoplankton ($>70\%$) are found associated with South Pacific Tropical Water (SPTW) between stations 2 and 5 (Fig. 6d). Elsewhere in the gyre, the proportion of picophytoplankton varies between 40 and 60% down to 250 m. Nanophytoplankton in the gyre system varies in concentrations and proportions that are comparable to the picophytoplankton (Figs. 6b and 6e), although below 250 m, it is found in proportions greater than 60% (essentially due to the quasi dominance of Hex). At the MAR station, nanophytoplankton is the predominant class. Surface waters at stations 17 and 18 also present relatively high proportions

of nanophytoplankton ($>60\%$), while minimal proportions are found in the SPTW area ($<30\%$) and in the upwelling zone. Microphytoplankton, as for fucoxanthin, points to the scarcity in diatom populations across the gyre system (Fig. 6c). Interestingly, a slight increase in the proportion of essentially fuco-containing phytoplankton is observed in the surface waters of the central gyre ($>10\%$, Fig. 6f) while proportions are less than 10% in the rest of the gyre system. The Marquesas waters are also enriched in fucoxanthin-containing microphytoplankton ($>20\%$). In the upwelling zone, microphytoplankton represents more than 60% of the TChla biomass. The contribution of peridinin to the microphytoplankton pool is generally low, but there are some exceptions: for example the Peri to Fuco ratio is particularly high (>2) in the SPTW area and at sites 15 and 20.

3.4 TChla biomass and pigment-based size classes: modelled versus in situ data

3.4.1 Global trends in Tchl_a

The vertical sections of the TChla concentrations obtained from in situ measurements and from the model are presented in Figs. 3 and 7, respectively. The comparison between these

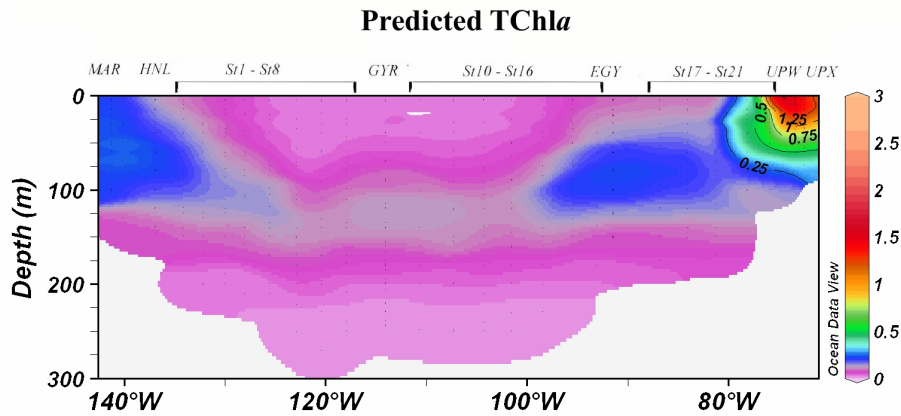


Fig. 7. Contour plot of the predicted TChla concentrations (mg m^{-3}) for the BIOSOPE cruise transect. (Ocean Data View (ODV) software, version 3.0.1, R. Schlitzer, <http://odv.awi-bremerhaven.de/>, 2005).

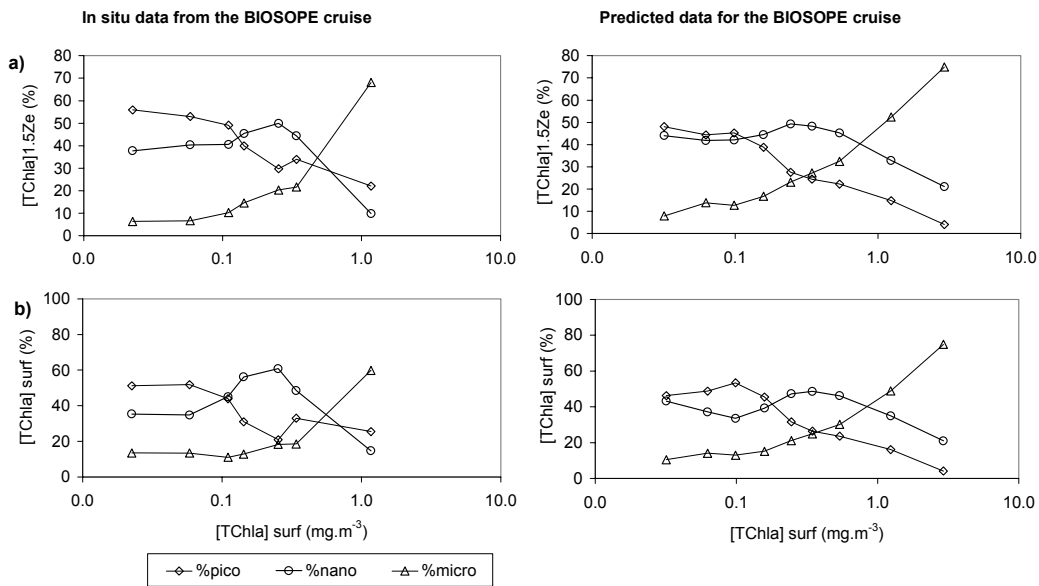


Fig. 8. Composition of the phytoplankton population as a function of surface TChla concentrations for in situ and model data. **(a)** integrated percentages of pico-, nano- and microphytoplankton between 0 and 1.5 Ze and **(b)** surface percentages of pico-, nano- and microphytoplankton.

two figures illustrates the capacity of the model to reproduce the general trends in the horizontal and vertical distribution of the TChla. Notably, the model simulates the gradient observed in the surface concentrations with extremely low values in the core of the gyre ($\approx 0.030 \text{ mg m}^{-3}$) and higher values at the extremities of the transect, i.e. in the vicinity of the Marquesas Islands and of the upwelling of Chile ($\approx 1.500 \text{ mg m}^{-3}$). It also reproduces the surface maximum at each end of the transect as well as the deepening of the maximum in the centre of the gyre. Besides these similarities however, the depth of the TChla maximum is significantly underestimated in the core of the gyre ($\approx 120 \text{ m}$ according to the model vs. 180 m following in situ measurements).

3.4.2 Global trends in pigment-based size classes

In a first approach we considered the contribution of the three pigment-based size classes to the total phytoplankton biomass as a function of the surface [TChla]. To do so, the same procedure as described in Uitz et al. (2006) was used. Namely, the average contribution of each phytoplankton size class was calculated for the surface layer on the one hand, and for the 0–1.5 Ze layer on the other hand, for nine trophic categories defined by successive intervals of surface [TChla]. The resulting contributions are compared to those obtained from the global dataset from which the model has been derived (Fig. 6 in Uitz et al., 2006). The changes

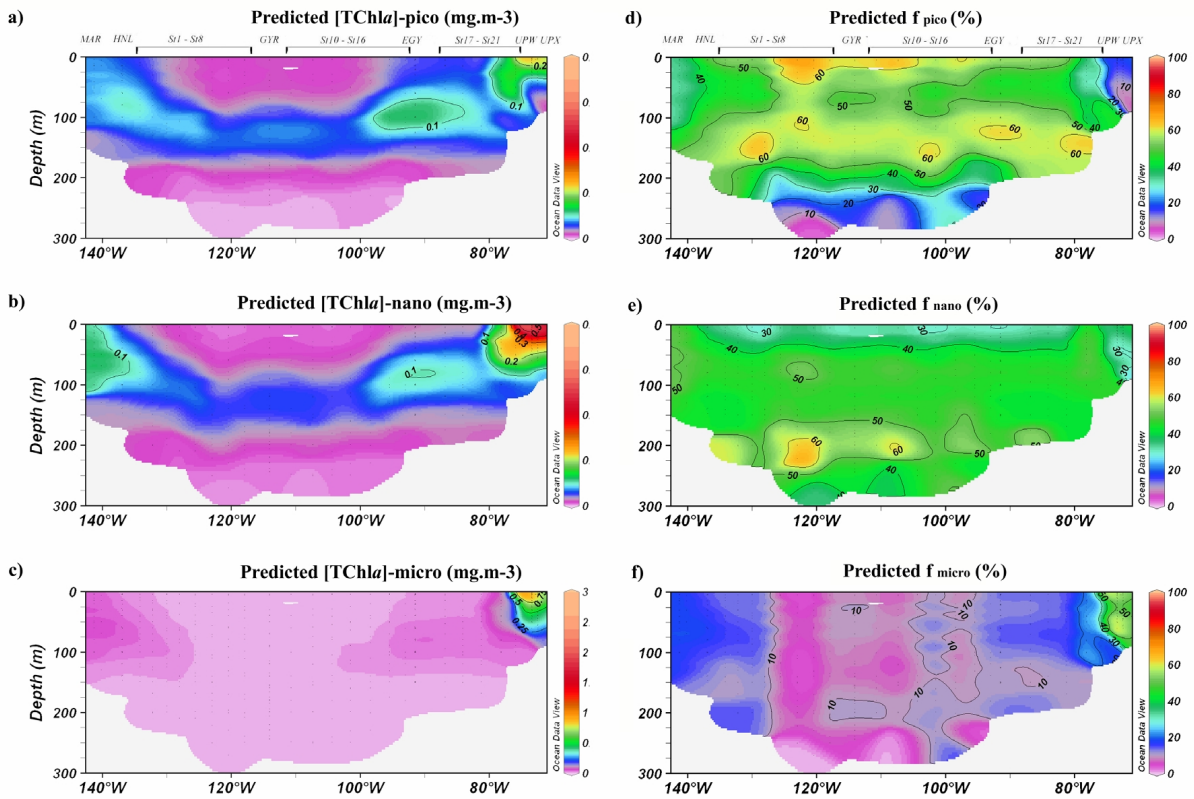


Fig. 9. Cross sections of the predicted TChla concentrations along the BIOSOPE transect for pico-, nano- and microphytoplankton, expressed in mg m^{-3} (a–c) and percentages (d–f).

in the contribution of the three pigment-based size classes as a function of the surface [TChla] display the same general trend for both datasets (Fig. 8). Indeed, the contribution of microphytoplankton tends to increase with the surface TChla concentration, and reaches up to 50–60% for a surface [TChla] of 1.000 mg m^{-3} . In contrast, picophytoplankton dominate in oligotrophic conditions ($\approx 50\%$ for a surface [TChla] of 0.030 mg m^{-3}) and nanophytoplankton in mesotrophic conditions ($\approx 50\%$ for a surface [TChla] of 0.500 mg m^{-3}).

3.4.3 Deviations with respect to the global trends

The comparison between in situ data and predictions shows that, at a first order, the model performs well for the wide range of trophic situations encountered along the BIOSOPE transect (Fig. 8). The sections of the absolute and relative TChla concentrations of micro-, nano- and picophytoplankton obtained from the model are presented in Fig. 9, to be compared to Fig. 6 (in situ data). In terms of absolute concentrations, the model displays similar values to those measured in situ. The global trends are also well represented in terms of relative values, as expected from Fig. 8. This exercise thus represents an a posteriori validation of the model considering that the BIOSOPE dataset was not included in

the database from which the model has been derived. In addition, this comparison exercise allows the identification of several features where the phytoplankton composition is not typical of the model-based composition associated to a given surface [TChla]. These particularities may be related to the very unique spatial and temporal features (large- or small-scale) that occurred within the study region. Within the following discussion, several areas, characterized by atypical pigment distributions and associations, will be depicted.

4 Discussion

4.1 General trends

4.1.1 Dominance of picophytoplankton in the South Pacific Subtropical Gyre

Between stations 1 and 16 (from 13.5° S ; 132.1° W to 31.4° S ; 93° W), picophytoplankton is generally the most abundant size class (50–60% of the phytoplankton biomass down to 250 m). This observation is consistent with other studies in tropical and subtropical areas of the world ocean (Claustre and Marty, 1995; Bidigare and Ondrusek, 1996; Mackey et al., 1996; Dandonneau et al., 2006). In these

strongly illuminated waters, cyanobacteria essentially dominate the phytoplankton populations. *Synechococcus* are more abundant at the surface and *Prochlorococcus* at depth (Fig. 11b and Fig. 11c). When DVChl*a* concentrations from the BIOSOPE cruise were compared with data from the Atlantic subtropical gyre systems (Uitz et al., 2006), it resulted that such low surface concentrations had never yet been measured and that, as for TChl*a*, the deep maximum concentration was significantly deeper than observed elsewhere (data not shown). The effect of photoacclimation (Falkowski and LaRoche, 1991; Partensky et al., 1996; Claustre and Marty, 1995) may explain this observation. It can also lead to an eventual increase of the accessory pigments to TChl*a* ratios with depth (MacIntyre et al., 2002). However this is not a rule, since the pigments do not all react similarly with changing irradiance. *Prochlorophytes* are known to reach maximal relative abundances in highly stratified and extremely nutrient-depleted waters (Partensky et al., 1999; Johnson and Howd, 2000). Either variations in community structure or photoadaptive processes within the cells (phenotypic versus genotypic modifications), may explain the observed vertical structure of the *prochlorophyte* population with divinyl chlorophyll-*a* prevailing in the upper 180 m (DCM included) while a layer of divinyl chlorophyll-*b*-rich water sits at the base of the DCM (DVChl-*b*/DVChl-*a* < 0.1 above 150 m and ≈ 2 at 300 m depth, see also Fig. 11a). Goericke and Repeta (1993) and Partensky et al. (1996) made similar observations in the North Atlantic. Moore and Chisholm (1999), Partensky et al. (1999), Johnson et al. (2006), Bouman et al. (2006) and Garczarek et al. (2006) support the hypothesis that several genetically different *prochlorophyte* populations coexist over a vertical light gradient. These ecotypes would be characterised by varying DVChl*b* to DVChl*a* ratios indicating their adaptation to low-light (below the thermocline) or high-light (in the upper mixed layer) environments. The extent of the depth reached by *prochlorophyte* populations may not only depend on light and on nutrients, but may also be limited by temperature. Indeed, in the SPSG, the divinyl chlorophyll-*a* and divinyl chlorophyll-*b* concentrations were always detected above the 11°C isotherm, as has been previously observed by Dandonneau et al. (2006) and Partensky et al. (1999).

4.1.2 Ubiquity of nanophytoplankton in the South Pacific

Throughout most of the SPSG, nanophytoplankton, essentially represented by Hex, corresponded to 40–50% of the TChl*a* biomass down to 200 m depth (Fig. 11d). The ubiquity of the nanophytoplankton class, even in conditions of hyper-oligotrophy and high irradiance, reflects a strong capacity for adapting to the extreme conditions encountered along the transect and as well as at great depths where nutrients become available. Caution must be taken with the definition of nanophytoplankton as it is essentially based on the presence of Hex and But. In the study area, especially at

Table 2. Average values \pm SD of the 0–1.5 Ze integrated TChl*a* contents (mg m^{-2}) associated to the total phytoplankton biomass and to the three pigment-based size classes: pico-, nano- and microphytoplankton between stations 1 and 16 for the gyre system and for stations MAR, EGY, UPW and UPX.

Stations	TChl <i>a</i>	[TChl <i>a</i>]-pico	[TChl <i>a</i>]-nano	[TChl <i>a</i>]-micro
St1–St16	20.3 \pm 2.1	11.6 \pm 1.7	7.4 \pm 0.8	1.3 \pm 0.3
MAR	30.2 \pm 2.8	7.1 \pm 0.1	15.7 \pm 1.6	7.4 \pm 1.4
EGY	23.0 \pm 0.5	11.6 \pm 0.5	9.7 \pm 0.4	1.7 \pm 0.1
UPW	79.2 \pm 22.7	3.8 \pm 1.6	8.7 \pm 3.4	66.7 \pm 18.3
UPX	37.4 \pm 6.9	17.8 \pm 2.1	3.0 \pm 0.2	16.5 \pm 4.5

the surface, these pigments which are typical for flagellates could however belong to smaller cells which may be part of the picophytoplankton pool. Further information would be needed to assess the real definition of size classes relative to the pigment composition in such oligotrophic waters.

4.1.3 Importance of photoheterotrophic bacteria in oligotrophic waters

BChl*a*-containing photosynthetic bacteria were most representative in the centre of the SPSG, with average surface BChl*a*/TChl*a* ratios of 2% progressively decreasing down to 0% at 170 m depth (Fig. 11f). These values are much lower than the range of 5 to 10% mentioned by Kolber et al. (2001). The results from the BIOSOPE cruise agree better with Cottrell et al. (2006) who measured ratios between 0.3% and 2.6% in the Mid-Atlantic Bight and are higher than those measured by Goericke (2002) in the oligotrophic California Current System (0.7%). This is consistent with parallel measurements done by Lami et al. (2007) who found high standing stocks of aerobic anoxygenic phototrophic (AAP) bacteria above the DCM in the SPSG.

4.1.4 The Marquesas Archipelago – HNLC transition zone

Comparison with the model data essentially focuses on the transition between the MAR and HNL sites, as the pigment distribution differs from one site to another. At the MAR site, the average integrated TChl*a* biomass between the surface and 1.5 Ze varied around 30.2 \pm 2.8 g m^{-2} (Table 2). Bidigare and Ondrusek (1996) measured values (between 0 and 150 m) ranging from 24 to 30 mg TChl a m^{-2} in the same area. Nanophytoplankton was the predominant size class (50–60%) between 0 and 175 m as equally predicted by the model. This is well represented by the Hex distribution. Above 80 m depth, the microphytoplankton pool had similar proportions to picophytoplankton (20–25% each), while below 80 m it decreased to less than 10% (Figs. 6d and f). The MAR site was also the only site of the transect (apart from the upwelling), where signs of diatom senescence could be found. Microscopic observations showed significant counts

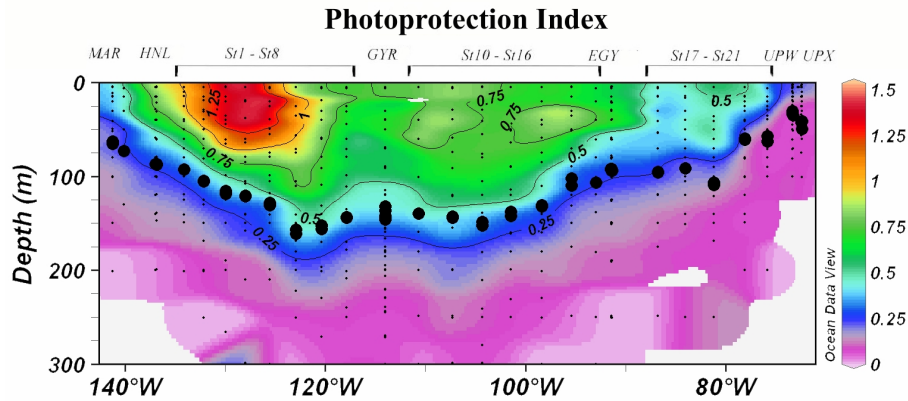


Fig. 10. Contour plot of the Photoprotection Index (PI) across the BIOSOPE transect. The large black dots represent the depth of the euphotic layer (Z_e). The small black dots represent the collected water samples at each station. (Ocean Data View (ODV) software, version 3.0.1, R. Schlitzer, <http://odv.awi-bremerhaven.de/>, 2005).

of diatoms and a low number of dinoflagellate populations (Gomez, personal communication, 2006). The proportion of peridinin also remained low, confirming the weak contribution of the dinoflagellate population. This is in agreement with previous observations in the Equatorial Pacific Ocean (Bidigare and Ondrusek, 1996). However precautions may need to be taken with the interpretation of the peridinin concentrations, as dinoflagellates that do not contain peridinin, like certain *Gymnodinium* sp., have already been observed in these waters (Chavez et al., 1990; Landry et al., 2000).

As expected, the HNL site, being “upstream” of the South Equatorial Current, was more typical of the stratified oligotrophic gyre waters, with a two fold increase in the proportion of picophytoplankton (Fig. 6d). A strong proportion of picophytoplankton, essentially prochlorophytes, prevailed around 130 m. An unusually high contribution of DVChl**b** was also observed at this depth. Nanophytoplankton represented about 30% of the total TChl**a** biomass (Fig. 6e). The proportion of microphytoplankton showed a discrete maximum around 60 m but remained below 12% (Fig. 6f), with a higher contribution of peridinin (dinoflagellates). It appears that the algal population at the HNL site is influenced by the proximity of the more hydrodynamically stable South Pacific Tropical Water formation area rather than the turbulent waters of the Marquesas Islands (Signorini et al., 1999).

4.2 Geographical particularities in the pigment distribution and associations

4.2.1 Extreme depth of the DCM in the Central South Pacific subtropical gyre

The chlorophyll maximum has rarely been observed to reach such remarkable depths in the global ocean as those encountered here. Although comprehensive, the dataset on which the model is based does not include data collected in such extreme oligotrophic conditions as those encountered during

the BIOSOPE cruise. Unsurprisingly, this made it difficult to predict the extent of the chlorophyll maximum in the centre of the gyre. Although some small nuances exist in the pigment distribution, the main and more important particularity of the SPG remains its exceptional transparency (Morel et al., 2007). This is likely the result of exceptional weak diffusive nutrient fluxes from the deep nutricline. Throughout the gyre, the integrated TChl**a** concentrations between 0 and $1.5Z_e$ varied around $20.3 \pm 2.1 \text{ mg m}^{-2}$ (Table 2) and fall within the range of those measured between 0 and 250 m by Claustre and Marty (1995) in the North Tropical Atlantic Ocean. This implies that although the phytoplankton biomass can develop at larger depths than in other parts of the world ocean, the biomass integrated down to $1.5Z_e$ seemingly remains comparable to other subtropical gyre systems. The phytoplankton community therefore follows the same general trends as observed for other gyres with the noticeable difference that the distribution is more extended (diluted) over the geometric depth. Actually with respect to euphotic depth (the ratio Z/Z_e) the DCM in the SPG is located deeper than in other gyres. The DCM is generally associated to the depth of the euphotic zone in other subtropical gyres (Letelier et al., 2004; Uitz et al., 2006), while for the most oligotrophic stations of the SPG, it was located at $\sim 1.2Z_e$ (i.e. at 190 m for $Z_e=160$ m). Consequently, phytoplankton at the level of the DCM and below has developed the most extreme adaptation characteristics with respect to light.

The adaptation to these extreme optical conditions can also be investigated through light intensity, characterised by the photoprotection index PI:

$$\text{PI} = (\text{Diadinoxanthin} + \text{Diatoxanthin} + \text{Zeaxanthin}) / [\text{TChl}a], \quad (4)$$

As expected, the values of the PI increase towards the surface, but more interestingly, the depths of the euphotic layer along the cruise track appear to closely follow the vertical variations in the PI (Fig. 10).

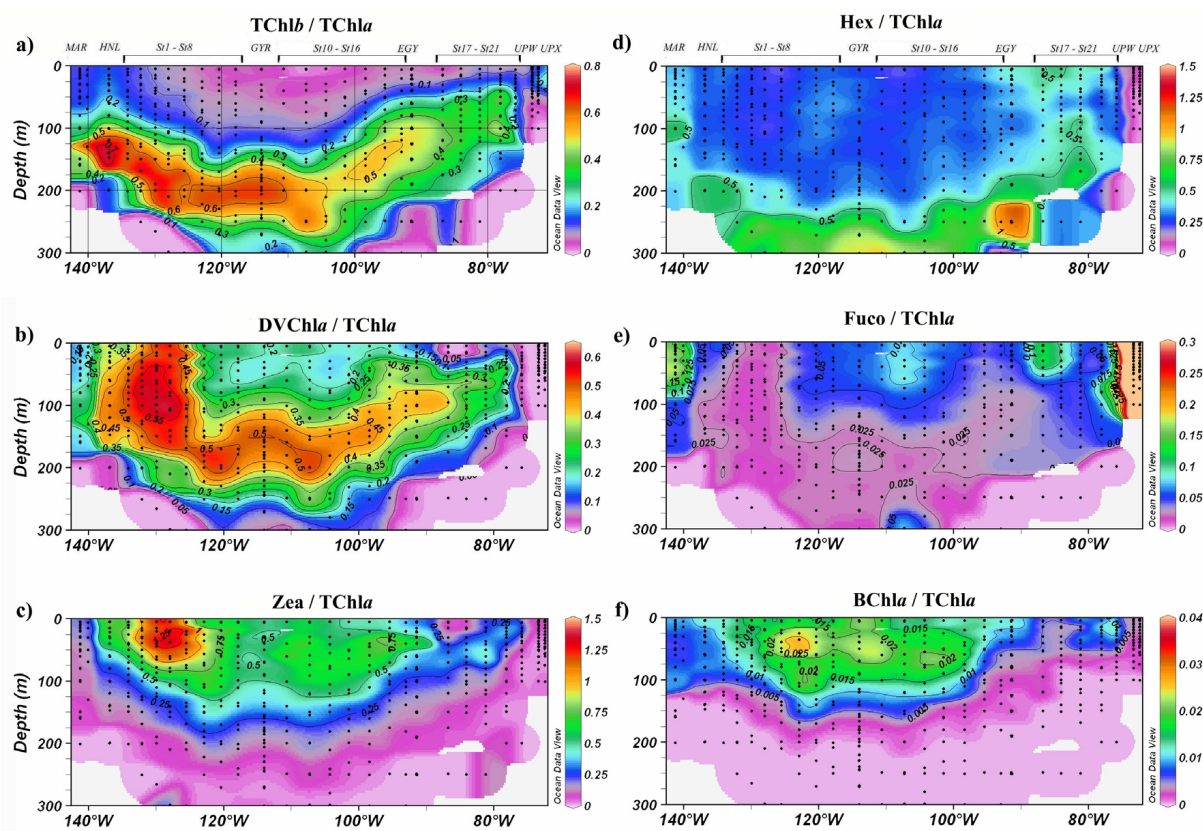


Fig. 11. Cross sections for pigment concentrations normalised to Total chlorophyll-*a* across the BIOSOPE cruise transect. (a) Total chlorophyll-*b*/TChl-*a*; (b) Divinyl Chlorophyll-*a*/TChl-*a*; (c) Zeaxanthin/TChl-*a*; (d) 19'-Hexanoyloxyfucoxanthin/TChl-*a*; (e) Fucoxanthin/TChl-*a*; (f) Bacteriochlorophyll-*a*/TChl-*a*.

4.2.2 A deep nanoflagellate population

A sudden increase in the proportion of nanophytoplankton was observed at the base of the DCM (Fig. 11d). This feature has been observed in other subtropical gyre systems (Claustre and Marty, 1995; Monger et al., 1999), but the reasons for its existence are still unclear. Claustre and Marty (1995) suggest that this deep nanoflagellate population can develop close to the nutricline, which is the case here. Other types of measurements from the cruise indicated that this deep layer was particularly rich in coccoliths (Beaufort et al., 2007). Twardowski et al. (2007) observed a high backscattering ratio in this layer and suggest that this population may correspond to the coccolithophorid *Florisphaera profunda*.

4.2.3 Slight increase in microphytoplankton in the centre of the SPSG

The microphytoplankton group was extremely sparse in the SPSG. Nevertheless, in the 0–80 m surface layer, a slight increase in the proportion of microphytoplankton, essentially represented by fucoxanthin (Fig. 11e), was observed at the centre of the gyre (particularly station 11). In contrast,

Gomez (2007), in accordance with the model results, describes a distinct decrease of the diatom population towards the centre of the gyre and towards the surface. Therefore according to microscopic observations this small increase of fucoxanthin should not originate from a diatom population (Gomez, personal communication), unless the diatom cells are smaller than 15 μm (lower limit of detection for the microscopic method).

Certain endosymbiont cyanobacteria, attached to particular diatom genera, directly fix dinitrogen and can supply all the nitrogen required to their host (Carpenter, 2002). Venrick (1974) and Scharek et al. (1999) have reported that several diatom species of the genera *Hemiaulus* or *Rhizosolenia* in association with the diazotroph cyanobacteria *Richestia intracellularis* are able to survive in oligotrophic surface waters. Indeed, although in low abundance, *Hemiaulus hauckii* were observed by microscopy to be the only diatom species at the surface at station 12 (Gomez, personal communication, 2006). Nevertheless, very little is yet known about these symbioses. Other large species of diatoms (*Ethmodiscus*, *Rhizosolenia* mats) or dinoflagellates (*Pyrocystis*) can migrate between the nutricline and surface waters in

nutrient-poor conditions (Villareal et al., 1999; Singler and Villareal, 2005), but apart from the presence of *Nitzschia* and *Dactyliosolen* between 200 and 300 m depth in the gyre, no significant microscopic observations are available. An alternative explanation may be the presence of other Fuco-containing phytoplankton groups, such as haptophytes or pelagophytes, but no other associated pigments behave like Fuco in this area, except for Peri which shows higher proportions in the surface waters of the SPSG. Hardy et al. (1996) and Gomez (personal communication, 2006) have observed small dinoflagellates to occur in the surface waters of the central gyre. Certain species of dinoflagellates are known to contain Fuco, especially when Peri is absent (Morden and Sherwood, 2002). So even though Fuco and Peri do not correlate well, one can hypothesise that the Fuco contribution in these waters may partly originate from dinoflagellate populations.

4.2.4 Very strong signature of prochlorophytes in the South Tropical Surface Water

The North-western border of the South Pacific Subtropical Gyre is under the influence of the South Equatorial Current (SEC) and represents typical HNLC (High Nutrient Low Chlorophyll) conditions. Between stations 2 and 5, the reasons for the particularly high proportion of picophytoplankton (Fig. 6d), and more precisely *Prochlorococcus*, down to 150 m, seem unclear. Their development is nevertheless associated to the remarkably high-salinity waters (36.5) of the South Tropical Surface Water (STSW), where a stronger evaporation rate relative to precipitation occurs (Johnson and McPhaden, 1999) and surface nutrient levels remain, as in the rest of the gyre system, below detection limits (Raimbault, 2007). This water mass can be characterised by a very specific prochlorophyte-dominated picophytoplanktonic population. As a consequence, the *Zea*/TChl*a* ratios are also exceptionally high (greater than 1) above 65 m depth (Fig. 11c). It is also the only part of the transect where the relative Fuco concentration represents less than 2.5% of the TChl*a* biomass (Fig. 11e). As the surface TChl*a* biomass in this zone is not exceptional in comparison to the rest of the gyre, the model does not predict such an unusual distribution in the phytoplankton population. The prevailing conditions and the exceptional phytoplankton population in this area would definitely deserve further investigation.

4.2.5 High variability in community structure in the upwelling area

Only the upwelling region was characterised by a proportion of microphytoplankton above 30% (Fig. 6f). This was also reflected by the model data (Fig. 9f). However both sites seem to have been very different in a taxonomical point of view, a difference which could not be predicted by the model. Table 2 summarizes, for the 0 to 1.5 Ze layer, the differences

observed between these 2 sites, with a higher and more variable integrated TChl*a* biomass at UPW than at UPX, the former being dominated by the microphytoplankton and the latter by equivalent proportions of pico- and microphytoplankton. The offshore UPW station was characteristic of a typically mature spring bloom with higher biomass concentrations essentially represented by diatoms which had probably been advected offshore from the upwelling zone. This is confirmed by the nutrient concentrations (Raimbault et al., 2007) that showed near-depletion in the surface waters of the UPW site and which may attribute the decrease of phytoplankton biomass towards the surface as a beginning of nutrient starvation. Furthermore, signs of pigment degradation related to senescence and grazing were highest for this site (Fig. 5c). Stuart et al. (2004) had similar results along the Chilean coast, i.e. typical upwelling features with high phytoplankton biomass (above 10 mg m^{-3}) and microphytoplankton-predominant populations, especially above the shelf break, and lower concentrations over the continental shelf and offshore regions. Only one site in their study presented unusually high relative concentrations of Chl*b* and *Zea*.

The surface waters of the coastal UPX site were dominated by a picoeukaryotic community (49 to 70% of picophytoplankton between the surface and 30 m depth), while it represented less than 10% of the TChl*a* biomass at the diatom-dominated UPW site. The pigments associated to the picoeukaryotic chlorophytes, prasinophytes and cryptophytes were essentially found in the upwelling zone only, with absolute and relative concentrations several fold higher at the UPX site than at UPW. The flow cytometry data also indicated a maximum in concentrations of picoeukaryotes at this site (Grob, 2007). According to the temperature profiles, UPX was seemingly the site of recent upwelling of cold deep waters and the observed phytoplankton community was probably at an early stage of development. Experimental tests by Duarte et al. (2000a and b) on a Mediterranean community showed how increasing nutrient inputs lead to an initial autotrophic response of picophytoplankton (particularly *Synechococcus*) which is later rapidly replaced by a stronger and more robust population of microphytoplankton. Furthermore, Larsen et al. (2004) and Bratbak et al. (1990) also witnessed an increase in autotrophic picoeukaryotes and/or cyanobacteria preceding a diatom spring bloom. Claustre et al. (1994) observed a similar event along a geostrophic front, where a ubiquitous flagellate biomass, associated to recently upwelled water, was observed to develop rapidly before being dominated by a slower developing diatom population. The picophytoplankton population at UPX was dominated by picoeukaryotes and not cyanobacteria (very low zeaxanthin concentrations) nor flagellates (the nanophytoplankton class varied at background levels at less than 10%, values which are largely overestimated by the model), but the observations of Claustre et al. (1994), Duarte et al. (2000a, b) and Larson et al. (2004) could corroborate the idea that this young picophytoplankton community had quickly responded to a recent

input of nutrients at the surface before being taken over by a diatom-dominated population. These transient communities are not usually observed in eutrophic zones as they probably occur at small time-scales. They are thus difficult to measure and even more to forecast with global models like the one used in this study.

5 Conclusions

As expected, the surface waters of the South Pacific Subtropical Gyre are the site of extremely low concentrations of phytoplankton biomass, requiring highly sensitive analytical techniques. The HPLC analytical method applied in this study was especially modified in order to adapt to such low concentrations and due to the low limits of detection obtained, an accurate and precise coverage of the different phytoplankton pigments with taxonomical significance has been achieved.

A phytoplankton pigment parameterisation, based on remotely sensed surface TChl a concentrations was applied to the BIOSOPE transect and the predicted values were compared to the in situ data. In a first approach, the general patterns produced by the model were relatively well validated by the in situ data across such contrasting environments. However, in detail, this has revealed certain areas where the phytoplankton populations deviate from their typical composition that would be expected from the surface TChl a concentrations. These are specific temporal or spatial features that cannot be depicted by a global parameterisation. The pigment signatures observed during the BIOSOPE cruise thus point to new issues and questions which could be the object of upcoming studies regarding the development of phytoplankton populations in the extreme conditions encountered in the ultra-oligotrophic center of the gyre, in the high salinity SPTW formation area or in eutrophic upwelling zones in general.

The outcome of such a comparison is a very promising new methodology for identifying atypical structures: indeed the model used here could be applied to data from other parts of the global ocean and could thus become a useful tool for rapidly pinpointing pigment associations and distributions that deserve special interest.

Acknowledgements. We thank the captain and crew of the R/V Atalante for their pleasant cooperation during the BIOSOPE cruise. We also appreciate the time and effort provided by B. Gentili for computations. D. Tailliez and C. Marec are warmly thanked for their efficient help in CTD rosette management and data processing. This is a contribution of the BIOSOPE project of the LEFE-CYBER program. This research was funded by the Centre National de la Recherche Scientifique (CNRS), the Institut des Sciences de l'Univers (INSU), the Centre National d'Etudes Spatiales (CNES), the European Space Agency (ESA), The National Aeronautics and Space Administration (NASA) and the Natural Sciences and Engineering Research Council of Canada (NSERC).

Edited by: E. Boss

References

- Beaufort, L., Couapela, M., Bucheta, N., and Claustre, H.: Calcite production by Coccolithophores in the South Pacific Ocean: from desert to jungle, *Biogeosciences Discuss.*, 4, 3267–3299, 2007, <http://www.biogeosciences-discuss.net/4/3267/2007/>.
- Bidigare, R. R. and Ondrusek, M. E.: Spatial and temporal variability of phytoplankton pigment distributions in the central equatorial Pacific Ocean, *Deep-Sea Res. II*, 43(4–6), 809–833, 1996.
- Bouman, H. A., Ulloa, O., Scanlan, D.J., Zwirgmaier, K., Li, W. K. W., Platt, T., Stuart, V., Barlow, R., Leth, O., Clementson, L., Lutz, V., Fukasawa, M., Watanabe, S., and Sathyendranath, S.: Oceanographic Basis of the Global Surface Distribution of *Prochlorococcus* Ecotypes, *Science*, 312, 918–921, 2006.
- Bratbak, G., Heldal, G. M., Norland, S., and Thingstad, T. F.: Viruses as partners in spring bloom microbial trophodynamics, *Appl. Environ. Microbiol.*, 56, 1400–1405, 1990.
- Carpenter, E. J.: Marine Cyanobacterial symbioses, *Biol. Environ.*, 102B, 1, 15–18, 2002.
- Chavez, F. P., Buck, K. R., and Barber, R. T.: Phytoplankton taxa in relation to primary production in the Equatorial Pacific, *Deep-Sea Res.*, 37, 11A, 1733–1752, 1990.
- Claustre, H.: The trophic status of various oceanic provinces as revealed by phytoplankton pigment signatures, *Limnol. Oceanogr.*, 39, 5, 1206–1210, 1994.
- Claustre, H., Kerhervé, P., Marty, J. C., Prieur, L., Videau, C., and Hecq, J. H.: Phytoplankton dynamics associated with a geostrophic front: ecological and biogeochemical implications, *J. Mar. Res.*, 52, 711–742, 1994.
- Claustre, H. and Maritorea, S.: The many shades of ocean blue, *Science*, 302, 1514–1515, 2003.
- Claustre, H. and Marty, J. C.: Specific phytoplankton biomasses and their relation to primary production in the tropical North Atlantic, *Deep-Sea Res. I*, 42, 8, 1476–1493, 1995.
- Claustre, H., Sciandra, A., and Vaultot, D.: Introduction to the special section: bio-optical and biogeochemical conditions in the South East Pacific in late 2004 – the BIOSOPE cruise, *Biogeosciences Discuss.*, 5, 605–640, 2008, <http://www.biogeosciences-discuss.net/5/605/2008/>.
- Cottrell, M. T., Mannino, A., and Kirchman, D. L.: Aerobic anoxygenic phototrophic bacteria in the Mid-Atlantic Bight and the North Pacific gyre, *Appl. Environ. Microbiol.*, 72, 1, 557–564, 2006.

- Dandonneau, Y., Deschamps, P. Y., Nicolas, J. M., Loisel, H., Blanchot, J., Montel, Y., Thieuleux, F., and Becu, G.: Seasonal and interannual variability of ocean colour and composition of phytoplankton communities in the North Atlantic, Equatorial Pacific and South Pacific, *Deep-Sea Res. II*, 51, 303–318, 2004.
- Dandonneau, Y., Montel, Y., Blanchot, J., Giraudeau, J., and Neveux, J.: Temporal variability in phytoplankton pigments, picoplankton and coccolithophores along a transect through the North Atlantic and tropical southwestern Pacific, *Deep-Sea Res. I*, 53, 4, 689–712, 2006.
- Duarte, C. M., Agusti, S., and Agawin, N. S. R.: Response of a Mediterranean phytoplankton community to increased nutrient inputs: a mesocosm experiment, *Mar. Ecol. Progress Ser.*, 195, 61–70, 2000a.
- Duarte, C. M., Agusti, S., Gasol, J. M., Vaqué, D., and Vazquez-Dominguez, E.: Effect of nutrient supply on the biomass structure of planktonic communities: an experimental test on a Mediterranean coastal community, *Mar. Ecol. Progress Ser.*, 206, 87–95, 2000b.
- Falkowski, P. G. and LaRoche, J.: Acclimation to spectral irradiance in algae, *J. Phycol.*, 27, 8–14, 1991.
- Garczarek, L., Dufresne, A., Rousvoal, S., West, N., Mazard, S., Marie, D., Claustre, H., Raimbault, P., Post, A., and Partensky, F.: High Vertical and Low Horizontal Microdiversity of *Prochlorococcus* Genotypes in the Mediterranean Sea in Summer, *FEMS Microbiol. Ecol.* doi:10.1111/j.1574-6941.2007.00297.x, 2006.
- Gieskes, W. W. C., Kraay, G. W., Nontji, A., Setiapermana, D., and Sutomo, D.: Monsoonal alternation of a mixed and a layered structure in the phytoplankton of the euphotic zone of the Banda Sea (Indonesia): A mathematical analysis of algal pigment fingerprints, *Netherlands J. Sea Res.*, 22, 123–137, 1988.
- Goericke, R.: Bacteriochlorophyll-*a* in the ocean: is anoxygenic bacterial photosynthesis important?, *Limnol. Oceanogr.*, 47, 1, 290–295, 2002.
- Goericke, R. and Repeta, D. J.: The pigments of *Prochlorococcus marinus*: the presence of divinyl chlorophyll *a* and *b* in a marine prokaryote, *Limnol. Oceanogr.*, 37, 2, 425–433, 1992.
- Goericke, R. and Repeta, D. J.: Chlorophylls-*a* and *b* and divinyl chlorophylls-*a* and *b* in the open subtropical North Atlantic Ocean, *Mar. Ecol. Progress Ser.*, 101, 3, 307–313, 1993.
- Gómez, F., Claustre, H., Raimbault, P., and Souissi, S.: Two High-Nutrient Low Chlorophyll phytoplankton assemblages: the tropical central Pacific and the offshore Perú-Chile Current, 4, 1535–1554, 2007.
- Grob, C., Ulloa, O., Claustre, H., Alarcon, G., Huot, Y., and Marie, D.: Contribution of picoplankton to the particulate attenuation coefficient (cp) and organic carbon concentration (POC) in the eastern South Pacific, 4, 1461–1497, 2007.
- Guillard, R. R. L., Murphy, L. S., Foss, P., and Liaaen-Jensen, S.: *Synechococcus* spp. as likely zeaxanthin-dominant ultra-phytoplankton in the North Atlantic, *Limnol. Oceanogr.*, 30, 2, 412–414, 1985.
- Hardy, J., Hanneman, A., Behrenfeld, M., and Horner, R.: Environmental biogeography of near-surface phytoplankton in the south-east Pacific ocean, *Deep-Sea Res. I*, 43, 10, 1647–1659, 1996.
- Hooker, S. B., Van Heukelem, L., Thomas, C. S., Claustre, H., Ras, J., Barlow, R., Sessions, H., Schluter, L., Perl, J., Trees, C., Stuart, V., Head, H., Clementson, L., Fishwick, J., Llewellyn, C., and Aiken, J.: The second SeaWiFS HPLC Analysis Round-Robin Experiment (SeaHARRE-2), NASA, Goddard Space Flight Center, Maryland, Technical Memorandum NASA/TM-2005-212787, 112 pp., 2005.
- Huot, Y., Babin, M., Bruyant, F., Grob, C., Twardowski, M. S., and Claustre, H.: Does chlorophyll-*a* provide the best index of phytoplankton biomass for primary productivity studies?, *Biogeosciences*, 4, 853–868, 2007, <http://www.biogeosciences.net/4/853/2007/>.
- Jeffrey, S. W. and Vesk, M.: Introduction to marine phytoplankton and their pigment signatures, in: *Phytoplankton pigment in oceanography: Guidelines to modern methods*, edited by: Jeffrey, S. W., Mantoura, R. F. C., and Wright, S. W., UNESCO, 33–84, 1997.
- Johnson, G. C. and McPhaden, M. J.: Interior pycnocline flow from the Subtropical to the Equatorial Pacific Ocean, *J. Phys. Oceanogr.*, 29, 12, 3073–3089, 1999.
- Johnson, Z. and Howd, P.: Marine photosynthetic performance forcing and periodicity for the Bermuda Atlantic Time Series, 1989–1995, *Deep-Sea Res. I*, 47, 8, 1485–1512, 2000.
- Johnson, Z. I., Zinser, E. R., Coe A., McNulty N. P., Malcolm E., Woodward S., and Chisholm S. W.: Niche partitioning among *Prochlorococcus* ecotypes along Ocean-scale environmental gradients, *Science*, 311, 1737–1740, 2006.
- Kolber, Z. S., Plumley, F. G., Lang, A. S., Beatty, J. T., Blankenship, R. E., VanDover, C. L., Vetriani, C., Koblizek, M., Rathgeber, C., and Falkowski, P. G.: Contribution of aerobic photoheterotrophic bacteria to the carbon cycle in the ocean, *Science*, 292, 2492–2495, 2001.
- Lami, R., Cottrel, M. T., Ras, J., Ulloa, O., Obernosterer, I., Claustre, H., Kirchman, D. L., and Lebaron, P.: High abundances of aerobic anoxygenic photosynthetic bacteria in the South Pacific Ocean, *Appl. Environ. Microbiol.*, 73, 13, 4198–4205, 2007.
- Landry, M. R., Ondrusek, M. E., Tanner, S. J., Brown, S. L., Constantinou, J., Bidigare, R. R., Coale, K. H., and Fitzwater, S.: Biological response to iron fertilization in the eastern equatorial Pacific (IronEx II). I. Microplankton community abundances and biomass, *Mar. Ecol. Progress Ser.*, 201, 27–42, 2000.
- Larsen, A., Fønnes Flaten, G. A., Sandaa, R. A., Castberg, T., Thyraug, R., Erga, S. R., Jacquet, S., and Bratbak, G.: Spring phytoplankton bloom dynamics in Norwegian coastal waters: Microbial community succession and diversity, *Limnol. Oceanogr.*, 49, 1, 180–190, 2004.
- Letelier, R. M., Karl, D. M., Abbott, M. R., and Bidigare, R. R.: Light driven seasonal patterns of chlorophyll and nitrate in the lower euphotic zone of the North Pacific Subtropical Gyre, *Limnol. Oceanogr.*, 49(2), 508–519, 2004.
- Longhurst, A. R.: *Ecological geography of the sea*, Academic Press, London, 398 pp., 1998.
- MacIntyre, H. L., Kana, T. M., Anning, T., and Geider, R.: Photoacclimation of photosynthesis irradiance response curves and photosynthetic pigments in microalgae and cyanobacteria, *J. Phycol.*, 38, 17–38, 2002.
- Mackey, M. D., Mackey, D. J., Higgins, H. W., and Wright, S. W.: CHEMTAX – a program for estimating class abundances from chemical markers: Application to HPLC measurements of phytoplankton, *Mar. Ecol. Progress Ser.*, 144, 265–283, 1996.
- Mahowald, N. M., Baker, A. R., Bergametti, G., Brooks, N., Duce, R. A., Jickells, T. D., Kubilay N., Prospero, J. M.,

- and Tegen, I.: Atmospheric global dust cycle and iron inputs to the ocean, *Global Biogeochem. Cy.*, 19, GB4025, doi:10.1029/2004GB002402, 2005.
- Monger, B. C., Landry, M. R., and Brown, S. L.: Feeding selection of heterotrophic marine nanoflagellates based on the surface hydrophobicity of their picoplankton prey, *Limnol. Oceanogr.*, 44, 8, 1917–1927, 1999.
- Moore, L. R., Goericke, R., and Chisholm, S. W.: Comparative physiology of *Synechococcus* and *Prochlorococcus*: influence of light and temperature on growth, pigments, fluorescence and absorptive properties, *Mar. Ecol. Progress Ser.*, 116, 259–275, 1995.
- Moore, L. and Chisholm S.W.: Photophysiology of the Marine Cyanobacterium *Prochlorococcus*: Ecotypic Differences among Cultured Isolates, *Limnol. Oceanogr.*, 44, 3, 1, 628–638, 1999.
- Morden, C. W. and Sherwood, A. R.: Continued evolutionary surprises among dinoflagellates, *Proc. Natl. Acad. Sci. USA.*, 99, 18, 11 558–11 560, 2002.
- Morel, A. and Berthon, J. F.: Surface pigments, algal biomass profiles and potential production of the euphotic layer: relationships revisited in view of remote sensing applications, *Limnol. Oceanogr.*, 34, 1545–1562, 1989.
- Morel, A. and Maritorea, S.: Bio-optical properties of oceanic waters: a reappraisal, *J. Geophys. Res.*, 106, C4, 7163–7180, 2001.
- Morel, A., Gentili, B., Claustre, H., Babin, M., Bricaud, A., Ras, J., and Tieche, F.: Optical properties of the “clearest” natural waters, *Limnol. Oceanogr.*, 52, 1, 217–229, 2007.
- O’Reilly, J. E., Maritorea, S., Mitchell, B. G., Siegel, D. A., Carder, K. L., Garver, S. A., Kahru, M., and McClain, C.: Ocean color chlorophyll algorithms for SeaWiFS, *J. Geophys. Res.*, 103, C11, 24 937–24 954, 1998.
- Parsons, T. R. and Strickland, J. D. H.: Discussion of spectrophotometric determination of marine plankton pigments with revised equations of ascertaining chlorophyll-*a* and carotenoids, *J. Mar. Res.*, 21, 3, 155–163, 1963.
- Partensky, F., Blanchot, J., Lantoiné, F., Neveux, J., and Marie, D.: Vertical structure of picophytoplankton at different trophic sites of the tropical northeastern Atlantic Ocean, *Deep-Sea Res. I*, 43, 8, 1191–1213, 1996.
- Partensky, F., Hess, W. R., and Vaulot, D.: *Prochlorococcus*, a Marine Photosynthetic Prokaryote of Global Significance, *Microbiol. Mol. Biol. R.*, 63, 1, 106–127, 1999.
- Prézelin, B. B., Hofmann, E. E., Mengelt, C., and Klinck, J. M.: The linkage between Upper Circumpolar Deep Water (UCDW) and phytoplankton assemblages on the west Antarctic Peninsula continental shelf, *J. Mar. Res.*, 58, 165–202, 2000.
- Raimbault, P., Garcia, N., and Cerrutti, F.: Distribution of inorganic and organic nutrients in the South Pacific Ocean. Evidence for long-term accumulation of organic matter in nitrogen-depleted waters, 4, 3041–3087, 2007.
- Scharek, R., Latasa, M., Karl, D. M., and Bidigare, R. R.: Temporal variations in diatom abundance and downward vertical flux in the oligotrophic North Pacific gyre, *Deep-Sea Res. I*, 46, 1051–1075, 1999.
- Signorini, S. R., McClain, C. R., and Dandonneau, Y.: Mixing and phytoplankton bloom in the wake of the Marquesas Islands, *Geophys. Res. Lett.*, 26, 3121–3124, 1999.
- Singler, H. R. and Villareal, T. A.: Nitrogen inputs into the euphotic zone by vertically migrating *Rhizosolenia* mats, *J. Plankton Res.*, 27, 6, 545–556, 2005.
- Stuart, V., Ulloa O., Alarcon, G., Sathyendranath, S., Major, H., Head, E. J. H., and Platt, T.: Bio-optical characteristics of phytoplankton populations in the upwelling system off the coast of Chile, *Rev. Chil. Hist. Natl.*, 77, 87–105, 2004.
- Twardowski, M. S., Claustre, H., Freeman, S. Stramski, D., and Huot, Y.: Optical Backscattering Properties of the “Clearest” Natural Waters, *Biogeosciences Discuss.*, 4, 2441–2491, 2007, <http://www.biogeosciences-discuss.net/4/2441/2007/>.
- Uitz, J., Claustre, H., Morel, A., and Hooker, S.: Vertical distribution of phytoplankton communities in open ocean: an assessment based on surface chlorophyll, *J. Geophys. Res.*, 111, C08005, doi:10.1029/2005JC003207, 2006.
- Van Heukelem, L. and Thomas, C. S.: Computer-assisted high-performance liquid chromatography method development with applications to the isolation and analysis of phytoplankton pigments, *J. Chromatogr. A*, 910, 31–49, 2001.
- Venrick, E. L.: The distribution and significance of *Richelia intracellularis* Schmidt in the North Pacific Central Gyre, *Limnol. Oceanogr.*, 19, 3, 437–445, 1974.
- Vidussi, F., Claustre, H., Manca, B. B., Luchetta, A., and Marty, J. C.: Phytoplankton pigment distribution in relation to upper thermocline circulation in the eastern Mediterranean Sea during winter, *J. Geophys. Res.*, 106, C9, 19 939–19 956, 2001.
- Villareal, T. A., Joseph, L., Brzezinski, M. A., Shipe, R. F., Lipschultz, F., and Altabet, M. A.: Biological and chemical characteristics of the giant diatom *Ethmodiscus* (Bacillariophyceae) in the central north Pacific gyre, *J. Phycol.*, 35, 896–902, 1999.
- Wagener, T., Guieu, C., Losno, R., Bonnet S., and Mahowald, N.: Revisiting atmospheric dust export to the South Hemisphere ocean, *Global Biogeochem. Cy.*, doi:10.1029/2007GB002984, in press, 2008.
- Wright, S. W. and Jeffrey, S. W.: Fucoxanthin pigment markers of marine phytoplankton analysed by HPLC and HPTLC, *Mar. Ecol. Progress Ser.*, 38, 259–266, 1987.
- Yentsch, C. S. and Menzel, D. W.: A method for the determination of phytoplankton chlorophyll and phaeophytin by fluorescence, *Deep-Sea Res.*, 10, 221–231, 1963.

Contribution of picoplankton to the total particulate organic carbon concentration in the eastern South Pacific

C. Grob^{1,2,3}, O. Ulloa², H. Claustre³, Y. Huot³, G. Alarcón², and D. Marie⁴

¹Graduate Programme in Oceanography, Universidad de Concepción, Concepción, Chile

²Department of Oceanography and Center for Oceanographic Research in the eastern South Pacific, Universidad de Concepción, Casilla 160-C, Concepción, Chile

³CNRS, Laboratoire d'océanographie de Villefranche, 06230 Villefranche-sur-Mer, France; Université Pierre et Marie Curie-Paris 6, Laboratoire d'océanographie de Villefranche, 06230 Villefranche-sur-Mer, France

⁴Station Biologique, CNRS, INSU et Université Pierre et Marie Curie, 29482 Roscoff Ceder, France

Received: 27 February 2007 – Published in Biogeosciences Discuss.: 9 May 2007

Revised: 6 August 2007 – Accepted: 1 October 2007 – Published: 15 October 2007

Abstract. *Prochlorococcus*, *Synechococcus*, picophytoeukaryotes and bacterioplankton abundances and contributions to the total particulate organic carbon concentration, derived from the total particle beam attenuation coefficient (c_p), were determined across the eastern South Pacific between the Marquesas Islands and the coast of Chile. All flow cytometrically derived abundances decreased towards the hyper-oligotrophic centre of the gyre and were highest at the coast, except for *Prochlorococcus*, which was not detected under eutrophic conditions. Temperature and nutrient availability appeared important in modulating picophytoplankton abundance, according to the prevailing trophic conditions. Although the non-vegetal particles tended to dominate the c_p signal everywhere along the transect (50 to 83%), this dominance seemed to weaken from oligo- to eutrophic conditions, the contributions by vegetal and non-vegetal particles being about equal under mature upwelling conditions. Spatial variability in the vegetal compartment was more important than the non-vegetal one in shaping the water column particle beam attenuation coefficient. Spatial variability in picophytoplankton biomass could be traced by changes in both total chlorophyll *a* (i.e. mono + divinyl chlorophyll *a*) concentration and c_p . Finally, picophytoeukaryotes contributed ~38% on average to the total integrated phytoplankton carbon biomass or vegetal attenuation signal along the transect, as determined by size measurements (i.e. equivalent spherical diameter) on cells sorted by flow cytometry and optical theory. Although there are some uncertainties as-

sociated with these estimates, the new approach used in this work further supports the idea that picophytoeukaryotes play a dominant role in carbon cycling in the upper open ocean, even under hyper-oligotrophic conditions.

1 Introduction

Global estimates indicate that about half of the Earth's primary production (PP) takes place in the ocean (Field et al., 1998). Of a mean global marine PP of 50.7 Gt C y^{-1} estimated through ocean-colour-based models (Carr et al., 2006), 86% would occur in the open ocean (Chen et al., 2003). Here the photosynthetic biomass is dominated by three main picophytoplanktonic (<2–3 μm) groups (e.g. Li, 1995): cyanobacteria of the genera *Prochlorococcus* (Chisholm et al., 1988) and *Synechococcus* (Waterbury et al., 1979), and eukaryotes belonging to diverse taxa (Moon-van der Staay et al., 2001).

Although cyanobacteria, especially *Prochlorococcus* (Li and Wood, 1988; Chisholm et al., 1988), tend to dominate in terms of numerical abundance, it has been shown that eukaryotic phytoplankton (usually <3.4 μm) dominates the ultraplankton (<5 μm) photosynthetic biomass in the northern Sargasso Sea (Li et al., 1992) and in the eastern Mediterranean Sea (Li et al., 1993). Across the North and South Atlantic Subtropical Gyres (Zubkov et al., 1998, 2000) and eastern South Pacific (Grob et al., 2007) picophytoeukaryotes also constituted a considerable fraction of the picophytoplanktonic carbon biomass.

Correspondence to: C. Grob
(mgrob@profc.udec.cl)

Using flow cytometry cell sorting combined with ^{14}C measurements, Li (1994) made the only simultaneous group-specific primary production rates measurements available so far in the literature for *Prochlorococcus*, *Synechococcus* and picophytoeukaryotes. Even though he could only apply this methodology at three different stations in the North Atlantic Ocean and at a single depth per station, this author's results showed that picophytoeukaryotes contribution to picophytoplankton primary production increased as the *Prochlorococcus* to picophytoeukaryotes abundances ratio decreased. At a coastal Pacific site in the Southern California Bight, on the other hand, Worden et al. (2004) reported that picophytoeukaryotes had the highest picophytoplankton growth rates and contributions to the net community production and carbon biomass on annual bases.

Picophytoeukaryotes can therefore make a significant contribution to the picophytoplanktonic PP and carbon biomass (see above). Carbon being the universal currency in marine ecological modelling, looking inside the pico-autotrophic "black box" to determine the distribution of carbon biomass among the different groups becomes fundamental to better understand the respective role of these groups in the global carbon cycle. Recent biogeochemical models have made a significant step forward on this subject by incorporating not only different plankton functional types, but also different groups within these functional types (e.g. cyanobacteria, picophytoeukaryotes, nitrogen fixers) in order to reproduce some of the ecosystem's variability (e.g. Bisset et al., 1999; Le Quéré et al., 2005). Different picophytoplanktonic groups have different physiological characteristics such as optimal specific rates of photosynthesis, adaptation to light, photosynthetic efficiencies and maximum specific growth rates (Veldhuis et al., 2005, and references therein). Knowing where one group dominates over the others could therefore help choosing the appropriate physiological parameters to estimate PP from surface chlorophyll *a* concentrations retrieved from space and improve such estimates at the large scale.

The measurement of the particle beam attenuation coefficient (c_p) has proven to be a very powerful tool in determining particle load and particulate organic carbon (POC) concentrations at the global (e.g. Gardner, 2006) as well as at the regional scale (e.g. Claustre et al., 1999; Oubelkheir et al., 2005). High frequency measurements of c_p signal can also be used to derive rates of change in particulate organic stocks like gross and net community production (Claustre et al., 2007). In situ c_p profiles associated with the simultaneous cytometric determination of the different phytoplanktonic groups and bacterioplankton (Bacteria + Archaea) abundances have the potential to allow the estimation of the contribution of these groups to the bulk c_p , and hence to POC. Group-specific contributions to POC can therefore be estimated from their contributions to c_p . In the equatorial Pacific, for instance, picophytoeukaryotic cells would dominate the vegetal contribution to c_p (Chung et al., 1996; DuRand

and Olson, 1996; Claustre et al., 1999). These estimations require however that the mean cell size and refractive index of each group are known or at least assumed (Claustre et al., 1999, and references therein). Total and group-specific beam attenuation coefficients can be obtained at relatively short time scales, but also have the advantage of being amenable to large scale in situ surveys on carbon stocks and cycling, and even to global estimation, since bulk oceanic bio-optical properties can be retrieved from space (e.g. Gardner, 2006).

In the present work we tried to answer the following questions: (1) What is the contribution of the different picoplanktonic groups to POC in the upper ocean? and (2) How does the spatial variability in these group's contributions influence the spatial changes in POC in the upper ocean? For this, we studied the waters of the eastern South Pacific, which present an extreme gradient in trophic conditions, from the hyper-oligotrophic waters of the central gyre to the eutrophic coastal upwelling waters off South America. Using flow cytometry cell sorting we were able to isolate different picophytoplankton populations in situ to obtain their mean cell sizes (as equivalent spherical diameters), which allowed us to improve estimations on the group-specific attenuation coefficients, and therefore on group-specific contributions to POC.

2 Methods

A total of 24 stations were sampled between the Marquesas Islands ($\sim 8.4^\circ\text{S}$; 141.2°W) and the coast of Chile ($\sim 34.6^\circ\text{S}$; 72.4°W) during the French expedition BIOSOPE (BIogeochemistry and Optics SOUTh Pacific Experiment) in austral spring time (26 October to 11 December 2004) (Fig. 1). Temperature, salinity and oxygen profiles were obtained with a conductivity-temperature-depth-oxygen profiler (CTDO, Seabird 911 Plus). Nutrient concentrations (nitrate, nitrite, ammonium, phosphate and silicate) were determined onboard (see Raimbault et al., 2007). Pigment concentrations from noon profiles (local time) were determined using High Performance Liquid Chromatography (HPLC). For HPLC analyses, water samples were vacuum filtered through 25 mm diameter and $0.7\ \mu\text{m}$ porosity Whatman GF/F glass fibre filters (see Ras et al., 2007), where on average 97% of *Prochlorococcus* cells are retained (Chavez et al., 1995). The above implies a maximum error of 3% on the total divinyl-chlorophyll *a* concentrations (dv-chl*a*, pigment that is specific only to this group) determined using this technique. Daily integrated surface total irradiance was determined from on-board calibrated measurements.

All stations reported here were sampled at local noon time at 6 to 14 different depths from the surface down to 300 m (Fig. 1). The position of the deepest sampling depth was established relative to the position of the bottom of the photic layer, Z_e (m) defined as the depth where the irradiance is reduced to 1% of its surface value. Five stations of very different trophic conditions, here referred to as long stations,

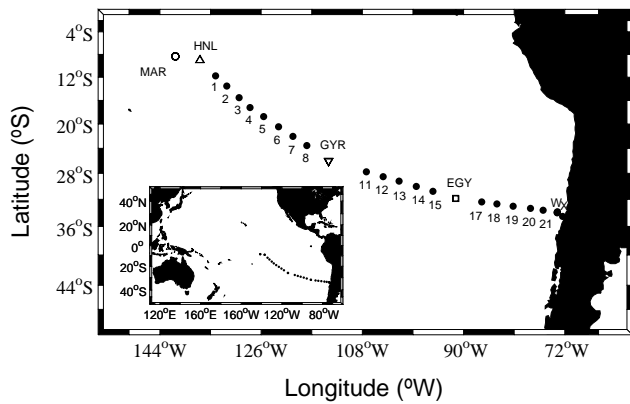


Fig. 1. BIOSOPE transect. In this study we include data from stations 1–8, 11–15 and 17–21, MAR, HNL, GYR, EGY, UPW (W) and UPX (X).

were also sampled at high frequency (i.e. every 3 h) during 2 to 4 days: (1) mesotrophic (MAR, Marquesas Islands), (2) high nutrient-low chlorophyll (HNL, $\sim 9.0^\circ$ S and 136.9° W), (3) hyper-oligotrophic (GYR, $\sim 26.0^\circ$ S and 114.0° W), (4) oligotrophic (EGY, $\sim 31.8^\circ$ S and 91.5° W) and (5) eutrophic (UPW, highly productive upwelling region, $\sim 34.0^\circ$ S and 73.3° W) (Fig. 1). The coastal-most station (UPX) was additionally sampled to compare it with UPW's upwelling condition (Fig. 1).

Our results are presented in terms of oligo-, meso- and eutrophic conditions according to surface total chlorophyll *a* concentrations (Tchl_a, chlorophyll *a* + divinyl chlorophyll *a*) of ≤ 0.1 , > 0.1 and ≤ 1 , and > 1 mg m^{-3} , respectively (Antoine et al., 1996). This division has been used to characterize the trophic status of the ocean from space and we consider it as appropriate to describe the large spatial patterns investigated during the BIOSOPE cruise.

2.1 Picoplankton analyses

Prochlorococcus, *Synechococcus* and picophytoeukaryotes abundances were determined on fresh samples on board with a FACSCalibur (Becton Dickinson) flow cytometer. For bacterioplankton counts (Bacteria + Archaea), samples fixed either with paraformaldehyde at 1% or glutaraldehyde at 0.1% final concentration and quick-frozen in liquid nitrogen were stained with SYBR-Green I (Molecular Probes) and run in the same flow cytometer within two months after the end of the cruise. Reference beads (Fluoresbrite YG Microspheres, calibration grade $1.00 \mu\text{m}$, Polysciences, Inc) were added to each sample before acquiring the data with the Cell Quest Pro software (Becton Dickinson) in logarithmic mode (256 channels). During data acquisition, between 5×10^3 and 300×10^3 events were registered in order to count at least 500 cells for each picoplanktonic group. The error associated with abundances determined using flow cytometry is $\leq 5\%$ (D. Marie, unpublished data). The data

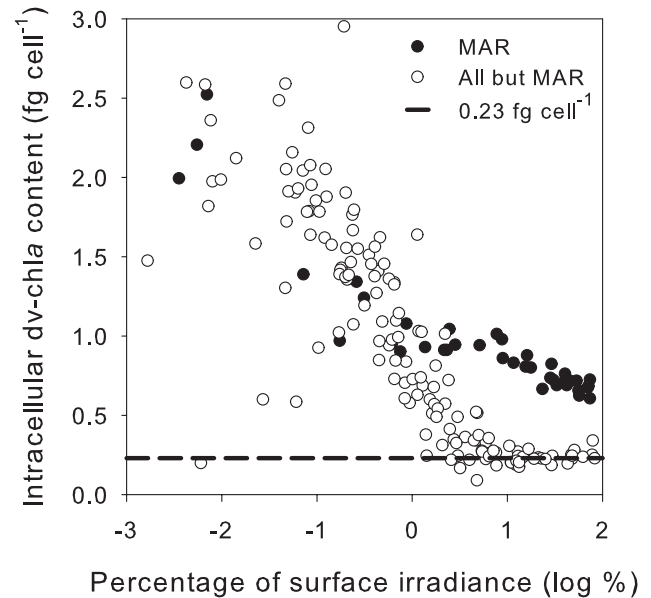


Fig. 2. *Prochlorococcus* intracellular dv-chla content (fg cell^{-1}) as a function of the percentage of surface irradiance at MAR (filled circles) and the rest of the transect (empty circles). Dashed line indicates the average surface intracellular dv-chla content established at $0.23 \text{ fg cell}^{-1}$.

were then analysed with the Cytowin software (Vaulot, 1989) to separate the picoplanktonic populations based on their scattering and fluorescence signals, according to Marie et al. (2000) (see Supp. Mat.: www.biogeosciences.net/4/837/2007/bg-4-837-2007-supplement.pdf).

Surface *Prochlorococcus* abundance for weakly fluorescent populations (i.e. $\sim 7\%$ of total samples) was estimated by fitting a Gaussian curve to the data using Cytowin. When their fluorescence was too dim to fit the curve (e.g. surface and sub-surface samples at the center of the gyre) their abundance was estimated from dv-chla concentrations by assuming an intracellular pigment content of $0.23 \text{ fg cell}^{-1}$ (see Supp. Mat.). This intracellular dv-chla content corresponds to the mean value obtained for cells in the surface layer (above $\sim 5\%$ of surface light) by dividing the HPLC-determined dv-chla by the cell number estimated from flow cytometry, considering all but the MAR data (Fig. 2). At the GYR station, *Synechococcus* and picophytoeukaryotes abundances above 100 m were only available for the first morning profile (samples taken above 90 m for the other GYR profiles are unfortunately not available). This profile showed that both groups' abundances were homogeneous over the first 100 m, so we assumed the abundances measured at 90–100 m to be representative of the abundances within the 0–100 m layer. All picoplankton abundances were then integrated from the surface to $1.5 Z_e$ rather than to Z_e , because deep chlorophyll maxima (DCM) were observed between these two depths at the center of the gyre.

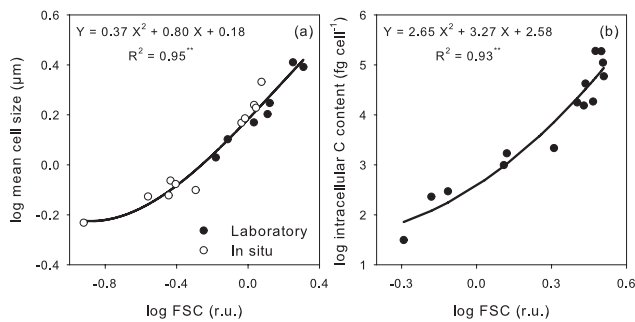


Fig. 3. Log-log relationships established between the flow cytometric forward scatter signal (FSC), expressed in units relative to reference beads (relative units, r.u.), and mean cell size in μm (a) and intracellular carbon (C) content in fg cell^{-1} (b). In (a), mean cell sizes measured on natural populations isolated in situ (empty circles) as well as on populations from culture (filled circles) are included. Mean intracellular carbon contents in (b) were obtained from culture cells. Carbon measurements were performed on triplicate with $\leq 5\%$ of standard deviation. ** indicates $p < 0.0001$.

In order to establish a relationship between actual sizes (i.e. mean cell sizes actually measured) and the mean forward scatter cytometric signal normalized to the reference beads (FSC in relative units, r.u.; see Supp. Mat.: www.biogeosciences.net/4/837/2007/bg-4-837-2007-supplement.pdf), in situ *Prochlorococcus*, *Synechococcus* and picophytoeukaryotes populations were sorted separately on board with a FACS Aria flow cytometer (Becton Dickinson). Each sorted population was then analysed with a Multisizer 3 Coulter Counter (Beckman Coulter) for size (μm) and with the FACS Calibur flow cytometer for FSC. Several *Synechococcus* and picophytoeukaryotes populations isolated in situ could be measured with the Coulter Counter. *Prochlorococcus* size, on the other hand, could only be determined for one population because they were at the detection limit of the instrument. A similar analysis was performed on monospecific cultures of various picophytoplankton species (without pre-sorting) to combine both in situ and laboratory measurements to establish a log-log polynomial relationship between FSC and size (Fig. 3a). We believe that even though the left-most end of the fitted curve is driven by a sole data point, it is still very useful to the relationship because it represents the actual mean cell size of a natural *Prochlorococcus* population (i.e. $0.59 \mu\text{m}$), corresponding to a mean FSC of 0.02 r.u. Based on this relationship established within the picophytoplankton size range, we calculated the upper size limit for the FSC settings we used during the whole cruise at $3 \mu\text{m}$ (i.e. $\text{FSC}=0.88$ r.u.).

Also using culture cells, we established a direct relationship between the mean cytometric FSC signal and intracellular carbon content to estimate *Synechococcus* and picophytoeukaryotes carbon biomass (Fig. 3b). To obtain intracellular carbon contents, a known volume of each cul-

ture population was filtered onto GF/F filters previously pre-combusted at 400°C , in triplicate. One blank filter per culture was put aside to be used as control. The number of phytoplankton and contaminating bacterioplankton cells retained in and passing through the filters were determined using flow cytometry (see Supp. Mat.: www.biogeosciences.net/4/837/2007/bg-4-837-2007-supplement.pdf). The filters were then dried at 60°C for 24 h, fumigated with concentrated chlorhydric acid for 6 to 8 h to remove inorganic carbon and dried again for 6 to 8 h. Each filter was finally put in a tin capsule and analysed with a Carbon-Hydrogen-Nitrogen (CHN) autoanalyzer (Thermo Finnigan, Flash EA 1112) (see Supp. Mat.: www.biogeosciences.net/4/837/2007/bg-4-837-2007-supplement.pdf). Carbon contents were estimated based on a calibration curve performed using Acetanilide.

Considering both size and carbon content derived from FSC, a conversion factor (in $\text{fgC } \mu\text{m}^{-3}$) was established for *Synechococcus* and then applied to the mean cell size estimated for *Prochlorococcus* to obtain the intracellular carbon content of that group. Picophytoplankton carbon biomass was then calculated by multiplying cell abundance and intracellular carbon content for each group.

2.2 Beam attenuation coefficients specific for each picoplankton group

Profiles of the total particle beam attenuation coefficient at 660 nm (c_p , m^{-1}), a proxy for POC (e.g. Claustre et al., 1999), were obtained with a C-Star transmissometer (Wet Labs, Inc.) attached to the CTD rosette. Procedures for data treatment and validation have been described elsewhere (Loisel and Morel, 1998; Claustre et al., 1999). Inherent optical properties of sea water (IOP's), such as c_p , depend exclusively on the medium and the different substances in it (Preisendorfer, 1961). The vegetal (c_{veg}) and non-vegetal (c_{nveg}) contribution (Eq. 1) to the particle beam attenuation coefficient can therefore be expressed as

$$c_p = c_{\text{veg}} + c_{\text{nveg}} \quad (1)$$

whereas the *Prochlorococcus* (c_{proc}), *Synechococcus* (c_{syn}), picophytoeukaryotes (c_{euk}) and larger phytoplankton ($> 3 \mu\text{m}$, c_{large}) contribution to the vegetal signal (Eq. 2) can be described by

$$c_{\text{veg}} = c_{\text{proc}} + c_{\text{syn}} + c_{\text{euk}} + c_{\text{large}} \quad (2)$$

Bacterioplankton (c_{bact}), heterotrophs (c_{het}) and detritus (c_{det} = non living particles) contribute to the non-vegetal component (Eq. 3) as follows,

$$\begin{aligned} c_{\text{nveg}} &= c_p - c_{\text{veg}} \\ &= c_{\text{bact}} + c_{\text{het}} + c_{\text{det}} \\ &= c_{\text{bact}} + 2c_{\text{bact}} + c_{\text{det}} \\ &= 3c_{\text{bact}} + c_{\text{det}} \end{aligned} \quad (3)$$

where c_{het} is assumed to be approximately $2c_{\text{bact}}$ (Morel and Ahn, 1991). This assumption was adopted in order to be able to estimate the fraction of total particulate organic carbon corresponding to detritus, which is the group of particles contributing to c_{p} that is not directly measured, i.e. the unaccounted c_{p} (see below; Eq. 4).

Since particulate absorption is negligible at 660 nm (Loisel and Morel, 1998), beam attenuation and scattering are equivalent, so we can estimate c_{proc} , c_{syn} , c_{euk} , c_{large} and c_{bact} by determining the group-specific scattering coefficients b_i (m^{-1}) = $N_i [s_i Q_{bi}]$, where $i = \text{proc, syn, euk, large or bact}$. We used flow cytometry to retrieve both picophytoplankton cell abundance (N_i , cells m^{-3}) and mean cell sizes (through FSC, see Sect. 2.1). Mean geometrical cross sections (s , $\text{m}^2 \text{ cell}^{-1}$) were calculated from size, while Q_{bi} (660), the optical efficiency factors (dimensionless), were computed through the anomalous diffraction approximation (Van de Hulst, 1957) assuming a refractive index of 1.05 for all groups (Claustre et al., 1999). For *Prochlorococcus* and *Synechococcus* we used mean sizes obtained from a few samples, whereas for the picophytoeukaryotes we used the mean cell size estimated for each sample (see Supp. Mat.: www.biogeosciences.net/4/837/2007/bg-4-837-2007-supplement.pdf). For samples where picophytoeukaryotes abundance was too low to determine their size we used the nearest sample value, i.e. the mean cell size estimated for the sample taken immediately above or below the missing one. This approximation was applied to $\sim 26\%$ of the samples and although it may seem a large fraction, it corresponds mostly to deep samples where cell abundance was very low. Low cell abundances will result in low biomasses and it is therefore unlikely that the error associated with this approximation will introduce important errors in the carbon biomass estimates. For bacterioplankton we used a value of $0.5 \mu\text{m}$, as used by Claustre et al. (1999). Finally, once c_{veg} , c_{bact} and therefore c_{het} are determined, c_{det} is obtained directly by difference (Eq. 4).

$$\begin{aligned} c_{\text{det}} &= c_{\text{veg}} - c_{\text{bact}} - c_{\text{het}} \\ &= c_{\text{veg}} - c_{\text{bact}} - 2c_{\text{bact}} \\ &= c_{\text{veg}} - 3c_{\text{bact}} \end{aligned} \quad (4)$$

Contributions to c_{p} by larger phytoplanktonic cells in the western and eastern part of the transect were estimated by assuming that peaks larger than $3 \mu\text{m}$ in the particle size distribution data obtained either with the Coulter Counter or with a HIAC optical counter (Royco; Pacific Scientific) corresponded to autotrophic organisms (see Supp. Mat.: www.biogeosciences.net/4/837/2007/bg-4-837-2007-supplement.pdf). Coulter Counter data were only available for 1 (surface samples, $\leq 5 \text{ m}$) to 3 different depths. Thus, in order to obtain water column profiles for MAR, HNL, EGY and UPW, the estimated c_{large} were extrapolated by assuming $c_{\text{large}}=0$ at the depth where no peak $>3 \mu\text{m}$ was detected (usually below 50 m). When

only surface data were available, c_{large} was assumed to be negligible at the depth where chlorophyll fluorescence became lower than the surface one. Group-specific attenuation signals were integrated from the surface down to $1.5 Z_e$ (water column, $c_{0-1.5Z_e}$) and from the surface to 50 m (surface layer, $c_{0-50 \text{ m}}$) to estimate their contribution to integrated c_{p} .

Finally, $c_{\text{p}}(660)$ was converted to particulate organic carbon (POC) by using the empirical relationship established by Claustre et al. (1999) for the tropical Pacific (Eq. 5), which has proven to be valid as part of BIOSOPE (see Stramski et al., 2007).

$$\text{POC (mg m}^{-3}\text{)} = c_{\text{p}}(\text{m}^{-1}) \times 500 \text{ (mg m}^{-2}\text{)} \quad (5)$$

Through the above relationship c_{p} explains $\sim 92\%$ of the variance in POC concentration (Claustre et al., 1999). To evaluate the ability of *Tchl a* and c_{p} to trace spatial changes in picophytoplankton biomass along the transect, we used local noon time data within the integration depth (0 to $1.5 Z_e$) from the stations where no large phytoplankton cells were detected with the particle counters (Coulter or HIAC), i.e. stations 3 to 15+GYR. We chose these stations because we do not have intracellular carbon content data for larger cells to include in the photosynthetic carbon biomass estimates.

3 Results

The sampled transect included South Pacific Tropical Waters (SPTW), with a clear salinity maximum extending from the surface down to 150 m between HNL and GYR, Eastern South Pacific Central Waters (ESPCW) characterized by salinities of 34.5 to 36 (Fig. 4a) and temperatures of 15 to 20°C at the centre of the gyre (GYR to EGY) and colder and fresher waters at the Chilean coast (Claustre et al., 2007). Limits between oligo-, meso- and eutrophic conditions were set at 133, 89 and 74.5°W according to the measured surface chlorophyll *a* concentrations, as explained above. Under oligotrophic conditions nitrate concentrations were close to $0 \mu\text{M}$ or undetectable between the surface and 150–200 m, and still very low ($\sim 2.5 \mu\text{M}$) between the latter depth and $1.5 Z_e$ (Fig. 4b). Expectedly, nutrient concentrations were higher under mesotrophic conditions and highest near the coast (see Raimbault et al., 2007), whereas phosphate was never a limiting factor (Moutin et al., 2007).

The hyper-oligotrophic centre of the South Pacific Subtropical Gyre (SPSG), i.e. the clearest waters of the world's ocean (Morel et al., 2007), was characterized by extremely low surface *Tchl a* concentrations ($<0.03 \text{ mg m}^{-3}$; see Ras et al., 2007) and undetectable nutrient levels (see Raimbault et al., 2007), greatly differing from the Marquesas Islands' mesotrophic conditions and the typical High Nutrient – Low Chlorophyll situation (i.e. HNL) encountered at the borders of the gyre, and the upwelling conditions observed at the coast.

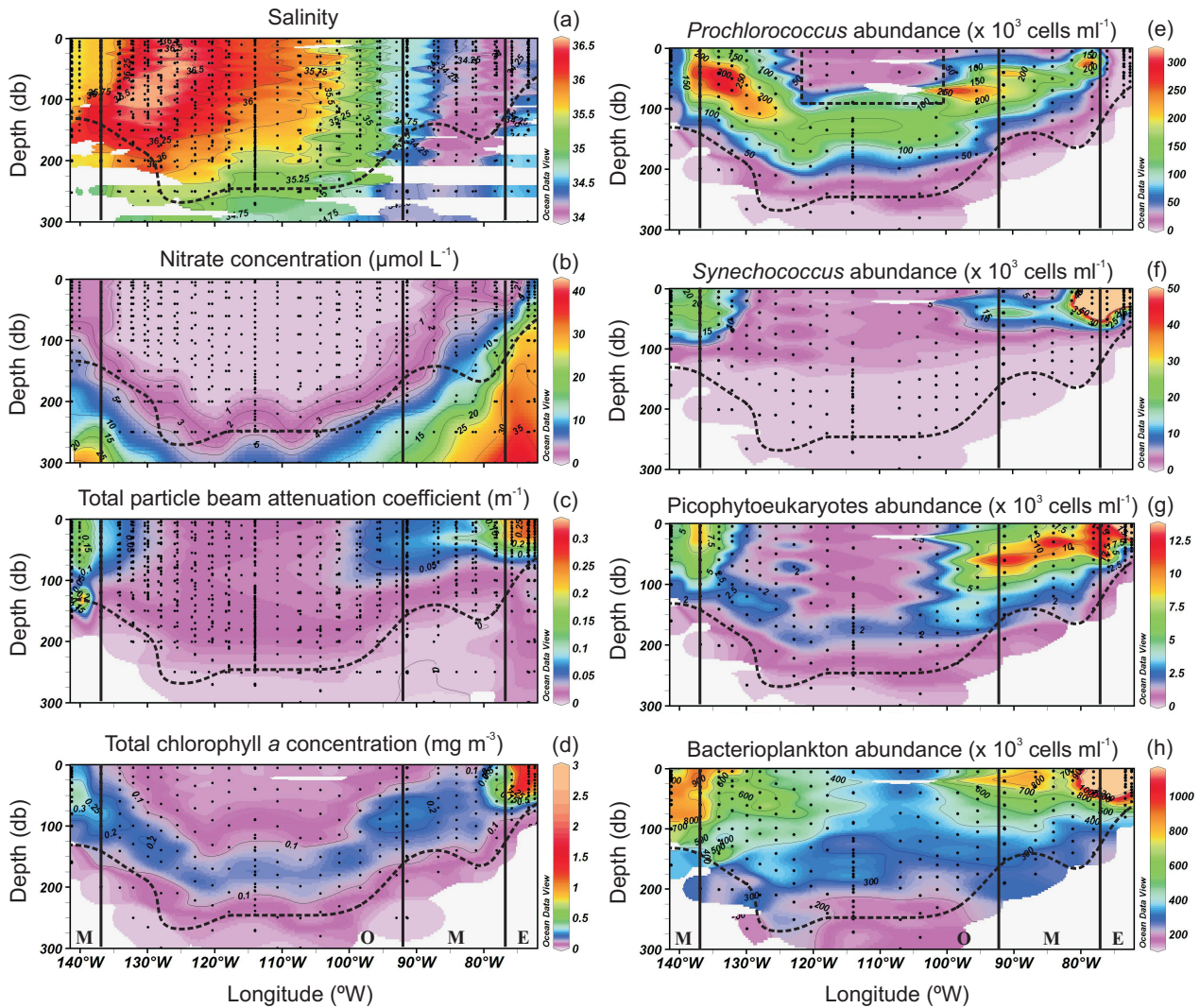


Fig. 4. Salinity (a), nitrate concentration in $\mu\text{mol L}^{-1}$ (b), total particle beam attenuation coefficient in m^{-1} (c), total chlorophyll *a* concentration in mg m^{-3} (d) *Prochlorococcus* (e), *Synechococcus* (f), picophytoeukaryotes (g) and bacterioplankton (h) abundances ($\times 10^3$ cells ml^{-1}). Vertical black lines indicate from left to right the limits between meso- (M), oligo- (O), meso- (M) and eutrophic (E) conditions. Horizontal black dashed line corresponds to the depth of the 1.5 Ze. Black dashed square in (e) indicates where *Prochlorococcus* abundances were estimated from dv-chla concentration.

3.1 Picoplankton numerical abundance

All groups' abundances tended to decrease towards the centre of the gyre. *Prochlorococcus* was highest at the western (up to 300×10^3 cells ml^{-1} around 50 m, associated with SPTW) and eastern (up to 200×10^3 cells ml^{-1} in the 50 to 100 m layer) borders of the oligotrophic region (Fig. 4e). Peaks in *Synechococcus* (up to 190×10^3 cells ml^{-1} ; Fig. 4f), picophytoeukaryotes ($10\text{--}70 \times 10^3$ cells ml^{-1} ; Fig. 4g) and bacterioplankton abundances (up to 2×10^6 cells ml^{-1} ; Fig. 4h) were registered near the coast. Deep *Prochlorococcus* ($100\text{--}150 \times 10^3$ cells ml^{-1} between 50 and 200 m; Fig. 4e) and picophytoeukaryotes ($\sim 2 \times 10^3$ cells ml^{-1} between 150

and 200 m; Fig. 4g) maxima were recorded at the centre of the gyre following the pattern of Tchl*a* concentrations (~ 0.15 mg m^{-3} ; Fig. 4d), above the deep chlorophyll maximum (DCM) for the former and within the DCM depth range for the latter (Figs. 4e and g). *Synechococcus* reached lower depth ranges than the rest of the groups everywhere along the transect (Fig. 4f). In terms of chlorophyll biomass, the importance of the DCM at the centre of the gyre is highlighted when comparing the surface-to-DCM average ratios for the different long stations: 0.67 ± 0.13 at MAR, 0.44 ± 0.04 at HNL, 0.12 ± 0.02 at GYR and 0.27 ± 0.02 at EGY.

Water column integrated picoplankton abundance (0 to 1.5 Ze) was strongly dominated by bacterioplankton along

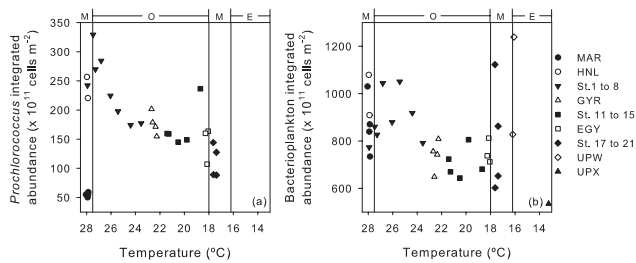


Fig. 5. *Prochlorococcus* (a), and bacterioplankton (b) integrated abundances (0 to 1.5 Ze, $\times 10^{11}$ cells m^{-2}) as a function of surface temperature, which was representative of the general eastward decrease in water temperature within the integration depth (0 to 1.5 Ze) along the transect. Vertical lines indicate the limits established between meso- (M), oligo- (O) and eutrophic (E) conditions.

Table 1. Correlation matrix for log integrated (0 to 1.5 Ze) picoplankton abundances (*Proc* = *Prochlorococcus*, *Syn* = *Synechococcus*, *Euk* = picophytoeukaryotes and *Bact* = bacterioplankton; $\times 10^{11}$ cells m^{-2}) and log integrated total chlorophyll *a* (*Tchl*_{*a*}; $mg m^{-2}$), considering the entire transect. Picophytoeukaryotes = *Proc* + *Syn* + *Euk*; picoplankton = *Proc* + *Syn* + *Euk* + *Bact*.

	<i>Proc</i>	<i>Syn</i>	<i>Euk</i>	<i>Bact</i>	<i>Tchl</i> _{<i>a</i>}
<i>Proc</i>	1.00	n.s.	n.s.	n.s.	-0.42*
<i>Syn</i>	-	1.00	0.68**	n.s.	0.82**
<i>Euk</i>	-	-	1.00	n.s.	n.s.
<i>Bact</i>	-	-	-	1.00	0.46*
Picophytoeukaryotes	-	-	-	-	0.58*
Picoplankton	-	-	-	-	0.61**

Upper right values show correlation coefficients with their corresponding level of significance:
 ** significance level <0.0001; * significance level <0.05; n.s., not statistically significant

the whole transect ($83 \pm 7\%$ of total picoplanktonic cells), followed by *Prochlorococcus* when present (up to 27% under oligotrophic conditions), the contributions by *Synechococcus* (0.1 to 3.7%) and picophytoeukaryotes (0.2 to 3.1%) being almost negligible. When not considering MAR, *Prochlorococcus* showed an evident positive relationship with surface temperature (Fig. 5a), which was representative of the general eastward decrease in water temperature within the integration depth (0 to 1.5 Ze) along the transect (see Claustre et al., 2007). Picophytoeukaryotes and *Synechococcus* abundances did not follow the surface temperature trend. Bacterioplankton, on the other hand, followed the *Prochlorococcus* pattern under oligotrophic conditions (Fig. 5b).

When considering the entire data set, *Prochlorococcus* integrated abundance was negatively correlated to *Tchl*_{*a*}, whereas bacterioplankton and *Synechococcus* (strongest correlation) were both positively correlated to this variable (Table 1). Bacterioplankton abundance covaried with phyto-

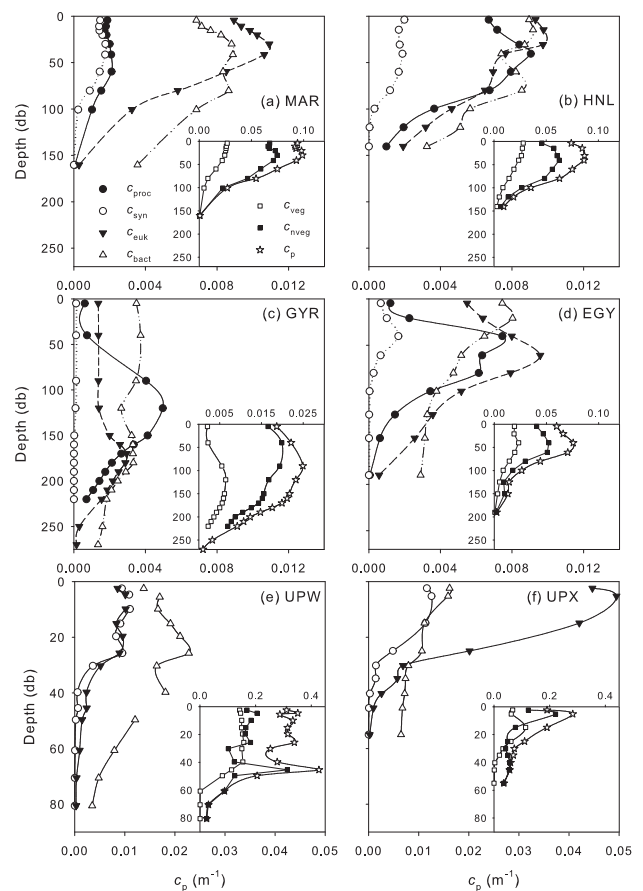


Fig. 6. Mean group-specific particle beam attenuation coefficients for *Prochlorococcus* (c_{proc}), *Synechococcus* (c_{syn}), picophytoeukaryotes (c_{euk}), bacterioplankton (c_{bact}). Insets contain the vegetational (c_{veg}), non-vegetational (c_{nveg}), and total particle beam attenuation coefficient (c_p) in m^{-1} . For MAR (a), HNL (b), GYR (c), EGY (d), UPW (e) and UPX (f). Note that UPW and UPX scales are equal to each other and different from the rest. For MAR, HNL, GYR and EGY all scale are the same except for GYR's c_p , c_{veg} and c_{nveg} .

plankton biomass (Table 1). Except for *Synechococcus* and picophytoeukaryotes, no statistically significant correlations were observed between picoplanktonic groups (Table 1).

3.2 Picoplankton contributions to c_p , a proxy for POC

Mean pico- and large phytoplankton cell sizes used to estimate the group-specific attenuation cross sections are summarized in Table 2 and compared with values from the literature. These values and the standard errors associated with them (Table 2) were obtained using the relationship established between mean FSC and cell size (Fig. 3a). The largest size difference between previous studies and the present one was observed for the picophytoeukaryotes (Table 2). For this group, the attenuation coefficients

Table 2. Picoplankton mean cell size (μm), volume (μm^3) and intracellular carbon content (fgC cell^{-1}).

Group	Mean cell size (μm)	Mean cell volume (μm^3)	Intracellular carbon content (fgC cell^{-1})	Reference
<i>Prochlorococcus</i>	0.68±0.08	0.17	29±11***	1
	0.74	0.21	–	2
	0.7	0.18	–	3
	0.63±0.2	0.13	29	4
<i>Synechococcus</i>	0.86±0.1* and 1.16±0.02**	0.33 and 0.82	60±19* and 140±9**	1
	0.90	0.38	–	2
	1.2	0.90	–	3
	0.95±0.31	0.45	100	4
Picophytoeukaryotes	1.74±0.13 (range = 1.37 to 1.99)	2.76	730±226 (range = 257 to 1266)	1
	1.26	1.05	–	2
	2.28	6.21	–	3
	2.35	6.8	1500	4
Large phytoplankton	3.3 (MAR) to ~20 (UPW)	18.8 to 4189	–	1
	10 to 22	523.6 to 5575.28	–	2
	6 to 13	113.1 to 1150.35	–	5
Bacterioplankton	0.5	0.07	–	1, 3
	0.56	0.09	–	2
	0.46±0.14	0.05	–	4
	0.50 to 0.65	0.07 to 0.13	–	6
	0.15 to 0.73	0.002 to 2	–	7

¹ This study

² Chung et al. (1998); Equatorial Pacific

³ Claustre et al. (1999); Tropical Pacific Ocean

⁴ Zubkov et al. (2000); North and South Atlantic Subtropical Gyres

⁵ Oubelkheir et al. (2005); Mediterranean Sea

⁶ Ulloa et al. (1992); Western North Atlantic

⁷ Gundersen et al. (2002); Bermuda Atlantic Time Series (BATS)

* For most of the transect and ** for UPX, the most coastal station

*** Obtained using the conversion factor $171\pm 15 \text{ fg C } \mu\text{m}^3$ derived from *Synechococcus* (see Sect. 2.1)

were determined by changes in both size (decreasing towards the coast; see Supp. Mat.: www.biogeosciences.net/4/837/2007/bg-4-837-2007-supplement.pdf) and abundance, when considering a constant refractive index. As a result, for instance, an average decrease in mean cells size of $0.22 \mu\text{m}$ ($0.0056 \mu\text{m}^3$) from MAR to HNL (see Supp. Mat.: www.biogeosciences.net/4/837/2007/bg-4-837-2007-supplement.pdf) counteracts the higher cell abundance in the latter (Fig. 6g; Table 2) to modulate c_{euk} along the transect (Figs. 6 and 7). In the case of *Prochlorococcus*, the mean value presented in Table 2 was obtained from samples taken at different depths along the entire transect, except at the centre of the gyre where the FSC signal could only be retrieved at depth. Larger cell sizes for this group were always found in deeper samples (not shown).

Along the transect, the shape and magnitude of the vertical c_p profiles were mainly determined by the non-vegetal compartment, with c_p and c_{nveg} presenting the same vertical pattern at all long stations (Fig. 6). At MAR and HNL, c_p was rather homogeneous in the top 50 m and declined be-

low this depth, whereas c_{nveg} decreased systematically with depth (Figs. 6a and b). At GYR c_p and c_{nveg} subsurface maxima were both observed around 100 m, these two variables being highest around 40 m at EGY (Figs. 6c and d). Both c_p and c_{veg} tended to be lower under hyper- and oligotrophic conditions at the centre of the gyre and were highest at UPW (Fig. 6). Both *Prochlorococcus* (when present) and picophytoeukaryotes usually presented subsurface maxima in their attenuation coefficients (e.g. at GYR around 125 m for the former and between 150 and 250 m for the latter; Fig. 6c) except at UPW, where c_{euk} tended to decrease below 30 m (Fig. 6e). UPX profiles were included to highlight the differences observed with UPW, the other upwelling station (Figs. 6e and f). No large phytoplankton peaks ($>3 \mu\text{m}$) were detected between Station 3 and 15, including GYR.

Total and group-specific integrated attenuation coefficients (0 to $1.5Z_e$) tended all to decrease from the western side towards the center of the gyre and increased again towards the coast (Fig. 7a). The integrated non-vegetal attenuation coefficient (detritus + bacterioplankton

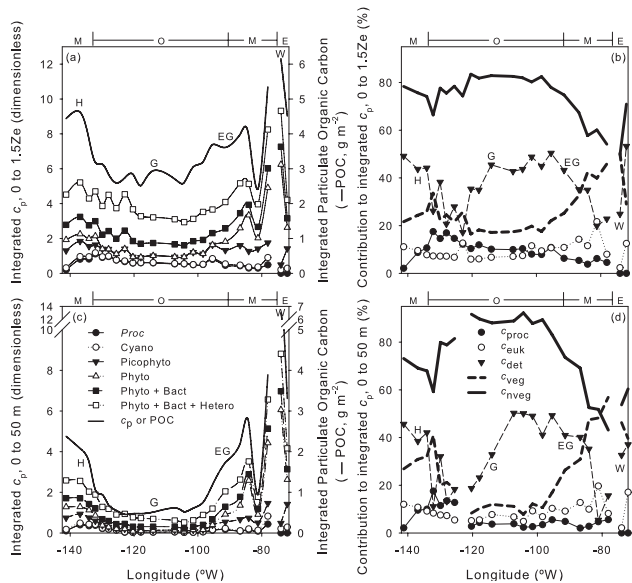


Fig. 7. Integrated attenuation coefficients for *Prochlorococcus* (*Proc*), *Proc + Synechococcus* (Cyano), Cyano + picophytoeukaryotes (Picophyto), Picophyto + nanophytoplankton (Phyto), Phyto + bacterioplankton (Phyto + Bact), Phyto + Bact + heterotrophic protists (Phyto + Bact + Hetero) and Phyto + Bact + Hetero + detritus (c_p) in the 0 to 1.5 Ze layer (a) and the 0 to 50 m layer (c). The contributions by *Prochlorococcus* (c_{proc}), picophytoeukaryotes (c_{euk}), detritus (c_{det}), vegetal (c_{veg}) and non-vegetal (c_{nveg}) particles to the corresponding total integrated attenuation coefficients are shown in (b) and (d). The top black lines in (a) and (c) correspond to the total integrated particle beam attenuation coefficient (c_p , left hand axis) and particulate organic carbon concentration (POC, right hand axis) estimated from c_p using Claustre et al. (1999) relationship (see Sect. 2.2; Eq. 5). M, O and E stand for meso-, oligo- and eutrophic conditions (top of each panel). H, G, EG and W indicate HNL, GYR, EGY and UPW stations.

+ heterotrophic organisms) was quite variable, constituting $\geq 70\%$ of $c_{0-1.5Ze}$ in most of the transect, reaching the highest (83%) and lowest (50%) contributions at GYR and UPW, respectively (Fig. 7b). Detritus being estimated by difference (Eq. 4), c_{det} and c_{veg} 's contributions to $c_{0-1.5Ze}$ followed a general opposite trend, presenting similar values near the meso-oligotrophic limits (~ 128 and 87° W) (Fig. 7b). Detritus contribution to $c_{0-1.5Ze}$ was always $\leq 50\%$, the lowest values being associated with highest vegetal contributions (Fig. 7b). Interestingly, between the two extreme trophic conditions encountered at GYR (hyper-oligotrophic; see Claustre et al., 2007) and UPW (eutrophic), $c_{0-1.5Ze}$ and integrated c_{veg} increased ~ 2 - and 6-fold, respectively, whereas integrated c_{nveg} and c_{det} were only ~ 1.2 - and 1.1-fold higher at the upwelling station (Fig. 7a). Furthermore, in terms of contribution to $c_{0-1.5Ze}$, c_{veg} was ~ 3 times higher at UPW, c_{nveg} and c_{det} representing only about half of the percentage estimated at GYR (Fig. 7b).

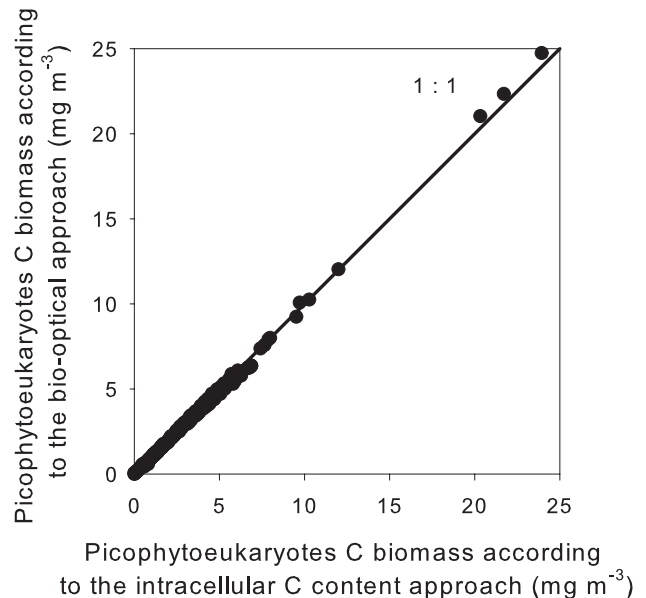


Fig. 8. Picophytoeukaryotes carbon biomass estimated from intracellular carbon content (see Sect. 2.1) compared to that estimated by calculating c_{euk} contribution to c_p , the latter assumed to be equivalent to POC (see Sect. 2.2). Note that both approaches gave very similar results. 1:1 indicates the 1-to-1 line relating both estimates.

Mean integrated *Prochlorococcus* (when present) and picophytoeukaryotes contributions to $c_{0-1.5Ze}$ for the whole transect were equivalent (9.7 ± 4.1 and $9.4 \pm 3.8\%$, respectively), although the latter were clearly more important under mesotrophic conditions in both absolute values (Fig. 7a) and relative terms (Fig. 7b). *Synechococcus* attenuation coefficients were too low (Fig. 7a) to contribute significantly to c_p (only $1.0 \pm 1.0\%$ on average), so we did not include them in Fig. 7b. Bacterioplankton attenuation coefficients varied little along the transect and were always lower than all phytoplankton combined (Fig. 7b). Large phytoplankton attenuation coefficients were lower than that of the picophytoplankton (cyanobacteria and picophytoeukaryotes combined) in the western part of the transect and higher or similar near the coast (Fig. 7a), their contributions to c_p following the same trend (included in c_{veg} 's contribution, Fig. 7b).

When comparing $c_{0-1.5Ze}$ to c_{0-50m} and their integrated group-specific attenuation coefficients, it becomes clear that not considering data below 50 m leads to very different results in most of the transect and especially at the centre of the gyre (Figs. 7a and c). For instance, whereas at UPW $c_{0-1.5Ze}$ and c_{0-50m} were equivalent, the former is 2- and the latter 13-fold higher than the corresponding GYR integrated values (Figs. 7a and c). Similarly, there was a 2-fold difference in c_{veg} 's contributions to $c_{0-1.5Ze}$ and c_{0-50m} at the centre of the gyre (Figs. 7b and d).

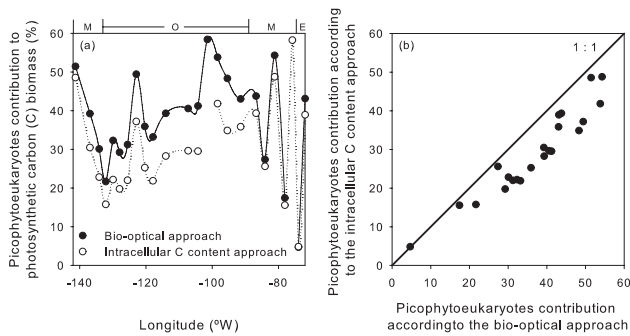


Fig. 9. Picophytoeukaryotes contribution to the photosynthetic carbon biomass as derived from c_{euk} 's contribution to c_{veg} by applying Eq. (5) (bio-optical method) and as obtained using intracellular carbon contents in Table 2 to estimate picophytoplankton carbon biomass (a). When comparing the results obtained using both approaches, it can clearly be seen that the contributions estimated using the intracellular carbon (C) content approach are lower than those estimated using the bio-optical approach, with almost all data points being below the 1-to-1 line relating both estimates (b).

3.3 Phytoplanktonic carbon biomass stocks and spatial variability

To avoid the use of carbon conversion factors from the literature, in the present work we used two different approaches to estimate the picophytoeukaryotes carbon biomass: (1) from intracellular carbon content (Fig. 3b; see Sect. 2.1) and (2) calculating c_{euk} contribution to c_{p} , the latter assumed to be equivalent to POC (see Sect. 2.2). Both approaches gave very similar results (Fig. 8), indicating that the premise that all picophytoeukaryotic organisms have the same refractive index (~ 1.05) is valid for the sampled transect, even if we know that this group is usually constituted by diverse taxa (Moonvan der Staay et al., 2001). The above provides strong support for the use of optical techniques and theory to determine picophytoeukaryotes carbon biomass, under the sole condition of using actual mean cell sizes.

The deconvolution of c_{p} indicates that at the centre of the gyre (~ 120.36 to 98.39° W or Station 7 to 14+GYR) the photosynthetic biomass, which was dominated by picophytoplankton, constituted $\sim 18\%$ of the total integrated c_{p} or POC (Fig. 7b). Even more interestingly, when looking at the vegetal compartment alone, $\sim 43\%$ of this photosynthetic biomass would correspond to the picophytoeukaryotes (Fig. 9a; filled circles). Let us now assume that the contribution to integrated c_{p} by all phytoplanktonic groups is representative of their contribution to POC, as proven for the picophytoeukaryotes (see above). Under this assumption, picophytoeukaryotes would constitute 51% of the total phytoplankton carbon biomass (large phytoplankton included) at MAR, about 39% at HNL and GYR and 43% at EGY (Fig. 9a; filled circles). At UPW, however, where mean integrated POC estimated from c_{p} (see Sect. 2.2) was $\sim 6 \text{ g m}^{-2}$ (right axis on

Fig. 7a), picophytoeukaryotes would only constitute 5% of the photosynthetic biomass (Fig. 9a; filled circles). When considering the whole transect, picophytoeukaryotes mean contribution to the total photosynthetic carbon biomass (i.e. c_{euk} 's mean contribution to c_{p}) was $\sim 38\%$.

Intracellular carbon contents used to estimate picophytoplankton biomass through the relationship established with FSC (Fig. 3b) are given in Table 2. Contributions to POC by *Prochlorococcus* and *Synechococcus* were ~ 1.7 and 1.5 times higher when estimated using this approach rather than attenuation coefficients (not shown). Using these higher values for cyanobacteria and assuming that the contribution by large phytoplankton is equivalent to c_{large} 's contribution to c_{p} , picophytoeukaryotes mean contribution to the total photosynthetic carbon biomass along the transect would be $\sim 30\%$, representing ~ 28 instead of 43% at the centre of the gyre (Fig. 9a; empty circles). These contributions are slightly lower than the ones estimated through the optically-based approach, with almost all data points being below the 1-to-1 line relating both estimates (Fig. 9b).

Regarding spatial variability, both *Tchl a* ($r=0.67$, $p<0.001$) and c_{p} ($r=0.53$, $p<0.001$) were correlated to the dominant picophytoplankton carbon biomass, i.e. *Prochlorococcus* + picophytoeukaryotes, between Stations 3 and 15, GYR included (Fig. 10). The results of a t-test on the z-transformed correlation coefficients (Zokal and Rohlf, 1994) indicates that both correlations are not significantly different ($p>0.05$). Therefore, *Tchl a* and c_{p} were equally well correlated to the picophytoplanktonic biomass. *Synechococcus* biomass, on the other hand, was negatively correlated to *Tchl a* (Fig. 10a) and positively to c_{p} (Fig. 10b). However, despite the differences observed between this cyanobacterium and the other two groups, correlation coefficients calculated for total picophytoplankton biomass (i.e. dominant + *Synechococcus*; not shown) were not significantly different ($p>0.05$) from those calculated for the dominant groups (Fig. 10). *Synechococcus* had no influence on the general relationships because of its negligible biomass. *Tchl a* and c_{p} were therefore useful in tracing total picophytoplanktonic carbon biomass in the part of the transect where no large phytoplankton was detected (i.e. Stations 3 to 15+GYR).

4 Discussion and conclusion

4.1 Picoplankton abundance

Macroecological studies indicate that 66% of the variance in picophytoplankton abundance can be explained by temperature (the dominant factor), nitrate and chlorophyll *a* concentration (Li, 2007). It has also been established that higher *Prochlorococcus* abundances are observed in more stratified waters, whereas *Synechococcus* and picophytoeukaryotes are more abundant when mixing prevails (e.g. Blanchot and

Rodier, 1996; Shalapyonok et al., 2001). Across the eastern South Pacific Ocean temperature, especially for *Prochlorococcus* and bacterioplankton (Fig. 5), and nitrate concentration along the transect (see Fig. 4b) appear important in modulating picophytoplankton abundance, their influence varying according to the prevailing trophic conditions.

As expected (e.g. Gasol and Duarte, 2000), integrated bacterioplankton abundances covaried with phytoplankton biomass (Table 1). Integrated picophytoeukaryotes abundance was the only one to vary independently from *Tchl a* when considering the whole transect (Table 1), suggesting that the factors controlling picophytoplankton population, such as sinking, sensitivity to radiation, grazing, viral infection, etc. (Raven, 2005) acted differently on this group. Thus, the ecology of picophytoeukaryotes needs to be studied in further detail. Across the eastern South Pacific, surface bacterioplankton concentrations were similar to those found by Grob et al. (2007) at 32.5° S. However, in the deep layer of the hyper-oligotrophic part of the gyre (200 m) this group was 2.5 times more abundant than published by Grob et al. (2007). Given the correlation between integrated bacterioplankton abundance and *Tchl a* concentration (Table 1), the latter could be attributed to the presence of deep *Prochlorococcus* and picophytoeukaryotes maxima that were not observed by Grob et al. (2007). Such deep maxima are a recurrent feature in the oligotrophic open ocean (Figs. 4e and g; Table 3). Along the transect, picophytoplankton abundances were usually within the ranges established in the literature for oligo-, meso- and eutrophic regions of the world's ocean (see Table 3). It is worth noticing that our estimates for surface *Prochlorococcus* abundance were, to our knowledge, the lowest ever estimated for the open ocean (see Table 3), although a possible underestimation cannot be ruled out.

The presence of the mentioned groups under extreme poor conditions suggests a high level of adaptation to an environment where inorganic nutrients are below detection limit. Although little is known on picophytoeukaryotes metabolism, several cyanobacteria ecotypes have been shown to grow on urea and ammonium (Moore et al., 2002). Ammonium uptake at the centre of the gyre was low but still detectable (Raimbault et al., 2007). Considering that heterotrophic bacteria would be responsible for ~40% of this uptake in marine environments (Kirchman, 2000), the possibility of surface picophytoplankton growing on this form of nitrogen at the centre of the gyre cannot be discarded.

4.2 Picoplankton contribution to c_p

The larger increase of integrated c_{veg} as compared to c_{nveg} observed between extreme trophic conditions (see Sect. 3.2) indicates that across the eastern South Pacific spatial variability in the vegetal compartment was more important than the non-vegetal one in shaping the water column optical properties, at least the particle beam attenuation coefficient. As expected (e.g. Chung et al., 1996; Loisel and Morel, 1998;

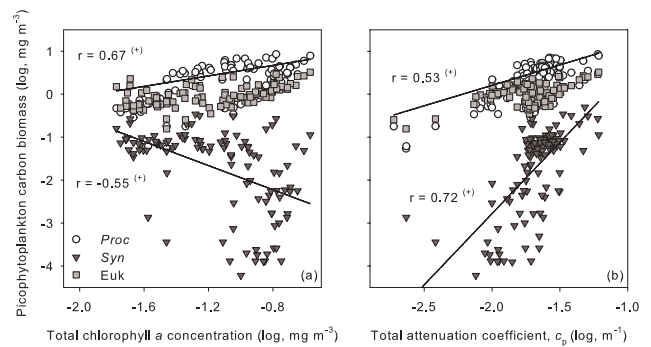


Fig. 10. Log-log relationships for *Prochlorococcus* (*Proc*), *Synechococcus* (*Syn*) and picophytoeukaryotes (*Euk*) carbon biomass (mg m^{-3}) with total chlorophyll *a* concentration in mg m^{-3} (a) and total particle beam attenuation coefficient in m^{-1} (b). Only data from Stations 3 to 15 and GYR, where no large phytoplankton cells were detected, and between the surface and 1.5 Ze are included (see Sect. 2.2). Correlation coefficients (r) were calculated for the sum of *Proc* and *Euk* (upper values) and for *Syn* carbon biomass (lower values) with *Tchl a* (a) and c_p (b). $(^{*})$ indicates $p < 0.001$.

Claustre et al., 1999), c_p and c_{veg} tended to be lower under hyper- and oligotrophic conditions at the centre of the gyre and were highest at UPW. Here, the highest c_p and c_{veg} were associated with mature upwelling conditions characterized by the highest primary production (Moutin et al., 2007) and *Tchl a* (Fig. 4d), and low nutrient concentration (Fig. 4b; Raimbault et al., 2007).

Although the non-vegetal particles tended to dominate the c_p signal, and therefore POC, regardless of trophic condition (Fig. 7b; e.g. Chung et al., 1998; Claustre et al., 1999; Oubelkheir et al., 2005), this dominance seems to weaken from oligo- to eutrophic conditions (Claustre et al., 1999; this study). Here we showed that under mature upwelling conditions (UPW) the contribution by vegetal and non-vegetal particles may even be equivalent (Fig. 7b), in contrast with the invariant ~80% c_{nveg} contribution estimated by Oubelkheir et al. (2005) for different trophic conditions. We therefore emphasize the importance of using complementary data to interpret bio-optical measurements since, for instance, the ~2.3-fold difference in c_{veg} 's contribution to c_p observed between our UPW results and those published by Oubelkheir et al. (2005) seems to be related to the state of development of the upwelling event (mature versus early).

At the hyper-oligotrophic centre of the gyre, c_{euk} contribution to $c_{0-1.5Ze}$ was equivalent to the one possibly overestimated (because of the larger cell size assumed) by Claustre et al. (1999). The above highlights the importance of making good size estimates when decomposing the total attenuation signal since, for example, a difference of 1.02 μm in size leads to a 10-fold difference in the scattering cross-section calculated for picophytoeukaryotes (Claustre et al., 1999; Oubelkheir et al., 2005). In the present

Table 3. *Prochlorococcus*, *Synechococcus* and picophytoeukaryotes abundances ($\times 10^3$ cells ml^{-1}) registered during spring time in different regions of the world's ocean under varying trophic conditions.

Trophic condition	<i>Prochlorococcus</i>	<i>Synechococcus</i>	Picophytoeukaryotes	Reference
Hyper-oligotrophic	16–18*	1.2–1.6*	0.76–1.3*	1 (GYR)
	150–160 (125 m)	0.8–1.4 (125 m)	1.8–2.3 (175 m)	
Oligotrophic	35–40*	6.9–8.6*	4.5–4.9*	1 (EGY)
	200–250 (50–75 m)	20 (50 m)	14 (60 m)	
	240 (0 to 100 m)	1.5 (0 to 100 m)	0.8–1 (0 to 100 m)	2
	30*	0.7*	0.5*	
	200 (120 m)	1–1.5 (50–125 m)	2 (140–150 m)	4
	100–150*	3–30*	0.6–2*	
	100 (120 m)	1 (120–160 m)	1–2 (80–120 m)	5
	115*	0.2–1 (0 to 100 m)	0.25–0.5*	
	150–200 (50–100 m)		Up to 3 (100 m)	6
	60 (0 to 100 m)	2.5 (0 to 50–100 m)	2–4*	
HNL	200 (surf)	10–28 (surf)	5–9 (0 to 80 m)	1
	270 (30–60 m)	25 (50 m)		
				3
	150–300 (0 to 80 m)	3–5 (0 to 80 m)	0.6–1 (0 to 100 m)	
	200 (0 to 50 m)	8 (0 to 100 m)	3 (0 to 100 m)	
Mesotrophic	100 (80 m)			8
	200 (30 and 60 m)	15 and 13 (30 and 60 m)	6 and 5 (30 and 60 m)	
	50–60 (0 to 80 m)	17–20 (0 to 60 m)	3–5 (0 to 80 m)	1 (MAR)
	30–200*	5–44*	3–18*	
	1–40 (100 m)	0.2–3 (100 m)	0.4–4 (100 m)	6
Eutrophic	–	60–200	5–10	
	–	50–250	10–60	
	–	Up to 150	Up to 80–90	10

* Surface data

1 This study

2 Campbell and Vaulot (1993); Subtropical North Pacific (ALOHA)

3 Vaulot et al. (1999); Subtropical Pacific (16° S; 150° W). These authors considered their surface *Prochlorococcus* abundances as “severely underestimated”.

4 Zubkov et al. (2000); North and South Atlantic Subtropical Gyres

5 Veldhuis and Kraay (2004); Eastern North Atlantic Subtropical Gyre

6 Grob et al. (2007); Eastern South Pacific

7 Mackey et al. (2002); Equatorial Pacific

8 Landry et al. (2003); Equatorial Pacific

9 Worden et al. (2004); Southern California Bight, North Pacific

10 Sherr et al. (2005); Oregon upwelling ecosystem, North Pacific

work, picophytoplankton populations were isolated on board by flow-cytometry cell sorting in order to measure their actual sizes using a particle counter (see Sect. 2.1). It is the first time to our knowledge that such direct measurements have been made in the field. For future studies we recommend to measure the different picophytoplankton mean cell sizes in situ for at least a few samples, including surface and deep populations in order to consider possible vertical variability. If these samples are taken under different oceanographic conditions, we also recommend including samples from each one of these conditions.

By establishing a relationship with FSC to estimate actual picophytoplankton cell size (Fig. 3a), we confirmed that picophytoeukaryotes were more important contributors to c_p than cyanobacteria under both meso- and eutrophic conditions (Claustre et al., 1999). The uncertainties in this relationship are larger for cyanobacteria (lower part of the curve; Fig. 3a) than for picophytoeukaryotes. However, *Prochlorococcus* and *Synechococcus*' mean cell sizes measured in situ were ≤ 0.59 (only one isolated population could be measured with the Coulter Counter, the rest being too small) and ≤ 0.87 μm , respectively (see

Table A, Supp. Mat.: www.biogeosciences.net/4/837/2007/bg-4-837-2007-supplement.pdf). We therefore believe that these group's mean cell sizes, and therefore their contributions to c_p along the transect, may have been at most over- rather than underestimated by this relationship. Differences in cell size (Table 2) would also explain the much lower *Synechococcus* contribution to c_p observed in the hyper-oligotrophic centre of the gyre compared to that published by Claustre et al. (1999) for the tropical Pacific (16° S, 150° W).

Only data collected at local noon time were used to estimate group-specific attenuation coefficients, to avoid errors associated with the natural diel variability that has been observed in the refractive index of picophytoplankton cells from culture (e.g. Stramski et al., 1995; DuRand and Olson, 1998; DuRand et al., 2002). Here we showed that the premise that all picophytoeukaryotes are homogeneous spheres with the same refractive index of 1.05 (assumptions of the anomalous diffraction approximation) is valid for the sampled transect when actual mean cell sizes are used. In the case of *Synechococcus*, a high refractive index of 1.083 (Aas, 1996) would only increase this group's mean attenuation cross-section by an almost negligible 6%. Given their low abundance compared to the other groups, the resulting increase in their contribution to c_p would be even lower.

If *Prochlorococcus* were to have a refractive index of 1.06 for instance, their mean attenuation cross-section would be 43% higher than the one calculated here. Nevertheless, the resulting *Prochlorococcus*' contribution to c_p for the entire transect would only be $4\pm 2\%$ higher. However, this group's contribution to c_{veg} would increase by $18\pm 2\%$ on average, constituting up to 99% of the vegetal compartment under hyper-oligotrophic conditions. Such high contribution contradicts both HPLC (dv-*chl*a to Tchl*a* ratios of ~ 0.2 to 0.5; see Ras et al., 2007) and flow cytometry data (see *Synechococcus* and picophytoeukaryotes abundances; Figs. 4f and g) and appears hence not possible. We therefore believe that the assumption of a refractive index of 1.05 for cyanobacteria is appropriate for the purposes of the present work. It is worth noticing that lower refractive indexes for these two groups would only reduce their contribution to c_p (and therefore POC) and c_{veg} , the contribution by picophytoeukaryotes resulting even more important than stated in this work.

Regarding mean cell size, deep *Prochlorococcus* cells are larger than surface ones (e.g. Li et al., 1993; this study). The former are better represented than the latter in the data set used to estimate mean *Prochlorococcus* cell size for the transect, since surface FSC signals could not be retrieved for a large area at the centre of the gyre. We therefore consider that the mean cell size used here for this group could be at most overestimated, i.e. biased towards a larger value due to the fewer surface data available. Hence, picophytoeukaryotes' contributions to c_{veg} could only be underestimated. The above highlights the importance of this group in terms of photosynthetic biomass in the open ocean.

Definitively the largest uncertainties in the deconvolution of c_p are related to the determination c_{bact} and c_{het} , which have a direct influence on c_{det} 's estimates (see Sect. 2.2, Eq. 4). First, bacterioplankton cells were assumed to have a mean cell size of $0.5\ \mu\text{m}$. Taking the minimum and maximum sizes presented in Table 2 (i.e. 0.46 and $0.73\ \mu\text{m}$), the scattering cross section for bacterioplankton would be $\sim 28\%$ lower and 4.5 times higher than the one used here, respectively. The lower scattering cross sections for these two groups would imply an underestimation of detritus' contribution to c_p of only $11\pm 3\%$ on average for the entire transect. A scattering cross section 4.5 times higher (i.e. $0.73\ \mu\text{m}$ of mean cell size) would imply contributions $\geq 100\%$ to c_p , and therefore POC, by bacteria and heterotrophic protists alone, which seems unrealistic. Using a mean cell size of $0.6\ \mu\text{m}$, i.e. the average value between 0.46 and $0.73\ \mu\text{m}$, leads to the same kind of overestimation of the heterotrophic contributions to c_p . Based on the above, we consider the assumption of a $0.5\ \mu\text{m}$ mean cell size for bacterioplankton to be appropriate for our estimates, since at most it would slightly underestimate detritus.

Following Claustre et al. (1999), here we assumed that $c_{het}=2\ c_{bact}$ (see Sect. 2.2, Eq. 3). The range reported by Morel and Ahn (1993) for this conversion factor is 1.8 to 2.4. Using these values instead of 2 would result in an average increase and decrease in c_{det} 's contribution to c_p across the eastern South Pacific of $2\pm 1\%$ and $4\pm 2\%$, respectively, which in both cases is negligible. It is worth noticing that even if larger errors were associated with the assumptions made in this work regarding bacterioplankton and heterotrophic protists, our results and conclusions regarding picophytoeukaryotes contributions to c_p , and therefore POC, and to the photosynthetic carbon biomass across the eastern South Pacific would not change.

4.3 Phytoplankton carbon biomass stocks and spatial variability

One of the most important observations of the present study is that spatial variability in the open-ocean, where no large phytoplankton was detected, picophytoplankton carbon biomass can be traced by changes in both Tchl*a* and c_p (Fig. 10). While chlorophyll concentration has widely been used as a proxy for photosynthetic carbon biomass, the use of c_p is more controversial. For instance, although c_p seems to be a better estimate of phytoplankton biomass than Tchl*a* in Case I waters (Behrenfeld and Boss, 2003) and within the mixed layer of the eastern Equatorial Pacific (Behrenfeld and Boss, 2006), chlorophyll concentration would work better in subtropical stratified waters (Huot et al., 2007). Our results indicate that Tchl*a* and c_p would be equally useful estimates of photosynthetic carbon biomass in the South Pacific gyre, where it is mainly constituted by picophytoplankton ($\leq 3\ \mu\text{m}$). However, it is important to highlight that in order to estimate the photosynthetic carbon biomass from c_p it is

necessary to have information or make some assumptions on the contributions by vegetal and non-vegetal particles to this coefficient. In this case, picophytoplankton biomass and c_p were positively correlated such as that the former could be retrieved from the latter. Despite of the stated limitations, the bio-optical approach used in the present work could be a good alternative for large scale open ocean surveys, especially considering that c_p measurements are much less time-consuming than determining chlorophyll concentration and can also be obtained at a much higher vertical resolution. Further research should be done to test the ability of c_p in tracing phytoplankton biomass in the ocean.

Although when present *Prochlorococcus* largely dominates in terms of abundance, the picophytoeukaryotes would constitute $\sim 38\%$ on average of the total integrated phytoplankton carbon biomass (*Prochlorococcus* + *Synechococcus* + picophytoeukaryotes + large phytoplankton) estimated from c_{euk} 's contribution to c_{veg} (Fig. 9a, filled circles; see Sect. 3.3). Furthermore, under oligotrophic conditions this group constituted $\sim 43\%$ of the photosynthetic carbon biomass. Previous studies indicate that picophytoeukaryotes largely dominate the vegetal compartment in the equatorial Pacific (DuRand et al., 1996; Claustre et al., 1999) and the picophytoplanktonic carbon biomass across the eastern South Pacific along 32.5° S (Grob et al., 2007). Here we showed that this group constitutes a very important and in some cases a dominant fraction of c_{veg} across the eastern South Pacific, confirming the findings by Grob et al. (2007). The above also agrees with what has been observed in the North and South Atlantic Subtropical Gyres (Zubkov et al., 2000). Picophytoeukaryotes also dominated the picophytoplanktonic carbon biomass in the coastal region, as previously indicated by Worden et al. (2004) and Grob et al. (2007).

Picophytoeukaryotes contributions obtained by estimating cyanobacteria biomass from intracellular carbon content were probably underestimated compared to those obtained using the bio-optical approach (Fig. 9b) because of the conversion factor used for *Prochlorococcus* (Table 2). We believe that establishing a relationship between intracellular carbon content and FSC for this cyanobacterium, as we did for *Synechococcus* and picophytoeukaryotes, would lead to contributions similar to those estimated using attenuation coefficients. It is worth noticing that higher or lower cyanobacteria carbon biomasses would only modify the y-intercept of the biomass relationships with *Tchl a* and c_p (Fig. 10), but not their slope or their strength.

When normalized to $1 \mu\text{m}^3$, maximal growth rates estimated for picophytoeukaryotes are higher than for *Prochlorococcus* (Raven, 2005, and references therein). Considering that the former are ~ 16 times larger than the latter in terms of mean cell volume, the amount of carbon passing through the picophytoeukaryotes could be very important. For the same reason, this group could also be the most important contributor to export fluxes in the open ocean, since picophytoplankton share of this carbon pathway

seems to be much more important than previously thought (Richardson and Jackson, 2007; Barber, 2007). The role of this group in carbon and energy flow would therefore be crucial.

Picophytoeukaryotes carbon biomass in the open ocean seems to be much more important than previously thought. Across the eastern South Pacific, this group's biomass is almost equivalent to that of *Prochlorococcus* under hyper-oligotrophic conditions and even more important under mesotrophic ones. The role of picophytoeukaryotes in biogeochemical cycles needs to be evaluated in the near future. Further attention needs to be focused on this group.

Acknowledgements. This work was supported by the Chilean National Commission for Scientific and Technological Research (CONICYT) through the FONDAP Program and a graduate fellowship to C. Grob; the ECOS (Evaluation and Orientation of the Scientific Cooperation, France)-CONICYT Program, the French program PROOF (Processus Biogéochimiques dans l'Océan et Flux), Centre National de la Recherche Scientifique (CNRS), the Institut des Sciences de l'Univers (INSU), the Centre National d'Etudes Spatiales (CNES), the European Space Agency (ESA), the National Aeronautics and Space Administration (NASA) and the Natural Sciences and Engineering Research Council of Canada (NSERC). This is a contribution of the BIOSOPE project of the LEFE-CYBER program. D. Tailliez and C. Bournot are warmly thanked for their efficient help in CTD rosette management and data processing. We also thank the scientific party and the Captain and crew of the RV L'Atalante during the BIOSOPE Expedition; F. Thièche for her help with laboratory work; L. Farías and M. Gallegos for organic carbon analyses, B. Gentili for PAR data processing and R. Wiff for help with statistical analyses.

Edited by: E. Boss

References

- Aas, E.: Refractive index of phytoplankton derived from its metabolite composition, *J. Plankton Res.*, 18, 2223–2249, 1996.
- Antoine, D., André, J. M., and Morel, A.: Oceanic primary production II. Estimation at global scale from satellite (Coastal Zone Color Scanner) chlorophyll, *Global Biogeochem. Cycles*, 10, 57–69, 1996.
- Barber, R. T.: Picoplankton Do Some Heavy Lifting, *Science*, 315, 777–778, 2007.
- Behrenfeld, M. J. and Boss, E.: The beam attenuation to chlorophyll ratio: an optical index of phytoplankton physiology in the surface ocean?, *Deep Sea Res. Part I*, 50, 1537–1549, 2003.
- Behrenfeld, M. J. and Boss, E.: Beam attenuation and chlorophyll concentration as alternative optical indices of phytoplankton biomass, *J. Mar. Res.*, 64, 431–451, 2006.
- Bissett, W. P., Walsh, J. J., Dieterle, D. A., and Carder, K. L.: Carbon cycling in the upper waters of the Sargasso Sea: I. Numerical simulation of differential carbon and nitrogen fluxes, *Deep Sea Res. I*, 46, 205–269, 1999.
- Blanchot, J. and Rodier, M.: Picophytoplankton abundance and biomass in the western Tropical Pacific Ocean during the 1992

- El Nino year: Results from flow cytometry, *Deep-Sea Res.*, 43, 877–896, 1996.
- Campbell, L. and Vault, D.: Photosynthetic picoplankton community structure in the subtropical North Pacific Ocean near Hawaii (station ALOHA), *Deep Sea Res. I*, 40, 2043–2060, 1993.
- Carr, M.-E., Friedrichs, M. A. M., Schmeltz, M., Aita, M. N., Antoine, D., Arrigo, K. R., Asanuma, I., Aumont, O., Barber, R., Behrenfeld, M., Bidigare, R., Buitenhuis, E. T., Campbell, J., Ciotti, A., Dierssen, H., Dowell, M., Dunne, J., Esaias, W., Gentili, B., Gregg, W., Groom, S., Hoepffner, N., Ishizaka, J., Kameda, T., Quéré, C. L., Lohrenz, S., Marra, J., Mélin, F., Moore, K., Morel, A., Reddy, T. E., Ryan, J., Scardi, M., Smyth, T., Turpie, K., Tilstone, G., Waters, K., and Yamanaka, Y.: A comparison of global estimates of marine primary production from ocean color, *Deep Sea Res. II*, 53, 741–770, 2006.
- Chavez, F. P., Buck, K. R., Bidigare, R. R., Karl, D. M., Hebel, D., Latasa, M., and Campbell, L.: On the chlorophyll a retention properties of glass-fiber GF/F filters, *Limnol. Oceanogr.*, 40, 428–433, 1995.
- Chen, C.-T. A., Liu, K.-K., and MacDonald, R. W.: Continental margin exchanges. *Ocean Biogeochemistry*, in: *The Role of the Ocean Carbon Cycle in Global Change*, edited by: Fasham, M. J. R., IGBP Book Series, Springer, 53–97, 2003.
- Chisholm, S. W., Olson, R. J., Zettler, E. R., Goericke, R., Waterbury, J. B., and Welschmeyer, N. A.: A novel free-living prochlorophyte occurs at high cell concentrations in the oceanic euphotic zone, *Nature*, 334, 340–343, 1988.
- Chung, S. P., Gardner, W. D., Richardson, M. J., Walsh, I. D., and Landry, M. R.: Beam attenuation and microorganisms: spatial and temporal variations in small particles along 140° W during the 1992 JGOFS EqPac transects, *Deep Sea Res. II*, 43, 1205–1226, 1996.
- Chung, S. P., Gardner, W. D., Landry, M. R., Richardson, M. J., and Walsh, I. D.: Beam attenuation by microorganisms and detrital particles in the Equatorial Pacific, *J. Geophys. Res.*, 103(C6), 12 669–12 681, 1998.
- Claustre, H., Morel, A., Babin, M., Cailliau, C., Marie, D., Marty, J. C., Tailliez, D., and Vault, D.: Variability in particle attenuation and chlorophyll fluorescence in the Tropical Pacific: Scales, patterns, and biogeochemical implications, *J. Geophys. Res.*, 104(C2), 3401–3422, 1999.
- Claustre, H., Huot, Y., Obernosterer, I., Gentili, B., Tailliez, D., and Lewis, M.: Gross community production and metabolic balance in the South Pacific Gyre, using a non-intrusive bio-optical method, *Biogeosciences Discuss.*, 4, 3089–3121, 2007, <http://www.biogeosciences-discuss.net/4/3089/2007/>.
- DuRand, M. D. and Olson, R. J.: Contributions of phytoplankton light scattering and cell concentration changes to diel variations in beam attenuation in the equatorial Pacific from flow cytometric measurements of pico-, ultra- and nanoplankton, *Deep Sea Res. Part II*, 43, 891–906, 1996.
- DuRand, M. D. and Olson, R. J.: Diel patterns in optical properties of the chlorophyte *Nannochloris* sp.: Relating individual-cell to bulk measurements, *Limnol. Oceanogr.*, 43, 1107–1118, 1998.
- DuRand, M. D., Green, R. E., Sosik, H. M., and Olson, R. J.: Diel variations in optical properties of *Micromonas pusilla* (Prasinophyceae), *J. Phycol.*, 38, 1132–1142, 2002.
- Falkowski, P. G., Barber, R. T., and Smetacek, V.: *Biogeochemical Controls and Feedbacks on Ocean Primary Production*, Science, 200–206, 1998.
- Field, C. B., Behrenfeld, M. J., Randerson, J. T., and Falkowski, P.: Primary Production of the Biosphere: Integrating Terrestrial and Oceanic Components, *Science*, 281, 237–240, 1998.
- Gardner, W. D., Mishonov, A. V., and Richardson, M. J.: Global POC concentrations from in-situ and satellite data, *Deep Sea Res. II*, 53, 718–740, 2006.
- Gasol, J. M. and Duarte, C. M.: Comparative analyses in aquatic microbial ecology: how far do they go?, *FEMS Microbiol. Ecol.*, 31, 99–106, 2000.
- Grob, C., Ulloa, O., Li, W. K. W., Alarcón, G., Fukasawa, M., and Watanabe, S.: Picoplankton abundance and biomass across the eastern South Pacific Ocean along latitude 32.5° S, *Mar. Ecol. Prog. Ser.*, 332, 53–62, 2007.
- Gundersen, K., Heldal, M., Norland, S., Purdie, D. A., and Knap, A. H.: Elemental C, N, and P cell content of individual bacteria collected at the Bermuda Atlantic Time-series Study (BATS) site, *Limnol. Oceanogr.*, 47, 1525–1530, 2002.
- Huot, Y., Babin, M., Bruyant, F., Grob, C., Twardowski, M. S., and Claustre, H.: Does chlorophyll *a* provide the best index of phytoplankton biomass for primary productivity studies?, *Biogeosciences Discuss.*, 4, 707–745, 2007, <http://www.biogeosciences-discuss.net/4/707/2007/>.
- Kirchman, D. L.: Uptake and regeneration of inorganic nutrients by marine heterotrophic bacteria, in: *Microbial ecology of the oceans*, edited by: Kirchman, D. L., Wiley-Liss, New York, 261–288, 2000.
- Landry, M. R., Brown, S. L., Neveux, J., Dupouy, C., Blanchot, J., Christensen, S., and Bidigare, R. R.: Phytoplankton growth and microzooplankton grazing in high-nutrient, low-chlorophyll waters of the equatorial Pacific: Community and taxon-specific rate assessments from pigment and flow cytometric analyses, *J. Geophys. Res.*, 108, 8142–8156, 2003.
- Le Quéré, C., Harrison, S. P., Prentice, I. C., Buitenhuis, E. T., Aumont, O., Bopp, L., Claustre, H., Cunha, L. C. D., Geider, R., Giraud, X., Klaas, C., Kohfeld, K. E., Legendre, L., Manizza, M., Platt, T., Rivkin, R. B., Sathyendranath, S., Uitz, J., Watson, A. J., and Wolf-Gladrow, D.: Ecosystem dynamics based on plankton functional types for global ocean biogeochemistry models, *Global Change Biol.*, 11, 2016–2040, 2005.
- Li, W. K. W., Zohary, T., Yacobi, Y. Z., and Wood, A. M.: Ultraphytoplankton in the eastern Mediterranean Sea: Towards deriving phytoplankton biomass from flow cytometric measurements of abundance fluorescence and light scatter, *Mar. Ecol. Prog. Ser.*, 102, 79–87, 1993.
- Li, W. K. W.: Primary production of prochlorophytes, cyanobacteria, and eucaryotic ultraphytoplankton: Measurements from flow cytometric sorting, *Limnol. Oceanogr.*, 39, 169–175, 1994.
- Li, W. K. W.: Composition of ultraphytoplankton in the Central North Atlantic, *Mar. Ecol. Prog. Ser.*, 122, 1–8, 1995.
- Li, W. K. W.: *Plankton Populations and Communities*, in: *Marine Macroecology*, edited by: Witman, J. and Kaustuv, R., University of Chicago Press, in press, 2007.
- Loisel, H. and Morel, A.: Light scattering and chlorophyll concentration in case 1 waters: A reexamination, *Limnol. Oceanogr.*, 43, 847–858, 1998.
- Mackey, D. J., Blanchot, J., Higgins, H. W., and Neveux, J.: Phytoplankton abundances and community structure in the equatorial Pacific, *Deep Sea Res. II*, 49, 2561–2582, 2002.

- Marie, D., Partensky, F., Simon, N., Guillou, L., and Vault, D.: Flow cytometry analysis of marine picoplankton, in: *Living Colors: Protocols in Flow Cytometry and Cell sorting*, edited by: Diamond, R. A. and DeMaggio, S., p. 421–454, 2000.
- Moon van der Staay, S. Y., Wachter, R. D., and Vault, D.: Oceanic 18S rDNA sequences from picoplankton reveal unsuspected eukaryotic diversity, *Nature*, 409, 607–610, 2001.
- Moore, L. R., Post, A. F., Rocap, G., and Chisholm, S. W.: Utilization of different nitrogen sources by the marine cyanobacteria *Prochlorococcus* and *Synechococcus*, *Limnol. Oceanogr.*, 47, 989–996, 2002.
- Morel, A. and Ahn, Y.-H.: Optics of heterotrophic nanoflagellates and ciliates: A tentative assessment of their scattering role in oceanic waters compared to those of bacterial and algal cells, *J. Mar. Res.*, 49, 177–202, 1991.
- Morel, A., Ahn, Y.-W., Partensky, F., Vault, D., and Claustre, H.: *Prochlorococcus* and *Synechococcus*: a comparative study of their size, pigmentation and related optical properties, *J. Mar. Res.*, 51, 617–649, 1993.
- Morel, A., Gentili, B., Claustre, H., Babin, M., Bricaud, A., Ras, J., and Tièche, F.: Optical properties of the "clearest" natural waters, *Limnol. Oceanogr.*, 52, 217–229, 2007.
- Moutin, T., Karl, D. M., Duhamel, S., Rimmelin, P., Raimbault, P., Van Mooy, B. A. S., and Claustre, H.: Phosphate availability and the ultimate control of new nitrogen input by nitrogen fixation in the tropical Pacific Ocean, *Biogeosciences Discuss.*, 4, 2407–2440, 2007, <http://www.biogeosciences-discuss.net/4/2407/2007/>.
- Not, F., Valentin, K., Romari, K., Lovejoy, C., Massana, R., Töbe, K., Vault, D., and Medlin, L. K.: Picobiliphytes: A Marine Picoplanktonic Algal Group with Unknown Affinities to Other Eukaryotes, *Science*, 315, 253–255, 2007.
- Oubelkheir, K., Claustre, H., and Babin, A. S.: Bio-optical and biogeochemical properties of different trophic regimes in oceanic waters, *Limnol. Oceanogr.*, 50, 1795–1809, 2005.
- Preisendorfer, R. W.: Application of radiative transfer theory to light measurements in the sea, *Monogr.*, 10, 11–30, Int Union Geod Geophys, Paris, 1961.
- Raimbault, P., Garcia, N., and Cerutti, F.: Distribution of inorganic and organic nutrients in the South Pacific Ocean – evidence for long-term accumulation of organic matter in nitrogen-depleted waters, *Biogeosciences Discuss.*, 4, 3041–3087, 2007, <http://www.biogeosciences-discuss.net/4/3041/2007/>.
- Ras, J., Claustre, H., and Uitz, J.: Spatial variability of phytoplankton pigment distributions in the Subtropical South Pacific Ocean: comparison between in situ and predicted data, *Biogeosciences Discuss.*, 4, 3409–3451, 2007, <http://www.biogeosciences-discuss.net/4/3409/2007/>.
- Raven, J. A., Finkel, Z. V., and Irwin, A. J.: Picophytoplankton: bottom-up and top-down controls on ecology and evolution, *Vie Milieu*, 55, 209–215, 2005.
- Richardson, T. L. and Jackson, G. A.: Small Phytoplankton and Carbon Export from the Surface Ocean, *Science*, 315, 838–840, 2007.
- Shalapyonok, A., Olson, R. J., and Shalapyonok, L. S.: Arabian Sea phytoplankton during Southwest and Northeast Monsoons 1995: composition, size structure and biomass from individual cell properties measured by flow cytometry, *Deep-Sea Res. Part II*, 48, 1231–1261, 2001.
- Sherr, E. B., Sherr, B. F., and Wheeler, P. A.: Distribution of coccoid cyanobacteria and small eukaryotic phytoplankton in the upwelling ecosystem off the Oregon coast during 2001 and 2002, *Deep Sea Res. II*, 52, 317–330, 2005.
- Sokal, R. R. and Rohlf, F. J.: *Biometry the principles and practice of statistics in biological research*, W. H. Freeman and Company, New York, 1994.
- Stramski, D., Shalapyonok, A., and Reynolds, R.: Optical characterization of the oceanic unicellular cyanobacterium *Synechococcus* grown under a day-night cycle in natural irradiance, *J. Geophys. Res.*, 100, 13 295–13 307, 1995.
- Stramski, D., Reynolds, R. A., Babin, M., Kaczmarek, S., Lewis, M. R., Röttgers, R., Sciandra, A., Stramska, M., Twardowski, M. S., and Claustre, H.: Relationships between the surface concentration of particulate organic carbon and optical properties in the eastern South Pacific and eastern Atlantic Oceans, *Biogeosciences Discuss.*, 4, 3453–3530, 2007, <http://www.biogeosciences-discuss.net/4/3453/2007/>.
- Ulloa, O., Sathyendranath, S., Platt, T., and Quiñones, R. A.: Light scattering by marine heterotrophic bacteria, *J. Geophys. Res.*, 97, 9619–9629, 1992.
- Van de Hulst, H. C.: *Light scattering by small particles*, Wiley, New York, 1957.
- Vault, D.: CYTOPC: Processing software for flow cytometric data, *Signal and Noise*, 2, 8, 1989.
- Vault, D. and Marie, D.: Diel variability of photosynthetic picoplankton in the equatorial Pacific, *J. Geophys. Res.*, 104(C2), 3297–3310, 1999.
- Veldhuis, M. J. W. and Kraay, G. W.: Phytoplankton in the subtropical Atlantic Ocean: towards a better assessment of biomass and composition, *Deep Sea Res. I*, 51, 507–530, 2004.
- Veldhuis, M. J. W., Timmermans, K. R., Croot, P., and Wagt, B. V. D.: Picophytoplankton; a comparative study of their biochemical composition and photosynthetic properties, *J. Sea Res.*, 53, 7–24, 2005.
- Waterbury, J. B., Watson, S. W., Guillard, R. R. L., and Brand, L. E.: Widespread occurrence of a unicellular, marine planktonic, cyanobacterium, *Nature*, 277, 293–294, 1979.
- Worden, A. Z., Nolan, J. K., and Palenik, B.: Assessing the dynamics and ecology of marine picophytoplankton: The importance of the eukaryotic component, *Limnol. Oceanogr.*, 49, 168–179, 2004.
- Zubkov, M. V., Sleight, M. A., Burkill, P. H., and Leakey, R. J. G.: Picoplankton community structure on the Atlantic Meridional Transect: a comparison between seasons, *Prog. Oceanogr.*, 45, 369–386, 2000.

Distribution of micro-organisms along a transect in the South-East Pacific Ocean (BIOSOPE cruise) using epifluorescence microscopy

S. Masquelier and D. Vaultot

Station Biologique de Roscoff, UMR 7144, CNRS et Université Pierre et Marie Curie, Place G. Tessier, 29682, Roscoff, France

Received: 6 July 2007 – Published in Biogeosciences Discuss.: 7 August 2007

Revised: 18 January 2008 – Accepted: 1 February 2008 – Published: 4 March 2008

Abstract. The distribution of selected groups of micro-organisms was analyzed along a South-East Pacific Ocean transect sampled during the BIOSOPE cruise in 2004. The transect could be divided into four regions of contrasted trophic status: a High Nutrient Low Chlorophyll (HNLC) region (mesotrophic) near the equator, the South-East Pacific Ocean gyre (hyper-oligotrophic), a transition region between the gyre and the coast of South America (moderately oligotrophic), and the Chile upwelling (eutrophic). The abundance of phycoerythrin containing picocyanobacteria (PE picocyanobacteria), autotrophic and heterotrophic eukaryotes (classified into different size ranges), dinoflagellates, and ciliates was determined by epifluorescence microscopy after DAPI staining. Despite some apparent loss of cells due to sample storage, distribution patterns were broadly similar to those obtained by flow cytometry for PE picocyanobacteria and picoeukaryotes. All populations reached a maximum in the Chile upwelling and a minimum near the centre of the gyre. The maximum abundance of PE picocyanobacteria was $70 \times 10^3 \text{ cell mL}^{-1}$. Abundance of autotrophic eukaryotes and dinoflagellates reached 24.5×10^3 and 20 cell mL^{-1} , respectively. We observed a shift in the size distribution of autotrophic eukaryotes from $2\text{--}5 \mu\text{m}$ in eutrophic and mesotrophic regions to less than $2 \mu\text{m}$ in the central region. The contribution of autotrophic eukaryotes to total eukaryotes was the lowest in the central gyre. Maximum concentration of ciliates (18 cell mL^{-1}) also occurred in the Chile upwelling, but, in contrast to the other groups, their abundance was very low in the HNLC zone and near the Marquesas Islands. Two key findings of this work that could not have been observed with other techniques are the high percentage of PE picocyanobacteria forming colonies in the HNLC region and the observation of numerous dinoflagellates with bright green autofluorescence.

1 Introduction

Unicellular picoplanktonic prokaryotes and eukaryotes less than $2 \mu\text{m}$ in size (Sieburth et al., 1978) are found in marine ecosystems at concentrations ranging from 10^2 to 10^5 and 10^2 to $10^4 \text{ cell mL}^{-1}$, respectively. They play a fundamental role (Azam et al., 1983; Sherr and Sherr, 2000), in particular, in oligotrophic waters (Hagström et al., 1988; Marañón et al., 2001) where their small size associated to the reduced diffusion boundary layer and large surface area per unit volume are an advantage to acquire nutrients (Raven, 1998). The photosynthetic component of picoplankton, i.e. *Prochlorococcus* and *Synechococcus* cyanobacteria and picoeukaryotic algae, are important contributors to the microbial community of the euphotic zone in many marine environments (Mackey et al., 2002; Pérez et al., 2006). Heterotrophic protists play a pivotal role in mediating organic flux to higher trophic levels in pelagic ecosystems (Azam et al., 1983; Fenchel, 1982; Hagström et al., 1988). Among the heterotrophic protists, ciliates and dinoflagellates are important grazers of picoplankton (Christaki et al., 2002).

In the Pacific Ocean, picoplankton has been analyzed both in the Equatorial region and the North gyre (e.g. Campbell et al., 1997; Mackey et al., 2002) but not in the South gyre. The latter is the most oligotrophic environment of the world oceans based on SeaWiFS imagery which provides estimates of average surface chlorophyll *a* concentrations down to 0.02 mg m^{-3} (Morel et al., 2007). The BIOSOPE (Biogeochemistry and Optics South Pacific Experiment) cruise explored this region sailing from the Marquesas Islands to the coast of Chile. Along this transect, a gradient in trophic conditions was encountered, from hyper-oligotrophic (gyre) to very eutrophic waters (Chile upwelling). The present study relied on epifluorescence microscopy to assess the distribution in this region of phycoerythrin containing picocyanobacteria (called PE picocyanobacteria throughout the paper), autotrophic and heterotrophic eukaryotes (in particular dinoflagellates and ciliates). In contrast to faster



Correspondence to: D. Vaultot
(vaultot@sb-roscoff.fr)

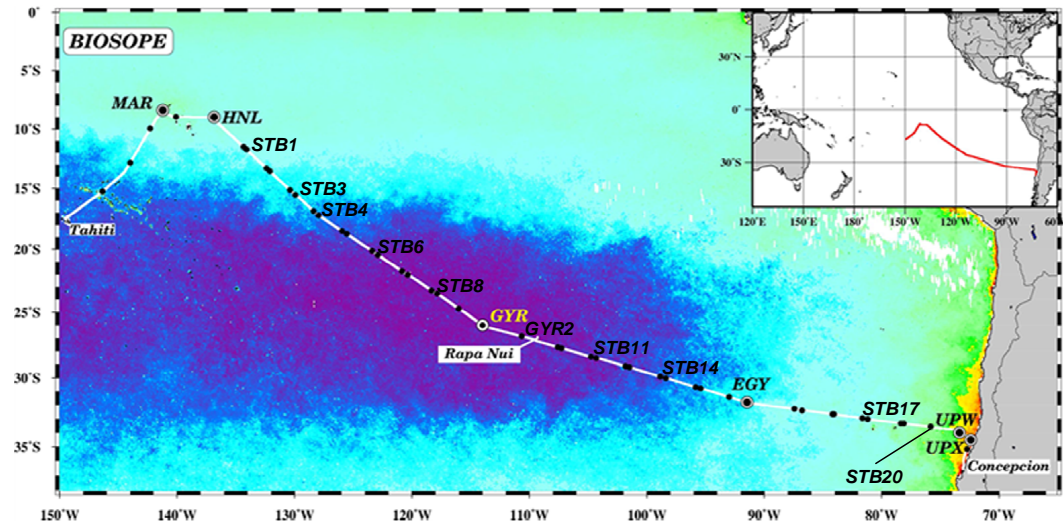


Fig. 1. Map of the BIOSOPE cruise track superimposed on a SeaWiFS ocean colour composite, dark purple indicating extremely low values (0.018 mg m^{-3}) of total chlorophyll *a*. Figure modified from Claustre et al. (2007). Stations analyzed by DAPI staining are labelled.

Table 1. Concentrations of the different populations enumerated in the present study. Values are averages for the six depths sampled at each station.

Station	Latitude-Longitude	Picocyanobacteria containing phycoerythrin mL^{-1}	Total eukaryotes mL^{-1}	Autotrophic eukaryotes mL^{-1}	Heterotrophic eukaryotes mL^{-1}	Total dinoflagellates mL^{-1}	Autotrophic dinoflagellates mL^{-1}	Heterotrophic dinoflagellates mL^{-1}	Green dinoflagellates mL^{-1}	Total ciliates mL^{-1}
MAR1	08°23 S–141°14 W	3486	1520	1292	228	105	56	48	4.6	<1.5
HLN1	09°00 S–136°51 W	2818	2312	1836	476	93	61	32	4.2	3
STB1	11°44 S–134°06 W	1612	1895	1165	730	111	62	50	4.5	1.5
STB3	15°00 S–129°55 W	413	1423	737	686	59	28	31	4.2	3.5
STB4	17°13 S–127°58 W	374	1267	736	531	57	26	32	7.0	1.5
STB6	20°26 S–122°54 W	6	1413	726	687	37	19	17	2.2	1.5
STB8	23°32 S–117°52 W	37	937	521	416	31	12	19	3.5	4.5
GYR2	25°58 S–114°00 W	46	806	541	265	43	21	22	3.5	1.5
STB11	27°45 S–107°16 W	34	1050	526	525	31	10	21	6.5	<1.5
STB14	30°02 S–98°23 W	142	1314	854	460	55	22	33	8.5	4.2
EGY2	31°50 S–91°27 W	1734	3083	2481	602	82	47	35	6.5	1.9
STB17	32°23 S–86°47 W	1104	2607	2086	521	94	46	48	12	5.2
STB20	33°21 S–78°06 W	10 726	1760	1195	566	92	44	48	6.7	3
UPW1	34°01 S–73°21 W	40 548	3396	2526	870	122	63	59	15	10
UPX2	34°37 S–72°27 W	18 548	14 088	12 211	1877	151	47	104	38	6.6

enumeration techniques such as flow cytometry, epifluorescence microscopy allows (1) to discriminate specific group of organisms such as dinoflagellates, (2) to recognize cell organization such as colonies, and (3) to regroup organisms into size classes. We attempted to relate the distribution of the different types of organisms to oceanographic conditions.

2 Material and methods

2.1 Oceanographic context

The BIOSOPE cruise took place on board the French NO “I’Atalante” in the South-East Pacific Ocean from 26th October to 11th December 2004 (Fig. 1). The transect inves-

tigated extended from the Marquesas Islands (South Pacific Tropical Waters; SPTW) to the coast of Chile, through the Eastern South Pacific Central Waters (ESPCW) which include the centre of the Pacific gyre (Claustre et al., 2008). The transect can be divided into four contrasted trophic zones (from West to East): a High Nutrient Low Chlorophyll (HNLC) zone (mesotrophic) near the equator, the South-East Pacific gyre (hyper-oligotrophic) proper, the transition zone between the gyre and the coastal region (moderately oligotrophic), and the Chile upwelling (very eutrophic). In the hyper oligotrophic zone, nitrate concentrations were nearly undetectable between the surface and 150–200 m and remained very low ($\sim 2.5 \mu\text{M}$) below this depth (Fig. 2 in Raimbault et al., 2007). Nitrate concentrations were higher in the HNLC zone and maximum in the Chile upwelling

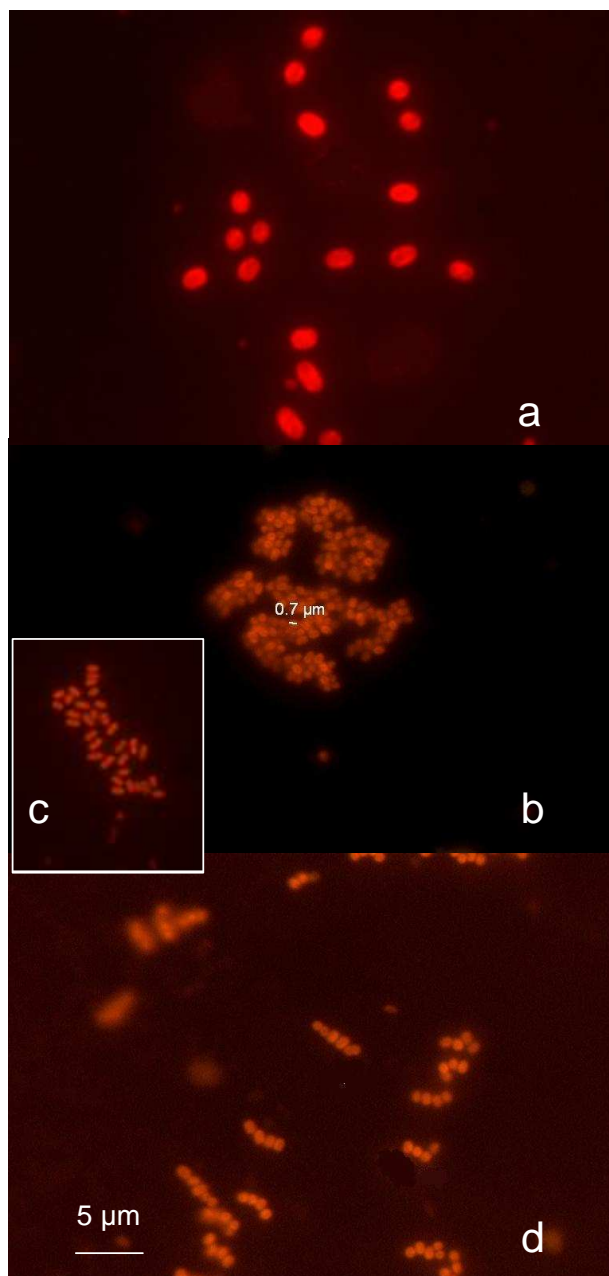


Fig. 2. Pictures of single (a), and colonial PE picocyanobacteria (b–d). Colony of more than 100 cells (b). Colony of 20–30 cells (c). Chain forming cells (d). Pictures taken under green light excitation on samples of stations MAR1 at 80 m (a), MAR1 at 40 m (b), HNL1 at 60 m (c), and STB3 at 60 m (d).

(Fig. 2 in Raimbault et al., 2007). Phosphate was apparently never a limiting factor (Fig. 2 in Raimbault et al., 2007).

2.2 DAPI staining and epifluorescence microscopy

Fifteen stations (Fig. 1 and Table 1) were sampled at six depths with a conductivity-temperature-depth (CTD) rosette

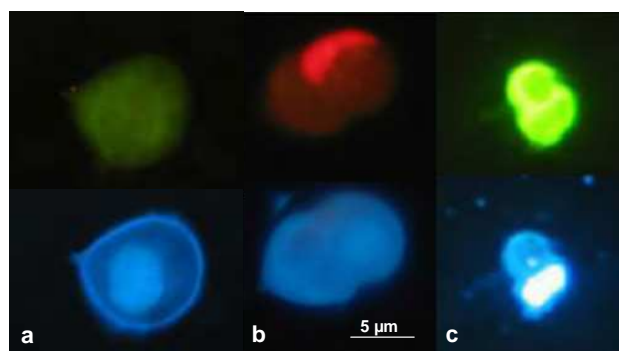


Fig. 3. Heterotrophic (a), autotrophic (b), and green fluorescing dinoflagellates (c) observed under blue light excitation (top) and UV light excitation (bottom). Pictures taken at stations STB3 (20 m), UPW and STB7 (5 m), respectively.

system equipped with 12 L Niskin bottles. In general, two samples were collected in the surface layer, three around the chlorophyll maximum and one below. Water was pre-filtered through a 200 μm mesh to remove zooplankton, large phytoplankton, and particles before further filtrations.

Water samples (100 mL) were fixed with glutaraldehyde (0.25% final concentration) and filtered through 0.8 μm pore size filters. This porosity was selected to avoid high densities of bacteria on the filter which would have rendered visualisation of the larger and less dense eukaryotes more difficult. Samples were stained with 4'6-diamidino-2-phenylindole (DAPI, 5 $\mu\text{g mL}^{-1}$ final concentration) (Porter and Feig, 1980) and stored at -20°C for a minimum of 12 months before counting. Counts were performed with an Olympus BX51 epifluorescence microscope (Olympus Optical CO, Tokyo, Japan) equipped with a mercury light source and an x100 UVFL objective. Pictures of dinoflagellates were taken on board the ship on the freshly prepared slides using a BH2 Olympus microscope with an x40 objective and a Canon G5 digital camera. Pictures of PE containing picocyanobacteria were taken in the laboratory on the BX51 Olympus microscope with a Spot RT-slider camera (Diagnostics Instruments, Sterling Heights, MI).

Prochlorococcus cannot be counted reliably by epifluorescence microscopy because of their small size and rapidly fading fluorescence. Therefore, only isolated and colonial PE picocyanobacteria (Fig. 2) were counted based on the orange fluorescence of phycoerythrin excited under green light (530–550 nm). DAPI staining allowed us to discriminate eukaryotic from prokaryotic organisms. Under UV light (360/420 nm), eukaryotic cell nucleus appeared as a separate blue organelle, while for prokaryotes, no nucleus was visible and cells appeared uniformly stained. The red fluorescence of chlorophyll under blue light (490/515 nm) allowed us to discriminate autotrophic (photosynthetic) from heterotrophic eukaryotes. However, it was not possible to distinguish truly autotrophic organisms from organisms that had ingested

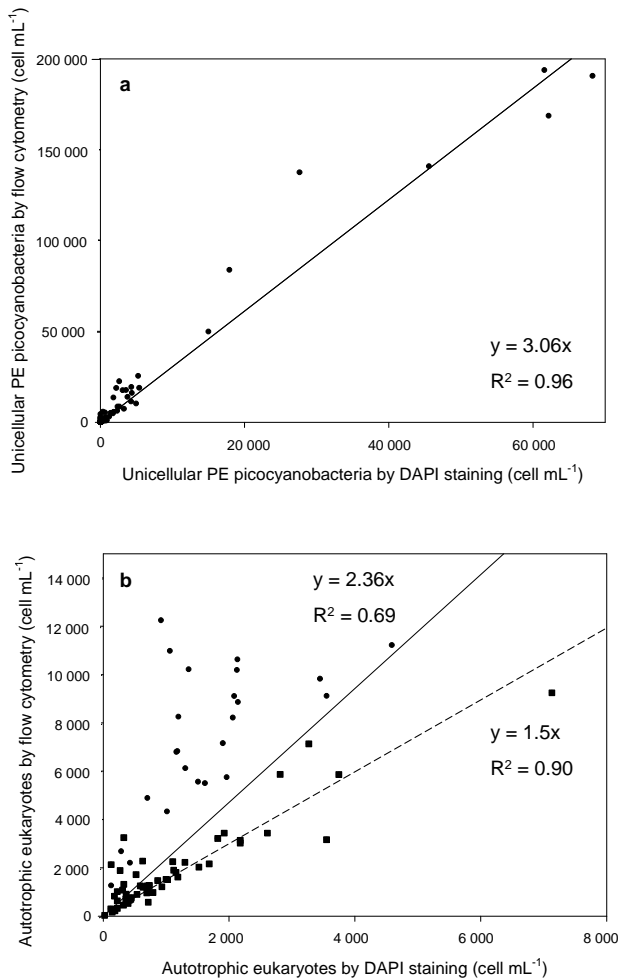


Fig. 4. Relationship between abundance (cell mL^{-1}) measured by flow cytometry (Grob et al., 2007) and estimated by DAPI counting for unicellular PE picocyanobacteria (a), and autotrophic eukaryotes (b). In panel (b) circles correspond to data from surface to 40–60 m depth depending on samples. Squares correspond to data from 40–60 m depth to 300 m depth. (a) $R^2=0.96$, $n=80$; (b) Solid line takes into account all data (circles and squares); $R^2=0.69$, $n=80$. Dashed line takes into account only squares; $R^2=0.90$, $n=56$.

chlorophyll-containing cells. Ten fields and a minimum of 100 cells were counted per slide. Eukaryotes were classified according to three diameter ranges: (i) smaller than $2 \mu\text{m}$, (ii) between $2 \mu\text{m}$ and $5 \mu\text{m}$, (iii) larger than $5 \mu\text{m}$. Among eukaryotes larger than $5 \mu\text{m}$, ciliates and dinoflagellates were counted separately. Dinoflagellates were discriminated by their shape, their size (between $5 \mu\text{m}$ and $100 \mu\text{m}$), and the presence of a nucleus with condensed chromatin. Autotrophic and heterotrophic dinoflagellates were discriminated according to the red fluorescence of chlorophyll under blue light of the former (Figs. 3a and b). Among heterotrophic dinoflagellates, some were characterized by an intense green fluorescence under blue light (Fig. 3c), as reported previously (Shapiro et al., 1989), and counted sepa-

rately. Ciliates were discriminated by their shape, their size (between $20 \mu\text{m}$ and $100 \mu\text{m}$), and the presence of cilia and multiple nuclei. No distinction between different types of ciliates was attempted. Because of their low abundance, 50 fields per slide were counted for dinoflagellates and ciliates such that the minimum concentration detectable was 1.5 cell mL^{-1} .

2.3 Data representation

Contour maps showing the distributions of the different populations were drawn using the Ocean Data View software (Schlitzer, 2003) with averaging VG gridding length-scales of 100 for both X and Y.

3 Results

3.1 Comparison between microscopy and flow cytometry

In order to validate our microscopy counts, we compared them to counts of *Synechococcus* cyanobacteria and photosynthetic eukaryotes done by flow cytometry (Grob et al., 2007) at the same stations (Fig. 4). There was a relatively good correlation between the two methods, such that global distribution trends were identical. However, slopes were significantly larger than one indicating that microscopy was underestimating the actual concentrations. For PE picocyanobacteria ($R^2=0.96$; $n=80$), abundance found by microscopy was 3 times lower than measured by flow cytometry (Fig. 4a). For photosynthetic eukaryotes, the correlation was moderate ($R^2=0.69$; $n=80$) when all the data were considered, although the slope was lower than for cyanobacteria (Fig. 4b). When only data below 40–60 m were included, the correlation was significantly better ($R^2=0.90$; $n=56$) and the slope less pronounced.

3.2 PE picocyanobacteria

In surface, abundance of PE picocyanobacteria (Fig. 5a) reached a maximum ($70 \cdot 10^3 \text{ cell mL}^{-1}$) near the coast of Chile (station UPW1) and a minimum (less than 500 cell mL^{-1}) in the middle of the South-East Pacific gyre. Their abundance increased again near the Marquesas Islands. In the vertical dimension, abundance decreased slightly down to circa 100 m and cells quickly disappeared below (Fig. 5a). Interestingly, a large fraction of the PE picocyanobacteria belonged to colonial forms in the vicinity of the Marquesas Islands and in the HNLC zone (Fig. 5b). In this region, this fraction could reach up to 50% near the surface and 5 to 10% between 25 and 100 m, while it dropped below 5% almost everywhere else. Three types of colony could be observed (Fig. 2): (i) groups of 20–30 cells, (ii) groups of more than 100 cells, (iii) short chains. None of these forms seemed to be preferentially observed in any given region.

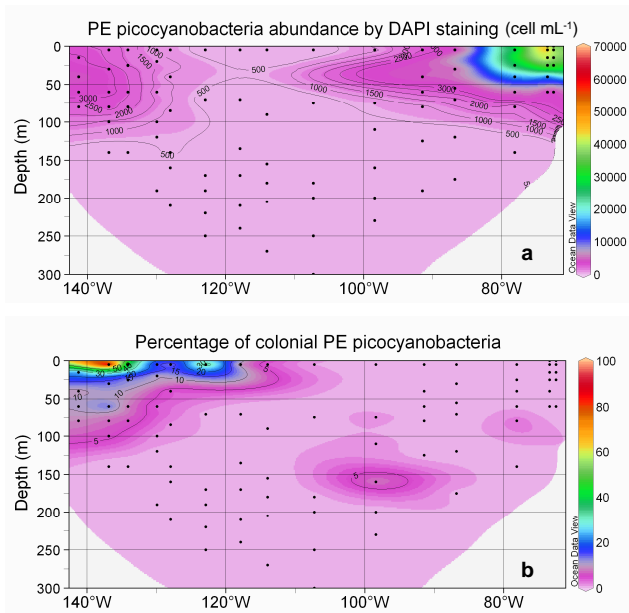


Fig. 5. Abundance obtained by DAPI counting for unicellular PE picocyanobacteria (cell mL^{-1}) (a), and percentage of unicellular PE picocyanobacteria in colony (b). Black dots correspond to samples analysed. Contour plots generated with the software Ocean Data View.

3.3 Eukaryotes

Maximum abundance of total eukaryotes ($26 \times 10^3 \text{ cell mL}^{-1}$) occurred in the Chile upwelling near the surface (station UPX2, 25 m) and minimum (276 cell mL^{-1}) in the gyre at depth (station GYR2, 270 m) (Fig. 6a). In the surface layer, abundance was minimal in the center of the gyre and increased both eastward and westward. The maxima of total eukaryotes coincided roughly with the depth of chlorophyll maximum (DCM, see Fig. 3 in Raimbault et al., 2007). Below 200 m, concentrations were always lower than $1000 \text{ cell mL}^{-1}$. The distributions of total eukaryotes and autotrophic eukaryotes were very similar with a maximum in the Chile upwelling and a minimum in the surface of the gyre (Fig. 6b). These similar distributions were a mere consequence of the fact that autotrophic eukaryotes were much more abundant than heterotrophic ones around the DCM (Fig. 6c). The size distribution of autotrophic eukaryotes varied dramatically throughout the transect (Figs. 7 and 8): in the surface of the gyre, cells smaller than $2 \mu\text{m}$ accounted for less than 10% while, they dominated (50–70%) in the DCM of the gyre as well as east of the gyre (Fig. 7a). In the Chile upwelling (station UPX2, 25 m), they accounted for up to 80% of the total eukaryotes. In contrast, their contribution was much lower in the HNLC region where larger eukaryotes between $2 \mu\text{m}$ and $5 \mu\text{m}$ accounted for 40% to 60% of the population (Fig. 7b). This size class was also dominant near the surface in the transition zone between the

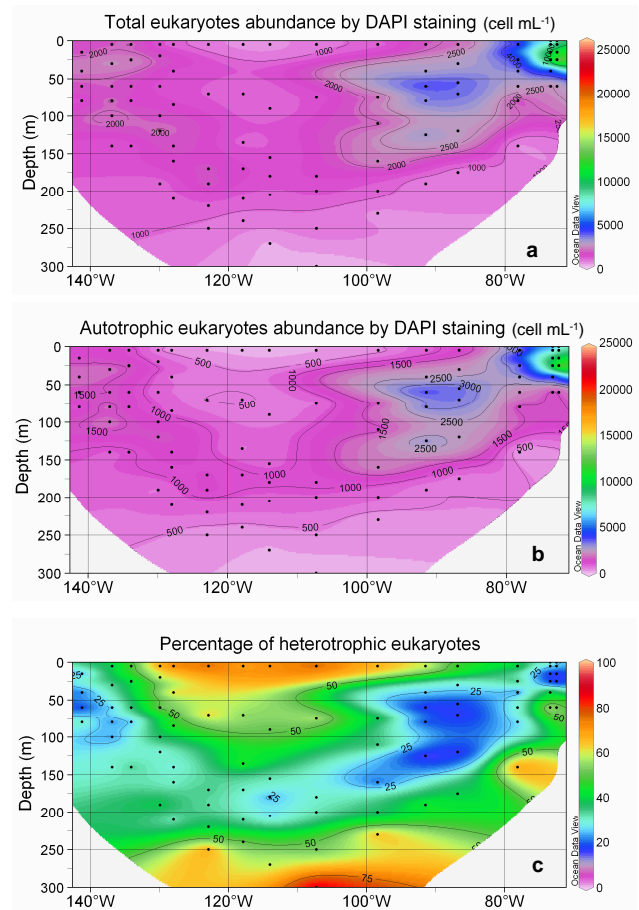


Fig. 6. Abundance obtained by DAPI counting of total eukaryotes (cell mL^{-1}) (a), autotrophic eukaryotes (cell mL^{-1}) (b), and percentage of heterotrophic eukaryotes in comparison with total eukaryotes (c). Legend as in Fig. 5.

gyre and the upwelling. Cells larger than $5 \mu\text{m}$ accounted for less than 10% of autotrophic eukaryotes everywhere along the transect, except near the Marquesas Islands where they contributed slightly more (Fig. 7c).

The relative proportion of heterotrophic eukaryotes was the highest in the 0–50 m layer of the gyre (75–80%), while in the DCM it dropped to 25% (Fig. 6c). In the DCM, cells smaller than $2 \mu\text{m}$ accounted for 28% (east of the gyre) to 40% (in the gyre) of heterotrophic eukaryotes (Fig. 8). The contribution of cells between $2 \mu\text{m}$ and $5 \mu\text{m}$ did not vary much (about 50%) while cells larger than $5 \mu\text{m}$ accounted for up to 14% of total heterotrophic eukaryotes in the HNLC region and for about 10% elsewhere.

In the 0–100 m layer, dinoflagellate abundance (Fig. 9a) increased towards the HNLC region (maximum observed: 200 cell mL^{-1} at station STB1, 25 m) and the Chile upwelling, and decreased towards the gyre (minimum observed: 10 cell mL^{-1} at station GYR2, 270 m). In relative terms, autotrophic dinoflagellates dominated around the

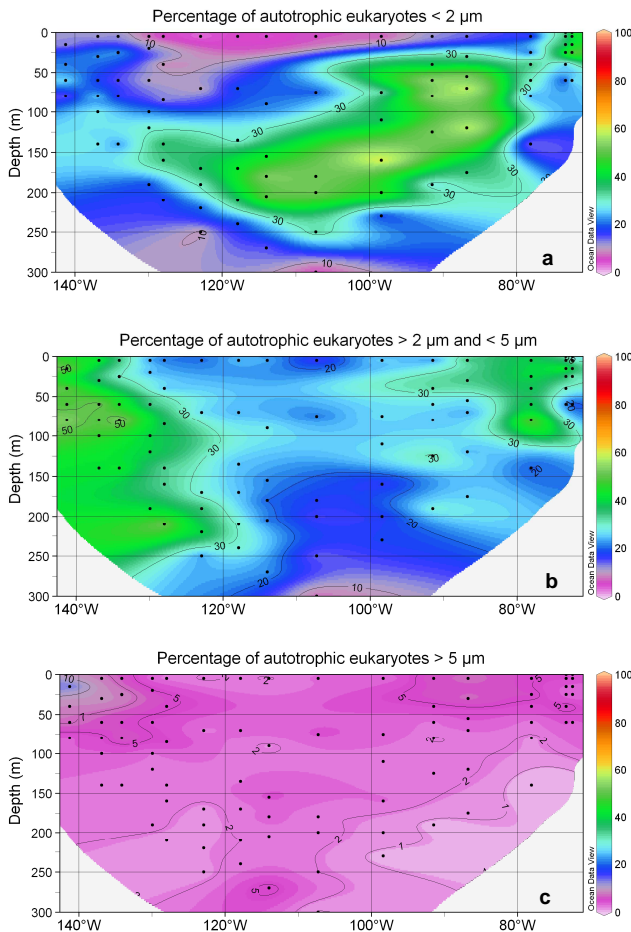


Fig. 7. Fraction of autotrophic eukaryotes smaller than $2 \mu\text{m}$ (a), between $2 \mu\text{m}$ and $5 \mu\text{m}$ (b), and larger than $5 \mu\text{m}$ (c) in comparison with the total eukaryotes. Legend as in Fig. 5.

Marquesas Islands (up to 80% of total dinoflagellates, at station STB1, 80 m depth) and in the Chile upwelling (70% at station UPW1, 15 m depth) (Fig. 9b). The maximum of percentage of autotrophic dinoflagellates (50%–80%) followed the DCM except at station STB8 where the highest percentage (50%) occurred at 70 m whereas the DCM was found much below at 170 m (Compare Fig. 9b in the present study and Fig. 3 in Raimbault et al., 2007). In the Chile upwelling, the maximum of autotrophic dinoflagellates (50% at station UPX2 in surface and 70% at station UPW1 at 15 m) occurred above the DCM. The percentage of autotrophic dinoflagellates was the lowest (5%–25%) in the surface of the gyre and below 250 m.

Heterotrophic dinoflagellates contribution ranged from 20% to 95% of the total (Fig. 9c) and consisted mostly (75% on average) of cells smaller than $15 \mu\text{m}$ in size (data not shown). Vertical profiles showed that maximum abundances of heterotrophic dinoflagellates followed the DCM only at some stations in the gyre (STB3, STB6 and STB8, Fig. 10).

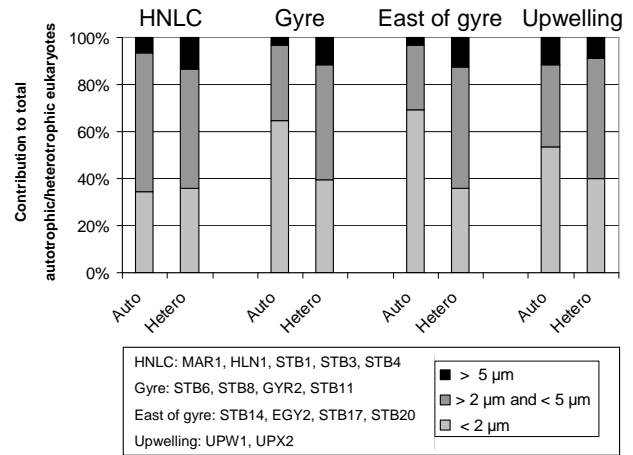


Fig. 8. Contribution of the different size classes to the abundance of autotrophic (Auto) and heterotrophic (Hetero) eukaryotes at the depth of chlorophyll maximum for the HNLC, Gyre, East of gyre and Chile upwelling regions.

At other stations, the maximum abundance of heterotrophic dinoflagellates was observed above the DCM, except in the upwelling (station UPX2) where the maximum was found below. At station EGY2 (east of gyre), the lowest concentration of heterotrophic dinoflagellates (18 cell mL^{-1}) occurred in the DCM.

Green fluorescing dinoflagellates (Fig. 3c) accounted for up to 50% of the heterotrophic dinoflagellates in surface east of the gyre and at depth in the Chile upwelling. They accounted for 5 to 25% of heterotrophic dinoflagellates in the HNLC zone and in surface in the Chile upwelling (Fig. 9d).

Ciliate abundance reached a maximum (18 cell mL^{-1}) in the Chile upwelling (station UPW1, 40 m depth) and a minimum in the HNLC region (Fig. 11). Abundance increased towards the Chile upwelling and decreased towards the gyre as for most other groups. However, in contrast to most other groups, ciliates also remained quite low towards the HNLC zone and the Marquesas Islands. Vertically, at many stations, ciliate maxima corresponded to dinoflagellate minima (Fig. 10).

4 Discussion

Differences between abundances estimated by microscopy vs. flow cytometry observed in this study could be due to several reasons. First, some cells smaller than $0.8 \mu\text{m}$ (e.g. some *Synechococcus*) could have passed through the $0.8 \mu\text{m}$ filter used here. The loss of eukaryotic cells is however likely to be negligible since the smallest known eukaryote *Ostreococcus tauri* has a size of $0.8 \mu\text{m}$ (Courties et al., 1994). Furthermore, according to Sherr et al. (2005), 16% of *Synechococcus* and only 2% of picoeukaryote cells may pass through a $1 \mu\text{m}$ filter. This may explain why the slope in the Fig. 4 is

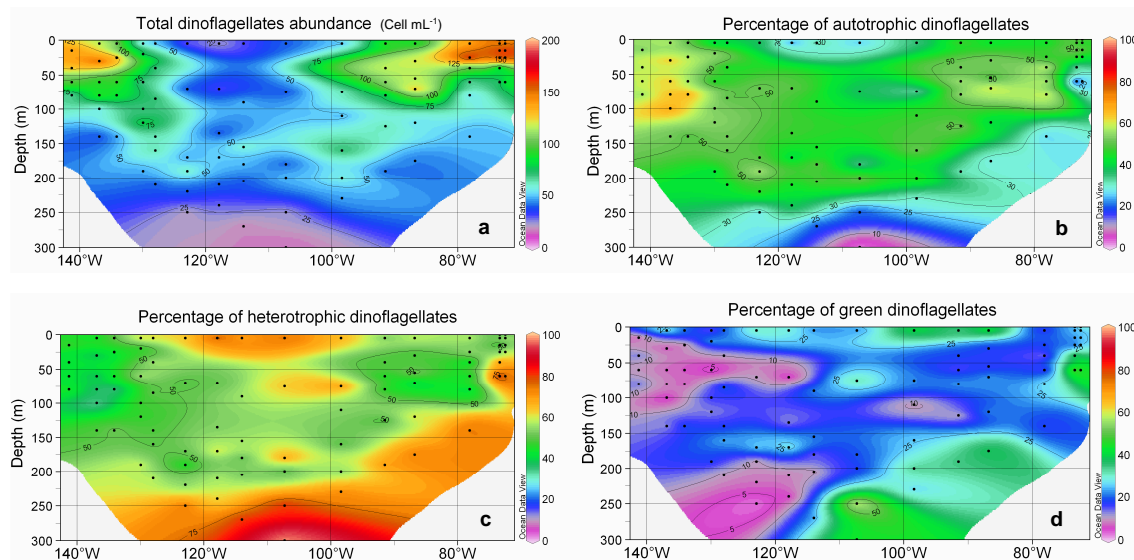


Fig. 9. Total dinoflagellates (cell mL⁻¹) (a), percentage of autotrophic dinoflagellates over total dinoflagellates (b), percentage of heterotrophic over total dinoflagellates (c), and percentage of green dinoflagellates over total heterotrophic dinoflagellates (d). Legend as in Fig. 5.

larger for PE picocyanobacteria than for eukaryotes. Second, samples for microscopy were stored for more than a year at -20°C before counting while samples for flow cytometry were analyzed fresh on board. Gundersen et al. (1996) and Putland et al. (1999) found significant losses for bacteria and for unicellular cyanobacteria after one month and three months, respectively, of sample storage at -20°C . Third, such storage conditions may cause a degradation of chlorophyll and an underestimation of red fluorescing organisms (Chavez et al., 1990). Therefore, abundances of unicellular PE picocyanobacteria and autotrophic eukaryotes may be underestimated, while the proportion of heterotrophic eukaryotes could be higher than in the initial samples. In fact, we observed that organisms from surface samples had less intense chlorophyll fluorescence than those of deeper samples (as expected due to photoacclimation). Moreover, this fluorescence faded faster. Therefore the distinction between autotrophic and heterotrophic organisms near the surface was not always easy. This could explain the lower correlation and higher slopes between flow cytometry and epifluorescence abundances for samples above 40–60 m (Fig. 4).

The low abundance of PE picocyanobacteria in the gyre and their higher abundance in the Chile upwelling, a region rich in nutrients and characterized by mixed waters, is in agreement with many studies (for a review see Partensky et al., 1999). Interestingly, up to 50% of the PE picocyanobacteria counted by microscopy appeared to be colonial near the Marquesas Islands and in the HNLC region (Figs. 2 and 5b). Comparison with flow cytometry data showed that at least 33% of the PE picocyanobacteria were retained by the $0.8\ \mu\text{m}$ filter, assuming that no cells were lost because of sam-

ple fixation and conservation (Fig. 4). Therefore, colonial PE picocyanobacteria would represent at least 15% (i.e. 33% of 50%) of all PE picocyanobacteria.

The high proportion of colonial PE picocyanobacteria near the Marquesas Islands and in the HNLC region could be due to a preference of colony-forming cyanobacteria for high nutrient waters (Paerl, 2000). However, the fact that we observed only 1% of colonial PE picocyanobacteria in the Chile upwelling seems to indicate that other factors have to be taken into account. Some cyanobacteria encountered in marine systems form colonies (Graham and Wilcox, 2000) but these are usually much larger than those we observed. It is, for example, the case for *Trichodesmium* that has been previously observed in the Equatorial Pacific (Capone et al., 1997). Interestingly, unicellular PE picocyanobacteria forming chains (cf. Fig. 2d) were isolated in culture from the HNLC station at 30 m and 100 m depth (Le Gall et al., 2008) but the other morphotypes observed in the field were not obtained. Since there was some evidence of nitrogen fixation activity in this area (Raimbault and Garcia, 2007), it is tempting to hypothesize that these colonial PE picocyanobacteria could be nitrogen-fixing. However, Raimbault and Garcia (2007) showed that important nitrogen fixation was also observed in the center of the gyre and in the Chile upwelling where very few colonies were observed. Furthermore, small cyanobacteria having the capacity to fix nitrogen do not seem to form colonies (Zehr et al., 2001). Their morphotype (spherical 3–10 μm cells) has been rarely observed in our samples (data not shown). Alternatively, colony formation could be an adaptation to the structure of the predator community in this region, such as the higher dinoflagellates

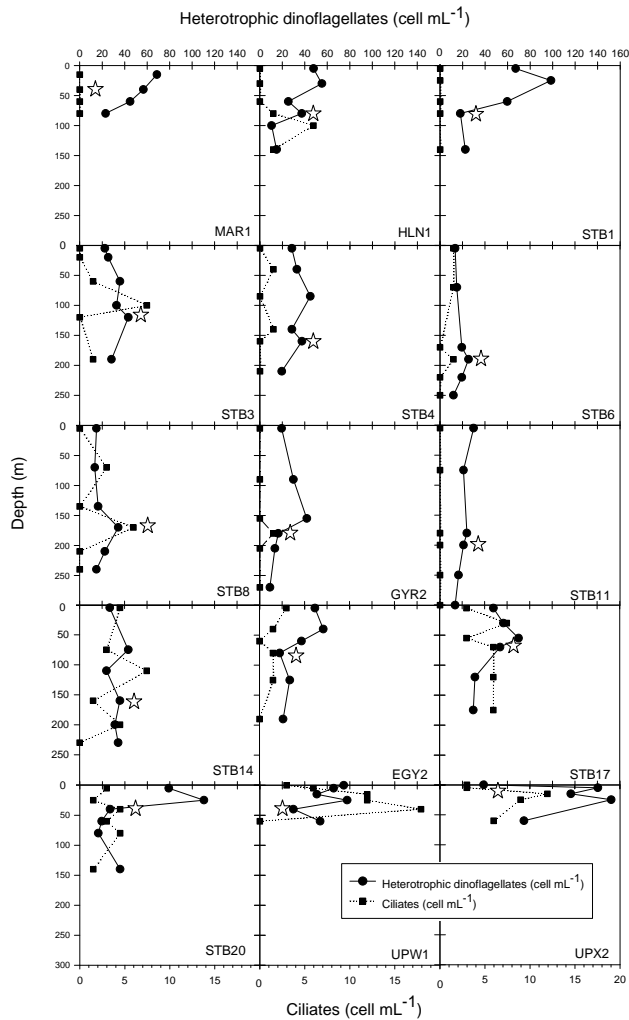


Fig. 10. Vertical profiles of concentration (cell mL^{-1}) of total heterotrophic dinoflagellates (solid line) and ciliates (dotted line). Stars indicate the depth of chlorophyll maximum.

to ciliates ratio. Indeed, cells forming colonies could take advantage of the positive aspects of increased size, in particular lower grazing pressure, without paying the full cost of decreased metabolism and reduced growth which is associated with large individual cell size (Nielsen, 2006). In the light of our observations, it could be interesting to extend counts of colonial picocyanobacteria to other oceanic regions in order to better understand how this fraction varies with oceanographic conditions.

The present study is consistent with estimates by Ras et al. (2007) based on HPLC pigment data and assumptions concerning the size range of different taxonomic groups (Claustre, 1994; Vidussi et al., 2001). They found that the contribution of picophytoplankton (in terms of percentage of total chlorophyll *a*) was the highest in the gyre itself and east of gyre, while nanophytoplankton dominated in the HNLC zone and the Chile upwelling. However, their method tends to underestimate the contribution of picophytoplank-

ton and to overestimate the contribution of macrophytoplankton. For example, they only took into account for the picoplankton size group pigments characterizing cyanobacteria and Chlorophyta. However, Prymnesiophyceae may also contribute significantly to picoeukaryotic population (Moon-Van Der Staay et al., 2001; Not et al., 2005). Indeed, Prymnesiophyceae cells characterized by two chloroplasts were observed in our DAPI samples (data not shown). Conversely, Ras et al. (2007) include pigments of dinoflagellates and diatoms in the microplankton size range (20–200 μm), while many dinoflagellates and some diatoms smaller than 20 μm (data not shown) have been detected along the South-East Pacific transect, as observed previously along 110° W (Hardy et al., 1996). Therefore, the contribution of microphytoplankton could be overestimated.

During the BIOSOPE cruise, Gómez et al. (2007) found dinoflagellate abundance always lower than 1 cell mL^{-1} , except at station 20 where a bloom of dinoflagellates was observed ($\sim 4 \text{ cell mL}^{-1}$ between surface and 5 m depth), and at station UPW ($\sim 2 \text{ cell mL}^{-1}$). These counts from acidified lugol's fixed samples are much lower than ours (Table 1). These differences could originate from differences in the size of the dinoflagellates that were counted in these two studies. We counted dinoflagellates which were between 5 μm and 50 μm in diameter while Gómez et al. (2007) only counted dinoflagellates larger than 15 μm . Hardy et al. (1996) showed that dinoflagellates larger than 20 μm accounted only for 10 to 30% of total dinoflagellates in the Pacific gyre. In our samples (data not shown), the contribution of dinoflagellates larger than 15 μm to total dinoflagellates in terms of abundances was below 1% near the Marquesas Islands, 1% in the upwelling zone, 2% in the HNLC zone and around the station EGY, and reached a maximum of 3% at station ST20 where a bloom was observed by Gómez et al. (2007).

Globally, the abundance of dinoflagellates (Fig. 9) decreased towards the hyper-oligotrophic zone and increased towards the mesotrophic and eutrophic zones. This is in agreement with Leterme et al. (2006) who showed that the dinoflagellate abundances increased with trophic status in the NE Atlantic Ocean. The observed increase in heterotrophic dinoflagellates contribution with depth is coherent with previous observations in the Equatorial Pacific (Chavez et al., 1990). Heterotrophic dinoflagellates were always much more abundant than ciliates as shown previously in the Sargasso Sea (Lessard and Murrell, 1996) and the North-East Equatorial Pacific (Yang et al., 2004). Although it is generally admitted that heterotrophic nanoflagellates are the major grazers of picoplankton (Mackey et al., 2002; Sato et al., 2007), predation by heterotrophic dinoflagellates could also be important (Sanders et al., 2000; Sherr et al., 1991).

Green fluorescing dinoflagellates were initially observed by Shapiro et al. (1989) in the North-West Atlantic, but little reported since then. Recently, Tang and Dobbs (2007) showed that green autofluorescence is a common feature

of dinoflagellates, diatoms, green algae, cyanobacteria and raphidophytes. They observed that this green autofluorescence is stronger in fixed cells, not stable over time, and that its intensity varies with organisms (the strongest signal is observed for dinoflagellates). Shapiro et al. (1989) found that green fluorescing dinoflagellates could contribute from 4 to 100% to heterotrophic dinoflagellates while Chavez et al. (1990) found that in the Equatorial Pacific, 32% of heterotrophic dinoflagellates on average produced bright green fluorescence. The data reported here (maximal concentrations in excess of 60 cell mL^{-1} and maximum contribution up to 50 %, Fig. 9) are in agreement with these previous studies. The origin of this bright green fluorescence (Fig. 3c) still remains intriguing. Shapiro et al. (1989) hypothesized that it could be due to a flavoprotein. The isolation by Fujita et al. (2005) of a flavoprotein from the green-fluorescing flagellum of the brown alga *Scytosiphon lomentaria* lends support to this hypothesis. Kim et al. (2004) showed that the infection of the thecate dinoflagellate *Gonyaulax spinifera* by *Amoebophrya*, a parasitic dinoflagellate, induces a bright green autofluorescence in infected cells. This fluorescence is, however, much more localised than in the green dinoflagellates observed in our samples (Fig. 3c). Another attractive possibility could be the presence of a cytoplasmic green fluorescing protein (GFP, Wilson and Hastings, 1998).

Ciliate abundances reported here (Table 1) are comparable to those reported from other similar marine systems ranging from oligotrophic to eutrophic (Beers et al., 1980; Leakey et al., 1996; Lessard and Murrell, 1996; Yang et al., 2004). Focusing only on tintinnid ciliates, Dolan et al. (2007) observed during the BIOSOPE cruise much lower concentrations ranging from 0.002 and $0.04 \text{ cell mL}^{-1}$ between 5 and 300 m. However, tintinnids generally account only for 5–10% of all ciliates (Dolan and Marrasé, 1995). Comparing our data with values from Table 2 of Dolan et al. (2007) results in a proportion of tintinnids (0.05%) smaller, for example, than in the Catalan Sea (Dolan and Marrasé, 1995). However, maxima and minima of tintinnid and total ciliates occurred simultaneously, in the upwelling and in the gyre, respectively.

The distribution pattern of ciliates (Fig. 11) agrees with previous observations in the North Western Indian Ocean (Leakey et al., 1996) where the lowest abundances were observed in oligotrophic waters and the highest in the most productive waters. The different patterns of vertical distribution of ciliates observed in the present study could be explained by the fact that no distinction has been made between the different types of ciliates (mixotrophic and heterotrophic ciliates). In the Catalan Sea, the distribution of heterotrophic ciliate is closely related to the DCM while mixotrophic ciliates display a more complicated vertical pattern and their distribution may vary from system to system (Dolan and Marrasé, 1995).

Nano-ciliates ($<20 \mu\text{m}$) have been identified as potentially important grazers of picoplankton (Sherr and Sherr, 1987;

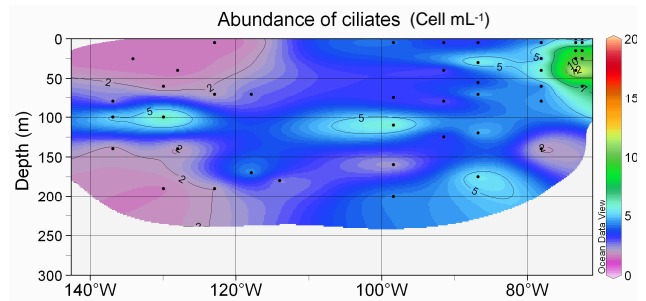


Fig. 11. Abundance of ciliates (cell mL^{-1}). Legend as in Fig. 5.

Sherr et al., 1991) and account in general from 50 to 95% of total ciliates in a variety of marine ecosystems (Beers et al., 1980; Montagnes et al., 1988; Yang et al., 2004). However, in our study, we observed very few nanociliates as the size of the majority of ciliates felled into a 50–100 μm range (data not shown). That could be explained by the fixation method used in our study: Leakey et al. (1994) demonstrated that the use of glutaraldehyde as fixative could lead to a loss of cells as high as 70% among aloricate ciliates relative to lugol's iodine while tintinnid numbers did not vary significantly between fixative treatments. However, Dolan and Marrasé (1995), observed only 8% of nanociliates in the Catalan Sea in June 1993 while lugol's iodine was used as fixative.

In conclusion, although assessing the abundance of the different microbial groups by DAPI microscopy is slow and labour-intensive and despite some cell loss following long-term sample storage, the present data set highlights some characteristics of the microbial community in the South-East Pacific Ocean that have escaped more rapid techniques such as flow cytometry. This includes in particular the importance of colonial PE containing picocyanobacteria in the HNLC area and the large contribution of green fluorescing dinoflagellates in some regions, such as between the gyre and the coast of South America.

Acknowledgements. D. Tailliez and C. Bournot are warmly thanked for their efficient help in CTD rosette management and data processing. D. Marie, M. Viprey and L. Garczarek are acknowledged for their help during the cruise. This is a contribution to the BIOSOPE project (LEFE-CYBER program). This research was funded by the Centre National de la Recherche Scientifique (CNRS), the Institut des Sciences de l'Univers (INSU), the Centre National d'Etudes Spatiales (CNES), the European Space Agency (ESA), the National Aeronautics and Space Administration (NASA) and the Natural Sciences and Engineering Research Council of Canada (NSERC). Additional funds were provided by the ANR Biodiversity project PICOFUNPAC. S. Masquelier was supported by a doctoral fellowship (BFR05/027) from the Ministère de la Culture, de l'Enseignement Supérieur et de la Recherche of Luxembourg.

Edited by: M. Dai

References

- Azam, F., Fenchel, T., Field, J. G., Gray, J. S., Meyer-Reil, L. A., and Thingstad, F.: The ecological role of water column microbes in the sea, *Mar. Ecol.-Prog. Ser.*, 10, 257–263, 1983.
- Beers, J. R., Reid, M. H., and Stewart, G. L.: Microplankton population structure in Southern California nearshore waters in late spring, *Mar. Biol.*, 60, 209–226, 1980.
- Campbell, L., Liu, H. B., Nolla, H. A., and Vaultot, D.: Annual variability of phytoplankton and bacteria in the subtropical North Pacific Ocean at station Aloha during the 1991–1994 ENSO event, *Deep-Sea Res. I*, 44, 167–192, 1997.
- Capone, D. G., Zehr, J. P., Paerl, H. W., Bergman, B., and Carpenter, E. J.: *Trichodesmium*, a globally significant marine cyanobacterium, *Science*, 276, 1221–1229, 1997.
- Chavez, F. P., Buck, K. R., and Barber, R. T.: Phytoplankton taxa in relation to primary production in the Equatorial Pacific, *Deep-Sea Res. II*, 37, 1733–1752, 1990.
- Christaki, U., Courties, C., Karayanni, H., Giannakourou, A., Mavrelas, C., Kormas, K. A., and Lebaron, P.: Dynamic characteristics of *Prochlorococcus* and *Synechococcus* consumption by bacterivorous nanoflagellates, *Microb. Ecol.*, 43, 341–352, 2002.
- Claustre, H.: The trophic status of various oceanic provinces as revealed by phytoplankton pigment signatures, *Limnol. Oceanogr.*, 39, 1206–1210, 1994.
- Claustre, H., Huot, Y., Obernosterer, I., Gentili, B., Tailliez, D., and Lewis, M.: Gross community production and metabolic balance in the South Pacific Gyre, using a non intrusive bio-optical method, *Biogeosciences Discuss.*, 4, 3089–3121, 2007, <http://www.biogeosciences-discuss.net/4/3089/2007/>.
- Claustre, H., Sciandra, A., and Vaultot, D.: Introduction to the special section: Bio-optical and biogeochemical conditions in the South East Pacific in late 2004 – the BIOSOPE cruise, *Biogeosciences Discuss.*, 5, 605–640, 2008, <http://www.biogeosciences-discuss.net/5/605/2008/>.
- Courties, C., Vaquer, A., Trousselier, M., Lautier, J., Chrétiennot-Dinet, M.-J., Neveux, J., Machado, C., and Claustre, H.: Smallest eukaryotic organism, *Nature*, 370, 255, 1994.
- Dolan, J. R. and Marrasé, C.: Planktonic ciliate distribution relative to a deep chlorophyll maximum: Catalan Sea. N.W. Mediterranean, June 1993, *Deep-Sea Res. I*, 42, 1965–1987, 1995.
- Dolan, J. R., Ritchie, M. E., and Ras, J.: The "neutral" community structure of planktonic herbivores, tintinnid ciliates of the microzooplankton, across the SE Tropical Pacific Ocean, *Biogeosciences*, 4, 297–310, 2007, <http://www.biogeosciences.net/4/297/2007/>.
- Fenchel, T.: Ecology of heterotrophic microflagellates. II. Bioenergetics and growth, *Mar. Ecol.-Prog. Ser.*, 8, 225–231, 1982.
- Fujita, S., Iseki, M., Yoshikawa, S., Makino, Y., Watanabe, M., Motomura, T., Kawai, H., and Murakami, A.: Identification and characterization of a fluorescent flagellar protein from the brown alga *Scytosiphon lomentaria* (Scytosiphonales, Phaeophyceae): a flavoprotein homologous to old yellow enzyme, *Eur. J. Phycol.*, 40, 159–167, 2005.
- Gómez, F., Claustre, H., Raimbault, P., and Souissi, S.: Two High-Nutrient Low-Chlorophyll phytoplankton assemblages: The tropical central Pacific and the offshore Perú-Chile current, *Biogeosciences*, 4, 1101–1113, 2007, <http://www.biogeosciences.net/4/1101/2007/>.
- Graham, L. and Wilcox, L.: *Algae*, Prentice Hall, Inc. Upper Saddle River, NJ, 630 pp., 2000.
- Grob, C., Ulloa, O., Claustre, H., Huot, Y., Alarcon, G., and Marie, D.: Contribution of picoplankton to the total particulate organic carbon concentration in the Eastern South Pacific, *Biogeosciences*, 4, 837–852, 2007, <http://www.biogeosciences.net/4/837/2007/>.
- Gundersen, K., Bratbak, G., and Heldal, M.: Factors influencing the loss of bacteria in preserved seawater samples, *Mar. Ecol.-Prog. Ser.*, 137, 305–307, 1996.
- Hagström, Azam, F., Andersson, A., Wikner, J., and Rassoulzadegan, F.: Microbial loop in an oligotrophic pelagic marine ecosystem: possible roles of cyanobacteria and nanoflagellates in the organic fluxes, *Mar. Ecol.-Prog. Ser.*, 49, 171–178, 1988.
- Hardy, J., Hanneman, A., Behrenfeld, M., and Horner, R.: Environmental biogeography of near-surface phytoplankton in the South-east Pacific Ocean, *Deep-Sea Res. I*, 43, 1647–1659, 1996.
- Kim, S., Park, M. G., Yih, W., and Coats, D. W.: Infection of the bloom-forming thecate dinoflagellates *Alexandrium affine* and *Gonyaulax spinifera* by two strains of *Amoebophrya* (Dinophyta), *J. Phycol.*, 40, 815–822, 2004.
- Le Gall, F., Marie, D., Garczarek, L., Viprey, M., and Vaultot, D.: Picoplankton diversity in the South East Pacific from cultures, *Biogeosciences*, 5, 203–214, 2008, <http://www.biogeosciences.net/5/203/2008/>.
- Leakey, R. J. G., Burkill, P. H., and Sleigh, M. A.: A comparison of fixatives for the estimation of abundance and biovolume of marine planktonic ciliate populations, *J. Plankton Res.*, 16, 375–389, 1994.
- Leakey, R. J. G., Burkill, P. H., and Sleigh, M. A.: Planktonic ciliates in the Northwestern Indian ocean: their abundance and biomass in waters of contrasting productivity, *J. Plankton Res.*, 18, 1063–1071, 1996.
- Lessard, E. J. and Murrell, M. C.: Distribution, abundance and size composition of heterotrophic dinoflagellates and ciliates in the Sargasso Sea near Bermuda, *Deep-Sea Res. I*, 43, 1045–1065, 1996.
- Leterme, S. C., Seuront, L., and Edwards, M.: Differential contribution of diatoms and dinoflagellates to phytoplankton biomass in the NE Atlantic Ocean and the North Sea, *Mar. Ecol.-Prog. Ser.*, 312, 57–65, 2006.
- Mackey, D. J., Blanchot, J., Higgins, H. W., and Neveux, J.: Phytoplankton abundances and community structure in the Equatorial Pacific, *Deep-Sea Res. II*, 49, 2561–2582, 2002.
- Marañón, E., Holligan, P. M., Barciela, R., González, N., Mouriño, B., Pazó, M. J., and Varela, M.: Patterns of phytoplankton size structure and productivity in contrasting open-ocean environments, *Mar. Ecol.-Prog. Ser.*, 216, 43–56, 2001.
- Montagnes, D. J. S., Lynn, D. H., Roff, J. C., and Taylor, W. D.: The annual cycle of heterotrophic planktonic ciliates in the waters surrounding the isles of shoals, Gulf of Maine: an assessment of their trophic role, *Mar. Biol.*, 99, 21–30, 1988.
- Moon-van der Staay, S. Y., De Wachter, R., and Vaultot, D.: Oceanic 18S rDNA sequences from picoplankton reveal unsuspected eukaryotic diversity, *Nature*, 409, 607–610, 2001.
- Morel, A., Gentili, B., Claustre, H., Babin, M., Bricaud, A., Ras, J., and Tieche, F.: Optical properties of the "clearest" natural waters, *Limnol. Oceanogr.*, 52, 217–229, 2007.
- Nielsen, S. L.: Size-dependent growth rates in eukaryotic and prokaryotic algae exemplified by green algae and cyanobacte-

- ria: Comparisons between unicells and colonial growth forms, *J. Plankton Res.*, 28, 489–498, 2006.
- Not, F., Massana, R., Latasa, M., Marie, D., Colson, C., Eikrem, W., Pedrós-Alió, C., Vaultot, D., and Simon, N.: Late summer community composition and abundance of photosynthetic picocoeukaryotes in Norwegian and Barents Seas, *Limnol. Oceanogr.*, 50, 1677–1686, 2005.
- Paerl, H. W.: *Marine plankton, The ecology of cyanobacteria: Their diversity in time and space*, Kluwer Academic Publishers, Dordrecht, The Netherlands, 121–148, 2000.
- Partensky, F., Hess, W. R., and Vaultot, D.: *Prochlorococcus*, a marine photosynthetic prokaryote of global significance, *Microb. Mol. Biol. R.*, 63, 106–127, 1999.
- Pérez, V., Fernández, E., Marañón, E., Morán, X. A. G. and Zubkov, M. V.: Vertical distribution of phytoplankton biomass, production and growth in the Atlantic subtropical gyres, *Deep-Sea Res. I*, 53, 1616–1634, 2006.
- Porter, K. G. and Feig, Y. S.: The use of DAPI for identifying and counting aquatic microflora, *Limnol. Oceanogr.*, 25, 943–948, 1980.
- Putland, J. and Rivkin, R.: Influence of storage mode and duration on the microscopic enumeration of *Synechococcus* from a cold coastal ocean environment, *Aquat. Microb. Ecol.*, 17, 191–199, 1999.
- Raimbault, P. and Garcia, N.: Carbon and nitrogen uptake in the South Pacific Ocean: Evidence for efficient dinitrogen fixation and regenerated production leading to large accumulation of dissolved organic matter in nitrogen-depleted waters, *Biogeosciences Discuss.*, 4, 3531–3579, 2007, <http://www.biogeosciences-discuss.net/4/3531/2007/>.
- Raimbault, P., Garcia, N., and Cerutti, F.: Distribution of inorganic and organic nutrients in the South Pacific Ocean-evidence for long-term accumulation of organic matter in nitrogen-depleted waters, *Biogeosciences Discuss.*, 4, 3041–3087, 2007, <http://www.biogeosciences-discuss.net/4/3041/2007/>.
- Ras, J., Uitz, J. and Claustre, H.: Spatial variability of phytoplankton pigment distribution in the South East Pacific, *Biogeosciences Discuss.*, 4, 3409–3451, 2007, <http://www.biogeosciences-discuss.net/4/3409/2007/>.
- Raven, J. A.: The twelfth Tansley lecture. Small is beautiful: The picophytoplankton, *Funct. Ecol.*, 12, 503–513, 1998.
- Sanders, R. W., Berninger, U. G., Lim, E. L., Kemp, P. F., and Caron, D. A.: Heterotrophic and mixotrophic nanoplankton predation on picoplankton in the Sargasso Sea and on Georges Bank, *Mar. Ecol.-Prog. Ser.*, 192, 103–118, 2000.
- Sato, M., Yoshikawa, T., Takeda, S., and Furuya, K.: Application of the size-fractionation method to simultaneous estimation of clearance rates by heterotrophic flagellates and ciliates of pico- and nanophytoplankton, *J. Exp. Mar. Biol. Ecol.*, 349, 334–343, 2007.
- Schlitzer, R.: ODV software, <http://www.awi-bremerhaven.de/GEO/ODV>, 2003.
- Shapiro, L. P., Haugen, E. M., and Carpenter, E. J.: Occurrence and abundance of green-fluorescing dinoflagellates in surface waters of the Northwest Atlantic and Northeast Pacific Oceans, *J. Phycol.*, 25, 189–191, 1989.
- Sherr, B. F. and Sherr, E. B.: High rates of consumption of bacteria by pelagic ciliates, *Nature*, 325, 710–711, 1987.
- Sherr, E. B. and Sherr, B. F.: Marine microbes an overview, in: *Microbial Ecology of the Oceans*, edited by: Kirchman, D. L., New York, Wiley-Liss, Inc., 13–46, 2000.
- Sherr, E. B., Sherr, B. F., and Wheeler, P. A.: Distribution of coccoid cyanobacteria and small eukaryotic phytoplankton in the upwelling ecosystem off the Oregon coast during 2001 and 2002, *Deep-Sea Res. II*, 52, 317–330, 2005.
- Sherr, E. F., Sherr, B. F., and McDaniel, J.: Clearance rates of $6\ \mu\text{m}$ fluorescently labeled algae (FLA) by estuarine protozoa: Potential grazing impact of flagellates and ciliates, *Mar. Ecol. Prog. Ser.*, 69, 81–92, 1991.
- Sieburth, J. M., Smetacek, V., and Lenz, J.: Pelagic ecosystem structure: Heterotrophic compartments of the plankton and their relationship to plankton size fractions, *Limnol. Oceanogr.*, 23, 1256–1263, 1978.
- Tang, Y. Z. and Dobbs, F. C.: Green autofluorescence in dinoflagellates, diatoms, and other microalgae and its implications for vital staining and morphological studies, *Appl. Environ. Microbiol.*, 73, 2306–2313, 2007.
- Vidussi, F., Claustre, H., Manca, B. B., Luchetta, A., and Marty, J. C.: Phytoplankton pigment distribution in relation to upper thermocline circulation in the Eastern Mediterranean Sea during winter, *J. Geophys. Res.*, 106, 19 939–19 956, 2001.
- Wilson, T. and Hastings, J. W.: Bioluminescence, *Annu. Rev. Cell Dev. Bi.*, 14, 197–230, 1998.
- Yang, E. J., Choi, J. K., and Hyun, J. H.: Distribution and structure of heterotrophic protist communities in the Northeast Equatorial Pacific Ocean, *Mar. Biol.*, 146, 1–15, 2004.
- Zehr, J. P., Waterbury, J. B., Turner, P. J., Montoya, J. P., Omeregic, E., Steward, G. F., Hansen, A., and Karl, D. M.: Unicellular cyanobacteria fix N_2 in the subtropical North Pacific Ocean, *Nature*, 412, 635–638, 2001.

Picoplankton diversity in the South-East Pacific Ocean from cultures

F. Le Gall¹, F. Rigaut-Jalabert¹, D. Marie¹, L. Garczarek¹, M. Viprey¹, A. Gobet^{1,2}, and D. Vaultot¹

¹Station Biologique de Roscoff, UMR 7144, CNRS et Université Pierre et Marie Curie, Place G. Tessier, 29682, Roscoff, France

²present address: Max Planck Institute for Marine Microbiology, Celsius Strasse 1, 28359 Bremen, Germany

Received: 4 July 2007 – Published in Biogeosciences Discuss.: 7 August 2007

Revised: 3 January 2008 – Accepted: 18 January 2008 – Published: 15 February 2008

Abstract. In late 2004, the BIOSOPE cruise sailed between the equatorial influenced waters off the Marquesas Islands and the nutrient enriched waters of the Chilean upwelling. Along the way, it explored the Southeast Pacific gyre centred around Easter Island, which is probably the most oligotrophic oceanic region on earth. During this cruise, we undertook a vigorous effort to isolate novel photosynthetic picoplanktonic eukaryotes. Two strategies were attempted on board: enrichment of filtered samples with culture medium and sorting of specific populations by flow cytometry based on size and chlorophyll fluorescence. Over 1900 pre-cultures were started and then further purified by flow cytometry, serial dilution or pipette isolation to yield a total of 212 strains. These strains were characterized morphologically and for more than 50% of them, genetically, through partial sequencing of the 18 S rRNA gene.

Among the characterized strains, the largest number belongs to stramenopiles (Heterokontophyta) with a record of 38 strains belonging to the species *Pelagomonas calceolata* (Pelagophyceae). Strains from the recently described genera *Bolidomonas* and *Florenciella* have been re-isolated for the first time since their description. Two other abundant groups are the Chlorophyta, especially Prasinophyceae, and the Haptophyta, especially the genera *Phaeocystis* and *Emiliana*. A limited number of heterotrophic flagellates have also been isolated, all of them belonging to groups containing known species. Finally, over a dozen of unicellular cyanobacterial *Synechococcus* strains have been obtained, some forming unusual short chains.

Overall our strategy was quite successful since it allowed us to isolate a large number of picoplankton strains. Still it failed in two respects. First, apparently very few novel taxa have been obtained. One set of strains is related to *Prasino-*

derma coloniale (Prasinococcales, Prasinophyceae) but their sequences are sufficiently different from the latter to probably belong to a new genus or species. The sequences of two other strains, unfortunately later lost, were phylogenetically affiliated to stramenopile environmental sequences, probably corresponding to a new algal class. Second, very few strains have been obtained from the very oligotrophic central gyre itself. In order to be successful, future work in similar waters should probably combine flow cytometry sorting with culture media and cultivation approaches specifically developed for oligotrophic water species.

1 Introduction

Although the existence of very small algal cells had been known for more than 150 years (Nägeli, 1849), it was only 30 years ago, that their importance in marine waters was recognized (Johnson and Sieburth, 1982; Waterbury et al., 1979), leading to the definition of picoplankton, designating cells with size between 0.2 and 2 μm (Sieburth et al., 1978). It was soon realized that a significant fraction of photosynthetic biomass and primary production could be attributed to these tiny cells (Li et al., 1983; Platt et al., 1983). This small size fraction was found to be more important as chlorophyll concentration decreased, i.e. as the degree of oligotrophy increased (Herbland et al., 1985). Within photosynthetic picoplankton, prokaryotes appeared early on as much less diversified than eukaryotes since they are dominated by only two major cyanobacteria genera: *Prochlorococcus* and *Synechococcus*. This probably explains why we now know much more about photosynthetic picoplanktonic prokaryotes than eukaryotes. In particular, the genetic diversity of these prokaryotes has been quite well characterized (Fuller et al., 2003; Rocap et al., 2002), representatives of key genotypes have been isolated in culture, and more recently quite a few genomes have been sequenced (Palenik et al., 2003; Rocap



Correspondence to: D. Vaultot
(vaultot@sb-roscoff.fr)

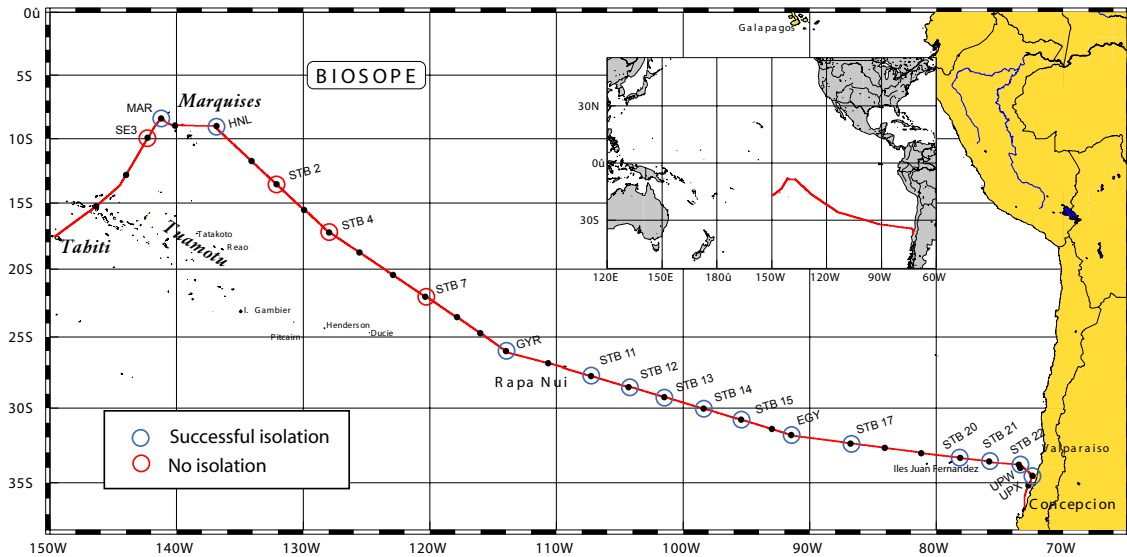


Fig. 1. BIOSOPE cruise track displaying the location of stations sampled for cultures.

et al., 2003). It is now possible to map the distribution of key groups of cyanobacteria in oceanic waters and to assess the existing relationships between genotypes and ecotypes (Johnson et al., 2006).

For photosynthetic picoeukaryotes, the situation is, in many respects, much less advanced, one reason being their very wide phylogenetic diversity. They belong to at least four major lineages: Chlorophyta, Haptophyta, stramenopiles (or Heterokontophyta) and Alveolata. Moreover, extensive studies of their genetic diversity from environmental samples started less than 10 years ago (López-García et al., 2001; Moon-van der Staay et al., 2001). To date, less than 25 species have been described for which cell size is always smaller than $3\ \mu\text{m}$ (Vaulot et al., 2008¹). Among these, knowledge about “flagship” species such as *Ostreococcus* and *Micromonas* (both belonging to the order Mamiellales, Prasinophyceae) is progressing fast since the genomes of several “ecotypes” have already been (or are currently) sequenced (Derelle et al., 2006; Palenik et al., 2007). Their oceanic distribution can be mapped using techniques such as fluorescent in situ hybridization (Not et al., 2005) or quantitative PCR (Marie et al., 2006). However, this only constitutes the tip of the iceberg as molecular approaches, in particular the analysis of 18S rDNA genetic libraries from the natural environment, have pointed out to a very wide diversity at all taxonomic levels (Vaulot et al., 2008¹). For example, a new division of photosynthetic eukaryotes, the picobiliphytes, has been recently discovered (Not et al., 2007). Many phylogenetic groups are only known from their sequences. This is the case for example for Prasinophyceae clade VII B (Guillou

et al., 2004) or for *Chrysochromulina*-related clades within the prymnesiophytes (Moon-van der Staay et al., 2000). For all these taxonomic groups, there is a critical need to obtain cultured representatives. This concern is especially acute in open ocean oligotrophic regions due to the difficulty to isolate and maintain organisms adapted to low nutrient conditions that are often outgrown by fast dividing “weed” species.

The BIOSOPE cruise that sailed through the center of the South East Pacific gyre, probably the most oligotrophic place on earth, offered an opportunity to obtain cultures from this unique environment. We performed sample enrichment with diluted culture medium following filtration to separate the smaller picoplankton cells from the rest of the plankton, a strategy that allowed us in the past to obtain novel taxa (Vaulot et al., 2004). We also targeted specifically photosynthetic picoeukaryotes by using flow cytometry sorting directly on board the ship. In the end, we obtained 212 cultures that have been integrated to the Roscoff Culture Collection (RCC, <http://www.sb-roscoff.fr/Phyto/RCC/>), more than half of which were characterized genetically by sequencing partially the 18S rRNA gene. These cultures encompass representatives of six major phylogenetic divisions: Cyanobacteria, Chlorophyta (mostly Prasinophyceae), stramenopiles, Haptophyta, Alveolata (dinoflagellates), Euglenozoa (bodonids). A significant fraction of these cultures are picoplanktonic, although for some groups such as the Alveolata, only large species were obtained.

¹Vaulot, D., Eikrem, W., Viprey, M., and Moreau, H.: The diversity of eukaryotic marine picophytoplankton, *FEMS Microbiol. Rev.*, submitted, 2008.

Table 1. Sampling stations and depths (in general two depths were selected corresponding to the two columns labelled min and max). The last three columns provide the number of starter cultures for each station obtained by either filtration on $0.6\ \mu\text{m}$, filtration on $3\ \mu\text{m}$, or by flow cytometry sorting.

Station	Depth min (m)	Depth max (m)	Cultures filtration < $0.6\ \mu\text{m}$	Cultures filtration < $3\ \mu\text{m}$	Cultures flow cytometry sorting
SE3	15	70			288
MAR	10	60	10	20	288
HLN	30	100	48	48	96
STB2	30	100			192
STB4	40	140			192
STB7	5	175			240
GYR2	5	500		8	72
STB11	0	200		12	48
STB12	40	180			48
STB13	0	160		16	
STB14	5	150			72
STB15	100	100			48
EGY2	5	80	32		112
STB17	0	20			19
STB20	5	45	16		8
STB21	5	5			4
UPW1	5	35	16		20
UPX	0	40	16		7

2 Material and methods

2.1 Sampling

Samples were taken in general at two depths (surface layer and vicinity of the chlorophyll maximum when present) at selected stations along the BIOSOPE cruise track (Fig. 1 and Table 1) using Niskin bottles mounted on a CTD frame. The oceanographic context of the cruise is described in Claustre et al. (2008).

2.2 Primary cultures

We used two different strategies to obtain starter cultures. The first one was based on filtered seawater enriched with nutrients. The second one relied on single cell sorting by flow cytometry, targeting specific cell populations based on their size and pigment fluorescence. As cultures were examined several times during the cruise, many variations were attempted in an effort to increase final culture yield.

2.2.1 Growth conditions used on board

All cultures were incubated on board in a thermostatic cabinet set at 20°C . Two light levels were obtained with 2 Sylvania 18 W tubes: white light around $140\ \mu\text{mol photons m}^{-2}\ \text{s}^{-1}$ and blue light (Moon Light Blue paper, M.E.S, Nantes, France) around $8\ \mu\text{mol photons m}^{-2}\ \text{s}^{-1}$. We used three types of medium:

K (Keller et al., 1987) for photosynthetic eukaryotes, Pro2 (Moore and Chisholm, 1999) for photosynthetic prokaryotes (*Prochlorococcus* and *Synechococcus*), and rice-based (Cowling, 1991) for heterotrophic eukaryotes which were grown in the dark. Multi-well plates were wrapped with parafilm in order to avoid any evaporation during growth.

2.2.2 Enrichment cultures

About 500 mL of sample seawater was filtered by simple gravity through two superposed (in an effort to provide more tight size fractionation) Nuclepore filters of 47 mm diameter, with either $0.6\ \mu\text{m}$ or $3\ \mu\text{m}$ porosity (Whatman International Ltd, Maidstone, UK). The filtrate was partitioned into 50 mL culture flasks (Sarstedt, Orsay, France) or, at one station (HLN), into individual wells of 24-well plates to which we added either 1/10 or 1/100 of full strength K or Pro2 medium. In order to try to promote nitrogen fixing organisms, some cultures were started by simply amending sea water with iron (as FeCl_3) and phosphorus (as KH_2PO_4) at final concentrations of 3 nM and $0.4\ \mu\text{M}$, respectively.

2.2.3 Cultures sorted by flow cytometry

Samples were run either un-concentrated or concentrated between 5 and 100-fold by tangential flow filtration using a 100 000 MWCO (Regenerated Cellulose – RC ref VF20C4) Vivaflow 200 cassette. Concentration was sometimes necessary so that rarer cells formed well defined populations in

flow cytometry cytograms. Between 1 to 500 000 cells were sorted using a FACSaria (Becton Dickinson, San Jose CA) flow cytometer either into 24 or 48-well plates or directly into 10 mL polystyrene tubes pre-filled with medium diluted 100 times (Table S1, Supplement: <http://www.biogeosciences.net/5/203/2008/bg-5-203-2008-supplement.pdf>). Different cell populations were discriminated based on side scatter as well as orange and red fluorescence following excitation at 488 nm (20 mW). Sorting was done either in purity or yield mode.

2.3 Primary culture processing and establishment of strains

On board the ship, primary cultures (either enriched or flow sorted) were checked for growth once or twice (depending on how early in the cruise they were started) using flow cytometry and inverted microscopy. Cultures that displayed growth but appeared mixed were sorted a second time.

A first set of cultures were transferred back to Roscoff on the occasion of change of crew at Easter Island at mid-cruise. At the end of the cruise, cultures from the early part of the cruise (i.e. about two months old) that showed no evidence of containing photosynthetic cells based on flow cytometry analysis were discarded. Cultures grown in multi-well plates were transferred to 10 mL polystyrene tubes. All cultures were brought back to Roscoff in the dark at ambient temperature in isothermal boxes to minimize temperature shocks. Cultures were exposed to moderate light when possible during the transit and then rushed to the Roscoff culture room on arrival.

Once transferred back to Roscoff, cultures were monitored based on colour as well as with optical microscopy and flow cytometry. Cultures were purified either by serial dilution, solid medium plating, or individual cell pipetting under an inverted microscope. Strains that appeared to be pure were transferred to normal strength medium: PCR-S11 (Rippka et al., 2000), K, and rice for cyanobacteria, autotrophic, and heterotrophic eukaryotes, respectively. They were then entered into the Roscoff Culture Collection (RCC) database under new accession numbers (Table S1, Supplement: <http://www.biogeosciences.net/5/203/2008/bg-5-203-2008-supplement.pdf>).

2.4 Strain characterization

Strains deposited to the RCC were characterized by optical microscopy. For each strain, pictures were taken on live cultures with an Olympus BX51 microscope with a $\times 100$ objective using differential interference contrast (DIC) with a SPOT RT-slider digital camera (Diagnostics Instruments, Sterling Heights, MI). Average cell dimension of each culture was determined from the pictures. Flagellated cells were also photographed after adding one drop of lugol to visualize flagellum shape, length and number. Cyanobacteria were identified by their colour and shape. The morphology of

a few strains was confirmed by whole-mount transmission electron microscopy. Cells were fixed for 15 min with 1% glutaraldehyde (final concentration). A drop of fixed cells was deposited onto formvar-coated grids. Once the drop had dried, grids were rinsed with distilled water. Cells on grids were stained with a saturated solution of uranyl acetate for 20 min and rinsed with distilled water. Photomicrographs were taken with a JEOL JEM-1200EX electron microscope.

A subset of strains was characterized by their partial 18S ribosomal RNA gene sequence. Cultures were grown in 50 mL flasks for 1–2 weeks depending on the growth of each strain and recovered by centrifugation at $11\,000\times g$ for 10 min. DNA was extracted using 3% Cetyl Trimethyl Ammonium Bromide (CTAB, Doyle and Doyle, 1990). DNA was then stored at -80°C .

The 18S rRNA gene was amplified by polymerase chain reaction (PCR) using the primer set Euk328f and Euk329r (Romari and Vaultot, 2004) and the HotStarTaq Master Mix (Qiagen, Courtaboeuf, France). For PCR, a 15 min initial activation step of the polymerase at 95°C , was followed by 40 cycles including 1 min of denaturation at 94°C , 45 s of annealing at 57°C and 75 s extension at 72°C . The PCR program was finished by a final extension of 10 min at 72°C followed by cooling at 4°C . PCR products were purified with the Qiaquick PCR purification kit (Qiagen) and controlled by electrophoresis on a 1% agarose gel. Partial 18S rRNA gene sequences were determined from purified PCR products by using Big Dye Terminator V3.1 (Applied Biosystems, Foster city, CA, USA) and the internal primer Euk 528f (Elwood et al., 1985) run on an ABI prism 3100 sequencer (Applied Biosystems, Courtaboeuf, France).

Sequences were compared to those available in public database with NCBI BLAST web application. Sequences were also automatically aligned using the ARB program (Ludwig et al., 2004) to a set of more than 20 000 high quality pre-aligned eukaryotic sequences (Pruesse et al., 2007) available from the Silva web site (SSURef database: www.arb-silva.de). After manual refinement of the alignment, sequences were added to the reference tree provided with the SSURef database using the quick parsimony addition option. Sequences with high similarities were grouped together using Fast Group II (http://biome.sdsu.edu/fastgroup/fg_tools.htm) with the sequence match parameter set at 80% and one or two representative sequences per group were chosen along with the closest publicly available sequence. Phylogeny analysis was performed on aligned sequences with MEGA4 (<http://www.megasoftware.net/>, Tamura et al., 2007). A neighbour-joining tree was computed from 394 common positions based on Kimura 2-parameter model distances using 1000 bootstrap replications. Sequences have been submitted to GenBank under accession number EU106736-EU106852.

3 Results and discussion

3.1 Isolation success

All together more than 1900 starter cultures were established during the BIOSOPE cruise (Table 1) either as enrichment cultures following filtration through either 0.6 or 3 μm or by sorting specific populations into individual wells or tubes. From one to three purification steps were in general necessary to obtain pure cultures (Table S1, Supplement: <http://www.biogeosciences.net/5/203/2008/bg-5-203-2008-supplement.pdf>). For example, enrichment cultures started at the beginning of the cruise were sorted at the end of the cruise and then purified by serial dilution back in the laboratory.

In the end, we obtained 188 autotrophic and 24 heterotrophic cultures which have been deposited to the RCC (Table S2, Supplement: <http://www.biogeosciences.net/5/203/2008/bg-5-203-2008-supplement.pdf>). Among these, 13 were subsequently lost and 25 remain not pure to this date. The latter are mostly autotrophic strains contaminated by heterotrophic eukaryotes. Cruise coverage was quite unequal with many strains obtained in mesotrophic regions and in the Chilean upwelling and much fewer from the central gyre (Fig. 1 and Table S1, Supplement: <http://www.biogeosciences.net/5/203/2008/bg-5-203-2008-supplement.pdf>). This reflects probably the difficulty to obtain cultures representative of extreme oligotrophic conditions, since nutrient additions even at relatively low concentrations are always much higher than those found in the environment. However this unbalanced coverage is not only the consequence of the environment but also of practical considerations. Cultures started early during the cruise had a chance to be screened before the end of the cruise and therefore could be re-purified on-board the ship. Conversely, cultures started late in the cruise were transported during their initial acclimation phase. Refinements in culturing conditions that were implemented late in the cruise based upon results obtained in the first part of the cruise may also explain why our success rate was better by the end of the cruise. For example, at the beginning of the cruise, starter cultures were sorted into 24 or 48-well plates. By mid-cruise, as we did not observe any growth under these conditions, we decided to switch to sorting into 10-mL tubes which seemed to result in higher success rates.

Sorting was an important element since more than 65% of the final cultures had undergone at least one sorting step. The strategy that yielded most pure strains was first to establish an enrichment culture with either 0.6 or 3 μm filtered samples followed by sorting sometimes later. In this case, it was often not necessary to perform further purification by serial dilution, saving this labour-intensive step. Sorting directly from natural samples was rarely sufficient to produce pure cultures and in most cases a second purification step had to be undertaken. It is difficult to determine whether sorting was

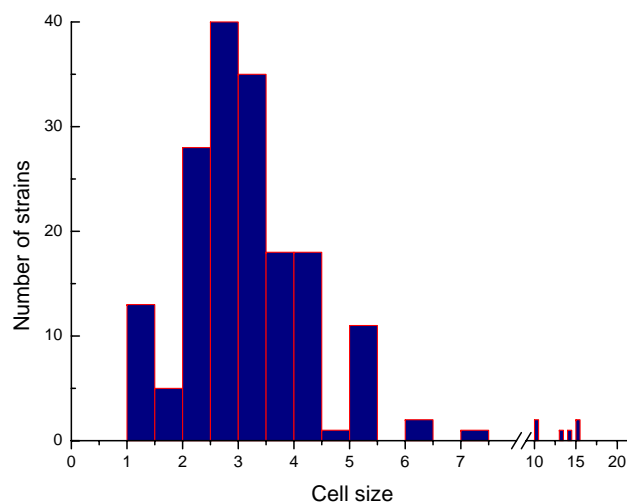


Fig. 2. Histogram of average sizes for all RCC cultures recovered from the BIOSOPE cruise.

successful in isolating the initially targeted population. We sorted sub-populations on the base of side scatter and chlorophyll but each of these sub-populations does not appear to be uniform genetically and consists probably of a mixture of several taxa belonging to different algal classes as established by 18S cloning and sequencing of sorted cells (X. Shi and D. Marie, unpublished).

3.2 Culture diversity

All purified cultures were examined by light microscopy, imaged digitally and their average size was determined (Fig. 2 and Tables S1 and S2, Supplement: <http://www.biogeosciences.net/5/203/2008/bg-5-203-2008-supplement.pdf>). No attempts were made to record measurements for a large number of cells in each culture and size data are therefore only indicative. They confirm, however, that our efforts to target picoplankton were successful since the mode size for the culture set lies between 2.5 and 3 μm .

A large, randomly chosen, subset of cultures (115, Tables S1 and S2, Supplement: <http://www.biogeosciences.net/5/203/2008/bg-5-203-2008-supplement.pdf>) was analysed phylogenetically by sequencing either partially or, in a few cases, totally the 18S rRNA gene. A few other cultures were identified based on their phenotypic characteristics (cyanobacteria, microplanktonic species).

Representatives of cyanobacteria and of three major eukaryotic divisions containing photosynthetic organisms (stramenopiles, Chlorophyta, and Haptophyta) have been obtained in culture with the former most prevalent and the latter two in almost equal proportions (Table 2). For these groups, a large fraction of the strains were picoplanktonic. This contrasts with the Alveolata for which only two larger sized (15 μm) dinoflagellate cultures could be isolated

Table 2. Number of strains identified for the different phylogenetic groups.

Division	Class	Genus	Number	Total per division	
Cyanobacteria	Cyanophyceae	<i>Synechococcus</i>	13	13	
Chlorophyta	Prasinophyceae	<i>Micromonas</i>	2	30	
	Prasinophyceae	<i>Prasinococcus</i>	1		
	Prasinophyceae	<i>Prasinoderma</i>	2		
	Prasinophyceae	<i>cf. Prasinoderma</i>	9		
	Prasinophyceae	<i>Pycnococcus</i>	5		
	Prasinophyceae	Unknown	8		
	Trebouxiophyceae	<i>Picochlorum</i>	3		
	Stramenopiles	Bacillariophyceae	<i>Chaetoceros</i>		1
Bacillariophyceae	<i>Minutocellus</i>	1			
Bacillariophyceae	<i>Thalassiosira</i>	1			
Bolidophyceae	<i>Bolidomonas</i>	1			
Dictyochophyceae	<i>Florenciella</i>	2			
Pelagophyceae	<i>Pelagomonas</i>	38			
Pelagophyceae	Unknown	2			
Unknown	Unknown	2			
Bicosoecid	<i>Caecitellus</i>	4			
Bicosoecid	<i>Cafeteria</i>	3			
Bicosoecid	Unknown	3			
Haptophyta	Prymnesiophyceae	<i>Emiliana</i>	12	28	
Prymnesiophyceae	<i>Phaeocystis</i>	14			
Prymnesiophyceae	Unknown	2			
Alveolata	Dinophyceae	<i>Prorocentrum</i>	2	2	
Kinetoplastida	Bodonid	Unknown	2	2	

(see Tables S2, Supplement: <http://www.biogeosciences.net/5/203/2008/bg-5-203-2008-supplement.pdf>).

Thirteen strains of unicellular rod-shaped cyanobacteria have been obtained tentatively identified as *Synechococcus*. No *Prochlorococcus* was obtained despite the use of the *Prochlorococcus* specific Pro2 medium. Some of these cyanobacterial strains form short chains, exhibiting sometimes very elongated cells (Fig. 3, RCC 1027) contrasting the usual *Synechococcus* morphology (Fig. 3, RCC 1022). Such strains mostly originated from the HNLC station near the Marquesas Islands (see Supplement: <http://www.biogeosciences.net/5/203/2008/bg-5-203-2008-supplement.pdf>, Table S1). Interestingly, samples from this region displayed an unusually high fraction of chain-forming and colonial picocyanobacteria (Masquelier and Vaultot, 2007). Phylogenetic analyses of the 16S rRNA gene will be necessary to determine the exact nature of these strains.

Chlorophyta, and more specifically Prasinophyceae, are important contributors to picoplankton and many strains have been isolated from marine waters in the past, some of them belonging to yet undescribed species (Guillou et al., 2004; Vaultot et al., 2004). Thirty Chlorophyta strains have been isolated during BIOSOPE, mostly Prasinophyceae. Among these, 11 are related to *Prasinoderma coloniale* (Prasinococ-

cales), a picoplanktonic species that can form colonies surrounded by mucus. These strains display the bilobed cup-shaped chloroplasts characteristics of *P. coloniale* (Hasegawa et al., 1996). However most of our strains do not seem to form colonies as *P. coloniale* does. Interestingly, one group of 9 sequences appears to form a separate clade (Fig. 4) with only 94.7% identity to *P. coloniale*, in contrast to the two other strains sharing 99.6% identity with *P. coloniale*. These sequences possess large and highly similar insertions at least 330 bp long inside the 18S rRNA gene starting at nucleotide position 862 of the *P. coloniale* sequence. Phenotypically, strains from these group appear slightly smaller (see Table S2, Supplement: <http://www.biogeosciences.net/5/203/2008/bg-5-203-2008-supplement.pdf>) than those closely related to *P. coloniale*. They were isolated from near-surface waters at a variety of stations, while the two strains more closely related to *P. coloniale* originated from the Marquesas area. A culture closely related to *Prasinococcus capsulatus*, a species that also belongs to the order Prasinococcales, has been recovered from the chlorophyll maximum at the GYR station. Cells display a polysaccharide capsule around the cell (Fig. 3, RCC 859), typical of this species (Miyashita et al., 1993). Five Prasinophyceae closely related to the picoplanktonic species *Pycnococcus provasolii* (Pseudocourfieldiales) have been isolated from two mid-depth

samples in the Chilean upwelling. Eight strains belong to clade VII of the Prasinophyceae (Guillou et al., 2004), a group which contains some cultured strains such as CCMP 1205 but for which no species has been described formally. All these strains consist of small (2 to 4 μm) spherical cells lacking discriminating features (Fig. 3, RCC 857). Two sets of strains originated from surface waters and one set from 100 m in the HNLC zone. Two Prasinophyceae strains from the Chilean upwelling belong to clade C of the very ubiquitous species *Micromonas pusilla* (Guillou et al., 2004). They possess an unusually long flagellum (Fig. 3, RCC 913) that could be a diagnostic feature for that clade (F. Jouenne, personal communication). We also isolated from one sample of the Chilean upwelling three cultures representative of another green algal class, the Trebouxiophyceae. These strains are phylogenetically related to the recently established genus *Picochlorum* (Fig. 4) that now regroups salt-tolerant species previously classified within the genus *Nanochlorum* (Henley et al., 2004).

All Haptophyta cultures are part of the class Prymnesiophyceae. Fourteen strains belong to the genus *Phaeocystis*. Among these, three from the upwelling region (RCC 908, 925 and 935) are closely related (>99.5% sequence similarity) to *P. jahnii*. This species has been recently described from the Mediterranean Sea (Zingone et al., 1999) and forms loose colonies. Nine strains from the Marquesas, east of the gyre and upwelling regions (RCC 851, 870, 882, 940, 992, 993, 1000, 1006, 1003) are closely related (>99.5% sequence similarity) to *P. globosa* that forms spherical colonies (Fig. 3, RCC 851). Another *Phaeocystis* strain (RCC 861) is more distantly (98%) related to *P. globosa*. For the last strain (RCC 849), no sequence is available. We also isolated 12 strains of *Emiliana huxleyi*, a few calcifying (Fig. 3, RCC 867) and most naked (Fig. 3, RCC 951), corresponding probably to diploid and haploid stages, respectively (Houdan et al., 2003). Two other unidentified coccolithophorids have also been obtained from the Marquesas and central gyre regions. Interestingly all Haptophyta strains were isolated from the top of euphotic zone (between 5 and 60 m).

Among stramenopiles, 38 cultures are closely related to the picoplanktonic species *Pelagomonas calceolata* (Pelagophyceae). The 37 available sequences share more than 99% similarity over 335 common positions and 34 are even 100% identical to each other. More than half of the strains are flagellated (Fig. 3, RCC 879), fitting the original description of the species (Andersen et al., 1993), while the other do not display any evidence of a flagellum. However, the presence of a flagellum could reflect life cycle stages rather than taxonomical differences. Interestingly, both flagellated and non-flagellated strains with identical 18S rDNA sequences have been isolated from the same sample: e.g. RCC 883 and 884 originated from 100 m at the HLN station and share 100% sequence similarity over 697 positions. The presence of a thin theca characteristics of the species (Andersen et al., 1993) was confirmed by electron microscopy on strain

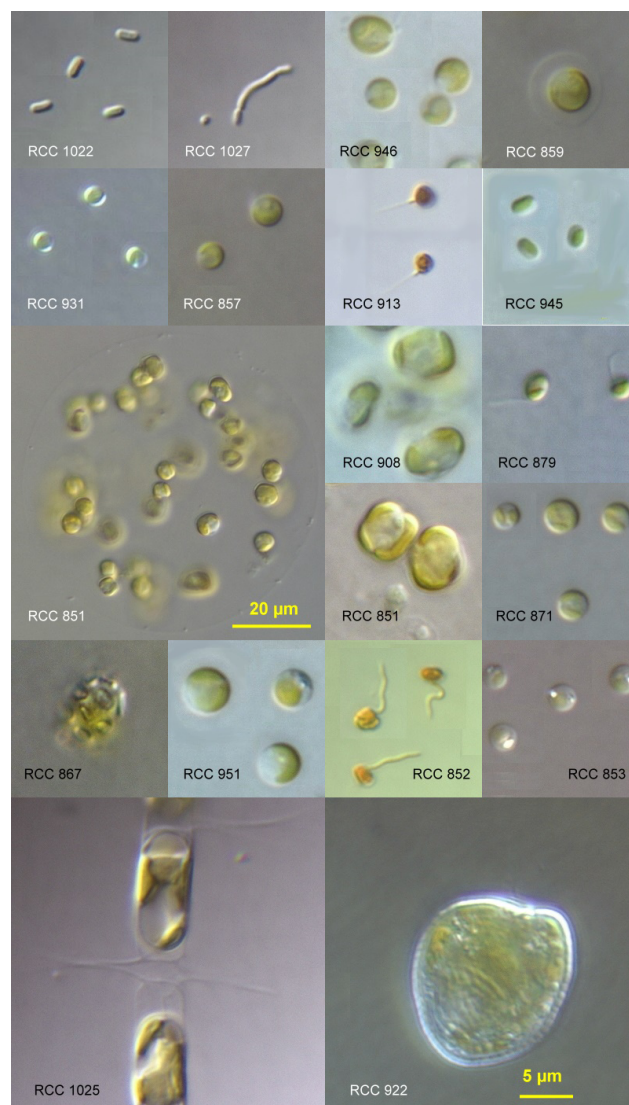


Fig. 3. Microscopy images of a selection of strains recovered during the BIOSOPE cruise. Scale bar is 5 μm for all images except for the *Phaeocystis* colony (RCC 851). From top to bottom and from left to right. Cyanobacteria: RCC 1022 and 1027. Note the elongated shape and short chains made by RCC 1027. Prasinophyceae: *Prasinoderma* sp. (RCC 946), *Prasinococcus capsulatus* (RCC 859), *Pycnococcus provasolii* (RCC 931), undescribed species belonging to clade VII (RCC 857), and *Micromonas pusilla* (RCC 913). Trebouxiophyceae: *Picochlorum* sp. (RCC 945). Prymnesiophyceae: *Phaeocystis* sp. (RCC 851 and 908, note colonial form) and *Emiliana huxleyi* (RCC 867, calcifying, and RCC 951, not calcifying). Pelagophyceae: *Pelagomonas calceolata* (RCC 879, flagellated lugol fixed, and RCC 871, spherical). Bolidophyceae: *Bolidomonas* sp. (RCC 852, lugol fixed). Heterokontophyta: unknown species (RCC 853). Diatom: *Chaetoceros* sp. (RCC 1025). Dinoflagellate: *Prorocentrum minimum* (RCC 922).

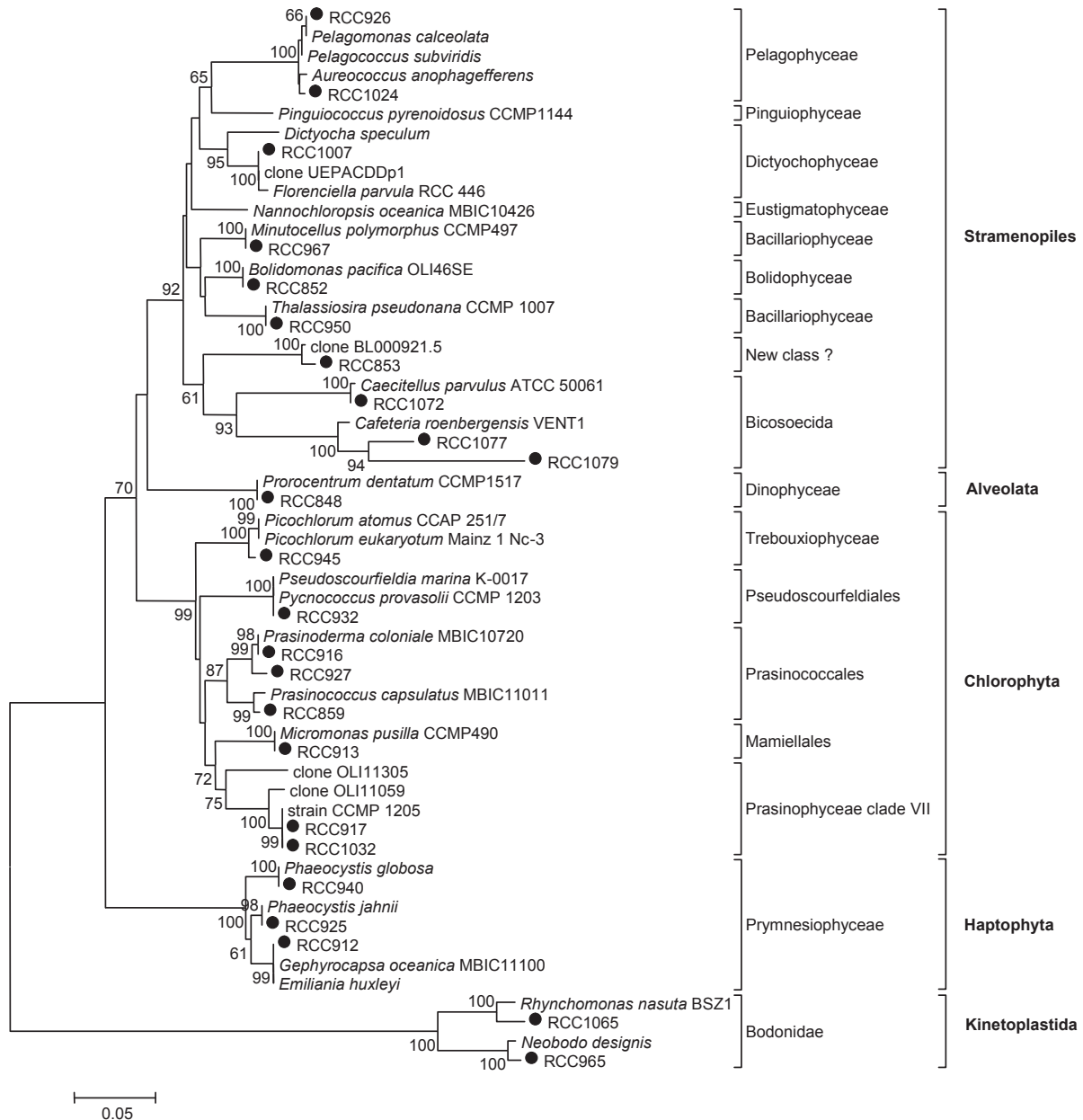


Fig. 4. Phylogenetic analysis of selected strains recovered during the BIOSOPE cruise. One or two 18S rDNA sequences from each taxonomic group was selected following clustering with Fast Group II (see Material and Methods). Neighbour-joining optimal tree with the sum of branch length = 1.74 shown. The percentage of replicate trees in which the associated taxa clustered together in the bootstrap test (1000 replicates) is displayed next to the branches. Only values larger than 60% are shown. The tree is drawn to scale, with branch lengths in the same units as those of the evolutionary distances used to infer the phylogenetic tree. The evolutionary distances were computed using the Kimura 2-parameter method and are in the units of the number of base substitutions per site. All positions containing gaps and missing data were eliminated from the dataset (complete deletion option). There were a total of 394 positions in the final dataset. Phylogenetic analyses were conducted with MEGA4 (<http://www.megasoftware.net/>).

RCC 879. *P. calceolata* was isolated at a variety of stations (Marquesas, HLNC, center of gyre, east of gyre and upwelling) both in surface and at 100 m, demonstrating that this species is truly ubiquitous in oceanic waters. Interestingly in the center of the South East gyre, *Pelagomonas* strains

were isolated from very deep samples down to 160 m. Two Pelagophyceae strains (RCC 986 and 1024) with 18S rDNA sequences displaying slightly lower similarity to *P. calceolata* (Fig. 4) were recovered at 60 m depth from the Marquesas region. Both are picoplanktonic and spherical, not

displaying any specific morphological features. We isolated a novel strain with high similarity to *Bolidomonas pacifica*, a species that belongs to the recently described class of the Bolidophyceae (Guillou et al., 1999), closely related to the diatoms. Its morphology (presence of 2 heterokont flagella) was confirmed by electron microscopy. This is quite interesting since to our knowledge this is the first novel isolate from this class since its initial discovery. In the same manner, we isolated from Marquesas surface waters, two strains very closely related by their 18S rDNA sequence to the recently described Dictyochophyceae picoplanktonic species *Florenciella parvula* (Eikrem et al., 2004). Similarity was also confirmed by electron microscopy. Two photosynthetic stramenopile strains could not be assigned to any specific class. Their 18S sequences share some homology with both *Pinguicoccus* (Pinguiphyceae) and *Nannochloropsis* (Eustigmatophyceae) and are almost identical to an environmental 18S sequence (BL000921.5) recovered from Blanes Bay in the Mediterranean Sea (Fig. 4). They could belong to a new class, although the presence of refractive intracellular granules (Fig. 3, RCC 853) is quite reminiscent of what is observed in *Nannochloropsis*. Unfortunately, these strains have been lost in early 2007 following a breakdown in the air conditioning system of our culture facility. Their loss, which was almost the only one from a quite large collection, attests of their sensitivity to change in environmental conditions and may explain why representatives of this group have not been isolated before.

Three diatoms, belonging to the genera *Chaetoceros* (Fig. 3, RCC 1025), *Thalassiosira* and *Minutocellus* were obtained from the upwelling region. The latter strain is quite interesting since its very small size (about 3 μm) connects it to picoplankton. Two dinoflagellates belonging to the genus *Prorocentrum*, *P. minimum* (Fig. 3, RCC 922) and *P. dentatum*, were isolated from surface waters, east of the gyre.

Twelve heterotrophic strains from dark cultures growing on rice medium have been identified by their 18S rDNA sequences. Ten belong to the bicosoecid lineage of the stramenopiles. Three cultures are quite closely related to the genus *Caecitellus* and four more distantly related to *Cafeteria*. The two remaining strains were closely related to the bodonid (Euglenozoa) genera *Rhynchomonas* and *Neobodo*. All these heterotrophic genera are quite often recovered in cultures (Arndt et al., 2003).

4 Conclusions

Our large scale effort to isolate picoplanktonic strains from the Southeast Pacific Ocean allowed us to obtain of 212 novel cultures, a large number of which are of picoplanktonic size. The final number of cultures obtained is substantially higher than in previous efforts such as those linked to the PROSOPE and MINOS cruises in the Mediterranean Sea or the OLIPAC cruise in the Equatorial Pacific Ocean for which we obtained

between 46 and 90 strains for each (Vaulot et al., 2004). Our initial intent was to use mostly flow cytometry sorting to establish strains. However as we experienced technical problems with flow cytometry in the first few days of the cruise and as we observed subsequently that the yield of the initially sorted samples was quite low, we decided to combine flow cytometry sorting with more classical enrichments. This proved to be quite a good recipe. In particular sorting based on photosynthetic pigment fluorescence appears to be a good way to prevent contamination of cultures by heterotrophic eukaryotes, a problem plaguing some of our previous efforts. The application of sorting either before or after enrichment did not appear to affect dramatically the type of taxa isolated (see Table S1, Supplement: <http://www.biogeosciences.net/5/203/2008/bg-5-203-2008-supplement.pdf>).

The final diversity achieved is quite wide since we obtained representatives of most major photosynthetic divisions (Table 2). However it is clear that we globally failed to obtain representatives of environmental sequences for which no culture is available yet. One interesting group of novel cultures was constituted by stramenopile strains RCC 853 and 862 from the central gyre which sequences were closely related to an environmental sequence from the Mediterranean Sea (Fig. 4). Although these sequences had some affinities, based on BLAST, to Eustigmatophyceae and their morphology was somewhat similar to the latter, they probably belonged to a novel class. Despite the fact that further studies are prevented since these strains have been lost, the strategy used (flow cytometry sorting followed by serial dilution) could be tried again to re-isolate them. Another interesting group is constituted by 9 cultures originating from the region east of the gyre and from the upwelling that are related to *Prasinoderma* but form a new clade clearly separated from the species *P. coloniale* (Fig. 4). They could belong to a new species within the genus *Prasinoderma* or form a new genus. Interestingly, they are apparently not related to any published environmental sequence. All the other cultures obtained are related to described species or at least to established cultures. In particular, we have been successful at re-isolating two genera *Bolidomonas* and *Florenciella* that our group had previously isolated and described (Eikrem et al., 2004; Guillou et al., 1999), but that had never been obtained again in culture since their initial isolation. Interestingly, *B. pacifica* was initially isolated from exactly the same region (between 2 and 16° S) as the new strain (9° S). In contrast, the only *F. parvula* strain available previously originated from English Channel coastal waters, a very different environment from that of the new strains. Moreover the 18S sequences of the latter differ slightly from that of *F. parvula* and they could belong to a novel species within this genus. Some of the cultures recovered correspond to ubiquitous species that were obtained from a wide range of environments. This is in particular the case for the two Haptophyta genera *Emiliania*, isolated from two of the four major regions investigated (Marquesas, east of gyre) and *Phaeocystis* isolated from three regions

(Marquesas, east of the gyre, Chilean upwelling) mostly in surface waters. For the latter genus, our strains may correspond to at least two different species, *P. globosa* and *P. jahni*. However, the largest number of strains obtained for a single taxon correspond to *Pelagomonas* isolated from a record of 13 different samples along the entire cruise track ranging from oligotrophic (St B13) to eutrophic (UPX) and from surface (5 m) to very deep (160 m) samples. Although the similarity of their 18S rRNA gene sequence is very high, it is likely that these strains present quite different growth responses to factors such as nitrogen supply or light levels and belong to different ecotypes, as observed previously for example for the genus *Ostreococcus* (Rodríguez et al., 2005).

From a biogeographic point of view, it is quite difficult to make any firm conclusion from this work. Many cultures belonging to a given taxonomic group were isolated from a variety of conditions and no specific pattern could be uncovered. Although there were some taxa unique to the central part of the gyre itself (Stations 3 to 15) such as *Prasinococcus* and the potentially novel class mentioned earlier, one should emphasize the low number of strains isolated from this region. This is probably linked to the fact that the media we used (K, Pro2), that are quite successful in general to isolate and maintain a wide variety of picophytoplankton strains, fail to mimic the drastic oligotrophic conditions met in the gyre. Moreover future isolation effort may need to involve new culture approaches (Zengler et al., 2002) such as those successful to isolate fastidiously growing bacterial strains from the open ocean environment such as *Pelagibacter ubique* (aka SAR11) that had escaped cultivation for quite a long time (Rappé et al., 2002).

Acknowledgements. We wish to thank the crew of the NO Atalante for their critical help in repairing the FACSARIA flow cytometer during the cruise as well as for their constant availability. We are grateful to all participants to the BIOSOPE cruise, especially to H. Claustre and A. Sciandra, who coordinated the cruise and acted as chief scientists. Help for microscopy from F. Jouenne is kindly acknowledged. L. Guillou provided very helpful comments on several versions of the paper. Financial support for this work was provided by the following programs and companies: ANR Biodiversité (project PICOFUNPAC), CNRS INSU PROOF, Contrat de Plan Etat Région (Souchothèque de Bretagne), Becton Dickinson.

Edited by: A. Boetius

References

- Andersen, R. A., Saunders, G. W., Paskind, M. P., and Sexton, J.: Ultrastructure and 18S rRNA gene sequence for *Pelagomonas calceolata* gen. and sp. nov. and the description of a new algal class, the Pelagophyceae *classis nov.*, *J. Phycol.*, 29, 701–715, 1993.
- Arndt, H., Hausmann, K., and Wolf, M.: Deep-sea heterotrophic nanoflagellates of the Eastern Mediterranean Sea: qualitative and quantitative aspects of their pelagic and benthic occurrence, *Mar. Ecol. Prog. Ser.*, 256, 45–56, 2003.
- Claustre, H., Sciandra, A., and Vault, D.: Introduction to the special section: bio-optical and biogeochemical conditions in the South East Pacific in late 2004 – the BIOSOPE program, *Biogeosciences Discuss.*, 5, 605–640, 2008, <http://www.biogeosciences-discuss.net/5/605/2008/>.
- Cowling, A. J.: Free-living heterotrophic flagellates: methods of isolation and maintenance, including sources of strains in culture, in: *The Biology of Free-Living Heterotrophic Flagellates*, edited by: Patterson, D. J. and Larsen, J., Clarendon Press, 477–492, 1991.
- Derelle, E., Ferraz, C., Rombauts, S., Rouze, P., Worden, A. Z., Robbens, S., Partensky, F., Degroeve, S., Echeynie, S., Cooke, R., Saeys, Y., Wuyts, J., Jabbari, K., Bowler, C., Panaud, O., Piegue, B., Ball, S. G., Ral, J.-P., Bouget, F.-Y., Piganeau, G., De Baets, B., Picard, A., Delseny, M., Demaille, J., Van de Peer, Y., and Moreau, H.: Genome analysis of the smallest free-living eukaryote *Ostreococcus tauri* unveils many unique features, *Proc. Natl. Acad. Sci. USA*, 103, 11 647–11 652, 2006.
- Doyle, J. J. and Doyle, J. L.: Isolation of plant DNA from fresh tissue, *Focus*, 12, 13–15, 1990.
- Eikrem, W., Romari, K., Latasa, M., Le Gall, F., Throndsen, J., and Vault, D.: *Florenciella parvula* gen. and sp. nov. (Dictyochophyceae, Heterokontophyta) a small flagellate isolated from the English Channel, *Phycologia*, 43, 658–668, 2004.
- Elwood, H. J., Olsen, G. J., and Sogin, M. L.: The small-subunit ribosomal RNA gene sequences from the hypotrichous ciliates *Oxytricha nova* and *Stylonychia pustulata*, *Mol. Biol. Evol.*, 2, 399–410, 1985.
- Fuller, N. J., Marie, D., Partensky, F., Vault, D., Post, A. F., and Scanlan, D. J.: Clade-specific 16S ribosomal DNA oligonucleotides reveal the predominance of a single marine *Synechococcus* clade throughout a stratified water column in the Red Sea, *Appl. Environ. Microbiol.*, 69, 2430–2443, 2003.
- Guillou, L., Chrétiennot-Dinet, M.-J., Medlin, L. K., Claustre, H., Loiseaux-de Goër, S., and Vault, D.: *Bolidomonas*: a new genus with two species belonging to a new algal class, the Bolidophyceae (Heterokonta), *J. Phycol.*, 35, 368–381, 1999.
- Guillou, L., Eikrem, W., Chrétiennot-Dinet, M. J., Le Gall, F., Masana, R., Romari, K., Pedrós-Alió, C., and Vault, D.: Diversity of picoplanktonic prasinophytes assessed by direct nuclear SSU rDNA sequencing of environmental samples and novel isolates retrieved from oceanic and coastal marine ecosystems, *Protist*, 155, 193–214, 2004.
- Hasegawa, T., Miyashita, H., Kawachi, M., Ikemoto, H., Kurano, N., Miyachi, S., and Chihara, M.: *Prasinoderma coloniale* gen. nov. et sp. nov., a new pelagic coccoid prasinophyte from the western Pacific Ocean, *Phycologia*, 35, 170–176, 1996.
- Henley, W. J., Hironaka, J. L., Guillou, L., Buchheim, M. A., Buchheim, J. A., Fawley, M. W., and Fawley, K. P.: Phylogenetic analysis of the ‘*Nannochloris*-like’ algae and diagnoses of *Picochlorum oklahomensis* gen. et sp. nov. (Trebouxiophyceae, Chlorophyta), *Phycologia*, 43, 641–652, 2004.
- Herbland, A., Le Bouteiller, A., and Raimbault, P.: Size structure of phytoplankton biomass in the equatorial Atlantic Ocean, *Deep-Sea Res. I*, 32, 819–836, 1985.
- Houdan, A., Billard, C., Marie, D., Not, F., Saez, A. G., Young, J. R., and Probert, I.: Holococcolithophore-heterococcolithophore

- (Haptophyta) life cycles: flow cytometric analysis of relative ploidy levels, *Syst. Biodivers.*, 4, 453–465, 2003.
- Johnson, P. W. and Sieburth, J. M.: *In-situ* morphology and occurrence of eucaryotic phototrophs of bacterial size in the picoplankton of estuarine and oceanic waters, *J. Phycol.*, 18, 318–327, 1982.
- Johnson, Z. I., Zinser, E. R., Coe, A., McNulty, N. P., Woodward, E. M. S., and Chisholm, S. W.: Niche partitioning among *Prochlorococcus* ecotypes along ocean-scale environmental gradients, *Science*, 311, 1737–1740, 2006.
- Keller, M. D., Selvin, R. C., Claus, W., and Guillard, R. R. L.: Media for the culture of oceanic ultraphytoplankton, *J. Phycol.*, 23, 633–638, 1987.
- Li, W. K. W., Subba Rao, D. V., Harrison, W. G., Smith, J. C., Cullen, J. J., Irwin, B., and Platt, T.: Autotrophic picoplankton in the tropical ocean, *Science*, 219, 292–295, 1983.
- López-García, P., Rodríguez-Valera, F., Pedrós-Alió, C., and Moreira, D.: Unexpected diversity of small eukaryotes in deep-sea Antarctic plankton. *Nature*, 409, 603–607, 2001.
- Ludwig, W., Strunk, O., Westram, R., Richter, L., Meier, H., Yad-hukumar, Buchner, A., Lai, T., Steppi, S., Jobb, G., Forster, W., Brettske, I., Gerber, S., Ginhart, A. W., Gross, O., Grumann, S., Hermann, S., Jost, R., König, A., Liss, T., Lussmann, R., May, M., Nonhoff, B., Reichel, B., Strehlow, R., Stamatakis, A., Stuckmann, N., Vilbig, A., Lenke, M., Ludwig, T., Bode, A., and Schleifer, K. H.: ARB: a software environment for sequence data, *Nucleic Acids Res.*, 32, 1363–1371, 2004.
- Marie, D., Zhu, F., Balagué, V., Ras, J., and Vaulot, D.: Eukaryotic picoplankton communities of the Mediterranean Sea in summer assessed by molecular approaches (DGGE, TTGE, QPCR), *FEMS Microbiol. Ecol.*, 55, 403–415, 2006.
- Masquelier, S. and Vaulot, D.: Distribution of micro-organisms along a transect in the South-East Pacific Ocean (BIOSCOPE cruise) from epifluorescence microscopy, *Biogeosciences Discuss.*, 4, 2667–2697, 2007, <http://www.biogeosciences-discuss.net/4/2667/2007/>.
- Miyashita, H., Ikemoto, H., Kurano, N., Miyachi, S., and Chihara, M.: *Prasinococcus capsulatus* gen. et sp. nov., a new marine coccoid prasinophyte, *J. Gen. Appl. Microbiol.*, 39, 571–582, 1993.
- Moon-van der Staay, S. Y., De Wachter, R., and Vaulot, D.: Oceanic 18S rDNA sequences from picoplankton reveal unsuspected eukaryotic diversity, *Nature*, 409, 607–610, 2001.
- Moon-van der Staay, S. Y., van der Staay, G. W. M., Guillou, L., Vaulot, D., Claustre, H., and Medlin, L. K.: Abundance and diversity of prymnesiophytes in the picoplankton community from the equatorial Pacific Ocean inferred from 18S rDNA sequences, *Limnol. Oceanogr.*, 45, 98–109, 2000.
- Moore, L. R. and Chisholm, S. W.: Photophysiology of the marine cyanobacterium *Prochlorococcus*: Ecotypic differences among cultured isolates, *Limnol. Oceanogr.*, 44, 628–638, 1999.
- Nägeli, C.: Gattungen einzelliger Algen physiologisch und systematisch bearbeitet, 139 pp., 1849.
- Not, F., Valentin, K., Romari, K., Lovejoy, C., Massana, R., Töbe, K., Vaulot, D., and Medlin, L.: Picobiliphytes, a new marine picoplanktonic algal group with unknown affinities to other eukaryotes, *Science*, 315, 252–254, 2007.
- Not, F., Massana, R., Latasa, M., Marie, D., Colson, C., Eikrem, W., Pedrós-Alió, C., Vaulot, D., and Simon, N.: Late summer community composition and abundance of photosynthetic picoeukaryotes in Norwegian and Barents seas, *Limnol. Oceanogr.*, 50, 1677–1686, 2005.
- Palenik, B., Brahmsha, B., Larimer, F. W., Land, M., Hauser, L., Chain, P., Lamerdin, J., Regala, W., Allen, E. E., McCarren, J., Paulsen, I., Dufresne, A., Partensky, F., Webb, E. A., and Waterbury, J.: The genome of a motile marine *Synechococcus*, *Nature*, 424, 1037–1042, 2003.
- Palenik, B., Grimwood, J., Aerts, A., Rouze, P., Salamov, A., Putnam, N., Dupont, C., Jorgensen, R., Derelle, E., Rombauts, S., Zhou, K., Otillar, R., Merchant, S. S., Podell, S., Gaasterland, T., Napoli, C., Gendler, K., Manuell, A., Tai, V., Vallon, O., Piganeau, G., Jancek, S., Heijde, M., Jabbari, K., Bowler, C., Lohr, M., Robbins, S., Werner, G., Dubchak, I., Pazour, G. J., Ren, Q., Paulsen, I., Delwiche, C., Schmutz, J., Rokhsar, D., Van de Peer, Y., Moreau, H., and Grigoriev, I. V.: The tiny eukaryote *Ostreococcus* provides genomic insights into the paradox of plankton speciation, *Proc. Natl. Acad. Sci. USA*, 104, 7705–7710, 2007.
- Platt, T., Subba-Rao, D. V., and Irwin, B.: Photosynthesis of picoplankton in the oligotrophic ocean, *Nature*, 300, 701–704, 1983.
- Pruesse, E., Quast, C., Knittel, K., Fuchs, B. M., Ludwig, W., Peplies, J., and Glockner, F. O.: SILVA: a comprehensive online resource for quality checked and aligned ribosomal RNA sequence data compatible with ARB, *Nucleic Acids Res.*, 35, 7188–7196, 2007.
- Rappé, M. S., Connon, S. A., Vergin, K. L., and Giovannoni, S. J.: Cultivation of the ubiquitous SAR11 marine bacterioplankton clade, *Nature*, 418, 630–633, 2002.
- Rippka, R., Coursin, T., Hess, W., Lichtle, C., Scanlan, D. J., Palinska, K. A., Itean, I., Partensky, F., Houmard, J., and Herdman, M.: *Prochlorococcus marinus* Chisholm et al. 1992 subsp. *pastoris* subsp. nov. strain PCC 9511, the first axenic chlorophyll a_2/b_2 -containing cyanobacterium (Oxyphotobacteria), *Int. J. Syst. Evol. Microbiol.*, 50, 1833–1847, 2000.
- Rocap, G., Distel, D. L., Waterbury, J. B., and Chisholm, S. W.: Resolution of *Prochlorococcus* and *Synechococcus* ecotypes by using 16S-23S ribosomal DNA internal transcribed spacer sequences, *Appl. Environ. Microbiol.*, 68, 1180–1191, 2002.
- Rocap, G., Larimer, F. W., Lamerdin, J., Malfatti, S., Chain, P., Ahlgren, N. A., Arellano, A., Coleman, M., Hauser, L., Hess, W. R., Johnson, Z. I., Land, M., Lindell, D., Post, A. F., Regala, W., Shah, M., Shaw, S. L., Steglich, C., Sullivan, M. B., Ting, C. S., Tolonen, A., Webb, E. A., Zinser, E. R., and Chisholm, S. W.: Genome divergence in two *Prochlorococcus* ecotypes reflects oceanic niche differentiation, *Nature*, 424, 1042–1047, 2003.
- Rodríguez, F., Derelle, E., Guillou, L., Le Gall, F., Vaulot, D., and Moreau, H.: Ecotype diversity in the marine picoeukaryote *Ostreococcus* (Chlorophyta, Prasinophyceae), *Environ. Microbiol.*, 7, 853–859, 2005.
- Romari, K. and Vaulot, D.: Composition and temporal variability of picoeukaryote communities at a coastal site of the English Channel from 18S rDNA sequences, *Limnol. Oceanogr.*, 49, 784–798, 2004.
- Sieburth, J. M., Smetacek, V., and Lenz, J.: Pelagic ecosystem structure: heterotrophic compartments of the plankton and their relationship to plankton size fractions, *Limnol. Oceanogr.*, 23, 1256–1263, 1978.
- Tamura, K., Dudley, J., Nei, M., and Kumar, S.: MEGA4: Molecular Evolutionary Genetics Analysis (MEGA) Software Version

- 4.0, Mol. Biol. Evol., msm092, 2007.
- Vaulot, D., Le Gall, F., Marie, D., Guillou, L., and Partensky, F.: The Roscoff Culture Collection (RCC): a collection dedicated to marine picoplankton, *Nova Hedwigia*, 79, 49–70, 2004.
- Waterbury, J. B., Watson, S. W., Guillard, R. R. L., and Brand, L. E.: Wide-spread occurrence of a unicellular, marine planktonic, cyanobacterium, *Nature*, 277, 293–294, 1979.
- Zengler, K., Toledo, G., Rappe, M., Elkins, J., Mathur, E. J., Short, J. M., and Keller, M.: Cultivating the uncultured, *Proc. Natl. Acad. Sci. USA*, 99, 15 681–15 686, 2002.
- Zingone, A., Chrétiennot-Dinet, M. J., Lange, M., and Medlin, L.: Morphological and genetic characterization of *Phaeocystis cordata* and *P. jahmii* (Prymnesiophyceae), two new species from the Mediterranean Sea, *J. Phycol.*, 35, 1322–1337, 1999.

Calcite production by coccolithophores in the south east Pacific Ocean

L. Beaufort¹, M. Couapel¹, N. Buchet¹, H. Claustre², and C. Goyet³

¹CEREGE, Aix-Marseille Université – CNRS, BP80 cedex4, 13545 Aix en Provence, France

²CNRS, Laboratoire d’océanographie de Villefranche, 06230 Villefranche-sur-Mer, France; Université Pierre et Marie Curie-Paris 6, Laboratoire d’océanographie de Villefranche, 06230 Villefranche-sur-Mer, France

³Université de Perpignan, 52, Avenue Paul Alduy, 66860 Perpignan, France

Received: 5 September 2007 – Published in Biogeosciences Discuss.: 17 September 2007

Revised: 10 June 2008 – Accepted: 3 July 2008 – Published: 4 August 2008

Abstract. BIOSOPE cruise covered an oceanographic transect through the centre of the South Pacific Gyre (SPG) from the Marquesas archipelago to the Peru-Chile upwelling (PCU). Water samples from 6 depths in the euphotic zone were collected at 20 stations. The concentrations of suspended calcite particles, coccolithophores cells and detached coccoliths were estimated together with size and weight using an automatic polarizing microscope, a digital camera, and a collection of softwares performing morphometry and pattern recognition. Some of these softwares are new and described here for the first time. The coccolithophores standing stocks were usually low and reached maxima west of the PCU. The coccoliths of *Emiliania huxleyi*, *Gephyrocapsa* spp. and *Crenalithus* spp. (Order Isochrysidales) represented more than 30% of all the suspended calcite particles detected in the size range 0.1–46 μm (22% of PIC in term of calcite weight). These species grew preferentially in the Chlorophyll maximum zone. In the SPG their maximum cell concentrations were recorded between depth of 150 and 200 m, which is unusually deep for these taxa. The weight of coccoliths and coccospheres were correlated to their size. Large and heavy coccoliths and coccospheres were found in regions with relatively high fertility in the Marquesas Island and in the PCU. Small and light coccoliths and coccospheres were found west of the PCU. This distribution is strongly related to ocean chemistry in particular to alkalinity and to carbonate ions concentration. The biotic (coccolithophores production) influence on calcification is mainly driven at the local scale (depth) whereas the abiotic (carbonate chemistry) plays its most important role at the regional (horizontal) level. Here 94% of the variability of coccolith and coccosphere weight can be explained by a change in 7 environmental variables.

1 Introduction

Coccolithophores represent an important group of unicellular algae. They are abundant both at high latitudes, where they form large blooms detectable by satellites (Brown and Yoder, 1994; Balch et al., 2007), and at low latitudes in oligotrophic (e.g. Okada and McIntyre, 1979; Winter et al., 1994) and upwelling (e.g. Winter et al., 1994; Giraudeau and Bailley, 1995) areas. They are responsible for about half of the total oceanic carbonate production (Milliman, 1993). Carbonate precipitation, settling (including ballasting aggregates containing organic matter), burial, and dissolution are key processes of the oceanic carbon cycle (e.g. Archer et al., 2000). Yet, despite their major role in the CO₂ cycle, many aspects of calcite production by coccolithophores are not well constrained. In particular the environmental impact on the secretion of coccoliths are poorly understood because direct field observations are scarce (Balch and Kilpatrick, 1996). Several laboratory and mesocosms experiments have shown a decrease in the production of calcium carbonate by coccolithophores when atmospheric CO₂ increases (e.g. Riebesell et al., 2000; Engel et al., 2005). This is because an increase of CO₂ in the atmosphere causes a decrease of oceanic water pH, with potentially dramatic consequences for oceanic calcifiers (Feely et al., 2004; Orr et al., 2005). It is therefore critical to determine how coccolithophores are calcifying in today’s Ocean.

The South Pacific Gyre (SPG) is the most oligotrophic and one of the least sampled ocean areas (Claustre and Martorena, 2003), particular for coccolithophores. The primary objective of BIOSOPE (Biogeochemistry and Optics South Pacific Experiment) was to study the South Pacific Gyre along a transect through the central part of the SPG to the Peru-Chile Upwelling (PCU). The Isochrysidales represent, numerically, the most important order of coccolithophores. We document, along this transect, variations of



Correspondence to: L. Beaufort
(beaufort@cerege.fr)

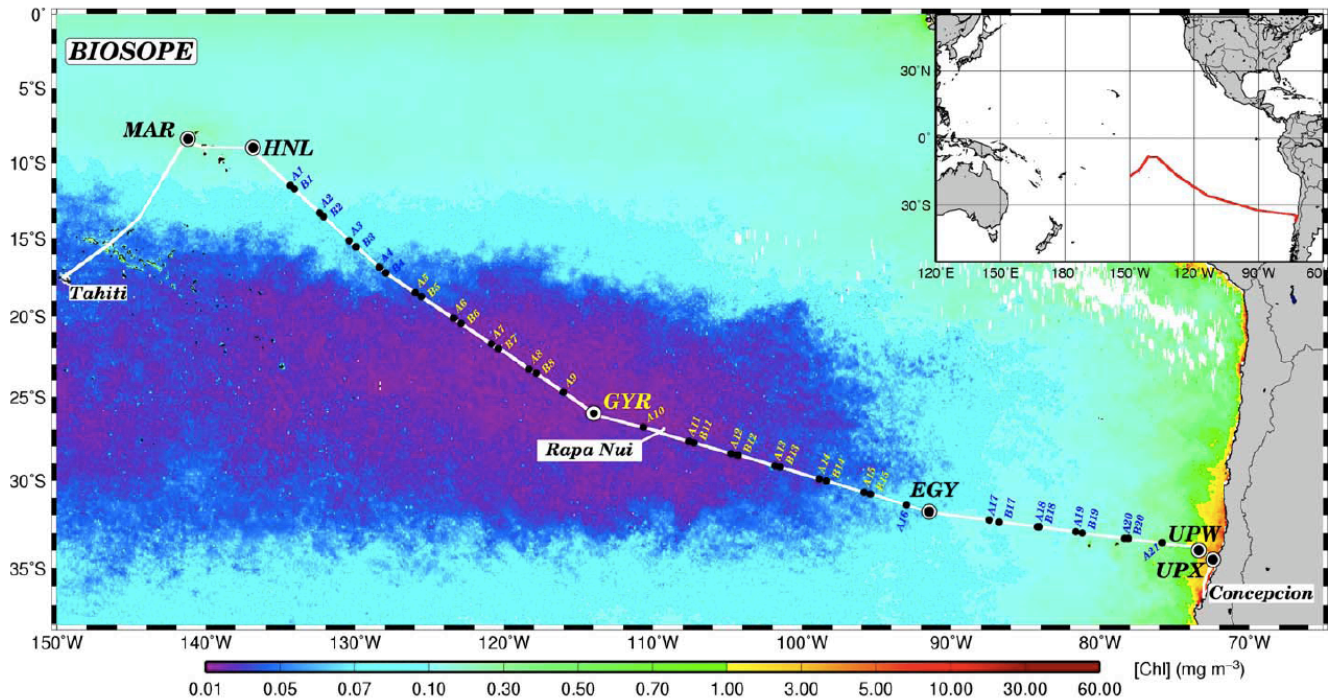


Fig. 1. Location map showing the transect and stations where water samples were taken at 6 depths, superimposed on the SeaWiFS composite (November–December 2004) for surface Chlorophyll concentration. Inset: geographic location of the transect in the Pacific Ocean.

Isochrysidales standing stock, as well as the absolute abundance of detached coccoliths and other small suspended calcite particles. The calcite stock produced by Isochrysidales was estimated using recently developed methods based both on microscopy automation and the birefringence properties of calcite. The size and weight of the coccospheres and coccoliths, was investigated in order to describe how Isochrysidales were calcifying in contrasting natural trophic environments, in particular in relation to calcite saturation state.

2 1-Material and methods

2.1 Setting

The BIOSOPE cruise (26 October to 11 December 2004) was conducted on board RV Atalante and covered a transect of about 8000 km in the South East Pacific. This enabled us to sample a full oceanic spectrum from the most oligotrophic oceanic waters in the south Pacific gyre to the fertile coastal waters of Chile (Fig. 1). Two features may explain why the broad South Pacific Gyre possesses the lowest surface chlorophyll concentration estimated through satellite imagery ($0.019 \text{ mg Chl-}a \text{ m}^{-3}$). It has the largest pycnocline depth recorded in the world ocean hydrological database ($>200 \text{ m}$), and the flux of atmospheric dust (e.g., iron) is extremely low (Claustre et al., 2008). In contrast, the PCU sys-

tem and the Marquesas archipelago (sub-equatorial area) are bathed by nutrient richer waters.

The sea surface temperature and salinity recorded during the cruise varied between 13° and 28°C and from 34 to 36.5, respectively, with higher values toward the west and lower values toward the east.

2.2 Sampling

Twenty stations were sampled for biogeochemical parameters (Claustre et al., 2008). At every station, samples for coccolithophores were taken depending on the position of the Deep Chlorophyll Maximum (DCM). At most stations, water samples were taken at 6 water depths: one sample at 5 m (i.e., just below the surface), two samples between 5 m and the DCM, one sample at the DCM, and two samples below the DCM. The DCM is located near the pycnocline which is considered as one of most important ecological boundaries in the ocean (Longhurst, 1998). The sampling strategy thus enabled us to study coccolithophores above and below this significant ecotone. In most cases, four liters of seawater were filtered on a nitrate cellulose membrane (47 mm diameter) having a pore size of $0.45 \mu\text{m}$. The membranes were quickly dried and stored at room temperature. Once in the laboratory, a quarter of each membrane was mounted between slide and cover slip and fixed with Canada balsam, which rendered the

membrane optically transparent. Additionally a small fragment of the filter was examined using a Hitachi 3000N Scanning Electron Microscope (SEM).

At the last four stations of the transect (i.e. in the PCU) the filter membrane diameter was 23 mm. Four liters of water were still filtered so the amount of particles on these filters was extremely high, leading to the possibility that significant amounts of coccoliths were concealed by large particles. Thus absolute abundances could not be reliably estimated for these stations.

2.3 Coccolithophore determination and species counts

The composition of the coccolithophore assemblages was determined using SEM at magnification of about 6000x and a Polarizing Microscope (PM) Zeiss Axioscop at a magnification of 1000x. Species abundances were estimated by counting more than 300 coccospheres in counted field of views (70 on average). The number of field of view was never lower than 10 even when coccolithophores were abundant on the PM.

2.4 Grabbing frames

A Polarizing Microscope (LEICA DMRBE) with a 50X oil immersion objective was used for automatic scanning of the microscope preparations in cross-polarized light. Microscope stage motions and focus were automated. For each sample, a 2 Megapixel Spot Insight camera grabbed forty fields of view. Each frame is $240 \times 180 \mu\text{m}^2$ with a pixel area of $0.0225 \mu\text{m}^2$. The amount of light going through the sample was held constant.

2.5 Analyzing calcite particles:

We developed a new software using routine LabView (National Instruments) that automatically detects and measures all birefringent particles from grabbed frames, hereafter called “*Particle Analyser*”. It takes advantage of the fact that some crystals are birefringent (they are illuminated in cross-polarized light) whereas other crystals and the preparation background remain dark. There is a relation between the thickness and the brightness of crystals, which can after calibration be expressed as a transfer function (Beaufort, 2005). The *Particle Analyser* opens all the frames in a sample, counts the number of objects brighter than background, and measures their surface. We placed a lower threshold at 3 pixels ($0.07 \mu\text{m}^2$) to get rid off background noise; and set an upper threshold at 74000 pixels ($1683 \mu\text{m}^2$ equivalent to circular particles having a $46 \mu\text{m}$ diameter; e.g., a foraminifera). This upper-threshold is high enough to include all particles in the size range of nanoplankton, including aggregates. The number (N) of particles ml^{-1} is calculated by

$$N = N_t \cdot S_m / (N_f \cdot S_f \cdot V_f) \quad (1)$$

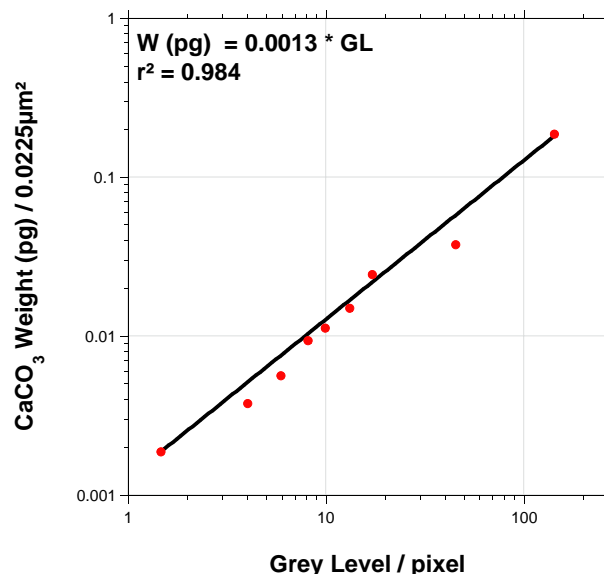


Fig. 2. Transfer function of Grey Levels into calcite weight. The x-axis represents the Grey Level value measure on average of one pixel. The y-axis gives the calcite weight (in pg) put onto the membrane per surface unit (here the area of one pixel). The line represents the best regression going through the origin.

where V_f is the volume filtered in milliliter, S_m is the surface area of the membrane, N_f is the number of the grabbed frames, S_f is the surface area of the grabbed frames, and N_t is the total number of particles analysed per sample.

The *Particle Analyser* automatically measures the “lightness” (L) of all frames as the sum of all grey levels (GL) pixel values. A transfer function was established following the protocol established in (Beaufort, 2005), but applied to samples prepared with cellulosic membranes instead of smear slides. In recalibrating we poured different (precisely weighted) amounts of pure calcite powder into known volumes of water. These suspensions were filtered on membranes of the same type as used for the BIOSOPE samples, and processed as described above. The relation between GL and weight on the membrane now serves as a transfer function (Fig. 2).

$$w = 0.0013 \cdot GL \quad (2)$$

where w is the weight in pg per pixel ($0.0225 \mu\text{m}^2$).

The calcite weight ml^{-1} (W) is calculated as following:

$$W = w \cdot N_p \cdot S_m / (N_f \cdot S_f \cdot V_f) \quad (3)$$

Where N_p is the number of pixel per frame ($=2 \cdot 10^6$). The values are given in pg ml^{-1} . Particulate Inorganic Carbon (PIC) is often given in $\text{mmol CaCO}_3 \text{m}^{-3}$. PIC values for the fraction $<46 \mu\text{m}$ ($\text{PIC}_{<46\mu}$) in this unit are obtained by dividing W by 10^5 .

Four different sources of error may be associated with this method:

1. The main source of error results from the patchiness of the distribution of particles on the membrane. Only a portion of the membrane is measured.
2. The error on the estimate of the light measure is extremely small and considered negligible.
3. High sediment loads on the membrane produce particle aggregation and is a potential source of error (underestimation of the weight) but for the open ocean waters investigated during BIOSOPE this problem did not occur.
4. Focus may be the cause of a small error on absolute values. Frames out of focus were excluded from the analysis.

The overall error associated with this method when dealing with carbonated sediments is estimated at ~12% (Beaufort, 2005), although no estimate regarding the measurements of PIC from water samples is available as yet.

2.6 Automated analysis of coccoliths and coccosphears: taxonomic recognition and size analysis

Coccoliths and coccosphears were automatically detected by SYRACO, a software developed in C++ at CEREGE (Dollfus and Beaufort, 1999; Beaufort and Dollfus, 2004). Based on Artificial Neural Networks (ANN) SYRACO is adapted to pattern recognition. In this study the ANN has been trained by the SYRACO learning algorithm, on a training set composed of two classes: (1) elliptical placoliths (essentially *Emiliania huxleyi*, *Gephyrocapsa oceanica* and other small placoliths in the genus *Gephyrocapsa* and *Crenalithus*; or *Reticulofenestra* for some authors), and (2) spherical coccosphears smaller than 10 μm in diameter bearing relatively birefringent, elliptical placoliths having a size of about 1/2 to 1/4 of the coccosphere. The great majority of taxa having these characteristics belongs to the Order of Isochrysidales. The training set is a monospecific sample from the Southern Indian Ocean with only coccosphears of *E. huxleyi*. However ANN has a large generalisation capability such that the coccosphere recognition used here is not species specific. Coccosphears from other orders (Syracosphaerales, Zygodiscales and Coccolithales) are generally not recognized by this ANN.

Because of the large generalisation capability of the ANN, a significant number of objects that resemble somewhat the targeted pattern are also included in the specific output frames. In the case of coccosphears, these foreign objects are “manually” erased from the frame. For the coccoliths, they are automatically eliminated from the analysis by a new software developed in LabView.

This software, hereafter called “*Coccolith Analyser*”, automatically measures coccoliths and coccosphears. It reads output frames where all the objects recognized as coccoliths are stored and analyses all of them. “*Coccolith Analyser*” is able to identify coccoliths based on 4 landmarks. If it determines that an object in the frame possesses these 4 landmarks, then it identifies it as a coccolith. If, on the contrary, it determines that an object does not possess these 4 landmarks, it discards the latter. With “*Coccolith Analyser*”, all objects incorrectly identified as coccoliths by SYRACO are eliminated. In the case of coccosphears, all the objects that were incorrectly identified as coccosphears by SYRACO were erased manually with “Adobe Photoshop” from the frames (we haven’t design yet a software capable to detect true coccosphere).

To check the reliability of SYRACO’s in estimating the abundance of coccosphears of Isochrysidales species in our samples, we compared SYRACO’s data with estimates based on direct counts of coccosphears using a polarizing microscope. We found that the two (automated and manual) estimates are highly correlated ($R=0.95$) (Fig. 3a). A slope of 2.2 could be interpreted as indicative that SYRACO misses about half of the coccosphears, but this is not the case. This slope reflects the fact that only few samples were taken at 4 stations (STB15 to STB18) located between 90 and 100° W an area where *E. huxleyi* coccosphears are extremely abundant and often contiguous. SYRACO is not capable of deciphering coccosphears in such groups. If the results from these 4 stations are excluded, the slope of the regression line is 0.98, indicating that the number of coccosphears of Isochrysidales species recognized by SYRACO is the same as recognized by direct human counts. Incidentally, this excellent fit confirms that only Isochrysidales are recognized by SYRACO (the slope is 1.75 when the entire (including not only the Isochrysidales but all the taxa) coccolithophore assemblage counted by human is used for comparison with SYRACO counts) (Fig. 3b). We estimated the abundance of coccoliths by directly counting the number of coccoliths contained in more than 10 fields of view ($=0.01 \text{ mm}^2$) in a total of 36 samples. Our estimates were then compared with those obtained by SYRACO. The estimates of coccolith abundance are significantly correlated for all stations (except STB15 to STB18), with a slope close to 1 and a $R>0.9$. For stations STB15 to STB18 the abundance of coccoliths was often $>800 \text{ ml}^{-1}$; aggregation of coccoliths prevents accurate counts of coccolith number in a frame by SYRACO. The abundance estimates reported in this paper are those determined by SYRACO for all samples except for those at Stations STB15 to STB18 for which manual counts were established. Our preference for SYRACO counts is that they are more representative of real values, counts being produced over a much larger area than is possible by humans. SYRACO counts are also more reproducible than human’s counts. It is important to note, however, that the patterns observed in BIOSOPE are the same whether established solely

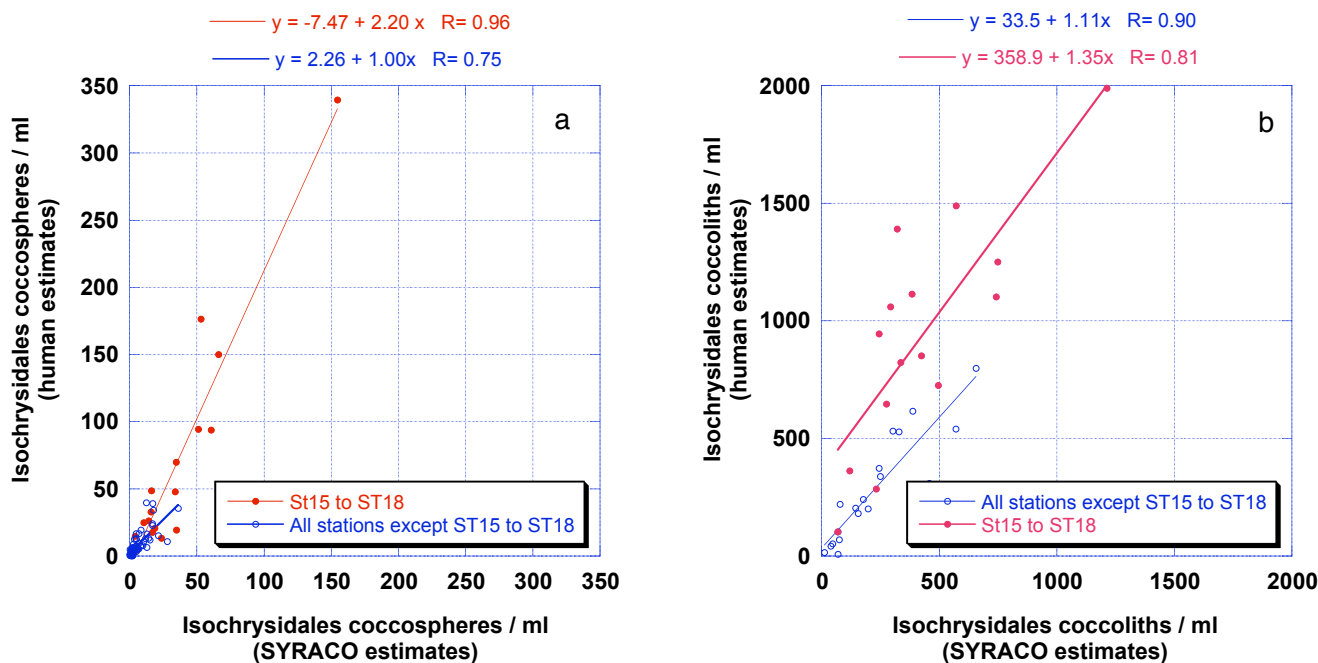


Fig. 3. Relation between “human” and “automated” (SYRACO) counts of Isochrysidales coccospheres (A) and coccoliths (B). In red are sample for 4 stations (STB15 to 18) where the density of Isochrysidales was too high (aggregation) for accurate automatic estimates. In blue are reported the other BIOSOPE stations.

from manual or automatic processes.

The *Coccolith Analyser* measures the grey level of objects, their diameter and surface, and tabulates the results. There is a bias of $0.6 \mu\text{m}$ in the measurement of the diameter of small, and dim objects, such as coccoliths. This is because we apply a minimum Grey Level threshold above background. This threshold erodes 2 pixels of the periphery of dim objects. Each pixel is $0.15 \mu\text{m}$, and 4 pixels are eroded in total when the long diameter is measured. Thus we added $0.6 \mu\text{m}$ to the measurement of coccolith length to compensate for this automatic loss. Another small bias in the measurements of the length of coccoliths of *E. huxleyi* exists, the distal shield being not detected in its entirety in cross-polarized light. Therefore the length of *E. huxleyi* presented here are slightly underestimated. We estimated this bias to a factor of 1.25 by comparing measures from the Coccolith analyzer and from SEM. The data presented here are uncorrected by this factor.

It should be noted that in the theoretical case of a pure *E. huxleyi* sample, the size distribution estimated by SYRACO would be narrower than that estimated with the *Calcite Analyser*. This is because SYRACO detects only well preserved, well-oriented and isolated coccoliths whereas the *Calcite Analyser* measures all particles, including aggregated, broken, out of focus and tilted coccoliths.

2.7 Chemical and physical parameters

The physical and chemical parameters used for comparison here were measured in situ during the cruise and are described in different papers in this volume. Temperature, salinity, fluorescence (Claustre et al., 2008) and backscattering (Twardowski et al., 2007) were measured precisely at location where water was collected for coccolithophores. Carbon chemistry was measured (Azouzi et al., 2007) at nearby locations but not exactly at the same water depth. We have selected the measurements available from the closest depths.

3 Results

3.1 Importance and composition of the Isochrysidales

Emiliania huxleyi and several species of the genera *Gephyrocapsa* and *Crenalithus* represent all the calcifying taxa of the marine Order Isochrysidales (de Vargas et al., 2007). SYRACO has been trained to recognize the Isochrysidales complex, which is therefore the focus of this paper. The specific composition of Isochrysidales varied significantly among BIOSOPE samples. Their variations have been studied in detail with both SEM and PM. East of Easter Island (about 110°W) the Isochrysidales dominated the coccolithophore community with relative abundance ranging from 60 to 100%. West of Easter Island the coccolithophore concentration diminished with the Isochrysidales representing

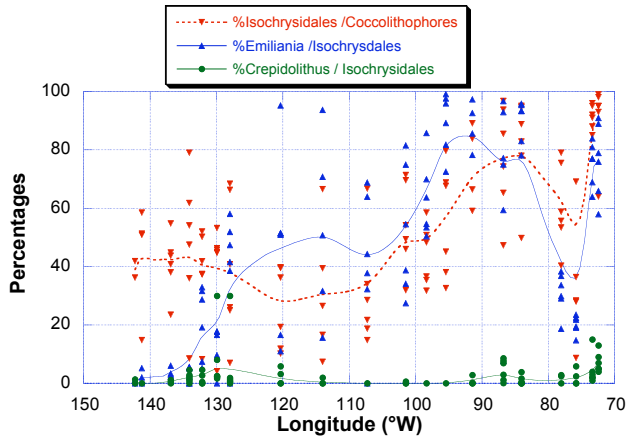


Fig. 4. Variations in the relative abundance of several coccolithophores taxa along the BIOSOPE transect. The data result from manual counts of coccospheres on the light microscope. The percentages of Isochrysidales in the coccolithophores are in red, the percentages of *E. huxleyi* in the Isochrysidales are in blue and the *Crepidolithus* (*Reticulofenestra* for some authors) are in green. The dots represent samples and the smooth lines show the stations means of these percentages.

40% on average of the coccolithophore community (Fig. 4). *Gephyrocapsa oceanica* dominated the Marquesas area. Between 130° W and 100° W the relative abundances of *Gephyrocapsa* and *Emiliania* were variable with a low number of *Emiliania*. From 100° W to the PCU, *Emiliania* dominated the communities. In some samples it constituted almost 100% of the coccolithophores. *Gephyrocapsa ericsonii* and *Crenalithus* always formed a minor part of the coccolithophore assemblages.

Because the version of SYRACO used in this study was trained to recognize only the coccoliths of the Order Isochrysidales, we relied on manual estimates for: 1) the percentages of the Isochrysidales coccospheres in the coccolithophores assemblages, and 2) the percentage of the various species in the Isochrysidales assemblages. To estimate the number of detached coccoliths of the different taxa, we combined the number of Isochrysidales coccoliths with our estimate of the coccolithophores taxonomic composition produced manually. Our first order assumption is that the number of detached coccoliths per coccosphere is the same in every species (which is not necessarily the case).

3.2 Spatial distribution of calcite particles

The concentrations of suspended calcite particles, and of detached coccoliths and coccospheres of the Isochrysidales Order showed very similar distribution patterns along the BIOSOPE transect (Fig. 5): maximum concentrations were found between 80° and 100° W, associated with the subtropical front (Claustre et al., 2008)

The concentration in coccospheres of Isochrysidales was generally low with an average of 11 ml^{-1} but it reached a maximum of 350 ml^{-1} in the eastern part of the transect, while the concentration of detached coccoliths ranged from 11 to $\sim 2000 \text{ ml}^{-1}$ with an average of 250. The concentration in suspended calcite particles was on average 733 ml^{-1} , and the total weight of calcite per milliliter was $11\,200 \text{ pg ml}^{-1}$ (or $\text{PIC}_{<46\mu} = 0.11 \text{ mmol CaCO}_3 \text{ m}^{-3}$). The corrected total weight of the Isochrysidales detached coccoliths and coccospheres was on average 2224 pg ml^{-1} (or $0.022 \text{ mmol CaCO}_3 \text{ m}^{-3}$), which represents 22% of the $\text{PIC}_{<46\mu}$. Large aggregates that may be rich in coccoliths composed a large part of remaining 78%.

The spatial distributions of coccospheres, detached coccoliths, and suspended calcite particles showed higher concentrations between 85° W and 100° W in the upper 80 m of the water column.

The observed pattern of density distribution of calcite particles is confirmed by the study of backscattering properties (Twardowski et al., 2007). The backscattering ratio (i.e. the ratio of backscattering to scattering) depends on the size distribution of particle assemblages (high when dominated by small particles and reciprocally) and on refractive index (high for particles with high refractive index, like calcite). This ratio approximately scales with the number of suspended calcite particles and the PIC estimated by the “*Calcite Analyser*” more specifically, it exhibits the two prominent scatterers of coccoliths at the exact same position than shown in the present analysis, and confirms the relative “patchy” distribution of these biogenic particles.

3.3 Grain size distribution of suspended calcite particles, detached coccoliths and coccospheres

Ninety five percent of the 416 000 suspended calcite particles analyzed from the BIOSOPE samples had a surface area $< 20 \mu\text{m}^2$ or a diameter $< 5 \mu\text{m}$ (in the 0.1–46 μm range). Their size distribution was unimodal and slightly skewed toward larger particles, with a mode at $3.2 \mu\text{m}^2$ (Fig. 6a). The distributions of detached coccoliths and coccospheres was also unimodals with modes at $3.2 \mu\text{m}^2$ and $40 \mu\text{m}^2$, respectively (Fig. 6a). Interestingly, the mode of the suspended calcite particles was the same as that of the detached coccoliths of Isochrysidales species. The number of detached coccoliths (mostly *E. huxleyi*, a few *Gephyrocapsa* and rare *Crenalithus*) represented 1/3 of all suspended calcite particles. At locations where coccoliths and coccospheres were extremely abundant, for instance at 30 m at Station 18 which corresponded to an almost monospecific bloom of *E. huxleyi*, the distribution of calcite particles and of coccoliths/coccospheres were very similar (Fig. 6b).

The concentrations of coccoliths are significantly correlated with the concentrations of calcite particles detected by the *Calcite Analyser* (Fig. 7). The Isochrysidales taxa, and in particular *E. huxleyi*, are the most important contributor

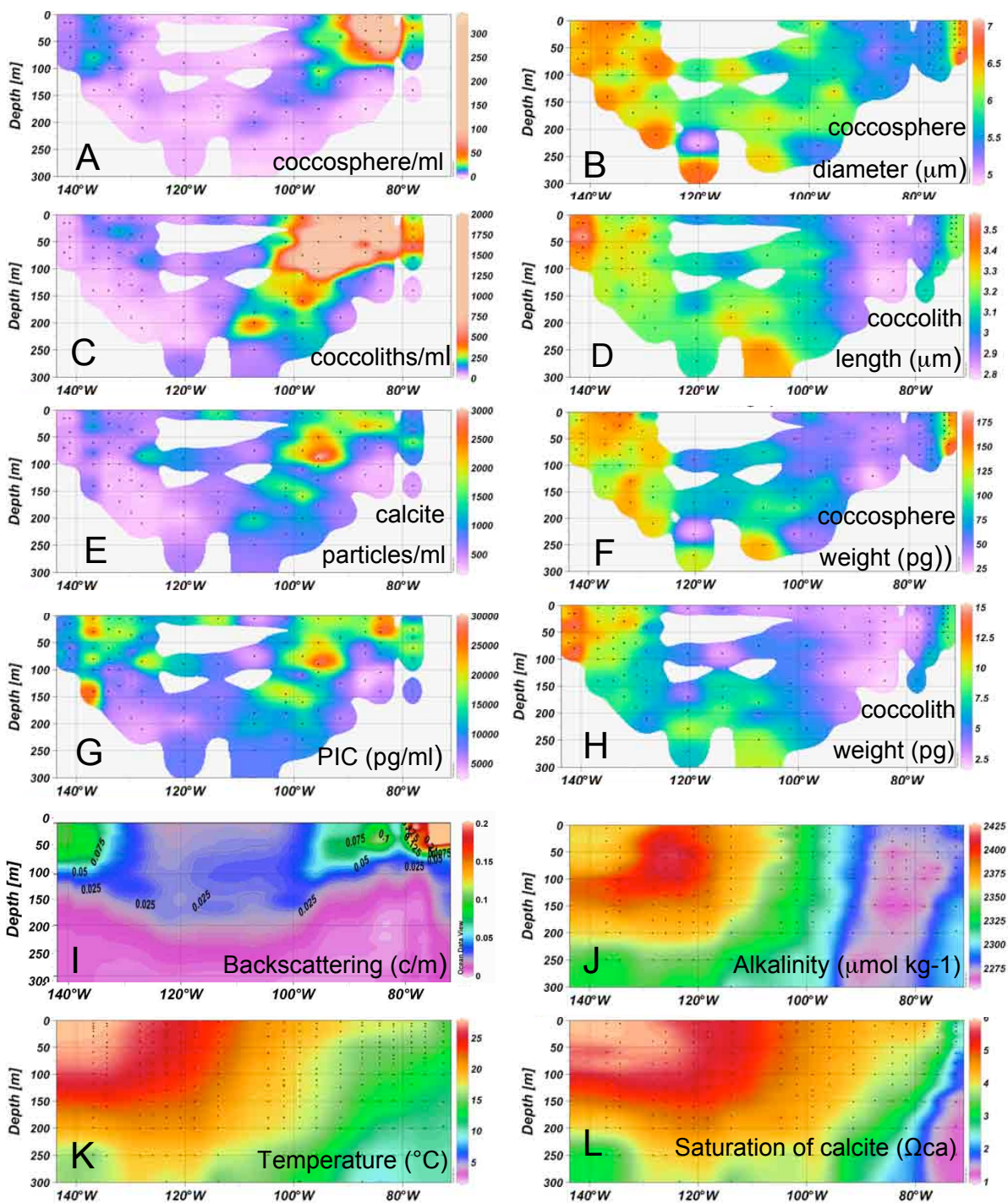


Fig. 5. Section along the BIOSOPE transect of (A) concentration in *Isochrysidales* coccospheres; (B) length of detached *Isochrysidales* coccoliths (μm); (C) concentration of detached *Isochrysidales* coccoliths; (D) Average diameter of *Isochrysidales* coccospheres (μm); (E); concentration in suspended calcite particles; (F) Average weight of detached *Isochrysidales* coccoliths (pg); (G) Total concentration of suspended calcite particles (PIC); (H) coccolith weight; (I) Attenuation coefficient (processed as described in Claustre et al., 2008) (m^{-1}); (J) Alkalinity ($\mu\text{mol kg}^{-1}$); (K); In situ temperature ($^{\circ}\text{C}$); (L) Saturation of Calcite (ΩCa).

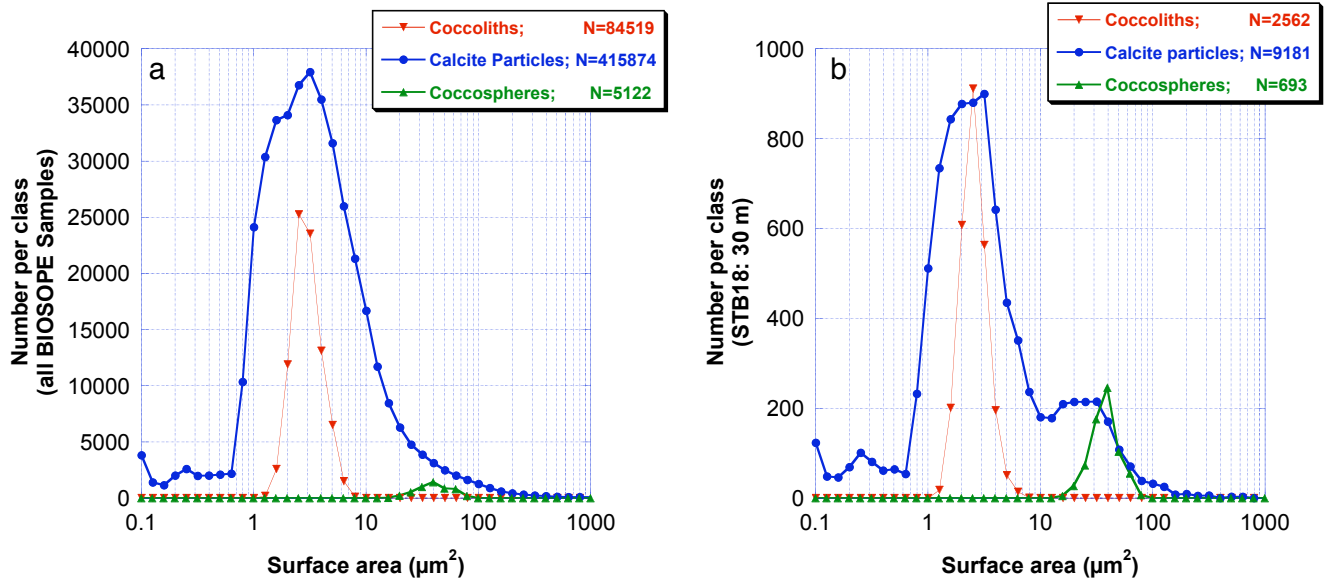


Fig. 6. Size Distribution of area of coccoliths (red), coccospheres (green) and calcite particles (blue) in all samples (A) and in sample taken at 30 m at Station 18 (B).

to this correlation. The non-*E. huxleyi* Isochrysidales and the non-Isochrysidales coccolithophores were less correlated with the carbonate particle density (Fig. 7). *Emiliania huxleyi* dominated the assemblages where the coccolith density and calcite particles were the highest, demonstrating that *E. huxleyi* were a major source of fine suspended calcite particles in the open ocean.

3.4 Size and weight distribution and number of coccoliths per coccosphere

The diameter and weight of the coccoliths and coccospheres show the same spatial distribution (Fig. 5). In general, both had higher values in the western part of the transect, decreased progressively toward the east until they reached their minima around 90° W, and slightly rose in the PCU (Fig. 8). There were significant correlations (Fig. 9) between the average length of coccoliths and the average diameter of coccospheres ($r=0.85$). The same was true for their weights ($r=0.88$). There were also significant correlations between the average of the weight and length of the coccoliths ($r=0.95$) and diameter of the coccosphere ($r=0.94$).

Assuming that the detached coccoliths have the same morphological characteristics as the attached coccoliths on the coccosphere, then the number of coccoliths per coccosphere was obtained by dividing the average weight of coccospheres by the average weight of the coccoliths. Doing so, we found an average of 15 coccoliths per coccospheres with standard deviation of 5. No clear pattern was found in the spatial distribution of that number.

3.5 Depth profiles

Morphometric and abundance data showed depth profiles which are similar to depth profiles of chlorophyll concentration. The maxima of abundance, weight, for both coccospheres and coccoliths were generally found associated with the chlorophyll maximum (Fig. 10). In consequence, the concentrations in coccolithophores and coccoliths, their weight and their size, were highest at shallow depth in the upwelling area, and deep in oligotrophic area. For example in the centre of the gyre, Isochrysidales taxa were most abundant between 150 and 200 m.

4 Discussion

4.1 Abundance distribution

The coccosphere stocks estimated in the South East Pacific were low, with a median value of 4000 cell l⁻¹. The lowest values were found at the centre of the South Pacific Gyre (GYR station). However in the centre of the gyre and at all stations, coccolithophores were continuously present down to the deepest sample (200–300 m) where sufficient light is remaining for the growth of some species (Claustre et al., 2008). The average Isochrysidales stock at Station GYR was 1250 cell per liter. This is equivalent to 375 × 10⁶ cells m⁻² in a 300 m deep water column; this value represents only the stock of marine Isochrysidales which represent a small coccolithophore fraction (1/3). These data imply that coccolithophore are in abundance even in the extreme oligotrophic environments that we investigated. The

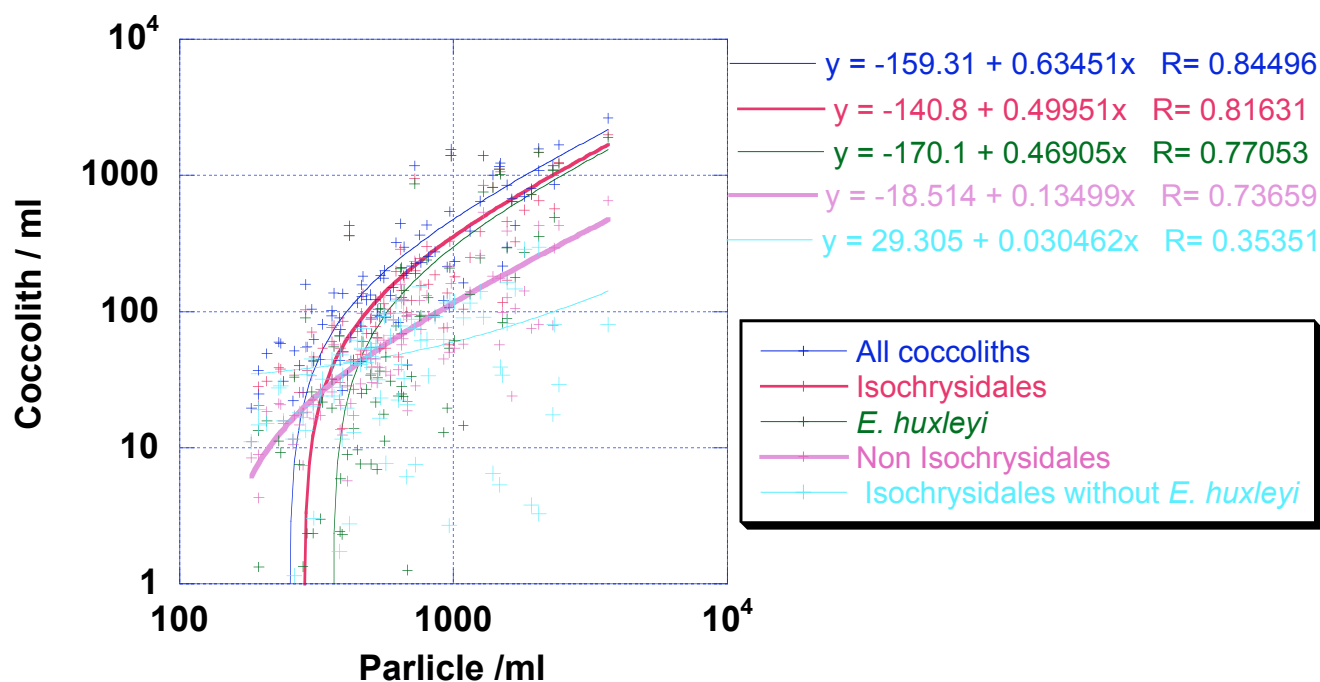


Fig. 7. Correlation between concentrations of suspended calcite particles and detached coccoliths of all coccolithophores taxa (deep blue), all Isochrysidales species (red), *E. huxleyi* (green), non-Isochrysidales coccolithophores taxa (purple), non-*E. huxleyi* Isochrysidales species (light blue). These numbers have been obtained by combining the concentration of Isochrysidales coccolith data (Fig. 5c) with the percentage of the different taxa estimated from coccosphere count shown in Fig. 4.

coccolithophore stocks estimated in this study are in the same range as previously reported for the more productive tropical Pacific, 1–240 cell ml⁻¹ (Hagino and Okada, 2006), 0–60 cell ml⁻¹ (Balch and Kilpatrick, 1996), 1–100 cell ml⁻¹ (Okada and Honjo, 1973; Ohkouchi et al., 1999), and 0–60 cell ml⁻¹ (Giraudeau and Beaufort, 2007). The highest cell density of *E. huxleyi* (240 cell ml⁻¹) in the South Equatorial Pacific was reported in the Peru Upwelling (~85° W–2° S) (Hagino and Okada, 2006). This is equivalent to what was found in BIOSOPE, where up to 350 cell ml⁻¹ were observed west of the PCU. The sample taken in the PCU on smaller membrane does not permit us to estimate the abundance of coccolithophores. One would nevertheless expect even higher abundance in this area because higher numbers of coccospheres of *E. huxleyi* are generally reported in the centre rather than outside of upwelling systems (Giraudeau and Bailley, 1995) where their abundance can reach several thousand of cell ml⁻¹ (Mitchell-Innes and Winter, 1987).

4.2 Deep production of marine Isochrysidales

Coccolithophores are growing at the boundary of their greatest depth habitat in the South Pacific Gyre. For example at Station STB11, *Florisphaera profunda* was found between

200 and 300 m. In the gyre, the maximum abundance of Isochrysidales occurred at about 120 m, i.e., deeper than usually found for coccoliths in oligotrophic area (e.g. Okada and Honjo, 1973; Okada and McIntyre, 1979). The fact that coccolithophores calcify at depth greater than 100 m represents a significant change from the proposed high-light niche of *E. huxleyi* (e.g. Nanninga and Tyrrell, 1996) and the observed restriction of calcification to shallower waters than silicification (Poulton et al., 2006). A possibility is that these coccospheres were not living cells but the sinking remains of coccolithophores that grew at shallower depths. Several lines of evidence argue against this: 1) the maximum abundances of coccospheres coincide with the Deep Chlorophyll Maxima (DCM) 2) the production in the upper photic zone is too low to fuel the coccosphere highest number at the DCM which is 3 times larger than at the surface. This is particularly true for *Florisphaera profunda*, which is found only below 200 m. 3) the community vertical structure is typical of oligotrophic area, 4) it is interesting to note that the DCM is not only the place of maximum abundance of Isochrysidales, but also an area in which they secrete heavier coccoliths and have larger cells. Why should a morphological change occur in dead assemblages during settling?

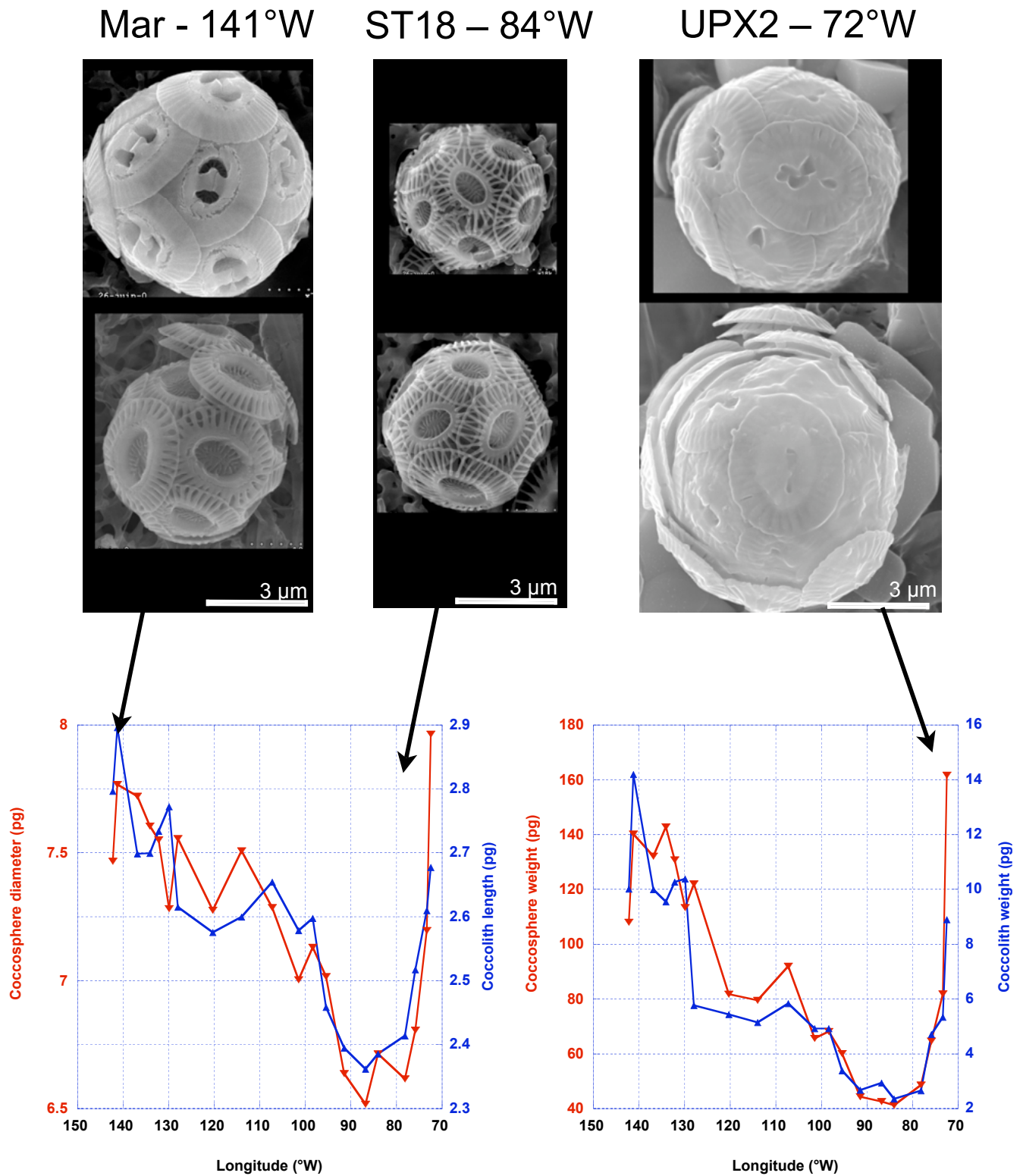


Fig. 8. Bottom left: Variability of *Isochrusidales* coccosphere diameter (red) and coccolith length (blue) averaged for every BIOSOPE station (average weighted by the concentration at each depth). Bottom right: variability of coccosphere (red) and coccolith (blue) weight averaged for each BIOSOPE station (average weighted by the concentration at each depth). Top: 6 SEM pictures (scale bars represents 3 μm: same scale in every picture) of typical *Isochrusidales* in 3 BIOSOPE stations.

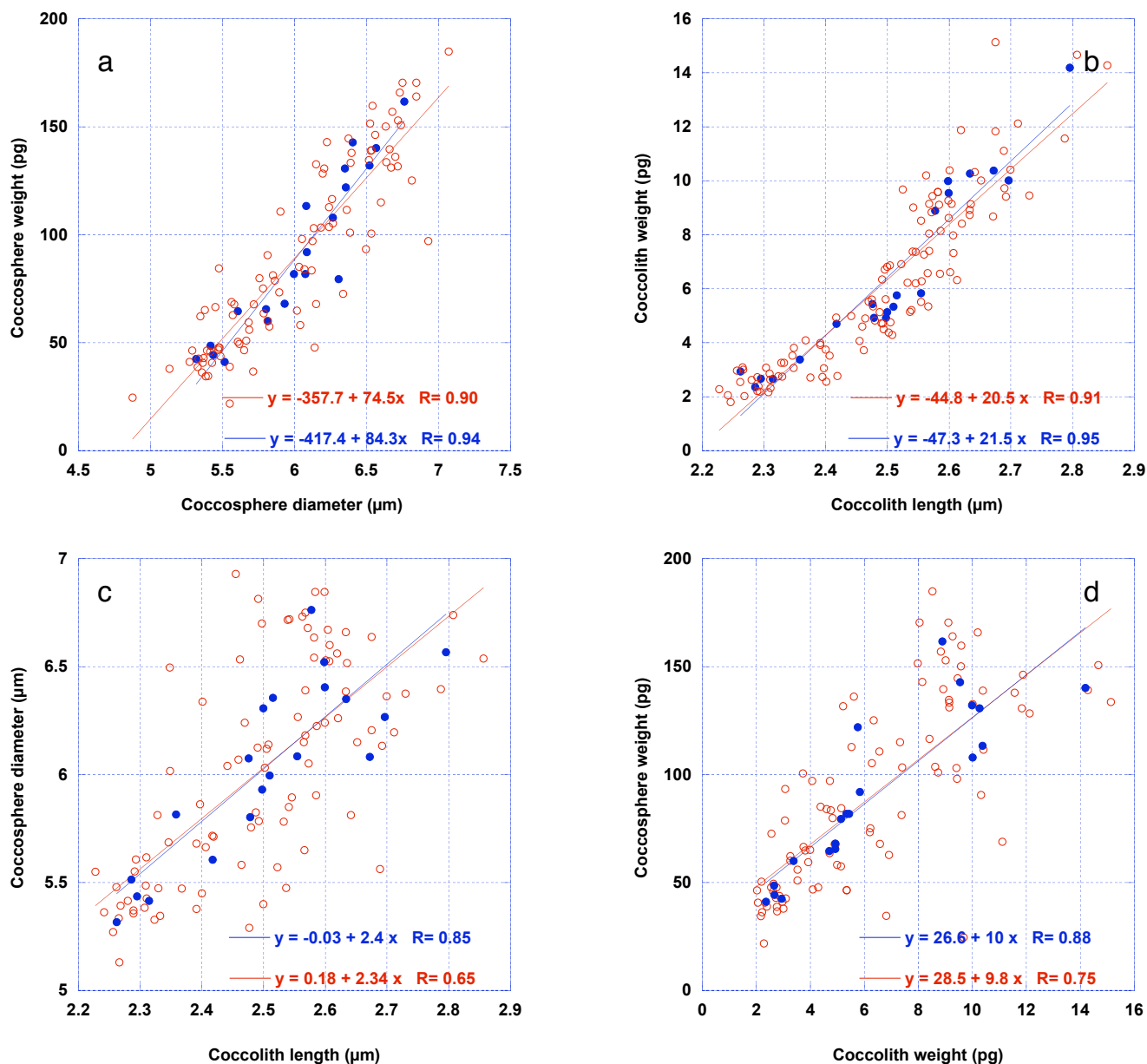


Fig. 9. Correlation between coccosphere diameter and weight (**A**), coccolith length and weight (**B**), coccolith length and coccosphere diameter (**C**) weight of coccolith and coccosphere (**D**) of *Isochrysidales* observed in BIOSOPE. Open red circles represent single BIOSOPE sample and the filled blue circles represent station average.

In conclusion, the system investigated can be considered as an endmember of oligotrophic systems with the deepest chlorophyll maximum and the clearest waters ever reported (Morel et al., 2007). The coccolithophores assemblage is typically adapted to these conditions with maximum cell density in general closely associated with the DCM. Furthermore it is very clear from pigment signature that below the chlorophyll maximum and up to depths of 250 and above, the dominant (sometimes the only) carotenoids is 19'-hexonyloxyfucoxanthin, the marker of prymnesiophyceae

(Ras et al., 2008, in their Fig. 11). This observation must be integrated with the layer of high backscattering ratio (the calcite marker) that is recorded at ~ 240 m (Twardowski et al., 2007) at the GYR station.

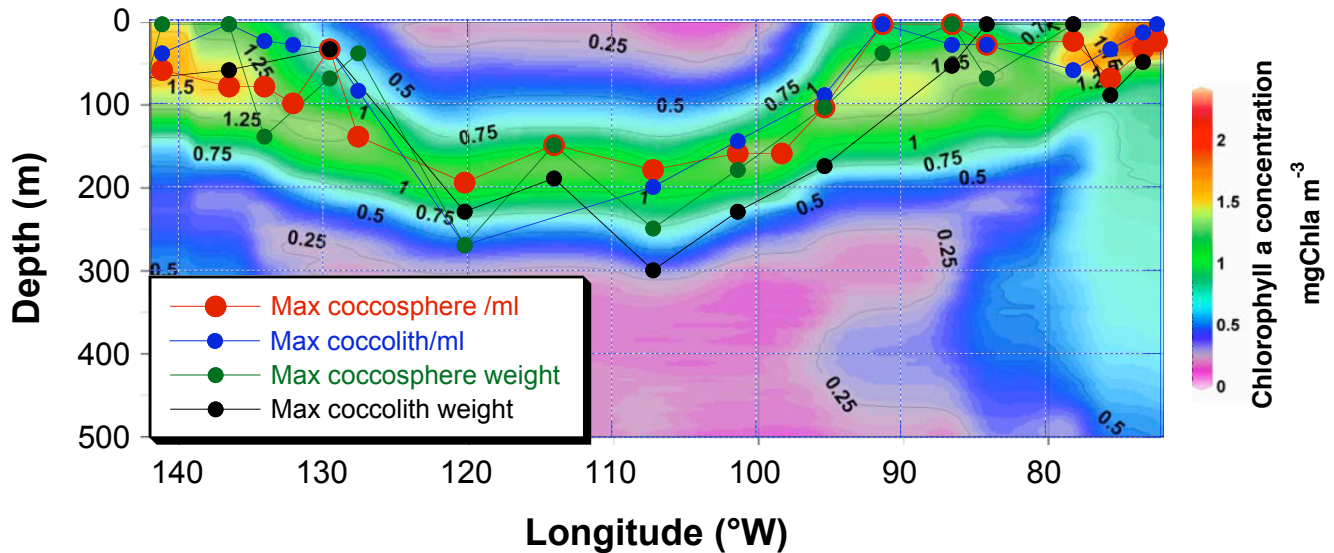


Fig. 10. Color section of the chlorophyll a concentration mg m^{-3} along the BIOSOPE transect with the position in depth where the maximum value at a given Station is observed for the Isochrysidales coccosphere density (red), detached coccolith density (blue), weight of coccosphere (green), weight of coccoliths (black).

4.3 Implication of deep production for alkenone paleothermometry

When the temperature difference between the water surface and the depth of maximum abundance of the Isochrysidales, is calculated, it appears that for 1/3 of the stations, the difference is greater than 2°C (Fig. 11). The Isochrysidales are the producers of alkenones used in paleoceanography as sea surface temperature (SST) proxy. Ohkouchi et al. (1999) described some discrepancies between SST estimates from North Pacific surface sediments and the observed SST at the same locations attributable to the fact that alkenones were produced in the DCM. Also, Conte et al. (2006) found some differences between the alkenone calibration curve based on surface sediments (Muller et al., 1998) and their calibration based on mixed-layer water measurements. But these differences were essentially recorded at high latitudes in absence of a DCM. Our results would indicate that it is may be excessive to infer SST from an alkenone record core taken below the South Pacific Gyre because alkenone would have been produced far below the surface (there are no suitable sediments to establish such a record in the Central Southern Pacific; Rea et al., 2006). But it has been shown that alkenones are produced exclusively in the mixed layer depth, and above the DCM in ALOHA Station in the oligotrophic North Pacific Gyre (Prahl et al., 2005). Either Station ALOHA is different from the South Pacific gyre (SPG) where *E. huxleyi* was abundant above DCM, or the secretion of alkenones by *E. huxleyi* is light dependent. In that case the deep production of Isochrysidales observed in SPG would not temper the SST reconstruction based on alkenones.

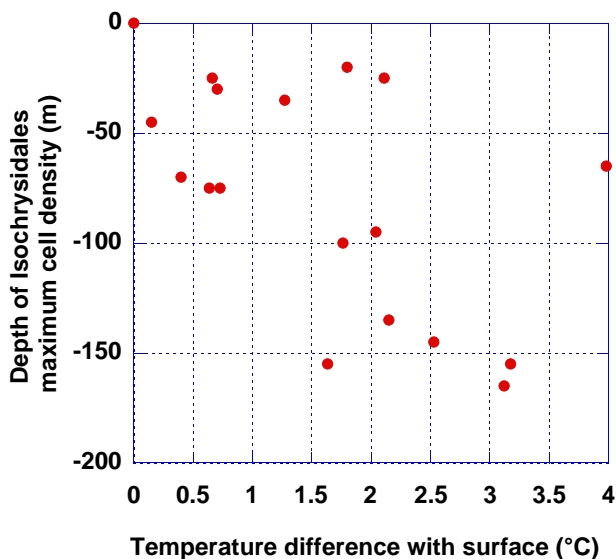


Fig. 11. Depth of Isochrysidales maximum density as a function of temperature difference between the depth of this maximum and surface.

4.4 *Emiliana huxleyi*: important calcite producer

The BIOSOPE PIC values are in the same range (0.05–0.35 mmol m⁻³) as previously reported for the Equatorial Pacific (Balch and Kilpatrick, 1996) if we exclude one value from the latter study of 1.33 mmol m⁻³ in the open ocean upwelling. One important finding of the present study is a strong relation between the numbers of coccoliths of *E. huxleyi* and the number of suspended calcite particles (hence PIC) (Fig. 7). The “cloud” of highest abundance of coccolithophores (Fig. 5a,c) was dominated by *E. huxleyi* (Fig. 4); it also was the place of highest PIC and of significant enhancement of backscattering (Fig. 5g, i). *Emiliana* has been sometimes considered as one of the most important calcite producers (e.g. Westbroek et al., 1993); but it has been also suggested that it represents only an insignificant part of the oceanic calcite production (Paasche, 2002; Ziveri et al., 2007), because this species secreted one of the lightest coccoliths (Beaufort and Heussner, 1999; Young and Ziveri, 2000). The BIOSOPE transect covers the diversity of trophic conditions potentially observable in open ocean waters, we show that a large part of the fine calcite particles is attributable to Isochrysidales coccoliths. Calcification in the Tropical Pacific is very high, (similar the rate of photosynthesis) and the turnover times of calcite in the euphotic zone ranges from 3 to 10 days (Balch and Kilpatrick, 1996). These high turnover rates of calcite induce a high ballasting of organic matter by carbonate particles and a decrease of PIC possibly associated with a depletion of Ca⁺⁺ ion in the euphotic zone (Balch et al., 2007). Because of the high abundance of detached coccoliths and of coccospheres, the ballasting due to *E. huxleyi* coccoliths must have been particularly efficient around 90° W–30° S. Ballasting could also have an effect on the alkalinity of the surface water. It is interesting to note that the area of highest standing stock of coccoliths present also has particularly low alkalinity. An inverse relation exists between alkalinity and PIC (Fig. 12), which is indicative of the effect of calcification on ocean surface alkalinity.

It is also interesting to note that the highest coccolith density was found in a scatter at depth greater than 30 m, the depth limit of detection of coccoliths by satellite. Hitherto coccolith blooms detected by satellite are always in regions of shallow organic production (high latitudes, continental shelves, and upwelling zones) (Brown and Yoder, 1994; Balch et al., 2007), therefore, the calcite density of this scatter will be largely underestimated, if ever detected, by satellite imagery.

4.5 Weight and size relation between coccolith and coccosphere

An interesting aspect of this study were the fact that there is a close relationship ($r=0.65$) between the diameters of the Isochrysidales coccoliths and coccospheres (Fig. 8). A factor

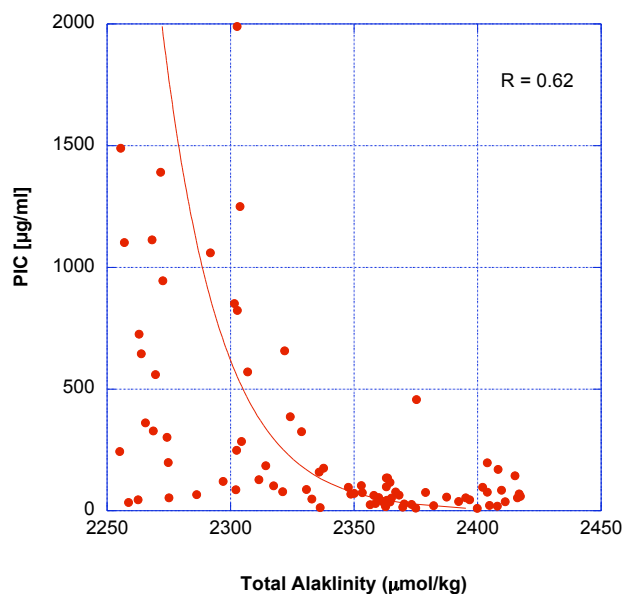


Fig. 12. Relation between the total weight of calcite particles and the total alkalinity.

of about ~ 2.4 (or ~ 1.9 taking into account the measurement bias for the coccolith length) can be used to estimate the diameter of a coccosphere from the length of a coccolith. Also the number of coccoliths per coccosphere is 15 on average without variations throughout the BIOSOPE transect. If the same relations were found elsewhere, these values would be useful in paleoceanographic studies for estimating the number and size of the cells of marine Isochrysidales from the number and length of their coccoliths.

4.6 Calcification, cell diameter and carbonate chemistry

The most calcified Isochrysidales are found in the high fertility zones of the Marquesas area and Peru-Chile Upwelling (PCU) (Figs. 5 and 8). Also we have shown that the maximal weight of both coccospheres and coccoliths are generally located in the DCM, which is close vicinity of the nitracline (Raimbault et al., 2008). These two observations may indicate that coccolithophores secrete more calcified coccoliths in higher fertility environments. This is in agreement with recent culturing and mesocosms experiments showing that *E. huxleyi* is more calcified in waters rich in *P* and *N* in batch cultures (Beaufort et al., 2007) or after addition of nutrients in mesocosms (Engel et al., 2005). However, these results contrast with those discussed in Paasche (2002). In BIOSOPE, the weights of the coccospheres and the coccoliths were weakly correlated with chlorophyll content and with stock of coccolith and coccosphere. Therefore other environmental factors than fertility or productivity might influence the calcification of coccolithophores.

The lightest coccoliths and coccospheres were recorded between 80 and 95° W, which is also exactly the place of the lowest alkalinity values in the upper 300 m of the BIOSOPE transect (Fig. 12). The concentration in carbonate ion was also particularly low in that area. These low values could be responsible, in part, for the low calcification of Isochrysidales cells. But this does not mean their growth was limited in such conditions because it is the place of highest concentrations of Isochrysidales coccoliths. In contrast, significant precipitation of calcite by *E. huxleyi*, revealed by highest PIC and coccolith concentrations, may have the effect of decreasing the dissolved carbonate concentration and the alkalinity of this area. Similarly, it has been recently suggested (Balch et al., 2007) that high PIC turnover such as recorded in the tropical Pacific, induces a depletion of calcium ion in the photic zone as a response of losses of PIC ballasted particles. We found a significant ($R=0.62$) reverse logarithmic correlation between the concentration of coccoliths and alkalinity. Significant linear positive correlation exists between alkalinity and the weight of coccolith and coccospheres ($R=0.84$ and $R=0.85$ respectively on the station averages or $R=0.59$ and $R=0.74$ respectively on all samples) (Fig. 13c and i). This highlights the likely fundamental importance of alkalinity on calcification. Except in the 3 upwelling stations, carbonate concentration and calcite saturation state appears to also share a strong influence on the coccolith and coccosphere weights (Fig. 13a, b, g and h). The partial pressure of CO₂ as well as pH does not appear to have significant impact on the degree of calcification of coccospheres and coccoliths ($R<0.03$) (Fig. 13d, e, j and k). This could be seen as contradicting with previous findings from culture and mesocosms experiments that predict a decrease of calcite production with increasing concentration of CO₂ (Riebesell et al., 2000; Engel et al., 2005). Recent culture experiments show that an increase of CO₂ may have a positive effect on calcification of *E. huxleyi* (Iglesias-Rodriguez et al., 2008) and other species (Langer et al., 2006). These experiments involve not only changes in CO₂ and pH, but also carbonate chemistry in very different ways depending on how the experiment was conducted. Our findings stress the importance of the entire carbonate system in the calcification of Isochrysidales.

The strong dependence of the concentration of carbonate ion on the coccolithophore calcification, has been recently illustrated by comparing Baltic and Black seas: the absence of coccoliths of *E. huxleyi* in the Baltic Sea result from low carbonate saturation states particularly during the winter (Tyrrell et al., 2008). In a comparison of numerical simulation and observed data from seasonal blooms in the Bering Sea, it has been shown that *E. huxleyi* production benefits greatly from an increase in the concentration of carbonate ion in the surface water resulting from the increase in phytoplankton production (Merico et al., 2006). These authors hypothesized that in a zone of seasonal blooms, *E. huxleyi* would calcify more after a spring bloom in response to the increase in carbonate ion concentration. This hypothesis

may explain why the heaviest coccospheres were observed in the eutrophic and mesotrophic areas of the BIOSOPE experiment. The least calcified Isochrysidales were found at the subtropical front in the highest coccosphere abundance zone of the BIOSOPE experiment. Because it is not a highly productive area, the production of coccoliths may have decreased the carbonate ion concentration, making calcification more difficult for *E. huxleyi*.

Multiple regression, applied to the weight of coccoliths or coccospheres with seven environmental parameters (total alkalinity, concentration of O₂, CO₃, and OH, temperature, salinity, and saturation of calcite (Ω_{Ca})), shows high correlations: $R=0.97$ (0.75) and 0.97 (0.82) respectively for the station averages (all samples) (Fig. 13f and l). The fact that the correlations are relatively less significant for the entire sample set than for the station average results not only from noise but also from the fact that at every station the maximum calcification was found at the maximum of coccolithophore density in the DCM (Fig. 10 and discussion above). Therefore the depth profiles of weight do not follow the carbonate chemistry profiles. The biotic (coccolithophores production) influence on calcification exist mainly at local scale (depth) whereas the abiotic (carbonate chemistry) plays a more important role at regional (horizontal) scale where 94% of the variability of coccolith and coccosphere weight can be explained by the change in these 7 independent variables. An important finding is that the degree of calcification of Isochrysidales strongly depends on environmental parameters. This relation was found at the "order" level rather than at the species level, suggesting that the specific composition of Isochrysidales could be related to carbon chemistry of the water. For example the fact that *G. oceanica* dominates around the Marquesas area could be related to the higher alkalinity of this area that presents an advantage for this relatively highly calcified species.

5 Conclusions

In most of the BIOSOPE stations the coccolithophore standing stocks were low, except in the vicinity of Peru Chile Upwelling system (80 to 100° W), where the Isochrysidales were highly abundant at mid photic zone depth (up to 350 000 coccospheres per liter between 30 and 60 m). This low abundance has been also reported in other studies conducted in the Tropical Pacific. In the South Pacific Gyre coccolithophores are rare at the surface but grow over the entire 0–300 m water column. The Isochrysidales coccoliths compose a significant fraction of PIC. The area of highest coccolithophore standing stock (80 to 100° W) here corresponds to the place of lowest alkalinity. There is a close relationship between the diameter of the coccoliths and length of the coccospheres of Isochrysidales. The most calcified Isochrysidales were found in the Marquesas area and in the Peru-Chile Upwelling (PCU) and the least calcified were found west of

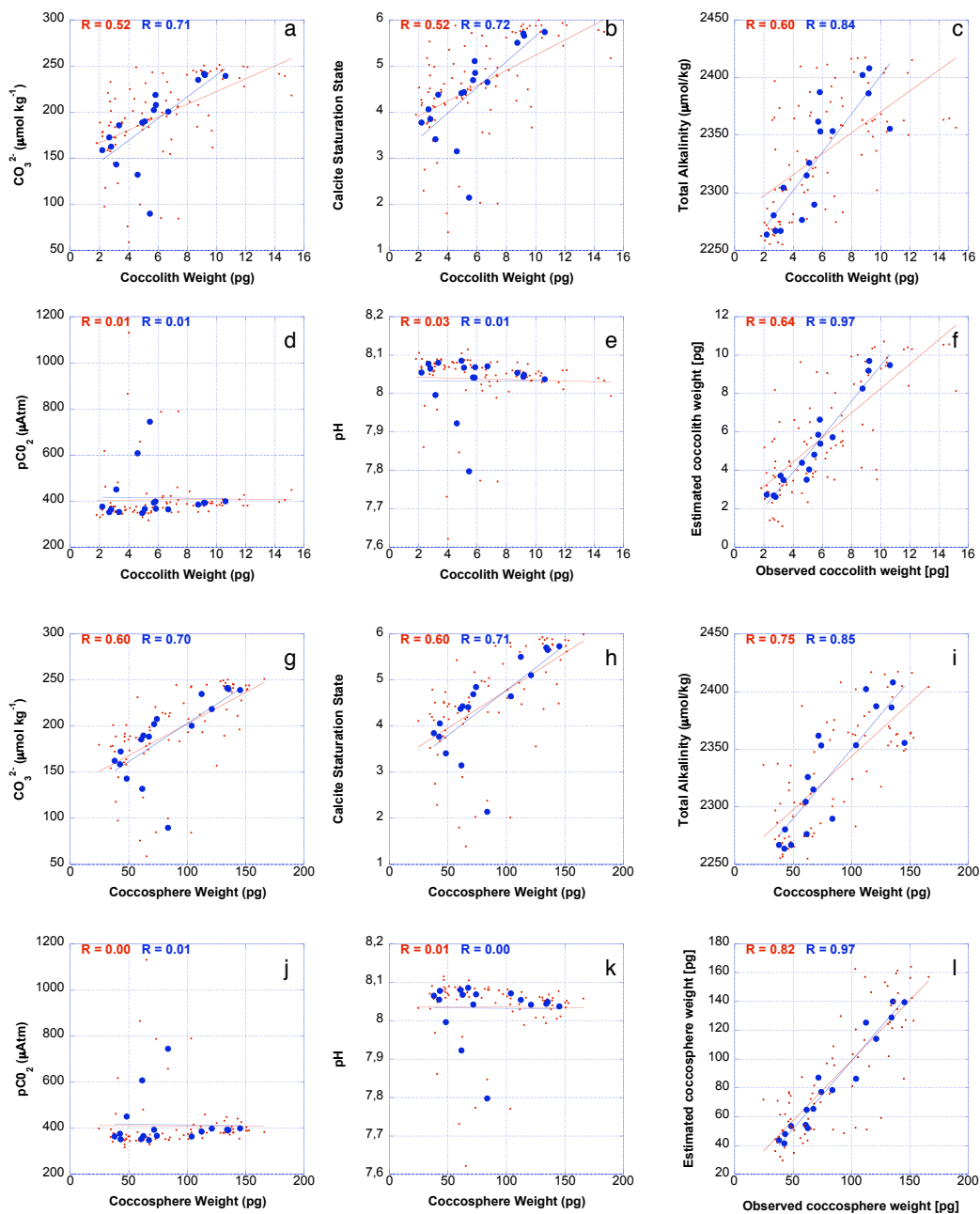


Fig. 13. Correlations between carbonate ion concentration (**a, g**), calcite saturation state (**b, h**), alkalinity (**c, i**), $p\text{CO}_2$ (**d, j**), pH (**e, k**) and the weight of Isochrysidales coccoliths (**a, b, c, d, e**) and coccospheres (**g, h, I, j, k**), and between observed and estimated weight of Isochrysidales coccoliths (**f**) and coccospheres (**l**). The entire suite of sample is represented in red, and the Station averages are represented in blue. The weights were estimated with the following equations:

$$\text{Coccolith weight} = 3.265 + (0.075 \cdot \text{Alkalinity}) - (0.040 \cdot [\text{O}_2]) - (0.380 \cdot \text{Temperature}) - (4.557 \cdot \text{Salinity}) + (0.207 \cdot [\text{CO}_3]) - 10.178 \cdot \Omega\text{Ca} + (2.268 \cdot [\text{OH}]) \quad (1)$$

$$\text{Coccosphere weight} = -1001.222 + (1.980 \cdot \text{Alkalinity}) + (0.078 \cdot [\text{O}_2]) + (4.448 \cdot \text{Temperature}) - (102.652 \cdot \text{Salinity}) - (0.952 \cdot [\text{CO}_3]) - (31.654 \cdot \Omega\text{Ca}) + (4.864 \cdot [\text{OH}]) \quad (2)$$

Those equations have been obtained by performing multiple regressions between these parameters and coccospheres and coccolith weight with the Station averages.

the PCU where the abundance of coccosphere is highest. The regional variability in the degree of calcification of Isochrysidales (weight of their coccoliths and coccospheres) strongly depends on environmental parameters (essentially the carbonate chemistry and the temperature). In area of high alkalinity the Isochrysidales secretes the heaviest coccospheres. The weight of Isochrysidales' coccoliths and coccospheres can be predicted at 94% from a set of 7 abiotic components.

Coccolithophores occur at great depths in the South Pacific Gyre: the maximum abundances of Isochrysidales were found between 150 and 170 m. The Deep Chlorophyll maximum is not only the place of maximum abundance of Isochrysidales, but also an area in which they secrete heavier coccoliths and have larger cells. Given the spatial extension of subtropical gyres, the role of coccolithophore in mediating particulate flux in these extreme oligotrophic waters may be significant when dealing with global ocean estimates.

Acknowledgements. Dominique Tailliez and Claudie Bournot are warmly thanked for their efficient help in CTD rosette management and data processing. We are thankful to Daniel Vaultot, Manon Viprey, and Laurence Garczarek for having filtered water samples for coccoliths during BIOSOPE cruise. We are thankful to Marie-Pierre Aubry and Amos Winter who made interesting comments on an earlier version of this paper. This is a contribution of the BIOSOPE project of the LEFE-CYBER program. BIOSOPE cruise was funded by the Centre National de la Recherche Scientifique (CNRS), the Institut des Sciences de l'Univers (INSU), the Centre National d'Etudes Spatiales (CNES), the European Space Agency (ESA), The National Aeronautics and Space Administration (NASA) and the Natural Sciences and Engineering Research Council of Canada (NSERC). This work is part of the pluridisciplinary project BOOM – Biodiversity of Open Ocean Microcalcifiers, funded by the “Institut Français de la Biodiversité” via the “Agence National de la Recherche”, grant ANR-05-BDIV-004.

Edited by: J. Middelburg

References

- Archer, D., Winguth, A., Lea, D., and Mahowald, N.: What caused the glacial/interglacial atmospheric pCO₂ cycles, *Rev. Geophys.*, 38, 159–189, 2000.
- Azouzi, L., Goncalves Ito, R., Touratier, F., and Goyet, C.: Anthropogenic carbon in the Eastern South Pacific Ocean, *Biogeosciences Discussions*, 4, 1815–1837, 2007.
- Balch, W. M. and Kilpatrick, K.: Calcification rates in the equatorial Pacific along 140° W, *Deep Sea Res. II*, 43, 971–993, 1996.
- Balch, W. M., Drapeau, D. T., Bowler, B. C., and Booth, E. S.: Prediction of pelagic calcification rates using satellite measurements, *Deep Sea Res. II*, 54, 478–495, 2007.
- Beaufort, L. and Heussner, S.: Coccolithophorids on the continental slope of the bay of Biscay. 1. Production, transport and contribution to mass fluxes, *Deep Sea Research II*, 46, 2147–2174, 1999.
- Beaufort, L. and Dollfus, D.: Automatic recognition of coccolith by dynamical neural network, *Mar. Micropaleont.*, 51(1–2), 57–73, 2004.
- Beaufort, L.: Weight estimates of coccoliths using the optical properties (birefringence) of calcite, *Micropaleontol.*, 51, 289–298, 2005.
- Beaufort, L., Probert, I., and Buchet, N.: Effects of acidification and primary production on coccolith weight: Implications for carbonate transfer from the surface to the deep ocean, *Geochemistry Geophysics Geosystems*, 8, Q08011, doi:10.1029/2006GC001493, 2007.
- Brown, C. W. and Yoder, J. A.: Coccolithophorid blooms in the global ocean., *J. Geophys. Res.*, 99(C4), 7467–7482, 1994.
- Claustre, H. and Maritorena, S.: The many shades of ocean blue, *Science*, 302, 1514–1515, 2003.
- Claustre, H., Sciandra, A., and Vaultot, D.: Introduction to the special section bio-optical and biogeochemical conditions in the South East Pacific in late 2004: the BIOSOPE program, *Biogeosciences*, 5, 679–691, 2008, <http://www.biogeosciences.net/5/679/2008/>.
- Claustre, H., Huot, Y., Obernosterer, I., Gentili, B., Tailliez, D., and Lewis, M.: Gross community production and metabolic balance in the South Pacific Gyre, using a non intrusive bio-optical method, *Biogeosciences*, 5, 463–474, 2008, <http://www.biogeosciences.net/5/463/2008/>.
- Conte, M. H., Sicre, M. A., Ruhlmann, C., Weber, J. C., Schulte, S., Schulz-Bull, D., and Blanz, T.: Global temperature calibration of the alkenone unsaturation index (uk'37) in surface waters and comparison with surface sediments, *Geochem. Geophys. Geosystems*, 7, Q02005, doi:10.1029/2005GC001054, 2006.
- de Vargas, C., Aubry, M. P., Probert, I., and Young, J.: Origin and evolution of coccolithophores: From coastal hunters to oceanic farmers, in: *Evolution of aquatic photoautotrophs*, edited by: Falkowski, P. G., and Knoll, A. H., Academic Press, New York, 456 pp., 2007.
- Dollfus, D. and Beaufort, L.: Fat neural network for recognition of position-normalised objects, *Neural Networks*, 12, 553–560, 1999.
- Engel, A., Zondervan, I., Aerts, K., Beaufort, L., Benthien, A., Chou, L., Delille, D., Gattuso, J. P., Harlay, J., Heemann, C., Hoffmann, L., Jacquet, S., Nejstgaard, J., Pizay, M. D., Rochelle-Newall, E., Schneider, U., Terbruggen, A., and Riebesell, U.: Testing the direct effect of CO₂ concentration on a bloom of the coccolithophorid *Emiliana huxleyi* in mesocosm experiments, *Limnol. Oceanogr.*, 50, 493–507, 2005.
- Feely, R. A., Sabine, C. L., Lee, K., Berelson, W., Kleypas, J., Fabry, V. J., and Millero, F. J.: Impact of anthropogenic CO₂ on the CaCO₃ system in the oceans, *Science*, 305, 362–366, 2004.
- Giraudeau, J. and Bailley, G. W.: Spatial dynamics of coccolithophore communities during an upwelling event in the southern Benguela system, *Continental Shelf Res.*, 15, 1825–1852, 1995.
- Giraudeau, J. and Beaufort, L.: Coccolithophores from extant population to fossil assemblages, in: *Developments in marine geology, proxies in late Cenozoic paleoceanography* edited by: Hilaire-Marcel, C. and de Vernal, A., Elsevier, Amsterdam, 409–439, 2007.
- Hagino, K. and Okada, H.: Intra- and infra-specific morphological variation in selected coccolithophore species in the Equatorial and Subequatorial Pacific Ocean, *Mar. Micropaleont.*, 58, 184–206, 2006.

- Iglesias-Rodriguez, M. D., Halloran, P. R., Rickaby, R. E. M., Hall, I. R., Colmenero-Hidalgo, E., Gittins, J. R., Green, D. R. H., Tyrrell, T., Gibbs, S. J., von Dassow, P., Rehm, E., Armbrust, E. V., and Boessenkool, K. P.: Phytoplankton calcification in a high-CO₂ world, *Science*, 336–340, doi:10.1126/science.1154122, 2008.
- Langer, G., M., Geisen, Baumann, K.-H., Kläs, J., Riebesell, U., Thoms, S., and Young, J. R.: Species-specific responses of calcifying algae to changing seawater carbonate chemistry, *Geochemistry, Geophysics, Geosystems*, 7, Q09006, doi:10.1029/2005GC001227, 2006.
- Longhurst, A.: Ecological geography of the sea, Academic Press, San Diego, 398 pp., 1998.
- Merico, A., Tyrrell, T. and Cokacar, T.: Is there any relationship between phytoplankton seasonal dynamics and the carbonate system?, *J. Mar. Syst.*, 59, 120–142, 2006.
- Milliman, J. D.: Production and accumulation of calcium carbonate in the ocean - budget of a nonsteady state, *Global Biogeochem. Cycles*, 7, 927–957, 1993.
- Mitchell-Innes, B. A. and Winter, A.: Coccolithophores : A major phytoplankton component in mature upwelled waters off the cape peninsula, south africa in march, 1983, *Mar. Biol.*, 95, 25–30, 1987.
- Morel, A., Gentili, B., Claustre, H., Babin, M., Bricaud, A., Ras, J., and Tieche, F., : Optical properties of the “Clearest” Natural waters, *Limnol. Oceanogr.*, 52, 217–229, 2007.
- Muller, P. J., Kirst, G., Ruhland, G., von Storch, I., and Rossel-Mele, A.: Calibration of the alkenone paleotemperature index uk’37 based on core-top from the Eastern South Atlantic and the global ocean (60° N–60° S), *Geochim. Cosmochim. Acta.*, 62, 1757–1722, 1998.
- Nanninga, H. J. and Tyrrell, T.: Importance of light for the formation of algal blooms by *Emiliana huxleyi*, *Mar. Ecol. Prog. Ser.*, 136, 195–203, 1996.
- Ohkouchi, N., Kawamura, K., Kawahata, H., and Okada, H.: Depth ranges of alkenone production in the Central Pacific Ocean, *Global Biogeochem. Cycles*, 13, 695–704, 1999.
- Okada, H. and Honjo, S.: The distribution of oceanic coccolithophorids in the Pacific, *Deep Sea Res.*, 20, 355–374, 1973.
- Okada, H. and McIntyre, A.: Modern coccolithophores of the Pacific and North Atlantic oceans, *Micropaleontol.*, 23, 1–55, 1979.
- Orr, J. C., Fabry, V. J., Aumont, O., Bopp, L., Doney, S. C., Felly, R. A., Gananadesikan, A., Gruber, N., Ishida, A., Joos, F., Key, R., Lindsay, K., Maier-Reimer, E., Matear, R., Monfray, P., Mouchet, A., Najjar, R., Plattner, G.-K., Rodgers, K. B., Sabine, C. L., Sarmiento, J. L., Schlitzer, R., Slater, R. D., Totterdell, I. J., Weirig, M. F., Yamanaka, Y., and Yool, A.: Anthropogenic ocean acidification over the twenty-first century and its impact on calcifying organisms, *Nature*, 437, 681–687, 2005.
- Paasche, E.: A review of the coccolithophorid *Emiliana huxleyi* (Prymnesiophyceae), with particular reference to growth, coccolith formation, and calcification-photosynthesis interactions., *Phycologia*, 40, 503–529, 2002.
- Poulton, A. J., Sanders, R., Holligan, P. M., Stinchcombe, M. C., Adey, T. R., Brown, L., and Chamberlain, K.: Phytoplankton mineralization in the Tropical and Subtropical Atlantic Ocean, *Global Biogeochem. Cycles*, 20, GB4002, doi:10.1029/2006GB002712, 2006.
- Prahl, F. G., Popp, B. N., Karl, D. M., and Sparrow, M. A.: Ecology and biogeochemistry of alkenone production at Station ALOHA, *Deep Sea Res.*, 52, 699–719, 2005.
- Raimbault, P., Garcia, N., and Cerutti, F.: Distribution of inorganic and organic nutrients in the South Pacific Ocean – evidence for long-term accumulation of organic matter in nitrogen-depleted waters, *Biogeosciences*, 5, 281–229, 2008, <http://www.biogeosciences.net/5/281/2008/>.
- Ras, J., Claustre, H., and Uitz, J.: Spatial variability of phytoplankton pigment distribution in the South East Pacific, *Biogeoscience*, 5, 353–369, 2008.
- Rea, D., Lyle, M. W., Liberty, L. M., Hovan, S. A., Bolyn, M. P., Gleason, J. D., Hendy, I. L., Latimer, J. C., Murphy, B. M., Owen, R. M., Paul, C. F., Rea, T. H. C., Stancin, A. M., and Thomas, D. J.: Broad region of no sediment in the Southwest Pacific Basin, *Geology*, 34, 873–876, 2006.
- Riebesell, U., Zondervan, I., Rost, B., Tortell, P. D., Zeebe, R., and M., M. F. M.: Reduced calcification of marine plankton in response to increased atmospheric CO₂, *Nature*, 407, 364–367, 2000.
- Twardowski, M. S., Claustre, H., Freeman, S. A., Stramski, D., and Huot, Y.: Optical backscattering properties of the “clearest” natural waters, *Biogeoscience*, 4, 1041–1058, 2007.
- Tyrrell, T., Schneider, B., Charalampopoulou, A., and Riebesell, U.: Coccolithophores and calcite saturation state in the Baltic and Black seas, *Biogeosciences*, 5, 485–494, 2008, <http://www.biogeosciences.net/5/485/2008/>.
- Westbroek, P., Brown, C. W., Bleijswijk, J. v., Brownlee, C., Brummer, G. J., Conte, M., Egge, J., Fernandez, E., Jordan, R., Knap-pertsbusch, M., Stefels, J., Veldhuis, M., Wal, P. V. D., and Young, J.: A model system approach to biological climate forcing. The example of *Emiliana huxleyi*, *Global and Planetary Change*, 8, 27–46, 1993.
- Winter, A., Jordan, R. W., and Roth, P. H.: Biogeography of living Coccolithophores in oceanic waters, in: *Coccolithophores*, edited by: Winter, A. and Siesser, W. G., Cambridge University Press, Cambridge, 161–177, 1994.
- Young, J., and Ziveri, P.: Calculation of coccolith volume and its use in calibration of carbonate flux estimates, *Deep Sea Res.*, 47, 1679–1700, 2000.
- Ziveri, P., de Bernardi, B., Baumann, K.-H., Stoll, H. M., and Mortyn, G. P.: Sinking of coccolith carbonate and potential contribution to organic carbon ballasting in the deep ocean, *Deep Sea Research Part II: Topical Studies in Oceanography*, 54, 659–675, 2007.

Two High-Nutrient Low-Chlorophyll phytoplankton assemblages: the tropical central Pacific and the offshore Perú-Chile Current

F. Gómez¹, H. Claustre^{2,3}, P. Raimbault¹, and S. Souissi⁴

¹Laboratoire d’Océanographie et de Biogéochimie, CNRS UMR 6535, Centre d’Océanologie de Marseille, Université de la Méditerranée, 163 avenue de Luminy, 13288 Marseille, France

²UPMC Univ. Paris 06, UMR 7093, Laboratoire d’Océanographie de Villefranche, 06230 Villefranche-sur-Mer, France

³CNRS, UMR 7093, LOV, 06230 Villefranche-sur-Mer, France

⁴Station Marine de Wimereux, Université des Sciences et Technologies de Lille-Lille1, FRE 2816 ELICO CNRS, 28 avenue Foch, BP 80, 62930 Wimereux, France

Received: 11 April 2007 – Published in Biogeosciences Discuss.: 14 May 2007

Revised: 5 October 2007 – Accepted: 27 November 2007 – Published: 14 December 2007

Abstract. The phytoplankton ($>15\ \mu\text{m}$) composition and abundance was investigated along a ~ 8000 km transect between the Marquesas Islands Archipelago and the Chilean coasts off Concepción. In the southern limit of the central Equatorial Pacific (at 8°S , 141°W), in High-Nutrient Low-Chlorophyll (HNLC) warm waters, the microphytoplankton assemblage was dominated by the lightly silicified diatoms *Pseudo-nitzschia delicatissima* and *Rhizosolenia bergonii*. The morphology of these species, a small pennate diatom that exhibited a tendency to form “ball of needles” clusters and large centric diatom ($>500\ \mu\text{m}$ long), are interpreted as two anti-grazing strategies in an environment dominated by small micrograzers. Surprisingly, this a priori typical HNLC phytoplankton assemblage was also found in the temperate offshore waters of the Perú-Chile Current between 2000 and 600 km off Chile. This observation suggests that a common set of environmental factors (obviously other than temperature and salinity) are responsible for the establishment and maintaining of this distinctive phytoplankton in these geographically and hydrologically distant regions. Both regions are characterized by a surface nitrate-silicic acid ratio ranging from 1–3. Occasionally *Rhizosolenia bergonii* showed frustules anomalously fragmented, likely the result of extreme weakly silicified phytoplankton. We suggest that silicon deficiency may be responsible of the occurrence of HNLC phytoplankton assemblage in the tropical central Pacific as well as the offshore Perú-Chile Current during the austral summer.

1 Introduction

The equatorial upwelling region in the central and eastern Pacific constitutes a large area of the so-called the High Nutrient Low Chlorophyll (HNLC) waters, representing a strong source of CO_2 to the atmosphere (Chavez and Toggweiler, 1995). Grazing control, ammonium inhibition of nitrogen uptake, limitations in silicic acid, micronutrient (iron) or light, lack of neritic bloom-forming diatoms among other hypothesis have been invoked to explain these paradoxical HNLC conditions (Chavez et al., 1991; Coale et al., 1996; Dugdale and Wilkerson, 1998). The microscope observations in the upwelling region of the central and eastern equatorial Pacific revealed a recurrent phytoplankton assemblage mainly composed of the small pennate diatom *Pseudo-nitzschia delicatissima* and the large centric diatom *Rhizosolenia bergonii* (Hasle, 1960).

The iron-hypothesis has challenged new studies in the equatorial upwelling region that have been focused, in particular, on biogeochemical fluxes and parameters such as biomass estimates and rate measures of primary and secondary production following the iron fertilization. These studies were nevertheless accompanied by scarce investigations on the large phytoplankton composition (Kaczmarek and Fryxell, 1994; Iriarte and Fryxell, 1995). They were often limited to identifications at suprageneric levels (Chavez and Buck, 1990) or focused on the species identification during iron-enriched incubation experiments (Fryxell and Kaczmarek, 1995).

The Perú-Chile or Humboldt Current originates when a part of the water that flows toward the east across the sub-Antarctic Ocean is deflected toward the north as it approaches South America. It flows northward along the coast

Correspondence to: F. Gómez
(fernando.gomez@fitoplancton.com)

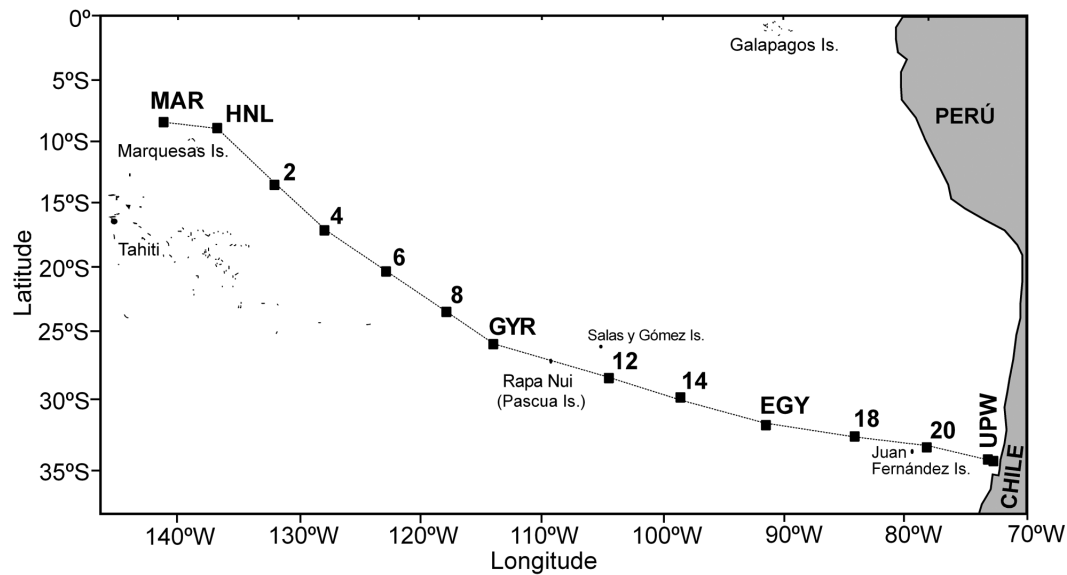


Fig. 1. Map of the stations occupied (solid squares) in the SE Pacific Ocean.

of Chile, Perú and Ecuador, and is associated with the economically most important coastal upwelling of the world's oceans (Longhurst, 1998). The coastal phytoplankton of the region is well documented (e.g. Rivera, 1983; Avaria and Muñoz, 1987). In contrast, the phytoplankton from the open waters of SE Pacific is one of the least known and documented of the world's oceans (Balech, 1962), reflecting the general undersampling of this remote area (Longhurst, 1998; Claustre and Maritorena, 2003). Very few recent investigations have been dedicated to the study of the picophytoplankton in the subtropical SE Pacific in latitudinal transects crossing the equator (DiTullio et al., 2003) or a few surface net samples with scarce detail on the phytoplankton specific composition (Hardy et al., 1996).

Within this context, we examined the composition and abundance of phytoplankton in relation to physical and chemical properties in the SE Pacific Ocean as part of a multidisciplinary survey along a transect of ~8000 km covering contrasted trophic conditions: HNLC waters of the Marquesas Islands Archipelago, hyper oligotrophic waters of the South Pacific Gyre (SPG), and more eutrophic conditions in the Perú-Chile Current (PCC) and the Chilean coastal upwelling. The present study focuses on the HNLC phytoplankton assemblage (HNLC-PA) near the Marquesas Islands Archipelago, the southern limit of the equatorial upwelling region that unexpectedly was also observed in a vast region of the temperate waters of the SE Pacific off Chile. The similarity in HNLC phytoplankton assemblage between two distant geographical and hydrological regions is analyzed and interpreted in the context of possible driving factors precluding this a priori paradoxical situation.

2 Methods

The data were collected during the BIOSOPE (Biogeochemistry and Optics South Pacific Experiment) cruise on board R/V L'Atalante from 26 October–12 December 2004. The ship was equipped with a 75 kHz RDI Acoustic Doppler Current Profiler (ADCP). Water sampling and measurements of temperature and salinity were made using a SeaBird SBE 911plus CTD/Carousel system fitted with an in situ Aquatracka III Chelsea fluorometer and Niskin bottles. The percentage of surface irradiance at each depth was calculated from the underwater PAR (Photosynthetic Active Radiation, 400–700 nm) profiles performed by a PNF-300 Profiling Natural Fluorometer sensor (Biospherical Instruments, Inc.). The limit of the euphotic zone corresponds to the depth where PAR is reduced to 1% of its surface value. Major nutrients and chlorophyll *a* were measured as described in Raimbault et al. (2007).

For microplankton analysis, samples were collected at 14 stations from 5–280 m depth (Fig. 1). One hundred samples were preserved with acidified Lugol's solution and stored at 5°C. A 500 ml aliquot of the sample was concentrated by sedimentation in glass cylinders. During a six-day settling period, the top 450 ml of the sample was slowly siphoned off with small-bore tubing. Fifty ml of the concentrate representing 500 ml of whole water sample was used for settlement in a composite settling chamber. The entire chamber was scanned at 200× magnification under an Olympus inverted microscope equipped with a digital camera. The specimens were photographed at 400× magnification with the Olympus DP70-BSW software. This methodology is suitable for the counting and identification of organisms higher than 15 μm. Diatoms and dinoflagellates were

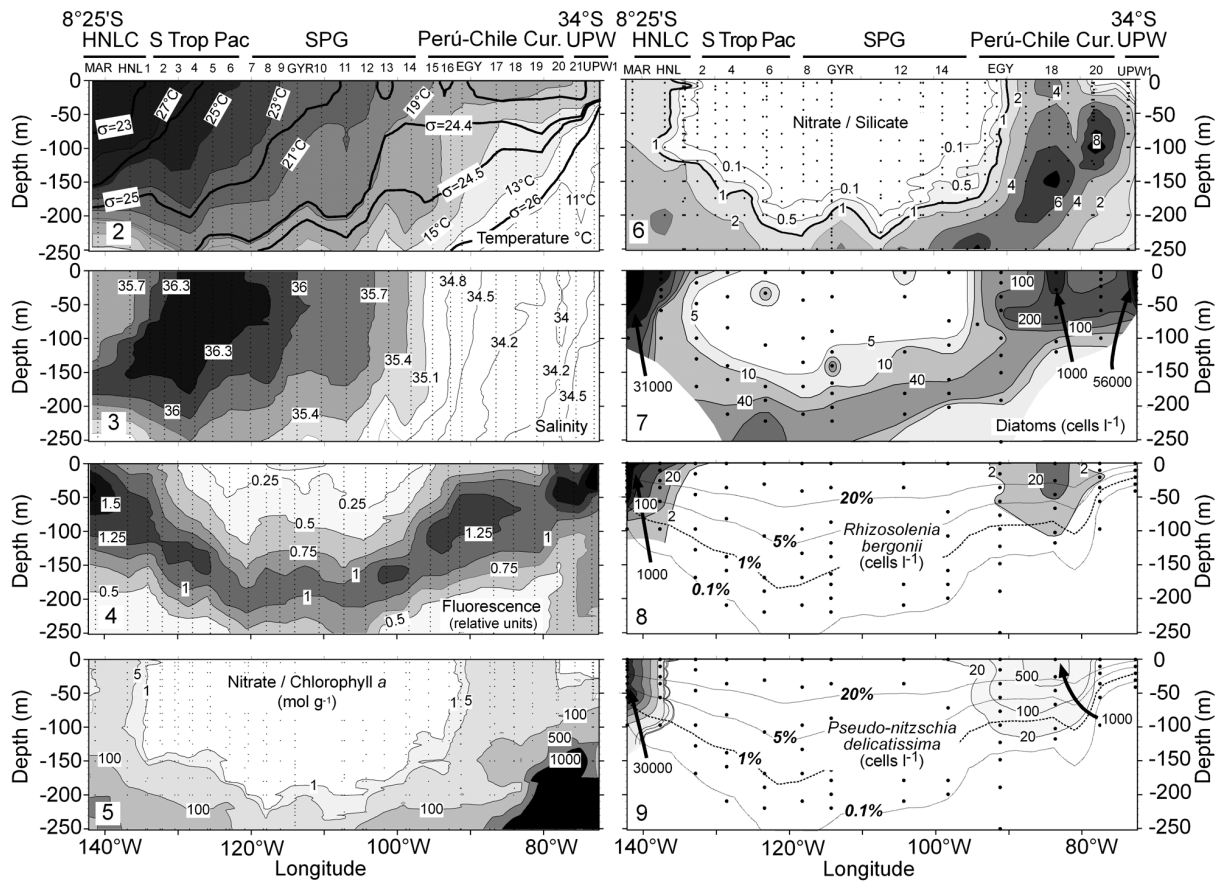


Fig. 2–9. Section plots of (2) temperature (°C) and the isopycnals lines labelled in units of sigma-t (density-1000)(kg m⁻³) are shown. (3) Salinity. (4) Fluorescence (relative units). (5) Nitrate-chlorophyll *a* ratio. (6) Nitrate-silicic acid ratio. (7) Abundance of diatoms. (8) *Rhizosolenia bergonii* and (9) *Pseudo-nitzschia delicatissima* (cells l⁻¹). The dashed lines represent the percentage of the surface irradiance.

well preserved, while most nanoplankton was lost due to preservation (i.e. coccolithophorids) or incomplete sedimentation. The organisms were identified to species level when possible.

3 Results

3.1 Tropical HNLC Phytoplankton assemblage

Waters surrounding the Marquesas Islands (8° S, 141° W) under the influence of the South Equatorial Current constituted the southern border of HNLC waters of the Equatorial Upwelling Region. Salinity ranged from 35.5–35.7 and the surface temperature reached 27.9°C. The vertical distribution of the fluorescence showed a wide maximum in the upper 50 m depth (Figs. 2–4). The concentrations of chlorophyll *a* (Chl *a*) were about 0.3–0.5 μg l⁻¹ with values of the nitrate-Chl *a* ratio higher than 5 (Fig. 5, Table 1).

Along 600 km between 8°23' S and 13°32' S extended the tropical HNLC-PA mainly represented small pennate diatom *Pseudo-nitzschia delicatissima* (30–80 μm in length,

2–3 μm in width) and the large centric diatom *Rhizosolenia bergonii* (>500 μm in length). The microphytoplankton abundance reached up to 31 000 cells l⁻¹ in the upper 60 m depth of the surrounding waters the Marquesas Islands Archipelago (Fig. 7). *Pseudo-nitzschia delicatissima* dominated the HNLC-PA with more than 85% of the total abundance. This threadlike and lightly sicilified species was relatively homogeneously distributed in the upper 60 m depth, and often forming clusters of 10–20 cells (Figs. 10–11). Other abundant colonial congeneric species were *Pseudo-nitzschia* cf. *subpacific*a (Fig. 12) and *Pseudo-nitzschia* cf. *pungens*. Strongly elongated cells (up to 2000 μm in length) of the pennate diatom *Thalassiothrix longissima* reached densities of 1200 cells l⁻¹ and other diatoms such as *Plagiotropis* spp. and *Haslea* spp. were abundant. *Rhizosolenia bergonii* was dominant and reached an abundance of 1000 cells l⁻¹ (maximum at 40–60 m depth, Figs. 13–14), followed by *Rhizosolenia acuminata* (120 cells l⁻¹). Although the abundance of these diatoms was low compared to *Pseudo-nitzschia* spp., it should be taken into account that they are very large and thick, and contribute importantly to

Table 1. Average values in the euphotic zone of chlorophyll *a* (Chl *a*, $\mu\text{g l}^{-1}$), nitrate (NO_3^- , μM), phosphate (PO_4^{3-} , μM), silicic acid (Si(OH)_4 , μM), nitrate-silicic acid ratio (N/Si), nitrate-phosphate ratio (N/P), abundance of diatoms ($> 15 \mu\text{m}$) and dinoflagellates ($> 15 \mu\text{m}$), units expressed as cells l^{-1} . Ze=depth of the euphotic zone calculated from the PNF-300 Profiling Natural Fluorometer sensor.

Station	HNLC-Marquesas		Tropical and South Pacific Gyre							Perú-Chile Current			Upw. UPW1
	MAR1	HNL	2	4	6	8	GYR3	12	14	EGY3	18	20	
Ze	66	90	124	136	157	144	155	152	136	94	87	48	31
Chl <i>a</i>	0.46	0.24	0.17	0.12	0.03	0.07	0.10	0.01	0.09	0.19	0.20	0.53	1.10
NO_3^-	1.48	1.52	0	0.04	0.02	0	0.01	0.01	0.01	0.30	4.08	2.18	2.38
PO_4^{3-}	0.46	0.36	0.17	0.14	0.12	0.13	0.15	0.15	0.05	0.16	0.42	0.41	0.63
Si(OH)_4	1.17	1.27	0.59	1.04	1.15	1.16	0.85	0.86	0.83	0.99	0.57	0.68	2.56
N/Si	1.27	1.25	0	0.04	0.02	0	0.01	0.01	0.01	0.32	7.10	3.16	0.86
N/P	3.23	4.34	0	0.30	0.19	0	0.06	0.04	0.13	1.61	9.73	4.64	3.62
DIATO	25103	148	8	4	10	1	9	14	15	89	662	176	342548
DINO	117	140	53	34	30	23	34	36	39	49	71	805	783



Fig. 10–19. Photomicrographs of microphytoplankton in the SE Pacific. (10–11) Clusters of *Pseudo-nitzschia delicatissima*, 20 m and 30 m depth. (12) *Pseudo-nitzschia* cf. *subpacificica*, 5 m depth. (13) “Normal” cell of *Rhizosolenia bergonii*, 60 m depth. (14) *R. bergonii* with fragmented frustule, 20 m depth. (10–14) 8°23' S; 141°14' W. (15) *R. bergonii* with fragmented frustule, 30 m depth. (16) *Rhizosolenia acuminata*, 5 m depth. (14–16) 9° S, 136°51' W; 30 and 5 m depth. (17) Curved cells of *R. bergonii* (13°32' S, 132°07' W, 5 m depth). (18) Auxospore of *R. bergonii*, 33°21' S, 78°06' W, 5 m depth. (19) Highly pigmented cells of *Rhizosolenia* sp. (17°13' S, 127°58' W, 210 m depth). Scale bar=50 μm .

the phytoplankton biomass. Other common centric diatoms were *Chaetoceros peruvianus* (200 cells l^{-1} near surface), *Chaetoceros atlanticus* var. *neapolitanus*, *Planktoniella sol*, *Bacteriastrium* cf. *elongatum* and *Asteromphalus heptactis*.

The dinoflagellates, ranging from 112–180 cells l^{-1} , showed a shallower distribution than the diatoms. The assemblage was rich on large autotrophic thecate species of the genus *Ceratium* (48–108 cells l^{-1}), mainly *C. tripos*, *C. furca*,

C. massiliense, *C. candelabrum*, and unarmoured dinoflagellates such as *Brachidinium capitatum* f. *Karenia papilionacea* (12–24 cells l⁻¹), *Pyrocystis* spp. and the prasino-phyte in phycome stage *Pterosperma moebii* (40 cells l⁻¹). Among the heterotrophic species, dinoflagellates (*Protoperidinium* and *Gyrodinium*) and choanoflagellates were abundant (Table 2).

At a station located 480 km eastwards (9° S, 136°51' W), diatom abundance decreased to 100–380 cells l⁻¹ (Fig. 7) and was dominated by *Rhizosolenia bergonii* that accounted for half of diatoms (Fig. 8). The abundance of *Pseudo-nitzschia delicatissima* was low (<140 cells l⁻¹) and the diatom clusters were not observed. The abundance of *R. bergonii* (180 cells l⁻¹) was less reduced than that of *P. delicatissima* in proportion to the previous station (Fig. 9). As occurred in the previous station, specimens of *R. bergonii* and *R. acuminata* showed the frustule anomalously fragmented in some concentric sections of the girdle (Figs. 14–16).

The decrease of the diatom abundance was associated with an increase of dinoflagellates (100–230 cells l⁻¹). The autotrophic species of *Ceratium* were replaced by heterotrophic species such as *C. teres*. The abundance of diatom-consumers dinoflagellates (*Protoperidinium* spp.) decreased and smaller heterotrophic species such as *Oxytoxum variable* and *Podolompa spinifera* were common.

To the south (13°32' S, 132°07' W), the HNLC-PA was present with a very low abundance (<50 cells l⁻¹) (Figs. 7–9). *Pseudo-nitzschia delicatissima* (20 cells l⁻¹), *Planktoniella sol*, a few specimens of *R. bergonii*, and *Thalassiothrix* sp. were encountered in the surface layer. Near the bottom of the euphotic (100–150 m depth, see Fig. 3), the salty South Tropical Pacific Waters coincided with highly pigmented specimens of *Rhizosolenia* cf. *imbricata* (Fig. 19), and *Nitzschia bicapitata* species complex at 170 m depth. The abundance of dinoflagellates ranged from 40–110 cells l⁻¹.

3.2 Temperate HNLC phytoplankton assemblage

Between 30° S and 32° S extended a subtropical front characterized by decrease of the salinity and temperature, and the shoaling of the isopicne of 1025.4 Kg m⁻³. The isohalines between 35.3 and 34.6 were vertically distributed in the upper 200 m. From 50–200 m depth, the isotherms were vertically distributed decreasing between 18°C and 16°C (Figs. 2–3). To the east, along the salinity frontal region the fluorescence increased and shoaled between 120 m and 70–80 m depth (Fig. 4). The nitrate-Chl *a* ratio showed values higher than 5 (Fig. 5).

The Perú-Chile Current is a width equatorward cold-water current. The isopicne of 1025.4 kg m⁻³ (Fig. 2) and the depth of the fluorescence maximum were horizontally distributed (Fig. 4). The PCC, delimited by isohaline of 34.3, was associated with fresher waters, especially between

78° W and 75° W (salinity ~34.1). Near the Juan Fernández Archipelago (650 km off Chile) the salinity decreased to 33.9 and isotherm of 11°C shoaled (Figs. 2–3). This fresher water mass found in the surface may correspond to the Eastern South Pacific Intermediate Water as defined by Schneider et al. (2003). In these conditions, the fluorescence increased and shoaled (Fig. 4). The ADCP measurements showed a northwards component between 92° W and 84° W, while the current was weak and often reverse towards the coasts of Chile.

Large phytoplankton was nearly absent in the upper 120 m of the vast region of the SPG with very deep maximum composed of *Nitzschia bicapitata* species complex, *Nitzschia* spp. and other small pennate diatoms. The large phytoplankton in the upper layer reappeared towards the western Perú-Chile Current. The surface phytoplankton assemblage found in the PCC coincided to that observed in the central tropical Pacific. About 2000 km off Chile under the influence of PCC (31°52' S, 91°24' W) the phytoplankton was constituted of the typical HNLC-PA in surface and deeper the diatom assemblage found in the oligotrophic waters of the SPG. In upper 100 m, the diatom abundance was 50–196 cells l⁻¹ composed of *Pseudo-nitzschia delicatissima* (160 cells l⁻¹), *Rhizosolenia bergonii* (8 cells l⁻¹), *R. acuminata* (6 cells l⁻¹), and a few specimens of *Plagiotropis* sp. and *Thalassiothrix* sp. Deeper than 100 m depth and parallel to the shoaling of the bottom of the euphotic zone, the abundance of the diatoms was low and composed of *Dactyliosolen* sp. (80–150 m depth), *Chaetoceros atlanticus* var. *neapolitanus* and *Thalassiosira* sp. (160 cells l⁻¹ at 80 m depth) (Fig. 7).

In the upper 60 m depth, the abundance of dinoflagellates ranged from 54–168 cells l⁻¹. The autotrophic dinoflagellates *Gonyaulax polygramma* (60 cells l⁻¹), *Ceratium fusus* (40 cells l⁻¹), *C. furca* were responsible of the surface maximum. Other autotrophic species were *C. tripos*, *C. azoricum*, *C. candelabrum*, *C. kofoidii* as observed in the warm HNLC region and brachidiniaceans. A diverse assemblage of heterotrophic dinoflagellates of more eutrophic conditions was present (Table 2).

In temperate waters ~1300 km off Chile (32°42' S, 84°04' W) the nitrate-silicic acid ratio was higher than 4 in the euphotic zone, with a maximum of 6 in the surface (Fig. 6, Table 1). The diatom assemblage was similar to that in HNLC conditions near the Marquesas Islands Archipelago. The diatom abundance showed values up to 1200 cells l⁻¹ in upper layer (Fig. 7) dominated by *Pseudo-nitzschia delicatissima* (900 cells l⁻¹), *Pseudo-nitzschia* cf. *subpacific* (120 cells l⁻¹), *Rhizosolenia bergonii* (50 cells l⁻¹) (Figs. 17–18), *Thalassiothrix* sp. (40 cells l⁻¹), *Planktoniella sol* (16 cells l⁻¹) and *Asteromphalus heptactis* (20 cells l⁻¹). *Dactyliosolen* sp. and *Chaetoceros atlanticus* var. *neapolitanus* were encountered below the surface phytoplankton assemblage. The abundance of dinoflagellates was low (40–78 cells l⁻¹), mainly composed of *Pronoctiluca pelagica* f. *spinifera*

Table 2. List of diatoms, dinoflagellates (> 15 μm) and large flagellates during the BIOSOPE cruise. HNLC=High-Nutrient Low-Chlorophyll region near the Marquesas Islands Archipelago; SPG=Tropical and South Pacific Gyre; PCC=Perú-Chile Current; UPW=Coastal upwelling off Concepción.

Diatom taxa	HNLC	SPG	PCC	UPW
<i>Asterionellopsis glacialis</i> (Castracane) Round				+
<i>Asterolampra marylandica</i> Ehrenberg		+		
<i>Asteromphalus flabellatus</i> (Brébisson) Greville	+	+	+	+
<i>Bacillaria</i> cf. <i>paxillifera</i> (O.F. Müller) Hendey	+			
<i>Bacteriastrum</i> cf. <i>comosum</i> Pavillard	+		+	
<i>Bacteriastrum</i> cf. <i>furcatum</i> Shadbolt	+			
<i>Bacteriastrum</i> sp1		+	+	
<i>Bacteriastrum</i> sp2				+
<i>Bacteriastrum</i> sp3		+		
<i>Chaetoceros affinis</i> Lauder				+
<i>Chaetocero atlanticus</i> var. <i>neapolitanus</i> (Schröder) Hustedt	+	+	+	
<i>Chaetoceros compressus</i> Lauder				+
<i>Chaetoceros curvisetus</i> Cleve				+
<i>Chaetoceros dadayi</i> Pavillard	+	+	+	
<i>Chaetoceros</i> cf. <i>diadema</i> (Ehrenberg) Gran				+
<i>Chaetoceros didymus</i> Ehrenberg				+
<i>Chaetoceros</i> cf. <i>diversus</i> Cleve		+		
<i>Chaetoceros lacinosus</i> Schütt				+
<i>Chaetoceros lauderi</i> Ralfs				+
<i>Chaetoceros lorenzianus</i> Grunow	+			+
<i>Chaetoceros peruvianus</i> Brightwell	+	+	+	
<i>Chaetoceros radicans</i> Schütt				+
<i>Chaetoceros rostratus</i> Lauder				+
<i>Chaetoceros</i> cf. <i>tenuissimus</i> Meunier				+
<i>Chaetoceros tetrastichon</i> Cleve	+	+		
<i>Chaetoceros</i> sp1		+		
<i>Chaetoceros</i> sp2		+		
<i>Chaetoceros</i> sp3	+	+		
<i>Chaetoceros</i> sp4		+		
<i>Chaetoceros</i> sp5		+		
<i>Corethron</i> cf. <i>criophilum</i> Castracane				+
<i>Coscinodiscus</i> sp.		+		
<i>Dactyliosolen</i> sp.		+	+	
<i>Dactyliosolen fragilissimus</i> (Bergon) Hasle				+
<i>Detonula pumila</i> (Castracane) Schütt				+
<i>Eucampia cornuta</i> (Cleve) Grunow				+
<i>Eucampia zodiacus</i> Ehrenberg				+
<i>Fragilariopsis doliolus</i> (Wallich) Medlin et Sims	+			
<i>Guinardia delicatula</i> (Cleve) Hasle				+
<i>Guinardia flaccida</i> (Castracane) Peragallo				+
<i>Guinardia striata</i> (Stolterfoth) Hasle				+
<i>Grossleriella tropica</i> Schütt		+		
<i>Hemiaulus hauckii</i> Grunow		+		
<i>Hemidiscus cuneiformis</i> Wallich	+			
<i>Lauderia annulata</i> Cleve				+
<i>Leptocylindrus danicus</i> Cleve				+
<i>Neostreptothea torta</i> f. <i>triangularis</i> Stosch		+		
<i>Nitzschia bicapitata</i> species complex	+	+	+	
<i>Nitzschia longissima</i> (Brébisson) Ralfs	+		+	+

Table 2. Continued.

Diatom taxa	HNLC	SPG	PCC	UPW
<i>Nitzschia</i> sp. (? <i>braarudii</i>)		+	+	
<i>Odontella</i> cf. <i>longicrucis</i> (Greville) Hoban				+
<i>Plagiotropis</i> sp.	+	+	+	
<i>Plagiotropis</i> sp. (? <i>lepidoptera</i>)	+	+	+	
<i>Planktoniella sol</i> (Wallich) Schütt				
<i>Proboscia alata</i> (Brightwell) Sundström	+	+	+	+
<i>Pseudotriceratium cinnamomeum</i> (Greville) Grunow		+		
<i>Pseudo-nitzschia delicatissima</i> (Cleve) Heiden <i>sensu</i> Hasle 1960	+	+	+	
<i>Pseudo-nitzschia</i> cf. <i>pungens</i> (Grunow <i>ex</i> Cleve) Hasle	+		+	
<i>Pseudo-nitzschia</i> cf. <i>subpacifica</i> (Hasle) Hasle	+		+	+
<i>Pseudo-nitzschia</i> sp1		+		
<i>Pseudo-nitzschia</i> sp2				+
<i>Pseudo-nitzschia</i> sp3				+
cf. <i>Pseudoeumotia</i> sp.		+	+	
<i>Rhizosolenia acuminata</i> (Peragallo) Gran				
<i>Rhizosolenia bergonii</i> Peragallo	+	+	+	
<i>Rhizosolenia</i> cf. <i>castracanei</i> Peragallo		+		
<i>Rhizosolenia clevei</i> var. <i>communis</i> Sundström		+		
<i>Rhizosolenia</i> cf. <i>imbricata</i> Brightwell		+		+
<i>Rhizosolenia</i> cf. <i>imbricata</i> var. <i>shrubsolleyi</i> (Cleve) Schröder		+		+
<i>Rhizosolenia setigera</i> Brightwell				+
<i>Rhizosolenia styliformis</i> Brightwell	+	+		
<i>Skeletonema</i> sp.				+
<i>Thalassionema nitzschioides</i> (Grunow) Mereschkowsky		+		+
<i>Thalassionema</i> cf. <i>pseudonitzschioides</i> (Schuette <i>et</i> Schrader) Hasle		+		+
<i>Thalassionema elegans</i> Hustedt	+	+		
<i>Thalassionema</i> sp.		+		
<i>Thalassiosira anguste-lineata</i> (A. Schmidt) Fryxell <i>et</i> Hasle				+
<i>Thalassiosira</i> cf. <i>decipiens</i> (Grunow) Jørgensen				+
<i>Thalassiosira</i> cf. <i>oestrupii</i> (Ostenfeld) Hasle	+		+	
<i>Thalassiosira subtilis</i> (Ostenfeld) Gran	+		+	+
<i>Thalassiosira</i> sp.			+	
<i>Thalassiothrix longissima</i> Cleve <i>et</i> Grunow	+	+	+	+
<i>Thalassiothrix</i> cf. <i>heteromorpha</i> Karsten	+	+	+	
Dinoflagellate taxa				
cf. <i>Amphidoma caudata</i> Halldal	+			
<i>Amphisolenia bidentata</i> Schröder		+	+	
<i>Amphisolenia globifera</i> Stein	+	+	+	
cf. <i>Blephaerocysta</i> sp.	+	+	+	
<i>Brachidinium capitatum</i> F.J.R. Taylor f. <i>Asterodinium</i>	+	+	+	+
<i>Brachidinium capitatum</i> F.J.R. Taylor f. <i>Brachidinium</i>	+	+	+	
<i>Brachidinium capitatum</i> F.J.R. Taylor f. <i>Karenia papilionacea</i>	+	+	+	+
<i>Brachidinium capitatum</i> F.J.R. Taylor f. <i>Microceratium</i>		+		
<i>Ceratium arietinum</i> Cleve		+		
<i>Ceratium azoricum</i> Cleve	+		+	+
<i>Ceratium belone</i> Cleve			+	
<i>Ceratium breve</i> (Ostenfeld <i>et</i> Schmidt) Schröder	+			
<i>Ceratium candelabrum</i> (Ehrenberg) Stein	+		+	
<i>Ceratium carnegiei</i> Graham <i>et</i> Bronikowsky	+		+	
<i>Ceratium carriense</i> Gourret	+	+	+	
<i>Ceratium</i> cf. <i>lineatum</i> (Ehrenberg) Cleve	+			

Table 2. Continued.

Dinoflagellate taxa	HNLC	SPG	PCC	UPW
<i>Ceratium contortum</i> (Gourret) Cleve			+	
<i>Ceratium declinatum</i> (Karsten) Jørgensen	+	+		
<i>Ceratium divaricatum</i> (Lemmermann) Kofoid var. <i>divaricatum</i>			+	
<i>Ceratium divaricatum</i> var. <i>balechii</i> (Meave, Okolodkov et Zamudio) Hernández-Becerril	+			+
<i>Ceratium extensum</i> (Gourret) Cleve		+	+	
<i>Ceratium falcatum</i> (Kofoid) Jørgensen	+			
<i>Ceratium furca</i> (Ehrenberg) Claparède et Lachmann	+	+	+	+
<i>Ceratium fusus</i> (Ehrenberg) Dujardin	+	+	+	+
<i>Ceratium gibberum</i> Gourret	+	+	+	
<i>Ceratium horridum</i> (Cleve) Gran				+
<i>Ceratium kofoidii</i> Jørgensen	+	+	+	
<i>Ceratium lanceolatum</i> Kofoid			+	
<i>Ceratium limulus</i> Gourret			+	
<i>Ceratium massiliense</i> (Gourret) Jørgensen	+	+	+	
<i>Ceratium pentagonum</i> Gourret	+	+	+	+
<i>Ceratium platycorne</i> Daday		+		
<i>Ceratium praeolongum</i> (Lemmermann) Kofoid			+	
<i>Ceratium pulchellum</i> Schröder				+
<i>Ceratium symmetricum</i> Pavillard		+	+	
<i>Ceratium teres</i> Kofoid	+	+		
<i>Ceratium trichoceros</i> (Ehrenberg) Kofoid	+	+	+	+
<i>Ceratium tripos</i> (O.F. Müller) Nitzsch	+	+	+	+
<i>Ceratocorys bipes</i> (Cleve) Kofoid			+	
<i>Ceratocorys horrida</i> Stein			+	
<i>Citharistes</i> sp.	+			
<i>Cladopyxis brachiolata</i> Stein	+	+	+	
<i>Cladopyxis</i> sp.	+	+	+	+
<i>Cochlodinium</i> sp.		+	+	+
<i>Craspedotella pileolus</i> Kofoid		+		
<i>Craspedotella</i> sp.	+	+	+	+
<i>Dicroerisma psilonereia</i> F.J.R. Taylor et Cattell	+	+	+	
<i>Dinophysis acuminata</i> Claparède et Lachmann				+
<i>Dinophysis</i> cf. <i>swezyae</i> Kofoid et Skogsberg		+		
<i>Dinophysis fortii</i> Pavillard			+	
<i>Dinophysis mucronata</i> (Kofoid et Skogsberg) Sournia	+		+	
<i>Dinophysis schuettii</i> Murray et Whitting		+	+	
<i>Erythrosideinium agile</i> (Hertwig) P.C. Silva	+	+	+	+
cf. <i>Gonyaulax birostris</i> Stein			+	
<i>Gonyaulax polygramma</i> Stein	+	+	+	
<i>Gymnodinium fusus</i> Schütt/ <i>Gyrodinium falcatum</i> Kofoid et Swezy	+	+	+	
<i>Gymnodinium</i> sp1				+
<i>Gymnodinium</i> sp2		+		
<i>Gyrodinium</i> spp.	+			+
<i>Gyrodinium spirale</i> (Bergh) Kofoid et Swezy	+	+	+	+
<i>Histioneis</i> cf. <i>crateriformis</i> Stein		+	+	
<i>Histioneis</i> cf. <i>pulchra</i> Kofoid			+	
<i>Histioneis</i> cf. <i>striata</i> Kofoid et Michener			+	
<i>Histioneis cleaveri</i> Rampi	+	+		
<i>Histioneis hyalina</i> Kofoid et Michener	+			
<i>Histioneis joergensenii</i> Schiller		+		
<i>Histioneis longicollis</i> Kofoid			+	

Table 2. Continued.

Dinoflagellate taxa	HNLC	SPG	PCC	UPW
cf. <i>Histiophysis</i> sp.			+	
<i>Karenia</i> cf. <i>bicuneiformis</i> Botes, Sym et Pitcher		+		
<i>Karenia</i> cf. <i>mikimotoi</i> (Miyake et Kominami ex Oda) G. Hansen et Moestrup	+		+	
<i>Karenia</i> spp.	+	+	+	+
<i>Kofoidinium pavillardii</i> J. Cachon et M. Cachon	+	+	+	
<i>Kofoidinium</i> sp.	+	+	+	
<i>Kofoidinium velelloides</i> Pavillard	+	+	+	
<i>Leptodiscus medusoides</i> Hertwig			+	
cf. <i>Metaphalacroma skogsbergii</i> Tai in Tai et Skogsberg			+	
<i>Nematodinium</i> sp.	+	+	+	
<i>Ornithocercus magnificus</i> Stein		+	+	
<i>Ornithocercus quadratus</i> Schütt	+	+	+	
<i>Ornithocercus</i> sp.	+	+		
<i>Oxytoxum</i> cf. <i>crassum</i> Schiller	+	+	+	
<i>Oxytoxum</i> cf. <i>frenquellii</i> Rampi			+	
<i>Oxytoxum</i> cf. <i>laticeps</i> Schiller	+	+		+
<i>Oxytoxum</i> cf. <i>longum</i> Schiller		+	+	
<i>Oxytoxum challengeroides</i> Kofoid		+		
<i>Oxytoxum constrictum</i> (Stein) Bütschli		+	+	
<i>Oxytoxum curvatum</i> (Kofoid) Kofoid	+	+	+	
<i>Oxytoxum curvicaudatum</i> Kofoid		+	+	
<i>Oxytoxum diploconus</i> Stein	+	+	+	
<i>Oxytoxum longiceps</i> Schiller	+	+	+	
<i>Oxytoxum scolopax</i> Stein	+	+	+	+
<i>Oxytoxum</i> sp1			+	
<i>Oxytoxum</i> sp2	+			
<i>Oxytoxum</i> sp3		+		
<i>Oxytoxum</i> sp4			+	
<i>Oxytoxum tessellatum</i> (Stein) Schütt	+	+	+	
<i>Oxytoxum variabile</i> Schiller	+	+	+	
<i>Phalacroma rotundatum</i> (Claparède et Lachmann) Kofoid et Michener			+	
<i>Phalacroma</i> sp1	+	+	+	
<i>Phalacroma</i> sp2	+			
<i>Phalacroma</i> sp3		+		
<i>Phalacroma</i> sp4		+		
<i>Phalacroma</i> sp5		+	+	
<i>Podolampas bipes</i> Stein	+	+	+	
<i>Podolampas elegans</i> Schütt		+	+	+
<i>Podolampas palmipes</i> Stein	+	+	+	
<i>Podolampas</i> sp.	+			
<i>Podolampas spinifera</i> Okamura	+	+	+	+
<i>Polykrikos</i> cf. <i>schwartzii</i> Bütschli		+	+	+
cf. <i>Pomatodinium impatiens</i> J. Cachon et Cachon-Enjumet	+		+	
<i>Pronoctiluca pelagica</i> Fabre-Domergue	+	+		
<i>Pronoctiluca pelagica</i> Fabre-Domergue f. <i>spinifera</i>	+	+	+	+
<i>Prorocentrum</i> cf. <i>compressum</i> (Bailey) Abé ex Dodge	+			
<i>Prorocentrum dentatum</i> Schiller	+	+		
<i>Prorocentrum rostratum</i> Stein	+	+	+	
<i>Prorocentrum</i> sp.			+	
<i>Protoperidinium</i> cf. <i>conicum</i> (Gran) Balech	+			
<i>Protoperidinium</i> cf. <i>curtipes</i> (Jørgensen) Balech	+		+	+

Table 2. Continued.

Dinoflagellate taxa	HNLC	SPG	PCC	UPW
<i>Protoperidinium</i> cf. <i>depressum</i> (Bailey) Balech				+
<i>Protoperidinium</i> cf. <i>divergens</i> (Ehrenberg) Balech	+			
<i>Protoperidinium</i> cf. <i>murrayi</i> (Kofoid) Hernández-Becerril	+		+	
<i>Protoperidinium</i> cf. <i>obtusum</i> (Karsten) Parke et Dodge	+			
<i>Protoperidinium</i> cf. <i>ovatum</i> Pouchet		+		
<i>Protoperidinium</i> cf. <i>steinii</i> (Jørgensen) Balech	+	+	+	+
<i>Protoperidinium</i> sp.	+			+
<i>Ptychodiscus noctiluca</i> Stein	+		+	
<i>Pyrocystis fusiformis</i> (Wyville Thomson ex Haeckel) Blackman	+			
<i>Pyrocystis lumula</i> (Schütt) Schütt	+	+	+	
<i>Pyrocystis noctiluca</i> J. Murray ex Haeckel	+	+	+	
cf. <i>Pyrocystis obtusa</i> Pavillard	+		+	
<i>Pyrophacus steinii</i> (Schiller) Wall et Dale			+	+
<i>Scaphodinium mirabile</i> Margalef	+	+	+	
<i>Scaphodinium</i> sp.		+		
<i>Scrippsiella</i> sp.		+		+
<i>Spatulodinium pseudonociluca</i> (Pouchet) J. Cachon et M. Cachon			+	+
<i>Spatulodinium</i> sp1		+	+	
<i>Spatulodinium</i> sp2		+		
cf. <i>Spiraulax jolliffei</i> (Murray et Whitting) Kofoid		+	+	
<i>Torodinium teredo</i> (Pouchet) Kofoid et Swezy	+	+	+	+
Large flagellate taxa				
<i>Dictyocha fibula</i> Ehrenberg	+		+	+
<i>Pterosperma moebii</i> (Jørgensen) Ostefeld	+	+	+	
<i>Pterosperma cuboides</i> Gaarder		+		
<i>Halosphaera viridis</i> Schmitz		+		
<i>Solenicola setigera</i> Pavillard	+	+	+	+

(40 cells l⁻¹), *Ptychodiscus noctiluca*, *Ornithocercus magnificus*, *Phalacroma rotundatum*, *Gyrodinium falcatum*, *Gonyaulax polygramma* (12 cells l⁻¹), *Ceratium fusus*, and *Dinophysis fortii* (8 cells l⁻¹) (Table 2).

About 650 km off Chile, a sampling station (33°21' S, 78°06' W) located 30 km north from the Robinson Crusoe Island, Juan Fernández Archipelago, was visited. The salinity reached a minimum of 33.9 in the surface. The ADCP measurements showed an eastwards drift and the surface warm waters run above the entrainment of fresher waters. This – surface stratified upwelling – resulted on a red tide of dinoflagellates with a surface abundance of 4400 cells l⁻¹. The main component of the red tide was the non-toxic autotrophic dinoflagellate *Gonyaulax polygramma* that reached 3800 cells l⁻¹ at 5 m depth, 530 cells l⁻¹ at 25 m, and nearly disappeared below this depth. Other autotrophic dinoflagellates were *Ceratium azoricum* (90 cells l⁻¹), *C. massiliense*, *C. gibberum*, *C. limulus*, *Ptychodiscus noctiluca* and brachidiniaceans. The heterotrophic dinoflagellates reached a high abundance, mainly composed of *Protoperidinium* cf. *curtipes* (120 cells l⁻¹), *Ornithocercus quadratus*, *Gyrodinium spirale* in the upper 5–15 m depth as well as kofoidiniaceans (*Kofoidinium* and *Spatulodinium*). Dinoflagellates such as *Oxytoxum longum* and *Pronociluca*

pelagica f. *spinifera* were encountered at mid-depths. The abundance of diatoms ranged from 100–600 cells l⁻¹ (Fig. 7) with *Pseudo-nitzschia delicatissima*, *Rhizosolenia bergonii* (4 cells l⁻¹), and *Pseudo-nitzschia* cf. *subpacificica* in the surface layer, *Thalassiosira* sp. (180 cells l⁻¹) at 25 m depth and *Dactyliosolen* sp. at 60 m depth were encountered (Table 2).

4 Discussion

4.1 High Nutrient-Low Chlorophyll phytoplankton assemblages

The HNLC-PA in the southeast Pacific was dominated by the lightly silicified diatoms *Pseudo-nitzschia delicatissima* and *Rhizosolenia bergonii* that were encountered in the Marquesas Islands Archipelago at 8° S with a surface temperature of 28° C and salinity 35.5, and between 2000 and 600 km off the Chilean coast at 33° S with a surface temperature of 17° C and salinity of 34 (Figs. 2–3, 8–9). The western side of the PCC did not appear in the literature as one of the HNLC regions of the world's oceans. The HNLC-PA showed scarce differences in these geographically distant regions. Only a few tropical species such as the dinoflagellate genus

Citharistes was absent in temperate waters (Table 2). HNLC diatoms such as *Planktoniella sol* or *Rhizosolenia bergonii* are commonly reported along the South American coastal waters associated with warm waters especially during the El Niño conditions (Avaria and Muñoz, 1987; Rodríguez et al., 1996). Based on a single survey and with a paucity of information in the literature in offshore waters in the region, the present study does not allow to establish the occurrence of the HNLC-PA in the western PCC as a permanent feature. In the SE Pacific the HNLC-PA was encountered in two regions of contrasted temperature and salinity values. Other trophic or ecological factor(s) may determinate the occurrence of the HNLC-PA in these two distant regions.

4.1.1 Grazing and the HNLC-PA

One of the explanations for the HNLC paradox is that phytoplankton populations are strictly controlled by the zooplankton (Frost and Franzen, 1992; Leising et al., 2003). In the equatorial Pacific, Roman and Gauzens (1997) suggested that the scarce copepods mainly grazed on protozoa. Landry et al. (1995) reported that grazing by microzooplankton dominates phytoplankton losses, and that large diatoms are not easily exploited by protistan consumers (ciliates, dinoflagellates, etc). The microscope observations in the present study showed a very low abundance of copepods, although the scarce volume examined (0.5 l) were insufficient to provide a statistically valid estimation of the early stages of copepods abundance. The ciliates and heterotrophic dinoflagellates (*Gyrodinium* spp. and *Protoperidinium* spp.) were abundant.

The two most successful species in the HNLC regions of the SE Pacific, *Pseudo-nitzschia delicatissima* and *Rhizosolenia bergonii*, seems to develop two different anti-grazing strategies. *Pseudo-nitzschia delicatissima*, and occasionally *Nitzschia longissima* increased their sizes by forming clumps or “ball of needles” of $\sim 100 \mu\text{m}$ in diameter disposed in all directions (Figs. 10–11). This diatom behavior was already described by Hasle (1960) and Buck and Chavez (1994). The aggregation of these diatoms suggests an anti-grazing adaptation in an environment dominated by micrograzers. On the other hand, centric diatoms such as *Rhizosolenia bergonii* and *R. acuminata* reached sizes $> 500 \mu\text{m}$ in length, being far of the prey size spectra of most micrograzers.

Other diatom species are not exclusive of the HNLC conditions, although they are favoured in these eutrophic conditions. Diatoms showed strongly elongated frustules or extensions. For example *Thalassiothrix longissima* is thin, but reached $2000 \mu\text{m}$ in length. *Planktoniella sol* secretes a large hyaline ring that increases its size. *Chaetoceros peruvianus* is a uni-cellular species with long spine-bearing setae. Colonial species such as *Chaetoceros atlanticus* var. *neapolianus* and *Bacteriastrium* cf. *elongatum* showed a similar strategy with long setae.

Beyond the size increase or aggregation of the diatoms as possible response to small grazers, it should be taken into account that the assemblage was dominated by *Pseudo-nitzschia*, a genus that contains numerous species able to produce the domoic acid. Reactive aldehydes produced by diatoms have been reported to reduce the fecundity and egg hatching success of copepods (Ianora et al., 2003). The effects of the compounds produced by diatoms such as the domoic acid, if produced, on the abundance of copepods in the HNLC region need further research.

4.1.2 Lightly silicified diatoms near the surface?

A rigid and thick frustule of diatoms is considered to be the main anti-grazing strategy against copepods. If copepods are not abundant in HNLC conditions, lightly silicified diatoms may be favoured. The dominant diatoms of the HNLC regions are characterized by thin frustules and the lack siliceous ornamentation requiring a superfluous silicon uptake. *Pseudo-nitzschia delicatissima* and *R. bergonii* easily dissolved their lightly silicified frustules and these diatoms are nearly absent from the sediments (Kolbe, 1954). At first sight, a lightly silicified frustule may be a response to an environment where the silicic acid bioavailability is low. In the present study the HNLC-PA appeared in two regions with different hydrographical conditions, but apparent similar trophic conditions. The *P. delicatissima*-*R. bergonii* assemblage (Figs. 8–9) was associated with a nitrate-silicic acid ratio that ranged from 1–3 in the euphotic zone of the two HNLC regions (Fig. 6, Table 1). The elemental composition of the diatoms is characterized by nitrogen-silicic acid ratio of 1 (Brzezinski, 1985). It can be expected that the diatoms uptake the nutrients from the surrounding waters with a similar ratio. Values of the nitrate-silicic acid ratio higher than 1, may imply a silicon limitation for the diatom growth. However, the nutrient limitation is a complex issue, and only the nutrient ratios are not suitable to infer limitations. Based on silicic acid uptake measurements, Leynaert et al. (2001) reported direct evidence that the diatoms are Si-limited in the central equatorial Pacific.

It is evident that the diatoms must be adapted to optimize the silicic acid utilization. Large frustules such as those in *R. bergonii* and *R. acuminata* may allow to escape of most of micrograzers. The balance between large frustules avoiding the micrograzers and a thin frustule that allowed to economize the scarce silicic acid available may result in deficiencies in the formation and maintenance of the frustule. In the present study, specimens of *Rhizosolenia bergonii* and *R. acuminata* were curved instead of the usual rigid frustules and sections of the frustules appeared anomalously fragmented (Figs. 12–15). This phenomenon did not occur with other diatoms and the plasmalemma of the diatom appeared retracted in the regions where the frustule is fragmented. The portion of the frustule closer to the diatom nucleus did not usually appear fragmented (Figs. 14–15). Consequently this

phenomenon of fragmentation of the frustule occurred before the fixation of the samples, discarding an artifact due to the fixation methodology. This is evidence that the silicic acid is an element limiting the large diatoms *R. bergonii* and *R. acuminata* in the HNLC regions of the South Pacific Ocean.

The possible deficiency of silicic acid may determinate the presence of other phytoplankton components of the HNLC-PA. Chavez (1989) included the absence of neritic bloom-forming diatoms among the factors to explain the HNLC paradox. Although colonial diatoms such as *Chaetoceros lorenzianus* were observed in the present study, well silicified neritic diatoms (i.e. *Detonula*, *Leptocylindrus*, *Guinardia*, etc.) that are dominant in mesotrophic coastal waters were absent in the HNLC regions. The typical neritic diatoms may be less competitive in the HNLC regions versus the lightly silicified diatoms. For example *Planktoniella sol* has developed an organic ring-like wing that does not contain silica. Beyond the diatoms, other phytoplankton groups such as silicoflagellates have an internal silica skeleton. *Dityocha* is often a common component of the phytoplankton in the north Pacific Gyre (Venrick, 1992; Scharek et al., 1999), were nearly absent during this survey in the SE Pacific. The open SE Pacific is far from the terrestrial inputs of dissolved silicon. The Antarctic waters spread along the deep SE Pacific Ocean. The waters of the PCC showed a nitrate-silicic acid ratio higher than 1 that may be associated to a Si-deficiency (Fig. 6). At the bottom of the euphotic zone the nitrate-silicic acid ratio was also higher than 1 (Fig. 6). Compared to the other oceanic regions, the SE Pacific seems to show deficiencies of the stock of silicic acid compared to other major nutrients. However, it is uncertain whether silicic acid is the main factor that determinate the dominant HNLC-PA and the diatoms of the bottom of the euphotic zone in the SPG.

Leynaert et al. (2001) hypothesized that silicon and iron limitations may interact. Iron is an essential component for the synthesis of chlorophyll and the nitrate reductase of the primary producers. It is unknown whether the iron from the Marquesas Islands Archipelago is the main responsible of the increase of the abundance of *Pseudo-nitzschia* and/or the increase is mainly due to the entrainment of deep major nutrients due the “island mass effect” (Signorini et al., 1999). In the present study, offshore the Marquesas Islands Archipelago, the dominance of the small *Pseudo-nitzschia* decreased and larger centric diatoms such as *R. bergonii* showed higher abundance (Fig. 8). In the proximity of islands the major nutrients and iron inputs is expected to be more continuous, favouring smaller diatoms such as *Pseudo-nitzschia*. In offshore waters, the pulsating enrichment events may favour species with big vacuoles such as *R. bergonii* able to accumulate nutrients for oligotrophic periods. Several studies showed that the domoic acid produced by *Pseudo-nitzschia* binds iron and copper (Rue and Bruland, 2001; Wells et al., 2005). The domoic acid is a strong organic ligand that facilitates the iron uptake of *Pseudo-nitzschia*

spp. According to Wells et al. (2005) this may explain why *Pseudo-nitzschia* spp. have persistent populations in oceanic HNLC regions.

Other characteristic of the HNLC diatoms is that they are restricted to surface waters and they did not form the typical sub-surface maximum as usual in other diatoms. For example species considered as deep flora such as *Planktoniella sol* (Sournia, 1982) showed a surface distribution in the HNLC regions of the present study. Under unfavourable surface conditions the diatoms are expected to sink to deep waters. However, in the transition of the warm HNLC region to oligotrophic conditions (13°32' S–132°07' W) *Rhizosolenia bergonii* remained near the surface despite the nitrate stock was depleted (Figs. 7–8, Table 1). It is uncertain the factor that determinate the surface distribution of these diatoms. Near the surface, the irradiance is higher and atmospheric inputs of iron are available. Iron is required for the photosynthetic electron transport system and chlorophyll molecule biosynthesis. At deeper waters (low irradiance), it can be expected that diatoms will require the synthesis of more chlorophyll and electron transport system molecules. Several studies reported that the iron requirements for diatoms increase at sub-saturating irradiances and decrease the efficiency of the utilization of iron (Sunda and Huntsman, 1995, 1997; Muggli and Harrison, 1997). Consequently in iron-depleted waters, the diatoms near the surface may grow with less iron requirements than in deeper waters. The hypothesis that the iron-stress would determinate the vertical distribution of HNLC diatoms requires further research. Other features such as the anti-grazing strategies and the physiology of HNLC species *Pseudo-nitzschia delicatissima* and *Rhizosolenia bergonii* need to be investigated.

Environmental factors, other than temperature and salinity, are responsible for the establishment and the persistence of a weakly silicified diatom assemblage in two geographically and hydrologically distant regions, the tropical central Pacific and the western limit of the Perú-Chile Current during the austral summer. The nitrate-silicic acid ratio ranging from 1–3 in the euphotic zone and frustules anomalously fragmented in *Rhizosolenia bergonii* suggest that Si-deficiency may be responsible of the HNLC-PA. Further studies are required to establish the factors that favour the occurrence of this distinctive phytoplankton assemblage.

Acknowledgements. D. Tailliez and C. Bournot are warmly thanked for their efficient help in CTD rosette management and data processing. We thank J. Ras for collection assistance. F. Gómez is supported by a post-doctoral grant of the Ministerio Español de Educación y Ciencia #2007-0213. This is a contribution of the BIOSOPE project of the LEFE-CYBER program.

Edited by: S. Pantoja

References

- Avaria, S. and Muñoz, P.: Effects of the 1982-1983 El Niño on the marine phytoplankton off Northern Chile, *J. Geophys. Res.*, 92, 14 369–14 382, 1987.
- Balech, E.: Tintinnoidea y Dinoflagellata del Pacífico según material de las expediciones Norpac y Downwind del Instituto Scripps de Oceanografía, *Rev. Mus. Argent. Cienc. Nat. "B. Rivadavia"*. *Cienc. Zool.*, 7, 1–253, 1962.
- Brzezinski, A. M.: The Si:C:N ratio of marine diatoms: interspecific variability and the effect of some environmental variables, *J. Phycol.*, 21, 347–357, 1985.
- Buck, K. R. and Chavez, F. P.: Diatom aggregates from the open ocean, *J. Plankton Res.*, 16, 1149–1457, 1994.
- Chavez, F. P.: Size distribution of phytoplankton in the central and eastern tropical Pacific, *Global Biogeochem. Cycles*, 3, 27–35, 1989.
- Chavez, F. P. and Buck, K. R.: Phytoplankton taxa in relation to primary production in the equatorial Pacific, *Deep-Sea Res.*, 37, 1733–1752, 1990.
- Chavez, F. P., Buck, K. R., Coale, K. H., Martin, J. H., Ditullio, G. R., Welshchmeyer, N. A., Jacobsen, A. C., and Barber, R. T.: Growth rate, grazing, sinking, and iron limitation of equatorial Pacific phytoplankton, *Limnol. Oceanogr.*, 36, 1816–1833, 1991.
- Claustre, H. and Maritorea, S.: The many shades of ocean blue, *Science*, 302, 1514–1515, 2003.
- Coale, K. H., Johnson, K. S., Fitzwater, S. E., et al.: A massive phytoplankton bloom induced by an ecosystem-scale iron fertilization experiment in the Equatorial Pacific Ocean, *Nature*, 383, 495–501, 1996.
- DiTullio, G. R., Geesey, M. E., Jones, D. R., Daly, K. L., Campbell, L., and Smith, O. S.: Phytoplankton assemblage structure and primary productivity along 170° W in the South Pacific Ocean, *Mar. Ecol. Prog. Ser.*, 255, 55–80, 2003.
- Dugdale, R. C. and Wilkerson, F. P.: Silicate regulation of new production in the equatorial Pacific upwelling, *Nature*, 391, 270–273, 1998.
- Frost, B. W. and Franzen, N. C.: Grazing and iron limitation in the control of phytoplankton stock and nutrient concentration: a chemostat analogue of the Pacific equatorial upwelling zone, *Mar. Ecol. Progr. Ser.*, 83, 291–303, 1992.
- Fryxell, G. A. and Kaczmarek, I.: Specific variability in Fe enrichment cultures from the equatorial Pacific, *J. Plankton Res.*, 16, 755–769, 1995.
- Hardy, J., Hanneman, A., Behrenfeld, M., and Horner, R.: Environmental biogeography of near-surface phytoplankton in the south-east Pacific Ocean, *Deep-Sea Res. I*, 43, 1647–1659, 1996.
- Hasle, G. R.: Phytoplankton and ciliate species from the tropical Pacific, *Skrifter utgitt av Det Norske Videnskaps-Akademi i Oslo. I, Matematisk-Naturvidenskabelig Klasse*, 2, 1–50, 1960.
- Ianora, A., Poulet, S. A., and Miralto, A.: The effects of diatoms on copepod reproduction: A review, *Phycologia*, 42, 351–363, 2003.
- Iriarte, J. L. and Fryxell, G. A.: Microplankton at the equatorial Pacific (140° W) during the JGOFS EqPac Time Series studies: March to April and October 1992, *Deep-Sea Res. II*, 42, 559–583, 1995.
- Kaczmarek, I. and Fryxell, G. A.: The genus *Nitzschia*: Three new species from the equatorial Pacific Ocean, *Diatom. Res.*, 9, 87–98, 1994.
- Kolbe, R. W.: Diatom from the Equatorial Pacific cores, Swedish Deep-Sea Exped. 1947-1948, Repts. 6, 3–49, 1954.
- Landry, M. R., Constantinou, J., and Kirshtein, J.: Microzooplankton grazing in the central equatorial Pacific during February and August, 1992, *Deep-Sea Res. II*, 42, 657–671, 1995.
- Leising, A. W., Gentleman, W. C., and Frost, B. W.: The threshold feeding response of microzooplankton within Pacific high-nitrate low-chlorophyll ecosystem models under steady and variable iron input, *Deep-Sea Res. II*, 50, 2877–2894, 2003.
- Leynaert, A., Tréguer, P., Christiane Lancelot, C., and Rodier, M.: Silicon limitation of biogenic silica production in the Equatorial Pacific, *Deep-Sea Res.*, I 48, 639–660, 2001.
- Longhurst, A. R.: *Ecological Geography of the Sea*, Academic Press, London, 1998.
- Muggli, D. L. and Harrison, P. J.: Effects of iron on two oceanic phytoplankters grown in natural NE subarctic Pacific seawater with no artificial chelators present, *J. Exp. Mar. Biol. Ecol.*, 212, 225–237, 1997.
- Raimbault, P., Garcia, N. and Cerutti, F.: Distribution of inorganic and organic nutrients in the South Pacific Ocean - evidence for long-term accumulation of organic matter in nitrogen depleted waters. *Biogeosciences Discuss.*, 4, 3041–3087, 2007
- Rivera, P. A.: Guide for references and distribution for the class Bacillariophyceae in Chile between 18° S and 58° S, *Bibliotheca Diatomologica*, 3, 1–386, 1983.
- Rodríguez, L., Escribano, R., Grone, G., Irribarren, C., and Castro, H.: Ecología del fitoplancton en la Bahía de Antofagasta (23° S), Chile, *Rev. Biol. Mar. Valparaíso*, 31, 65–80, 1996.
- Roman, M. R. and Gauzens, A. L.: Copepod grazing in the equatorial Pacific, *Limnol. Oceanogr.*, 42, 623–634, 1997.
- Rue, E. L. and Bruland, K. W.: Domoic acid binds iron and copper: a possible role for the toxin produced by the marine diatom *Pseudo-nitzschia*, *Mar. Chem.*, 76, 127–134, 2001.
- Scharek, R., Latasa, M., Karl, D. M., and Bidigare, R. R.: Temporal variations in diatom abundance and downward vertical flux in the oligotrophic North Pacific gyre, *Deep-Sea Res.*, I 46, 1051–1075, 1999.
- Schneider, W., Fuenzalida, R., Rodríguez-Rubio, E., Garcés-Vargas, J., and Bravo, L.: Characteristics and formation of Eastern South Pacific Intermediate Water, *Geophys. Res. Lett.*, 20 30, 1581, doi:10.1029/2003GL017086, 2003.
- Signorini, S. R., McClain, C. R., and Dandonneau, Y.: Mixing and phytoplankton bloom in the wake of the Marquesas Islands, *Geophys. Res. Lett.*, 26, 3121–3124, 1999.
- Sournia, A.: Is there a shade flora in the marine plankton?, *J. Plankton Res.*, 4, 391–399, 1982.
- Sunda, W. G. and Huntsman, S. A.: Iron uptake and growth limitation in oceanic and coastal phytoplankton, *Mar. Chem.*, 50, 189–206, 1995.
- Sunda, W. G. and Huntsman, S. A.: Interrelated influence of iron, light and cell size on marine phytoplankton growth, *Nature*, 390, 389–392, 1997.
- Venrick, E. L.: Phytoplankton in an oligotrophic ocean: observations and questions, *Ecol. Monogr.*, 52, 129–154, 1982.
- Wells, M. L., Trick, C. G., Cochlan, W. P., Hughes, M. P. and Trainer, V. L.: Domoic acid: The synergy of iron, copper, and the toxicity of diatoms, *Limnol. Oceanogr.*, 50, 1908–1917, 2005.

Factors limiting heterotrophic bacterial production in the southern Pacific Ocean

F. Van Wambeke¹, S. Bonnet², T. Moutin³, P. Raimbault³, G. Alarcón⁴, and C. Guieu²

¹Laboratoire de Microbiologie, Géochimie et Ecologie Marines (LMGEM), CNRS, UMR 6117, Université de la Méditerranée, Campus de Luminy – Case 901, 13 288 Marseille cedex 9, France

²CNRS, Laboratoire d’océanographie de Villefranche, 06 230 Villefranche-sur-Mer, France; Université Pierre et Marie Curie - Paris6, Laboratoire d’océanographie de Villefranche, 06 230 Villefranche-sur-Mer, France

³Laboratoire d’Océanographie et de Biogéochimie (LOB), CNRS, UMR 6535, Université de la Méditerranée, Campus de Luminy – Case 901, 13 288 Marseille cedex 9, France

⁴Department of Oceanography & Center for Oceanographic Research in the eastern South Pacific, University of Concepcion, Casilia 160-C, Concepcion, Chile

Received: 26 September 2007 – Published in Biogeosciences Discuss.: 16 October 2007

Revised: 21 February 2008 – Accepted: 8 May 2008 – Published: 19 May 2008

Abstract. The role of potential factors limiting bacterial growth was investigated along vertical and longitudinal gradients across the South Eastern Pacific Gyre. The effects of glucose, nitrate, ammonium and phosphate additions on heterotrophic bacterial production (using leucine technique) were studied in parallel in unfiltered seawater samples incubated under natural daily irradiance. The enrichments realized on the subsurface showed three types of responses. From 141° W (Marquesas plateau) to approx 125° W, bacteria were not bottom-up controlled, as confirmed by the huge potential of growth in non-enriched seawater (median of enhancement factor $\times 39$ in 24 h). Within the Gyre (125° W–95° W), nitrogen alone stimulated leucine incorporation rates (median $\times 4.2$), but rapidly labile carbon (glucose) became a second limiting factor (median $\times 37$) when the two elements were added. Finally from the border of the gyre to the Chilean upwelling (95° W–73° W), labile carbon was the only factor stimulating heterotrophic bacterial production. Interaction between phytoplankton and heterotrophic bacterial communities and the direct versus indirect effect of iron and macronutrients on bacterial production were also investigated in four selected sites: two sites on the vicinity of the Marquesas plateau, the centre of the gyre and the Eastern border of the gyre. Both phytoplankton and heterotrophic bacteria were limited by availability of nitrogen within the gyre, but not by iron. Iron limited phytoplankton at Marquesas plateau and at the eastern border of the gyre. However

48 h enrichment experiments were not sufficient to show any clear limitation of heterotrophic bacteria within Marquesas plateau and showed a limitation of these organisms by labile carbon in the eastern border of the Gyre.

1 Introduction

Heterotrophic bacteria generally meet their energy and elemental needs from utilisation of organic matter, which includes essential elements like C, N, P and Fe. However, in oligotrophic environments, elemental needs are sometimes not satisfied only by utilization of organic matter and heterotrophic bacteria can compete with phytoplankton for mineral nutrients like N, P or Fe (Kirchman, 1994; Tortell et al., 1999; Thingstad, 2000). To examine factors limiting heterotrophic bacterial growth, seawater samples are generally amended with various components (organic molecules, macro nutrients, iron), alone or in combination. After 24–48 h, some bacterial parameters are examined, the main one primarily being bacterial production (either with thymidine or leucine technique). Different elements have been shown to stimulate bacterial production: phosphorus in the Atlantic Ocean (Sargasso Sea: Cotner et al., 1997, Gulf of Mexico: Pomeroy et al., 1995) and in the Mediterranean Sea (Eastern: Zohary and Robarts, 1998; Thingstad et al., 2005; Western: Van Wambeke et al., 2002), nitrogen in the South West Pacific Ocean (French Polynesia: Torrétón et al., 2000), labile organic carbon in the Equatorial and Subarctic Pacific (Kirchman, 1990; Kirchman and Rich, 1997), iron in the Southern ocean (Pakulski et al., 1996, Tortell et al., 1996).



Correspondence to: F. Van Wambeke
(france.van-wambeke@univmed.fr)

From a punctual observation, it is difficult to generalize because within a given area, temporal and vertical variability have been shown (Sala et al., 2002; Van Wambeke et al., 2002). In addition, the simple point of view of “one single” resource limiting factor has evolved: i) co-limitation often occurs: carbon – iron (Tortell et al., 1999; Church et al., 2000; Kirchman et al., 2000), carbon – phosphorus (Sala et al., 2002, Van Wambeke et al., 2002), carbon – nitrogen (Torréon et al., 2000) ii) among heterotrophs, organic molecules might act as nutrients for building biomass but also as energy resources; this observation is at the origin of the concept of energy limitation (Kirchman, 1990, Donachie et al., 2001) and iii) direct versus cascade effects: are bacteria directly stimulated, or do they benefit from a surplus phytoplankton production also affected by the relieving of one key nutrient? (Palkuski et al., 1996; Church et al., 2000; Cochlan, 2001; Oliver et al., 2004; Obernosterer et al., 2008b).

In the South Pacific Gyre, extreme isolation from terrestrial influence results in a permanent situation of hyperoligotrophy (Claustre et al., 2008). Picoplanktonic organisms, both heterotrophic and photoautotrophic, dominate community metabolism in this area (Grob et al., 2007). Bacterial production is very low in the centre of the gyre and relies upon autochthonous, photosynthetically derived organic matter as well as on changes in solar radiations as shown by the diel variability of bacterial production (Van Wambeke et al., 2008a; b). Photo-autotrophic production is limited by nitrogen availability within the centre of the Gyre and is particularly adapted to the very low amounts of dissolved iron present (Bonnet et al., 2008). In contrast, iron limits phytoplanktonic production within the Marquesas plateau. In addition, bulk DOC stock is particularly important in the south Pacific Gyre (Raimbault et al., 2008). One might expect dynamics of bacterial production to be also affected by the lack of inorganic nutrients or iron and the limiting factors to change across this vast, unexplored region of the eastern south Pacific. The purpose of this study was thus to determine which factors limited heterotrophic bacterial growth across a broad survey along longitudinal and vertical gradients from Marquesas Plateau to the Chilean upwelling.

2 Materials and methods

To follow bottom-up factors controlling heterotrophic bacteria, prefiltration of samples should be ideal. However, particularly in oligotrophic environments, organic material devoted to bacterial growth is provided continuously through regenerating processes by higher size-class organisms, so that bottom up control is influenced by preying organisms. This is particularly evidenced within the center of the south Pacific Gyre site where the Redfield *f* ratio is close to zero, but becomes slightly positive only when considering atmospheric di-nitrogen fixation (Raimbault and Garcia, 2008). In this case, the response of all members of the community

is needed to fully appreciate the complexity of changes in trophic regulations and nutrient transfers resulting from addition of nutrients. Another problem is the representativeness of the activity associated to a pre-filtered bacterial fraction (within the gyre, on average 36% of the bacterial production was associated to the $>0.6 \mu\text{m}$ fraction, unpub. results). Finally, we chose to maintain whole seawater samples to keep the possibility to study simultaneously effect of amendments on both autotrophic and heterotrophic compartment and to explore potentially direct versus indirect effects.

In order to identify the factors limiting heterotrophic bacterial production, two different sets of experiments were performed, one under trace metal clean condition (TMC), and the other under non trace metal clean conditions (non TMC).

2.1 TMC

These experiments were performed at four experimental sites. These stations represented different trophic regimes (Table 1): the mesotrophic area associated to the plume of the Marquesas Island (141.14° W, 8.19° S) (MAR), the adjacent medium nitrate, low chlorophyll waters (136.97° W, 9.04° S) (HNL), the hyperoligotrophic waters associated with the central part of the South Pacific gyre (114.02° W, 26.04° S) (GYR) and the oligotrophic eastern side of the gyre (91.39° W, 31.89° S) (EGY). The GYR site has been selected from ocean color images as having the lowest surface chlorophyll concentration in the world ocean. Details of these on-deck incubations are fully described in Bonnet et al. (2008). All experimental setups were performed using strict trace metal clean techniques (Bruland et al., 1979) inside a clean container. Briefly, seawater was collected at 30-meter depth using a Teflon pump system and dispensed into acid-washed (Suprapur Merck HCL) transparent polycarbonate bottles. Under a laminar flow hood, nutrients were added alone and in combination to final concentrations of $1 \mu\text{M NH}_4^+$ (from ammoniac reagent) + $2 \mu\text{M NaNO}_3$, $0.3 \mu\text{M NaH}_2\text{PO}_4$, 2 nM FeCl_3 , $10 \mu\text{M C-glucose}$ (Table 2). The bottles were incubated in an on-deck incubator with circulating surface seawater at appropriated irradiance (50% ambient light level). The difference between circulated surface water temperature and 30 m depth temperature was negligible at the three sites investigated (no more than 1°C). Three bottles for each treatment were randomly selected and sampled destructively at 24 h and 48 h. A large set of parameters were measured to follow nutrient concentrations, phytoplankton response (cytometric counts, variable fluorescence, chlorophyll, particulate primary production, Bonnet et al., 2008), bacterial abundance and heterotrophic bacterial production.

2.2 Non TMC

We also investigated more systematically factors influencing leucine incorporation rates using non TMC

Table 1. Initial conditions of “trace metal clean” experiments.

BN: bacterial abundances.

PP: primary production.

	T°C	NO ₃	NH ₄	PO ₄	SiOH ₄	Fe	DOC*	Chl- <i>a</i>	PP	BN	leu inc rate
		μM	μM	μM	μM	nM	μM	mg m ⁻³	mgC m ⁻³ d ⁻¹	×10 ⁵ ml ⁻¹	pmol L ⁻¹ h ⁻¹
MAR	27.7	1.97	0.32	0.37	0.97	0.13	70	0.18	nd	9.6	26
HNL	27.7	1.82	0.04	0.31	0.91	0.14	70	0.11	9.1	8.9	27
GYR	22.1	bdl	bdl	0.11	0.55	0.1	118	0.03	1.8	4.1	18
EGY	18.0	0.04	0.008	0.17	1.02	0.1	98	0.07	6.5	7.5	15

nd: not determined,

bdl: below detection limits, T°C: temperature

* DOC concentrations come from the analysis of sea water sample collected at the nearest (in time) CTD cast.

Table 2. Summary of enrichment conditions.Fe: iron, NH₄: ammonium, NO₃: nitrate, Si: orthosilicic acid, PO₄: phosphate, GLU: glucose.

experiment	code	Fe	NH ₄	NO ₃	Si	PO ₄	C-GLU	Incubation sampling
MAR*	C							24–48 h in situ simulated 50% light screen
	Fe	2 nM						
	N		1 μM	2 μM	2 μM**	0.3 μM		
	all	2 nM	1 μM	2 μM	2 μM**	0.3 μM		
HNL*	C							24–48 h in situ simulated 50% light screen
	Fe	2 nM						
	N		1 μM	2 μM	2 μM**	0.3 μM		
	FeN	2 nM	1 μM	2 μM	2 μM**	0.3 μM		
	G						10 μM C	
GFFe	2 nM					10 μM C		
GYR*	C							24–48 h in situ simulated 50% light screen
	EGY*	Fe	2 nM					
	N		1 μM	2 μM				
	FeN	2 nM	1 μM	2 μM				
	all	2 nM	1 μM	2 μM		0.3 μM		
	G						10 μM C	
	GFFe	2 nM					10 μM C	
routine	C							
bioassays***	P					0.25 μM		
	N		1 μM	1 μM				
	G						10 μM	
	NPG		1 μM	1 μM		0.25 μM	10 μM	

* “trace metal clean” conditions of manipulation.

** Si addition resulted in a slight contamination in Fe of about 0.1 nM.

*** non “trace metal clean” conditions of manipulation.

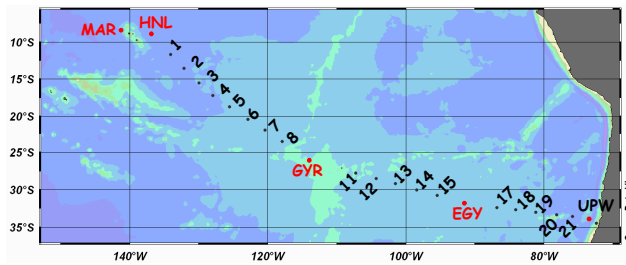


Fig. 1. Transect of the BIOSOPE cruise from the Marquesas Islands to Chile. In red, stations where “trace metal clean” enrichment experiments were processed, in black, stations used for “non metal clean” bioassays. Numbers indicate short-term stations, for which only numbers have been indicated to simplify presentation, not the complete code as in Table 3. For instance 1 is STB1 and 21 is STA21.

experiments, i.e. incubated water sampled from Niskin bottles and manipulated in a classical laboratory. Nutrients were added in order to obtain a final concentration of $1 \mu\text{M NH}_4\text{Cl} + 1 \mu\text{M NaNO}_3$, $0.25 \mu\text{M Na}_2\text{HPO}_4$, $10 \mu\text{M C}$ -glucose (Table 2). Transparent polycarbonate flasks of 60 ml were used and incubated on average 24 h in simulated in situ conditions (on deck incubator, neutral screens). For the longitudinal trend (141°W to 72°W , Fig. 1), seawater was sampled at one single depth varying from 5 to 30 m according the CTD profile. The depths chosen were always within the mixed layer, and corresponded to 50% incident light. We also investigated factors limiting BP along vertical profiles at sites GYR, EGY and UPW. The latter site corresponded to the upwelling area off the Chilean Coast (73.2°W , 33.5°S , Fig. 1). For those experiments, for each depth sampled, five 60 ml polycarbonate flasks (C, P, N, G, NPG) were incubated in a running seawater bath covered with a neutral screen corresponding to the incident light level. The deeper depth sampled was below the euphotic zone and was incubated in the dark in the incubator at in situ temperature. In situ light conditions were then correctly reproduced (excluding UV effects), whereas a slight difference could be obtained with temperature: up to 3°C difference at GYR (for the 185 m sample corresponding to 1% incident light: 19°C in situ, 22° during incubation), 2°C at EGY and 2.2° at UPW.

Samples for bacterial abundances were fixed with paraformaldehyde at 1% and quick frozen in liquid nitrogen. Within 2 months after the cruise, they were analyzed with SYBR Green I and run on a FACSCalibur flow cytometer as described in Grob et al. (2007). Bacterial production was determined using ^3H leucine technique coupled with the centrifuge method with full methodological description in Van Wambeke et al. (2008a). Briefly, 1.5 ml seawater samples or sub-samples from incubated flasks were incubated in the dark for 1 to 2 h after addition of 20 nM leucine. The terms “heterotrophic bacteria” and “heterotrophic bacterial production” are used in the whole text by simplicity but sensus

stricto refers to heterotrophic prokaryotes and heterotrophic prokaryotic production, respectively. Indeed, prokaryotes include Bacteria and Archaea; and it has been shown that some organisms in both groups are able to incorporate leucine (Kirchman et al., 2007).

Nutrients were analyzed following standard colorimetric methods on board (Raimbault et al., 2008). Chlorophyll-*a* (Chl-*a*) concentrations given for the enrichment experiments were analyzed fluorimetrically as described in Bonnet et al. (2008) whereas pigment concentrations were measured systematically at each station during the transect using HPLC method (Ras et al., 2008). Particulate primary production was measured on board in running seawater baths covered with a 50% neutral screen. Incubations periods lasted on average 5 h during morning time hours. Detailed methodology and assumption used to convert hourly to daily rates are fully described in Duhamel et al. (2007).

We used a non parametric test, the Mann-Whitney test in TMC experiments. Because this test lacks statistical power with small samples, we used it only when triplicate data where available in order to maintain comparison purpose. When comparing the effect of one enrichment to the control on a given variable, untransformed data were compared. When comparing the degree of stimulation reached for one given enrichment between 2 variables, the enrichment factor (i.e., ratio of rate (or stock) in enriched batch to the rate (or stock) in control unamended) were compared. The Wilcoxon signed-rank test was used in non TMC experiments.

3 Results

3.1 Initial conditions prior to enrichment experiments

A large gradient of nutrient concentrations and chlorophyll *a* was observed along the transect (Table 3). Nitrate concentrations ranged from undetectable values to $3.6 \mu\text{M}$ (station STB 18), whereas soluble reactive phosphorus was always detectable and above 120 nM (Moutin et al., 2008). Chl-*a* varied almost by 2 orders of magnitude (0.02 mg m^{-3} in the centre of the gyre to 14.8 mg m^{-3} in the Chilean upwelling system). Leucine incorporation rates ranged from 10 to $164 \text{ pmol L}^{-1} \text{ h}^{-1}$. Higher values of nutrients, Chl-*a* and leucine incorporation rates were obtained at the eastern part of the transect, within the Chilean upwelling (stations STB20, STA21, site UPW). Stations between STB6 and STB15 displayed lower Chl-*a* stocks and leucine incorporation rates (means $\pm \text{sd}$ $0.027 \pm 0.009 \text{ mg Chl-}a \text{ m}^{-3}$, $11.9 \pm 1.2 \text{ pmol L}^{-1} \text{ h}^{-1}$, respectively). Vertical profiles of dissolved iron indicated low ($0.13 \pm 0.03 \text{ nM}$) and constant concentrations from the surface to 80 m throughout most of the transect (site STB4 to STB14, including GYR), and increased notably from station STA21 to the Chilean coast, to reach 0.4 to 1.2 nM in surface waters (also see Blain et al., 2008).

Table 3. Initial conditions prevailing in sea water samples used for routine bioassays. SST: sea surface temperature (used in running sea water baths during incubations), Chl *a*: Chlorophyll *a*, Leu inc rate: incorporation rates of leucine into proteins, ld: below detection limits.

station	depth m	Longitude ° W	Latitude ° S	date	SST °C	NO ₃ μM	NH ₄ μM	PO ₄ nM	Chl- <i>a</i> mg m ⁻³	Leu inc rate pmol L ⁻¹ h ⁻¹
MAR	5	141°14	08°19	29-oct.		1.68*	0.33*		0.168	50.9
STB1	10	134°05	11°44	3-nov.	27.8	0.70 (5 m)	0.03	313	0.112	30.9
STB2	15	132°06	13°33	4-nov.	27.4	ld	0.01	208	0.088	29
STB3	15	129°55	15°32	5-nov.	27.1	0.046	0.004	193	0.055	21.4
STB4	15	127°58	17°14	6-nov.	26.5	ld	ld	213	0.050	21
STB5	20	125°33	18°44	7-nov.	25.7	ld	ld	163	0.038	15.9
STB6	25	122°53	20°27	8-nov.	24.5	ld	0.008	178	0.018	11.9
STB7	20	120°22	22°03	9-nov.	24.3	0.046	ld	143	0.022	13.4
STB8	30	117°53	23°33	10-nov.	23.4	ld	ld	128	0.026	12.4
GYR	30	114°00	25°58	12-nov.	22.1	ld	0.02*	128	0.028	10.8
STB11	30	107°17	27°46	20-nov.	21.3	ld	ld*	123	0.032	12.4
STB12	30	104°18	28°32	21-nov.	21.2	ld	0.001*	133	0.022	11.2
STB13	25	101°28	29°13	22-nov.	20	ld	0.003*	123	0.023	10.6
STB14	20	98°23	30°02	23-nov.	19.8	0.048	ld*	138	0.027	10.5
STB15	15	95°25	30°47	24-nov.	18.7	ld	0.015*	153	0.048	13.9
EGY	15	91°27	31°49	26-nov.	18.1	0.006*	0.006*	178	0.074	17
STB17	15	86°47	32°23	1-dec.	17.3	2.65*	0.116*	313*	0.116	20.3
STB18	15	84°04	32°40	2-dec.	17.4	3.64	0.119*	388	0.147*	16.6
STB19	15	81°12	33°01	3-dec.	17.2	2.76	0.132*	373	0.066	17.5
STB20	5	78°07	33°21	4-dec.	17.6	0.095		268	0.274	51.5
STA21	5	75°49	33°36	5-dec.	16.8	0.071		358	0.218	54.6
UPW1	5	73°22	33°59	6-dec.	15.9				1.481*	145.4
UPW2	5	73°21	33°55	7-dec.		0.289		508	1.394	163.7

* refers to data acquired on another CTD cast sampled in an interval of few hours on the same site.

3.2 TMC experiments

3.2.1 Heterotrophic versus autotrophic response.

The extent of stimulation of phytoplankton and bacterial biomasses and productions following various amendments varied according to the station and the element tested. Roughly, phytoplankton was significantly stimulated by Fe addition alone but also N addition alone at the MAR and HNL sites, by N at the GYR site, and responded mostly to Fe+N (FeN, all) additions at the EGY site (Table 4). Leucine incorporation rate was particularly stimulated by glucose at the HNL site and by N at the GYR site. Stimulations were less significant at MAR and EGY sites: Fe alone, but also N alone stimulated leucine activity at the MAR site, whereas it was glucose at the EGY site (Fig. 2, Table 4).

Besides the information concerning the limiting factor(s), we obtained the following general features: bacterial numbers did not increase or, when increasing, always increased less than leucine incorporation rates (HNL site in G and GFe, $p < 0.05$ for all comparisons of enrichment factors). Chlorophyll stocks either increased in the same proportion as the primary production (GYR 24 h in N, FeN and all for instance), or increased in less proportion than primary produc-

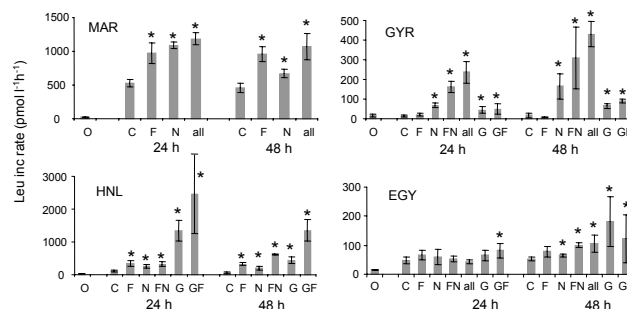


Fig. 2. Evolution of leucine incorporation rates on bioassay experiments made under “trace metal clean” conditions. Means \pm sd of triplicate bottles sampled after 24 and 48 h of incubations. For MAR and HNL enrichments were O: initial conditions, C: control non enriched, F: +iron, N: + nitrates+ammonium+phosphates+silicates, all: nitrates+phosphates+silicates+iron, G: +glucose, GF: glucose+iron. For GYR and EGY N was only nitrate+ammonium, FN was nitrate+ammonium+iron and all nitrates+ammonium+phosphates+iron. *: response significantly different from the control at the same time, Mann Whitney test, $p < 0.05$.

Table 4. Summary of the factors of increase obtained after 24 and 48h incubations in “trace metal clean” experiments. Results are expressed as the ratio of the mean value obtained divided by the mean value obtained in the non-amended control at the same time. For the lines corresponding to non-amended controls (C), the italic values indicate the factor of increase relative to the control at time zero. Enrichment codes correspond to Table 2. The parameters and their units before comparison are: chlorophyll-*a* (Chl-*a*, mg m⁻³), bacterial abundance (BN, cells ml⁻¹), heterotrophic nanoflagellate abundances (HNAN, cells ml⁻¹), ¹⁴C-primary production (PP, mg C m⁻³ d⁻¹), leucine incorporation rates (Leu pmol L⁻¹ h⁻¹), primary production per unit Chl-*a* (spec PP, mgC mg Chl a⁻¹ d⁻¹) and leucine incorporation rate per cell (spec Leu, × 10⁻²¹ mol cell⁻¹ h⁻¹). Empty places: parameter not sampled.

		24 h						48 h							
		Chl-A	BN	HNAN	PP	Leu	sp PP	sp Leu	Chl-A	BN	HNAN	PP	Leu	sp PP	sp Leu
MAR	C	<i>1.5</i>	<i>1.1</i>			<i>20.1</i>		<i>17.6</i>	<i>2</i>				<i>17.4</i>		
	Fe	1.6**	1.1**			1.8**		1.7**	3.0**				2.1**		
	N	1.7**	1.1**			2.1**		1.8**	1.7**				1.5**		
	all	2.2**	1.2**			2.2**		2.0**	8.7**				2.3**		
HNL	C	<i>1.4**</i>	<i>1.1**</i>	<i>1.2</i>	<i>1.1</i>	<i>4.2**</i>	<i>0.8**</i>	<i>3.8**</i>	<i>1.3**</i>	<i>1.2**</i>	<i>1.3</i>	<i>0.8**</i>	<i>2.6**</i>	<i>0.6**</i>	<i>2.2</i>
	Fe	1.4**	1	1.1	2.8**	3.1**	2.0**	3.3**	3.6**	0.9	1.2	5.5**	4.6**	1.5**	5**
	N	1.9**	1	1.8	3.9**	2.3**	2.1**	2.2**	4.5	1	2.1	5.7**	2.7**	1.1	2.7**
	FeN	1.9**	0.9	1.7	4.3**	2.9**	2.3**	3.1**	6.1	1	2	9.5**	8.7**	1.4	9.1**
	G		1.1**	1.4		11.9**		10.5**		1.1**	1.4		6.3**		5.5**
	Gfe		1.2**	1.2		21.7**		18.8**		1.1**	1.4		19.1**		16.3**
GYR	C	<i>1.1</i>	<i>0.9</i>	<i>1.1</i>	<i>0.4**</i>	<i>0.8</i>	<i>0.4</i>	<i>0.9</i>	<i>0.7</i>		<i>1.1</i>	<i>0.5**</i>	<i>1</i>	<i>0.7</i>	
	Fe	1.5	1	1	1.1	1.4	0.6	1.4	1	1	1	0.7**	0.5	0.7	
	N	2.2**	1	1.1	2.1**	4.6**	0.9	4.7**	3.1	1.4	1.4	4.2**	8.9**	1.4	
	FeN	2.3**	1	1.1	2.4**	11.0**	1.1	11.0**	4	1.6	1.6	5.4**	16.9**	1.4	
	all	2.1**	1	2	2.0**	16.0**	0.9	15.9**	3.3	1.8	1.8	4.5**	23.4**	1.4	
	G		1	1.1		3**		3.1		1.4	1.4		3.5**		
	GFe		1	1		3.4**		3.5**		1.5	1.5		4.9**		
EGY	C	<i>1.9**</i>	<i>1.1</i>	<i>1.1</i>	<i>0.7**</i>	<i>3.1**</i>	<i>0.4**</i>	<i>2.7</i>	<i>1.8**</i>	<i>1.1</i>	<i>1.1</i>	<i>0.8**</i>	<i>3.5**</i>	<i>0.4**</i>	<i>3.1</i>
	Fe	0.9	1	1.2	1	1.4	1.1	1.4	1.4	1.1	1.6	1.3**	1.5	1.3	1.3
	N	1.2**	1	1.3	1.1**	1.3	0.9	1.3	1.6**	1	1.9	1.9**	1.2**	1.2**	1.2**
	FeN	1.2**	1	1.2	1.5**	1.1	1	1.1	2.6**	1	2	3.8**	1.9**	1.5**	1.8**
	all	1.3**	1	1.6	1.8**	0.9	1.4**	1	3.0**	1.2	2.4	4.5**	2**	1.5**	1.7**
	G		1	1.2		1.4		1.4		1	1.4		3.5**		3.4**
	GFe	–	1	1.1		1.8**		1.7**		1	1.7	–	2.3		2.4

** Indicates a response significantly different at $p < 0.05$ after Mann Whitney test. This test was made only when triplicate data were available for both pairs of data set compared (bold characters).

tion (HNL 24 h in Fe, N, FeN; HNL 48 h in Fe; GYR 48 h in N, FeN; EGY 48 h in N, FeN, all, $p < 0.05$ for all these comparisons of enrichment factors). In addition, chlorophyll stocks increased after 48 h up to a factor of 6 (FeN at the HNL site), whereas bacterial abundances never increased more than a factor of 1.2 (“all” at the EGY site, GFe at the HNL site and “all” at the MAR site). Factors of increase of leucine specific activities were consequently very close to those of the fluxes, whereas primary production per unit of chlorophyll, when increasing, increased, on average of × 1.6 less than photosynthesis rates (Table 4).

Out of these general trends, the intensity of the heterotrophic response differed from the intensity of autotrophic response. For instance, at the GYR site, both photosynthesis and heterotrophic production were stimulated after N additions (alone and combined: N, FeN, “all”), but leucine incorporation rates increased up to 8 times more than primary

production (GYR “all”, after 24 h, × 16 and × 2, respectively, Table 4, all these differences at 24h and 48h between enrichment factors on leucine activity vs PP were significant at $p < 0.05$). On the opposite, in the treatments N (24, 48 h) and FeN (24 h) at the HNL site, and FeN (24, 48 h) and “all”(24, 48 h) in the treatments at the EGY site, primary production increased on average 1.6 times more than leucine incorporation rates (differences of enrichment factors significant at $p < 0.05$). It must be noticed that these latter cases corresponded to situations where phytoplankton and heterotrophic bacteria were not stimulated primarily by the same factor (i.e. N or Fe for phytoplankton and glucose for bacteria).

3.2.2 Iron control on Heterotrophic Bacteria

At the MAR site, the most significant increase was obtained in the non-amended control (× 20 in 24 h), whereas Fe alone,

macronutrients N+P+Si (“N”) or a combination of all the nutrients Fe+N+P+Si (“all”) lead to similar significant but low response (1.8 to 2.2 times higher than the control at the same time). There was no other additional effect after 48 h. At the HNL site, only the glucose and glucose+Fe additions resulted in a drastic increase of leucine incorporation rates ($\times 11$ and $\times 21$), visible 24 h after enrichment, although significant, but lower stimulations were obtained after Fe, N, and FeN enrichments. At the GYR site, Fe+N (FeN), and a combination of all the nutrients Fe+N+P (all) resulted in a significantly higher leucine incorporation rates after 24 h ($\times 11$, $\times 16$, respectively) and 48 h ($\times 16$, $\times 23$, respectively). The leucine incorporation rate was also enhanced after N addition alone, but on a lower extent, and not by Fe alone. Glucose (alone or in combination with Fe) results in a significant, but low increase of leucine incorporation rate, even after 48h. At the EGY site, however, only glucose additions stimulated significantly leucine incorporation rates at 24 h ($\times 1.8$ in GFe at 24 h). Significant increases of leucine activity were seen also after 48 h in N, FeN and “all” ($\times 1.2$ to $\times 1.9$) but to a lesser extent than after glucose addition ($\times 3.5$, Table 4, Fig. 2).

The results obtained in the framework of these trace metal clean experiments allowed us to draw some conclusions: i) iron was never a single factor limiting bacterial production, ii) when stimulation by iron occurred, response in the un-amended control (MAR site), in glucose amended samples (HNL) was greater, suggesting that the stimulation of bacterial production after iron addition was a cascade effect. Consequently, we assumed that effects of N, P and glucose additions could be studied more systematically along the transect by using “non TMC” technique, and 24 h incubations should be long enough to detect some stimulation, if occurring.

3.3 Non TMC experiments

3.3.1 Longitudinal variability of nutrient control on Heterotrophic Bacteria

Along the horizontal transect in the mixed layer, P alone stimulated leucine incorporation rates only in 1 case over 23 tested (station STB4, $\times 2.2$ higher than the control). However, in that bioassay the addition of N ($\times 3.4$) and G alone ($\times 2.6$) also resulted in an increase of leucine incorporation rates. We thus discarded phosphorus as a potentially limiting factor everywhere on the transect. At the opposite, effects of N, glucose and NPG additions on leucine incorporation rates showed three groups of responses. In the western part, from the MAR site to station STB5, the leucine incorporation rate was greatly stimulated simply by confinement during 24 h in a polycarbonate bottle (see example of STB1, Fig. 3). On average, the median factor of increase of leucine incorporation rates was 39 (Fig. 4a). This is in agreement with the TMC experiments conducted at the MAR site (Fig. 2). The median values of stimulation factors were $\times 1.4$, $\times 1.1$ and $\times 2.6$ for glucose, N and NPG addition, respectively (Fig 4b). In this

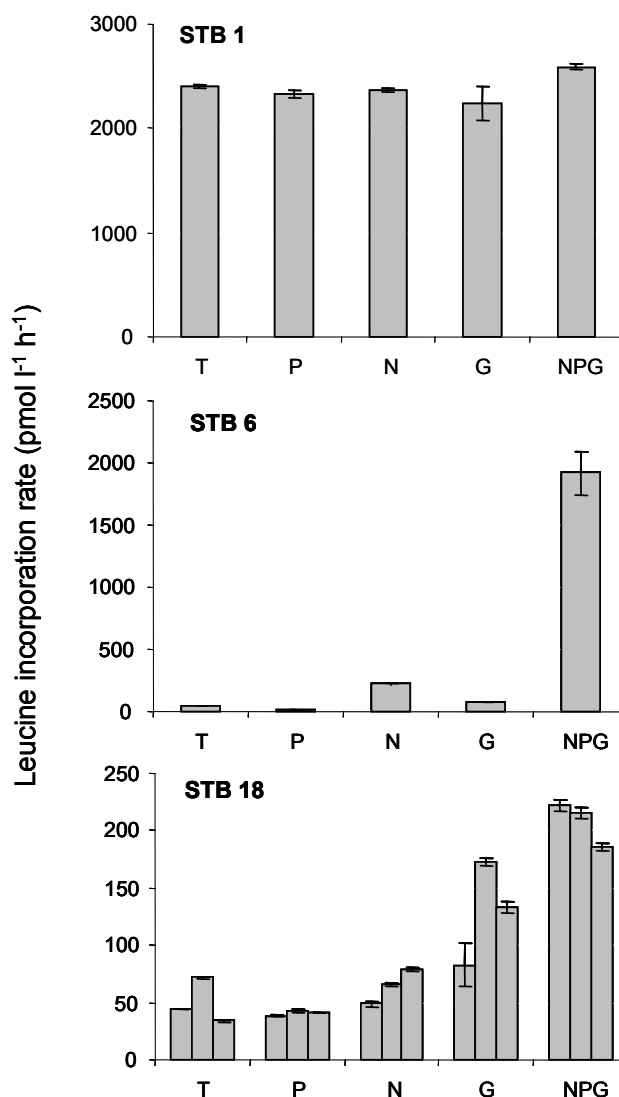


Fig. 3. Typical results obtained from “non metal clean” bioassays. C: control, P:+phosphates, N:+nitrites+nitrates, G:+glucose, NPG: all 4 elements. Error bar represents variability within duplicate leucine measurements in a single flask. At station STB18, triplicate flasks were incubated. Station STB1: no stimulation, STB6: slight stimulation with N, big stimulation with NPG, STB18: stimulation with glucose.

group of stations, the leucine incorporation rates increased significantly only in the control (Wilcoxon signed-rank test, $p < 0.05$). In the second group of stations (STB6 to STB15, including the GYR site, see example of STB6, Fig. 3), the leucine incorporation rates increased less ($\times 1.1$ to $\times 5.3$) in the non-amended control (Fig. 4a). The median values of stimulation factors for glucose, N and NPG additions were $\times 1.4$, $\times 4.2$ and $\times 37.2$, respectively (Fig. 4b). In this group of stations, the leucine incorporation rates increased significantly in the control, in N and NPG –amended samples (Wilcoxon signed-rank test, $p < 0.01$). For the last group of

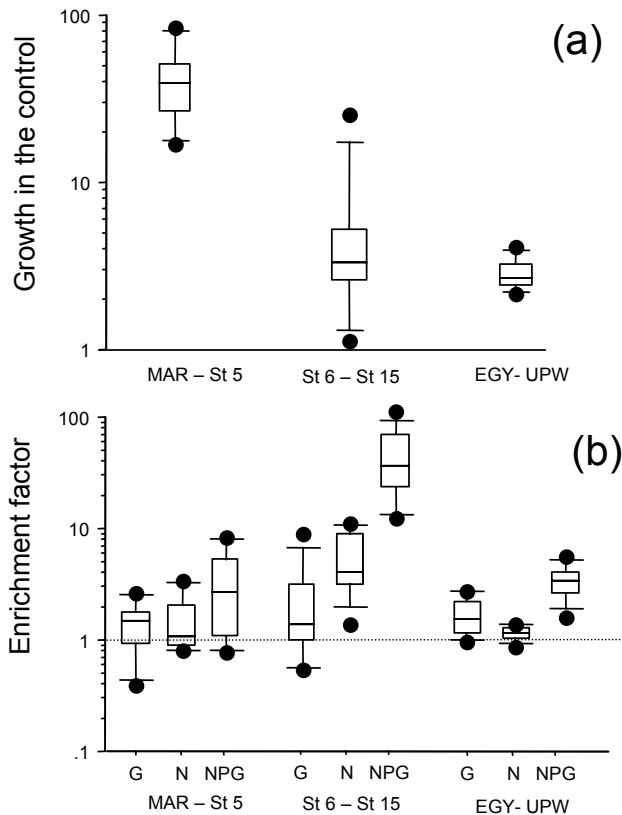


Fig. 4. Mean results on bioassays realized in sub surface waters, varying from 5 m (MAR, UPW areas) to 30 m (GYR area). **(a)** Box-plot distribution of the factor of enrichment in the non enriched control after 24h incubation under in situ-simulated conditions. **(b)** Box-plot distribution of enrichment factors obtained after 24 h incubation in presence of nitrate+ammonium (N), glucose (G) and phosphates+nitrates+ammonium+glucose (NPG). Enrichment factor is the leucine incorporation rate after 24h amendments compared to the leucine incorporation rate in the non-amended control at the same time. MAR – St 5 group (site MAR and stations STB1 to STB5, $n=6$), St 6-St 15 group (stations STB6 to STB8, site GYR, stations STB11 to STB15, $n=9$), EGY-UPW (site EGY, stations STB17 to STA21, UPW1, UPW2, $n=8$). The middle line in the box is the median value. Limits of the box: upper 75th percentile, lower 25th percentile; limits of the error bar: 90th and 10th percentiles; dots: outliers.

stations (EGY to UPW2), the leucine incorporation rates also increased slightly in the non-amended control ($\times 2.1$ to $\times 2.7$ in 24 h between station EGY and STA21, but $\times 4.1$ and $\times 3.5$ at stations UPW1 and UPW2). The median values of stimulation factors for glucose, N and NPG additions were $\times 1.6$, $\times 1.1$ and $\times 3.4$, respectively (Fig. 4b, see example of STB18, Fig. 3). In this last group of stations, the leucine incorporation rates increased significantly in the control, in G and NPG – amended samples (Wilcoxon signed-rank test, $p < 0.05$).

3.3.2 Vertical variability of nutrient control on Heterotrophic Bacteria

There were also varying stimulation factors of leucine incorporation rates along vertical profiles. At the GYR site, leucine incorporation rates increased after N addition at all depths tested, even if nitrate was significantly detected below 150 m ($0.15 \mu\text{M}$ at 185 m, $3.6 \mu\text{M}$ at 245 m, Fig. 5). Glucose, however, has a higher effect than N at 185 m ($\times 83$ versus $\times 4$) and 245 m ($\times 495$ versus $\times 190$, respectively). At the EGY site, the stimulation factor of leucine incorporation rates after 24 h addition of glucose progressively increased between 80 m and 250 m ($\times 4$ up to $\times 105$). Stimulation by N alone was non existent or low ($\times 2.2$ at 40 m, $\times 2.6$ at 250 m), although nitrogen was still undetectable above 40 m. Stimulation by NPG also increased from the surface layer ($\times 1.1$ – $\times 2.9$ above 30 m) to 250 m ($\times 49$). At the UPW site, only effects of G and NPG were visible, being more or less constant and with poor increases (factors < 4) below 10 m. At 5 m depth, none of the nutrients (alone or in combination) stimulated leucine incorporation rates.

4 Discussion

4.1 Abundance or production to track limitation?

Because both abundance and leucine incorporation rates have been followed, one question is arising: What is the best indicator for tracking factors limiting heterotrophic bacterial growth? The increase in leucine incorporation rates, when present, is either due to stimulation of a greater percentage of active population, or the stimulation of the specific growth rate of individual cells, or some combination of these two processes, whereas bacterial abundance is also regulated by grazing when intact sea water is manipulated, and should increase more rapidly in pre-filtered samples. Indeed, bacterial abundance responds generally less than production to enrichments in unfiltered samples (Kirchman, 1990; Pomeroy et al., 1995; Graneli et al., 2004). In our experiments, bacterial abundances showed a response up to $\times 1.2$ after enrichments, whereas leucine incorporation rates increased up to 23 times (Table 4), confirming these previous results. Within surface water at the GYR site, only 25% of the “DAPI-labelled bacteria” showed distinct silver grains after microautoradiography coupled to hybridization in situ (Obenosterer et al., 2008a) suggesting inexistent or very low protein synthesis rate by a majority of the cells before enrichments. When adding the limiting factor, bacteria recovered stoichiometric equilibrium and/or energy capacity which gave them the capacity to assimilate leucine again. Such unbalanced growth is often the explanation for the strong changes generally observed with the thymidine or the leucine technique, compared to that of abundances (Carlson and Ducklow, 1996). Thus the increase of leucine incorporation rate does not mean

immediately a change in population. However, rapid growth of gamma-proteobacteria after FeN and “all” additions (Van Wambeke, unpub. results) was observed at the GYR site after 48 h of enrichments. A shift in bacterial population is generally an obligatory consequence of long term confinement and enrichments (Pinhassi et al., 2006). The number of heterotrophic flagellates increased, suggesting that bacterial predation was also enhanced after some stimulation of heterotrophic bacteria (GYR site, N enrichments, Table 4), and consequently regulated bacterial abundances. In conclusion, the leucine incorporation rates were thus better indicators than abundances for tracking factors limiting bacterial growth. Nevertheless, responses could have been different in terms of intensity or delay with other tracers of heterotrophic activity or using pre-filtered samples (Carlson and Ducklow, 1996; Donachie et al., 2001).

4.2 Direct versus indirect limitation

There has been much debate about direct (suppression of a real limiting factor) or indirect (stimulation of phytoplankton by the added component which induces a surplus of DOM production fuelling heterotrophic bacteria) effects of iron and other macronutrients limitation on heterotrophic bacteria (Table 5).

The timing and magnitude of responses of phytoplanktonic parameters (primary production, chlorophyll biomass) compared to that of heterotrophic bacteria in the experiment performed under TMC have helped to argue for possible direct or indirect effect of nutrient additions. If iron alone induced a positive stimulation of leucine activity within the Marquesas plateau (MAR site), addition of other nutrients N+P+Si (“all”) without Fe stimulated leucine activity at the same level (factor 2 compared to the control at the same time, Fig. 2). In addition, chlorophyll biomass increased compared to the control, by a factor equivalent to that of leucine activity in 24 h, and even more after 48h (factor 3, Table 4). It is thus probable that the effect of Fe on leucine activity was indirect. The major effect obtained at the MAR site is however obtained in the non-amended control ($\times 20$ at the MAR site in the “trace metal clean” conditions, Fig. 2), although chlorophyll biomass increased only by $\times 1.5$ in this control (Table 4). It is possible that sufficient amounts of labile DOC were present, allowing a rapid bacterial growth without any enrichment, which implies that heterotrophic bacteria were not limited at all after a 24 h confinement at the MAR site. The capacity of bacteria to grow on bulk DOC was also seen in the vicinity of MAR site, up to 125° W, as a strong growth in the non-amended controls was observed up to station STB5 (Fig. 4a). Interpretation of growth in a non-amended control is difficult because the use of batch experiments last for a few days. This implies to take into account bottle effect: underestimation of the levels of the trophic web, and possible destruction of fragile cells during handling that fuels labile organic resources for heterotrophic

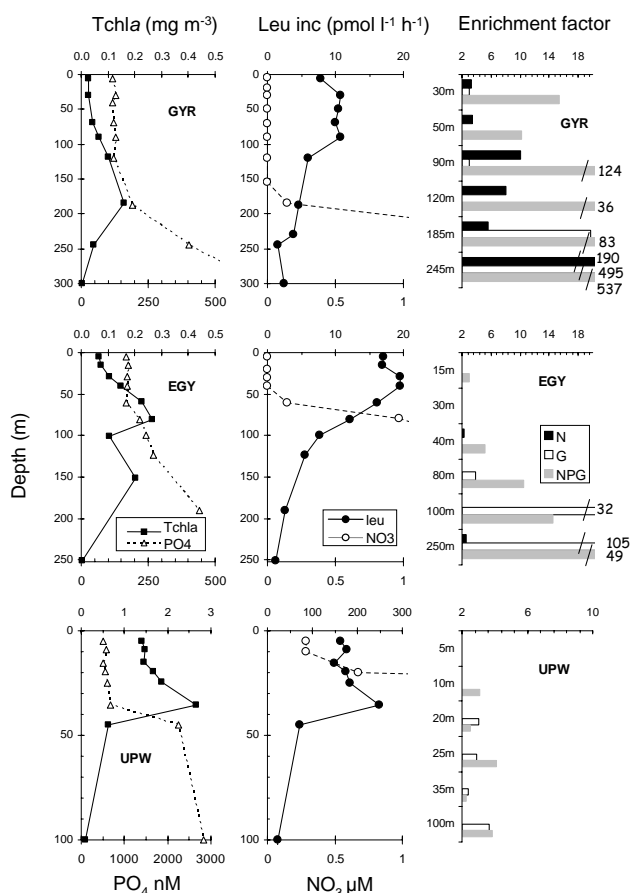


Fig. 5. Distribution of *in situ* chlorophyll a, leucine incorporation rates, nitrate and phosphate concentrations along vertical profiles, at sites GYR, EGY and UPW and responses to bioassays. Bioassays are expressed in terms of stimulation factor after N, G and NPG additions (leucine activity divided by leucine activity in the control at the same time). Only stimulation factors greater than 2 were plotted.

bacteria. However, all the other experiments have been performed in the same conditions, and the non-amended control did not increase that much. Possible other explanations are the change in the top-down control of bacteria or non steady state of bacterial growth at the time of the sampling at these stations. Day-to-day changes in *in situ* primary production, as well as *in situ* specific leucine incorporation rates have been observed during occupation of the MAR site (Van Wambeke et al., 2008a) and argue for this second hypothesis.

At the GYR site, the addition of iron did not result in any significant increase of photosynthesis rates (Table 4). Although dissolved iron was low and constant along most of the transect (~ 0.1 nM in surface), it was shown that phytoplankton was acclimated to iron deprivation in the centre of the gyre (Bonnet et al., 2008). N addition alone (nitrate+ammonium) or in combinations (FeN, “all”) have all stimulated chlorophyll and primary production (24 and 48 h).

Table 5. Review of factors enhancing some bacterial variables among different oceanic environments (Leu, Tdr: production based on Leucine and Thymidine technique, BN: bacterial numbers, BS: bacterial size, EEA: ectoenzymatic activities, O₂: respiration, BGE: bacterial growth efficiencies, DIV: diversity). DCM deep chlorophyll maximum, PE-DOM: filtrate of heat killed plankton extract (>335 μm), Me+Vit: trace metals+vitamins, glu: glucose, DFAA: dissolved free amino acids, NH₄: ammonium, NO₃: nitrate, Fe: iron. Co refers to colimitation. * in situ fertilization experiments. When carbon is limiting, and when the information was available, the terms in italic (*resource, not clear and energy*) refer to the authors' conclusions about energy versus resource limitation.

area	date	parameter followed	nutrients tested	limitation by	effect direct vs. cascade	
Gulf of Mexico to Mississippi. river plume	Jan June 1993	Leu, BN, O ₂	NH ₄ , PO ₄ , Me, +Vit, glu	P		Pomeroy et al., 1995
Sargasso Sea off Bermuda	Jul oct 92, Mar Jul 93, Jan 94	Leu, Tdr, BN, BS	NH ₄ , PO ₄ , glu, DFAA, algal lysate	<i>C (resource)</i>		Carlson and Ducklow, 1996
Med Sea, Western, Ionian, Levantine	June and Sept 99	Leu	NO ₃ , PO ₄ , glu	co C-P, P		Van Wambeke et al., 2002
Med Sea, Catalano-Balearic Basin, surface, DCM	Jun 95, Jun Sept 96	Leu, BN	NO ₃ , PO ₄ , glu	P, co C-P C, N		Sala et al., 2002
Med Sea, Ionian, Cretan, Levantine Basins	Jan Feb 1995	Tdr, BN	PO ₄ , NH ₄ , Fe, EDTA	P		Zohary and Robarts, 1998
Med Sea, Levantine (Cyprus Gyre)		Leu, BN	PO ₄	P	direct	Thingstad et al., 2005
Subarctic Pacific, gulf of Alaska	Sept 1987, May Aug 1988	Tdr, Leu, BN	NH ₄ , DFAA, glu, protein, alkylamines	<i>C (energy)</i>		Kirchman, 1990
Subtropical North Pacific, St ALOHA	Dec 96-Apr 98	glucose uptake, EEA	NH ₄ , NO ₃ , leu, his, glu	co N-C (<i>not clear</i>)		Donachie et al., 2001
Eastern North Pacific, California current	June Oct 1992	O ₂ , BN, BGE	PE-DOM, glu, NH ₄ , urea, PO ₄ , DFAA	<i>C (energy)</i>		Cherrier et al., 1996
Eastern North Pacific, California current	June 96, June 97	Leu, BN	Fe		not clear	Hutchins et al., 1998
Eastern Equatorial Pacific, IRONEX II	May 1995	Leu, BN	Fe *	Fe	not clear	Cochlan, 2001
South East Pacific, Tuamotu atolls	Nov 95, Mar 96	Tdr	NH ₄ , PO ₄ , glu	N, C, P, co C-N		Torréon et al., 2000
Ocean around atolls				C	direct	
South Eastern Pacific Gyre (this study)	Nov-Dec 2005	Leu, BN	Fe, NH ₄ +NO ₃ , PO ₄ , glu	N	direct	This study
Antarctic, Gerlashe Strait	October 1995		Fe	Fe	direct	Palkulski et al., 1996
Southern Ocean, Atlantic sector	austral summer 97/98	Leu, BN	NH ₄ PO ₄ glu	C		Tortell et al., 1996
Southern Ocean, Atlantic sector, EISENEX	Nov 2000	Leu, Tdr, BN, EEA, DIV	Fe*	Fe	not clear	Arrieta et al., 2004

The leucine incorporation rate in the GYR site is statistically higher in N and G enriched sample than in the control ($\times 4.6$ and $\times 3$ enrichment factor at 24 h, $\times 8.9$ and $\times 3.5$ at 48 h, respectively, $p < 0.05$, Table 4). The growth after N addition is not higher than that after G addition at 24 h, but it is at 48 h ($p < 0.05$). Thus, based on a 48 h response, it seems that N addition provides better possibility to grow to heterotrophic bacteria than addition of glucose alone. This trend is confirmed from non TMC experiments made along different stations inside the gyre (STB6-STB15). In these experiments, the increase of leucine incorporation rates after glucose addition is lower than that obtained after N addition (Wilcoxon signed-rank test, $p = 0.038$, $n = 9$ pairs of comparison, box plots Fig. 4b). These results suggest that the limitation by N of bacterial production within the gyre is direct.

But other observations suggest that labile carbon acts sequentially as a second limiting factor. Indeed, within the surface waters of stations STB6-STB15, addition of glucose alone did not stimulate leucine incorporation rates (Wilcoxon signed-rank test between C and G enriched samples, $n = 9$ pairs of comparison, $p = 0.07$), but addition of N alone did (comparison C-N, $p < 0.01$). However, leucine incorporation rates increased statistically much more in NPG amended samples than in N amended samples (Fig. 4, median of increasing factor switched from $\times 4.2$ to $\times 37$, Wilcoxon signed-rank test between N and NPG enriched samples, $n = 9$ pairs of comparison, $p < 0.01$). Considering further that P never stimulated bacteria, we infer that in the area between 122° W and 95° W, labile organic carbon rapidly becomes a limiting factor after N addition.

Within the deep chlorophyll maximum (DCM), however, glucose is the first limiting nutrient, not N (Fig. 5). A similar switch from a mineral nutrient within surface layer to organic

C limitation within DCM has been evidenced in the Mediterranean Sea (Sala et al., 2002; Van Wambeke et al., 2002).

The rapidity of the response of heterotrophs versus autotrophs after relieving the N limiting nutrient in the South Pacific gyre could have consequences on the metabolic balance of this environment. Recently, it has been shown that 5–10% of deep sea water mixed with water from the nutrient-limited mixed layer of the North Pacific Gyre provided a set of nutrient enrichment sufficient to significantly enhance the net community production after 5 days (Mc Andrew et al., 2007). Thus, the question arises here if, in our nitrogen enrichment experiments made at the GYR site, photosynthesis was also notably favoured compared to respiration. Oxygen budgets were not measured in our experiments, but as our stimulation factors were much greater with leucine incorporation rates than particulate primary production, our results would suggest the opposite (i.e. enrichment would favour net heterotrophy at the GYR site). Nevertheless, the leucine incorporation rate is not respiration, and possible changes in leucine conversion factors, as well as in bacterial growth efficiencies with time could not be ruled out. Indeed, the relieving of a factor limiting heterotrophic bacteria enhances bacterial growth efficiency (Carlson and Ducklow, 1996). Also, our experiments lasted only 48 h, whereas significant chlorophyll biomass and net community production occurred only after 4–5 days in the Mc Andrew et al. (2007) experiments. Finally, the rates at which autotrophic and heterotrophic cells developed in our experiment might have been influenced by enzymatic properties of uptake systems for ammonium and nitrate which differs inside these two groups, heterotrophic bacteria being favoured by ammonium addition, whereas only nitrate were provided by deep sea water enrichments in Mc Andrew et al. (2007) approach.

4.3 Carbon versus energy limitation of heterotrophic bacteria

Because the organic molecule tested is also often an energy-rich molecule easily entering catabolic pathways (e.g. glucose), one could wonder if this carbon source is tracking carbon resource limitation or energy limitation (Table 4). Free glucose (not combined) is rare in this area (Sempéré et al., 2008), suggesting that this molecule plays an important role in energy restoration once added. DOC is probably highly refractory, due to strong UV radiation effects (Tedetti et al., 2007). Indeed, it has been shown that growth of heterotrophic bacteria at the GYR site after a one day UV exposure of DOM is partly inhibited (Sempéré et al., 2008). It is probable that the limitation in N and energy prevents the synthesis of enzymes able to degrade the bulk accumulated DOC present in this area ($118 \mu\text{M}$ at GYR, Table 1, Raimbault et al., 2008). Indeed, in addition to changes in populations (Pinhassi et al., 2006), induction of some genes after the relieving of some limiting nutrients has been observed (Arietta et al., 2004). Bacteria were described as energy limited in the South Pacific (Kirchman, 1990), and in the Eastern North Pacific (Cherrier et al., 1996), but resource limited in the Sargasso Sea (Carlson and Ducklow, 1996). In addition, conflicting interpretation are sometimes given to the same observation, for instance when comparing enhancement of bacterial activity after amino acids addition or with glucose+ammonium addition (Kirchman, 1990; Carlson and Ducklow, 1996; Donachie et al., 2001). It is probably impossible to dissociate notions of energy versus resource limitation in nature and varying conclusions given probably rely on the quality of organic matter present and the parameter tracking heterotrophic activity.

In the centre of the South Pacific Gyre, nitrogen was a common primarily factor limiting phytoplankton and bacteria. Competitive advantages for N between bacteria and phytoplankton might thus exist and vary with irradiance levels, which had not been considered in this study. Indeed, it has also been suggested that the factors limiting bacteria could change at a daily scale (Shiah, 1999; Kuipers et al., 2000). DOC produced by phytoplankton release could be a major source of carbon and energy for bacteria. The huge needs of nitrogen and energy source for heterotrophic bacteria, as well as their strong plasticity to grow again once limitation is relieved, are probably the key factors explaining the strong coupling between phytoplankton and bacteria as seen on diel cycles (Van Wambeke et al., 2008b).

5 Conclusions

A large set of enrichment experiments was performed here along a 8000 km transect, sometimes along vertical profiles, allowing a broad generalization of the observed trends over a large spatial scale of the South Pacific Ocean in an aus-

tral summer situation. Our enrichment experiments have shown that iron was never the single nutrient limiting bacterial production. From the vicinity of the Marquesas Islands to approx 125°W , the high response in the control suggests no limitation. Nitrogen was the first factor limiting heterotrophic bacterioplankton within the surface layers in the centre of the south Pacific Gyre, with labile carbon acting sequentially as a second limiting factor. Overall the surface layers around the eastern border of the South Pacific Gyre (91°W to the upwelling off Chile), labile carbon was the primarily factor limiting heterotrophic bacterial production.

Because the weak horizontal advection in the centre of the South Pacific Gyre and because intense seasonal convective mixing is excluded (Raimbault et al., 2008), this suggests that the situation of nitrogen limitation could be permanent throughout the entire year. However, nitrogen was a common primarily factor limiting both phytoplankton and bacteria, which probably had consequences on their relationships at short time scales. The heterotrophic bacterioplankton of the South Pacific Gyre lives in a very dynamic situation which is difficult to determine adequately, and current methods and tools for detecting limiting factors on short incubation time are urgently needed.

Acknowledgements. This work was supported by French program PROOF (Processus biologiques dans l'océan et flux), Centre National de la Recherche Scientifique (CNRS). This is a contribution of the BIOSOPE project of the LEFE-CYBER program. We also thank Stéphane Blain and Flavienne Bruyant for help in sample processing of trace metal clean experiments, Carolina Grob for collecting bacterial abundance samples on board, Hervé Claustre for leadership of this program, and 2 anonymous reviewers who helped to improve this ms.

Edited by: M. Dai

References

- Arrieta, J., Weinbauer, M., Lute, C., and Herndl, G.: Response of bacterioplankton to iron fertilization in the southern Ocean, *Limnol. Oceanogr.*, 49, 799–808, 2004.
- Blain, S., Bonnet, S., and Guieu, C.: Dissolved iron distribution in the tropical and sub tropical South Eastern Pacific, *Biogeosciences*, 5, 269–280, 2008, <http://www.biogeosciences.net/5/269/2008/>.
- Bonnet, S., Guieu, C., Bruyant, F., Prášil, O., Van Wambeke, F., Raimbault, P., Moutin, T., Grob, C., Gorbunov, M., Zehr, J. P., Masquelier, S., Garczarek, L., and Claustre, H.: Nutrient limitation of primary productivity in the Southeast Pacific (BIOSOPE cruise), *Biogeosciences*, 5, 215–2225, 2008, <http://www.biogeosciences.net/5/215/2008/>.
- Bruland, K. W., Franks, R. P., Knauer, G. A. and Martin, J. H.: Sampling and analytical methods for the determination of Cu, Cd, Zn, and Ni at the nanogram per liter level in sea water, *Anal. Chim. Acta*, 105, 234–245, 1979.

- Carlson, C. A. and Ducklow, H. W.: Growth of bacterioplankton and consumption of dissolved organic carbon in the Sargasso Sea, *Aquat. Microb. Ecol.*, 10, 69–85, 1996.
- Cherrier, J., Bauer, J. E., and Druffel, E. R. M.: Utilization and turnover of labile dissolved organic matter by bacterial heterotrophs in eastern North Pacific surface waters, *Mar. Ecol. Prog. Ser.*, 139, 267–279, 1996.
- Church, M., Hutchins, D., and Ducklow, H. W.: Limitation of bacterial growth by dissolved organic matter and iron in the Southern Ocean, *Appl. Environ. Microbiol.*, 66, 455–466, 2000.
- Claustre, H., Sciandra, A., and Vault, D.: Introduction to the special section Bio-optical and biogeochemical conditions in the South East Pacific in late 2004: the BIOSOPE program, *Biogeosciences*, 5, 679–691, 2008, <http://www.biogeosciences.net/5/679/2008/>.
- Cochlan, W. P.: The heterotrophic bacterial response during a mesoscale iron enrichment experiment (IronEx II) in the Eastern equatorial Pacific Ocean, *Limnol. Oceanogr.*, 46, 428–435, 2001.
- Cotner, J., Ammermann, J., Peele, E., and Bentzen, E.: Phosphorus-limited bacterioplankton growth in the Sargasso Sea, *Aquat. Microb. Ecol.*, 13, 141–149, 1997.
- Duhamel, S., Moutin, T., Van Wambeke, F., Van Mooy, B., Rimmelin, P., Raimbault, P., and Claustre, H.: Growth and specific P-uptake rates of bacterial and phytoplanktonic communities in the Southeast Pacific (BIOSOPE cruise), *Biogeosciences*, 4, 941–956, 2007, <http://www.biogeosciences.net/4/941/2007/>.
- Donachie, S. P., Christian, J. R., and Karl, D. M.: Nutrient regulation of bacterial production and ectoenzyme activities in the subtropical North Pacific Ocean, *Deep-Sea Res. II*, 48, 1719–1732, 2001.
- Granéli, W., Carlsson, P., and Bertilsson, S.: Bacterial abundance, production and organic carbon limitation in the Southern Ocean (39–62° S, 4–14° E) during the austral summer 1997/1998, *Deep-Sea Res. II*, 51, 2569–2582, 2004.
- Grob, C., Ulloa, O., Claustre, H., Huot, Y., Alarcón, G., and Marie, D.: Contribution of picoplankton to the total particulate organic carbon concentration in the eastern South Pacific, *Biogeosciences*, 4, 837–852, 2007, <http://www.biogeosciences.net/4/837/2007/>.
- Hutchins, D. A., DiTullio, G. R., Zhang, Y., and Bruland, K. W.: An Iron limitation mosaic in the California upwelling regime, *Limnol. Oceanogr.*, 43, 1037–1054, 1998.
- Kirchman, D. L.: The uptake of inorganic nutrients by heterotrophic bacteria, *Microb. Ecol.*, 28, 255–271, 1994.
- Kirchman, D. L.: Limitation of bacterial growth by dissolved organic matter in the subarctic Pacific, *Mar. Ecol. Prog. Ser.*, 62, 47–54, 1990.
- Kirchman, D. L. and Rich, J.: Regulation of bacterial growth rates by dissolved organic carbon and temperature in the Equatorial Pacific Ocean, *Microb. Ecol.*, 33, 11–20, 1997.
- Kirchman, D. L., Meon, M., Cottrell, M. T., Hutchins, D. A., Weeks, D., and Bruland, K. W.: Carbon versus iron limitation of bacterial growth in the California upwelling regime, *Limnol. Oceanogr.*, 45, 1681–1688, 2000.
- Kirchman, D. L., Elifantz, H., Dittel, A., Malmstrom, R., and Cottrell, M.: Standing stocks and activity of Archaea and Bacteria in the western Arctic Ocean, *Limnol. Oceanogr.*, 52, 495–507, 2007.
- Kuipers, B.: Diel periodicity of bacterioplankton in the euphotic zone of the subtropical Atlantic Ocean, *Mar. Ecol. Prog. Ser.*, 201, 13–25, 2000.
- McAndrew, P., Bjorkman, K., Church, M., Morris, P., Jachowski, N., Williams, P. J. le B., and Karl, D.: Metabolic response of oligotrophic plankton communities to deep water nutrient enrichment, *Mar. Ecol. Prog. Ser.*, 332, 63–75, 2007.
- Moutin, T., Karl, D. M., Duhamel, S., Rimmelin, P., Raimbault, P., Van Mooy, B. A. S., and Claustre, H.: Phosphate availability and the ultimate control of new nitrogen input by nitrogen fixation in the tropical Pacific Ocean, *Biogeosciences*, 5, 95–109, 2008, <http://www.biogeosciences.net/5/95/2008/>.
- Obernosterer, I., Catala, P., Lami, R., Caparros, J., Ras, J., Bricaud, A., Dupuy, C., Van Wambeke, F. and Lebaron, P.: Biochemical characteristics and bacterial community structure of the sea surface microlayer in the South Pacific Ocean, *Biogeosciences*, 5: 693–705, 2008a.
- Obernosterer, I., Christaki, U., Lefèvre, D., Catala, P., Van Wambeke, F., and Lebaron, P.: Rapid bacterial mineralization of organic carbon produced during a phytoplankton bloom induced by natural iron fertilization in the Southern Ocean, *Deep-Sea Res. II*, 55, 777–789, 2008b.
- Olivier, J. L., Barber, R. T., Smith, W. O., and Ducklow, H. W.: The heterotrophic bacterial response during the southern Ocean Iron Experiment (SOFEX), *Limnol. Oceanogr.*, 49, 2129–2140, 2004.
- Pakulski, J. D., Coffin, R. B., Kelley, C. A., Holder, S. L., Downer, R., Aas, P., Lyons, M. M., and Jeffrey, W. H.: Iron stimulation of Antarctic bacteria. *Nature*, 383, 133–134, 1996.
- Pinhassi, J., Gómez-Consarnau, L., Alonso-Sáez, L., Sala, M., Vidal, M., Pedrós-Alió, C., and Gasol, J.: Seasonal changes in bacterioplankton nutrient limitation and their effects on bacterial community composition in the NW Mediterranean Sea, *Aquat. Microb. Ecol.*, 44, 241–252, 2006.
- Pomeroy, L. R., Sheldon, J. E., Sheldon, W. M., and Peters, F.: Limits to growth and respiration of bacterioplankton in the Gulf of Mexico, *Mar. Ecol. Prog. Ser.*, 117, 259–268, 1995.
- Raimbault, P., Garcia, N.: Evidence for efficient regenerated production and dinitrogen fixation in nitrogen-deficient waters of the South Pacific Ocean: impact on new and export production estimates, *Biogeosciences*, 5, 323–338, 2008.
- Raimbault, P., Garcia, N., and Cerutti, F.: Distribution of inorganic and organic nutrients in the South Pacific Ocean - Evidence for long-term accumulation of organic matter in nitrogen-depleted waters, *Biogeosciences*, 5, 281–298, 2008, <http://www.biogeosciences.net/5/281/2008/>.
- Ras, J., Claustre, H., and Uitz, J.: Spatial variability of phytoplankton pigment distributions in the Subtropical South Pacific Ocean: comparison between in situ and predicted data, *Biogeosciences*, 5, 353–369, 2008, <http://www.biogeosciences.net/5/353/2008/>.
- Sala, M. M., Peters, F., Gasol, J. M., Pedrós-Alió, C., Marrasé, C., and Vaqué, D.: Seasonal and spatial variations in the nutrient limitation of bacterioplankton growth in the northwestern Mediterranean, *Aquat. Microb. Ecol.*, 27, 47–56, 2002.
- Shiah, F. K.: Diel cycles of heterotrophic bacterioplankton abundance and production in the ocean surface waters, *Aquat. Microb. Ecol.*, 17, 239–246, 1999.
- Sempéré, S., Tedetti, M., Charrière, B., Panagiotopoulos, C. and

- Van Wambeke, F.: Molecular distribution and bacterial availability of dissolved sugars in the south East Pacific, *Biogeosciences Discuss.*, 5, 725–750, 2008, <http://www.biogeosciences-discuss.net/5/725/2008/>.
- Tedetti, M., Sempéré, R., Vasilkov, A., Charrière, B., Nérini, D., Miller, W. L., Kawamura, K., and Raimbault, P.: High penetration of ultraviolet radiation in the south east Pacific waters, *Geophys. Res. Lett.*, 34, L12610, doi:10.1029/2007GL029823, 2007.
- Thingstad, T.: Control of bacterial growth in idealized food webs, in: *Microbial Ecology of the Oceans*, edited by: Kirchman, D. L., Wiley-Liss, New York, 239–260, 2000.
- Thingstad, T., Krom, M., Mantoura, F., Flaten, G., Groom, S., Herut, B., Kress, N., Law, C., Pasternak, A., Pitta, P., Psarra, S., Rassoulzadegan, F., Tanaka, T., Tselepidis, A., Wassmann, P., Woodward, M., Riser, C., Zodiatis, G., and Zohary, T.: Nature of phosphorus limitation in the ultraoligotrophic eastern Mediterranean, *Science*, 309, 1068–1071, 2005.
- Tortell, P. D., Maldonado, M. T., Granger, J., and Price, N. M.: Marine bacteria and biogeochemical cycling of iron in the oceans, *FEMS Microb. Ecol.*, 29, 1–11, 1999.
- Tortell, P. D., Maldonado, M. T., and Price, N. M.: The role of heterotrophic bacteria in iron-limited ecosystems. *Nature*, 383, 330–332, 1996.
- Torréton, J.-P., Talbot, V., and Garcia, N.: Nutrient stimulation of bacterioplankton growth in Tuamotu atoll lagoons, *Aquat. Microb. Ecol.*, 21, 125–137, 2000.
- Van Wambeke, F., Christaki, U., Giannakourou, A., Moutin, T., and Souvemerzoglou, K.: Longitudinal and vertical trends of bacterial limitation by phosphorus and carbon in the Mediterranean Sea, *Microb. Ecol.*, 43, 119–133, 2002.
- Van Wambeke, F., Obernosterer, I., Moutin, T., Duhamel, S., Ulloa, O., and Claustre, H.: Heterotrophic bacterial production in the South East Pacific: Longitudinal trends and coupling with primary production, *Biogeosciences*, 5, 157–169, 2008a, <http://www.biogeosciences.net/5/157/2008/>.
- Van Wambeke, F., Tedetti, M., Duhamel, S., and Sempéré, R.: Diel variability of heterotrophic bacterial production and UV doses in the South East Pacific, *Biogeosciences Discuss.*, 5, 435–462, 2008b, <http://www.biogeosciences-discuss.net/5/435/2008/>.
- Zohary, T., and Robarts, R. D.: Experimental study of microbial P limitation in the eastern Mediterranean, *Limnol. Oceanogr.*, 43, 387–395, 1998.

Distribution and bacterial availability of dissolved neutral sugars in the South East Pacific

R. Sempéré, M. Tedetti, C. Panagiotopoulos, B. Charrière, and F. Van Wambeke

Laboratoire de Microbiologie, Géochimie et Ecologie Marines (LMGEM), UMR 6117, CNRS, Université de la Méditerranée, Centre d'Océanologie de Marseille, Campus de Luminy, Case 901, 13 288 Marseille Cedex 9, France

Received: 3 December 2007 – Published in Biogeosciences Discuss.: 14 February 2008

Revised: 23 April 2008 – Accepted: 18 July 2008 – Published: 25 August 2008

Abstract. The distribution and bacterial availability of dissolved neutral sugars were studied in the South East Pacific from October to December 2004 during the BIOSOPE cruise. Four contrasting stations were investigated: Marquesas Islands (MAR), the hyper-oligotrophic South Pacific Gyre (GYR), the eastern part of the Gyre (EGY), and the coastal waters associated to the upwelling area off Chile (UPW). Total (free and combined) dissolved neutral sugar (TDNS) concentrations were in the same order of magnitude at MAR (387 ± 293 nM), GYR (206 ± 107 nM), EGY (269 ± 175 nM), and UPW (231 ± 73 nM), with the highest and lowest concentrations found at MAR (30 m, 890 nM) and EGY (250 m, 58 nM), respectively. Their contribution to dissolved organic carbon (TDNS-C \times DOC⁻¹%) was generally low for all sites varying from 0.4% to 6.7% indicating that South East Pacific surface waters were relatively poor in neutral sugars. Free dissolved neutral sugar (FDNS; e.g. sugars analyzed without hydrolysis) concentrations were very low within the detection limit of our method (5–10 nM) accounting for <5% of the TDNS. In general, the predominant sugars within the TDNS pool were glucose, xylose, arabinose, and galactose, while in the FDNS pool only glucose was present. TDNS stock to bacterial production ratios (integrated values from the surface to the deep chlorophyll maximum) were high at GYR with respect to the low primary production, whereas the opposite trend was observed in the highly productive area of UPW. Intermediate situations were observed for MAR and EGY. Bioavailability of dissolved organic matter (DOM) exposed to natural solar radiation was also experimentally studied and compared to dark treatments. Our results showed no or little detectable effect of sunlight on DOM bacterial assimilation in surface waters of UPW and GYR, while a significant stimulation was found in MAR and

EGY. The overall results clearly suggest that DOM is less labile at GYR compared to UPW, which is consistent with the observed accumulation of dissolved organic carbon and the elevated C/N ratios reported by Raimbault et al. (2008).

1 Introduction

Sugars are among the most abundant components in seawater constituting structural and storage compounds (Painter, 1983; Parsons et al., 1984; Benner and Kaiser, 2003) of marine organisms and generally account 20–40 dry wt. % of plankton, 17 dry wt. % of bacteria (Stouthamer, 1977), 2–30% of dissolved organic matter (DOM; Pakulski and Benner, 1994; Benner, 2002), and 50–70% of the high molecular weight DOM (> 1 kDa; Benner et al., 1992; Aluwihare et al., 1997). Two major categories of sugars have been identified in DOM: Monosaccharides (free monomers) and polysaccharides (neutral sugars released after acid hydrolysis). Concentrations of free sugars have been found extremely low (<50 nM) compared to the dissolved polysaccharides (200–800 nM) (Benner, 2002 and references therein). Of the free sugars glucose appears to be quantitatively most important although arabinose and fructose have also been detected (Rich et al., 1996, 1997; Skoog et al., 1999; Kirchman et al., 2001). Only few vertical profiles of dissolved sugars in seawater have been already published (Skoog and Benner, 1997; Amon and Benner, 2003) and there is a limited number of studies dealing with the bacterial reactivity of polysaccharides and monosaccharides (free glucose) in the water column for different trophic regimes (Rich et al., 1996; Skoog et al., 1999; Kirchman et al., 2001).

The South East Pacific waters encompass a wide range of primary productivity ranging from the most oligotrophic and clearest waters of the world ocean in the central part of the South Pacific Gyre (SPG) (Claustre and Maritorea, 2003; Morel et al., 2007; Tedetti et al., 2007) to the highly eutrophic



Correspondence to: R. Sempéré
(richard.sempere@univmed.fr)

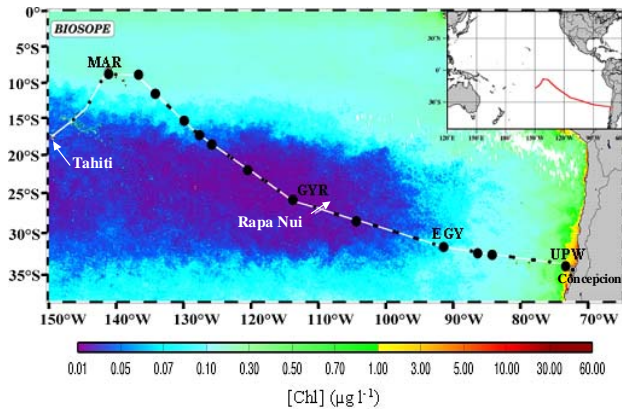


Fig. 1. Map of the BIOSOPE cruise track superimposed on a Sea-viewing Wide Field-of-view Sensor (SeaWiFS) composite for November and December showing the chlorophyll concentration in the upper layer. The long (3–6 days) stations studied for dissolved neutral sugar content, bacterial production, DOM-photodegradation and -biodegradation experiments are Marquesas Islands (MAR), center of the South Pacific Gyre (GYR), East of the South Pacific Gyre (EGY) and upwelling off Chile (UPW). Rapa Nui is Easter Island. <http://www.obs-vlfr.fr/proof/vt/op/ec/biosope/bio.htm>.

upwelling area off Chile (Carr, 2002). However, very little is known about DOM dynamics in the South Pacific and there is no report dealing with sugar distribution in the SPG. Such a study could help to evaluate DOM characteristics in terms of bacterial cycling and abiotic degradation (solar radiation).

This paper aims to provide data on the molecular distribution of sugars in the DOM pool in the South East Pacific waters at four contrasting stations and to understand its photochemical and bacterial reactivity.

2 Material and methods

2.1 Sampling

Sampling was performed along a 8000 km transect in the South East Pacific during the BIOgeochemistry and Optics SOuth Pacific Experiment (BIOSOPE) cruise (24 October–11 December 2004). To study the molecular distribution and bacterial availability of dissolved neutral sugars, we collected

1. depth profile samples (0–500 m) and
2. large volume samples (20 l) for DOM-photodegradation and -biodegradation experiments.

Four stations were sampled: Marquesas Islands (MAR), center of the SPG (GYR), East of the SPG (EGY), and the upwelling of Chile (UPW) (Fig. 1; Table 1). Biogeochemical and physical characteristics of these sampling sites are described in detail elsewhere (Claustre et al., 2008). Surface

and underwater solar irradiance measurements were also performed at these stations.

Discrete seawater samples were taken with 12 l Niskin bottles mounted on a CTD/rosette and washed with 1 M HCl and Milli-Q water before the cruise. Rubber made ribbons and o-rings of the original Niskin bottles were replaced with silicon ribbons and Viton o-rings, respectively. Samples for dissolved sugar and bacterial production (BP) measurement were collected at six depths (maximum depth sampled: 160 m in MAR, 270 m in GYR, 250 m in EGY, and 500 m in UPW) close to solar noon (bio-optical CTD cast) directly (without tubing) from the Niskin bottles into pre-combusted (450°C, 6 h) 500-ml glass bottles, first or after gas sampling to avoid organic carbon contamination. The bottles were rinsed two times with the respective water samples before filling. Following collection, seawater for dissolved sugar analysis was filtered through 0.2- μm polycarbonate filters (Nuclepore, 47 mm filter diameter) which were washed with a few ml of 1 M HCl, 2 l of Milli-Q water, and 150 ml of sample prior to filtration. Samples were transferred to 5 ml polypropylene tubes (prewashed with 1 M HCl and Milli-Q water) and stored in the dark at -18°C . BP measurements were made on unfiltered seawater. For DOM-photodegradation and -biodegradation experiments, samples were collected at two depths (5 m and deep chlorophyll maximum (DCM), except in MAR: 5 and 160 m) at midnight in 20 l Nalgene carboy bottles using Teflon tubing. Samples were immediately processed in a temperature controlled laboratory on board. Plastic gloves were worn and care was taken to minimize contamination during sampling and the following procedure. Glassware filtration material was pre-combusted before the cruise and rinsed with 1 M HCl and Milli-Q water after each sample. Sampling information is summarized in Table 1.

2.2 DOM-photodegradation and -biodegradation experiments

After sampling, seawater was filtered through precombusted GF/F filters (Whatman, diameter: 142 mm) using a peristaltic pump with acid-cleaned silicon tubing and then through acid-cleaned Whatman POLYCAP AS 0.2 μm (820-cm²) filter capsules to exclude bacteria and others microorganisms. Seawater was also filtered under a low vacuum (<50 mm Hg) through 0.8 μm polycarbonate filters (Nuclepore, diameter: 47 mm) to prepare the bacterial inoculum whilst excluding predators. The filters were washed with 150 ml of 1 M HCl (filter capsule and Nuclepore), 2 l of Milli-Q water and 150 l of sample (filter capsule, Nuclepore and GF/F) prior to filtration. The 0.2 μm filtered seawater (here after called DOM-solution) was distributed into precombusted 5 l glass bottles and stored at 4°C in the dark until morning. DOM-solutions were transferred into 100 ml quartz and Pyrex Winkler flasks and exposed on the ship deck for one day (~ 8 h around solar noon) to natural solar radiation in a recirculating water

Table 1. Site location, date of sampling, deep chlorophyll maximum (DCM), depth of the euphotic zone (Z_e , 1% surface PAR), bacterial and primary productions integrated down to DCM (I-BP and I-PP) after Van Wambeke et al. (2008a) at the four stations in the South East Pacific. For depths sampled for DOM-photodegradation and biodegradation experiments, temperature (T), salinity (SAL), total chlorophyll- a (TChl- a) concentration after Ras et al. (2008), bacterial abundance (BA) and leucine incorporation rates (LEU) are also indicated. The maximum depths were 3623 m, 3013 m, 3393 m and 4825 m for MAR, GYR, EGY, and UPW sampling stations, respectively.

Site	Latitude	Longitude	Date	Z_e	I-BP	I-PP	depth	T	SAL	TChl- a	BA	LEU
				m	mg C m ⁻² d ⁻¹	mg C m ⁻² d ⁻¹	m	°C		μg l ⁻¹	x 10 ⁵ ml ⁻¹	pmol l ⁻¹ h ⁻¹
MAR*	08°21' S	141°16' W	27 ^a , 28 ^b , 29 ^c Oct.	70	144	683	5 m	27.9	35.55	0.27	8.25	44.0
							DCM (60 m)	27.7	35.55	0.38	9.17	29.4
							160 m*	22.4	35.99	0.018	2.55	2.3
GYR	26°03' S	114°00' W	12 ^b , 14 ^a , 15 ^c Nov.	160	50	159	5 m	22.6	36.01	0.019	3.36	8.2
							DCM (175 m)	19.05	35.51	0.18	3.12	6.6
EGY	31°50' S	091°27' W	26 ^b , 28 ^{a,c} Nov.	88	55	196	5 m	18.1	34.69	0.064	8.68	13.2
							DCM (80 m)	16.1	34.61	0.23	3.95	14.7
UPW	34°01' S	073°21' W	06 ^{a,c} , 07 ^b Dec.	34	226	4362	5 m	15.7	34.24	1.46	12.5	226
							DCM (40 m)	13.3	34.31	3.06	12.7	396

* 160 m, is the depth of the second DOM-photodegradation and -biodegradation experiment at MAR site

^a Sampling for T , SAL, dissolved neutral sugar, BA and LEU profiles (bio-optical CTD cast, close to solar noon)

^b Sampling for DOM-photodegradation and -biodegradation experiments (0:00 CTD cast). Surface solar irradiance was measured continuously during the exposure period (~ 8 h around solar noon)

^c Underwater solar irradiance measurements (close to solar noon)

bath (0.1 m depth). Surface water temperatures ranged from 16°C (UPW) to 28°C (MAR) (Table 1). Samples were irradiated in duplicates for two light conditions: so-called “Full Sun” (FS: total solar radiation in quartz flasks) and “Dark” (Pyrex flasks wrapped with aluminum foil). Before and immediately after irradiation of DOM-solutions, aliquots were taken in FS and Dark samples for free dissolved neutral sugar (FDNS) measurements and stored in 5 ml polypropylene tubes (prewashed with 1 M HCl and Milli-Q water) in the dark at -18°C. During DOM-photodegradation, the bacterial inoculum was kept in the dark at in situ temperature. Quartz and Pyrex flasks were precombusted before the cruise and extensively washed with 1 M HCl and Milli-Q water between different sets of samples during the cruise.

Bacterial response to the DOM changes after photodegradation was quantified through biodegradation experiments. After irradiation, the DOM-solutions were mixed with the (unirradiated) bacterial inocula (1/6, inoculum/DOM-solution final ratio) and then dispensed in duplicate into several precombusted 100-ml Pyrex Winkler flasks and incubated in the dark at in situ temperature. No nutrients were added in the mixed solutions in order to measure the response of bacteria under “natural” conditions. Subsamples were taken and analyzed for BP at time 0, 24, 48, and 72 h of incubation. For each experiment, killed controls were made by addition of HgCl₂ (final concentration: 10 mg l⁻¹), incubated with other samples and analyzed at the end of the experiment for BP.

2.3 Total dissolved neutral sugars (TDNS)

After a quick defrosting, samples (4 ml) for total (free and combined) dissolved neutral sugar (TDNS) analysis were transferred into precombusted Pyrex vials and hydrolyzed under N₂ with 0.1 M HCl at 100°C for 20 h (Burney and Sieburth, 1977). After hydrolysis, samples were not neutralized (to avoid contaminations from the addition of calcium carbonate) but directly desalted using AG2-X8 and AG50W-X8 Bio-Rad ion exchange resins according to Mopper et al. (1992). The reactions between resins and acidified samples (pH 1) favored the elimination of carbonates (which were released into the sample by anionic exchange with chloride) into CO₂, allowing a partial neutralization of sugar samples (pH 3–4.5 after desalting). A portion of the initial sample was also directly desalted (see above) without hydrolysis in order to estimate the amount of FDNS.

The samples were injected into a WATERS-HPLC system through a manual Rheodyne valve equipped with a 200 μl sample loop. The mobile phase consisted of a mixture 95/5 (v/v) of low-carbonate NaOH (20 mM, Baker) and Milli-Q water which was pumped at a flow rate of 0.7 ml min⁻¹ on isocratic mode. Neutral sugars were separated on a Dionex Carbopac PA-1 anion exchange column (4×250 mm) with 19 mM NaOH at 17°C (column temperature) and were detected by a Decade electrochemical detector (Antec Leyden BV) using a gold working electrode and a Pd reference electrode (Panagiotopoulos et al., 2001; Panagiotopoulos and Sempéré, 2005). A 1 M NaOH solution was added to the eluent stream by a post-column pump at a flow rate of 0.2 ml min⁻¹ to increase detector sensitivity. To avoid

Table 2. 10% irradiance depths ($Z_{10\%}$) in the UVB (305 nm), UVA (325, 340, 380 nm) and visible (412, 443, 490, 565 nm) spectral domains at the four stations in the South East Pacific.

Site	$Z_{10\%}$ (m)							
	305 nm	325 nm	340 nm	380 nm	412 nm	443 nm	490 nm	565 nm
MAR	9.6	17.1	23.3	37.0	39.2	41.9	49.2	26.8
GYR	21.4	40.4	57.4	108.9	107.0	113.1	97.4	36.5
EGY	11.8	22.7	28.3	53.4	47.1	49.0	54.4	27.4
UPW	3.0	4.9	5.8	8.8	9.9	10.6	14.5	17.8

absorption of carbonates by NaOH, eluent solutions were degassed before use and constantly purged with helium at a flow rate of 4 ml min^{-1} .

Recoveries of desalting, estimated in spiked (20–100 nM) sodium chloride solutions ranged from 72 to 80% for fucose, rhamnose, arabinose, mannose, xylose and ribose, and between 85–100% for galactose and glucose, respectively. Procedural blanks run with desalted sodium chloride solutions, showed only small peak of glucose ($\sim 5 \text{ nM}$), even though a systematic peak induced by desalting was coeluted with fructose avoiding its quantification. The detection limit was 5–10 nM for all sugars. Analytical errors determined from duplicate analysis were $< 8\%$ for all sugars except ribose (15%). Concentrations of dissolved sugars presented in this study are corrected for the blank values (glucose).

2.4 Bacterial production (BP)

BP was estimated from the incorporation rate of ^3H -leucine into proteins using the centrifugation method (Smith and Azam, 1992). The detailed protocol is fully described in Van Wambeke et al. (2008a). Briefly, 1.5 ml duplicate samples were incubated in the dark for 1–2 h with 20 nM addition of leucine. The experimental error was calculated as half the difference between two duplicates and averaged 6% of BP rates. The leucine-carbon conversion factor used was 1.5 kg C per mole leucine incorporated.

2.5 Surface and underwater solar irradiance

Two profiles of downward irradiance were made at each station (Fig. 1) close to solar noon using a Satlantic MicroPro free-fall profiler equipped with OCR-504 downward irradiance in the UVB (305 nm), UVA (325, 340 and 380 nm), and visible (412, 443, 490 and 565 nm) spectral domains. Surface irradiance was simultaneously measured at the same channels on the ship deck using other OCR-504 irradiance sensors to account for the variations of cloud conditions during the cast, as well as to monitor UV and visible irradiances during the exposure period for the DOM-photodegradation experiments. A detailed description of optical measurements and determination of 10% irradiance depth ($Z_{10\%}$ in m) is given elsewhere (Tedetti et al., 2007).

2.6 Statistical analyses

The Mann-Whitney test was used to evaluate the differences between biogeochemical parameters among the four sites, as well as to compare leucine incorporation rates between dark and full sun treatments in the DOM-photodegradation and biodegradation experiments. The significance threshold was set at $p < 0.05$.

3 Results and discussion

3.1 General observations

The main biogeochemical characteristics of the four stations are presented in Table 1. DCM ranged from 40 m (UPW) to 175 m (GYR) and was very close to the corresponding depth of euphotic zone [Z_{eu} , the depth of 1% surface photosynthetically available radiation (PAR)]. Total Chlorophyll-*a* (TChl-*a*) concentrations within subsurface and DCM depths as well as BP and primary production (PP) values integrated to DCM (I-BP and I-PP) showed large variations between the stations (Table 1). At the GYR station, TChl-*a*, I-BP, and I-PP values were low compared to the other stations, which further confirm its hyper-oligotrophic status. In this area, PP was strongly nutrient-limited because of the absence of terrestrial inputs and because of the depth of nutricline ($0.01 \mu\text{MN}$ at $\sim 160 \text{ m}$; Raimbault et al., 2008). At the MAR station, TChl-*a* (0.27 and $0.38 \mu\text{g l}^{-1}$ for 5 m and 60 m, respectively), and I-PP ($683 \text{ mg C m}^{-2} \text{ d}^{-1}$) values were higher than those previously observed in this high nutrients low chlorophyll area (Signorini et al., 1999), probably due to the vertical input of dissolved iron from subsurface waters (Blain et al., 2008). From October to March, wind-driven coastal upwelling fertilizes the surface waters off Chile leading to one of the most productive areas in the world ocean (Carr, 2002). In the same way, $Z_{10\%}$ in the UVB, UVA, and visible spectral domains showed great variability with the highest values recorded in GYR (21 m at 305 nm to 113 m at 443 nm) and the lowest values measured in UPW (3 m at 305 nm to 18 m at 565 nm) (Table 2). The values reported in GYR suggest that this area likely contains the clearest oceanic waters of the world ocean (Morel et al., 2007; Tedetti et al., 2007).

3.2 Concentration levels of TDNS and FDNS

Concentrations of TDNS (free and combined) in depth profiles ranged from 58 nM (EGY, 250 m) to 890 nM (MAR, 30 m), the second maximum value reached being observed at EGY (492 nM at 80 m). Two general trends can be observed in a first approach:

1. the depth profile patterns followed those of TChl-*a* for MAR and EGY, although a significant correlation between TChl-*a* and TDNS was observed only at EGY ($r=0.95$, $p<0.01$). This probably reflects the high contribution from autotrophic organisms from cellular release processes (Fig. 2). There were no other significant correlations (considering sites individually or all together) neither with TChl-*a* (as source), nor with DOC (as bulk stock), nor with leucine incorporation rates (as measure of DOC uptake processes).
2. TDNS concentrations at the highly eutrophic site of UPW (149–328 nM) were not as much elevated as someone may expect for an eutrophic regime. Indeed, the maximum value in UPW was lower than that observed in the highly oligotrophic GYR (79–389 nM). This feature was kind of surprising because TChl-*a*, and I-PP values were one order of magnitude higher in UPW than in GYR (Fig. 2; Table 1).

Similar TDNS concentrations in the upper 500 m (180–800 nM) have been already observed in Equatorial Pacific (Skoog and Benner, 1997), Northeastern Pacific and Sargasso Sea (Borch and Kirchman, 1997), Central Arctic (Rich et al., 1997), Ross Sea (Kirchman et al., 2001), as well as in ultrafiltrated DOM samples (20–661 nM) collected from Equatorial Pacific and Arctic Oceans (Skoog and Benner, 1997; Amon and Benner, 2003). It is worth to note that higher sugar concentrations (1000–4000 nM) above the thermocline were reported only for coastal samples (e.g. inshore the Oregon coast; Borch and Kirchman, 1997, Arctic estuarine samples; Amon and Benner, 2003). Our TDNS concentration results are not comparable to those obtained by colorimetric techniques [3-methyl-2-benzothiazolinone hydrazone (MBTH) or 2,4,6-tripyridyl-s-triazine (TPTZ)] because these techniques include in their analysis a much broader spectrum of sugars including methylsugars, aminosugars, uronic acids etc. These compounds were outside the analytical window of the HPAEC-PAD technique under our current analytical conditions (Borch and Kirchman, 1997; Skoog and Benner, 1997; Panagiotopoulos and Sempéré, 2005).

Although our sugar measurements were made only in the upper layers and we did not obtain data from the entire water column, we expect that sugar concentrations will decrease with depth. Reported literature data below the thermocline ranged from 90 to 450 nM for Northeastern Pacific, Equatorial Pacific and Sargasso Sea (Borch and Kirchman, 1997; Skoog and Benner, 1997), and from 31–68 nM for deep Arctic water samples (Amon and Benner, 2003). These results

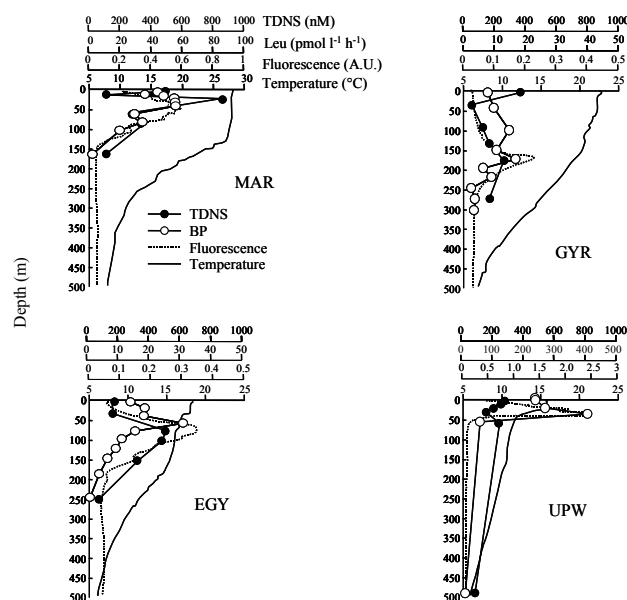


Fig. 2. Depth profiles of total dissolved neutral sugars (TDNS in nM), leucine incorporation rates (LEU, $\text{pmol l}^{-1} \text{h}^{-1}$), chlorophyll fluorescence (arbitrary unit), and temperature ($^{\circ}\text{C}$) at the four stations in the South East Pacific.

are in good agreement with our deepest TDNS concentrations (110 nM at 160 m for MAR, 185 nM at 270 m for GYR, 58 nM at 250 m for EGY and 149 nM at 500 m for UPW).

FDNS concentrations were within the detection limit of the PAD (5–10 nM) in most of the sites and ranged from undetectable to 35 nM (MAR, 30 m). Our results are much lower than those found in the Equatorial Pacific (20–110 nM; Rich et al., 1996), and Central Arctic (31–68 nM; Rich et al., 1997) but similar to that reported in Gulf of Mexico (3–7 nM; Skoog et al., 1999), and Ross Sea (0–14 nM; Kirchman et al., 2001). FDNS comprised a small fraction of TDNS in all stations and generally were <5% of the TDNS.

3.3 TDNS and FDNS yields

TDNS yields were calculated by dividing TDNS-C by dissolved organic carbon (DOC) (Raimbault et al., 2008) and as such are presented as a percentage of DOC ($\text{TDNSC} \times \text{DOC}^{-1} \%$). TDNS yields ranged from 0.4 (GYR, 40 m) to 6.7% (MAR, 30 m). At MAR higher TDNS yields were measured ($3.3\% \pm 2.2\%$; significantly higher than the other sites, $p<0.05$), which probably reflects a terrestrial influence. Indeed, Signorini et al. (1999) reported the importance of the Marquesas Island mass effect in the stimulation of PP up to 1000 km downstream from the island. Our results are in good agreement with previous values reported from the Equatorial Pacific (1–7%, Rich et al., 1996; 2–6%, Skoog and Benner, 1997), Ross Sea (1–11%, Kirchman et al., 2001), and Central Arctic (2–20%, Rich et al., 1997).

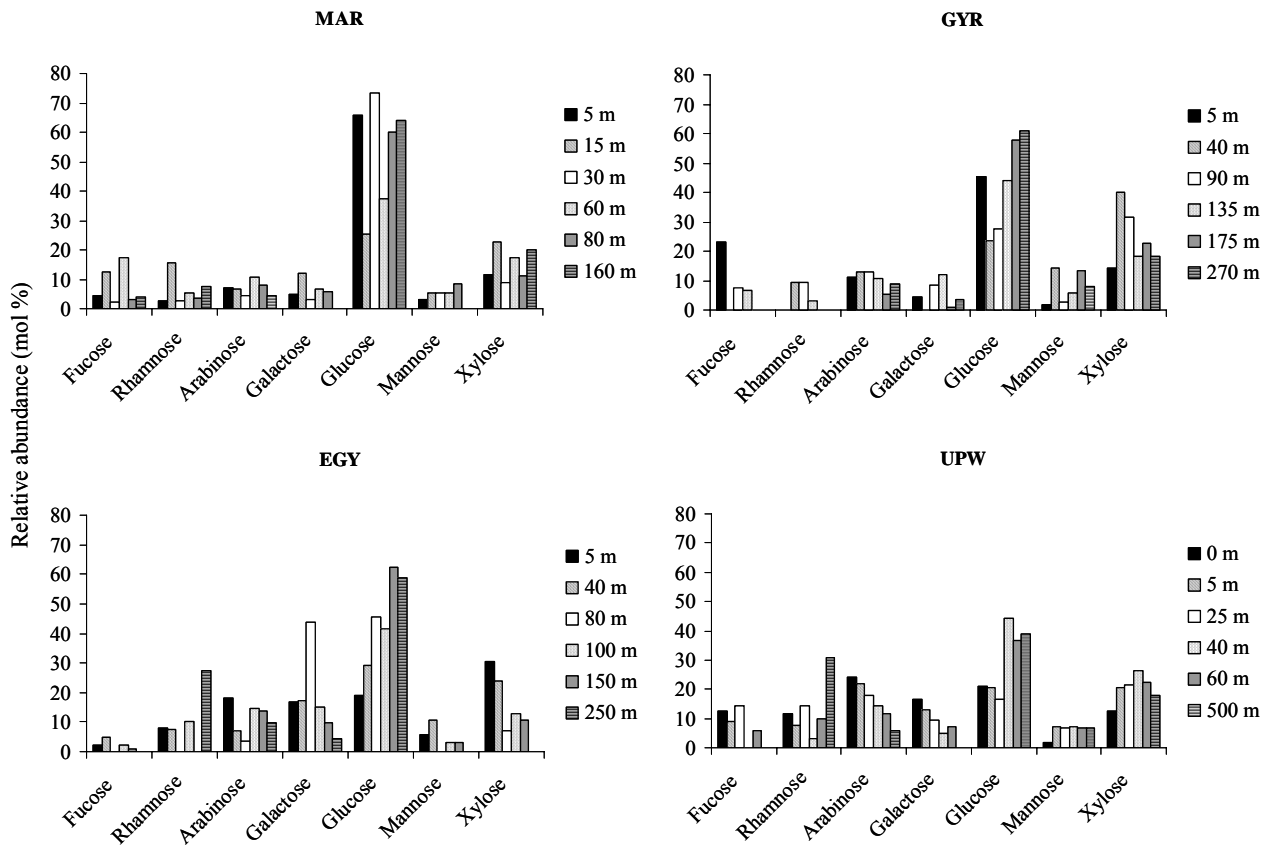


Fig. 3. Relative abundance of total dissolved neutral sugars (TDNS in mol %) at the four stations in the South East Pacific.

3.4 Molecular composition of TDNS and FDNS

Three major sugar classes were detected in South East Pacific samples including the aldohexoses (glucose, galactose and mannose), deoxysugars (fucose and rhamnose), and aldopentoses (arabinose and xylose). Concentrations of ribose (aldopentose) are not reported here because they were very low and often not detected (Fig. 3). Aldohexoses were in most of the sites the most abundant compound class (30–727 nM) followed by aldopentoses (27–131 nM), and deoxysugars (<10–91 nM). Glucose was very often the most abundant (15–77% of the TDNS) followed by xylose (7–40%), arabinose (4–24%), and galactose (3–44%). Mannose, fucose and rhamnose were less abundant accounting <10% of the total sugar pool. Note that xylose was predominant at 40 and 90 m at GYR and at 5 m water depth of the EGY stations, whereas arabinose was predominant at UPW in the first 0–25 m (Fig. 3).

Our results indicated that glucose was clearly the most abundant sugar at greater depths (>40 m), and that its relative abundance increase with depth in GYR and in EGY (Fig. 3). The dominance of glucose within the TDNS pool was reported from several oceanic regions including the Equatorial Pacific (0–4000 m, 21–61%; Skoog and Benner, 1997), Sar-

gasso Sea (surface, 35%; Borch and Kirchman, 1997), Central Arctic (0–40 m, 39%; Rich et al., 1997), and Antarctic (0–60 m, 35–37%; Kirchman et al., 2001). Glucose was also the only detectable sugar within the FDNS pool with concentrations ranging from 2 to 10 nM in most of the sites (see above). The 100% abundance of glucose in the FDNS pool for our South East Pacific samples is in agreement to that reported in Gulf of Mexico (Skoog et al., 1999), and Ross Sea (Kirchman et al., 2001). Other studies carried out in the Equatorial Pacific and central Arctic indicated that glucose (47–79%), fructose (15–16%), and arabinose (5–15%) were present in the FDNS pool (Rich et al., 1996; Rich et al., 1997).

3.5 Sugar stocks in relation with biological activity

TDNS stocks integrated to the DCM ranged from 612 (UPW) to 2190 mg C m⁻² (MAR). Intermediate values were found at GYR and EGY (2154 and 1439 mg C m⁻²).

Because DCMs depths were very different among sites direct comparison of integrated TDNS stocks is not possible. However, these results indicate that sugars are, relatively to BP, more abundant in the euphotic layer in the SPG (GYR) and on its border (EGY) than in zones of higher PP (MAR and UPW; Fig. 4). Because sugars are by-products of PP

Table 3. Doses (surface irradiances integrated over time) received by the DOM-solutions during the photodegradation experiments in the UVB (305 nm), UVA (325, 340, 380 nm) and visible (412, 443, 490, 565 nm) spectral domains at the four stations in the South East Pacific.

Site	Sky	Dose (kJ m^{-2})							
		305 nm	325 nm	340 nm	380 nm	412 nm	443 nm	490 nm	565 nm
MAR	sunny	2.2	11.9	16.2	22.9	36.8	41.6	47.0	43.9
GYR	cloudy	1.4	7.7	10.5	14.5	22.9	25.1	27.5	25.2
EGY	cloudy	1.3	7.4	10.1	13.8	21.8	23.9	26.2	23.8
UPW	sunny	2.5	13.5	18.4	25.9	41.3	46.6	52.7	49.0

and are essentially consumed by bacteria, our results indicate large variability across the transect between dissolved sugars production by PP and derived processes and its utilization by bacteria.

Excess-dissolved sugars relative to BP in oligotrophic to hyperoligotrophic (GYR, EGY) waters might be explained by the accumulation of recalcitrant sugars due to rapid diagenetic processes governed by microorganisms and/or to nutrient deficiency which results in low bacterial activity. Our results clearly showed low TDNS/BP ratios in highly productive area (UPW, MAR; Fig. 4) suggesting that TDNS are rapidly exhausted by bacterial consumption. On the other hand, in the less productive areas (GYR and EGY), TDNS are relatively abundant with respect to BP (Fig. 4), and therefore accumulate in the surface layer. These results are consistent with Raimbault et al. (2008) observations indicating high concentrations of DOC as well as elevated DOM C/N ratios in the euphotic zone (GYR: 16–18; EGY: 13–18), significantly higher ($p < 0.01$) compared to MAR (12–15). Such features might be related to a malfunctioning of the microbial loop with severely nutrient limited heterotrophic bacteria (Thingstad et al., 1997). Indeed, Van Wambeke et al. (2007) using enrichment experiments, reported clear BP limitation by nitrogen at GYR. Because of low horizontal advection as well as low seasonal convective mixing at GYR (Raimbault et al., 2008), BP nitrogen limitation is likely to be predominant all over the year (Van Wambeke et al., 2007), leading to an accumulation of sugar-rich DOC in surface waters.

3.6 Bacterial responses to DOM photodegradation

Solar doses (surface irradiances integrated over time) received by the DOM-solutions during the photodegradation experiments are presented in Table 3. Doses were higher at MAR and UPW (sunny days), ranging from ~ 2.2 (305 nm) to 52.7 kJ m^{-2} (490 nm), than at GYR and EGY (cloudy days), ranging from ~ 1.3 (305 nm) to 27.5 kJ m^{-2} (490 nm; Table 3). A complete assessment of solar UV doses is provided in Van Wambeke et al. (2008b). DOM-photodegradation and -biodegradation experiments indicated different effects of solar radiation on the DOM bioavailability to heterotrophic bacteria (Fig. 5). At MAR and EGY, surface DOM photodegradation led to a significant stimulation

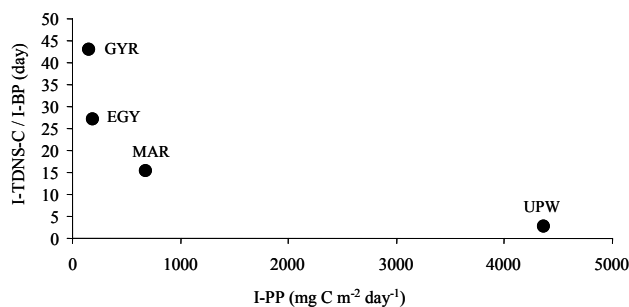


Fig. 4. Relationship between I-TDNS-C/I-BP ratios [total dissolved neutral sugars expressed in carbon units integrated down to DCM (I-TDNS-C in mg C m^{-2}) and bacterial production integrated down to DCM (I-BP in $\text{mg C m}^{-2} \text{ day}^{-1}$)] and primary production integrated down to DCM (I-PP in $\text{mg C m}^{-2} \text{ day}^{-1}$) at the four stations in the South East Pacific.

of leucine incorporation rates by 150 and 133%, respectively (FS compared to Dark, $p < 0.05$ for both comparisons). However, the photodegradation of DOM collected deeper (180 m at MAR and 80 m at EGY) increased significantly leucine incorporation rates only at EGY (by 80%, $p < 0.05$; Fig. 5). Van Wambeke et al. (2007) found that heterotrophic bacteria were not bottom-up controlled at MAR, whereas they were limited by labile DOC (e.g. glucose) at EGY. We did not detect any significant photochemical production of FDNS during the photodegradation experiments. Therefore, the stimulation of leucine incorporation rates after the DOM irradiation may be explained by the photochemical production of (other) bioavailable low molecular weight organic compounds such as aldehydes or organic acids that have been shown to be the major DOM-derived photoproducts (Kieber et al., 1990; Moran and Zepp, 1997; Mopper and Kieber, 2002). At GYR, surface DOM photodegradation did not significantly change leucine incorporation rates ($p > 0.05$). This was maybe due to the very low content in chromophoric (photoreactive) DOM in surface waters of the SPG (Morel et al., 2007) that prevents any photochemical processes to occur. On the other hand, Van Wambeke et al. (2007) observed that at GYR, BP was limited by nitrogen and not labile DOC. Thus, even though some organic photoproducts might have been released from DOM irradiation, they could not in turn substantially increase BP. The photodegradation of DOM collected in the

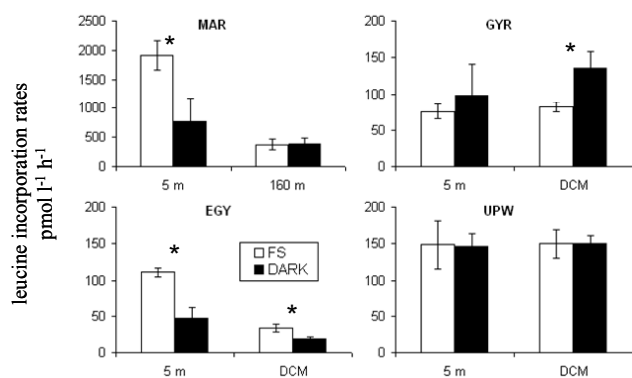


Fig. 5. Leucine incorporation rates ($\text{pmol leu l}^{-1} \text{ h}^{-1}$) after 48 h (MAR) or 72 h (GYR, EGY, UPW) incubation of irradiated DOM-solution ($0.2\text{-}\mu\text{m}$ filtered seawater) with a bacterial non-irradiated inoculum ($0.8\text{-}\mu\text{m}$ filtered seawater, inoculum/DOM-solution final ratio 1/6,) at the four stations in the South East Pacific. Samples were collected at two depths, i.e. 5 m and DCM, except in MAR (5 and 160 m). DOM-solutions were irradiated under natural solar radiation (~ 8 h around solar noon) in full sun (FS, white bars) or kept in the dark (Dark, black bars). Error bars represent standard deviations for pooled measurements of duplicate subsample for each duplicate experiment.

* Significant differences (Mann Whitney test, $p < 0.05$) between full sun and dark treatments.

DCM of GYR significantly inhibited BP by 40% ($p < 0.05$; Fig. 5). This decrease could be related to the photochemical production of biorefractory compounds (Kieber et al., 1997). DOM irradiation in UPW resulted no significant difference in BP for both surface and DCM samples ($p > 0.05$ for both comparisons; Fig. 5). This absence of response may be attributed to the high amount of labile carbon initially present in the upwelling system, i.e. heterotrophic bacteria were not limited in carbon before DOM photodegradation. These different bacterial responses to DOM photodegradation reflect differences in the nature and chemical composition of DOM before irradiation (Moran and Covert, 2003).

4 Summary and conclusion

This study showed a diversity of TDNS amounts in the South East Pacific waters. At all sites investigated, TDNS make up only 0.4 to 6.7% of DOC. Although TDNS variations were very large along vertical profiles, maximum values were reached at stations of intermediate trophic status like MAR and EGY, but not the more eutrophic (UPW). In this highly productive area of the Chile upwelling where both PP and BP were particularly elevated, high turnover of labile DOM was reflected by low TDNS/IBP ratios. There was no noticeable effect of solar radiation on DOM bacterial assimilation in such environments probably because of the high water mixing. In contrast, TDNS concentrations relative to bacterial production were higher in the center of the SPG (GYR) and

to a lesser extent in the eastern border of the SPG (EGY). We found that at GYR, TDNS were accumulated with respect to the low primary and heterotrophic bacterial productions, and reinforce the idea of limitation of bacterial growth by nitrogen (Van Wambeke et al., 2007). Such feature is consistent with the DOC accumulation (Raimbault et al., 2008) and likely considering the relatively old character of the surface DOM revealed by its elevated C/N ratios (Raimbault et al., 2008). The DOM which accumulates in the surface waters of GYR, does not seem to be photoreactive as indicated by the photo (bio)degradation experiments. Indeed, it has been hypothesized that DOM in this area was continuously photobleached in the surface waters due to the high level of stratification and to high surface UV irradiances (Morel et al., 2007). Other stations, EGY and MAR, showed moderate TDNS concentrations and turnover regarding bacterial and primary productions.

Acknowledgements. We are grateful to the captain and crew of the RV “L’Atalante” for excellent service during the BIOSOPE cruise. We acknowledge H. Claustre and A. Sciandra as chief scientists of the cruise, as well as C. Bournot, D. Taillez and D. Merien for CTD operations. We thank J. Raas and P. Raimbault for providing TChl-*a* and DOC data, respectively. We also acknowledge T. Moutin and S. Duhamel for providing primary production data and the two referees for improving the MS. K. Mopper gave a substantial help to our group for improving the quality of the desalination procedure. This research was funded by CNRS-PROOF projects (BIOSOPE and UVECO), and the Region of Provence Alpes Côte d’Azur.

Edited by: A. Boetius

References

- Aluwihare, L. I., Repeta, D. J., and Chen, R. F.: A major biopolymeric component to dissolved organic carbon in seawater, *Nature*, 387, 166–167, 1997.
- Amon, R. M. W. and Benner, R.: Combined neutral sugar as indicators of the diagenetic state of dissolved organic matter in the Arctic Ocean, *Deep-Sea Res. Pt. I*, 50, 151–169, 2003.
- Blain, S., Bonnet, S., and Guieu, C.: Dissolved iron distribution in the tropical and sub tropical South Eastern Pacific, *Biogeosciences*, 5, 269–280, 2008, <http://www.biogeosciences.net/5/269/2008/>.
- Benner, R. and Kaiser, K.: Abundance of amino sugars and peptidoglycan in marine particulate and dissolved organic matter, *Limnol. Oceanogr.*, 48, 118–128, 2003.
- Benner, R., Pakulski, J. D., McCarthy, M., Hedges, J. I., and Hatcher, P. G.: Bulk chemical characteristics of dissolved organic matter in the ocean, *Science*, 255, 1562–1564, 1992.
- Benner, R.: Chemical composition and reactivity, in: *Biogeochemistry of Marine Dissolved Organic Matter*, edited by: Hansell, D. and Carlson, C., Academic Press, New York, USA, 59–90, 2002.
- Borch, N. H. and Kirchman, D. L.: Concentration and composition of dissolved combined neutral sugars (polysaccharides) in seawater determined by HPLC-PAD, *Mar. Chem.*, 57, 85–95, 1997.

- Burney, C. M. and Sieburth, J. M.: Dissolved carbohydrates in seawater – II: A spectrometric procedure for total carbohydrate analysis and polysaccharide estimation, *Mar. Chem.*, 5, 15–28, 1977.
- Carr, M. E.: Estimation of potential productivity in Eastern Boundary currents using remote sensing, *Deep-Sea Res. Pt. II*, 49, 59–80, 2002.
- Claustre, H. and Maritorena, S.: The many shades of ocean blue, *Science*, 302, 1514–1515, 2003.
- Claustre, H., Sciandra, A., and Vaultot, D.: Introduction to the special section bio-optical and biogeochemical conditions in the South East Pacific in late 2004: the BIOSOPE program, *Biogeosciences*, 5, 679–691, 2008, <http://www.biogeosciences.net/5/679/2008/>.
- Kieber, R. J., Hydro, L. H., and Seaton, P. J.: Photooxydation of triglycerides and fatty acids in seawater: implication toward the formation of marine humic substances, *Limnol. Oceanogr.*, 42, 1454–1462, 1997.
- Kieber, R. J., Zhou, X., and Mopper, K.: Formation of carbonyl compounds from UV-induced photodegradation of humic substances in natural waters: Fate of riverine carbon in the sea, *Limnol. Oceanogr.*, 35, 1503–1515, 1990.
- Kirchman, D. L., Meon, B., Ducklow, H. W., Carlson, C. A., Hansell, D. A., and Steward, G.: Glucose fluxes and concentrations of dissolved combined sugars (polysaccharides) in the Ross Sea and Polar Front Zone, Antarctica, *Deep-Sea Res. Pt. II*, 48, 4179–4197, 2001.
- Mopper, K. and Kieber, D. J.: Photochemistry and the cycling of carbon, sulphur, nitrogen and phosphorus, in: *Biogeochemistry of marine dissolved organic matter*, edited by: Hansell, D. A. and Carlson, C. A., Academic Press, San Diego, CA, USA, 455–507, 2002.
- Mopper, K., Schultz, C., Chevolut, L., Germain, C., Revuelta, R., and Dawson, R.: Determination of sugars in unconcentrated seawater and other natural waters by liquid chromatography, *Environ. Sci. Technol.*, 26, 133–137, 1992.
- Moran, M. A. and Covert, J. S.: Photochemically mediated linkages between dissolved organic matter and bacterioplankton, in: *Aquatic ecosystems: interactivity of dissolved organic matter*, edited by: Findlay, S. E. G. and Sinsabaugh, R. L., Academic Press, San Diego, CA, USA, 243–262, 2003.
- Moran, M. A. and Zepp, R. G.: Role of photoreactions in the formation of biologically labile compounds from dissolved organic matter, *Limnol. Oceanogr.*, 42, 1307–1316, 1997.
- Morel, A., Gentili, B., Claustre, H., Babin, M., Bricaud, A., Ras, J., and Tieche F.: Optical properties of the “clearest” natural waters, *Limnol. Oceanogr.*, 52, 217–229, 2007.
- Painter, T. J.: Algal polysaccharides, in: *Polysaccharides*, edited by: Aspinall, G. O., Academic, New York, USA, 195–285, 1983.
- Pakulski, J. and Benner, R.: Abundance and distribution of carbohydrates in the ocean, *Limnol. Oceanogr.*, 39, 930–940, 1994.
- Panagiotopoulos, C. and Sempéré, R.: Molecular distribution of carbohydrates in large marine particles, *Mar. Chem.*, 95, 31–49, 2005.
- Panagiotopoulos, C., Sempéré, R., Lafont, R., and Kerhervé, P.: Effects of temperature in the determination of monosaccharides by using an anion-exchange column, *J. Chromatogr.*, 920, 13–22, 2001.
- Parsons, T. R., Takahashi, M., and Hargrave, B.: *Biological oceanographic processes*, Pergamon, Oxford, UK, 1984.
- Raimbault, P., Garcia, N., and Cerutti, F.: Distribution of inorganic and organic nutrients in the South Pacific Ocean – evidence for long-term accumulation of organic matter in nitrogen-depleted waters, *Biogeosciences*, 5, 281–298, 2008, <http://www.biogeosciences.net/5/281/2008/>.
- Ras, J., Claustre, H., and Uitz, J.: Spatial variability of phytoplankton pigment distributions in the Subtropical South Pacific Ocean: comparison between in situ and predicted data, *Biogeosciences*, 5, 353–369, 2008, <http://www.biogeosciences.net/5/353/2008/>.
- Rich, J. H., Ducklow, H. W., and Kirchman, D. L.: Concentrations and uptake of neutral monosaccharides along 140° W in the equatorial Pacific: contribution of glucose to heterotrophic bacterial activity and the DOM flux, *Limnol. Oceanogr.*, 41, 595–604, 1996.
- Rich, J. H., Gosselin, M., Sherr, E., Sherr, B., and Kirchman, D. L.: High bacterial production, uptake and concentrations of dissolved organic matter in the central Arctic Ocean, *Deep-Sea Res. Pt. II*, 44, 1645–1663, 1997.
- Signorini, S. R., McClain, C. R., and Dandonneau, Y.: Mixing and phytoplankton bloom in the wake of the Marquesas Islands, *Geophys. Res. Lett.*, 26, 3121–3124, 1999.
- Skoog, A. and Benner, R.: Aldoses in various size fractions of marine organic matter: Implications for carbon cycling, *Limnol. Oceanogr.*, 42, 1803–1813, 1997.
- Skoog, A., Biddanda, B., and Benner, R.: Bacterial utilization of dissolved glucose in the upper water column of the Gulf of Mexico, *Limnol. Oceanogr.*, 44, 1625–1633, 1999.
- Smith, D. C. and Azam, F.: A simple, economical method for measuring bacterial protein synthesis rates in sea water using 3H-Leucine, *Mar. Microb. Food Webs*, 6, 107–114, 1992.
- Stouthamer, A. H.: Energetic aspects of the growth of microorganisms, *Symp. Soc. Gen. Microbiol.*, 27, 285–315, 1977.
- Tedetti, M., Sempéré, R., Vasilkov, A., Charrière, B., Nérini, D., Miller, W. L., Kawamura, K., and Raimbault, P.: High penetration of ultraviolet radiation in the south east Pacific waters, *Geophys. Res. Lett.*, 34, L12610, doi:10.1029/2007GL029823, 2007.
- Thingstad, T. F., Hagstrom, A., and Rassoulzadegan, F.: Accumulation of degradable DOC in surface waters: Is it caused by a malfunctioning microbial loop?, *Limnol. Oceanogr.*, 42, 398–404, 1997.
- Van Wambeke, F., Bonnet, S., Moutin, T., Raimbault, P., Alarcón, G., and Guieu, C.: Factors limiting heterotrophic bacterial production in the southern Pacific Ocean, *Biogeosciences*, 5, 833–845, 2008, <http://www.biogeosciences.net/5/833/2008/>.
- Van Wambeke, F., Obernosterer, I., Moutin, T., Duhamel, S., Ulloa, O., and Claustre, H.: Heterotrophic bacterial production in the South East Pacific: longitudinal trends and coupling with primary production, *Biogeosciences*, 5, 1–13, 2008a, <http://www.biogeosciences.net/5/1/2008/>.
- Van Wambeke, F., Tedetti, M., Duhamel, S., and Sempéré, R.: Diel variability of heterotrophic bacterial production and UV doses in the South East Pacific, *Biogeosciences Discuss.*, 5, 435–462, 2008b, <http://www.biogeosciences-discuss.net/5/435/2008/>.

Phospholipid synthesis rates in the eastern subtropical South Pacific Ocean

B. A. S. Van Mooy¹, T. Moutin², S. Duhamel^{2,3}, P. Rimmelin², and F. Van Wambeke³

¹Dept. of Marine Chemistry and Geochemistry, Woods Hole Oceanographic Institution, MS #4, Woods Hole, MA 02543, USA

²Laboratoire d'Océanographie et de Biogéochimie, UMR-CNRS 6535, Case 901, Centre d'Océanologie de Marseille, Université de la Méditerranée – Campus de Luminy, 13 288 Marseille cedex 9, France

³Laboratoire de Microbiologie, Géochimie et Ecologie Marines, UMR-CNRS 6117, Case 901, Centre d'Océanologie de Marseille, Université de la Méditerranée – Campus de Luminy, 13 288 Marseille Cedex 9, France

Received: 17 July 2007 – Published in Biogeosciences Discuss.: 20 August 2007

Revised: 11 December 2007 – Accepted: 4 January 2008 – Published: 6 February 2008

Abstract. Membrane lipid molecules are a major component of planktonic organisms and this is particularly true of the microbial picoplankton that dominate the open ocean; with their high surface-area to volume ratios, the synthesis of membrane lipids places a major demand on their overall cell metabolism. Specifically, the synthesis of cell membrane phospholipids creates a demand for the nutrient phosphorus, and we sought to refine our understanding of the role of phospholipids in the upper ocean phosphorus cycle. We measured the rates of phospholipid synthesis in a transect of the eastern subtropical South Pacific from Easter Island to Concepcion, Chile as part of the BIOSOPE program. Our approach combined standard phosphorus radiotracer incubations and lipid extraction methods. We found that phospholipid synthesis rates varied from less than 1 to greater than 200 pmol PL⁻¹ h⁻¹, and that phospholipid synthesis contributed between less than 5% to greater than 22% of the total PO₄³⁻ incorporation rate. Changes in the percentage that phospholipid synthesis contributed to total PO₄³⁻ uptake were strongly correlated with the ratio of primary production to bacterial production, which supported our hypothesis that heterotrophic bacteria were the primary agents of phospholipid synthesis. The spatial variation in phospholipid synthesis rates underscored the importance of heterotrophic bacteria in the phosphorus cycle of the eastern subtropical South Pacific, particularly the hyperoligotrophic South Pacific subtropical gyre.

1 Introduction

Cell membrane lipids form the interface between a cell and its environment, and, as such, house many of the enzyme and transporter systems that are required to harvest energy and material from the environment. Microbial picoplankton (i.e. plankton <2 μm) have higher cell surface area to cell volume ratios than larger plankton, and therefore we would expect cell membrane lipids to be a particularly important biochemical component of picoplankton. The picoplanktonic community dominates the surface waters of the open ocean (e.g. Cho and Azam, 1990) and is composed of diverse populations of picoeukaryotes, cyanobacteria and heterotrophic bacteria (e.g. Campbell and Vaultot, 1993; Cavender-Bares et al., 2001).

Membrane lipids generally compose 15 to 25% of the carbon in planktonic cells (Wakeham et al., 1997), and, as such, their synthesis constitutes a substantial fraction of overall community anabolism and carbon demand. The synthesis of one class of membrane lipids, the phospholipids, creates an additional burden to planktonic cells because it creates a demand for nutrient phosphorus. In the surface waters of the North Pacific subtropical gyre (NPSG) the synthesis of phospholipids was shown to consume 18 to 28% of the PO₄³⁻ taken up by the total planktonic community (Van Mooy et al., 2006). However, the demand for phosphorus created by phospholipid synthesis does not appear to be equally distributed among the various types of plankton that compose the total planktonic community. For example, the synthesis of phospholipids constitutes less than a few percent of overall phosphorus demand by *Prochlorococcus*, the picocyanobacterium that dominates the phytoplanktonic community of the NPSG and South Pacific subtropical gyre (SPSG) (Björkman et al., 2000; Campbell et al., 1994; Van Mooy et al., 2006; Grob et al., 2007). In addition to phospholipids,



Correspondence to: B. A. S. Van Mooy
(bvanmooy@whoi.edu)

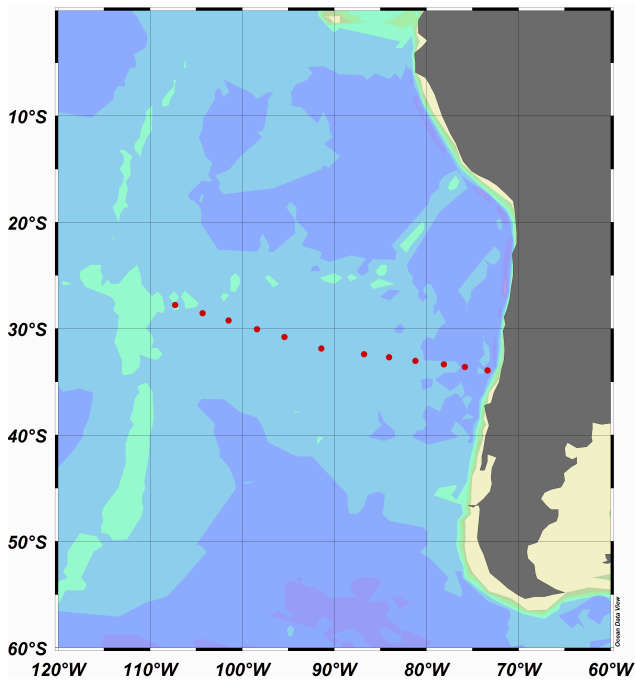


Fig. 1. Map of stations where phospholipid synthesis rates were determined during the second leg of the BIOSOPE cruise.

cyanobacterial membranes also contain abundant glycolipids and sulfolipids (Wada and Murata, 1998). Moreover, these organisms appear to have the ability to substitute sulfolipids for phospholipids when nutrient phosphorus concentrations are low in the environment (Benning, 1998). The observation that sulfolipids were the most abundant membrane lipid in the surface waters of the NPSG, led Van Mooy et al. (2006) to hypothesize that cyanobacteria employ few phospholipids and that heterotrophic bacteria were the organisms primarily responsible for phospholipid synthesis.

We sought to examine the importance of phospholipid synthesis to picoplankton under a range of biological and chemical conditions, with the intention of refining our understanding of the biological origin of phospholipids and the role of phospholipid synthesis within the overall upper ocean phosphorus cycle. We encountered such a range of conditions on the second leg of the BIOSOPE cruise, which was a transect between the hyperoligotrophic waters of SPSG and the nutrient-rich waters upwelled off Chile. We quantified phospholipid synthesis rates at several depths at twelve different stations, and compared these data to chlorophyll fluorescence, primary production rates, and heterotrophic bacterial production rates. These data add further support to the hypothesis that phospholipids are primarily of heterotrophic bacterial origin, and as such, phospholipid synthesis rates are a molecular proxy for the relative role of heterotrophic bacteria in the upper ocean phosphorus cycle.

2 Methods

2.1 Sampling

Data in this paper were obtained during the second leg of the BIOSOPE cruise between Easter Island and Concepcion, Chile aboard the R/V *L' Atalante* (Fig. 1; Claustre et al., 2007²²). Seawater was collected using Niskin bottles at depths corresponding to either 100, 50, 15, 3, 1 or 0.3% of surface photosynthetically available radiation (PAR).

2.2 Incubations

We collected 250 ml samples of seawater directly from the Niskin bottle into acid-washed polycarbonate bottles. These bottles were then spiked with 0.37 MBq of $^{33}\text{PO}_4^{3-}$ (Amersham), which was an amendment of approximately 130 pmol L^{-1} of $^{33}\text{PO}_4^{3-}$ and was less than 1% of ambient concentrations of PO_4^{3-} at all stations (Moutin et al., 2008; Duhamel et al., 2007). The bottles were then incubated in an on deck incubator at surface seawater temperatures but at in situ PAR. Incubations were started at approximately noon local time and terminated shortly after sundown by filtration on 0.2 μm pore size alumina membranes (Whatman).

2.3 Phospholipid extraction and analysis

Following filtration, the membranes were immediately immersed in a glass centrifuge tube containing a Bligh and Dyer (1959) extraction mixture, which consisted of 1.5 ml of dichloromethane, 3 ml of methanol and 1.2 ml of 0.1 X phosphate buffered saline (PBS) solution and stored overnight at -20°C . The following day, 1.5 ml of dichloromethane and 1.5 ml MilliQ water (Millipore) were added. The samples were centrifuged and the lower organic phase, containing the phospholipids, was recovered. These total phospholipid extracts were used to determine the $^{33}\text{PO}_4^{3-}$ uptake rates into the total phospholipids: 500 μL of the extract was mixed with 10 mL of UltimaGold scintillation cocktail (PerkinElmer) in a 20 ml polyethylene scintillation vial. The ^{33}P radioactivity was determined on a Tricarb scintillation counter (Packard) using standard methods (Duhamel et al., 2006).

2.4 Calculations

The steady state production rates of phospholipids were determined as follows:

$$P = \left(\frac{A/S}{t} \right) \quad (1)$$

Where P is the hourly production rate of phospholipids ($\text{pmol PL}^{-1} \text{h}^{-1}$), A is the ^{33}P radioactivity of the phospholipid extract (dpm), S is the specific ^{33}P radioactivity of PO_4^{3-} in the incubations ($\text{dpm} (\text{pmol PL}^{-1})^{-1}$), and t is the

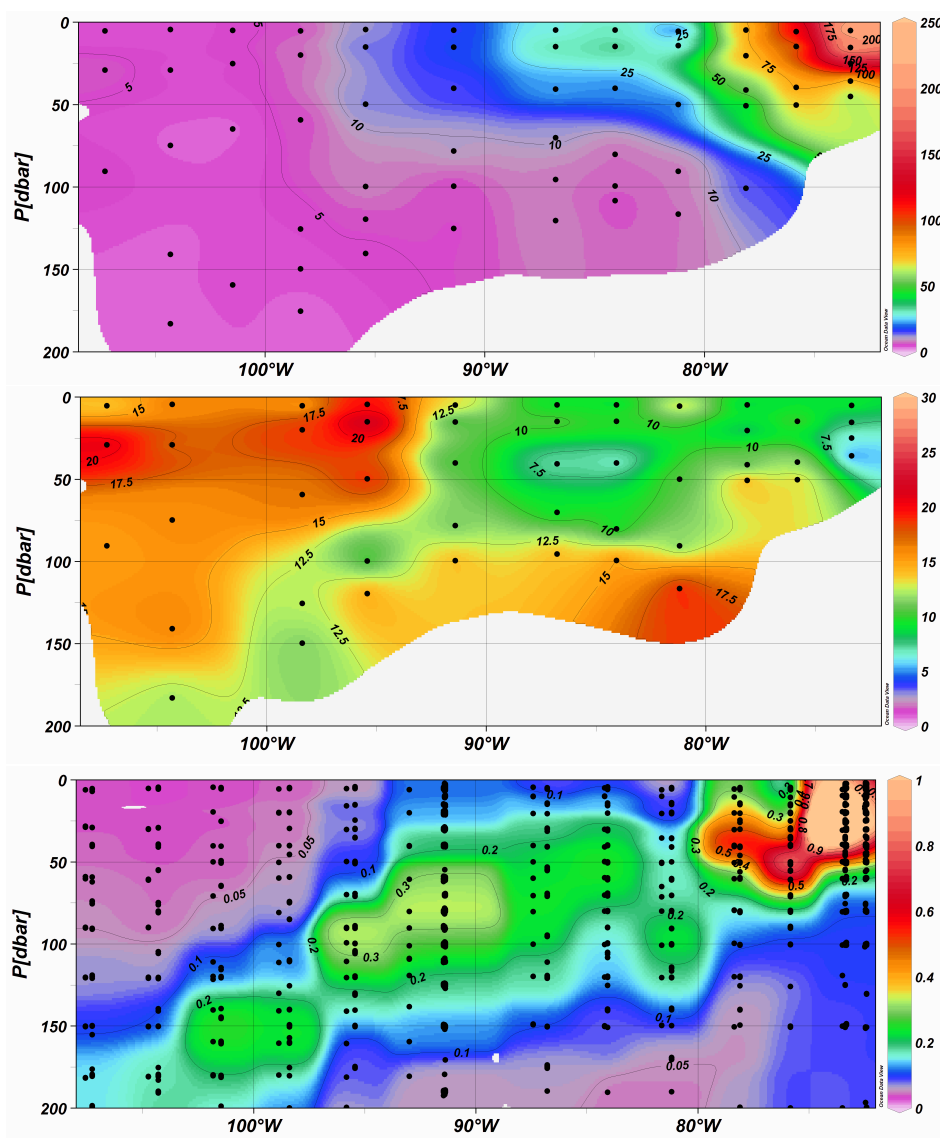


Fig. 2. Northward looking sections between Easter Island and Concepcion, Chile of: (a) phospholipid synthesis rate in units of $\text{pmol PL}^{-1} \text{h}^{-1}$, (b) contribution of phospholipid synthesis to total PO_4^{3-} incorporation in percent, and (c) in vivo fluorescence in relative units.

length of the incubation (h). The steady-state assumption is valid since the incubation time (approximately 8 h) was short compared to the turnover time of PO_4^{3-} (weeks or longer; Moutin et al., 2008). Phosphate concentrations were reported by Moutin et al. (2008). Water from the same Niskin bottles was also used to determine the total PO_4^{3-} incorporation rates using standard methods (Moutin et al., 2008). Contribution of phospholipid production rates to the total PO_4^{3-} incorporation rates were expressed as percent by taking the quotient of the two values and multiplying by 100. Only one phospholipid synthesis rate measurement was made at each depth, except at $30^\circ \text{S } 98^\circ \text{W}$ where samples were conducted in trip-

licate and coefficient of variation was found to be 6.2%. Data were plotted using Ocean Data View software (Schlitzer, R., Ocean Data View, <http://odv.awi-bremerhaven.de>, 2004).

2.5 Additional measurements

Chlorophyll fluorescence data were obtained in situ using a Chelsea Aquatrack MkIII fluorometer and are expressed in relative units. Heterotrophic bacterial production (BP) hourly rates were determined using ^3H -leucine incubation and standard microcentrifuge-based protocols as described by Van Wambeke et al. (2007a). Primary production (PP) rates were determined as hourly dissolved inorganic carbon

uptake rates into particulate material using $\text{H}^{14}\text{CO}_3^-$ incubations as described by Duhamel et al. (2007). Rates of BP, PP and phospholipid synthesis were determined from waters sampled during the same cast and usually from the same Niskin bottles.

3 Results

PO_4^{3-} was present in abundance at every station and depth that we examined (Moutin et al., 2008) and was never the nutrient that limited either phytoplanktonic or bacterial production (Bonnet et al., 2007; Van Wambeke et al., 2007b). Concentrations of PO_4^{3-} ranged from 123 to 668 nmol PL^{-1} . Rates of BP and PP ranged from 3 to 385 $\text{ng CL}^{-1} \text{hr}^{-1}$ and 9 to 1612 $\text{ng CL}^{-1} \text{hr}^{-1}$ respectively, and both rates generally decreased with depth and from west to east (Van Wambeke et al., 2007a).

Phospholipid synthesis rates ranged from 1 $\text{pmol PL}^{-1} \text{h}^{-1}$ in the SPSG to $>200 \text{pmol PL}^{-1} \text{h}^{-1}$ off the coast of Chile (Fig. 2a). In general, the phospholipid synthesis rates were relatively constant in the hyperoligotrophic waters west of 98°W , but increased dramatically eastward of this longitude. Moreover, phospholipid synthesis rates were relatively constant with depth west of 98°W , but east of this, the rates strongly decreased with depth. When expressed as a percentage of total PO_4^{3-} uptake (Fig. 2b), the phospholipid synthesis rates ranged from 4% to 23% of the total PO_4^{3-} uptake rate, with the average being $14 \pm 5\%$ (mean \pm s.d.; $n=48$). Highest percentages were observed in the upper mixed layer of the SPSG, while the lowest rate percentages were observed off the coast of Chile. There was a deep minimum layer in these rate percentages that gradually shoaled between 105°W and 90°W ; east of this, minimum values were observed in a layer centered at about 50 m depth with slightly higher percentages above and markedly higher percentages below. This pattern closely resembled that of chlorophyll fluorescence (Fig. 2c), which showed a maximum layer that shoaled from west to east and centered at about 50 m east of 90°W .

4 Discussion

During the second leg of the BIOSOPE cruise we encountered a broad range of oceanographic conditions and this was reflected in the phospholipid synthesis rates that we measured, which spanned nearly two orders of magnitude (Fig. 2a). As expected, the rates increased from west to east in conjunction with increasing rates of biomass production (Van Wambeke et al., 2007a). The phospholipid synthesis rates in the SPSG were generally $\leq 5 \text{pmol PL}^{-1} \text{h}^{-1}$, which is an order of magnitude slower than observed in the NPSG where the rates ranged from 40 to 120 $\text{pmol PL}^{-1} \text{h}^{-1}$ (Van Mooy and Devol, 2008; Van Mooy et al., 2006). As temperature and PO_4^{3-} availability are not drastically different be-

tween these two locations, We ascribe the difference in phospholipid synthesis rates to the more subdued rates of PP and BP in the SPSG. Thus, phospholipid synthesis rates in the SPSG reflected the extreme hyperoligotrophic conditions in this region (Claustre et al., 2007^{??}).

When viewed as a percentage of total PO_4^{3-} uptake, it is clear that phospholipid synthesis was a major component of the upper ocean phosphorus cycle across the entire transect (Fig. 2). However, this was particularly true in the near-surface waters of SPSG, where values in excess of 15% were consistently observed. So despite the fact that overall phospholipid synthesis rates were an order of magnitude slower in the SPSG than in the NPSG, the relative percentages that phospholipid synthesis contributed to total PO_4^{3-} uptake were very similar to those in the NPSG, which were also in excess of 15% (Van Mooy et al., 2006). It has been argued that heterotrophic bacteria are the primary source of phospholipids in the NPSG (Van Mooy et al., 2006), and we suggest here that the common percentage of phospholipid synthesis in the NPSG and SPSG reflects the common planktonic community structure of these environments, where heterotrophic bacteria compose the majority of total planktonic cells (Björkman et al., 2000; Campbell et al., 1997; Grob et al., 2007).

We observed a layer where phospholipid synthesis contributed $<15\%$ of total PO_4^{3-} uptake, which coincided with a layer of maximum chlorophyll fluorescence (Figs. 2b, c). At the station at 92°W , chlorophyll fluorescence was highest between 50 and 100 m depth, and Grob et al. (2007) observed maxima in the abundances of picoeukaryotes and *Prochlorococcus* in this same depth interval. This low contribution of phospholipid synthesis to total PO_4^{3-} incorporation coupled with the abundance of *Prochlorococcus* suggests that production by phytoplankton contributed disproportionately less to phospholipid synthesis than heterotrophic bacteria. In culture studies, cyanobacteria have been shown to use very little of total PO_4^{3-} uptake for phospholipid synthesis (Cuhel and Waterbury, 1984; Van Mooy et al., 2006). Cyanobacteria and picoeukaryotes are also often very rich in membrane lipids that do not contain phosphorus, such as sulfolipids, glycolipids, and betaine lipids (e.g. Bell and Pond, 1996; Kato et al., 1996; Van Mooy et al., 2006; Wada and Murata, 1998). In the NPSG, RNA synthesis accounted for about half of total PO_4^{3-} uptake and, as such, was a much larger biochemical sink for PO_4^{3-} than phospholipid synthesis (Van Mooy and Devol, 2008; Van Mooy et al., 2006). Thus we interpret the minimum layer in percent phospholipid synthesis as a layer where nucleic acid synthesis by phytoplankton dilutes phospholipid synthesis by heterotrophic bacteria. Further support for this interpretation comes from the data from the below the chlorophyll maximum: due to the decrease in PP with depth the relative contribution of heterotrophic bacteria to total biomass production would presumably be greater below the chlorophyll maximum than at shallower depths, and,

indeed, phospholipid synthesis contributes a greater percentage of total PO_4^{3-} uptake below the chlorophyll maximum (Fig. 2b).

If phytoplankton did indeed make a disproportionately smaller contribution to phospholipid synthesis than heterotrophic bacteria, then we would expect the percent contribution of phospholipid synthesis to total PO_4^{3-} uptake to have been lowest where phytoplankton contributed the most to overall biomass production. To determine whether this was true, we examined the relationship between the ratio of PP to BP (PP:BP) and the percent contribution of phospholipid synthesis to total PO_4^{3-} incorporation by plotting these data versus one another (Fig. 3); all of these parameters are methodologically independent. We performed a linear regression of the data and found that nearly half of the variance ($r^2=0.49$; $P<0.01$) in the percent contribution of phospholipid synthesis to total PO_4^{3-} uptake could be explained by the variance in PP:BP. This is a remarkable relationship considering the immense diversity in the populations of both phytoplankton and heterotrophic bacteria across this nearly 3000 km transect. Furthermore, the relationship is not driven simply by data from the uniquely hyperoligotrophic SPSG portion of the transect, since data points from west of 98° W span almost the entire range of values. The y-intercept, where PP:BP is zero, predicts that heterotrophic bacteria alone dedicate $21.1\pm 8.3\%$ (mean \pm s.d.) of total PO_4^{3-} uptake to phospholipid synthesis. In contrast, we regressed the data with an inverse first order equation ($r^2=0.46$; $P<0.01$; not shown) to represent the approach to infinite PP:BP, and the percent contribution of phospholipid synthesis to total PO_4^{3-} uptake by phytoplankton alone was predicted to be $7.2\pm 7.7\%$. This analysis supports our hypothesis that heterotrophic bacteria are a more important source of phospholipid synthesis than phytoplankton. Admittedly, the population differences of the endmember communities probably impact the estimates of percent phospholipid synthesis by phytoplankton and heterotrophic bacteria. For example, the highest ratios of PP:BP occur east of 98° W outside of the hyperoligotrophic gyre and outside of the area dominated by *Prochlorococcus* (Grob et al., 2007), which could explain why the estimate of 7.2% from the regression is so much higher than the 0.4% observed in axenic strains of *Prochlorococcus* (Van Mooy et al., 2006). As PO_4^{3-} was present in abundance, it is reasonable to expect that phytoplankton were free to employ optimal proportions of phospholipids versus glycolipids and sulfolipids in their membranes. It is important to recognize that the “sulfolipid-phospholipid substitution hypothesis” of Benning (1998) predicts that phytoplankton would have the biochemical motivation to synthesize even fewer phospholipids under conditions where phosphorus is the limiting nutrient, such as in the Mediterranean Sea (Moutin et al., 2002; Thingstad et al., 2005).

Given that heterotrophic bacteria were responsible for the majority of phospholipid synthesis we can use the synthe-

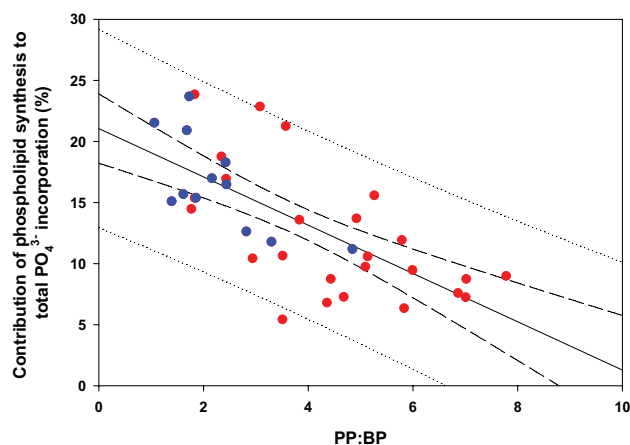


Fig. 3. Plot of percent contribution of phospholipid synthesis to total PO_4^{3-} uptake vs. the ratio of primary production to bacterial production (PP:BP). Blue points are west of 98° W and the red points are east of 98° W. Solid line is linear regression, dashed line is 95% confidence interval of the regression, and dotted line is 95% prediction interval.

sis rate data to constrain the role of this group of organisms within the overall phosphorus cycle observed during the BIOSOPE cruise. First, it is clear that heterotrophic bacteria play an important role in the phosphorus cycle of the SPSG, which agrees with Duhamel et al. (2007) who found that plankton $<0.6 \mu\text{m}$ were responsible for the about a third of PO_4^{3-} uptake. Second there were two patches where phospholipid synthesis contributed $<7.5\%$ of total PO_4^{3-} uptake (Fig. 2b) and these represent areas where phytoplankton production played a more dominant role in the cycling of phosphorus. This type of information has important implications for understanding the distribution of phytoplanktonic vs. bacterial sinks for PO_4^{3-} in the eastern subtropical South Pacific Ocean and, in turn, for understanding sources and sinks of other biolimiting nutrients (e.g. Deutsch et al., 2007). Finally, the phospholipid synthesis data clearly show that heterotrophic bacteria dominated the phosphorus cycle in the lower part of the euphotic zone.

5 Conclusions

We found that phospholipid synthesis was a major component of the upper ocean phosphorus cycle during the BIOSOPE cruise. Phospholipid synthesis made the greatest percentage contribution to total PO_4^{3-} incorporation in the surface waters of the SPSG, and the least in the upwelled waters off of Chile. Furthermore, there was a layer in minimum phospholipid synthesis percentage values that corresponded to the layer of maximum chlorophyll concentrations. Regression analyses showed a strong relationship between the variance in phospholipid percentages and variance in PP:BP. These analyses also predicted that heterotrophic bacteria may

utilize more than a fifth of their total PO_4^{3-} uptake for the synthesis of phospholipids, while phytoplankton may utilize only several percent. Thus phospholipid synthesis is a term in the phosphorus cycle that is dominated by heterotrophic bacteria, and the distribution of the phospholipid synthesis rate during the BIOSOPE cruise confirmed that heterotrophic bacteria play a very important role in the phosphorus cycle of the SPSG.

Acknowledgements. The authors wish to thank the chief scientists of the BIOSOPE cruise H. Claustre and A. Sciandra as well as the captain and crew of the *L'Atlante*. This is a contribution of the BIOSOPE project of the French LEFE-CYBER program. B. A. S. Van Mooy was funded by the National Science Foundation (OCE-0646944), the Grayce B. Kerr Fund and The Penzance Endowed Fund in Support of Assistant Scientists and the Ocean Life Institute at Wood Hole Oceanographic Institution.

Edited by: S. W. A. Naqvi

References

- Bell, M. V. and Pond, D.: Lipid composition during growth of motile and coccolith forms of *Emiliana huxleyi*, *Phytochemistry*, 41, 465–471, 1996.
- Benning, C.: Biosynthesis and function of the sulfolipid sulfoquinovosyl diacylglycerol, *Annu. Rev. Plant Physiol. Plant Mol. Biol.*, 49, 53–75, 1998.
- Björkman, K., Thomson-Bulldis, A. L., and Karl, D. M.: Phosphorus dynamics in the North Pacific subtropical gyre, *Aquat. Microb. Ecol.*, 22, 185–198, 2000.
- Bligh, E. G. and Dyer, W. J.: A rapid method of total lipid extraction and purification, *Can. J. Biochem. Physiol.*, 37, 911–917, 1959.
- Bonnet, S., Guieu, C., Bruyant, F., Prasil, O., Raimbault, P., Van Wambeke, F., Gorbunov, M., Zehr, J. P., Grob, C., Masquelier, S., Garczarek, L., and Claustre, H.: Nutrients controlling primary productivity in the South East Pacific (BIOSOPE cruise), *Biogeosciences Discuss.*, 4, 2733–2759, 2007, <http://www.biogeosciences-discuss.net/4/2733/2007/>.
- Campbell, L. and Vault, D.: Photosynthetic Picoplankton Community Structure in the Subtropical North Pacific-Ocean near Hawaii (Station Aloha), *Deep-Sea Res. I*, 40, 2043–2060, 1993.
- Campbell, L., Nolla, H. A., and Vault, D.: The importance of *Prochlorococcus* to community structure in the central north Pacific Ocean, *Limnol. Oceanogr.*, 39, 954–961, 1994.
- Campbell, L., Liu, H., Nolla, H. A., and Vault, D.: Annual variability of phytoplankton and bacteria in the subtropical North Pacific Ocean at Station ALOHA during the 1991-1994 ENSO event, *Deep-Sea Res. I*, 44, 167–192, 1997.
- Cavender-Bares, K. K., Karl, D. M., and Chisholm, S. W.: Nutrient gradients in the western North Atlantic Ocean: Relationship to microbial community structure and comparison to patterns in the Pacific Ocean, *Deep-Sea Res. I*, 48, 2373–2395, 2001.
- Cho, B. C. and Azam, F.: Biogeochemical significance of bacterial biomass in the ocean's euphotic zone, *Mar. Ecol. Prog. Ser.*, 63, 253–259, 1990.
- Cuhel, R. L. and Waterbury, J. B.: Biochemical composition and short term nutrient incorporation patterns in a unicellular marine cyanobacterium, *Synechococcus* (WH7803), *Limnol. Oceanogr.*, 29, 370–374, 1984.
- Deutsch, C., Sarmiento, J. L., Sigman, D. M., Gruber, N., and Dunne, J. P.: Spatial coupling of nitrogen inputs and losses in the ocean, *Nature*, 445, 163–167, 2007.
- Duhamel, S., Zeman, F., and Moutin, T.: A dual-labeling method for the simultaneous measurement of dissolved inorganic carbon and phosphate uptake by marine planktonic species, *Limnol. Oceanogr. Meth.*, 4, 416–425, 2006.
- Duhamel, S., Moutin, T., Van Wambeke, F., Van Mooy, B., Rimmelin, P., Raimbault, P., and Claustre, H.: Growth and specific P-uptake rates of bacterial and phytoplanktonic communities in the Southeast Pacific (BIOSOPE cruise), *Biogeosciences*, 4, 913–925, 2007, <http://www.biogeosciences.net/4/913/2007/>.
- Grob, C., Ulloa, O., Claustre, H., Huot, Y., Alarcón, G., and Marie, D.: Contribution of picoplankton to the total particulate organic carbon concentration in the eastern South Pacific, *Biogeosciences*, 4, 837–852, 2007, <http://www.biogeosciences.net/4/837/2007/>.
- Kato, M., Sakai, M., Adachi, K., Ikemoto, H., and Sano, H.: Distribution of betain lipids in marine algae, *Phytochemistry*, 42, 1341–1345, 1996.
- Moutin, T., Thingstad, T. F., Wambeke, V., Marie, D., Slawyk, G., Raimbault, P., and Claustre, H.: Does competition for nanomolar phosphate supply explain the predominance of the cyanobacterium *Synechococcus*?, *Limnol. Oceanogr.*, 47, 1562–1567, 2002.
- Moutin, T., Karl, D. M., Duhamel, S., Rimmelin, P., Raimbault, P., Van Mooy, B. A. S., and Claustre, H.: Phosphate availability and the ultimate control of new nitrogen input by nitrogen fixation in the tropical Pacific Ocean, *Biogeosciences*, 5, 95–109, 2008, <http://www.biogeosciences.net/5/95/2008/>.
- Thingstad, T. F., Krom, M. D., Mantoura, R. F. C., Flaten, G. A. F., Groom, S., Herut, B., Kress, N., Law, C. S., Pasternak, A., Pitta, P., Psarra, S., Rassoulzadegan, F., Tanaka, T., Tselepidis, A., Wassman, P., Woodward, E. M. S., Wexels Riser, C., Zodiatis, G., and Zohary, T.: Nature of phosphorus limitation in the ultra-oligotrophic eastern Mediterranean, *Science*, 309, 1068–1071, 2005.
- Van Mooy, B. A. S., Rocop, G., Fredricks, H. F., Evans, C. T., and Devol, A. H.: Sulfolipids dramatically decrease phosphorus demand by picocyanobacteria in oligotrophic marine environments, *Proc. Natl. Acad. Sci.*, 103, 8607–8612, 2006.
- Van Mooy, B. A. S. and Devol, A. H.: Assessing nutrient limitation of *Prochlorococcus* at ALOHA by using an RNA capture method, *Limnol. Oceanogr.*, 53, 78–88, 2008.
- Van Wambeke, F., Obernosterer, I., Moutin, T., Duhamel, S., Ulloa, O., and Claustre, H.: Heterotrophic prokaryotic production in the South East Pacific: Longitudinal trends and coupling with primary production, *Biogeosciences Discuss.*, 4, 2761–2791, 2007a.
- Van Wambeke, F., Bonnet, S., Moutin, T., Raimbault, P., Alarçon G., and Guieu, C.: Factors limiting heterotrophic prokaryotic production in the southern Pacific Ocean, *Biogeosciences Discuss.*, 4, 3799–3828, 2007b.

Wada, H. and Murata, N.: Membrane lipids in cyanobacteria. Lipids in photosynthesis: structure, function and genetics, edited by: Siegenthaler, P.-A. and Murata, N., Kluwer Academic, 65–81, 1998.

Wakeham, S. G., Hedges, J. I., Lee, C., Peterson, M. L., and Hernes, P. J.: Compositions and transport of lipid biomarkers through the water column and surficial sediments of the equatorial Pacific Ocean, *Deep-Sea Res. II*, 44, 2131–2162, 1997.

Biochemical characteristics and bacterial community structure of the sea surface microlayer in the South Pacific Ocean

I. Obernosterer^{1,2}, P. Catala^{1,2}, R. Lami^{1,2}, J. Caparros^{1,2}, J. Ras³, A. Bricaud³, C. Dupuy⁴, F. van Wambeke^{5,2}, and P. Lebaron^{1,2}

¹Université Pierre et Marie Curie-Paris6, UMR7621; F66650 Banyuls-sur-Mer, France

²CNRS, UMR7621, F-66650 Banyuls-sur-Mer, France

³CNRS, Laboratoire d'Océanographie de Villefranche, 06230 Villefranche sur Mer, France; Université Pierre et Marie Curie-Paris6, Laboratoire d'Océanographie de Villefranche, 06230 Villefranche sur Mer, France

⁴Université de la Rochelle, Pôle Science, CRELA, UMR6217, Av. Michel Crépeau, 17042 La Rochelle cedex 01, France

⁵Laboratoire de Microbiologie, Géologie et Ecologie Marine (LMGEM), CNRS 6117, Université de la Méditerranée, Campus de Luminy – Case 901, 13288 Marseille cedex 9, France

Received: 10 July 2007 – Published in Biogeosciences Discuss.: 22 August 2007

Revised: 23 April 2008 – Accepted: 23 April 2008 – Published: 6 May 2008

Abstract. The chemical and biological characteristics of the surface microlayer were determined during a transect across the South Pacific Ocean in October-December 2004. Concentrations of particulate organic carbon (1.3 to 7.6-fold) and nitrogen (1.4 to 7-fold), and POC:PON ratios were consistently higher in the surface microlayer as compared to surface waters (5 m). The large variability in particulate organic matter enrichment was negatively correlated to wind speed. No enhanced concentrations of dissolved organic carbon were detectable in the surface microlayer as compared to 5 m, but chromophoric dissolved organic matter was markedly enriched (by 2 to 4-fold) at all sites. Based on pigment analysis and cell counts, no consistent enrichment of any of the major components of the autotrophic and heterotrophic microbial community was detectable. CE-SSCP fingerprints and CARD FISH revealed that the bacterial communities present in the surface microlayer had close similarity (>76%) to those in surface waters. By contrast, bacterial heterotrophic production (³H-leucine incorporation) was consistently lower in the surface microlayer than in surface waters. By applying CARD-FISH and microautoradiography, we observed that *Bacteroidetes* and *Gammaproteobacteria* dominated leucine uptake in the surface microlayer, while in surface waters *Bacteroidetes* and *Alphaproteobacteria* were the major groups accounting for leucine incorporation. Our results demonstrate that the microbial community in the surface microlayer closely resembles that of the surface

waters of the open ocean. Even a short residence in the surface microlayer influences leucine incorporation by different bacterial groups, probably as a response to the differences in the physical and chemical nature of the two layers.

1 Introduction

The air-water interface is a site of dynamic exchange processes of gaseous, liquid and particulate matter between the atmosphere and aquatic environments (Liss et al., 1997). The atmospheric-aquatic boundary layer, comprised of a series of sub-layers that are generally summarized as the sea surface microlayer (1–1000 μm), plays a pivotal role in these transfer processes. The enrichment of the surface microlayer in organic and inorganic matter affects physical features of the air-sea interface such as the surface tension, and thus air-sea fluxes (Frew, 1997). The potential contribution of biological activity in the surface microlayer to air-water exchange processes is far less known. The partial pressure of CO₂ in the top layer (2 cm) of the ocean was recently reported to be linked to microbial community metabolism (Calleja et al., 2005). The consistently enhanced rates of respiration in samples collected from the surface microlayer in different coastal and offshore marine environments support this notion (Garabétian, 1990; Obernosterer et al., 2005; Reinthaler et al., 2008). The biogenic gases dimethylsulfoxide (DMSO) and dimethylsulfoniopropionate (DMSP) were markedly enriched in the surface microlayer as compared to surface waters during calm wind conditions (Zemmelink et al., 2005). These observations could indicate that important biological



Correspondence to: I. Obernosterer
(ingrid.obernosterer@obs-banyuls.fr)

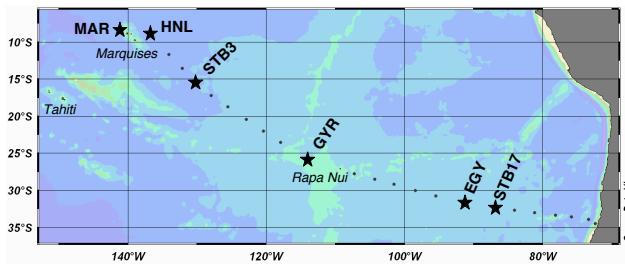


Fig. 1. Cruise track and sampled stations of the BIOSOPE (Biogeochemistry and Optics South Pacific Ocean Experiment) project. Stations where the sea surface microlayer was collected are indicated by stars.

processes at the air-water interface differ from those in surface waters, however, their impact on air-sea fluxes remains to be determined.

Whether organisms inhabiting the surface microlayer act as sources or sinks for various components will strongly depend on the abundance and activity of the different members of the microbial community. Reports on these biological features display large variability among studies, with enrichments, depletions or no differences observed (Agogu e et al., 2004 and references therein). This is most likely due to the spatial and temporal variability in the development of the surface microlayer. The utilization of different sampling devices that collect layers of varying thickness could also account for the differences observed. Another important issue to be addressed is the specificity of the autotrophic and heterotrophic community inhabiting the surface microlayer. Phytoneston has long been viewed as a unique group of organisms inhabiting the surface film of aquatic environments (see review by Zaitsev, 1997), but this idea has recently been challenged. Based on the tight relationship between the abundance of different groups of the plankton community in surface waters and that in the surface microlayer, the upward transport of organisms by physical processes rather than the in situ development has been suggested the source for their presence in the surface microlayer (Joux et al., 2006).

Only recently have molecular tools allowed to address the question whether heterotrophic bacteria inhabiting the surface microlayer display a specific community structure. The only two studies available up to date reveal contrasting conclusions (Agogu e et al., 2004; Franklin et al., 2005). Based on different sampling techniques and molecular approaches, the bacterial community structure associated with the surface microlayer was found to be similar in the coastal Mediterranean Sea (Agogu e et al., 2004) or distinctly different in the North Sea (Franklin et al., 2005) to that from surface waters.

The objective of the present study was to evaluate by two complementary molecular-based techniques whether the top layer of the ocean is inhabited by a distinct bacterioneuston community. Our aim was to describe the bacterial community structure in relation to major biological and chemical

features that characterized the surface microlayer in contrasting marine environments across the South Pacific Ocean.

2 Material and methods

2.1 Study sites

The BIOSOPE (BIogeochemistry and Optics South Pacific Experiment) cruise track crossed the South Pacific Ocean from the Marquise Islands to Chile (Claustre et al., 2008¹). The surface microlayer was sampled at 6 stations ranging from oligotrophic to ultraoligotrophic in the center of the South Pacific Gyre (Fig. 1). The sampled sites were located in the vicinity of the Marquise Islands (Station MAR), in High-Nutrient-Low-Chlorophyll waters east of the Marquise Islands (Station HNL), in the center of the South Pacific Gyre (Station GYR), in the eastern part of the South Pacific Ocean (Station EGY), and in the western (STB3) and eastern (STB17) part of the South Pacific Ocean (Fig. 1, Table 1). Wind speed was recorded every 10 s. Sea surface microlayer collection was done during calm wind conditions ($<3 \text{ m s}^{-1}$) and the mean wind speed 6h prior to sampling varied between 0.5 and 2.6 m s^{-1} at the different stations.

2.2 Surface microlayer sampling

We used a metal screen (Garrett, 1965) to collect the surface microlayer (250–400 μm) as described previously (Obernosterer et al., 2005). Sampling was done from a dinghy, roughly 0.5 nautical miles upwind from the research vessel. To prevent the collection of water adhering to the frame, the first 100 ml of water draining from the metal screen were rejected. Prior to collection, the metal screen was rinsed several times with the respective sample water. Surface water was collected at 5 m using a 5-l Niskin bottle. Samples collected in the surface microlayer and in surface waters were transferred to 9-l polycarbonate (PC) carboys. Prior to sampling, the PC carboys were rinsed with 1 N HCl, Milli-Q water and 3 times with the respective water samples.

2.3 Particulate organic carbon (POC) and nitrogen (PON) and dissolved organic carbon (DOC)

For POC-analysis, duplicate 700–1000-ml samples were filtered onto combusted (450°C for 5 h) Whatman GF/F filters. The filters were rinsed with $\sim 2 \text{ ml}$ of Milli-Q water to remove salts, then stored frozen (-20°C) until analysis. POC and PON measurements were performed on a 2400 Perkin Elmer CHN analyzer. The error for duplicate samples of POC and PON was, on average, 4% and 12%, respectively.

¹Claustre, H., Sciandra, A., and Vaultot, D.: Introduction to the special section: bio-optical and biogeochemical conditions in the South East Pacific in late 2004 – the BIOSOPE cruise, submitted to Biogeosciences Discuss., 2008.

Table 1. Date and local time of the day of the surface microlayer collection and general characteristics of the study sites. Phytoplankton biomass (chl-*a*) is integrated over the euphotic zone. Mean wind speed for 6 h prior to the surface microlayer collection is given. Ze – depth of the euphotic zone.

Station	Date	Time of the Day	Ze (m)	chl- <i>a</i> (mg m ⁻²) ¹	Wind speed (m s ⁻¹)
MAR	29 Oct. 2004	10:00–11:00	78	21	2.6
HNL	1 Nov. 2004	13:30–14:30	90	17	2.6
STB3	5 Nov. 2004	15:00–16:00	134	16	1.9
GYR-2	12 Nov. 2004	12:00–13:00	160	11	1.9
GYR-4	14 Nov. 2004	13:30–14:30	142	7	2.0
EGY	28 Nov. 2004	09:00–10:30	94	15	0.5
STB17	1 Dec. 2004	13:30–14:30	96	15	1.4

¹ Data are from Ras et al. (2008)

For DOC-analysis, GF/F filtered samples were preserved by adding 100 μ l H₃PO₄ (35%) to 20 ml subsamples. The samples were stored in combusted glass vials with Teflon-lined screw caps in the dark at 4°C until analyzed. DOC measurements were performed on a Shimadzu TOC-V-CSH (Benner and Strom, 1993). Prior to injection, DOC samples were sparged with CO₂-free air for 6 min to remove inorganic carbon. Hundred μ l of sample were injected in triplicate and the analytical precision was ~2%. Standards were prepared with acetanilid. The error for duplicate DOC samples was, on average, 1%.

2.4 Chromophoric Dissolved Organic Matter (cDOM)

The absorption coefficients of cDOM were measured throughout the ultraviolet-visible domain (280–735 nm) using the multiple path length, liquid core waveguide system UltraPath (WPI Inc.), with a pathlength of 2 m. Samples were filtered immediately after collection, in dim light, using 0.2 μ m Millipore filters pre-rinsed with Milli-Q water. Filtered samples were then placed in the automatic sampler (maintained in the dark), and pumped into the sample cell of the Ultrath instrument. Absorbance spectra were measured with reference to a salt solution (35 PSU), prepared with High Pressure Liquid Chromatographie (HPLC)-quality water and granular NaCl, to match the salinity and refractive index of samples. Between measurements, the cell was flushed successively with diluted detergent, high reagent grade MeOH, 2 M HCl, and Milli-Q water, and the cleanliness of the tube was controlled using a reference value for the transmittance of the reference water. As the absorption coefficients of pure water vary with temperature (especially in the infra-red), we minimized the temperature differences between the reference and the sample. The presence of microbubbles in the sample cell was also avoided by using a peristaltic pump and a debubbler.

2.5 Pigment analysis

Three to six liters of seawater were filtered onto GF/F filters (25 mm diameter) and the filters were stored in liquid nitrogen until HPLC-analysis according to Van Heukelem and Thomas (2001). A detailed description of the pigment extraction and analysis is given in Ras et al. (2008).

2.6 Enumeration of heterotrophic bacteria, autotrophic prokaryotic and eukaryotic cells by flow cytometry

Three-ml subsamples were fixed with 2% formaldehyde (final conc.), stored for 30 min at 4°C, then frozen in liquid nitrogen and stored at –80°C until analysis. For flow cytometric analysis of heterotrophic bacteria, samples were stained with the nucleic acid dye SYBR Green-I (Molecular Probes) at 0.025% (vol/vol) final concentration (Lebaron et al., 2001). Counts were performed on a FACS-Calibur flow cytometer (Becton Dickinson, San Jose, CA) equipped with a 488 nm wavelength, 15 mW Argon laser. Stained bacteria were excited at 488 nm wavelength and discriminated according to their right angle-light scatter (SSC, related to cell size) and green fluorescence at 530±15 nm wavelength. Based on a plot of green versus red fluorescence we distinguished photosynthetic from non-photosynthetic prokaryotes. Enumeration of autotrophic cells was performed according to Marie et al. (2000). *Synechococcus* spp. was discriminated by its strong orange fluorescence (585±21 nm) and pico- and nanoeukaryotes were discriminated by their scatter signals of the red fluorescence (>670 nm). The coefficient of variation among replicate samples is generally <5% (Agogue et al., 2004). To convert bacterial abundance to bacterial biomass we applied a conversion factor of 12.4 fg C cell⁻¹ (Fukuda et al., 1998).

2.7 Enumeration of nanoflagellates

Plastidic and heterotrophic nanoflagellates were determined after staining with Primulin according to Sherr et al. (1993).

Twenty to one hundred ml of raw seawater were fixed with 2% formaldehyde (final conc.) and filtered onto 0.8 μm black PC membrane filters (25 mm filter diameter). The filter was subsequently rinsed with two 1-ml aliquots of 0.1 M Trizma HCl (pH 4.0). The filter was covered with Primulin (250 g ml⁻¹, 0.1 M Trizma-HCl) and incubated in the dark for 15 min. After removing the Primulin solution by filtration, the filter was rinsed again with 0.1 M Trizma HCl, before being mounted onto a glass slide. Heterotrophic and autotrophic nanoflagellates were subsequently visualized using UV and blue light excitation, respectively, using an epifluorescence microscope (x 1000, Zeiss, Axiovert Mot plus).

2.8 Bacterial heterotrophic production

Bacterial production was determined by [³H] leucine incorporation applying the centrifugation method (Smith and Azam 1992). Briefly, 1.5 ml samples were incubated with a mixture of [4,5-³H]leucine (Amersham, specific activity 160 Ci mmol⁻¹) and nonradioactive leucine at final concentrations of 7 and 13 nM, respectively. Samples were incubated in the dark at the respective in situ temperatures for 2–3 h. Linearity of leucine incorporation over this time period was tested at the three stations. Incubations were terminated by the addition of trichloroacetic acid (TCA, Sigma) to a final concentration of 5%. To facilitate the precipitation of proteins, bovine serum albumine (BSA, Sigma, 100 mg l⁻¹ final concentration) was added prior to centrifugation at 16 000 g for 10 min (Van Wambeke et al., 2002). After discarding the supernatant, 1.5 ml of 5% TCA were added and the samples were subsequently vigorously shaken on a vortex and centrifuged again. The supernatant was discarded, 1.5 ml of PCS liquid scintillation cocktail (Amersham) added and the radioactivity incorporated into bacterial cells was counted aboard with a Packard LS 1600 Liquid Scintillation Counter. The variation between two replicate measurements was on average $\pm 10\%$ from the mean.

2.9 Catalyzed reporter deposition – fluorescence in situ hybridization and microautoradiography (MICRO-CARD-FISH)

At three stations (MAR, GYR and STB17) the bacterial community structure and the activity of the major bacterial groups was determined applying MICRO-CARD-FISH. Raw seawater samples (50 ml) were incubated with [4,5-³H]leucine (Amersham, specific activity 160 Ci mmol⁻¹) at a final concentration of 20 nM in the dark at in situ temperature for 2–4 h. The incubation was terminated by adding paraformaldehyde (PFA, 2% final concentration), and controls were fixed with PFA (2% final concentration) prior to incubation with ³H-leucine. Samples were stored at 4°C in the dark for 12 h before filtration onto 0.2 μm PC filters (25 mm filter diameter, Nuclepore). The filters were stored at -20°C until treated by CARD-FISH using the protocols

described in Pernthaler et al. (2002) and Sekar et al. (2003). Filters were embedded in low-melting-point agarose (0.2% final concentration), dried, dehydrated (96% EtOH, 1 min) and treated with lysozyme (Fluka, 10 mg ml⁻¹, 100 mM Tris [pH 8], 50 mM EDTA) for 1 h at 37°C to allow cell wall permeabilization. The filters were subsequently washed in Milli-Q water and dehydrated in ethanol (96%) for 1 min.

We determined the relative contribution of the major bacterial groups using the probes ALF968 (5'-GGT AAG GTT CTG CGC GTT-3') for *Alphaproteobacteria*, GAM42a (5'-GCC TTC CCA CAT CGT TT-3') for *Gammaproteobacteria*, and CFB319a (5'-TGG TCC GTG TCT CAG TAC-3') for *Bacteroidetes*, and a mix of the the probes EUB338I (5'-GCT GCC TCC CGT AGG AGT-3'), EUB338II (5'-GCA GCC ACC CGT AGG TGT-3') and EUB338III (5'-GCT GCC ACC CGT AGG TGT-3') for the identification of *Bacteria*. The negative control (NON338, 5'-ACT CCT ACG GGA GGC AGC-3') was used to determine non-specific binding. Probe working solution was added at a final concentration of 2.5 ng μl^{-1} and the hybridization was done at 35°C for 2 h.

For the microautoradiographic development, we followed the protocol described by Cottrell and Kirchman (2000). Briefly, the previously hybridized filter sections were placed onto slides coated with photographic emulsion (type NTB-2; Kodak, diluted 1:1 with Milli-Q water). The photographic emulsion was heated at 43°C for 30–60 min before utilization. The slides were then dried (for 15 min) on an ice-cold aluminum plate and kept in a dark box during exposure at 4°C. The slides were developed for 2 min (Dektol developer [1:1 dilution with Milli-Q water], Kodak), rinsed with Milli-Q water for 10 s, fixed for 6 min (Fixer Tmax, Kodak) and again rinsed for 6 min in Milli-Q water. After having dried the slides in a desiccator for 12 h, filter sections were peeled off and the cells were counterstained with a DAPI mix (4 parts Citifluor, 1 part Vectashield (Vector Laboratories) with DAPI at a final concentration of 0.5 $\mu\text{g ml}^{-1}$). To determine the appropriate exposure time for samples collected in the surface microlayer and surface waters, slides were developed after 12 h, 24 h, 36 h, 48 h, 72 h and 96 h at Stations GYR and STB17. At both stations, the percent of DAPI-stained cells associated with silver grains increased during the first 48 h and remained stable thereafter. We subsequently used an exposure time of 48 h. The slides were examined under a Olympus AX70 epifluorescence microscope and an image analysis system as described in Cottrell and Kirchman (2003). For each slide, 20 fields were enumerated, resulting in a minimum of 500 DAPI-stained cell counts. Mean values and the standard errors among the cell counts of 20 fields are presented. To determine the contribution of different bacterial groups to leucine incorporation, the number of probe-positive cells associated with silver grains was divided by the number of DAPI-stained cells associated with silver grains.

2.10 Capillary electrophoresis – single strand conformation polymorphism (CE-SSCP)

At all stations CE-SSCP was performed on DNA extracts to obtain molecular fingerprints of the surface microlayer and surface waters. Seawater samples ($<3\ \mu\text{m}$ size fraction, 0.5 l) were filtered onto $0.2\ \mu\text{m}$ PC filters (47 mm, Nuclepore) and filters were kept frozen (-80°C) until nucleic acid extraction. Nucleic Acid extraction was performed as described previously (Ghiglione et al., 2005). Primers used for polymeric chain reaction (PCR) were the specific bacterial primers w49dir ($5' -\text{A CGG TCC AGA CTC CTA CGG G}-3'$; Delbès et al., 2000) and w34rev ($5' -\text{TTA CCG CGG CTG CTG GCA C}-3'$; Lee et al., 1996) synthesized commercially (Eurogentec). Primer w34 was fluorescently 5'-labelled with phosphoramidite (TET, Eurogentec). Primers were designed to target a short sequence (around 200 pb), allowing a good resolution of the CE-SSCP signal (V3 region of 16S rDNA, *Escherichia coli* positions 329–533, Brosius et al., 1981). Amplifications were performed in $50\ \mu\text{l}$, with $1\ \mu\text{l}$ of DNA, $0.3\ \mu\text{M}$ of each primer, $0.8\ \text{mM}$ dNTPs, and 1X buffer (Promega), before adding 1.0 U of *pfu* polymerase (Promega). Samples were amplified (Robocycler 96, Stratagene) with the following program: 94°C (3min) for denaturation, 25 cycles at 94°C (denaturation, 30 s), 61°C (annealing, 25 s), 72°C (extension, 30 s), before a final extension at 72°C (10 min). The amplicon size was checked on agarose gel (2%), and the PCR products were purified using a PCR purification kit (Qiagen).

2.10.1 CE-SSCP electrophoresis

CE-SSCP was performed according to a previously described protocol (Ghiglione et al., 2005) on the Genetic Analyser ABI310 (Applied Biosystems). Briefly, each sample was diluted between 2- and 40-fold in sterile Tris-borate-EDTA (TBE) ($10\ \text{mM}$ Tris, $1\ \text{mM}$ EDTA) to obtain $10\ \text{ng}\ \mu\text{l}^{-1}$ of PCR product. From this resulting dilution, $1\ \mu\text{l}$ of PCR product was mixed with $0.1\ \mu\text{l}$ of an internal size standard (GeneScan-400 Rox, Applied Biosystems) and $18.9\ \mu\text{l}$ of deionised formamide (Applera), before heating (94°C , 10 min) and cooling in a water/ice bath (10 min). Samples were electrokinetically injected (5 s, 12 kV) into a capillary ($47\ \text{cm}\times 50\ \mu\text{m}$) filled with 5.6% GeneScan polymer (Applied Biosystems) gel containing 10% autoclaved glycerol in sterile TBE buffer ($90\ \text{mM}$ Tris-borate, $2\ \text{mM}$ EDTA [pH 8.0]). Samples migrated for 30 min (15 kV, 30°C). Phosphoramidite (TET)-labelled fragments were detected by a laser with a virtual filter C (detection wavelengths 532, 537 and 584 nm). Data collection was performed with the ABI Prism 310 collection software (Applied Biosystems).

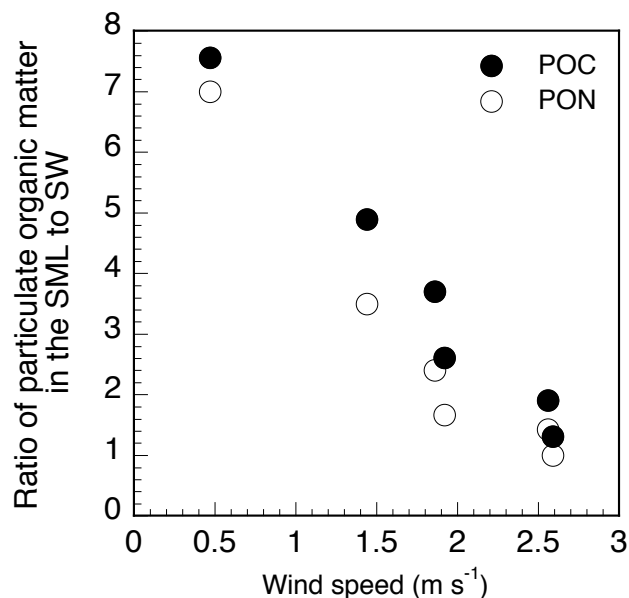


Fig. 2. Relation between the ratio of particulate organic carbon (POC) and nitrogen (PON) in the surface microlayer (SML) to that in surface waters (SW) and the mean wind speed 6 h prior to sampling.

2.10.2 CE-SSCP fingerprints analysis

Electrophoregrams were aligned with the GeneScan analysis software by fixing positions of the internal standard (GeneScan-400 Rox, Applied Biosystems) with a second-order least-square curve (i.e. linear regression). Peak detection on environmental fingerprints was realized using the first derivative of a polynomial curve fitted to the data within a window that was centred on each data point (GeneScan analysis software). Peaks overlapping were observable on the obtained fingerprints, to avoid artefacts in peak enumeration we used a high polynomial degree (10) to increase peak sensitivity. The peak amplitude threshold was fixed at 50 and applied for both Rox and TET fluorescent dyes.

3 Results

3.1 Particulate and dissolved organic matter

The surface microlayer was markedly enriched in particulate organic matter, by factors varying between 1.3 and 7.6 for POC, and between 1.4 and 7 for PON (Table 2). The variability in particulate organic matter enrichment was largely explained by wind history. The ratio of POC in the surface microlayer to that of surface waters (i.e. the enrichment factor) was negatively correlated to the mean wind speed 6 h prior to sampling ($r^2=0.97$, $n=6$, $p<0.0001$, Fig. 2). This was also the case for the PON enrichment factor ($r^2=0.93$, $n=6$, $p=0.0004$). No relationship between the concentration

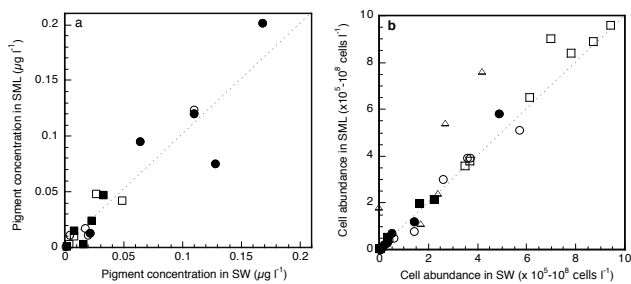


Fig. 3. Relation between (a) pigment concentration and (b) the abundance of autotrophic and heterotrophic cells in the surface microlayer (SML) and in surface waters (SW). Data of all pigment analyses and all cell counts are pooled. (a) filled circles: chl-*a*; empty circles: chl-*b*; filled squares: chl-*c*; empty squares: Divinyl chl-*a*. (b) filled circles: *Synechococcus* spp. ($\times 10^7 l^{-1}$); empty circles: Pico/Nanoeukaryotes ($\times 10^6 l^{-1}$); filled squares: Plastidic Nanoflagellates ($\times 10^6 l^{-1}$); empty squares: Heterotrophic bacteria ($\times 10^8 l^{-1}$); empty triangles: Heterotrophic nanoflagellates ($\times 10^5 l^{-1}$). Dashed line indicates the 1:1 line.

of particulate organic matter in the surface microlayer and in surface waters was detectable. C/N ratios of particulate organic matter were by 1.1 to 1.6-fold higher in the surface microlayer than at 5 m, indicating preferential accumulation of carbon-rich organic matter. Concentrations of dissolved organic carbon did not display any particulate pattern (Table 2). By contrast, cDOM was enriched in the surface microlayer by 2-fold at Stations MAR, HNL, STB3 and GYR, and by 4-fold at Station EGY (Table 2).

3.2 Autotrophic and heterotrophic components of the sea surface microlayer

The components of the microbial community determined in the present study did not exhibit any consistent pattern in terms of biomass or abundance in the surface microlayer as compared to surface waters (Fig. 3). Concentrations of chlorophyll-*a* in the surface microlayer exceeded those at 5 m at Stations MAR and EGY by factors of 1.2 and 1.5, respectively. At Stations HNL, GYR and STB17 concentrations of chlorophyll-*a* in the surface microlayer were similar or depleted compared to those at 5 m (Table 3). The group specific pigments chlorophyll-*b* (Chlorophytes) and chlorophyll-*c* (Chromophytes) revealed a similar trend as chlorophyll-*a* with pronounced enrichments only at Station EGY (by 2.8- and 1.9-fold, respectively). Concentrations of divinyl chlorophyll-*a* indicated an enrichment of *Prochlorococcus* in the surface microlayer at Stations MAR (by 1.8-fold) and EGY (by 1.3-fold), similar to that of *Synechococcus* based on cell abundances (by 1.2- and 1.4-fold, respectively) (Tables 3 and 4). Pico- and nanoeukaryotes displayed similar abundances in the surface microlayer and in surface waters. Plastidic and heterotrophic nanoflagellates were more abundant (by 1.2- to 4-fold) in the surface microlayer

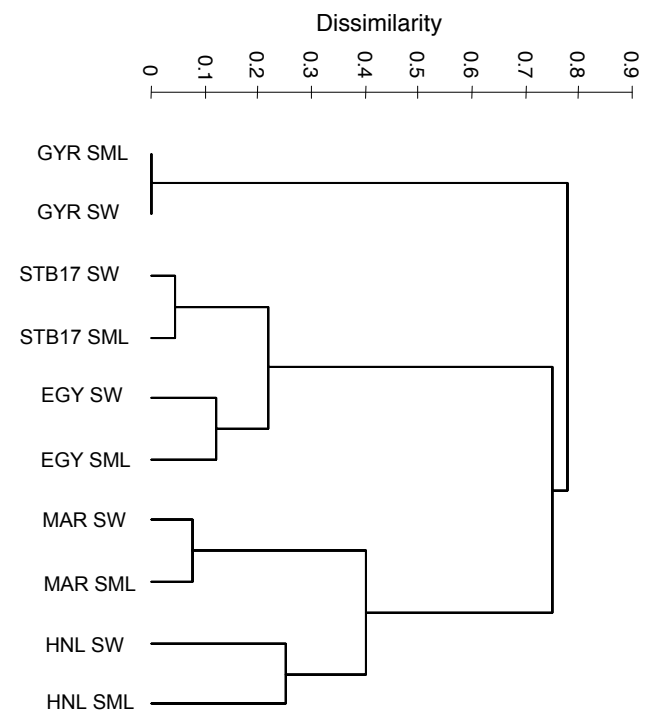


Fig. 4. UPGMA dendrogram generated from the CE-SSCP profiles from the surface microlayer (SML) and surface waters (SW). Scale bar indicates the dissimilarity.

in 3 out of 5 surface microlayer samplings. Phaeopigments were below the limit of detection in the surface microlayer and in surface waters of all stations. No marked enrichment of heterotrophic bacterial abundances was detectable in the surface microlayer (mean 1.04, range 1.01–1.08), except for Station EGY where abundances exceeded those at 5 m by 1.3-fold (Table 4).

3.3 Bacterial community structure

The CE-SSCP fingerprints revealed overall close similarity (>76%) of the bacterial community structure between the surface microlayer and surface waters (Fig. 4). The UPGMA dendrogram is based on the comparison of the presence or absence of peaks (thereafter referred to as ribotype) among the CE-SSCP fingerprints. The number of peaks represented on the fingerprints ranged between 13 and 24. Minor, but noticeable differences between the surface microlayer and surface waters were detectable at Stations EGY and STB17, owing to the presence of two distinct ribotypes in the surface microlayer. At Station HNL, a few minor ribotypes distinguished the CE-SSCP profile from the surface microlayer to that of surface waters.

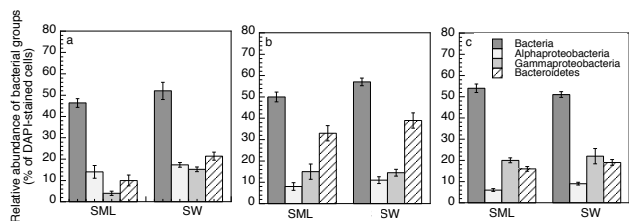
At Stations MAR, GYR and STB17 we compared the relative contribution of major bacterial groups in the surface microlayer and surface waters, using in situ hybridization. The percent DAPI-stained cells identified by a combination of the

Table 2. Concentration of particulate organic carbon (POC) and nitrogen (PON), dissolved organic carbon (DOC) and chromophoric dissolved organic matter (cDOM) in the sea surface microlayer (SML) and in surface waters (SW). n.d. – not determined.

		MAR	HNL	STB3	GYR-2	EGY	STB17
POC (μM)	SML	10.3	11.5	14.8	7.3	25.7	23.0
	SW	5.4	8.8	4.0	2.8	3.4	4.7
PON (μM)	SML	1.0	1.0	1.2	0.5	4.2	2.8
	SW	0.7	1.0	0.5	0.3	0.6	0.8
POC:PON	SML	10.8	11.5	12.7	14.6	6.2	8.3
	SW	7.6	8.5	7.9	8.4	5.2	6.0
DOC (μM)	SML	80	85	94	81	105	88
	SW	85	92	88	78	99	88
cDOM ($\text{Abs}_{350\text{nm}}\text{m}^{-1}$)	SML	0.072	0.097	0.051	0.036	0.073	n.d.
	SW	0.037	0.050	0.027	0.016	0.014	n.d.

Table 3. Concentrations of chlorophyll-*a* (chl-*a*), *b* (chl-*b*), *c* (chl-*c*) and Divinyl chl-*a* in the sea surface microlayer (SML) and surface waters (SW). BD – below limit of detection.

		MAR	HNL	GYR-4	EGY	STB17
chl- <i>a</i> ($\mu\text{g l}^{-1}$)	SML	0.201	0.075	0.013	0.095	0.12
	SW	0.168	0.128	0.021	0.064	0.11
chl- <i>b</i> ($\mu\text{g l}^{-1}$)	SML	0.017	0.011	0.001	0.011	0.124
	SW	0.017	0.020	0.001	0.004	0.110
chl- <i>c</i> ($\mu\text{g l}^{-1}$)	SML	0.047	0.003	0.001	0.015	0.024
	SW	0.033	0.016	0.002	0.008	0.023
Divinyl chl- <i>a</i> ($\mu\text{g l}^{-1}$)	SML	0.048	0.042	0.003	0.010	BD
	SW	0.027	0.049	0.004	0.008	BD

**Fig. 5.** Relative contribution of *Bacteria* and major bacterial groups to total DAPI-stained cells in the surface microlayer (SML) and in surface waters (SW) at Stations MAR (a), GYR (b) and STB17 (c). The control probe NON was on average 2% of DAPI-stained cells. Mean values \pm SE are given.

three probes EUB338I, EUB338II and EUB338III varied between 46–54% and 51–65% in the surface microlayer and in surface waters, respectively (Fig. 5). Our detection rate of *Bacteria* is in the lower range of values reported in the literature, and it is also lower than those we observed in the coastal and off-shore Mediterranean Sea and in the Southern Ocean (70–90%, unpublished data). The low metabolic activity and the small size of bacterial cells, and possibly also an inef-

ficient cell-wall permeabilization could account for the low detection rate observed in the present study.

The slightly lower percentage of DAPI-stained cells identified as *Bacteria* in the surface microlayer probably reflects the lower heterotrophic bacterial activity in this layer as compared to surface waters (see below). The sum of the relative contributions of *Alpha*-, and *Gammaproteobacteria* and *Bacteroidetes* amounted to $82\pm 20\%$ (mean \pm SD, $n=3$) in the surface microlayer and equaled (mean \pm SD, $100\pm 10\%$) the percent EUB positive cells in surface waters. Overall, no differences in the relative contribution of the major bacterial groups were detectable between the surface microlayer and surface waters (Fig. 5). At Station MAR, *Alpha*-, and *Gammaproteobacteria* and *Bacteroidetes* had similar relative contributions in both layers. At Station GYR *Bacteroidetes* were the dominant phylogenetic group (33 to 39% of DAPI-stained cells), and at STB17 *Bacteroidetes* (16 to 19% of DAPI-stained cells) and *Gammaproteobacteria* (20 to 22% of DAPI-stained cells) dominated in terms of abundance the heterotrophic bacterial community.

Table 4. Abundance of the major components of the microbial community in the sea surface microlayer (SML) and surface waters (SW). n.d. – not determined; b.d. – below limit of detection. * - data are based on flow cytometric analysis; ** – data are based on microscopic observations.

		MAR	HNL	STB3	GYR-2	GYR-4	EGY	STB17
<i>Synechococcus spp.</i> * ($\times 10^7 l^{-1}$)	SML	5.8	1.2	0.3	0.1	0.02	0.7	0.2
	SW	4.9	1.4	0.3	0.1	0.04	0.5	0.2
Pico/Nanoeukaryotes* ($\times 10^6 l^{-1}$)	SML	3.9	5.1	0.8	0.5	0.4	3.0	3.9
	SW	3.6	5.7	1.4	0.6	0.4	2.6	3.7
Plastidic Nanoflagellates** ($\times 10^5 l^{-1}$)	SML	19.9	21.5	5.3	0.4	0.4	n.d.	n.d.
	SW	16.6	22.2	3.5	0.1	0.6	n.d.	n.d.
Heterotrophic bacteria* ($\times 10^8 l^{-1}$)	SML	9.6	8.9	6.5	3.8	3.6	9.0	8.4
	SW	9.4	8.7	6.1	3.7	3.5	7.0	7.8
Heterotrophic nanoflagellates** ($\times 10^5 l^{-1}$)	SML	7.6	5.4	1.1	1.8	2.4	n.d.	n.d.
	SW	4.2	2.7	1.7	b.d.	2.4	n.d.	n.d.

3.4 Contribution of major bacterial groups to bulk leucine incorporation

By contrast to the heterotrophic bacterial abundance, distinct differences in bacterial heterotrophic production, as determined by 3H -leucine incorporation, were detectable between the two layers. Bacterial leucine incorporation in the surface microlayer accounted for 5% to 80% ($n=6$) of that at 5 m and the inhibition of bacterial heterotrophic production in the surface microlayer was most pronounced at low wind speeds (Fig. 6). An exception to this pattern was Station HNL, where leucine incorporation in the surface microlayer was enhanced by 20% as compared to surface waters. Only a small fraction of DAPI-stained cells incorporated leucine in the surface microlayer (4–13%) in comparison to surface waters (19–33%), further indicating the inhibition of the bacterial activity in the surface microlayer.

Different bacterial groups were responsible for bulk leucine incorporation in the surface microlayer as compared to surface waters at Stations GYR and STB17 (Fig. 7). At Station GYR, *Bacteroidetes* clearly dominated leucine uptake in the surface microlayer (43% of DAPI-stained cells associated with silver grains), while in surface waters both *Alphaproteobacteria* and *Bacteroidetes* (26% and 36%, respectively, of DAPI-stained cells associated with silver grains) had similar contributions to leucine uptake. At Station STB17, *Gammaproteobacteria* and *Bacteroidetes* dominated leucine uptake in the surface microlayer (28% and 25% respectively, of DAPI-stained cells associated with silver grains), while the three bacterial groups studied contributed equally to leucine uptake in surface waters (13% to 16% of DAPI-stained cells associated with silver grains) (Fig. 7).

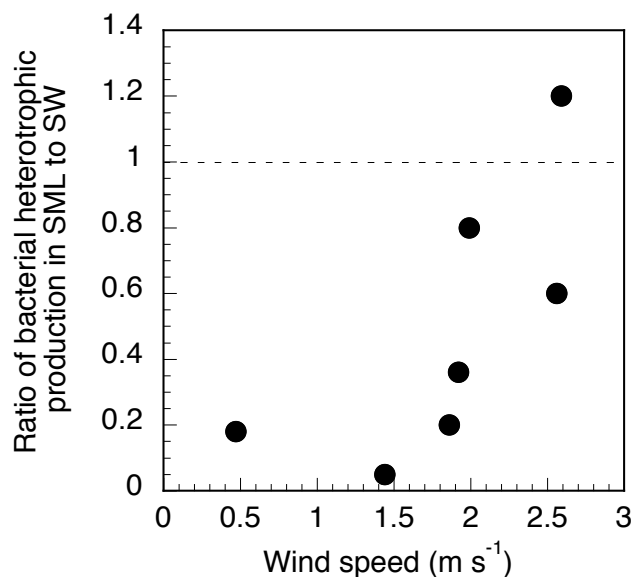


Fig. 6. Relation between the ratio of bacterial heterotrophic production in the surface microlayer (SML) to surface waters (SW) and the mean wind speed 6h prior to sampling.

4 Discussion

The thickness of the surface microlayer sampled, and thus its definition for a given study, depends on the sampling device applied. The metal screen we used in the present study collects the upper 250–440 μm water layer (Garrett 1965), while the layers collected by the glass plate (Harvey and Burzell 1972) and the rotating drum (Harvey 1966) are thinner (60–100 μm). For specific microbiological studies membranes are used to collect the upper 1 to 40 μm (Kjelleberg et al., 1979). These differences are mainly due to the physical mechanisms to sample the uppermost layer of aquatic systems, with some devices being more selective than oth-

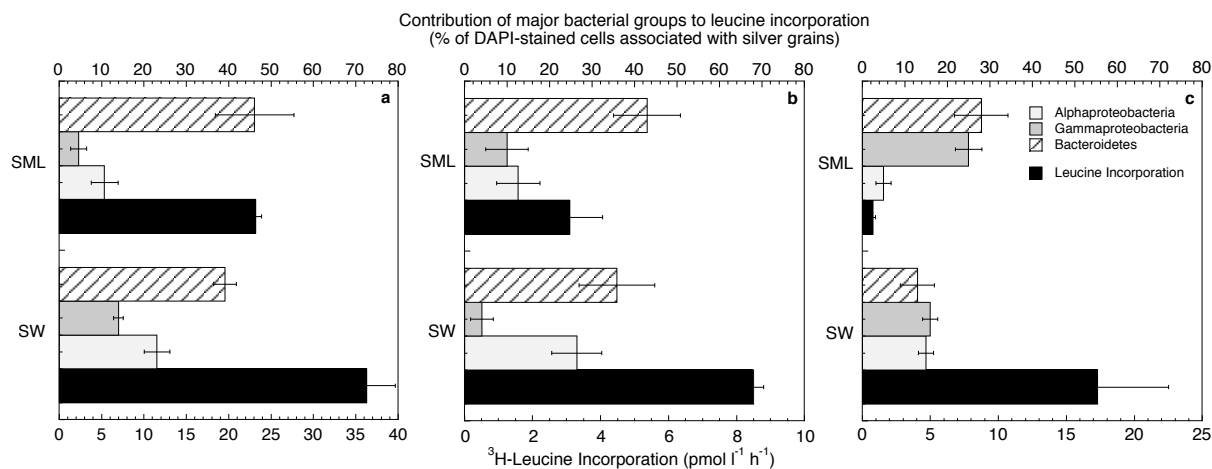


Fig. 7. Bulk ^3H -leucine incorporation and relative contribution of bacterial groups to leucine-incorporation in the surface microlayer (SML) and in surface waters (SW) at Stations MAR (a), GYR (b) and STB17 (c). For ^3H -leucine incorporation, mean values \pm variation of duplicate incubations, and for the relative contribution of bacterial groups mean values \pm SE are given.

ers. Based on a large data set of chemical (Momzikoff et al., 2004) and biological (Agogu e et al., 2004) parameters collected both with the metal screen and the glass plate in the coastal Mediterranean Sea, no significant differences in the enrichment factors between the two samplers were observed. Kuznetsova et al. (2004) report a more efficient collection of surface microlayer dissolved and particulate material by the screen than by the drum, despite the thinner layer sampled by the latter. These studies demonstrate that the collection of the surface microlayer to study the parameters considered herein are most likely not biased due to dilution with surface waters, despite the larger thickness of the layer sampled. Our choice of the screen sampler is driven by the efficient, non-selective sampling of a relatively large water volume for chemical and biological analyses.

The marked accumulation of particulate organic matter at the sea surface observed in the present study was not accompanied by any pronounced enrichment in photo- or heterotrophic organisms. This suggests that detrital particles, including colloidal aggregates, transparent exopolymeric particles (TEP), and submicron particles most likely constitute an important fraction of the surface microlayer biofilm. The higher C:N ratios of particulate organic matter observed in the present and previous studies (Nishizawa, 1971; Taguchi and Nakajima, 1971) further support this notion. The enrichment in particulate organic matter was strongly controlled by wind history, but independent of particulate organic matter concentrations in surface waters, suggesting that physical processes, such as turbulent mixing, transport by rising bubbles or buoyant particles were important for the surface microlayer formation. The most pronounced accumulation of particulate organic matter was observed at Station EGY where calm wind conditions ($\leq 2 \text{ m s}^{-1}$) prevailed over roughly 18 h prior to surface microlayer collection. It was

interesting to note that at this site the C:N ratio of particulate organic matter in the surface microlayer was similar to that in surface waters (Table 2). Station EGY was the only site where a pronounced enrichment in cell abundance and biomass of autotrophic and heterotrophic organisms was observed (Tables 3 and 4). These observations could indicate the transport of fresh material to the ocean surface, but they could also reflect photo- and heterotrophic biomass production in the surface microlayer when calm wind conditions exist over an extended time period. The latter idea is, however, not supported by results from the present study, as the inhibition in bacterial heterotrophic production in the surface microlayer was most pronounced at calm sea conditions (Fig. 6). This suggests that wind-induced physical processes determine not only the amount, but to some extent also the characteristics of the particulate organic matter that accumulates at the air-water interface.

The chemical characteristics of surface microlayer dissolved organic matter (DOM) appear to contrast the observations on particulate organic matter. Recent studies performed in the open Atlantic and the western Mediterranean Sea report a pronounced enrichment in dissolved free amino acids and a substantially lower C:N ratio in the DOM from the surface microlayer as compared to that from surface waters (Kuznetsova et al., 2004; Reinthaler et al., 2008). Interestingly, Reinthaler et al. (2008) concluded that the bioreactivity of the surface microlayer DOM was low, despite the high contribution of amino acids to DOC and DON. Selective accumulation, and also in situ production were both suggested to account for the enrichment in amino acids in the surface microlayer (Kuznetsova et al., 2004; Reinthaler et al., 2008). The consistently higher concentrations of chromophoric DOM (cDOM) in the surface microlayer observed in the present and previous studies (Carlson, 1983) are

clearly indicative for the selective accumulation of DOM at the air-water interface. Removal of cDOM by photomineralization and photobleaching is most likely rapid in the surface microlayer, the observation that cDOM is consistently enriched strongly suggests the continuous supply from bulk seawater by selective scavenging.

In the present study, bacterial heterotrophic production was clearly reduced in the surface microlayer as compared to surface waters. Previous studies support (Sieburth et al., 1976; Carlucci et al., 1986) or contrast (Dietz et al., 1976; Bell and Albright, 1982; Bailey et al., 1983; Williams et al., 1986; Agogu e et al., 2004; Reinthaler et al., 2008) this observation. A more consistent pattern among studies is observed on rates of bacterial (<0.8 μm fraction) or microbial community respiration in the surface microlayer, generally exceeding those in surface waters by several-fold (Garab etian 1990; Obernosterer et al., 2005; Reinthaler et al., 2008). These contrasting responses most likely reflect the different characteristics of the surface microlayer. The enrichment in organic and inorganic matter renders the surface microlayer a potentially favorable habitat for heterotrophic bacteria, at the same time it is exposed to drastic changes in temperature, pH, salinity and also to high intensities of solar radiation, in particular ultraviolet radiation. Based on the short incubation time, bacterial heterotrophic production provides an instantaneous response to the conditions in the surface microlayer. By contrast, respiration measurements require 12 h–24 h incubations in the dark and they more likely reflect the potential of organic matter originating from the surface microlayer in sustaining bacterial metabolism.

Bacterial growth rates could further indicate the activity of the bacterial community in the surface microlayer. Bacterial growth rates are commonly calculated on the basis of total bacterial cell abundance even though several independent approaches have shown that only a fraction of the bacterial community can be considered active (Gasol et al., 1999; Lebaron et al., 2001; Zubkov et al., 2001). The microautoradiographic observations performed in the present study allowed us to estimate the fraction of active cells, accounting for roughly 10% and 25% of DAPI-stained cells in the surface microlayer and surface waters, respectively. Assuming that this percentage represents the active part of the bacterial community, growth rates in the surface microlayer (0.6 d^{-1}) exceeded those in surface waters (0.3 d^{-1}) by a factor of two. Could this indicate that only a few bacterial groups are active in the surface microlayer accounting for most of the bacterial heterotrophic production in this particular environment?

Our results from the fingerprints and the in situ hybridization suggest that the surface microlayer is not inhabited by a particular bacterioneuston community. Two complementary approaches, a PCR-based (i.e. CE-SSCP) and a PCR-independent method (i.e. CARD-FISH) support this notion. The overall close similarity of the CE-SSCP fingerprints, each represented by 13–24 ribotypes, indicate that the bacterial community structure in the surface microlayer strongly

resembles that in surface waters. Even though the probes we used in the present study provide information on a low phylogenetic level, the results from the in situ hybridization appear to support this conclusion. Given the low bacterial growth rates determined in the present study, and the relatively short time period over which the surface microlayer persists, an in situ development of a specific bacterioneuston community is unlikely. Physical processes are mainly responsible for the formation of the surface microlayer, with upward transport of particulate material being a predominant process. The differences that we observed in the fingerprints between the two layers is most likely owing to the selective enrichment of the surface microlayer by specific ribotypes. Likely candidates are bacteria attached to particles that are transported to the air-sea interface. The structure of the bacterial community attached to particles in the water column differs from that of free-living bacteria (Acinas et al., 1999; Riemann and Winding, 2001; Ghiglione et al., 2007) and *Bacteroidetes* were found to have an important contribution to the bacterial communities associated with aggregates (DeLong et al., 1993; Ploug et al., 1999; Simon et al., 2002). Marine aerosol particles have also been observed to be enriched in bacteria, and their transport in the atmosphere has been suggested a potentially important dispersal mechanism (Aller et al., 2005).

Our conclusion on the close similarity between the bacterial community structure in the surface microlayer and surface waters is supported by results from samples collected in the same way from the coastal Mediterranean Sea (Agogu e et al., 2004), but they contrast the conclusion of a study conducted in the coastal North Sea (Franklin et al., 2005). These authors utilized hydrophilic membranes to collect surface microlayer bacteria, and based on 16S rRNA clone libraries they observed a lower bacterial diversity in the surface microlayer as compared to surface waters (Franklin et al., 2005). The potentially selective adsorption of bacteria onto hydrophilic membranes as discussed in Agogu e et al. (2004), could at least partly account for the different conclusions obtained by these studies.

In contrast to the similarity between the two layers in terms of community structure and abundance of major bacterial groups, differences in the composition of the active community were detectable. This was particularly pronounced at Station STB17 where *Bacteroidetes* and *Gammaproteobacteria* dominated the active community in the surface microlayer, while the three bacterial groups investigated contributed equally to the active community in surface waters (Fig. 7). Even though these bacterial groups contain each a diverse assemblage of sub-groups, they have been attributed specific characteristics, based on different experimental approaches. There is for instance increasing evidence that members of the *Bacteroidetes* group play an important role in the degradation of complex polymeric substances (Cottrell and Kirchman, 2000; Kirchman 2002; Cottrell et al., 2005). Several members belonging to the planktonic heterotrophic *Gammaproteobacteria* were characterized as

“opportunistic” due to their ability to rapidly respond to nutrient enrichment (Pinhassi and Berman, 2003). Pronounced growth of *Gammaproteobacteria* was detectable in nitrogen-amended incubations at Station GYR (Van Wambeke et al., personal communication). The dominance of *Bacteroidetes* and *Gammaproteobacteria* in the active community in the surface microlayer could reflect the rapid response of members of these bacterial groups to changes in the growth conditions, such as the enrichment and composition of organic and inorganic matter. These results suggest that even short time periods in the surface microlayer result in differences in bacterial groups accounting for leucine incorporation, probably as a response to the differences in the physical and chemical nature of the two layers.

In the open ocean, the organic matter accumulating at the air-sea interface originates predominantly from phytoplankton primary production. The vertical flux of phytoplankton-derived organic carbon to the ocean surface has, to the best of our knowledge, never been evaluated. The potential importance of an upward flux of organic matter has been illustrated by studies on buoyant particles. TEP-rich microaggregates, for example, have been reported to ascend at velocities as fast as $0.1\text{--}1\text{ m d}^{-1}$ to the ocean surface (Azetsu-Scott and Passow, 2004). The accumulation of organic matter at the sea surface impacts its physical structure and consequently the gas transfer rates. Photochemical mineralization of surface microlayer organic matter could have important consequences for the air-sea gas exchange (Obernosterer et al., 2005). The results from the present study suggest that heterotrophic bacteria in the surface microlayer do not represent an assemblage specific to this environment. The strong inhibition of bacterial biomass production in the surface microlayer indicates a lack of adaptation of the bacterial community, most likely due to its short residence time. This could lead to the conclusion that heterotrophic bacteria do not have a major contribution to the degradation of surface microlayer organic matter. This idea, however, contrasts the conclusion drawn from bacterial and community respiration rates based on bottle incubation experiments (Calleja et al., 2005; Obernosterer et al., 2005; Reinthaler et al., 2008). To better understand and determine the importance of biological processes for the air-sea exchange, clearly novel techniques allowing in situ measurements of biological fluxes at the air-water interface are required.

Acknowledgements. We are grateful to S. Blain, D. Marie and A. Sciandra for their help with the surface microlayer sampling. We thank the chief scientists H. Claustre and A. Sciandra, and the captain and the crew of the *R/V Atalante* for their support aboard. D. Taillez kindly provided the wind speed data. Two anonymous reviewers helped improve an earlier version of the manuscript. Financial support for this work came from the French National program PROOF (INSU/CNRS).

Edited by: A. Boetius

References

- Acinas, S. G., Anton, J., and Rodriguez-Valera, F.: Diversity of free-living and attached bacteria in offshore Mediterranean waters as depicted by analysis of genes encoding 16S rRNA, *Appl Environ. Microbiol.*, 65, 514–522, 1999.
- Agogué, H., Casamayor, E. O., Joux, F., Obernosterer, I., Dupuy, C., Lantoiné, F., Catala, P., Weinbauer, M. G., Reinthaler, T., Herndl, G. J., and Lebaron, P.: Comparison of samplers for the biological characterization of the sea surface microlayer, *Limnol. Oceanogr. Methods*, 2, 213–225, 2004.
- Aller, J. Y., Kuznetsova, M. R., Jahns, C. J., and Kemp, P. F.: The sea surface microlayer as a source of viral and bacterial enrichment in marine aerosols, *Aerosol Science*, 36, 801–812, 2005.
- Azetsu-Scott, K. and Passow, U.: Ascending marine particles: Significance of transparent exopolymer particles (TEP) in the upper ocean, *Limnol. Oceanogr.*, 49, 741–748, 2004.
- Bailey, C. A., Neihof, R. A., and Tabor, P. S.: Inhibitory effect of solar radiation on amino acid uptake in Chesapeake Bay bacteria, *Appl. Environ. Microbiol.*, 46, 44–49, 1983.
- Bell, C. R. and Albright, L. J.: Bacteriological investigation of the neuston and plankton in the Fraser River estuary, *British Columbia, Estuar. Coast. Shelf Sciences*, 15, 385–394, 1982.
- Benner, R. and Strom, M.: A critical evaluation of the analytical blank associated with DOC measurements by high-temperature catalytic oxidation, *Mar. Chem.*, 41, 153–160, 1993.
- Brosius, J., Dull, T., Sleeter, D. D., and Noller, H. F.: Gene organization and primary structure of a ribosomal RNA operon from *Escherichia coli*, *J. Molecular Biology*, 148, 107–127, 1981.
- Calleja, M. L., Duarte, C. M., Navarro, N., and Agustí, S.: Control of air-sea CO₂ disequilibria in the subtropical NE Atlantic by planktonic metabolism under the ocean skin, *Geophys. Res. Lett.*, 32, 2005.
- Carlson, D. J.: Dissolved organic materials in surface microlayers: Temporal and spatial variability and relation to sea state, *Limnol. Oceanogr.*, 28, 415–431, 1983.
- Carlucci, A. F., Craven, D. B., Robertson, K. J., and Williams, P. M.: Surface-film microbial populations: diel amino acid metabolism, carbon utilization, and growth rates, *Mar. Biol.*, 92, 289–297, 1986.
- Cottrell, M. T. and Kirchman, D. L.: Natural assemblages of marine proteobacteria and members of the *Cytophaga-Flavobacter* cluster consuming low- and high-molecular-weight dissolved organic matter, *Appl. Environ. Microbiol.*, 66, 1692–1697, 2000.
- Cottrell, M. T. and Kirchman, D. L.: Contribution of major bacterial groups to bacterial biomass production (thymidine and leucine incorporation) in the Delaware estuary, *Limnol. Oceanogr.*, 48, 168–178, 2003.
- Cottrell, M. T., Yu, L., and Kirchman, D. L.: Sequence and expression analyses of *Cytophaga*-like hydrolases in a Western arctic metagenomic library and the Sargasso Sea, *Appl Environ Microbiol.*, 71, 8506–8513, 2005.
- Delbès, C., Moletta, R., and Godon, J.: Monitoring of activity dynamics of an aerobic digester bacterial community using 16S rRNA polymerase chain reaction-single-strand conformation polymorphism analysis, *Environ Microbiol.*, 2, 506–515, 2000.
- DeLong, E. F., Franks, D. G., and Alldredge, A. L.: Phylogenetic diversity of aggregate-attached vs. free-living marine bacterial assemblages, *Limnol. Oceanogr.*, 38, 924–934, 1993.

- Dietz, A. S., Albright, L. J., and Tuominen, T.: Heterotrophic activities of bacterioneuston and bacterioplankton, *Can. J. Microbiol.*, 22, 1699–1709, 1976.
- Franklin, M. P., McDonald, I. R., Bourne, D. G., Owens, N. J. P., Upstill-Goddard, R. C., and Murrell, J. C.: Bacterial diversity in the bacterioneuston (sea surface microlayer): the bacterioneuston through the looking glass, *Environ Microbiol*, 7, 723–736, 2005.
- Frew, N. M.: The role of organic films in air-sea gas exchange, 121–172, in: *The sea surface and global change*, edited by: Liss, P. S. and Duce, R. A., Cambridge University Press, 1997.
- Fukuda, R., Ogawa, H., Nagata, T., and Koike, I.: Direct determination of carbon and nitrogen contents of natural bacterial assemblages in marine environments, *Appl. Environ. Microbiol.*, 64, 3352–3358, 1998.
- Garabétian, F.: Production de CO₂ à l'interface air-mer, Une approche par l'étude des phénomènes respiratoires dans la microcouche de surface, *Int Rev ges Hydrobiol*, 76, 219–229, 1990.
- Garrett, W. D.: Collection of slick-forming materials from the sea surface, *Limnol. Oceanogr.*, 10, 602–605, 1965.
- Gasol, J. M., Zweifel, U. L., Peters, F., Fuhrman, J. A., and Hagström, A.: Significance of size and nucleic acid content heterogeneity as measured by flow cytometry in natural planktonic bacteria, *Appl. Environ. Microbiol.*, 65, 4475–4483, 1999.
- Ghiglione, J.-F., Larcher, M., and Lebaron, P.: Spatial and temporal scales of variation in the bacterioplankton community structure in the NW Mediterranean Sea, *Aquat. Microb. Ecol.*, 40, 229–240, 2005.
- Ghiglione, J.-F., Mevel, G., Pujo-Pay, M., Mousseau, L., Lebaron, P., and Goutx, M.: Diel and seasonal variations in abundance, activity, and community structure of particle-attached and free-living bacteria in NW Mediterranean Sea, *Microb Ecol*, 54, 217–231, 2007.
- Harvey, G. W.: Microlayer collection from the sea surface: a new method and initial results, *Limnol. Oceanogr.*, 11, 608–614, 1966.
- Harvey, G. W. and Burzell, L. A.: A simple microlayer method for small samples, *Limnol. Oceanogr.*, 17, 156–157, 1972.
- Joux, F., Agogue, H., Obernosterer, I., Dupuy, C., Reinthaler, T., Herndl, G. J., and Lebaron, P.: Microbial community structure in the sea surface microlayer at two contrasting coastal sites in the northwestern Mediterranean Sea, *Aquat. Microb. Ecol.*, 42, 91–104, 2006.
- Kirchman, D. L.: The ecology of Cytophaga-Flavobacteria in aquatic environments, *FEMS Microbiology Ecology*, 39, 91, 2002.
- Kjelleberg, S., Stenström, T. A., and Odham, G.: Comparative study of different hydrophobic devices for sampling lipid surface films and adherent microorganisms, *Mar. Chem.*, 53, 21–25, 1979.
- Kuznetsova, M., Lee, C., Aller, J., and Frew, N.: Enrichment of amino acids in the sea surface microlayer at coastal and open ocean sites in the North Atlantic Ocean, *Limnol. Oceanogr.*, 49, 1605–1619, 2004.
- Lebaron, P., Servais, P., Agogue, H., Courties, C., and Joux, F.: Does the high nucleic acid content of individual bacterial cells allow us to discriminate between active cells and inactive cells in aquatic systems?, *Appl. Environ. Microbiol.*, 67, 1775–1782, 2001.
- Lee, D. H., Zo, Y. G., and Kim, S. J.: Non-radioactive method to study genetic profiles of natural bacterial communities by PCR-single-strand-conformation polymorphism, *Appl. Environ. Microbiol.*, 62, 3112–3120, 1996.
- Liss, P. S., Watson, A. J., Bock, E. J., Jaehne, B., Asher, W. E., Frew, N. M., Hasse, L., Korenowski, G. M., Merlivat, L., Phillips, L. F., Schluessel, P., and Woolf, D. K.: Physical processes in the microlayer and the air-sea exchange of trace gases, 1–33, in: *The sea surface and global change*, edited by: Liss, P. S. and Duce, R. A., Cambridge University Press, 1997.
- Marie, D., Simon, N., Guillon, L., Partensky, F., and Vaultot, D.: Flow cytometry analysis of marine picoplankton, 421–454, in: *Living Color: Protocols in flow cytometry and cell sorting*, edited by: Maggio, D., Springer Verlag, 2000.
- Momzikoff, A., Brinis, A., Dallot, S., Gondry, G., Saliot, A., and Lebaron, P.: Field study of the chemical characterization of the upper ocean surface using various samplers, *Limnol. Oceanogr. Methods*, 2, 374–386, 2004.
- Nishizawa, S.: Concentration of organic and inorganic material in the surface skin at the Equator, 155° W, *Bull. Plankton Soc. Japan*, 18, 42–44, 1971.
- Obernosterer, I., Catala, P., Reinthaler, T., Herndl, G. J., and Lebaron, P.: Enhanced heterotrophic activity in the surface microlayer of the Mediterranean Sea, *Aquat. Microb. Ecol.*, 39, 293–302, 2005.
- Pernthaler, A., Pernthaler, J., and Ammann, R.: Fluorescence in situ hybridization and catalyzed reporter deposition for the identification of marine bacteria, *Appl. Environ. Microbiol.*, 86, 3094–3101, 2002.
- Pinhassi, J. and Berman, T.: Differential growth response of colony-forming Alpha- and Gammaproteobacteria in dilution culture and nutrient addition experiments from Lake Kinneret (Israel), the Eastern Mediterranean Sea, and the Gulf of Eilat, *Appl. Environ. Microbiol.*, 69, 199–211, 2003.
- Ploug, H., Grossart, H. P., Azam, F., and Joergensen, B. B.: Photosynthesis, respiration and carbon turnover in sinking marine snow from surface waters of Southern California Bight: implications for the carbon cycle in the ocean, *Mar. Ecol. Prog. Ser.*, 179, 1–11, 1999.
- Ras, J., Claustre, H., and Uitz, J.: Spatial variability of phytoplankton pigment distributions in the Subtropical South Pacific Ocean: comparison between in situ and modelled data, *Biogeosciences*, 5, 353–369, 2008, <http://www.biogeosciences.net/5/353/2008/>.
- Reinthaler, T., Sintes, E., and Herndl, G. J.: Dissolved organic matter and bacterial production and respiration in the sea-surface microlayer of the open Atlantic and the western Mediterranean Sea, *Limnol. Oceanogr.*, 53, 122–136, 2008.
- Riemann, L. and Winding, A.: Community Dynamics of Free-living and Particle-associated Bacterial Assemblages during a Freshwater Phytoplankton Bloom, *Microb. Ecol.*, 42, 274–285, 2001.
- Sekar, R., Pernthaler, A., Pernthaler, J., Warnecke, F., Posch, T., and Amann, R.: An improved protocol for quantification of freshwater Actinobacteria by fluorescence in situ hybridization, *Appl. Environ. Microbiol.*, 69, 2928–2935, 2003.
- Sherr, E. B., Caron, D. A., and Sherr, B. F.: Staining of heterotrophic protists for visualization via epifluorescence microscopy, 213–227, in: *Handbook of methods for aquatic microbial ecology*, edited by: Kemp, P. F., Sherr, B. F., Sherr, E. B., and Cole, J. J., Lewis Publishers, 1993.

- Sieburth, J. M. N., Willis, P.-J., Johnson, K. M., Burney, C. M., Lavoie, D. M., Hinga, K. R., Caron, D. A., French Iii, F. W., Johnson, P. W., and Davis, P. G.: Dissolved organic matter and heterotrophic microneuston in the surface microlayers of the North Atlantic, *Science*, 194, 1415–1418, 1976.
- Simon, M., Grossart, H. P., Schweitzer, B., and Ploug, H.: Microbial ecology of organic aggregates in aquatic ecosystems, *Aquat. Microb. Ecol.*, 28, 175–211, 2002.
- Smith, D. C. and Azam, F.: A simple, economical method for measuring bacterial protein synthesis rates in sea water using ^3H - Leucine, *Mar. Microb. Food Webs.*, 6, 107–114, 1992.
- Taguchi, S. and Nakajima, K.: Plankton and seston in the sea surface of three inlets of Japan, *Bull. Plankton Soc., Japan*, 18, 20–36, 1971.
- Van Heukelem, L. and Thomas, C. S.: Computer-assisted high-performance liquid chromatography method development with applications to the isolation and analysis of phytoplankton pigments, *J. Chromatography A.*, 901, 31–49, 2001.
- Van Wambeke, F., Christaki, U., Giannakourou, A., Moutin, T., and Souvemerzoglou, K.: Longitudinal and vertical trends of bacterial limitation by phosphorus and carbon in the Mediterranean Sea, *Microb. Ecol.*, 43, 119–133, 2002.
- Williams, P. M., Carlucci, A. F., Henrichs, S. M., Vleet, E. S. V., Horrigan, S. G., Reid, F. M. H., and Robertson, K. J.: Chemical and microbiological studies of sea-surface films in the southern gulf of California and off the west coast of Baja California, *Mar. Chem.*, 19, 17–98, 1986.
- Zaitsev, Y.: Neuston of seas and oceans, 371–382, in: *The sea surface and global change*, edited by: Liss, P. S. and Duce, R. A., Cambridge University Press, 1997.
- Zemmelink, H. J., Houghton, L., Sievert, S. M., Frew, N. M., and Dacey, J. W. H.: Gradients in dimethylsulfide, dimethylsulfoniopropionate, dimethylsulfoxide, and bacteria near the sea surface, *Mar. Ecol. Prog. Ser.*, 295, 33–42, 2005.
- Zubkov, M. V., Fuchs, B. M., Burkhill, P. H., and Amann, R.: Comparison of cellular and biomass specific activities of dominant bacterioplankton groups in stratified waters of the Celtic Sea, *Appl. Environ. Microbiol.*, 67, 5210–5218, 2001.

The “neutral” community structure of planktonic herbivores, tintinnid ciliates of the microzooplankton, across the SE Tropical Pacific Ocean

J. R. Dolan¹, M. E. Ritchie², and J. Ras³

¹Marine Microbial Ecology Group, Laboratoire d’Océanographie de Villefranche, Université Paris6 CNRS UMR 7093, BP 28, Station Zoologique, 06230 Villefranche-sur-Mer, France

²Syracuse University, Department of Biology, 108 College Place, Syracuse NY 13244, USA

³Marine Optics and Remote Sensing Group, Laboratoire d’Océanographie de Villefranche, Université Paris6 CNRS UMR 7093, 06230 Villefranche-sur-Mer, France

Received: 5 February 2007 – Published in Biogeosciences Discuss.: 13 February 2007

Revised: 7 May 2007 – Accepted: 23 May 2007 – Published: 7 June 2007

Abstract. We assessed the community characteristics of a group of planktonic herbivores across a species-rich area, the SE Pacific Ocean. A series of 22 stations between the Marquise Islands (7° S 142° W) and the coast of Chile (35° S 73° W) was sampled during the BIOSOPE cruise in 2004. We examined the relationships between taxonomic diversity, morphological diversity, patterns of tintinnid species assemblage, and phytoplankton abundance. Tintinnid community characteristics were estimated from large volume (20–60 l) discrete depth sampling and phytoplankton were characterized based on HPLC pigment signatures. Across the transect, average water column concentrations of tintinnids ranged from 2–40 cells l⁻¹ or 8–40 ng C l⁻¹, and were positively related to chlorophyll *a* concentrations which varied between 0.07–2 μg l⁻¹. Large numbers of tintinnid taxa were found, 18–41 species per station, yielding a total of 149 species. Among stations, morphological and taxonomic diversity metrics co-varied but were not significantly related to phytoplankton diversity estimated using a pigment-based size-diversity metric. Taxonomic diversity of tintinnids, as H’ or Fishers’ alpha, was inversely related to chlorophyll concentration and positively to the depth of the chlorophyll maximum layer. Species abundance distributions were compared to geometric, log-series and log-normal distributions. For most stations, the observed distribution most closely matched log-series, coherent with the neutral theory of random colonization from a large species pool. Occurrence rates of species were correlated with average abundance rather than specific characteristics of biomass or lorica oral diameter (mouth) size. Among stations, species richness was cor-

related with both the variety of mouth sizes (lorica oral diameters) as well as numbers of species per mouth size, also consistent with random colonization.

1 Introduction

In the early 20th century, oceanographic and biological surveys identified the SE Pacific as extraordinarily species-rich (e.g., the Agassiz Expedition of 1904–1905 and the Carnegie Expedition of 1928–1929). With the decline of survey campaigns, the zone was very rarely sampled (Hasle, 1959). The few modern research efforts or major programs in the SE Pacific (such as Eastropac in the late 1960’s), in common with other oceanic areas, were process studies, focused on parameters such as biomass estimates and rate measures of primary and secondary production. Interestingly, from these studies a paradigm has emerged stressing the apparent efficiency of tropical and subtropical food webs. Algal biomass is quite low, occasionally lower than one might expect given concentrations of nutrients (i.e., zones of high nutrient low chlorophyll, HNLC) and nearly all the primary production is consumed. The efficiency of grazers, especially protists, is often invoked as an explanation, at least partial (e.g., Leising et al. 2003) for the maintenance of low algal biomasses. The efficiency of both primary producers and secondary consumers may be related to the diversity of tropical and subtropical pelagic systems. However, the existence or importance of the link between trophic efficiency and diversity in planktonic communities is difficult to evaluate because community characteristics have received very little attention, especially with regard to the primary consumers, the microzooplankton.

Correspondence to: J. Dolan
(dolan@obs-vlfr.fr)

Table 1. Station locations and tintinnid sampling. Cruise track shown in Fig. 1. Layer denotes depth layer sampled in meters, $n(Z)$ the number of discrete depth sampled within the layer and $\sum \text{Vol}$ the total volume (l) screened through a $20 \mu\text{m}$ mesh plankton concentrator.

Station	Location	Date	Layer	$n(Z)$	$\sum \text{Vol}$
SE3	9°56' S 142°15' W	10/25/04	15–70	2	10
MAR1	8°22' S 141°15' W	10/27/04	15–80	4	20
HLN1	9°00' S 136°52' W	11/01/04	5–140	6	30
STB1	11°45' S 134°05' W	11/03/04	5–140	6	30
STB2	13°31' S 132°08' W	11/04/04	5–130	4	20
STB3	15°30' S 129°54' W	11/05/04	5–130	5	25
STB4	17°13' S 127°57' W	11/06/04	5–210	6	30
STB6	20°25' S 122°55' W	11/08/04	5–250	6	30
STB8	23°31' S 117°51' W	11/10/04	5–240	6	58
GYR2	26°01' S 114°01' W	11/13/04	5–270	6	60
STB11	27°45' S 107°16' W	11/20/04	5–300	5	25
STB12	28°30' S 104°16' W	11/21/04	5–280	6	60
STB13	29°12' S 101°28' W	11/22/04	5–230	6	60
STB14	30°01' S 98°23' W	11/23/04	5–230	6	56
STB15	30°46' S 95°26' W	11/24/04	5–175	6	60
EGY2	31°50' S 91°27' W	11/26/04	5–190	6	35
STB17	32°23' S 86°47' W	12/01/04	5–175	6	55
STB18	32°41' S 84°04' W	12/02/04	5–140	6	54
STB20	33°21' S 78°06' W	12/04/04	5–140	6	60
STB21	33°38' S 75°50' W	12/05/04	5–90	6	60
UPW2	33°52' S 73°32' W	12/07/04	0–50	6	60
UPX2	34°38' S 72°78' W	12/10/04	0–60	6	39

These grazers have long been identified as the likely dominant consumers of algal production, given their relatively high biomass compared to metazoan grazers, especially in systems such as the SE Pacific (Beers and Stewart, 1971). Here we focus on large-scale geographic patterns across the SE Pacific Ocean for a particular group of these organisms members of the ciliate suborder Tintinnia, tintinnid ciliates of the microzooplankton, which are united ecologically as grazers on pico and nanplankton.

Tintinnid ciliates are characterized by the possession of a tube or vase-shaped shell or lorica into which the ciliate cell can contract. They are generally a minority component of the microzooplankton, representing 5–10% of ciliate numbers (e.g., Dolan and Marassé, 1995) but occasionally dominate the microzooplankton (Karayanni et al., 2005). Tintinnids, as loricate choreotrich ciliates, are considered a monophyletic group in traditional ciliate classification schemes (Lynn and Small, 2000) and based on results of molecular work (e.g., Agatha and Strüder-Kypke, 2007; Agatha et al., 2005; Snoeyenbos-West et al., 2002). The group is species-rich with over 700 species distinguished in the monographs of Kofoid and Campbell (1929, 1939), a large portion of which (>200) were newly described from samples gathered during the Agassiz expedition to the Pacific.

Similar to foraminifera and radiolarians, species descriptions have been based on skeletal or shell (lorica) architecture. However, species in some genera are known to be polymorphic (e.g. Laval-Peuto, 1983; Williams et al., 1994).

Characteristics of the lorica are not only of taxonomic but also ecological significance. The diameter of the mouth end of the lorica, the lorica oral diameter (LOD), is related to the size of the food items ingested by the ciliate. Heinbokel (1978) noted that the largest prey ingested were about half the LOD and Dolan et al. (2002) found that tintinnid feeding rates were maximal on prey sizes equal to about 25% of LOD. Thus, in tintinnid ciliates the lorica distinguishes species both taxonomically and ecologically. Not surprisingly then, morphological diversity, in terms of LOD sizes, and taxonomic diversity co-vary both spatially and temporally.

Between the Moroccan upwelling system and the Eastern Mediterranean, taxonomic and morphological diversity of tintinnids showed parallel trends (Dolan et al., 2002). Diversity increased from the upwelling area into the Western Mediterranean and declined slightly towards the oligotrophic Eastern Mediterranean. Both taxonomic and morphological (LOD) diversity were correlated with a chlorophyll size-diversity estimate. In temperate systems, seasonal changes in the average LOD of tintinnid communities are well-known (e.g., Verity, 1987). In a recent study of the seasonal changes in a tropical lagoon, median LOD of the tintinnid community shifted with the fraction of chlorophyll $a > 10 \mu\text{m}$ (Dolan et al., 2006). The numbers of species were relatable to numbers of LOD size-classes and taxonomic diversity was correlated with LOD size-class diversity.

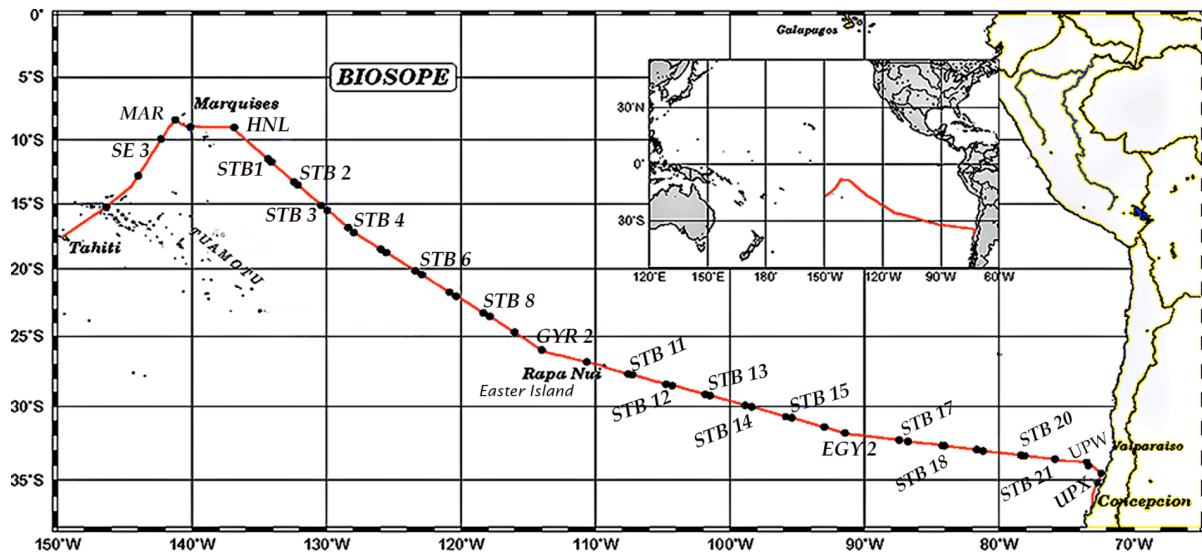


Fig. 1. BIOSOPE cruise track showing stations at which samples for tintinnid ciliates were obtained. Station locations and sampling dates are given in Table 1.

Here we examine patterns of community assembly across the SE Pacific. The areas sampled included zones with highest recorded species richness of tintinnids (>100 spp, for some stations in Kofoid and Campbell (1939)). The SE Pacific ranges from the clearest waters of the world ocean (Morel et al., 2007) to the productive upwelling system of Chile. Using data from stations across a large geographic scale and range of phytoplankton concentrations, the questions addressed were: 1) Is diversity related to resource level? 2) Are taxonomic and morphological diversity linked across large scales and species pools? 3) Is resource (phytoplankton) size-structure related to tintinnid community structure under low resource conditions? 4) What factors are controlling community assemblies? The questions were addressed by estimating diversity metrics of tintinnid communities, defined as sets of species occurring in a particular place and time (Fauth et al., 1996), both taxonomic and morphological, at each of the 22 stations sampled. Phytoplankton concentrations and composition were estimated using pigment analysis. Species abundance plots were constructed and compared to modeled distributions representing distinct patterns of species assemblies. The different model species abundance distributions are associated with different assumptions about the ecological equivalence of species and factors regulating the occurrence and abundance of individual species. The neutral model in which site-specific interactions and ecological differences between species are relatively unimportant was compared to models in which resource monopolization or species-interactions control community composition.

2 Methods

2.1 Tintinnid sampling and sample analysis

Station locations, sampling dates and depth strata sampled are given in Table 1. The cruise track is shown in Fig. 1. For tintinnids, usually 6 depths were sampled between the surface and just below the chlorophyll maximum depth (based on CTD fluorescence profiles) using a 20 l Niskin bottle. At each station, 5–10 l volumes of sample from each depth (total volumes for each station are given in Table 1) was concentrated to 20 ml by slowly and gently pouring the water through a 20 μ m mesh Nitex screen fixed to the bottom of a 10 cm dia. PVC tube. We have found that using a 20 μ m concentrator yields higher numbers of tintinnids than settling whole water samples, in agreement with Pierce and Turner (1994), and have used the method in previous studies (Cariou et al., 1999; Dolan and Gallegos, 2001). Concentrated water samples were fixed with Lugol's solution (2% final conc.). Aliquots (2–10 ml) of concentrated sample were settled in sedimentation chambers and subsequently, the entire surface of the chamber was examined using an inverted microscope at 200x total magnification. All material from all the samples was examined.

Tintinnid identifications were made based on lorica morphology and following Kofoid and Campbell (1929, 1939), Hada (1938) and Marshall (1969). Species of certain genera are known to be capable of displaying different lorica morphologies (e.g., Gold and Morales, 1976; Davis, 1981; Laval-Peuto, 1983; Wasik, 1988; Williams et al., 1994). We adopted a what we term a 'conservative' approach, that is pooling apparent varieties. However, only a

few of the 149 species encountered in this study appeared potentially variable and may, or may not, represent single species (*Dadayiella ganymedes-bulbosa-acuta*, *Tintinnopsis rapa-parva*, *Favella* spp., *Climacocylis* spp). Empty lorica were not enumerated. For each station, data from all samples were pooled. Average cell concentrations were calculated from total counts divided by total original water sample volumes. Concentrations in terms of carbon were estimated by 1) calculating lorica volumes for each species based on combinations of simple geometric forms (entire or fractional cylinders, cones, hemispheres), 2) converting lorica volume to carbon units using the empirical conversion factor 0.05 pg C per μm^3 of lorica volume reported by Verity and Langdon (1984).

2.2 Tintinnid diversity metrics

Taxonomic diversity was estimated for each sample as the Shannon index (ln-based, e.g., Magurran, 2004) and species richness. Morphological diversity was estimated by placing species into size-classes of lorica oral diameter (LOD). Each species was assigned the average dimensions reported in Koifoid and Campbell (1929, 1939), Campbell (1942) and Marshall (1969). LOD is considered the most conservative characteristic of tintinnid loricas (Laval-Peuto and Brownlee, 1986). Size-class diameters were binned over 4 μm intervals beginning with the overall smallest diameter encountered and continuing to the largest diameter encountered in a given sample. For each sample, morphological diversity was estimated as the number of size-classes occupied and a Shannon index of morphological diversity calculated using numbers and proportional importance of different size-classes (ln-based). Statistical relationships between diversity, concentration estimates, station occupation rates and morphological characteristics were examined using nonparametric Spearman Rank Correlation.

2.3 Tintinnid rank abundance curves

We constructed log-rank abundance curves for the tintinnid assemblages of each station by calculating relative abundance for each species and ranking species from highest to lowest and plotting ln(relative abundance) vs. rank. Then, for each assemblage, we constructed hypothetical log-rank abundance curves that could fit the data by using parameters of the particular assemblage. We constructed curves for three different models of community organization: geometric series, log-series, and log-normal.

A geometric series distribution represents the result of the priority exploitation of resources by species arriving sequentially in a community (Whittaker, 1972), and is modeled by assuming that each species' abundance is proportional to a fixed proportion p of remaining resources. Thus the relative abundance of the i th species is $(1-p)p^{i-1}$. For the tintinnid samples we used the relative abundance of the most abundant

species to estimate p . This differs from the approach recommended by Magurran (2004), which is to use the relative abundance p_i of the lowest-ranked species to iteratively calculate p in the equation: $p_i = (1-p)p^{i-1}$ where i is species rank. We felt that this curve-fitting approach forces the fitted line for the predicted geometric series to not have a minimum relative abundance less than that of the rarest species and tests simply whether the logarithm of relative abundances follows a straight line with species rank. Our method is more consistent with the original hypothesized mechanism of the geometric series (Whittaker, 1972; MacArthur, 1972) which is that the relative abundance of the most dominant species is equal to the proportion of resources or niche space it utilizes and that all lower ranked species will use the same proportion of remaining resources or niche species.

A log-series distribution represents the result of random dispersal from a larger community, such as a metacommunity in Hubbell's neutral theory (Hubbell, 2001). In a community exhibiting a log-series distribution, species having abundance n occur with frequency $\alpha x^n/n$, where x is a fitted parameter and α is Fisher's alpha, a measure of species diversity that is independent of total community abundance. For a given community with N total individuals and S species, x can be found (Magurran, 2004) by iteratively solving the following equation for x : $S/N = -\ln(1-x)(1-x)/x$ and then finding Fisher's alpha as $\alpha = N(1-x)/x$. For the tintinnid assemblages, we simply used the observed S and N for each sample to calculate x and α .

A log-normal species abundance distribution is thought to result from a large number of species of independent population dynamics with randomly varying (in either space or time) exponential growth, such that $N(i) \propto e^{r_i}$ where r_i is a random variable. Since $N(i)$ is a function of an exponential variable, $\ln(N(i))$ should be normally distributed (May, 1975). Alternatively, species in a community that are limited by multiple factors that act on population size in a multiplicative fashion should also exhibit a lognormal distribution of abundances. We calculated the expected lognormal species abundance distribution for each tintinnid sample by calculating the mean and standard deviation of ln(abundance) and generating three expected abundance distributions for the S species in the sample using the lognormal distribution macro program in an Excel[®] spreadsheet. We then calculated the mean abundance for each species, ranked from highest to lowest, and then calculated relative abundance.

For each station assemblage, the observed rank abundance distribution was compared to these three hypothetical models using a Bayesian approach: an Akaike Goodness of fit test (Burnham and Anderson, 2002). In this test, an Akaike Information Criterion (AIC) was determined as the natural logarithm of the mean (sum divided by S) of squared deviations between observed and predicted ln(relative abundance) for all ranked S species plus an additional term to correct for the number of estimated parameters, k (1 for geometric

series and 2 each for logseries and lognormal distributions): $(S+k)/(S-k-2)$. The lower the calculated AIC value, the better the fit. A difference of 1 in AIC corresponds roughly to a three-fold difference in fit, so this test statistic is sensitive enough for our data to judge the fit of the three different models.

2.4 Phytoplankton pigment sampling and analysis

Seawater samples from 10 depths at each station (except SE3 for which no samples were taken) were collected from the 12 L Niskin bottles of the rosette sampler. Volumes between 5.6 and 1 L (depending on the trophic conditions) were filtered onto 25 mm GF/F filters, and the filters stored in liquid nitrogen at -80°C until analysis on land. The samples were extracted in 3 mL methanol for a minimum of 1 h, with filter disruption by ultra-sonication. The clarified extracts were injected onto an *Agilent Technologies* 1100 series High Performance Liquid Chromatography (HPLC) system equipped with a refrigerated auto sampler and a column thermostat, according to a modified version of the method described by Van Heukelem and Thomas (2001). Separation was achieved within 28 min during a gradient elution between a Tetrabutylammonium acetate:Methanol mixture (30:70) and 100% methanol. The chromatographic column, a Zorbax-C8 XDB (3×150 mm) was maintained at 60°C . Chlorophyll *a*, divinyl chlorophyll *a* and derived products were detected at 667 nm and the other accessory pigments at 450 nm using a diode array detector. (Detection limits for chlorophyll *a* were 0.0001 mg m^{-3} , injection precision was 0.4%). The different pigments were identified using both their retention times and absorption spectra. Quantification involved an internal standard correction (Vitamin E acetate) and a calibration with external standards provided by *DHI Water and Environment* (Denmark).

Total chlorophyll *a* (TChl*a*) was assigned as the sum of chlorophyll *a*, divinyl chlorophyll *a* and chlorophyllide *a*. Seven diagnostic pigments (DP) were used to divide the phytoplankton population quantitatively, relative to the TChl*a* concentration, into three main size classes: picophytoplankton, nanophytoplankton and microphytoplankton using the following 4 equations according to Uitz et al. (2006):

- (1) **Pico ($\text{mg TChl}a \cdot \text{m}^{-3}$)** = TChl*a* (0.86 zeaxanthin + 1.01 chlorophyll *b* + 1.01 divinyl chlorophyll *b*)/DP
- (2) **Nano ($\text{mg TChl}a \cdot \text{m}^{-3}$)** = TChl*a* (0.35 19'-butanoyloxyfucoxanthin + 1.27 19'-hexanoyloxyfucoxanthin + 0.60 alloxanthin)/DP
- (3) **Micro ($\text{mg TChl}a \cdot \text{m}^{-3}$)** = TChl*a* (1.41 fucoxanthin + 1.41 peridinin)/DP
- (4) **DP** = (0.86 zeaxanthin + 1.01 chlorophyll *b* + 1.01 divinyl chlorophyll *b* + 0.35 19'-butanoyloxyfucoxanthin + 1.27 19'-hexanoyloxyfucoxanthin + 0.60 alloxanthin + 1.41 fucoxanthin + 1.41 peridinin)

Table 2. Tintinnid summary data. Data were pooled for each station. Thus, total number of tintinnids examined denoted by \sum cells, average concentrations of cells and carbon equivalents were calculated by dividing station sums by original sample volumes (see Table 1).

Station	\sum cells	Cells l^{-1}	ng C l^{-1}
SE3	107	10.7	51
MAR1	548	27.4	16
HLN1	480	16	70
STB1	235	7.8	29
STB2	82	4.1	18
STB3	105	4.2	24
STB4	98	3.9	16
STB6	101	3.5	4
STB8	115	2.0	4
GYR2	190	3.2	10
STB11	53	2.1	4
STB12	250	4.3	5
STB13	324	5.4	21
STB14	276	4.9	4
STB15	235	3.9	13
EGY2	354	6.6	37
STB17	314	5.0	22
STB18	376	7.0	158
STB20	1670	28.7	73
STB21	805	13.4	23
UPW2	2540	42.3	216
UPX2	665	17.1	50

Concentrations were integrated throughout the depth strata corresponding to that sampled for tintinnids. The size fractionated Chl*a* concentrations (pico, nano and micro) transformed into % total chlorophyll were used to estimate an index of the size-diversity of chlorophyll (Shannon index, ln-based). Statistical relationships were examined using non-parametric Spearman Rank Correlation. Pigment concentrations calculated using only data from the depths at which tintinnids were sampled gave very similar results. Here we present the pigment data based on all data available for the depth strata considered.

3 Results

3.1 Concentrations across the transect

Tintinnid and phytoplankton concentrations co-varied (Fig. 2). Average tintinnid concentrations ranged from about 2–42 cells l^{-1} and 4–216 ng C l^{-1} (Table 2). Concentrations of chlorophyll similarly varied over about 2.5 orders of magnitude, ranging 0.08–1.7 $\mu\text{g chl}a \text{ l}^{-1}$. Phytoplankton, based on pigment concentrations (Table 3), appeared to be roughly divided between pico-sized taxa and nano-sized

Table 3. Summary of phytoplankton pigment data. Layer denotes segment (m) of the water column sampled at 7–10 discrete depths (generally 9). CMD is the chlorophyll maximum depth (m) based on the chlorophyll vertical profile, $\Sigma\text{Chl } a$ is the average chlorophyll a concentration ($\mu\text{g l}^{-1}$) throughout the layer sampled. Total chlorophyll was partitioned into 3 size fractions (see methods); $p\text{Chl } a$, $n\text{Chl}$, μchl are, respectively, estimated average pico-sized, nano-sized and micro-size chlorophyll a concentrations as % total chlorophyll a throughout the layer sampled. Phytoplankton samples were not taken for Station SE3.

Station	Layer	CMD	$\Sigma\text{Chl } a$	$p\text{Chl}$	$n\text{Chl}$	μChl
MAR1	4–80	41	0.370	20.80	49.52	29.60
HLN1	4–140	79	0.191	57.53	33.64	8.82
STB1	4–140	100	0.165	55.45	35.98	8.61
STB2	5–130	100	0.137	62.20	31.62	5.18
STB3	4–120	120	0.115	65.69	29.25	5.06
STB4	5–210	158	0.113	62.44	32.14	5.42
STB6	5–250	190	0.076	59.76	34.34	5.90
STB8	5–240	209	0.079	53.34	39.73	6.93
GYR2	5–270	180	0.082	52.3	41.16	6.54
STB11	5–300	199	0.080	53.98	38.88	7.19
STB12	4–280	211	0.077	53.34	40.22	6.54
STB13	5–230	160	0.087	49.4	44.43	6.17
STB14	5–230	160	0.093	57.05	36.74	6.22
STB15	5–175	105	0.139	56.94	36.36	6.70
EGY2	5–190	80	0.143	50.93	42.67	6.40
STB17	6–175	95	0.138	34.99	52.62	12.40
STB18	4–140	50	0.153	39.49	48.53	12.00
STB20	5–140	40	0.247	46.00	38.78	15.20
STB21	15–90	51	0.413	25.64	50.76	23.60
UPW2	3–50	40	1.697	3.31	8.14	88.60
UPX2	3–60	3	0.716	45.27	7.61	47.10

taxa, with a minor contribution of micro-sized taxa at all stations except for the Marquise Island (MAR1) and upwelling stations (UPW, UPX).

3.2 Relationships among tintinnid diversity metrics and phytoplankton pigment parameters

Each of the tintinnid diversity metrics employed, taxonomic or morphological, were correlated with at least one other metric (Table 4). For example, species richness was high at all stations, ranging from 19 to 40 species, and correlated with the number lorica size-classes and the Shannon index H' . Values of Fisher's alpha were correlated with those of H' as well as the diversity of LOD (oral size classes). In contrast, there were few relationships among tintinnid diversity metrics and phytoplankton parameters (Table 5). Tintinnid taxonomic diversity as H' or Fisher's alpha was positively related to the depth of the chlorophyll maximum (Fig. 3). Fisher's alpha was also negatively related to average chlorophyll concentration and tintinnid concentration. The depth of the chlorophyll maximum layer was negatively related to av-

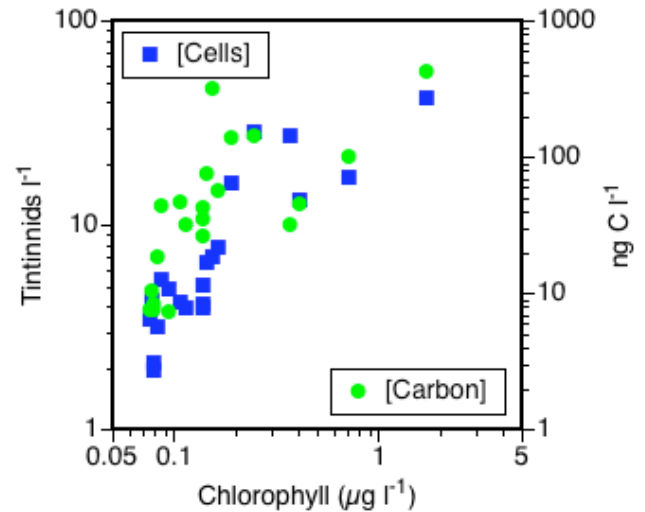


Fig. 2. Scatter plot of the relationship between phytoplankton concentration (as chlorophyll) and tintinnid ciliate abundance in terms of cells of carbon units among the stations. Data shown appears in Tables 2 and 3.

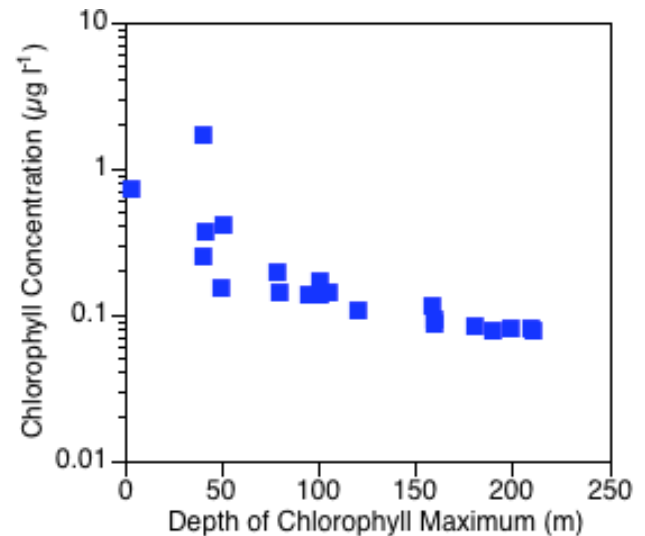


Fig. 3. Relationship between average chlorophyll concentration and the depth of the chlorophyll maximum layer among the stations sampled.

erage chlorophyll concentration (Table 3 and Fig. 4). Overall, tintinnid diversity appeared to be negatively related to resource availability as chlorophyll a and positively related to resource dispersion, in the form of the depth of the chlorophyll maximum layer.

3.3 Rank abundance distributions

Results of the analyses of species abundance distributions are summarized in Table 6 and examples of observed and

Table 4. Spearman rank correlation relationships (Rho values) among metrics of taxonomic and morphological diversity of tintinnids. For each station, estimates of taxonomic and morphological diversity were based on a pooled sample consisting of all individuals encountered in all samples from the station. Taxonomic metrics were numbers of species, the Shannon index, ln-based (H') and Fisher's alpha. Morphological metrics were numbers of lorica oral diameters (in $4\ \mu\text{m}$ size-classes) and the Shannon index of the diversity of lorica oral diameters (LOD- H'), calculated by substituting size-classes for species (see methods for details). For all pairs, $n=22$; asterisks denote significant relationships ($p=.01$). Note that measures of taxonomic diversity and morphological diversity co-vary positively.

	Taxonomic			Morphological	
	# species	H'	Fishers's alpha	# LOD s-c	LOD H'
# species	–	0.597*	0.318	0.727*	0.364
H'	0.597*	–	0.704*	0.396	0.550
Fisher's alpha	0.318	0.704*	–	0.176	0.596*
# LOD s-c	0.727*	0.396	0.176	–	0.415
LOD H'	0.364	0.550	0.596*	0.415	–

Table 5. Spearman rank correlation relationships (Rho values) among metrics of the diversity of tintinnids, their concentration and characteristics of the phytoplankton. For each station, estimates of taxonomic and morphological diversity were based on a pooled sample consisting of all individuals encountered in all samples from the station. Taxonomic metrics were numbers of species, the Shannon index, ln-based (H') and Fisher's alpha. Morphological metrics were numbers of lorica oral diameters (in $4\ \mu\text{m}$ size-classes) and the Shannon index of the diversity of lorica oral diameters (LOD- H'), calculated by substituting size-classes for species (see methods for details). Concentrations represent average water column integrated values. Chlorophyll H' , the phytoplankton size diversity parameter, reflects the relative contributions of micro, nano and pico-size cells to total chlorophyll. For all pairs, $n=21$; asterisks denote significant relationships ($p=.01$). Overall, diversity appears negatively related to tintinnid and chlorophyll concentrations and positively related to the depth of the chlorophyll maximum layer which declines with chlorophyll concentration (see Table 3).

	Taxonomic			Morphological	
	# species	H'	Fishers's alpha	# LOD s-c	LOD H'
log [tintinnids]	0.189	–0.195	–0.633*	0.250	–0.208
[chlorophyll]	0.051	–0.518	–0.709*	0.107	–0.372
chlorophyll H'	0.071	0.335	0.386	0.195	0.320
Depth Chl Max	0.027	0.587*	0.785*	–0.033	0.434

modeled distributions shown in Fig. 5. There was no obvious relationship between the type of rank abundance distribution and phytoplankton or tintinnid concentrations. The geometric series, describing a sequential monopolization of resources, described well only one tintinnid assemblage, that of St 17 which was highly dominated by a single species of *Eutintinnus*. The log-series, resembling that predicted by Hubbell's neutral theory (Hubbell, 2001), provided the best match to the observed pattern in 17 of the 21 stations. The log-normal distribution, thought to result from complex species interactions, provided the best fit for 3 of the stations.

4 Discussion

In agreement with reports from survey campaigns (Kofoid and Campbell, 1929, 1939; Campbell, 1949) we found the tintinnid assemblages of the SE Pacific to be very species-rich. Compared to recent geographic surveys of other areas,

we recorded 149 species compared to a total of 87 tintinnid species found along a transect from 42°N to 42°S from Italy through the Indian Ocean to New Zealand (Modigh et al., 2003), or the 70–80 species recorded from west to east Mediterranean transects (Dolan et al., 2000, 2002). We found about 30 species per location and this taxonomic diversity was paired with morphological diversity. Chlorophyll concentrations were quite low and the phytoplankton was dominated by small cells, except for stations those in or near the upwelling zone (Table 3), consistent with expectations from similar areas of the Pacific (Mackey et al., 2002).

The relationships of diversity of these micrograzers and food resources were similar to those found examining trends across the Mediterranean in the late spring/early summer (Dolan, 2000). Total abundance of tintinnids increased with chlorophyll while diversity decreased. The depth of the chlorophyll maximum layer, inversely related to chlorophyll concentration, was positively related to tintinnid diversity

Table 6. Results of analysis of the species abundance distributions. For the tintinnid community of each station, the log-rank abundance curve was compared to model-derived geometric, log normal and log-series curves using the Akaike test. Asterisks denote the lowest AIC value indicating the closest fit.

Station	log Normal	log Series	geometric	# spp	Dominant sp (% \sum cells)
MAR1	-0.032	-1.199*	7.24	37	<i>Steenstrupiella steenstrupii</i> (29%)
HLN1	-1.29*	0.074	7.68	35	<i>Steenstrupiella steenstrupii</i> (22%)
STB1	-1.63*	-0.603	8.06	40	<i>Proplectella perpusilla</i> (20%)
STB2	-0.22	-1.02*	5.30	19	<i>Steenstrupiella gracilis</i> (37%)
STB3	-1.72*	-1.24	7.23	31	<i>Cantheriella pyramidata</i> (25%)
STB4	-0.61	-1.88*	7.08	21	<i>Salpingella attenuata</i> (15%)
STB6	-0.36	-1.71*	8.89	22	<i>Steenstrupiella gracilis</i> (19%)
STB8	-0.48	-2.05*	7.50	27	<i>Parundella aculeata</i> (17%)
GYR2	-1.15	-2.09*	7.69	30	<i>Cantheriella pyramidata</i> (17%)
STB11	-0.74	-1.69*	6.76	19	<i>Salpingella decurtata</i> (17%)
STB12	-0.20	-0.54*	8.53	38	<i>Salpingella decurtata</i> (12%)
STB13	-1.17	-1.17	8.53	41	<i>Steenstrupiella steenstrupii</i> (14%)
STB14	0.63	-1.88*	8.00	36	<i>Salpingella curta</i> (18%)
STB15	-1.00	-1.57*	6.34	38	<i>Salpingella faurei</i> (16%)
EGY2	-1.33	-2.65*	6.42	38	<i>Protohabdonella striatura</i> (14%)
STB17	1.55	0.66	0.26*	19	<i>Eutintinnus apertus</i> (71%)
STB18	0.83	-1.39*	3.12	23	<i>Eutintinnus fraknoi</i> (50%)
STB20	-1.54	-2.37*	4.59	29	<i>Protohabdonella curta</i> (26%)
STB21	1.40	-0.77*	4.64	18	<i>Protohabdonella curta</i> (31%)
UPW2	-0.46	-1.03*	4.82	30	<i>Eutintinnus tubulosa</i> (39%)
UPX2	0.69	0.41*	6.15	32	<i>Condenellopsis pusilla</i> (47%)

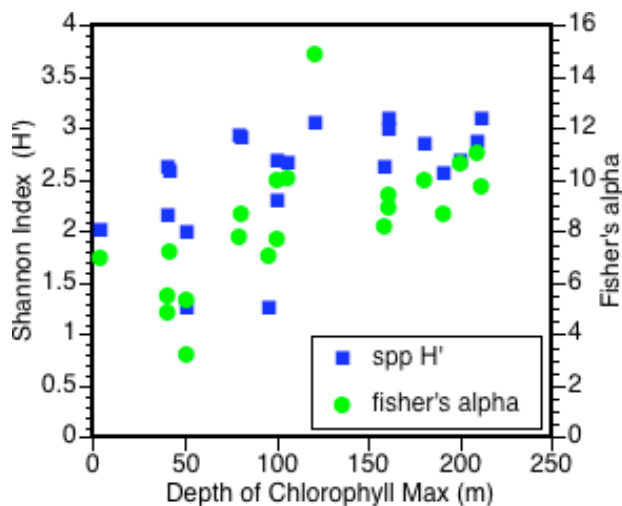


Fig. 4. Relationship between taxonomic diversity of the tintinnid community and the depth of the chlorophyll maximum layer.

(Dolan, 2000). In a subsequent study, based on samples taken at different stations in early fall from the Atlantic coast of Morocco to the Eastern Mediterranean, the only significant relationships found were between chlorophyll size-diversity and tintinnid diversity (Dolan et al., 2002). While

in the SE Pacific average concentrations of chlorophyll encountered were of a range very similar to that reported in the Mediterranean transects, tintinnid abundances were lower by about half compared to the Mediterranean (Dolan, 2000; Dolan et al., 2002). The apparent variable relationships between tintinnid diversity and resources as chlorophyll led us to examine the patterns of species assembly using rank abundance distributions. The different patterns of rank abundance we examined as possibilities (geometric, log-series and log-normal) are thought to reflect different mechanisms governing the assemblage of individual communities. The distinct distributions thus reflect different assumptions concerning the ecological equivalence of species and factors regulating the abundance of individual species. Our goal was to determine which pattern dominated and if species abundance pattern was variable.

The geometric series represents a community in which dominant species limit the occurrence of rare species (e.g., May, 1975). The most abundant species monopolizes, in proportion to its abundance, part of the limiting resource; the second ranked species, in proportion to its abundance, monopolizes a part of the remaining resource, and so on, to the least abundant species. All resources are exploited and the total number of species is then largely controlled by the degree of dominance exerted by the most abundant species. The geometric pattern is found, for example, in the early

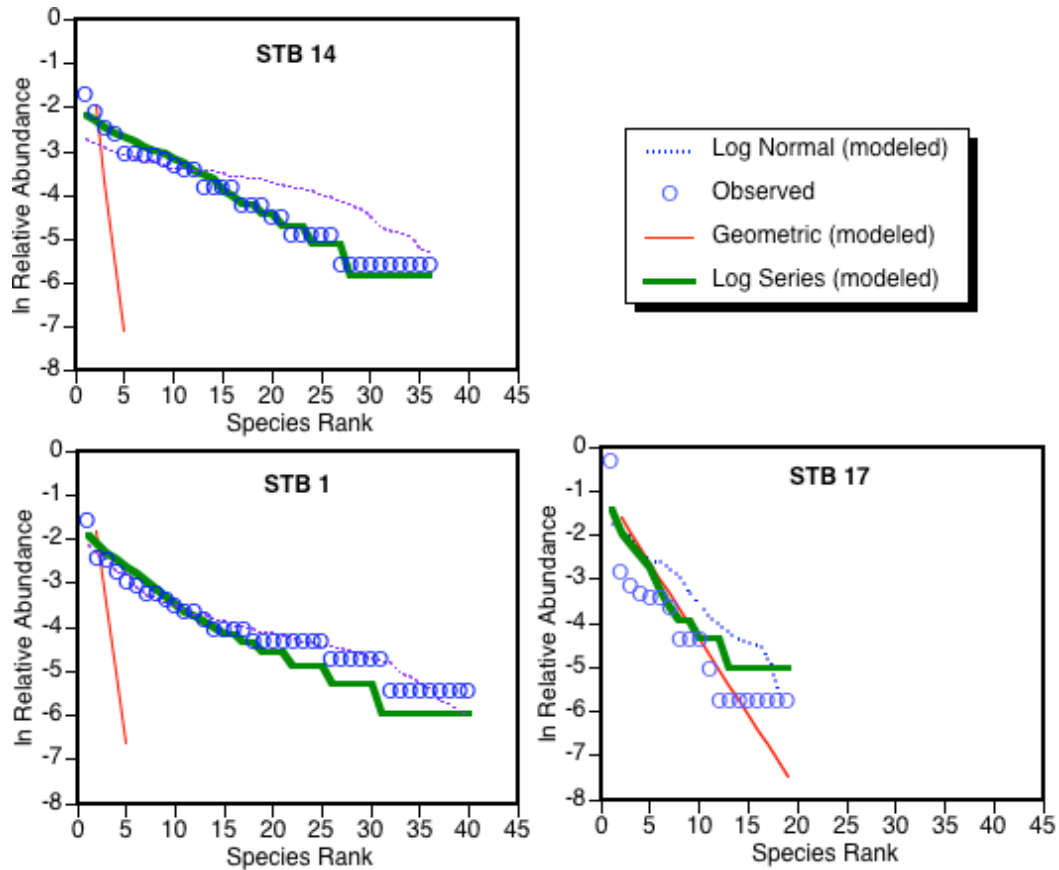


Fig. 5. Examples of species abundance distributions. Station STB 14 shows the most common pattern (15 of 21 data sets) of the log-series distribution providing the closest fit to the actual data. STB 1 was one of 3 data sets in which a log-normal distribution best matched the observed species abundance. STB 17, highly dominated by a single species (Table 4) was the only station for which the geometric distribution provided the closest fit.

successional stages among terrestrial plant communities or in relatively extreme environments (e.g. Whittaker, 1972).

A log-normal distribution represents a community in which populations are subjected to random variations or are affected by several interacting factors. It can result from a large number of species of independent population dynamics with randomly varying exponential growth, in either space or time (e.g., Huisman and Weissing, 1999). Alternatively, species in a community that are limited by multiple factors that act on population size in a multiplicative fashion should also exhibit a lognormal distribution of abundances. The log-normal species abundance distribution is the most common pattern exhibited by large assemblages (Magurran, 2004).

The log-series distribution of species abundance is predicted from Hubbell's neutral model. Local communities are part of a metacommunity, a larger widely dispersed (in space and time) group of trophically similar forms (Hubbell, 2001). With unlimited immigration, species abundance for a given community will resemble that of the larger metacommunity and will follow a log-series distribution (Magurran, 2004). Similar to the geometric series, ecological equiva-

lence of species is assumed but in contrast dispersal plays a determining role. Log-series distributions characterize a large variety of organisms (e.g., Hubbell, 2001; Alonso et al., 2006). Among planktonic organisms, marine diatoms, a group of ecologically similar organisms, show log-series distributions, but not dinoflagellates, a group which includes autotrophic, heterotrophic and mixotrophic species (Pueyo, 2006).

The tintinnid communities of the SE Pacific were not well-described by a geometric series, as this model predicted a much more rapid than observed decline in relative abundance with decreasing rank than did either log-series or log-normal models. The single exception was a community a single species represented 71% of cell numbers (Table 4). The log-series models fit the data best (lowest AIC) in 17 of 21 cases, which suggests that tintinnid communities are structured by dispersal limitation and exhibit weak if any competition at other than local (perhaps <1 m) scales. The log-normal distribution fit the data best in 3 cases which were not obviously distinct in any manner from the other communities.

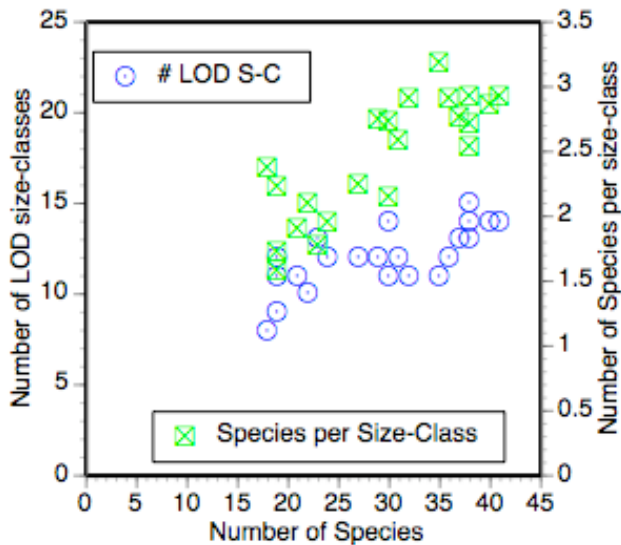


Fig. 6. Species packing in tintinnid communities across the SE Pacific Ocean. Comparing the different stations, both the number of mouth sizes, lorica oral diameter LOD in $4\ \mu\text{m}$ size – class intervals, and the average number of species per mouth size increased with the number of species.

Magurran (2004) has argued that species abundance distributions are difficult to compare for samples with less than 30 species, because small samples may represent a sampling of the right-hand “tail” of a lognormal distribution and therefore not detect species from the left-hand tail that are essentially “veiled” to the observer. However, we found that for communities with <30 species, the fit of the log-series distribution actually improved (AIC declined) as species richness increased. Although some station data may reflect partial samples of communities that are otherwise described best with a log-normal distribution, the consistent best fit of the log-series distribution to the tintinnid data, particularly for communities with low total abundance and/or high species richness, could reflect the prevalence of mechanisms, such as neutral dispersal (Hubbell 2001), that lead to a log-series distribution.

The neutral model, due largely to its assumption of ecological equivalency among species within a community, has generated a great deal of controversy (for recent examples see Holyoak and Loreau, 2006; McGill et al., 2006; Alonso et al., 2006). There are differences of ecological significance between tintinnid species, for example LOD is related to the size of prey most efficiently grazed. However, in the SE Pacific competitive interactions may not be important simply because the food resources are insufficient or of the inappropriate size. Ritchie (1997) predicted theoretically that scarce food can lead to effective dispersal limitation rather than competition because each consumer population may not encounter all available food items within some specified time. Such a mechanism might explain why SE Pacific tintinnid communities appear to be random collections of species.

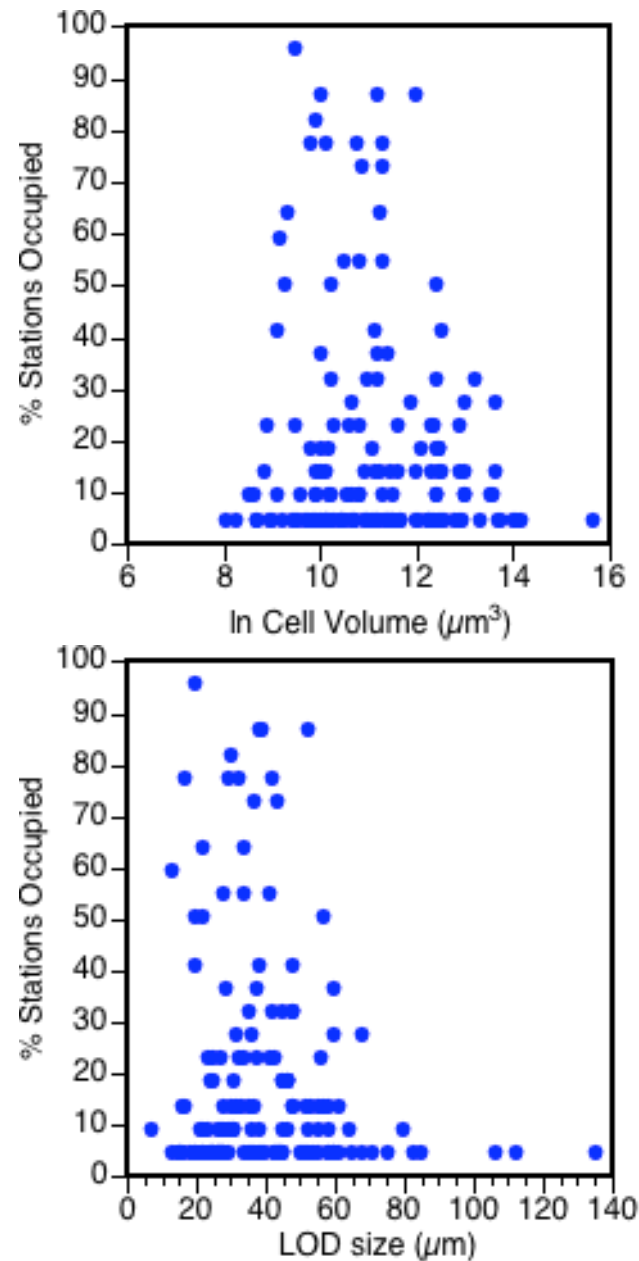


Fig. 7. Scatter plots of occurrence rates of tintinnid species, as a % of stations occupied, among the stations and morphological characteristics. The top panel shows the lack of relationship of occurrence rate and lorica volume (Rho value= -0.003 , $p=0.97$) and the bottom panel shows a similar lack of relation with LOD size (Rho value= -0.028 , $p=0.73$). Thus, neither lorica volume nor oral diameter appear linked to average occurrence.

To further test whether tintinnid communities are structured by resource partitioning versus dispersal in the SE Pacific, we examined the relationship between numbers of species in a community and numbers of distinct LOD size-classes composing the community and the number of species

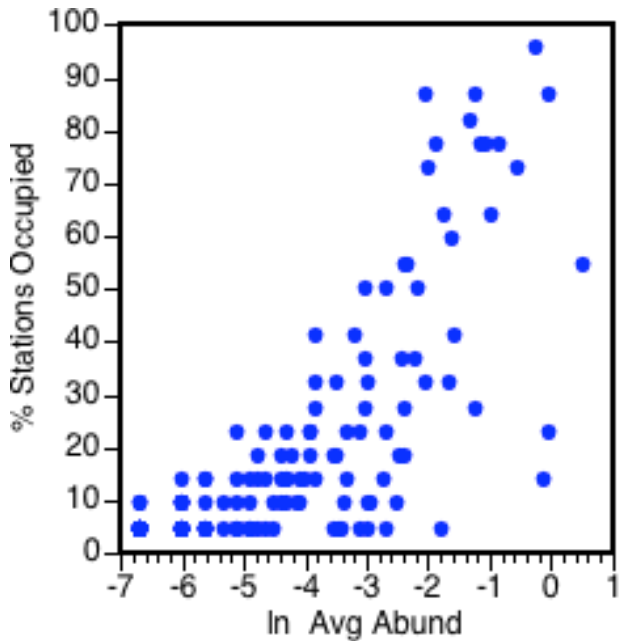


Fig. 8. Scatter plot of occurrence rate of tintinnid species, as a % of stations occupied, against average abundance across all the stations. The positive relationship between average abundance and occurrence (Rho value of 0.796, $p < 0.0001$) supports the idea that overall population size determines occurrence rate. Recall that morphology appears to be unrelated to occurrence rate (Fig. 7).

per LOD size-class within the community. We reasoned that if resource partitioning were strong, species-richness would reflect either larger ranges of allowed morphologies (more size-classes) or more species sharing the same resources (more species per size-class) but probably not both. We hypothesized that if species were added to communities at random, species-rich communities would exhibit both more size classes as well as more species per size class. Among the communities, we found that species numbers increase with numbers of distinct size-classes present and species per size-class of LOD (Fig. 6).

We also examined the importance of individual species characteristics in determining occurrence, by plotting occurrence rate, as % stations occupied, against lorica volume or LOD for each species and found no relationships (Fig. 7). On the other hand, occupation rate was positively related to average abundance across all stations (Fig. 8). This last relationship is expected if occurrence of a species at a given site is dependent only on the large-scale population size of the species. The species with high occupation rates did not share any obvious morphological characteristics (Fig. 9). These species can be described as wide-spread, having all been found in both the Mediterranean and New Caledonia (Dolan, 2000; Dolan et al., 2006).

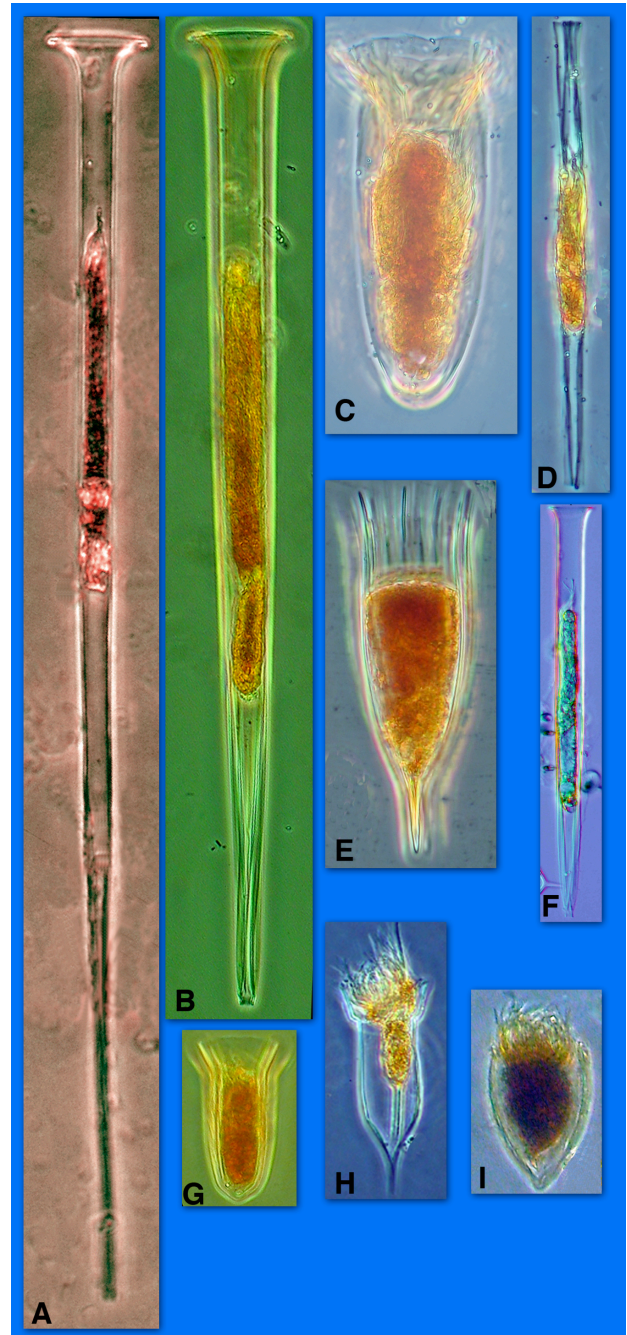


Fig. 9. Photomicrographs of tintinnid species found in over 75% of the stations sampled: *Salpingella attenuata* (A), *Salpingella acuminata* (B), *Amphorella* (*Amphorides*) *quadrilineata* (C), *Salpingella faureii* (D), *Dadayiella ganymedes* (E), *Salpingella decurtata* (F), *Cantheriella pyrimidata* (G), *Ormsella trachelium* (H), *Protorhabdonella simplex* (I). *Dadayiella ganymedes* (E) is 100 μm in total length. Note that these wide-spread species do not share any obvious morphological characteristics.

Overall we found evidence that tintinnid communities in the SE Pacific could be described by Hubbell's neutral theory. The patterns we found could be specific to the conditions we encountered of sparse resources combined with a large species pool. In this regard it is worth recalling that diversity increased among the stations with the depth of the chlorophyll maximum layer and decreased with the concentration of chlorophyll. High diversity was found with little food spread over a wide area coupled with low abundances of tintinnids, providing little opportunity for inter-specific relationships.

The neutral theory serves well as a null hypothesis when examining patterns of community composition. On the other hand, evidence supporting (as opposed to not disproving) dispersal limitation requires comparison of spatially distinct communities along some reasonable gradient with regard to dispersal (e.g. Condit et al., 2002). Our data for the SE Pacific do not permit an examination of actual dispersal using for example species decay. The stations sampled were across distinct water masses and current systems. In future investigations we hope to sample coherently within a single set of hydrological conditions (e.g., Thompson and Alder, 2005).

Our study re-visited a region and documented a surprising variety of forms, many of which were described from very few specimens and so whose existence could be doubted (Dolan, 2006). The correspondence of these forms with species is another question entirely. Cytological work on common coastal forms of *Tintinnopsis* suggests that there are likely about twice as many species catalogued (based on lorica morphology) as actually distinguishable via ciliary pattern (Agatha and Riedel-Lorjé, 2006; Laval-Pueto and Brownlee, 1986). Our data show that substituting morphological categories for classical species designations yields very similar results with regard to estimates of diversity or patterns of community assembly. Clearly, the next step is the use of genetic categories along with (or rather than) classical species designations, morphology will remain of interest as the means by which an organism interacts with its environment and other organisms.

5 Conclusions

Large numbers of tintinnid taxa were found, 18–41 species per station, with a total species pool of 149. While, morphological and taxonomic diversity metrics of tintinnid communities co-varied they were not significantly related to phytoplankton diversity estimated using a pigment-based size-diversity metric. Taxonomic diversity of tintinnids, as H' or Fishers' alpha, was inversely related to chlorophyll concentration and positively to the depth of the chlorophyll maximum layer. The species abundance distributions compared to geometric, log-series and log-normal distributions showed that for most stations, the observed distribution most closely matched log-series, coherent with the neutral theory of ran-

dom colonization from a large species pool. Occurrence rates of species were correlated with average abundance rather than specific characteristics of biomass or lorica oral diameter (mouth) size. Among stations, species richness was correlated with both the variety of mouth sizes (lorica oral diameters) as well as numbers of species per mouth size, also consistent with random colonization.

Acknowledgements. The samples for this work were taken by L. Garczarek and M. Viprey of the Roscoff Oceanic Plankton Group and we are truly grateful for it represented a large amount of work. The BIOSOPE cruise was admirably organized and managed by H. Claustre and financed through the French national program "PROOF". Financial support was also provided by the Marplan project, part of the MARBEF Network of Excellence (Contract No. GOCE-CT-2003-505446). This is contribution MPS-07031 of MARBEF. The manuscript profited from the comments of the official reviewers (G. A. Thompson, G. B. McManus, G. Chust, X. Irigoien) as well as colleagues generous with their time (R. Colwell, B. McGill, B. Hawkins, T. Fenchel, J. Huisman, J. Henjes). However, we retain credit for all errors of fact and interpretation.

Edited by: W. Kiessling

References

- Agatha, S. and Riedel-Lorjé, J. C.: Redescription of *Tintinnopsis cylindrica*, Daday 1887 (Ciliophora, Spirotricha) and unification of tintinnid morphology, *Acta Protozool.*, 45, 137–151, 2006.
- Agatha, S. and Stüder-Kypke, M. C.: Phylogeny of the order Choreotrichida (Ciliophora, Spirotricha, Oligotrichea) as inferred from morphology, ultrastructure, ontogenesis, and SSrRNA gene sequences, *Eur. J. Protistol.*, 43, 37–63, 2007.
- Agatha, S., Strüder-Kypke, M. C., Beran, A., and Lynn, D. H.: *Pelagostrobilidium neptuni* (Montagnes and Taylor, 1994) and *Strombidium biarmatum* nov. spec. (Ciliophora, Oligotrichea): phylogenetic position inferred from morphology, ontogenesis, and gene sequence data, *Eur. J. Protistol.*, 41, 65–83, 2005.
- Alonso, D., Etienne, R. S., and McKane, A. J.: The merits of neutral theory, *Trends Ecol. Evol.*, 21, 451–457, 2006.
- Beers, J. R. and Stewart, G. L.: Microzooplankton in the plankton communities of the upper waters of the eastern tropical Pacific, *Deep-Sea Res.*, 18, 861–883, 1971.
- Burnham K. P. and Anderson D. R.: Model selection and multi-model inference: a practical information-theoretic approach, Springer, New York, 2002
- Campbell, A. S. : The Oceanic Tintinnina of the plankton gathered during the last cruise of the Carnegie, Carnegie Institution of Washington, Washington D.C., Publication 537, 1942.
- Cariou, J. B., Dolan, J. R., and Dallot, S.: A preliminary study of tintinnid diversity in the NW Mediterranean Sea, *J. Plank. Res.*, 21, 1065–1075, 1999.
- Condit, R., Pitman, N., Leigh, E. G., Chave, J., Terborgh, J., Foster, R. B., Nunez, P. B., Aguilar, S., Valencia, R., Villa, G. Muller-Landau, H. C., Losos, E., and Hubbell, S. P.: Beta-diversity in tropical forest trees, *Science*, 295, 666–669, 2002.

- Davis, C. C.: Variations of lorica shape in the genus *Ptychocylis* (Protozoa: Tintinnia) in relation to species identification, *J. Plank. Res.*, 3, 433–443, 1981.
- Dolan, J. R.: Tintinnid ciliate diversity in the Mediterranean Sea: longitudinal patterns related to water column structure in late spring-early summer, *Aquat. Microb. Ecol.*, 22, 20–30, 2000.
- Dolan, J. R.: Re-discovered beauty – new images for old descriptions - tropical tintinnids of the genus *Xystonellopsis* (Ciliophora, Tintinnia), *Protist*, 157, 251–253, 2006.
- Dolan, J. R. and Gallegos, C. L.: Estuarine diversity of tintinnids (planktonic ciliates), *J. Plank. Res.*, 23, 1009–1027, 2001.
- Dolan, J. R. and Marassé, C.: Planktonic ciliate distribution relative to a deep chlorophyll maximum: Catalan Sea, N.W. Mediterranean, June 1993, *Deep-Sea Res.* 1, 42, 1965–1987, 1995.
- Dolan, J. R., Claustre, H., Carlotti, F., Plounevez, S., and Moutin, T.: Microzooplankton diversity: relationships of tintinnid ciliates with resources, competitors and predators from the Atlantic coast of Morocco to the eastern Mediterranean, *Deep-Sea Res.* 1, 49, 1217–1232, 2002.
- Dolan, J. R., Jacquet, S., and Torrétón, J.-P.: Comparing taxonomic and morphological biodiversity of tintinnids (planktonic ciliates) of New Caledonia, *Limnol. Oceanogr.*, 51, 950–958, 2006.
- Fauth, J. E., Bernardo, C., Camara, M., Resetarits, W. J., Van Burskik, J., and McCollim, S. A.: Simplifying the jargon of community ecology: a conceptual approach, *Am. Nat.*, 147, 282–286, 1996.
- Gold, K. and Morales, E. A.: Studies on the sizes, shapes, and the development of the lorica of agglutinated tintinnida, *Biol. Bull.*, 150, 377–392, 1976.
- Hada, Y.: Studies on the Tintinnoinea from the Western Tropical Pacific, *J. Fac. Sci. Hokkaido Imper. Univ. Ser. IV Zool.*, 6, 87–190, 1938.
- Hasle, G. R.: A quantitative study of phytoplankton from the equatorial Pacific, *Deep-Sea Res.*, 6, 38–59, 1959.
- Heinbokel, J. F.: Studies on the functional role of tintinnids in the Southern California Bight. II. Grazing rates of field populations, *Mar. Biol.*, 47, 191–197, 1978.
- Holyoak, M. and Loreau, M.: Reconciling empirical ecology with neutral community models, *Ecology*, 87, 1370–1377, 2006.
- Hubbell, S. R.: The unified neutral theory of biodiversity and biogeography, Princeton, USA, Princeton University Press, 2001.
- Huisman, J. and Weissing, F. J.: Biodiversity of plankton by species oscillations and chaos, *Nature*, 402, 407–410, 1999.
- Karayanni, H., Christaki, U., Van Wambeke, F., Denis, M., and Moutin, T.: Influence of ciliated protozoa and heterotrophic nanoflagellates on the fate of primary production in the northeast Atlantic Ocean, *J. Geophys. Res.-Oceans*, 110(C7), C07S1, doi:10.1029/2004JC002602, 2005.
- Kofoed, C. A. and Campbell, A. S.: A conspectus of the marine and fresh-water ciliata belonging to the suborder tintinnoinea, with descriptions of new species principally from the Agassiz expedition to the eastern tropical Pacific 1904–1905, *Univ. Calif. Publ. Zool.*, 34, 1–403, 1929.
- Kofoed, C. A. and Campbell, A. S.: The Tintinnoinea of the eastern tropical Pacific, *Bull. Mus. Compar. Zool. Harvard Coll.*, 84, 1–473, 1939.
- Laval-Peuto, M.: Sexual reproduction in *Favella ehrenbergii* (Ciliophora, Tintinnia): taxonomic implications, *Protistologica*, 19, 503–512, 1983.
- Laval-Peuto, M. and Brownlee, D. C.: Identification and systematics of the tintinnia (Ciliophora): evaluation and suggestions for improvement, *Ann. Inst. Océanogr. Paris*, 62, 69–84, 1986.
- Lynn, D. H. and Small, E. B.: Phylum Ciliophora, in: An illustrated guide to the protozoa, edited by: Lee, J. J., Leedale, G. F., and Bradbury, P., Lawrence, USA, Society of Protozoologists, 371–656, 2002.
- MacArthur, R. H.: Geographical Ecology: Patterns in the Distribution and Abundance of Species, Harper and Row, New York, 1972.
- Mackey, D. J., Blanchot, J., Higgins, H. W., and Neveux, J.: Phytoplankton abundances and community structure in the equatorial Pacific, *Deep-Sea Res.* II, 49, 2561–2582, 2002.
- Magurran, A. E.: Measuring Biological Diversity, London, UK, Blackwell Publishing, 2004.
- Marshall, S. M.: Protozoa, order Tintinnia, Conseil International pour l'Exploration de la Mer, Copenhagen, Denmark, CIEM, Fiches d'Identification de Zooplancton, fiches, 117–127, 1969.
- May, R. M.: Patterns of species abundance and diversity, in: Ecology and evolution of communities, edited by: Cody, M. L. and Diamond, J. M., Boston, USA, Harvard University Press, 81–120, 1975.
- McGill, B. J., Maurer, B. A., and Weiser, M. D.: Empirical evaluation of neutral theory, *Ecology*, 87, 1411–1423, 2006.
- Modigh, M., Castalado, S., Saggiomo, M., and Santarpia, I.: Distribution of tintinnid species from 42° N to 43° S through the Indian Ocean, *Hydrobiologia*, 503, 251–262, 2003.
- Morel, A., Gentili, B., Claustre, H., Babin, M., Bricaud, A., Ras, J., and Tièche, F.: Optical properties of the “clearest” natural waters, *Limnol. Oceanogr.*, 52, 217–229, 2007.
- Pierce, R. W. and Turner, J. T.: Plankton studies in Buzzards Bay, Massachusetts, USA. IV. Tintinnids, 1987 to 1988, *Mar. Ecol. Prog. Ser.*, 112, 235–240, 1994.
- Pueyo, S.: Diversity: between neutrality and structure, *Oikos*, 112, 392–405, 2006.
- Leising, A. W., Gentleman, W. C., and Frost, B. W.: The threshold feeding response of microzooplankton within Pacific high-nitrate low-chlorophyll ecosystem models under steady and variable iron input, *Deep-Sea Res.* II, 50, 2877–2894, 2003.
- Ritchie, M. E.: Population dynamics in a landscape context: sources, sinks, and metapopulations, in: Wildlife and Landscape Ecology, edited by: Bissonette, J. A., Springer, New York, USA, 160–184, 1997.
- Snoeybos-West, O. L. O., Salcedo, T., McManus, G. B., and Katz, L.: Insights into the diversity of choreotrich and oligotrich ciliates (class Spirotrichea) based on genealogical analyses of multilocus loci, *Int. J. Syst. Evol. Microbiol.*, 52, 1901–1913, 2002.
- Thompson, G. A. and Alder, V. A.: Pattern in tintinnid species composition and abundance in relation to hydrological conditions of the southwestern Atlantic during austral spring, *Aquat. Microb. Ecol.*, 40, 85–101, 2005.
- Uitz, J., Claustre, H., Morel, A., and Hooker, S.: Vertical distribution of phytoplankton communities in open ocean: an assessment based on surface chlorophyll, *J. Geophys. Res.*, 111, C08005, doi:10.1029/2005JC003207, 2006.
- Van Heukelem, L. and Thomas, C. S.: Computer-assisted high-performance liquid chromatography method development with applications to the isolation and analysis of phytoplankton pigments, *J. Chromatogr. A*, 910, 31–49, 2001.

- Verity, P. G.: Abundance, community composition, size distribution, and production rates of tintinnids in Narragansett Bay, Rhode Island. *Est. Coast. Shelf Sci.*, 24, 671–690, 1987.
- Verity, P. G. and Langdon, C.: Relationships between lorica volume, carbon, nitrogen, and ATP content of tintinnids in Narragansett Bay, *J. Plank. Res.*, 6, 859–868, 1984.
- Wasik, A.: Antarctic tintinnids: their ecology, morphology, ultrastructure and polymorphism, *Acta Protozool.*, 37, 5–15, 1988.
- Williams, R., McCall, H., Pierce, R. W., and Turner, J. T.: Speciation of the tintinnid genus *Cymatocylis* by morphometric analysis of the loricae, *Mar. Ecol. Prog. Ser.*, 107, 263–272, 1994.
- Whittaker, R. H.: Evolution and measurement of species diversity, *Taxon*, 21, 213–251, 1972.

Nitrous oxide distribution and its origin in the central and eastern South Pacific Subtropical Gyre

J. Charpentier^{1,2}, L. Farias², N. Yoshida^{3,4}, N. Boontanon^{4,5}, and P. Raimbault⁶

¹Programa de Postgrado, Departamento de Oceanografía, Facultad de Ciencias Naturales y Oceanográficas, Universidad de Concepción, Chile

²Departamento de Oceanografía & Centro Oceanográfico del Pacífico Sur (COPAS), Universidad de Concepción, Concepción, Chile

³Frontier Collaborative Research Center, Tokyo Institute of Technology, Midori-ku, Yokohama, Japan

⁴SORST project, JST, Kawaguchi, Saitama, Japan

⁵Faculty of Environment and Resource Studies, Mahidol University 999 Phuttamonthon 4 Road, Phuttamonthon, Salaya, Nakhon Pathom 73170, Thailand

⁶Laboratoire d'Océanographie et de Biogéochimie (CNRS UMR 6535), Centre d'Océanologie de Marseille, Campus de Luminy, Marseille Cedex, France

Received: 10 May 2007 – Published in Biogeosciences Discuss.: 25 May 2007

Revised: 22 August 2007 – Accepted: 12 September 2007 – Published: 13 September 2007

Abstract. The mechanisms of microbial nitrous oxide (N_2O) production in the ocean have been the subject of many discussions in recent years. New isotopomeric tools can further refine our knowledge of N_2O sources in natural environments. This study compares hydrographic, N_2O concentration, and N_2O isotopic and isotopomeric data from three stations along a coast-perpendicular transect in the South Pacific Ocean, extending from the center (Sts. GYR and EGY) of the subtropical oligotrophic gyre ($\sim 26^\circ \text{S}$; 114°W) to the upwelling zone (St. UPX) off the central Chilean coast ($\sim 34^\circ \text{S}$). Although $\text{AOU}/\text{N}_2\text{O}$ and NO_3^- trends support the idea that most of the N_2O (mainly from intermediate water (200–600 m)) comes from nitrification, N_2O isotopomeric composition (intramolecular distribution of ^{15}N isotopes) expressed as SP (site preference of ^{15}N) shows low values (10 to 12‰) that could be attributed to the production through of microbial nitrifier denitrification (reduction of nitrite to N_2O mediated by ammonium oxidizers). The coincidence of this SP signal with high – stability layer, where sinking organic particles can accumulate, suggests that N_2O could be produced by nitrifier denitrification inside particles. It is postulated that deceleration of particles in the pycnocline can modify the advection - diffusion balance inside particles, allowing the accumulation of nitrite and O_2 depletion suitable for nitrifier denitrification. As lateral advection seems to be relatively insignificant in the gyre, in situ nitrifier denitrification could account for 40–50% of the N_2O produced in this

layer. In contrast, coastal upwelling system is characterized by O_2 deficient condition and some N deficit in a eutrophic system. Here, N_2O accumulates up to 480% saturation, and isotopic and isotopomer signals show highly complex N_2O production processes, which presumably reflect both the effect of nitrification and denitrification at low O_2 levels on N_2O production, but net N_2O consumption by denitrification was not observed.

1 Introduction

N_2O exists in the atmosphere at trace levels. However, this “greenhouse gas” is of great environmental importance. It is 170 to 300 times more efficient (per molecule) than CO_2 (Manne and Richels 2001) in trapping infrared radiation and accounts for 5–6% of the greenhouse effect (Law and Ling 2001). The oceans are a net source of N_2O for the atmosphere, with an estimated average annual emission of 6 Tg N year⁻¹, corresponding to 20% of the global emissions (Nevison et al., 1995).

The relative importance of the biological processes producing N_2O remains unclear. Nitrification is a chemotrophic process by which NH_4^+ and NO_2^- are aerobically oxidized to fix inorganic carbon. These reactions are carried out in two stages by different groups of microorganisms (Ward 2000). The first stage is ammonium oxidation to nitrite, carried out by microorganisms called ammonium-oxidizers. In this reaction, hydroxylamine acts as an intermediate and has been proposed as a precursor of N_2O , although the biochemical

Correspondence to: J. Charpentier
(jcharpentier@prof.udec.cl)

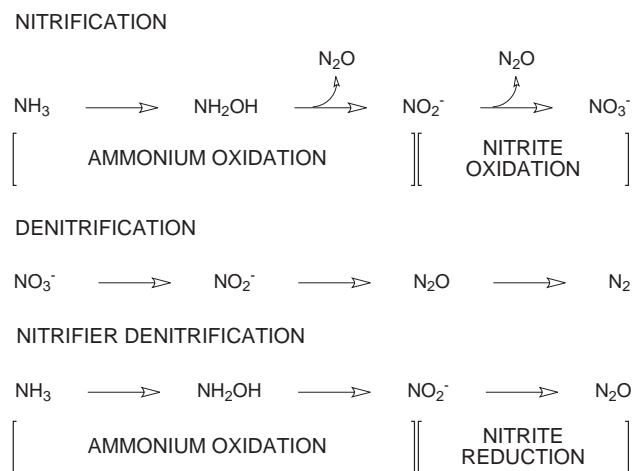


Fig. 1. Outline of different pathways of N_2O production. Adapted from Wrage et al. (2001).

mechanism by which it is formed is not clear (Naqvi and Noronha, 1991; Ostrom et al., 2000). Recent works have shown that certain *Archaea* can also oxidize ammonium to nitrite with a metabolism similar to that of bacterial ammonium oxidation (Konneke et al., 2005). The second stage is nitrite oxidation to nitrate, with nitric oxide acting as an intermediate and possible precursor of N_2O . This process is carried out by organisms called nitrite-oxidizers.

Conventional denitrification is the reduction of oxidized inorganic nitrogen (NO_3^- , NO_2^- , NO , N_2O) to gaseous nitrogen forms (N_2 , N_2O), and involves a loss of fixed-nitrogen from the system. This process is carried out by several organisms as a respiration process under suboxic (<0.1 ml/L O_2) conditions, with nitrate as the electron acceptor (Knowles, 1982). For this reason, denitrification is enhanced in O_2 minimum areas (Codispoti et al., 2001; Gruber and Sarmiento, 1997) or in areas where large accumulation of particulate organic matter takes place, such as the pycnocline (Allredge and Cohen 1987). Denitrification occurs in several stages, during which N_2O is an intermediate, unlike nitrification. Thus, N_2O can be both produced and consumed during denitrification (Elkins et al., 1978). Under suboxic conditions (<0.1 ml/L), N_2O produced by denitrification is almost entirely reduced to N_2 , whereas at the oxycline, where the O_2 concentration is near 0.5 ml/L, the N_2O production rate significantly increases and the reduction of N_2O to nitrogen is inhibited (Castro and Farías, 2004).

Moreover, certain species of nitrifying bacteria can produce N_2O under O_2 stress conditions (< 1 ml/L) by means of ammonium oxidation to nitrite, which in turn is reduced to N_2O ; this process is called “nitrifier denitrification” (Poth and Focht, 1985). This process is carried out by ammonium oxidizers like *Nitrosomona europaea* (Ritchie and Nicholas, 1972; Shaw et al., 2006). Biochemical studies show that the second part of this process indeed corresponds to denitrifica-

tion, and that the involved enzymes could be the same (Poth and Focht, 1985). Otherwise, the genomes of ammonium oxidizing archaea also present nitrite reductase and nitric oxide reductase genes, potentially allowing them to carry out nitrifier denitrification (Hallam et al., 2006; Treusch et al., 2005). Figure 1 shows a general outline of these processes.

Recently, some additional processes have been recognized as a part of the marine nitrogen cycle, particularly the anammox reaction ($\text{NO}_2^- + \text{NH}_4^+ \rightarrow \text{N}_2 + 2\text{H}_2\text{O}$), which result in a loss of nitrogen from the system as nitrogen gas (N_2). Kartal et al. (2007) found that *Kuenenia stuttgartiensis*, an anammox bacterium, can produce small quantities of N_2O as a byproduct of anammox.

The typical vertical distribution of N_2O in the open ocean shows that it is directly correlated with nitrate and inversely correlated with O_2 (Nevison et al., 2003; Oudot et al., 2002). Since nitrification is favored at low O_2 concentrations (Carlucci and McNally, 1969; Goreau et al., 1980), this distribution has usually been interpreted as an indirect evidence that nitrification is the dominant process in oceanic N_2O formation. Isotopic data, however, show that $\delta^{15}\text{N}(\text{N}_2\text{O})$ values are higher than expected for N_2O produced by nitrification in areas where the relationship between O_2 , N_2O , and nitrate indicates that nitrification is the dominant process (Dore et al., 1998; Kim and Craig, 1990; Naqvi et al., 1998; Ostrom et al., 2000; Yoshida, 1988; Yoshida et al., 1989).

The determination of N_2O isotopomers (i.e., the intramolecular distribution of ^{15}N in the linear NNO molecule) offers a useful and relatively new tool for elucidating N_2O production mechanisms (Toyoda and Yoshida 1999). $\delta^{15}\text{N}^\alpha$ is the relative isotopic abundance of ^{15}N for the central position and $\delta^{15}\text{N}^\beta$ for the terminal position. Site preference (SP) is defined as follows:

$$S.P. = \delta^{15}\text{N}^\alpha - \delta^{15}\text{N}^\beta \quad (1)$$

Since N_2O precursors contain only one nitrogen atom (NO_2^- , NO , NH_2OH) and excluding the possibility that different chemical species combine to form N_2O , the isotopomer distribution in N_2O should be independent of the $\delta^{15}\text{N}$ of the precursors. It can, therefore, be determined by the biochemical reaction step in which equivalence between both nitrogen atoms is lost (Toyoda et al., 2002). This is the main advantage of the N_2O isotopomer ratio over the conventional $\delta^{15}\text{N}$ ratio. Nevertheless, the lack of knowledge of the specific biochemical mechanisms involved in N_2O production makes it difficult to “predict” which isotopomer signature corresponds to which particular processes (Schmidt et al., 2004). The few works that present isotopomer results in marine environments have found positive SP values associated with nitrification (Popp et al., 2002; Toyoda et al., 2002) or denitrification (Westley et al., 2006; Yamagishi et al., 2005). The main problem in interpreting these results is the context of N_2O production processes and how these processes influence the isotopomer signal.

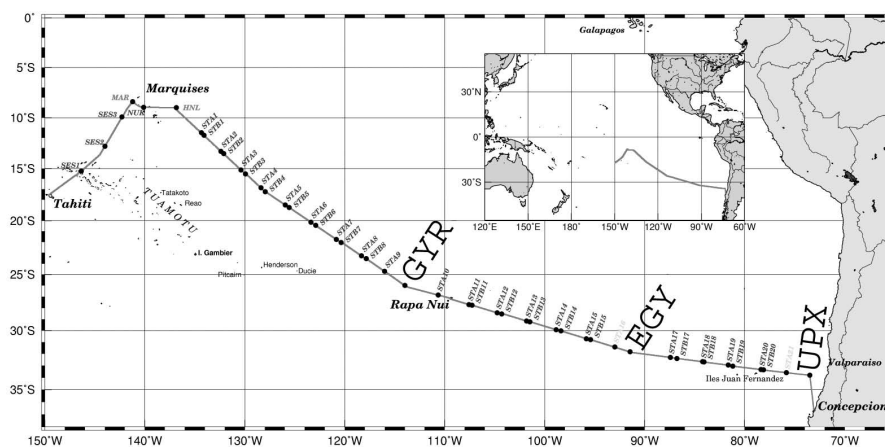


Fig. 2. Sampled stations during Biosope Cruise, GYR, EGY and UPX are indicated in bigger letters.

The South Pacific Central Gyre has been described as the most oligotrophic zone in the world ocean (Claustre and Maritorena, 2003), with an extreme nutrient (N, Fe) limitation (Bonnet et al., 2007); it is also one of the least studied areas of the ocean (Daneri and Quiñones, 2001). In contrast, the central Chile upwelling system is one of the most productive marine environments in the world, with a high supply of nitrate and other nutrients due to an upwelling regime and coastal contribution through land runoff, which supports a high rate of new production (Daneri et al., 2000). In addition, this area contains the southernmost extension of the O₂ minimum zone (OMZ), fed from the equator by the Peru Chile Undercurrent (PCUC); the OMZ has a significant influence on the water column community (Morales et al., 1996). Thus, the transect stretching from the center of the gyre to the Chilean coast is an ideal area for studying the variety of processes that produce N₂O along an extreme gradient.

The main objective of this work is to try to elucidate the changes in N₂O production processes in relation to different environmental conditions in the water column through a comparison of the different environments encountered during the BIOSOPE cruise (Fig. 2). To accomplish this, we employ a combination of isotopic and isotopomeric N₂O measurements along with oceanographic and biogeochemical data.

2 Methods

2.1 Sampling

All samples were collected during the BIOSOPE cruise (October–December 2004 or early austral spring) on board the R/V L'Atalante. The stations chosen in this work – GYR (26.07° S, 113.99° W), EGY (31.90° S, 91.41° W), and UPX (34.58° S, 72.43° W) – are representatives of different zones along the trophic gradient. GYR is within the South Pacific Central Gyre, EGY is on the eastern border of the gyre, and

UPX is in the coastal upwelling zone, 33 km from the shore (Fig. 2).

Temperature and salinity profiles were obtained with a Seabird SBE 911 + CTD. Fluorescence (as Relative Fluorescence Unit, RFU) was measured in situ from a Chelsea AquaTracka fluorometer, attached to the CTD rosette-sampler system. Sampling was done one hour before sunrise, with twelve-Liter Niskin bottles attached to a CTD-O rosette. Particle content was measured by an Underwater Video Profiler (UVP) system as described in Gorsky et al. (2000). Particle size was measured as Equivalent Spherical Diameter (ESD) in mm (Stemmann et al., 2000).

Seawater samples were collected for isotopic and N₂O concentration analyses as well as for O₂ and nutrient analyses. The samples for isotopes, isotopomers, and N₂O analyses were transferred directly into 125-ml glass flasks, preserved with HgCl₂, and sealed with butyl rubber stoppers following the method described in Yamagishi et al. (2001).

2.2 Nitrous oxide, oxygen, nitrate, and phosphate determination

N₂O was determined in the seawater samples used for the isotopic analysis with gas chromatography and mass spectrometry detection. The method is well described in Toyoda et al. (2005).

O₂ was measured in situ with a Seabird SBE 43 O₂ meter. The O₂ sensor was calibrated with Winkler titrations. Nitrate was immediately analyzed on board following two methods depending on the concentration range. For low concentrations (nM range), the method described in Raimbault et al. (1990) was used, whereas for higher concentrations (μM range), the method of Armstrong et al. (1967) was used. Phosphate was analyzed immediately on board by the method described in Tréguer and LeCorre (1975). The Apparent O₂ Utilization (AOU) value was obtained by subtracting the measured value of the O₂ concentration from the

saturation value computed for the temperature and salinity of the seawater (Murray and Riley, 1969), whereas the difference between the N_2O saturation concentration and its measured concentration ($\Delta\text{N}_2\text{O}$) in the seawater was used to infer its production (positive) or consumption (negative) (Yoshinari, 1976).

2.3 Isotopic and isotopomeric determinations

Isotopic and isotopomeric determinations were carried out at the Tokyo Institute of Technology using a Finnigan MAT 252 mass spectrometer following the method described in Toyoda and Yoshida (1999). For this, N_2O was extracted from samples by sparging with helium and then introduced into a preconcentration-gas chromatography-isotopic ratio mass spectrometry system. $\delta^{15}\text{N}$ (α and β) and $\delta^{18}\text{O}$ (N_2O) were determined in relation to the atmospheric nitrogen and Vienna Standard Mean Ocean Water (VSMOW), respectively. N_2O isotopomers were determined based on the analysis of ionic mass fragments (NO^+ and N_2O^+) formed by the electronic impact of N_2O . This determination was possible since NO^+ fragments contain the central nitrogen (α), which allows the conversion of the fragment ratios into isotopic ratios of $^{14}\text{N}^{15}\text{NO}$ and $^{15}\text{N}^{14}\text{NO}$. Although there is a rearrangement reaction during the ionic fragmentation process, its magnitude can be determined and corrections applied. Precision of the measurements is typically better than 0.5‰ for $\delta^{15}\text{N}_{\text{bulk}}$ and $\delta^{18}\text{O}$, and better than 1‰ for $\delta^{15}\text{N}^\alpha$ and $\delta^{15}\text{N}^\beta$ (Toyoda et al., 2005). Isotopomeric ratios were calculated with the following expressions:

$$^{15}\text{R}^\alpha = \frac{[^{14}\text{N}^{15}\text{N}^{16}\text{O}]}{[^{14}\text{N}^{14}\text{N}^{16}\text{O}]} \quad (2)$$

$$^{15}\text{R}^\beta = \frac{[^{15}\text{N}^{14}\text{N}^{16}\text{O}]}{[^{14}\text{N}^{14}\text{N}^{16}\text{O}]} \quad (3)$$

$$\delta^{15}\text{N}^\alpha = \left\{ \frac{^{15}\text{R}^\alpha}{^{15}\text{R}^\alpha (\text{std}) - 1} \right\} \times 1000 \quad (4)$$

$$\delta^{15}\text{N}^\beta = \left\{ \frac{^{15}\text{R}^\beta}{^{15}\text{R}^\beta (\text{std}) - 1} \right\} \times 1000 \quad (5)$$

Furthermore, the definition of $\delta^{15}\text{N}_{\text{bulk}} = (\delta^{15}\text{N}^\alpha + \delta^{15}\text{N}^\beta)/2$ allowed us to compare the relative abundance of the isotopomers α and β with the relative isotopic abundance of ^{15}N .

2.4 Data analysis

The Brunt-Vaisälä frequency (BVF) was determined using temperature and salinity data. For better data interpretation, BVF profiles were visually fitted to an eight-term Gaussian model included in MATLAB software. The mixed layer was determined by averaging the depths of

four criteria as described in the official data source of the Biosope cruise (http://www.obs-vlfr.fr/proof/php/bio_log_basicfiles.php). The photic layer is defined as the depth at which the surface light irradiance is reduced to 1% of its surface value. This determination was made by averaging readings from four different sensors.

3 Results and discussion

3.1 General water column characteristics

The three studied stations are located along a gradient from very oligotrophic to highly eutrophic systems and are found in different oceanographic regimes with the following characteristics. The GYR station is located at the center of South Pacific Gyre, with severe oligotrophy (Claustre and Mariotorena, 2003). The fluorescence peak (0.23 RFU) at this station occurs at ~ 180 m, just below the bottom of the photic layer (164 m). The shallower pycnocline is located at 10 m. A second, thicker pycnocline is observed between 100 and 500 m, as shown by the BVF plot in Fig. 3a.

The EGY station is located on the eastern border of the South Pacific Gyre, in a less oligotrophic environment. The fluorescence peak (0.34 RFU at 52 m) is shallower and more pronounced than at the previous station, well above the depth of the photic layer (92 m). The shallower pycnocline is located at 26 m and the BVF plot shows a second, thicker pycnocline between 120 and 400 m (Fig. 3b). Both GYR and EGY stations are located in a zone in which surface and subsurface waters (0–500 m) are mainly dominated by East South Pacific Central Water (ESPCW), which is characterized by wide temperature and salinity ranges. The ESPCW is formed in the middle of the South Pacific close to 40°S (Emery and Meincke 1986).

The UPX station is located off the coast of central Chile in a highly productive environment. The chlorophyll fluorescence peak (0.81 RFU) at this station is found at 32 m, but fluorescence is still high at the surface (0.70 RFU). The peak is close to the base of the photic layer (37 m) and the mixed layer (36 m). The BVF plot showed a high stability zone from 20 to 60 m depth (Fig. 3c). Changes in the values and shapes of the chlorophyll profiles from west to east clearly showed the expected differences in productivity due to the enhanced nutrient supply. The central Chile coast is characterized by the upwelling of nutrient-rich, low O_2 Equatorial Subsurface Water (ESSW) (Strub et al., 1995).

Circulation at this coastal station is greatly affected by horizontal advection that brings nutrient-enriched waters to this latitude in the form of ESSW, which is transported by the PCUC. Indeed, the PCUC has been detected as far south as 48°S (Silva and Neshyba, 1979). The SW wind stress on the surface layer causes upwelling of nutrient-rich, low-oxygen waters followed by increased productivity that provides favourable conditions for N_2O production (Cornejo

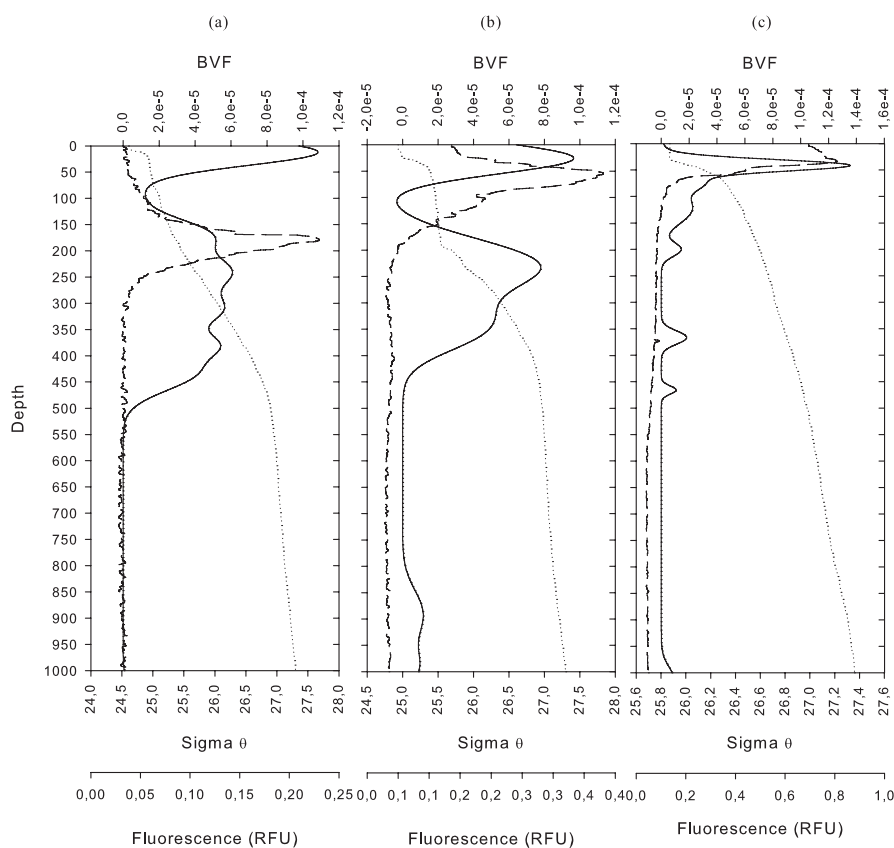


Fig. 3. Vertical profiles at stations (a): GYR, (b): EGY and (c): UPX. The parameters shown are: Potential density (dotted line), Brunt-Vaisälä frequency (continuous line), and Fluorescence (dashed line).

et al., 2006). Thus, N_2O produced in subsurface waters is brought to the surface through advection and mixing, enhancing N_2O fluxes to the atmosphere.

3.2 Nitrous oxide, oxygen, and nutrient behavior

Vertical distributions of N_2O and O_2 are shown in Fig. 4. N_2O is slightly oversaturated at GYR and EGY from the surface to ≈ 200 m ($\approx 114\%$ and $\approx 105\%$, respectively), and is highly oversaturated below this depth ($\approx 230\%$, at both stations) (Figs. 4a, b). N_2O profiles at GYR and EGY are almost mirrored by the O_2 profiles, indicating that the amount of N_2O produced in the water column is strongly driven by the O_2 concentration. At the UPX station, the whole water column is highly N_2O -oversaturated from 230% at the surface to 480% at the N_2O maximum at 350 m. At this station, the O_2 concentrations display a strong depletion up to $\approx 10 \mu\text{mol/Kg}$ between 150 m and 300 m and do not show a clear relationship with the N_2O profile.

Nitrate and phosphate profiles are shown in Fig. 5. At the GYR and EGY stations, both nutrients have very similar profiles, with low concentrations in the first 200 m. Below this depth, the nitrate concentrations gradually increase to $40 \mu\text{mol/Kg}$ (1000 m) at GYR and $35 \mu\text{mol/Kg}$ (400 m)

at EGY. At both stations (GYR, EGY), abrupt increases in nitrate and phosphate concentrations close to 400 m coincide with maxima in the N_2O concentrations, suggesting an increase in the rate of nitrification at this depth. At the UPX station, nitrate concentrations are high at the surface (Fig. 5c) due to the upwelling of nutrient-rich water (Daneri et al., 2000). Although the nitrate and phosphate profiles show similar trends, the profiles appear to be more complicated than at the oceanic stations. N_2O and nitrate show very similar profiles at this station, suggesting that the N_2O production-consumption processes are the same as for nitrate.

The PO_4^{3-} vs NO_3^- plots (Figs. 5a, b, insets) suggest that at stations GYR and EGY both nutrients behave according to the Redfield ratio, indicating that nitrogen oxidative processes are predominant. At UPX, the plot (Fig. 5c, inset) suggests nitrate removal by denitrification since there is a phosphate excess in relation to nitrate according to the Redfield ratio.

In order to obtain information about the processes involved in N_2O cycling throughout the water column, scatter diagrams of AOU vs. $\Delta\text{N}_2\text{O}$ and AOU vs. NO_3^- below the photic layer (200–600 m) at GYR and EGY are presented (Figs. 6a, b). $\Delta\text{N}_2\text{O}$ correlated positively with AOU at both

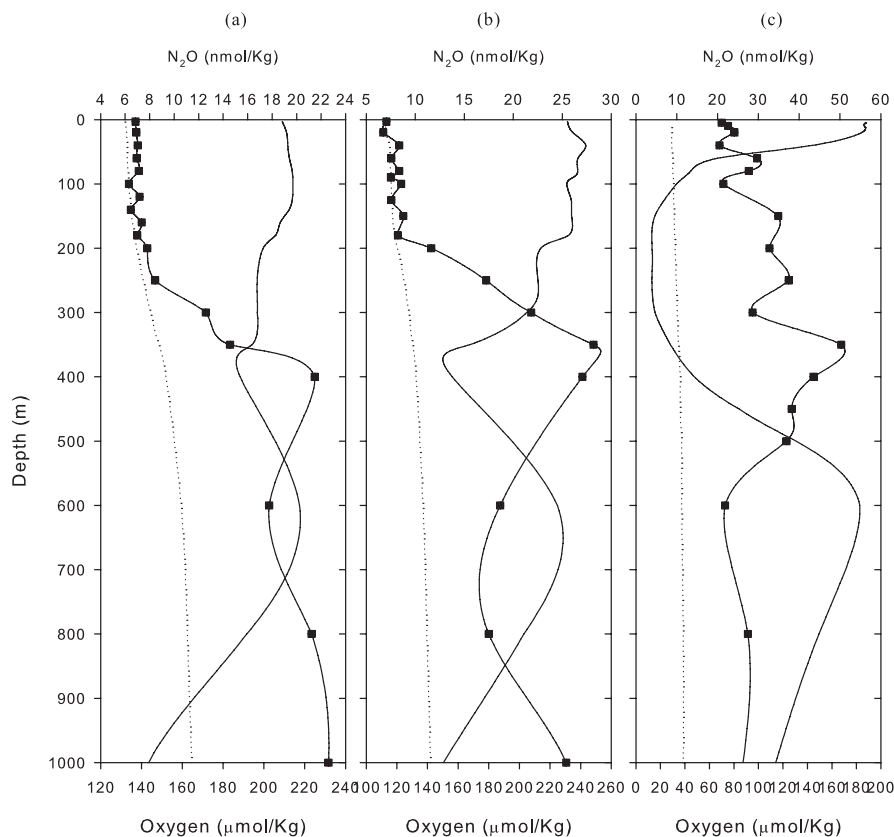


Fig. 4. Vertical profiles at stations (a): GYR, (b): EGY (c): UPX. The parameters shown are: N₂O saturation (dotted line), N₂O (squares) and O₂ (continuous line).

stations, indicating that more N₂O is produced while O₂ is consumed. NO₃⁻ also correlated positively with AOU, supporting the view that, N₂O and nitrate production are produced mainly from nitrification. The ratio of N₂O production to O₂ consumption (on a molar basis), referred to as the N₂O oxidative ratio, was 1.76×10^{-4} and 1.42×10^{-4} for GYR and EGY station respectively. Since NO₃⁻ regeneration was also linearly related to AOU, it was possible to calculate the ratio of N₂O production to NO₃⁻ production (expressed as a percentage on the mol-N basis) as 0.088% and 0.15% for GYR and EGY stations respectively. The N₂O oxidative ratio (i.e., produced N₂O per mol of respired O₂) and the N₂O reaction yields (i.e., produced N₂O per mol of produced NO₃⁻) are close to the oceanic values reported by Cohen and Gordon (1979) for the North East Pacific.

3.3 $\delta^{15}\text{N}_{\text{bulk}}$, $\delta^{18}\text{O}$, and isotopomers of nitrous oxide

The $\delta^{15}\text{N}_{\text{bulk}}$ has been defined as equivalent to conventional $\delta^{15}\text{N}$ (Toyoda and Yoshida 1999). Surprisingly, variations of this parameter at the three stations are relatively small. In contrast, the SP signal shows great variability, which provides more information about the processes occurring in the water column. At the GYR and EGY stations, the SP values

in the mixed layer are close to the expected atmospheric N₂O value ($19 \pm 2\text{‰}$) (Yoshida and Toyoda, 2000), indicating that surface N₂O originates mainly from ocean-atmosphere interactions (Figs. 7a, b). At UPX, however, the SP value in the mixed layer ($\approx 14\text{‰}$) is lower than in the air, indicating the influence of N₂O upwelled with subsurface waters (Fig. 7c). Although the accepted value for the SP of atmospheric N₂O was determined in air samples from the North West Pacific, the high mixing rates of tropospheric gases and the high residence times of atmospheric N₂O over 120 years (Liao et al., 2004) make the value given by Yoshida and Toyoda (2000) a good approximation.

Site preference between the shallow pycnocline and the base of the photic layer shows high variability. Assimilatory nitrate reduction has been mentioned as a source of N₂O in surface waters (Oudot et al., 1990). However, not enough information is available to establish whether this process is actually occurring. At UPX, where the mixed layer coincides with the photic layer, SP and $\delta^{18}\text{O}$ (N₂O) values over the pycnocline are quite stable.

Below the photic zone, SP profiles at GYR and EGY show conspicuous minima (11.5‰, 8.5‰) at 350 m and 250 m, respectively, followed by a gradual increase up to 22‰ in

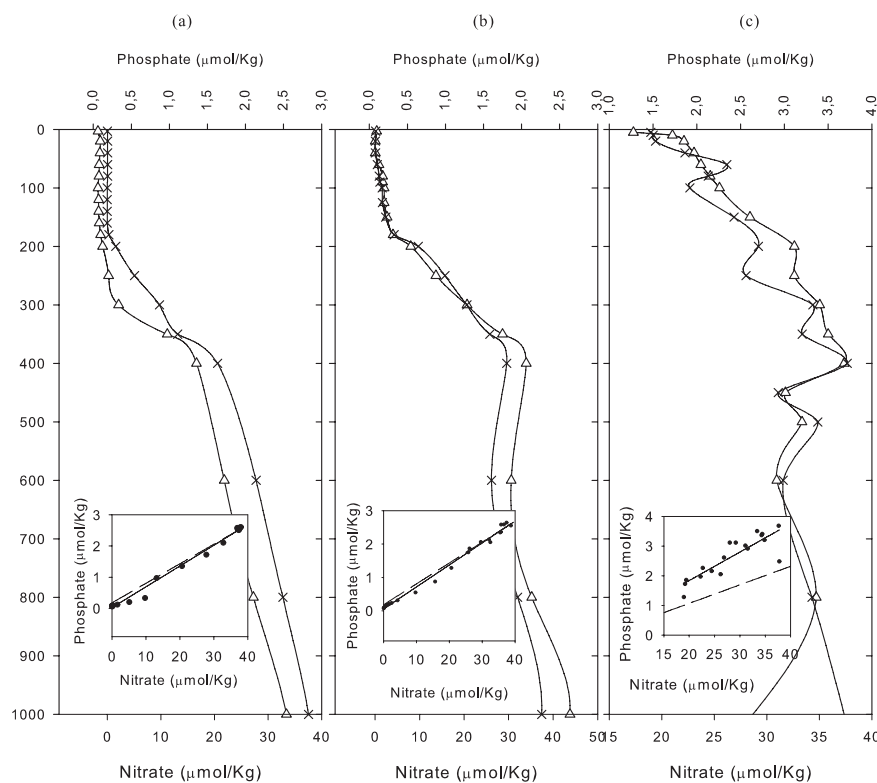


Fig. 5. Vertical profiles at stations (a): GYR, (b): EGY (c): UPX. The parameters shown are: Nitrate (cross) and phosphate (open triangle). Insets show nitrate v/s phosphate ratio. Solid line shows linear regression of data, dashed line shows the equation deduced from Redfield N:P ratio (16:1) (Gruber and Sarmiento, 1997).

deeper waters. Such a minimum is also observed at UPX at a very shallow depth (40 m) within the upper pycnocline. Below the pycnocline, SP values do not show a clear depth trend. Since SP is independent from the $\delta^{15}\text{N}$ of its precursors, or the extent of the reaction, and is only dependant on the reaction mechanism, the observed changes in SP in the water column must be associated with changes in the mechanistic sources of N_2O (Toyoda et al., 2002). The SP minima at oceanic and coastal stations must be influenced by a particular process that produces low SP N_2O .

It is unlikely that the SP minimum values are being transported from nutrient-rich coastal waters. The Ekman transport in east oceanic margins is determined by the Rossby radius of deformation, whose maximum reach at mid-latitudes is 200 to 300 km for very unstratified coastal waters (Csanady, 1982). Otherwise, as has been previously mentioned, surface and subsurface waters (0–500 m) of the Subtropical South Pacific Gyre are dominated by ESPCW, produced close to 40°S (Emery and Meincke, 1986).

The coincidence that all SP minima (at three stations) with high density gradient layers (see Figs. 3, 7) where particles are likely to accumulate indicates that N_2O production at this point should be, at least in part, associated with the accumulation of such particles. Studies have demon-

strated that temporal oxygen-depleted microsites are possible in marine snow in the absence of light (Alldredge and Cohen, 1987; Ploug, 2001; Ploug et al., 1997). The O_2 consumption around sinking particles strongly depends on the advection-diffusion balance driven by sinking velocities (Csanady, 1986; Kiørboe et al., 2001), with higher O_2 depletion associated with slower-falling particles.

Although the stations GYR and EGY are located in a very oligotrophic area, the accumulation of sinking particles at the steepest density gradient layer inside the pycnocline (see Brunt-Vaisälä frequency plots, Fig. 3) should allow the formation of aggregates suitable for nitrogen reductive processes, as proposed by Yoshida et al. (1989). Figure 8 shows the particle count between 0.052 mm and 8.438 mm of ESD (a wide range of marine snow sizes) at three sampled stations (C. Gorsky and M. Picheral, personal communication). At the GYR and EGY stations, small particle accumulation is observed at 300 m (≈ 35 part/L) and 50 m (≈ 45 part/L), respectively, roughly coincident with high stability zones. The particle content at EGY below the photic zone shows no significant accumulation; the mean particle content between 200 m and 400 m is ≈ 22 part/L. High particle contents at the UPX station are also closely related to the stability profile.

Toyoda et al. (2002) proposed that nitrification should

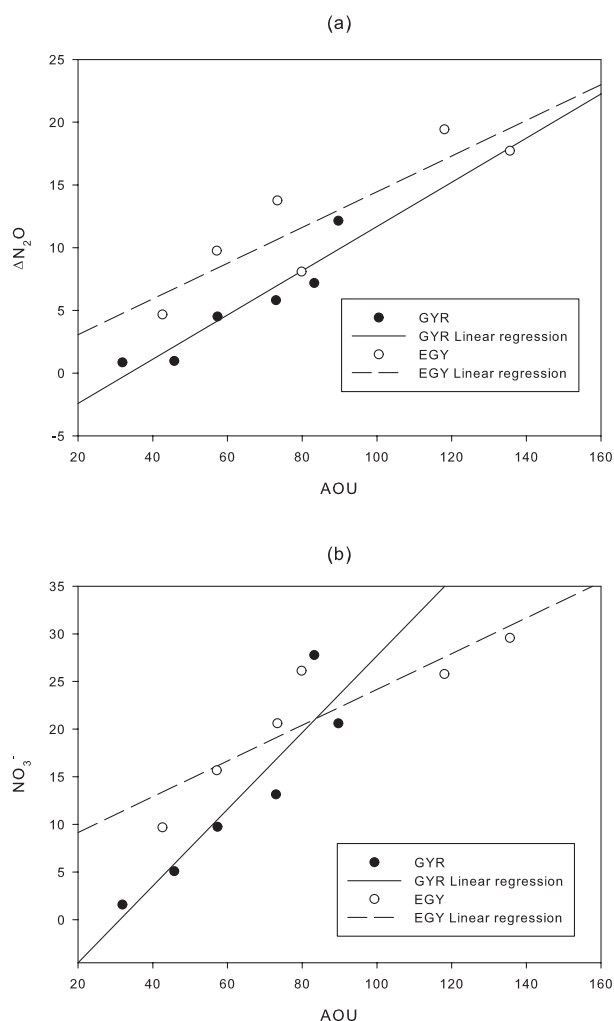


Fig. 6. (a) AOU v/s ΔN_2O at GYR and EGY stations from 200 to 600 m, the linear regression model for each line was GYR: $y = -5.94 + 0.176x$, $r^2 = 0.87$; EGY: $y = 0.22 + 0.142x$, $r^2 = 0.79$. (b) AOU v/s NO_3^- at GYR and EGY stations from 200 to 600 m, the linear regression model for each line was GYR: $y = -12.0 + 0.403x$, $r^2 = 0.85$; EGY: $y = 5.4 + 0.188x$, $r^2 = 0.81$.

yield $\delta^{15}N^\alpha$ enriched N_2O due to the existence of a hyponitrite (-ONNO-) intermediary followed by the selective breakage of the NO bond where the lightest isotopes are located, based on the ZPE (zero point energy) for N_2O (Zuñiga et al., 2003). This mechanism has been described for some nitric oxide reductases (Hendriks et al., 2000; Wasser et al., 2002). Culture experiments carried out by Sutka et al. (2006) show that ammonium oxidation carried out by ammonium oxidizers (i.e. *Nitrosomona europaea*, *Nitrosospira multiformis*) produces N_2O enriched in $\delta^{15}N^\alpha$, with average SP values of 33‰. Despite the lack of conclusive evidence about this specific mechanism in nitrification, if we assume that nitrification is the main process of N_2O production, at least at the oceanic stations, positive SP values below the photic layer can be attributed to nitrification.

These results, as well as other culture experiments carried out by Sutka et al. (2003, 2006) show that, under O_2 stress, nitrifier denitrification mediated by ammonium oxidizers (i.e. *Nitrosomona europaea* and *Nitrosospira multiformis*), produces N_2O with an average SP value of zero. This means that there is no selectivity of nitrogen atoms during N_2O production. Evidence of sequential mechanisms of N_2O production by nitrite reductive processes in bacteria has been reported several times in the biochemical literature (Aeressens et al., 1986; Averill and Tiedje, 1982; Weeg-Aeressens et al., 1988; Zafriou et al., 1989). Such mechanisms involve the successive addition of one molecule of precursor (NO_2^- or NO) to the enzyme. The resulting ^{15}N distribution must be statistically determined by the entrance of the precursor, contrary to the selective effect of simultaneous mechanisms proposed by Toyoda et al. (2002).

Although it has been pointed out that nitrifier denitrification occurs under O_2 stress, Shaw et al. (2006) demonstrated that bacteria of the genera *Nitrosospira* and *Nitrosomona* are capable of producing N_2O via nitrifier denitrification in the presence of nitrite, even in aerobic environments. Nitrifier denitrification has not been studied in marine environments, and its possible ecological role is far from being established. Wrage et al. (2001) proposed thermodynamic reasons for the occurrence of nitrifier denitrification due to the negative Gibbs free energy for the $NH_4^+ \rightarrow NO_2^- \rightarrow N_2O$ processes, which are favoured at low pH. Poth and Focht (1985) have proposed that nitrifier denitrification in soil can act as a nitrite detoxification mechanism. Nitrite has been shown to be toxic for ammonium oxidizers since it reduces ammonium monooxygenase activity (Stein and Arp, 1998). Therefore, we propose that nitrite accumulation around sinking particles due to the sudden loss of speed in the pycnocline potentially activates nitrifier denitrification enzymes on ammonium oxidizers.

It is important to emphasize that $\delta^{15}N^\alpha$ enrichment due to denitrifying N_2O consumption in anoxic microsites of particles in oceanic environments, as previously pointed out (Yoshida et al., 1989), is not expected because N_2O reduction only occurs at very low O_2 concentrations (Castro and Farías, 2004; Elkins et al., 1978). Very large aggregates are necessary for the occurrence of highly anoxic microsites in particles and this is unlikely in open oligotrophic or even mesotrophic environments. If this process occurs, its effect must be negligible.

$\delta^{18}O$ (N_2O) is always hard to elucidate due to its dependence on the isotopic signature of precursors. The $\delta^{18}O$ (N_2O) profile below the mixed layer at GYR and EGY and below 500 m at UPX are similar in shape to the SP, as previously observed by Toyoda et al. (2002) and Popp et al. (2002), indicating that $\delta^{18}O$ (N_2O) is also driven by N_2O production mechanisms. The primary source of O in the N_2O produced by ammonium oxidation is dissolved O_2 (Ostrom et al., 2000), since it is expected that $\delta^{18}O$ (N_2O) will be greater than 40‰. Furthermore, the preferential breakage of

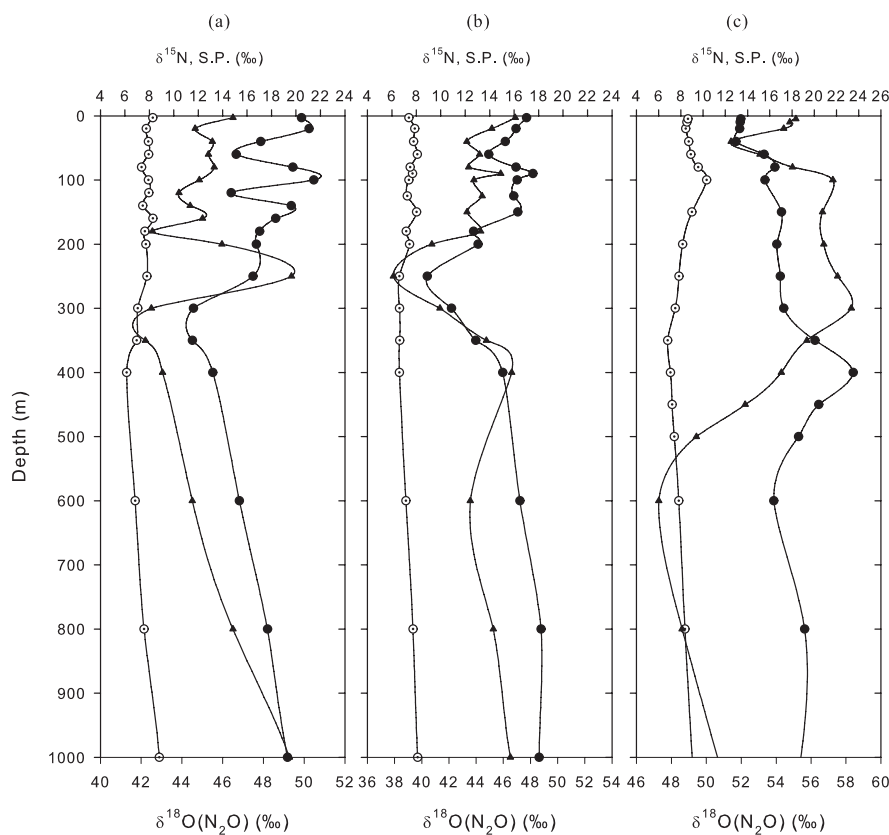


Fig. 7. Vertical profiles at stations (a): GYR, (b): EGY (c): UPX. The parameters shown are: $\delta^{15}\text{N}_{\text{bulk}}$, (open circle): Site preference (solid circle), $\delta^{18}\text{O}(\text{N}_2\text{O})$ (solid triangle).

bonds of the lightest isotopes during the intermediate hypolimnetic step should drive the $\delta^{18}\text{O}(\text{N}_2\text{O})$, as occurs with $^{15}\text{N}^{\alpha}$ enrichment (Schmidt et al., 2004). The source of the oxygen atom in N_2O produced by nitrite reduction is nitrite (Aeressens et al., 1986; Averill, 1996). Therefore, if this (nitrite) is produced in situ by ammonium oxidizers, it must be isotopically depleted compared to ammonium and O_2 . Thus, the resulting N_2O must be depleted in ^{18}O . This explains why $\delta^{18}\text{O}(\text{N}_2\text{O})$ is lighter in the deeper pycnocline, even when dissolved O_2 should be isotopically enriched due to the respiration of organic matter accumulated in this pycnocline, supporting nitrifier denitrification hypotheses as a N_2O source in these regions.

The behavior of SP and $\delta^{18}\text{O}(\text{N}_2\text{O})$ below the pycnocline at UPX is more complicated than at the oceanic stations. Maximum values of $\delta^{18}\text{O}(\text{N}_2\text{O})$ between 56‰ and 60‰ coincide with the O_2 minimum zone (OMZ). This can be interpreted as the influence of the isotopic enrichment of O_2 due to respiration. From this, it can be concluded that the main source of N_2O is nitrification. Otherwise, SP in the OMZ ($\approx 17\text{‰}$) is diminished related to the N_2O released by nitrification at the oceanic station ($\approx 22\text{‰}$), probably due to the influence of nitrifier denitrification. In any case, these two

processes could be running simultaneously. The SP maximum is observed at 400 m, coinciding with the nitrate maximum and the rising O_2 concentration below the OMZ, and slightly deeper than the N_2O maximum ($50.29 \text{ nmol Kg}^{-1}$). This suggests an enhancement of the extent of nitrification at this depth. It must be considered that the coastal zone is a highly dynamic environment, with significant meridional transport and isotopic, isotopomeric, and concentration values that could be influenced by non-local processes. In fact, minima of $\delta^{18}\text{O}(\text{N}_2\text{O})$, SP, and N_2O are found at UPX (600 m), as is an O_2 maximum; this parameter seems to be related to the core of a water mass identified at this depth ($S \approx 34.3$ and $T \approx 5.5^\circ\text{C}$).

3.4 Contribution of nitrifier denitrification

At GYR and EGY, it is possible to identify at least 3 sources of N_2O according to the shape of the SP profiles. A first source can be attributed to mixing with the air in the shallow mixed layer, where the average SP at both stations is about 17‰, slightly below the value expected for the atmosphere ($19 \pm 2\text{‰}$) (Yoshida and Toyoda, 2000). A second source is represented by the SP signal below 1000 m, which averaged 22‰, and a third source is located at the SP minimum

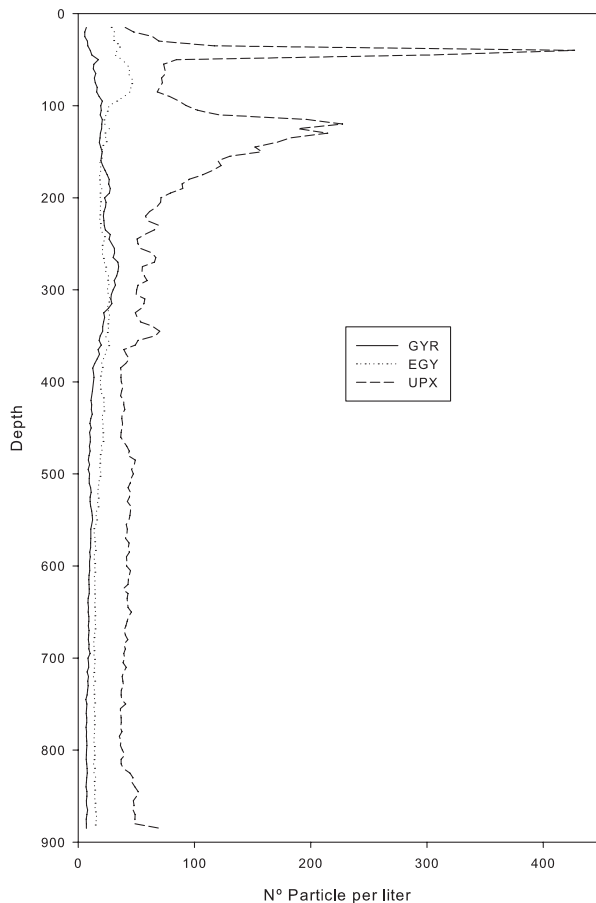


Fig. 8. Particle content at the stations : GYR (continuous line), EGY (dotted line) and UPX (dashed line).

located at 320 m and 250 m at the GYR and EGY stations, respectively.

Assuming that there is no significant contribution from air-sea transfer below the pycnocline, and that SP values below 1000 m are representative only of ammonium oxidation, it is possible to build a simple two-box model to elucidate the contribution of ammonium oxidation and nitrite reduction to the minimum SP zone at GYR and EGY using SP values. The fraction of N_2O produced by nitrifier denitrification (F) can be determined as follows:

$$F = \frac{SP_{IM} - SP_{ao}}{SP_{nr} - SP_{ao}} \quad (6)$$

where SP_{IM} is the SP value at the site preference minimum, SP_{ao} is the SP value attributable to ammonium oxidation (equal to the SP value below 1000 m), and SP_{nr} is the SP value attributable to nitrite reduction, equal to zero, based on the biochemical literature discussed above, and the values obtained in cultures with induced nitrifier denitrification (Sutka et al., 2004; Sutka et al., 2006). The assumption that

SP values below 1000 m are representative of nitrification is supported by the $\delta^{15}N^{\alpha}$ enrichment predicted for this process and the agreement of the nitrate-phosphate ratio with the Redfield ratio for those stations shown in Fig. 5. If we assume that our hypothesis about N_2O production through nitrifier denitrification is correct, the calculated F values of 0.4 and 0.5 (GYR and EGY, respectively) indicate that nitrifier denitrification pathways can be an important source of N_2O , even in oligotrophic and well-oxygenated waters.

At UPX, the N_2O production processes seems to be more complicated than at the oceanic stations. Coastal environments are commonly highly dynamic and highly influenced by horizontal advection. Because of this, the model applied here to the oceanic station should not be valid for the coastal station. Nevertheless, nitrifier denitrification could be an important source of N_2O to the atmosphere, in view of the SP-depleted N_2O present in the mixed layer (related to the expected atmospheric SP values).

4 Conclusions and perspectives

Our results show that N_2O sources in the ocean are far from being identified. Even in very stable oligotrophic environments, different mechanisms could coexist. In this sense, new tools like N_2O isotopomer determination provide new information about nitrogen cycling processes.

The SP signal supporting the evidence of the occurrence of nitrifier denitrification in highly oligotrophic environments is one of the most striking contributions of this work. Particular chemical dynamics of this process under such conditions, as well the role of particles should be the subject of further challenging studies.

The importance of the occurrence of nitrifier denitrification in oceanic environments for the whole nitrogen cycle may be enormous, considering that the Central South Pacific Gyre represents a major part of the South Pacific. Moreover, such conditions are found in the other oceans, thus rendering this process a potentially significant contributor to the oceanic N_2O budget.

Acknowledgements. Dominique Tailliez and Claudie Bournot are warmly thanked for their efficient help in CTD rosette management and data processing. The authors thank G. Gorsky and M. Picheral for allowing us to use their UVP data; O. Ulloa, G. Alarcon, M. Gallegos, and the crew of the R. V. L'Atalante for their help during the BIOSOPE Cruise. J. Charpentier thanks V. Molina, A. Montecinos, and S. Hormazabal for their help during the writing of this manuscript. This is a contribution of the BIOSOPE project of the LEFE-CYBER program. This research was funded by the Centre National de la Recherche Scientifique (CNRS), the Institut des Sciences de l'Univers (INSU), the Centre National d'Etudes Spatiales (CNES), the European Space Agency (ESA), the National Aeronautics and Space Administration (NASA), and the Natural Sciences and Engineering Research Council of Canada (NSERC). Financial assistance was provided by the FONDAP-COPAS center (Project No. 150100007). J. Charpentier was supported by a grant

from the MECESUP UCO002 project. This work was supported by the Chilean National Commission for Scientific and Technological Research through FONDECYT grant 1050743 (L. Farias).

Edited by: S. W. A. Naqvi

References

- Aeressens, E., Tiedje, J., and Averill, B.: Isotope labelling studies on the mechanism of N-N bond formation in denitrification, *J. Biol. Chem.*, 261, 9652–9656, 1986.
- Allredge, A. L. and Cohen, Y.: Can Microscale Chemical Patches Persist in the Sea? Microelectrode Study of Marine Snow, Fecal Pellets, *Science*, 235, 689–691, 1987.
- Armstrong, F. A., Stearns, C. R., and Strickland, D. H.: The measurement of upwelling and subsequent biological processes by means of the Technicon Autoanalyzer and associated equipment, *Deep Sea Res.*, 14, 381–389, 1967.
- Averill, B. A.: Dissimilatory Nitrite and Nitric Oxide Reductases, *Chem. Rev.*, 96, 2951–2964, 1996.
- Averill, B. A. and Tiedje, J. M.: The chemical mechanism of microbial denitrification, *FEBS Lett.*, 138, 8–12, 1982.
- Bonnet, S., Guieu, C., Bruyant, F., Pril, O., Van Wambeke, F., Raimbault, P., Grob, C., Moutin, T., Gorbunov, M. Y., Zehr, J. P., Masquelier, S. M., Garczarek, L., and Claustre, H.: Nutrients limitation of primary productivity in the Southeast Pacific (BIOCOPE cruise), *Biogeosciences Discuss.*, 4, 2733–2759, 2007, <http://www.biogeosciences-discuss.net/4/2733/2007/>.
- Carlucci, A. F. and McNally, P. M.: Nitrification by Marine Bacteria in Low Concentrations of Substrate and Oxygen, *Limnol. Oceanogr.*, 14, 736–739, 1969.
- Claustre, H. and Maritorena, S.: OCEAN SCIENCE: The Many Shades of Ocean Blue, *Science*, 302, 1514–1515, 2003.
- Castro, M. and Farias, L.: N₂O cycling at the core of the oxygen minimum zone off northern Chile, *Mar. Ecol. Prog. Ser.*, 280, 1–11, 2004.
- Codispoti, L. A., Brandes, J. A., Christensen, J. P., Devol, A. H., Naqvi, S. W. A., Paerl, H. W., and Yoshinari, T.: The oceanic fixed nitrogen and nitrous oxide budgets: Moving targets as we enter the anthropocene?, *Sci. Mar.*, 65, 85–105, 2001.
- Cohen, Y. and Gordon, L. I.: Nitrous oxide production in the ocean, *J. Geophys. Res.*, 84, 347–353, 1979.
- Cornejo, M., Farias, L., and Paulmier, A.: Temporal variability in N₂O water content and its air-sea exchange in an upwelling area off central Chile (36 degrees S), *Mar. Chem.*, 101, 85–94, 2006.
- Csanady, G. T.: Circulation in the coastal ocean. Dordrecht, D. Reidel, pp. 279, 1982.
- Csanady, G. T.: Mass Transfer to and from Small Particles in the Sea, *Limnol. Oceanogr.*, 31, 237–248, 1986.
- Daneri, G., Dellarossa, V., Quinones, R., Jacob, B., Montero, P., and Ulloa, O.: Primary production and community respiration in the Humboldt Current System off Chile and associated oceanic areas, *Mar. Ecol. Prog. Ser.*, 197, 41–49, 2000.
- Daneri, G. and Quinones, R.: Undersampled Ocean systems : a plea for an international study of biogeochemical cycles in the Southern Pacific Gyre and its boundaries, *U.S. JGOFS Newsletter*, 11, 9, 2001.
- Dore, J. E., Popp, B. N., Karl, D. M., and Sansone, F. J.: A large source of atmospheric nitrous oxide from subtropical North Pacific surface waters, *Nature*, 396, 63–66, 1998.
- Elkins, J. E., Wofsy, S. C., McElroy, M. B., Kolb, C. E., and Kaplan, W. A.: Aquatic sources and sinks for nitrous oxide., *Nature*, 275, 602–606, 1978.
- Emery, W. J. and Meincke, J.: Global Water masses: summary and review, *Oceanol. Acta*, 9, 383–391, 1986.
- Goreau, T. J., Kaplan, W. A., Wofsy, M. B., McElroy, M. B., Valois, F. W., and Watson, S. W.: Production of NO₂⁻ and N₂O by nitrifying bacteria at reduced concentrations of oxygen, *Appl. Environ. Microbiol.*, 40, 526–532, 1980.
- Gorsky, G., Picheral, M., and Stemmann, L.: Use of the Underwater Video Profiler for the Study of Aggregate Dynamics in the North Mediterranean, *Est. Coast. Shelf Sci.*, 50, 121–128, 2000.
- Gruber, N. and Sarmiento, J. L.: Global patterns of marine fixation and denitrification, *Global Biogeochem. Cycles*, 11, 235–266, 1997.
- Hallam, S. J., Mincer, T. J., Schleper, C., Preston, C. M., Roberts, K., Richardson, P. M., and DeLong, E. F.: Pathways of Carbon Assimilation and Ammonia Oxidation Suggested by Environmental Genomic Analyses of Marine Crenarchaeota, *PLoS Biology*, 4, e95, 2006.
- Hendriks, J., Oubrie, A., Castresana, J., Urbani, A., Gemeinhardt, S., and Saraste, M.: Nitric oxide reductases in bacteria, *Biochim. Biophys. Acta*, 1459, 266–273, 2000.
- Kartal, B., Kuypers, M. M. M., Lavik, G., Schalk, J., Op den Camp, H. J. M., Jetten, M. S. M., and Strous, M.: Anammox bacteria disguised as denitrifiers: nitrate reduction to dinitrogen gas via nitrite and ammonium, *Environ. Microbiol.*, 9, 635–642, 2007.
- Kim, K. R. and Craig, H.: Two-isotope characterization of N₂O in the Pacific Ocean and constraints on its origin in deep water, *Nature*, 347, 58–61, 1990.
- Kjørboe, T., Ploug, H., and Thygesen, U.: Fluid motion and solute distribution around sinking aggregates. I. Small-scale fluxes and heterogeneity of nutrients in the pelagic environment, *Mar. Ecol. Prog. Ser.*, 211, 1–13, 2001.
- Knowles, R.: Denitrification, *Microbiol. Rev.*, 46, 43–70, 1982.
- Konneke, M., Bernhard, A. E., de la Torre, J. R., Walker, C. B., Waterbury, J. B., and Stahl, D. A.: Isolation of an autotrophic ammonia-oxidizing marine archaeon, *Nature*, 437, 543–546, 2005.
- Law, C. S. and Ling, R. D.: Nitrous oxide flux and response to increased iron availability in the Antarctic Circumpolar Current, *Deep-Sea Res. II*, 48, 2509–2527, 2001.
- Liao, T., Camp, C., and Yung, Y.: The seasonal cycle of N₂O, *Geophys. Res. Lett.*, 31, L17108, doi:10.1029/2004GL020345, 2004.
- Manne, A. S. and Richels, R. G.: An alternative approach to establishing trade-offs among greenhouse gases, *Nature*, 410, 675–677, 2001.
- Morales, C., Blanco, J., Braun, M., Reyes, H., and Silva, N.: Chlorophyll-a distribution and associated oceanographic conditions in the upwelling region off northern Chile during the winter and spring 1993, *Deep Sea Res. I*, 43, 267–289, 1996.
- Murray, C. N. and Riley, J. P.: The solubility of gases in distilled water and sea water–II. Oxygen, *Deep Sea Res.*, 16, 311–320, 1969.
- Naqvi, S. W. A. and Noronha, R. J.: Nitrous oxide in the Arabian Sea, *Deep-Sea Res. A*, 38, 871–890, 1991.

- Naqvi, S. W. A., Yoshinari, T., Jayakumar, D. A., Altabet, M. A., Narvekar, P. V., Devol, A. H., Brandes, J. A., and Codispoti, L. A.: Budgetary and biogeochemical implications of N₂O isotope signatures in the Arabian Sea, *Nature*, 394, 462–464, 1998.
- Nevison, C., Butler, J. H., and Elkins, J. W.: Global distribution of N₂O and the Δ N₂O-AOU yield in the subsurface ocean, *Global Biogeochem. Cycles*, 17, 30–1–30–18, 2003.
- Nevison, C. D., Weiss, R. F., and Erickson, D. J., III.: Global oceanic emissions of nitrous oxide, *J. Geophys. Res.*, 100, 809–820, 1995.
- Ostrom, N. E., Russ, M. E., Popp, B., Rust, T. M., and Karl, D. M.: Mechanisms of nitrous oxide production in the subtropical North Pacific based on determinations of the isotopic abundances of nitrous oxide and di-oxygen, *Chemosphere - Global Change Sci.*, 2, 281–290, 2000.
- Oudot, C., Andrie, C., and Montel, Y.: Nitrous oxide production in the tropical Atlantic Ocean, *Deep-Sea Res.*, 37, 183–202, 1990.
- Oudot, C., Jean-Baptiste, P., Fourre, E., Mormiche, C., Guevel, M., Ternon, J.-F., and Le Corre, P.: Transatlantic equatorial distribution of nitrous oxide and methane, *Deep-Sea Res. I*, 49, 1175–1193, 2002.
- Ploug, H.: Small-Scale Oxygen Fluxes and Remineralization in Sinking Aggregates, *Limnol. Oceanogr.*, 46, 1624–1631, 2001.
- Ploug, H. and Kühl, M., Buchholz-Cleven, B. and Jørgensen, B.: Anoxic aggregates – an ephemeral phenomenon in the pelagic environment?, *Aquat. Microb. Ecol.*, 13, 285–294, 1997.
- Popp, B., Westley, M., Toyoda, S., Miwa, T., Dore, J., Yoshida, N., Rust, T., Sansone, F., Russ, M., Ostrom, N. and Ostrom, P.: Nitrogen and oxygen isotopomeric constraints on the origins and sea-to-air flux of N₂O in the oligotrophic subtropical North Pacific gyre, *Global Biogeochem. Cycles*, 16, 1064–1073, 2002.
- Poth, M. and Focht, D.: ¹⁵N Kinetic analysis of N₂O production by *Nitrosomonas europaea*: an examination of nitrifier denitrification, *Appl. Environ. Microbiol.*, 49, 1134–1141, 1985.
- Raimbault, P., Slawyk, G., Coste, B., and Fry, J.: Feasibility of using an automated colorimetric procedure for the determination of seawater nitrate in the 0 to 100 nM range: Examples from field and culture, *Mar. Biol.*, 104, 347–351, 1990.
- Ritchie, G. A. and Nicholas, D. J.: Identification of the sources of nitrous oxide produced by oxidative and reductive processes in *Nitrosomonas europaea*, *Biochem. J.*, 126, 1181–1191, 1972.
- Schmidt, H. L., Werner, R. A., Yoshida, N., and Well, R.: Is the isotopic composition of nitrous oxide an indicator for its origin from nitrification or denitrification? A theoretical approach from referred data and microbiological and enzyme kinetic aspects, *Rapid Commun. Mass Spectrom.*, 18, 2036–2040, 2004.
- Shaw, L. J., Nicol, G. W., Smith, Z., Fear, J., Prosser, J. I., and Baggs, E. M.: *Nitrosospira spp.* can produce nitrous oxide via a nitrifier denitrification pathway, *Environ. Microbiol.*, 8, 214–222, 2006.
- Silva, N. and Neshyba, S.: On the southernmost extension of the Peru-Chile undercurrent, *Deep Sea Res.*, 26, 1387–1393, 1979.
- Stein, L. Y. and Arp, D. J.: Loss of Ammonia Monooxygenase Activity in *Nitrosomonas europaea* upon Exposure to Nitrite, *Appl. Environ. Microbiol.*, 64, 4098–4102, 1998.
- Stemann, L., Picheral, M., and Gorsky, G.: Diel variation in the vertical distribution of particulate matter (>0.15 mm) in the NW Mediterranean Sea investigated with the Underwater Video Profiler, *Deep-Sea Res. I*, 47, 505–531, 2000.
- Strub, T., Mesias, J. M., Monecino, V., Rutlland, J., and Salinas, S.: Coastal Ocean Circulation off Western South America, in: *The Sea*, edited by: Robinson, A. R. and Brinks, K. H., New York, John Wiley and Sons, 11, 273–213 1995.
- Sutka, R., Ostrom, N., Ostrom, P., Gandhi, H., and Breznak, J.: Nitrogen isotopomer site preference of N₂O produced by *Nitrosomonas europaea* and *Methylococcus capsulatus* Bath, *Rapid Commun. Mass Spectrom.*, 17, 738–745, 2003.
- Sutka, R., Ostrom, N., Ostrom, P., Gandhi, H., and Breznak, J.: Erratum: Nitrogen isotopomer site preference of N₂O produced by *Nitrosomonas europaea* and *Methylococcus capsulatus* Bath, *Rapid Commun. Mass Spectrom.*, 18, 1411–1412, 2004.
- Sutka, R. L., Ostrom, N. E., Ostrom, P. H., Breznak, J. A., Gandhi, H., Pitt, A. J., and Li, F.: Distinguishing Nitrous Oxide Production from Nitrification and Denitrification on the Basis of Isotopomer Abundances, *Appl. Environ. Microbiol.*, 72, 638–644, 2006.
- Toyoda, S., Mutoke, H., Yamagishi, H., Yoshida, N., and Tanji, Y.: Fractionation of N₂O isotopomers during production by denitrifier, *Soil Biol. Biochem.*, 37, 1535–1545, 2005.
- Toyoda, S. and Yoshida, N.: Determination of Nitrogen Isotopomers of Nitrous Oxide on a Modified Isotope Ratio Mass Spectrometer, *Anal. Chem.*, 71, 4711–4718, 1999.
- Toyoda, S., Yoshida, N., Miwa, T., Matsui, Y., Yamagishi, H., Tsunogai, U., Nojiri, Y., and Tsurushima, N.: Production mechanism and global budget of N₂O inferred from its isotopomers in the western North Pacific, *Geophys. Res. Lett.*, 29, 25–28, 2002.
- Tréguer, P. and LeCorre, P.: Manuel d'analyses des sels nutritifs dans l'eau de mer (Utilisation de l'Autoanalyser II). Brest, Laboratoire de Chimie Marine, Université de Bretagne Occidentale, pp. 110 pp, 1975.
- Treusch, A. H., Leininger, S., Kletzin, A., Schuster, S. C., Klenk, H.-P., and Schleper, C.: Novel genes for nitrite reductase and Amo-related proteins indicate a role of uncultivated mesophilic crenarchaeota in nitrogen cycling, *Environ. Microbiol.*, 7, 1985–1995, 2005.
- Ward, B.: Nitrification and the marine nitrogen cycle, in: *Microbial Ecology of the Oceans*, edited by: Kirchman, D., New York, Wiley – Liss, 427–453, 2000.
- Wasser, I. M., de Vries, S., Moëgne-Loccoz, P., Schröder, I., and Karlin, K.: Nitric Oxide in Biological Denitrification: Fe/Cu Metalloenzyme and Metal Complex NO_x Redox Chemistry, *Chem. Rev.*, 102, 1201–1234, 2002.
- Weeg-Aerssens, J. M., Tiedje, J. M., and Averill, B. A.: Evidence from isotope labeling studies for a sequential mechanism for dissimilatory nitrite reduction, *J. Am. Chem. Soc.*, 110, 6851–6856, 1988.
- Westley, M. B., Yamagishi, H., Popp, B. N., and Yoshida, N.: Nitrous oxide cycling in the Black Sea inferred from stable isotope and isotopomer distributions, *Deep Sea Res. II*, 53, 1802–1816, 2006.
- Wrage, N., Velthof, G. L., van Beusichem, M. L., and Oenema, O.: Role of nitrifier denitrification in the production of nitrous oxide, *Soil Biol. Biochem.*, 33, 1723–1732, 2001.
- Yamagishi, H., Miwa, T., Toyoda, S., Tsunogai, U., and Yoshida, N.: A method for the Measurement of Dissolved Nitrous Oxide Isotopomers in Natural Waters. 1st International Symposium on Isotopomers, Yokohama, Japan, 2001.
- Yamagishi, H., Yoshida, N., Toyoda, S., Popp, B., Westley, M.,

- and Watanabe, S.: Contributions of denitrification and mixing on the distribution of nitrous oxide in North Pacific, *Geophys. Res. Lett.*, 32, L04603, doi:10.1029/2006JG000227, 2005.
- Yoshida, N.: ^{15}N -depleted N_2O as a product of nitrification, *Nature*, 335, 528–529, 1988.
- Yoshida, N., Morimoto, H., Hirano, M., Koike, I., Matsuo, S., Wada, E., Saino, T., and Hattori, A.: Nitrification rates and ^{15}N abundances of N_2O and NO_3^- in the western North Pacific, *Nature*, 342, 895–897, 1989.
- Yoshida, N. and Toyoda, S.: Constraining the atmospheric N_2O budget from intramolecular site preference in N_2O isotopomers, *Nature*, 405, 330–334, 2000.
- Yoshinari, T.: Nitrous oxide in the sea, *Mar. Chem.*, 4, 189–202, 1976.
- Zafiriou, O., Hanley, Q., and Snyder, G.: Nitric oxide and nitrous oxide production and cycling during dissimilatory nitrite reduction by *Pseudomonas perfectomarina*, *J. Biol. Chem.*, 264, 5694–5699, 1989.
- Zuñiga, J., Bastida, A., and Requena, A.: Theoretical calculations of vibrational frequencies and rotational constants of the N_2O isotopomers, *J. Mol. Spectrosc.*, 217, 43–58, 2003.

Evidence for efficient regenerated production and dinitrogen fixation in nitrogen-deficient waters of the South Pacific Ocean: impact on new and export production estimates

P. Raimbault and N. Garcia

Laboratoire de Microbiologie, Géochimie et Ecologie Marine (UMR 6117 CNRS), Centre d'Océanologie de Marseille, Université de la Méditerranée, Campus de Luminy, 13288 Marseille, France

Received: 24 July 2007 – Published in Biogeosciences Discuss.: 5 October 2007

Revised: 8 January 2008 – Accepted: 24 January 2008 – Published: 5 March 2008

Abstract. One of the major objectives of the BIOSOPE cruise, carried out on the R/V *Atalante* from October–November 2004 in the South Pacific Ocean, was to establish productivity rates along a zonal section traversing the oligotrophic South Pacific Gyre (SPG). These results were then compared to measurements obtained from the nutrient – replete waters in the Chilean upwelling and around the Marquesas Islands. A dual $^{13}\text{C}/^{15}\text{N}$ isotope technique was used to estimate the carbon fixation rates, inorganic nitrogen uptake (including dinitrogen fixation), ammonium (NH_4) and nitrate (NO_3) regeneration and release of dissolved organic nitrogen (DON). The SPG exhibited the lowest primary production rates ($0.15 \text{ g C m}^{-2} \text{ d}^{-1}$), while rates were 7 to 20 times higher around the Marquesas Islands and in the Chilean upwelling, respectively. In the very low productive area of the SPG, most of the primary production was sustained by active regeneration processes that fuelled up to 95% of the biological nitrogen demand. Nitrification was active in the surface layer and often balanced the biological demand for nitrate, especially in the SPG. The percentage of nitrogen released as DON represented a large proportion of the inorganic nitrogen uptake (13–15% in average), reaching 26–41% in the SPG, where DON production played a major role in nitrogen cycling. Dinitrogen fixation was detectable over the whole study area; even in the Chilean upwelling, where rates as high as $3 \text{ nmoles l}^{-1} \text{ d}^{-1}$ were measured. In these nutrient-replete waters new production was very high ($0.69 \pm 0.49 \text{ g C m}^{-2} \text{ d}^{-1}$) and essentially sustained by nitrate levels. In the SPG, dinitrogen fixation, although occurring at much lower daily rates ($\approx 1\text{--}2 \text{ nmoles l}^{-1} \text{ d}^{-1}$), sustained up to 100% of the new production ($0.008 \pm 0.007 \text{ g C m}^{-2} \text{ d}^{-1}$) which was two orders of magnitude lower than that measured in the upwelling. The annual N_2 -fixation of the South Pacific

is estimated to $21 \times 10^{12} \text{ g}$, of which $1.34 \times 10^{12} \text{ g}$ is for the SPG only. Even if our “snapshot” estimates of N_2 -fixation rates were lower than that expected from a recent ocean circulation model, these data confirm that the N-deficiency South Pacific Ocean would provide an ideal ecological niche for the proliferation of N_2 -fixers which are not yet identified.

1 Introduction

The nitrogen cycle in the oceanic gyres has been studied ever since the pioneering work of Menzel and Ryther in the Sargasso Sea (Menzel and Ryther, 1960; Ryther and Menzel, 1961). Several years later, Dugdale and Goering (1967) defined new and regenerated nitrogen and hence new production, fuelled by allochthonous N-sources (mainly NO_3^-) supplied by diffusion from the nitracline. Regenerated production, on the other hand, is fuelled by autochthonous N-sources (mainly NH_4^+), derived from biological processes (Harrison et al., 1987). The fraction of primary production derived from “new nutrients” is termed the *f*-ratio (Eppley and Peterson, 1979) and when in a steady state, accounts for the proportion of production available for export. Historically, measurements of the nitrogen cycle were primarily based on ^{15}N tracer techniques. New production estimates, computed in terms of carbon using the *f*-ratio and primary production, have shown considerable variations (Aufdenkampe et al., 2002), due to inaccuracies in estimating *f* and NO_3^- assimilation (Priscu and Downes, 1985; Ward et al., 1989; Gentilhomme and Raimbault, 1994; Raimbault et al., 1999; Diaz and Raimbault, 2000; Aufdenkampe et al., 2001).

The main sources of error in classical ^{15}N uptake experiments are still being debated, in particular nitrogen regeneration and the release of dissolved organic nitrogen (DON), which have evoked several revisions on the concepts of new and regenerated production. Ammonium regeneration is the



Correspondence to: P. Raimbault
(patrick.raimbault@univmed.fr)

main source of regenerated nitrogen in the euphotic zone. By studying ammonium isotopic dilution (recycling of unlabeled substrate) during ^{15}N incubation experiments, Glibert et al. (1982), and Harrison et al. (1987) showed that ammonium regeneration can result in significant underestimations of regenerated production, which would also bias the assessment of the f-ratio. Nitrification (the oxidation of NH_4 to NO_3 by bacteria) is also an important variable, responsible for maintaining the deep sea nitrate reservoir and also believed to provide a source of “in situ” regenerated nitrate at the base of the euphotic zone (where phytoplankton is light limited and competes for NH_4^+ ; see review in Ward 2000). Until recently, nitrification was considered to be restricted to specific environments but over the last decade it has been found to be more widely distributed (Zehr and Ward, 2002; Lomas and Lipschultz, 2006). The failure in estimating dissolved inorganic nitrogen (DIN) taken up by phytoplankton and released as DON presents another and not entirely resolved source of error in DIN uptake rates (Bronk et al., 1994; Slawyk and Raimbault, 1995). However, the impact of such processes is rarely reported as a possible factor for overestimation in new production calculations. Finally, oceanographers have traditionally viewed the upward eddy-diffusive flux of nitrate as the exclusive source of new nitrogen supporting the export flux of biogenic particles in the open oceans. In fact, the ubiquitous pool of dinitrogen gas (N_2) dissolved in the sea can represent a significant source of new nitrogen. Recently, estimates of biological nitrogen fixation have been revised and are much higher than originally thought (Galloway et al., 1995; Grüber and Sarmiento, 1997; Capone and Carpenter, 1982). In the north subtropical and tropical Atlantic and Pacific Oceans, it has been estimated that N_2 fixation contributes to 50–180% of the nitrate flux into the photic zone (Capone et al., 2005), demonstrating that a large proportion of new primary production is fuelled by N_2 fixation rather than from deep nitrate diffusing from the deeper layers into the photic zone. While the large size classes (*Trichodesmium* and diatoms containing endosymbiotic *Richelia*) are thought to be responsible for the vast majority of N_2 fixation, recent work by Zehr et al. (2001) has found a *nifH* gene in the nanoplanktonic fraction. These small diazotrophic organisms, while present at low cellular concentration, could sustain a large proportion of the new production under nitrate-deplete conditions (Montoya et al., 2004; Falcon et al., 2004; Garcia et al., 2006, 2007). Representing 60% of the global ocean’s area, the subtropical open-ocean ecosystems are the largest coherent biomes of our planet and the biogeochemical processes they support have global consequences (Karl, 2002). These environments provide an ideal ecological niche for the development of nitrogen-fixing organisms. To date, studies dedicated to nutrient control on nitrogen fixation have concentrated on the Northern Hemisphere and there is very little data available for the Southern Hemisphere, which contains the largest ocean area globally. Deutsch et al. (2007), using an ocean

circulation model associated with the climatological distribution of nitrate and phosphate, demonstrated that nitrogen rates were highest in the Pacific Ocean and were closely related to the generation of nitrogen-deficient waters. In this context, the BIOSOPE (BIOgeochemistry and Optics South Pacific Experiment) cruise was scheduled to provide a complete data set of biogeochemical parameters in the South Pacific Ocean, characterized by a marked nitrogen-deficiency (Deutsch et al., 2007; Raimbault et al., 2007). In addition, the South Pacific Central Gyre has been described as the most oligotrophic zone in the world’s oceans (Claustre and Maritorena, 2003), exhibiting extreme nutrient limitation. It is also one of the least studied areas of the Ocean (Daneri and Quinones, 2001). The 8000-km transect, stretching from the Marquesas Islands to the Chilean coast and crossing the centre of the South Pacific Gyre, was chosen because it is an ideal area for studying primary production and new production along extreme trophic gradients. This work focuses on the geographical distribution of photosynthetic carbon fixation, nitrogen assimilation (including dinitrogen fixation and release of dissolved organic nitrogen) and nitrogen regeneration in the photic zone of the South Pacific Ocean and across a section spanning a wide range of trophic status (from nutrient enriched to severely nutrient impoverished), in order to estimate primary production and the f-ratio correctly, i.e. determining the part that was sustained by “new” nitrogen. Additionally, it provides an objective methodological approach for estimating new production in oligotrophic systems.

2 Methods

This work was carried out on board the R/V *Atalante* during October–November 2004. Data was collected during the BIOSOPE (BIOgeochemistry and Optics South Pacific experiment) cruise carried out in the southeast Pacific Ocean along a transect stretching from the Marquesas archipelago to the Chilean coast (between 146.36 W and 72.49° W, Fig. 1).

Twenty-four short-stay stations were sampled along an 8000-km transect crossing different oceanic regimes. These were the mesotrophic area associated with the plume off the Marquesas Island (141° W–134° W), the adjacent high nitrate – low chlorophyll waters (132°–123° W), the ultra-oligotrophic waters associated with the central part of the south Pacific gyre (123° W–101° W), the oligotrophic eastern side of the gyre (101° W–81° W) and the Chilean upwelling (80° W–72° W). In addition, six experimental sites were specifically investigated with long-stay, fixed stations (over 2–5 days), representing sites of different trophic regimes: MAR = Marquesas archipelago (141.3° W; 8.4° S); HLNC = High Nutrient Low Chlorophyll area east of the Marquesas islands (136.8° W; 9° S); GYR = centre of the South Pacific Gyre (114° W, 26° S); EGY = eastern border of the gyre (91.4° W, 31.8° S), UPW and UPX situated in the area of a Chilean upwelling (73° W–34° S and 72.4° W–34.5° S). The

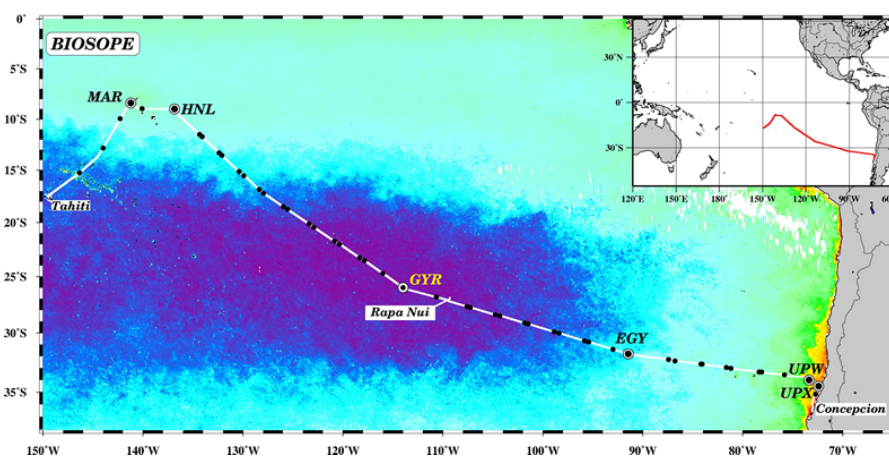


Fig. 1. Map showing the location of the BIOSOPE cruise from Marquises Island to Chile superimposed on a SeaWiFS surface Chl-*a* composite (November–December 2004). Locations of CTD casts are indicated by dark points and long time experimental stations by large circles. (MAR=141.3° W; 8.4° S; HLN=136.8° W; 9° S; GYR=114° W; 26° S); EGYR = eastern border of the gyre (91.4° W, 31.8° S; UPW=73° W–34° S and UPX=72.4° W–34.5° S).

station situated in the gyre was selected using ocean colour images, and has the lowest surface chlorophyll concentration in the world's ocean.

Nutrient measurements were performed at every station of the grid. For nitrate and nitrite determination, samples were taken into 250-ml polyethylene flasks and analyzed on board immediately using a semiautomatic Technicon Autoanalyser[®] II, according to Raimbault et al. (1990), for both low-nitrate waters (<500 nmoles l⁻¹; detection limit = 3 nmoles l⁻¹) and for high-nitrate waters (>500 nmoles l⁻¹; detection limit = 0.05 μmoles l⁻¹) according to Tréguer and le Corre (1975). Ammonium concentrations (40 ml collected in 50 ml Schott glass bottles) were measured using the fluorometric method (Holmes et al., 1999; detection limit = 0.005 μmoles l⁻¹).

At each productivity station, rates of carbon fixation (primary production), nitrate and ammonium uptake and dinitrogen fixation (diazotrophy) were measured using a dual ¹³C/¹⁵N isotopic technique. For this purpose, three 580-ml samples were collected before sunrise at 6 depths between the surface and 1% light irradiance/incidence and poured into acid-cleaned polycarbonate flasks. Bottles were rinsed after use with 10% HCl, then with distilled water from a Milli Q ion exchange unit. Labelled ¹³C sodium bicarbonate (NaH¹³CO₃ – 6 g 250 ml⁻¹ deionized water – 99 at % ¹³C, EURISOTOP) was added to each bottle in order to obtain an ≈10% final enrichment (0.5 ml 580 ml⁻¹ sea water). ¹⁵N₂ gas (99 at % ¹⁵N, EURISOTOP) was then bubbled into gas tight bottles (2 ml of gas 580 ml⁻¹ sea water). We added a fixed quantity of ¹⁵N₂ gas and calculated the enrichment of each bottle on the basis of its volume and the solubility of N₂. We used the equations provided by Weiss (1970) to calculate the initial N₂ concentration, assuming equilibrium

with the atmosphere. The ¹⁵N₂ enrichments ranged between 22% and 25% in seawater, where temperatures varied from 15°C (in the upwelling) to 27°C (in the subequatorial zone). The samples were then carefully shaken to ensure rapid equilibration between ¹⁵N₂ and natural N₂.

Nitrogen ¹⁵N-tracer additions, K¹⁵NO₃ or ¹⁵NH₄Cl (99% at ¹⁵N), were 10% or 20% of the ambient concentration based on real-time measurements. In nutrient impoverished waters, when concentrations were lower than the detection limit, additions of ¹⁵N were fixed at ~17 nmoles l⁻¹ for ¹⁵N-NO₃ and 43 nmoles l⁻¹ for ¹⁵N-NH₄.

Incubations were carried out immediately following tracer addition, just before dawn in an on-deck incubator. This consisted of 6–7 opaque boxes, each with a light screen, allowing 50%, 25%, 15%, 8%, 4%, 1% and 0.3% light penetration. The incubator was maintained at sea-surface temperature using pumped sea water. At each of the 5 experimental sites, incubations were performed in situ on a drifting rig situated at the same depth from which the samples were collected. After 24 h (dawn to dawn), final concentrations of NO₃⁻ and NH₄⁺ were measured and samples were filtered through pre-combusted (450°C) Whatman GF/F filters (25 mm in diameter, nominal porosity ≈0.7 μm), using a low vacuum pressure (<100 mm Hg). The ¹⁵N-NH₄ filtrates were collected in Duran Schott glass flasks and poisoned with 1 ml HgCl₂ (6 g l⁻¹) in order to prevent bacterial activity during storage; 200-ml aliquots of these filtrates were also filtered through 0.2 μm Teflon membranes. ¹⁵N-nitrate filtrates were collected during in situ experiments, only. In this case 300 ml of GF/F filtrate was filtered through 0.2-μm Teflon membranes and stored as above. Following filtration, filters were placed into 2-ml glass tubes, dried for 24 h in a 60°C oven and stored dry until laboratory analysis. These filters were

used to determine the final $^{15}\text{N}/^{13}\text{C}$ enrichment ratio in the particulate organic matter and the concentrations of particulate carbon and particulate nitrogen.

The dual isotopic enrichment analysis was performed on an Integra-CN mass spectrometer, calibrated using glycine references for every batch of 10–15 samples. The accuracy of our analytical system was also regularly verified using reference materials from the International Atomic Energy Agency (IAEA, Analytical Quality Control Services). The mean ^{15}N atom % did not vary between 0.2 and 10 $\mu\text{moles N}$. Thus, the low background of the system gave an accurate analyse for samples containing low nitrogen concentrations (0.1–0.2 μmole), values often observed in surface oligotrophic waters. The ^{15}N isotope enrichment of a sample is reported in terms of the ratio of ^{15}N atom % excess overtime, over the ^{15}N atom % in non-enriched samples taken from the same phytoplankton population at time zero. The value of time zero enrichment is vital and was determined using samples (same volume as the incubated sample) which were filtered immediately after isotope addition. For N_2 experiments, the time zero value, established using 8 samples, was $0.3676 \pm 0.007\%$. For $^{15}\text{N}\text{-NO}_3$ and $^{15}\text{N}\text{-NH}_4$ experiments, time 0 enrichment was $0.372 \pm 0.007\%$. We considered the results to be significant when ^{15}N excess enrichments were greater than 0.014% (two times the standard deviation obtained with time zero samples).

The transport rate of ^{15}N -labelled dissolved inorganic nitrogen (DIN), from the DIN pool to the PON pool, i.e. the net DIN uptake ($\rho_{\text{DIN}}^{\text{net}}$ in $\text{nmoles l}^{-1} \text{d}^{-1}$) was computed, according to Dugdale and Wilkerson (1986), from Eq. (1):

$$\rho_{\text{DIN}}^{\text{net}} = \frac{R_{\text{PON}}}{R_{\text{DIN}} \times T} \times [\text{PON}], \quad (1)$$

where R_{PON} and R_{DIN} represent the ^{15}N atom % excess enrichment in the PON and DIN pools, respectively, $[\text{PON}]$ represents the final PON concentration and T represents the incubation time (in days). To correct ammonium uptake rates for isotopic dilution, we made R_{DIN} in Eq. (1) equal to the mean value obtained between initial and final R_{NH_4} . According to these experimental conditions, the detection limit for nitrogen uptake, calculated from significant enrichment (0.014% in excess) and lowest particulate nitrogen (0.2 $\mu\text{mole N}$) is estimated from Eq. (1) to be $0.12 \text{ nmol l}^{-1} \text{d}^{-1}$ for nitrogen-fixation (mean $R_{\text{DIN}} \approx 24\%$) and $0.03 \text{ nmol l}^{-1} \text{d}^{-1}$ for nitrate and ammonium uptake in nutrient-depleted waters ($R_{\text{DIN}} \approx 100\%$).

Carbon fixation rates were calculated according to Slawyk and Collos (1984), with a time 0 enrichment of $1.113 \pm 0.005\%$ ($n=8$). This time 0 value is little higher than the natural abundance for phytoplankton (1.089), due to residual traces of ^{13}C tracer. It should be noted that the ^{13}C enrichment of samples was less problematic than the ^{15}N enrichment, since inorganic carbon is assimilated by the whole phytoplankton population and excess values ranged

from 0.3 to 3.6%. Fixation rates for ^{13}C , i.e. primary production, were calculated from the mean of three replicates and are expressed in $\mu\text{g C l}^{-1} \text{d}^{-1}$. Applying a similar calculation as that for nitrogen, the detection limit is estimated to be $0.35 \mu\text{g C l}^{-1} \text{d}^{-1}$.

GF/F filtrates from the $^{15}\text{NH}_4$ incubations were used to measure the final ^{15}N enrichment 1) in the DIN pool and 2) in the $<0.7 \mu\text{m}$ organic matter pool, as outlined by Raimbault et al. (1999). In this procedure, all forms of DIN are removed from the sample as $(\text{NH}_4)_2\text{SO}_4$, by successive diffusion and reduction processes. The first diffusion step enables us to quantify the final ^{15}N enrichment of the ammonium pool, and the estimation of the isotope dilution of the tracer due to NH_4 regeneration. During the second diffusion, the ^{15}N enrichment of the nitrate pool in the ammonium filtrates enables us to quantify the oxidation of ammonium to nitrate (nitrification). During the third diffusion, the ^{15}N enrichment was determined in the fraction passing through GF/F to estimate the rate of $^{15}\text{N}\text{-NH}_4$ accumulation in the $<0.7 \mu\text{m}$ organic matter (dissolved organic nitrogen + $<0.7 \mu\text{m}$ particulate nitrogen). The $<0.2 \mu\text{m}$ filtrates from $^{15}\text{N}\text{-NH}_4$ and $^{15}\text{N}\text{-NO}_3$ experiments were used to measure ^{15}N enrichment in the $<0.2 \mu\text{m}$ fraction which only contains dissolved organic nitrogen (DON), in order to estimate tracer loss in terms of DON ($\rho_{\text{DIN}}^{\text{loss}}$).

Ammonium regeneration rates (r_{NH_4} in $\text{nmoles l}^{-1} \text{d}^{-1}$) were estimated according to Laws (1984):

$$r_{\text{NH}_4} = \frac{[\text{NH}_4]_I + [\text{NH}_4]_F}{2 * T} * \ln \left(\frac{R_{\text{ONH}_4}}{R_{f\text{NH}_4}} \right), \quad (2)$$

where $[\text{NH}_4]_I$ and $[\text{NH}_4]_F$ represent initial and final concentrations of ammonium during the incubation experiment. R_{ONH_4} and $R_{f\text{NH}_4}$ are the initial and final excess enrichments in $^{15}\text{N}\text{-NH}_4$ for the incubation period.

Nitrification rates (ρ_{NIT} in $\text{nmoles l}^{-1} \text{d}^{-1}$) were computed according to Raimbault et al. (1999):

$$\rho_{\text{NIT}} = \frac{R_{\text{NO}_3}}{R_{\text{NH}_4} \times T} \times [\text{NO}_3], \quad (3)$$

where R_{NO_3} is the ^{15}N atom % excess enrichment in the $(\text{NO}_3^- + \text{NO}_2^-)$ pool, R_{NH_4} is the mean ^{15}N atom % excess enrichment of the NH_4^+ pool, and $[\text{NO}_3]$ is the final NO_3^- concentration in the filtrate.

The measurement of ^{15}N abundance in the organic matter collected in the $<\text{GF/F}$ filtrate ($R_{<\text{GF/F}}$) enabled us to calculate ammonium uptake in the $<0.7 \mu\text{m}$ fraction ($\rho_{\text{NH}_4}^{<\text{GF/F}}$), calculated as following (Eq. 4):

$$\rho_{\text{NH}_4}^{<\text{GF/F}} = \frac{R_{<\text{GF/F}}}{R_{\text{NH}_4} \times T} \times [\text{PON}_{<\text{GF/F}}], \quad (4)$$

where $R_{<\text{GF/F}}$ and R_{NH_4} are the ^{15}N atom % excess enrichment of the $<\text{GF/F}$ fraction and final ammonium pool, respectively, and $[\text{PON}_{<\text{GF/F}}]$ is the final particulate nitrogen in the GF/F filtrate. The measurement of ^{15}N abundance in

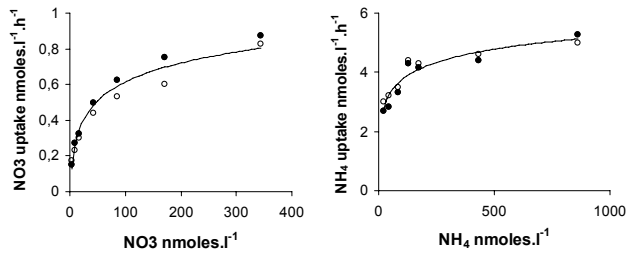


Fig. 2. Rates of nitrate and ammonium uptake ($\text{nmol L}^{-1} \text{h}^{-1}$) as a function of nitrate and ammonium additions in nutrient-depleted waters. Experiments were performed during two successive days with surface waters of the South Pacific Gyre (114°W – 26°S).

the extracellular DON pool (R_{DON}) enabled us to calculate the DIN (nitrate or ammonium) lost ($\rho_{\text{DIN}}^{\text{loss}}$) as DON (Eq. 5), calculated as outlined by Slawyk et al. (1998):

$$\rho_{\text{DIN}}^{\text{loss}} = \frac{R_{\text{DON}}}{R_{\text{DIN}} \times T} \times [\text{DON}], \quad (5)$$

where R_{DON} and R_{DIN} are the ^{15}N atom % excess enrichment of the extracellular DON and DIN pool, respectively, and $[\text{DON}]$ is the final extracellular DON concentration. The quantification of the $\rho_{\text{DIN}}^{\text{loss}}$ offers the possibility for calculating the gross uptake rate $\rho_{\text{DIN}}^{\text{gross}}$ as the sum of the net DIN uptake and the DIN loss:

$$\rho_{\text{DIN}}^{\text{gross}} = \rho_{\text{DIN}}^{\text{net}} + \rho_{\text{DIN}}^{\text{loss}}. \quad (6)$$

During this study, nitrate and ammonium concentrations were often lower than the detection limit (especially in the South Pacific Gyre) and it was experimentally impossible to reduce the addition of the tracer to the ideal level ($<10\%$ of ambient concentration). In these nutrient conditions, the tracer addition violates the general assumption that the tracer addition does not disturb the steady-state of the system and could well have evoked a major perturbation in the nitrate and ammonium uptake (Allen et al., 2002; Harrison et al., 1996). Despite this, the use of kinetic parameters, described by Harrison et al. (1996), enabled us to account for the uptake rate enhancement according to the following equation given by Rees et al. (1999),

$$\rho N_H = \rho N_0 / [N_{sp} / (K_s + N_{sp}) \times (K_s + N_A) / N_A], \quad (7)$$

where N is nitrate or ammonium, ρN_0 is the original uptake rate ($\text{nmol L}^{-1} \text{d}^{-1}$), ρN_H is the uptake rate adjusted for enhancement of tracer, N_{sp} is the ambient + tracer nutrient (nmol), N_A is the ambient nutrient and K_s is the half-saturation constant. In this case, N_A was assumed to be 3 nmol L^{-1} for nitrate and 5 nmol L^{-1} for ammonium, corresponding to the detection limit of our analytical procedures. To quantify the affinity constant K_s , two kinetic studies were performed with 6 graduated additions of ^{15}N -labeled substrate (Fig. 2). A Monod equation

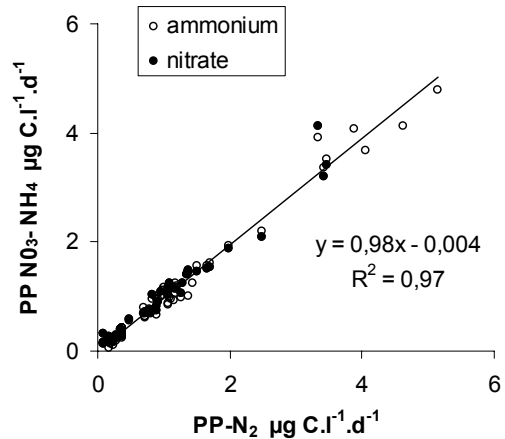


Fig. 3. Comparison between primary production ($\text{mg C m}^{-3} \text{d}^{-1}$) measured in nutrient-depleted samples, e.g. without nutrient additions (PP N_2), and those ($\text{PP NO}_3\text{-NH}_4$) spiked with nitrate (17 nmol L^{-1}) or ammonium (43 nmol L^{-1}). The solid line is the model II linear regression.

$[V = VmS / (K_s + S)]$ was assumed, where V is the uptake rate for substrate concentration S , Vm is the saturated uptake rate and K_s , the affinity constant, e.g. the substrate concentration at half Vm . The kinetics constant K_s , needed for the use of Rees et al.'s model, was derived from the Wolf plot linear transformation of S/V vs. S . K_s obtained during 4 experiments performed in nitrogen-depleted waters (12.9 and 15 nmol L^{-1} for nitrate and ammonium, respectively) were a little lower than those measured in other oceanic waters (around $25\text{--}30 \text{ nmol L}^{-1}$) by Sahlsten (1987) and Harrison et al. (1996). As a first approximation, we assumed that DIN losses as DON ($\rho_{\text{DIN}}^{\text{loss}}$) and nitrification (ρ_{NIT}) could be activated in the same way as net uptake rates and we applied the same procedure of correction to these processes.

In addition, spiked nutrient additions in nutrient-limited waters could also stimulate ^{13}C fixation. Thus samples enriched with $^{15}\text{N-N}_2$, which did not significantly change the N_2 concentration of the samples, were used as a control for the stimulation of primary production by ^{15}N -tracer additions in oligotrophic waters (Fig. 3). Model II gives a regression coefficient of 0.98 , revealing no significant stimulation of primary production by low nutrient addition, at least over the 24 h experiments. As the ^{13}C isotope is not routinely used for estimating marine productivity, especially in oligotrophic oceanic areas, our results (PP^{13}C) also offered the opportunity to carry out an extensive comparison with classical primary production measurements using a ^{14}C tracer (PP^{14}C) in the same conditions (T. Moutin, personal communication). On pooling all the data collected during in situ experiments and using the model II linear regression, we noted the significant relationships ($\text{PP}^{13}\text{C} = 1.02 \text{ PP}^{14}\text{C} + 0.14$, $r^2 = 0.98$; $n = 50$), which indicated the efficiency of the ^{13}C procedure in quantifying the photosynthetic carbon fixation in oligotrophic waters.

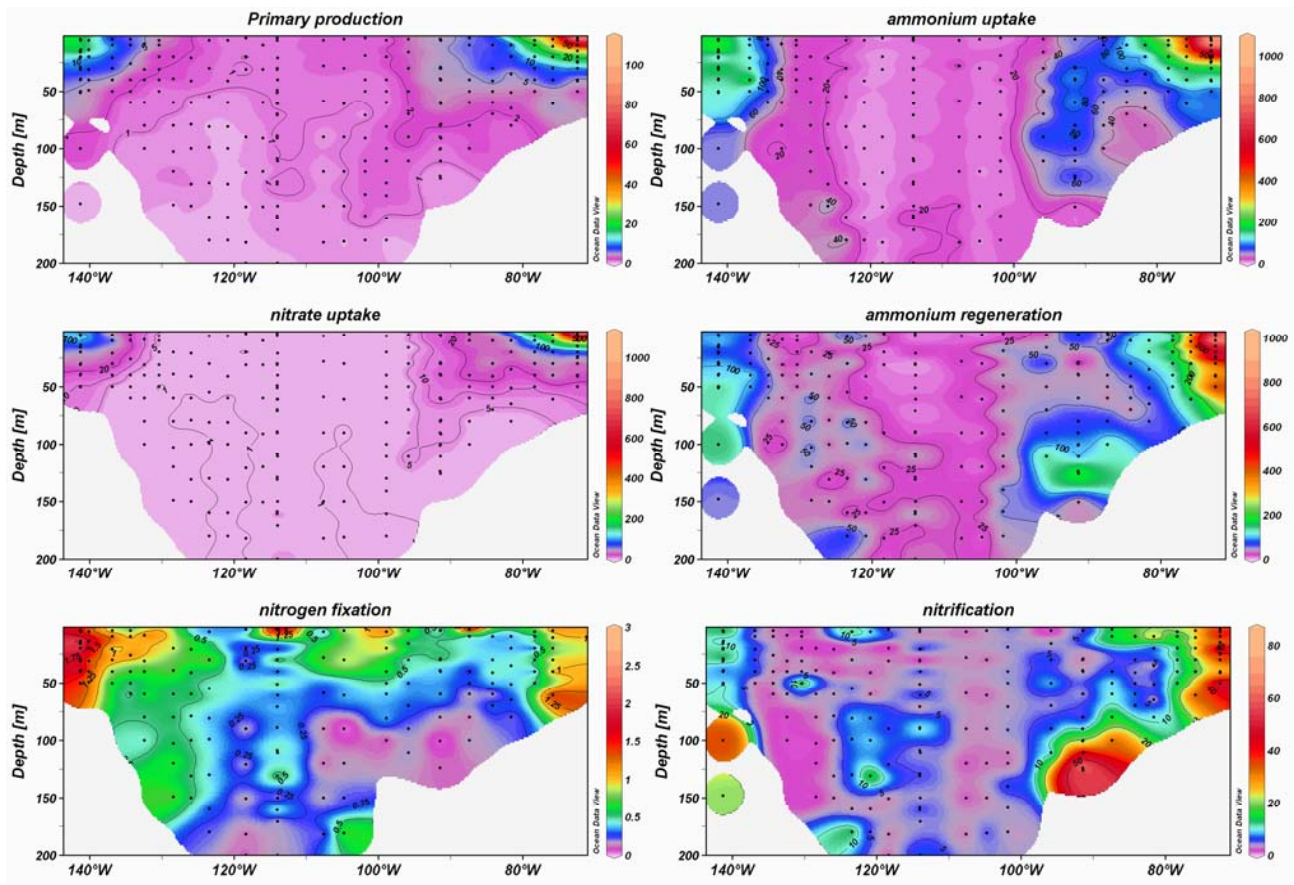


Fig. 4. Zonal sections of primary production ($\mu\text{g C l}^{-1} \text{d}^{-1}$), nitrate uptake ($\text{nmoles l}^{-1} \text{d}^{-1}$), ammonium uptake ($\text{nmoles N l}^{-1} \text{d}^{-1}$), nitrogen fixation ($\text{nmoles N l}^{-1} \text{d}^{-1}$), ammonium regeneration ($\text{nmoles N l}^{-1} \text{d}^{-1}$) and nitrification ($\text{nmoles N l}^{-1} \text{d}^{-1}$), along the BIOSOPE Transect. (Ocean Data View software (ODV), version 3.1; Reiner Schlitzer; <http://odi.awi-bremerhaven.de/2005>).

Surface light levels and the thickness of the euphotic layer were measured around noon using a spectroradiometer (LI.1800U.W, LI-COR instrument; Morel et al., 2007). The depth of the euphotic zone (Z_e) was defined as the depth where the downward photosynthetic available radiation (PAR) irradiance was reduced to 1% of its surface value; For CTD casts performed early in the morning, Z_e was computed using in situ TChl-*a* concentration profiles (see Ras et al., 2007), according to the model developed by Morel and Maritorea (2001).

3 Results

A detailed description of the geographical distribution of nutrients and biomass during this study can be found in Raimbault et al. (2007). Briefly, the zonal distribution of surface nitrate showed minimal values (lower than the detection limit of 3 nmoles l^{-1}) between 125° W and 95° W , i.e. in the South Pacific Gyre (SPG). Other regions (Marquesas Islands and Chilean upwelling) showed significant nitrate concentrations ($>0.5 \mu\text{moles l}^{-1}$) in the surface. Chlorophyll biomass fol-

lowed this general trend with very low values in the center of the SPG ($0.023 \mu\text{g l}^{-1}$), with levels reaching $0.3 \mu\text{g l}^{-1}$ near the Marquesas Islands and $1 \mu\text{g l}^{-1}$ in the Chilean upwelling. The photic layer located at $40\text{--}50 \text{ m}$ around the Marquesas and upwelling regions deepened in the centre of the SPG, reaching 160 m between 120° W and 105° W , which could be expected in the clearest natural waters of the world (Morel et al., 2007; Tedetti et al., 2007). The incident solar radiation was more or less constant during the cruise ($41 \pm 7 \text{ Em}^{-2} \text{ s}^{-1}$) with the exception of three very cloudy days (9 to 11 November 2004, e.g. from 120° W to 117° W), where incident radiation decreased to $14\text{--}20 \text{ Em}^{-2} \text{ s}^{-1}$.

Primary production and nitrogen uptake rates followed the same general distribution, responding to the nutrient variations observed in the photic layer along the transect (Fig. 4). A large central area was characterized by very low primary production rates and this was surrounded by two small regions: the subequatorial Marquesas region (in the west) where primary production reached $10 \mu\text{g C l}^{-1} \text{d}^{-1}$ in surface waters, and a part of the Chilean upwelling in the east, which was the most productive area, primary

production reaching more than $50 \mu\text{g C l}^{-1} \text{d}^{-1}$. For the most part, the transect (e.g. the South Pacific Gyre = SPG) was characterized by very low carbon fixation rates, less than $2 \mu\text{g C l}^{-1} \text{d}^{-1}$ between 130 and 95°W . Vertical variations in primary production were insignificant in the centre of the SPG, with the rates remaining more or less constant ($\approx 1\text{--}2 \mu\text{g C l}^{-1} \text{d}^{-1}$) from the surface to the base of the photic layer. Nitrate and ammonium uptake rates followed the same general pattern as primary production. Nitrate uptake ranged from $100\text{--}500 \text{ nmoles l}^{-1} \text{d}^{-1}$ in the upwelling to less than $5 \text{ nmoles l}^{-1} \text{d}^{-1}$ in the SPG. Intermediate values were found near the Marquesas Islands ranging from 20 and $100 \text{ nmoles l}^{-1} \text{d}^{-1}$. Ammonium uptake rates (corrected from isotopic dilution) were always significantly higher than nitrate uptake rates. The upwelling presented the highest uptake rates (up to $500 \text{ nmoles l}^{-1} \text{d}^{-1}$), intermediate levels (up to $100 \text{ nmoles l}^{-1} \text{d}^{-1}$) were observed around the Marquesas Island and very low rates ($<40 \text{ nmoles l}^{-1} \text{d}^{-1}$) in the SPG. As for primary production, vertical distribution of ammonium uptake, as well as nitrate uptake were quite homogeneous in the SPG, with very low vertical variation and no clear surface or subsurface maximum. However, contrary to primary production, noticeable rates of ammonium and nitrate uptake (>60 and $>5 \text{ nmoles l}^{-1} \text{d}^{-1}$, respectively) were detected, reaching depths of 100 m on the eastern edge of the SPG between 90 and 100°W .

Dinitrogen fixation rates showed a particular distribution, with rates always lower than ammonium and nitrate uptake. Firstly, the vertical extension of this biological process was more important to the west (until 150 m) than to the east of the investigated area. Secondly, nitrogen fixation was essentially located near the surface in the SPG, where a clear surface maximum ($>1 \text{ nmoles l}^{-1} \text{d}^{-1}$) was detected. Rates decreased rapidly with depth and were $<0.5 \text{ nmoles l}^{-1} \text{d}^{-1}$ below 50 m . The geographical gradient was weak since maximum surface rates measured in the upwelling ($3.6 \text{ nmoles l}^{-1} \text{d}^{-1}$) were only two folds higher than the maximum rates measured in the SPG ($1.8 \text{ nmoles l}^{-1} \text{d}^{-1}$). The Marquesas Island was marked by intermediate nitrogen fixation ($\approx 2 \text{ nmoles l}^{-1} \text{d}^{-1}$).

Ammonium regeneration rates showed the same regional variations. This process was very active in surface water near the upwelling ($>200 \text{ nmoles l}^{-1} \text{d}^{-1}$), as well as around the Marquesas Islands with rates $>100 \text{ nmoles l}^{-1} \text{d}^{-1}$ until 135°W . Surface values decreased to $20 \text{ nmoles l}^{-1} \text{d}^{-1}$ in the SPG, but remained more or less constant between the surface and 200 m . As for ammonium uptake, a subsurface maximum (located around 125 m) was detected on the eastern edge (90°W) of the SPG. The significant ammonium regeneration measured at all stations, regardless of the trophic level, induced great variations of ammonium enrichment during the 24-h incubations. Figure 5 demonstrates that if isotopic dilution is not taken into account, then there is a massive underestimation of ammonium uptake of more than 50%. Moreover, there was no relationship between the mag-

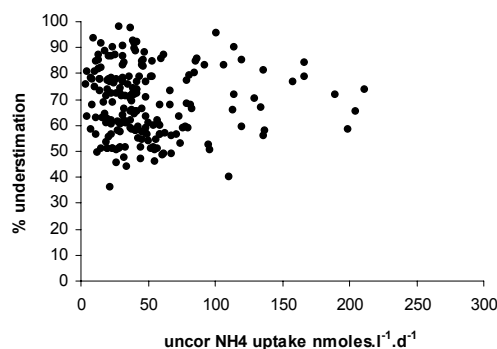


Fig. 5. Percentage of underestimation of ammonium uptake (% underestimation) when isotopic dilution is not included for calculating rates versus ammonium uptake rates not corrected from the isotopic dilution (uncor NH_4 uptake).

nitude of the underestimation and the uptake rates, clearly indicating that estimates of isotopic dilution are necessary in order to quantify ammonium uptake over 24-h incubations, even in oligotrophic waters.

Nitrification showed a similar pattern to that of ammonium regeneration, indicating a tight coupling between the two processes, although rates, always significant, were globally one order of magnitude lower than those of ammonium regeneration. Highest nitrification rates ($>30 \text{ nmoles l}^{-1} \text{d}^{-1}$) were observed in the upwelling with a westward extension to 90°W . The subsurface patch of ammonium regeneration at 90°W was also marked by active nitrification (up to $40 \text{ nmoles l}^{-1} \text{d}^{-1}$). The Marquesas region was characterized by relatively low nitrification rates ($5\text{--}10 \text{ nmoles l}^{-1} \text{d}^{-1}$), while the lowest, but detectable values ($<5 \text{ nmoles l}^{-1} \text{d}^{-1}$) were measured in the SPG. As observed for preceding biological processes, nitrification was again homogeneous throughout the water column with no significant maximum in the oligotrophic central region. Nitrate uptake in comparison to nitrification generally dominated the upper layer, except in the SPG, where both rates were similar. At the base of the photic layer, nitrification rates were 2 to 10 times higher than the corresponding nitrate uptake rates, especially in the upwelling area.

A significant proportion of the ammonium was assimilated by the particulate matter passing through the GF/F filters (Fig. 6). This $<0.7 \mu\text{m}$ ammonium uptake was significant in the upwelling region, with rates higher than $25 \text{ nmoles l}^{-1} \text{d}^{-1}$ and up to $170 \text{ nmoles l}^{-1} \text{d}^{-1}$, but also significant in the SPG (10 to $20 \text{ nmoles l}^{-1} \text{d}^{-1}$). Some of the $<0.7 \mu\text{m}$ uptake was ultimately found in the $<0.2 \mu\text{m}$ fraction, i.e. in the dissolved organic nitrogen pool, rates here defined as ρ_{loss} . Ammonium losses in terms of DON were again highest in the upwelling area (50 to $100 \text{ nmoles l}^{-1} \text{d}^{-1}$), but highly significant in the oligotrophic SPG (5 to $20 \text{ nmoles l}^{-1} \text{d}^{-1}$). The lowest rates ($<5 \text{ nmoles l}^{-1} \text{d}^{-1}$) were measured in the western part of

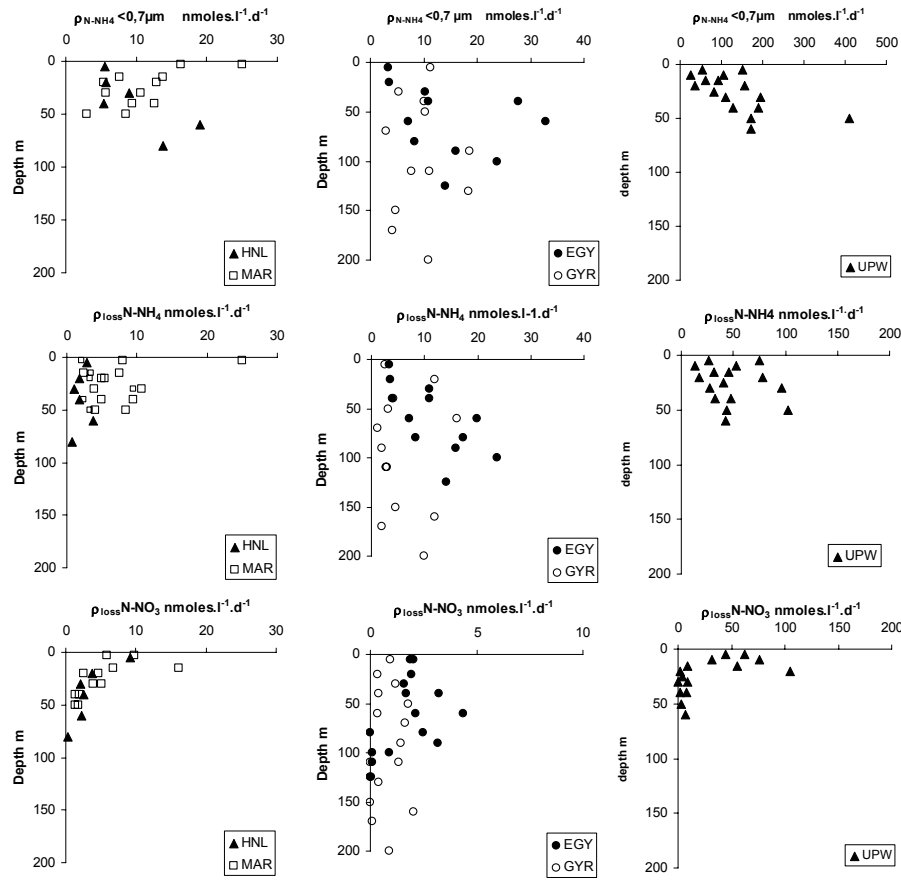


Fig. 6. Vertical profiles of ammonium uptake in the $<GF/F$ fraction ($\rho_{\text{NH}_4} < 0.7 \mu\text{m}$; upper panels), loss of ^{15}N -ammonium in terms of DON in the $<0.2 \mu\text{m}$ fraction ($\rho_{\text{loss NH}_4}$; middle panels) and loss of ^{15}N -nitrate in terms of DON in the $<0.2 \mu\text{m}$ fraction ($\rho_{\text{loss NO}_3}$; lower panels) at the five experimental sites.

the area. The nitrate losses were lowest in the SPG (1 to $5 \text{ nmoles l}^{-1} \text{ d}^{-1}$) and highest in the surface waters of the upwelling. Some data in the SPG appeared close to zero and could be explained by the very low uptake rates of labeled nitrogen and then the very low excess enrichment in the $<0.2 \mu\text{m}$ DON pool (close to 0.01%). Loss of nitrate generally tended to decrease rapidly with depth, as observed in the most productive region (Marquesas Islands and Chilean upwelling). The mean DIN percentage loss showed important regional variations (Table 1). The lowest productive system (SPG) revealed the most important loss of recent nitrogen uptake ($>20\%$), while in the other regions percentage losses were less than 15%. It should be noted that the percentage of N-nitrate losses were equivalent to those of N-ammonium losses, except around the Marquesas Islands (Mar and HLN sites).

Several corrections have been applied to the f-ratio to take into account several processes that are rarely measured during nitrogen uptake experiments, such as nitrification, DIN loss and nitrogen fixation. Nitrification (as a source of nitrate) can induce overestimations of new production by

adding NO_3^- to the nitrate pool, with some being derived from regenerated production (Dore and Karl, 1996; Ward et al., 1989; Priscu and Downes, 1985; Dugdale and Goering, 1967). Thus, the fraction of nitrate produced by nitrification (ρ_{NIT}) has to be subtracted from the total nitrate uptake (ρ_{NO_3}) in order to truly assess the uptake of “new” nitrate as classically defined by Dugdale and Goering (1967). As nitrogen fixation rates (ρ_{N_2}) were available, they were included in the estimate of new production (P_{new}), calculated as follows:

$$P_{\text{new}} = \rho_{\text{N}_2} + (\rho_{\text{NO}_3} - \rho_{\text{NIT}}). \quad (8)$$

When nitrification rates were higher than nitrate uptake ($\rho_{\text{NO}_3} - \rho_{\text{NIT}} < 0$), P_{new} was estimated to be equal to ρ_{N_2} . According to this assumption, the f-ratio can be calculated as follows:

$$f = \frac{\rho_{\text{N}_2} + \rho_{\text{NO}_3} - \rho_{\text{NIT}}}{[\rho_{\text{N}_2} + \rho_{\text{NO}_3} + \rho_{\text{NH}_4^+}]}. \quad (9)$$

As ρ_{loss} was not available for all stations (especially from ^{15}N - NO_3 experiments), gross uptake rates were not used in the calculation of the f-ratio, which was only estimated with

Table 1. Percentages (mean values integrated over the photic layer) of ammonium uptake in the <GF/F filtrate ($\rho_{<0.7\mu\text{m}}$) and loss in terms of DON ($\rho_{\text{DON}<0.2\mu\text{m}}$) from ammonium and nitrate relative to gross uptake rates ($\rho_{\text{gross}} = \rho_{\text{net}} + \rho_{\text{DON}<0.2\mu\text{m}}$) for the five investigated oceanic regions. Values from nitrate values are available from only in situ profiles performed on the 5 experimental sites.

Area	Ammonium % ρ_{gross}		Experimental site	Ammonium % ρ_{gross}		Nitrate % ρ_{gross}
	$\rho_{<0.7\mu\text{m}}$	$\rho_{\text{DON}<0.2\mu\text{m}}$		$\rho_{<0.7\mu\text{m}}$	$\rho_{\text{DON}<0.2\mu\text{m}}$	$\rho_{\text{DON}<0.2\mu\text{m}}$
MAR (141°–134° W)	7±4	4±2	12° S–138° W	6±3	4±2	11±4
HNL (133°–123° W)	17±14	10±9	9° S–136° W	7±4	1±1	10±7
SPG (123°–101° W)	41±19	28±13	26° S–114° W	26±14	20±7	19±12
EGY (100°–81° W)	25±15	15±13	32° S–91° W	16±14	12±7	11±9
UPW (80°–72° W)	26±36	12±9	34° S–73° W	55±61	16±14	12±8

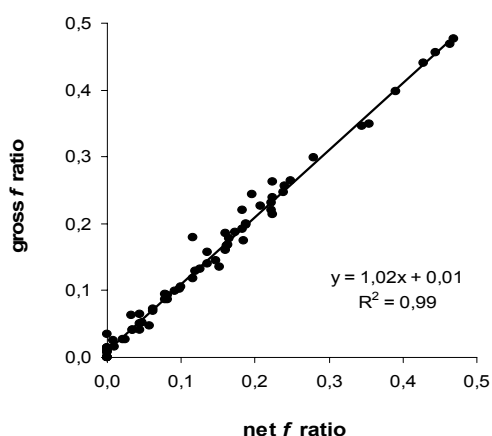


Fig. 7. Comparison of f-ratio calculating from gross nitrogen uptake (gross f-ratio) and from net nitrogen uptake rates (net f-ratio). The linear regression line was obtained from model II regression.

the net uptake rates. Using data from in situ experiments, where both losses of N-nitrate and N-ammonium were measured, the model II regression analysis gives a slope of 1.02 (Fig. 7). The slope was not significantly different from 1, indicating that by including DIN loss one does not change the estimates of the f-ratios. To assess the influence of nitrification and N_2 -fixation on the magnitude of the f-ratio, we compared the f-ratio calculation, according to Eq. (5), to those calculated without nitrification ($f_{-\text{NIT}}$) or without N_2 -fixation ($f_{-\text{N}_2}$). The possible overestimation due to the noninclusion of uptake of urea could not be evaluated, since fluxes of this organic nitrogen compound have not been investigated in this area.

The geographical variations of the f-ratios (averaged over the photic layer) reflect the zonal evolution of the trophic states (Fig. 8), with highest values (>0.30) observed in the upwelling. Waters surrounding the Marquesas Islands were characterized by f-ratios ranging between 0.1 and 0.2. In the SPG, the f-ratio was generally lower than 0.1, with very low

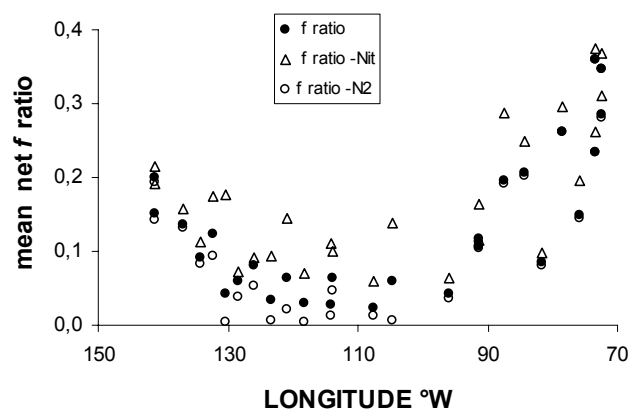


Fig. 8. Zonal evolution of net f-ratio calculating without nitrification (f-ratio – Nit), without dinitrogen fixation (f-ratio – N_2), or including both processes (f-ratio).

values (0.02) found in the centre. The exclusion of nitrification rates ($f_{-\text{NIT}}$) significantly increased the f-values in the SPG (0.08–0.15). In the other regions nitrification, although acting at significant rates, did not modify the mean f-ratio. In the same way, the influence of nitrogen fixation was only sensitive in the SPG. In this oligotrophic area, $f_{-\text{N}_2}$ down to very low values (often close to 0) clearly indicated that nitrogen fixation was the main process providing new nitrogen in this upper layer.

4 Discussion

This study confirms previous satellite observations suggesting very low productivity in the SPG, i.e. in the clearest waters of the world's ocean (Morel et al., 2007; Tedetti et al., 2007). Nixon (1995) assigned annual rates of carbon fixation of <100, 100 to 300 and 300 to 500 $\text{g C m}^{-2} \text{y}^{-1}$ in oligotrophic, mesotrophic and eutrophic areas, respectively. Following this criterion and assuming that our measured rates remained constant over the year, the upwelling

Table 2. Mean and standard deviation of integrated rates over the photic layer of nitrate (ΣNO_3), primary production (ΣPP), nitrate uptake ($\Sigma\rho\text{NO}_3$), ammonium uptake ($\Sigma\rho\text{NH}_4$), nitrogen fixation ($\Sigma\rho\text{N}_2$), carbon/nitrogen ratio during uptake (C/N), ammonium regeneration (r_{NH_4}) and nitrification (ρ_{NIT}) pooled for each studied oceanic area.

Area	ΣNO_3 mmoles m^{-2}	ΣPP $\text{g m}^{-2} \text{d}^{-1}$	$\Sigma\rho\text{NO}_3$	$\Sigma\rho\text{NH}_4$ mmoles $\text{m}^{-2} \text{d}^{-1}$	$\Sigma\rho\text{N}_2$	C/N	$\Sigma\rho\text{NH}_4$ mmoles $\text{m}^{-2} \text{d}^{-1}$	Σr_{NH_4}	$\Sigma\rho_{\text{NIT}}$
MAR (141°–134° W)	128±24	0.66±0.1	2.2±1.1	8.7±3.6	0.11±0.03	6.3±2.6	6.3±1.6	5.8±1.9	0.82±0.4
HNL (133°–123° W)	49±73	0.25±0.12	0.5±0.7	4.6±4.3	0.07±0.07	5.2±2.2	2.6±0.8	4.8±3.1	0.61±0.7
SPG (123°–101° W)	0.84±1.3	0.15±0.05	0.06±0.06	2.1±1.0	0.06±0.03	6.1±2.3	1.2±0.6	3.5±1.9	0.76±0.4
EGY (100°–81° W)	141±67	0.33±0.6	0.82±0.4	6.0±2.3	0.03±0.005	4.4±1.4	2.9±0.4	6.3±2.0	0.81±0.5
UPW (80°–72° W)	285±310	1.8±1.3	8.6±6.8	20±10	0.09±0.06	4.9±0.9	6.2±2.0	19 11	1.31±0.6

(660 $\text{g C m}^{-2} \text{y}^{-1}$) could be described as eutrophic, the Marquesas region as mesotrophic (270 $\text{g C m}^{-2} \text{y}^{-1}$), and the SPG (36 $\text{g C m}^{-2} \text{y}^{-1}$) as an “ultra” oligotrophic system.

The zonal variation of integrated rates over the euphotic layer, using the trapezoidal method, revealed some specific patterns (Table 2). For example, the increase in primary production and nitrogen uptake was not as pronounced as the increase in nutrient availability. Although integrated nitrate concentrations increased by a factor of 100 and 300 from the oligotrophic zone (0.9 mmoles m^{-2}) to the Marquesas or to upwelling regions (128 mmoles m^{-2} and up to 285 mmoles m^{-2} , respectively), integrated carbon fixation rates increased only by 10 to 20 fold. Nitrogen fixation appeared more or less constant around 0.03–0.11 $\text{mmoles m}^{-2} \text{d}^{-1}$, while integrated nitrate uptake increased 10 or 50 fold between the SPG (0.2 $\text{mmoles m}^{-2} \text{d}^{-1}$) and the Marquesas region (2.9 $\text{mmoles m}^{-2} \text{d}^{-1}$) or the upwelling (11 $\text{mmoles m}^{-2} \text{d}^{-1}$). The C/N uptake ratios were always lower than the conventional 6.6 Redfield ratio (Table 2). Such low C/N uptake ratios may suggest that some nitrogen assimilation (especially ammonium) was due to heterotrophic organisms. The importance of submicron heterotrophic organisms was emphasized by the large quantity of $^{15}\text{N-NH}_4$ found in the <GF/F filtrates, i.e. the <0.7 μm size fraction, following 24-h incubations (Table 1). The low efficiency of the GF/F filters for PON retention compared to 0.2- μm membranes is now well-documented in a variety of marine environments (Altabet, 1990; Libby and Wheeler, 1997; Slawyk and Raimbault, 1995; Raimbault et al., 2000; Fernandez et al., 2007) and has been confirmed during this study (Raimbault et al., 2007). Our experiments showed that the use of GF/F filters can result in severe underestimations of ammonium uptake during high productivity, as well as under oligotrophic conditions. This emphasizes the importance of discussing the use of GF/F and 0.2- μm filters for tracer addition experiments. GF/F filters do, however, collect all particles containing chlorophyll, i.e. photosynthetic organisms (Chavez et al., 1995; Raimbault et al., 2007) and this heterotrophic ammonium uptake should not be included in the estimates for regenerated primary production. Con-

sequently, the underestimation of gross ammonium uptake rates by filtering through GF/F filters should not have any consequences for the f-ratio estimation. There are no current data available giving information on the possible nitrate uptake by the <0.7 μm size fraction; however, a study conducted in the equatorial Pacific has shown that submicron particles passing through the GF/F filters do not assimilate nitrate (Raimbault et al., 2000).

As our C/N uptakes deviate from the Redfield ratio, no relationship was found between new production estimates obtained using the ^{13}C fixation rates, multiplied by the independently estimated f-ratio, and those computed using direct measurements of new nitrogen multiplied by the 6.6 Redfield ratio (Table 3). The two estimates often disagreed by 25–50%, with the lowest (0.007–0.008 $\text{g C m}^{-2} \text{d}^{-1}$) and highest (0.53–0.69 $\text{g C m}^{-2} \text{d}^{-1}$) values found in the SPG and in the upwelling, respectively. The extremely low f-ratio obtained in the SPG (0.05±0.03) confirms that most of the primary production, which maintained relatively significant rates over the 0–180 m water column, was supported by regenerated nitrogen. This is indicated by the relatively high values of ammonium uptake (2.1 $\text{mmoles m}^{-2} \text{d}^{-1}$), as well as by significant ammonium and nitrate regeneration rates, 3.5 and 0.76 $\text{mmoles m}^{-2} \text{d}^{-1}$, respectively (Table 2). Rates of NH_4 regeneration are rare for oceanic waters but our results are in the range of the data available (e.g. Bode et al., 2002; Raimbault et al., 1999; Fernandez and Raimbault, 2007). Ammonium regeneration showed high rates (up to 500 $\text{nmoles l}^{-1} \text{d}^{-1}$) in the high productive Marquesas and upwelling regions (MAR and UPW), but significant activity was also measured in the SPG (10–20 $\text{nmoles l}^{-1} \text{d}^{-1}$); these rates were able to sustain the biological demand. This observation was substantiated by the picoplankton abundance which was strongly dominated by heterotrophic bacterioplankton along the whole transect (Grob et al., 2007).

Another important finding was the magnitude of the nitrification process in the euphotic layer. Although the potential significance of “regenerated” nitrate in the euphotic zone has been acknowledged for some time (Dugdale and Goering, 1967; Ward et al., 1989; Dore and Karl, 1996) and nitrification studies have been performed in a variety

Table 3. Mean and standard deviation of integrated rates over the photic layer of chlorophyll-*a* (ΣT_{chlo}), *f*-ratio calculated with net uptake rates of dissolved inorganic nitrogen (f_{net}), new production calculated by multiplied rates of dissolved inorganic nitrogen rates by the Redfield ratio 6.6 (New PP) or by multiplying the primary production by the *f*-ratio ($\text{PP} \times f$) for the five investigated oceanic regions. Mean “net *f*-ratio” (f_{net}) and “gross *f*-ratio” (f_{gross}) are compared with data obtained during in situ experiments performed at 5 experimental sites.

Area	T_{chlo} mg m^{-2}	f_{net} mean	New PP $\text{g C m}^{-2} \text{d}^{-1}$	$\text{PP} \times f$ $\text{g C m}^{-2} \text{d}^{-1}$	experimental sites	f_{net}	f_{gross}
MAR (141°–134° W)	27±5	0.18±0.04	0.18±0.10	0.13±0.02	12° S–138° W	0.18	0.19
HNL (133°–123° W)	18±4	0.08±0.04	0.04±0.06	0.02±0.02	9° S–136° W	0.09	0.10
SPG (123°–101° W)	11±2	0.05±0.03	0.008±0.007	0.007±0.007	26° S–114° W	0.05	0.06
EGY (100°–81° W)	16±4	0.12±0.07	0.07±0.03	0.04±0.03	32° S–91° W	0.11	0.11
UPW (80°–72° W)	44±28	0.27±0.08	0.69±0.49	0.53±0.47	34° S–73° W	0.27	0.28

of marine environments (Ward et al., 1984; Codispoti and Christensen, 1985; Ward and Zafriou, 1988), observations in the open ocean are rare (Lomas and Lipschultz, 2006). Nitrification rates presented here (Table 2) are in the range of previous observations (e.g. Ward and Zafriou, 1988; Bianchi et al., 1994; Raimbault et al., 1999; Fernandez and Raimbault, 2007). Regeneration processes were active throughout the water column, even in the oligotrophic waters of the SPG and were largely able to sustain the phytoplanktonic demand in the photic layer (Table 2). Rates measured in the top 100 m suggest that about 80 to 100% of nitrate uptake in the surface waters was supported by nitrification in the SPG. This result confirms the significant role of nitrification in the upper layers of oceanic waters, as previously reported in the equatorial Pacific, where 20 to 100% of the total nitrate demand was fueled by nitrification (Raimbault et al., 1999) and 142% at station ALOHA (Dore and Karl, 1996). The role of nitrification in providing regenerated nitrate in the euphotic zone has been confirmed by recent findings in the Atlantic, as well as in the Mediterranean Sea, where nitrification can support 25 to 100% of the new production (Diaz and Raimbault, 2000; Fernandez and Raimbault, 2007). A logical conclusion is that there could be overestimations in new production data when all the nitrogen regeneration processes are not taken into account. In terms of integrated values over the photic layer, overestimation was only significant in the SPG, where rates of new nitrate assimilation were lower than expected, even close to zero. Consequently, average *f*-ratio values were very low in the SPG but there were no zero values since significant new production was sustained by N_2 -fixation, which appeared as the only source of new nitrogen in the upper layer of the SPG (Fig. 8).

Along the investigated area, primary production remained quantitatively related to new production (Fig. 9), revealing that a threefold increase in total production in oligotrophic waters would result in a tenfold increase of new production. Such a relationship between primary production and new production corresponds with the data of Dugdale et al. (1992) and Raimbault et al. (1999) for the equatorial Pacific (until 16° S), but were much lower (up to 10 fold) than those esti-

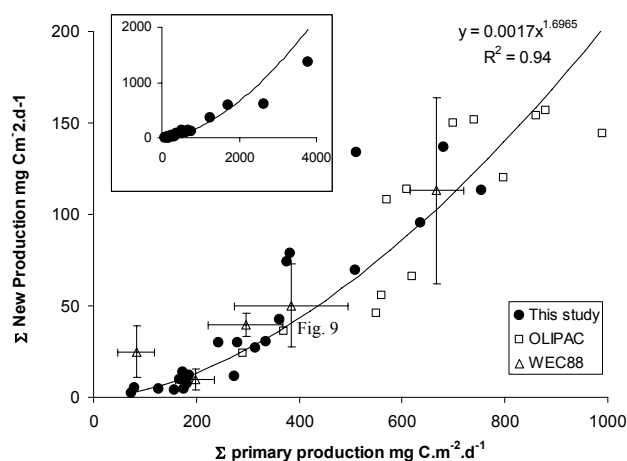


Fig. 9. Plot of integrated new production (Σ New production) versus integrated primary production (Σ primary production). OLIPAC data are from Raimbault et al. (1999); WEC 88 data are from Dugdale et al. (1992). The power relationship is calculated from data of this study (dark points). Insert shows present data for primary production higher than $1000 \text{ mg C m}^{-2} \text{d}^{-1}$.

ated by the model of Eppley and Peterson (1979). Moreover, in this very oligotrophic water, exhibiting strong nutrient gradients, there was no evident pattern between nitrate concentration and new production, as suggested by Platt and Harrison (1985). When mean *f*-ratio values are plotted against integrated primary productivity values there is a positive relationship (Fig. 10). The initial linearly slope (0.0003) for new production $< 500 \text{ mg m}^{-2} \text{d}^{-1}$ ($\approx 200 \text{ mg m}^{-2} \text{y}^{-1}$) is close to that of Dugdale et al. (1992) for the equatorial Pacific (0.00063 ± 0.00036), but much lower than the 0.0025 proposed by Eppley and Peterson (1979). The model proposed by Eppley and Peterson (1979) does not work in these oceanic waters, as nitrate uptake in coastal regions is very different from that in oligotrophic waters.

The *f*-ratio provides an indirect estimation of export rates of particulate organic matter toward the deep ocean only when suitable time scales are considered. This concept is

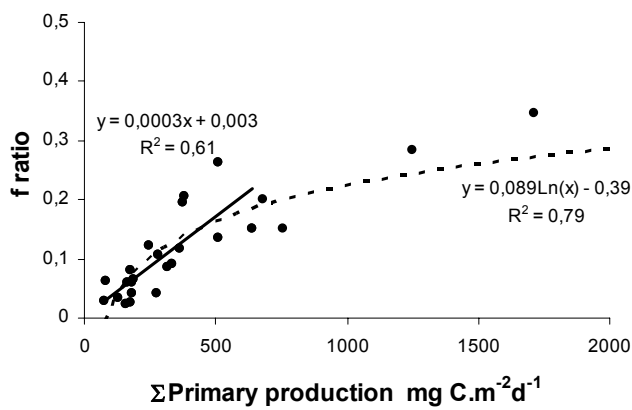


Fig. 10. Plot of mean f-ratio (f-ratio) versus integrated primary production (Σ primary production). Dashed curve is the best relationship calculated for all the data. Straight line is the linear relationship calculated for primary production lower than $500 \text{ mg C m}^{-2} \text{ d}^{-1}$.

supported by the assumption that the input by advection and diffusion of nitrate towards the surface should be balanced by the losses of particulate and dissolved matter to the deep sea. Sinking fluxes of POC ($0.14\text{--}1.15 \text{ mg C m}^{-2} \text{ d}^{-1}$) and PON ($0.04\text{--}0.2 \text{ mg N m}^{-2} \text{ d}^{-1}$) measured in the SPG by sediment traps (J. C. Miquel, personal communication) appear to be much lower than the new production rates obtained using tracer uptake experiments ($7\text{--}8 \text{ mg C m}^{-2} \text{ d}^{-1}$; $1.7 \text{ mg N m}^{-2} \text{ d}^{-1}$). There are several reasons to explain this discrepancy. The main one is the export of dissolved organic matter (by vertical mixing or horizontal advection) which can exceed fluxes of sinking particles and thus appear as the major fate of new production (Copin-Montégut and Avril, 1993; Peltzer and Hayward, 1996). According to Toggweiler (1989), the most realistic balance is obtained when half of the new production sustained by upwelled nutrients goes into a pool of dissolved organic compounds. In fact, our data demonstrated that a significant part of the DIN taken up was lost as dissolved organic nitrogen (DON) during the 24-h incubation experiments. It is difficult to ascertain whether the ^{15}N -tracer detected in the DON pool was transferred solely by the direct and active release from living phytoplankton cells. The ^{15}N excess enrichment in the DON pool may have resulted from cell rupture, by sloppy-feeding, and from cell analysis due to viral infection (Bronk et al., 1994; Procter and Fuhrman, 1990). Pooling all available data, DI^{15}N ultimately found in the extracellular DON pool (ρ_{loss}) represented, on average, 13 to 15% of the nitrate and ammonium, respectively. Values were often higher in the SPG, up to 46% in the subsurface layer. It appears that the $\rho_{\text{net}}:\rho_{\text{gross}}$ ratios were in the range of values found in literature, i.e. between the low loss rates ($<15\%$) found in the equatorial Pacific (Raimbault et al., 1999, 2000) and the very high ones (74%) found in the Southern California Bight by Bronk and Glibert (1991). They are also in the same order of magnitude as those found

in the Mediterranean Sea during spring (Diaz and Raimbault, 2000) and in the Atlantic Ocean (Fernandez and Raimbault, 2007).

However, one should keep in mind that ρ_{loss} does not represent the total flux of nitrogen from the particulate organic matter (PON) in the DON pool (Slawyk et al., 2000). The true DON release (ρ_{DON}) is greater than our measured loss of DIN (ρ_{loss}). Quantification of ρ_{DON} depends on the ^{15}N enrichment in the intracellular DON ($R_{\text{DON}i}$). $R_{\text{DON}i}$ is not experimentally accessible, but it is related to the initial ^{15}N enrichment DIN pool (R_{DIN}), according the relationship defined by Raimbault et al. (2000),

$$\rho_{\text{DON}} = \rho_{\text{loss}} \times R_{\text{DIN}}/R_{\text{DON}i} \quad (10)$$

Due to of the dilution of the ^{15}N tracer by intracellular nitrogen during uptake, $R_{\text{DIN}}/R_{\text{DON}i}$ is greater than 1. This relationship indicates that; 1) the total fluxes of organic nitrogen from particulate matter to extracellular DON would be higher than the loss of tracer in the form of DON, as measured here and 2) the lower the final enrichment of the intracellular DON pool, the greater the difference between DIN loss and DON release. Assuming phytoplanktonic growth rates calculated from the residence time of chlorophyll-containing particles (Raimbault et al., 2007), the $R_{\text{DIN}}/R_{\text{DON}i}$ ratio would be 3 to 6 folds higher in the SPG than in the productive regions (Marquesas Islands and Chilean upwelling). Consequently, we can hypothesize that production of DON was proportionally much higher in the oligotrophic waters than in productive systems, and consequently, this process could be a significant way for export production in the SPG.

The availability of high-precision isotope ratio mass spectrometers, combined with sensitive field tracer methods (Montoya et al., 1996) enable $^{15}\text{N}_2$ -tracer incubations to be carried out on unconcentrated natural water samples, with minimal disturbance of the system. However, measurements of N_2 -fixation in oceanic waters are rare and the data reported here are the first available for the South Pacific. The iron supply from atmospheric dust deposition at the sea surface has been hypothesized to favour N_2 -fixation in the areas influenced by the continents, e.g. the Atlantic Ocean. N_2 -fixation, due to high phosphorus requirements, could lead to a decrease in the soluble reactive phosphorus until a shift from N to P limitation occurs, as hypothesized by Béthoux and Copin-Montégut (1986) and Karl et al. (2002) for the Mediterranean Sea and the North Pacific Oceanic, respectively. Elevated N to P in the dissolved inorganic is often considered as indicative of N_2 fixation (Grüber and Sarmiento, 1997). From this point of view, the waters of the South Pacific, characterized by very low dust depositions (Mahowald et al., 1999) and by having sufficient phosphorus concentrations and very low nitrate/phosphate ratios (Raimbault et al., 2007) do not seem to be favourable regions for N_2 -fixers. Nevertheless, significant rates were measured throughout the transect, confirming results from recent work using ocean

circulation modelling (Deutsch et al., 2007). N_2 -fixation was the weakest, but the most stable biological process along the 8000-km investigated area, in spite of large deviations in nutrient biomass and primary productivity. In the SPG, N_2 -fixation ($0.06 \text{ mmol m}^{-2} \text{ d}^{-1}$) was essentially located in the upper layer (0–50 m), where irradiance was higher and atmospheric deposition, even though very weak in this region, was more readily available. The highest N_2 -fixation rates (0.09 – $0.11 \text{ mmol m}^{-2} \text{ d}^{-1}$) were observed around the Marquesas Islands and in the Chilean upwelling (Table 2). The most surprising feature was the high N_2 -fixation rates found in the cold and nutrient-replete waters along the Chilean coast, since nitrogen fixation is commonly associated with certain cyanobacteria, essentially *Trichodesmium* sp., that inhabit the warm and nutrient-depleted subtropical waters (Capone et al., 2005; Mahaffey et al., 2005). But this observation confirms the result of Deutsch et al.'s model (2007) that provides evidence that biological fixation could also be intimately linked with marine nitrogen removal in the South Pacific Ocean.

Unfortunately, the organisms responsible for this process were not identified in this study. The organisms responsible for N_2 fixation are taxonomically, physiologically, and ecologically diverse, including bacteria (phototrophs, heterotrophs, chemolithotrophs) heterocystous and nonheterocystous cyanobacteria and Archeae (Karl et al., 2002). But much of the oceanic research about N_2 fixation has been focused on the filamentous cyanobacteria *Trichodesmium* (Capone et al., 2005). However, due to the absence of diazotrophic *Trichodesmium* populations during this cruise, we can postulate that N_2 -fixation was executed by nanoplanktonic and picoplanktonic organisms, recently revealed by new molecular biological techniques (Zehr et al., 1998, 2000) and by direct measurements (Montoya et al., 2004; Garcia et al., 2007; Biegala and Raimbault, 2008). The discovery of potentially important marine diazotrophs other than *Trichodesmium* opens up a new area when studying the importance of nitrogen fixation in the ocean. Due to their ability to fix N, these nanoplanktonic cyanobacteria can contribute substantially to the input of new nitrogen into nutrient-depleted waters, even if the rates of fixation measured are typically quite low relative to the apparent N demand of the ecosystem. Our integrated values (30 – $910 \mu\text{mol m}^{-2} \text{ d}^{-1}$) are the same order of magnitude as found in the literature concerning dinitrogen fixation by nanoplankton, with the exception of the high value ($3955 \mu\text{mol m}^{-2} \text{ d}^{-1}$) found along the Australian coasts by Montoya et al. (2004). Zehr et al. (2001) give an integrated value of $92 \mu\text{mol m}^{-2} \text{ 12 h}^{-1}$ for the North Pacific. This value is a little higher than those measured by Montoya et al. (2004) in the same region (24 – $66 \mu\text{mol m}^{-2} \text{ d}^{-1}$). Similar results have been found in the Southwest Pacific around New Caledonia (Garcia et al., 2007), with nitrogen fixation occurring in the $<10 \mu\text{m}$ fraction, i.e. not associated with *Trichodesmium* populations, ranging from 40–

$300 \mu\text{mol m}^{-2} \text{ d}^{-1}$. Falcon et al. (2004) found a daily range of 62 – $167 \mu\text{mol m}^{-2} \text{ d}^{-1}$ for the north Atlantic. Recent equivalent rates ($\approx 50 \mu\text{mol m}^{-2} \text{ d}^{-1}$) were obtained in the Mediterranean Sea during the oligotrophic summer period (Garcia et al., 2006), representing up to 40% of new production. These small nanoplanktonic cyanobacteria were not observed during the BIOSOPE cruise. But high density populations of phycoerythrin containing cyanobacteria were detected along the transect, with a maximum being observed in the Chilean upwelling, and most of these cyanobacteria (up to 50% in the SPG) forming colonies (Masquelier and Vaultot, 2007). Thus, as suggested by these authors, it is tempting to hypothesize that these colonial cyanobacteria could be the organisms responsible of the observed N_2 -fixation. N_2 -fixation sustained a large fraction of new production (up to 100%) in the oligotrophic SPG and this nitrogen pool represents a potentially important nitrogen source for other organisms in the pelagic food web, especially where any input of other forms of new nitrogen is excluded. The light $\delta^{15}\text{N}$ isotopic signal observed in the SPG (Raimbault et al., 2007) suggests that nitrogen fixation provides a local dominant supply of nitrogen to phytoplankton in this isolated region, where the vertical flux of nitrate from below the thermocline is extremely low due to the deep thermocline. Finally, our observations confirmed the global distribution diagnosed by Deutsch et al. (2007), providing evidence that elevated N_2 -fixation rates are closely linked to areas of denitrification, as encountered along the Peruvian and Chilean coasts. According to the model of Deutsch et al. (2007), annual fixation rates in the SPG and in the Chilean upwelling range from 40 – $160 \text{ mmol m}^{-2} \text{ y}^{-1}$ and 20 – $120 \text{ mmol m}^{-2} \text{ y}^{-1}$, respectively. Our direct measurements, assuming no seasonal variation, are at the low end of these ranges ($22 \pm 12 \text{ mmol m}^{-2} \text{ y}^{-1}$ and $33 \pm 22 \text{ mmol m}^{-2} \text{ y}^{-1}$, respectively). The basin scale N_2 -fixation for the South Pacific Gyre, representing 1.1% of the global oceanic surface (4.10^6 km^2), is estimated to be about $1.34 \times 10^{12} \text{ g N y}^{-1}$ and corresponds to about 1% of the global N_2 -fixation calculated by Deutsch et al. (2007). Finally, our direct estimates of N_2 fixation for the entire South Pacific basin ($21.10^{12} \text{ g yr}^{-1}$) was two folds lower than expected by Deutsch et al. (2007). This apparent inconsistency could be due to uncertainties regarding ocean circulation and precise nutrient distribution (Deutsch et al., 2007) and also seasonal variations of N_2 -fixation as observed in the southwest and North Pacific (Garcia et al., 2007; Dore et al., 2002). Nevertheless, our basin-scale budget are close to recent estimates for the North Atlantic Ocean (4.2 to $85 \times 10^{12} \text{ g yr}^{-1}$, compiled in Hansell et al., 2007), considered as an important region of N_2 fixation given the enhanced inputs of atmospheric dust from the Sahara. This indicates that the South Pacific Ocean would provide an ideal ecological niche for the proliferation of N_2 -fixers (still unknown), even if our “snapshot” estimates of N_2 -fixation rates were lower than could be expected from the ocean circulation model. Finally, oceanic N-fixation is a

process which is more important than initially thought and not restricted to the warm- and nutrient-depleted tropical areas. This source of new nitrogen will support net production and export of organic matter from the euphotic zone, with a direct effect on the carbon cycle. This fact leads to relevant consequences in relation to the N₂ fixation–climate feedback hypothesis proposed by Michaels et al. (2001). Clearly, the budget of N₂ fixation remains highly uncertain and so more widespread research needs to be carried out on marine N-fixers in order to quantify their role in the global oceanic biogeochemistry cycle.

Acknowledgements. This is a contribution of the BIOSOPE project of the LEFE-CYBER program, funded by the Centre National de la recherche Scientifique (CNRS), the Institut des Sciences de l'Univers (INSU), the Centre National d'Etudes Spatiales (CNES), The European Space Agency (ESA), the National Aeronautics and Space Administration (NASA) and the natural Sciences and Engineering Research Council of Canada (NSERC). This work is fund in part by the French Research and Education Council. The Biosope cruise program was managed by H. Claustre and A. Sciandra. We thank the crew of the R/V Atalante for outstanding shipboard support operations. Data concerning euphotic layer depth and surface light intensity were kindly provided by H. Claustre. D. Taillez and C. Bournot are warmly thanked for their efficient help in CTD rosette management and data processing. J. C. Miquel provided sediment trap data, and T. Moutin provided data of primary production from ¹⁴C experiments. The authors gratefully thank the two anonymous referees who helped to make substantial improvements in the manuscript and T. Bentley for her linguistic and scientific advice.

Edited by: S. W. A. Naqvi

References

- Allen, A. E., Howard-Jones, M. H., Booth, M. G., Frischer, M. E., Verity, P. G., Bronk, D. A., Sanderson, M. P.: Importance of heterotrophic bacterial assimilation of ammonium and nitrate in the Barents Sea during summer, *J. Marine Syst.*, 38, 93–108, 2002.
- Altabet, M.: Organic C, N and stable isotopic composition of particulate matter collected on glass-fiber and aluminum oxide filters, *Limnol. Oceanogr.*, 35(4), 902–909, 1990.
- Aufdenkampe, A. K., McCarthy, J. J., Rodier, M., Navarrette, C., Dunne, J., and Murray, J. W.: Estimation of new production in the Tropical Pacific, *Global Biogeochem. Cy.*, 15, 101–113, 2001.
- Aufdenkampe, A. K., McCarthy, J. J., Navarrette, C., Rodier, M., Dunne, J., and Murray, J. W.: Biogeochemical controls on new production in the tropical pacific, *Deep. Sea. Res. II*, 49, 2619–2648, 2002.
- Béthoux, J. P. and Copin-Montégut, G.: Biological fixation of atmospheric nitrogen in the Mediterranean Sea, *Limnol. Oceanogr.*, 31, 1353–1358, 1986.
- Bianchi, M., Feliatra, F., Tréguer, P., Vincendeau, M., and Morvan, J.: Nitrification rates, ammonium and nitrate distribution in upper layers of the water column and in sediments of the Indian sector of the Southern Ocean, *Deep Sea Res. II*, 44(5), 1017–1032, 1997.
- Biegala, I. C. and Raimbault, P.: High abundance of diazotrophic picocyanobacteria (<3 μm) in a South-West Pacific coral lagoon, *Aquat. Microb. Ecol.*, in press, 2008.
- Bode, A., Castro, C., Doval, M. D., and Varela, M.: New and regenerated production and ammonium regeneration in the western Bransfield region (Antarctica) during phytoplankton bloom conditions in summer, *Deep Sea Res. II*, 49, 787–804, 2002.
- Bronk, D. A. and Glibert, P.: A ¹⁵N tracer method for the measurement of dissolved organic nitrogen release by phytoplankton, *Mar. Ecol. Prog. Ser.*, 77, 171–182 1991.
- Bronk, D. A., Glibert, P., and Ward, B. B.: Nitrogen uptake, dissolved organic nitrogen release and new production, *Science*, 256, 1843–1846, 1994.
- Capone, D. G. and Carpenter, E. J.: Nitrogen fixation in the marine environment, *Science*, 217, 1140–1142, 1982.
- Capone, D. G., Burns, J. A., Montoya, J. P., Subramaniam, A., Mahaffey, C., Gunderson, T., Michaels, A. F., and Carpenter, E. J.: Nitrogen fixation by *Trichodesmium* spp.: An important source of new nitrogen to the tropical and subtropical North Atlantic Ocean, *Global Biogeochem. Cy.*, 19, GB2024, doi:10.1029/2004GB002331, 2005.
- Carlson, C. A., Ducklow, H. W., and Michaels, A. F.: Annual flux of dissolved organic carbon from the euphotic zone in the north-western Sargasso Sea, *Nature*, 371, 405–408, 1994.
- Chavez, F. P., Buck, K. R., Bidigare, R. R., Karl, D. M., Hebel, D., Latasa, M., and Campbell, L.: On the chlorophyll a retention properties of glass-fiber GF/F filters, *Limnol. Oceanogr.*, 40, 428–433, 1995.
- Claustre, H. and Maritorea, S.: Ocean Science: The many shades of ocean blue, *Science*, 302, 1514–1515, 2003.
- Codispoti, L. A. and Christensen, J. P.: Nitrification, denitrification and nitrous oxide cycling in the eastern tropical South Pacific Ocean, *Mar. Chem.*, 16(4), 277–300, 1985.
- Copin-Montégut, G. and Avril, B.: Vertical distribution and temporal variation of dissolved organic carbon in the North-Western Mediterranean Sea, *Deep-Sea Res.*, 40, 1963–1972, 1993.
- Daneri, G. and Quinones, R. A.: Undersamples ocean systems: appeal for an international study of biogeochemical cycles in the Southern Pacific gyre and its boundaries, *U.S. JGOFS Newsletter* January 2001, 9, 2001.
- Deutsch, C., Sarmiento, J.L., Sigman, D. M., Gruber, N., and Dunne, J. P.: Spatial coupling of nitrogen inputs and losses in the ocean, 445(7124), 163–167, 2007.
- Diaz, F. and Raimbault, P.: Nitrogen regeneration and dissolved organic nitrogen release during spring in a NW Mediterranean coastal zone (Gulf of Lions): implications for the estimations of f-ratio and new production, *Mar. Ecol. Progr. Ser.*, 197, 53–66, 2000.
- Dore, J. E. and Karl, D. M.: Nitrification in the euphotic zone as a source of nitrite, nitrate, and nitrous oxide at Station ALOHA, *Limnol. Oceanogr.*, 41, 1619–1628, 1996.
- Dore, J. E., Brum, J. R., Tupas, L. M., and Karl, D. M.: Seasonal and interannual variability in sources of nitrogen supporting export in the oligotrophic subtropical North Pacific Ocean, *Limnol. Oceanogr.*, 47(6), 1595–1607, 2002.
- Dugdale, R. C. and Goering, J. J.: Uptake of new and regenerated forms of nitrogen in primary productivity, *Limnol. Oceanogr.*,

- 12, 196–206, 1967.
- Dugdale, R. W. and Wilkerson, F. P.: The use of ^{15}N to measure nitrogen uptake in eutrophic oceans: experimental considerations, *Limnol. Oceanogr.*, 31, 673–689, 1986.
- Dugdale, R. W., Wilkerson, F. P., Chavez, F. P., and Barber, R. T.: Estimating new production in the equatorial Pacific at 150°W , *J. Geophys. Res.*, 97, 681–686, 1992.
- Dugdale, R. C. and Goering, J. J.: Uptake of new and regenerated forms of nitrogen in primary productivity, *Limnol. Oceanogr.*, 12, 196–206, 1967.
- Dugdale, R. C. and Wilkerson, F. P.: The use of ^{15}N to measure nitrogen uptake in eutrophic oceans, experimental considerations, *Limnol. Oceanogr.*, 31(4), 673–689, 1986.
- Dugdale, R. C., Wilkerson, F. P., Barber, R., and Chavez, F.: Estimating new production in the equatorial Pacific Ocean at 150°W , *J. Geophys. Res.*, 97(C1), 681–686, 1992.
- Eppley, R. W. and Peterson, B. J.: Particulate organic matter flux and planktonic new production in the deep ocean, *Nature*, 282, 677–680, 1979.
- Falcon, L. I., Carpenter, E. J., Cipriano, F., Bergman, B., and Capone, D. G.: N_2 fixation by unicellular bacterioplankton from the Atlantic and Pacific oceans: phylogeny and in situ rates, *Appl. Environ. Microbiol.*, 765–770, 2004.
- Fernandez, C. and Raimbault, P.: Nitrogen regeneration in the NE Atlantic Ocean and its impact on seasonal new, regenerated and export production, *Mar. Ecol. Progr. Ser.*, 337, 79–92, 2007.
- Galloway, J. N., Schlesinger, W. H., Levy, H., Michaels, A., and Schnoor, J. L.: Nitrogen fixation: Anthropogenic enhancement-environmental response, *Global Biogeochem. Cy.*, 9, 235–252, 1995.
- Garcia, N., Raimbault, P., Gouze, E., and Sandroni, V.: Dinitrogen fixation and primary production in Western Mediterranean Sea, *C. R. Biol.*, 329(9), 742–750, 2006.
- Garcia, N., Raimbault, P., and Sandroni, V.: Seasonal nitrogen fixation and primary production in Southwest Pacific (New Caledonia): Some evidence for nanoplanktonic diazotrophy and rapid transfer of newly fixed nitrogen to picoplankton organisms, *Mar. Ecol. Progr. Ser.*, 343, 25–33, 2007.
- Gentilhomme, V. and Raimbault, P.: Absorption et régénération de l'azote dans a zone frontale du courant algérien (Méditerranée Occidentale): Réévaluation de la production nouvelle, *Oceanol. Acta.*, 17, 555–562, 1994.
- Glibert, P. M., Lipschultz, F., McCarthy, J. J., and Altabet, M. A.: Isotope dilution models of uptake and remineralization of ammonium by marine plankton, *Limnol. Oceanogr.*, 27, 639–650, 1982.
- Grob, C., Ulloa, O., Claustre, H., Huot, Y., Alarcón, G., and Marie, D.: Contribution of picoplankton to the total particulate organic carbon concentration in the eastern South Pacific, *Biogeosciences*, 4, 837–852, 2007, <http://www.biogeosciences.net/4/837/2007/>.
- Grüber, N. and Sarmiento, J.: Global patterns of marine nitrogen fixation and denitrification, *Global Biogeochem. Cy.*, 11, 235–266, 1997.
- Hansell, D. A., Olson, D. B., Dentener, F., and Zamora, L. M.: Assessment of excess nitrate development in the subtropical North Atlantic, *Mar. Chem.*, 106, 562–579, doi:10.1016/j.marchem.2007.
- Harrison, W. G., Platt, T., and Lewis, M. R.: f-ratio and its relationship to ambient nitrate concentration in coastal waters, *J. Plankton Res.*, 9(1), 235–248, 1987.
- Harrison, W. G., Harris, L. R., and Irwin, B. D.: The kinetic of nitrogen utilization in the oceanic mixed layer: nitrate and ammonium interactions at nanomolar concentrations, *Limnol. Oceanogr.*, 41, 16–32, 1996.
- Holmes, M. R., Aminot, A., Kerouel, R., Hooker, B. A., and Peterson, J. B.: A simple and precise method for measuring ammonium in marine and freshwater ecosystems, *Can. J. Fish Aquat. Sci.*, 56, 1801–1808, 1999.
- Karl, D. M.: Nutrients dynamics in the deep blue sea, *Trends Microbiol.* 10, 410–418, 2002.
- Karl, D. M., Michaels, A., Bergman, B., et al.: Dinitrogen fixation in the world's oceans, *Biogeochemistry*, 57/58, 47–98, 2002.
- Karl, D. M., Letelier, R., Tupas, L., Dore, J., and Christian, J. D. H.: The role of nitrogen fixation in biochemical cycling in the subtropical North Pacific Ocean, *Nature*, 386, 533–538, 1997.
- Laws, E.: Isotope dilution models and the mystery of the vanishing ^{15}N , *limnol. Oceanogr.*, 29, 379–386, 1984.
- Libby, P. S. and Wheeler, P. A.: Particulate and dissolved organic nitrogen in the central and eastern Equatorial Pacific, *Deep-Sea Res.*, 44, 345–361, 1996.
- Lomas, M. W. and Lipschultz, F.: Forming the primary nitrite maximum: nitrifiers or phytoplankton?, *Limnol. Oceanogr.*, 51, 2453–2467, 2006.
- Mahaffey, C., Michaels, A. F., and Capone, D. G.: The conundrum of marine nitrogen fixation, *Am. J. Sci.*, 305, 546–595, 2005.
- Mahowald, N.: Dust sources and deposition during the last glacial maximum and current climate: A comparison of model results with paleodata from ice cores and marine sediments, *J. Geophys. Res.-Atmos.*, 104, 15 895–15 916, 1999.
- Maita, Y. and Yanada, M.: Vertical distribution of total dissolved nitrogen and dissolved organic nitrogen in seawater, *Geochem. J.*, 24, 245–254, 1990.
- Masquelier, S. and Vaultot, D.: Distribution of micro-organisms along a transect in the South-East Pacific Ocean (BIO SOPE cruise) from epifluorescence microscopy, *Biogeosciences Discuss.*, 4, 2667–2697, 2007, <http://www.biogeosciences-discuss.net/4/2667/2007/>.
- Menzel, D. W. and Ryther J. H.: The annual cycle of primary production in the Sargasso Sea off Bermuda, *Deep Sea Res.*, 6, 351–367, 1960.
- Menzel, D. W. and Ryther, J. H.: The composition of particulate organic matter in the western north Atlantic, *Limnol. Oceanogr.*, 9, 179–186, 1964.
- Michaels, A. F., Karl, D. M., and Capone, D. G.: Element stoichiometry, new production and nitrogen fixation, *Oceanography*, 14, 68–77, 2001.
- Montoya, J. P., Voss, M., Kähler, P., and Capone, D. G.: A simple, high precision, high sensitivity tracer assay for N_2 fixation, *Appl. Environ. Microb.*, 62, 986–993, 1996.
- Montoya, J. P., Holl, C. M., Zehr, J. P., Hansen, A., Villareal, T. A., and Capone, D. G.: High rates of N_2 fixation by unicellular diazotrophs in the oligotroph Pacific, *Nature*, 430, 1027–1031, 2004.
- Morel, A. and Maritorena, S.: Bio-optical properties of oceanic waters: a reappraisal, *J. Geophys. Res.*, 106(C4), 7163–7180, 2001.
- Morel, A., Gentili, B., Claustre, H., Babin, M., Bricaud, A., Ras, J., and Tieche, F.: Optical properties of the clearest natural waters,

- Limnol. Oceanogr., 52, 217–229, 2007.
- Nixon, S. W.: Coastal eutrophication: a definition, social causes and future concerns, *Ophelia*, 41, 199–220, 1995.
- Peltzer, E. T. and Hayward, N. A.: Spatial and temporal variability of total organic carbon along the 140° W in the equatorial Pacific ocean in 1992, *Global Biogeochem. Cy.*, 6, 45–76, 1996.
- Platt, T. and Harrison, W. G.: Biogenic fluxes of carbon and oxygen in the ocean, *Nature*, 318, 55–58, 1985.
- Priscu, J. C. and Downes, M. T.: Nitrogen uptake, ammonium oxidation and nitrous oxide (N₂O) levels in the coastal waters of western Cook Strait, New Zealand, *Estuary. Coast Shel Sci.*, 20, 529–542, 1985.
- Procter, L. M. and Fuhrman, J. A.: Viral mortality of marine bacteria and cyanobacteria, *Nature*, 343, 1327–1332, 1990.
- Raimbault, P., Slawyk, G., Coste, B., and Fry, J.: Feasibility of using an automated colorimetric procedure for the determination of seawater nitrate in the 0 to 100 nM range: Examples from field and culture, *Mar. Biol.*, 104, 347–351, 1990.
- Raimbault, P., Garcia, N., and Cerutti, F.: Distribution of inorganic and organic nutrients in the South Pacific Ocean – evidence for long-term accumulation of organic matter in nitrogen-depleted waters, *Biogeosciences Discuss.*, 4, 3041–3087, 2007, <http://www.biogeosciences-discuss.net/4/3041/2007/>.
- Raimbault, P., Slawyk, G., Boudjellal, B., Coatanoan, C., Conan, P., Coste, B., Garcia, N., Moutin, T., and Pujo-Pay, M.: Carbon and nitrogen uptake and export in the equatorial Pacific at 150° W: Evidence of an efficient regenerated production cycle, *J. Geophys. Res.*, 104(C2), 3341–3356, 1999.
- Raimbault, P., Slawyk, G., and Garcia, N.: Comparison between chemical and isotopic measurements of biological nitrate utilization: further evidence of low new production levels in the equatorial Pacific, *Mar. Biol.*, 136, 1147–1155, 2000.
- Ras, J., Claustre, H., and Uitz, J.: Spatial variability of phytoplankton pigment distributions in the Subtropical South Pacific Ocean: comparison between in situ and predicted data, *Biogeosciences Discuss.*, 4, 3409–3451, 2007, <http://www.biogeosciences-discuss.net/4/3409/2007/>.
- Redfield, A. C., Ketchum, B. H., and Richards, F. A.: The influence of organisms on the composition of seawater, in: *The Sea*, edited by: Hill, M. N., Wiley, 26–77, 1963.
- Rees, A. P., Joint, I., and Donald, D. M.: Early spring bloom phytoplankton-nutrient dynamics at the Celtic Sea Shelf edge, *Deep Sea Res.*, 46, 483–510, 1999.
- Ryther, J. H. and Menzel, D. W.: The seasonal and geographical range of primary production in the Western Sargasso sea, *Deep Sea Res.*, 6, 235–238, 1960.
- Sahlsten, E.: Nitrogenous nutrition in the euphotic zone of the central North Pacific Gyre, *Mar. Biol.*, 96, 433–439, 1987.
- Slawyk, G. and Collos, Y.: ¹³C and ¹⁵N uptake by marine phytoplankton III. Interactions in euphotic zone profiles of stratified oceanic areas, *Mar. Ecol. Prog. Ser.* 19, 223–231, 1984.
- Slawyk, G. and Raimbault, P.: Simple procedure for the simultaneous recovery of dissolved inorganic and organic nitrogen in ¹⁵N-tracer experiments and improving the isotopic mass balance, *Mar. Ecol. Prog. Ser.*, 124, 289–299, 1995.
- Slawyk, G., Raimbault, P., and Garcia, N.: Measuring gross uptake of ¹⁵N labeled nitrogen by marine phytoplankton without particulate matter collection: Evidence of low ¹⁵N losses to the dissolved organic nitrogen pool, *Limnol. Oceanogr.*, 43(7), 1734–1739, 1998.
- Slawyk, G., Raimbault, P., and Garcia, N.: Use of ¹⁵N to measure dissolved organic nitrogen release by marine phytoplankton (reply to comment by Bronk and Ward), *Limnol. Oceanogr.*, 45(8), 884–1886, 2000.
- Tedetti, M., Sempéré, R., Vasilkov, A., Charrière, B., Nérini, D., Miller, W. L., Kawamura, K., and Raimbault, P.: High penetration of ultraviolet radiation in the South East Pacific waters, *Geophys. Res. Lett.*, 34, L12610, doi: 10.29/2007/GL029823, 2007.
- Toggweiler, J. R.: Is the downward dissolved organic matter (DOM) flux important in carbon export, in: *Productivity of the ocean: Present and past*, edited by: Berger, W. H., Smetacek, V. S., and Wefer, G., Wiley-Intersci., New-York, 65–84, 1989.
- Tréguer, P. and LeCorre, P.: Manuel d'analyses des sels nutritifs dans l'eau de mer: Utilisation de l'Autoanalyseur II Technicon, Univ. of Bretagne Occidentale, Lab. de Chim. Mar., Brest, France, 1975.
- Ward, B. B.: Nitrification and the marine nitrogen cycle, in: *Microbial ecology of the oceans*, edited by: Kirchman, D., Wiley-Liss Inc., 427–454, 2000.
- Ward, B. B., Talbot, M. C., and Perry, M. J.: Contributions of phytoplankton and nitrifying bacteria to ammonium and nitrite dynamics in coastal waters, *Cont. Shelf Res.*, 3, 383–398, 1984.
- Ward, B. B., Kilpatrick, K. A., Renger, E. H., and Eppley, R. W.: Biological nitrogen cycling in the nitracline, *Limnol. Oceanogr.*, 34(3), 493–513, 1989.
- Ward, B. B. and Zafriou, O. C.: Nitrification and nitric oxide in the oxygen minimum of the eastern tropical North Pacific, *Deep Sea Res.*, 35(7), 1127–1442, 1988.
- Weiss, R. F.: The solubility of nitrogen, oxygen and argon in water and seawater, *Deep Sea-Res.*, 17, 721–735, 1970.
- Zehr, J. P., Mellon, M. T., and Zani, S.: New nitrogen fixing microorganisms detected in oligotrophic oceans by the amplification of nitrogenase (*nifH*) genes, *Appl. Environ. Microbiol.*, 64, 3444–3450, 1998.
- Zehr, J. P., Carpenter, E. J., and Villareal, T. A.: New perspectives on nitrogen-fixing microorganisms in tropical and subtropical oceans, *Trends Microbiol.*, 8, 68–73, 2000.
- Zehr, J. P. and Ward, B. B.: Nitrogen cycling in the Ocean: New perspectives on processes and paradigms, *Appl. Environ. Microbiol.*, 68(3), 1015–1024, 2002.
- Zehr, J. P., Waterbury, J. P., Turner, P. J., Montoya, J. P., Omoregie, E., Steward, G. F., Hansen, A., and Karl, D. M.: Unicellular cyanobacteria fix N₂ in the subtropical North Pacific Ocean, *Nature*, 412 635–638, 2001.

Nutrient limitation of primary productivity in the Southeast Pacific (BIOSOPE cruise)

S. Bonnet¹, C. Guieu¹, F. Bruyant², O. Prášil³, F. Van Wambeke⁴, P. Raimbault⁴, T. Moutin⁴, C. Grob¹, M. Y. Gorbunov⁵, J. P. Zehr⁶, S. M. Masquelier⁷, L. Garczarek⁷, and H. Claustre¹

¹Laboratoire d'Océanographie de Villefranche, UMR 7093, CNRS and Université Pierre et Marie Curie, BP 08 06238 Villefranche sur mer Cedex, France

²Dalhousie University—Department of Oceanography, 1355 Oxford Street Halifax, NS, B3H 4J1, Canada

³Institute of Microbiology ASCR, Opatovický mlýn, 37981 Trebon and University of South Bohemia, Zámek, 37333 Nové Hrad, Czech Republic

⁴Centre d'Océanologie de Marseille - Campus de Luminy, 13288 Marseille Cedex 09, France

⁵Rutgers University, Institute of marine and Coastal Sciences, 71 Dudley road, New Brunswick, N. J. 08901-8521, USA

⁶University of California Santa Cruz, Ocean Sciences Department, 1156 high street, Santa Cruz, CA 95064, USA

⁷Station Biologique de Roscoff, UMR 7144, CNRS and Univ. Pierre et Marie Curie, BP 74, 29682 Roscoff Cedex, France

Received: 2 July 2007 – Published in Biogeosciences Discuss.: 9 August 2007

Revised: 19 November 2007 – Accepted: 11 January 2008 – Published: 20 February 2008

Abstract. Iron is an essential nutrient involved in a variety of biological processes in the ocean, including photosynthesis, respiration and dinitrogen fixation. Atmospheric deposition of aerosols is recognized as the main source of iron for the surface ocean. In high nutrient, low chlorophyll areas, it is now clearly established that iron limits phytoplankton productivity but its biogeochemical role in low nutrient, low chlorophyll environments has been poorly studied. We investigated this question in the unexplored southeast Pacific, arguably the most oligotrophic area of the global ocean. Situated far from any continental aerosol source, the atmospheric iron flux to this province is amongst the lowest of the world ocean. Here we report that, despite low dissolved iron concentrations ($\sim 0.1 \text{ nmol l}^{-1}$) across the whole gyre (3 stations located in the center and at the western and the eastern edges), primary productivity are only limited by iron availability at the border of the gyre, but not in the center. The seasonal stability of the gyre has apparently allowed for the development of populations acclimated to these extreme oligotrophic conditions. Moreover, despite clear evidence of nitrogen limitation in the central gyre, we were unable to measure dinitrogen fixation in our experiments, even after iron and/or phosphate additions, and cyanobacterial *nifH* gene abundances were extremely low compared to the North Pacific Gyre. The South Pacific gyre is therefore unique with respect to the physiological status of its phytoplankton populations.

1 Introduction

The production of organic matter in the sea is sustained by a continuous supply of essential macro- (C, N, P) and micronutrients (metals, vitamins). The nutrients requirements vary among different phytoplanktonic species. According to the Liebig's law, organic matter production is controlled by the element that is available in the lowest concentration relative to the growth requirements. This simple view is now replaced by the realization that multiple resources simultaneously limit phytoplankton growth in some parts of the ocean (Arrigo, 2005). Global environmental forcings, including human-induced climate change, could potentially modify the nutrient delivery processes to the ocean, leading to fundamental changes in the diversity and functioning of the marine food web. It is thus fundamental to understand which nutrients control primary productivity in the open ocean to predict the biogeochemical consequences of global change. Representing 60% of the global ocean's area, the subtropical open-ocean ecosystems are the largest coherent biomes on our planet, and the biogeochemical processes they support are of global importance (Emerson et al., 1997; Karl, 2002). The development of permanent time series stations in the North tropical Atlantic and Pacific over the past two decades have led to a revolution in the understanding of the mechanisms and controls of nutrient dynamics in these remote environments. These oceanic gyres provide ideal ecological niche for the development of nitrogen-fixing organisms (e.g. Karl et al., 2002). In the North subtropical and tropical Atlantic and Pacific oceans, it has been estimated that dinitrogen fixation is equivalent to 50–180% of the flux

Correspondence to: S. Bonnet
(sbonnet@usc.edu)

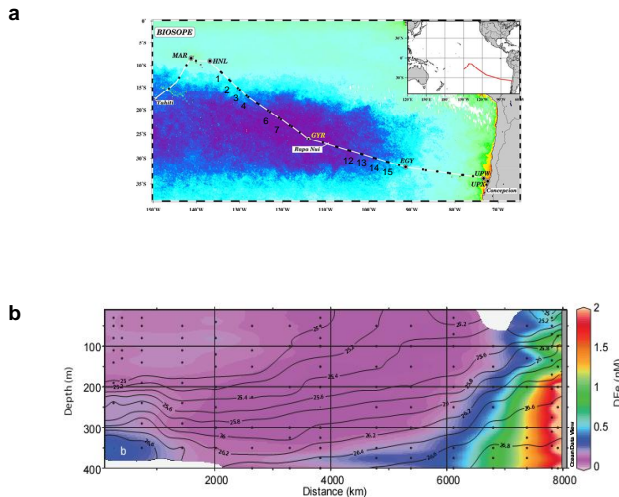


Fig. 1. (a) Transect of the BIOSOPE cruise from the Marquesas Islands to Chile superimposed on a SeaWiFS surface Chl-*a* composite image (November–December 2004), and location of the short (numbers) and long-stations of the cruise (MAR, HNL, GYR, EGY, UPW, UPX). This study reports results of bioassay experiments performed at stations HNL, GYR and EGY. (b) Dissolved iron concentrations (0–400 m) (nmol l^{-1}) along the BIOSOPE transect from Marquesas Islands (left) to Chile (right).

of NO_3^- into the euphotic zone (Karl et al., 1997; Capone et al., 2005), demonstrating that a large part of new primary productivity is fuelled by N_2 fixation, rather than NO_3^- diffusing from deeper layer into the euphotic zone. Dinitrogen fixation requires the iron-rich nitrogenase complex, therefore N_2 -fixing organisms have high iron (Fe) requirements compared to phytoplankton growing on nitrate or ammonium (Raven, 1988; Kustka et al., 2003). Dinitrogen fixation in oceanic gyres has been seen to be controlled by Fe availability, as well as phosphate, which can (co)limit the process (Sanudo-Wilhelmy et al., 2001; Mills et al., 2004). However, all studies dedicated to the nutrient control of primary productivity and dinitrogen fixation have focused so far on the Northern Hemisphere and there are few data available in the Southern Hemisphere.

The South Pacific gyre, which is the largest oceanic gyre of the global ocean, had been particularly undersampled (Claustre et al. see introduction of this issue). This unique environment appears from satellite imagery and ocean colour to have the lowest chlorophyll-*a* (Chl-*a*) concentrations of the global ocean and thus represents an end-member of oceanic hyper-oligotrophic conditions (Claustre and Maritorena, 2003). In contrast to the oceanic gyres located in the Northern Hemisphere, the South Pacific Gyre is far removed from any continental source (anthropogenic and natural desert aerosols) and receives amongst the lowest atmospheric Fe flux in the world (Wagener et al., 2008). Consequently, the phytoplankton community as a whole, and particularly nitrogen-fixing

organisms have been suggested to be Fe-limited (Falkowski et al., 1998; Berman-Frank et al., 2001; Moore et al., 2002), but direct experiment were lacking.

The BIOSOPE cruise provided the first spatially extensive experiment in the Southeast Pacific. We conducted nutrient addition bioassays, designed to investigate which nutrient (N, P and/or Fe) controls primary productivity, photosynthetic efficiency and dinitrogen fixation along a trophic gradient in the Southeast Pacific. A complementary paper (Van Wambeke et al. this issue) examines the factors that control heterotrophic bacterial growth in the same area.

2 Material and methods

This research was carried out onboard the R/V *Atalante* in October–November 2004. The experiments were performed at three stations (Fig. 1a) located in the western edge (station HNL, $9^\circ \text{ S } 136^\circ \text{ W}$), in the center (station GYR, $26^\circ \text{ S } 114^\circ \text{ W}$) and in the southeastern edge of the gyre (station EGY, $34^\circ \text{ S } 92^\circ \text{ W}$).

All experimental setups were performed under strict trace metal clean conditions inside a clean container. Seawater was collected at 30 m depth using a trace metal-clean Teflon pump system and dispensed into 21 to 33 (depending on the number of treatments) acid-washed 4.5 l transparent polycarbonate bottles. Under a laminar flow hood, nutrients or dust were added either alone or in combination: +Fe, +NPSi and +FeNPSi at station HNL, +Fe, +N, +P, +FeN, +FeNP and +dust at stations GYR and EGY. The final concentrations were $1 \mu\text{mol l}^{-1} \text{NH}_4^+$, $2 \mu\text{mol l}^{-1} \text{NaNO}_3^-$, $0.3 \mu\text{mol l}^{-1} \text{NaH}_2 \text{PO}_4$, $2 \text{nmol l}^{-1} \text{FeCl}_3$ and 0.25mg l^{-1} of dust. Despite the fact that Saharan dust deposition events are unlikely to occur in the Southeast Pacific, the dust used in this experiment was the Saharan soils collected and characterized by Guieu et al. (2002) in order to allow a comparison with earlier efforts (Mills et al., 2004; Blain et al., 2004; Bonnet et al., 2005). Each fertilization was performed in triplicate. The bottles were immediately capped with parafilm, sealed with PVC tape, and incubated for 48 h in an on-deck incubator with circulating surface seawater at appropriated irradiance (50% ambient light level). For each station, the incubation started in the morning. After two selected time points during the course of the experiment ($T_1=24 \text{ h}$; $T_2=48 \text{ h}$), three replicates of each treatment were sacrificed in order to measure the following parameters: variable fluorescence, Chl-*a* concentrations, epifluorescence microscopy counts and flow cytometry. For rate measurements such as primary productivity and dinitrogen fixation, subsamples of each 4.5 l microcosms have been used after each time point (24 h and 48 h) for parallel incubations (see below). For each parameter, treatment means were compared using a one-way ANOVA and a Fisher PLSD means comparison test.

2.1 Nutrient analysis

Ambient nutrient concentrations have been measured at each of the three stations before the incubation experiments as well as during the incubations. Concentrations of nitrate, nitrite, phosphate and silicate have been analysed using a Technicon Autoanalyser II (Treguer and Le Corre, 1975). All the measurements have been done onboard, except for the silicate samples, which were poisoned (mercuric chloride $1 \mu\text{g ml}^{-1}$) and analyzed on land. Measurements in the nanomolar range (lower detection limit = 3 nmoles l^{-1}) were obtained from the sensitive method described by Raimbault et al. (1990). Nitrate at submicromolar levels (detection limit: $0.05 \mu\text{moles l}^{-1}$) and phosphate (detection limit: $0.02 \mu\text{moles l}^{-1}$) were measured according to Armstrong et al. (1967). Ammonium concentrations were measured as described by Holmes et al. (1999), with a detection limit of 5 nmoles l^{-1} .

2.2 Dissolved iron (DFe) concentrations

DFe concentrations were measured on 19 vertical profiles (0–400 m) along the 8000 km transect. They were analyzed by Flow Injection Analysis with online preconcentration and chemiluminescence detection (FIA-CL) (adapted from Obata et al., 1993). The mean blank, calculated from daily determinations, equaled $69 \pm 18 \text{ pmol l}^{-1}$ ($n=19$) and the detection limit was 54 pmol l^{-1} . Each sample was analyzed in triplicate. When at least two of the three runs agreed within expected reproducibility (10%), the average of the two or three concordant runs was taken as a correct concentration. If the concentration obtained deviated too much from the profile continuum expectations and seemed to be contaminated, one of the other sampled bottles was then analyzed (in triplicate) (see Blain et al. this issue, for more details on the methodology).

2.3 Dinitrogen fixation

At the last time point of each experiment, 0.6 ml of each microcosms have been subsampled. 1 ml of $^{15}\text{N}_2$ gas (99% $^{15}\text{N}_2$ EURISOTOP) was introduced to each 0.6 l polycarbonate bottle through a Teflon-lined butyl rubber septum using a gas-tight syringe according to Montoya et al. (1996). After 24 h of incubation, the samples were filtered under low vacuum (100 mm Hg) through a precombusted (24 h at 450°C) 25-mm GF/F filter and dried at 60°C . Filters were stored in a desiccator until analysed. Determination of ^{15}N enrichments was performed with an Integra-CN PDZ EUROPA mass spectrometer. The background natural abundance determined on 8 unlabelled samples was $0.367 \pm 0.007\%$ for N. Only excess enrichments larger than twice the standard deviation (0.014% for N) were considered as significant. The spectrometer was calibrated in order to detect the low levels of particulate nitrogen encountered; it was calibrated with

glycin references every batch of 10–15 samples. The accuracy of our analytical system was also regularly verified using reference materials from the International Atomic Energy Agency (IAEA, Analytical Quality Control Services). Based on the lowest nitrogen level determined by our mass spectrometer ($0.2 \mu\text{moles}$), the detection limit for dinitrogen fixation was $0.3 \mu\text{moles l}^{-1}$. Dinitrogen fixation rates ($r\text{N}$ in $\text{nmoles N l}^{-1} \text{ t}^{-1}$) were computed from an equation based on final particulate nitrogen (Dugdale and Wilkerson, 1986) (see Raimbault and Garcia, this issue for more details on the methodology).

2.4 Primary productivity

After each time point, primary production was measured on 250 ml subsamples of each microcosm as described by Moutin and Raimbault (2002). Each subsample was inoculated with 0.37 MBq of $\text{NaH}^{14}\text{CO}_3$ (Amersham CFA3) and incubated in a on-deck incubator (50% ambient light level) for four to seven hours around noon. Three samples were filtered immediately after inoculation for radioactivity determination at T0, and $250 \mu\text{l}$ were sampled randomly from three bottles and stored with $250 \mu\text{l}$ of ethanolamine to determine the quantity of added tracer (Q_i). After incubation, the samples were filtered on GF/F filters, covered with $500 \mu\text{l}$ of HCl 0.5 mol l^{-1} and stored for pending analysis in the laboratory. In the laboratory, samples were dried for 12 h at 60°C , 10 ml of ULTIMAGOLD-MV (Packard) were added to the filters and the radioactivity measured after 24 h with a Packard Tri carb 2100 TR liquid scintillation analyser. The hourly rate of primary production (PP) was calculated as:

$$\text{PP}(\text{mgC m}^{-3}\text{h}^{-1}) = (\text{dpm} - \text{dpm}_{(t_0)}) / (\text{dpm}_{(Q_i)} \times 1000) \times 25000 / T$$

with T = incubation duration.

2.5 Flow cytometry

Cytometric analyses for picophytoplankton were performed on fresh samples with a FACSCalibur (Becton Dickinson) flow cytometer. Populations were differentiated based on their scattering and fluorescence signals (Marie et al., 2000). Samples were acquired for 3 minutes at $\sim 80 \mu\text{l min}^{-1}$ (~ 12 to 100×10^3 cells) using Cell Quest Pro software and data were analysed using the Cytowin software (see http://www.sb-roscoff.fr/Phyto/index.php?option=com_docman\&task=cat.view\&gid=118\&Itemid=112). Forward scatter (FSC) and chlorophyll-*a* fluorescence (FL3) cytometric signals were normalized to reference beads (Fluoresbrite® YG Microspheres, Calibration Grade $1.00 \mu\text{m}$, Polysciences, Inc) and then used as indicators of mean cell size and intracellular chlorophyll content, respectively (e.g. Campbell and Vaulot 1993). Significant changes in mean FSC and FL3 after incubation under the different treatments (48 h) was evaluated through ANOVA analyses.

2.6 Epifluorescence microscopy counts

Counts were performed with a Olympus BX51 epifluorescence microscope. Water samples (100 ml) were fixed with glutaraldehyde (0.25% final concentration) and filtered through 0.8 μm pore size filters. Samples were stained with 4'-6-diamidino-2-phenylindole (DAPI, 5 $\mu\text{g ml}^{-1}$ final concentration). Eukaryotes were identified and counted by standard epifluorescence microscopy (Porter and Feig, 1980).

2.7 Variable fluorescence

Chlorophyll variable fluorescence of phytoplankton was measured using the custom-built benchtop Fluorescence Induction and Relaxation (FIRE) system (Gorbunov and Falkowski, 2005). The excitation light was provided by 4 blue light-emitting diodes, LEDs, (central wavelength 450 nm, 30 nm bandwidth, with the peak optical power density of 2 W cm^{-2}). The variable fluorescence sequences were processed to calculate minimum (F_o) and maximum (F_m) fluorescence (measured in the dark), as the quantum efficiency of PSII (F_v/F_m), according to Kolber et al. (1998). Measurements were made on dark-adapted samples (30 min). The background fluorescence signal (blank) was measured using 0.2 μm filtered seawater and was subtracted from the measured variable fluorescence.

2.8 Abundance of nitrogen fixers

Water samples (3 l) were filtered through 3 μm pore size filters (GE Osmonics) and subsequently through 0.2 μm pore size Supor filters (PALL corp.). Both filters were processed to determine the N_2 -fixing microorganisms in the $>3 \mu\text{m}$ and $<3 \mu\text{m}$ size fractions. DNA was extracted from the filters (Church et al., 2005) with the addition of a bead-beating step prior to the lysis step. The *nifH* gene was amplified with nested PCR primers (*nifH1*, *nifH2*, *nifH3* and *nifH4*) (Church et al., 2005). The amplification products were cloned into pGEM®-T vectors (Promega). Plasmid DNA was isolated with Montage kits (Millipore) and the cloned inserts were sequenced at the University of California-Berkeley Sequencing facility. Quantitative PCR for Group A and B unicellular cyanobacterial *nifH* was performed as described in Church et al. (2005).

2.9 Determination of pigments

2.8 l of seawater were filtered onto GF/F filters and immediately stored in liquid nitrogen then at -80°C until analysis on land which was performed according to the procedure described in Ras et al. (2007). Pigment grouping into pigment-base size classes was performed according to Uitz et al. (2006).

3 Results

3.1 Initial nutrient concentrations and phytoplankton composition

The initial nutrient concentrations and phytoplanktonic species composition for these bioassay experiments are given in Table 1. Fe vertical profiles indicated low (below $0.134 \pm 0.05 \text{ nmol l}^{-1}$) and constant DFe concentrations from the surface to 400 m depth throughout the entire transect (station MAR throughout station EGY, $n=110$), except in the Chilean coastal upwelling zone (Fig. 1b, see also Blain et al. this issue). Surface DFe concentrations were $0.14 \pm 0.02 \text{ nmol l}^{-1}$, $0.10 \pm 0.01 \text{ nmol l}^{-1}$ and $0.10 \pm 0.01 \text{ nmol l}^{-1}$, respectively for the HNL, GYR and EGY stations (Table 1). In contrast, macronutrients and Chl-*a* concentrations differed markedly among stations, with Chl-*a* concentrations being $0.029 \pm 0.01 \text{ mg m}^{-3}$ in NO_3^- -depleted waters of GYR and 0.103 ± 0.02 and $0.110 \pm 0.01 \text{ mg m}^{-3}$ respectively at EGY and HNL, where NO_3^- concentrations were higher (0.02 ± 0.02 and $1.66 \pm 0.11 \mu\text{mol l}^{-1}$; Table 1). Waters were phosphate-replete along the whole transect with concentrations always above $0.11 \mu\text{mol l}^{-1}$.

The phytoplankton community structure was dominated by picophytoplankton at the three stations, where it represented 58%, 49% and 47% of the total Chl-*a* (Table 1), respectively at HNL, GYR and EGY. Cyanobacteria, mainly belonging to the *Prochlorococcus* genera, dominated picophytoplankton. Phytoplankton pigment distribution along the transect is described in Ras et al. (2007).

3.2 Biological response during the incubation experiments

For all the parameters measured in this experiments, the stimulation by nutrients was considered to be significant when the ANOVA comparison of distribution of triplicate treatments gave values of $p < 0.05$. The significant responses (different from the control) are indicated by an asterisk on Fig. 2.

3.2.1 Photosynthetic quantum efficiency of photosystem II

The western part of the gyre (station HNL) was characterized by low F_v/F_m (0.16 ± 0.01) at T0 (Table 1), indicating an apparently low yield of photosynthesis. Iron was found to be the nutrient that controls photosynthetic efficiency at that station, as indicated by the increase of 65% of F_v/F_m after an Fe addition ($p < 0.05$; Fig. 2). The station located at the eastern side of the gyre (station EGY) exhibited medium F_v/F_m values at T0 (0.30 ± 0.02) (Table 1) that increased significantly ($p < 0.05$) after Fe addition, but in a lower proportion compared to station HNL (30%; Fig. 2). In contrast, the center of the South Pacific Gyre was characterized by high F_v/F_m at T0 (0.51 ± 0.03) (Table 1). This value did not increase after Fe, N, P or dust addition ($p > 0.05$, Fig. 2). The

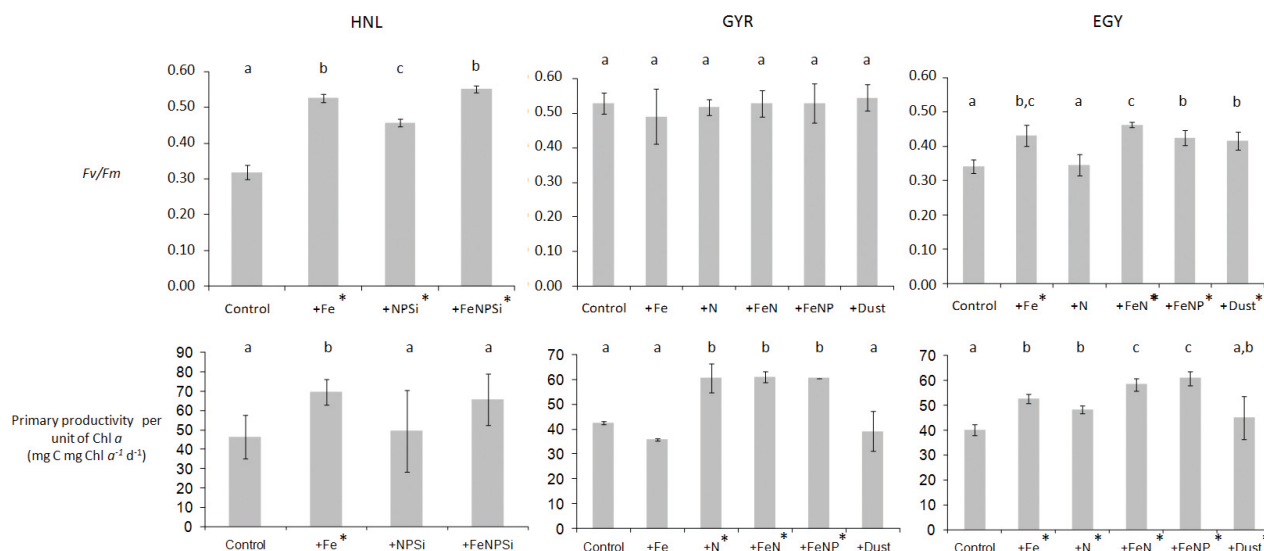


Fig. 2. Effect of nutrient additions during bioassay experiments performed at the three stations (HNL, GYR, EGY) (a) Photochemical efficiency of photosystem II (F_v/F_m) after 24 h incubation, (b) Primary productivity per unit chlorophyll-*a* ($\text{mg C mg Chl-}a^{-1} \text{d}^{-1}$) after 48 h of incubation. F_v/F_m and carbon fixation were measured from separate triplicate bottles, such that nine bottles were incubated for each nutrient treatment. The error bars represent the standard deviation from triplicate incubations. Treatment means were compared using a one-way ANOVA and a Fisher PLSD means comparison test. Means that are significantly different from the control are labelled with an asterisk and means that are not significantly different are labelled with the same letter ($p < 0.05$).

Table 1. Initial conditions for bioassay experiments. % pico-, nano- and microphytoplankton correspond to the biomass proportion of total Chl-*a* associated with each size class of phytoplankton calculated as described in Uitz et al. (2006).

	Experiment 1 HNL	Experiment 2 GYR	Experiment 3 EGY
Latitude Longitude	9°04'S 136°97'W	26°04'S 114°02'W	31°89'S 91°39'W
Chl- <i>a</i> (mg m^{-3})	0.11±0.05	0.029±0.01	0.103±0.02
NO_3^- ($\mu\text{mol l}^{-1}$)	1.66±0.11	<0.003	0.02±0.02
NO_2^- ($\mu\text{mol l}^{-1}$)	0.03±0.00	< 0.003	0.01±0.00
NH_4^+ ($\mu\text{mol l}^{-1}$)	0.03±0.00	0.006±0.00	< 0.005
PO_4^{3-} ($\mu\text{mol l}^{-1}$)	0.30±0.01	0.11±0.02	0.14±0.06
SiOH_4 ($\mu\text{mol l}^{-1}$)	1.31±0.12	0.98±0.09	1.21±0.17
DFe (nmol l^{-1})	0.14±0.02	0.10±0.01	0.10±0.01
F_v/F_m	0.16±0.01	0.51±0.03	0.30±0.01
% pico-	58	49	47
% nano-	31	48	43
% micro-	11	13	10

addition of macronutrients without Fe had a positive effect at station HNL, but did not have any effect at station EGY, where only a Fe addition (alone or in combination) resulted in an increase of F_v/F_m . The dust treatment also had a positive effect on F_v/F_m at the station EGY.

3.2.2 Rate measurements

Primary productivity

At station HNL, only the addition of Fe resulted in a significant increase of primary productivity (+50%, $p < 0.05$), whereas at station GYR, only the treatments having nitrogen (+N, +FeN and +FeNP) resulted in a positive response (+45%, $p < 0.05$). At station EGY, all treatments

Table 2. Abundance of diazotrophs (gene copies per liter) determined by QPCR for samples collected at 13 stations between HNL and EGY (ND: Non Detectable). The depth at which the *nifH* gene was detectable is indicated between parentheses. The nitrogen fixation rates ($\text{nmol l}^{-1} \text{d}^{-1}$) measured at the three stations during the incubation experiments are also indicated. ^a Data obtained from Church et al. (2005) at 25 m depth in December 2002 (Aloha station). ^b Data from Dore et al. (2002).

Station	< 3 μm		> 3 μm		N_2 fixation rates
	Group A	Group B	Trichodesmium	Chaetoceros/Calothrix	
HNL	27 (5 m)	ND	ND	ND	
1	ND	ND	ND	ND	
2	ND	ND	ND	30 (70 m)	ND
3	ND	ND	ND	ND	
4	ND	ND	ND	ND	
6	–	ND	ND	ND	
7	ND	ND	ND	ND	
GYR	184 (5 m)	ND	ND	ND	ND
12	–	ND	ND	ND	
13	ND	ND	ND	ND	
14	ND	–	–	–	
15	ND	ND	ND	ND	
EGY	ND	ND	ND	ND	ND
ALOHA	10000–00000 ^a	1000 ^a	1000–10000 ^a	–	0.07–2.21 ^b

with a source of Fe or N resulted in a positive increase (+25%). The addition of both Fe and N resulted in a higher response (+50%), indicating a clear Fe and N co-limitation. At stations GYR and EGY, the addition of P together with Fe and N did not result in a significantly higher response than the addition of Fe and N alone, indicating that P is not limiting.

Dinitrogen fixation

$^{15}\text{N}_2$ assimilation consistently remained below the detection limit at the three stations in our incubation experiments (Table 2), indicating the absence of dinitrogen fixation, even after dust, Fe, and FeP additions.

3.2.3 Abundance of nitrogen fixers

Water samples from 13 stations situated between HNL and EGY (Fig. 1a) were examined for presence of N_2 -fixing microorganisms by amplification of the *nifH* gene. After amplification, cloning and sequencing the nitrogenase genes, our results indicate the absence of the filamentous cyanobacteria *Trichodesmium*, or any large (3–7 μm) unicellular putative nitrogen fixing cyanobacteria (Group B). The results suggest however the presence of low numbers of Group A cyanobacterial phylotypes at two stations (less than 200 copies l^{-1} , Table 2), and low numbers of non-cyanobacterial *nifH* sequences (*Vibrio* diazotrophicus and proteobacteria), that must explain the significant dinitrogen fixation rates measured by Raimbault et al. (2007) during

the transect. It must be noted that the molecular data for both ends of the transect (data not related to these incubations) indicate the presence of larger number of cyanobacteria close to the Marquesas archipelago (up to 342 copies l^{-1} Group B, 45 copies l^{-1} *Trichodesmium* and 178 copies l^{-1} *Chaetoceros/Calothrix*) and close to the Chilean upwelling (108 copies l^{-1} Group B and 20 copies l^{-1} *Trichodesmium*). These higher densities of diazotrophs are consistent with the higher dinitrogen fixation rates measured by Raimbault et al. (2007) at both ends of the transect.

3.2.4 Cell numbers

Epifluorescence microscopy confirmed the absence of the two phylotypes *Trichodesmium* and unicellular from Group B at any station and treatment, which is in agreement with molecular biology data. Concerning non nitrogen-fixing organisms, the addition of Fe or Fe and/or macronutrients at stations HNL resulted in a significant ($p < 0.05$) increase in *Synechococcus* and picoeukaryotes abundances (Table 3). At station EGY, all treatments containing nitrogen had a positive effect on picoeukaryotes, *Prochlorococcus* and *Synechococcus* abundances. At station GYR, only the +N and +Fe and N treatments induced a significant increase in picoeukaryotes abundances. The other treatments did not have any effect on this group, nor on *Synechococcus*. However, larger *Synechococcus* fluorescence (FL3) and forward light scatter (FSC) cytometric signals indicated at station GYR an increase in relative cell size and intracellular chlorophyll-*a* content after addition of N, Fe and N and FeNP ($p < 0.05$ for

Table 3. Evolution of the abundances of *Prochlorococcus*, *Synechococcus* and picophyto-eukaryotes after 48 h of incubation at the three stations studied, for each treatment (cells ml⁻¹; mean±SD). The standard deviation (SD) is calculated on the triplicates. At station GYR, *Prochlorococcus* fluorescence was too dim to allow us to detect changes in either the abundance or cytometric signals. Treatment means were compared using a one-way ANOVA and a Fisher PLSD means comparison test. Means that are significantly different from the control ($p<0.05$) are labelled with an asterisk.

HNL station						
Sample	Prochlorococcus/ml		Synechococcus/ml		Picoeukaryotes/ml	
Control	264133 ±	17091	30096 ±	677	10140 ±	371
Fe	116928 ±	1858	47740 ±	1256*	15502 ±	1039*
NPSi	420368 ±	43935*	60892 ±	4157*	23309 ±	1056*
FeNPSi	142137 ±	12420	61178 ±	1726*	18243 ±	1398*
GYR station						
Sample	Prochlorococcus/ml		Synechococcus/ml		Picoeukaryotes/ml	
Control	nd		1704 ±	272	572 ±	109
Fe	nd		1873 ±	176	518 ±	37
N	nd		1659 ±	119	775 ±	144*
FeN	nd		1491 ±	79	916 ±	106*
FeNP	nd		1546 ±	55	678 ±	113
Dust	nd		2012 ±	129	625 ±	33
EGY station						
Sample	Prochlorococcus/ml		Synechococcus/ml		Picoeukaryotes/ml	
Control	158798 ±	6284	18743 ±	512	6422 ±	162
Fe	102588 ±	3761	15963 ±	795	5724 ±	141
N	253317 ±	19927*	20521 ±	900*	8642 ±	589*
FeN	129818 ±	12825	18129 ±	669	7960 ±	237*
FeNP	127752 ±	7424	17400 ±	454	8694 ±	186*
Dust	138278 ±	nd	17936 ±	481	8288 ±	312*

Table 4. Cytometric signals obtained at station GYR for each treatment. Significant changes in mean FSC and FL3 after incubation under the different treatments (48 h) was evaluated using a one-way ANOVA. Significant data ($p<0.05$) are labelled with an asterisk. Abbreviations: Proc (Prochlorococcus), Syn (Synechococcus), Euk (picophytoeukaryotes), SSC (side scattered light intensity), FSC (Forward scattered light intensity), FL3 (chlorophyll-*a* fluorescence).

	Fe	N	Fe and N	All	Dust
SSC Proc.	0.065*	0.013*	0.024*	0.034*	0.016*
FSC Syn.	0.470	0.012*	0.006*	0.009*	0.858
SSC Syn.	0.792	0.805	0.374	0.444	0.400
FL3 Syn.	0.230	0.021*	0.020*	0.018*	0.708
FSC Euk.	0.646	0.011*	0.259	0.221	0.883
SSC Euk.	0.663	0.002*	0.124	0.048*	1.000
FL3 Euk.	0.096	0.032*	0.117	0.01*	0.595

FSC and FL3, Table 4). The presence of cyanobacteria in the size range 1 to 3 μm was later confirmed by epifluorescence microscopy counts.

4 Discussion

4.1 The role of Fe

The data indicate that Fe is the nutrient that controls photosynthetic efficiency and primary productivity outside the gyre, at station HNL. These results are in accordance with the patterns found in other HNLC waters (e.g. Boyd et al., 2000). Around Marquesas, Behrenfeld and Kolber (1999) also found low values of F_v/F_m with a pronounced decrease at night; in our experiments, the addition of Fe eliminated the nocturnal decrease and increased F_v/F_m values. In the central gyre (GYR), the high F_v/F_m value (0.51 ± 0.03) was however unexpected due to the low dissolved Fe concentrations. This value is close to the maximum value observed in the ocean (Falkowski et al., 2004) and did not increase after Fe or dust addition. Behrenfeld et al. (2006) found the same pattern (high F_v/F_m , absence of nocturnal decrease) in the North Tropical Pacific, but the ambient dissolved Fe concentrations there are two to seven times higher (Boyle et al., 2005) than in the South Pacific Gyre, where our experiments were carried out. Our data also indicate that the addition of Fe did not change Chl-*a* concentrations or primary productivity ($p>0.05$), indicating that, in contrary to the HNL sta-

tion, the photoautotrophic community was not Fe-limited in the gyre. This suggests that the natural assemblage is acclimated to Fe deprivation.

Flow cytometry measurements identified *Prochlorococcus* as a prominent component of the prokaryote-dominated phytoplankton assemblage at station GYR (20 000 cells ml⁻¹), whereas in terms of carbon biomass, picophytoeukaryotes dominated (0.89 mg C m⁻³, i.e. 2.6-fold higher than *Prochlorococcus*). Although *Synechococcus* abundance was similar to that of *Prochlorococcus* (1400 cells ml⁻¹), their contribution to the phytoplanktonic carbon biomass was negligible (0.06 mg C m⁻³). To maintain high carbon fixation rates in such a low Fe environment, the organisms must have developed ecophysiological strategies to survive the shortage of Fe, including Fe scavenging systems (Geider and la Roche, 1994), efficient Fe transport systems over the plasma membrane (Katoh et al., 2001) or gene regulation systems consisting in rearrangements of photosynthetic apparatus (Sandström et al., 2002).

In summary, although DFe concentrations were identical at the three stations, our data clearly show contrasting physiological responses to Fe additions. Cultures experiments conducted under Fe limited conditions exhibit either low (~0.1) or high (~0.5) F_v/F_m depending on whether growth is balanced or unbalanced (Price, 2005). The high F_v/F_m values measured in the center of the gyre (GYR) are a clear indication that the phytoplankton assemblages are well acclimated to the stable environmental conditions of low N and low Fe. In contrast, station HNL (situated in the southern limit of the equatorial upwelling and embedded in the westward flowing South Equatorial Current) and station EGY (corresponding to a transition zone between the salty Eastern South Pacific Central Waters and the waters influenced by fresher Subantarctic Surface Waters (Emery and Meincke, 1986) are less steady environments, with low F_v/F_m values and increased F_o possibly due to the presence of specific Fe-stress pigment-protein complexes (Behrenfeld et al., 2006). This might also suggest an unbalanced growth (Parkhill et al., 2001) in environment with occasional spikes of nutrients.

It is interesting to note that a dust addition did not cause any increase of primary productivity at station EGY, while an iron addition resulted in a positive response. This absence of response can be interpreted by the fact that only 0.1% of the iron in the dust dissolved, which is ten times lower than the dissolution found with the same amount of the same dust in the Mediterranean waters by Bonnet and Guieu (2004). This difference can be interpreted by the difference in organic ligands concentrations between the Pacific and the Mediterranean waters (Bonnet, 2005).

4.2 From Fe to nitrogen limitation

Dissolved Fe concentrations were low and constant along the three stations studied, but the data clearly show a progression from Fe limitation in station HNL towards nitrogen limita-

tion in station GYR. Station EGY, located on the southeastern edge of the gyre, is a transition station where primary productivity is Fe and N co-limited. In the center of the gyre (station GYR), nitrogen is the nutrient that controls primary productivity. The addition of a nitrogen source resulted in an increase in the abundance of picophytoeukaryotes and an increase in relative cell size and intracellular Chl-*a* content of *Synechococcus* ($p < 0.05$). It is interesting to note that bacterial production is also directly enhanced after a nitrogen addition (by a factor of 9 after 48 h, see Van Wambeke et al. this issue).

Perhaps the most intriguing part of this study is the absence of dinitrogen fixation in our experiments, even after dust, Fe and/or P additions. These results suggest that neither P nor Fe limit dinitrogen fixation at 30 m depth. It must be noted that Raimbault and Garcia (2007) measured low dinitrogen fixation rates at 30 m in the central gyre (stations GYR), revealing the weakness of the process at this depth. However, these authors measured significant N₂ fixation rates in subsurface waters (~1 nmol l⁻¹ d⁻¹), which is in accordance with the molecular data (Table 2) and recent modelling efforts (Deutsch et al. 2007). At the other stations located between stations HNL and EGY, diazotrophic heterotrophic bacteria detected by molecular tools must be responsible of the dinitrogen fixation rates measured at regular stations by Raimbault and Garcia (2007). It has to be noted that the density of diazotrophic cyanobacteria are extremely low compared to those of the North Pacific Gyre (ALOHA station in December, 10 000 to 100 000 copies l⁻¹). The absence of *Trichodesmium* and Group B phylotypes also contrasts with amplification from oligotrophic waters of the tropical North Pacific Ocean, where cyanobacterial *nifH* genes from these two groups are abundant, even during the winter season (see Table 2; Church et al., 2005). In this area, dinitrogen fixation rates are high throughout the water column (Dore et al., 2002) and provide a major source of newly fixed nitrogen to the euphotic zone, sustaining up to 50% of new primary production, and drives the system towards P- and/or Fe-limitation (Karl et al., 1997; Sohm et al.¹). The scarcity of nitrogen fixing organisms in the South Pacific Gyre may be one of the origins of the relatively large phosphate concentrations (always above 0.11 μmol l⁻¹; Moutin et al., 2007), as well as the N controlled status of the phytoplankton and bacterial communities. However, the other potential sources of nitrogen for the South Pacific Gyre are small and dinitrogen fixation may nonetheless represent the main source of new nitrogen in the system (Raimbault and Garcia, 2007): the vertical flux of NO₃⁻ from below the thermocline is extremely low compared to other gyres (10 to 12 times lower than the one measured in the North Atlantic gyre; Capone

¹Sohm, J., Krauk, J., Mahaffey, C., Capone, D. G.: Diagnostics of phosphorus stress in the cyanobacterium *Trichodesmium* reveal the northwest Atlantic is more severely P limited than the tropical Pacific, *Limnol. Oceanogr.*, submitted, 2008.

et al., 2005), and potential atmospheric deposition of nitrogen is almost absent according to the aerosols measurements performed in this area by Wagener et al. (2008).

5 Conclusions

This paper is an attempt to analyse which are the nutrients that control primary productivity in the Southeast Pacific. A gradient in the nutrient control of phytoplanktonic communities is described, from an Fe-controlled system (on the edge of the gyre) towards a nitrogen-controlled system (in the center of the gyre). By combining physiological data, rate processes measurements and molecular approaches, this unique nutritional status of the phytoplankton populations is described for the first time in the gyre. Autotrophic communities are indeed adapted to living under extremely low Fe levels; these results add a new perspective on life in extreme environments and give a new perspective to so-called HNLC areas of the world ocean. In addition, we show for the first time that nitrogen fixing cyanobacteria are scarce in the South Pacific Gyre. Due to the extremely low Fe-rich dust inputs at the surface waters of the gyre, these waters constitute a “low iron” environment (Blain et al. this issue). It is hypothesized that this region is not a favourable environment for common photoautotrophic nitrogen fixing organisms (e.g. *Trichodesmium*), as they have elevated Fe quotas relative to non-diazotrophic phytoplankton (Kustka et al., 2003). However, the factors controlling dinitrogen fixation are still poorly understood and further studies are needed to understand the distribution of these organisms and their biogeochemical impact in the ocean.

Acknowledgements. Dominique Tailliez and Claudie Bournot are warmly thanked for their efficient help in CTD rosette management and data processing. This is a contribution of the BIOSOPE project of the LEFE-CYBER program. This research was funded by the Centre National de la Recherche Scientifique (CNRS), the Institut des Sciences de l’Univers (INSU), the Centre National d’Études Spatiales (CNES), the European Space Agency (ESA), The National Aeronautics and Space Administration (NASA), the Academy of Sciences (AVCR) and the Ministry of Education (MSMT) of the Czech Republic, and the Natural Sciences and Engineering Research Council of Canada (NSERC).

Edited by: J.-P. Gattuso

References

- Armstrong, F. A. J., Stearns, C. R., and Strickland, J. D. H.: The measurement of upwelling and subsequent biological processes by means of the Technicon AutoAnalyzer and associated equipment, *Deep Sea Res.*, 14(3), 381–389, 1967.
- Arrigo, K. R.: Marine micro-organisms and global nutrient cycles, *Nature*, 437(7057), 349–355, 2005.
- Behrenfeld, M. J. and Kolber, Z. S.: Widespread iron limitation of phytoplankton in the South Pacific Ocean, *Science*, 238 840–843, 1999.
- Behrenfeld, M. J., Worthington, K., Sherell, R. M., et al.: Controls on tropical Pacific ocean productivity revealed through nutrient stress diagnostic, *Nature* 442, 1025–1028, 2006.
- Berman-Frank, I., J., Cullen, J., Hareli, Y., et al.: Iron availability, cellular iron quotas, and nitrogen fixation in *Trichodesmium*, *Limnol. Oceanogr.*, 46, 1249–1277, 2001.
- Blain, S., Bonnet, S., and Guieu, C.: Dissolved iron distribution in the tropical and sub tropical Southeastern Pacific, *Biogeosciences Discuss.*, 4, 2845–2875, 2007, <http://www.biogeosciences-discuss.net/4/2845/2007/>.
- Bonnet, S. and Guieu, C.: Dissolution of atmospheric iron in seawater. *Geophys. Res. Lett.*, 31, L03303, doi:10.1029/2003GL018423, 2004.
- Bonnet S., Guieu C., Chiaverini J., et al.: Impact of atmospheric inputs on the autotrophic communities in a low nutrient low chlorophyll system, *Limnol. Oceanogr.*, 50(6), 1810–1819, 2005.
- Bonnet, S.: The role of atmospheric iron in oligotrophic environments. Ph.D. thesis, University Pierre et Marie Curie, Paris 6, 207 pp., 2005.
- Boyd, P. W., Watson, A. J., Law, C. S., et al.: A mesoscale phytoplankton bloom in the polar Southern Ocean stimulated by iron fertilization, *Nature*, 407, 695–702, 2000.
- Boyle, E., Bergquist, B. A., Kayser, R. A., and Mahowald, N.: Iron, manganese, and Lead at Hawaii Ocean Time-series station ALOHA: Temporal variability and an intermediate water hydrothermal plume, *Geochim. Cosmochim. Act.*, 69, 933–952, 2005.
- Campbell, L. and Vault, D.: Photosynthetic picoplankton community structure in the subtropical North Pacific Ocean near Hawaii (station ALOHA). *Deep-Sea Res.*, 40, 2043–2060, 1993.
- Capone, D. G., Burns, J. A., Montoya, J. P. et al.: New nitrogen input to the tropical North Atlantic Ocean by nitrogen fixation by the cyanobacterium, *Trichodesmium* spp., *Global Biogeochem. Cy.*, 19, GB2024, doi:10.1029/2004GB002331, 2005.
- Church, M. J., Jenkins, B. D., Karl, D. M., and Zehr, J. P.: Vertical distributions of nitrogen-fixing phylotypes at Stn ALOHA in the oligotrophic North Pacific Ocean. *Aquat. Microb. Ecol.*, 38(1), 3–14, 2005.
- Claustre, H. and Maritorena, S.: The many shades of ocean blue, *Science*, 302, 1514–1515, 2003.
- Deutsch, C., Sarmiento, J. L., Sigman, D. M., et al.: Spatial coupling of nitrogen inputs and losses in the ocean, *Nature*, 445, 163–167, 2007.
- Dore, J. E., Brum, J. R., Tupas, L. M., and Karl, D. M.: Seasonal and Interannual Variability in Sources of Nitrogen Supporting Export in the Oligotrophic Subtropical North Pacific Ocean. *Limnol. Oceanogr.*, 47, 1595–1607, 2002.
- Dugdale, R. C. and Wilkerson, F. P.: The use of ¹⁵N to measure nitrogen uptake in eutrophic oceans, experimental conditions. *Lim-*

- nol. *Oceanogr.*, 31 673–689, 1986.
- Emerson, S., Quay, P., Karl, D., et al.: Experimental determination of the organic carbon flux from open-ocean surface waters, *Nature*, 389, 951–954, 1997.
- Emery, W. J. and Meincke, J.: Global water masses: summary and review. *Oceanol. Acta.*, 9, 383–391, 1986.
- Falkowski, P. G., Katz, M. E., Knoll, A. H., et al.: The Evolution of Modern Eukaryotic Phytoplankton., *Nature*, 305, doi: 0.1126/science.1095964, 354–360, 2004.
- Falkowski, P. G., Barber, R. T., and Smetacek, V.: Biogeochemical controls and feedbacks on primary production, *Science*, 281, 200–206, 1998.
- Falkowski, P. G.: Evolution of the nitrogen cycle and its influence on the biological sequestration of CO₂ in the Ocean, *Nature*, 387, 272–275, 1997.
- Geider, J. G. and La Roche, J.: The role of iron in phytoplankton. photosynthesis, and the potential for iron-limitation of primary production in the sea. *Photosynth. Res.*, 39, 275–301, 1994.
- Guieu C., Loye-Pilot, M.-D., Ridame, C., and Thomas, C.: Chemical characterization of the Saharan dust end-member; some biological implications for the western Mediterranean, *J. Geophys. Res.*, 107(D15), 4258, doi:10.1029/2001JD000582, 2002.
- Gorbunov, M. Y. and Falkowski, P. G.: Fluorescence Induction and Relaxation (FIRE) Technique and Instrumentation for Monitoring Photosynthetic Processes and Primary Production in Aquatic Ecosystems. *Photosynthesis: Fundamental Aspects to Global Perspectives*. A. v. d. E. a. D. Bruce, Allen Press: 1029–1031, 2005.
- Holmes, M. R., Aminot, A., Kerouel, R., Hooker, B. A., and Peterson, J. B.: A simple and precise method for measuring ammonium in marine and freshwater ecosystems, *Can. J. Fish. Aquat. Sci.*, 56, 1801–1808, 1999.
- Karl, D. M., Letelier, R., Tupas, L., et al.: The role of nitrogen fixation in biogeochemical cycling in the subtropical North Pacific Ocean, *Nature*, 388, 533–538, 1997.
- Karl, D. M.: Nutrient dynamics in the deep blue sea, *Trends Microbiol.*, 10, 410–418, 2002.
- Karl, D., Michaels, A., Bergman, B., Capone, D., Carpenter, E., Letelier, R., Lipschultz, F., Paerl, H., Sigman, D., and Stal, L.: Dinitrogen Fixation in the World's Oceans, *Biogeochem.*, 57, 47–98, 2002.
- Katoh, H., Hagino, N., Grossman, A. R., and Ohawa, T.: Gens essential to iron transport in the cyanobacterium *synechocystis* sp. strain PCC 6803, *J. Bacteriol.*, 183(9), 2779–2784, 2001.
- Kolber, Z., Prasil, O., and Falkowski, P.: Measurements of variable chlorophyll fluorescence using fast repetition technique I. Defining methodology and experimental protocols, *Biochim. Biophys. Acta.*, 1367, 88–106, 1998.
- Kustka, A. B., Carpenter, E. J., Sañudo-Wilhelmy, S., and Sunda, W. G.: Iron requirements for N₂ and NH₄⁺ supported growth in cultures of *Trichodesmium* (IMS 101): comparison with nitrogen fixation rates and Fe: C ratios of field populations, *Limnol. Oceanogr.*, 48, 1869–1884, 2003.
- Marie, D., Partensky, F., Simon, N., et al.: Flow cytometry analysis of marine picoplankton. living colors: protocols in flow cytometry and cell sorting, D. S. Diamond RA, New York, Springer-Verlag, 421–454, 2000.
- Mills, M. M., Ridame, C., Davey, M., et al.: Iron and phosphorus co-limit nitrogen fixation in the eastern tropical North Atlantic, *Nature*, 429, 292–294, 2004.
- Montoya, J. P., Voss, M., Kaehler, P., and Capone, D. G.: A simple, high precision tracer assay for dinitrogen fixation, *App. Environ. Microb.*, 62, 986–993, 1996.
- Moore, J. K., Doney, S. C., Glover, D. M., Fung, I. Y.: Iron cycling and nutrient-limitation patterns in surface waters of the World Ocean, *Deep-Sea Research Part II-Topical Studies in Oceanography*, 49, 463–507, 2002.
- Moutin, T. and Raimbault, P.: Primary production, carbon export and nutrients availability in western and eastern Mediterranean Sea in early summer 1996, *J. Marine Syst.*, 33–34, 273–288, 2002.
- Moutin T., Karl, D. M., Duhamel, S., Rimmelin, P., Raimbault, P., Van Mooy, B. A. S., and Claustre, H.: Phosphate availability and the ultimate control of new nitrogen input by nitrogen fixation in the tropical Pacific Ocean, *Biogeosciences Discuss.*, 4, 2407–2440, 2007, <http://www.biogeosciences-discuss.net/4/2407/2007/>.
- Obata, H., Karatani, H., and Nakayama, E.: Automated determination of iron in seawater by chelating resin concentration and chemiluminescence detection, *Anal. Chem.*, 5, 1524–1528, 1993.
- Parkhill, J. P., Maillet, G., and Cullen, J. J.: Fluorescence-based maximal quantum yield for PSII as a diagnostic of nutrient stress, *J. Phycol.*, 17, 517–529, 2001.
- Price, N. M.: The elemental stoichiometry and composition of an iron-limited diatom. *Limnol. Oceanogr.*, 50, 1159–1171, 2005.
- Porter, K. G. and Feig, Y. S.: The use of DAPI for identifying and counting aquatic microflora, *Limnol. Oceanogr.*, 25, 943–948, 1980.
- Raimbault P., Slawyk G., Coste B., and Fry J.: Feasibility of using an automated colorimetric procedure for the determination of seawater nitrate in the 0 to 100 nmol l⁻¹ range: examples from field and culture, *Mar. Biol.*, 104, 347–351, 1990.
- Raimbault, P. and Garcia, N.: Carbon and nitrogen uptake in the South Pacific Ocean: Evidence for efficient dinitrogen fixation and regenerated production leading to large accumulation of dissolved organic matter in nitrogen-depleted waters, *Biogeosciences Discuss.*, 4, 3531–3579, 2007, <http://www.biogeosciences-discuss.net/4/3531/2007/>.
- Ras J., Claustre, H., and Uitz, J.: Spatial variability of phytoplankton pigment distributions in the Subtropical South Pacific Ocean: comparison between in situ and predicted data, *Biogeosciences Discuss.*, 4, 3409–3451, 2007, <http://www.biogeosciences-discuss.net/4/3409/2007/>.
- Raven, J. A.: The iron and molybdenum use efficiencies of plant growth with different energy, carbon and nitrogen source, *New Phytol.*, 109, 279–287, 1988.
- Sandström, S., Ivanov, A. G., Park, Y., et al.: Iron stress responses in the cyanobacterium *Synechococcus* sp. PCC7942, *Physiol. Plantarum*, 116(2), 255–263, doi:10.1034/j.1399-3054.2002.
- Sañudo-Wilhelmy, S. A., Kustka, A. B., Gobler, C. J., et al.: Phosphorus limitation of nitrogen fixation by *Trichodesmium* in the central Atlantic Ocean, *Nature*, 411, 66–69, 2001.
- Tréguer P. and Le Corre P.: Manuel d'analyse des sels nutritifs dans l'eau de mer. Utilisation de l'AutoAnalyser II Technicon. 2nd ed., Univ. Bretagne Occidentale, Laboratoire de Chimie marine, Brest, France, 1–110, 1975.
- Uitz, J., Claustre, H., Morel, A., and Hooker, S. B.: Vertical distri-

- bution of phytoplankton communities in open ocean: an assessment based on surface chlorophyll, *J. Geophys. Res-oceans*, 111, C08005, doi:10.1029/2005JC003207, 2006.
- Van Wambeke F., Bonnet S., Moutin T., Raimbault P., Alarçon G., and Guieu C.: Factors limiting heterotrophic prokaryotic production in the Southern Pacific Ocean, *Biogeosciences Discuss.*, 4, 3799–3828, 2007, <http://www.biogeosciences-discuss.net/4/3799/2007/>.
- Wagener, T., Guieu, C., Losno, R., Bonnet, S., and Mahowald, N.: Revisiting Atmospheric dust export to the South Hemisphere Ocean, *Global Biogeochemical Cycles*, in press, doi:10.1029/2007GB002984, December 2007.
- Zehr, J. P., Waterbury, J. B., Turner, P. J., et al.: New nitrogen-fixing unicellular cyanobacteria discovered in the North Pacific subtropical gyre, *Nature*, 412, 635–638, 2001.

Dissolved iron distribution in the tropical and sub tropical South Eastern Pacific

S. Blain^{1,*}, S. Bonnet², and C. Guieu²

¹Laboratoire d'Océanographie et de Biogéochimie, Campus de Luminy, case 901, 13288 Marseille cedex, France

²Laboratoire d'océanographie de Villefranche sur mer, Quai de la darse, Villefranche sur mer, France

*present address: UPMC Univ. Paris 06, UMR 7621, Laboratoire d'Océanographie Biologique, 66650 Banyuls/mer, France

Received: 13 July 2007 – Published in Biogeosciences Discuss.: 24 August 2007

Revised: 20 December 2007 – Accepted: 18 January 2008 – Published: 27 February 2008

Abstract. Dissolved iron (DFe) distributions ($<0.2\ \mu\text{m}$) were determined in the upper water column (0–400 m) of the south eastern tropical and subtropical Pacific, in October–November 2004. Data were collected along a transect extending from the Marquesas Islands to the Chilean coast with most of the stations located in the south Pacific gyre. The concentrations of DFe presented large variability with highest values observed at both extremities of the transect. In the Chilean upwelling, DFe concentrations ranged between 1.2–3.9 nM. These high values result from inputs from the continental margin and are likely maintained by anoxic conditions in the water corresponding to the Oxygen Minimum Zone (OMZ). In subsurface waters near the Marquesas, that were also associated with the extension of the OMZ, DFe concentrations varied between 0.15–0.41 nM. Vertical transport of this water by mesoscale activity eastward of the archipelago may explain the dissymmetric east-west distribution of chlorophyll-*a* evidenced by satellite images. Using the new tracer $\text{Fe}^* = \text{DFe} - r_{\text{Fe:P}}(\text{PO}_4^{3-})$ we show that DFe was in deficit compared to PO_4^{3-} resulting from the remineralisation of organic matter. This suggests that the Marquesas islands and the surrounding plateau are not a significant source of DFe. In the gyre, DFe concentrations in the upper 350 m water column were around 0.1 nM and the ferricline was located well below the nitracline. These low concentrations reflect the low input of DFe from the atmosphere, from the ventilation of the upper thermocline with water containing low DFe, and from the low biological activity within this ultra oligotrophic gyre.

1 Introduction

Iron is now recognised as an important element involved in numerous biochemical processes in the ocean. In High Nutrient Low Chlorophyll (HNLC) regions, iron is the proximate control of organic matter production as was clearly demonstrated by artificial iron fertilisation experiments (Boyd et al., 2007). A natural iron fertilisation experiment carried out in the largest HNLC region, the Southern Ocean (Blain et al., 2007), has revealed that the carbon export is extremely sensitive to iron inputs, much more than previously thought from artificial iron fertilisation experiments. Evidence for iron limitation of biological productivity was also found in other environments including coastal upwelling (Hutchins and Bruland, 1998), mesotrophic (Blain et al., 2004) and oligotrophic (Sedwick et al., 2005) systems. Oligotrophic systems generally provide an ideal ecological niche for the development of nitrogen-fixing organisms (e.g. (Capone et al., 2005; Karl, 2002)). Due to the high cellular iron quota in diazotrophs compared to non diazotrophic phytoplankton (Kustka et al., 2003), iron availability also exerts a control on nitrogen fixation and new primary productivity (Mills et al., 2004; Moore and Doney, 2007).

The distribution of dissolved iron (DFe) in seawater depends on the nature and the magnitude of the sources and sinks and on the transport mechanisms. The two major external sources of iron to the ocean are dust deposition from the atmosphere (Jickells et al., 2005) and inputs from the sediments (Elrod et al., 2004; Johnson et al., 1999). The fingerprint of dust deposition was clearly detectable in the DFe surface concentrations in different regions (Bonnet and Guieu, 2006; Boyle et al., 2005; Guieu et al., 2002; Sedwick et al., 2005). However, the magnitude of the atmospheric source of DFe is still very difficult to quantify because it requires determining both the flux of deposition and the solubility of dust. Qualitative evidence of the input from the sediment has mainly been reported for continental shelf or



Correspondence to: S. Blain
(stephane.blain@obs-banyuls.fr)

along the continental margin (Laës et al., 2007; Martin et al., 1989). But again the magnitude of the source is not well constrained due to the few quantitative studies on 2007. Elrod et al. (2004) pointed out large discrepancies between fluxes measured in benthic chambers and those inferred from DFe profiles in pore waters. Besides these two major sources, hydrothermalism (Boyle et al., 2005), pack ice or iceberg melting (Sedwick and Di Tullio, 1997) can locally also impact the vertical DFe distribution. The major sinks in the ocean are the net biological uptake and scavenging by sinking particles. The combination of mixing and sinking tends to rapidly decrease DFe concentrations at locations away from the source. This horizontal trend was fitted by an exponential law with e -fold (Bucciarelli et al., 2001; Johnson et al., 1997). However, in deep waters where scavenging is reduced due to the low abundance of particles, DFe can be transported over long distances (Laës et al., 2003).

In regions where dust deposition is low, the deep ocean is the main reservoir of DFe for surface waters. In this context, the determination of DFe fluxes resulting from diapycnal and deep winter mixing is crucial to quantify the input of new iron to the surface layer and to compare it with the iron demand of phytoplankton (Blain et al., 2007). In some areas, vertical upwelling may also be a major pathway for transporting iron from the deep sea to the surface layer (Johnson et al., 1999). Although no direct observation is available, vertical movement induced by mesoscale or sub-mesoscale activities may also promote upward iron transport.

During the past decade, models that include different degrees of complexity for the iron cycle and for the coupling with other biogeochemical cycles were developed (Aumont et al., 2003; Johnson et al., 1997; Moore et al., 2004; Parekh et al., 2005; Weber et al., 2007). They are used to test the sensitivity of the iron cycle to processes like scavenging, dissolution, complexation with organic ligands, and allow drawing some conclusions on the factors that control the iron distribution in seawater and the subsequent effect on biological processes (i.e. primary production, nitrogen fixation). The validation of these models is largely dependent on the spatial and temporal coverage of DFe distributions in the global ocean. The most recent compilation of iron data in the world ocean (Parekh et al., 2005) shows that although the number of data available is rapidly growing, some large regions are still poorly or not at all sampled. This is the case for the south eastern subtropical Pacific which is also largely under-sampled for most of the other biogeochemical and biological parameters. The BIOSOPE cruise has filled this gap with a long transect extending from the Marquesas archipelago to the Chilean coast. We report here the DFe concentrations in the upper 400m of the water column. The vertical and horizontal distributions are discussed in relation with the possible sources and sinks of iron.

2 Material and methods

2.1 Fe determination

The BIOSOPE cruise took place in October–November 2004. The upper water column (0–400 m) was sampled at 19 stations (Table 1) along the 8000 km transect (Fig. 1a). From the surface to 50 m, seawater was collected using a clean Teflon pump connected to a PVC tube attached to a Kevlar cable. In-line filtration was performed through a $0.2\ \mu\text{m}$ cartridge (Sartorius Sartobran-P-capsule $0.45\ \mu\text{m}$ prefilter and $0.2\ \mu\text{m}$ final filter) in a clean laboratory container.

Below 50 m, samples were collected with acid-cleaned 121 Teflon-coated GO-Flo bottles mounted on a Kevlar cable (length 450 m) and tripped by Teflon messengers. The bottles were then brought to a clean van for sub sampling. The GO-Flo bottles were gently pressurised with high purity nitrogen allowing on-line filtration through Sartobran cartridges ($0.2\ \mu\text{m}$ with a $0.4\ \mu\text{m}$ prefilter, Sartorius). All the filtered samples for DFe analysis were collected in duplicate, in acid-cleaned 60 ml low density polyethylene bottles and immediately acidified with ultrapure HCl ($60\ \mu\text{l}$, $9.5\ \text{mM}$ final concentration, Merck, ultrapur[®]) under a class 100 laminar flow hood. The samples were left for at least 24 h before analysis.

The concentrations of DFe were measured on board by Flow Injection Analysis with chemiluminescence detection (adapted from Obata et al., 1993). The pH of the acidified samples was adjusted to 5 using Ultrapur ammonia and a 3-times purified ammonium acetate buffer before loading for 120 s on the 8 hydroxyquinoline (8 HQ) preconcentration column (1 cm long). The mean blank, calculated from daily determinations, equalled $69 \pm 18\ \text{pM}$ ($n=19$) and the detection limit was $54\ \text{pM}$. The accuracy was assessed by re-analysing one vertical profile (6 samples) of the BIOSOPE cruise during the KEOPS cruise (Blain et al., 2008) in parallel with the new reference material from the SAFE cruise (North Pacific gyre, same period as BIOSOPE). Both profiles analyzed during BIOSOPE and KEOPS were not statistically different (t -test, $p < 0.01$), indicating a good accuracy of the method.

2.2 Ancillary measurements

Temperature, salinity, and dioxygen (O_2) were determined from CTD casts performed at each station. Samples for nutrient analyses were collected both from GO-Flo and Niskin casts. The comparison between both data sets was used to detect possible malfunctioning of the GO-Flo bottles (e.g. leaks). Dioxygen was measured by the Winkler method with potentiometric endpoint detection. Nitrate and phosphate concentrations were measured using a Technicon Autoanalyser II (Tréguer and Le Corre, 1975). For low nitrate concentrations, the method described in (Raimbault et al., 2007) was used. All the nutrient data presented in this paper are from GO-Flo bottles allowing the direct comparison with DFe.

Table 1. Data.

Station	mon/day/yr	Lon (° E)	Lat (° S)	Depth (m)	DFe (nM)	NO _x (μM)	PO ₄ (μM)				
MAR3	10/29/2004	-141.2777	-8.3213	10	0.19						
				30	0.17						
				50	0.18	2.26	0.36				
				80	0.14	3.03	0.41				
				110	0.19	3.81	0.46				
				140	0.15	7.14	0.61				
				190	0.12	9.51	0.86				
				240	0.20	13.1	1.45				
NUK1	10/30/2004	-140.1076	-8.9768	350	0.42	18.4	2.38				
				30	0.16	0.04	0.24				
				50	0.16	0.01	0.24				
				80	0.19	0.82	0.29				
				110	0.13	5.34	0.57				
				130	0.17	5.57	0.6				
				HNL2	11/02/2004	-136.9761	-9.046	10	0.15		
								30	0.14		
50	0.15	2.26	0.35								
80	0.19	2.26	0.36								
110	0.17	0.92	0.43								
140	0.18	4.1	0.5								
190	0.14	5.77	0.64								
240	0.23	13.5	1.5								
STA2	11/04/2004	-132.3949	-13.3054	290	0.18	16.7	2.43				
				350	0.33	17.8	2.63				
				50	0.13	0.02	0.19				
				80	0.16	0.02	0.19				
				110	0.17	0.03	0.16				
				140	0.19	0.29	0.21				
				190	0.13	1.41	0.43				
				240	0.16	5.04	0.59				
STA4	11/06/2004	-128.3849	-16.871	290	0.11	8.38	0.9				
				350	0.17	26.7	2.38				
				40	0.20	0	0.17				
				80	0.24	0	0.17				
				120	0.17	0	0.17				
				150	0.15	0.89	0.29				
				200	0.12	1.55	0.32				
				250	0.11	2.75	0.4				
STA6	11/08/2004	-123.4107	-20.1288	300	0.09	6.93	0.84				
				350	0.13	9.99	1.56				
				50	0.11	0.01	0.15				
				110	0.18	0.02	0.13				
				150	0.13	0	0.13				
				225	0.13	1.45	0.28				
				300	0.10	5.03	0.52				
				350	0.16	9.65	1.08				
STA8	11/10/2004	-118.3248	-23.2879	400	0.12	12.2	1.66				
				50	0.15	0	0.13				
				100	0.12	0	0.15				
				200	0.12	0.01	0.15				
				300	0.11	4.38	0.48				
				325	0.12	6.6	0.64				
				350	0.12	8.87	0.88				
				400	0.14	12.3	1.44				
GYR2	11/13/2004	-114.0241	-26.0195	30	0.12	0					
				50	0.11	0	0.11				
				80	0.13	0	0.11				
				100	0.12	0	0.12				
				150	0.10	0.95	0.19				
				200	0.11	3.4	0.41				
				300	0.10	6.92	0.71				
				325	0.11	8.46	0.85				
350	0.10	9.92	1.11								
400	0.15	12.0	1.67								

Table 1. Continued

Station	mon/day/yr	Lon (° E)	Lat (° S)	Depth (m)	DFe (nM)	NO _x (μM)	PO ₄ (μM)
GYR3	11/14/2004	-114.0159	-26.0444	50	0.11	0	0.09
				100	0.11	0	0.1
				150	0.10	0.01	0.12
				200	0.09	1.5	0.24
				250	0.09	4.98	0.43
				300	0.10	8.46	0.66
				350	0.09	15.2	0.99
				400	0.24	19.5	1.26
STA12	11/21/2004	-104.7419	-28.4308	50	0.15	0	0.11
				100	0.13	0	0.11
				150	0.12	0	0.11
				200	0.13	0.48	0.18
				250	0.11	5.47	0.46
				300	0.10	9.6	0.77
				350	0.29	16.9	1.24
				400	0.5	22.9	1.5
STA14	11/23/2004	-98.8609	-29.9175	50	0.09	0	0.09
				100	0.08	0	0.09
				150	0.09	0.19	0.1
				200	0.09	1.03	0.15
				250	0.06	6.11	0.46
				300	0.07	9.86	0.81
				350	0.09	15.8	1.13
				400	0.22	19.7	1.38
EGY4	11/29/2004	-91.3954	-31.8962	30	0.10	0.04	0.17
				70	0.09	1.02	0.26
				100	0.08	1.26	0.24
				150	0.10	1.98	0.3
				200	0.10	5.68	0.5
				250	0.11	11.1	1.02
				300	0.17	18.1	1.42
				400	0.21	28.4	1.88
STA18	12/02/2004	-84.2061	-32.6689	250	0.29	30.9	2.05
				300	0.31	33	2.15
				100	0.13	6.46	0.48
				150	0.13	9.92	0.72
				200	0.14	12.7	1.06
				250	0.23	22.7	1.54
				300	0.33	27.0	1.77
STA20	12/04/2004	-78.0989	-33.3694	350	0.89	34.4	2.28
				375	0.92	34.1	2.25
				400	0.93		
				50	0.08	3.08	0.32
				130	0.10	14.0	0.93
				200	0.53	24.8	2.03
				250	1.16	32.3	2.53
				300	1.14	35.4	2.57
STA22	12/06/2004	-73.4962	-33.8009	325	1.11	36.7	2.53
				350	1.30	37.2	2.52
				375	1.33	37.0	2.4
				400	1.34	36.3	2.31
				10	0.32		
				30	0.45		
				50	0.26		
				70	0.48		
				100	0.67	27.7	2.03
				135	0.68	29.6	2.08
				170	0.99	32.3	2.43
205	1.23	35	2.53				
240	1.36	36.8	2.51				
275	1.44	39.6	2.63				
310	1.61	40	2.68				
345	1.7	40	2.56				
400	1.34	39.6	2.43				

Table 1. Continued

Station	mon/day/yr	Lon (° E)	Lat (° S)	Depth (m)	DFe (nM)	NO _x (μM)	PO ₄ (μM)
				30	1.20	19.1	1.62
				75	1.35	26.9	2.43
				100	1.98	27.3	2.61
				150		27.9	2.65
UPX	12/09/2004	-72.4047	-34.5471	200	3.39	28.8	2.61
				250	3.25	30	2.63
				300	3.18	31.2	2.61
				350	2.66	32.3	2.63
				400	2.78	34.9	2.63

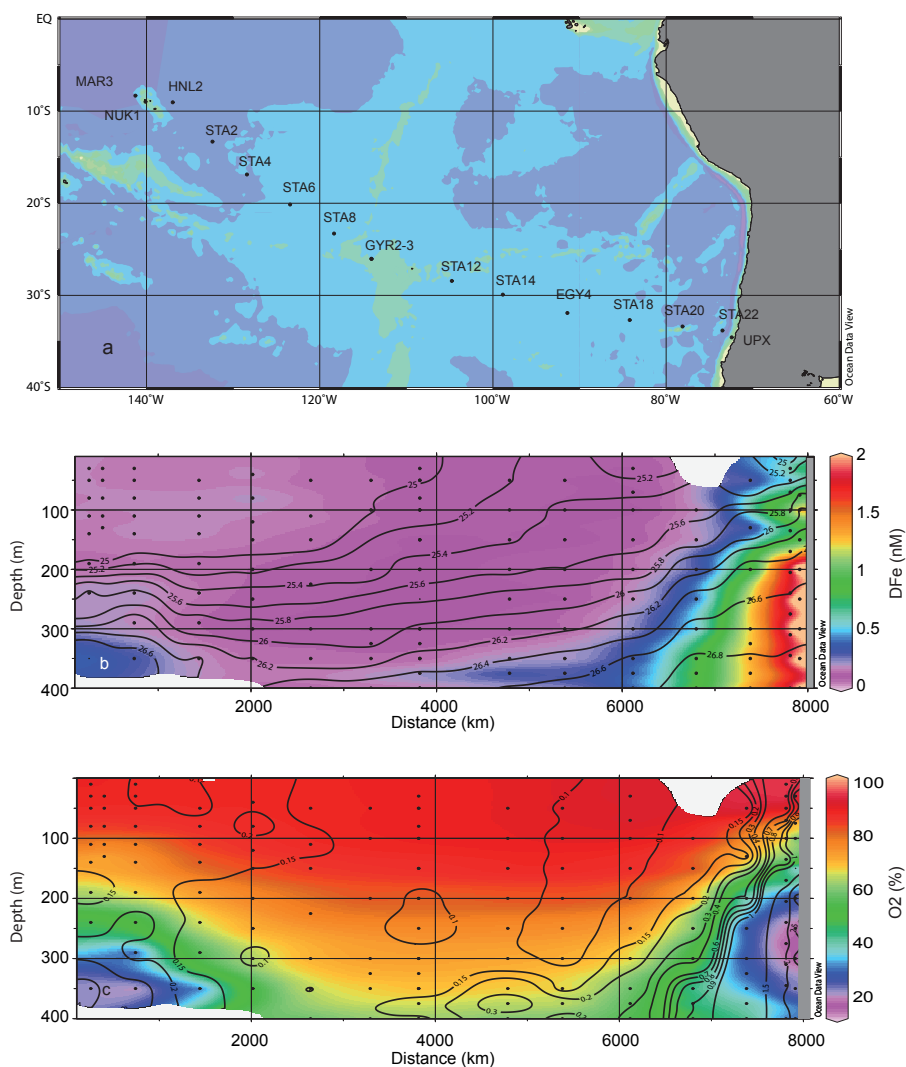


Fig. 1. Position of sampled stations during the BIOSOPE cruise (a), two dimensional distribution of DFe (b) and two dimensional distribution of the percentage of O₂ saturation (c). The black lines denote the depths of the iso-density (γ) (b) and the DFe concentrations (c).

3 Results and discussion

The two-dimensional distribution of DFe along the BIOSOPE transect is presented in conjunction with the iso-

density lines (Fig. 1b) and overlaid on the percentage of O₂ saturation (Fig. 1c). The concentrations of DFe ranged over almost two orders of magnitude from 0.061 nM to 3.39 nM (Table 1). In the following section we first present and

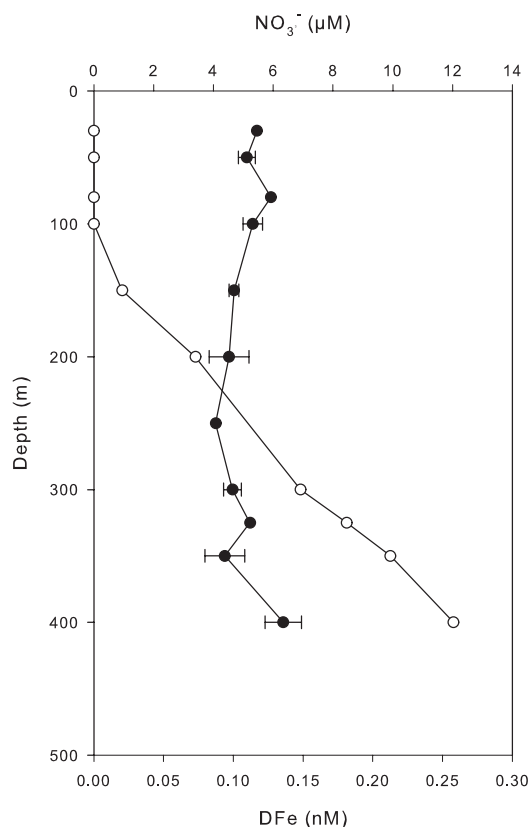


Fig. 2. Vertical distribution of DFe (black dots) and nitrate (white dots) at the station GYR. For DFe, mean values ($n=2$) \pm one standard deviation are given.

discuss the vertical distribution of DFe in three different environments: the upwelling zone including the stations where the Oxygen Minimum Zone (OMZ) was present (stations UPX, STA18, STA20 and STA22), the HNLC region close to the Marquesas islands (stations MAR3, NUK and HNL2), and the gyre (stations STA2-14 and GYR1-2 and EGY4). When possible, the DFe distributions were compared with other sites with similar oceanographic regimes. In the second part of the paper, we consider the relationship between DFe and the major nutrients to discuss the status of iron as limiting factor in the different regions and the possible role of the OMZ in maintaining high DFe concentrations in the sub surface water of the low latitudes of the South Pacific.

3.1 The vertical distribution of DFe in typical oceanographic environments

3.1.1 The coastal upwelling region

The Chilean coastal upwelling region had the highest DFe concentrations measured during the cruise (Fig. 1, Table 1). The station UPX, located in the core of the upwelling, was characterised by high values of nitrate ($19.1 \mu\text{M}$) and phos-

phate ($1.2 \mu\text{M}$) at 30 m. The concentration of DFe at this depth was also high (1.2 nM) and increased up to 3.39 nM at 200 m. In surface waters, DFe decreased rapidly with distance from shore and DFe concentrations at STA20 were $<0.1 \text{ nM}$, typical for oceanic surface waters with low iron supply. Below the mixed layer, the decrease in DFe from in-shore to offshore stations was also marked. At 250 m, DFe at STA18 was 10 fold lower than at station UPX. However, if compared to surface water, the decrease was not as abrupt and, below 200 m, concentrations $>1 \text{ nM}$ were still measured at STA20 and STA22. High DFe concentrations are also reported for the Peru upwelling (from 2° S to 18° S), (Bruland et al., 2005), but large variability was observed near the bottom depending on the size of the shelf. Concentrations of DFe as high as 50 nM were associated with the widest shelf in the north, but in the southern part, where the shelf was narrow, the concentrations in near bottom suboxic waters were an order of magnitude lower ($1.4\text{--}4.3 \text{ nM}$). We did not measure the concentrations of DFe above the Chilean shelf, but at station UPX at 100 m, which is roughly the depth of the continental shelf in this region, DFe was 2 nM . This is in the same range as in the southern part of the Peru upwelling and could also be explained by the quite narrow shelf off Chile.

In the upwelling zone, the highest concentrations of DFe were measured between 200 and 400 m, close to the shelf break. This part of the water column is suboxic (Fig. 1c) and associated with the relatively salty water mass of the Equatorial Sub-Surface Water (ESSW) (Blanco et al., 2001). In fact, this under-counter current is flowing poleward along the entire South American continent starting at around 5° S (Brink et al., 1983). When the current flows over a wide shelf it is in contact with the organic-rich shelf sediments and DFe concentrations are high. By contrast, when the current flows over a narrow shelf or along the steep continental slope, the concentrations are an order of magnitude lower but still high compared to open ocean concentrations. The suboxic conditions that prevailed are favourable conditions to maintain iron in solution in the reduced form Fe(II) which is more soluble than Fe(III). High concentration of Fe(II) have been reported (Hong and Kester 1986) off the Peru coast in samples close to the bottom, but also at stations located offshore at depth coinciding with the upper portion of the oxygen minimum.

3.1.2 The oligotrophic gyre

The DFe concentrations at the station GYR (26° S , 114° W) are low and homogenous ($0.104 \pm 0.012 \text{ nM}$, $n=15$, 2 profiles) between the surface and 350 m (Fig. 2). DFe vertical profiles are reported at stations located in the other subtropical gyres in the Atlantic and the Pacific (Fig. 3). In the North Pacific gyre, at station ALOHA ($22^\circ 45' \text{ N}$, $158^\circ 00' \text{ W}$), the near surface DFe concentrations are in the range $0.2\text{--}0.7 \text{ nM}$ (Boyle et al., 2005). In the western part of the subtropical North Atlantic gyre, at a station ($31^\circ 25' \text{ N}$, $63^\circ 25' \text{ W}$) near BATS (Bermuda Atlantic Time-Series Station), large

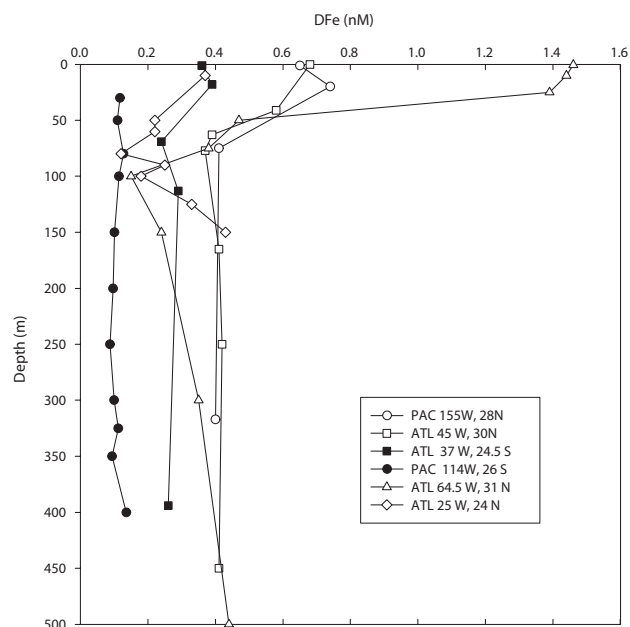


Fig. 3. Vertical profiles of DFe at different tropical and subtropical stations. Black symbols are for stations located in the Southern Hemisphere and open symbols for stations located in the Northern Hemisphere.

seasonal variations were observed ranging from 1–2 nM to 0.1–0.2 nM (Sedwick et al., 2005). In the centre of this gyre (30°00' N, 45°00' W), DFe varied between 0.37–0.68 nM (Bergquist and Boyle, 2006), and in eastern part of the gyre, in an area extending from the Canary Islands to the Cap Verde Islands, DFe surface concentrations were in the range 0.2–1.2 nM (Sarhou et al., 2003). In all these studies, the DFe variations in surface waters were attributed to the variability in dust deposition. Only few data are available for the South Atlantic gyre. At 25° S, 37° W, a mean DFe concentration of 0.37 ± 0.03 nM was reported in the depth stratum 0–52 m (Bergquist and Boyle, 2006). In the Guinea gyre, DFe in surface water was significantly lower (0.12 ± 0.08 nM) (Sarhou et al., 2003).

The current study reveals that the concentrations in the south east Pacific subtropical gyre are among the lowest reported so far. This is consistent with the very low atmospheric iron deposition of 0.11 ± 0.05 nmol m⁻² d⁻¹ measured during the cruise (Wagener et al., 2008). The atmospheric data revealed a very low seasonality over the BIOSOPE area, with a small maximum during spring (Wagener et al., 2008). The values of dust deposition were 12- to 3000-times lower than the dust deposition reported at BATS and ALOHA (Measures et al., 2005; Sedwick et al., 2005) and 7- to 7000-times lower than the estimates in the subtropical north east Atlantic (Sarhou et al., 2003).

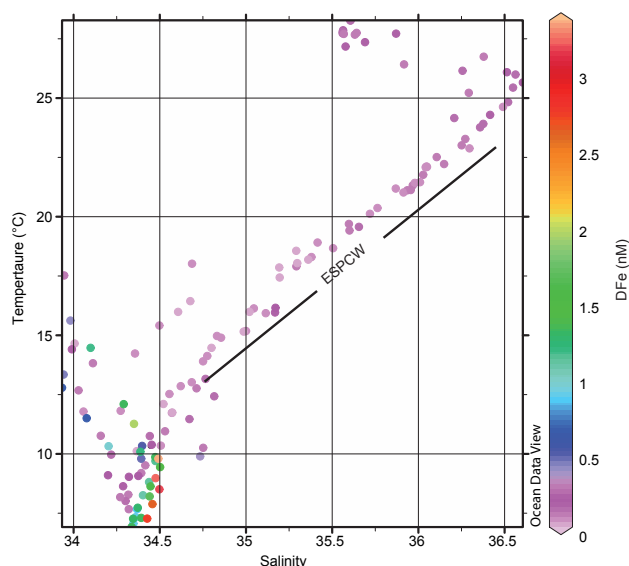


Fig. 4. Temperature versus salinity diagram with the colour of the dots scaled to DFe concentrations (see color bar). The black line denotes the occurrence of the Eastern South Pacific Central Water (ESPCW).

At the station GYR, a small increase of DFe was observed between 350 and 400 m (Fig. 2). This might denote the beginning of the ferricline but this cannot be confirmed due to the lack of DFe measurements at deeper depths. Even though uncertainties exist concerning the exact position of the ferricline, it is clear that it was located well below the nitracline (Fig. 2). The nutricline results from the mixing between the surface water, that is nutrient-depleted due to biological activity, and the subsurface water, that is refuelled by mineralization of sinking organic material. Lateral transport of nutrients (spreading along isopycnal surface or lateral advection) can alter the one-dimensional model. The lack of DFe vertical gradients between 0 and 350 m suggests that both the consumption of DFe in surface waters and the remineralisation in subsurface waters were low. This is consistent with the extremely low biomass and productivity in the hyper-oligotrophic surface waters of the gyre (Raimbault et al., 2007). The thermocline of the south east Pacific gyre is mainly ventilated by the Eastern South Pacific Central Water ESPCW characterised by a temperature-salinity relationship that spans over a large range (Fig. 4). This water mass contains low DFe concentrations (<0.2 nM). The water mass was formed in the region between 180–150° W (Sprintall and Tomczak, 1992) where no measurements of DFe are available. However, low DFe concentrations are expected in this area due to the low dust deposition. The surface waters located above the ESPCW have a low productivity resulting in low particle export below the mixed layer. DFe produced by mineralization of sinking particles is therefore modest in the ESPCW. Consequently, the ventilation of the

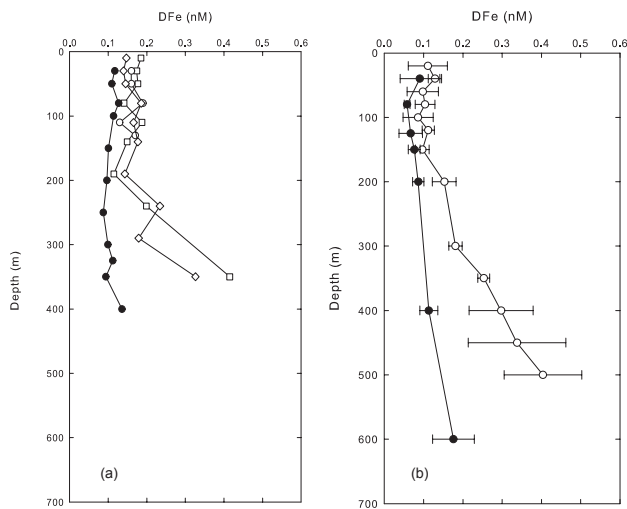


Fig. 5. Comparison of the vertical DFe distribution at stations in the vicinity of archipelagi and typical oceanic stations. **(a)** Vertical profiles of DFe near the Marquesas islands (open symbols) and in the centre of the South East Pacific gyre (station GYR, black symbols). **(b)** Vertical profiles of DFe at a station above the Kerguelen plateau (white dots) ($58^{\circ}38' \text{ S}$, $72^{\circ}05' \text{ E}$), and at an HNLC station ($51^{\circ}39' \text{ S}$, $78^{\circ}00' \text{ E}$) south east of the plateau (black dots) (Blain et al., 2007).

upper thermocline cannot be a large source of DFe for subsurface water in the gyre. The same conclusion was drawn by Bergquist and Boyle (2006) to explain the relatively low DFe concentrations measured in the pycnocline in the southern subtropical Atlantic gyre that is ventilated by water formed at higher latitudes where dust deposition is expected to be low.

3.1.3 The Marquesas islands

Vertical profiles of DFe were collected west, within and east of the Marquesas archipelago (Fig. 5a). The vertical distributions of DFe were very similar at the three stations studied. The mean concentration in the upper 80 m was $0.16 \text{ nM} \pm 0.02 \text{ nM}$ ($n=11$). This was not significantly different ($p=0.01$) of the mean DFe ($0.13 \pm 0.03 \text{ nM}$ ($n=9$)) in the upper 80 m of the gyre (STA4-14 and GYR1-2). Chlorophyll-*a* concentrations inferred from satellite images, (http://www.obs-vlfr.fr/proof/php/bio_satellite_imagery.php), clearly show a strong contrast between surface waters east and west of the island. This was also confirmed by in situ measurements (Raimbault et al., 2007). It was suggested that this dissymmetry might be caused by natural iron enrichment of the HNLC water down stream the islands, similarly to the blooms in the vicinity of other islands in HNLC systems, like Galapagos (Gordon et al., 1998) or Kerguelen (Blain et al., 2007).

At a first glance it is tempting to attribute the iron source to the vicinity of the island (Signorini et al., 1999). However, the vertical profile at the shallow station (NUK) located be-

tween two islands did not significantly differ from the DFe profiles at deep ocean stations located east or west of the island (Fig. 5a). There is no significant increase of DFe in surface water and this rules out the land drainage as an important source of DFe, at least at the time of the cruise. On an interannual time scale, the detailed analysis of the variation of the rainfall at the Marquesas islands do not indicate a high correlation with the Chl-*a* inferred from satellite (Martinez and Maamaatuaiahutapu 2004). In addition to the possible input of DFe originating from the island, Signorini et al. (1999) suggested that the hydrothermal flux through old volcanic formations might also be a source of DFe. The fingerprint of hydrothermal activity in DFe vertical profiles was detectable off Hawaii (Boyle et al., 2005) at station ALOHA. At this site, the increase in dissolved and particulate Fe at around 1000 m correlated well with the highest concentration of $\delta^3\text{He}$ (Boyle et al., 2005). Such data do not exist for the Marquesas island, but the absence of high DFe concentrations close to the island do not support the hypothesis of hydrothermal fluid injection into the water column.

A clear increase in DFe below 200 m was detectable at the western and eastern stations (Fig. 5a). This vertical DFe gradient was considerably steeper than at the station GYR. The origin of the enrichment in DFe near the Marquesas will be discussed in the next section, but it is interesting to compare the data in Fig. 5a with data collected in the Southern Ocean (Fig. 5b) near the Kerguelen plateau, where natural iron fertilisation of surface waters has clearly been demonstrated (Blain et al., 2007). The surface waters above and outside the plateau had similar concentrations but the gradient of DFe below 150 m was steeper above the Kerguelen plateau where the bloom occurred compared to outside the plateau where concentrations of Chl-*a* were low. The deep reservoir of DFe was made available for phytoplankton by different mechanisms including diapycnal vertical mixing and deep winter mixing.

If DFe was responsible for the east-west difference in biomass near the Marquesas islands, mechanisms for upward transport of DFe should only exist eastward of the island. An analysis for the period 1997–2002 of sea surface height anomaly (Martinez and Maamaatuaiahutapu, 2004), Chl-*a*, wind speed and SST indicates that the bloom was strongly correlated with the total surface current (Eckman plus geostrophic), the high values of the current being associated with high values of Chl-*a*. These authors concluded that the origin of the bloom was the result of the interaction between the chain of islands and the mean flow of water masses, but the underlying mechanisms such as wind driven upwelling or mixing due to friction could not be established. Recent investigations in the vicinity of Hawaii (Benitez-Nelson et al., 2007) demonstrated that wind driven mesoscale cyclonic eddies that form in the lee of islands increased nutrient supply and primary production following the doming of isopycnal surfaces. Within oceanic eddies interaction of the wind with the underlying eddy-driven flow can

also create episodic eddy driven upwelling supplying nutrients for surface water (Mcgillicuddy et al., 2007). All these processes have the potential to generate the complex dissymmetric and mesoscale patterns of Chl-*a* observed around the Marquesas islands but more detailed field studies are required to elucidate the correct mechanisms.

3.2 Application of the tracer Fe*

The remineralisation of organic matter (OM) is a major source of macro or micro-nutrients in subsurface waters. This process is associated with the consumption of oxygen and the apparent oxygen utilisation (AOU) can provide a quantitative estimate of the amount of material that has been remineralised. We have used our data with $z > 80$ m to construct the plots of PO_4^{3-} , NO_3^- and DFe versus AOU that are shown in Fig. 6a, b and c, respectively. The concentrations of PO_4^{3-} are well correlated with AOU ($r^2=0.9317$) showing that the remineralisation of POP directly translates into DIP and that PO_4^{3-} can be used as a good tracer for the remineralisation in the studied areas. The correlation is so not obvious for NO_3^- when the entire data set is considered. This is mainly due to loss of nitrate by denitrification or anammox in the zone where the O_2 concentrations are low. No clear relation can be established between DFe and AOU (Fig. 6c). This is not surprising because the whole data set included regions where the DFe distribution was obviously impacted by processes other than remineralisation (e.g. iron input from the shelf in the upwelling region). However, a more detailed examination has revealed that there was a good linear correlation between DFe and AOU, or PO_4^{3-} , for the stations 18 to 22 that were typical of the OMZ. The slope of the curve, representing the typical remineralisation ratio, was $r_{(\text{Fe}/\text{P})\text{OMZ}}=0.99\pm 0.11 \text{ mmol mol}^{-1}$. The intercept of the regression line was $-1.23\pm 0.11 \text{ nmol l}^{-1}$, reflecting possible excess of preformed PO_4^{3-} compared to DFe in this water mass. To reveal the balance between physical transport and scavenging, Parekh et al. (2005) defined $\text{Fe}^*=(\text{DFe})-r_{\text{Fe}/\text{P}}(\text{PO}_4^{3-})$ which subtracts the contribution of remineralisation of OM to DFe. A positive Fe^* implies that there is enough iron to support the complete consumption of PO_4^{3-} when this water is brought to the surface, and a negative Fe^* implies a deficit. We have applied this definition (using the same value of $r_{\text{Fe}/\text{P}}=0.47 \text{ mol mol}^{-1}$ used in their work) to calculate Fe^* along the transect (Fig. 7). Positive values were observed in the upwelling region. Most other stations of the transect presented Fe^* lightly negative, except in the subsurface water near the Marquesas and near 400 m in the gyre where Fe^* was clearly negative. Fe^* relies on the choice of $r_{\text{Fe}/\text{P}}$ which is not well constrained. The ratio $r_{\text{Fe}/\text{P}}$ very likely depends on the degree of iron limitation of phytoplankton that has synthesized the OM (Sunda 1997). In iron-limited regimes the ratio ($0.2\text{--}0.5 \text{ mmol mol}^{-1}$) could be lower than in non iron-limited regions ($0.7\text{--}1.4 \text{ mmol mol}^{-1}$). The direct measurement of the elemental composition of diatoms collected

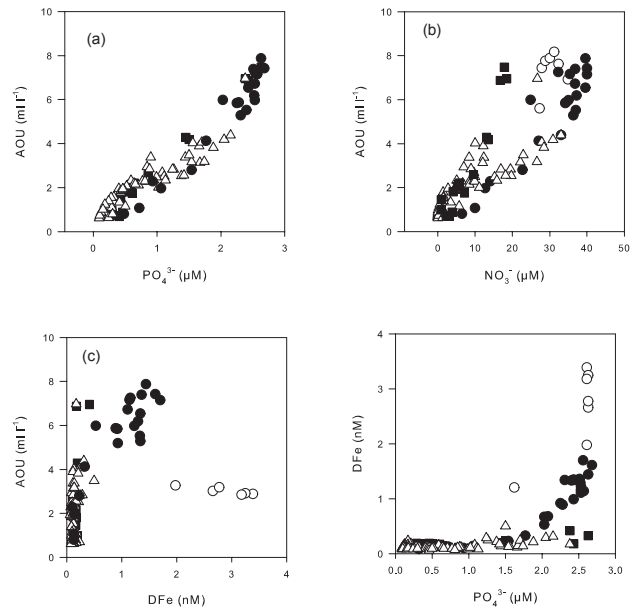


Fig. 6. Property-property diagrams for stations STA18-22 (black circles), stations UPX (white circles), stations MAR3, NUK and HNL2 (black squares), station STA2-14, GYR 2-3 and EGY (white triangles).

inside and outside the fertilised patch of SOFEX (Twining et al., 2004) confirmed this trend. For diatoms the mean Fe/P ratios were $0.71 \text{ mmol mol}^{-1}$ and $1.9 \text{ mmol mol}^{-1}$ in low and high Fe environments, respectively. In our study, $r_{\text{Fe}/\text{P}}$ was certainly not constant along the transect as shown by the large scatter in the data (Fig. 6d). However, the variability in the $r_{\text{Fe}/\text{P}}$ between 1 to 0.2 mol mol^{-1} does not change our conclusion that $\text{Fe}^* < 0$ and $\text{Fe}^* > 0$ occurred in subsurface waters near Marquesas and close to the Chilean coast, respectively. The qualitative examination of the distribution of DFe (Fig. 1b, c), of the vertical profiles at stations MAR3 and HNL2 (Fig. 5a), and the comparison with the distribution of DFe near Kerguelen island (Fig. 5b) suggest that there may be a source of DFe near the islands. The negative Fe^* does not confirm this idea because there was less DFe than predicted from the remineralisation of the organic matter independent of the $r_{\text{Fe}/\text{P}}$ values applied. The samples with negative Fe^* are located in waters with low O_2 (Fig. 1c). The occurrence of the OMZ is a major feature of the water column in the South East Pacific. The biological or physical origin of the OMZ has been debated in the past (Wirtki 1962), but there is now a consensus that three major processes contribute to its formation. 1) high phytoplankton production at the surface, 2) a sharp permanent pycnocline and 3) a sluggish circulation leading to old age for subpycnocline waters. During our cruise, the OMZ was clearly identified along the Chilean coast but a global distribution of O_2 in the eastern Pacific (Fig. 20 in Fiedler and Talley, 2006) shows that the subsurface waters of the stations near Marquesas are part of the

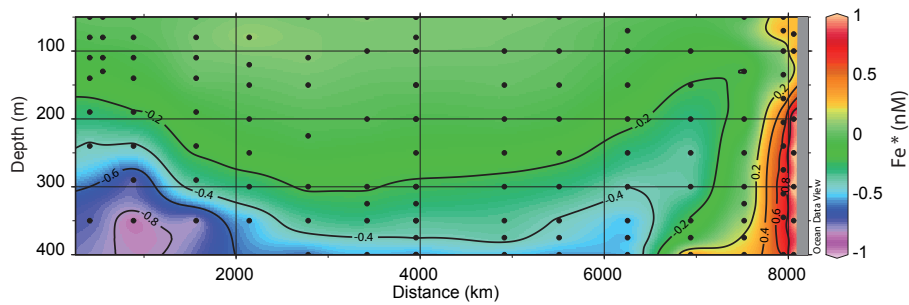


Fig. 7. Two dimensional distribution of Fe^* calculated as $\text{DFe} - r_{\text{Fe}/\text{P}} (\text{PO}_4^{3-})$ with $r_{\text{Fe}/\text{P}} = 0.47 \text{ mmol mol}^{-1}$.

wide OMZ extending westward from the continent. Therefore, in this region, the most appropriate ratio to be used in the calculation of Fe^* would be 1, as determined above for the remineralisation of OM in the OMZ. This leads to largely negative values of $\text{Fe}^* < -1 \text{ nM}$ in the OMZ near Marquesas, showing that the scavenging and slow circulation in sub pycnocline waters had dramatically reduced the concentration of DFe compared to PO_4^{3-} . Johnson et al. (1997) have shown that the length scale for the reduction of DFe versus the distance of the source can be estimated from $1/\text{slope}$ of the linear plot of $\text{Ln}(\text{DFe}) = f(\text{distance from the source})$. This corresponds to the distance at which DFe was reduced by 37% compared to the source. At 1000 m, offshore the Californian coast, the length scale was 5000 km. If we apply the same approach at 350 m using the value at stations STA20 (1.3 nM) and MAR3 (0.4 nM) we obtain a similar distance (4400 km). In both cases, the length scales were estimated at depth where the O_2 concentrations were low. The reducing conditions probably contributed to maintain iron in solution.

3.3 Potential impact of DFe distribution on biology

The objective of the present paper was to describe and discuss the DFe distributions, but we briefly mention two potentially important implications in terms of biological activity.

- i) If we assume that the relatively high biomass observed downstream the Marquesas island is due to vertical inputs of DFe from subsurface waters (see Sect. 3.1.3), the negative Fe^* values in these waters imply that the amount of DFe supplied was still in deficit compared to phosphate leading to the significant amount of unused nutrient ($0.3 \mu\text{M}$ of PO_4^{3-} and $2.2 \mu\text{M}$ of NO_3^-) in surface waters.
- ii) Our data show that DFe was low in the entire South Pacific gyre, but NO_3^- was also extremely low (Raimbault et al., 2007). The limitation of primary production by Fe on the edges of the gyre was demonstrated by deck incubation experiments (Bonnet et al., 2007). By contrast, evidence for severe nitrogen limitation of primary production was observed in the centre of the gyre (Bon-

net et al., 2007). It has been hypothesised that DFe may also regulate the rate of nitrogen fixation in such low nitrate environments. During incubation experiments carried out in the centre of the South Pacific gyre, iron addition did not stimulate nitrogen fixation (Bonnet et al., 2007; Raimbault et al., 2007). This result seems to be at odds with the possible limitation of the nitrogen fixation by iron availability. However the lack of response in this short term experiment could also be due to the quasi absence of N-fixing populations. Temporally more detailed information is required to fully understand the role of Fe on primary producers in these oligotrophic waters.

Acknowledgements. We thank the captain, the officers and the crew of the R/V Atalante. We also thank P. Raimbault who performed the nutrient analysis of the Go-Flo samples, H. Claustre, leader of BIOSOPE and chief scientist of the leg1, and chief scientist A. Sciandra of the leg2. The manuscript profited from the comments of two anonymous reviewers. This is a contribution of the BIOSOPE project, funded by CNRS-INSU (LEFE CYBER-program), CNES, ESA and NASA.

Edited by: J. Middelburg

References

- Aumont, O., Maier-Reimer, E., Blain, S., and Monfray, P.: An ecosystem model of the global ocean including Fe, Si, P co limitations, *Global Biogeochem. Cy.*, 17, 1060, doi:10.1029/2001GB001745, 2003.
- Benitez-Nelson, C., Bidigare, R. C., Dickey, T. D., Landry, M. R., Leonard, C. L., Brown, S. L., Nencioli, F., Rii, Y. M., Maiti, K., Becker, J. W., Biddy, T. S., Black, W., Cai, W.-J., Carlson, C. A., Chen, F., Kuwahara, V. S., Lmahaffey, C., McAndrew, P. M., Quay, P. D., Rappé, M. S., Selph, K. E., Simmonds, M. P., and Yang, E. J.: Mesoscale eddies drive increased silica export in the subtropical Pacific ocean, *Science*, 316, 1017–1021, 2007.
- Bergquist, B. A. and Boyle, E. A.: Dissolved iron in the tropical and subtropical atlantic ocean, *Global Biogeochem. Cy.*, 20, GB1015, doi:10.1029/2005GB002505, 2006.
- Blain, S., Guieu, C., Claustre, H., Leblanc, K., Moutin, T., Quéguiner, B., and Sarthou, G.: Availability of iron and ma-

- for nutrients for phytoplankton in the north-east Atlantic ocean, *Limnol. Oceanogr.*, 49, 2095–2104, 2004.
- Blain, S., Quéguiner, B., Armand, L., Belviso, S., Bombled, B., Bopp, L., Bowie, A., Brunet, C., Brussaard, K., Carlotti, F., Christaki, U., Corbière, A., Durand, I., Ebersbach, F., Fuda, J. L., Garcia, N., Gerringa, L. J. A., Griffiths, F. B., Guigue, C., Guillerm, C., Jacquet, S., Jeandel, C., Laan, P., Lefèvre, D., Lomonaco, C., Malits, A., Mosseri, J., Obernosterer, I., Park, Y. H., Picheral, M., Pondaven, P., Remenyi, T., Sandroni, V., Sarthou, G., Savoye, N., Scouarnec, L., Souhault, M., Thuillers, D., Timmermans, K. R., Trull, T., Uitz, J., Van-Beek, P., Veldhuis, M. J. W., Vincent, D., Viollier, E., Vong, L., and Wagener, T.: Effect of natural iron fertilisation on carbon sequestration in the Southern Ocean, *Nature*, 446, 1070–1075, 2007.
- Blain, S., Sarthou, G., and Laan, P.: Distributions of dissolved iron during the natural iron fertilisation experiment KEOPS (Kerguelen Island, Southern Ocean), *Deep Sea Res. II*, doi:10.1016/j.dsr2.2007.12.008, in press, 2008.
- Blanco, J. L., Thomas, A. C., Carr, M. E., and Strub, P. T.: Seasonal climatology of hydrographic conditions in the upwelling region off northern Chile, *J. Geophys. Res.*, 106, 11 456–11 467, 2001.
- Bonnet, S. and Guieu, C.: Atmospheric forcing on the annual iron cycle in the western Mediterranean sea, *J. Geophys. Res.*, 111, C09010, doi:10.1029/2005JC003213, 2006.
- Bonnet, S., Guieu, C., Bruyant, F., Prášil, O., Van Wambeke, F., Raimbault, P., Grob, C., Moutin, T., Gorbunov, M. Y., Zehr, J. P., Masquelier, S. M., Garczarek, L., and Claustre, H.: Nutrients limitation of primary productivity in the Southeast Pacific (BIOCOPE cruise) *Biogeosciences Discuss.*, 4, 2733–2759, 2007, <http://www.biogeosciences-discuss.net/4/2733/2007/>.
- Boyd, P. W., Jickells, T., Law, C., Blain, S., Boyle, E. A., Buesseler, K. O., Coale, K. H., Cullen, J. J., De Baar, H. J. W., Follows, M., Harvey, M., Lancelot, C., Levasseur, M., Owens, N. J. P., Pollard, D. A., Rivkin, R. B., Sarmiento, J. L., Schoemann, V., Smetacek, V., Takeda, S., Tsuda, A., Turner, D. R., and Watson, A.: Mesoscale iron enrichment experiments 1993–2005: Synthesis and future directions, *Science*, 315, 612–617, 2007.
- Boyle, E. A., Bergquist, B. A., Kayser, R. A., and N., M.: Iron, manganese, and lead at Hawaii Ocean Time-series station ALOHA: Temporal variability and an intermediate water hydrothermal plume, *Geochimica et Cosmochimica Acta*, 69, 933–952, 2005.
- Brink, K. H., Halpern, D., Huyer, A., and Smith, R. L.: The physical environment of the Peruvian upwelling system, *Prog. Oceanogr.*, 12, 285–305, 1983.
- Bruland, K. W., Rue, E., Smith, G. J., and Di Tullio, G. R.: Iron, macronutrient and diatom blooms in the Peru upwelling regime: brown and blue waters off Peru, *Mar. Chem.*, 93, 81–103, 2005.
- Bucciarelli, E., Blain, S., and Tréguer, P.: Iron and manganese in the wake of the Kerguelen Islands (Southern Ocean), *Mar. Chem.*, 73, 21–36, 2001.
- Capone, D. G., Burns, J. A., Montoya, J. P., Michaels, A. F., Subramanian, A., and Carpenter, E. J.: New nitrogen input to the tropical North Atlantic Ocean by nitrogen fixation by the cyanobacterium, *trichodesmium* spp., *Global Biogeochem. Cy.*, 19, GB2024, doi:10.1029/2004GB002331, 2005.
- Elrod, V. A., Berelson, W. M., Coale, K. H., and Johnson, K.: The flux of iron from continental shelf sediments: a missing source for global budgets, *Geophys. Res. Lett.*, 31, L12307, doi:10.1029/2004GL020216, 2004.
- Fiedler, P. C., and Talley, L. D.: Hydrography of the eastern tropical Pacific: a review, *Prog. Oceanogr.*, 69, 143–180, 2006.
- Gordon, R. M., Johnson, K. S., and Coale, K. H.: The behaviour of iron and other trace elements during the ironEx-I and PlumEx experiments in the Equatorial Pacific, *Deep Sea Res. II*, 45, 995–1041, 1998.
- Guieu, C., Bozec, Y., Blain, S., Ridame, C., Sarthou, G., and Leblond, N.: Impact of high Saharan dust inputs on dissolved iron distributions in the Mediterranean sea, *Geophys. Res. Lett.*, 29, 1911, doi:10.1029/2001GL014454, 2002.
- Hong, H. and Kester, D. R.: Redox state of iron in the offshore waters of Peru, *Limnol. Oceanogr.*, 31, 512–534, 1986.
- Hutchins, D. A. and Bruland, K. W.: Iron-limited diatom growth and Si:N uptake ratios in a coastal upwelling regime, *Nature*, 393, 561–564, 1998.
- Jickells, T. D., An, Z. S., Andersen, K. K., Baker, A. R., Bergametti, G., Brooks, N., Cao, J. J., Boyd, P. W., Duce, R. A., Hunter, K. A., Kawahata, H., Kubilay, N., Laroche, J., Liss, P. S., Mahowald, N., Prospero, J. M., Ridgwell, A. J., Tegen, I., and Torres, R.: Global Iron Connections Between Desert Dust, Ocean Biogeochemistry, and Climate, *Science*, 308, 67–71, 2005.
- Johnson, K., Chavez, F. P., and Friederich, G. E.: Continental-shelf sediment as a primary source of iron for coastal phytoplankton, *Nature*, 398, 697–700, 1999.
- Johnson, K. S., Gordon, R. M., and Coale, K. H.: What controls dissolved iron concentrations in the world ocean? *Mar. Chem.*, 57, 137–161, 1997.
- Karl, D. M.: Nutrient dynamics in the deep blue sea, *Trends Microbiol.*, 10, 410–418, 2002.
- Laës, A., Blain, S., Laan, P., Achterberg, E. P., Sarthou, G., and De Baar, H. J. W.: Deep dissolved iron profiles in the eastern North Atlantic in relation to water masses, *Geophys. Res. Lett.*, 30, 1902, doi:10.1029/2003GL017902, 2003.
- Laës, A., Blain, S., Laan, P., Ussher, S., Achterberg, E. P., Tréguer, P., and De Baar, H. J. W.: Sources and transport of dissolved iron and manganese along the continental margin of the Bay of Biscay, *Biogeosciences*, 4, 181–194, 2007.
- Martin, J. H., Gordon, R. M., Fitzwater, S. E., and Broenkow, W. W.: VERTEX: phytoplankton/iron studies in the Gulf of Alaska, *Deep-Sea Res. I*, 36, 649–680, 1989.
- Martinez, E. and Maamaatuaiahutapu, K.: Island mass effect in the Marsueas islands: time variation, *Geophys. Res. Lett.*, 31, L18307, doi:10.1029/2004GL020682, 2004.
- McGillicuddy, D. J., Anderson, L. A., Bates, N. R., Bidy, T. S., Buesseler, K. O., Carlson, C. A., Davis, C. S., Ewart, C., Falkowski, P. G., Goldthwait, S. A., Hansell, D. A., Jenkins, W. J., Johnson, R., Kosnyrev, V. K., Ledwell, J. R., Li, Q. P., Siegel, D. A., and Steinberg, D. K.: Eddy/wind interactions stimulate extraordinary mid-ocean plankton blooms, *Science*, 316, 1021–1026, 2007.
- Measures, C. I., Brown, M. T., and Wink, S.: Dust deposition to the surface waters of the western and central North Pacific inferred from surface water dissolved aluminum concentrations, *Geochem. Geophys. Geosyst.*, 6, Q09M03, doi:10.1029/2005GC000922, 2005.
- Mills, M. M., Ridame, C., Davey, M., La Roche, J., and Geider, J. G.: Iron and phosphorus co-limit nitrogen fixation in the eastern

- tropical North Atlantic, *Nature*, 429, 292–294, 2004.
- Moore, J. K. and Doney, S. C.: Iron availability limits the ocean nitrogen inventory stabilizing feedback between marine denitrification and nitrogen fixation, *Global Biogeochem. Cy.*, 21, GB2001, doi:10.1029/2006GB002762, 2007.
- Moore, J. K., Doney, S. C., and Lindsay, K.: Upper ocean dynamics and iron cycling in a global three-dimensional model, *Global Biogeochem. Cy.*, 18, GB4028, doi:10.1029/2004GB002220, 2004.
- Parekh, P., Follows, M., and Boyle, E. A.: Decoupling of iron and phosphate in the global ocean, *Global Biogeochem. Cy.*, 19, GB2020, doi:10.1029/2004GB002280, 2005.
- Raimbault, P., Slawick, G., Coste, B., and Fry, J.: Feasibility of using an automated colorimetric procedure for the determination of seawater nitrate in the 0 to 100 nM range: examples from field and culture, *Mar. Biol.*, 104, 347–351, 1900.
- Raimbault, P. and Garcia, N.: Carbon and nitrogen uptake in the South Pacific Ocean: evidence for efficient dinitrogen fixation and regenerated production leading to large accumulation of dissolved organic matter in nitrogen-depleted waters, *Biogeosciences Discuss.*, 4, 3531–3579, 2007, <http://www.biogeosciences-discuss.net/4/3531/2007/>.
- Sarthou, G., Baker, A. R., Blain, S., Achterberg, E. P., Boye, M., Bowie, A. R., Croot, P., Laan, P., De Baar, H. J. W., Jickells, T. D., and Worsfold, P. J.: Atmospheric iron deposition and sea-surface dissolved iron concentrations in the eastern Atlantic Ocean, *Deep-Sea Res. I*, 50, 1339–1352, 2003.
- Sedwick, P. N., Church, T. M., Bowie, A. R., Marsay, C. M., Ussher, S. J., Achilles, K. M., Leathaby, P. J., Johnson, R. J., Sarin, M. M., and McGillicuddy, D. J.: Iron in the Sargasso Sea (BATS region) during summer: Eolian imprint, spatio-temporal variability, and ecological implications., *Global Biogeochem. Cy.*, 19, GB4006, doi:10.1029/2004GB002445, 2005.
- Sedwick, P. N. and Di Tullio, G. R.: Regulation of algal blooms in Antarctic shelf waters by the release of iron from melting sea ice, *Geophys. Res. Lett.*, 24, 2515–2518, 1997.
- Signorini, S. R., McClain, C., and Dandonneau, Y.: Mixing and phytoplankton bloom in the wake of the Marquesas Islands, *Geophys. Res. Lett.*, 26, 3121–3124, 1999.
- Sprintall, J. and Tomczak, M.: Evidence of the barrier layer in the surface layer of the tropics, *J. Geophys. Res.*, 97, 7305–7316, 1992.
- Sunda, W.: Control of dissolved iron concentration in the world ocean: A comment, *Mar. Chem.*, 57, 169–172, 1997.
- Tréguer, P. and Le Corre, P.: Manuel d'analyse des sels nutritifs dans l'eau de mer. Utilisation de l'AutoAnalyser II Technicon, 2nd ed., Université de Bretagne Occidentale, 1975.
- Twining, B. S., Baines, S. B., Fisher, N. S., and Landry, M. R.: Cellular iron contents of plankton during the Southern Ocean Iron Experiment (SOFEX), *Deep-Sea Res. I*, 51, 1827–1850, 2004.
- Wagener, T., Guieu, C., Losno, R., Bonnet, S., and Mahowald, N.: Revisiting atmospheric dust export to the southern hemisphere ocean: biogeochemical implication, *Global Biogeochem. Cy.*, doi:10.1029/2007GB002984, in press, 2008.
- Weber, L., Völker, C., Oschlies, A., and Burchard, H.: Iron profiles and speciation of the upper water column at the Bermuda Atlantic time-series study site: a model based sensitivity study, *Biogeosciences*, 4, 689–706, 2007, <http://www.biogeosciences.net/4/689/2007/>.
- Wirtki, K.: The oxygen minima in relation to ocean circulation, *Deep-Sea Res. I*, 11–23, 1962.

Distribution of inorganic and organic nutrients in the South Pacific Ocean – evidence for long-term accumulation of organic matter in nitrogen-depleted waters

P. Raimbault, N. Garcia, and F. Cerutti

Laboratoire de Microbiologie, Géochimie et Ecologie Marine (UMR 6117 CNRS), Centre d'Océanologie de Marseille, Université de la Méditerranée, Campus de Luminy, 13288 Marseille, France

Received: 23 July 2007 – Published in Biogeosciences Discuss.: 30 August 2007

Revised: 6 December 2007 – Accepted: 25 January 2008 – Published: 3 March 2008

Abstract. During the BIOSOPE cruise the RV *Atalante* was dedicated to study the biogeochemical properties in the South Pacific between the Marquesas Islands (141° W–8° S) and the Chilean upwelling (73° W–34° S). Over the 8000 km covered by the cruise, several different trophic situations were encountered, in particular strong oligotrophic conditions in the South Pacific Gyre (SPG, between 123° W and 101° W). In this isolated region, nitrate was undetectable between the surface and 160–180 m and only trace quantities (<20 nmoles l⁻¹) of regenerated nitrogen (nitrite and ammonium) were detected, even in the subsurface maximum. Integrated nitrate over the photic layer, which reached 165 m, was close to zero. Despite this severe nitrogen-depletion, phosphate was always present in significant concentrations (≈ 0.1 μ moles l⁻¹), while silicic acid was maintained at low but classical oceanic levels (≈ 1 μ moles l⁻¹). In contrast, the Marquesas region (MAR) to the west and Chilean upwelling (UPW) to the east were characterized by high nutrient concentrations, one hundred to one thousand fold higher than in the SPG. The distribution of surface chlorophyll reflected the nitrate gradient, the lowest concentrations (0.023 nmoles l⁻¹) being measured at the centre of the SPG, where integrated value throughout the photic layer was very low (≈ 10 mg m⁻²). However, due to the relatively high concentrations of chlorophyll-*a* encountered in the DCM (0.2 μ g l⁻¹), chlorophyll-*a* concentrations throughout the photic layer were less variable than nitrate concentrations (by a factor 2 to 5). In contrast to chlorophyll-*a*, integrated particulate organic matter (POM) remained more or less constant along the study area (500 mmoles m⁻², 60 mmoles m⁻² and 3.5 mmoles m⁻² for particulate organic carbon, particulate organic nitrogen and particulate organic phosphorus,

respectively), with the exception of the upwelling, where values were two fold higher. The residence time of particulate carbon in the surface water was only 4–5 days in the upwelling, but up to 30 days in the SPG, where light isotopic $\delta^{15}\text{N}$ signal noted in the suspended POM suggests that N₂-fixation provides a dominant supply of nitrogen to phytoplankton. The most striking feature was the large accumulation of dissolved organic matter (DOM) in the SPG compared to the surrounding waters, in particular dissolved organic carbon (DOC) where concentrations were at levels rarely measured in oceanic waters (>100 μ moles l⁻¹). Due to this large pool of DOM in the SPG photic layer, integrated values followed a converse geographical pattern to that of inorganic nutrients with a large accumulation in the centre of the SPG. Whereas suspended particulate matter in the mixed layer had a C/N ratio largely conforming to the Redfield stoichiometry (C/N ≈ 6.6), marked deviations were observed in this excess DOM (C/N ≈ 16 to 23). The marked geographical trend suggests that a net in situ source exists, mainly due to biological processes. Thus, in spite of strong nitrate-depletion leading to low chlorophyll biomass, the closed ecosystem of the SPG can accumulate large amounts of C-rich dissolved organic matter. The implications of this finding are examined, the conclusion being that, due to weak lateral advection, the biologically produced dissolved organic carbon can be accumulated and stored in the photic layer for very long periods. In spite of the lack of seasonal vertical mixing, a significant part of new production (up to 34%), which was mainly supported by dinitrogen fixation, can be exported to deep waters by turbulent diffusion in terms of DOC. The diffusive rate estimated in the SPG (134 μ moles C m⁻² d⁻¹), was quite equivalent to the particles flux measured by sediments traps.

Correspondence to: P. Raimbault
(patrick.raimbault@univmed.fr)

1 Introduction

The warm oligotrophic regions of the open ocean are subject to smaller seasonal temperature variations than temperate waters, and are permanently underlain by a strong thermocline. Therefore they are regarded as the least variable and the least productive surface waters of the sea. However, as they represent 60% of the global oceanic area, the subtropical open-ocean ecosystems are the largest coherent biomes of our planet and the biogeochemical processes they support have global consequences (Karl, 2002). A comprehensive evaluation of both inorganic and organic nutrient pools is important in order to understand the production and fate of organic matter in these large oceanic areas. Rates of inorganic nutrient assimilation reported for oligotrophic waters are subject to large errors (McCarthy, 1980) as conventional nutrient analysis are unable to measure the extremely low concentrations that exist over the vast areas of the open ocean. Over the last 15 years, international programs have advanced our understanding of these vast marine ecosystems; however the South Pacific remains one of the least studied areas of the Ocean (Daneri and Quinones, 2001). This region has been described as the most oligotrophic zone in the world's oceans (Dandonneau et al., 2006) having the lowest surface chlorophyll concentrations, observed using satellite imagery (Claustre and Maritorena, 2003) and confirmed by exhibiting the clearest oceanic waters of the world (Morel et al., 2007).

The BIOSOPE (BIOgeochemistry and Optics South Pacific Experiment) cruise provided the first spatially extensive experiment in the South East Pacific. The 8000 km transect, stretching from the Marquesas Islands to the Chilean coast and crossing the centre of the SPG, is an ideal area for studying organic and inorganic nutrients along an extreme trophic gradient. The main objective of this work is to describe inorganic and organic distributions by comparing the different environmental conditions covered by the BIOSOPE cruise. Since ambient concentrations are often below the detection limit of conventional analytical procedures (Brzezinski, 1985; Garside 1985; Sahlsten, 1987; Raimbault et al., 1999) the more sensitive methods of Garside (1982), Raimbault et al. (1990) and Holmes et al. (1999) have to be employed in order to detect the trace nutrients. In this paper we describe spatial and vertical distributions of inorganic and organic nutrients in the South Pacific in particular in the oligotrophic SPG. Pools of carbon, nitrogen and phosphorus essential for production in the upper layer are analyzed producing the first broad data base for this unexplored oceanic region.

2 Materials and methods

Data was collected during the BIOSOPE cruise carried out on board the R/V *Atalante* between October–November

2004 in the southeast Pacific Ocean along a transect between the Marquesas archipelago and the Chilean coasts (from 146.36° W–15.24° S to and 72.49° W–34.7° S, Fig. 1). Twenty four short-term (8 h) stations were studied during transit. In addition, six experimental sites were specifically investigated with long fixed stations (over 2–5 days), representing sites of different trophic regimes: MAR = Marquesas archipelago (141.3° W; 8.4° S); HLNC=High Nutrient Low Chlorophyll area east of the Marquesas islands (136.8° W; 9° S); GYR = centre of the South Pacific gyre (114° W, 26° S); EGY=eastern border of the gyre (91.4° W, 31.8° S), UPW and UPX situated in the area of Chilean upwelling (73° W–34° S and 72.4° W–34.5° S). Sampling sites in the gyre were selected using ocean colour images, and exhibited the lowest surface chlorophyll concentrations found in the world's oceans. High vertical resolution environmental data were collected between 0 and 500 m using a conductivity temperature-depth-oxygen profiler (CTDO, Seabird 911 plus) with a rosette supporting 12-l Niskin bottles equipped with silicon rubber closures.

2.1 Inorganic nutrients

Nutrient samples for nitrate, nitrite, phosphate and silicic acid determination, were collected into 20 ml polyethylene flasks and 250 ml polycarbonate bottles at each station. Samples in the 20 ml polyethylene flasks were immediately poisoned with mercuric chloride ($10 \mu\text{g ml}^{-1}$), according to Kirkwood (1992), and stored for subsequent laboratory analysis. Ambient nitrate, nitrite and phosphate concentrations were measured immediately by pumping the 250 ml sample through a Technicon AutoAnalyzer®. Nitrate and nitrite concentrations in the nanomolar range (lower detection limit= 3 nmoles l^{-1}) were obtained using the sensitive method of Raimbault et al. (1990). Nitrate at submicromolar levels (detection limit $0.05 \mu\text{moles l}^{-1}$) and phosphate (detection limit $0.02 \mu\text{moles l}^{-1}$) were measured according to the method of Armstrong et al. (1967). Ammonium concentrations (40 ml collected into 50 ml Schott glass flasks) were measured using the sensitive method of Holmes et al. (1999) having a detection limit of 5 nmoles l^{-1} .

Silicic acid concentrations as well as duplicate nitrate and phosphate concentrations were determined in the laboratory (Tréguer and LeCorre, 1975) on the poisoned samples four months after sampling. To ensure the reproducibility of nutrient measurements between analyses, in-house standards were used, which were regularly compared to the commercially available products (OSIL). Precision was also tested, through participation in the European inter-calibration exercise QUASIMEME (<http://www.quasimeme.org>).

2.2 Phytoplanktonic biomass

250 ml of seawater was filtered through 25 mm Whatmann GF/F filters (nominal pore size around $0.7 \mu\text{m}$) immediately

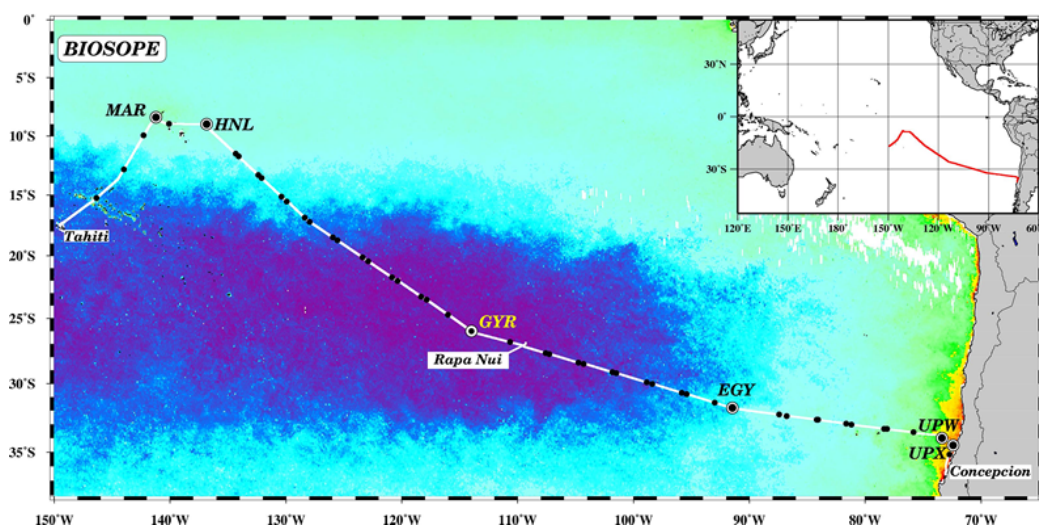


Fig. 1. Map showing the location of the BIOSOPE cruise from Marquises Island to Chile superimposed on a SeaWiFS surface Chl-*a* composite. Locations of CTD casts are indicated by dark spots and long time experimental stations by large circles. (MAR=141.3° W; 8.4° S; HLN=136.8° W; 9° S; GYR = 114° W, 26° S); EGYR=eastern border of the gyre (91.4° W, 31.8° S; UPW=73° W–34° S and UPX=72.4° W–34.5° S).

Table 1. Values for reagent blanks and blank filters (not including reagent blank) obtained during the analysis of dissolved and particulate organic matter using wet oxidation or high temperature combustion.

	C	Wet oxidation		High temperature combustion	
		N	P	C	N
		$\mu\text{moles.l}^{-1}$		μmoles	
Reagent blank	5.9±0.3	0.2±0.08	0.03±0.01		
DIW	4.2±0.6	<D.L.	<D.L.		
		$\mu\text{moles/filter}$		$\mu\text{moles/filter}$	
Blank filter Teflon (47 mm)	2.2±0.85	0.05±0.07	0.008±0.005		
Blank filter GF/F (25 mm)	0.63±0.18	0.03±0.02	0.003±0.003	0.9±0.3	0.13±0.05

after sampling, and placed in glass tubes containing 5 ml of pure methanol as described by Raimbault et al. (2004). Following 20–30 min of extraction, fluorescence of the extract was determined on a Turner Fluorometer 110 equipped with the Welschmeyer kit to avoid chlorophyll-*b* interference (Welschmeyer, 1994). As the monochromatic fluorescence method cannot separate divinyl chlorophyll from chlorophyll-*a*, results are given in terms of total chlorophyll-*a* concentration (Tchl-*a*), i.e. the sum of chlorophyll-*a* and divinyl chlorophyll-*a*. The blank “methanol + filter” was close to zero giving a very low detection limit of around $0.01 \mu\text{g l}^{-1}$. Calibrations were made using a pure Sigma chlorophyll-*a* standard.

2.3 Organic nutrients

Samples for particulate organic carbon (POC), particulate organic nitrogen (PON) and particulate organic phospho-

rus (POP) were filtered onto a $0.2 \mu\text{m}$ Teflon membrane. The hydrophobic Teflon membranes were washed with 1 ml ethanol just before filtration and then rinsed with milliQ water. Between 580 to 1200 ml of sample was filtered, dependant on the quantity of particulate matter in the sample. Following filtration, filters were washed with $100 \mu\text{l}$ of H_2SO_4 (0.5 N) to remove any inorganic carbon. The filters were then stored in 25 ml Schott glass bottles for subsequent laboratory analysis. Blank filters were prepared for each set of samples by washing the filter with 1 ml ethanol and rinsing with 600 ml of $<0.2 \mu\text{m}$ seawater. Determination of POC, PON and POP was carried out simultaneously on the same sample using the wet-oxidation procedure according to Raimbault et al. (1999a). Filter blanks are given in Table 1. Values were slightly higher than those published by Raimbault et al. (1999a) but remain three to ten fold lower than the samples. Samples for particulate carbon (PC) and particulate nitrogen (PN) were filtered onto

Whatman GF/F filters and values were obtained using dual isotopic $^{13}\text{C}/^{15}\text{N}$ experiments (see Raimbault and Garcia, 2007). The filters were not acidified and PC and PN measurements were obtained using high combustion (900°C) on a CN Integra mass spectrometer. Samples for total organic matter determination were collected directly from the Niskin bottles into 50 ml Glass Schott bottles. Samples were immediately acidified with 100 μl H_2SO_4 0.5 N and stored for analytical determination in the laboratory. Prior to oxidation, samples were bubbled with a high purity oxygen/nitrogen gas stream for 15 min. Persulfate wet-oxidation was used to digest the organic matter in these unfiltered samples, according to Raimbault et al. (1999b). The calibration was made according to the range of the marine content observed. Total organic nitrogen and total organic phosphorus was calculated as total nitrogen and phosphorus minus dissolved inorganic nitrogen (nitrate+nitrite+ammonium) or phosphate measured in the same samples. Dissolved organic carbon (DOC), dissolved organic nitrogen (DON) and dissolved organic phosphorus (DOP) were calculated from these total organic fractions by subtracting values of POC, PON and POP obtained from the $>0.2 \mu\text{m}$ fractions (see above). The analytical accuracy was close to 5, 0.5 and 0.05 $\mu\text{mole l}^{-1}$ for DOC, DON and DOP, respectively. Deep Sargasso Sea reference water was used to verify the analytical calibration (45 $\mu\text{moles C l}^{-1} \pm 0.5$ SE, Hansell Laboratory, Bermuda Biological Station for Research). All reagents and sample blanks were prepared using fresh Millipore Milli-Q plus® water. Mean blank values are presented in Table 1.

2.4 Natural abundance of particulate ^{15}N measurements ($\delta^{15}\text{N}$)

Water samples were drawn into 10 l polyethylene bottles and the contents filtered immediately online, onto pre-combusted Whatman, GF/F filters which were placed into glass tubes and dried at 60°C. Some large samples (1000–1500 l) were also collected using an in situ pump and a fraction of the glass fiber filter, corresponding to 10–15 l of seawater, was treated as above. In the laboratory, each filter was rolled into a pellet and fed into a mass-spectrometer (CN-Integra tracer-mass) to analyse the stable isotopic composition of the particulates ($\delta^{15}\text{N}$). An organic standard (glycine) was used to calibrate the PN measurements and to track the consistency of the Dumas combustion. The $\delta^{15}\text{N}$ of this standard was $4.88 \pm 0.39\%$ ($n=24$) for nitrogen levels ranging from 20 to 140 μg . In addition, two NIST-certified organic ^{15}N reference materials (IAEA 310 A $\delta^{15}\text{N}=47\%$; IAEA 310 B, $\delta^{15}\text{N}=245\%$) were used to insure the accuracy of the isotopic measurements. The values for these analysis were $47.3 \pm 0.27\%$ and $243 \pm 0.46\%$ for IAEA310 and IAEA 310b, respectively. Analytical precision determined with these reference materials was 0.03%. The standard reference was atmospheric N_2 gas ($^{15}\text{N}/^{14}\text{N}=0.003663$; $\delta^{15}\text{N}=0\%$).

Surface light levels and the thickness of the euphotic layer were measured around local noon using a spectroradiometer (LI.1800U.W, LI-COR instrument; Morel et al., 2007). The depth of the euphotic zone (Z_e) is defined as the depth where the downward photosynthetic available radiation (PAR) irradiance is reduced to 1% of its surface value. For CTD casts performed early in the morning, Z_e was computed using in situ TChl-*a* concentration profiles (see Ras et al., 2007) according to the model developed by Morel and Maritorena (2001).

Data shown throughout this paper are limited to the 0–300 m water column.

3 Results

3.1 Hydrological background

The general distribution of temperature and salinity are presented and described in Claustre et al. (2008) and Ras et al. (2007). Briefly, surface temperature generally decreased from the Marquesas site (27.8°C) to the Chilean coast (18°C). Surface temperatures were greater than 25°C up to 125° W and greater than 20°C up to 100° W. The 15°C isotherm remained below 250 m until 100° W rapidly becoming shallower thereafter and reaching the surface along the Chilean coast. Salinity patterns (Fig. 2) generally followed those of temperature, decreasing from west (37.75) to east (34.5); but a maximum (>36.5) and minimum (<34.25) were noted around 130° W and 90° W, respectively. These specific water masses are referred to as the South Pacific Tropical Waters (SPTW) and Eastern South Pacific Intermediate Waters (ESPIW). The waters surrounding the Marquesas Islands (8°–141° W) were influenced by the South Equatorial current and constituted the southern boundary of High Nutrient Low Chlorophyll (HNLC) waters of the equatorial upwelling region (Andrié et al., 1993). Salinity ranged from 35.5–35.7 and surface temperatures reached 27.9°C. The Peru-Chile current, delimited by an isohaline of 34.3 was associated with fresher waters, especially between 78° W and 75° W (salinity around 34.1).

3.2 Inorganic nutrient distribution

The distribution of major inorganic nutrients (nitrate, phosphate and silicate) is shown in Fig. 2. In contrast to temperature, the nutrient isolines sunk deeper from west to east up until 110° W. Thus, the concentrations of deep and surface nutrients tended to be symmetrically distributed around the center of the investigated area, with lowest concentrations found in the central region (110° W). The Marquesas region (moving westward to 135° W), located at the southern limit of the equatorial Pacific, was characterized by rich superficial waters with nitrate concentrations greater than 1 $\mu\text{moles l}^{-1}$. The 2 $\mu\text{moles l}^{-1}$ isoline, indicated the start of the nitracline

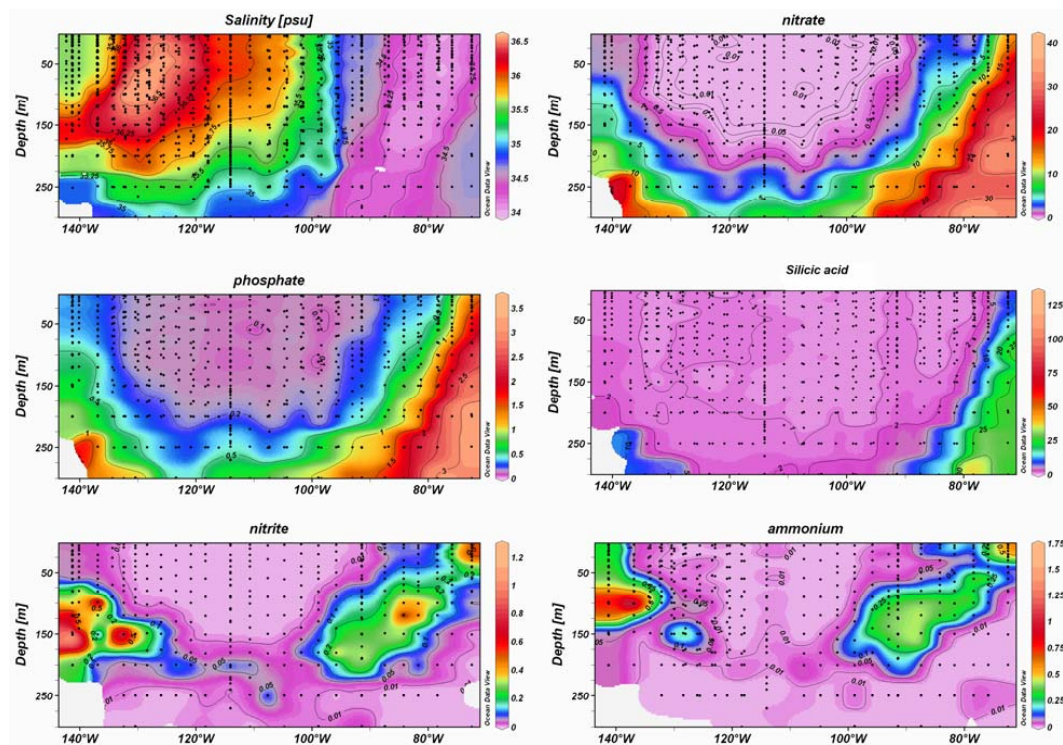


Fig. 2. Longitudinal section of salinity, nitrate, phosphate, silicic acid, nitrite and ammonium along the BIOSOPE Transect. Units for nutrients are $\mu\text{moles l}^{-1}$. (Ocean Data View software (ODV), version 3.1, Reiner Schlitzer, <http://odv.awi.de>).

at 55 m. Phosphate was also present in significant concentrations ranging between 0.3 and 0.5 $\mu\text{moles l}^{-1}$. To the east of the Marquesas island (135° W to 130° W), nitrate was still detectable in the surface but there was a significant variation in the nitrate level with depth, with concentrations decreasing from 1 to 0.05 $\mu\text{moles l}^{-1}$ between the surface and 100 m. Phosphate concentrations in the surface were close to 0.2 $\mu\text{moles l}^{-1}$. Here, the nitracline was deeper, reaching 60–70 m. The centre of investigated area (South Pacific Gyre=SPG; 125° W to 100° W) was characterized by very nutrient-depleted water. Surface nitrate concentrations were always lower than 0.010 $\mu\text{moles l}^{-1}$ and often undetectable ($<0.003 \mu\text{moles l}^{-1}$) in the upper 100 m layer, or the upper 160 m layer between 120° W and 110° W. Moving eastward from 108° W, the depth at which nitrate concentrations reached 0.01 $\mu\text{moles l}^{-1}$ reduced, getting close to the surface at 96° W. This defines the eastern limit of the SPG. As in the case of nitrate, surface concentrations of phosphate were minimal in the SPG ($\approx 0.1 \mu\text{moles l}^{-1}$). However, despite complete nitrate-depletion, surface waters were phosphate-replete over the whole transect. Further west, surface nutrient concentrations increased rapidly reaching maximum values in the Chilean upwelling region. The 5 $\mu\text{moles l}^{-1}$ nitrate isoline outcropped at the surface at 76° W. This defines the western limit of the upwelling. Silicic acid distribution showed the same general pattern as that of nitrate, although

surface concentrations along the transect were less variable, ranging from 1 to 2 $\mu\text{moles l}^{-1}$, and up to 10 $\mu\text{moles l}^{-1}$ in the upwelling. Concentrations were lowest in the SPG, but always close to 1 $\mu\text{moles l}^{-1}$. Thus, like phosphate, complete silicic acid-depletion was never observed.

Regenerated forms of nitrogen, such as nitrite and ammonium (Fig. 2), showed particular distribution patterns characterized by the presence of subsurface maxima located at each extremity of the transect. Nitrite was generally undetectable or present in very low concentrations at the surface ($<0.05 \mu\text{moles l}^{-1}$), except in the upwelling region where superficial concentrations reached 0.1 $\mu\text{moles l}^{-1}$ (up to 0.5 $\mu\text{moles l}^{-1}$). A well-marked maximum was located at 120 m in the western area, with concentrations reaching 0.5 $\mu\text{moles l}^{-1}$. This subsurface maximum disappeared in the SPG (between 120° W and 105° W) and only some traces of nitrite ($<0.05 \mu\text{moles l}^{-1}$) were detected below the euphotic zone (200 m), associated with the 0.5 $\mu\text{moles l}^{-1}$ nitrate isoline. A second maximum was observed around 150 m, from 100° W. However, in contrast to the western maximum, nitrite concentrations rarely reached 0.5 $\mu\text{moles l}^{-1}$ and remained close to 0.25 $\mu\text{moles l}^{-1}$, except in surface upwelling waters. Whatever the depth of the nitracline (depth where nitrate ranged between 0.01 and 0.05 $\mu\text{mole l}^{-1}$), the primary nitrite maximum was about 10 to 20 m deeper than the top of the nitracline.

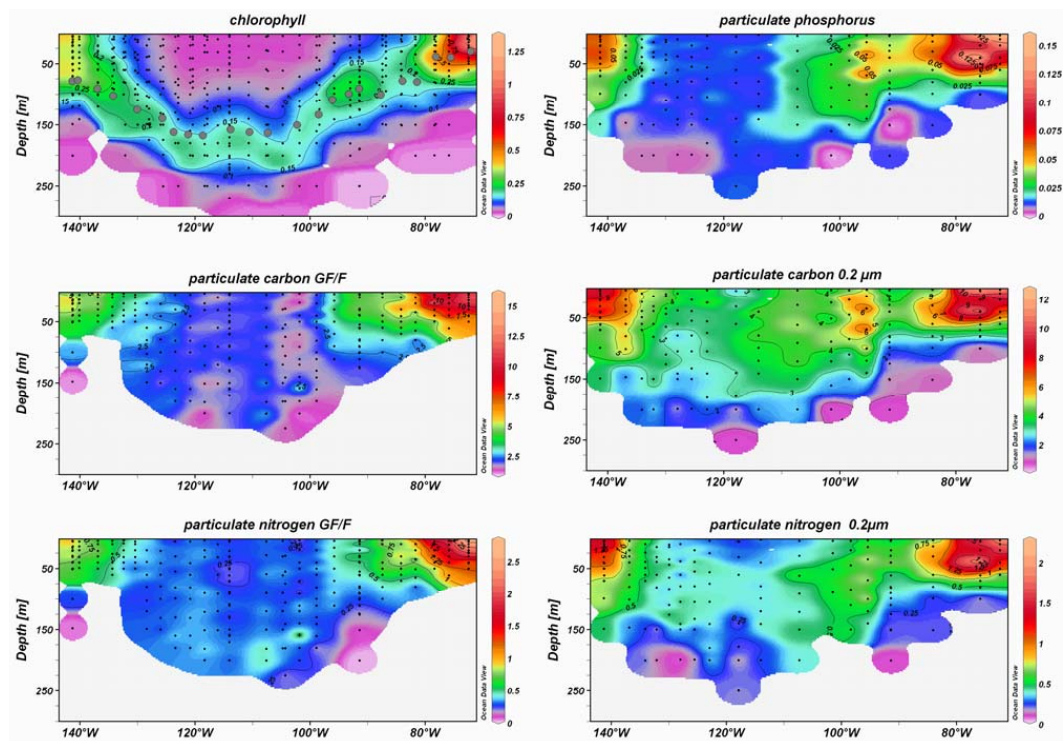


Fig. 3. Vertical sections of total chlorophyll-*a* (Chlorophyll in $\mu\text{g l}^{-1}$), particulate phosphorus, $>0.2 \mu\text{m}$ particulate organic carbon and particulate nitrogen and $>\text{GF/F}$ particulate carbon and particulate nitrogen (units are in $\mu\text{moles l}^{-1}$). Dark spots on chlorophyll section indicate the 1% light penetration depth. (Ocean Data View software (ODV), version 3.1, Reiner Schlitzer, <http://odv.awi.de>).

Ammonium concentrations followed the same general trend. Highest concentrations (up to $0.5 \mu\text{moles l}^{-1}$) being located in the subsurface in the Marquesas zone, although the maximum concentration was shallower than the nitrite maximum (100 m instead of 150 m). High surface concentrations ($>0.3 \mu\text{moles l}^{-1}$) were also measured in this region. The SPG was characterized by undetectable ammonium concentrations through most of the superficial layer. A very weak and narrow maximum, with trace concentrations of ammonium ($0.010 \mu\text{moles l}^{-1}$), was detected around 180 m, more or less associated with the narrow nitrite maximum. The western ammonium maximum was also located just above the nitrite maximum. Concentrations ranged from 0.25 to $0.3 \mu\text{moles l}^{-1}$. The eastern boundary of the SPG was also characterized by a deep ammonium maximum (80–100 m), with lower concentrations than those observed in the western region ($<0.25 \mu\text{moles l}^{-1}$). The upwelling area was defined by surface concentrations $>0.25 \mu\text{moles l}^{-1}$. Concentrations of both regenerated nitrogen forms followed similar trends to those of the macronutrients, with “hot spots” to the west and east of the investigated transect. The SPG was entirely N-depleted, indicating low nitrogen regeneration activity or a tight coupling between regeneration and phytoplankton and bacteria uptake.

3.3 Biomass distribution

Vertical distributions of biomass are shown in Fig. 3 as total chlorophyll-*a* (TChl-*a*), particulate organic carbon (POC), particulate organic nitrogen (PON) and particulate organic phosphorus (POP). In situ chlorophyll-*a*, in accordance with ocean colour imagery, showed considerable variations across the South Pacific. TChl-*a* distribution and concentration are roughly equivalent to those found by Ras et al. (2007) who used the HPLC procedure. The extremities of the transect exhibited the highest biomass, located in the surface, while very low chlorophyll concentrations were measured at the center of the SPG. The lowest concentration ($0.023 \mu\text{g l}^{-1}$) was found in the surface at 114°W . This value is close to the lowest measured at this site ($0.017 \mu\text{g l}^{-1}$) by Ras et al. (2007). In contrast, in the waters off the Marquesas Islands, surface Tchl-*a* were ten folds higher ($0.3 \mu\text{g l}^{-1}$) and higher than values previously observed in the subequatorial area at other times of the year (Signorini et al., 1999). In the Chilean upwelling, surface Tchl-*a* was much higher (up to $3 \mu\text{g l}^{-1}$). The SPG was also characterized by a deep chlorophyll maximum (DCM) at 160 and 180 m between 120°W and 100°W . The depth of the DCM decreased progressively eastward and westward, reaching the surface at the Chilean upwelling, but restricted to 50 m in the Marquesas area. While the DCM was generally found just above the 1% light penetration depth in

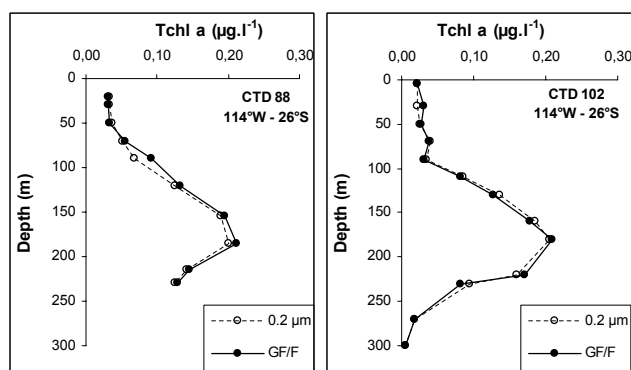


Fig. 4. Vertical profiles of chlorophyll-*a* (Tchl-*a*) made with GF/F filters and 0.2 µm Teflon membranes.

the Marquesas area and east of 110° W, the entire DCM was well below the limit of the photic zone in the SPG. Within this DCM, chlorophyll concentrations were confined to a narrow range (0.15 to 0.20 µg l⁻¹) whatever the depth; and no significant relationship was found between the depth of the DMC and chlorophyll concentration.

Previous work has indicated that GF/F filters are not efficient in collecting all the chlorophyll particles, especially in very oligotrophic waters (Dickson and Wheeler, 1993). This investigation, carried out in one of the most oligotrophic areas of the world, enabled us to test the efficiency of the GF/F filters. Two comparison profiles carried out at the most oligotrophic site (114° W and 26° S) clearly demonstrated that pre-combusted GF/F filters were as efficient as the 0.2 µm Teflon membranes (Fig. 4) in determining chlorophyll concentrations, even in these very poor oceanic waters dominated by small picophytoplankton (Grob et al., 2007). This observation contradicts Dickson and Wheeler's results and confirms those of Chavez et al. (1995) that GF/F filters are adequate for collecting TChl-*a* in the open oligotrophic ocean.

Biomass in terms of particulate organic carbon, particulate nitrogen and particulate phosphorus collected on 0.2 µm Teflon membranes (Fig. 3) showed very different patterns to those of chlorophyll. The Marquesas waters and upwelling areas were again the richest regions with superficial concentrations of POC, PON and POP higher than 6, 1 and 0.05 µmoles l⁻¹, respectively. The SPG revealed very low values throughout the water column (POC < 4 µmoles l⁻¹, PON < 0.5 µmoles l⁻¹, POP < 0.02 µmoles l⁻¹) with no pronounced subsurface maximum as observed for chlorophyll. The eastern area of the SPG (between 110° W and 90° W) was richer than the western area, with POC, PON and POP higher than 5, 0.5 and 0.025 µmoles l⁻¹, respectively. Although surface concentrations were higher near the Marquesas Islands and in the upwelling region than in the SPG, the differences were less than twofold, compared with the ten and thousand fold differences found in surface TChl-*a*

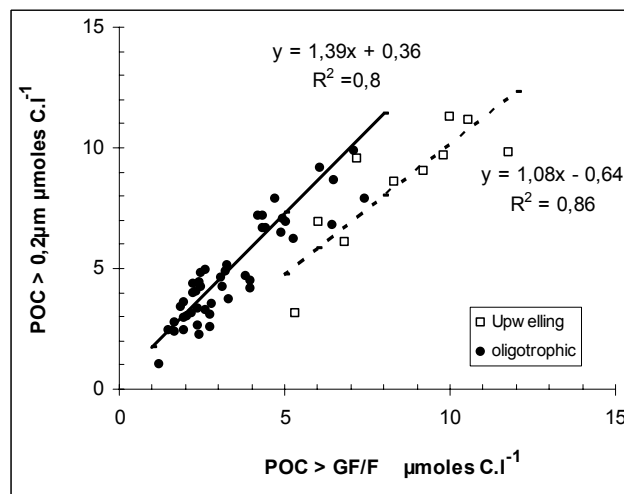


Fig. 5. Comparison between particulate organic carbon measured on 0.2 µm Teflon membranes by a wet-oxidation method (POC in µmoles l⁻¹) and particulate carbon on GF/F filters measured using High temperature combustion (PC in µmoles l⁻¹). Linear relationships are obtained using model II regression.

and nitrate concentrations, respectively. Depth distributions of POC, PON and POP were uniform over the photic zone, lacked pronounced subsurface maxima, but showed a characteristic decrease to the bottom of the euphotic zone. Particulate carbon and particulate nitrogen collected on GF/F filters described the same geographical pattern (Fig. 3). Maximum biomass was found in surface upwelling waters and in the Marquesas vicinity while a homogeneous vertical distribution was observed in the SPG.

The estimates of POM in the >0.2 µm size fraction (collected on Teflon filters) and in the >0.7 µm size fraction (approximate GF/F filter pore size) were compared by calculating the geometric mean model II regression, which take into account the measurement errors in both variables. Results obtained from upwelling waters appeared significantly different from other waters (Fig. 5) and were treated separately. On average, >0.2 µm POC and PON were 1.38, 1.24 times higher than the corresponding 0.7 µm estimates (Table 2), indicating that a large proportion of POC/PON particles were <0.7 µm and therefore the GF/F filters were shown to be underestimating the values. In some cases, this underestimation reached 50%, i.e. in the SPG. In the case of N-replete water from the upwelling, the linear regression slope was not significantly different from 1, indicating that there was no significant biomass lower than 0.7 µm.

When all the data were pooled the relationship between POC versus PON and POC versus POP were close to the Redfield ratio for the >0.2 µm fraction and for the >0.7 µm GF/F filter fraction (Table 2). However, intercepts of the regression equations for the 0.2 µm teflon and GF/F filter comparisons showed that particles in the <0.7 µm filtrate

Table 2. Comparative study of retention efficiency of 0.2 μm Teflon membrane and GF/F Whatman® filters (approximate 0.7 μm pore size) for collection of particulate carbon (POC and PC), particulate nitrogen (PON), particulate phosphorus (POP) and chlorophyll (Tchl-*a*). Coefficient regression and coefficient correlation are obtained from model II regression.

All BIOSOPE data, except upwelling (141°–82° W)			upwelling (81° W–74° W)		
	r^2	n		r^2	n
$\text{POC}_{0.2\mu\text{m}}=1.38\text{PC}_{0.7\mu\text{m}}+0.36$	0.80	52	$\text{POC}_{0.2\mu\text{m}}=1.08\text{PC}_{0.7\mu\text{m}}-0.6$	0.85	10
$\text{PON}_{0.2\mu\text{m}}=1.24\text{PON}_{0.7\mu\text{m}}+0.04$	0.75	52	$\text{PON}_{0.2\mu\text{m}}=1.08\text{PON}_{0.7\mu\text{m}}-0.36$	0.98	10
$\text{POC}_{0.2\mu\text{m}}=6.19\text{PON}_{0.2\mu\text{m}}+0.94$	0.66	133	$\text{POC}_{0.2\mu\text{m}}=5.9\text{PON}_{0.2\mu\text{m}}+0.10$	0.90	27
$\text{POC}_{0.2\mu\text{m}}=103\text{POP}_{0.2\mu\text{m}}+1.5$	0.629	133	$\text{POC}_{0.2\mu\text{m}}=74\text{POP}_{0.2\mu\text{m}}+0.66$	0.85	27
$\text{POC}_{0.2\mu\text{m}}=15.3\text{Tchl-}a+1.6$	0.40	93	$\text{POC}_{0.2\mu\text{m}}=4.9\text{Tchl-}a+3.8$	0.39	18
$\text{PON}_{0.2\mu\text{m}}=2.6\text{Tchl-}a+0.1$	0.60	92	$\text{PON}_{0.2\mu\text{m}}=0.9\text{Tchl-}a+0.58$	0.36	18
$\text{POP}_{0.2\mu\text{m}}=0.14\text{Tchl-}a-0.00$	0.48	92	$\text{POP}_{0.2\mu\text{m}}=0.07\text{Tchl-}a+0.038$	0.2	18
$\text{PC}_{0.7\mu\text{m}}=6.4\text{PON}_{0.7\mu\text{m}}+0.17$	0.87	207	$\text{PC}_{0.7\mu\text{m}}=6.3\text{PON}_{0.7\mu\text{m}}-1.74$	0.88	29
$\text{PC}_{0.7\mu\text{m}}=17.0\text{Tchl-}a+0.71$	0.31	207	$\text{PC}_{0.7\mu\text{m}}=7.9\text{Tchl-}a+2.85$	0.72	29
$\text{PON}_{0.7\mu\text{m}}=2.66\text{Tchl-}a+0.084$	0.44	207	$\text{PON}_{0.7\mu\text{m}}=1.25\text{Tchl-}a+0.73$	0.75	29
$\text{Tchl-}a_{0.2\mu\text{m}}=0.98\text{Tchl-}a_{0.7\mu\text{m}}+0.001$	0.99	23			

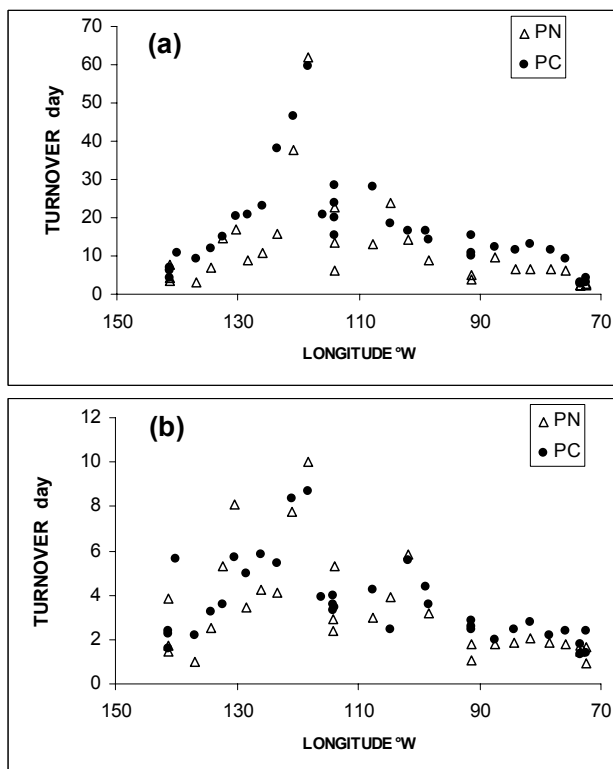


Fig. 6. Longitudinal evolution of turnover time (day) of particulate carbon (PC) and particulate nitrogen (PN) collected on GF/F filters, estimated as the PC/versus photosynthesis and PN /nitrogen uptake rates ratios. (a) total material collected on GF/F filters. (b) particles containing chlorophyll estimated from Tchl-*a* Vs PC and Tchl-*a* vs PN relationship (see Table 2).

have a C/N ratio slightly higher than the Redfield value (0.36/0.04=9). Consequently, the particulate matter in the

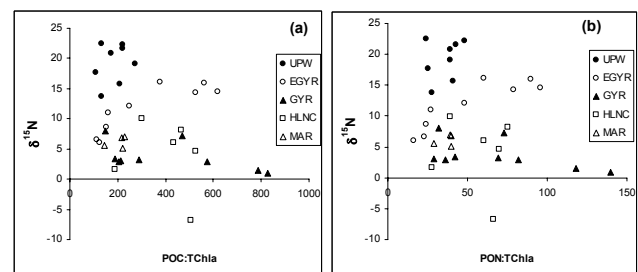


Fig. 7. Relationship between $\delta^{15}\text{N}$ PON (‰) with the ratio of POC:Tchl (a) and PON:Tchl (b). There is no significant relationship between $\delta^{15}\text{N}$ PON and the ratios, except for the east Gyre area (EGY) where $\delta^{15}\text{N}$ PON = 0.016 POC:Tchl + 6.5 with $r^2=0.73$ and $\delta^{15}\text{N}$ PON = 0.11 PON:Tchl + 6.1 with $r^2=0.76$.

<GF/F filtrate was essentially carbon rich with no chlorophyll particles. Using photosynthesis rates and nitrogen uptake (Raimbault and Garcia, 2007), we can calculate the residence time of PC and PN collected on GF/F filters in the photic zone (Fig. 6a) as proposed by Copin-Montégut and Copin-Montégut (1978). Average residence times of less than 10 days were found in the Marquesas Island waters and around 4–5 days in the upwelling, while values increased to more than 30 days in the SPG. It should be noted that carbon turnover times were 10 to 15% higher than those of nitrogen. Using POM vs Tchl-*a* relationships (Table 2), the turnover time of photosynthetic particles, containing chlorophyll, can be estimated (Fig. 6b). In this case, residence times were close to 1 day in the upwelling, 2 to 3 days in the Marquesas sector and ranged from 4 to 6 days in the SPG.

The distribution of the natural ^{15}N isotope ($\delta^{15}\text{N}$) can provide useful information regarding the origin of this organic matter. The abundance of this stable isotope of nitrogen (^{15}N) has been widely employed for N cycle studies in

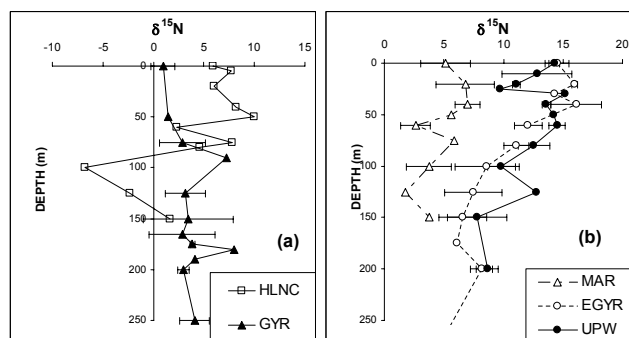


Fig. 8. Vertical profiles of ^{15}N natural abundance ($\delta^{15}\text{N}$) in suspended particulate matter within the euphotic zone obtained at 5 sites in the South East Pacific. (MAR=141.3° W; 8.4° S; HLNC=136.8° W; 9° S; GYR=114° W, 26° S); EGY=eastern border of the gyre (91.4° W, 31.8° S; UPW=73° W–34° S).

the oceans (e.g. Wada and Hattori, 1991), as differences in the natural abundance $^{15}\text{N}:^{14}\text{N}$ ratio (0.3663%) between organic matter pools can be used to constrain the source materials from which they were derived, but only in absence of trophic bias. It is well known that inclusion of particulate matter derived from higher trophic levels than phytoplankton, i.e. zooplankton, would add PON enriched in ^{15}N (Minagawa and Wada, 1984) and not chlorophyll to the particulate biomass. Thus, as proposed by Waser et al. (2000) and Mahaffey et al. (2004), this trophic bias appears important if a positive relationship between the ratio of POC:Chlorophyll or PON:chlorophyll and $\delta^{15}\text{N}$ is observed. Figures 7a and 7b revealed that there was no such relationship in the regions investigated, except for samples from east Gyre (EGY). Consequently, suspended PON in the latest region was assumed to reflect some influence of trophic transfer and can not be presented as the composition of phytoplankton. For the other regions, the range of $\delta^{15}\text{N}$ in the suspended particulate matter collected on GF/F filters varied greatly in the superficial layer but seemed to display coherent patterns with the trophic gradient (Fig. 8). The western area of the transect (MAR and HNLC sites) showed typical values of 5–6‰ for marine phytoplankton found in oceanic regions that are not strongly affected by upwelling or derived N-inputs (Altabet and McCarthy, 1986). This value was close to those of $\delta^{15}\text{N}\text{-NO}_3$ (6.5‰) reported in the central Pacific (Liu and Kaplan, 1989). Large negative values were found in deep waters around (140° W) associated with high nitrite and ammonium concentrations (Fig. 2). This could be due to biological utilization of regenerated nitrogen generally characterized by negative isotope fractionation (Hoch et al., 1992), since ammonium excreted by zooplankton is depleted in ^{15}N (Checkley and Miller, 1989). The Central South Pacific Gyre was characterized by low $\delta^{15}\text{N}$, close to 2‰, which is the signature of enhanced dinitrogen fixation (Minagawa and Wada, 1984; Dore et al., 2002). The highest $\delta^{15}\text{N}$ values (up to

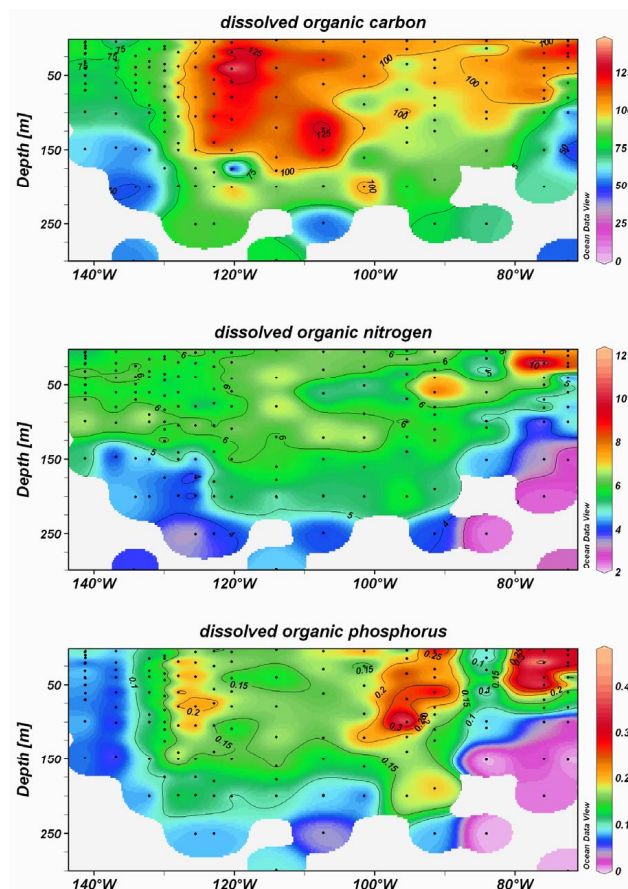


Fig. 9. Vertical section of dissolved organic carbon (DOC), dissolved organic nitrogen (DON) and dissolved organic phosphorus (DOP). Units are $\mu\text{moles l}^{-1}$ (Ocean Data View software (ODV), version 3.1, Reiner Schlitzer, <http://odv.awi.de>).

15‰) were found in the upwelling area. These values overlap those generally observed in oceanic waters, indicating the use of a nitrogen source enriched in ^{15}N . In fact, it is well known that $\delta^{15}\text{N}$ in the nitrate pool increases as concentrations decrease, because of the rapid utilization of the light isotope ^{14}N , which is preferentially assimilated during photosynthesis. Consumption of nitrate during the early stages of the upwelling, when diatoms grow actively, will be accompanied by a significant isotopic fractionation leading to a large increase in $\delta^{15}\text{N}$ (up to 30‰), when residual nitrate reaches 10 to 20% of the initial concentration (Montoya and Mc Carthy, 1995). Phytoplankton using this residual ^{15}N -enriched nitrate for growth, as occurred in offshore upwelling water sampled during this study, could exhibit a heavier nitrogen signature. Another explanation could be the biological use of enriched ^{15}N -nitrate coming from the denitrification layer, as $\delta^{15}\text{N}$ in the nitrate pool can reach 20‰ during this process (Cline and Kaplan, 1975).

3.4 Distribution of dissolved organic nutrients

The vertical profiles of dissolved organic carbon (DOC), dissolved organic nitrogen (DON) and dissolved organic phosphorus (DOP) are shown in Fig. 9. The main feature was the high DOC concentration ($>100 \mu\text{moles.l}^{-1}$) exhibiting a patchy maximum in the superficial layer (0–150 m) in the SPG (between 125°W and 100°W). This DOC concentration was slightly higher than those measured in the surface waters of the upwelling ($100 \mu\text{moles.l}^{-1}$). The lowest surface concentrations ($<80 \mu\text{moles.l}^{-1}$) were found in the Marquesas area. Classical low DOC values ($<60 \mu\text{moles.l}^{-1}$) were measured at depths below 70 m in the Marquesas and upwelling regions, and only below 250–300 m in the central region. The DOC concentrations in deeper waters ($>500 \text{ m}$) presented no significant variations ($47 \pm 5 \mu\text{moles.l}^{-1}$) and were consistent with values found in various oceanic regions (Hansell and Carlson, 1998). The lowest value ($42.7 \mu\text{moles.l}^{-1}$) was measured at 3000 m (114°W – 26°S). DON concentrations were uniformly distributed in the photic layer and no subsurface maximum was observed. The general pattern of DON showed no significant geographical variation, with concentrations ranging from 5.5 to $6 \mu\text{moles.l}^{-1}$ throughout the 0–150 m water column, with the exception of the upwelling where concentrations reached $9 \mu\text{moles N.l}^{-1}$ near the surface. Classical low residual concentrations ($<3 \mu\text{moles.l}^{-1}$) were measured below 250 m. The lowest value (2.7 – $3 \mu\text{moles.l}^{-1}$) was measured below 1200 m. DOP exhibited a more variable distribution with two marked maxima at the eastern edge of the SPG and in the upwelling ($>0.2 \mu\text{moles.l}^{-1}$). Elsewhere, superficial values ranged between 0.10 and $0.15 \mu\text{moles.l}^{-1}$. The isoline $0.1 \mu\text{moles.l}^{-1}$ was generally located around 20 m with the exception of the upwelling region where it reached 100 m. DOP decreased rapidly below 250 m becoming abruptly, undetectable. Contrary to carbon and nitrogen, phosphorus is more quickly liberated from dead material (Menzel and Ryther, 1964; Clark et al., 1999). As a consequence, in the open ocean, the proportion of detrital P in the phosphorus pool is low (Faul et al., 2005), and no DOP was detected in the deep waters. Due to total inorganic nitrogen depletion DON accounted for almost 100% of the nitrogen in the surface water of the SPG, while DOP accounted for 20 to 50% of total phosphorus.

Another view of the geographical distribution of the major biogeochemical parameters can be demonstrated using the pattern of integrated values over the euphotic zone (Ze). The distribution of integrated nitrate (Fig. 10) confirms the main characteristic of the SPG, i.e. complete depletion of inorganic nitrogen. Integration over Ze was close to zero between 130 and 100°W . Integrated chlorophyll followed the same geographical trend, with very low values in the SPG, where Ze integration was lower than 10 mg m^{-2} . It should be noted that a large proportion of chlorophyll (up to 50%) was located below the 1% light penetration depth,

with the exception of the upwelling and Marquesas regions. Consequently, in the SPG, integrated Tchl-*a* over 1.5 Ze was twofold higher than content over Ze. In contrast to nitrate and chlorophyll, integrated particulate organic matter (in terms of POC, PON and POP) did not show a clear geographical gradient. Integrated values over Ze, remained more or less constant along the transect, except in the upwelling system, where values significantly increased. The ranges were 400–500, 50–75 and 2–4 mmoles m^{-2} for POC, PON and POP, respectively. In the upwelling, content increased significantly reaching 900, 180 and 10 mmoles m^{-2} for POC, PON and POP, respectively.

In contrast, integrated dissolved organic carbon (ΣDOC), dissolved organic nitrogen (ΣDON) and dissolved organic phosphate (ΣDOP), exhibited lowest values in the upwelling and Marquesas regions (5000, 500 and 15 mmoles m^{-2} , for ΣDOC , ΣDON and ΣDOP over the photic zone, respectively). The highest values were measured in the centre of the gyre between 115 and 105°W , where ΣDOC , ΣDON and ΣDOP reached 17 000, 900 and 30 mmoles m^{-2} , respectively. Over the photic layer, the integrated inorganic and organic dissolved nutrient data exhibited a clearly opposing trend in the South Pacific

4 Discussion

The BIOSOPE transect crossed the central region of the South Pacific, while extreme stations were influenced either by the Marquesas Islands or Chilean upwelling. As initially expected and confirmed by satellite imagery, the Central South Pacific Gyre is a very oligotrophic area (Claustre and Maritorena, 2003), characterized by a strong depletion in inorganic nitrogen and very low phytoplanktonic biomass. Since the development of sensitive analytical procedures, it has been shown that nitrate concentrations of subtropical surface waters over much of the world's oceans, including the subtropical gyres, is often at sub-micromolar concentrations (3 to $<50 \text{ nmoles.l}^{-1}$). Using a chemiluminescent method, Garside (1985) and Eppley et al. (1990) previously found nitrate concentrations $<10 \text{ nM}$ in the Sargasso Sea and in the subtropical Pacific. These concentrations, which would be depleted in a few hours by the ambient assemblages of phytoplankton, were low but not zero. For these authors, these residual concentrations were kept greater than zero due to some physical process such as atmospheric inputs and nighttime convection. We could assume that all of these processes occur at very low rates in the South Pacific Gyre (SPG) leading to a permanent and complete nitrate depletion (nitrate content over the photic layer was close to $0 \mu\text{moles m}^{-2}$). More, top-down wind-driven mixing of the water column seldom deepens the mixed layer below 100 m, and measurable increases of nitrate concentration in surface waters were unlikely over the year in the SPG, as the nitracline was below 160 m.

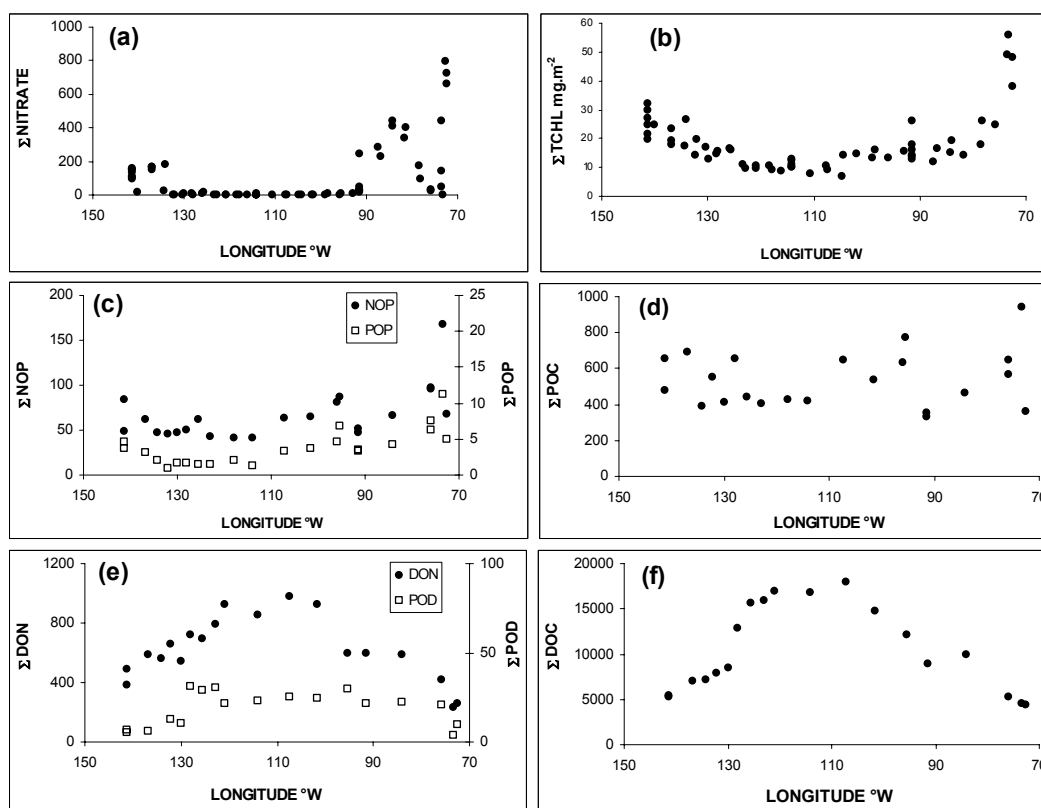


Fig. 10. Geographical distribution of nitrate (Σ nitrate), total chlorophyll-*a* (Σ TCHL), dissolved organic carbon (Σ DOC), dissolved organic nitrogen (Σ DON), dissolved organic phosphorus (Σ DOP), particulate organic carbon (Σ POC), particulate organic nitrogen (Σ PON) and particulate organic phosphorus (Σ POP) integrated over the photic zone ($Z_e=1\%$ surface light).

Similarly, the very low concentrations of nitrite and ammonium and the lack of a significant subsurface maximum, generally found in all stratified systems, were unexpected. It has been hypothesized that subsurface ammonium maxima are produced by local imbalances between ammonium regeneration and uptake, caused by active regeneration at the base of the photic zone where ammonium uptake by the phytoplankton is inhibited by low light intensities. In the present case, ammonium concentrations below the detection limit could be due to the lack of regeneration activity, or to a tight coupling between regeneration and ammonium uptake and ammonium oxidation (=nitrification). Brandhorst (1958) and Wada and Hattori (1971) suggested that nitrite originates from bacterial oxidation of ammonia. Vaccaro and Ryther (1960) first proposed that the appearance of nitrite near the nitracline would be caused by the reduction of nitrate by phytoplankton. Reasoning from laboratory experiments (Raimbault, 1986), argued that increases in nitrite concentrations are expected when phytoplankton starved of nitrogen, are exposed to increased concentrations of nitrate and decreased temperature and irradiances, such as those occurring at the base of the photic layer. The primary nitrite maximum generally occurs in a light limited regime where nitrate

is abundant and can define precisely the deep layer of the euphotic zone in which light becomes a limiting factor on primary production (Voituriez and Herbland, 1977). Thus, the primary nitrite maximum widely distributed in the ocean (Vaccaro and Ryther, 1960; Olson, 1981) has often been considered as an indicator of new production through phytoplankton excretion, or bacterial oxidation of organic matter, as well as a signature of the depth at which light limitation occurs (Ward et al., 1989). In a recent review, Lomas and Lipschultz (2006) concluded for the predominance of excretion from phytoplankton growing on nitrate, while bacterial nitrification likely playing only a supporting role. In return, the very low concentration of nitrite as observed at the base of the photic layer in the SPG, could reveal a very low diffusion of nitrate, as well as the lack of significant new production (nitrate uptake by phytoplankton) both in the DCM and in the nitracline.

In spite of the marked depletion in inorganic nitrogen leading to undetectable concentrations throughout the 0–160 m water column, phosphate concentrations, while being lower than those found near to the Marquesas Islands and Chilean coast, remained $>0.1 \mu\text{moles l}^{-1}$ in the SPG. The significant amounts of phosphate in the superficial nitrate-depleted

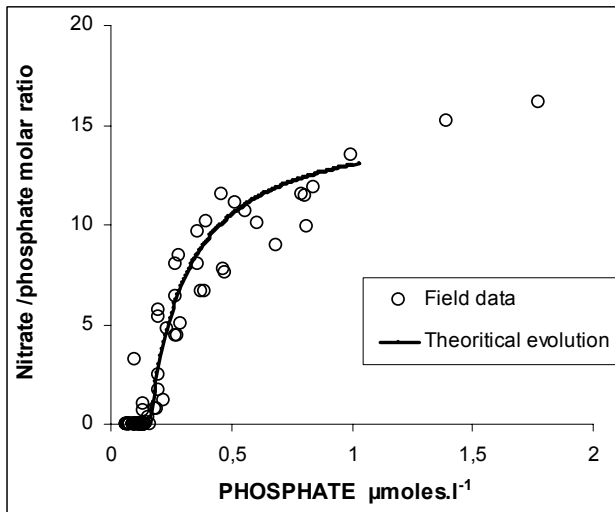


Fig. 11. Nitrate/phosphate ratio versus phosphate concentration in the SPG; Open circles=field data. The curve fits the theoretical relationship obtained from phosphate and nitrate utilization by phytoplankton, according to the Redfield ratio (15.5), of deep nutrients coming from below the photic zone with a nitrate:phosphate ratio ≈ 12 –13.

layer of this tropical region confirmed previous observations made at 150° W and 16° S (Raimbault et al., 1999c). The reason for this excess phosphate and/or the deficit in nitrate (around $2 \mu\text{moles l}^{-1}$ when applying the N/P Redfield ratio) is not clear. But it reflects the general feature of nitrate and phosphate distribution in the world ocean, where nutrient-depleted waters usually contain a small residue of phosphate (Tyrell, 1999). This has led to the biological concept that dissolved inorganic nitrogen (mainly nitrate) is the most limiting nutrient and that nitrogen dynamics are important for controlling phytoplankton productivity. However, the geochemists point of view would suggest that phosphate could be the ultimate limiting factor in aquatic systems, because of the nitrogen-fixers, which can use the available atmospheric dinitrogen. This scheme has been experimentally demonstrated in lakes, but not in the ocean (Smith, 1983). In return, according to this hypothesis, the residual phosphate found in the South east Pacific could demonstrate very low fixation of nitrogen, although available inorganic phosphorus offers favorable conditions for nitrogen-fixers. In fact low $\delta^{15}\text{N}$ in POM confirms that nitrogen fixation is an important process in the SPG, but the rates are too low to drive phosphate depletion (Raimbault and Garcia, 2007), at least during the season investigated here. It should be noted that nitrate/phosphate ratios were less than the Redfield's constant of 16 (Redfield et al., 1963) down to 400–500 m, indicating that the deep reservoir of nutrients was also nitrogen deficient. The eastern Pacific Ocean near the Chilean coast is one of the major areas of denitrification in the world oceans (Codispoti et al., 1976). Deutsch et al. (2001) argue that denitrification

inside the oxygen minimum zone of the Peru-Chilean upwelling generates nitrogen-deficient waters which carry surplus phosphorus. Due to the isolation of the SPG, nutrient input into the euphotic zone appears to be mainly through diffusive process, which in this case could bring in nitrate and phosphate with a low N/P ratio (around 12–13). This observation suggests that the biological utilization of deep nutrients by phytoplankton with a typical N/P requirement of 15.5 would decrease the N/P ratios to very low values. Our field data closely fit such a theoretical removal of nutrients (Fig. 11), suggesting that phytoplankton consumption of N-deficient nutrient pools would be the probable cause of such a phosphate residual value ($\approx 0.1 \mu\text{moles l}^{-1}$) in the photic layer.

The nitrate/silicic acid ratio (NO_3/Si) generally ranged between 1 and 4 over the whole transect except in the SPG, where nitrate depletion gave a ratio close to 0. A high NO_3/Si ratio (>5 and up to 8) was observed in the low salinity tongue located at 95° W. In comparison to the Redfield ratio and to the phytoplankton requirement (Fleming, 1940), these values indicate a deficit in silicic acid relative to nitrate (when detectable) in the 0–300 m superficial layer, especially in the euphotic zone. A strong deficit in silicic acid was noticeable in the western area near the upwelling zone. According to the elemental composition of diatoms, characterized by the N/Si ratio of 1 (Brzezinski, 1985), it is expected that diatoms will take up nutrients from surrounding waters with a similar ratio. Thus, values of NO_3/Si ratio higher than 1 may imply silicate-limitation.

Changes in the values and shapes of the chlorophyll profiles from west to east clearly show the expected differences in productivity driven by nutrient availability. The hyper oligotrophic centre of the SPG make up the clearest water of the world's ocean (Morel et al., 2007) and is characterized by extremely low surface Tchl-*a* concentrations ($<0.03 \mu\text{g l}^{-1}$). In this region, primary production was strongly nutrient limited considering the absence of terrestrial inputs (Jickells et al., 2005) and the depth of the nitracline (around 160–180 m). Nevertheless, the decrease in chlorophyll content between the upwelling and SPG was much lower (about four-fold) than the decrease in nitrate content (hundred to thousand fold). A chlorophyll maximum, permanently associated with the nitracline, was always detectable with values never lower than $0.20 \mu\text{g l}^{-1}$, at least ten-fold greater than measured in the upper layer. When the data was pooled no correlation was found between the magnitude of the DCM and nutrient concentration. Vertical distribution of POM was nearly always homogeneous without a subsurface maximum layer. With exception of the upwelling waters, the chlorophyll maximum was never associated with an increase of biomass in terms of carbon, nitrogen or phosphorus. Moreover, while surface concentrations reflected the oligotrophic conditions with lowest values in the SPG (by a factor 2), the integrated values over the photic zone did not reveal such marked trophic gradients. In fact, the photic layer of the SPG contains slightly

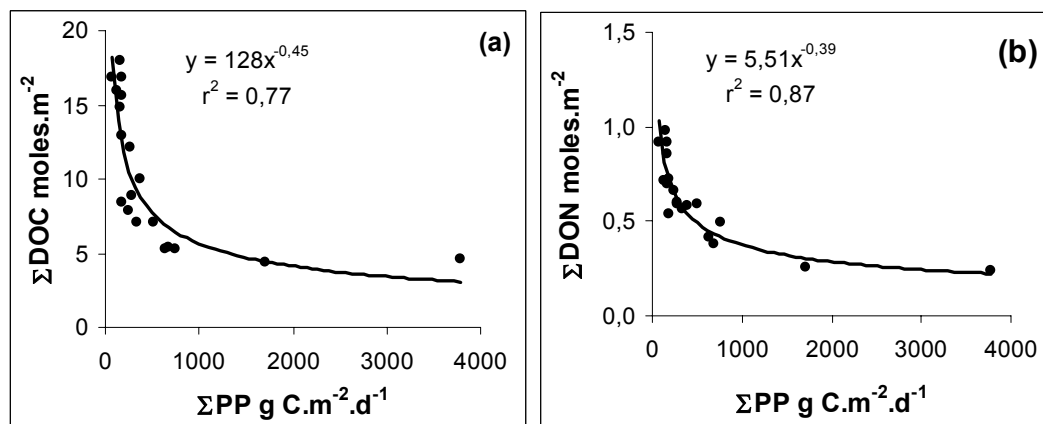


Fig. 12. Contents of dissolved organic carbon ((a): ΣDOC) and dissolved organic nitrogen ((b): ΣDON) over the photic layer versus integrated primary production (ΣPP).

less POM than the upwelling, but as much as the Marquesas areas. However, all of these oceanic regions were characterized by very different turnover times for particulate matter, as well as by different nitrogen sources as indicated by the natural abundance of $\delta^{15}\text{N}$. The SPG was characterized by particulate matter having very long residence times (20 days). However, values found in the upwelling and the Marquesas region (5 to 10 days) were close to those noted in the Central north Pacific (Laws et al., 1987) and in the equatorial Pacific (Eppley et al., 1992). The low $\delta^{15}\text{N}$ of PON (2‰) suggests a greater role of N_2 fixation in supporting production in the SPG, as typically observed in subtropical oceans (Minagawa and Wada, 1986), whereas a higher ratio (5–6‰) indicated a greater role of nitrate in the surrounding regions. Because $\delta^{15}\text{N}$ remained very low throughout the photic layer in the SPG, it is clear that (1) vertical mixing does not penetrate the nitracline, and (2) primary production in the superficial layer would be essentially supported by nitrogen regeneration and by N_2 -fixation (Raimbault and Garcia, 2007), both processes lower $\delta^{15}\text{N}$ values.

With the exception of the upwelling, POC and PON collected on $0.2\ \mu\text{m}$ membranes were higher than those retained on GF/F filters, confirming that the use of GF/F filters can greatly underestimate the concentration of particulate matter, especially in oceanic oligotrophic waters where the underestimation can be up to 50% (Altabet, 1990; Libby and Wheeler, 1997; Raimbault et al., 2000; Fernandez and Raimbault, 2007). However, the GF/F filters were proven to be efficient in collecting chlorophyll, so we can postulate that the organic matter in the $<0.7\ \mu\text{m}$ GF/F filtrate was essentially made up of carbon-rich particles ($\text{POC}/\text{PON} > 6.6$), but without chlorophyll.

The final unexpected result was the large dissolved organic matter (DOM) accumulation in the surface waters of the vast central region of the SPG. DON and DOP concentrations were similar to those generally observed in oceanic

waters of the Pacific Ocean (Karl et al., 1993; Raimbault et al., 1999) in spite of very low concentrations of inorganic nutrients. In contrast, our range of DOC found in the SPG ($>100\ \mu\text{moles l}^{-1}$) overlapped concentrations generally observed in surface oceanic waters and were about 10 to 20% higher than maximal values reported for the North Pacific Gyre (Church et al., 2002). Nevertheless, levels greater than $100\ \mu\text{moles l}^{-1}$ (up to $140\ \mu\text{moles l}^{-1}$) have been previously reported in the North Atlantic (Kepkey and Wells, 1992), although in this case, high DOC concentrations were associated with very high chlorophyll concentrations ($>10\ \mu\text{g l}^{-1}$). The marked geographical gradient suggests a net in situ source exists, mainly attributed to biological processes since this DOC accumulation was close to the surface layer where elevated primary production was observed (Raimbault and Garcia, 2007). This excess, much higher than the total particulate organic content, was greatest at the western edge of the SPG, associated with a high turnover rate of POM. The C:N ratio of the particles varied little along the transect, ranging from 5 to 7. In contrast, the global relationship between DOC and DON was significantly higher ($\text{DOC} = 10.14\ \text{DON} + 0.31$; $r^2 = 0.35$; $n = 250$). Excluding old recalcitrant DOM ($43\ \mu\text{moles l}^{-1}$ DOC, and $3\ \mu\text{moles l}^{-1}$ DON), the C/N ratio of the “freshly formed DOM” (excess DOM in surface water relative to deep water) was around 16–23, which is close to the range (20–23) found in the North Pacific by Kähler and Koeve (2001) and Karl and Tien (1997). In short, DOM with a C:N ratio far greater than Redfield’s value (low-N DOM or C-rich DOM) was accumulated in the surface water with a magnitude that increased exponentially with levels of oligotrophy as noted here by the rates of primary production (Fig. 12).

It has been assumed that the bulk of DOC (as well as DON and DOP) has its fundamental origin in surface ocean waters via such processes as phytoplankton excretion, lysis or solubility of living and detrital POM, and sloppy feeding

Table 3. Comparison of gradient and turbulent diffusion of nutrients through the thermocline, calculated from vertical diffusion coefficients ($K_z=0.76\pm 0.81\text{ m}^2\text{ d}^{-1}$) and gradients of organic (dissolved organic carbon=DOC, dissolved organic nitrogen=DON and dissolved organic phosphorus=DOP) or inorganic nutrients (nitrate, phosphate) in the SPG (122° W – 101° W). Upward fluxes are considered as positive and downward fluxes as negative.

	Gradient $\mu\text{moles m}^{-4}$	Diffusive fluxes $\mu\text{moles m}^{-2}\text{ d}^{-1}$
Nitrate	75 ± 22	$+57.4\pm 10$
Phosphate	5.9 ± 2	$+4.5\pm 1.1$
DOC	176	-134
DON	6.6	-5
DOP	0.4	-0.3

at various trophic levels. Therefore this DOC concentration is the result of a large array of production, consumption and transformation processes due to biological activity (Williams, 1975). Phytoplankton are the major producers (Biersmith and Benner, 1998) releasing 5–10% of the total photosynthetic carbon production under rapid growth conditions, and considerably more under nutrient limited growth, because carbon fixation may exceed incorporation into cell material (Carlson, 2002). DOC production is also influenced by the phytoplankton community composition (Bidanda and Benner, 1997) and is greatly enhanced by grazing of protists and copepods (Strom et al., 1997). Biological release of DOC and DON during field experiments has been reported for different types of marine waters (Karl et al., 1998; Bronk and Glibert, 1993; Bronk and Glibert, 1994; Bronk et al., 1994; Raimbault et al., 1999b; Fernandez and Raimbault, 2007). In a tightly coupled system with a rapid turnover, a fraction of this DOC is labile and will fuel heterotrophic and photo-heterotrophic production. But, over longer time scales, biological production and accumulation of DOC and DON seem to be evident in oceanic regions (Avril, 2002; Libby and Wheeler, 1997), processes which would be favoured by nutrient depletion (Kähler and Koeve, 2001). In seasonal studies of the dynamics of inorganic and organic nitrogen, Buttler et al. (1979), Maita and Yanada (1990) and Libby and Wheeler (1997) found an inverse relationship between nitrate concentration and DON in the English channel, the sub arctic Pacific water, and in the Equatorial Pacific, respectively. Zweifel et al. (1993) showed that the addition of nutrients to samples from a nutrient-depleted system promoted DOC breakdown, which also implies that the lack of nutrients favours DOC preservation. Cauwet et al. (2002) reported that during nutrient deficiency, bacteria are unable to utilize a carbon-rich organic substrate like carbohydrates. Therefore as suggested by Thingstad et al. (1997) and Tanaka and Rassoulzadegan (2002), this surface accumulated DOC could indicate long term mal-

functioning of the microbial loop; this could be related to bacteria-phytoplankton competition for inorganic nutrients that reduce DOC remineralization in nutrient-depleted water.

According to Eppley and Peterson (1979), annual new production must balance the organic particle flux from the euphotic zone to the deep waters. Thus, particulate export in the sea is traditionally considered to vary with new production, increasing with the input of nitrate from deep waters that penetrates through the nitracline. Under ecological conditions where large amounts of DOM are produced in response to inorganic nutrient limitation, such as those described in this study, the traditional particulate matter biological pump may be completed with the export of dissolved matter (Copin-Montégut and Avril, 1993; Carlson et al., 1994; Toggweiler, 1989). Several studies in oceanic environments have shown DOC accumulation over the productive period in the upper water column where it is homogenized. This DOC, accumulates from summer to autumn, then disappears from the surface layer during destratification and winter mixing (Copin-Montégut and Avril, 1993; Carlson et al., 1994). Except some Ekman wind-driven circulation which can lead to lateral transport of significant part of DOM (Roussenov et al., 2006; Mahaffey et al., 2004), horizontal advection can be neglected in the centre of the SPG that can be considered as at rest. Intense seasonal convective mixing is excluded enabling the SPG to maintain high DOC concentrations and act as a large and a long-term reservoir of biological carbon. Another route for DOC transfer is via the diffusive mode, which could persist in this permanent stratified water. Assuming that nutrient flux (inorganic or inorganic) in or out of the mixed layer is linearly correlated to the gradient ($\delta\text{nutrient}/\delta z$, units= $\mu\text{mol m}^{-4}$) from the bottom of the mixed layer by a vertical diffusion coefficient (K_z ; units= $\text{m}^2\text{ d}^{-1}$), we can calculate the diffusive vertical fluxes ($F_{\text{nutrients}}$; units $\mu\text{mol m}^{-2}\text{ d}^{-1}$) using the following equation: $F_{\text{nutrient}}=K_z \delta\text{Nutrient}/\delta z$.

K_z is the diffusion coefficient obtained from the following equation: $K_z=0.24 \varepsilon/N^2$, where ε (units, $\text{m}^{-2}\text{ s}^{-3}$) is the turbulent kinetic energy dissipation and N (units, s^{-1}) is the buoyancy (Brünt-Väisälä) frequency (Oakey, 1982). Values for ε as well as for K_z are rarely experimentally available, especially in oceanic waters. However, assuming the only nitrate source for phytoplankton growth comes from deep water via turbulent diffusion, we can propose that the biological nitrate uptake is equal to this diffusive flux, as suggested by King and Devol (1979). Using integrated nitrate uptake rates measured in the SPG ($60\ \mu\text{moles m}^{-2}\text{ d}^{-1}$; Raimbault and Garcia, 2007) and nitrate gradients from the top of the thermocline ($75.4\pm 22\ \mu\text{moles m}^{-4}$), the K_z value is estimated ($0.76\pm 0.81\text{ m}^2\text{ d}^{-1}=0.09\pm 0.1\text{ cm}^2\text{ s}^{-1}$). This value agrees with previous results obtained from oceanic waters (Eppely et al., 1979; King and Devol, 1979; Lewis et al., 1986) ranging from 0.06 to $0.75\text{ cm}^2\text{ s}^{-1}$. The diffusive fluxes of inorganic and organic dissolved nutrients in the SPG calculated using this K_z value, are presented in

Table 3. Turbulent fluxes for DOC, DON and DOP are estimated to be 134, 5 and 0.3 $\mu\text{moles m}^{-2} \text{d}^{-1}$, respectively. These DOC and DON fluxes were equivalent to the particle flux measured simultaneously, using drifting sediment traps placed just below the photic zone ($12\text{--}96 \mu\text{moles C m}^{-2} \text{d}^{-1}$; $2.8\text{--}14 \mu\text{moles N m}^{-2} \text{d}^{-1}$, J. C. Miquel, personal communication). When considering the mean primary production in the SPG ($0.15 \text{ g m}^{-2} \text{d}^{-1}$; Raimbault and Garcia, 2007), this calculated downward DOC flux represents a low proportion of the total primary production ($\approx 2\%$), but a large fraction (34%) of the new production as calculated from integrated nitrate uptake ($60 \times 6.6 = 396 \mu\text{moles C m}^{-2} \text{d}^{-1}$). Assuming these values are constant throughout the year, we can deduce an annual diffusive export of $0.44 \text{ g C m}^{-2} \text{y}^{-1}$, a lower value than that obtained by Avril (2002) for the Mediterranean sea during the oligotrophic stratified period ($1 \text{ g C m}^{-2} \text{y}^{-1}$). Global DOC export (vertical mixing+turbulent mixing) is estimated to be 1.7 GT/year (Six and Maier-Reimer, 1996), a value consistent with the oceanic “missing” CO_2 sink quantified to be about 1.8 GT C.y^{-1} (Siegenthaler and Sarmiento, 1993). According to Avril (2002) about 10% ($170 \times 10^6 \text{ T.y}^{-1}$) of this global DOC export could be due to diffusion processes. The diffusive export of the entire South Pacific gyre, representing 1.1% of the global oceanic surface (4.10^6 km^2), is estimated to be about $2.5 \times 10^6 \text{ TC}$ and could represent about 1.5% of the global DOC diffusive flux. Assuming DOC release rates are 4 to 10% of gross production, levels generally reported in the literature (Mingelbier et al., 1994) and a 2% loss by diffusion (see above), the excess DOC in the centre of the SPG ($10\,000 \text{ mmoles C m}^{-2} = 120 \text{ g C m}^{-2}$) would correspond to an accumulation over a period of 41 to 124 years. Therefore our present calculation suggests a significant role of the SPG in the global biogeochemical budget of carbon, for (1) long-term storage in surface waters and (2) significant export to deep water.

5 Conclusions

As expected from satellite imagery, the South Pacific Gyre (SPG) transected by the BIOSOPE cruise, is a very oligotrophic area characterized by a strong depletion of inorganic nitrogen and very low phytoplanktonic biomass. The distribution of hydrological parameters and inorganic nutrients clearly showed that the organic parameters (particulate or dissolved) varied much less than might be expected from nutrient distributions. The most important feature observed was the large accumulation of dissolved organic matter, reflecting the specific functioning of the productivity system and the biological CO_2 pump. The SPG can store and preserve a large quantity of low-N organic material in the photic layer. The surface waters of the SPG, once described as a “monotonous and unchanging oceanic desert” (Claustre and Maritorea, 2003), could be home to a dynamic ecosystem

exhibiting high accumulation of carbon-rich dissolved organic matter. The concept of new production and the Redfield constant appears to be strongly influenced by carbon dynamics and was not linearly coupled with that of nitrogen. Moreover, assuming that there is no real steady-state for carbon cycling, a large quantity of atmospheric carbon, fixed by photosynthesis, can ultimately be accumulated over long periods in the surface layer and not immediately exported. Consequently understanding both the DOC production rates and the chemical composition of this accumulated pool is essential before accurate biogeochemical and metabolic models can be formulated for this ultra-oligotrophic system of the South Pacific Gyre.

Acknowledgements. This is a contribution of the BIOSOPE project of the LEFE-CYBER program, funded by the Centre National de la recherche Scientifique (CNRS), the Institut des Sciences de l’Univers (INSU), the Centre National d’Etudes Spatiales (CNES), The European Space Agency (ESA), the National Aeronautics and Space Administration (NASA) and the natural Sciences and Engineering Research Council of Canada (NSERC). This work is fund in part by the French Research and Education Council. The Biosope cruise program was managed by H. Claustre and A. Sciandra. We thank the crew of the R/V Atalante for outstanding shipboard support operations. Data concerning Euphotic Layer Depths was kindly provided by H. Claustre and J. Ras. D. Taillez and C. Bournot are thanked for their efficient help in CTD rosette management and data processing, as is J. C. Miquel for providing particulate samples from an in situ pump. The authors gratefully thank the two anonymous referees who helped to make substantial improvements in the manuscript and T. Bentley for her linguistic and scientific advice.

Edited by: S. Pantoja

References

- Altabet, M.: Organic C, N and stable isotopic composition of particulate matter collected on glass-fibre and aluminium oxide filters, *Limnol. Oceanogr.*, 35, 902–909, 1990.
- Altabet, M. A. and McCarthy, J. J.: Vertical patterns in ^{15}N natural abundance in PON from the surface waters of warm-core rings, *J. Mar. Res.*, 44, 203–225, 1986.
- Andrié, C., Bouloubassi, I., Cornu, H., Fichez, R., Pierre, C., and Rougerie, F.: Chemical tracer studies in coral reef interstitial waters (French Polynesia), Implications for endo-upwelling circulation, in: *Proceedings of the 7th Coral Reef International Symposium*, edited by: Richmond, R. H., Univ of Guam press, 1165–1173, 1993.
- Armstrong, F. A. J., Stearns, C. R., and Strickland, J. D. H.: The measurement of upwelling and subsequent biological processes by means of the Technicon AutoAnalyzer and associated equipment, *Deep-Sea Res.*, 14(3), 381–389, 1967.
- Avril, B.: DOC dynamics in the northwestern Mediterranean Sea (DYFAMED Site), *Deep-Sea Res.*, 49, 2163–2182, 2002.
- Biddanda, D. and Benner, R.: Carbon, nitrogen and carbohydrate fluxes during the production of particulate and dissolved organic

- matter by marine phytoplankton, *Limnol. Oceanogr.*, 42, 506–518, 1997.
- Biersmith, A. and Benner, R.: Carbohydrates in phytoplankton and freshly produced dissolved organic matter, *Mar. Chem.*, 63, 131–144, 1988.
- Brzezinski, M. A.: Vertical distribution of ammonium in stratified oligotrophic waters, *Limnol. Oceanogr.*, 33, 1176–1182, 1988.
- Brandhorst, W.: Nitrite accumulation in the north-east tropical Pacific, *Nature*, London, 182, 679, doi:10.2038/182179aO, 1958.
- Bronk, D. A. and Glibert, P. M.: Application of a ^{15}N tracer method to the study of dissolved organic nitrogen uptake during spring and summer in Chesapeake Bay, *Mar. Biol.*, 115, 501–508, 1993.
- Bronk, D. A. and Glibert, P. M.: The fate of missing ^{15}N differs among marine systems, *Limnol. Oceanogr.*, 39, 189–194, 1994.
- Bronk, D. A., Glibert, P. M., and Ward, B. B.: Nitrogen uptake, dissolved organic nutrient release and new production, *Science*, 256, 1843–1846, 1994.
- Butler, E. I., Knox, S., and Liddcoat, M. I.: The relationship between inorganic and organic nutrients in seawater, *J. Mar. Biol. Assoc. UK*, 59, 239–250, 1979.
- Carlson, C. A.: Production and removal processes, in: *Biogeochemistry of marine dissolved organic matter*, edited by: Hansell, D. A. and Carlson, C.A., Academic press, Amsterdam, 91–151, 2000.
- Carlson, C. A., Ducklow, H. W. and Michaels, A. F.: Annual flux of dissolved organic carbon from the euphotic zone in the north-western Sargasso Sea, *Nature*, 371, 405–408, 1994.
- Carr, M. E.: Estimation of potential productivity in eastern boundary current using remote sensing, *Deep-Sea Res. Pt. II*, 49, 59–80, 2002.
- Cauwet, G., Déliat, G., Krastev, A., Shtereva, G., Becquevort, S., Lancelot, C., Momzikoff, A., Saliot, A., Cociasu, A., and Popa, L.: Seasonal DOC accumulation in Black Sea: a regional explanation for a general mechanism, *Mar. Chem.*, 79, 193–205, 2002.
- Chavez, F. P., Buck, K. R., Bidigare, R. R., Karl, D. M., Hebel, D., Latasa, M., and Campbell, L.: On the chlorophyll *a* retention properties of glass-fiber GF/F filters, *Limnol. Oceanogr.*, 40, 428–433, 1995.
- Chekley, D. M. and Miller, C. A.: Nitrogen isotope fractionation by oceanic zooplankton, *Deep-Sea Res.*, 36, 1449–1456, 1989.
- Church, M. J., Ducklow, H. W., and Karl, D. M.: Multiyear increases in dissolved organic matter inventories at station ALOHA in the North Pacific subtropical gyre, *Limnol. Oceanogr.*, 47, 1–10, 2002.
- Clark, L., Ingall, E. D., and Benner, R.: Marine organic phosphorus cycling: Novel insights from nuclear magnetic resonance, *Am. J. Sci.*, 299, 724–737, 1999.
- Claustre, H. and Maritorena, S.: Ocean Science: The many shades of ocean blue, *Science*, 302, 1514–1515, 2003.
- Claustre, H., Sciandra, A., and Vaultot, D.: Introduction to the special section: bio-optical and biogeochemical conditions in the South east Pacific late 2004 – the BIOSOPE cruise, *Biogeosciences Discuss.*, 5, 605–640, 2008, <http://www.biogeosciences-discuss.net/5/605/2008/>.
- Cline, J. D. and Kaplan, I. R.: Isotopic fractionation of dissolved nitrate during denitrification in the eastern tropical North Pacific Ocean, *Mar. Chem.*, 3, 271–299, 1975.
- Copin-Montégut, G. and Avril, B.: Vertical distribution and temporal variation of dissolved organic carbon in the North-Western Mediterranean Sea, *Deep-Sea Res.*, 40, 1963–1972, 1993.
- Copin-Montégut, C. and Copin-Montégut, G.: The chemistry of particulate matter from the south Indian and Antarctic oceans, *Deep-Sea Res.*, 25, 911–931, 1978.
- Dandonneau, Y., Montel, Y., Blanchot, J., Giraudeau, J., and Neveux, J.: Temporal variability in phytoplankton pigments, picoplankton and coccolithophores along a transect through the North Atlantic and tropical southwestern Pacific, *Deep-Sea Res. Pt. I*, 53, 689–712, 2006.
- Daneri, G. and Quinones, R. A.: Undersamples ocean systems: appeal for an international study of biogeochemical cycles in the Southern Pacific gyre and its boundaries, *U.S. JGOFS Newsletter January 2001*: 9, 2001.
- Denman, K. L. and Gargett, A. E.: Time and space scales of vertical mixing and advection of phytoplankton in the upper ocean, *Limnol. Oceanogr.*, 28, 801–815, 1983.
- Deutsch, C., Gruber, R., Key, R. M., Sarmiento, J. L., and Ganachaud, A.: Denitrification and N_2 fixation in the Pacific ocean, *Global Biogeochem. Cy.*, 15, 483–506, 2001.
- Dickson, M. L. and Wheeler, P. A.: Chlorophyll *a* concentrations in the north Pacific: Does a latitudinal gradient exist?, *Limnol. Oceanogr.*, 38, 1813–1818, 1993.
- Dore, J. E., Brum, J. R., Tupas, L. M., and Karl, D. M.: Seasonal and interannual variability in sources of nitrogen supporting export in the oligotrophic subtropical North Pacific Ocean, *Limnol. Oceanogr.*, 47, 1595–1607, 2002.
- Eppley, R. C., Chavez, F. and Barber, R.: Standing stocks of particulate carbon and nitrogen in the Equatorial Pacific at 150°W , *J. Geophys. Res.*, 97, 655–661, 1992.
- Eppley, R. W., Garside, C., Renger, R. W., and Orellana, E.: Variability of nitrate concentration in nitrogen-depleted subtropical surface waters, *Mar. Biol.*, 107, 53–60, 1990.
- Eppley, R. W. and Peterson, B. J.: Particulate organic matter flux and planktonic new production in the deep ocean, *Nature*, 282, 677–680, 1979.
- Eppley, R. W., Renger, E. G., and Harrison, W. G.: Nitrate and phytoplankton production in southern California coastal waters, *Limnol. Oceanogr.*, 24, 483–494, 1979.
- Faul, K. L., Paytan, A., and Delaney, M. L.: Phosphorus distribution in sinking oceanic particulate matter, *Mar. Chem.*, 97, 307–333, 2005.
- Fernandez, C. and Raimbault, P.: Nitrogen regeneration in the NE Atlantic Ocean and its impact on seasonal new, regenerated and export production, *Mar. Ecol.-Prog. Ser.*, 337, 79–92, 2007.
- Fleming, R. H.: The composition of plankton and units for reporting population and production, 6th Pacific Science Congress, 5, 535–540, 1940.
- Garside, C.: A chemoluminescent technique for the determination of nanomolar concentrations of nitrate and nitrite in seawater, *Mar. Chem.*, 11, 159–167, 1982.
- Garside, C.: The vertical distribution of nitrate in open ocean water, *Deep-Sea Res.*, 32, 723–732, 1985.
- Grob, C., Ulloa, O., Claustre, H., Alarcon, G., Huot, Y., and Marie, D.: Contribution of picoplankton to the particulate attenuation coefficient (*cp*) and organic carbon concentration (*POC*) in the eastern South Pacific, *Biogeosciences*, 4, 837–852, 2007, <http://www.biogeosciences.net/4/837/2007/>.

- Holmes, M. R., Aminot, A., Kerouel, R., Hooker, B. A., and Peterson, J. B.: A simple and precise method for measuring ammonium in marine and freshwater ecosystems, *Can. J. Fish. Aquat. Sci.*, 56, 1801–1808, 1999.
- Hoch, M. M. P., Fogel, M. L., and Kirchman, D. L.: Isotope fractionation associated with ammonium uptake by marine bacterium, *Limnol. Oceanogr.*, 37, 1447–1459, 1992.
- Hansell, D. A. and Carlson, C. A.: Deep ocean gradients in the concentration of dissolved organic carbon, *Nature*, 395, 263–266, 1998.
- Jickells, T. D., An, Z. S., Andersen, K. K., et al.: Global iron connections between desert dust, ocean biogeochemistry and climate, *Science*, 30, 67–71, 2005.
- Kähler, P. and Koeve, W.: Marine dissolved organic matter: can its C:N ratio explain carbon over consumption?, *Deep-Sea Res. Pt. I*, 48, 49–62, 2001.
- Karl, D. M.: Nutrients dynamics in the deep blue sea, *Trends Microbiol.*, 10, 410–418, 2002.
- Karl, D. M., Tien, G., Dore, J., and Winn, D.: Total dissolved nitrogen and phosphorus concentrations at US-JGOFDS Station ALOHA: Redfield reconciliation, *Mar. Chem.*, 41, 203–208, 1993.
- Karl, D. M. and Tien, G.: Temporal variability in dissolved phosphorus concentrations in the subtropical North Pacific Ocean, *Mar. Chem.*, 56, 77–96, 1997.
- Karl, D. M., Hebel, D. V., and Björkman, K.: The role of dissolved organic matter release in the productivity of the oligotrophic North Pacific Ocean, *Limnol. Oceanogr.*, 43, 1270–1286, 1998.
- Kepkay, P. E. and Wells, M. L.: Dissolved organic carbon in the North Atlantic surface waters, *Mar. Ecol.-Progr. Ser.*, 80, 275–283, 1992.
- King, F. D. and Devol, A. H.: Estimates of vertical eddy diffusion through the thermocline from phytoplankton nitrate uptake rates in the mixed layer of the eastern pacific, *Limnol. Oceanogr.*, 24, 645–651, 1979.
- Kirkwood, D. S.: Stability of solutions of nutrients salts during storage, *Mar. Chem.*, 38, 151–164, 1992.
- Law, E. A., DiTullio, G. R., Betzer, P. R., Karl, D. M. and Carder, K. L.: Autotrophic production and elemental fluxes at 26° N, 155° W in the north pacific subtropical gyre, *Deep-Sea Res.*, 36, 103–120, 1987.
- Lewis, M. R., Harrison, W. G., Oakey, N. S., Hebert, D., and Platt, T.: Vertical nitrate fluxes in the oligotrophic ocean, *Science*, 234, 870–872, 1986.
- Libby, P. S. and Wheeler, P. A.: Particulate and dissolved organic nitrogen in the central and eastern Equatorial Pacific, *Deep-Sea Res.*, 44, 345–361, 1996.
- Liu, K. K. and Kaplan, I. R.: The eastern tropical north Pacific as a source of ¹⁵N-enriched nitrate in seawater off Southern California, *Limnol. Oceanogr.*, 34, 820–830, 1989.
- Lomas, M. W. and Lipschultz, F.: Forming the primary nitrite maximum: nitrifiers or phytoplankton?, *Limnol. Oceanogr.*, 51, 2453–2467, 2006.
- Longhurst, A. R.: *Ecological geography of the Sea*, Academic press, London, 398 pp., 1998.
- Mahaffey, C., Williams, R., and Wolf, G.: Physical supply of nitrogen to phytoplankton in the Atlantic Ocean, *Global Biogeochem. Cy.*, 18, GB1034, doi:10.1029/2003GB002129, 2004.
- Maita, Y. and Yanada, M.: Vertical distribution of total dissolved nitrogen and dissolved organic nitrogen in seawater, *Geochemical J.*, 24, 245–254, 1990.
- McCarthy, J. I.: Nitrogen and phytoplankton ecology, in: *The physiological ecology of phytoplankton*, edited by: Morris, I., Blackwell, 191–233, 1980.
- Menzel, D. W. and Ryther, J. H.: The composition of particulate organic matter in the western north Atlantic, *Limnol. Oceanogr.*, 9, 179–186, 1964.
- Minagawa, M. and Wada, E. Z.: Nitrogen isotopes ratios of red tide organisms in the east China Sea: A characterization of biological nitrogen fixation, *Mar. Chem.*, 19, 245–259, 1984.
- Mingelbier, A., Klein, B., Claereboudt, R., and Legendre, L.: Measurement of daily primary production using 24 h incubations with the 14C method: a caveat, *Mar. Ecol.-Progr. Ser.*, 113, 301–309, 1994.
- Montoya, J. P. and McCarthy, J. J.: Isotopic fractionation during nitrate uptake by phytoplankton grown in continuous culture, *J. Plankton Res.*, 17, 439–464, 1995.
- Morel, A. and Maritorena, S.: Bio-optical properties of oceanic waters: a reappraisal, *J. Geophys. Res.*, 106(C4), 7163–7180, 2001.
- Morel, A., Gentili, B., Claustre, H., Babin, M., Bricaud, A., Ras, J., and Tiedeche F.: Optical properties of the clearest natural waters, *Limnol. Oceanogr.*, 52, 217–229, 2007.
- Oakey, N. S.: Determination of the rate of dissipation of turbulent energy from simultaneous temperature and velocity shear microstructure measurements, *J. Phys. Oceanogr.*, 12, 256–271, 2002.
- Olson, R. J.: Differential photoinhibition of marine nitrifying bacteria: a possible mechanism for the formation of the primary nitrite maximum, *J. Mar. Res.*, 39, 227–238, 1981.
- Raimbault, P.: Effect of temperature on nitrite excretion by three marine diatoms during nitrate uptake, *Mar. Biol.*, 92, 149–155, 1986.
- Raimbault, P. and Garcia, N.: Carbon and nitrogen uptake in the South Pacific Ocean: Evidence for efficient dinitrogen fixation and regenerated production leading to large accumulation of dissolved organic matter in nitrogen-depleted waters, *Biogeosciences Discuss.*, 4, 3531–3579, 2007, <http://www.biogeosciences-discuss.net/4/3531/2007/>.
- Raimbault, P., Slawyk, G., Coste, B., and Fry, J.: Feasibility of using an automated colorimetric procedure for the determination of seawater nitrate in the 0 to 100 nM range: Examples from field and culture. *Mar. Biol.*, 104, 347–351, 1990.
- Raimbault, P., Pouvesle, W., Sempéré, R., Diaz F., and Garcia, N.: A simple procedure for simultaneous analysis of total and dissolved organic forms of carbon, nitrogen and phosphorus in seawater using the wet-oxidation technique, *Mar. chem.*, 66, 161–169, 1999.
- Raimbault, P., Diaz, F., and Boudjellal, B.: Simultaneous determination of particulate forms of carbon, nitrogen and phosphorus collected on filters using a semi-automatic wet-oxidation procedure, *Mar. Ecol.-Progr. Ser.*, 180, 289–295, 1999.
- Raimbault, P., Slawyk, G., Boudjellal, B., Coatanoan, C., Conan, P., Coste, B., Garcia, N., Moutin, T., and Pujo-Pay, M.: Carbon and nitrogen uptake and export in the equatorial pacific at 150° W: Evidence of an efficient regenerated production cycle, *J. Geophys. Res.*, 104(C2), 3341–3356, 1999.

- Raimbault, P., Slawyk, G., and Garcia, N.: Comparison between chemical and isotopic measurements of biological nitrate utilization: further evidence of low new production levels in the equatorial Pacific, *Mar. Biol.*, 136, 1147–115, 2000.
- Raimbault, P., Neveux, J. and Lantoiné, F.: Dosage rapide de la chlorophylle *a* et des phaeopigments *a* par fluorimétrie après extraction au méthanol, Comparaison avec la méthode classique d'extraction à l'acétone, *Oceanis*, 30(2), 189–205, 2004.
- Ras, J., Claustre, H., and Uitz, J.: Spatial variability of phytoplankton pigment distributions in the subtropical South Pacific Ocean: a comparison between in situ and modelled data, *Biogeosciences Discuss.*, 4, 3409–3451, 2007.
- Redfield, A. C., Ketchum, B. H., and Richards, F. A.: The influence of organisms on the composition of seawater, in: *The Sea* Wiley, edited by: Hill, M. N., 26–77, 1963.
- Roussinov, V., Williams, R. G., Mahaffey, C., and Wolff, G. A.: Does the transport of dissolved organic nutrients affect export production in the Atlantic Ocean?, *Global Biogeochem. Cy.*, 20, GB3002, doi:10.1029/2005GB002510, 2006.
- Sahlsten, E.: Nitrogen nutrition in the euphotic zone of the central north Pacific gyre, *Mar. Biol.*, 96, 433–439, 1987.
- Siegenthaler, U. and Sarmiento, J. L.: Atmospheric carbon dioxide and the ocean, *Nature*, 365, 119–125, 1993.
- Signorini, S. R., McClain, C. R., and Dandonneau, Y.: Mixing and phytoplankton bloom in the wake of Marquesas Islands, *Geophys. Res. Lett.*, 26, 3121–3214, 1999.
- Six, K. D. and Maier-Reimer, E.: Effects of plankton dynamics on seasonal carbon fluxes in an ocean general circulation model, *Global Biogeochem. Cy.*, 10(4), 559–583, 1996.
- Smith, S. V.: Phosphorus versus nitrogen limitation in the marine environment, *Limnol. Oceanogr.*, 29, 1149–1160, 1983.
- Strom, S. L., Benner, R., Ziegler, S., and Magg, M. J.: Planktonic grazers are potentially important source of marine dissolved organic carbon, *Limnol. Oceanogr.*, 42, 1364–1374, 1997.
- Tanaka, T. and Rassoulzadegan, F.: Full-depth profile (0–2000 m) of bacteria, heterotrophic nanoflagellates and ciliates in the NW Mediterranean Sea: Vertical partitioning of microbial trophic structures, *Deep-Sea Res.*, 49, 2093–2107, 2002.
- Thingstad, T. F., Hagstrom, A., and Rassoulzadegan, F.: Accumulation of degradable DOC in surface waters: is it caused by malfunctioning microbial loop?, *Limnol. Oceanogr.*, 42, 398–404, 1997.
- Toggweiler, J. R.: Is the downward dissolved organic matter (DOM) flux important in carbon export, in: *Productivity of the ocean: Present and past*, edited by: Berger, W. H., Smetacek, V. S., and Wefer, G., Wiley-Intersci., New-York, 65–84, 1989.
- Tréguer, P. and LeCorre, P.: Manuel d'analyses des sels nutritifs dans l'eau de mer: Utilisation de l'Autoanalyseur II Technicon, Univ. of Bretagne Occidentale, Lab. de Chim. Mar., Brest, France, 1975.
- Tyrrell, T.: The relative influence of nitrogen and phosphorus on oceanic primary production, *Nature*, 400, 525–531, 1999.
- Vaccaro, R. F. and Ryther, J. H.: Marine phytoplankton and the distribution of nitrite in the sea, *J. Cons. Perm. Int. Explor. Mer.*, 26, 260–271, 1960.
- Voituriez, B. and Herbland, A.: Production primaire, nitrate, nitrite dans l'Atlantique tropical, II Distribution du nitrate et production du nitrite, *Cah. ORSTOM, Sér. Océanogr.*, 15, 57–66, 1997.
- Wada, E. and Hattori, A.: Nitrite metabolism in the euphotic zone of the central Pacific Ocean, *Limnol. Oceanogr.*, 16, 766–772, 1971.
- Wada, E. and Hattori, A.: Natural abundance of ^{15}N in particulate organic matter in the North Pacific Ocean, *Geochim. Cosmochim. Ac.*, 40, 249–251, 1976.
- Ward, B. B., Kilpatrick, K. A., Renger, E., and Eppley, R. W.: Biological cycling in the nitracline, *Limnol. Oceanogr.*, 34, 493–513, 1989.
- Waser, N. D. A., Harrison, W. C., Head, E.J.H., Nielsen, B., Lutz, V. A., and Calvert, S. E.: Geographic variations in the nitrogen isotope composition of surface particulate nitrogen and new production across the North Atlantic Ocean, *Deep-Sea Res.*, 47, 1207–1226, 2000.
- Welschmeyer, N. A.: Fluorometric analysis of chlorophyll *a* in the presence of chlorophyll *b* and pheopigments, *Limnol. Oceanogr.*, 39(8), 1985–1992, 1994.
- Williams, P. J. le B.: Biological and chemical aspects of dissolved material in sea water, in: *Chemical Oceanography*, 2nd Edition, Vol. 2, edited by: Riley, J. P. and Skirrow, G., Academic Press London, 301–362, 1975.
- Zweifel, U. L., Norman, B., and Hagstrom, A.: Consumption of dissolved organic carbon by bacteria and demand for inorganic nutrients, *Mar. Ecol.-Prog. Ser.*, 101, 23–32, 1993.

Phosphate availability and the ultimate control of new nitrogen input by nitrogen fixation in the tropical Pacific Ocean

T. Moutin¹, D. M. Karl², S. Duhamel¹, P. Rimmelin¹, P. Raimbault¹, B. A. S. Van Mooy³, and H. Claustre⁴

¹Laboratoire d'Océanographie et de Biogéochimie, UMR-CNRS 6535, Campus de Luminy, 13 288 Marseille Cedex 09, France

²Department of Oceanography, University of Hawaii, Honolulu, HI 96822, USA

³Department of Marine Chemistry and Geochemistry, Woods Hole Oceanographic Institution, Massachusetts, MA 02543, USA

⁴Laboratoire d'Océanographie de Villefranche, CNRS-INSU and UPMC, BP 08, 06238 Villefranche-sur-mer, France

Received: 19 July 2007 – Published in Biogeosciences Discuss.: 26 July 2007

Revised: 30 November 2007 – Accepted: 13 December 2007 – Published: 29 January 2008

Abstract. Due to the low atmospheric input of phosphate into the open ocean, it is one of the key nutrients that could ultimately control primary production and carbon export into the deep ocean. The observed trend over the last 20 years has shown a decrease in the dissolved inorganic phosphate (DIP) pool in the North Pacific gyre, which has been correlated to the increase in di-nitrogen (N₂) fixation rates. Following a NW-SE transect, in the Southeast Pacific during the early austral summer (BIOSOPE cruise), we present data on DIP, dissolved organic phosphate (DOP) and particulate phosphate (PP) pools along with DIP turnover times (T_{DIP}) and N₂ fixation rates. We observed a decrease in DIP concentration from the edges to the centre of the gyre. Nevertheless the DIP concentrations remained above 100 nmol L⁻¹ and T_{DIP} was more than 6 months in the centre of the gyre; DIP availability remained largely above the level required for phosphate limitation to occur and the absence of *Trichodesmium* spp and low nitrogen fixation rates were likely to be controlled by other factors such as temperature or iron availability. This contrasts with recent observations in the North Pacific Ocean at the ALOHA station and in the western Pacific Ocean at the same latitude (DIAPALIS cruises) where lower DIP concentrations (<20 nmol L⁻¹) and T_{DIP}<50 h were measured during the summer season in the upper layer. The South Pacific gyre can be considered a High Phosphate Low Chlorophyll (HPLC) oligotrophic area, which could potentially support high N₂ fixation rates and possibly carbon dioxide sequestration, if the primary ecophysiological controls, temperature and/or iron availability, were alleviated.

1 Introduction

New nitrogen (N) input by N₂ fixation has been recognized as a significant process influencing global oceanic productivity and the associated carbon fluxes (Karl et al., 1997; Falkowski, 1997). It is the primary process responsible for the input of N-containing compounds into the sea (Codispoti et al., 2001; Capone and Knapp, 2007) and can decouple N from other bioelement cycles which depend on ocean mixing; this decoupling has potentially important biogeochemical implications (Gruber, 2004; Karl, 2007). This input largely depends on the biomass of N₂ fixing organisms, which in turn depends on factors such as temperature (Capone et al., 1997; Staal et al., 2003; Breitbarth et al., 2007), iron (Falkowski, 1997; Kustka et al., 2002; Fu and Bell, 2003) and P availability (Karl et al., 1997; Sanudo-Wilhelmy et al., 2001; Moutin et al., 2005; Karl et al., in press). These factors are affected by human activity (increase in temperature, increase in nutrient input by rivers and changes in atmospheric Fe input, Tagliabue et al., 2007), so the input of N, via N₂ fixation, may change over time. Indeed, Karl et al. (1997) have observed an increase in diazotrophic biomass at the ALOHA station, in the Subtropical North Pacific gyre, along with a decrease in soluble reactive P (SRP which is equivalent to DIP in our study) and an apparent shift from N limitation to P limitation (Karl et al., 2001; Karl, 2007).

P availability is a crucial factor in controlling the process of N₂ fixation. It has long been considered, by “geochemists”, as the ultimate factor controlling primary production in the global ocean (Redfield et al., 1963; Tyrrell, 1999). Contrary to N, there is a negligible atmospheric reservoir of P so there is no alternative source when P runs out. Furthermore, P availability in the open ocean is probably less affected by human activity. P coming into the sea is mainly of river origin (Broecker and Peng, 1982). Riverine fluxes of

Correspondence to: T. Moutin
(thierry.moutin@univmed.fr)

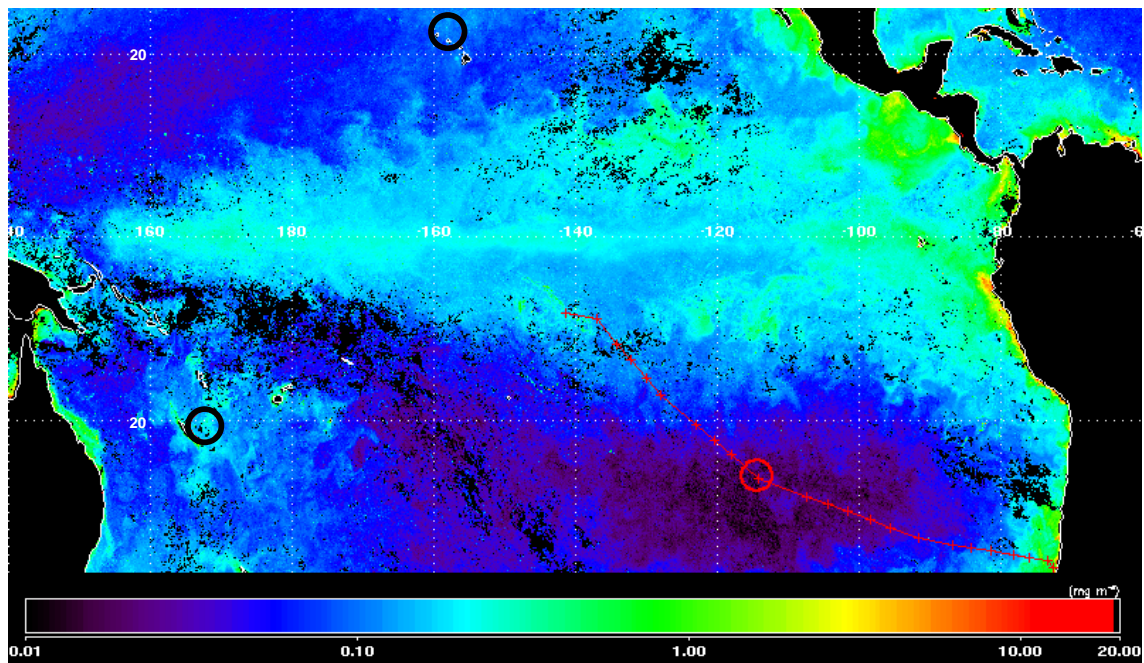


Fig. 1. Location of the stations sampled during the BIOSOPE cruise (November–December 2004) and of the three stations (red circle) where current P pools and availability are compared: a station in the centre of the South gyre (S-gyre station), ALOHA station frequently sampled since the 80's (N-gyre station) and a station sampled during the DIAPALIS cruises (2001–2002) in the SW Pacific Ocean (SW station).

P are also increasing (Meybeck, 1993; Moutin et al., 1998), however, due to its rapid consumption by biological or chemical processes in estuaries (Lucotte and Danglejan, 1988; Golterman and de Oude, 1991), P input by rivers, may have little impact on a global scale, at least over a decadal time scale. Most P is trapped in the superficial sediment (Van Den Broeck and Moutin, 2002; Paytan and McLaughlin, 2007) and may only have local impact. Thus, it is necessary to determine the current P availability in the open ocean to determine its role in the control of N₂ fixation, at the present time and in the near future.

We studied N₂ fixation, P pools and subsequent nutrient availability for planktonic species, following a NW–SE transect in the South Pacific Ocean during November–December 2004 (BIOSOPE cruise). N₂ fixation rate, and DIP, DOP and PP pools were measured together with DIP turnover times in the upper water column. Data from this cruise, particularly from the central gyre, which is one of the least studied major oceanic entities of the world's ocean, is compared with data obtained from the North Pacific gyre at the ALOHA station and a station in the South Western Pacific, where blooms of the N₂ fixing cyanobacterium *Trichodesmium*, are frequently observed (Dupouy et al., 2000). Other diazotrophs such as the recently described unicellular cyanobacteria (Zehr et al., 2001; Zehr et al., 2007) further emphasise the importance of the N₂ fixation process in the budget of new N. Nevertheless, current estimates suggest that *Trichodesmium* may be two- to threefold more abundant than

previously reported and may account for the missing sink of ~90 Tg N required to support the observed new production in the ocean (Davis and McGillicuddy, 2006; Levitan et al., 2007) and confirms the prevalent role of *Trichodesmium* previously reported “in the oligotrophic ocean” (Capone et al., 1997). We consider the current understanding of the factors controlling N₂ fixing organism biomass and the most probable temporal evolution of these factors, then discuss the predictable changes that may occur in N₂ fixation and DIP availability in the south equatorial Pacific.

2 Methods

2.1 Station locations, cruises, chronology and sample collection

The BIOSOPE cruise was carried out during November–December 2004 from the Marquesas Islands to the Chilean coast (Fig. 1). We sampled water along a 6000 km transect and the clearest ocean waters, near Easter Island (Morel et al., 2007) inside the South East Pacific gyre suggested to be the most oligotrophic and stable water body on the basis of remotely sensed ocean colour (Claustre and Maritorena, 2003). All samples were collected from a CTD rosette fitted with 20, 12-L Niskin bottles equipped with silicone rubber closures and tubing that had been carefully cleaned to avoid introducing toxic metals during sampling. Following water collection, samples were processed within 1 h.

Table 1. SST range (°C, monthly long-term mean data), and integrated (0–100 m integrals) P pools (mmol m⁻²) at the three studied stations. N-gyre (ALOHA station, <http://www.soest.hawaii.edu>) and SW station (Chenal des Loyauté station, <http://www.com.univ-mrs.fr/IRD/urcyano/identite/spdiap.htm>). *NOAA_OI_SST_V2 data provided by the NOAA/OAR/ESRL PSD, Boulder, Colorado, USA, from their Web site at <http://www.cdc.noaa.gov/>

		SW station	N-gyre station (ALOHA)	S-gyre station
		21° 30 S; 167° E	22°45 N; 158° W	26°05 S; 114° W
SST (°C) range*	Min–Max	23.1–27.3	23.4–26.4	20.7–25.1
I DIP (0–100 m)	Winter–Summer	9.65–5.40	5.07–5.06	12.45
I DOP (0–100 m)	Winter–Summer	26.45–21.35	21.66–23.69	16.28
I PP (0–100 m)	Winter–Summer	1.97–1.52	1.44–1.33	0.54

Data from the central station, inside the South Pacific gyre (S-gyre station), are compared with data obtained from the DIAPALIS cruises, at the chenal des Loyauté station (SW station) in 2002–2003, and data from the ALOHA station (N-gyre station) in the North Pacific in 2000–2001 (Table 1 and Fig. 1).

2.2 Analytical methods

2.2.1 N₂ fixation rate

One mL of ¹⁵N₂ gas (99% ¹⁵N₂ EURISOTOP) was introduced to each 0.6 L polycarbonate bottle through a Teflon-lined butyl rubber septum using a gas-tight syringe, following the protocol of Montoya et al. (1996). Following 24 h incubations, the samples were filtered under low vacuum (100 mm Hg) through precombusted (24 h at 450°C) 25 mm GF/F filters and dried at 60°C. Filters were stored in a desiccator until processed. Determination of ¹⁵N enrichments were performed using an Integra-CN PDZ EUROPA mass spectrometer. We measured a background natural abundance, determined from 8 unlabelled samples, of 0.367 ± 0.007%. Only excess enrichments higher than two times the standard deviation (0.014% for N) were considered significant. As we worked with low levels of particulate N (PN), we calibrated the spectrometer using the same conditions as for PN and the quality of the analysis was tested with standard molecules (glycine). Based on the lowest N level determined by our mass spectrometer (0.2 μmol), the detection limit for N₂ fixation was 0.12 nmol L⁻¹ d⁻¹. N₂ fixation rates (nmol L⁻¹ d⁻¹) were computed from an equation based on final PN (Dugdale and Wilkerson, 1986). A detailed description of the methodologies for ¹⁵N based measured rates including N₂ fixation rates is given in the paper of Raimbault and Garcia (2007).

2.2.2 P pools

Total P (TP) in seawater samples may be separated in three pools: the Dissolved Inorganic P (DIP) pool, the Dissolved Organic P (DOP) pool and the Particulate P (PP) pool.

The DIP pool was estimated on board using the molybdenum blue reaction (Strickland and Parsons, 1972), on 50 mL samples, using a 10 cm length-cuvette in a spectrophotometer (Cecil CE 1011), at 880 nm, following a 30 min reaction time. Concentrations were expressed in nmol L⁻¹. The lower limit of detection for DIP by this method was 20 nmol L⁻¹. Only one sample was analysed per depth with the exception of the S-gyre station where triplicate samples were analysed. The new MAGIC 25 procedure (Rimmelin and Moutin, 2005) was used on triplicate samples to determine DIP concentration (detection limit=0.8±0.5 nmol L⁻¹) and arsenate concentration at the S-gyre station. The arsenate concentration was 10.8 nmol L⁻¹ (sd=8.6, n=21). Because this is lower than the detection limit outlined in the Strickland and Parsons (1972) procedure for DIP measurement and is not constant (relatively high standard deviation), no arsenate correction was taken into account for DIP measurement.

The PP pool was determined by the filtration of 1-L samples through polycarbonate filters (0.2 μm; 47 mm) at very low pressure. Pressure was increased to get a drop by drop filtration but never exceeded 0.1 bar. PP was measured by standard DIP analysis at 880 nm, following high temperature persulfate wet-oxidation at 120°C and 1 bar (Pujopay and Raimbault, 1994) which converts all inorganic and organic non-reactive P compounds to DIP. Only one sample was analysed per depth with the exception of the S-gyre station where duplicate samples were analysed. Using a concentration factor of 40 (final volume=25 mL), the detection limit was 0.5 nmol L⁻¹.

Total P (TP) was estimated from 40 mL duplicate seawater samples, using the same high-temperature persulfate wet-oxidation pre-treatment as for PP. DIP was then analysed as previously described. The measurement of DOP in seawater requires simultaneous measurements of DIP and TP. DOP was assumed to be equal to ([TP]–[DIP+PP]). The precision and accuracy of the DOP estimates decreased with increasing depth, as DIP concentrations became the dominant component in the total dissolved nutrient pools.

2.2.3 Turnover times of DIP

The DIP turnover time (T_{DIP}) is the ratio of DIP concentration to DIP uptake rate. Thingstad et al. (1993) derived the following relationship for T_{DIP} : $r(t)=1-e^{-t/T}$, where r is the fraction of added radioactivity absorbed, t the incubation time and T the turnover time. This equation has been rearranged in order to give a direct calculation for turnover time: $T=-t/\ln(1-R(t))$ where $R(t)=(R_f-R_b)/R_t$, R_f , the radioactivity on the filter, R_b , the radioactivity of the blank, and R_t , total tracer added. T_{DIP} was determined using ^{33}P tracer (H_3PO_4 in dilute hydrochloric acid; Amersham BF 1003; specific activity $>3000\text{ Ci mmol}^{-1}$). The working solution of ^{33}P -DIP was prepared by diluting the tracer in Milli-Q water filtered through pre-washed $0.2\ \mu\text{m}$ filters, immediately before use. 300 mL of seawater was dispensed into acid-washed Milli-Q and sample rinsed polycarbonate bottles, and incubated with $25\ \mu\text{Ci}$ carrier-free $^{33}\text{PO}_4$ working solution to give a total activity of $0.08\ \mu\text{Ci mL}^{-1}$. Less than $0.03\ \text{nmol L}^{-1}$ of P was added to each sample. The bottles were then placed in an on-deck incubator and maintained at constant temperature using a continuous circulation of surface seawater, at 50, 25, 15, 7, 3 and 1% incident light. The same protocol was used for duplicate 300 mL samples where $300\ \mu\text{L HgCl}_2$ ($20\ \text{g L}^{-1}$) had been added as a control for non-biological uptake. Incubations were stopped by the addition of $600\ \mu\text{L}$ of non-radioactive KH_2PO_4 ($10\ \text{mmol L}^{-1}$). The optimal incubation time (4 to 5 h) was determined from a prior time-series experiment. Sample counts were at least 10 times greater than the blanks, less than 10% of the radioactivity in the samples was consumed, and incubations did not exceed several hours in order to minimize the increase in bacterial production caused by confinement (Van Wambeke et al., 2007). DIP turnover times were measured in 50 mL duplicate sub-samples from each bottle. Filtrations were carried out on 25 mm polycarbonate filters ($0.2\ \mu\text{m}$), placed on DIP-saturated support GF/F filters, using a low-vacuum pressure <0.2 bars. Filters were not washed with filtered seawater at the end of the filtration, but pressure was briefly increased to 0.6 bars, to remove non cellular radioactivity from the filter. Filters were then placed in low-potassium 6 mL glass scintillation vials (Wheaton) with 6 mL of scintillation liquid (Ultima gold MV, Packard) and the radioactivity of the filters measured using a scintillation counter Packard Tri-Carb® 2100TR. Initial radioactivity was measured on 5 replicates of $5\ \mu\text{L}$ of working solution alongside each experiment in order to verify the amount of ^{33}P added to each sample.

2.2.4 Labile DOP

We used the Strickland and Parsons (1972) procedure to measure the labile DOP within the gyre. This pool was assumed to be composed mainly of P monoesters and thus, to be easily hydrolysed by alkaline phosphatase. At each station from the

NW edge to the centre of the gyre, 50 mL triplicate surface (50% of incident light depth) samples were incubated with 1 mL of a fresh and pure solution of *Escherichia coli* alkaline phosphatase (Sigma P-4252, $0.2\ \text{U mL}^{-1}$) and 1 mL of Tris buffer solution 0.5 M (pH=8). Following 2 h incubation at 30°C , the DIP concentration was measured. A further set of triplicate surface samples was used to determine the initial DIP concentration. The labile DOP concentration is the difference between these two measurements. For each series of measurements, a blank sample was processed as well as a control with $1\ \mu\text{mol L}^{-1}$ of a glucose-6-phosphate solution in order to confirm enzymatic efficiency.

2.2.5 Excess DIP relative to nitrate concentration

Ambient nitrate + nitrite and nitrite were measured immediately on collection by pumping the sample from the sampling polyethylene bottle directly through the Technicon AutoAnalyzer. Nitrate and nitrite concentrations in the nanomolar range (lower detection, $3\ \text{nmol L}^{-1}$) were obtained using the sensitive method of Raimbault et al. (1990). For submicromolar concentrations, the classical Technicon AutoAnalyser method was used (Tréguer and LeCorre, 1975). The recently defined variable P^* (Deutsch et al., 2007) was calculated: $\text{P}^*=\text{PO}_4-\text{NO}_3/\text{rr}$ ($\text{rr}=\text{Redfield ratio}=16$), $\text{PO}_4=\text{DIP}$ in this study. While nutrient uptake by non-N₂-fixing organisms will on average consume NO_3 and PO_4 in a proportion that conserves P^* , N₂ fixation will extract PO_4 alone, driving a water parcel towards lower P^* (Deutsch et al., 2007).

3 Results

3.1 P pools and availability in the tropical Pacific Ocean

3.1.1 Spatial distribution (SE Pacific Ocean)

DIP, DOP and PP concentrations in surface waters were highest near the Marquesas Islands and near the Chilean coast (Fig. 2a, b, c). For the 3 distinct pools, there is an obvious decrease in concentration from the edge to the centre of the gyre, reaching minimum values of 120 and $150\ \text{nmol L}^{-1}$ for the DIP and DOP pools respectively, and less than $10\ \text{nmol L}^{-1}$ for PP. Duhamel et al. (2007) have argued that the PP pool is mainly associated with living biomass in the centre of the gyre. Values of PP less than $10\ \text{nmol L}^{-1}$ suggest extremely low biomass as confirmed by total chlorophyll *a* (TChl*a*) concentrations reaching $0.017\ \text{mg m}^{-3}$ in surface waters in the centre of the gyre (Ras et al., 2007). In the upper layer from the edge to the centre of the gyre, the decreases in DIP and PP concentrations are approximately one order of magnitude, compared to a factor of 2.5 for the DOP pools. The DIP/DOP concentration ratio is close to one in the centre of the gyre. The mean labile DOP concentration (P monoesters) inside the gyre at 5 meter depth was below the detection limit of $20\ \text{nmol L}^{-1}$. DIP turnover

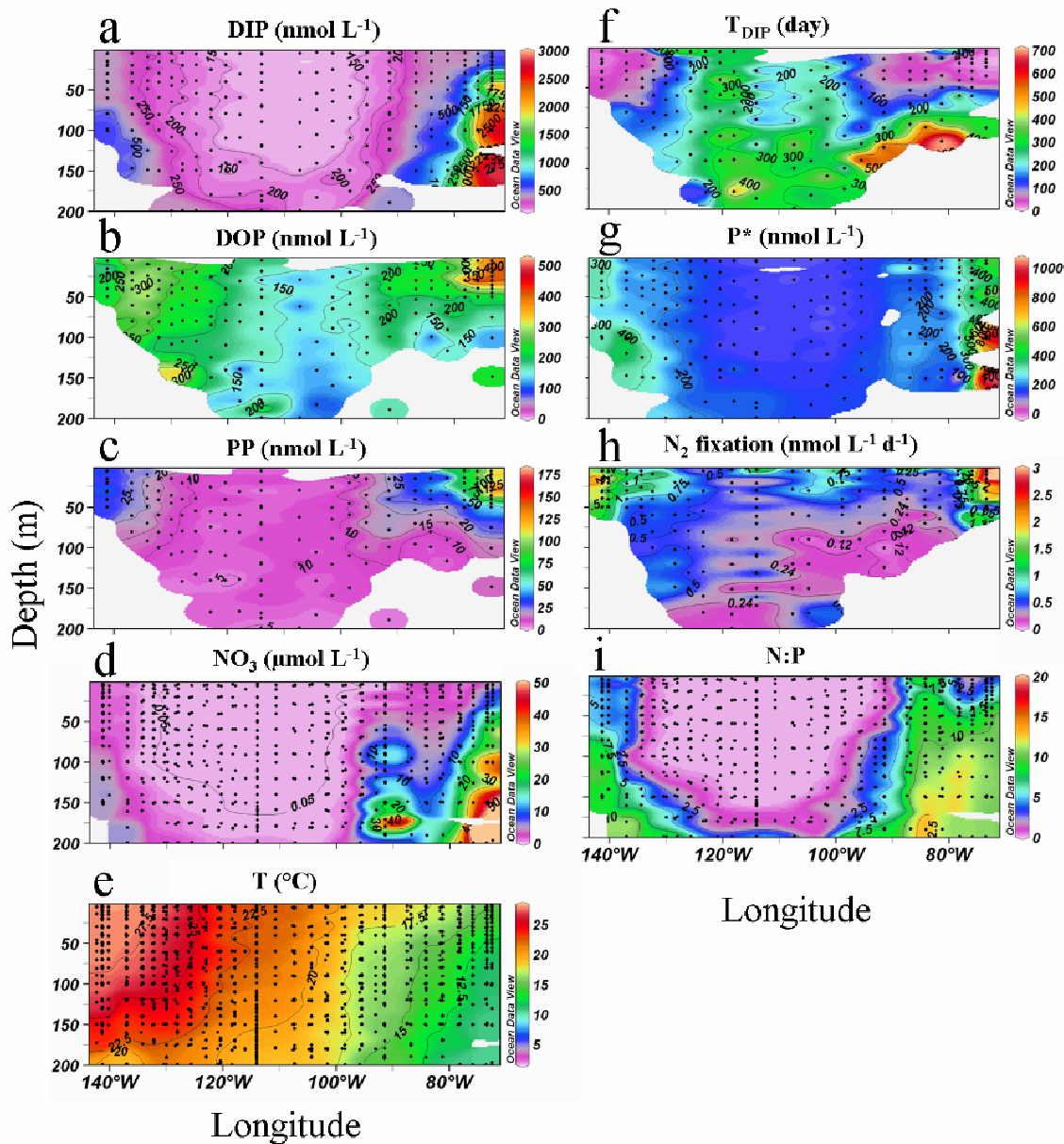


Fig. 2. (a) DIP, (b) DOP, (c) PP, (d) NO_3^- , (e) Temperature, (f) DIP turnover time, (g) P^* , (h) N_2 fixation rates and (i) NO_3^-/DIP measured during the BIOSOPE cruise (November–December 2004) in the South Pacific between the Marquesas Islands and the Chilean coast. ODV (Schlitzer, 2002) was used to generate the distribution maps.

times varied from several days at the edge, to around 200 days in the gyre (Fig. 2f). Higher P^* values were observed near the Chilean coast below 100 m depth ($\sim 1000 \text{ nmol L}^{-1}$) and close to the Marquesas Islands ($\sim 500 \text{ nmol L}^{-1}$). Values of less than 200 nmol L^{-1} were observed in the centre of the South Pacific gyre (Fig. 2g) where the nitrate concentrations became $< 50 \text{ nmol L}^{-1}$ (Fig. 2d). A significant relationship ($p < 0.001$; non parametric Pearson test) was obtained between N_2 fixation and P^* ($\text{N}_2 \text{ fixation} = 6.37 P^* - 0.41$, $N = 136$, $r^2 = 0.49$) using all data collected during the BIOSOPE cruise.

3.1.2 Vertical depth profile inside the gyre (S-gyre station)

DIP concentrations are homogeneous having a mean value of $127.0 \text{ nmol L}^{-1}$ ($\text{sd} = 7.1$, $n = 42$) in the surface waters (0–150 m) and increasing with depth below 150 m (Fig. 3f) at the S-gyre station. The DIP concentration versus depth gradient between 150 and 250 m is $3.5 \mu\text{mol m}^{-4}$. DIP concentrations in surface waters are above the detection limits of the standard method (Strickland and Parsons, 1972). No significant difference was observed with the high sensitivity MAGIC 25 method (Rimmelin and Moutin, 2005) thus enabling us to

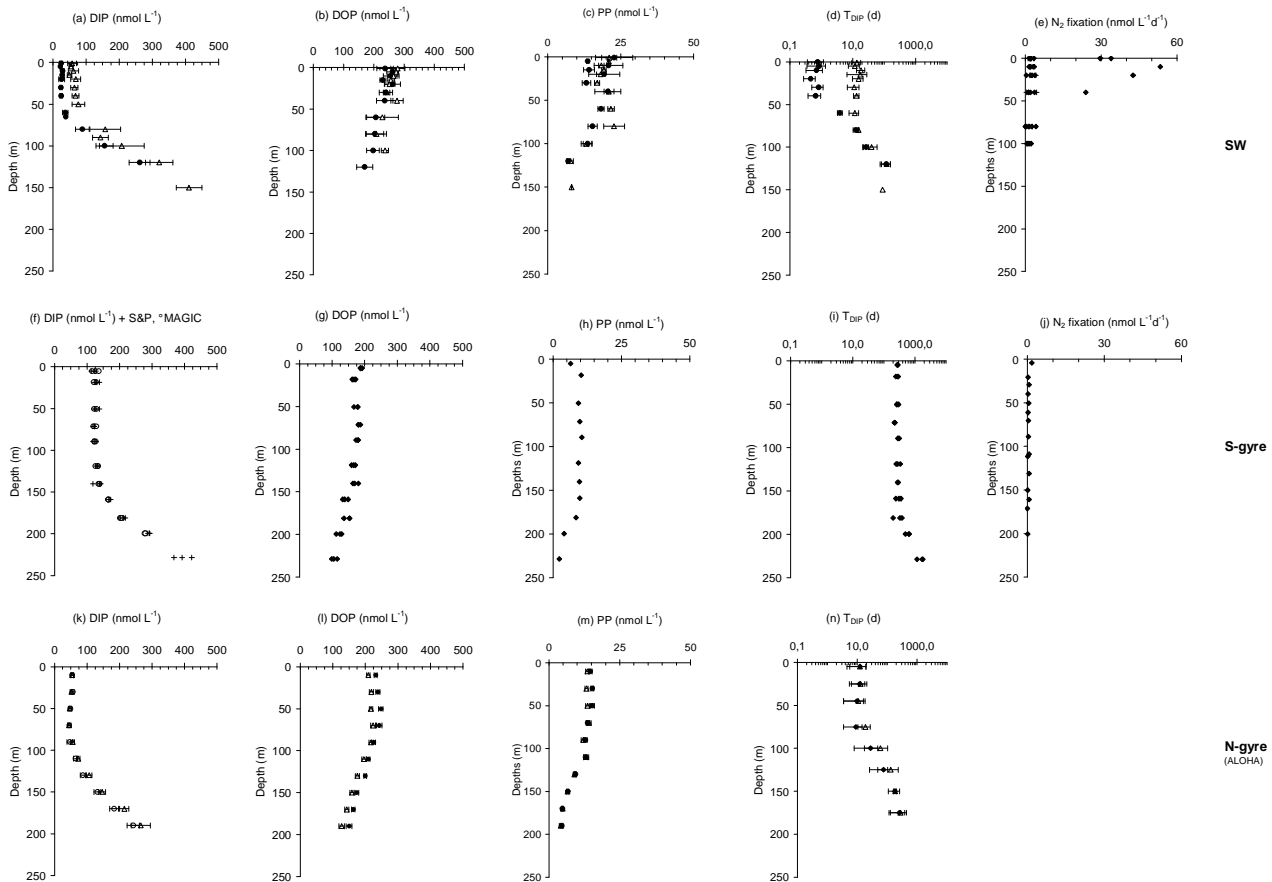


Fig. 3. Current Dissolved Inorganic P (DIP), Dissolved Organic P (DOP), Particulate P (PP) concentrations, DIP turnover time and N₂ fixation rates vs depth at the three stations studied in the South, N-gyre (ALOHA station, http://www.soest.hawaii.edu/HOT_WOCE/ftp.html) and SW station (Chenal des Loyauté station, <http://www.com.univ-mrs.fr/IRD/urcyano/identite/spdiap.htm>). Summer and Winter (Δ) concentrations are indicated when available.

validate our detailed protocol for a 25 times MAGIC pre-concentration procedure. DIP turnover times are homogeneous with a mean value of 273 days ($sd=29$, $n=21$) in surface waters (Fig. 3i).

DOP concentrations are highest in near surface waters with a mean value of $175.5 \text{ nmol L}^{-1}$ ($sd=9.2$, $n=21$) and decrease with increasing water depth (Fig. 3g). DOP dominates in the surface water, accounting for 58% of the total dissolved P pool. DIP becomes the dominant component of the total dissolved pool below 150 m. The mean DOP concentration from duplicate deep water samples (600–2000 m) is 61.0 nmol L^{-1} ($sd=16.5$, $n=8$). PP concentrations follow the same pattern as DOP concentrations with a mean value of 9.3 nmol L^{-1} ($sd=1.5$, $n=6$) in surface waters decreasing as water depth increased (Fig. 3h). A maximum in PP was not observed at the depth of the deep chlorophyll maximum (180 m). Values below 200 m were similar to the mean concentration from duplicate deep water samples (600–2000 m) of 1.0 nmol L^{-1} ($sd=0.3$, $n=8$).

3.1.3 Comparison with depth profiles from the SW and N-gyre Pacific stations

In the upper layer, the maximum values of DIP and for T_{DIP} are recorded at the S-gyre station. Depths trends similar to those at the S-gyre station, are observed for DIP, DOP and PP at the SW (Fig. 3a, b, c) and N-gyre (Fig. 3k, l, m) stations; the only exception is the sharp decrease in DIP concentration, observed at the SW station (Fig. 3a), during the summer period. The average decrease in DIP concentration between austral winter and austral summer in the upper 40 m of the water column was 35 nmol L^{-1} at the SW station. This difference corresponds to a minimum value as DIP concentration was generally below the 20 nmol L^{-1} detection limit of the classical Strickland and Parsons, 1972 method. No MAGIC measurements are available but indirect estimations of the DIP concentrations from T_{DIP} measurements (Van Den Broeck et al., 2004) indicated sub-nanomolar concentrations during the summer period. There was no corresponding increase in either the PP pool or the DOP pool, although large

differences in the concentration of the DOP pool were observed during both the winter and summer periods. DIP turnover times (Fig. 3d) vary from approximately 10 days in winter to a few hours in summer in near surface waters.

No clear seasonal variations were observed in the DIP pool at the N-gyre station (ALOHA, Fig. 3k). DIP concentrations were lower (by a factor of 2–2.5) than concentrations measured in the mixed layer of the S-gyre station. DOP concentrations were slightly above the DOP concentrations measured at the S-gyre station and very close to those measured at the SW station. The PP concentrations at the N-gyre station were higher (by a factor of 1.5) than those in the more oligotrophic S-gyre station and close to or lower than those at the SW-station. DIP turnover times were around 10 days near the sea surface at the N-gyre station, close to those observed during the winter season at the SW station and no marked variations between the summer and winter seasons are observed.

3.2 Current distribution of N₂ fixation

The N₂ fixation in surface waters during the BIOSOPE cruise yielded maximum values, around 4 nmol L⁻¹ d⁻¹, near the Chilean coast, intermediate values near the Marquesas Islands (1.2–2.8 nmol L⁻¹ d⁻¹) and low values, just above the detection limit of the method employed (0.12 nmol L⁻¹ d⁻¹), inside the gyre (Fig. 2h). Integrated depth profiles gave a value of ~142 μmol N m⁻² d⁻¹ near the Chilean coast (1 in situ depth profile between 0 and 40 m) and 48 and 135 μmol N m⁻² d⁻¹ at the S-gyre station (2 in situ depth profiles between 0 and 200 m taken on two days). A doubling of the mean irradiance intensity and similar variations of ammonium and nitrate uptake rates were also observed between the two different days. Maximum N₂ fixation rates were found in the upwelling area where N:P ratio close to 10 (Fig. 2i) and ample Fe concentrations (1.2–3.9 nM) are found (Blain et al., 2007), and temperatures did not exceed 16°C (Fig. 2e). The N₂ fixation rates are maximal near the surface within the gyre and decrease with depth indicating that light could play a role in controlling this process. At present we do not know the species responsible for these fluxes. *Trichodesmium*, a large filamentous N₂ fixing microorganism that often forms large easily identified colonies, was not observed. Bonnet et al. (2007) found the presence of extremely low numbers of Group A cyanobacterial phylogenotypes (see their Table 2).

The N₂ fixation rates at the SW station (DIAPALIS cruises) were highly variable within seasons and ranged between 151–703 μmol N m⁻² d⁻¹ (Garcia et al., 2007). The maximum values correspond to a *Trichodesmium* specific bloom that occurred during the summer period (Fig. 3e) when temperatures were above 26°C. At the N-gyre station ALOHA, higher N₂ fixation rates than those measured in the South Pacific gyre have already been reported and these appear to be associated with *Trichodesmium* blooms (Dore et

al., 2002). At least two independent microbial assemblages and ecosystem processes contribute to N₂ fixation in the NP gyre, namely the “background state” wherein a relatively low but relatively constant rate supported by pico and nano-diazotrophs, and the aperiodic “bloom state” wherein large filamentous, colonial and aggregate forming diazotrophs (*Trichodesmium* and/or endosymbiont-containing diatoms) dominate the new N cycle (Karl et al., in press). It is estimated that the summer bloom is responsible for up to 38% of the annual N₂ fixation at ALOHA station (J. Dore, personal communication). Based on a variety of independent estimates including nitrogenase activity by acetylene reduction method, *Trichodesmium* abundance, N:P mass balance, and ¹⁵N isotope balance, an annual N₂ fixation rate of 31–51 mmol N m⁻² year⁻¹ was estimated for the Pacific Ocean near Hawaii (Karl et al., 1997). N₂ fixation at Station ALOHA would equate to 3–4% of the total N demand for the microorganisms that inhabit that ecosystem. However, when compared to estimates of new production or to N exports by sinking particles and migrant zooplankton, N₂ fixation appears to be a significant (40–60%) source of new N (Karl et al., in press) since export from oligotrophic ecosystems is low. When compared to estimates of new production with ¹⁵N, N₂ fixation accounted for up to 50% in the South Pacific gyre (Raimbault and Garcia, 2007). The N₂ fixation rates measured inside the SP gyre are close to the averaged 0.25 ± 0.05 nmol N L⁻¹ d⁻¹ measured in oligotrophic waters of the NP Ocean where water temperatures are typically below 20–25°C (Needoba et al., 2007). Integrated rates in the SP gyre are similar to those reported by Falcon et al. (2004) for the tropical NA in summer (62 μmol N m⁻² d⁻¹, SE=21, n=30) and February 2001 (167 μmol N m⁻² d⁻¹, SE=49, n=30) and in the subtropical NP (84 ± 50 μmol N m⁻² d⁻¹).

4 Discussion

4.1 P availability in the contemporary ocean

4.1.1 Availability of DIP

DIP is directly available for all microbes and its concentration can be considered as the first criterion to evaluate P availability. DIP is not completely exhausted from the upper water at the N-gyre station (ALOHA) or in the South Pacific gyre, but DIP concentrations reach <20 nM concentration during the summer season at the SW station. As these DIP concentrations at the SW station are close to or even below detection limits of classical chemical analyses (20 nM), the study of DIP turnover times can provide additional information on nutrient availability: DIP turnover time is the most broadly-applicable measurement of DIP availability because it has the potential to identify variations in P availability even when DIP concentrations become analytically undetectable (Moutin et al., 2002; Moutin et al., 2005).

Table 2. DIP turnover time (mean and standard deviation in hours) in upper ocean surface waters (0–20 m or at the depth of 50% of incident light*), D5S1N5 is for 5 depths (D5), 1 station sampled (S1), 5 samples (N5), as an example. **=median value. See also (Tanaka et al., 2006) for others T_{DIP} measurements in the Mediterranean Sea.

Winter	Spring	Summer	Fall	Area	Year of sampling	References
396 (370)	3.9 (2.4)	1.6 (0.9)		Mediterranean Sea		
D1S9N9	D1S17N17	D1S20N20		Lion gulf	1997–1998	Moutin et al. (2000)
			10.5 and 7.6	Alboran	1999	Moutin et al. (2002)
			D1S2N2			
			1.7 (1.5)	Western basin	1999	Moutin et al. (2002)
			D1S5N5			
			1.2 (0.5)	Eastern basin (Ionian)	1999	Moutin et al. (2002)
			D1S4N4			
2.9 and 6.7				Eastern basin (Ionian)	1996	Zohary and Robarts (1998)
D1S2N2						
4.1 (1.6)				Eastern basin (Levantin)	1996	Zohary and Robarts (1998)
D1S5N5						
11		5		Atlantic Ocean		
D1S1N1		D1S1N1		Sargasso Sea (BATS)	1992–1993	Cotner et al. (1997)
230 (38)	1.3 (0.4)		217	Gascogne gulf		Labry et al. (2002)
D1S3N3	D1S4N4		D1S1N1			
			82 (25)	Marocco upwelling	1999	Moutin, unpublished
			D3S1N3			
1182 (382)	152 (55)		168 (110)	North Eastern	2000–2001	Moutin, unpublished
D2S3N6	D2S4N8		D2S4N8	(between Azore islands and Spain)		
				Pacific Ocean		
504 (175)	107 (37)	10.8 (2.4)	4.0 (0.3) and 68 (2)	South Western	2002–2003	Van den Broeck et al. (2004)
D5S1N5	D5S1N5	D3S2N6	D5S1N5			
672**	456**	744**		Northern central	1973–1974	Perry and Eppley (1981)
S5	S6	S4		(within a degree of 30° N, 155° W)		
	504 (399)	144	72	Northern central gyre	1996–1997	Björkman et al. (2000)
	D1S1N3	D1S1N1	D1S1N1	(ALOHA)		
	216 and 48			Northern central gyre	1996–1997	Björkman et al. (2000)
	D1S2N2			(Climax)		
514 and 500	291 (36)	93 (35)	405 (31)	Northern central gyre	2000–2001	Björkman et al. (2003)
D2S1N2	D2S3N6	D2S2N4	D2S2N4	(ALOHA)		
149	120	221		Northern central gyre	2002–2004	Van Mooy, unpublished
D1S1	D1S2	D1S1		(ALOHA)		
	936 (451)			South equatorial	2004	This study*
	D1S3N6			(Marqueous Island)		
	2086 (1202)			Western transition area	2004	This study*
	D1S5N10					
	5589 (1472)			Transect inside the southern gyre	2004	This study*
	D1S8N16					
	1964 (1003)			Eastern transition area	2004	This study*
	D1S5N10					
	464 (305)			Chilean upwelling	2004	This study*
	D1S3N6					

DIP turnover times represent the ratio between DIP concentration and DIP uptake by the microbial assemblage. Despite the DIP concentrations being much lower in the centre of the South gyre than those found near the Marquesas Islands and Chilean coast, the larger T_{DIP} indicates that DIP availability, compared to the planktonic species requirement within the gyre, is greater than in the upwelling region. The turnover time is also the time it would take for all the ambient DIP to be taken up assuming no additional

input (Ammerman et al., 2003). Without any additional external sources or input by regeneration, it would take 200 days to exhaust all available DIP in the gyre, while it may only take 10 days in the Chilean upwelling and at the N-gyre station (ALOHA). Nonetheless, T_{DIP} in the Southern and Northern gyres suggest a P sufficiency that is contrary to what has been observed in the very P-depleted Mediterranean Sea, Sargasso Sea and South Western Pacific during the summer season (Table 2) where T_{DIP} of less than 10 h

were observed (Table 2). Nevertheless, short DIP turnover times of around 2 days (Bjorkman et al., 2000, Table 2) and a long term decrease in DIP availability (Karl et al., 1997; Karl et al., 2001) have also been reported at the ALOHA station. The comparison between DIP turnover times obtained by Perry and Eppley (1981) in the central Pacific gyre in the 70's, and current estimations (Table 2) confirm the decrease in DIP availability, particularly during the summer season. The large differences in T_{DIP} measurements observed in oligotrophic areas (Table 2) enable us to distinguish the High P Low Chlorophyll (HPLC) oligotrophic areas (SP gyre) and Low P Low Chlorophyll (LPLC) oligotrophic areas (Sargasso Sea, Mediterranean Sea). The ALOHA station in the NP gyre appears to be an intermediary or transient state of DIP availability.

4.1.2 Availability of DIP and N₂ fixation

Low DIP availability may control the growth and biomass of N₂ fixing organisms. A critical DIP turnover time of 50 h, giving favourable and unfavourable growth conditions for *Trichodesmium*, was determined during the DIAPALIS survey in the SW Pacific ocean (Moutin et al., 2005). It was demonstrated that the sharp decrease in DIP availability in the early summer season could explain most of the numerous and periodic sea surface accumulations of *Trichodesmium* observed, and more importantly, the prevalent role of DIP availability in the control of N input by N₂ fixation in this area (Moutin et al., 2005). The DIP turnover times of around 10 days measured at the N-gyre station (ALOHA, Fig. 3n) suggests a higher P deficiency than in the South Pacific gyre (T_{DIP} around 200 days and DIP concentrations $>100 \text{ nmol l}^{-1}$), but this is not strong enough to provoke *Trichodesmium* decay (obtained for $T_{DIP} <50 \text{ h}$ equivalent to DIP concentration $<10 \text{ nmol l}^{-1}$ at the SW station). Thus, another factor must prevent the complete exhaustion of DIP and may currently control N₂ fixation by *Trichodesmium* at the N-gyre station (ALOHA). Nevertheless, episodic *Trichodesmium* blooms followed by severe DIP depletion have already been observed at the N-gyre station (Letelier, ASLO meeting 2006).

Due to their smaller size, small diazotrophs are probably more efficient in taking up DIP from the surrounding water and as a consequence, are probably less affected by DIP depletion. It is likely that the current high DIP availability in the SP gyre may not control N₂ fixation, at least during the studied period (November–December). Strong seasonal variations in DIP availability are not expected as this is an area where the lowest sea surface chl *a* concentrations in the world's oceans are determined from space throughout the year (Claustre and Maritorena, 2003).

4.1.3 Availability of DOP

For the most part DOP is not directly available to living organisms as it cannot be taken into the cell in this form (Cembella et al., 1984; Bjorkman and Karl, 2003; Paytan and McLaughlin, 2007). Organic P must first be converted to DIP. The labile fraction of the DOP pool inside the South Pacific gyre was $<20 \text{ nmol l}^{-1}$ suggesting that only a small fraction of the DOP pool was available (through alkaline phosphatase activity). At the SW station during the summer period, DIP concentrations reached $<20 \text{ nmol l}^{-1}$. However, no significant change was observed in the DOP concentrations (Fig. 3b), which suggests that most of the DOP pool in the upper surface is not readily available, even after several months of severe DIP depletion. Moreover, despite the variations in DIP concentrations and turnover times at all three stations, the DOP concentration was around 200 nmol l^{-1} at all three suggesting that the DOP reservoir is not a particularly dynamic reservoir of P in upper ocean waters. The South Pacific gyre appears to be an ocean as close as can be expected (Lewis, personal communication). Thus, the DOP pool in the S-gyre station may mainly be formed by an accumulation of older organic molecules with low bioavailability.

Even though most of the DOP pool is not readily available, it may play a determinant role in phytoplankton growth. It is probable that the turnover of the available DOP pool is rapid. It has been estimated that DOP utilization can be of the same order of magnitude as DIP utilization in the upper water column at ALOHA (Bjorkman and Karl, 2003). Recent evidence also indicates that certain compounds in the DOP pool, particularly the phosphonates, which may account for 25% of the high molecular weight DOP pool (Clark et al., 1998; Kolowitz et al., 2001), may be used (Dyhrman et al., 2006), but we know little about its global significance and there is a major scope for future research in the field of P availability.

4.1.4 Relative availability of DIP pool vs availability of DIN (DIN: Dissolved Inorganic Nitrogen which is equivalent to nitrate in our study)

P^* is a convenient estimate of the excess in DIP relative to DIN, when it is assumed that these nutrients are utilised following Redfield proportions (N:P=16). P^* variations in the South Pacific are close to those expected by Deutsch et al. (2007). They argue that denitrification in the oxygen minimum zones (OMZs) generates DIP-enriched and DIN-deficient waters. These waters subsequently undergo a disproportionate loss of DIP as they are upwelled and transported into the adjacent gyres. The eastern Pacific Ocean near the Chilean coast is one of the three major areas of denitrification in the world's oceans (Codispoti and Richards, 1976). Thus, it may explain the high P^* observed (Fig. 2g). North of 14° S, the waters are under the influence of the equatorial regime (Claustre et al. this volume). Following

general circulation models, water near the Marquesas Islands (Fig. 2g) are influenced by waters upwelled near the equator. This may also explain the high P* values observed in this area. The decrease in P* toward the centre of the gyre corresponds to the trend observed by Deutsch et al. (2007): downstream of the OMZs, surface waters that initially carry a surplus of phosphorus (because of subsurface denitrification) lose this excess gradually through N₂ fixation. This may be attributed to N₂ fixation restoring the system to a “Redfieldian” balance as already suggested by Redfield (1934) and Capone and Knapp (2007).

The model by Deutsch et al. (2007) for N₂ fixation rates along the studied transect, with minimum values found on the edge and maximum values in the centre of the gyre, is contrary to our observations. They calculated a basin-wide N₂ fixation rate for the Pacific of 48 mmol N m⁻² yr⁻¹ similar to previous estimates ~50 mmol N m⁻² yr⁻¹, Redfield et al. (1963), with maximum values of up to 120 mmol N m⁻² yr⁻¹ inside the South Pacific gyre. Assuming no seasonal variations (i.e. 120000/365 ~ 330 μmol N m⁻² d⁻¹) and a maximum depth of 200 m available for N₂ fixation inside the gyre, this rate is equivalent to 1.7 nmol N L⁻¹ d⁻¹, a value at least 2.5 times greater than the mean rate measured in this study (0.24 and 0.67 nmol N L⁻¹ d⁻¹). The annual rate calculated near the Chilean coast by Deutsch et al. (2007) is under 20 mmol N m⁻² yr⁻¹. Assuming no seasonal variations (i.e. 20000/365 ~ 55 μmol N m⁻² d⁻¹) and a maximum depth of ~40 m available for N₂ fixation in the upwelling, this rate is equivalent to ~1 nmol N L⁻¹ d⁻¹, a value that is around 4 times lower than the measured value. Thus, even if the calculated (Deutsch et al., 2007) and observed (Fig. 2g) P* distributions are very similar, the N₂ fixation rates measured in the South Pacific gyre are not consistent with the predicted rates. Some of the discrepancy between observed N₂ fixation rates and model outputs is certainly due to uncertainties in ocean circulation and care should be taken, also, that the trend suggested by Deutsch et al. (2007) may not directly be reflected in a snap shot observation. The strong relationship between P* and N₂ fixation rates observed (Fig. 2g and h) may further strengthen the idea that biological N₂ fixation and marine N removal are tightly coupled (Deutsch et al., 2007): N₂ fixation begins, and is highest, when upwelled waters reach the surface near the Chilean coast. The waters do not need to be transported to the warmer adjacent gyre to lose most of their excess P. N₂ fixation in the surface waters increases the deficit in DIP relative to DIN (decrease in P*). However, N₂ fixation is not the only process driving the decrease in P* in the water. The export of material with a N:P ratio lower than the Redfield ratio will give the same pattern. It is not known whether the greater depth of the synthesis of material that is vertically exported outside the upwelling zone produces exported material with a higher P content.

Deutsch et al. (2007) argue that the ratio of N to P in seawater may be the central factor regulating N₂ fixation and

that Fe rich dust may not exert as much influence on marine N₂ fixation (Capone and Knapp, 2007) as is currently assumed (Berman-Frank et al., 2001). The close link between denitrification and N₂ fixation is convincing but another simple explanation for the higher N₂ fixation rates near the Chilean coast could be that there is less competition for nutrients so enabling N₂ fixing organisms to thrive independently from the DIN:DIP ratio.

4.2 N₂ fixation distribution and controls other than P availability

The remaining relatively high DIP concentration in the centre of the SP gyre suggests a control other than DIP availability for N₂ fixation. It is probably related to temperature or Fe availability. Indeed, the Fe requirement of N₂ fixers must be provided by the upper photic water column and the temperature must be adequate to enable growth or N₂ fixation.

4.2.1 Temperature

There are numerous studies showing a correlation between *Trichodesmium* abundance and temperature (Capone et al., 1997; Lugomela et al., 2002; Chen et al., 2003; Moutin et al., 2005). The relationship between *Trichodesmium* distribution and sea surface temperature (SST) is so “commonly accepted” that the observed temperature distribution range (20–30°C) is used to constrain N₂ fixation in oceanic biogeochemical circulation models (OCBM) (Fennel et al., 2002; Hood et al., 2004). Temperatures above 26°C are necessary for *Trichodesmium* bloom development (Carpenter et al., 2004). The correlation between water temperature and *Trichodesmium* abundance is generally attributed to oceanographic features associated with warm waters, such as a shallow mixed layer, high light regimes and oligotrophic nutrient conditions, rather than to a direct physiological response to the temperature itself (Hood et al., 2004). Nevertheless, it was recently demonstrated that the *Trichodesmium* strain IMS-101 are adapted to optimum growth temperatures of between 24 and 30°C tolerating temperatures from 20 to 34°C (Breitbarth et al., 2007). Thus, as suggested by Capone et al. (1997), seawater temperature sets a physiological constraint on the geographical distribution of *Trichodesmium* (Breitbarth et al., 2007). Most of the numerous sea surface accumulations of *Trichodesmium* observed in the South western Pacific Ocean near New Caledonia occurred during the spring and early summer periods when temperatures were above 25°C. Monthly, mean SST's reached a maximum of 25.1°C during summer at the S-gyre station reaching 27.3 and 26.4°C at the SW and N-gyre Pacific stations, respectively. SST's were less than 25°C over a large part of the South Pacific gyre during the BIOSOPE cruise (Fig. 2e) and may explain the current absence of *Trichodesmium* in the SP gyre.

Other N₂ fixing organisms may not be affected by temperature. Indeed, N₂ fixers can be encountered at temperatures close to freezing (Zielke et al., 2002; Pandey et al., 2004). Then, another control for these species is needed to explain the low N₂ fixation rates inside the gyre, or at least to explain why DIP is not completely exhausted from the upper layer.

4.2.2 Fe availability

Numerous experimental studies attribute a dominant role of Fe availability in the control of diazotroph growth (Paerl, 1994; Falkowski, 1997; Kustka et al., 2002; Mills et al., 2004). A high Fe requirement of the enzyme nitrogenase is believed to prevent N₂ fixing organisms from alleviating widespread N limitation (Falkowski, 1997). Atmospheric input of dust, which is highly enriched in Fe relative to other nutrients, plays a significant role in the distribution of *Trichodesmium* (Orcutt et al., 2001) and on the decoupling between N-P-Fe-Si biogeochemical cycles in the ocean (Karl, 2002). High rates of N₂ fixation in the North Atlantic were considered to be the result of the unusually high growth rates of N₂ fixers, stimulated by the high Fe availability (Wu et al., 2000; Deutsch et al., 2007). Contrary to the oceanic gyres situated in the Northern Hemisphere, Fe-rich dust deposition is extremely low in the South Pacific gyre (Wagener et al., 2008) and dissolved Fe concentrations of $0.13 \pm 0.03 \text{ nmol l}^{-1}$ inside the upper water (0–80 m) of the gyre (Blain et al., 2007) may prevent the development of N₂ fixing organisms. Nevertheless, enrichment experiments showed that primary production was N-limited at the S-gyre station and no N₂ fixation was measured following dust, Fe and/or P additions (Bonnet et al., 2007). The lack of response could be related to sampling at a depth of 30 m depth using a peristaltic pump, a depth where N₂ fixation rates were extremely low and close to the detection limit of the method.

4.3 P availability and the ultimate control of N₂ fixation in the tropical Pacific ocean

Following the most probable temporal changes (over a few decades) for factors controlling N₂ fixation, several scenarios have been considered for N input via N₂ fixation and the ultimate P availability for the South Pacific Ocean:

4.3.1 Increase in temperature

The expected increase in temperature will increase stratification but is not likely to modify the upwelling intensity near the Chilean coast and thus, changes in N₂ fixation will probably occur elsewhere. If the presence of *Trichodesmium* spp. is controlled by seawater temperature, any increase in temperature will increase its distribution. Breitbarth et al. (2007) predicted an 11% areal increase of *Trichodesmium*'s potential geographic distribution following a modelled SST increase of up to 3° C by 2090, but a simultaneous decrease in the area characterized by optimum growth. High SSTs are predicted

for the western Pacific which is a characteristic province for present-day *Trichodesmium* abundance (LaRoche and Breitbarth, 2005). In this area where *Trichodesmium* biomass is already controlled by P availability, no change in N₂ fixation with increasing temperature is expected. Nevertheless, the increasing widespread high sea surface temperature is expected to increase the distribution area of *Trichodesmium* driving the system towards the ultimate P control over a larger area. An increasing trend in N₂ fixation associated with a decreasing trend in P availability may therefore be expected in the South western ocean.

4.3.2 Increase in Fe dust deposition

The dominant external input of Fe to the surface of the open ocean is the transport of aeolian dust, from the great deserts of the world (Jickells et al., 2005) and this appears to be very sensitive to climate changes (Mahowald et al., 2006). The effect of dust/Fe in subtropical gyres is a reduction in Fe limitation on N₂ fixation so increasing primary production (Falkowski et al., 1998). A higher Fe supply to the sea surface has been hypothesized to favour N₂ fixation in the continentally influenced Atlantic Ocean (Wu et al., 2000) as well as in the South Western Pacific Ocean (Van Den Broeck et al., 2004) and probably the Mediterranean Sea (Bonnet and Guieu, 2006). The increasing atmospheric input of Fe in the Northern Hemisphere has been believed to cause the decreasing trend of P availability at the N-gyre station ALOHA (Karl et al., 2001). A similar trend may be expected for the South Pacific.

4.3.3 An extension of the geographical area of denitrification

Deutsch et al. (2007) suggest that N₂ fixation is closely coupled to the generation of N-deficient waters in areas of denitrification (timescale of year to decades) and are mainly dependent on the N:P ratios of the water upwelled near the coast. As denitrification occurs mainly in suboxic zones with $[\text{O}_2] < 5 \mu \text{ mol l}^{-1}$ (Codispoti et al., 2001), any change in the spread of these areas will have significant impact on the N₂ fixation rate inside the gyres. The most probable future change is an extension of the geographical areas of denitrification. This will generate a higher volume of DIN deficient waters and consequently, according to Deutsch et al. (2007) a higher N₂ fixation rate in the South Pacific and a strengthening control of the carbon cycle by P availability.

5 Conclusions

We found that P availability was largely above the level required for P limitation on N₂ fixation in the South Pacific gyre. This is in contrast to recent observations in the SW Pacific Ocean over the same latitude. We suggest a geographical trend for limitation on N₂ fixation, from P limitation in

the West to temperature and/or Fe limitation in the central and South East Pacific Ocean. The South Pacific gyre can be considered a High P Low Chlorophyll (HPLC) oligotrophic area, which could potentially support high N₂ fixation rates if the primary control temperature and/or Fe availability were alleviated. A decrease in P availability due to an increasing input of N by N₂ fixation is the most probable decadal trend to occur following climate change.

As already mentioned by Deutsch et al. (2007), environmental controls on N₂ fixation and thus its probable response to past and future climate change would be much clearer if we knew the geographic distribution of this process in the ocean. The poor correlation between their model output and our observations for N₂ fixation in the South Pacific area emphasizes the importance of studying the geographical distribution of N₂ fixation as well as the main factors controlling this process. Increased understanding of the factors controlling the growth and biomass of N₂ fixing organisms is needed in the field in order to constrain the models.

Acknowledgements. The authors thank the crew of the R/V L'Atalante for outstanding shipboard support operations. D. Taillez and C. Bournot are warmly thanked for their efficient help in CTD rosette management and data processing, A. Sciandra for his leadership during the second leg and T. Lefevre for English correction. This is a contribution of the BIOSOPE project of the LEFE-CYBER program. This research was funded by the Centre National de la Recherche Scientifique (CNRS), the Institut des Sciences de l'Univers (INSU), the Centre National d'Etudes Spatiales (CNES), the European Space Agency (ESA), The National Aeronautics and Space Administration (NASA) and the Natural Sciences and Engineering Research Council of Canada (NSERC). This work is funded in part by the French Research and Education council. Data from the N-gyre station (ALOHA) originates from Hawaii Ocean Time-series observations supported by the U.S. National Science Foundation under Grant OCE- 0326616 and from the Gordon and Betty Moore Foundation.

Edited by: S.W.A. Naqvi

References

- Ammerman, J. W., Hood, R. R., Case, D. A., and Cotner, J. B.: Phosphorus Deficiency in the Atlantic: An Emerging Paradigm, *Oceanography. Eos Trans.*, 84, 169–170, 2003.
- Berman-Frank, I., Cullen, J. T., Shaked, Y., Sherrell, R. M., and Falkowski, P. G.: Iron availability, cellular iron quotas, and nitrogen fixation, *Trichodesmium*. *Limnology and Oceanography*, 46, 1249–1260, 2001.
- Bjorkman, K., Thomson-Bulldis, A. L., and Karl, D. M.: Phosphorus dynamics in the North Pacific subtropical gyre, *Aquatic Microbial Ecology, Aquat. Microb. Ecol.*, 22, 185–198, 2000.
- Bjorkman, K. M. and Karl, D. M.: Bioavailability of dissolved organic phosphorus in the euphotic zone at station ALOHA, North Pacific Subtropical Gyre, *Limnol. Oceanogr.*, 48, 1049–1057, 2003.
- Blain, S., Bonnet, S., and Guieu, C.: Dissolved iron distribution in the tropical and sub tropical South Eastern Pacific, *Biogeosciences Discuss.*, 4, 2845–2875, 2007, <http://www.biogeosciences-discuss.net/4/2845/2007/>.
- Bonnet, S. and Guieu, C.: Atmospheric forcing on the annual iron cycle in the western Mediterranean Sea: A 1-year survey, *J. Geophys. Res.-Oceans.*, 111, C09010, doi:10.1029/2005JC003213, 2006.
- Bonnet, S., Guieu, C., Bruyant, F., Prášil, O., Van Wambeke, F., Raimbault, P., Grob, C., Moutin, T., Gorbunov, M. Y., Zehr, J. P., Masquelier, S. M., Garczarek, L., and Claustre, H.: Nutrients limitation of primary productivity in the Southeast Pacific (BIOSOPE cruise), *Biogeosciences Discuss.*, 4, 2733–2759, 2007, <http://www.biogeosciences-discuss.net/4/2733/2007/>.
- Breitbarth, E., Oschlies, A., and LaRoche, J.: Physiological constraints on the global distribution of *Trichodesmium* – effect of temperature on diazotrophy, *Biogeosciences*, 4, 53–61, 2007, <http://www.biogeosciences.net/4/53/2007/>.
- Broecker, W. S. and Peng, T. H.: *Tracers in the sea*, Lamont-Doherty Geological Observatory, Columbia University, 690 pp., 1982.
- Capone, D. G. and Knapp, A. N.: Oceanography – A marine nitrogen cycle fix?, *Nature*, 445, 159–160, 2007.
- Capone, D. G., Zehr, J. P., Paerl, H. W., Bergman, B., and Carpenter, E. J.: *Trichodesmium*, a globally significant marine cyanobacterium, *Science*, 276, 1221–1229, 1997.
- Carpenter, E. J., Subramaniam, A., and Capone, D. G.: Biomass and primary productivity of the cyanobacterium *Trichodesmium* spp. in the tropical N Atlantic ocean, *Deep-Sea Res. Part I – Oceanographic Research Papers*, 51, 173–203, 2004.
- Cembella, A. D., Antia, N. J., and Harrison, P. J.: The Utilization of Inorganic and Organic Phosphorus-Compounds as Nutrients by Eukaryotic Microalgae – a Multidisciplinary Perspective. 1. *Crc Critical Reviews, Microbiology*, 10, 317–391, 1984.
- Chen, Y. L. L., Chen, H. Y., and Lin, Y. H.: Distribution and downward flux of *Trichodesmium* in the South China Sea as influenced by the transport from the Kuroshio Current, *Mar. Ecol.-Prog. Ser.*, 259, 47–57, 2003.
- Clark, L. L., Ingall, E. D., and Benner, R.: Marine phosphorus is selectively remineralized, *Nature*, 393, 426–426, 1998.
- Claustre, H. and Maritorea, S.: The many shades of ocean blue, *Science*, 302, 1514–1515, 2003.
- Codispoti, L. A. and Richards, F. A.: Analysis of Horizontal Regime of Denitrification in Eastern Tropical North Pacific, *Limnol. Oceanogr.*, 21, 379–388, 1976.
- Codispoti, L. A., Brandes, J. A., Christensen, J. P., Devol, A. H., Naqvi, S. W. A., Paerl, H. W., and Yoshinari, T.: The oceanic fixed nitrogen and nitrous oxide budgets: Moving targets as we enter the anthropocene?, *Sci. Mar.*, 65, 85–105, 2001.
- Cotner, J. B., Ammerman, J. W., Peele, E. R., and Bentzen, E.: Phosphorus-limited bacterioplankton growth in the Sargasso Sea, *Aquat. Microb. Ecol.*, 13, 141–149, 1997.
- Davis, C. S. and McGillicuddy, D. J.: Transatlantic abundance of the N-2-fixing colonial cyanobacterium *Trichodesmium*, *Science*, 312, 1517–1520, 2006.
- Deutsch, C., Sarmiento, J. L., Sigman, D. M., Gruber, N., and Dunne, J. P.: Spatial coupling of nitrogen inputs and losses in the ocean, *Nature*, 445, 163–167, 2007.

- Dore, J. E., Brum, J. R., Tupas, L. M., and Karl, D. M.: Seasonal and interannual variability in sources of nitrogen supporting export in the oligotrophic subtropical North Pacific Ocean, *Limnol. Oceanogr.*, 47, 1595–1607, 2002.
- Dugdale, R. C. and Wilkerson, F. P.: The Use of ¹⁵N to Measure Nitrogen Uptake in Eutrophic Oceans – Experimental Considerations, *Limnol. Oceanogr.*, 31, 673–689, 1986.
- Duhamel, S., Moutin, T., Van Wambeke, F., Van Mooy, B., Rimelin, P., Raimbault, P., and Claustre, H.: Growth and specific P-uptake rates of bacterial and phytoplanktonic communities in the Southeast Pacific (BIOPEPE cruise), *Biogeosciences*, 4, 941–956, 2007, <http://www.biogeosciences.net/4/941/2007/>.
- Dupouy, C., Neveux, J., Subramaniam, A., Mulholland, M. R., Montoya, J. P., Campbell, L., Carpenter, E. J., and Capone, D. G.: Satellite Captures Trichodesmium Blooms in the southwestern Tropical Pacific, *EOS*, 81, 13–16, 2000.
- Dyrhman, S. T., Chappell, P. D., Haley, S. T., Moffett, J. W., Orchard, E. D., Waterbury, J. B., and Webb, E. A.: Phosphate utilization by the globally important marine diazotroph Trichodesmium, *Nature*, 439, 68–71, 2006.
- Falcon, L. I., Carpenter, E. J., Cipriano, F., Bergman, B., and Capone, D. G.: N₂ fixation by unicellular bacterioplankton from the Atlantic and Pacific oceans: Phylogeny and in situ rates, *Appl. Environ. Microb.*, 70, 765–770, 2004.
- Falkowski, P. G.: Evolution of the nitrogen cycle and its influence on the biological sequestration of CO₂ in the ocean, *Nature*, 387, 272–275, 1997.
- Falkowski, P. G., Barber, R. T., and Smetacek, V.: Biogeochemical controls and feedbacks on ocean primary production, *Science*, 281, 200–206, 1998.
- Fennel, K., Spitz, Y. H., Letelier, R. M., Abbott, M. R., and Karl, D. M.: A deterministic model for N₂ fixation at stn. ALOHA in the subtropical North Pacific Ocean, *Deep-Sea Research Part II-Topical Studies, Oceanography*, 49, 149–174, 2002.
- Fu, F. X. and Bell, P. R. F.: Factors affecting N₂ fixation by the cyanobacterium Trichodesmium sp GBR-TRL1101, *Fems Microbiol. Ecol.*, 45, 203–209, 2003.
- Garcia, N., Raimbault, P., and Sandroni, V.: Seasonal nitrogen fixation and primary production in the Southwest Pacific: nanoplankton diazotrophy and transfer of nitrogen to picoplankton organisms, *Mar. Ecol.-Prog. Ser.*, 343, 25–33, 2007.
- Golterman, H. L. and de Oude, N. T.: Eutrophication of Lakes, Rivers and Coastal Seas, in: *The Handbook of Environmental Chemistry*, edited by: Hutzinger, O., Springer-Verlag, Berlin, 79–124., 1991
- Gruber, N.: The dynamics of the marine nitrogen cycle and its influence on atmospheric CO₂, *The ocean carbon cycle and climate*, Kluwer Academic, 97–148, 2004
- Hood, R. R., Coles, V. J., and Capone, D. G.: Modeling the distribution of Trichodesmium and nitrogen fixation in the Atlantic Ocean, *J. Geophys. Res.-Oceans*, 109, C06007, doi:10.1029/2002JC001754, 2004.
- Jickells, T. D., An, Z. S., Andersen, K. K., Baker, A. R., Bergametti, G., Brooks, N., Cao, J. J., Boyd, P. W., Duce, R. A., Hunter, K. A., Kawahata, H., Kubilay, N., laRoche, J., Liss, P. S., Mahowald, N., Prospero, J. M., Ridgwell, A. J., Tegen, I., and Torres, R.: Global iron connections between desert dust, ocean biogeochemistry and climate, *Science*, 308, 67–71, 2005.
- Karl, D., Letelier, R., Tupas, L., Dore, J., Christian, J., and Hebel, D.: The role of nitrogen fixation in biogeochemical cycling in the subtropical North Pacific Ocean, *Nature*, 388, 533–538, 1997.
- Karl, D. M.: Nutrient dynamics in the deep blue sea, *Trends in Microbiology*, *Trends Microbiol.*, 10, 410–418, 2002.
- Karl, D. M.: The marine phosphorus cycle, in: *Manual of Environmental Microbiology*, Third Edition, edited by: Hurst C. J. et al., American Society for Microbiology, Washington D.C., 523–539, 2007.
- Karl, D. M., Bidigare, R. R., Church, M. J., Dore, J. E., Letelier, R. M., Mahaffey, C., and Zehr, J.: The nitrogen cycle in the North Pacific trades biome: An evolving paradigm, edited by: Capone, D. G., Carpenter, E. J., Mulholland, M. and Bronk, D. A., *Nitrogen in the Marine Environment*, New York, Academic Press., in press.
- Karl, D. M., Bjorkman, K. M., Dore, J. E., Fujieki, L., Hebel, D. V., Houlihan, T., Letelier, R. M., and Tupas, L. M.: Ecological nitrogen-to-phosphorus stoichiometry at station ALOHA, *Deep-Sea Research Part II-Topical Studies in Oceanography, Deep-Sea Res. Part II-Top*, *Stud. Oceanogr.*, 48, 1529–1566, 2001.
- Kolowitz, L. C., Ingall, E. D., and Benner, R.: Composition and cycling of marine organic phosphorus, *Limnol. Oceanogr.*, 46, 309–320, 2001.
- Kustka, A., Carpenter, E. J., and Sanudo-Wilhelmy, S. A.: Iron and marine nitrogen fixation: progress and future directions, *Res. Microbiol.*, 153, 255–262, 2002.
- Labry, C., Herbland, A., and Delmas, D.: The role of phosphorus on planktonic production of the Gironde plume waters in the Bay of Biscay, *J. Plankton Res.*, 24, 97–117, 2002.
- LaRoche, J. and Breitbarth, E.: Importance of the diazotrophs as a source of new nitrogen in the ocean, *J. Sea Res.*, 53, 67–91, 2005.
- Levitan, O., Rosenberg, G., Setlik, I., Setlikova, E., Grigel, J., Klepetar, J., Prasil, O., and Berman-Frank, I.: Elevated CO₂ enhances nitrogen fixation and growth in the marine cyanobacterium Trichodesmium, *Glob. Change Biol.*, 13, 531–538, 2007.
- Lucotte, M. and Danglejan, B.: Processes Controlling Phosphate Adsorption by Iron Hydroxides in Estuaries, *Chem. Geol.*, 67, 75–83, 1988.
- Lugomela, C., Lyimo, T. J., Bryceson, I., Semesi, A. K., and Bergman, B.: Trichodesmium in coastal waters of Tanzania: diversity, seasonality, nitrogen and carbon fixation, *Hydrobiologia*, 477, 1–13, 2002.
- Mahowald, N. M., Muhs, D. R., Levis, S., Rasch, P. J., Yoshioka, M., Zender, C. S., and Luo, C.: Change in atmospheric mineral aerosols in response to climate: Last glacial period, preindustrial, modern, and doubled carbon dioxide climates, *J. Geophys. Res.-Atmos.*, 111, 2006.
- Meybeck, M.: C, N, P and S in rivers: from sources to global in: inputs, Interaction of C, N, P and S biogeochemical cycles and global change, edited by: Wollast, F. T. M. R. and Chou, L., Springer Verlag, 163–193, 1993.
- Mills, M. M., Ridame, C., Davey, M., La Roche, J., and Geider, R. J.: Iron and phosphorus co-limit nitrogen fixation in the eastern tropical North Atlantic, *Nature*, 429, 292–294, 2004.
- Montoya, J. P., Voss, M., Kahler, P., and Capone, D. G.: A simple, high-precision, high-sensitivity tracer assay for N₂ fixation, *Appl. Environ. Microb.*, 62, 986–993, 1996.
- Morel, A., Gentili, B., Claustre, H., Babin, M., Bricaud, A., Ras,

- J., and Tieche, F.: Optical properties of the “clearest” natural waters, *Limnol. Oceanogr.*, 52, 217–229, 2007.
- Moutin, T.: Cycle biogéochimique du phosphate: rôle dans le contrôle de la production planctonique et conséquence sur l’exportation du carbone de la couche éclairée vers l’océan profond, *Océanis*, 36, 643–660, 2000.
- Moutin, T., Raimbault, P., Golterman, H. L., and Coste, B.: The input of nutrients by the Rhone river into the Mediterranean Sea: Recent observations and comparison with earlier data, *Hydrobiologia*, 374, 237–246, 1998.
- Moutin, T., Van Den Broeck, N., Beker, B., Dupouy, C., Rimmelin, P., and Le Bouteiller, A.: Phosphate availability controls *Trichodesmium* spp. biomass in the SW Pacific Ocean, *Mar. Ecol.-Prog. Ser.*, 297, 15–21, 2005.
- Moutin, T., Thingstad, T. F., Van Wambeke, F., Marie, D., Slawyk, G., Raimbault, P., and Claustre, H.: Does competition for nanomolar phosphate supply explain the predominance of the cyanobacterium *Synechococcus*?, *Limnol. Oceanogr.*, 47, 1562–1567, 2002.
- Needoba, J. A., Foster, R. A., Sakamoto, C., Zehr, J. P., and Johnson, K. S.: Nitrogen fixation by unicellular diazotrophic cyanobacteria in the temperate oligotrophic North Pacific Ocean, *Limnol. Oceanogr.*, 52, 1317–1327, 2007.
- Orcutt, K. M., Lipschultz, F., Gundersen, K., Arimoto, R., Michaels, A. F., Knap, A. H., and Gallon, J. R.: A seasonal study of the significance of N₂ fixation by *Trichodesmium* spp. at the Bermuda Atlantic Time-series Study (BATS) site, *Deep-Sea Res. Part II-Topical Studies, Oceanography*, 48, 1583–1608, 2001.
- Paerl, H. W., Prufert-Bebout, L. E., and Guo, C.: Iron-stimulated N₂ fixation and growth in Natural and Cultured Populations of the Planktonic Marine Cyanobacteria *Trichodesmium* spp., *Appl. Environ. Microb.*, 60, 1044–1047, 1994.
- Pandey, K. D., Shukla, S. P., Shukla, P. N., Giri, D. D., Singh, J. S., Singh, P., and Kashyap, A. K.: Cyanobacteria in Antarctica: Ecology, physiology and cold adaptation, *Cell. Mol. Biol.*, 50, 575–584, 2004.
- Paytan, A. and McLaughlin, K.: The oceanic phosphorus cycle, *Chem. Rev.*, 107, 563–576, 2007.
- Perry, M. J. and Eppley, R. W.: Phosphate-Uptake by Phytoplankton in the Central North Pacific-Ocean, *Deep-Sea Res. Part a-Oceanographic Research Papers*, 28, 39–49, 1981.
- Pujopay, M. and Raimbault, P.: Improvement of the Wet-Oxidation Procedure for Simultaneous Determination of Particulate Organic Nitrogen and Phosphorus Collected on Filters, *Mar. Ecol.-Prog. Ser.*, 105, 203–207, 1994.
- Raimbault, P. and Garcia, N.: Carbon and nitrogen uptake in the South Pacific Ocean: evidence for efficient dinitrogen fixation and regenerated production leading to large accumulation of dissolved organic matter in nitrogen-depleted waters, *Biogeosciences Discuss.*, 4, 3531–3579, 2007, <http://www.biogeosciences-discuss.net/4/3531/2007/>.
- Raimbault, P., Slawyk, G., Coste, B., and Fry, J.: Feasibility of Using an Automated Colorimetric Procedure for the Determination of Seawater Nitrate in the 0 to 100 Nm Range – Examples from Field and Culture, *Mar. Biol.*, 104, 347–351, 1990.
- Ras, J., Claustre, H., and Uitz, J.: Spatial variability of phytoplankton pigment distributions in the Subtropical South Pacific Ocean: comparison between in situ and predicted data, *Biogeosciences Discuss.*, 4, 3409–3451, 2007, <http://www.biogeosciences-discuss.net/4/3409/2007/>.
- Redfield, A. C.: On the proportions of organic derivatives in sea water and their relation to the composition of plankton, in: James Johnstone Memorial Volume, edited by: Daniel, R. J., University Press, 176–192, 1934.
- Redfield, A. C., Ketchum, B. H., and Richards, F. A.: The influence of organisms on the composition of sea-water, in: THE SEA, Ideas and Observations on Progress in the Study of the Seas, edited by: Hill, M. N., Interscience publishers a division of John Wiley and Sons, 26–77, 1963.
- Rimmelin, P. and Moutin, T.: Re-examination of the MAGIC method to determine low orthophosphate concentration in sea-water, *Anal. Chim. Acta*, 548, 174–182, 2005.
- Sanudo-Wilhelmy, S. A., Kustka, A. B., Gobler, C. J., Hutchins, D. A., Yang, M., Lwiza, K., Burns, J., Capone, D. G., Raven, J. A., and Carpenter, E. J.: Phosphorus limitation of nitrogen fixation by *Trichodesmium* in the central Atlantic Ocean, *Nature*, 411, 66–69, 2001.
- Schlitzer, R.: Interactive analysis and visualization of geoscience data with Ocean Data View, *Computers and Geosciences*, 28, 1211–1218, 2002.
- Staal, M., Meysman, F. J. R., and Stal, L. J.: Temperature excludes N-2-fixing heterocystous cyanobacteria in the tropical oceans, *Nature*, 425, 504–507, 2003.
- Strickland, J. D. H. and Parsons, T. R.: A practical handbook of seawater analysis, 2nd ed., *Bull. Fish. Res. Bd. Can.*, 310 pp., 1972.
- Tagliabue, A., Bopp, L., and Aumont, O.: Ocean biogeochemistry exhibits contrasting responses to a large scale reduction in dust deposition, *Biogeosciences*, 5, 11–24, 2008, <http://www.biogeosciences.net/5/11/2008/>.
- Tanaka, T., Henriksen, P., Lignell, R., Olli, K., Seppala, J., Tamminen, T., and Thingstad, T. F.: Specific Affinity for Phosphate Uptake and Specific Alkaline Phosphatase Activity as Diagnostic Tools for Detecting Phosphorus-limited Phytoplankton and Bacteria, *Estuaries Coasts*, 29, 1226–1241, 2006.
- Thingstad, T. F., Skjoldal, E. F., and Bohne, R. A.: Phosphorus Cycling and Algal-Bacterial Competition in Sandsfjord, Western Norway, *Mar. Ecol.-Prog. Ser.*, 99, 239–259, 1993.
- Tréguer, P. and LeCorre, P.: Manuel d’analyse des sels nutritifs dans l’eau de mer (Utilisation de l’autoAnalyseur II), Université de Bretagne Occidentale, Laboratoire d’Océanographie chimique, 110, 1975.
- Tyrrell, T.: The relative influences of nitrogen and phosphorus on oceanic primary production, *Nature*, 400, 525–531, 1999.
- Van Den Broeck, N. and Moutin, T.: Phosphate in the sediments of the Gulf of Lions (NW Mediterranean Sea), relationship with input by the river Rhone, *Hydrobiologia*, 472, 85–94, 2002.
- Van Den Broeck, N., Moutin, T., Rodier, M., and Le Bouteiller, A.: Seasonal variations of phosphate availability in the SW Pacific Ocean near New Caledonia, *Mar. Ecol.-Prog. Ser.*, 268, 1–12, 2004.
- Van Wambeke, F., Obernosterer, I., Moutin, T., Duhamel, S., Ulloa, O., and Claustre, H.: Heterotrophic bacterial production in the South East Pacific: longitudinal trends and coupling with primary production, *Biogeosciences Discuss.*, 4, 2761–2791, 2007, <http://www.biogeosciences-discuss.net/4/2761/2007/>.
- Wagener, T., Guieu, C., Losno, R., Bonnet, S., and Mahowald, N.: Revisiting atmospheric dust export to the South Hemisphere

- ocean, *Global Biogeochem. Cy.*, doi:10.1029/2007GB002984, in press, 2008.
- Wu, J. F., Sunda, W., Boyle, E. A., and Karl, D. M.: Phosphate depletion in the western North Atlantic Ocean, *Science*, 289, 759–762, 2000.
- Zehr, J. P., Waterbury, J. B., Turner, P. J., Montoya, J. P., Omoregie, E., Steward, G. F., Hansen, A., and Karl, D. M.: Unicellular cyanobacteria fix N₂ in the subtropical North Pacific Ocean, *Nature*, 412, 635–638, 2001.
- Zehr, J. P., Montoya, J. P., Jenkins, B. D., Hewson, I., Mondragon, E., Short, C. M., Church, M. J., Hansen, A., and Karl, D. M.: Experiments linking nitrogenase gene expression to nitrogen fixation in the North Pacific subtropical gyre, *Limnol. Oceanogr.*, 52, 169–183, 2007.
- Zielke, M., Ekker, A. S., Olsen, R. A., Spjelkavik, S., and Solheim, B.: The influence of abiotic factors on biological nitrogen fixation in different types of vegetation in the High Arctic, Svalbard, *Arct. Antarct. Alp. Res.*, 34, 293–299, 2002.
- Zohary, T. and Robarts, R. D.: Experimental study of microbial P limitation in the eastern Mediterranean, *Limnol. Oceanogr.*, 43, 387–395, 1998.

Growth and specific P-uptake rates of bacterial and phytoplanktonic communities in the Southeast Pacific (BIOSOPE cruise)

S. Duhamel^{1,2}, T. Moutin¹, F. Van Wambeke², B. Van Mooy³, P. Rimmelin¹, P. Raimbault¹, and H. Claustre⁴

¹Aix-Marseille Université, Laboratoire d'Océanographie et de Biogéochimie, LOB-UMR 6535 CNRS, OSU/Centre d'Océanologie de Marseille, 13288 Marseille, Cedex 09, France

²Aix-Marseille Université, Laboratoire de Microbiologie, Géochimie et Ecologie Marines, LMGEM-UMR 6117 CNRS, OSU/Centre d'Océanologie de Marseille, 13288 Marseille, Cedex 09, France

³Department of Marine Chemistry and Geochemistry, Wood Hole Oceanographic Institution, MS #4, Wood Hole, MA 02543, USA

⁴CNRS, Laboratoire d'océanographie de Villefranche, 06230 Villefranche-sur-Mer, France; Université Pierre et Marie Curie-Paris 6, Laboratoire d'océanographie de Villefranche, 06230 Villefranche-sur-mer, France

Received: 15 June 2007 – Published in Biogeosciences Discuss.: 27 June 2007

Revised: 18 September 2007 – Accepted: 18 October 2007 – Published: 8 November 2007

Abstract. Predicting heterotrophic bacteria and phytoplankton specific growth rates (μ) is of great scientific interest. Many methods have been developed in order to assess bacterial or phytoplankton μ . One widely used method is to estimate μ from data obtained on biomass or cell abundance and rates of biomass or cell production. According to Kirchman (2002), the most appropriate approach for estimating μ is simply to divide the production rate by the biomass or cell abundance estimate. Most methods using this approach to estimate μ are based on carbon (C) incorporation rates and C biomass measurements. Nevertheless it is also possible to estimate μ using phosphate (P) data. We showed that particulate phosphate (PartP) can be used to estimate biomass and that the P uptake rate to PartP ratio can be employed to assess μ . Contrary to other methods using C, this estimator does not need conversion factors and provides an evaluation of μ for both autotrophic and heterotrophic organisms. We report values of P-based μ in three size fractions (0.2–0.6; 0.6–2 and $>2\ \mu\text{m}$) along a Southeast Pacific transect, over a wide range of P-replete trophic status. P-based μ values were higher in the 0.6–2 μm fraction than in the $>2\ \mu\text{m}$ fraction, suggesting that picoplankton-sized cells grew faster than the larger cells, whatever the trophic regime encountered. Picoplankton-sized cells grew significantly faster in the deep chlorophyll maximum layer than in the upper part of the photic zone in the oligotrophic gyre area, suggesting that picoplankton might outcompete $>2\ \mu\text{m}$ cells in this particular high-nutrient, low-light environment. P-based μ attributed to free-living bacteria (0.2–0.6 μm) and picoplankton (0.6–2 μm) size-fractions were relatively low ($0.11\pm 0.07\ \text{d}^{-1}$ and

$0.14\pm 0.04\ \text{d}^{-1}$, respectively) in the Southeast Pacific gyre, suggesting that the microbial community turns over very slowly.

1 Introduction

A fundamental aim in ecology and hence, biological oceanography and limnology, is to understand and predict the abundance of organisms and their temporal change (Banse, 2002). An assessment of the ecological role of both autotrophic and heterotrophic marine micro-organisms depends, to a significant extent, on estimates of their specific growth rate (μ) (Azam et al., 1983). Bacterial or primary production is the synthesis of bacteria or phytoplankton biomass, respectively. Production can be expressed as the rate of synthesis of cells or cell mass: $\text{production}=\mu\times\text{biomass}$, where μ is the specific growth rate of the population expressed in units of inverse time t^{-1} (Ducklow, 2000). Phytoplankton μ estimates vary widely from values of around $0.1\text{--}0.3\ \text{d}^{-1}$ (Letelier et al., 1996; Marañón et al., 2000, 2005) to $1\text{--}2\ \text{d}^{-1}$ (Laws et al., 1987; Quevedo and Anadon, 2001). Bacterial μ estimates also vary widely, from very low values $0.004\text{--}0.25\ \text{d}^{-1}$ (Sherr et al., 2001; Van Wambeke, 2007b) to higher values of around $2\text{--}10\ \text{d}^{-1}$ (Ducklow, 1983; Jones et al., 1996). Studies comparing bacterial and phytoplankton μ are scarce and show significant differences between bacterial and phytoplankton μ (Jones et al., 1996).

Numerous methods have been developed to measure μ (Brock, 1971). Direct and indirect methodologies of varying accuracy have been used to estimate phytoplankton and

Correspondence to: S. Duhamel
(solange.duhamel@univmed.fr)

heterotrophic bacterial μ . The two most common direct methods, applicable to both heterotrophic bacteria and phytoplankton, are (1) to observe the frequency of dividing cells (Hagstrom et al., 1979) and (2) the dilution technique (Landry and Hassett, 1982; Quevedo and Anadon, 2001). Direct methods are difficult to set up on board so microbial growth rates are commonly calculated from production and standing stock data (Ducklow, 2000). According to Kirchman (2002), the most appropriate approach for estimating μ of microbial assemblages is the simplest, that is, dividing the production rate by the biomass estimate (B). This ratio called the “specific uptake rate” (V^{SP}) is a carbon (C), nitrogen (N) or phosphate (P)-based measurement of μ corresponding to the cell specific or biomass specific uptake of C, N or P (Lipschultz, 1995; Dickson and Wheeler, 1995; Ducklow, 2000). V^{SP} is an expression of the μ . These two parameters are not necessarily equal and V^{SP} must be considered as an estimator of μ . Both μ and V^{SP} are determined by resource limitation, temperature and predation (Brock, 1971; Thingstad, 2000). The most common indirect methods for measuring phytoplankton μ are ^{14}C -pigment labelling (Redalje and Laws, 1981; Welschmeyer et al., 1991; Jones et al., 1996; Cailiau et al., 1996), cell cycle analysis (Vaulot, 1992; Liu et al., 1999) and the use of equations linking autotrophic production (AP) and autotrophic cell abundance or biomass (AB) (Smith et al., 2000; Marañon, 2005). In such equations, AP is deduced from $\text{NaH}^{14}\text{CO}_3$ incorporation rate measurements (Steemann-Nielsen, 1951) in the particulate fraction (i.e. biomass production) which does not include significant losses from respiration or excretion, when short term incubations are processed. The most common indirect method for studying heterotrophic bacterial μ is the use of equations linking heterotrophic bacterial production (HBP) and heterotrophic bacterial cell abundance or biomass (HBB). In such equations, HBP is generally deduced from the incorporation of ^3H -thymidine (Fuhrman and Azam, 1980, 1982) and ^3H -leucine (Kirchman et al., 1985) into DNA and proteins, respectively, with appropriate conversion factors for biomass production. More recently, measurements of the incorporation rates of $^{33}\text{PO}_4$ into phospholipids (particularly phosphatidylglycerol: PG and phosphatidylethanolamine: PE) specific to bacterioplankton have been used (Van Mooy et al., 2006).

Phytoplankton μ is frequently estimated by dividing AP (measured using the ^{14}C method) by various AB estimators such as Chlorophyll a (Chla), particulate organic carbon (POC) and C content using microscopy or flow cytometry measurements (Eppley, 1972; Vadstein et al., 1988; Malone et al., 1993; Marañon et al., 2000, 2005; Moreira-Turcq, 2001). The use of Chla and POC as AB proxies is debatable (Le Floch et al., 2002; Sobczak et al., 2002; Huot et al., 2007) and C content estimates are dependant on conversion factors. These conversion factors can vary greatly between studies. Similarly, the evaluation of bacterial μ based on the HBP to HBB ratio requires the use of sev-

eral conversion factors (to convert the incorporation of ^3H -leucine or ^3H -thymidine to C equivalents and to convert cell number to biomass equivalents). These conversion factors vary with different studies (Riemann et al., 1990). Furthermore, method comparisons can show significant differences between μ estimates (Laws et al., 1984).

If $\mu = \text{production/biomass}$, then there is a direct relationship between incorporation rate per cell and μ (Kirchman, 2002). Although biomass and production estimators are usually expressed in terms of C, it is also possible to express them in terms of N or P as C, N and P are major cellular constituents linked via the “Redfield ratio” (Redfield, 1963; Berman, 1980; Laws et al., 1984). PartP is released from decaying material more efficiently than C and N (Loh and Bauer, 2000) and seems to be decomposed or remineralized essentially at the same rate as chlorophyll (Menzel and Ryther, 1964). As a consequence, in the open ocean, the proportion of detrital P in PartP is low (Faul et al., 2005). Phosphate uptake rates are commonly measured using the ^{32}P or ^{33}P method, which quantifies the amount of P that is taken up by both heterotrophic and autotrophic cells. Measuring the dissolved inorganic P (DIP) uptake rates provides an estimate for planktonic production, assuming DIP is the sole source of P and there is no, or negligible luxury uptake (Thingstad et al., 1996). Thus, particulate P (PartP) and P uptake rate can be used as estimators of planktonic biomass and production, respectively.

We estimated μ from production to biomass ratios expressed in terms of P and discussed the bias associated with using C and P-based μ estimations. Combining P uptake rates and PartP measurements with size fractionations, we determined the DIP specific uptake rate ($V_{\text{DIP}}^{\text{SP}}$) in three size fractions corresponding to heterotrophic bacteria, picophytoplankton and nano-microphytoplankton (0.2–0.6; 0.6–2 and $>2 \mu\text{m}$, respectively), following an East-West transect along the Southeast Pacific ocean. This area presents a gradient in trophic conditions, from the extremely oligotrophic Southeast Pacific gyre, the largest and most poorly investigated province of the world ocean (Claustre and Maritorena, 2003; Claustre et al., 2007¹), to the highly productive Chilean upwelling region. The measurement of $V_{\text{DIP}}^{\text{SP}}$ in the different fractions enabled us to compare bacterial to phytoplankton μ using the same method and enabled us to study the variation in dynamics between 2 major groups of phytoplankton.

¹Claustre, H., Sciandra, A., and Vaulot, D.: Introduction to the special section: bio-optical and biogeochemical conditions in the South East Pacific in late 2004 – the BIOSOPE cruise, Biogeosciences, in preparation, 2007.

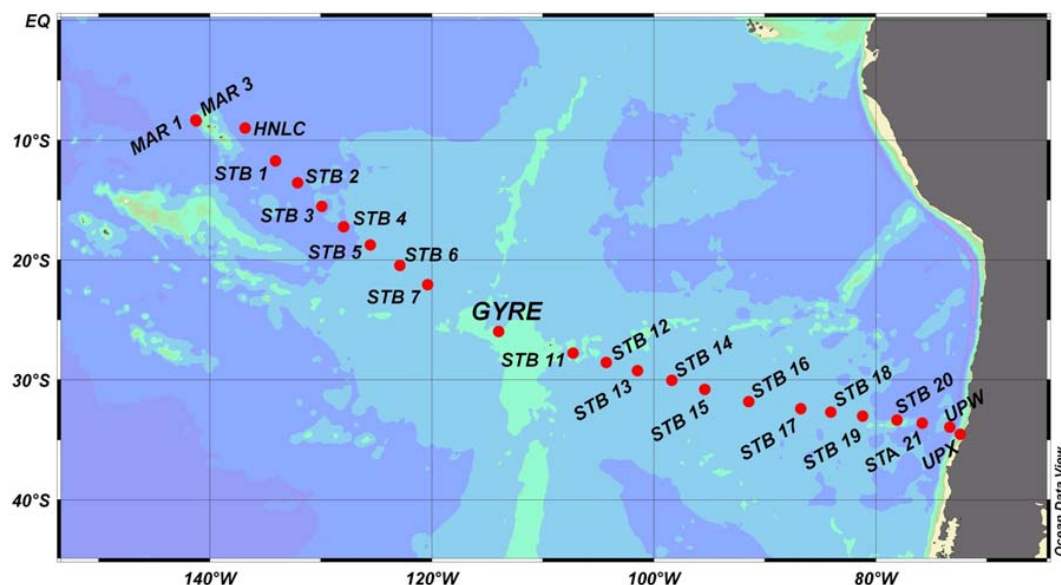


Fig. 1. Station names and locations of the BIOSOPE cruise transect in the South East Pacific Ocean (October–December 2004). MAR 1 and MAR 3 (in the vicinity of Marquesas Islands), HNLC (High Nutrient Low Chlorophyll area), GYRE (the central part of the Southeast Pacific gyre), and UPW and UPX (the Chilean upwelling) are long stations (3–4 days) abbreviated according their location; STB1–STA21 are short stations (1 day).

2 Materials and methods

2.1 Station locations, sample collection and hydrological characteristics

This work was conducted during the BIOSOPE (BIogeochemistry and Optics SOUTh Pacific Experiment) cruise in the Southeast Pacific Ocean (between 146.36° W and 72.49° W; Fig. 1). The cruise was carried out aboard “l’Atalante” from October to December 2004. High resolution profiles of temperature, conductivity, salinity, oxygen and fluorescence were obtained using a CTDO profiler (Seabird 911 Plus) from a depth of 0 to 500 m (See Claustre et al. and Ras et al., 2007, for hydrodynamical entities, hydrographic conditions and pigment distribution). Seawater samples were collected at 6 different depths corresponding to 50, 25, 15, 7, 3 and 1% surface irradiance, respectively. Samples were collected in 12 l Niskin bottles attached to a rosette CTD system, at 09:00 a.m. (local time). Subsamples were collected without pre-filtration, into clean, sample-rinsed polycarbonate bottles.

2.2 Analytical methods

Particulate phosphate (PartP) was measured using the Strickland and Parsons procedure (1972) for standard DIP, following high-temperature persulfate wet-oxidation at 120°C and 1 bar (Pujo-Pay and Raimbault, 1994). Sequential filtration was carried out on 1 to 1.2 l samples through different porosity polycarbonate filters (0.2, 0.6, and 2 µm; 47 mm) using Sartorius systems and very low vacuum (drop by drop). The

0.2 and 0.6 µm filters in the lower Sartorius system were separated by a nylon separator (NY8H04700, Millipore) previously treated using persulfate wet-oxidation to lower blank values. Immediately after filtration, the filters (and the separator for the 0.2 µm filter) were put into 20 ml Teflon bottles. 2.5 ml of reagent (140 ml of NaOH 1.5 M, 30 g of H₃BO₃, 360 ml of demineralised water) was added and the mineralization processed (autoclave 30 min, 1 bar). After cooling down to ambient temperature, DIP was measured in the same bottles. All reagents were prepared with pro analysis Merck™ Reagent Grade chemicals and with Milli-QTM high purity demineralised water. All utensils were washed with 10% hydrochloric acid and rinsed three times with demineralised water.

Particulate organic carbon concentration was determined by the wet-oxidation procedure (Raimbault et al., 1999), following the filtration of 1.2 l of seawater through 0.2 µm teflon membranes.

Chlorophyll a (Chl a) concentration was determined by the serial filtration of 1 to 1.2 l samples following the same filtration method as for PartP. Immediately after filtration, the filters were put in cryotubes with 5 ml of methanol for pigment extraction (30 min, 4°C) (Herbland et al., 1985). The fluorescence was measured using a Turner designs 10-AU-005-CE fluorimeter equipped with a chlorophyll a Kit (F4T45.B2 lamp) according to Welschmeyer (1994).

Picophytoplankton (*Prochlorococcus*, *Synechococcus* and picophytoeukaryotes) and bacterial abundance were determined according to Grob et al. (2007) using a FACSCalibur (Becton Dickinson) flow cytometer. Picophytoplankton

abundance was determined in situ on fresh samples while bacterioplankton samples were fixed with a final concentration of either 1% paraformaldehyde or 0.1% glutaraldehyde and frozen in liquid nitrogen. Samples were then processed according to Marie et al. (2000a,b). At each sampling depth, defined by the Chla and P and C uptake rates measurements, 2 mL samples were filtered through 0.6 μm polycarbonate filters. The filtrate was then analysed using flow cytometry and compared to the total in the corresponding sample.

Carbon and phosphate uptakes were determined using the $^{33}\text{P}/^{14}\text{C}$ dual labelling method (Duhamel et al., 2006). Duplicate samples (300 ml) were collected into sample-rinsed, polycarbonate bottles (Nalgene) for each sampling depth. An additional duplicate sample (300 ml) of surface water was incubated with 300 μl of HgCl_2 (20 g l^{-1}) to act as a control for non-biological assimilation (Kirkwood 1992). The samples were inoculated with 1080 kBq carrier-free ^{33}P (<40 pmol l^{-1} final concentration – orthophosphate in dilute hydrochloric acid; Amersham BF 1003; half-life 25.383 \pm 0.040 days; Duhamel et al., 2006), and 3.7 MBq ^{14}C (bicarbonate aqueous solution; Amersham CFA3; half-life 5700 \pm 30 years; Duhamel et al., 2006). Samples were incubated under simulated conditions for 4 to 5 h. Incubation boxes equipped with light filters (nickel screens) were used to reproduce the light level at the sample depths (50 – 25 – 15 – 7 – 3 – 1% of transmitted light). Following incubation, 600 μl of KH_2PO_4 (10 mmol l^{-1}) was added to each flask in order to stop labelled DIP assimilation. Samples were kept in the dark to stop DIC uptake. Fractions of 50 ml were filtered through 25 mm polycarbonate membranes (0.2, 0.6 and 2 μm) which had been placed on GF/F filters soaked with saturated KH_2PO_4 , using a low-pressure suction (<0.2 bars). When all samples were filtered, the pressure was increased to 0.6 bars for 5 s in order to eliminate unincorporated ^{33}P . Filters were placed into scintillation vials (Wheaton low-potassium 6 ml glass-clear vials with screw-cap foil liner) with 150 μl of HCl (0.5 mol l^{-1}) in order to eliminate any unincorporated ^{14}C . After 12 h, 6 ml of scintillation liquid (Ultimagold MV scintillation liquid, Packard) was added to each vial before the first count. Counting (count per minute - cpm) was carried out on a Packard Tri-Carb® 2100TR scintillation counter. In order to separate the activity due to ^{33}P from that of ^{14}C , we applied the method using the different half-lives of the two isotopes (For more details, see Duhamel et al., 2006). A second count was made a year later, samples having been preserved in the dark at room temperature. C and P uptake rate measurements in each size fraction (0.2–0.6; 0.6–2 and >2 μm) were obtained using difference calculations.

Bacterial production was determined by [^3H]-leucine incorporation using the centrifugation method (Smith and Azam, 1992) according to Van Wambeke et al. (2007b). A factor of 1.5 kg C mol leucine $^{-1}$ was used to convert the incorporation of leucine to carbon equivalents, assuming no isotopic dilution (Kirchman, 1993).

2.3 Daily rates

The daily C uptake rates have been calculated using the method of Moutin et al. (1999). The model enables a conversion factor to be calculated which permits net hourly DIC uptake rates ($\text{nmol l}^{-1} \text{h}^{-1}$) to be transformed into net daily rates ($\text{nmol l}^{-1} \text{d}^{-1}$). The model takes into account the geographical position (latitude and longitude), the sampling date, the time of dawn, incubation start time and the time the incubation ended (GMT). The model of Moutin et al. (1999) that previously took theoretical solar radiation into account has been modified to take into account the surface irradiance measured on board.

Daily P uptake rates have been calculated simply by multiplying the hourly rate by 24. Indeed, in several studies (Perry and Eppley, 1981; Moutin et al., 2002), P uptake was shown to be constant over 24 h.

2.4 Specific uptake rate estimates

Specific uptake rates (V^{SP}) have been calculated by dividing heterotrophic bacterial production (HBP), C uptake rates (V_{DIC}) or P uptake rates (V_{DIP}) by heterotrophic bacterial biomass (HBB), phytoplankton biomass (AB) and particulate P (PartP), respectively. $V_{\text{DIP}}^{\text{SP}}$ corresponds to the V_{DIP} to PartP ratio, $V_{\text{DIC}}^{\text{SP}}$ corresponds to the V_{DIC} to AB ratio, HBP:HBB corresponds to the HBP to HBB ratio. A conversion factor of 10 fgC cell $^{-1}$ (Christian and Karl, 1994; Caron et al., 1995) has been used to convert heterotrophic bacterial abundance (counted by flow cytometry) to C equivalent. AB has been calculated using two methods. The first one uses a cell-number-to-biomass conversion factor. We chose the Campbell et al. (1997) estimates for *Prochlorococcus*, *Synechococcus* and Picoeukaryotes (Table 1). The second method uses a Chla-to-biomass conversion factor. For stations outside the gyre, we chose 70 gC gChla $^{-1}$, the average value found for subtropical Atlantic Ocean total phytoplankton (Veldhuis and Kraay, 2004). For stations inside the gyre, we used a Chla-to-biomass conversion factor varying with PAR (Photosynthetically Active irradiance): 185, 120, 90, and 20 gC gChla $^{-1}$ for 50 and 25%, 15%, 7%, and 3 and 1% of PAR, respectively. These factors were chosen in accordance with the results obtained by Veldhuis and Kraay (2004) at their most oligotrophic station in the Atlantic tropical gyre.

The $V_{\text{DIP}}^{\text{SP}}$ have been calculated for four size fractions: 0.2–0.6; 0.6–2; >2 and >0.6 μm . We will develop arguments to show that they correspond to heterotrophic bacteria ($V_{\text{DIP}<0.6}^{\text{SP}}$), picophytoplankton ($V_{\text{DIP}0.6-2}^{\text{SP}}$), nanophytoplankton ($V_{\text{DIP}>2}^{\text{SP}}$) and total phytoplankton ($V_{\text{DIP}>0.6}^{\text{SP}}$), respectively. V^{SP} are expressed as daily rates (d^{-1}) so are comparable with the values found in the literature.

Table 1. Review of values of biovolume-to-biomass and cell-number-to-biomass conversion factors.

Biovolume-to-biomass conversion factor		
Biovolume:B (g of C cm ⁻³)	Organisms - location	Reference
0.121	Bacteria seawater or cultures	Watson et al., 1977
0.38±0.05	Heterotrophic bacteria - pebble beach (Long Island) or culture	Lee and Fuhrman, 1987
Cell-number-to-biomass conversion factor		
Cell:B (fg of C cell ⁻¹)	Organisms - location	Reference
20±0.8	Heterotrophic bacteria - pebble beach (Long Island) or culture	Lee and Fuhrman, 1987
5.9 to 47.9	Heterotrophic bacteria - coastal environments	Fukuda et al., 1998
13	Heterotrophic bacteria - subtropical Pacific Ocean	Fukuda et al., 1998
12.4	Heterotrophic bacteria - Oceanic environments	Fukuda et al., 1999
10	Heterotrophic bacteria - subtropical Pacific Ocean	Christian and Karl, 1994
15	Heterotrophic bacteria - Sargasso Sea	Caron et al., 1995
5.83	Heterotrophic bacteria - Northern Adriatic Sea (warm period)	La Ferla and Leonardi, 2005
42.17	Heterotrophic bacteria - Northern Adriatic Sea (cold period)	La Ferla and Leonardi, 2005
20	Heterotrophic bacteria - Station ALOHA	Campbell et al., 1997
65±67	<i>Prochlorococcus</i> CCMP 1378: considering C content varies with light for cultures switched from low light to high light	Cailliau et al., 1996
48±10	<i>Prochlorococcus</i> CCMP 1378: considering C content varies with light for cultures switched high light to low light	Cailliau et al., 1996
49±9	<i>Prochlorococcus</i> CCMP 1378: considering C content is independent of light	Cailliau et al., 1996
27±6	<i>Prochlorococcus</i> PCC 9511 grown under a daily light cycle	Claustre et al., 2002
53	<i>Prochlorococcus</i> - Station ALOHA	Campbell et al., 1997
46	<i>Prochlorococcus</i> - cultures <i>Prochlorococcus</i> MED4	Bertilsson et al., 2003
29	<i>Prochlorococcus</i> - Atlantic transect from 50° N to 50° S	Zubkov et al., 1998
279.1±84.2	<i>Synechococcus</i> - cultures <i>Synechococcus</i> WH8102	Six et al., 2004
250	<i>Synechococcus</i> - Station ALOHA	Campbell et al., 1997
92	<i>Synechococcus</i> - cultures <i>Synechococcus</i> WH8012	Bertilsson et al., 2003
100	<i>Synechococcus</i> - Atlantic transect from 50° N to 50° S	Zubkov et al., 1998
2108	Picoeukaryote - Station ALOHA	Campbell et al., 1997
1500	Picoeukaryote - Atlantic transect from 50° N to 50° S	Zubkov et al., 1998

3 Results

3.1 Cytometry data

Bacteria were separated from phytoplankton by filtering through 0.6 μm filters so as to determine bacterial V_{DIP}^{SP} in the 0.2–0.6 μm fraction. The percentages of bacterial cells passing through a 0.6-μm-filter were counted using flow cytometry in order to assess the accuracy of the results. On comparing total and <0.6 μm sample counts, we found that on average, 91±10% of the heterotrophic bacteria passed through the 0.6-μm-filter whatever the trophic regime (n=90; all euphotic-layer depths included). This value was in the same range as those obtained in other studies (~80%; Obernosterer et al., 2003). Flow cytometry mea-

surements revealed that *Prochlorococcus* (when detectable), *Synechococcus* and Picoeucaryotes cells had an average size of 0.68±0.08 μm; 0.86±0.1 μm and 1.74±0.13 μm, respectively over the entire transect (Results from Grob et al., 2007). The average cell size of *Synechococcus* found at the upwelling stations was 1.16±0.02 μm. Despite of this, cytometry counts showed that 34±24% of the *Prochlorococcus* cells and 3±5% of the *Synechococcus* cells were found in the <0.6 μm fraction.

3.2 Evaluating the use of particulate phosphate as an estimator of living biomass

Figure 2 shows a typical example of the vertical distribution of PartP and Chla concentrations compared to the vertical

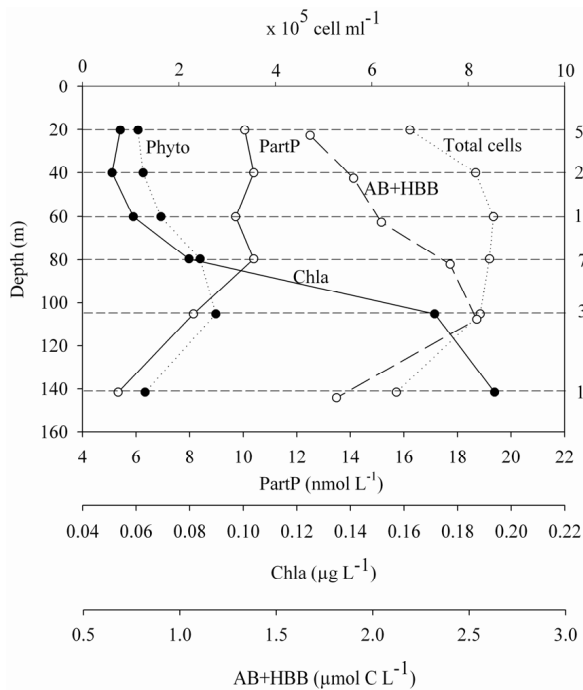


Fig. 2. Example of vertical distribution of biological properties at station STB4 (127.97° W; 17.23° S): particulate phosphate (PartP), chlorophyll a (Chla), total phytoplankton counted by flow cytometry: *Prochlorococcus* + *Synechococcus* + picoeukaryotes (phyto), total cells (heterotrophic bacteria + phytoplankton) counted by flow cytometry (Total cells) and total C biomass estimates based on cell counts (AB+HBB).

distribution of cell counts by flow cytometry and total C biomass estimate based on cell counts (AB+HBB). In the upper 80 m, PartP concentrations were fairly constant, varying between 10.0 and 10.4 nmol l⁻¹ from the surface to a depth of 7% PAR. PartP concentrations decreased to 5.3 nmol l⁻¹ at the depth of 1% PAR while Chla concentrations increased from 0.05 to 0.19 µg l⁻¹ from the surface waters down to 1% of PAR, respectively. In contrast to Chla, PartP did not show a deep concentration maximum (Fig. 2). Phytoplankton cell counts using flow cytometry showed an increase from 1.1 × 10⁵ to 2.8 × 10⁵ cells ml⁻¹ from surface water to the depth of 3% of PAR and a decrease to 1.3 × 10⁵ cells ml⁻¹ at the depth of 1% of PAR. In the same way, total cytometric counts (bacteria + phytoplankton) showed an increase from 6.8 × 10⁵ to 8.5 × 10⁵ cells ml⁻¹ from the surface water to the depth of 15% of PAR and a decrease to 6.5 × 10⁵ cells ml⁻¹ at the depth of 1% of PAR. The total C biomass (AB+HBB) estimated from cell counts using flow cytometry and conversion factors from Campbell et al. (1997) for the different groups of organisms (heterotrophic bacteria, *Prochlorococcus*, *Synechococcus* and picoeukaryotes) increased between 50 and 3% of PAR, ranging from 1.68 to 2.64 µmol C l⁻¹, before decreasing to 1.81 µmol C l⁻¹. Variations in PartP concentration throughout the euphotic zone are closer to that of

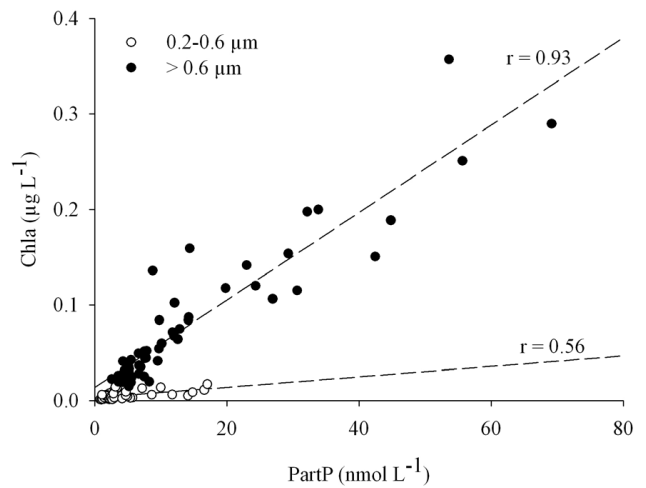


Fig. 3. Relations between Chlorophyll a (Chla) and particulate phosphate (PartP) at depth corresponding to a range of PAR levels between 50% and 15%, for two size fractions: 0.2–0.6 µm and >0.6 µm.

cell concentration and total C biomass, estimate based on cell counts, than to Chla concentration.

Chla is largely used to estimate phytoplankton biomass (Trembaly and Legendre, 1994; Uitz et al., 2006). However, as illustrated in Fig. 2, the C:Chla ratio varies with light (Taylor et al., 1997). In comparing biomass estimates to Chla concentration only data between 50 and 15% of transmitted light have been considered to avoid any bias associated with photoacclimation. PartP and Chla data were compared in the <0.6 and >0.6 µm fractions (Fig. 3) in order to verify that the PartP in these fractions was representative of the bacteria and phytoplankton biomasses, respectively. Most of the PartP in the >0.6 µm fraction correlated to Chla, supporting the hypothesis that it is essentially made up of phytoplankton biomass (Fig. 3). The relationship between Chla and PartP in the 0.2–0.6 µm fraction was less significant than in the >0.6 µm fraction ($r=0.56$, $P<0.001$; and $r=0.93$, $P<0.001$, respectively; Fig. 3), indicating that PartP variability (69% and 14%, respectively) is not related to Chla variability in the 0.2–0.6 µm fraction. Indeed, the *Prochlorococcus* cells that passed through the 0.6 µm filter contributed to PartP and Chla concentrations in the 0.2–0.6 µm fraction, but the correlation between these two parameters is comparatively weak and indicates that it is mainly free-living bacteria (i.e. organisms that do not contain Chla) that contribute to PartP in this <0.6 µm fraction.

Menzel and Ryther (1964) determined the detrital proportion of PartP using a regression between PartP, particulate C and Chla, for the same group of samples. We made such comparisons (Fig. 4a, c, d; eutrophic stations have been omitted to avoid regressions being drawn by high values.). The correlation between Chla and PartP concentration data was better ($r=0.87$, $p<0.001$, Fig. 4c) than that between Chla and

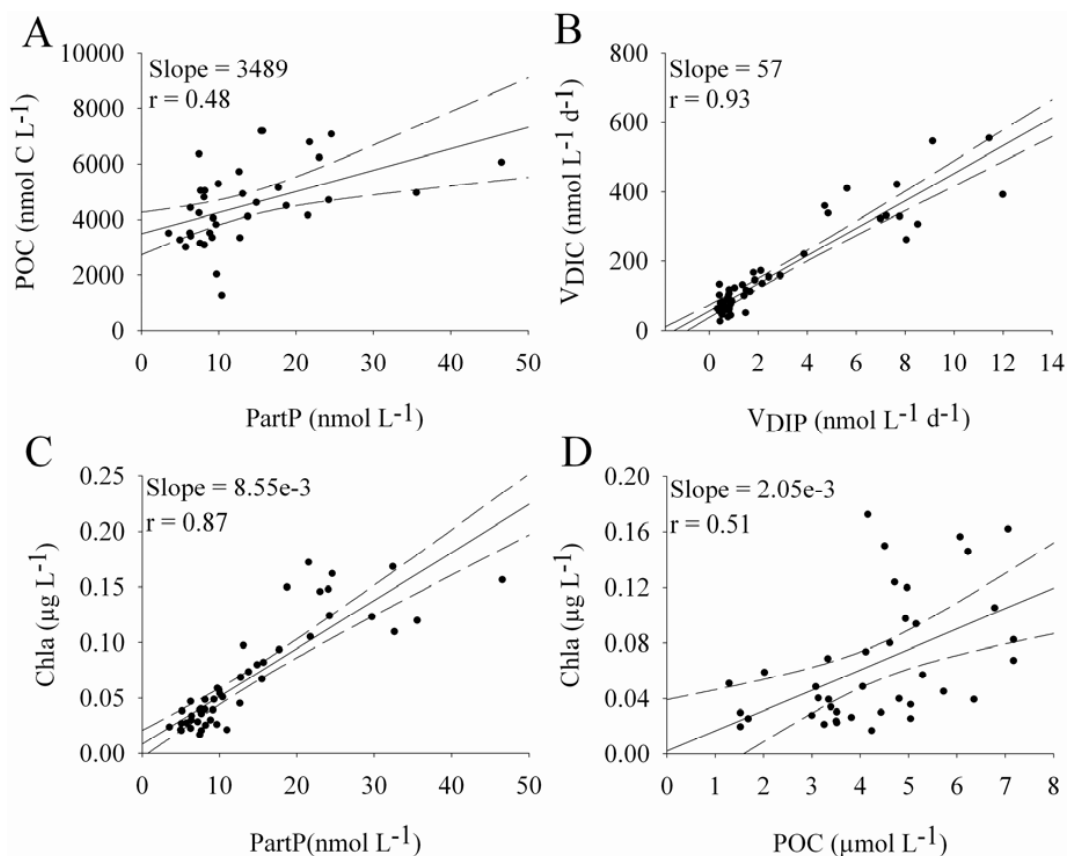


Fig. 4. Relations between particulate carbon (POC) and phosphate (PartP) (A), between carbon (V_{DIC}) and phosphate (V_{DIP}) uptake rates (B) between chlorophyll a (Chla) and PartP (C) and between Chla and POC (D). Data from 50 to 15% of PAR and between HNLC and STB18 stations. “slope” and “r” corresponds to the slope and the regression coefficient, respectively. The dotted lines correspond to the 95% confident range of the regression line (full line).

POC ($r=0.51$, $p<0.05$, Fig. 4d), supporting the hypothesis that PartP is a better indicator of living biomass than POC. As found by Menzel and Ryther (1964), the regressions between PartP and POC, when extrapolated toward the origin, indicated significant amounts of C in the absence of P whilst the regression between PartP and Chla intercepted at the origin, indicating that Chla and PartP were decomposed or mineralized at essentially the same rate, whilst POC was more refractory. The comparison of the regression slope between POC and PartP concentration and between V_{DIC} and V_{DIP} (Fig. 4a, b) also supports the hypothesis that P is more rapidly mineralized from dead material than C. Indeed, if POC and PartP are representative of C and P living biomass, then the C to P incorporation rate ratio should be in the same range as the POC to PartP ratio. The regression slope between POC and PartP concentration was 3489 (Fig. 4a) and 57 between V_{DIC} and V_{DIP} (Fig. 4b). This difference can be explained by the longer turnover rates of POC than those of PartP.

3.3 Evaluation of the use of V_{DIP}^{SP} as an estimator of bacteria and phytoplankton growth rates

We compared euphotic-layer averaged values of V^{SP} obtained from different methods (Fig. 5). For bacteria, we compared the values of $V_{DIP<0.6}^{SP}$ and of HBP:HBB (Fig. 5a). $V_{DIP<0.6}^{SP}$ values were 1.2 to 9.5 times higher than HBP:HBB values in productive areas (MAR-STB6 and STB15-UPX, respectively) while in the centre of the gyre (STB7-STB14), $V_{DIP<0.6}^{SP}$ values were 1.2 to 2.2 times lower than HBP:HBB values. Between MAR and STA21 stations, HBP:HBB values were quite low and constant ($0.11\pm 0.04\text{ d}^{-1}$) while $V_{DIP<0.6}^{SP}$ values varied widely from 0.04 to 1.11 d^{-1} depending the trophic regime encountered. As a consequence, the correlation between HBP:HBB ratio and $V_{DIP<0.6}^{SP}$ values, even excluding the “original” upwelling sites, was not significant ($r^2=0.08$, $p>0.05$). For phytoplankton, we compared the values of $V_{DIC>0.6}^{SP}$ and of $V_{DIP>0.6}^{SP}$. $V_{DIC>0.6}^{SP}$ can be obtained using a Chla-to-biomass or cell-number-to-biomass conversion factor. Using cell-number-to-biomass conversion factors according to Campbell et al. (1994, 1997) we found

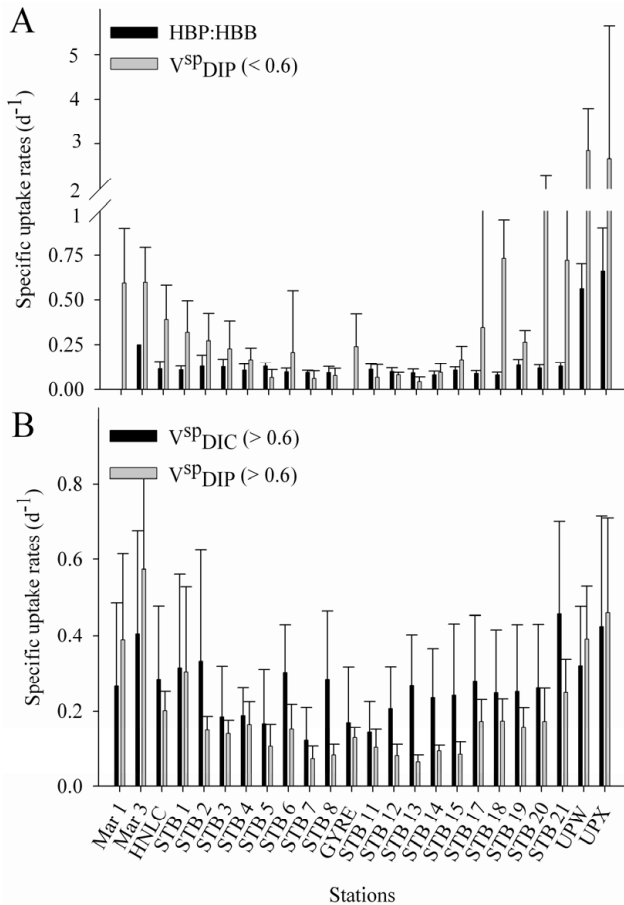


Fig. 5. (A) Bacterial specific uptake rates calculated from HBP:HBB ratio and V_{DIP}^{sp} in the fraction $<0.6 \mu\text{m}$. (B) Phytoplankton specific uptake rates calculated from V_{DIC}^{sp} and V_{DIP}^{sp} in the fraction $>0.6 \mu\text{m}$. Average specific uptake rates values on the photic zone. Autotrophic biomass calculated from Chl_a using a C:Chl_a conversion factors as describe in the Materials and Methods section. Heterotrophic bacterial biomass calculated from bacterial cells abundance converted to C equivalent using a conversion factor of 10 fgC cell^{-1} .

V_{DIC}^{sp} values on average 2 and 12 times higher than using a Chl_a-to-biomass conversion factors. Greatest differences were found in meso- and eutrophic areas. Using the Chl_a-to-biomass conversion factors from Veldhuis and Kraay (2004), $V_{DIC>0.6}^{sp}$ values were 1 to 4 and 0.6 to 1.8 times higher than $V_{DIP>0.6}^{sp}$ in the gyre and in the meso- and eutrophic areas, respectively (Fig. 5b). The major bias linked with the determination of V_{DIC}^{sp} is the choice of conversion factor. Indeed, when considering the extreme values of the C:Chl_a ratio in the surface layer in the equatorial Pacific ocean (40 and $200 \text{ g C Chl}_a^{-1}$, Chavez et al., 1996), values of V_{DIC}^{sp} can vary up to a factor 5. In the same way, we calculated V_{DIC}^{sp} using different cell-number-to-biomass conversion factors. Using conversion factors provided by Campbell et al. (1997) or by

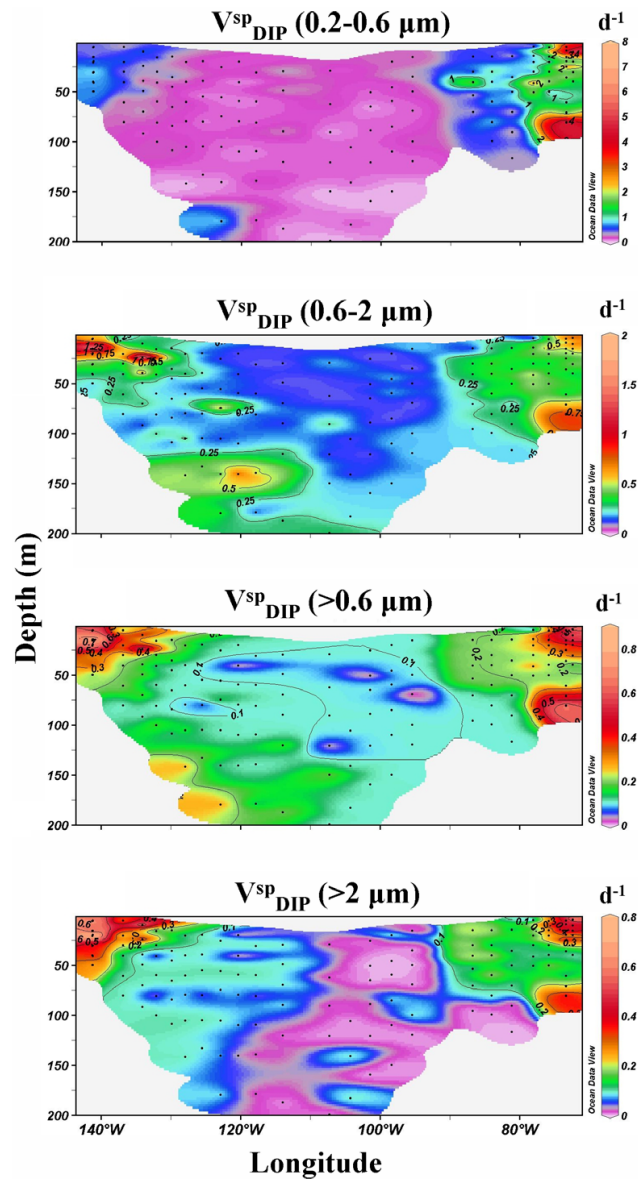


Fig. 6. Vertical and longitudinal distribution of the daily specific uptake of DIP (V_{DIP}^{sp}) along the BIOSOPE transect for four size classes: 0.2–0.6; 0.6–2; >0.6 and $>2 \mu\text{m}$.

Bertilsson et al. (2003) for *Prochlorococcus*, *Synechococcus* and picoeucaryotes (see Table 1), we found that V_{DIC}^{sp} values were on average 20% higher using Campbell's value.

3.4 Estimates of bacteria and phytoplankton V_{DIP}^{sp} in the Southeast Pacific gyre

The different size fractions showed significant vertical and longitudinal variations of V_{DIP}^{sp} along the transect ($P < 0.001$; Fig. 6). Highest values were found in productive areas while lower values were found in the upper part of the photic zone in the gyre area. In productive areas, the 0.2–0.6 μm fraction,

assumed to be composed mostly of free-living heterotrophic bacteria, showed the highest euphotic zone mean values of V_{DIP}^{SP} (0.6 ± 0.3 to $3 \pm 1 \text{ d}^{-1}$) while in the gyre area, the $0.6\text{--}2 \mu\text{m}$ fraction, assumed to consist of picophytoplankton cells, showed the highest euphotic zone mean values of V_{DIP}^{SP} (0.10 ± 0.04 to $0.20 \pm 0.11 \text{ d}^{-1}$). Whatever the station, the $>2 \mu\text{m}$ fraction had the lowest V_{DIP}^{SP} euphotic zone mean values ($0.02 \pm 0.07\text{--}0.6 \pm 0.2 \text{ d}^{-1}$). The variation of V_{DIP}^{SP} with depth in the $0.6\text{--}2 \mu\text{m}$ fraction was quite different from that of the $>2 \mu\text{m}$ fraction, particularly in the western part of the gyre area. Here, the $>2 \mu\text{m}$ fraction showed fairly constant V_{DIP}^{SP} values with depth (no significant difference was found between V_{DIP}^{SP} values in the deep chlorophyll maximum layer (DCML) and the upper layer of the euphotic zone, $P=0.161$), while the $0.6\text{--}2 \mu\text{m}$ fraction exhibited significantly higher values of V_{DIP}^{SP} in the DCML ($P<0.001$). The smaller size fraction ($0.2\text{--}0.6 \mu\text{m}$) exhibited quite low values throughout the euphotic zone in the oligotrophic area ($0.11 \pm 0.07 \text{ d}^{-1}$) and no significant tendency with depth was observed ($P<0.001$).

4 Discussion

Quantifying heterotrophic bacteria and phytoplankton μ in the ocean is vitally important for understanding many oceanographic processes since μ and mortality of individual populations control the ultimate composition of the assemblage (Banse, 1991). This, in turn, controls a large number of ecosystem properties, such as export of organic matter, nutrient utilization and production patterns. Understanding μ is critical to our understanding of the biotic responses to environmental forcing. The physiological responses are an integral component in mechanistic models in predicting ecosystem trophodynamics. Nevertheless, studies of heterotrophic bacteria and phytoplankton assemblages are scarce, especially in the Southeast Pacific. We measured DIP uptake rates and PartP concentrations in three size fractions: $0.2\text{--}0.6$, $0.6\text{--}2$ and $>2 \mu\text{m}$ in order to assess in situ specific growth rates of bacteria and two size fractions of phytoplankton. Firstly, we discuss the production and biomass estimators; secondly, we discuss the P-based μ estimates obtained in the Southeast Pacific.

4.1 Biomass estimators

The distribution of phytoplankton is commonly described in terms of Chla (Huot et al., 2007). Because the Chla content varies between species, light and nutrients (Philips et al., 1995; Sciandra et al., 1997; Finkel et al., 2004; Pérez et al., 2006; Moore et al., 2006), it is not an ideal biomass estimator (Breton et al., 2000; Le Floch et al., 2002). POC cannot be used directly as it contains a high proportion of detrital matter (Sobczak et al., 2002; Fig. 4a and d). The AB in terms of C is never directly determined but derived from

other variables: Chla, biovolumes or cell numbers which are then transformed using appropriate conversion factors. This entails a critical step in the estimation of AB: the choice of conversion factor. C:Chla values vary over a wide range even at species level. As an example, in the subtropical Atlantic ocean, Veldhuis and Kraay (2004) found C:Chla ratios ranging from 450 at the surface to 15 gC gChla^{-1} at 150 m, for *Prochlorococcus* populations and a C:Chla ratio of $30\text{--}80 \text{ gC gChla}^{-1}$ in surface waters for the collective eukaryotic phytoplankton, varying by a factor of 3–7 fold with depth. In most studies however, authors use values ranging between 30 and 55 gC gChla^{-1} to convert their Chla data into C biomass (Gasol et al., 1997; Lequeré et al., 2005; Houlbrèque et al., 2006). For phytoplankton, cell-number-to-C conversion factors can also vary significantly even at the species level (Table 1). We found significant differences ($P<0.001$) in V_{DIC}^{SP} estimates according to the choice of phytoplankton cell-number-to-C or C:Chla conversion factors. So although the use of a single conversion factor is the rule in field studies, it probably leads to significant errors in biomass estimates. Conversely, using appropriate cell or Chla to carbon conversion factors demands complex data analysis. Studies on heterotrophic bacterial communities have shown that the C cell content changes in relation to natural conditions and the physiological state of the bacterial assemblages (Table 1). Gundersen et al. (2002) showed that the outcome of HBB assessments is highly dependant on the choice of cell-specific conversion factors. In the same way, La Ferla and Leonardi (2005) demonstrated that the quantification of HBB based solely on abundance must be considered with caution because of the variability in cell volumes and morphotypes. Thus there is great uncertainty surrounding the estimate of C-based phytoplankton and heterotrophic bacterial μ , whatever the choice of biomass estimator.

P is an essential element required for life, used by all organisms. It is found in a variety of molecules with different cellular roles, ranging from storage of genetic information (nucleic acids: DNA, RNA) and energy (ATP, ADP, AMP) to structural composition (phospholipids). If the contribution of detrital P to PartP standing stocks is small enough, then PartP can be considered to reflect the standing stock of living material. Our results showed that PartP contained less detrital material than the POC (Fig. 4). This was indicated by significantly higher turnover rates of PartP compared to those of POC and a significant correlation between PartP and Chla concentrations. Similar observations have shown that P is preferentially released from both dissolved and particulate matter into the water column relative to other elements such as C and N (Menzel and Ryther, 1964; Knauer et al., 1979; Minster and Boulahdid, 1987; Clark et al., 1998, 1999; Loh and Bauer, 2000; Paytan et al., 2003). The use of PartP as a living biomass indicator is particularly well adapted to the open ocean. Indeed, in such areas, low values of detrital P are commonly found ($\sim 1\%$ in equatorial Pacific Ocean, Faul et al., 2005). Nevertheless, even if the fraction of detrital

P is negligible in the whole fraction, the size distribution of detrital P is not known and can affect the measurement of $V_{\text{DIP}}^{\text{SP}}$ in each size fraction. It has been shown that as the size of the organic matter decreases, the more refractory it becomes (the size-reactivity continuum hypothesis; Amon and Benner, 1996; Mannino and Harvey, 2000), therefore we can hypothesise that there is also a size-reactivity continuum in detrital matter that engender higher concentrations of detrital matter in the smallest fraction. For this reason, $V_{\text{DIP} < 0.6}^{\text{SP}}$ may be underestimated. The proportion of detrital P in PartP is high in coastal areas (Faul et al., 2005). Consequently, $V_{\text{DIP}}^{\text{SP}}$ is more likely to be underestimated in the upwelling area. The other main advantage of using P instead of Chla is that PartP takes both bacteria and phytoplankton into account. So if it is possible to separate bacterial P from phytoplankton P in PartP, then it would be possible to estimate bacterial and phytoplankton $V_{\text{DIP}}^{\text{SP}}$ in the same sample. Size fractionation was an adequate method for separating heterotrophic bacteria from phytoplankton, in our study, since more than 90% of bacterial cells passed through the 0.6 μm -filters. However, an increasing fraction of *Prochlorococcus* cells passed through when the water became ultraoligotrophic (in the centre of the gyre). Consequently, values of heterotrophic bacteria $V_{\text{DIP}}^{\text{SP}}$ in the gyre may be biased due to the influence of *Prochlorococcus* cells. Nevertheless, it was shown that DIC uptake in the 0.2–0.6 μm fraction was negligible (data not shown) and therefore the phytoplankton production in this fraction was negligible. Thus, production in terms of P in the 0.2–0.6 μm fraction can be mainly attributed to free-living heterotrophic bacteria. Therefore, $V_{\text{DIP} < 0.6}^{\text{SP}}$ gives a good representation of bacterial μ . In the $>0.6 \mu\text{m}$ size fractions, the nano and microzooplankton can account for some of the PartP concentration values. Gasol et al. (1997) showed that zooplankton C-biomass (protozooplankton + mesozooplankton) could account for 13–21% and 15–65% of the total C-biomass in coastal and open ocean areas, respectively. Consequently, this could be a non negligible source of phytoplankton $V_{\text{DIP}}^{\text{SP}}$ underestimation, particularly for the $>2 \mu\text{m}$ size fraction.

4.2 DIP uptake rate measurements

Assuming that the DIP represents biologically available orthophosphate, we measured P uptake rates (V_{DIP}) in three size fractions. Daily P uptake rates were calculated by multiplying the hourly rate by 24. P uptake is generally shown to be constant over 24 h (Perry and Eppley, 1981, Harrison, 1983; Moutin et al., 2002) but diurnal variations in P uptake have been observed in some studies (Eppley et al., 1971; Harrison et al., 1977; Currie and Kalff, 1984). For the majority of stations, time course experiments for ^{33}P uptake were linear over 24 h, however there were some variations in P uptake rates at some stations along the BIOSOPE transect (Duhamel et al., 2006). The methodological problems associated with 24 h incubation experiments can be significant

(Nalewajko and Garside, 1983, Harrison and Harris, 1986), especially in terms of losses. However, short incubation experiments should reduce the bias linked to such losses (see discussion in Duhamel et al., 2006). It is important to stress that even if the $<0.6 \mu\text{m}$ fraction is composed of solely heterotrophic bacteria, our data set does not prove that P is turning over at the same rate as the cells. Indeed, Nalewajko and Lean (1978) measured net phosphate uptake and influx rates in batch cultures of three algal cell cultures. They showed that short-term P fluxes always exceeded the net increase in P biomass, indicating that the cells release P compounds back into the medium. To the best of our knowledge, the study of Nalewajko and Lean (1978) has not been repeated, so this experiment should be repeated in a variety of field samples to verify that this phenomenon is not exclusively observed in cultures. C-based μ estimations are also submitted to such error type. Indeed, the release of assimilation products is common to C measurements. Claustre et al. (2007) propose that the release of DOC in the Southeast Pacific should be a major process which could explain the high community (bacteria + phytoplankton) production rates. The release of DOC by phytoplankton cells produces bias in the evaluation of C production (Wood et al., 1992) and subsequently for C-based μ estimations.

4.3 Growth rates estimates

In 1981, Perry and Eppley used the ^{33}P uptake rate to PartP ratio to estimate the growth rate of phytoplankton (Table 2), stating that DIP assimilation was mediated by phytoplankton (their data indicating low heterotrophic activity). In 1996, Thingstad et al. determined both heterotrophic bacteria and phytoplankton P-based generation times [(PartP \times ^{32}P uptake rate) \times $\ln(2)$] using 1 μm size fractionations (Table 2). From these different studies, where the proportion of detrital matter in the PartP was negligible, it was possible to put forward the hypothesis that DIP was the sole source of P and so $V_{\text{DIP}}^{\text{SP}}$ estimates could be used to assess bacteria and/or phytoplankton μ . Thus the idea of using P-based estimates of μ is not new. In this study we provide information on the variations in P-based μ values in a gradient of oligotrophy where the waters were P-repleted (DIP concentration and turnover time minimum values: 120 nmol l^{-1} and 7 d^{-1} , respectively; Moutin et al., 2007). Most estimates for C-based heterotrophic bacterial growth rates in the open ocean fall into a wide range from zero to 10 d^{-1} , whilst phytoplankton appears to grow at rates of no more than 2 d^{-1} (Table 2). We report a wide range in μ estimates ranging from 0 to 7 d^{-1} for heterotrophic bacteria and from 0 to 2 d^{-1} for phytoplankton. This range of values reflects the wide range of trophic status encountered during the BIOSOPE cruise.

Estimates of production to biomass ratio, based on the leucine incorporation technique and C conversion of bacterial abundance (HBP:HBB) were significantly lower than those estimated by $V_{\text{DIP} < 0.6}^{\text{SP}}$ in productive areas

Table 2. Review of values of surface water phytoplankton and bacteria growth rate (d^{-1}).

Growth rate (d^{-1})	Technique	Organisms - location	Reference
0.76 (0.57-1.07)	Dilution technique	Phytoplankton – North-east Atlantic	Quevedo and Anadon 2001
0.26 (0.19–0.36)	^{14}C method	Phytoplankton – eastern North Atlantic subtropical gyre	Maranon, 2005
0.51 (0.42–0.62)	^{14}C method	Phytoplankton – western North Atlantic subtropical gyre	Maranon, 2005
0.17 (0.13–0.22)	^{14}C method	Phytoplankton – South Atlantic subtropical gyre	Maranon, 2005
0.21 \pm 0.02	^{14}C method	Microphytoplankton – oligotrophic area – Atlantic ocean	Maranon et al., 2000
0.1–>1.5	Review	Phytoplankton – poor water of the open ocean	Eppley, 1981
0.0–2.9	Review	Phytoplankton assemblages	Furnas, 1990
0.3–0.53	^{14}C method	Phytoplankton – Station ALOHA – 22° 45' N; 158° 00' W	Letelier et al., 1996
1	Pigment labeling with ^{14}C	Phytoplankton – North Pacific subtropical gyre	Laws et al., 1987
0.3–0.6	Pigment labeling with ^{14}C	Cyanobacteria – Sargasso Sea off Bermuda	Goericke 1998
0.14	Specific DIP uptake rate	Phytoplankton – Central North Pacific Ocean	Perry and Eppley, 1981
3.5–8.8 d	P-based generation time	Phytoplankton (> 1 μm) – Bay of Aarhus (Denmark)	Thingstad et al., 1996
0.06–0.99	Specific DIP uptake rate	Picophytoplankton (0.6–2 μm) – Southeast Pacific 146.36° W, 72.49° W	This study
0.02–0.83	Specific DIP uptake rate	Nano-microphytoplankton (>2 μm) – Southeast Pacific 146.36° W, 72.49° W	This study
1.44	Seawater culture	Bacteria - North western Atlantic Ocean	Ducklow and Hill, 1985
0–0.45	Dilution technique	Bacteria - Gulf of Mexico	Jochem et al., 2004
2–10	Review	Bacteria	Ducklow, 1983
4.7	^3H -adenine method	Bacteria – North Pacific subtropical gyre	Jones et al., 1996
0.2–1.5	^3H -Thymidine method	Bacteria – western Black Sea	Morgan et al., 2006
0.03–1.1	^3H -Thymidine method	Bacteria – Danube – Black Sea	Becquevort et al., 2002
0.004–0.25	^3H -Leucine method	Bacteria - review	Van Wambeke et al., 2007
0.31 \pm 0.09	^3H -Leucine method	Bacteria – Northeast Pacific Ocean 44°38.3' N, 124°18.5' W	Sherr et al., 2001
0.03 \pm 0.01	^3H -Leucine method	Bacteria – Northeast Pacific Ocean 44°38.3' N, 124°48.0' W	Sherr et al., 2001
0.02 \pm 0.01	^3H -Leucine method	Bacteria – Northeast Pacific Ocean 44°38.65' N, 127°10' W	Sherr et al., 2001
0.1–0.45	^3H -Leucine method	Bacteria – eastern equatorial Pacific Ocean 4.6° S, 105° W	Cochlan, 2001
2.5–4.1	P-based generation time	Bacteria (0.2–1 μm) – Bay of Aarhus (Denmark)	Thingstad et al., 1996
0.06–4.28	Specific DIP uptake rate	Bacteria (0.2–0.6 μm) – Southeast Pacific 146.36° W, 72.49° W	This study

(MAR-STB6 and STB15-UPX, $P < 0.001$). Applying various methods (measurements of the natural abundance of nucleoid-containing cells by combined epifluorescence and phase-contrast microscopy; detection of the reduction of the fluorogenic dye, 5-cyano-2,3-ditolyl tetrazolium chloride; nucleic acid double staining (SYBR Green + propidium iodide); determination of membrane integrity by confocal laser-scanning microscopy), it has been shown that at any given time, a significant fraction of the bacterioplankton community has minimal or no metabolic activity (Zweifel and Hagström, 1995; Sherr et al., 1999; Gregori et al., 2001; Pirker et al., 2005). For this reason, μ estimates based on the HBP:HBB ratio could be underestimated. Our $V_{\text{DIP}}^{\text{SP}} < 0.6$ values were significantly higher in the productive areas than in the gyre area ($P < 0.001$). Morgan et al. (2006) also found that bacterial growth rates (with $\mu = \text{HBP}/\text{bacterial abundance}$, HBP deduced from ^3H -Thymidine method using conversion factor of $2 \times 10^{18} \text{ cells} \times [\text{mol TdR}]^{-1}$) were significantly greater on the shelf (0.8–1.8 d^{-1}) compared to the gyre (0.1–0.3 d^{-1}) in the western Black Sea.

Studies comparing bacterial and phytoplankton μ are few (Jones et al., 1996; Almeida et al., 2002). Measurements of $V_{\text{DIP}}^{\text{SP}}$ in the 0.2–0.6, 0.6–2 and >2 μm fractions have enabled us to make such comparisons. In oligotrophic environments, heterotrophic bacterial μ can be higher or lower than that of phytoplankton. For example, Pérez et al. (2006)

showed that in the upper water (mixed layer) of the subtropical Atlantic gyres, phytoplankton growth rates were 0.17 d^{-1} (from daily AP and picoplankton abundance transformed to B with the empirical conversion factors obtained by Zubkov et al. (2000), see Table 1). While in the same area, Zubkov et al. (2000) found that heterotrophic bacterial growth rates were 0.12 d^{-1} (using a conversion factor of 11.5 fg C per heterotrophic bacteria). In the upper 40 m of the North Pacific subtropical gyre, Jones et al. (1996) found 0.7 d^{-1} for phytoplankton (estimated from the Chla-labelling technique) and $\sim 1 \text{ d}^{-1}$ for heterotrophic bacteria (estimated from the incorporation of ^3H -adenine into DNA). We showed that picophytoplankton μ (0.14 \pm 0.04 d^{-1}) was higher than heterotrophic bacteria μ (0.11 \pm 0.07 d^{-1}) in the Southeast Pacific gyre and that values were in the same range as those found by Pérez et al. (2006) and Zubkov et al. (2000) in the Atlantic gyres, suggesting the presence of a microbial community with a very slow turnover. These relatively low values of μ for both phytoplankton and heterotrophic bacteria in the oligotrophic gyre area must be the result of nitrogen limitation on bacterial and primary production (Bonnet et al., 2007; Van Wambeke et al., 2007a). Slow phytoplankton μ in the subtropical Atlantic have been explained in terms of the observed assimilation numbers and C:Chla ratios in a review by Marañón (2005). The light-saturated, chlorophyll normalised photosynthesis rate

necessary to support a phytoplankton μ of 1 d^{-1} , would be well above those reported in the subtropical Atlantic (156 ± 16 and $205 \pm 17 \text{ mg C m}^{-2} \text{ d}^{-1}$, in the North and South Atlantic subtropical gyres, respectively; Pérez et al., 2006) and the Southeast Pacific gyre ($134 \pm 82 \text{ mg C m}^{-2} \text{ d}^{-1}$; Van Wambeke et al., 2007b). In coastal areas heterotrophic bacterial μ are often lower than that of phytoplankton (Laws et al., 1984; Revilla et al., 2000). In the productive areas (MAR-STB6 and STB15-UPX) of the Southeast Pacific, we found that organisms in the $<0.6 \mu\text{m}$ fraction had higher $V_{\text{DIP}}^{\text{SP}}$ values than organisms in the $>0.6 \mu\text{m}$ fraction, while in the hyperoligotrophic gyre, organisms in the $0.6\text{--}2 \mu\text{m}$ fraction yielded the highest $V_{\text{DIP}}^{\text{SP}}$ values. Thus it may be deduced that the picophytoplankton were better adapted than the nano-microphytoplankton and free living heterotrophic bacteria for growing in hyperoligotrophic conditions.

There are relatively few studies comparing μ for different size fractions of natural phytoplanktonic communities (Pérez et al., 2006). In coastal eutrophic ecosystems, large phytoplankton are reported to have faster growth rates than small-sized phytoplankton (Cermeno et al., 2005 – C-specific photosynthetic rates). Nevertheless, in the Chilean upwelling area, there was no significant difference between $V_{\text{DIP}}^{\text{SP}}$ for the two size-fractions of phytoplankton (0.5 ± 0.3 and $0.4 \pm 0.2 \text{ d}^{-1}$ for picophytoplankton and nano-microphytoplankton respectively, $P > 0.05$). We found that picophytoplankton ($0.6\text{--}2 \mu\text{m}$) grew 1 to 15 times faster than the nano-microphytoplankton ($>2 \mu\text{m}$) between the Marquesas Islands and Chile, with maximal differences in the gyre area. Differences in growth rates have been related to the specific composition of the planktonic community (Furnas, 1990). So the differences we observed could be related to differences between the taxonomic groups encountered along the BIOSOPE transect. Flow cytometry data showed high variations in the relative composition of picophytoplankton populations along the BIOSOPE transect (Grob et al., 2007). In the hyperoligotrophic region, the DCM corresponded to *Prochlorococcus* and picophytoeukaryotes maxima (Grob et al., 2007) as well as to the maximum growth rate values of the picophytoplankton size fraction (Fig. 6).

In most of the oligotrophic area, phytoplankton μ were found to be higher in the upper mixed layer than within the DCML (Malone et al., 1993 – with AP deduced from the ^{14}C labelling method and AB deduced using a C:Chla ratio or ^{14}C -Chla experiments; Quevedo and Anadon, 2001 – dilution method). We found that picophytoplankton grew significantly faster at the DCML than in the upper part of the photic zone in the hyperoligotrophic gyre (from STB7 to STB14; $P < 0.001$). Pérez et al. (2006) found the same trends in the subtropical Atlantic gyres with a μ in the $<2 \mu\text{m}$ fraction of $0.17 \pm 0.01 \text{ d}^{-1}$ in the mixed layer and $0.25 \pm 0.02 \text{ d}^{-1}$ in the DCML. However, they found that the large size fraction ($>2 \mu\text{m}$) grew faster in the mixed layer than in the DCML while we found no statistical difference for $V_{\text{DIP}}^{\text{SP}} > 2$

($P = 0.161$). Our results support the hypothesis of Pérez et al. (2006) that picoplankton could outcompete large cells in the high-nutrient, low-light environment of the DCML.

The evaluation of μ is still a subject of debate (Marañón, 2005). It is not possible to judge which technique is best for measuring μ , if indeed any one technique is capable of doing so, as each method measures a different aspect of growth. P-based μ estimates are one of the many ways to assess μ and by comparing the results obtained with those of the different existing methods can help to understand how quickly the cells grow in relation to their environment (Christian et al., 1982; Laws et al., 1984; Jespersen et al., 1992).

5 Conclusions

Growth rate is a fundamental property of all organisms and gives valuable information about the activity of microbial populations. The relative activity of bacteria and phytoplankton in oligotrophic oceans has significant implications for food-web structures, nutrient cycling pathways and for sinking fluxes of organic matter. Contrary to C-based approaches, the P-based approach enables us to assess bacterial and phytoplankton μ on the same sample in that size fraction can effectively isolate both heterotrophic and phytoplanktonic communities. We have characterized the vertical and longitudinal variability of P-based μ in three size fractions of plankton. Picophytoplankton ($0.6\text{--}2 \mu\text{m}$) grew faster than the large phytoplankton ($>2 \mu\text{m}$) over the Southeast Pacific transect, particularly in the centre of the gyre. Thus, cells smaller than $2 \mu\text{m}$ were better adapted for growing in a wide range of trophic conditions than those greater than $2 \mu\text{m}$. Heterotrophic bacteria ($0.2\text{--}0.6 \mu\text{m}$) showed higher variations in P-based μ with maximum rates in productive areas. Picophytoplankton grew faster than heterotrophic bacteria in the Southeast Pacific gyre with values in the range of those found in the Atlantic and North Pacific gyres by Pérez et al. (2006) and Zubkov et al. (2000), suggesting the presence of a microbial community with a slow turn over.

Acknowledgements. We express our gratitude to O. Ulloa, G. Alarcon and C. Grob for providing us cytometry data. We thank T. Bentley for help with improving the English. We also thank the crew of the R/V L'Atalante for outstanding shipboard support operations. D. Tailliez and C. Bournot are warmly thanked for their efficient help in CTD rosette management and data processing. This is a contribution to the BIOSOPE project of the LEFE-CYBER program. This research was funded by the Centre National de la Recherche Scientifique (CNRS), the Institut des Sciences de l'Univers (INSU), the Centre National d'Etudes Spatiales (CNES), the European Space Agency (ESA), The National Aeronautics and Space Administration (NASA) and the Natural Sciences and Engineering Research Council of Canada (NSERC). This work is funded in part by the French Research and Education council.

Edited by: A. Boetius

References

- Almeida, M. A., Cunha, M. A., and Alcântara, F.: Seasonal change in the proportion of bacterial and phytoplankton production along a salinity gradient in a shallow estuary, *Hydrobiologia*, 475–476, 251–262, 2002.
- Amon, R. M. W. and Benner, R.: Bacterial utilization of different size classes of dissolved organic matter, *Limnol. Oceanogr.*, 41, 41–51, 1996.
- Azam, F., Frenchel, T., Field, J. G., Gray, J. S., Meyer-Reil, L. A., and Thingstad, T. F.: The ecological role of water-column microbes in the sea, *Mar. Ecol.-Prog. Ser.*, 10, 257–263, 1983.
- Banse, K.: Rates of phytoplankton cell division in the field and in iron enrichment experiments, *Limnol. Oceanogr.*, 36, 1886–1898, 1991.
- Banse, K.: Should we continue to measure ¹⁴C-uptake by phytoplankton for another 50 years?, *Limnology and Oceanography: Bulletin*, 11, 45–46, 2002.
- Becquevort, S., Bouvier, T., Lancelot, C., Cauwet, G., Deliat, G., Egorov, V. N., and Popovichev, V. N.: The seasonal modulation of organic matter utilization by bacteria in the Danube-Black Sea mixing zone, *Estuar. Shelf S.*, 54, 337–354, 2002.
- Berman, T.: Multiple isotopic tracer methods in the study of growth, dynamics and metabolic processes in marine ecosystems, in: *Primary Productivity in the Sea*, edited by: Falkowski, P., Plenum Publishing, 213–229, 1980.
- Bertilsson, S., Berglund, O., Karl, D. M., and Chisholm, S. W.: Elemental composition of marine *Prochlorococcus* and *Synechococcus*: Implications for the ecological stoichiometry of the sea, *Limnol. Oceanogr.*, 48, 1721–1731, 2003.
- Bonnet, S., Guieu, C., Bruyant, F., Prasil, O., Raimbault, P., Max Y. Gorbunov, M., Zehr, J. P., Grob, C., Masquelier, S., Garczarek, L., Moutin, T., Van Wambeke, F., and Claustre, H.: Nutrients limitation of primary productivity in the Southeast Pacific (BIOCOPE cruise), *Biogeosciences Discuss.*, 4, 2733–2759, 2007, <http://www.biogeosciences-discuss.net/4/2733/2007/>.
- Breton, E., Brunet, C., Sautour, B., and Brylinski, J. M.: Annual variations of phytoplankton biomass in the Eastern English Channel: comparison by pigment signatures and microscopic counts, *J. Plankton Res.*, 22, 1423–1440, 2000.
- Brock, T. D.: Microbial growth rates in nature, *Bacteriol. Rev.*, 35, 39–58, 1971.
- Cailliau, C., Claustre, H., Vidussi, F., Marie, D., and Vault, D.: Carbon biomass and gross growth rates as estimated from ¹⁴C pigment labelling method during photoacclimation in *Prochlorococcus* CCMP1378), *Mar. Ecol.-Prog. Ser.*, 145, 209–221, 1996.
- Campbell, L., Liu, H., Nolla, H. A., and Vault, D.: Annual variability of phytoplankton and bacteria in the subtropical North Pacific Ocean at Station ALOHA during the 1991–1994 ENSO event, *Deep-Sea Res. Pt. I*, 44, 167–192, 1997.
- Campbell, L., Nolla, H. A., and Vault, D.: The importance of *Prochlorococcus* to community structure in the central North Pacific Ocean, *Limnol. Oceanogr.*, 39, 954–961, 1994.
- Caron, D. A., Dam, H. G., Kremer, P., Lessard, E. J., Madin, L. P., Malone, T. C., Napp, J. M., Peele, E. R., Roman, M. R., and Youngbluth, M. J.: The contribution of microorganisms to particulate carbon and nitrogen in surface waters of the Sargasso Sea near Bermuda, *Deep-Sea Res. Pt. I*, 42, 943–972, 1995.
- Cermeno, P., Maranon, E., Rodriguez, J., and Fernandez, E.: Large-sized phytoplankton sustain higher carbon-specific photosynthesis than smaller cells in a coastal eutrophic ecosystem, *Mar. Ecol.-Prog. Ser.*, 297, 51–60, 2005.
- Chavez, F. P., Buck, K. R., Service, S. K., Newton, J., and Barber, R. T.: Phytoplankton variability in the central and eastern tropical Pacific, *Deep-Sea Res. Pt. II*, 43, 835–870, 1996.
- Christian, J. R. and Karl, D. M.: Microbial community structure at the U.S. -Joint Global Ocean flux Study Station ALOHA: Inverse methods for estimating biochemical indicator ratios, *J. Geophys. Res.*, 99, 14 269–14 276, 10.1029/94JC00681, 1994.
- Christian, R. R., Hanson, R. B., and Newell, S. Y.: Comparison of methods for measurement of bacterial growth rates in mixed batch cultures, *Appl. Environ. Microb.*, 43, 1160–1165, 1982.
- Clark, L. L., Ingall, E. D., and Benner, R.: Marine organic phosphorus cycling: Novel insights from nuclear magnetic resonance, *Am. J. Sci.*, 2999, 724–737, 1999.
- Clark, L. L., Ingall, E. D., and Benner, R.: Marine phosphorus is selectively remineralized, *Nature*, 393, 426, 1998.
- Claustre, H. and Maritorena, S.: The Many Shades of Ocean Blue, *Science*, 302, 1514–1515, 2003.
- Claustre, H., Bricaud, A., Babin, M., Bruyant, F., Guillou, L., Le Gall, F., and Partensky, F.: Diel variations in *Prochlorococcus* optical properties, *Limnol. Oceanogr.*, 47, 1637–1647, 2002.
- Cochlan, W.: The heterotrophic bacterial response during a mesoscale iron enrichment experiment (IronEx II) in the eastern equatorial Pacific Ocean. *Limnology and Oceanography*, 46, 428–435, 2001.
- Currie, D. J. and Kalf, J.: The relative importance of bacterioplankton and phytoplankton in phosphorus uptake in freshwater, *Limnol. Oceanogr.*, 29, 311–321, 1984.
- Dickson, M.-L. and Wheeler, P. A.: Nitrate uptake rates in a coastal upwelling regime: A comparison of PN-specific, absolute, and Chl a-specific rates. *Limnology and Oceanography*, 40, 533–543, 1995.
- Ducklow, H. W.: Bacterial production and biomass in the oceans, in: *Microbial ecology of the oceans*, edited by: Kirchman, D. L., Wiley series in Ecological and Applied Microbiology, Ralph Mitchelk, Series Editor., 85–120, 2000.
- Ducklow, H. W.: Production and fate of bacteria in the oceans, *Bio-science*, 33, 494–501, 1983.
- Duhamel, S., Zeman, F., and Moutin, T.: A dual-labeling method for the simultaneous measurement of dissolved inorganic carbon and phosphate uptake by marine planktonic species, *Limnol. Oceanogr.-Meth.*, 4, 416–425, 2006.
- Eppley, R. W., Carlucci, A. F., Holm-Hansen, Kiefer, D., McCarthy, J. J., Venrick, E., and Williams, P. M.: phytoplankton growth and composition in shipboard cultures supplied with nitrate, ammonium, or urea as the nitrogen source, *Limnol. Oceanogr.*, 16, 741–751, 1971.
- Eppley, R. W.: Relations between nutrient assimilation and growth rate in phytoplankton with a brief review of estimates of growth rate in the ocean. in: *Physiological Bases of Phytoplankton Ecology*, edited by: Platt, T., *Can. Bull. Fish. Aquat. Sci.*, 210, 251–263, 1981.
- Eppley, R. W.: Temperature and phytoplankton growth in the sea, *Fish. B.-N.O.A.A.*, 70, 1063–1085, 1972.
- Faul, K. L., Paytan, A., and Delaney, M. L.: Phosphorus distribution in sinking oceanic particulate matter, *Mar. Chem.*, 97, 307–333, 2005.

- Finkel, Z. V., Irwin, A. J., and Schofield, O.: Resource limitation alters the 3/4 size scaling of metabolic rates in phytoplankton, *Mar. Ecol.-Prog. Ser.*, 273, 269–279, 2004.
- Fuhrman, J. A. and Azam, F.: Bacterioplankton secondary production estimates for coastal waters of British Columbia, Antarctica and California, *Appl. Environ. Microb.*, 39, 1085–1095, 1980.
- Fuhrman, J. A. and Azam, F.: Thymidine incorporation as a measure of heterotrophic bacterioplankton production in marine surface waters: Evaluation and field results, *Mar. Biol.*, 66, 109–120, 1982.
- Fukuda, R., Ogawa, H., Nagata, T., and Koike, I.: Direct determination of carbon and nitrogen contents of natural bacterial assemblages in marine environments, *Appl. Environ. Microb.*, 64, 3352–3358, 1998.
- Furnas, M. J.: In situ growth rates of marine phytoplankton: approaches to measurement, community and species growth rates, *J. Plankton Res.*, 12, 1117–1151, 1990.
- Gasol, J. M., Del Gioglio, P., and Duarte, C. M.: Biomass distribution in marine planktonic communities, *Limnol. Oceanogr.*, 42, 1353–1363, 1997.
- Goericke, R.: Response of phytoplankton community structure and taxon-specific growth rates to seasonally varying physical forcing in the Sargasso Sea off Bermuda, *Limnol. Oceanogr.*, 43, 921–935, 1998.
- Grégori, G., Citterio, S., Ghiani, A., Labra, M., Sgorbati, S., Brown, S., and Denis, M.: Resolution of viable and membrane-compromised bacteria in freshwater and marine waters based on analytical flow cytometry and nucleic acid double staining, *Appl. Environ. Microb.*, 67, 4662–4670, 2001.
- Grob, C., Ulloa, O., Claustre, H., Huot, Y., Alarcon, G., and Marie, D.: Contribution of picoplankton to the total particulate organic carbon (POC) concentration in the eastern South Pacific, *Biogeosciences*, 4, 837–852, 2007, <http://www.biogeosciences.net/4/837/2007/>.
- Gundersen, K., Heldal, M., Norland, S., Purdie, D. A., and Knap, A. H.: Elemental C, N, and P cell content of individual bacteria collected at the Bermuda Atlantic Time-series Study (BATS) site, *Limnol. Oceanogr.*, 47, 1525–1530, 2002.
- Hagstrom, A., Larsson, U., Horstedt, P., and Normark, S.: Frequency of dividing cells, a new approach to the determination of bacterial growth rates in aquatic environments, *Appl. Environ. Microb.*, 37, 805–812, 1979.
- Harrison, W. G. and Harris, L. R.: Isotope dilution and its effects on measurements of nitrogen and phosphorus by oceanic microplankton, *Mar. Ecol.-Prog. Ser.*, 27, 253–261, 1986.
- Harrison, W. G., Azam, F., Renger, E. H., and Eppley, R. W.: Some experiments on phosphate assimilation by coastal marine plankton, *Mar. Biol.*, 40, 9–18, 1977.
- Harrison, W. G.: The time-course of uptake of inorganic and organic nitrogen compounds by phytoplankton from the Eastern Canadian Arctic: A comparison with temperate and tropical populations, *Limnol. Oceanogr.*, 28, 1231–1237, 1983.
- Herbland, A., Le Bouteiller, A., and Raimbault, P.: Size structure of phytoplankton biomass in the equatorial Atlantic Ocean, *Deep-Sea Res. Pt. I*, 32, 819–836, 1985.
- Houlbrèque, F., Delesalle, B., Blanchot, J., Montel, Y., and Ferrier-Pagès, C.: Picoplankton removal by the coral reef community of La Prévoyante, Mayotte Island, *Aquat. Microb. Ecol.*, 44, 59–70, 2006.
- Huot, Y., Babin, M., Bruyant, F., Grob, C., Twardowski, M. S., Claustre, H.: Relationship between photosynthetic parameters and different proxies of phytoplankton biomass in the subtropical ocean, *Biogeosciences*, 4, 853–868, 2007, <http://www.biogeosciences.net/4/853/2007/>.
- Jespersen, A.-M., Nielsen, J., Riemann, B., and Sondergaard, M.: Carbon-specific phytoplankton growth rates: a comparison of methods, *J. Plankton Res.*, 14, 637–648, 1992.
- Jones, D. R., Karl, D. M., and Laws, E. A.: Growth rates and production of heterotrophic bacteria and phytoplankton in the North Pacific subtropical gyre, *Deep-Sea Res. Pt. I*, 43, 1567–1580, 1996.
- Kirchman, D. L., K'nees, E., and Hodson, R.: Leucine incorporation and its potential as a measure of protein synthesis by bacteria in natural aquatic systems, *Appl. Environ. Microb.*, 49, 599–607, 1985.
- Kirchman, D. L.: Calculating microbial growth rates from data on production and standing stocks, *Mar. Ecol.-Prog. Ser.*, 233, 303–306, 2002.
- Kirchman, D. L.: Leucine incorporation as a measure of biomass production by heterotrophic bacteria, in: *Handbook of methods in aquatic microbial ecology*, edited by: Kemp, P. F., Sherr, B. F., Sherr, E. B., and Cole, J. J., Boca Raton: Lewis, 509–512, 1993.
- Kirkwood, D. S.: Stability of solutions of nutrient salts during storage. *Mar. Chem.*, 38, 151–164, 1992.
- Knauer, G. A., Martin, J. H., and Bruland, K. W.: Fluxes of particulate carbon, nitrogen, and phosphorus in the upper water column of the northeast Pacific, *Deep-Sea Res.*, 26, 97–108, 1979.
- La Ferla, R. and Leonardi, M.: Ecological implications of biomass and morphotype variations of bacterioplankton: an example in a coastal zone of the Northern Adriatic Sea (Mediterranean), *Mar. Ecol.*, 26, 82–88 doi:10.1111/j.1439-0485.2005.00049.x, 2005.
- Landry, M. R. and Hassett, R. P.: Estimating the grazing impact of marine micro-zooplankton, *Mar. Biol.*, 67, 283–288, 1982.
- Laws, E. A., Ditullio, G. R., and Redalje, D. G.: High phytoplankton growth and production rates in the North Pacific subtropical gyre, *Limnol. Oceanogr.*, 32, 905–918, 1987.
- Laws, E. A., Redalje, D. G., Haas, L. W., Bienfang, P. K., Eppley, R. W., Harrison, W. G., Karl, D. M., and Marra, J.: High phytoplankton growth and production rates in oligotrophic Hawaiian coastal waters, *Limnol. Oceanogr.*, 29, 1161–1169, 1984.
- Le Floc'h, E., Gilbert, M., and Antoine, S.: An automatic device for in vivo absorption spectra acquisition and chlorophyll estimation in phytoplankton cultures, *J. Appl. Phycol.*, V14, 435–444, 2002.
- Le Quééré, C., Harrison, S., Prentice, I. C., Buitenhuis, E. T., Aumont, O., BOPP, L., Claustre, H., Cotrim Da Cunha, L., Geider, R., Giraud, X., Klass, C., Kohfeld, K. E., Legendre, k. L., Manizza, M., Platt, T., Rivkin, R. B., Sathyendranath, S., Uitz, J., Watson, Y. J., and Wofl - Glaro, D.: Ecosystem dynamics based on plankton functional types for global ocean biogeochemistry models, *Glob. Change Biol.*, 11, 1–25, doi:10.1111/j.1365-2486.2005.001004.x, 2005.
- Lee, S. and Fuhrman, J. A.: Relationships between biovolume and biomass of naturally derived marine bacterioplankton, *Appl. Environ. Microb.*, 53, 1298–1303, 1987.
- Letelier, R. M., Dore, J. E., Winn, C. D., and Karl, D. M.: Seasonal and interannual variations in photosynthetic carbon assimilation at Station, *Deep-Sea Res. Pt. II*, 43, 467–490, 1996.
- Lipschultz, F.: Nitrogen-specific uptake rates of marine phytoplank-

- ton isolated from natural populations of particles by flow cytometry, *Mar. Ecol.-Prog. Ser.*, 123, 245–258, 1995.
- Liu, H., Landry, M. R., Vault, D., and Campbell, L.: Prochlorococcus growth rates in the central equatorial Pacific: An application of the f_{max} approach *J. Geophys. Res.*, 104, 3391–3399, 1999.
- Loh, A. N., Bauer, J. E., and Druffel, E. R. M.: Variable ageing and storage of dissolved organic components in the open ocean, *Nature*, 430, 877–881, 2004.
- Malone, T. C., Pike, S. E., and Conley, D. J.: Transient variations in phytoplankton productivity at the JGOFS Bermuda time series station, *Deep-Sea Res. Pt. I*, 40, 903–924, 1993.
- Mannino, A. and Harvey, H. R.: Biochemical composition of particles and dissolved organic matter along an estuarine gradient: Sources and implications for DOM reactivity, *Limnol. Oceanogr.*, 45, 775–788, 2000.
- Maranon, E., Cermeno, P., and Perez, V.: Continuity in the photosynthetic production of dissolved organic carbon from eutrophic to oligotrophic waters, *Mar. Ecol.-Prog. Ser.*, 299, 7–17, 2005.
- Maranon, E., Holligan, P., Varela, M., Mourino, B., and Bale, A. J.: Basin-scale variability of phytoplankton biomass, production and growth in the Atlantic Ocean, *Deep-Sea Res. Pt. I*, 47, 825–857, 2000.
- Marie, D., Partensky, F., Simon, N., Guillou, L., and Vault, D.: Flow cytometry analysis of marine picoplankton, in: *Living Colors: Protocols in Flow Cytometry and Cell sorting*, edited by: Diamond, R. A., DeMaggio S., 421–454, 2000a.
- Marie, D., Simon, N., Guillou, L., Partensky, F., and Vault, D.: DNA, RNA analysis of phytoplankton by flow cytometry. In: *Current Protocols in Cytometry*, John Wiley & Sons, Inc., 1–18, 2000b.
- Menzel, D. W. and Ryther, J. H.: The composition of particulate organic matter in the western north Atlantic, *Limnol. Oceanogr.*, 9, 179–186, 1964.
- Minster, J. F. and Boulahdid, M.: Redfield ratios along isopycnal surfaces – a complementary study, *Deep-Sea Res.*, 34, 1981–2003, 1987.
- Moore, C. M., Ostrowski, M., Scanlan, D. J., Feren, K., and Sweetser, T.: Phytoplankton photoacclimation and photoadaptation in response to environmental gradients in a shelf sea, *Limnol. Oceanogr.*, 51, 936–949, 2006.
- Moreira-Turcq, P. F., Cauwet, G., and Martin, J. M.: Contribution of flow cytometry to estimate picoplankton biomass in estuarine systems, *Hydrobiologia*, 462, 157–168, 2001.
- Morgan, J. A., Quinby, H. L., and Ducklow, H. W.: Bacterial abundance and production in the western Black Sea, *Deep-Sea Res. Pt. II*, 53, 1945–1960, 2006.
- Moutin, T., Karl, D., Duhamel, S., Rimmelin, P., Raimbault, P., Van Mooy, B. and Claustre, H.: Phosphate availability and the ultimate control of nitrate input by nitrogen fixation in the tropical Pacific Ocean, *Biogeosciences Discuss.*, 4, 2407–2440, 2007, <http://www.biogeosciences-discuss.net/4/2407/2007/>.
- Moutin, T., Raimbault, P., and Poggiale, J.-C.: Production primaire dans les eaux de surface de la Méditerranée occidentale, *Calcul de la production journalière*, *C. R. Académie des Sciences* 322, 651–659, 1999.
- Moutin, T., Thingstad, T. F., Van Wambeke, F., Marie, D., Slawyk, G., Raimbault, P., and Claustre, H.: Does competition for nanomolar phosphate supply explain the predominance of the cyanobacterium *Synechococcus*?, *Limnol. Oceanogr.*, 47, 1562–1567, 2002.
- Nalewajko, C. and Garside, C.: Methodological problems in the simultaneous assessment of photosynthesis and nutrient uptake in phytoplankton as functions of light intensity and cell size, *Limnol. Oceanogr.*, 28, 591–597, 1983.
- Obernosterer, I., Kawasaki, N., and Benner, R.: P-limitation of respiration in the Sargasso Sea and uncoupling of bacteria from P-regeneration in size-fractionation experiments, *Aquat. Microb. Ecol.*, 32, 229–237, 2003.
- Paytan, A., Cade-Menun, B. J., McLaughlin, K., and Faul, K. L.: Selective phosphorus regeneration of sinking marine particles: evidence from $^{31}\text{P-NMR}$, *Mar. Chem.*, 82, 55–70, 2003.
- Perez, V., Fernandez, E., Maranon, E., Moran, X. A. G., and Zubkov, M. V.: Vertical distribution of phytoplankton biomass, production and growth in the Atlantic subtropical gyres, *Deep-Sea Res. Pt. I*, 53, 1616–1634, 2006.
- Perry, M. J. and Eppley, R. W.: Phosphate uptake by phytoplankton in the central North Pacific Ocean, *Deep-Sea Res.*, 28A, 39–49, 1981.
- Philips, E. J., Aldridge, F. J., Schelske, C. L., and Crisman, T. L.: Relationships between light availability, chlorophyll a, and tripton in a large, shallow subtropical lake, *Limnol. Oceanogr.*, 40, 416–421, 1995.
- Pirker, H., Pausz, C., Stoderegger, K. E., and Herndl, G. J.: Simultaneous measurement of metabolic activity and membrane integrity in marine bacterioplankton determined by confocal laser-scanning microscopy, *Aquat. Microb. Ecol.*, 39, 225–233, 2005.
- Pujo-Pay, M. and Raimbault, P.: Improvement of the wet-oxidation procedure for simultaneous determination of particulate organic nitrogen and phosphorus collected on filters, *Mar. Ecol.-Prog. Ser.*, 105, 203–207, 1994.
- Quevedo, M. and Anadon, R.: Protist control of phytoplankton growth in the subtropical north-east Atlantic, *Mar. Ecol.-Prog. Ser.*, 221, 29–38, 2001.
- Raimbault, P., Diaz, F., and Boudjellal, B.: Simultaneous determination of particulate forms of carbon, nitrogen and phosphorus collected on filters using a semi-automatic wet-oxidation procedure, *Mar. Ecol.-Prog. Ser.*, 180, 289–295, 1999.
- Ras, J., Uitz, J., and Claustre, H.: Spatial variability of phytoplankton pigment distributions in the Subtropical South Pacific Ocean: comparison between in situ and predicted data, *Biogeosciences Discuss.*, 4, 3409–3451, 2007, <http://www.biogeosciences-discuss.net/4/3409/2007/>.
- Redalje, D. G. and Laws, E. A.: A new method for estimating phytoplankton growth rates and carbon biomass, *Mar. Biol.*, 62, 73–79, 1981.
- Redfield, A. C., Ketchum, B. H., and Richards, F. A.: The influence of organisms on the composition of seawater, in: *The Sea*, edited by: Hill, M. N., 26–77, 1963.
- Revilla, M., Iriarte, A., Madariaga, I., and Orive, E.: Bacterial and Phytoplankton Dynamics along a Trophic Gradient in a Shallow Temperate Estuary, *Estuar. Coast. Shelf S.*, 50, 297–313, 2000.
- Riemann, B., Bell, R. T., and Jorgensen, N. O. G.: Incorporation of thymidine, adenine and leucine into natural bacterial assemblages, *Mar. Ecol.-Prog. Ser.*, 65, 87–94, 1990.
- Sciandra, A., Gostan, J., Collos, Y., Descola-Gros, C., Leboulanger, C., Martin-Jézéquel, V., Denis, M., Lefèvre, D., Copin-Montégut, C., and Avril, B.: Growth-compensating phenomena in continuous cultures of *Dunaliella tertiolecta* limited simulta-

- neously by light and nitrate, *Limnol. Oceanogr.*, 42, 1325–1339, 1997.
- Sherr, E. B., Sherr, B. F., and Sigmon, C. T.: Activity of marine bacteria under incubated and in situ conditions, *Aquat. Microb. Ecol.*, 20, 213–223, 1999.
- Sherr, E., Sherr, B., and Cowles, T.: Mesoscale variability in bacterial activity in the Northeast Pacific Ocean off Oregon, USA, *Aquat. Microb. Ecol.*, 25, 21–30, 2001.
- Six, C., Thomas, J. C., Brahmsha, B., Lemoine, Y., and Partensky, F.: Photophysiology of the marine cyanobacterium *Synechococcus* sp. WH8102, a new model organism, *Appl. Environ. Microb.*, 35, 17–29, 2004.
- Smith, D. C. and Azam, F.: A simple, economical method for measuring bacterial protein synthesis rates in seawater using 3H-leucine, *Marine Microbial Food Webs*, 6, 107–114, 1992.
- Smith, J. W. O., Marra, J., Hiscock, M. R., and Barber, R. T.: The seasonal cycle of phytoplankton biomass and primary productivity in the Ross Sea, Antarctica, *Deep-Sea Res. Pt. II*, 47, 3119–3140, 2000.
- Sobczak, W. V., Cloern, J. E., Jassby, A. D., and Muller-Solger, A. B.: Bioavailability of organic matter in a highly disturbed estuary: The role of detrital and algal resources, *PNAS*, 99, 8101–8105, 2002.
- Steeman-Nielsen, E.: Measurement of production of organic matter in the sea by means of carbon-14, *Nature*, 267, 684–685, 1951.
- Strickland, J. D. H. and Parsons, T. R.: A practical handbook of seawater analysis, *Bulletin of Fisheries Research Board of Canada*, 167, 49–55, 1972.
- Taylor, A., Geider, R., and Gilbert, F.: Seasonal and latitudinal dependencies of phytoplankton carbon-to-chlorophyll a ratios: results of a modelling study, *Mar. Ecol.-Prog. Ser.*, 152, 51–66, 1997.
- Thingstad, T. F., Riemann, B., Havskum, H., and Garde, K.: Incorporation rates and biomass content of C and P in phytoplankton and bacteria in the Bay of Aarhus (Denmark) June 1992, *J. Plankton Res.*, 18, 97–121, 1996.
- Thingstad, T. F.: Control of bacterial growth in idealized food webs, in: *Microbial ecology of the oceans*, edited by: Kirchman, D. L., Wiley series in Ecological and Applied Microbiology, Mitcheck, R. (Series Ed.), 229–260, 2000.
- Tremblay, J. and Legendre, L.: A model for the size-fractionated biomass and production of marine phytoplankton, *Limnol. Oceanogr.*, 39, 2004–2014, 1994.
- Uitz, J., Claustre, H., Morel, A., and Hooker, S. B.: Vertical distribution of phytoplankton communities in open ocean: An assessment based on surface chlorophyll, *J. Geophys. Res.*, 111, doi:10.1029/2005JC003207, 2006.
- Vadstein, O., Jensen, A., Olsen, Y., and Reinertsen, H.: Growth and phosphorus status of limnetic phytoplankton and bacteria, *Limnol. Oceanogr.*, 33, 489–503, 1988.
- Van Mooy, B. A. S., Rocap, G., Fredricks, H. F., Evans, C. T., and Devol, A. H.: Sulfolipids dramatically decrease phosphorus demand by picocyanobacteria in oligotrophic marine environments, *PNAS*, 103, 8607–8612, 2006.
- Van Wambeke, F., Bonnet, S., Moutin, T., Raimbault, P., Alarçon, G., and Guieu, C.: Factors limiting heterotrophic bacterial production in the southern Pacific Ocean, *Biogeosciences Discuss.*, 4, 3799–3828, 2007a.
- Van Wambeke, F., Obernosterer, I., Moutin, T., Duhamel, S., Ulloa, O., and Claustre, H.: Heterotrophic bacterial production in the South East Pacific: longitudinal trends and coupling with primary production, *Biogeosciences Discuss.*, 4, 2761–2791, 2007b.
- Vaulot, D.: Estimate of phytoplankton division rates by the mitotic index method: The fmax approach revisited, *Limnol. Oceanogr.*, 37, 644–649, 1992.
- Veldhuis, M. J. W. and Kraay, G. W.: Phytoplankton in the subtropical Atlantic Ocean: towards a better assessment of biomass and composition, *Deep-Sea Res. Pt. I*, 51, 507–530, 2004.
- Watson, S. W., Novitsky, T. J., Quinby, H. L., and Valois, F. W.: Determination of bacterial number and biomass in the marine environment, *Appl. Environ. Microb.*, 33, 940–946, 1977.
- Welschmeyer, N. A., Goericke, R., Strom, S., and Peterson, W. T.: Phytoplankton growth and herbivory in the subarctic Pacific: a chemotaxonomic analysis, *Limnol. Oceanogr.*, 36, 1631–1649, 1991.
- Welschmeyer, N. A.: Fluorimetric analysis of chlorophyll a in the presence of chlorophyll b and pheopigments, *Limnol. Oceanogr.*, 39, 1985–1992, 1994.
- Wood, A. M., Rai, H., Garnier, J., Kairesalo, T., Gresens, S., Orive, E., and Ravail, B.: Practical approaches to algal excretion, *Marine Microbial Food Webs*, 6, 21–38, 1992.
- Zubkov, M. V., Sleight, M. A., Burkill, P. H., and Leakey, R. J. G.: Picoplankton community structure on the Atlantic Meridional Transect: a comparison between seasons, *Prog. Oceanogr.*, 45, 369–386, 2000.
- Zweifel, U. L. and Hagstrom, A.: Total Counts of Marine Bacteria Include a Large Fraction of Non-Nucleoid-Containing Bacteria (Ghosts), *Appl. Environ. Microbiol.*, 61, 2180–2185, 1995.

Heterotrophic bacterial production in the eastern South Pacific: longitudinal trends and coupling with primary production

F. Van Wambeke¹, I. Obernosterer^{2,3}, T. Moutin⁴, S. Duhamel^{1,4}, O. Ulloa⁵, and H. Claustre⁶

¹Laboratoire de Microbiologie, Géochimie et Ecologie Marines (LMGEM), CNRS, UMR 6117, Université de la Méditerranée, Campus de Luminy – Case 901, 13288 Marseille cedex 9, France

²Université Pierre et Marie Curie-Paris6, Laboratoire ARAGO, Avenue Fontaulé, BP44, 66650 Banyuls-sur-Mer, France

³CNRS, UMR7621, Laboratoire d’Océanographie Biologique de Banyuls, Avenue Fontaulé, BP44, 66650 Banyuls-sur-Mer, France

⁴Laboratoire d’Océanographie et de Biogéochimie (LOB), CNRS, UMR 6535, Université de la Méditerranée, Campus de Luminy – Case 901, 13288 Marseille cedex 9, France

⁵Departamento de Oceanografía & Centro de Investigación Oceanográfica en el Pacífico Sur-Oriental, Universidad de Concepción, Casilla 160-C, Concepción, Chile

⁶CNRS, Laboratoire d’océanographie de Villefranche, 06230 Villefranche-sur-Mer, France ; Université Pierre et Marie Curie-Paris6, Laboratoire d’océanographie de Villefranche, 06230 Villefranche-sur-Mer, France

Received: 23 July 2007 – Published in Biogeosciences Discuss.: 15 August 2007

Revised: 7 January 2008 – Accepted: 7 January 2008 – Published: 8 February 2008

Abstract. Spatial variation of heterotrophic bacterial production and phytoplankton primary production were investigated across the eastern South Pacific Ocean (-141° W, -8° S to -72° W, -35° S) in November–December 2004. Bacterial production (^3H leucine incorporation) integrated over the euphotic zone encompassed a wide range of values, from $43\text{ mg C m}^{-2}\text{ d}^{-1}$ in the hyper-oligotrophic South Pacific Gyre to $392\text{ mg C m}^{-2}\text{ d}^{-1}$ in the upwelling off Chile. In the gyre (120° W, 22° S) records of low phytoplankton biomass ($7\text{ mg Total Chl a m}^{-2}$) were obtained and fluxes of in situ ^{14}C -based particulate primary production were as low as $153\text{ mg C m}^{-2}\text{ d}^{-1}$, thus equal to the value considered as a limit for primary production under strong oligotrophic conditions. Average rates of ^3H leucine incorporation rates, and leucine incorporation rates per cell ($5\text{--}21\text{ pmol l}^{-1}\text{ h}^{-1}$ and $15\text{--}56\times 10^{-21}\text{ mol cell}^{-1}\text{ h}^{-1}$, respectively) determined in the South Pacific gyre, were in the same range as those reported for other oligotrophic subtropical and temperate waters. Fluxes of dark community respiration, determined at selected stations across the transect varied in a narrow range ($42\text{--}97\text{ mmol O}_2\text{ m}^{-2}\text{ d}^{-1}$), except for one station in the upwelling off Chile ($245\text{ mmol O}_2\text{ m}^{-2}\text{ d}^{-1}$). Bacterial growth

efficiencies varied between 5 and 38%. Bacterial carbon demand largely exceeded ^{14}C particulate primary production across the South Pacific Ocean, but was lower or equal to gross community production.

1 Introduction

Over a broad range of aquatic systems, heterotrophic bacterial biomass varies less than phytoplankton biomass (Cole et al., 1988). The magnitude, variability and control of bacterial heterotrophic production has been well studied in the northern hemisphere (Ducklow, 2000; Landry and Kirchman, 2002), including the Arctic (Sherr et al., 2003; Kirchman et al., 2005). By contrast, the oceans in the southern hemisphere have been much less explored, except along several coasts and margins, and the Indian and the Antarctic Ocean. In the Pacific Ocean, results for heterotrophic bacterial production were mainly acquired in tropical and subtropical regions ($20^{\circ}\text{N}\text{--}20^{\circ}\text{S}$, Landry and Kirchman, 2002). The North Pacific Central gyre has been intensively studied, particularly the long term station HOTS (Hawaii Ocean Time Series, Karl et al., 2001). Overall, oligotrophic regions of the ocean are clearly the least well studied.

On the basis of remotely-sensed ocean color, the South Pacific central gyre appears to be the most oligotrophic and



Correspondence to: F. Van Wambeke
(france.van-wambeke@univmed.fr)

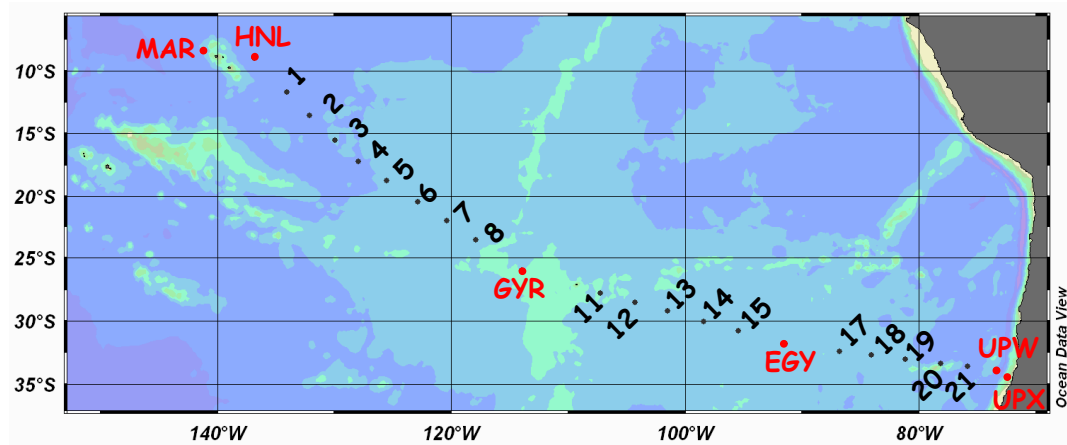


Fig. 1. Transect of the BIOSOPE cruise from the Marquesas Islands to Chile. Long-term process stations are indicated in red. Numbers indicates short-term stations, for which only numbers have been indicated to simplify presentation, and not the complete code as in Table 3. For instance 1 is STB1 and 21 is STA21.

stable water body (Claustre and Maritoner, 2003). To date, however, no investigation on the biogeochemistry of this water body has taken place. The aim of the BIOSOPE (Biogeochemistry and Optics South Pacific Experiment) project was to conduct a pluridisciplinary exploration of this gyre as well as their eastern (Chilean coastal upwelling) and western (Marquesas plateau) borders, allowing the examination of a very large range of trophic conditions. Hyperoligotrophic conditions were observed at the centre of the gyre, with the clearest natural waters ever described (Morel et al., 2007), and a deep chlorophyll maximum reaching 180 m (Ras et al., 2007). The aim of the present study was to determine the abundance and activity of heterotrophic bacteria across the South Pacific Ocean, and to relate bacterial heterotrophic activity to phytoplankton primary production. We further discuss the techniques involved for determining the coupling between primary and bacterial heterotrophic production.

2 Materials and methods

2.1 Strategy of sampling

The BIOSOPE cruise was conducted from 24 October to 11 December 2004 aboard R/V *Atalante* across the eastern South Pacific Ocean (Fig. 1). Stations of short (<5 h, 21 stations) and long (3 to 6 days, 6 stations) duration were sampled (Table 1). Stations occupied for less than 5 h were abbreviated chronologically (station type STB1 to STB20 and STA21, Fig. 1, Table 1). The stations of long duration were abbreviated according to their location: MAR (in the vicinity of Marquesas Islands), HNL (High Nutrients Low Chlorophyll waters in North Eastern area far from Marquise Islands), GYR (the central part of the South Pacific gyre), EGY (the eastern part of the South Pacific gyre) and, UPW and UPX (two sites chosen in the coastal upwelling

region of central Chile). At the short stations we systematically sampled at 09:00 h local time to avoid possible biases due to daily variability in heterotrophic bacterial abundance and activity. At the long stations, we checked the validity of our routine bacterial production protocols by time series and concentration kinetics. All samples were collected from a CTD-rosette system fitted with 20 12-l Niskin bottles equipped with Teflon rings. Samples were processed within 1 h of collection. Water samples used for in situ-simulated primary measurements (IPP_{deck}) came from the same rosette cast as that used for bacterial production (the 09:00 a.m. CTD cast). However some measurements of PP using the JGOFs protocol (in situ moored lines immersed for 24 h from dusk to dusk, IPP_{insitu}) were also performed sometimes at the long stations. In that case, samples were taken on a rosette before dusk. Besides measurements of bacterial abundance and production and primary production described below, other data presented in this paper include hydrographic properties (Claustre et al., 2008) and Total chlorophyll *a* (TChl_a=Chl_a+Divinyl-Chl_a, Ras et al., 2007).

2.2 Bacterial abundance

Water samples for flow cytometric analyses of non-chlorophyllous bacterioplankton populations, assumed to be mainly heterotrophic bacteria in the upper ocean, were fixed with paraformaldehyde at 1% and preserved in liquid nitrogen for further analysis in the laboratory. The protocol is fully described in Grob et al. (2007). Briefly, bacterioplankton samples were stained with SYBR-Green I and counted on a FACS Calibur (Becton Dickinson) flow cytometer.

2.3 Bacterial production

“Bacterial” production (BP – sensu stricto referring to heterotrophic prokaryotic production –) was determined by [³H]

Table 1. Main physical and biological characteristics of the stations sampled during the BIOSPE cruise. SST: sea surface temperature, Ze: depth of the euphotic zone (1% PAR), $Z_{10\%}$ (UV-B): the 10% UV-B irradiance depth (at 305 ± 2 nm) as determined in Tédetti et al. (2007), I TChl *a*: integrated Total chlorophyll *a*, IPP_{deck}: integrated particulate primary production (based on on-deck incubations, see methods), IBP_{Ze}: integrated bacterial heterotrophic production. All stocks and fluxes are integrated from the surface to the euphotic depth.

station	Longitude ° W	Latitude ° S	date	SST °C	Ze m	$Z_{10\%}$ (UVB) m	I TChl <i>a</i> mg m ⁻²	IPP _{deck} mgC m ⁻² d ⁻¹	IBP _{Ze} mgC m ⁻² d ⁻¹
MAR1	-141.24	-8.40	26 October	27.8	66	10	24	457	131
MAR3	-141.28	-8.33	28 October	27.8	70		21	683	144
HNL1	-136.85	-9.00	31 October	27.8	90	10	16	335	86
STB1	-134.10	-11.74	3 November	27.8	99	12	17	414	101
STB2	-132.11	-13.55	4 November	27.4	124		17	250	96
STB3	-129.93	-15.53	5 November	27.1	134	12	16	150	114
STB4	-127.97	-17.23	6 November	26.5	136	17	16	164	87
STB5	-125.55	-18.75	7 November	25.7	142	19	11	142	71
STB6	-122.89	-20.45	8 November	24.5	157		5	139	72
STB7	-120.38	-22.05	9 November	24.3	167	28	8	76	79
STB8	-117.89	-23.55	10 November	23.4	144		7	152	61
GYR2	-114.01	-25.97	12 November	22.1	160	21	11	159	50
STB11	-107.29	-27.77	20 November	21.3	152		8	97	62
STB12	-104.31	-28.54	21 November	21.2	152	19	7	98	49
STB13	-101.48	-29.23	22 November	20.0	145		8	125	43
STB14	-98.39	-30.04	23 November	19.8	136		10	138	47
STB15	-95.43	-30.79	24 November	18.7	108		12	219	57
EGY2	-91.46	-31.82	26 November	18.1	92	12	14	196	55
STB17	-86.78	-32.40	1 December	17.3	96	10	15	280	61
STB18	-84.07	-32.68	2 December	17.4	87	9	15	233	44
STB19	-81.20	-33.02	3 December	17.2	107		12	195	57
STB20	-78.12	-33.35	4 December	17.6	48		21	359	93
STA21	-75.83	-33.61	5 December	16.8	56		21	566	110
UPW2	-73.36	-33.93	7 December	15.9	34	3	59		226
UPX1	-72.41	-34.54	9 December	13.3	38		39	1446	392

leucine incorporation applying the centrifugation method (Smith and Azam, 1992). Duplicate 1.5 mL samples were incubated with a mixture of [4,5-³H]leucine (Amersham, specific activity 160 Ci mmol⁻¹) and nonradioactive leucine at final concentrations of 7 and 13 nM, respectively for active waters (>10 pmol leu l⁻¹ h⁻¹) and the opposite (7 nM cold, 13 nM labeled) for low activity waters. Samples were incubated in the dark at the respective in situ temperatures for 1–7 h according to expected activities, period during which we preliminarily checked that the incorporation of leucine was linear with time (e.g. at the centre of the gyre we incubated surface waters on average for 2 h, and the activity in dark incubated samples was linear up to 8 h, data not shown). Incubations were stopped by the addition of trichloroacetic acid (TCA) to a final concentration of 5%. To facilitate the precipitation of proteins, bovine serum albumin (BSA, Sigma, 100 mg l⁻¹ final concentration) was added prior to centrifugation at 16 000 g for 10 min. After discarding the supernatant, 1.5 ml of 5% TCA were added and the samples were subsequently vigorously shaken on a vortex and centrifuged again. The supernatant was discarded and 1.5 ml of PCS liq-

uid scintillation cocktail (Amersham) were added. The radioactivity incorporated into bacterial cells was counted in a Packard LS 1600 Liquid Scintillation Counter on board the ship. We checked effects of ethanol rinse and BSA addition in our protocol, because in most published studies BSA is not added and ethanol rinse is often used to remove unspecific ³H labelling (Wicks and Robarts, 1998; Ducklow et al., 2002; Kirchman et al., 2005) although sometimes ethanol rinse did not change the results (Van Wambeke et al., 2002; Granéli et al., 2004). There was no significant difference among the different treatments (+ or – ethanol, + or – BSA added, data not shown). As we also managed some size-fractionated BP measurements on some selected samples, we were also able to compare the filtration technique (20 ml incubated with 1 nM ³H-leucine +19 nM cold leucine, filtered through Millipore GS 0.2 μm filters, no ethanol rinse), with the centrifugation technique (BSA addition, no ethanol rinse). The model II regression was applied to compute the relationships between both techniques. With the whole data set ($n=88$, BP range 5–578 ng C l⁻¹ h⁻¹), the slope of “filtration” versus “centrifugation” was 1.04 ± 0.02 ,

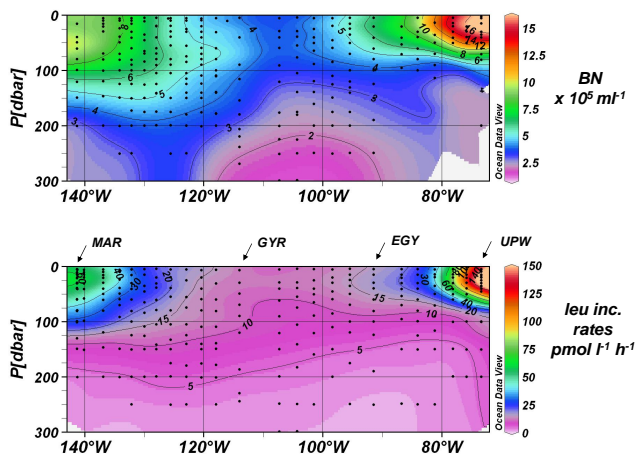


Fig. 2. Distribution of bacterial abundances (upper panel) and leucine incorporation rates (lower panel) along the BIOSOPE cruise transect. All CTD casts were performed around 09:00. The main characteristics of the stations sampled are presented in Table 1. The scale of leucine incorporation rates is limited to $150 \text{ pmol l}^{-1} \text{ h}^{-1}$ but higher values were obtained in the coastal upwelling region (see Fig. 3). Interpolation between sampling points in contour plots was made with the Ocean Data View program (VG gridding algorithm, Schlitzer, 2004).

and with only the $<50 \text{ ng C l}^{-1} \text{ h}^{-1}$ data set ($n=77$), the slope was 0.93 ± 0.04 (figure not shown). In both cases, the Y intercept was not significantly different from 0. We felt thus confident in comparing our measurements of leucine rates to results obtained with other protocols (centrifugation with no BSA or filtration technique).

A factor of $1.5 \text{ kg C mol leucine}^{-1}$ was used to convert the incorporation of leucine to carbon equivalents, assuming no isotopic dilution (Kirchman, 1993). Indeed, isotopic dilution ranged from 1.04 to 1.18 as determined on four occasions on concentration kinetics. Errors associated with the variability between replicate measurements (half the difference between the two replicates) averaged 13% and 6% for BP values less and more than $10 \text{ ng C l}^{-1} \text{ h}^{-1}$, respectively.

2.4 Particulate primary production

Primary production was determined: (1) by 24 h-in situ incubations according to the experimental protocol detailed in Moutin and Raimbault (2002), and (2) by short-term ($<5 \text{ h}$) on-deck incubations using incubators equipped with Nickel screens (50, 25, 15, 7, 3 and 1% of incident irradiance) (Duhamel et al., 2006). Rates of daily particulate primary production were obtained using two incubation methods: (i) in situ moored lines immersed during 24 h, and in that case daily rates were directly measured ($\text{PP}_{\text{in situ}}$) and (ii) using the conversion factors $\tau(T_i; T)$ according to Moutin et al. (1999) to calculate normalized (dawn-to-dawn) daily rates from the hourly rates measured in the on-deck incubators (PP_{deck}).

The conversion factors were calculated based on incident irradiance measured aboard.

2.5 Gross community production, dark community respiration and net community production

Rates of gross community production (GCP), dark community respiration (DCR) and net community respiration (NCP) were estimated from changes in the dissolved oxygen (O_2) concentration during light/dark incubations of unfiltered seawater (24 h) carried out in situ on moored lines. Seawater was collected at six depths in the euphotic zone and transferred to 9-l polycarbonate bottles. The biological oxygen demand (BOD) bottles (125 ml) were filled by siphoning, using silicon tubing. For DCR, the BOD bottles were placed in black bags. All BOD bottles (quadruplicate in the dark, quadruplicate in the light at each layer) were incubated in situ at the respective depth layers under natural irradiance levels from dusk to dusk using the same mooring line as for $\text{PP}_{\text{in situ}}$. The concentration of oxygen was determined by Winkler titration of whole bottles. Titration was done with an automated potentiometric end-point detection system (Metrohm DMS 716), following the recommendations of Carignan et al. (1998). DCR and NCP were calculated as the difference between initial and final O_2 concentrations in dark and light bottles, respectively. GCP was calculated as the difference between NCP and DCR. On two occasions (St 3 5 m, 125 m), respiration rates were also determined on filtered ($0.8 \mu\text{m}$) water samples.

2.6 Bacterial growth efficiency

The bacterial growth efficiency (BGE) was calculated from BP and DCR, assuming that bacterial respiration represented a constant proportion (f) of DCR, and applying a respiratory quotient (RQ) to convert O_2 -based measurements to carbon units:

$$\text{BGE} = \text{BP} / (\text{BP} + (f \times \text{RQ} \times \text{DCR}))$$

The choices of RQ and f are developed in the results section. The BGE were estimated from data of daily BP and DCR integrated over the euphotic zone. Vertical profiles for both parameters are available at the long stations MAR, HNL, GYR, UPW and UPX, where moored lines were deployed for 24 h in situ.

3 Results

3.1 Horizontal and vertical variation of bacterial production

Bacterial abundances ($0.8\text{--}20.7 \times 10^5 \text{ cells ml}^{-1}$) and leucine incorporation rates ($0.34\text{--}400 \text{ pmol leu l}^{-1} \text{ h}^{-1}$) varied over a large range across the 8000 km of the BIOSOPE transect (Fig. 2) and both variables were strongly correlated (relation log-log, $n=249$, $r=0.85$, $p<0.001$). The gradients of

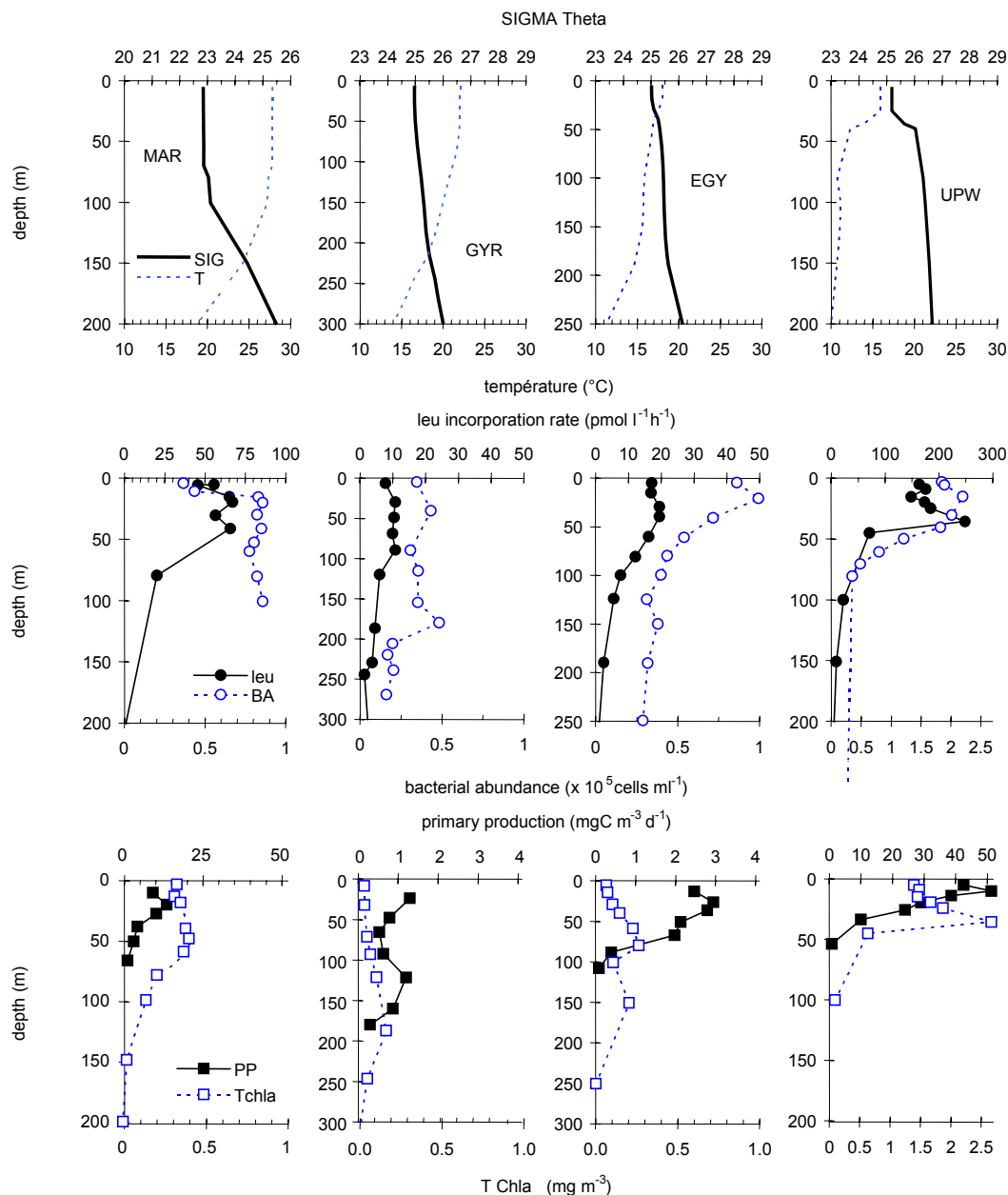


Fig. 3. Vertical distributions of temperature, sigma theta (upper panel), bacterial abundance, leucine incorporation rates (middle panel), Tchl_a, primary production (PP_{deck}, see methods, lower panel), at stations mesotrophic MAR (26 October), hyperoligotrophic GYR (12 November), oligotrophic EGYR (26 November), and eutrophic UPW (7 December). All variables are from the 09:00 CTD cast, except for bacterial abundance (the following 12:00 CTD cast).

bacterial abundances and leucine incorporation rates were particularly pronounced off Chile. Highest leucine incorporation rates were obtained in the coastal upwelling area (250 pmol l⁻¹ h⁻¹ at UPW at 35 m, Fig. 3; 400 pmol l⁻¹ h⁻¹ at UPX at 15 m, data not shown) and in the northwestern zone of the transect, close to the Marquesas Islands (60 pmol l⁻¹ h⁻¹ at MAR at 10–50 m). Leucine incorporation rates were substantially lower between STB6 to STB15

representing the gyre stations (maximum 15 pmol l⁻¹ h⁻¹). A similar pattern was detectable for chlorophyll (Ras et al., 2007) and concentrations of inorganic nutrients (Raimbault et al., 2007).

At the mesotrophic site MAR, sea surface temperature was 27.5°C and the mixed layer reached 70 m (Fig. 3). Leucine incorporation rates were highest between 10 and 50 m (59±8 pmol l⁻¹ h⁻¹) coinciding with the layer of

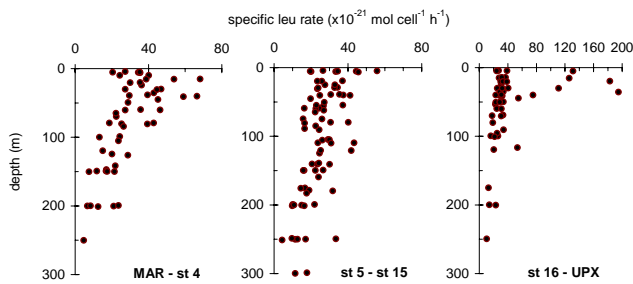


Fig. 4. Vertical distribution of specific leucine incorporation rates ($\times 10^{-21}$ mol leucine cell $^{-1}$ h $^{-1}$). Bacterial abundance and leucine incorporation rates were measured on water samples coming from the same CTD cast. MAR-st 4: MAR 3, HNLI, STB1, 2, 3, 4; st5-st15: STB5, 6, 7, 8, 11, 12, 13, 14; st16-UPW: STB15, 17, 18, 19, 20, 21, UPW2, UPX1. All these casts were sampled at 09:00 local time.

maximum primary production (20 m, $13 \mu\text{g C l}^{-1} \text{d}^{-1}$) and maximum TChla (50 m, $0.4 \mu\text{g l}^{-1}$). At the eutrophic site UPW, characterized by a shallow mixed layer (20 m) and relatively low surface water temperature (15.9°C), the maximum rates of leucine incorporation ($250 \text{ pmol l}^{-1} \text{h}^{-1}$) and primary production ($50 \mu\text{g C l}^{-1} \text{d}^{-1}$) were higher than those at the MAR site. Maximum leucine incorporation coincided with a narrow, high TChla peak ($2.6 \mu\text{g l}^{-1}$) at 35 m depth (Fig. 3). At the hyperoligotrophic GYR site, leucine incorporation was homogenous (mean \pm SD: $9.3 \pm 1.9 \text{ pmol l}^{-1} \text{h}^{-1}$) down to 120 m depth, similarly to primary production ($0.9 \pm 0.3 \mu\text{g C l}^{-1} \text{d}^{-1}$ between 20 and 160 m). Below 120 m, leucine incorporation progressively decreased to $1.4 \text{ pmol l}^{-1} \text{h}^{-1}$ at 250 m depth. No clear association with the deep, very small peak of TChla ($0.16 \mu\text{g l}^{-1}$) at 185 m depth was detectable at this site. At the oligotrophic site EGY, leucine incorporation rates were still very low, but exhibited a subsurface maximum around 40 m, coinciding with a peak of primary production around $3 \mu\text{g C l}^{-1} \text{d}^{-1}$.

In contrast to bulk leucine incorporation rates, cell-specific leucine incorporation rates varied within a rather narrow range ($10\text{--}70 \times 10^{-21}$ mol cell $^{-1}$ h $^{-1}$), except for the Chilean coast, where values reached up to 200×10^{-21} mol cell $^{-1}$ h $^{-1}$ (Fig. 4). From MAR to STB4, a sub-surface maximum was visible around 20–30 m with values ranging from 30 to 70×10^{-21} mol cell $^{-1}$ h $^{-1}$ (Fig. 4). Within the gyre (stations STB6 to STB15), specific leucine incorporation rates were rather constant down to the deep TChla maximum at around 160 m ($13\text{--}56 \times 10^{-21}$ mol cell $^{-1}$ h $^{-1}$).

Bacterial production (BP) integrated over the euphotic zone (IBP) ranged from 43 to $392 \text{ mg C m}^{-2} \text{d}^{-1}$ during the BIOSOPE cruise (Table 1). The large range of trophic conditions encountered is reflected by the integrated stocks of TChla in the euphotic zone ranging between 7 and 59 mg m^{-2} (Table 1) and the integrated fluxes of particulate primary production (IPP_{deck}) varying between 76 and $1446 \text{ mg C m}^{-2} \text{d}^{-1}$ (Table 1). As for volumetric values,

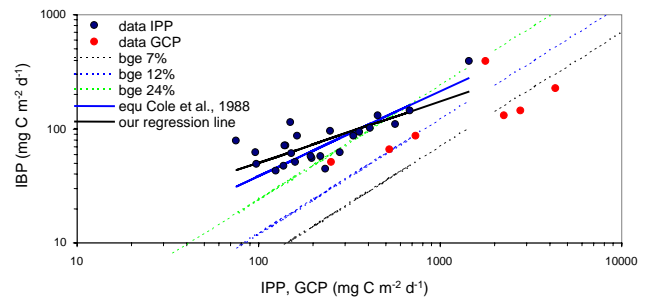


Fig. 5. Relation between bacterial production (IBP; y axis) and primary production (IPP, x axis), both expressed on an integrated basis for the euphotic zone (black dots). Relation between IBP and gross community production (GCP) are also indicated (red dots). Black line: regression line ($\text{Log IBP} = 0.542 \text{ Log IPP} + 0.615$) for all our data set ($n=24$, $r^2=0.59$, $p<0.0001$). Red line: regression line ($\text{Log IBP} = 0.746 \text{ Log IPP} + 0.093$) from Cole et al. (1988) calculated for pelagic systems. We used ordinary least square regression for comparison purposes, and also for the reasons evoked in Teira et al. (2001). The three dotted lines are relying on a couple of IBP, IPP points such that BCD equals IPP, ($\text{BCD} = \text{IBP}/\text{BGE} = \text{IPP}$), with assumed BGEs values of (from left to the right) 7% (green), 12% (blue), 24% (black).

highest values of IBP were obtained in the upwelling region off Chile ($226\text{--}392 \text{ mg C m}^{-2} \text{d}^{-1}$) corresponding roughly to the IBP obtained by Cuevas et al. (2004) – based on the thymidine technique – in the upwelling area off Concepcion in October 1999 ($268\text{--}561 \text{ mg C m}^{-2} \text{d}^{-1}$ for their coastal station at 73°W). At stations STB6 to STB15, encompassing the GYR sites, IBP was as low as $58 \pm 11 \text{ mg C m}^{-2} \text{d}^{-1}$ (mean \pm SD). Similarly, IPP_{deck} revealed lowest values at these stations ($134 \pm 42 \text{ mg C m}^{-2} \text{d}^{-1}$). Stations MAR and HNL, on the western part of the transect, presented intermediary values of IBP ($86\text{--}140 \text{ mg C m}^{-2} \text{d}^{-1}$) and IPP_{deck} ($318\text{--}683 \text{ mg C m}^{-2} \text{d}^{-1}$). IPP_{insitu}, determined only on a limited number of stations across the transect reflected the trend in IPP_{deck} ($r=0.89$, $n=5$) with higher values at MAR and UPX (1146 and $1344 \text{ mg C m}^{-2} \text{d}^{-1}$, respectively) and lower values at GYR ($154 \text{ mg C m}^{-2} \text{d}^{-1}$, Table 2). IPP_{insitu} was, on average, 1.3 fold higher than IPP_{deck} (range $0.92\text{--}1.67$, $n=5$). There was a significant log-log relationship between IBP and IPP_{deck} when all data were pooled ($\text{Log IBP} = 0.551 \text{ Log IPP} + 0.594$, $n=36$, $r^2=0.59$, $p<0.0001$) (Fig. 5). The ratio IBP to IPP_{deck}, however, was highly variable, ranging from 0.19 to 1.04 ($n=24$) across the cruise transect. For the GYR sites (STB 6 to STB15), the ratio IBP to IPP_{deck} was, on average, 0.48 ± 0.24 , and it was lower on the boundaries of the transect (for the eastern part, stations EGY to UPX: 0.24 ± 0.05 , for the western part, stations MAR to STB1: 0.25 ± 0.03).

Gross community production (GCP) integrated in the euphotic zone ranged from 29 to $505 \text{ mmol O}_2 \text{ m}^{-2} \text{d}^{-1}$ (Table 2) and was well correlated with IPP_{insitu} ($r=0.88$, $n=7$).

Table 2. Measured gross community production (GCP), dark community respiration (DCR), net community production (NCP), ^{14}C based particulate primary production (IPP_{deck} and $\text{IPP}_{\text{insitu}}$) at stations where all these parameters were available. Data are integrated over the euphotic zone (Ze). Errors correspond to water-column integrated standard deviations for GCP, DCR and NCP (quadruplicate incubations at each depth) and for $\text{IPP}_{\text{insitu}}$ (triplicate samples at each depth). For IBP and IPP_{deck} errors represent water column integrated values of the variability between duplicate measurements per depth. Note that the units vary according the variable ($\text{mmol O}_2 \text{ m}^{-2} \text{ d}^{-1}$ and $\text{mgC m}^{-2} \text{ d}^{-1}$).

	Ze m	IBP $\text{mgC m}^{-2} \text{ d}^{-1}$	DCR $\text{mmol O}_2 \text{ m}^{-2} \text{ d}^{-1}$	NCP $\text{mmol O}_2 \text{ m}^{-2} \text{ d}^{-1}$	GCP $\text{mmol O}_2 \text{ m}^{-2} \text{ d}^{-1}$	$\text{IPP}_{\text{deck}}^1$ $\text{mgC m}^{-2} \text{ d}^{-1}$	$\text{IPP}_{\text{insitu}}^1$ $\text{mgC m}^{-2} \text{ d}^{-1}$
MAR 1	66	131±4	71±18	193±32	264±37	457±17	702±136
MAR 3	70	171±10*	97±13	227±16	324±20	683±29	1146±123
HNL 1	90	86±4	42±17	44±21	86±28	318±33	518±28
GYR 2	160	50±3	66±19	-37±40	29±45	159±19	154±23
GYR 4	160	65±3*	74±30	-13±20	61±37	nd	203±15
UPW 2	34	226±9	76±12	429±19	505±24	nd	4362±306
UPX 1	38	392±3	245±21	-38±23	207±34	1446±46	1344±46

¹ IPP_{deck} : as in Table 1 (on-deck incubations), $\text{IPP}_{\text{insitu}}$: from 24 h in situ moored lines.

* The daily IBP were calculated cumulating data of different profiles measured every 3 h along a diel cycle (Van Wambeke et al., 2008). In other cases, daily BP was calculated from the 09:00 CTD cast assuming daily rates = 24 times hourly rates.

Integrated net community production (NCP) was again highest at the upwelling site UPW ($429 \pm 19 \text{ mmol O}_2 \text{ m}^{-2} \text{ d}^{-1}$) and at the stations close to the Marquesas islands (mean $210 \text{ mmol O}_2 \text{ m}^{-2} \text{ d}^{-1}$). Integrated fluxes of NCP were negative at UPX ($-38 \pm 23 \text{ mmol O}_2 \text{ m}^{-2} \text{ d}^{-1}$) and were close to balance at the GYR site ($-13 \pm 20 \text{ mmol O}_2 \text{ m}^{-2} \text{ d}^{-1}$ and $-37 \pm 40 \text{ mmol O}_2 \text{ m}^{-2} \text{ d}^{-1}$).

3.2 Dark community respiration and bacterial growth efficiency

Rates of dark community respiration (DCR) varied within a narrow range ($42\text{--}97 \text{ mmol O}_2 \text{ m}^{-2} \text{ d}^{-1}$) except for the high rates obtained at UPX ($245 \text{ mmol O}_2 \text{ m}^{-2} \text{ d}^{-1}$). Respiration in $0.8 \mu\text{m}$ filtered seawater was determined only at station STB5. Respiration rates in the $<0.8 \mu\text{m}$ size fraction and unfiltered seawater amounted to 0.62 ± 0.22 and $0.52 \pm 0.25 \mu\text{mol O}_2 \text{ l}^{-1} \text{ d}^{-1}$, respectively, at 5 m and to 0.46 ± 0.12 and $0.58 \pm 0.24 \mu\text{mol O}_2 \text{ l}^{-1} \text{ d}^{-1}$, respectively, at 125 m. Such comparison was made only in two occasions, and since it is risky to generalize these results, to determine the BCD we assume the following: (i) that heterotrophic bacterial respiration accounts entirely for DCR (BGE_{100}), (ii) or that it represents half of it (BGE_{50} , Table 3). For all stations considered, BGE_{100} and BGE_{50} ranged between 7 and 24% and between 14 and 38%, respectively. The application of respiratory quotients (RQ) reported in the literature (0.8–1.1; Robinson and Williams, 1999; Lefevre et al., in press) resulted in minor changes in the BGE for a given contribution of bacterial to community respiration (by 2 to 7%). Hence, the assumption on the fraction of DCR attributable to bacterial respiration has a greater impact on the variability

Table 3. Calculated bacterial growth efficiency (BGE), integrated gross community production (GCP, in carbon units), the ratio of $\text{IPP}_{\text{insitu}}/\text{GCP}$ and BCD/GCP at stations where all the parameters were available. BGEs were calculated using the following formula: $\text{BGE} = \text{BP}/(\text{BR} + \text{BP})$, where BR (bacterial respiration) was assumed to be equal to DCR (BGE_{100}) or half of it (BGE_{50}). DCR and IBP data considered are those given in Table 2. BGE_{corr} : BGE_{100} corrected for exponential growth in the flask during incubation.

	BGE_{50}^1 %	BGE_{100}^1 %	$\text{BGE}_{\text{corr}}^1$ %	GCP^2 $\text{mgC m}^{-2} \text{ d}^{-1}$	IPP/GCP^3 ratio	BCD/GCP^3 ratio
MAR 1	22–28	12–16	21–27	2259–2876	0.16–0.31	0.16–0.47
MAR 3	21–27	12–16	20–26	2778–3536	0.19–0.41	0.18–0.52
HNL 1	24–30	13–17	23–29	738–939	0.34–0.7	0.31–0.87
GYR 2	10–14	5.4–7.4	10–13	252–320	0.48–0.63	1.2–3.7
GYR 4	12–15	6.2–8.3	11–15	525–669	0.30–0.39	0.63–2.0
UPW 2	31–38	18–24	30–37	4328–5509	0.22–1	0.11–0.29
UPX 1	20–25	10–14	19–24	1774–2258	0.6–0.81	0.69–2.0

¹The range considers minimum – maximum values when applying Respiratory Quotients of 0.8 and 1.1.

²The range considers minimum – maximum values when applying Photosynthetic Quotients of 1.1 and 1.4.

³The range considers minimum – maximum values obtained according the BGEs, RQ and PQ used.

ity of the BGE than the choice of the respiratory quotient (RQ). Considering both assumptions (i.e. different contributions of bacterial to community respiration and RQs), the lowest BGEs were obtained at site GYR (5–15%), and BGEs increased in the upwelling area (UPW: 14–38%) and in the western part, at the MAR and HNL sites (12–28%, Table 3).

Table 4. Review of leucine incorporation rates, specific leucine incorporation rates (SA leu) and bacterial turnover rates (TR) in most oligotrophic mid-latitudes to equatorial areas. Temperature (T), conversion factors used to compute TR (leu CF), bacterial biomass conversion factor (BB CF) and Leucine concentration used are also indicated. Empty case: data not available. CK: concentration kinetic.

T^1 °C	Area		leu conc nM	Leu rate $\text{pmol l}^{-1} \text{h}^{-1}$	SA leu $10^{-21} \text{mol cell}^{-1} \text{h}^{-1}$	leu CF kgC mole^{-1}	BB CF fgC cell^{-1}	TR d^{-1}	reference
20–25	South East Pacific, center of the Gyre ⁴	Nov–Dec 2004	20	5–21	13–56	1.5	10	0.05–0.21	This study
30	South West pacific (Tuamotou Arch. 148°15 W, 14°55 S)	91–94	CK	36	71	1.7	15.3	0.13–0.19	Torréton and Dufour, 1996a
18	Northwestern Med, inshore offshore transect	June 1993 & June 1995	20	8–70	3.4–101	0.3–2.1			Gasol et al., 1998
22–24	Med longitudinal transect, ionian+levantine ²	June 1999	20	0.4–17	1–49	1.5	15	0.003–0.123	Van Wambeke et al., 2002
21–22	western			3–36	8–68			0.02–0.17	
26–27	Med longitudinal transect, ionian ³	Sep 1999	20	10–26	18–49	1.5	15	0.04–0.123	Van Wambeke et al., 2002
23–25	western			15–48	14–63			0.03–0.15	
25–28	Arabian Sea	Jan–Dec 1995		15–202	40–100				Ducklow et al., 2001
15	Atlantic NABE 40° N	April–May 1989	10	20–100	66–136*	1.1	20	0.08–0.1	Li et al., 1993
	45° N		10	20–200		3.4	20	0.2–0.4	
20	Sargasso Sea, BATS	spring	21	10–40		0.3–0.6	4.2–7.2	0.096	Carlson et al., 1996
25–26	(31°50 N, 64°10 W)	summer		10–30				0.079	
24–26		autumn		10–25				0.057	
18–21		winter		10–20				0.07	
18	North East Pacific, gyre edge off Oregon	summer 1997, 1998	20	15–33	14–21	0.4	20	0.02–0.04	Sherr et al., 2001
28	Equatorial Pacific along 140° W	Feb, Oct 1992			60–70**	3	20	0.109–0.163	Kirchman et al., 1995
28	Equator, Pac 140° W during El Niño	March 1992	10	25–55		2.3	20	0.15–0.25	Ducklow et al., 1995
25	Equator, Pac 140° W during non El Niño	Oct 1992	10	20–40		2.3	20	0.05–0.1	

¹Only surface temperatures are indicated when stratification is important, ²values from profiles down to depth of TChla maximum, ³ values from surface layers, ⁴for our study, values have been indicated for stations 5 to 14 within euphotic layer (down to Ze), *from related reference Ducklow et al. (1992), **from related reference Kirchman et al. (2005).

Keeping an average BGE of 7% as an estimate for the more oligotrophic sites, the ratio of the integrated bacterial carbon demand (BCD) to ¹⁴C-Primary production (IPP_{deck}, given in Table 1) in the gyre would range between 3.7 (STB15) and 14 (STB7) (median for stations STB6 to STB15: 5.7, $n=9$).

The calculation of the BGE is commonly based on bacterial heterotrophic production determined prior to the 24 h incubation. During the size fractionation experiment at station STB3 as well as during bioassay experiments (Van Wambeke et al., 2007), we observed, however, an increase in bacterial heterotrophic production during the 24 h incubation period (median factor of increase $\times 3.2$, $n=9$, STB6 to STB15, Van Wambeke et al., 2007). Such increases during DCR measurements were reported previously (Pomeroy et al., 1994). Estimates of the BGE can be corrected from this bias by assuming an exponential increase in bacterial production during the 24 h as follows: $(\text{BP}_{24} - \text{BP}_0) / (\text{Ln}(\text{BP}_{24}) - \text{Ln}(\text{BP}_0))$. Applying this correction, BGEs at the GYR sites range from 10 to 15% (Table 3). Consequently, the average BGE of 7% given above for the hyper-oligotrophic sites increases to 12%, resulting in a decrease in the range of the ratio BCD/IPP to 2.1–8.6 (median 3.3 for stations STB6 to STB15, $n=9$).

4 Discussion

The South Pacific Gyre is probably the most oligotrophic water body of the global ocean, a description that is up to date mainly based on satellite observations (Claustre and Maritoner, 2003). Several parameters determined dur-

ing the BIOSOPE-cruise (Claustre et al., 2008), such as water transparency (Morel et al., 2007) and phytoplankton biomass (7 mg TChla m^{-2} in the euphotic zone, Table 1, Ras et al., 2007) confirm the hyperoligotrophic character of this area. One question that we addressed in the present study was whether bacterial production rates are also the lowest reported for open seas and oligotrophic areas. For surface layers, most reported rates of leucine incorporation in oligotrophic areas do not decrease below a threshold of $\sim 10 \text{ pmol l}^{-1} \text{ h}^{-1}$ (Table 4). Lower leucine incorporation rates were measured in the eastern Mediterranean Sea (Levantine and Ionian Sea, range 0.4–17, mean $6.6 \pm 4.9 \text{ pmol l}^{-1} \text{ h}^{-1}$, Table 4), and in our study between STB6 and STB15 (range 5–21 $\text{pmol l}^{-1} \text{ h}^{-1}$, mean $10.8 \pm 2.9 \text{ pmol l}^{-1} \text{ h}^{-1}$). Both cases correspond to marine environments where the depth of the deep TChla maximum exceeds 150 m. Bacterial abundance varies less than bacterial heterotrophic production, thus the lowest cell-specific activities are again obtained for the Levantine Basin in the Mediterranean Sea ($1\text{--}49 \times 10^{-21} \text{ mol cell}^{-1} \text{ h}^{-1}$), and cell specific activities were in the same order of magnitude ($10\text{--}60 \times 10^{-21} \text{ mol cell}^{-1} \text{ h}^{-1}$) in the centre of the South Pacific Gyre, the western Mediterranean Sea, or the equatorial Pacific Ocean (Table 4).

The bacterial community turnover rate (the ratio of bacterial production (BP) to bacterial biomass (BB)) allows a comparison among studies independent of the technique (leucine or thymidine incorporation) used, but it requires the application of conversion factors for bacterial biomass and production. In the present study, we used 1.5 kgC per mol leucine incorporated, assuming no isotopic dilution, and

a low carbon per cell conversion factor specific for oligotrophic environments (10 fg C per cell, Christian and Karl, 1994; Fukuda et al., 1998). The application of these conversion factors allowed us to compare our bacterial community turnover rates ($0.05\text{--}0.21\text{ d}^{-1}$, Table 4, mean $0.11\pm 0.03\text{ d}^{-1}$, $n=63$) with many previous studies that used 3.1 kgC per mol leucine and 20 fg C per cell (Li et al., 1993; Kirchman et al., 1995). Lowest bacterial community turnover rates are still obtained for the eastern Mediterranean Sea ($0.003\text{--}0.123\text{ d}^{-1}$ based on leucine incorporation, Table 4 and $0.005\text{--}0.11\text{ d}^{-1}$ based on thymidine incorporation, Robarts et al., 1996). In the tropical, subtropical and temperate Pacific and Atlantic Oceans, a bacterial community turnover rate of $0.02\text{--}0.04\text{ d}^{-1}$ (Table 4) appears to be a minimum threshold based on theoretical leucine-carbon conversion factors. However, a recent investigation of empirical conversion factors along a coast-offshore transect in the Atlantic (Alonso-Saez et al., 2007) suggests a bias related to the high respiration of leucine (60–80%), in off shore stations leading to very low conversion factors ($0.02\text{--}0.36\text{ kg C mol leu}^{-1}$). Applying the mean of their empirical conversion factors ($0.17\text{ kg C mol leu}^{-1}$, Alonso-Saez et al., 2007) to our data set, bacterial turnover rates would range between 0.005 and 0.02 d^{-1} in the South Pacific Gyre. Based on microautoradiographic observations, the fraction of bacteria taking up leucine was determined to account for 19 to 33% of the bacterioplankton cells in surface waters in the gyre (Obernosterer et al., 2007). Assuming that this fraction represents the active bacterioplankton community, the turnover rate of the active population would be four-fold higher than any estimate based on the total counts. Considering all these assumptions, would lead to a possibly very large range of bacterial community growth rates, varying between 0.005 d^{-1} ($0.17\text{ kg C per mole}$, no correction for the active fraction) to 0.8 d^{-1} (1.5 kg C per mole , 25% of the bacteria active).

The fact that the bacterial community turnover rate is often low compared to that of phytoplankton is presently subject of debate (Duhamel et al., 2007 and references therein). Alternative techniques based on the turnover of a particular chemical pool or a cell compound were recently proposed to estimate turnover rates of heterotrophic bacterial cells. The turnover rate of the phosphate (P) pool in different size fractions, for instance, was examined during the BIOSOPE cruise (Duhamel et al., 2007). Based on the hypothesis that detrital particulate P is negligible, and assuming that the P assimilation rates and the P biomass in the $<0.6\text{ }\mu\text{m}$ fraction are mainly related to heterotrophic prokaryotes, these authors found a bacterial P-based turnover time of $0.11\pm 0.07\text{ d}^{-1}$ in the gyre. This value compares well with the mean bacterial turnover rate that we obtained in the centre of the gyre using theoretical conversion factors. Unexpected high turnover rates of bacteriochlorophyll-a were reported for the Atlantic ($0.7\text{--}1.1\text{ d}^{-1}$ in gyres centers, Koblizek et al., 2007). This pigment is characteristic for aerobic anoxygenic phototrophic bacteria, which were also abundant in the South

Pacific Gyre (Lami et al., 2007) at the time of the cruise. Such turnover rates derived from the analysis of a given chemical pool, if representative for cell turnover (Koblizek et al., 2007), further suggest that some components of the heterotrophic (including mixotrophs) bacterioplankton might have higher turnover rates than the whole consortium.

Our measurements of bacterial production, though among the lowest reported for the open ocean – excluding high latitude, cold waters – clearly do not represent minimum values. If bacterial activity is similar among open ocean oligotrophic environments, is this also the case for primary production? A comparison among studies is not simple due to differences in the incubation conditions. Our IPP_{deck} values were generally lower than those obtained by “standard” in situ incubations (IPP_{insitu}, Table 2). It is well known that it is difficult to reproduce natural irradiance conditions on board and thus, for the comparison with IPP from other studies, we will only refer to primary production determined from the in situ moored lines. It appears that considerably higher rates of IPP_{insitu} were obtained in the North Pacific Gyre at ALOHA ($200\text{--}900\text{ mg C m}^{-2}\text{ d}^{-1}$, Karl et al., 2001), and in the Sargasso Sea at BATS ($312\text{--}520\text{ mg C m}^{-2}\text{ d}^{-1}$ and $340\text{--}530\text{ mg C m}^{-2}\text{ d}^{-1}$, Steinberg et al., 2001 and Mourino-Carballido and McGillicuddy, 2006, respectively) as compared to the measurements of IPP_{insitu} in the centre of the South Pacific Gyre ($154\text{--}203\text{ mg C m}^{-2}\text{ d}^{-1}$). These previous estimates were derived from in situ dawn to dusk incubations, whereas our results are from 24 h incubations. As previously reported for the eastern Mediterranean Sea, an integrated primary production of about $150\text{ mg C m}^{-2}\text{ d}^{-1}$ may appear as a lower limit for primary production rates estimated by 24 h in situ incubations under strong oligotrophic conditions (Moutin and Raimbault, 2002). Thus the rates of primary production determined in the centre of the south Pacific gyre appear to be among the lowest reported.

We explored the phytoplankton-bacteria coupling by comparing the bacterial carbon demand (BCD) to primary production (IPP) and gross community production (GCP). These comparisons are often used to determine the potential fate of primary production through the microbial food web, but they often represent also the basis for defining the metabolic balance, presently a subject of debate (del Giorgio et al., 1997; Kirchman, 1997; del Giorgio and Duarte, 2002; Williams, 2004; Mc Andrew et al., 2007; Claustre et al., 2007a). We paid particular attention to the methodological biases related to these different estimates.

As suggested previously (Ducklow et al., 2000), we assumed linearity when converting bacterial heterotrophic production from hourly to daily rates. Taking into account the diurnal variability of BP we observed at selected stations (Van Wambeke et al., 2008), real daily rates were, on average, by 18% higher than those calculated from one single measurement made at 09:00 a.m. and assuming linearity over 24 h. The error introduced by not taking into account the diurnal variability is in the same order as the precision of the

bacterial production measurement in oligotrophic areas (13% for BP values lower than $10 \text{ ng C l}^{-1} \text{ h}^{-1}$, see methods).

Considering all these biases (e.g. diurnal variability in BP, BGE estimates), BCD could exceed ^{14}C based IPP in the gyre by factors varying between 2 to 8 (median 3.3, $n=9$). This is illustrated in Fig. 5 where most of our data points (IBP, IPP) are on the left side of the theoretical lines corresponding to situations where BCD equals IPP (Fig. 5), in particular with an assumed BGE of 7% and 12%. Two aspects should be considered about these results: first, BCD exceeded IPP at all stations, and second, a large variability of this ratio was obtained. Particulate PP based on ^{14}C measurements accounts for about 40–50% of gross photosynthesis (Karl et al., 1998; Moutin et al., 1999; Bender et al., 1999). In the present study, the ratio IPP/GCP (including the whole set of IPP_{deck} and IPP_{insitu} as given in Table 2) was 0.47 ± 0.25 (mean \pm SD) (Table 3), which confirms previous studies. Thus, the question arises how adequate the comparison between the BCD and ^{14}C -particulate primary production is? The present data set allowed us to compare the BCD to GCP, indicating that the ratio BCD/GCP is <1 or close to 1 (Table 3). Even in the centre of the gyre the two fluxes were close to balance. The same conclusion can be drawn from the fluxes of NCP (Table 2).

Processes like DOC production (by excretion, lysis, grazing processes) and respiratory losses are the main contributors to the difference between GCP and particulate PP. Estimates on the percent of primary production released as DOC vary largely among studies. Although some studies report a percentage of excretion constant across trophic gradients (Maranon et al., 2005); both laboratory (Mykkestadt, 1995; Obernosterer and Herndl, 1995) and field studies (Teira et al., 2001; Moran et al., 2002; Fernández et al., 2004), indicate an increase of the percent of primary production released as DOC in nutrient-limited environments. In the South Pacific Gyre primary production was strongly limited by nitrogen (Bonnet et al., 2007). We attempted to estimate DOC excretion by using empirical equations on DOC production and particulate primary production obtained in field studies (Baines and Pace, 1991; Moran et al., 2001; Teira et al., 2001; Moran et al., 2002). This approach is, however, limited because the rates of primary production analyzed are higher than those encountered in the South Pacific Ocean. Applying on our data set relationships which were obtained in oligotrophic conditions as close as possible as ours: southern Ocean – NE Atlantic (Moran et al., 2002) or NW Iberian coastal transition zone (Teira et al., 2001), the percentage of extracellular release would vary between $20\% \pm 6\%$ and $58\% \pm 11\%$ ($n=63$) in the South Pacific Gyre, respectively. This approach does not take into account the amount of DOC released that is respired by bacteria during the incubation period. This fraction is likely to be high given the low BGEs in oligotrophic environments. This suggests potentially high percentages of DOC production rates in the South Pacific Gyre.

A marked diurnal pattern in bacterial production determined from high-frequency sampling at three stations (MAR, GYR and EGY) was observed (Van Wambeke, 2008). Bacterial production was highest around midnight, decreased until the early afternoon, and then rapidly increased again. This pattern reflects an adjustment of heterotrophic bacterial production to in situ primary production and DOC production. Heterotrophic bacterial production is likely to be delayed by a few hours from that of phytoplankton due to inhibition by UV radiation around noon. Apart from this short time-lag, these results suggest a strong coupling between primary production and heterotrophic bacterial production.

The variability in the ratio BCD/IPP observed in the present study is more driven by the variability in IPP than by the variability in IBP (percentage of variation 32% for IPP_{deck} data, versus 19% for IBP data at stations 6 to 15 considered as oligotrophic, Table 1). The strong variability in IPP was not related to the position of the station only. At station GYR, IPP_{deck} and GCP varied both considerably during our visit, and this variability was linked to surface irradiance (Claustre et al., 2007). Day-to-day fluctuations of primary production and thus variability in the ratio of BCD/IPP are also reported from a Lagrangian experiment (Ducklow, 1999). Larger variability in primary production as compared to respiration was also observed during a one year study at station ALOHA (Williams et al., 2004). The lack of synchronicity between PP and BP has been proposed as an explanation for punctual high BCD/IPP ratios (Kirchman, 1997). Our results appear to support the hypothesis that short-term variability in PP frequently occurs, but that it is rarely determined due to the time scale on which oceanographic cruises are taking place (Williams et al., 2004). Indeed, rapid (<1 week) bursts of net autotrophy, decoupled from respiration, could appear as a consequence of mesoscale physical processes, as shown by recent investigation on the effects of deep-sea water enrichment in nutrient-limited surface waters of the North Pacific subtropical Gyre (Mc Andrew et al., 2007). During the BIOSOPE-cruise the balance between autotrophic and heterotrophic processes was also determined applying an optically based method to determine gross primary production (Claustre et al., 2007). These authors conclude that the South Pacific Gyre is in metabolic balance. Observations based on alternative techniques and higher frequency (Emerson et al., 2002) are probably required to provide valuable insights into the temporal variability of autotrophic and heterotrophic processes in the open ocean.

Acknowledgements. The authors thanks the crew of the R.V. Atalante for their help during the cruise, A. Sciandra for his leadership during the second leg., C. Bournot, D. Taillez and D. Merien for CTD operations, C. Grob and G. Alarcón for the analysis of bacterioplankton by flow cytometry, and P. Catala for GCP and DCR measurements during Leg 2. Two anonymous reviewers improved the manuscript through their criticism and are also acknowledged. OU was funded by the Chilean National

Commission for Scientific and Technological Research through the FONDAP program (grant 15010007) and the Millenium Scientific Initiative (grant EBMA P04/007). This research was founded by the French program PROOF (Processus Biogeochimiques dans l'Océan et Flux), Centre National de la Recherche Scientifique (CNRS), the Institut National des Sciences de l'Univers (INSU). This is a contribution to the BIOSOPE project of the LEFE CYBER program.

Edited by: T. J. Battin

References

- Alonso-Saez, L., Gasol, J. M., Aristegui, J., Vilas, J. C., Vaque, D., Duarte, C. M., and Agustí, S.: Large scale variability in surface bacterial carbon demand and growth efficiency in the subtropical northeast Atlantic Ocean, *Limnol. Oceanogr.*, 52, 533–546, 2007.
- Baines, S. B. and Pace, M. L.: The production of dissolved organic matter by phytoplankton and its importance to bacteria: Patterns across marine and freshwater systems, *Limnol. Oceanogr.*, 36, 1078–1090, 1991.
- Bender, M. L., Orchardo, J., Dickson, M. L., Barber, R., and Lindley, S.: In vitro O₂ fluxes compared with ¹⁴C production and other rate terms during the JGOFS Equatorial Pacific experiment, *Deep-Sea Res. Pt. I*, 46, 637–654, 1999.
- Carignan, R., Blais, A.-M., and Vis, C.: Measurement of primary production and community respiration in oligotrophic lakes using the Winkler method, *Can. J. Fish. Aquat. Sci.*, 55, 1078–1084, 1998.
- Carlson, C. A., Ducklow, H. W., and Sleeter, T. D.: Stocks and dynamics of bacterioplankton in the northwestern Sargasso Sea, *Deep-Sea Res. Pt. II*, 43, 491–515, 1996.
- Christian, J. R. and Karl, D. M.: Microbial community structure at the U.S.-Joint Global Ocean flux Study Station ALOHA: Inverse methods for estimating biochemical indicator ratios, *J. Geophys. Res.*, 99(C7), 14 269–14 276, 1994.
- Claustre, H., Huot, Y., Obernosterer, I., Gentili, B., Taillez, D., and Lewis, M.: Gross community production and metabolic balance in the south Pacific Gyre using a non intrusive bio-optical method, *Biogeosciences Discuss.*, 4, 3089–3121, 2007, <http://www.biogeosciences-discuss.net/4/3089/2007/>.
- Claustre, H. and Maritónera, S.: The many shades of ocean blue, *Science*, 302, 1514–1515, 2003.
- Claustre, H., Sciandra, A., Vulot, D., and Raimbault, P.: Introduction to the special section: bio-optical and biogeochemical conditions in the South East Pacific in late 2004 – the BIOSOPE program, *Biogeosciences Discuss.*, in press, 2008.
- Cole, J. J., Findlay, S., and Pace, M. L.: Bacterial production in fresh and saltwater ecosystems : a cross-system overview, *Mar. Ecol.-Prog. Ser.*, 43, 1–10, 1988.
- Cuevas, L. A., Daneri, G., Jacob, B., and Montero, P.: Microbial abundance and activity in the seasonal upwelling area off Concepción (36° S), central Chile: a comparison of upwelling and non-upwelling conditions, *Deep-Sea Res. Pt. II*, 51, 2427–2440, 2004.
- Del Giorgio, P. A. and Duarte, C. M.: Respiration in the open ocean, *Nature*, 420, 379–384, 2002.
- Ducklow, H. W., Kirchman, D. L., and Quinby, H. L.: Bacterioplankton cell growth and macromolecular synthesis in seawater cultures during the North Atlantic spring phytoplankton bloom, May, 1989, *Microb. Ecol.*, 24, 125–144, 1992.
- Ducklow, H. W., Quinby, H. L., and Carlson, C. A.: Bacterioplankton dynamics in the equatorial Pacific during the 1992 El Niño, *Deep-Sea Res. Pt. II*, 42, 621–638, 1995.
- Ducklow, H. W.: The bacterial component of the oceanic euphotic zone, *FEMS, Microb. Ecol.*, 30, 1–10, 1999.
- Ducklow, W. H.: Bacterial production and biomass in the oceans, in: *Microbial Ecology of the Oceans*, edited by: Kirchman, D. L., Wiley-Liss, New York, 85–120, 2000.
- Ducklow, H. W., Smith, D. C., Campbell, L., Landry, M. R., Quinby, H. L., Steward, G. F., and Azam, F.: Heterotrophic bacterioplankton in the Arabian Sea: Basinwide response to year-round high primary productivity, *Deep-Sea Res. Pt. II*, 48, 1303–1323, 2001.
- Ducklow, H. W., Kirchman, D. L., and Anderson, T. R.: The magnitude of spring bacterial production in the North Atlantic Ocean, *Limnol. Oceanogr.*, 47, 1684–1693, 2002.
- Ducklow, H. W., Dickson, M. L., Kirchman, D. L., Steward, G., Orchardo, J., Marra, J., and Azam, F.: Constraining bacterial production, conversion efficiency and respiration in the Ross Sea, Antarctica, January–February, 1997, *Deep-Sea Res. Pt. II*, 47, 32 227–33 247, 2000.
- Duhamel, S., Zeman, F., and Moutin, T.: A dual-labelling method for the simultaneous measurement of dissolved inorganic carbon and phosphate uptake by marine planktonic species, *Limnol. Oceanogr.-Meth.*, 4, 416–425, 2006.
- Duhamel, S., Moutin, T., Van Wambeke, F., Van Mooy, B., Rimmelin, P., Raimbault, P. and Claustre, H.: Growth and specific P-uptake rates of bacterial and phytoplanktonic communities in the Southeast Pacific (BIOSOPE cruise), *Biogeosciences*, 4, 941–956, 2007, <http://www.biogeosciences.net/4/941/2007/>.
- Emerson, S., Stump, C., Johnson, B., and Karl, D.: In situ determination of oxygen and nitrogen dynamics in the upper ocean, *Deep-Sea Res. Pt. I*, 49, 941–952, 2002.
- Fernández, M., Bianchi, M., and Van Wambeke, F.: Bacterial biomass, heterotrophic production and utilization of dissolved organic matter photosynthetically produced in the Almeria-Oran front, *J. Marine Syst.*, 5, 313–325, 1994.
- Fukuda, R., Ogawa, H., Nagata, T., and Koike, I.: Direct determination of carbon and nitrogen contents of natural bacterial assemblages in marine environments, *Appl. Environ. Microbiol.*, 64, 3352–3358, 1998.
- Gasol, J. M., Doval, M. D., Pinhassi, J., Calderon-Paz, J. I., Guixa-Boixareu, N., Vaque, D., and Pedros-Alí, C.: Diel variations in bacterial heterotrophic activity and growth in the northwestern Mediterranean Sea, *Mar. Ecol.-Prog. Ser.*, 164, 107–124, 1998.
- Granéli, W., Carlsson, P., and Bertilsson, S.: Bacterial abundance, production and organic carbon limitation in the Southern Ocean (39–62° S, 4–14° E) during the austral summer 1997/1998, *Deep Sea Res. Pt. II*, 51, 2569–2582, 2004.
- Grob, C., Ulloa, O., Claustre, H., Huot, Y., Alarcon, G., and Marie, D.: Contribution of picoplankton to the total particulate organic carbon concentration in the eastern South Pacific, *Biogeosciences*, 4, 837–852, 2007, <http://www.biogeosciences.net/4/837/2007/>.

- Karl, D. M., Hebel, D. V., and Bjorkman, K.: The role of dissolved organic matter release in the productivity of oligotrophic North Pacific Ocean, *Limnol. Oceanogr.*, 13, 1270–1286, 1998.
- Karl, D. M., Bidigare, R. R., and Letelier, R. M.: Long-term changes in plankton community structure and productivity in the North Pacific Subtropical Gyre: The domain shift hypothesis, *Deep-Sea Res. Pt. II*, 48, 1449–1470, 2001.
- Kirchman, D. L.: Leucine incorporation as a measure of biomass production by heterotrophic bacteria, in: *Handbook of methods in aquatic microbial ecology*, edited by: Kemp, P. F., Sherr, B. F., Sherr, E. B., and Cole, J. J., Boca Raton: Lewis, 509–512, 1993.
- Kirchman, D. L.: Microbial breathing lessons, *Nature*, 385, 121–122, 1997.
- Kirchman, D. L., Rich, J. H., and Barber, R. T.: Biomass and biomass production of heterotrophic bacteria along 140° W in the Equatorial Pacific: Effect of temperature on the microbial loop, *Deep-Sea Res. Pt. II*, 42, 603–619, 1995.
- Kirchman, D. L., Malmstrom, R. R., and Cottrell, M. T.: Control of bacterial growth by temperature and organic matter in the Western Arctic, *Deep-Sea Res. Pt. II*, 52, 3386–3395, 2005.
- Koblížek, M., Masin, M., Ras, J., Poulton, A. J., and Prasil, O.: Rapid growth of aerobic anoxygenic phototrophs in the oceans, *Environ. Microbiol.*, 9, 2401–2406, 2007.
- Lami, F., Cottrell, M., Ras, J., Ulloa, O., Obernosterer, I., Claustre, H., Kirchman, D., and Lebaron, P.: High abundances of aerobic anoxygenic photosynthetic bacteria in the South Pacific ocean, *Appl. Environ. Microbiol.*, 73, 4198–4205, 2007.
- Landry, M. R. and Kirchman, D. L.: Microbial community structure and variability in the tropical Pacific, *Deep-Sea Res. Pt. II*, 49, 2669–2693, 2002.
- Lefevre, D., Guigue, C., and Obernosterer, I.: The metabolic balance during a phytoplankton bloom induced by natural iron fertilization in the Southern Ocean (Kerguelen Plateau), *Deep Sea Res. Pt. II*, in press, 2008.
- Li, W. K. W., Dickie, P. M., Harrison, W. C., and Irwin, B. D.: Biomass and production of bacteria and phytoplankton during the spring bloom in the western north Atlantic Ocean, *Deep-Sea Res. Pt. II*, 40, 303–327, 1993.
- Maranon, E., Cermeno, P., and Perez, V.: Continuity in the photosynthetic production of dissolved organic carbon from eutrophic to oligotrophic waters, *Mar. Ecol.-Prog. Ser.*, 299, 7–17, 2005.
- McAndrew, P., Bjorkman, K., Church, M., Morris, P., Jachowski, N., Williams, P. J. Le B., and Karl, D.: Metabolic response of oligotrophic plankton communities to deep water nutrient enrichment, *Mar. Ecol.-Prog. Ser.*, 332, 63–75, 2007.
- Moran, X. A. G., Estrada, M., Gasol, J. M., and Pedros-Alio, C.: Dissolved primary production and the strength of phytoplankton-bacterioplankton coupling in contrasting marine regions, *Microbial Ecol.*, 44, 217–223, 2002.
- Moran, X. A., Gasol, J., Pedros-Alio, C., and Estrada, M.: Dissolved and particulate primary production and bacterial production in offshore Antarctic waters during austral summer: coupled or uncoupled?, *Mar. Ecol.-Prog. Ser.*, 222, 25–39, 2001.
- Morel, A., Gentili, B., Claustre, H., Babin, M., Bricaud, A., Ras, J., and Tieche, F.: Optical properties of the “clearest” natural waters, *Limnol. Oceanogr.*, 52, 217–229, 2007.
- Mourino-Carballido, B. and McGillicuddy Jr., D. J.: Mesoscale variability in the metabolic balance of the Sargasso Sea, *Limnol. Oceanogr.*, 51, 2675–2689, 2006.
- Moutin, T., Raimbault, P., and Poggiale, J. C.: Production primaire dans les eaux de surface de la Méditerranée occidentale: Calcul de la production journalière, *C. R. Acad. Sci. Paris, Sciences de la vie*, 322, 651–659, 1999.
- Moutin, T. and Raimbault, P.: Primary production, carbon export and nutrients availability in western and eastern Mediterranean Sea in early summer 1996, *J. Marine Syst.*, 33–34, 273–288, 2002.
- Mykkestad, S. M.: Release of extracellular products by phytoplankton with special emphasis on polysaccharides, *Sci. Total Environ.*, 165, 155–164, 1995.
- Obernosterer, I. and Herndl, G.: Phytoplankton extracellular release and bacterial growth: dependence on the inorganic N:P ratio, *Mar. Ecol.-Prog. Ser.*, 116, 247–257, 1995.
- Obernosterer, I., Catala, P., Lami, R., Caparros, J., Ras, J., Bricaud, A., Dupuy, C., Van Wambeke F., and Lebaron, P.: Biochemical characteristics and bacterial community structure of the sea surface microlayer in the South Pacific Ocean, *Biogeosciences Discuss.*, 4, 2809–2844, 2007, <http://www.biogeosciences-discuss.net/4/2809/2007/>.
- Pomeroy, L. R., Sheldon, J. E., and Sheldon, W. M.: Changes in Bacterial numbers and leucine assimilation during estimations of microbial respiratory rates in seawater by the precision Winkler method, *Appl. Environ. Microbiol.*, 60, 328–332, 1994.
- Raimbault, P., Garcia, N., and Cerutti, F.: Distribution of inorganic and organic nutrients in the South Pacific Ocean – evidence for long-term accumulation of organic matter in nitrogen-depleted waters, *Biogeosciences Discuss.*, 4, 3041–3087, 2007, <http://www.biogeosciences-discuss.net/4/3041/2007/>.
- Ras, J., Claustre, H., and Uitz, J.: Spatial variability of phytoplankton pigment distributions in the Subtropical South Pacific Ocean: comparison between in situ and predicted data, *Biogeosciences Discuss.*, 4, 3409–3451, 2007, <http://www.biogeosciences-discuss.net/4/3409/2007/>.
- Robarts, R. D., Zohary, T., Waiser, M. J., and Yacobi, Y. Z.: Bacterial abundance, biomass, and production in relation to phytoplankton biomass in the Levantine Basin of the southeastern Mediterranean Sea, *Mar. Ecol.-Prog. Ser.*, 137, 273–281, 1996.
- Sherr, E., Sherr, B., and Cowles, T.: Mesoscale variability in bacterial activity in the NorthEast Pacific Ocean off Oregon, USA, *Aquat. Microb. Ecol.*, 25, 21–30, 2001.
- Sherr, B. F. and Sherr, E. B.: Community respiration/production and bacterial activity in the upper water column of the central Arctic Ocean, *Deep-Sea Res. Pt. I*, 50, 529–542, 2003.
- Smith, D. C. and Azam, F.: A simple, economical method for measuring bacterial protein synthesis rates in sea water using 3H-Leucine, *Mar. Microb. Food Webs*, 6, 107–114, 1992.
- Steinberg, D. K., Carlson, C. A., Bates, N. R., Johnson, R. J., Michaels, A. F., and Knap, A. H.: Overview of the US JGOFS Bermuda Atlantic Time-series Study (BATS): a decade-scale look at ocean biology and biogeochemistry, *Deep-Sea Res. Pt. II*, 48, 1405–1447, 2001.
- Tedetti, M., Sempéré, R., Vasilkov, A., Charrière, B., Nérini, D., Miller, W. L., Kawamura, K., and Raimbault, P.: High penetration of ultraviolet radiation in the south east Pacific waters, *Geophys. Res. Lett.*, 34, L12610, doi:10.1029/2007GL029823, 2007.

- Teira, E., Serret, P., and Fernandez, E.: Phytoplankton size structure, particulate and dissolved organic carbon production and oxygen fluxes through microbial communities in the NW Iberian transition zone, *Mar. Ecol.-Prog. Ser.*, 219, 65–83, 2001.
- Torréon, J.-P. and Dufour, P.: Bacterioplankton production determined by DNA synthesis, protein synthesis, and frequency of dividing cells in Tuamotu Atoll Lagoons and surrounding ocean, *Microb. Ecol.*, 32, 185–202, 1996.
- Van Wambeke, F., Christaki, U., Giannakourou, A., Moutin, T., and Souvemerzoglou, K.: Longitudinal and vertical trends of bacterial limitation by phosphorus and carbon in the Mediterranean Sea, *Microb. Ecol.*, 43, 119–133, 2002.
- Van Wambeke, F., Bonnet, S., Moutin, T., Raimbault, P., Alarçon G., and Guieu, C.: Factors limiting heterotrophic prokaryotic production in the southern Pacific Ocean, *Biogeosciences Discuss.*, 4, 3799–3828, 2007, <http://www.biogeosciences-discuss.net/4/3799/2007/>.
- Van Wambeke, F., Tedetti, M., Duhamel, S., and Sempéré, R.: Diel variability of heterotrophic bacterial production and UV doses in the South East Pacific, *Biogeosciences Discuss.*, 5, 435–462, 2008, <http://www.biogeosciences-discuss.net/5/435/2008/>.
- Wicks, R. J. and Robarts, R. D.: Ethanol extraction requirement for purification of protein labeled with ³HLeucine in aquatic bacterial production studies, *Appl. Environ. Microbiol.*, 54, 3191–3193, 1988.
- Williams, P. J. Le B.: Microbial contribution to overall marine plankton metabolism: a direct measurement of respiration, *Oceanol. Acta*, 4, 359–364, 1981.
- Williams, P. J. Le B., Morris, P. J., and Karl, D. M.: Net community production and metabolic balance at the oligotrophic ocean site, station ALOHA, *Deep-Sea Res. Pt. I*, 51, 1563–1578, 2004.

Gross community production and metabolic balance in the South Pacific Gyre, using a non intrusive bio-optical method

H. Claustre^{1,2}, Y. Huot^{1,2}, I. Obernosterer³, B. Gentili^{1,2}, D. Tailliez^{1,2}, and M. Lewis⁴

¹UPMC Univ Paris 06, UMR 7093, Laboratoire d’Océanographie de Villefranche, 06230 Villefranche-sur-Mer, France

²CNRS, UMR 7093, LOV, 06230 Villefranche-sur-Mer, France

³Université Pierre et Marie Curie-Paris6, UMR7621, F66650 Banyuls-sur-Mer, France ; CNRS, UMR7621, F-66650 Banyuls-sur-Mer, France

⁴Department of Oceanography, Dalhousie University, Halifax, Nova Scotia B3H 4J1, Canada

Received: 30 July 2007 – Published in Biogeosciences Discuss.: 03 September 2007

Revised: 7 January 2008 – Accepted: 3 March 2008 – Published: 28 March 2008

Abstract. The very clear waters of the South Pacific Gyre likely constitute an end-member of oligotrophic conditions which remain essentially unknown with respect to its impact on carbon fixation and exportation. We describe a non-intrusive bio-optical method to quantify the various terms of a production budget (Gross community production, community losses, net community production) in this area. This method is based on the analysis of the diel cycle in Particulate Organic Carbon (POC), derived from high frequency measurements of the particle attenuation coefficient c_p . We report very high integrated rates of Gross Community Production within the euphotic layer (average of $846 \pm 484 \text{ mg C m}^{-2} \text{ d}^{-1}$ for 17 stations) that are far above any rates determined using incubation techniques for such areas. Furthermore we show that the daily production of POC is essentially balanced by the losses so that the system cannot be considered as net heterotrophic. Our results thus agree well with geochemical methods, but not with incubation studies based on oxygen methods. We stress to the important role of deep layers, below the euphotic layer, in contributing to carbon fixation when incident irradiance at the ocean surface is high (absence of cloud coverage). These deep layers, not considered up to now, might fuel part of the heterotrophic processes in the upper layer, including through dissolved organic carbon. We further demonstrate that, in these extremely clear and stratified waters, integrated gross community production is proportional to the POC content and surface irradiance via an efficiency index ψ_{GCP}^* , the water column cross section for Gross Community Production. We finally discuss our results in the context of the role of oligotrophic gyre in the global

carbon budget and of the possibility of using optical proxies from space for the development of growth community rather than primary production global models.

1 Introduction

Subtropical gyres are vast oceanic oligotrophic biomes representing 60% of the global ocean. Their metabolic state (magnitude of carbon fixation vs. respiration rates) and, consequently, their role in the global oceanic carbon cycle is still being debated (del Giorgio et al., 1997; Williams, 1998) which finds its roots in early discussions about the magnitude of carbon fixation in these systems (Jenkins, 1982; Lewis et al., 1986; Jenkins, 1988). On one hand, and based on in vitro biological techniques performed in the euphotic zone and having characteristic time scales of ~ 1 day, it is generally concluded that the ocean is in a net heterotrophic state: rates of carbon fixation are low and the whole community respiration rate (R) exceeds the gross primary production (GPP) (del Giorgio et al., 1997; del Giorgio and Duarte, 2002), so that the so-called Net Community Production ($\text{NCP} = \text{GPP} - \text{R}$) is always negative. On the other hand, studies based on geochemical tracer distributions with larger relevant space/time scales support net production and export rates one order of magnitude higher (Jenkins, 1982; Jenkins, 1988; Lewis et al., 1986; Hansell et al., 2004). As a result, the upper ocean ecosystems are considered on average to be autotrophic which suggests that in vitro experiments are affected by biases or not representative of larger space or time scales. Modelling studies conclude that mesoscale activity and the so-called eddy-pumping processes cannot explain the discrepancies between both approaches (Oschlies,



Correspondence to: H. Claustre
(claustre@obs-vlfr.fr)

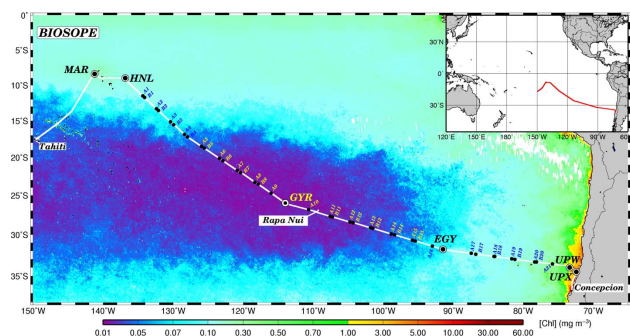


Fig. 1. Transect of the BIOSOPE cruise superimposed on a SeaWiFS composite image of Chl-*a* concentration in the upper layer for November–December 2004.

2002), and that unaccounted biological processes, such as N_2 -fixation (Gruber, 2005), export of dissolved organic carbon (Dietze and Oschlies, 2005) or episodic primary production events generally missed by classical sampling strategies (Karl et al., 2003; Williams et al., 2004), may be responsible. It has been suggested that primary production rates are as much as 3–5 times higher in these vast ocean regions than what has been estimated using classical strategies/methods (Karl et al., 2003). Given the vast extent of the oligotrophic gyres, the implications for carbon dynamics at the global scale are profound.

Siegel et al. (1989) presented the first data of a daily cycle in the attenuation coefficient, c_p , a proxy of particle load, in the upper layers (>100 m) of the oligotrophic waters of the North Pacific Gyre. Increase of particle load was observed during daytime, while a decrease of similar amplitude was observed during nighttime, allowing the conclusion that particle production was balanced at the daily scale. Since c_p is strongly correlated with Particulate Organic Carbon (POC) concentration (e.g. Gardner et al., 1993; Loisel and Morel, 1998) it can be calibrated to retrieve the diel variations in POC. Indeed, daily cycle in c_p must contain information about the various terms (gains, losses) involved in the upper ocean carbon budget. The seminal paper of Siegel was thus the starting point of subsequent studies where the diel cycle in c_p and its potential implication in terms of carbon fluxes in the upper oceanic layers were addressed. Analyses of these diel variations were later performed either from ship-based acquisition (e.g. Cullen et al., 1992; Cullen and Lewis, 1995; Walsh et al., 1995; Durand and Olson, 1996; Claustre et al., 1999) from mooring data (Marra, 1994; 1995; 2002) or from laboratory culture (e.g. Stramski and Reynolds, 1993; Stramski et al., 1995; Durand and Olson, 1998; Claustre et al., 2002). Most of these studies were motivated by a strong interest in developing and using a non-intrusive method to measure biogeochemical rates whose estimation normally requires sample manipulation and incubation. To our knowledge the comparison of c_p -based production with classical

incubation techniques has been carried out only once (Marra, 2002 for the North Atlantic Bloom Experiment) and they were found to provide similar estimates in this environment.

The first aim of the present study is to continue the investigation of the daily cycle in optically-resolved POC and its potential significance to quantify the various terms of the production budget. In the context of the metabolic balance of subtropical oligotrophic gyre, our study is here based on the South Pacific Gyre (SPG). This region is likely the most oligotrophic oceanic area (Claustre and Maritorea, 2003) of the global ocean with the clearest waters ever reported (Morel et al., 2007a) associated with undetectable surface nitrate and the deepest nitracline (Raimbault et al., 2008). Obviously, any conclusions reached about the carbon production terms in this oligotrophic condition end-member might constitute a reference for subtropical gyres as a whole. Therefore, as part of the BIOSOPE cruise (Claustre et al., 2008) which was carried out in the South East Pacific and crossed the SPG in its most oligotrophic part, we here focus on the analysis and interpretation of the diel cycle in c_p for a ~ 3000 km subset of the transect where the oligotrophic conditions appeared to be the most extreme.

2 Methods

2.1 Cruise description and station selection

The BIOSOPE cruise onboard RV *Atalante* took place during austral summer from 26 October to 11 December from the Marquesas Islands towards the Chilean coast. The ~ 8000 km transect encompassed a wide range of hydrodynamic and trophic conditions (Claustre et al., 2008). Two types of stations were investigated (Fig. 1), the so-called long (more than 2 days of occupation) and short (less than one day of occupation) stations. For the present study we will mainly focus on the most oligotrophic waters. They are here defined as those waters for which the euphotic zone depth (the depth where the Photosynthetically Available Radiation (PAR, in the range 400–700 nm) is reduced to 1% of its surface value) is greater than 100 m. Actually such criteria delineates waters with surface Chlorophyll-*a* (Chl-*a*) concentration lower than ~ 0.08 mg m^{-3} (Morel et al., 2007b, equation in the legend of their Fig. 9). Such waters represent $\sim 30\%$ of the global ocean (Antoine et al., 2005, their Fig. 8). In the area investigated during BIOSOPE, these oligotrophic stations include the long station GYR (Fig. 1), west of Easter Island. We will focus on this station to develop our approach and apply it elsewhere. From the real-time ocean color images, this station was selected as having the lowest surface Chl-*a* concentration (see also supplementary information, part 1 <http://www.biogeosciences.net/5/463/2008/bg-5-463-2008-supplement.pdf>). The GYR station was occupied for five days and eight casts a day were performed. Additionally, 13 “oligotrophic” short stations

(StB2 to StB15 and StB19, Fig. 1) were investigated and at least three casts were performed during the day period.

2.2 Particle attenuation coefficient: treatment and significance

The attenuation coefficient, c (m^{-1}) was determined using a Wetlabs C-star transmissiometer (25 cm path length and 660 nm wavelength) attached to the CTD rosette. Each cast was performed down to 500 m. Data treatment was performed as described in Loisel and Morel, 1998 and Claustre et al., 1999. Briefly, in order to take into account any possible variation due to change in the cleanliness of the optical window, attenuation coefficient profiles were corrected assuming that deep waters were optically stable and close to pure water ($c=0.364 \text{ m}^{-1}$). The average of attenuation coefficient between 450 and 500 m was thus taken as a reference for each cast.

In open ocean waters, the beam attenuation coefficient at 660 nm measured by a transmissiometer, once corrected for absorption by pure water, is essentially a measurement of the attenuation coefficient by particles, c_p (m^{-1}), because absorption coefficients by dissolved material are negligible at this wavelength (Loisel and Morel, 1998). Furthermore, the absorption by particles (detrital and vegetal) is also negligible so that c_p is equivalent to the particle scattering coefficient. Thus, the main source of variation in c_p is the numerical abundance and size of particles while second order sources are refractive index and shape of particles (Gardner et al., 1993). For a standard particle size distribution (Junge type with a -4 exponent), the particles to which the transmissiometer is most sensitive lie in the 0.5–10 μm size range (Stramski and Kiefer, 1991) which typically corresponds to the size domain of the living (pico- and nanophytoplankton, cyanobacteria, heterotrophic and photo-heterotrophic bacteria pico- and nano-zooplankton) and non-living particles (detritus). It has been suggested (Morel, 1988) and subsequently verified (e.g. Gardner et al., 1993; Loisel and Morel, 1998; Claustre et al., 1999) that c_p is linearly related to the particulate organic concentration, POC (mg m^{-3}). Some significant regional differences in this relationship have been reported. In particular a relationship with a slope of $502 \text{ mg C m}^{-3} \text{ m}^{-1}$ was reported for the North western part of South Pacific gyre (Claustre et al., 1999) which was at least twice larger than those found for other oceanic regions (Siegel et al., 1989; Walsh et al., 1995). As part of the present study and using 35 simultaneous c_p and POC measurements, the high slope was confirmed ($\text{POC}=502c_p+10$) and also recently corroborated by new regional relationships obtained for the North Pacific Gyre (slope=560) and the equatorial Pacific (slope=552) (Gardner et al., 2006). Therefore, the slightly rounded relationship $\text{POC}=500c_p$ proposed by (Claustre et al., 1999) is adopted for the present study. This conversion factor is equivalent to an attenuation cross section of $2 \text{ m}^2 \text{ gC}^{-1}$. The relative stability of the c_p vs. POC rela-

tionship over the diel cycle is critical when dealing with the inversion of the c_p diel cycle into carbon production terms. This aspect is investigated in more detail in supplementary information <http://www.biogeosciences.net/5/463/2008/bg-5-463-2008-supplement.pdf> (part 2).

2.3 Other measurements

Total sun radiation was measured onboard (every min) using an Eppley pyranometer. PAR (in energy units) was subsequently derived, assuming it represents 43% of the total irradiance at the ocean surface.

For the pigment analysis, 5.6 L of seawater were filtered onto GF/F filters which were subsequently stored in liquid nitrogen. Within 3 months after collection, pigments were extracted in methanol and analysed by HPLC using a method dedicated for low concentration samples (Ras et al., 2008). The HPLC absorbance detector was also set at 770 nm to detect bacteriochlorophyll-*a* (Bchl-*a*) (limit of quantitation of 0.0004 mg m^{-3}). The euphotic zone limit, Z_e (m) was derived from in situ radiometric measurements using a LICOR irradiance profiler (Morel et al., 2007a). On some occasions, when irradiances measurements were not performed, Z_e was derived from the vertical profile of Chl-*a* as described in Ras et al. (2008).

For the determination of particulate organic carbon (POC), up to 8.2 L of seawater were collected from Niskin bottles and filtered onto precombusted GF/F filters. Carbon Analysis was performed using a CEC 440HA Organic Elemental Analyzer after the filters had been treated with 0.25 ml of 10% HCl to remove inorganic carbon (Stramski et al., 2008).

On two occasions at the GYR station (12 November and 14 November), net community production and community respiration were measured using 24-h light and dark incubations, respectively, of unfiltered seawater in 120-ml biological oxygen demand (BOD) bottles. Seawater was collected at 6 depths in the upper 200 m and in situ incubations started at 06:00 a.m. The BOD bottles were filled by siphoning the seawater from 10-L acid-rinsed polycarbonate (PC) carboys, using silicon tubing and allowing the BOD bottles to overflow. Prior to sampling, the BOD bottles were rinsed with 1N HCl, Milli-Q water and seawater ($3\times$) from the respective depth layer. Measurements of net community production and respiration were performed in five replicate BOD bottles. Gross primary production and community respiration were calculated as the difference between the initial and final dissolved oxygen concentrations in the light and dark incubations, respectively. The concentration of dissolved oxygen was determined by Winkler titration of whole bottles. Titration was done with an automated potentiometric end-point detection system (Metrohm DMS 716). The mean standard error of the oxygen concentration determination was $0.15 \mu\text{mole O}_2 \text{ L}^{-1}$ (coefficient of variation of 0.061%).

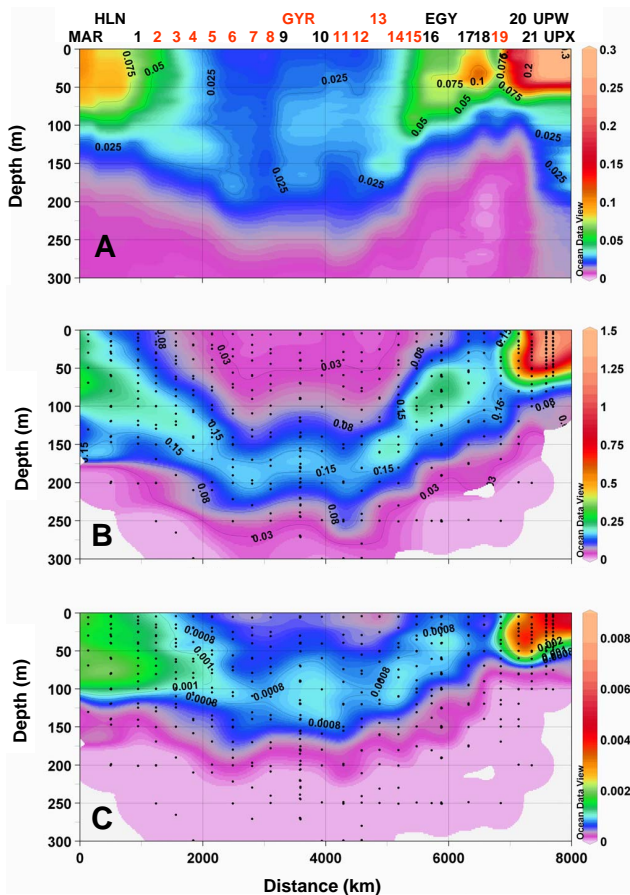


Fig. 2. Distribution of key biogeochemical quantities along the BIOSOPE transect. (a) The attenuation coefficient, c_p . (b) the concentration in Chl-*a* (sum of mono- and Divinyl-Chl-*a*) (c) the concentration in bacteriochlorophyll-*a* (mg m^{-3}). On the upper part of panel A are reported the positions of station (see also Fig. 1). The “oligotrophic stations” examined in this study are identified in red.

3 Results and discussion

3.1 Main patterns observed along the transect

The main hydrodynamic patterns crossed along the BIOSOPE transect are described in detail in Claustre et al. (2008). The distribution in c_p (Fig. 2) is in accordance with these patterns. At both extremities, in the vicinity of Marquesas islands (west) and associated with the Peru Chile Current (east), high c_p values are recorded in the upper layers (up to 0.5 m^{-1} in the upwelling conditions off the Chilean coast). In the central part of transect ($\sim \text{km } 2000$ to $\text{km } 4500$), associated with undetectable nitrates in the 0–150 m layer (Raimbault et al., 2008), low surface Chl-*a* and the presence of a pronounced deep Chl-*a* maximum (DCM, sometimes extending to 180 m and below), c_p takes its lowest values, especially at stations 7 and 8. Station 7 indeed represent the clearest waters of the cruise (Morel et al., 2007a) with

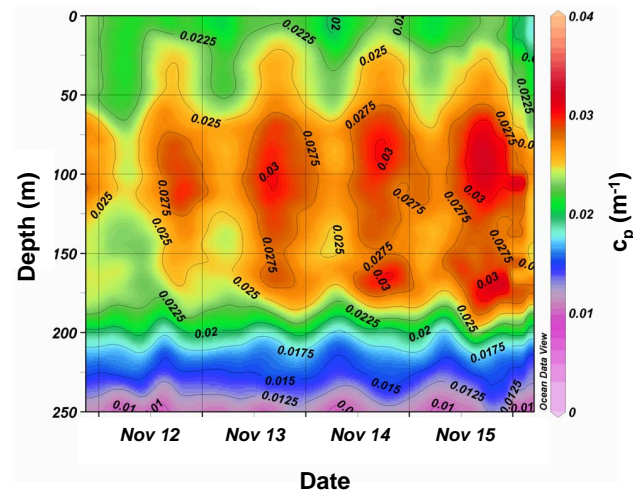


Fig. 3. Daily and vertical variations in c_p within the 0–300 m layer at the GYR station.

an euphotic zone depth extending down to ~ 170 m. From the GYR station to St14 there is a weak, but significant, relative maximum in c_p around ~ 100 m. The distribution of c_p in this layer roughly parallels that of BChl-*a*, an indicator of photoheterotrophs performing anoxygenic photosynthesis. Eastwards, outside the core of the oligotrophic part of the Gyre, station 19 still presents oligotrophic characteristics with an euphotic zone depth of ~ 105 m, surface Chl-*a* of $\sim 0.06 \text{ mg m}^{-3}$ and $c_p < 0.06 \text{ m}^{-1}$ in the upper layer. Actually, nutrient distribution at this station ($\sim 2.8 \text{ mM}$ at the surface) reveals that it corresponds to a High Nutrient Low Chl-*a* situation (Raimbault et al., 2008).

3.2 POC budget at the daily cycle: case study at the GYR station

3.2.1 The various terms of the budget

At the GYR station, high frequency CTD transmissiometry measurements allow the variations of c_p to be highlighted at the daily scale (Fig. 3). c_p measurements displayed conspicuous daily variations with a sunrise minimum and sunset maximum, an observation previously reported for other oligotrophic and mesotrophic areas (Siegel et al., 1989; Claustre et al., 1999). While this cycle was detectable down to 220–240 m, there are two zones in the upper layer, where this cycle is stronger: the zone of the DCM and the layer around ~ 100 m (zone of BChl-*a* maximum, see Fig. 2). Once calibrated in terms of POC and integrated over pre-defined layers (POC, see Fig. 4), the clear increase of POC during the day followed by a decrease of roughly similar amplitude at night, suggests that production and loss of POC are balanced over 24 h (see also supplementary information, part 2 <http://www.biogeosciences.net/5/463/2008/bg-5-463-2008-supplement.pdf>). In a less olig-

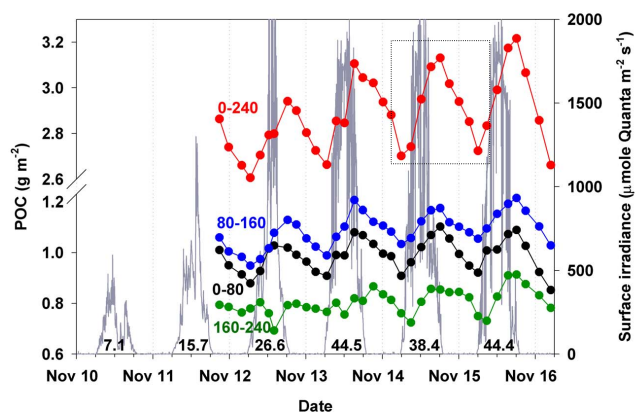


Fig. 4. Daily variations in integrated particulate organic carbon content, derived from c_p measurements, over various optical depth intervals. Red : 0–240 m corresponds to the range of 100%–0.1% of surface irradiance; Blue : 80–160 m (10%–1%); Black : 0–80 m (100%–10%); Green : 160–240 m (1%–0.1%). Surface irradiance is plotted as a grey line and the number inside each daily irradiance cycle refers to the daily dose of photons (moles quanta m^{-2}). The dotted square identifies the portion of the cycle which is used for the schematic presented in Fig. 5.

otrophic part of the South Pacific Gyre ($16^\circ S$, $150^\circ W$, with surface concentration of $\sim 0.07 \text{ mg Chl-}a \text{ m}^{-3}$), it was established that phytoplankton do not contribute to more than 20% of the POC stocks within the euphotic layer (Claustre et al., 1999), a value which was confirmed in the present study (Grob et al., 2007) throughout the gyre. While the fraction of the contribution to the total POC is low, it can be shown that growth rates typical of phytoplankton in such systems can account for a significant part of the daily variability in POC seen by the transmissiometer (see supplementary information part 2 <http://www.biogeosciences.net/5/463/2008/bg-5-463-2008-supplement.pdf>). The rest of the increase is due to other heterotrophic components (e.g. bacteria, flagellates) of the microbial community. Given that the increase in POC occurs during the day, the increase of heterotrophic biomass thus appears also stimulated (positively related) to photo-trophic processes. We thus propose that a budget of the various production and loss terms can be derived from the variations in the integrated content in POC at the daily scale (Fig. 5).

Over a given oceanic layer, the light stimulated Gross Community Production (GCP) seen by a transmissiometer (^{Opt}GCP , $\text{mg C m}^{-2} \text{ d}^{-1}$, the Opt prefix refers to optically-determined) is here defined as the sum of Gross Primary Production (GPP, excluding dissolved production) and of the production by the microbial (heterotrophic) community (which arise in part from dissolved phytoplankton production). The Net Community Production measured optically (^{Opt}NCP , $\text{mg C m}^{-2} \text{ d}^{-1}$) thus represents the difference between ^{Opt}GCP and community losses (^{Opt}CL , mg C m^{-2}

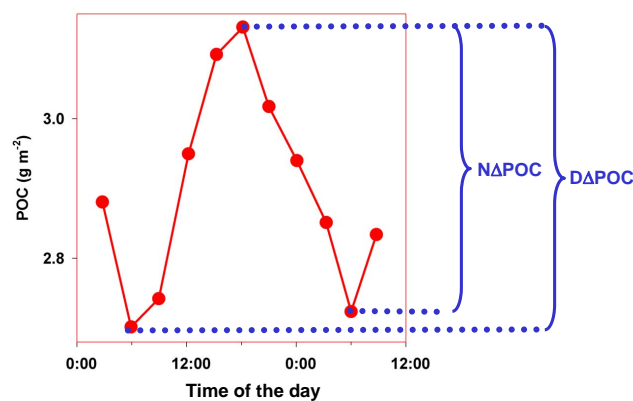


Fig. 5. Schematic of the various terms of the metabolic balance that can be inferred from the diel change in c_p or POC. The data corresponds to the third cycle presented in Fig. 4 (dotted square).

d^{-1}).

$$^{Opt}NCP = ^{Opt}GCP - ^{Opt}CL \quad (1)$$

Community loss processes primarily include respiration, however, other processes such as grazing and sinking must also contribute to the removal of particles (and hence POC) measured by a transmissiometer. Because NCP is strictly defined as the difference between GCP and respiration rate and since additional loss processes are taken into account by the optical method (i.e. ^{Opt}CL , $>$ respiration rate), ^{Opt}NCP likely underestimates NCP. In the hyperoligotrophic conditions studied, the additional loss terms are expected to be small and the underestimation of NCP by ^{Opt}NCP to be weak, if any. This is because such systems are characterized by a dominance of small particles (picophytoplankton, heterotrophic bacteria), whose grazers (e.g. nanoflagellates) are still in the size range detected by the transmissiometer (see also supplementary information, part 2 <http://www.biogeosciences.net/5/463/2008/bg-5-463-2008-supplement.pdf>). Furthermore sinking is expected to be negligible under such conditions.

For the duration of the night period (Nt , d), the Gross Community Production is null, so the night time decrease in POC, $\Delta PO C$ (mg m^{-2} , taken as a positive number), can be considered as an estimation of ^{Opt}CL , assumed to be the identical for the night and day period (in the same way that bacterial respiration is assumed to be constant for the O_2 in vitro technique relying on 24 h incubation):

$$^{Opt}CL = \Delta PO C / Nt \quad (2)$$

inserting Eq. (2) into (1):

$$^{Opt}GCP = ^{Opt}NCP + \Delta PO C / Nt \quad (3)$$

At this stage, another constraint can be imposed, which is derived from the observation of Fig. 4. Actually, over a full day, the daily increase in POC, $\Delta PO C$ (mg m^{-2}) roughly

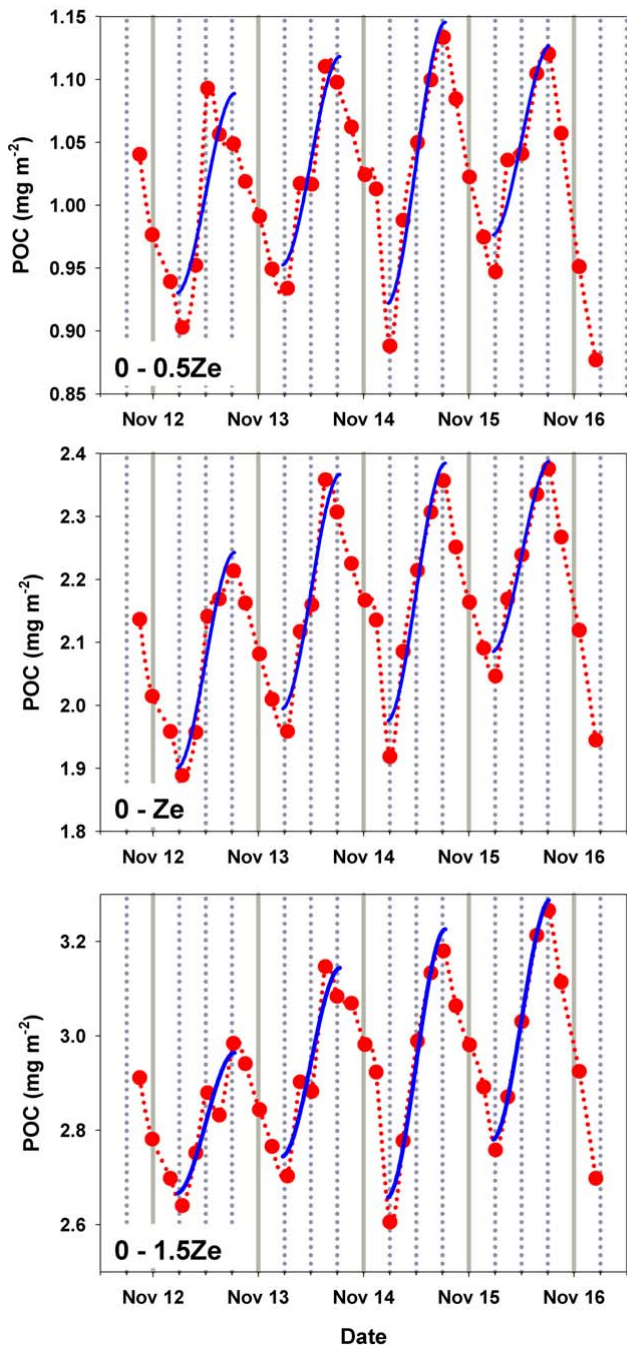


Fig. 6. Modelling diurnal variations in optically determined POC in various optical layers at the GYR station. The red dot corresponds to the data while the blue line represents the fitting of Eq. (1) to the data.

balances $N\Delta\text{POC}$. NCP presents slight positive and negative variations from day to day at station GYR (Fig. 4). However, over the 4 days of investigation the average NCP is not significantly different from zero. This thus implies that over the

four days:

$$D\Delta\text{POC} = N\Delta\text{POC} \quad (4)$$

Using this new constraint, OptGCP can be expressed as:

$$\text{OptGCP} = D\Delta\text{POC}/Nt = N\Delta\text{POC}/Nt \quad (5)$$

Equation (5) shows that, when the light-dark cycle is close to 12:12 ($Nt \sim 0.5$ d), OptGCP is roughly twice the loss rates. Furthermore, it shows that only the increase (or decrease) in POC during day (or night) time and the duration of the night is required to estimate OptGCP . This approximation is, of course, only valid in stable systems and will only hold in systems where biomass is not changing on the daily scale (i.e. $D\Delta\text{POC} = N\Delta\text{POC}$).

3.2.2 Model development

The sampling frequency at the GYR station was sufficient to encompass the full range of day-night variations in POC. This was not the case for other stations (see Fig. 2) which were sampled only 3 times during daytime. To obtain OptGCP from these data, we need to provide additional information in the form of a simple model. We base this model on the rather regular daily variations in POC observed at the GYR station, which suggests that they can be accurately modelled using an empirical formulation. A polynomial of third degree was chosen with the following constraints. The rates of change of POC are equal to zero at sunrise (t_{sr} , h) and sunset (t_{ss} , h), respectively and maximal (inflexion point) at noon (t_{no} , h). Using these constraints, the time variation in POC, $\text{POC}(t)$, can be modelled as:

$$[\text{POC}(t)] = [\text{POC}_{t_{no}}] + R\text{POC}_{t_{no}} (t - t_{no}) \left[\frac{1 - (t - t_{no})^2}{3(t_{sr} - t_{no})^2} \right] \quad (6)$$

where $[\text{POC}_{t_{no}}]$ (mg m^{-2}) and $R\text{POC}_{t_{no}}$ ($\text{mg m}^{-2} \text{h}^{-1}$) represents the $[\text{POC}]$ content and the instantaneous production in $[\text{POC}]$ at noon (t_{no} , h), respectively. Actually, $R\text{POC}_{t_{no}}$ represents the maximal instantaneous rate of change in POC. Equation (6) was fitted to the GYR data using the Gauss-Newton method. The model performs well for the four days of investigation and for the 3 layers investigated (Fig. 6). Actually fitted OptGCP compares well with measured OptGCP estimated from the difference between the minimal and maximal values (Fig. 7).

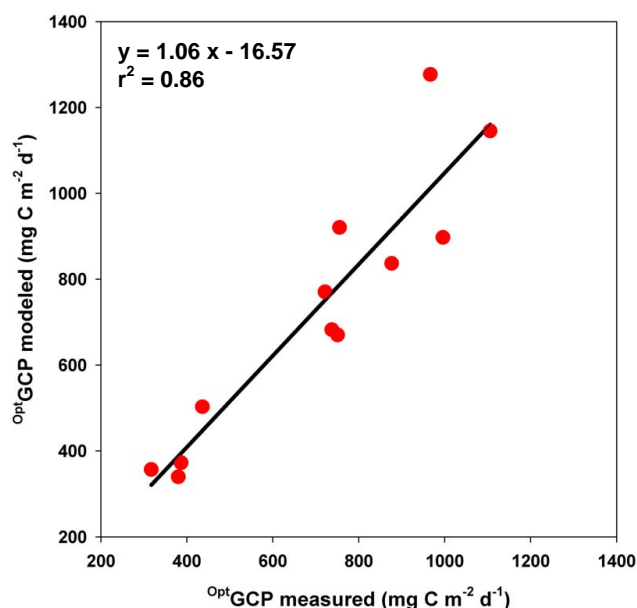
3.3 Gross and Net Community production in oligotrophic regime

The average OptGCP within the euphotic zone over four diel cycles is $\sim 734 (\pm 97) \text{ mg C m}^{-2} \text{ d}^{-1}$ (Table 1). This production is balanced by losses $[721 (\pm 159) \text{ mg C m}^{-2} \text{ d}^{-1}]$, and average NCP (over 4 days) is not significantly different from 0.

Table 1. Comparative carbon production and loss rates in the South Pacific Gyre.

		Process measured		Rate obtained	
		Oxygen method	Optical method	Oxygen method	Optical method
Gains	O ₂ -GPP		Opt ^t GCP	473±223	734±97
Losses	O ₂ -CR		Opt ^t CL	768±65	721±159
Balance	O ₂ -NCP		Opt ^t NCP	-295±158	14±73

Measurements were obtained using two techniques in the euphotic zone (0–160 m) at the GYR station. Values are expressed in $\text{mg C m}^{-2} \text{d}^{-1} \pm$ one standard deviation. A photosynthetic and respiratory quotient of 1.1 is assumed (Laws, 1991). CR: Dark community respiration.

**Fig. 7.** Comparison of fitted (using the polynomial model) and measured Opt^tGCP at the GYR station.

On days 1 and 3, using classical measurements of O₂ changes in light/dark bottles incubated over a 24-h period, Gross Primary Production (O₂-GPP) and Community Respiration (O₂-CR) were determined in the euphotic zone. O₂-GPP, once converted to carbon units with a photosynthetic quotient of 1.1 (Laws, 1991), is significantly lower [473 (± 223) $\text{mg C m}^{-2} \text{d}^{-1}$] than GCP (Table 1). By contrast, and assuming a respiratory quotient of 1.1, the CR of 768 (± 65) $\text{mg C m}^{-2} \text{d}^{-1}$ is in the same range as the loss rates determined by the optical method.

The net community production computed solely using O₂ measurements leads to the usual conclusion that the upper ocean is in metabolic deficit (O₂-NCP = -295 (± 158) $\text{mg C m}^{-2} \text{d}^{-1}$) (Table 1). Being the most oligotrophic oceanic region, it is not surprising that our O₂ based production rates are lower than those previously reported for the less oligotrophic North Pacific Gyre [O₂-GPP = 657 (± 52) $\text{mg C m}^{-2} \text{d}^{-1}$; O₂-CR = 920 (± 39) $\text{mg C m}^{-2} \text{d}^{-1}$] (Williams et al.,

2004). Our O₂-NCP values for the SPG are however essentially equivalent to those for the North Pacific Gyre [-270 (± 49) $\text{mg C m}^{-2} \text{d}^{-1}$]. Contrary to incubation methods, our optical method is non-intrusive as are geochemical approaches. In addition, unlike geochemical observations, we integrate over the same time scales (hours to day) as incubation measurements.

When the model is applied to all oligotrophic stations (using only three measurements a day), the high Opt^tGCP values recorded at GYR are confirmed (Fig. 8). On average, Opt^tGCP amounts 452±264, 846±484 and 1093±520 $\text{mg C m}^{-2} \text{d}^{-1}$ for 0–0.5 Ze, 0–Ze and 0–1.5 Ze layers, respectively. These high in situ estimates are comparable to the very high values of GPP (greater than 1 $\text{g m}^{-2} \text{d}^{-1}$) reported at station ALOHA using an in situ, non intrusive technique based on triple oxygen isotope measurements (Juraneck and Quay, 2005). Our results when compared to other BIOSOPE results, remain, however, higher than primary production rates measured at the GYR station using O₂ in vitro techniques. Furthermore these rates are much higher than the average rates derived for all the oligotrophic stations, using in vitro incubation with either ¹³C labelling (Raimbault and Garcia, 2007: 180±60 $\text{mg C m}^{-2} \text{d}^{-1}$) or ¹⁴C labelling (Van Wambeke et al., 2007: 153±48 $\text{mg C m}^{-2} \text{d}^{-1}$). It should be noted, that contrarily to O₂-based method, those measurements based on isotope labelling do not take into consideration Dissolved Organic Carbon (DOC) excretion, a process which can be of major significance in such systems (see later).

While optical measurements indicate that POC production is roughly balanced over 5 days, consistent with geochemical approaches, the oxygen measurements imply net heterotrophy. We argue below that photosynthetic processes occurring in extremely dim light conditions could explain, at least partly, the missing ~300 $\text{mg C m}^{-2} \text{d}^{-1}$ estimated with O₂ measurements (Table 1) to obtain the balanced production observed by the optical approaches.

Significant production rates were recorded in the deep layer (160–240 m) where the remaining light represents between 1% and 0.1% of surface radiation, i.e. below the so called euphotic zone (Table 2). A diurnal trend was not observed in this layer during our first day on station, which had experienced overcast conditions for at least 2 days (Fig. 4).

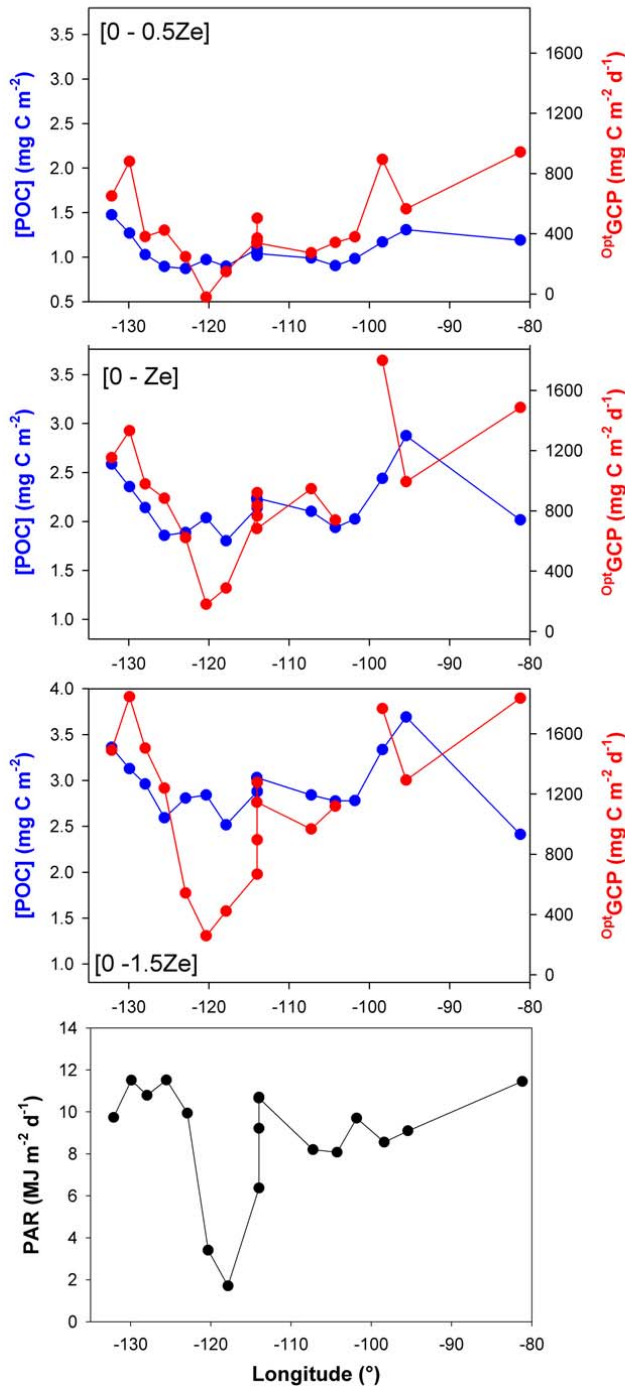


Fig. 8. Variations in POC and ^{Opt}GCP in oligotrophic stations along the BIOSOPE transect. Only stations reported in red in Fig. 2 are here considered. The three upper panels corresponds to three different photic layers. The lower panel presents daily dose of PAR.

A clear cycle became apparent, however, in the last three days (13–15 November). SPG surface waters are the clearest of the global ocean (Morel et al., 2007a), and thus short term fluctuations in surface irradiance are reflected in the 160–

240 m layer, and undoubtedly impact photosynthesis (and hence ^{Opt}GCP) at these depths. This process, although never demonstrated, was previously suggested for highly stratified oligotrophic systems (Karl et al., 2002). Actually in this deep layer, the ^{Opt}GCP increased by a factor of seven over the four days of investigation (from 45 mg to 319 mgC m⁻² d⁻¹) (Table 2). Over the same period, ^{Opt}GCP in the euphotic zone increased by 34% reflecting to some extent saturation of photosynthesis at high light intensities. Furthermore, on some days (e.g. cycle 4), production in the deep layer could account for more than the average discrepancy between the oxygen and optical method observed for the 0–160 m layer. Over the 4 days of investigation, the mean ^{Opt}GCP in this deep layer (176 mg C m⁻² d⁻¹, Table 2), which account for ~60% of this discrepancy. About 40% of this discrepancy remains to be explained.

The concentration of dissolved organic carbon (DOC) in the euphotic layer (~120 μM) is the highest ever reported for a subtropical gyre (Raimbault et al., 2008). It is indeed about 20% higher than maximal values reported for the North Pacific Gyre (Church et al., 2002), and values as high as 90 μM were still recorded at the 0.1% of surface radiation. Most of this DOC is likely of refractory nature and given the shape of the profile, these high concentrations must result from local production accumulating over time. For the North Pacific Gyre, it has been advanced that phototrophic production of DOC could represent up to 50% of GPP (Karl et al., 1998). The optical method does not measure this dissolved fraction directly. However, in a tightly coupled system with a rapid turnover, the labile fraction of this dissolved production can fuel heterotrophic and photo-heterotrophic production in the SPG, especially during the daylight period (Church et al., 2004; Karl et al., 1998) and this production will be observed optically. We observed a peak in c_p at ~100 m that is not associated with any Chl-*a* features (Fig. 2), and which shows clear daily oscillations and thus contribute to ^{Opt}GCP . This c_p maximum is collocated with the BChl-*a* maximum lying 80 m above the Chl-*a* maximum (see also Ras et al., 2008), a feature present throughout a large part of the SPG. BChl-*a*-containing bacteria can use both light and dissolved organic material to sustain their growth and carbon requirements (Sieracki et al., 2006). Furthermore, besides photoheterotrophy performed by these BChl-*a*-containing bacteria, it is very likely that other photoheterotrophic organisms might intervene in particulate organic carbon build-up (Church et al., 2004; Beja et al., 2001). These processes might be particularly important in the nutrient impoverished environments of subtropical gyres (Karl, 2002).

The fact that, in these extremely clear oligotrophic waters, processes below the so-called euphotic zone (1% depth) have not to date received much attention, might be surprising. Indeed, even if it is widely recognized that the deep chlorophyll maximum prevailing in oligotrophic gyre might be in large part the result of photo-adaptation processes, its presence nevertheless remains a clear indication that oxygen

Table 2. Day-to-day variations in the carbon production and loss rates in the South Pacific Gyre.

	OptGCP (0–240 m)	OptCL (0–240 m)	OptNCP (0–240 m)	OptGCP (160–240 m)	Surface irradiance
Cycle 1	663	607	56	45	26.6
Cycle 2	920	881	39	123	44.5
Cycle 3	911	888	23	219	38.4
Cycle 4	1148	1211	–63	319	44.4
Mean	910±198	897±247	14±53	176±119	

The 240 m depth corresponds to 1.5 times the euphotic depth as traditionally defined, and is a depth where 0.1% of surface irradiance is available. Production terms are expressed in $\text{mg C m}^{-2} \text{d}^{-1} \pm$ one standard deviation and surface irradiance in $\text{moles quanta m}^{-2} \text{d}^{-1}$.

photosynthesis does occur in deep layers. Actually, at the GYR station, more than 60% of the water Chl-*a* content was located in the layer comprised between the euphotic depth (Z_e) and $1.5Z_e$. The fact that other studies did not succeed to measure production (O_2 , ^{14}C) in very deep layers (below Z_e) is very likely linked to the difficulty of keeping “deep samples” in extremely dim light (not to say dark) conditions during sample processing at sea. We suggest here that in most cases, deep populations receive unavoidable light damage during their sampling, manipulation and during bottle deployment at sea. Our optical method, operating at the same time scale than *in vitro* measurements, is not intrusive (like geochemical ones) and thus avoid any light hazard of that sort.

During the present investigation, surface irradiance varied tremendously, by a factor of 6 (more than the seasonal variation in surface irradiance) over 6 days. Nevertheless, the investigated area remained in metabolic balance (even in slight autotrophic state) which means that such highly stratified systems have a large capacity to adapt and to stabilize their metabolic status under strongly variable environmental conditions (here light, which is likely the most important forcing variable in subtropical oligotrophic gyres).

4 Potential extrapolation of our observations

The estimations based on the bio-optical method presented here were conducted at a location and period representative of the most extreme oligotrophic conditions of the global ocean (see supplementary information, part 1 <http://www.biogeosciences.net/5/463/2008/bg-5-463-2008-supplement.pdf>). In this context, the rates estimated for this maximum of oligotrophy can be considered as a minimum reference for oligotrophic gyres in general (60% of the global ocean). From the OptGCP rates measured ($846 \pm 484 \text{ mg C m}^{-2} \text{d}^{-1}$) the annual carbon fixation rates for subtropical gyres are thus estimated to be at least 67 Pg for the euphotic layer. These values are equivalent or higher than estimates derived from bio-optical models for the global ocean (Antoine et al., 1996; Behrenfeld et al., 2005).

The subtropical gyres, therefore, might have a much larger impact than anticipated on ocean carbon cycle.

Furthermore, we believe that the method presented here is potentially useful in the context of bio-optical modelling of production. Bio-optical models for the estimation of depth integrated primary production are of the general form :

$$P = \text{PAR}(0^+) \times B \times \Psi \quad (7)$$

which expresses that the carbon fixation rate P ($\text{g C m}^{-2} \text{d}^{-1}$) is proportional to the product of the column integrated content of the biomass (B) of phototrophic organism by the irradiance at the ocean surface, $\text{PAR}(0^+)$. B is generally depicted by areal Chl-*a* ($\text{mg Chl-}a \text{ m}^{-2}$). Ψ is an efficiency term which convolves the irradiance absorption capability of B together with its efficiency in converting absorbed photons into chemical energy. Depending on the units chosen for $\text{PAR}(0^+)$ (quanta- or energy based), different ways of expressing Ψ have been proposed (Falkowski, 1981; Malone, 1987; Morel, 1991). The most simple expression of Ψ is achieved when B is expressed in terms of Chl-*a* concentration and $\text{PAR}(0^+)$ is expressed in $\text{MJ m}^{-2} \text{d}^{-1}$ and converted into reduced carbon equivalent (39 kJ gC^{-1}) such that Eq. (7) can be rewritten as :

$$\Psi^* = 39P / [\text{PAR}(0^+) \text{Chl-}a] \quad (8)$$

Ψ^* ($\text{m}^2 \text{g Chl-}a^{-1}$) is here defined as the chlorophyll specific water column photosynthetic cross section. For the global ocean, within the layer comprised between the surface and $1.5Z_e$, Ψ^* varies within a relatively narrow range around a central value of $\Psi^* = 0.070 \pm 0.035 \text{ m}^2 \text{gChl-}a^{-1}$. This means that 7% of the incident PAR is converted into stored chemical energy when 1g of Chlorophyll-*a* is present in the upper lit layers.

All the studies investigating such bulk water column efficiency indexes have only considered the biomass of photoautotrophic organisms depicted by Chl-*a*. The present study clearly demonstrates that phytoplankton alone cannot explain the daily increase in particulate carbon; heterotrophs (bacteria and possibly pico and nano-heterotrophs) as well as photo-heterotrophs also participate in this process.

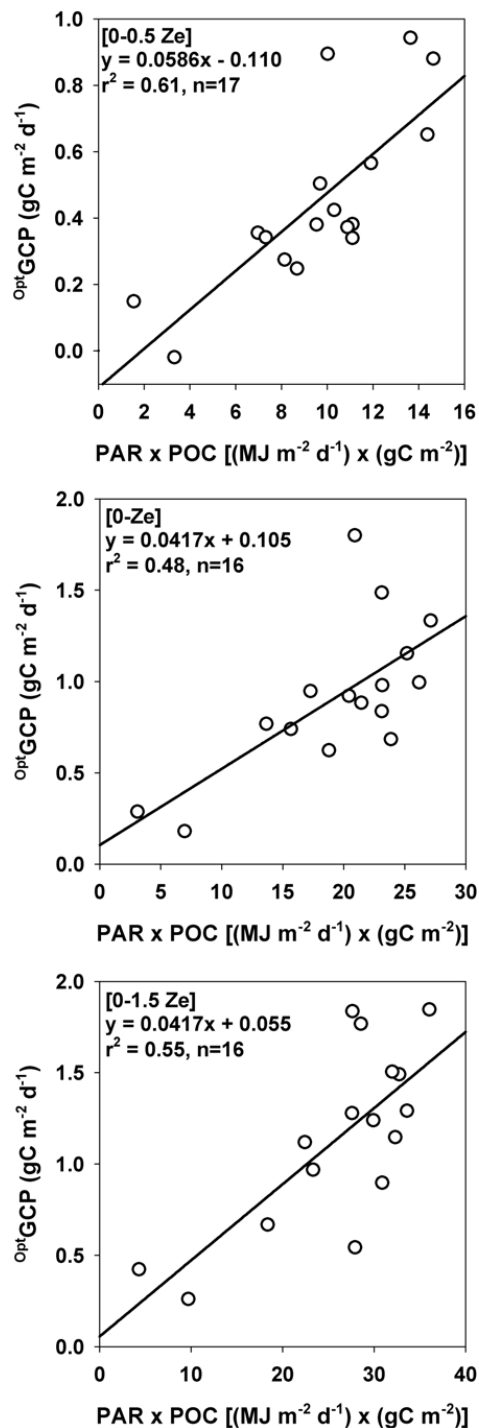


Fig. 9. The Estimation of ψ^*_{GCP} , the cross section for Growth Community Production in oligotrophic regime. ψ^*_{GCP} represents the slope of the regression between ^{Opt}GCP and the product of surface irradiance by the carbon content. Data from station 13 have been excluded from this analysis for the 0-Ze and 0–1.5 Ze layer because internal waves have made the DCM (and the associated c_p peak) shift from above Ze to below Ze between consecutive casts.

From Fig. 8, it is clear that ^{Opt}GCP in all investigated layers appear to be reduced in the vicinity of $120^\circ W$, when surface irradiance was drastically reduced ($2\ MJ\ m^{-2}\ d^{-1}$ vs. an average value over $10\ MJ\ m^{-2}\ d^{-1}$ for the other stations). Figure 9 provides an analyses, for each layer, of the possible dependency of ^{Opt}GCP with respect to biomass (here expressed in POC) and surface irradiance. Clearly ^{Opt}GCP appears proportional to the product of POC and surface irradiance. This coupling suggests that, in the same way that a photosynthetic cross section was defined earlier, the Gross Community Production cross section with respect to carbon can be defined, Ψ^*_{GCP} :

$$\Psi^*_{GCP} = 39^{Opt}GCP/[PAR(0^+)POC] \quad (9)$$

Actually the slopes of the regression presented in Fig. 9 have units of $m^2\ MJ^{-1}$. Using the conversion factor (between energy and carbon), Ψ^*_{GCP} is estimated to $2.28\ 10^{-3}$, $1.63\ 10^{-3}$ and $1.63\ 10^{-3}\ m^2\ gC^{-1}$ for 0–0.5 Ze, 0-Ze and 0–1.5 Ze layers, respectively. In other words, $\sim 0.2\%$ of the surface irradiance is converted to chemical energy when 1 g of POC is present. If the values are normalized by the generic $0.07\ m^2\ g\ Chl-a^{-1}$ for photosynthetic cross section a reasonable POC/Chl-*a* ratio of ~ 40 is estimated within the 0–1.5 Ze layer. This represents, at least, a partial validation of the estimations.

Beside the estimation of a carbon- rather than a Chl-*a*-based water column efficiency for production, the present approach has also a potential interest for the bio-optical modelling of production. Recently, it has been proposed that carbon-based, rather than Chl-*a*-based, models could be an improved way to estimate the rate of ocean carbon fixation from remote sensing data (Behrenfeld et al., 2005). The premise of carbon-based models is that the backscattering coefficient retrieved from space is an (accurate) estimation of phytoplankton carbon. This assumption is, however, questionable. Indeed, optical proxies (either c_p or b_{bp}) derived from either space or in situ measurements are primarily related to the particle load (POC content in oceanic waters), including together with phytoplankton, heterotrophic components (bacteria, flagellates) and also bio-detritus; thus their relationship to phytoplankton carbon is not straightforward, if any.

Therefore, because community production likely integrates the contribution of all organisms depicted by b_{bp} , the proper rate of carbon fixation that should be associated with this optical proxy of particle load would better be the community production rather than the sole primary production. It is interesting to note that using the carbon-based model, Behrenfeld et al. (2005) ends up with much higher primary production rates for the tropical ocean than using a Chl-*a*-based model, while the discrepancies are much lower for other oceanic areas. One possibility for such discrepancies is that phytoplankton carbon derived from space would be overestimated in tropical environments ; some dedicated stud-

ies have indeed clearly shown that the contribution of phytoplankton to c_p can be low in such oligotrophic environment (Claustre et al., 1999). The production rates derived for these environments would possibly be more closely related to gross community (phytoplankton and small heterotrophs) rather than to primary production rates.

Based on the use of optical proxies of biogenic particles (not exclusively phytoplankton) from space, we thus believe that a bio-optical model of Gross Community Production (GCP) would thus likely provide a more reliable estimate of carbon fixation, especially in oligotrophic tropical environments where microbial communities play an essential role. Indeed, GCP is a photo-driven process which, besides the POC formation by phytoplankton, also integrates DOC excretion and its subsequent use by microbial organisms. DOC release is certainly a key process (see Karl et al., 1998) that would require much more attention in view of implementing such models.

Acknowledgements. We thank the captain and crew of the R/V *Atalante* for their pleasant cooperation during the BIOSOPE cruise. C. Marec is warmly thanked for their efficient help in CTD rosette management and data processing. We are grateful to D. Stramski for providing POC data used for the calibration of the attenuation coefficient. This is a contribution of the BIOSOPE project of the LEFE-CYBER program. This research was funded by the Centre National de la Recherche Scientifique (CNRS), the Institut des Sciences de l'Univers (INSU), the Centre National d'Etudes Spatiales (CNES), the European Space Agency (ESA), the National Aeronautics and Space Administration (NASA) and the Natural Sciences and Engineering Research Council of Canada (NSERC).

Edited by: E. Boss

References

- Antoine, D., André, J. M., and Morel, A.: Oceanic primary production 2. Estimation at global scale from satellite (coastal zone color scanner) chlorophyll, *Global Biogeochem. Cyc.*, 10, 57–69, 1996.
- Antoine, D., Morel, A., Gordon, H. R., Banzon, V. F., and Evans, R. H.: Bridging ocean color observations of the 1980's and 2000's in search of long-term trends, *J. Geophys. Res.*, 110, C06009, doi:10.1029/2004JC002620, 2005.
- Behrenfeld, M. J., Boss, E., Siegel, D. A., and Shea, D. M.: Carbon-based ocean productivity and phytoplankton physiology from space, *Global Biogeochem. Cyc.*, 19, GB1006, doi:10.1029/2004GB002299, 2005.
- Beja, O., Spudich, E. N., Spudich, J. L., Leclerc, M., and DeLong, E. F.: Proteorhodopsin phototrophy in the ocean, *Nature*, 411, 786–789, 2001.
- Church, M. J., Ducklow, H., and Karl, D.: Multiyear increases in dissolved organic matter inventories at station ALOHA in the North Pacific Gyre, *Limnol. Oceanogr.*, 47, 1–10, 2002.
- Church, M. J., Ducklow, H. W., and Karl, D. A.: Light dependence of [H-3]leucine incorporation in the oligotrophic North Pacific ocean *Appl. Environ. Microbiol.*, 70, 4079–4087, 2004.
- Claustre, H. and Maritorena, S.: The many shades of ocean blue, *Science*, 302, 1514–1515, 2003.
- Claustre, H., Morel, A., Babin, M., Cailliau, C., Marie, D., Marty, J. C., Tailliez, D., and Vaultot, D.: Variability in particle attenuation and chlorophyll fluorescence in the Tropical Pacific: Scales, patterns, and biogeochemical implications, *J. Geophys. Res.*, 104, 3401–3422, 1999.
- Claustre, H., Bricaud, A., Babin, M., Bruyant, F., Guillou, L., Le Gall, F., Marie, D., and Partensky, F.: Diel variations in *Prochlorococcus* optical properties, *Limnol. Oceanogr.*, 47, 1637–1647, 2002.
- Claustre, H., Sciandra, A., and Vaultot, D.: Introduction to the special section: bio-optical and biogeochemical conditions in the South East Pacific in late 2004 – the BIOSOPE program, *Biogeosciences Discuss.*, 5, 605–640, 2008, <http://www.biogeosciences-discuss.net/5/605/2008/>.
- Cullen, J. J., Lewis, M. R., Davis, C. O., and Barber, R. T.: Photosynthetic characteristics and estimated growth rates indicate grazing is the proximate control of primary production in the equatorial Pacific, *J. Geophys. Res.*, 97, 639–654, 1992.
- del Giorgio, P. A. and Duarte, C. M.: Respiration in the open ocean, *Nature*, 420, 379–384, 2002.
- del Giorgio, P. A., Cole, J. J., and Cimleris, A.: Respiration rates in bacteria exceed phytoplankton production in unproductive aquatic systems, *Nature*, 385, 148, 1997.
- Dietze, H. and Oschlies, A.: Modeling abiotic production of apparent oxygen utilisation in the oligotrophic subtropical North Atlantic, *Ocean Dynam.*, 55, 28–33, 2005.
- DuRand, M. D. and Olson, R. J.: Contributions of phytoplankton light scattering and cell concentration changes to diel variations in beam attenuation in the equatorial Pacific from flow cytometric measurements of pico-, ultra- and nanoplankton, *Deep-Sea Res. II*, 43, 891–906, 1996.
- DuRand, M. D., and Olson, R. J.: Diel patterns in optical properties of the chlorophyte *nannochloris* sp.: Relating individual-cell to bulk measurements, *Limnol. Oceanogr.*, 43, 1107–1118, 1998.
- Falkowski, P. G.: Light-shade adaptation and assimilation numbers, *J. Plankton Res.*, 3, 203–216, 1981.
- Gardner, W. D., Walsh, I. D., and Richardson, M. J.: Biophysical forcing of particle production and distribution during a spring bloom in the North Atlantic, *Deep-Sea Res. Part II: Topical Studies in Oceanography*, 40, 171–195, 1993.
- Gardner, W. D., Mishonov, A. V., and Richardson, M. J.: Global POC concentrations from in-situ and satellite data, *Deep-Sea Res. II: Topical Studies in Oceanography*, 53, 718, 2006.
- Grob, C., Ulloa, O., Claustre, H., Alarcon, G., Huot, Y., and Marie, D.: Contribution of picoplankton to the particulate attenuation coefficient (c_p) and organic carbon concentration (POC) in the eastern South Pacific, *Biogeosciences Discuss.*, 4, 837–852, 2007, <http://www.biogeosciences-discuss.net/4/837/2007/>.
- Gruber, N.: A bigger nitrogen fix, *Nature*, 436, 786, 2005.
- Hansell, D., Ducklow, H., Macdonald, A. M., and O'Neil Baringer, M.: Metabolic poise in the north Atlantic ocean diagnosed from organic matter transports, *Limnol. Oceanogr.*, 49, 1084–1094, 2004.
- Jenkins, W. J.: Oxygen utilization rates in North Atlantic subtropical gyre and primary production in oligotrophic systems, *Nature*, 300, 246–248, 1982.

- Jenkins, W. J.: Nitrate flux into the euphotic zone near Bermuda, *Nature*, 331, 521–523, 1988.
- Juranek, L. W. and Quay, P. D.: In vitro and in situ gross primary and net community production in the North Pacific Subtropical Gyre using labeled and natural abundance isotopes of dissolved O₂, *Global Biogeochem. Cyc.*, 19, GB3009, doi:10.1029/2004GB002384, 2005.
- Karl, D.: Hidden in a sea of microbes, *Nature*, 415, 590–591, 2002.
- Karl, D., Bidigare, R. R., and Letelier, R.: Sustained and aperiodic variability in organic matter production and phototrophic microbial community structure in the North Pacific subtropical gyre, in: *Phytoplankton productivity, Carbon assimilation in marine and freshwater ecosystems*, edited by: P. J. L. Williams, D. N. Thomas, and C. S. Reynolds, Blackwell publishing, 222–264, 2002.
- Karl, D., Laws, E. A., Morris, P., Williams, P. J. L., and Emerson, S.: Metabolic balance of the open sea, *Nature*, 426, 32, 2003.
- Karl, D. M., Hebel, D. V., Bjorkman, K., and Letelier, R. M.: The role of dissolved organic matter release in the productivity of the oligotrophic North Pacific Ocean, *Limnol. Oceanogr.*, 43, 1270–1286, 1998.
- Laws, E. A., Redalie, D. G., Haas, L. W., Bienfang, P. K., Eppley, R. W., Harrison, W. G., Karl, D. M., and Marra, J.: High phytoplankton growth and production rates in oligotrophic hawaiian coastal waters, *Limnol. Oceanogr.*, 29, 1161–1169, 1984.
- Laws, E. A.: Photosynthetic quotients, new production and net community production in the open ocean, *Deep-Sea Res.*, 38, 143–167, 1991.
- Lewis, M. R., Harrison, W. G., Oakey, N. S., Hebert, D., and Platt, T.: Vertical Nitrate Fluxes In The Oligotrophic Ocean, *Science*, 224, 870–873, 1986.
- Loisel, H. and Morel, A.: Light scattering and chlorophyll concentration in case 1 waters: A reexamination, *Limnol. Oceanogr.*, 43, 847–858, 1998.
- Malone, T. C.: Primary production of the ocean water column as a function of surface light intensity, *Deep-Sea Res.*, 34, 139, 1987.
- Marra, J.: Primary production in the north atlantic: Measurements, scaling, and optical determinants, *Philosophical Transactions of the Royal Society of London B*, 348, 153–160, 1995.
- Marra, J.: Capabilities and merits of long-term bio-optical moorings, in: *Ocean optics*, edited by: Spinrad, R. W., Carder, K. L., and Perry, M. J., Oxford University Press, New York, 189–201, 1994.
- Marra, J.: Approaches for the measurement of plankton production, in: *Phytoplankton productivity, Carbon assimilation in marine and freshwater ecosystems*, edited by: Williams, P. J. L., Thomas, D. N., and Reynolds, C. S., Blackwell publishing, 78–108, 2002.
- Morel, A.: Optical modeling of the upper ocean in relation to its biogenous matter content (Case 1 waters), *J. Geophys. Res.*, 93, 10 749–10 768, 1988.
- Morel, A.: Light and marine photosynthesis: A spectral model with geochemical and climatological implications, *Progress in Oceanography*, 26, 263–306, 1991.
- Morel, A., Gentili, B., Claustre, H., Babin, M., Bricaud, A., Ras, J., and Tieche, F.: Optical properties of the “clearest” natural waters, *Limnol. Oceanogr.*, 52, 217–229, 2007a.
- Morel, A., Huot, Y., Gentili, B., Werdell, P. J., Hooker, S. B., and Franz, B. A.: Examining the consistency of products derived from various ocean color sensors in open ocean (Case 1) waters in the perspective of a multi-sensor approach, *Remote Sensing of Environment*, 111, 69–88, 2007b.
- Oschlies, A.: Can eddies make ocean deserts bloom?, *Global Biogeochem. Cy.*, 16, 1106, doi:10.1029/2001GB001830, 2002.
- Raimbault, P., Garcia, N., and Cerrutti, F.: Distribution of inorganic and organic nutrients in the south pacific ocean -evidence for long-term accumulation of organic matter in nitrogen-depleted waters, *Biogeosciences*, 5, 281–298, 2008, <http://www.biogeosciences.net/5/281/2008/>.
- Ras, J., Uitz, J., and Claustre, H.: Spatial variability of phytoplankton pigment distribution in the south east pacific, *Biogeosciences*, 5, 353–369, 2008, <http://www.biogeosciences.net/5/353/2008/>.
- Siegel, D. A., Dickey, T. D., Washburn, L., Hamilton, M. K., and Mitchell, B. G.: Optical determination of particulate abundance and production variations in the oligotrophic ocean, *Deep-Sea Res.*, 36, 211–222, 1989.
- Sieracki, M. E., Gilg, I. C., Thier, E. C., Poulton, N. J., and Goericke, R.: Distribution of planktonic aerobic anoxygenic phototrophic bacteria in the northwest Atlantic, *Limnol. Oceanogr.*, 51, 38–46, 2006.
- Stramski, D. and Kiefer, D. A.: Light scattering by microorganisms in the open ocean, *Progress in Oceanography*, 28, 343–383, 1991.
- Stramski, D. and Reynolds, R. A.: Diel variations in the optical properties of a marine diatom, *Limnol. Oceanogr.*, 38, 1347–1364, 1993.
- Stramski, D., Shalapyonok, A., and Reynolds, R. A.: Optical characterization of the oceanic unicellular cyanobacterium *Synechococcus* grown under a day-night cycle in natural irradiance, *J. Geophys. Res.*, 100, 13 295–13 307, 1995.
- Stramski, D., Reynolds, R. A., Babin, M., Kaczmarek, S., Lewis, M. R., Rottgers, R., Sciandra, A., Stramska, M., Twardowski, M. S., and Claustre, H.: Relationships between the surface concentration of particulate organic carbon and optical properties in the eastern south pacific and eastern atlantic oceans, *Biogeosciences*, 5, 171–201, 2008, <http://www.biogeosciences.net/5/171/2008/>.
- Van Wambeke, F., Obernosterer, I., Moutin, T., Duhamel, S., Ulloa, O., and Claustre, H.: Heterotrophic bacterial production in the south east pacific: Longitudinal trends and coupling with primary production, *Biogeosciences Discuss.*, 4, 2761–2791, 2007, <http://www.biogeosciences-discuss.net/4/2761/2007/>.
- Vaulot, D., Marie, D., Olson, R. J., and Chisholm, S. W.: Growth of *Prochlorococcus*, a photosynthetic prokaryote, in the equatorial pacific ocean, *Science*, 268, 1480–1482, 1995.
- Walsh, I. D., Chung, S. P., Richardson, M. J., and Gardner, W. D.: The diel cycle in the integrated particle load in the Equatorial Pacific: A comparison with primary production, *Deep-Sea Res.*, 42, 465–477, 1995.
- Williams, P. J. L., Morris, P. J., and Karl, D. M.: Net community production and metabolic balance at the oligotrophic ocean site, station ALOHA, *Deep-Sea Res.*, 51, 1563–1578, 2004.
- Williams, P. J. L.: The balance of plankton respiration and photosynthesis in the open oceans, *Nature*, 394, 55–57, 1998.

Distribution and fluxes of aggregates $>100 \mu\text{m}$ in the upper kilometer of the South-Eastern Pacific

L. Guidi^{1,2}, G. Gorsky¹, H. Claustre¹, J. C. Miquel³, M. Picheral¹, and L. Stemmann¹

¹Université Pierre et Marie Curie-Paris 6, Laboratoire d'Océanographie de Villefranche; CNRS, Laboratoire d'Océanographie de Villefranche, Villefranche-sur-Mer, France

²Department of Oceanography, Texas A and M University, College Station, Texas, TX, USA

³IAEA Marine Environment Laboratory, Monaco, Monaco

Received: 3 December 2007 – Published in Biogeosciences Discuss.: 20 February 2008

Revised: 7 August 2008 – Accepted: 13 August 2008 – Published: 29 September 2008

Abstract. Large sinking particles transport organic and inorganic matter into the deeper layers of the oceans. Between 70 and 90% of the aggregates exported from the surface mixed layer are disaggregated within the upper 1000 m. This decrease with depth indicates that fragmentation and remineralization processes are intense during sedimentation. Generally, the estimates of vertical flux rely on sediment trap data but difficulties inherent in their design limit the reliability of this information. During the BIOSOPE study in the south-eastern Pacific, 76 vertical casts using the Underwater Video Profiler (UVP) and deployments of drifting sediment traps provided an opportunity to fit the UVP data to sediment trap flux measurements. We applied the calculated UVP flux in the upper 1000 m to the whole 8000 km BIOSOPE transect. Comparison between the large particulate material (LPM) abundance and the estimated fluxes from both UVP and sediment traps showed different patterns in different regions. On the western end of the BIOSOPE section the standing stock of particles in the surface layer was high but the export between 150 and 250 m was low. Below this layer the flux values increased. High values of about 30% of the calculated UVP maximum surface zone flux were observed below 900 m at the HNLC station. The South Pacific Gyre exported about $2 \text{ mg m}^{-2} \text{ d}^{-1}$. While off Chilean coast 95% of the surface mixed layer matter was disaggregated, remineralized or advected in the upper kilometer, 20% of the surface zone flux was observed below 900 m near the Chilean coast. These results suggest that the export to deep waters is spatially heterogeneous and related to the different biotic and abiotic factors.

1 Introduction

The biological pump is the sum of biological processes by which atmospheric CO_2 fixed in photosynthesis is transferred from the euphotic layer to the ocean interior. Organic and inorganic matter is transported into the deep layers mainly by sinking particles (Volk and Hoffert, 1985). Small (micrometers range) particles settle slowly while large (>100 micrometers) particles are considered to settle more rapidly. Size is an important parameter, determining among others the sinking velocity, mass content and food potential of particles. Particle volume distribution measurements for aggregates in surface water show that most of the mass is encompassed in the 0.1–3 mm range (Jackson et al., 1997). Stemmann et al. (2007) showed that in the size range from microns to millimetres, the volume of large particles can equal the volume of the smaller ones. On the other hand, according to Richardson and Jackson (2007), picoplankton despite their small size (0.2–2.0 μm), may contribute more to oceanic carbon export than currently recognized. Picoplankton can aggregate, be incorporated into settling detritus or consumed as aggregates or as individual cells by higher trophic levels such as the pelagic filter-feeder tunicates or flux-feeder pteropods. These zooplankton short-circuit the microbial loop (Alldredge, 2005; Andersen et al., 1998; Gorsky et al., 1999; Noji et al., 1997) and transform small, slowly settling particles into rapidly sinking large particulate matter (LPM). Organic particles leaving the euphotic zone sink until they are remineralized or reach the ocean bottom. Numerous studies agree that relatively little of the organic matter that leaves the euphotic zone reaches the bottom. Particle flux at 1000 m is considered to be about 10% of that at 100 m (Betzer et al., 1984; Martin et al., 1987; Suess,



Correspondence to: G. Gorsky
(gorsky@obs-vlfr.fr)

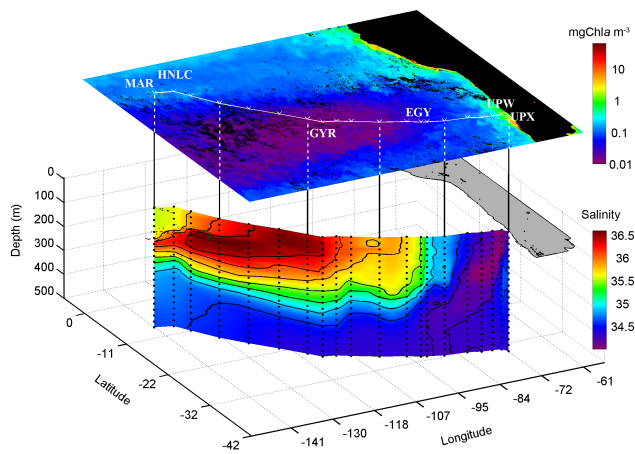


Fig. 1. Salinity section below the BIOSOPE transect superimposed on a SeaWiFS composite image of Chl-*a* concentration. The South American continent is in black and grey. Position of the 6 long-term stations is from left to right: MAR, HNLC, GYR, EGY, UPW and UPX stations.

1980). The decrease in concentration of particles with depth (Bishop and Edmond, 1976; Gardner and Walsh, 1990) implies that intense solubilizing processes of sinking particles occur in the water column during sedimentation. Particles can also be repackaged into larger, faster settling objects with lower concentrations and therefore more difficult to sample.

Estimates of sinking material rely primarily on the deployment of sediment traps (Asper, 1987; Buesseler et al., 2007a; Gardner et al., 2000; Honjo et al., 1984). Problems associated with the use of sediment traps, such as hydrodynamic flushing, swimmer contamination, and sample degradation, make trap measurements difficult to interpret (see Buesseler et al., 2007 for review). One way to increase the reliability of quantitative estimations of vertical export of the particulate matter is to deploy neutrally buoyant traps which drift in the sampled water mass to minimize the bias of advective effects (Buesseler et al., 2007a). In fact, most of the changes in flux with depth occur in the upper 1000 m (Lutz et al., 2002) and most of the processes that can bias flux estimates occur in this layer of the water column. On the other hand, little attention is given in the literature to the role of the particle size distribution although many particle properties fundamental in biogeochemical studies, such as sinking rate and carbon content, depend on accurate determinations of particle size (Burd et al., 2007).

Here we estimate the flux of particles by a method based on optical quantification of particles $>100\ \mu\text{m}$ (LPM) including the marine snow fraction (Gorsky et al., 2000; Guidi et al., 2007). As this methodology gives a detailed vertical assessment of the LPM abundance and size spectrum, we can estimate fluxes between the surface and the depth of 1000 m (the depth limit of the UVP used during the cruise).

The BIOSOPE (Biogeochemistry and Optics South Pacific Experiment) cruise covered a large range of contrasting hydrodynamic and trophic regimes along an ~ 8000 km transect from west of the Marquesas archipelago to the coastal waters of Chile (Claustre et al., 2008, this volume).

On the western end of the BIOSOPE transect, near Marquesas archipelago, an enhancement of the primary production is visible from satellite colour images. This level of production is often due to the island mass effect and has been explained by the dynamic interaction of the circulation and the topography (Martinez and Maamaatuaiahutapu, 2004, and references therein).

The South Pacific Gyre (SPG) is the largest subtropical anticyclonic gyre and the least described region of the ocean (Claustre and Maritorena, 2003; Longhurst, 1995). We know remarkably little about organic matter production and fate in it. The rare observations report very low chlorophyll concentrations (Chavez et al., 1995; Morel et al., 2007).

On the eastern end of the BIOSOPE transect a large biomass is exported offshore and to the deep layers near the Chilean coast fuelled by the Chilean upwelling (Claustre et al., 2008; Thomas, 1999).

The Underwater Video Profiler (UVP, see below for details) was used to assess the particle stock and size spectrum at a high vertical resolution. As part of the BIOSOPE program we fitted the UVP data to sediment trap flux measurements and applied the UVP flux estimations to the 76 profiles made during the BIOSOPE transect. We characterised the distribution of the large particulate matter (LPM) and the resulting fluxes in the 1000-m water column over the whole transect.

2 Methods

2.1 Zone of the study and data acquisition

The BIOSOPE cruise was conducted from 26 October to 11 December 2004. The detailed description of the cruise including the sampling strategy is reviewed in Claustre et al. (2008).

Within this spatial context, we examined the vertical distribution of the Large Particulate Matter (LPM $>100\ \mu\text{m}$ to 2 cm) using a non-destructive imaging system the Underwater Video Profiler (UVP) constructed in the Laboratoire d'Océanographie de Villefranche sur mer, France. The vertical deployments were conducted from the surface to the depth of 1000 m (Table 1) at a descent speed of 1 m/s. During the transect, 76 vertical profiles were completed from Marquesas archipelago to the coastal waters of Chile (Fig. 1).

The UVP coupled to a CTD SBE19 (Seabird Inc.) quantified and measured objects illuminated in a slab of water of known volume: 10.53 L. Object sizes are represented by the number of pixels. Size and volume calibrations were conducted in a sea-water tank using natural particles of different

Table 1. Location and time of the UVP deployments.

Station	Longitude	Latitude	Date	Time (UT)	Station	Longitude	Latitude	Date	Time (UT)
ES01	-144.001	-12.5	25-Oct-04	1:23 a.m.	STA13	-101.5	-29.09	22-Nov-04	11:31 a.m.
MAR01	-141.14	-8.25	26-Oct-04	1:24 p.m.	STA15	-95.501	-30.42	24-Nov-04	11:34 a.m.
MAR02	-141.16	-8.23	27-Oct-04	10:32 a.m.	STA16	-92.59	-31.25	25-Nov-04	10:18 a.m.
MAR02	-141.16	-8.23	27-Oct-04	11:06 a.m.	EGY02	-91.28	-31.49	26-Nov-04	6:45 a.m.
MAR02	-141.16	-8.22	28-Oct-04	1:45 a.m.	EGY02	-91.27	-31.5	27-Nov-04	3:07 a.m.
MAR02	-141.16	-8.22	28-Oct-04	2:19 a.m.	EGY03	-91.25	-31.52	27-Nov-04	6:07 a.m.
MAR03	-141.16	-8.201	28-Oct-04	10:53 a.m.	EGY03	-91.25	-31.52	27-Nov-04	6:41 a.m.
MAR03	-141.16	-8.201	28-Oct-04	11:27 a.m.	EGY03	-91.24	-31.52	27-Nov-04	7:08 p.m.
MAR04	-141.16	-8.19	29-Oct-04	10:06 a.m.	EGY03	-91.24	-31.52	27-Nov-04	9:05 p.m.
MAR04	-141.16	-8.19	29-Oct-04	10:40 a.m.	EGY03	-91.24	-31.52	27-Nov-04	9:39 p.m.
HLNC01	-136.52	-9.001	31-Oct-04	12:57 p.m.	EGY04	-91.25	-31.52	28-Nov-04	8:54 a.m.
HLNC01	-136.52	-9.01	01-Nov-04	1:25 a.m.	EGY04	-91.25	-31.52	28-Nov-04	9:11 p.m.
HLNC02	-136.53	-9.001	01-Nov-04	10:14 a.m.	EGY04	-91.25	-31.52	28-Nov-04	9:45 p.m.
HLNC02	-136.53	-9.001	01-Nov-04	10:48 a.m.	EGY05	-91.25	-31.54	29-Nov-04	6:18 a.m.
HLNC02	-136.59	-9.03	02-Nov-04	5:09 a.m.	EGY05	-91.25	-31.54	29-Nov-04	6:52 a.m.
HLNC03	-136.58	-9.04	02-Nov-04	10:15 a.m.	EGY05	-91.21	-31.54	29-Nov-04	12:03 p.m.
HLNC03	-136.58	-9.04	02-Nov-04	10:49 a.m.	EGY05	-91.22	-31.53	29-Nov-04	9:49 p.m.
STA01	-134.21	-11.31	03-Nov-04	2:12 p.m.	EGY06	-91.24	-31.54	30-Nov-04	9:07 a.m.
STA03	-130.23	-15.08	05-Nov-04	1:39 p.m.	STA17	-87.26	-32.18	01-Dec-04	10:31 a.m.
STA05	-125.57	-18.301	07-Nov-04	1:36 p.m.	STA18	-84.04	-31.42	02-Dec-04	8:40 p.m.
STA07	-120.51	-21.44	09-Nov-04	1:05 p.m.	STA19	-81.38	-32.57	03-Dec-04	10:25 a.m.
STA09	-116.01	-24.42	11-Nov-04	12:51 p.m.	STA20	-78.22	-33.19	04-Dec-04	10:21 a.m.
GYRE02	-113.59	-26.001	12-Nov-04	11:56 a.m.	STA21	-75.501	-33.35	05-Dec-04	9:57 a.m.
GYRE03	-114.01	-26.001	13-Nov-04	8:16 a.m.	UPW01	-73.23	-33.52	07-Dec-04	1:27 a.m.
GYRE03	-114.01	-26.001	13-Nov-04	8:50 a.m.	UPW02	-73.23	-33.58	07-Dec-04	5:12 a.m.
GYRE03	-114.001	-26.03	13-Nov-04	11:19 p.m.	UPW02	-73.23	-33.58	07-Dec-04	5:46 a.m.
GYRE03	-114.001	-26.03	13-Nov-04	11:53 p.m.	UPW02	-73.24	-33.58	07-Dec-04	8:08 a.m.
GYRE04	-114.02	-26.04	14-Nov-04	10:53 a.m.	UPW02	-73.21	-33.52	07-Dec-04	9:21 p.m.
GYRE04	-114.02	-26.04	14-Nov-04	11:27 a.m.	UPW02	-73.21	-33.52	07-Dec-04	9:55 p.m.
GYRE04	-114.01	-26.05	14-Nov-04	11:20 p.m.	UPW03	-73.18	-33.5	08-Dec-04	6:26 a.m.
GYRE04	-114.01	-26.05	14-Nov-04	11:54 p.m.	UPW03	-73.18	-33.5	08-Dec-04	7:00 a.m.
GYRE05	-114.01	-26.04	15-Nov-04	8:08 a.m.	UPX01	-72.24	-34.32	09-Dec-04	9:03 p.m.
GYRE05	-114.01	-26.04	15-Nov-04	8:42 a.m.	UPX02	-72.26	-34.36	10-Dec-04	1:30 a.m.
GYRE05	-114.01	-26.04	15-Nov-04	9:16 a.m.	UPX02	-72.27	-34.37	10-Dec-04	6:29 a.m.
GYRE05	-114.02	-26.04	15-Nov-04	11:25 p.m.	UPX02	-72.27	-34.37	10-Dec-04	7:03 a.m.
GYRE06	-114.001	-26.04	16-Nov-04	10:28 a.m.	UPX02	-72.301	-34.401	11-Dec-04	1:21 a.m.
STA10	-110.401	-26.51	17-Nov-04	12:22 p.m.	UPX03	-72.29	-34.39	11-Dec-04	8:10 a.m.
STA11	-107.35	-27.42	20-Nov-04	12:17 p.m.	UPX03	-72.29	-34.39	11-Dec-04	8:39 a.m.

types to determine the conversion between pixels to metric units (Stemmann et al., 2002). Images were recorded digitally at a rate of 12 images per second and processed with custom made image analysis software (Gorsky et al., 2000). The equivalent spherical diameter (ESD) of each particle was calculated assuming that the particle projected shape was a circle.

The resulting particles size distribution and flux data integrated over 5-m intervals were related to the simultaneously acquired CTD and fluorescence data.

This instrument was built for exhaustive optical estimation of

1. the stock of the particles $>100 \mu\text{m}$ (large particulate matter – LPM) from the surface to the depth of 1000 m and
2. their size distribution (Stemmann et al., 2007).

We estimated the LPM mass flux along the whole transect. As described more in details in Guidi et al. (2008), we integrated the mass flux over all the particles according to their sizes.

2.2 Flux estimates from the size spectrum of particles

The mass flux was calculated from size spectra using the method from Guidi et al. (2008). An extensive set of data with 118 flux measurements from sediment traps (model Technicap PPS5) both moored and drifting and concomitant profiles of aggregate abundance and size distributions were used to parameterize the relationships presented in Guidi et al. 2008 (see Table 4).

The assumption is that the total mass flux (F) is the mass flux spectrum integrated over all particle sizes. Using diameter (d) as a measure of particle size, then

$$F = \int_0^{\infty} n(d)m(d)w(d)dd \quad (1)$$

The mass (m) of a spherical particle is given by

$$m(d) = \alpha d^3 \quad (2)$$

where $\alpha = \pi \rho / 6$ and ρ is its average density.

Its settling rate (w) can be calculated using Stokes Law as follow:

$$w(d) = \beta d^2 \quad (3)$$

where $\beta = g(\rho - \rho_0)(18\nu\rho_0)^{-1}$, g is the gravitational acceleration, ρ_0 is the fluid density, and ν is the kinematic viscosity.

If both $w(d)$ and $m(d)$ are given by power relationships, so is the combined quantity,

$$w \cdot m = A \cdot d^b \quad (4)$$

For the above case of constant density (ρ) shown in Eqs. (2) and (3) the exponent b in Eq. (4) is equal to 5. In theory, the spectrum should be integrated over the whole range of particle sizes (i.e. 0 to the effective maximum particle size). In the present study, where the available size range is 100 μm to few cm, the spectrum was calculated over that range.

If the aggregates size distribution and the values of A and b are known, then a mass flux can be calculated from size spectra using Eqs. (1) and (4). The fluxes calculated this way can be compared to matching sediment trap values. Because the appropriate values of A and b are unknown, a minimization procedure was used to find those two values that provided the best fit between the two fluxes: sediment trap and particle size distribution flux derived.

We used the Matlab function `fminsearch` (The Mathworks, Inc., Natick, MA) to find the values of A and b of Eq. (4) that minimized the log-transformed differences (ΔF_c) between sediment trap and spectral-estimated fluxes:

$$\Delta F_c = \sum_i [\log(F_{T,i}) - \log(F_{E,i})]^2 \quad (5)$$

where $F_{T,i}$ is the sediment trap flux value and $F_{E,i}$ the associated flux based on Eq. (1) for the i th observation. The

logarithmic transformation was used to give equal weight to differences of small and large fluxes.

The minimization procedure yields only one pair of parameter values. We used a jack-knife procedure to estimate the errors of the estimates. The minimization was performed on 1000 subsamples one third the size of the original data set and composed of data pairs selected randomly from the original data set. The results provide us with the frequency distribution of A and b from which mean and standard deviations were calculated (Guidi et al., 2008: Table 4).

Note that the flux integration is only for particles between classes i to m available with the UVP, not 0–1 but 0–infinity symbol (horizontal 8) shown in Eq. (1).

Hence, knowing A and b (Eq. 4), aggregate with a given size (d) can be directly related to its mass flux. Estimated fluxes with UVP were compared to matching sediment trap observations at global scale. A minimization procedure using the Matlab function `fminsearch` (Mathworks Inc., Natick, MA) allowed to calculate A and b providing the best fit between the two fluxes, measured from sediment traps and estimated from particle size distributions (Guidi et al., 2008). Residues' normality between model (estimated UVP flux) and data (sediment traps) were tested and the model validated. The mass flux is given in units of dry weight (DW).

2.3 Sediment traps

Drifting surface tethered sediment traps were deployed at all 6 long-term stations (see Fig. 1 and Table 1 for geographical coordinates) for a period of 2 to 4 days. At each site, baffled conical sediment traps model Technicap PPS5 (1 m² surface collection) were deployed at 2 depths, ranging from 100–200 m depth at the eastern and western extremities of the cruise transect, to 200–400 m at the center of the South Pacific Gyre. The depth of trap deployments was decided based on the physico-chemical characteristics of the water column. Trap samples were preserved in a 2% formaldehyde solution in ambient seawater to prevent degradation or grazing of the collected particles.

3 Results

3.1 Hydrology

The general hydrology studied during the BIOSOPE cruise is described in Claustre et al. (2008). The surface salinity pattern varied over a large range, from the highly salty waters associated with the South Pacific Tropical Waters (SPTW) around 130° W (salinity of 36.6) towards the Eastern South Pacific Intermediate Water (ESPIW), at 78° W (salinity of ~34, Fig. 1). The South Equatorial Current (SEC) surrounding the Marquesas Islands (stations MAR) constituted the southern border of High Nutrients Low Chlorophyll (HNLC) waters of the equatorial upwelling region (see Claustre et al.,

2008, and the references herein). The South Pacific gyre (station GYR) was characterized by the strongly stratified Eastern South Pacific Central Waters (ESPCW). East of 100° W, the transition zone between the ESPCW and the waters, influenced by fresher Subantarctic Surface Waters (SASW, Fig. 1), marked the subtropical front. East of EGY stations a tongue of low salinity waters was observed at a depth of 300 m and flowed close to the surface near the coast.

East of 78° W, the ESPIW lies above the relatively saltier Equatorial Subsurface Water (EESW) that extends in the 100–400 m range. The ESPIW is part of the poleward Peru-Chile undercurrent (PCUC, stations UPW, UPX).

3.2 Distribution of the biogeochemical parameters

The distribution and amounts of total chlorophyll-*a* concentration (TChl-*a*) measured along the transect by different methods were similar (Raimbault et al., 2007; Ras et al., 2007). These in situ chlorophyll-*a* measurements matched the values derived from satellite imagery and showed considerable variations along the section. The highest concentrations of Tchl-*a* were recorded in surface layers at the western and eastern extremities; very low chlorophyll content was measured in the centre of the SPG. The lowest concentration occurred near the surface at 114° W (0.02 mg TChl-*a* m⁻³). Distribution of the in vivo fluorescence of TChl-*a* (Fig. 2) shows the range of variation of the autotrophic biomass along transect.

During the BIOSOPE cruise, the LPM distribution was generally correlated with the vertical distribution of fluorescence (Fig. 3) suggesting a direct relationship between the two parameters. Except the UPX station near the Chilean coast, this relationship was not evident in the deeper layers where the UVP maxima were certainly associated with the detrital or heterotrophic matter. LPM biovolume and abundance were the lowest respectively at the GYR, EGY and HNLC stations while near Chile the water column contained the highest volumes of LPM (Figs. 3 and 4). However, considering only the euphotic zone (see Claustre et al., 2008) the MAR and UPW stations displayed the highest maximum LPM values.

3.3 Sediment trap fluxes

Downward particle flux was very different at the several sites studied and, overall, varied by >2 orders of magnitude between stations. The lowest mass fluxes were measured at the GYR site and at the eastern site of it (2–28 mg m⁻² d⁻¹) as well as at the HNLC site (11–22 mg m⁻² d⁻¹). In the more productive waters of MAR particle flux were slightly higher (38–49 mg m⁻² d⁻¹). In contrast, particle fluxes were significantly higher at the 2 eastern stations off south-America, ranging from 54 to 630 mg m⁻² d⁻¹ at the UPW and UPX sites.

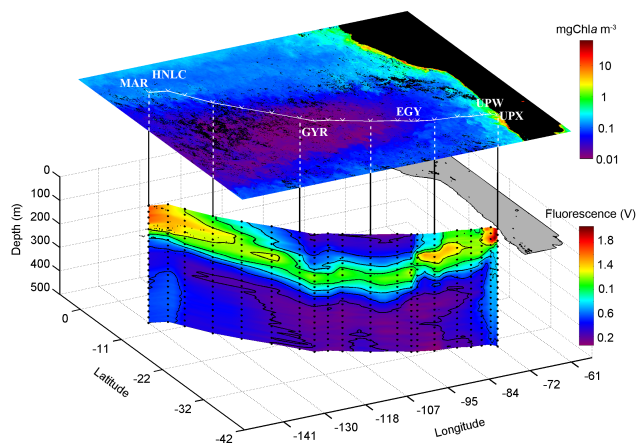


Fig. 2. In vivo fluorescence plot of Chl-*a* along the BIOSOPE section. Note the relatively high values at each end of the transect.

3.4 Comparison of LPM in the distinct zones along the BIOSOPE transect

LPM concentrations along the BIOSOPE transect (Fig. 4) reveal the following features:

1. high abundance of particles in the euphotic zone at the station MAR and relatively high concentration of particles from 150–300 m.
2. deep LPM maximum between 135 and 130° W,
3. a discontinuity in the abundance pattern at the vicinity of 100° W and
4. low particle densities in the low salinity ESPIW water mass (Figs. 1 and 4).

3.4.1 Western portion of the section

The mass flux estimated from size distribution profiles of the LPM along the BIOSOPE transect revealed a strong potential export in the first 150 m at the western end of the transect (Fig. 5). However, below this layer, between 150 and 300 m at the MAR station the LPM vertical flux was very low, forming a discontinuity stratum between the surface and the mesopelagic layers (Fig. 5). Despite the low vertical fluxes at this station (Fig. 5) the abundance of particles was high (Fig. 4). This observation may be explained by the small size and low settling velocities of these particles. The section between MAR and GYR is characterized by the increasing oligotrophy and by the deepening of the nutricline (Raimbault et al., 2007). The deep chlorophyll maximum (DCM) deepens also (Figs. 2 and 3) its base follows the 26 kg m⁻³ isopycnal (Claustre et al., 2008).

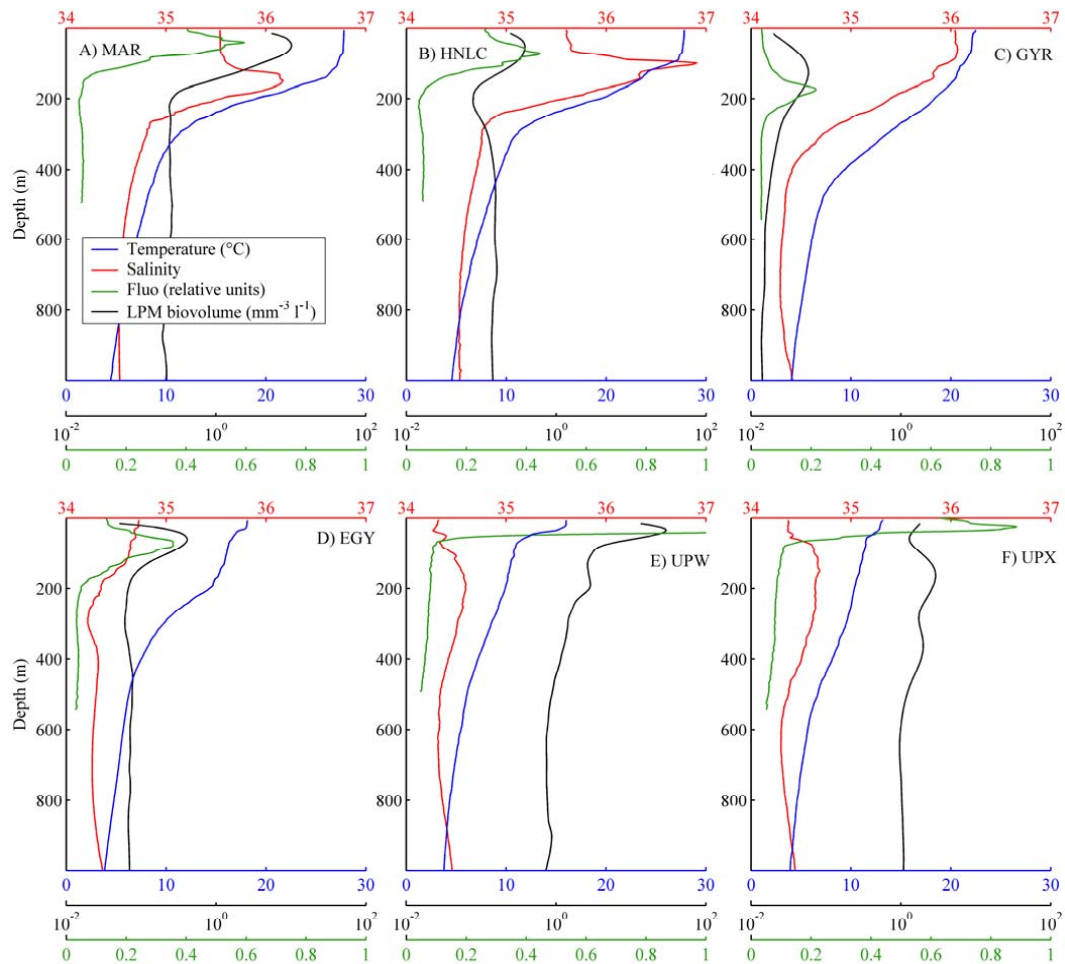


Fig. 3. Mean 0–1000 m profiles of the long-term stations displaying the temperature, salinity, fluorescence (RU) and the biovolumes (in $\text{mm}^{-3} \text{L}^{-1}$) of the LPM estimated from the UVP data. Note the logarithmic scale for the LPM data.

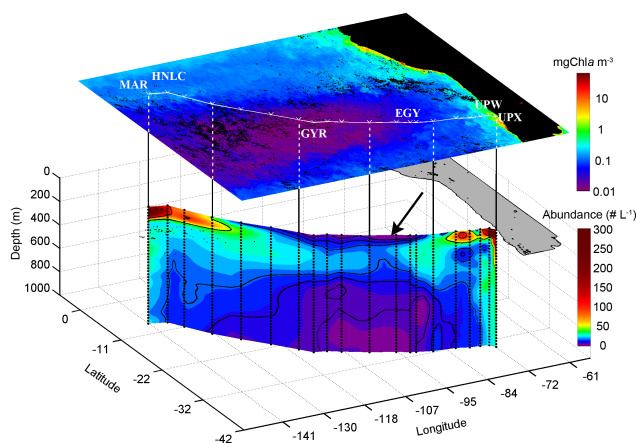


Fig. 4. Abundance of LPM $>100 \mu\text{m}$ in the first km of the BIOSOPE cruise. The arrow indicates the discontinuity zone in the abundance distribution of the large particulate matter.

3.4.2 The South Pacific gyre

As expected, the lowest values of particles abundance and the lowest export values were measured in and below the GYR. Abundances were higher in the 100–400-m layer than in the surface. The low biovolume and low fluxes indicate that particles in the SPG were small (Figs. 3 and 5). Eastwards, the strong salinity gradient delineated the limit of the SPG and indicated the presence of the subtropical frontal zone (Fig. 1). A discontinuity in the particle abundance pattern was observed in this zone and the vertical fluxes displayed the lowest values.

3.4.3 Eastern portion of the section

East of the EGY station, and below the ESPIW waters (at a depth of 250 m and below) the water mass had small particle abundance and low vertical flux values. A significant decrease in the concentration of particles was observed at the UPW station in the subsurface layer. Nevertheless, the

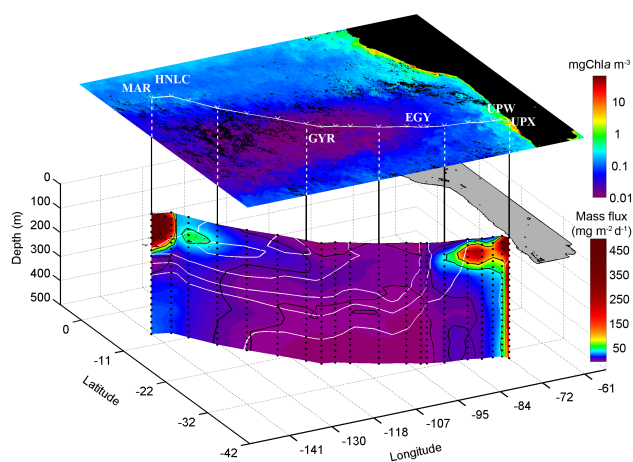


Fig. 5. Mass flux of LPM in $\text{mg DW m}^{-2} \text{d}^{-1}$ estimated from size measurements of every individual particle recorded during the vertical deployment of the UVP. Only data from 0–500 m are shown for better visualisation of the upper water column structures. The vertical resolution of the sampling was 10.5 L every 8 cm (see Guidi et al., 2007, for details). Isohalines are in white.

particulate volume and vertical export remained high. This result suggests that the contribution of the large particles was high. Near the Chilean coast the mixed layer was reduced and nutrient concentrations and the primary production were high. At the UPX station the Chl-*a* fluorescence signal was measurable even in the intermediate layers. The abundance of particles and the resulting vertical flux was high in the entire water column (Figs. 4 and 5).

4 Discussion

Marine particles vary in length from submicron colloidal particles to marine snow larger than tens of millimeter in diameter (Alldredge and Gotschalk, 1988; Fowler et al., 1987). The abundance of particles varies across this size range, with smaller particles generally being more abundant than larger ones (McCave, 1975). The particle mass however, tends to be concentrated in the larger particles (e.g., Jackson et al., 1997; McCave, 1975).

Here we are using particle diameter to estimate mass and settling rate values. We applied a minimization procedure to find the best fit between the UVP and sediment trap fluxes. Flux estimations made for the 76 UVP profiles were compared to the drifting sediment traps mass flux measurements (Fig. 6) made during the cruise. As the correlation between the optical assessment and the collected matter is good we are applying the flux estimates to all the 76 UVP profiles providing extensive information on the potential export in the different depths along the whole transect. Image acquisition is a conservative sampling method. With the improvement of the sediment trap methodology *sensu* Buesseler et

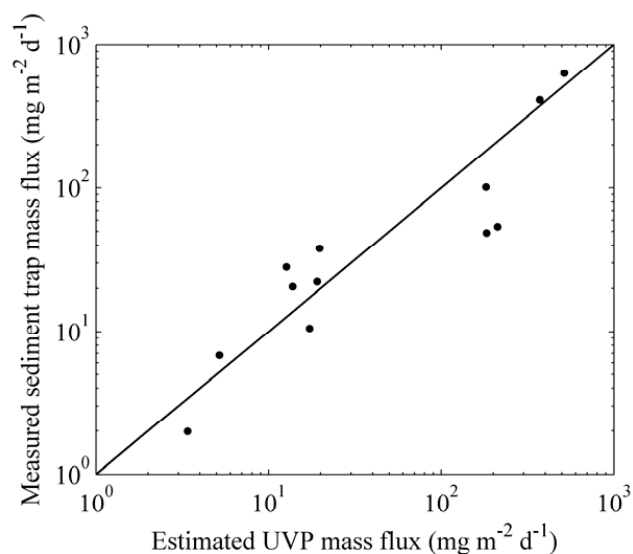


Fig. 6. Drifting sediment trap mass flux measurements versus the UVP estimated mass flux. The sediment traps were deployed below the mixed layer at 2 depths at each site, at 100–200 m depth at the extremities of the transect and at 200–400 m at the centre of the SPG.

al. (2007b) we will be able to ameliorate also the trap-UVP correlations and provide more precise flux data with high spatial and temporal resolution. This treatment can be done retrospectively and also on past data stored in the UVP data-bank (<http://www.obs-vlfr.fr/LOV/ZooPart/UVP/>).

4.1 Abundance vs. fluxes

4.1.1 Western portion of the section

On the western end of the BIOSOPE transect, (station MAR), the abundance of particulate matter in the surface zone is very high (Fig. 4). According to Gomez (2007), the small pennate cluster forming diatom *Pseudo-nitzschia delicatissima* and the large centric diatom *Rhizosolenia bergonii* were the main microphytoplanktonic constituents of this layer. Large, rapidly sinking phytoplankton, such as diatoms, are believed to control carbon flux from upper ocean layers (Michaels and Silver, 1988). However as pointed out by Gomez (2007) in the western and eastern part of the BIOSOPE transect, the surface layer diatom population was characterized by frustules with low silicate content because of the silicate-limited environment. This feature may also limit their ballasting efficiency.

Although the abundance profile shows a vertical continuum and the surface LPM maximum is the second highest on the whole transect (Fig. 4), the flux estimations calculated from the UVP data fitted to the drifting sediment trap measurements reveal that the export between 150 and 250 m is very low (Fig. 5). This discontinuity in the vertical flux

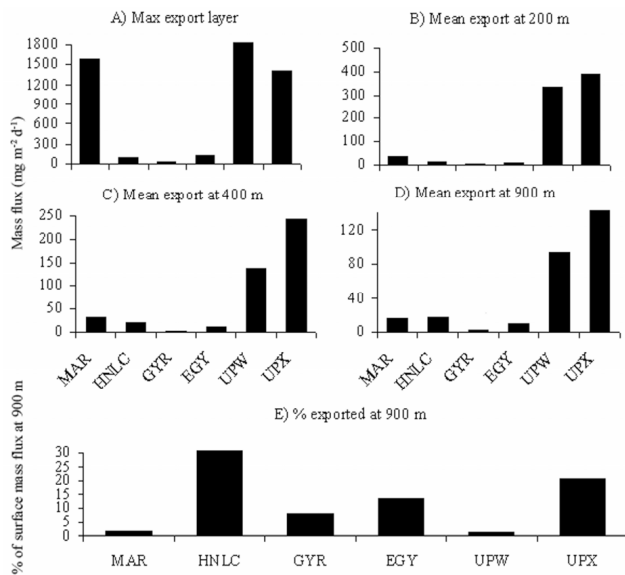


Fig. 7. Mean export at different depths and the % exported below 900 m related to the potential surface export maximum (UVP data fitted to sediment trap measurements).

clearly observed at the station MAR may be the result of different biological and physical factors. Large unknown transparent objects were detected by the UVP at the MAR site (see Fig. 7 in Stemmann et al., 2007). These circular-shaped objects were about 2–5 mm in diameter with concentrations between 1–10 objects L⁻¹. They were located throughout the upper 200 m but below 170 m their concentration decreased. If they were anomalous, low-density organism, they might increase the apparent flux values in the upper layer. Below, the particles population was composed of small size classes. The hydrology at the MAR site may also contribute to the discontinuity in the vertical export. The discontinuity stratum (150–250 m) corresponds to the zone of narrowing density field and is the site of strong advective processes (Figs. 3 and 4 in Claustre et al., 2008). These advective processes may be responsible of the change in the size structure of the particles population. Below this discontinuity layer the vertical flux values increase slightly. This feature is clearly visible in the Fig. 7.

An increase of the LPM flux was observed in the HNLC zone in the vicinity of 130° W. This increase may be associated with the deepening of the sub-surface isotherms (Claustre et al., 2008). About 30% of the maximum surface layer flux was observed below 900 m at the HNLC station. In fact, the mean export initially decreased at 200 m when compared to the maximum flux at the surface layer, but then it increased with depth (Figs. 3 and 7). The surface production at this region is weak: only about 99 mg m⁻² d⁻¹ in the maximum layer, but still about 20 mg m⁻² d⁻¹ below 900 m. The reason for the increase of exported mass at depth may be linked to other processes such as aggregation, advection or to the low

oxygen conditions. Furthermore, no significant difference was observed between the day and night fluxes that may be attributed to the vertical zooplankton migration (Stemmann et al., 2007). According to Claustre et al. (2008) in this area the currents were weak. Therefore, the hypothesis that the increase of large particles flux may be associated with suboxic conditions should be further explored. According to Claustre et al. (2008) this oxygen minimum reflects the signature of north-westwards propagation of the oxygen minimum zone developed along South America. Typically, these zones underlie regions of high biological productivity and thus high production of organic matter. The transition from oxic to anoxic conditions involves important biogeochemical shifts. In the absence of oxygen, nitrate is used to oxidize organic material (Stramma et al., 2008). Oxygen-poor conditions have far-reaching impacts on ecosystems because important mobile macroorganisms avoid or cannot survive in hypoxic zones. It is hypothesized that low oxygen is limiting the vertical migration of zooplankton (Morrison et al., 1999) and thus the fragmentation processes. This is a region of denitrification, and the presence and activities of bacteria may cause the increase in particles. On the other hand, the suboxic conditions might prevent the degradation of particulate matter. This hypothetical particle preservation could also occur in the Marquesas area. Below 200 m there is a good conservation of the mass flux. Mass flux estimated at 900 m is 70% of mass flux estimated at 200 m.

4.1.2 The South Pacific gyre

The SPG is known as a hyper-oligotrophic water mass (Claustre and Maritorena, 2003; Morel et al., 2007). The biological production in the surface zone is the lowest in the global ocean. Peaks of small particles centered at 100 m were associated with a *Prochlorococcus* sp. population (Grob et al., 2007). The deep chlorophyll maximum (DCM) located between 160–200 m was mainly composed of picophytoeukaryotes, although some coccolithophorid and diatom cells were also present (Beaufort et al., 2008; Gomez et al., 2007; Ras et al., 2007). The maximum phaeophorbide (a tracer for altered Chl-*a*) concentration was found also in this layer (Ras et al., 2007). Oligotrophic regions, where small cells dominate the production, can contribute significantly to the global carbon flux via detritus (Richardson and Jackson, 2007). The mass flux associated with the DCM was estimated from the UVP data as ~30 mg m⁻² d⁻¹. The export at 200 m was 20% of that in surface waters and about 8% at 900 m (~2 mg m⁻² d⁻¹). While considering the large geographical extent of the SPG, this extreme oligotrophic ecosystem is producing a non negligible amount of carbon. Due to the lack of seasonal vertical mixing and weak lateral advection, the biologically produced LPM carbon can be exported and trapped in the deep layers for long periods.

4.1.3 Eastern portion of the section

In the vicinity of 100° W, we observe a distinct discontinuity in the abundance distribution of the LPM (arrow in Fig. 4). This discontinuity corresponds to the uplifted isolines delineating the subtropical front as described in Claustre et al. (2008). At EGY, the DCM is located at the depth of 80 m but the export values are low, similar to the HNLC station. The mean surface layer maximum export is estimated as $127 \text{ mg m}^{-2} \text{ d}^{-1}$, and a slight increase of fluxes with depth can be observed (Fig. 7). About 13% of the surface export is measured below 900 m. This result constitutes 94% of the vertical flux estimated at 200 m. No difference was observed between the day and night fluxes.

The situation is quite different off and near the Chilean coast. High LPM concentrations are observed in the surface zone with a strong decrease below at the location of the low salinity waters (Fig. 1). This feature is not detected on the flux plot (Fig. 5). Therefore, the decrease in abundance is related to the small particle fraction. At the UPW station, the situation changed. The potential export from the Chl-*a* maximum estimated for the whole section is $7367 \text{ mg m}^{-2} \text{ d}^{-1}$. At depths of 200 m and 900 m only 4.6% and 1.5% respectively of this flux remained. Thus, 95% of the matter was remineralized, disaggregated to $<100 \mu\text{m}$ or advected. At both coastal stations the vertical zooplankton migration was significant. Near the Chilean coast, at the UPX stations, the vertical flux remained high in the entire water column. The surface maximum export was $1400 \text{ mg m}^{-2} \text{ d}^{-1}$, lower than the mean UPW surface maximum but in contrary to the latter, 20% of the surface layer flux was observed below 900 m (Fig. 7). Thus the remineralization processes differ in the two stations near the Chilean coast.

4.2 Export efficiency

Particulate export is a result of particle supply, production, consumption and aggregation/disaggregation. These processes are developed at different scales of variability including time lags between biological production and export. During settling, particles disaggregate, decompose and disappear. Some of the marine snow particles may be fragmented by the swimming activity of migrating zooplankton (Dilling and Alldredge, 2000; Goldthwait et al., 2004). Most are transformed into particles smaller than the $100 \mu\text{m}$ cutoff of the UVP and/or into dissolved matter by the processes of remineralization. Some may coalesce into larger particles by grazing or aggregation (Alldredge and Silver, 1988; Jackson and Burd, 2002). It is at depths between the surface euphotic zone and roughly 1000 m where most sinking particles are remineralized (Buesseler et al., 2007b). The variety of vertical profiles shows that there are variations in remineralization rates or advection rates with depth. Blooms of some species, like coccolithophores or diatoms and the consequent phytodetritus deposition, can cause episodic changes in rem-

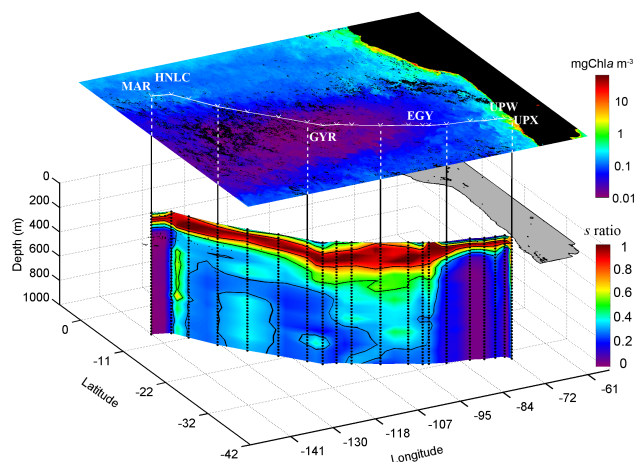


Fig. 8. The *s* ratio corresponding to the LPM mass flux (F) estimated at depth Z normalized by the flux estimated below Z_e ($s\text{-ratio}(Z) = F(Z)/F(Z_e)$). Here, Z_e is the depth where the mass flux is maximal (*s*-ratio is equal to 1 for Z_e : dark red).

ineralization length-scales (Nodder et al., 2007); blooms of filter-feeder thaliaceans, larvaceans or flux-feeder pteropods can change element ratios, sinking speeds and ballasting (Alldredge, 2005; Andersen et al., 1998; Boyd and Newton, 1995) or size distributions of particles (Gorsky et al., 1999). Zooplankton affect particle flux in the sea in a number of ways; they create or aggregate particles by feeding and producing sinking fecal pellets, disaggregate sinking particles by their feeding or swimming activities, remineralize sinking particles through their feeding and metabolism, and actively transport particulate and dissolved organic matter from the surface to depth by vertical migration (e.g., Fowler et al., 1987; Longhurst et al., 1990). Beyond the overall changes in particle flux with depth, changes in composition of the sinking material can have an impact on carbon gradients. Steinberg et al. (2008), compared losses of sinking POC measured by neutrally buoyant sediment traps with bacteria and zooplankton metabolic requirements in the subtropical Pacific and in the subarctic Pacific. Mesopelagic bacterial carbon demand was respectively 3- to 4-fold, and 10-fold greater than the loss of sinking POC flux, while zooplankton carbon demand was 1- to 2-fold, and 3- to 9-fold greater. Nevertheless, on the studied section and in the different trophic regimes UVP data indicate that particle export below 900 m was not negligible.

During the BIOSOPE transects in the different geographic zones the relative fluxes when compared to the surface maximums were different (Fig. 8). Higher proportion of particulate matter was mediated to the deep layers in the GYR region than in the rich surface layer MAR or UPW zones.

Sinking velocities determine the depth at which remineralization occurs, which in turn determines how soon remineralized nutrients and carbon will be returned to the surface

ocean (Sarmiento and Gruber, 2006). Particles of the same excess density settle at roughly the same speed principally because Reynolds number is very sensitive to particle size (Khelifa and Hill, 2006a, b). Although organic compounds are initially present in different proportions in the particles with different settling velocities, the degradation process can lead to uniform chemical compositions of particles (Goutx et al., 2007). This change reflects the processes of loss through enzymatic hydrolysis of source compounds and input of bacterial biomass. The settling speed may differ in the different regions due to the differences in the composition of primary and secondary producers. More studies should test the hypothesis on which our flux estimations are based, i.e., that at mesopelagic depths particles of similar size settle at a more or less uniform speed due to their similar composition.

5 Conclusions

Abundance and size spectrum of particles $> 100 \mu\text{m}$ were optically estimated from the surface to 1000 m and the mass flux of particles was calculated. The resulting mass fluxes estimated with the UVP were compared to drifting sediment trap data (at the 6 locations) and applied over the whole BIOSOPE transect.

The LPM abundance and the estimated fluxes varied considerably across the study area. At the MAR station the abundance profile showed a vertical continuum while the vertical flux decreased significantly between 150 and 250 m. This change could be due to an abundance of large, unidentified low-density objects that disappeared with depth, or due to intense hydrodynamic processes (Figs. 3 and 4 in Claustre et al., 2008) in this zone. Only about 2% of the upper zone LPM was exported below 900 m.

Contrastingly, about 30% of the maximum surface flux was observed below 900 m at the HNLC station. This feature may be associated with the suboxic conditions (Claustre et al., 2008).

In spite of relatively small values (from 7 to 15% of the surface layer maximum), the carbon export below the extreme oligotrophic SPG is not negligible. The lack of seasonal vertical mixing and weak lateral advection suggest that this material can be trapped in deep layers for long periods.

A discontinuity in the abundance distribution of the LPM is observed in the vicinity of 100°W and is associated with the intrusion of the subtropical front.

High LPM concentrations are observed in the upper layer off and near the Chilean coast. There is a strong decrease of particles abundance below this layer in the low salinity waters, but not in the vertical flux, suggesting a decrease in the small particle population only.

The potential export from the Chl-*a* maximum displays the highest value at the UPW station but at depths of 200 m and 900 m, only 4.6% and 1.5% respectively of this flux re-

mains. 95% of the matter is remineralized, disaggregated or advected away.

At the UPX station, the vertical flux remains high in the entire water column. In contrast to UPW, 20% of the surface flux is still observed below 900 m.

Variations in the estimated flux rates of LPM obtained in this study suggest that a wide variety of biotic and abiotic processes may drive the aggregation-disaggregation processes and influence the export of matter from mesopelagic layers. This conclusion suggests that LPM export to deep waters is heterogeneous and that optical methods allowing high spatial resolution studies should be utilized in deep sea habitats.

Acknowledgements. This work was supported by the French national programs LEFE and PNEC (ZOOPEC project). Special thanks to the crew of the ATALANTE French oceanographic vessel for their assistance with this research. We thank the two anonymous referees for the substantial improvement of the ms and M. Youngbluth for constructive discussions. The International Atomic Energy Agency is grateful for the support provided to its Marine Environment Laboratories by the Government of the Principality of Monaco.

Edited by: T. J. Battin

References

- Allredge, A.: The contribution of discarded appendicularian houses to the flux of particulate organic carbon from oceanic surface waters, in: Response of marine ecosystems to global change: Ecological impact of appendicularians, edited by: Gorsky, G., Youngbluth, M., and Deibel, D., GB Science Publishers-Editions Scientifiques GB, Paris, 309–326, 2005.
- Allredge, A. L. and Gotschalk, C.: In situ settling behavior of marine snow, *Limnol. Oceanogr.*, 33, 339–351, 1988.
- Allredge, A. L. and Silver, M. W.: Characteristics, dynamics and significance of marine snow, *Prog. Oceanogr.*, 20, 41–82, 1988.
- Andersen, V., Francois, F., Sardou, J., Picheral, M., Scotto, M., and Nival, P.: Vertical distributions of macroplankton and micronekton in the Ligurian and Tyrrhenian seas (Northwestern Mediterranean), *Oceanol. Acta*, 21, 655–676, 1998.
- Asper, V. L.: Measuring the flux and sinking speed of marine snow aggregates, *Deep-Sea Res. Part. I*, 34, 1–17, 1987.
- Beaufort, L., Couapel, M., Buchet, N., Claustre, H., and Goyet C.: Calcite, production by Coccolithophores in the south east Pacific Ocean, *Biogeosciences*, 5, 1101–1117, 2008, <http://www.biogeosciences.net/5/1101/2008/>.
- Betzer, P. R., Showers, W. J., Laws, E. A., Winn, C. D., Ditullio, G. R., and Kroopnick, P. M.: Primary productivity and particle fluxes on a transect of the equator at 153°W in the Pacific Ocean, *Deep-Sea Res. Part. I*, 31, 1–11, 1984.
- Bishop, J. K. B. and Edmond, J. M.: A new large volume filtration system for the sampling of oceanic particulate matter, *J. Mar. Res.*, 34, 181–198, 1976.
- Boyd, P. and Newton, P.: Evidence of the potential influence of planktonic community structure on the interannual variability of

- particulate organic-carbon flux, *Deep-Sea Res. Part. I*, 42, 619–639, 1995.
- Buesseler, K. O., Antia, A. N., Chen, M., Fowler, S. W., Gardner, W. D., Gustafsson, O., Harada, K., Michaels, A. F., van der Loeff, M. R., Sarin, M., Steinberg, D. K., and Trull, T.: An assessment of the use of sediment traps for estimating upper ocean particle fluxes, *J. Mar. Res.*, 65, 345–416, 2007a.
- Buesseler, K. O., Lamborg, C. H., Boyd, P. W., Lam, P. J., Trull, T. W., Bidigare, R. R., Bishop, J. K. B., Casciotti, K. L., Dehairs, F., Elskens, M., Honda, M., Karl, D. M., Siegel, D. A., Silver, M. W., Steinberg, D. K., Valdes, J., Van Mooy, B., and Wilson, S.: Revisiting carbon flux through the ocean's twilight zone, *Science*, 316, 567–570, 2007b.
- Burd, A. B., Jackson, G. A., and Moran, S. B.: The role of the particle size spectrum in estimating POC fluxes from 234th/238u disequilibrium, *Deep-Sea Res. Part. I*, 54, 897–918, 2007.
- Chavez, F. P., Buck, K. R., Bidigare, R. R., Karl, D. M., Hebel, D., Latasa, M., Campbell, L., and Newton, J.: On the chlorophyll-*a* retention properties of glass-fiber *gf/f* filters, *Limnol. Oceanogr.*, 40, 428–433, 1995.
- Claustre, H. and Maritorena, S.: The many shades of ocean blue, *Science*, 302, 1514–1515, 2003.
- Claustre, H., Sciandra, A., and Vaultot, D.: Introduction to the special section bio-optical and biogeochemical conditions in the South East Pacific in late 2004: the BIOSOPE program, *Biogeosciences*, 5, 679–691, 2008, <http://www.biogeosciences.net/5/679/2008/>.
- Fowler, S. W., Buat-Menard, P., Yokoyama, Y., Ballestra, S., Holm, E., and Van Nguyen, H.: Rapid removal of Chernobyl fallout from mediterranean surface waters by biological activity, *Nature*, 329, 56–58, 1987.
- Dilling, L. and Alldredge, A.: Fragmentation of marine snow by swimming macrozooplankton: A new process impacting carbon cycling in the sea. *Deep-Sea Res. Part. I*, 47, 1227–1245, 2000.
- Gardner, W. D. and Walsh, I. D.: Distribution of macroaggregates and fine-grained particles across a continental-margin and their potential role in fluxes, *Deep-Sea Res. Part. I*, 37, 401–411, 1990.
- Gardner, W. D., Richardson, M. J., and Smith, W. O.: Seasonal patterns of water column particulate organic carbon and fluxes in the ross sea, Antarctica, *Deep-Sea Res. Part. II*, 47, 3423–3449, 2000.
- Goldthwait, S., Yen, J., Brown, L., and Alldredge, A.: Quantification of marine snow fragmentation by swimming euphausiids, *Limnol. Oceanogr.*, 49, 940–952, 2004.
- Gomez, F.: On the consortium of the tintinnid *Eutintinnus* and the diatom *Chaetoceros* in the Pacific Ocean, *Mar. Biol.*, 151, 1899–1906, 2007.
- Gorsky, G., Chretiennot-Dinet, M. J., Blanchot, J., and Palazzoli, I.: Picoplankton and nanoplankton aggregation by appendicularians: Fecal pellet contents of *Megalocercus huxleyi* in the equatorial Pacific, *J. Geophys. Res.-Oceans*, 104, 3381–3390, 1999.
- Gorsky, G., Picheral, M., and Stemann, L.: Use of the Underwater Video Profiler for the study of aggregate dynamics in the North Mediterranean, *Estuar. Coast. Shelf Sci.*, 50, 121–128, 2000.
- Goutx, M., Moriceau, B., Lee, C., Liu, Z., Guigue, C., Dufflos, M., Tedetti, M., Sempere, R., Wakeham, S. G., and Xue, J.: Composition and degradation of marine particles with different settling velocities, *Limnol. Oceanogr.*, 52(4), 1645–1664, 2007.
- Grob, C., Ulloa, O., Claustre, H., Huot, Y., Alarcón, G., and Marie, D.: Contribution of picoplankton to the total particulate organic carbon concentration in the eastern South Pacific, *Biogeosciences*, 4, 837–852, 2007, <http://www.biogeosciences.net/4/837/2007/>.
- Guidi, L., Stemann, L., Legendre, L., Picheral, M., Prieur, L., and Gorsky, G.: Vertical distribution of aggregates (>110 μm) and mesoscale activity in the Northeastern Atlantic: effects on the deep vertical export of surface carbon, *Limnol. Oceanogr.*, 52, 7–18, 2007.
- Guidi, L., Jackson, G. A., Stemann, L., Miquel, J. C., Picheral, M., and Gorsky, G.: Relationship between particle size distribution and flux in the mesopelagic zone, *Deep-Sea Res. Part. I*, 55, 1364–1374, 2008.
- Honjo, S., Doherty, K. W., Agrawal, Y. C., and Asper, V. L.: Direct optical assessment of large amorphous aggregates (marine snow) in the deep ocean, *Deep-Sea Res. Part. I*, 31, 67–76, 1984.
- Jackson, G. A., Maffione, R., Costello, D. K., Alldredge, A. L., Logan, B. E., and Dam, H. G.: Particle size spectra between 1 μm and 1 cm at Monterey Bay determined using multiple instruments, *Deep-Sea Res. Part. I*, 44, 1739–1767, 1997.
- Jackson, G. A. and Burd, A. B.: A model for the distribution of particle flux in the mid-water column controlled by subsurface biotic interactions, *Deep-Sea Res. Part. II*, 49, 193–217, 2002.
- Khelifa, A. and Hill, P. S.: Models for effective density and settling velocity of flocs, *J. Hydraul. Res.*, 44, 390–401, 2006a.
- Khelifa, A. and Hill, P. S.: Kinematic assessment of floc formation using a Monte Carlo model, *J. Hydraul. Res.*, 44, 548–559, 2006b.
- Longhurst, A.: Seasonal cycles of pelagic production and consumption, *Prog. Oceanogr.*, 36, 77–167, 1995.
- Longhurst, A. R., Bedo, A. W., Harrison, W. G., Head, E. J. H., and Sameoto, D. D.: Vertical flux of respiratory carbon by oceanic diel migrant biota, *Deep-Sea Res.*, 37, 685–694, 1990.
- Lutz, M., Dunbar, R., and Caldeira, K.: Regional variability in the vertical flux of particulate organic carbon in the ocean interior, *Global Biochem. Cy.*, 16, 1–15, 2002.
- Martin, J. H., Knauer, G. A., Karl, D. M., and Broenkow, W. W.: Vertex: carbon cycling in the Northeast Pacific, *Deep-Sea Res.*, 34, 267–285, 1987.
- Martinez, E. and Maamaatuaiahutapu, K.: Island mass effect in the Marquesas Islands: Time variation, *Geophys. Res. Lett.*, 31, L18307, doi:10.1029/2004GL020682, 2004.
- McCave, I. N.: Vertical flux of particles in the ocean, *Deep-Sea Res.*, 22, 491–502, 1975.
- Michaels, A. F. and Silver, M. W.: Primary production, sinking fluxes and the microbial food web, *Deep-Sea Res.*, 35, 473–490, 1988.
- Morel, A., Gentili, B., Claustre, H., Babin, M., Bricaud, A., Ras, J., and Tieche, F.: Optical properties of the “clearest” natural waters, *Limnol. Oceanogr.*, 52, 217–229, 2007.
- Morrison, J. M., Codispoti, L. A., Smith, S. L., Wishner, K., Flagg, C., Gardner, W. D., Gaurin, S., Naqvi, S. W. A., Manghnani, V., Prosperie, L., and Gundersen, J. S.: The oxygen minimum zone in the Arabian Sea during 1995, *Deep-Sea Res. Part. II*, 46, 1903–1931, 1999.
- Nodder, S. D., Duineveld, G. C. A., Pilditch, C. A., Sutton, P. J., Probert, P. K., Lavaleye, M. S. S., Witbaard, R., Chang, F. H., Hall, J. A., and Richardson, K. M.: Focusing of phytodetritus deposition beneath a deep-ocean front, Chatham rise, New Zealand,

- Limnol. Oceanogr., 52, 299–314, 2007.
- Noji, T. T., Bathmann, U. V., von Bodungen, B., Voss, M., Antia, A., Krumbholz, M., Klein, B., Peeken, I., Noji, C. I. M., and Rey, F.: Clearance of picoplankton-sized particles and formation of rapidly sinking aggregates by the pteropod, *Limacina retroversa*, J. Plankton Res., 19, 863–875, 1997.
- Raimbault, P., Garcia, N., and Cerutti, F.: Distribution of inorganic and organic nutrients in the South Pacific Ocean – evidence for long-term accumulation of organic matter in nitrogen-depleted waters, Biogeosciences, 5, 281–298, 2008, <http://www.biogeosciences.net/5/281/2008/>.
- Ras, J., Claustre, H., and Uitz, J.: Spatial variability of phytoplankton pigment distributions in the Subtropical South Pacific Ocean: comparison between in situ and predicted data, Biogeosciences, 5, 353–369, 2008, <http://www.biogeosciences.net/5/353/2008/>.
- Richardson, T. L. and Jackson, G. A.: Small phytoplankton and carbon export from the surface ocean, Science, 315, 838–840, 2007.
- Sarmiento, J. L. and Gruber, N.: Ocean Biogeochemical Dynamics, Princeton University Press, Princeton, Woodstock, UK, 503 pp., 2006.
- Steinberg, D. K., Van Mooy, B. A. S., Buesseler, K. O., Boyd, P. W., Kobari, T., and Karl, D. M.: Microbial vs. zooplankton control of sinking particle flux in the oceans twilight zone, Limnol. Oceanogr., 53, 1327–1338, 2008.
- Stemmann, L., Gorsky, G., Marty, J. C., Picheral, M., and Miquel, J. C.: Four-year study of large-particle vertical distribution (0–1000 m) in the NW Mediterranean in relation to hydrology, phytoplankton, and vertical flux, Deep-Sea Res. Part. II, 49, 2143–2162, 2002.
- Stemmann, L., Eloire, D., Sciandra, A., Jackson, G. A., Guidi, L., Picheral, M., and Gorsky, G.: Volume distribution for particles between 3.5 to 2000 μm in the upper 200 m region of the South Pacific Gyre, Biogeosciences, 5, 299–310, 2008, <http://www.biogeosciences.net/5/299/2008/>.
- Stramma, L., Johnson, G. C., Sprintall, J., and Mohrholz, V.: Expanding Oxygen-Minimum Zones in the Tropical Oceans, Science, 320, 655–658, 2008.
- Suess, E.: Particulate organic-carbon flux in the oceans – surface productivity and oxygen utilization, Nature, 288, 260–263, 1980.
- Thomas, A. C.: Seasonal distributions of satellite-measured phytoplankton pigment concentration along the Chilean coast, J. Geophys. Res.-Oceans, 104, 25 877–25 890, 1999.
- Volk, T. and Hoffert, M. I.: Ocean carbon pumps: analysis of relative strengths and efficiencies in ocean-driven atmospheric CO₂ changes, in: The carbon cycle and atmospheric CO₂: natural variations archean to present, Proceedings of the Chapman Conference on Natural Variations in Carbon Dioxide and the Carbon Cycle, Tarpon Springs, FL, USA, 9–13 January 1984, A86-39426 18–46, 1985.

Volume distribution for particles between 3.5 to 2000 μm in the upper 200 m region of the South Pacific Gyre

L. Stemmann^{1,2}, D. Eloire³, A. Sciandra¹, G. A. Jackson⁴, L. Guidi^{1,2}, M. Picheral¹, and G. Gorsky¹

¹Laboratoire d'Océanographie de Villefranche (LOV), Observatoire Océanologique, BP 28, 06234 Villefranche sur mer Cedex, France

²Université Pierre et Marie Curie-Paris6, UMR 7093, Villefranche sur Mer, 06234 France, Laboratoire d'Océanographie de Villefranche (LOV), Observatoire Océanologique, BP 28, 06234 Villefranche sur mer Cedex, France

³Plymouth Marine Laboratory, Prospect Place, Plymouth, PL1 3DH, UK

⁴Department of Oceanography, Texas A&M University, College Station, TX 77843, USA

Received: 12 September 2007 – Published in Biogeosciences Discuss.: 27 September 2007

Revised: 3 January 2008 – Accepted: 1 February 2008 – Published: 3 March 2008

Abstract. The French JGOFS BIOSOPE cruise crossed the South Pacific Gyre (SPG) on a transect between the Marquesas Islands and the Chilean coast on a 7500 km transect (8°S – 34°S and 8°W – 72°W). The number and volume distributions of small ($3.5 < d < 30 \mu\text{m}$) and large particles ($d > 100 \mu\text{m}$) were analysed combining two instruments, the HIAC/Royco Counter (for the small particles) and the Underwater Video Profiler (UVP, for the large particles). For the HIAC analysis, samples were collected from 12 L CTD Rosette bottles and immediately analysed on board while the UVP provided an estimate of in situ particle concentrations and size in a continuous profile. Out of 76 continuous UVP and 117 discrete HIAC vertical profiles, 25 had both sets of measurements, mostly at a site close to the Marquesas Islands (site MAR) and one in the center of the gyre (site GYR). At GYR, the particle number spectra from few μm to few mm were fit with power relationships having slopes close to -4 . At MAR, the high abundance of large objects, probably living organisms, created a shift in the full size spectra of particles such that a single slope was not appropriate. The small particle pool at both sites showed a diel pattern while the large did not, implying that the movement of mass toward the large particles does not take place at daily scale in the SPG area. Despite the relatively simple nature of the number spectra, the volume spectra were more variable because what were small deviations from the straight line in a log-log plot were large variations in the volume estimates. In addition, the mass estimates from the size spectra are very sensitive to crucial parameters such as the fractal dimension and the POC/Dry Weight ratio. Using consistent values for

these parameters, we show that the volume of large particles can equal the volume of the smaller particles. However the proportion of material in large particles decreased from the mesotrophic conditions at the border of the SPG to the ultra-oligotrophy of the center in the upper 200 m depth. We expect large particles to play a major role in the trophic interaction in the upper waters of the South Pacific Gyre.

1 Introduction

The size distribution of particles is a fundamental property of marine systems, affecting ecological trophic interactions, the vertical transmission of solar energy and the downward transport of organic matter. Despite its fundamental importance, size distribution is difficult to measure because particles occur over a large range of size and composition, from sub-micrometer compact particles to large, cm-sized loose aggregates. Accurate characterization of the entire size distribution requires instruments with resolution fine enough to characterize the small particles but sampling volumes large enough to capture the large, rare aggregates. Such observations of large aggregates must be made in situ because due to their fragile structures they are easily disrupted when retrieved for shipboard observation. Until recently, only the retrieval and analysis of the smallest size fraction ($d < 100 \mu\text{m}$) was feasible. The lack of technology hindered the detection and sizing of larger aggregates. However, recent development of optic and in situ imaging technologies makes the measurement of the complete particle size spectra more rapid. The datasets produced by these instruments could be used in biogeochemical studies to assess particle biomasses and fluxes.



Correspondence to: L. Stemmann
(stemmann@obs-vlfr.fr)

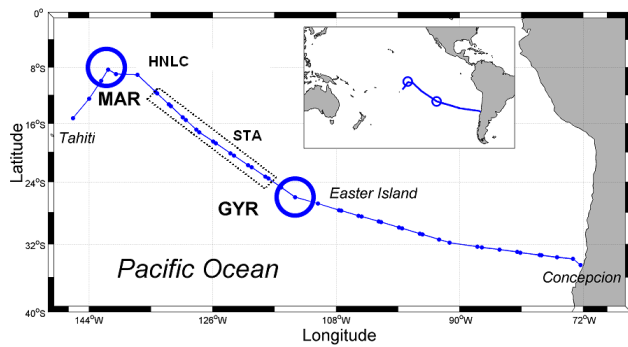


Fig. 1. Position of the short and long (large circle) stations during the BIOSOPE cruise.

Previous understanding was that the logarithm of particle concentration (expressed as a number spectrum) decreases almost proportionate to the logarithm of the particle diameter (d) with a slope of approximately 4 (Sheldon et al., 1972). Using this result, many authors have argued that there were equal volumes of living and non living particles in equal logarithmic size intervals for animals as large as the Loch Ness monster (Sheldon and Kerr, 1972). More recent analyses of a number spectra have combined different in situ instruments based on aperture impedance, imaging and optics (Jackson et al., 1995; Jackson et al., 1997; Mikkelsen et al., 2004). These observations of algal and detritic particles in both coastal waters and estuaries have challenged the above hypothesis. They show that most of the mass is found in aggregates larger than 100 μm and smaller than a few millimetres. To our knowledge, no particle size spectra for the range few μm to cm is yet available across surface oceans gyres.

The aims of the present study are to assess the vertical and temporal variability of the number and mass distributions of small ($3.5 < d < 30 \mu\text{m}$) and large particles ($d > 100 \mu\text{m}$) in the South Pacific Ocean. To do this, we analyse particle data from the French JGOFS BIOSOPE cruise that took place across the South Pacific Gyre (SPG). The size spectra of particles ranging from few μm to several mm were calculated from data collected using a HIAC/Royco Counter and the Underwater Video Profiler (Gorsky et al., 2000). With the observations, we were able to assess the contributions of both size fractions to the total biomass in different trophic conditions from the hyper-oligotrophic waters of the central gyre to the mesotrophic conditions of the Marquesas archipelago. In particular, we show the sensibility of the particle biomass assessment to the hypothesis made on the value of their porosity. The finding suggests that particle properties must be known before intensively using particle size spectra to assess biomass in biogeochemical studies.

2 Methods

2.1 Sampling sites

The French JGOFS BIOSOPE cruise sampled waters on a transect between the Marquesas Islands and the Chilean coast on a 7500 km transect (8°S – 34°S and 8°W – 72°W). The cruise was divided into two legs: Marquesas Archipelago (141°W , 8°S) to Easter Island (141°W , 26°S) and Easter Island to Concepcion, Chile (73°W , 35°S). Short duration stations (4 h, noted as STA for Leg 1 in Fig. 1) were located every 500 km and included measurement of biogeochemical and optical properties made by using 0–500 m vertical profiles of CTD-Rosette, optical devices, plankton nets. Three long duration stations during Leg 1 (4–5 days, noted as MAR, HNLC, GYR in Fig. 1) were located to sample contrasting systems more intensively by also using in situ pumps and sediment traps to collect particulate material. The particle size spectra from few μm to few mm were determined by combining data from a HIAC/Royco Counter and the Underwater Video Profiler (UVP). 76 UVP continuous casts during both Leg and 117 vertical discrete profiles for the HIAC (only during Leg 1) were performed. There were 25 UVP and HIAC combined profiles for Leg 1 and 15 combined profiles around the Marquesas Archipelago (MAR) and in the centre of the gyre near Easter Island (GYR). The profiles presented here are predominantly from MAR and GYR because of the additional information available from the time series measurements made there. Additional profiles are from the intermediate stations (5 profiles at HNLC, and 5 profiles at STA). MAR and GYR were chosen because they had the greatest difference in phytoplankton community structure and optical properties (Ras et al., 2007). The complete series of the UVP data from the upper 1000 m depth along the entire 8000 km transect are presented in (Guidi et al., 2008).

2.2 Particle-sizing instruments

Diameters d for particles $1.7 < d < 100 \mu\text{m}$ were determined on the ship using a HIAC/Royco particle counter (Pacific Scientific). The sensor's optical system (HRLD 400 HC) of the Hiac Counter (Model 3001) utilizes the principle of light-extinction for particle detection. The liquid sample flows through a sensor microcell where a laser beam is directed through a window at the sample. The light intensity is sensed by the light-extinction photodiode and used for automatic and continuous gain control of the sensor. When a particle is present within the sensor microcell, the particle blocks the laser beam from the photodetector. These pulses are proportional in amplitude to the light intensity of light extinction which is a measure of the particle size. The instrument reports the size as Equivalent Spherical Diameter (ESD). Size calibration is performed with latex beads of known size, but whose refractive index is greater than the refractive index of marine particles. Samples were collected from 12 L CTD

Rosette bottles and immediately analysed on board. The incidence of sample handling (rosette sampling in the water column, and sampling in the rosette) on the size spectra is difficult to evaluate. Because the total processing by the HIAC counter took approximately two hours for a 24 bottles rosette cast, the HIAC was placed on a rotating table to prevent particles falling to the bottom of sample bottles. Despite this, control tests showed that the concentration measured on the same seawater sample split among the 24 bottles of the device decreased by about 20%, presumably due to particle aggregation and/or dissolution during the counting. Surprisingly, this trend was not accompanied by a significant change of the particle size spectra slopes. The sequence of analysis always proceeded from shallowest to deepest samples, so that the measurements were systematically more biased for the latter. We have also examined the merging of Coulter and Hiac available size spectra in the size range where the two devices overlap. For most of the cases, the number spectra in this size range are similar for Hiac and Coulter. This may be an indirect indication that the sample manipulation for Hiac processing provides minimal bias. The final HIAC data for a given sample was calculated by averaging results from four 25 ml replicate measurements.

Larger particles ($d > 60 \mu\text{m}$) were enumerated in situ using the UVP. Two cameras of 732×570 pixel resolution and 12 Hz of frequency with different zoom lenses (25 and 8 mm) were positioned perpendicularly to an 8 cm thick light beam generated by two 54 W Chadwick Helmuth stroboscopes and took their images simultaneously. Only particles illuminated against a dark background were observable. The volumes sampled were 1.25 and 10.5 L for the high and low magnification cameras. The short flash duration (pulse duration = 30 μs) allowed a fast lowering speed (up to 1.5 m/s) without deterioration of image quality. The images of the UVP were analyzed after the deployment by custom-made software on a laboratory computer (Gorsky et al., 2000). Objects in each image were detected, sized and enumerated. The measurement is based on the lateral scattering of light from a particle; the instrument reports the particle size as a total number of pixels, which is converted to ESD. The UVP recorded images over the entire depth range that it was lowered, with one image acquired every 8 cm. In order to avoid contamination of the images by solar light, we have only used images obtained deeper than 40 m for day profiles.

We averaged UVP data collected within 2.5 m of the sampled depth to compare with samples collected with the Niskin sampler. Thus, the sampled volumes were effectively 100 ml, 75 L and 630 L for the HIAC and UVP (small and large zoom cameras) respectively in the Marquesas station. In the Gyre the UVP data were combined within 5 m of the depth because of the lower particle concentrations there, yielding sample volumes of 150 and 1260 L for the UVP cameras.

2.3 Calculating the number and mass size spectra

The particle size spectrum (n , particle number $\text{cm}^{-3} \text{cm}^{-1}$) is a useful description of the relationship between particle abundance and size. This relationship generally follows a power law function of the form:

$$n = bd^{-k} \quad (1)$$

where b is a constant, k the slope and d the particle diameter (Sheldon et al., 1972). The number spectrum, $n = dN/dd$, can be calculated from dN , the total number of particles per unit volume in a diameter range between d and $d+dd$ where dd is a small diameter increment.

Different instruments measure different particle properties and, hence, can give different estimates of particle diameter. For example, the Coulter Counter measures the change in electrical resistance when a particle passes through an orifice. The resistance is approximately proportional to the solid particle volume (the *conserved volume*) and excludes any water between the solid parts of an aggregate. The diameter of a sphere with that volume is the *conserved diameter*, d_c ; The diameter of the overall object, including any contained water is the *fractal diameter*, d_f . The two are related using fractal scaling (Jackson, 1990). For a solid object the two diameters are the same but they can be very different if the particle is porous, as marine aggregates are.

When we combine the data from the two instruments, we will discuss the possibility that the HIAC reports a conserved diameter and the UVP a fractal diameter. To convert between a number spectrum calculated using d_f (n_f) and one calculated using d_c (n_c) we use the following equation:

$$n_c = n_f \frac{dd_f}{dd_c} \quad (2)$$

The conversion of n_f to n_c requires a relationship between particle fractal diameter and conserved diameter. Fractal scaling provides such a relationship. The two key descriptors are an initial cell diameter d_1 and a fractal dimension for aggregates D_3 and the underlying hypothesis are that all aggregates are formed from the aggregation of a single type of particles (phytoplankton cells) and that the porosity of the aggregates is constant on the entire size spectra. To simplify the complexity of the natural assemblage of phytoplankton cells during the cruise, we assumed values of $d_1 = 5 \mu\text{m}$ because the nanophytoplankton were present at both sites. We have tested three different values of the fractal dimension (1.9, 2.3 and 3) for the conversion. The two first values have been estimated as being the minimum and average values obtained by comparing 118 UVP size spectra data obtained in different cruises with combined measured vertical flux in sediment traps using a Monte Carlo procedure (Guidi et al., 2008). This data set used to constrain the aggregate fractal dimension contains the sediment traps data of the BIOSOPE cruise. Using the vertical flux of particles to constrain the UVP size spectra is more accurate than using POC data because the

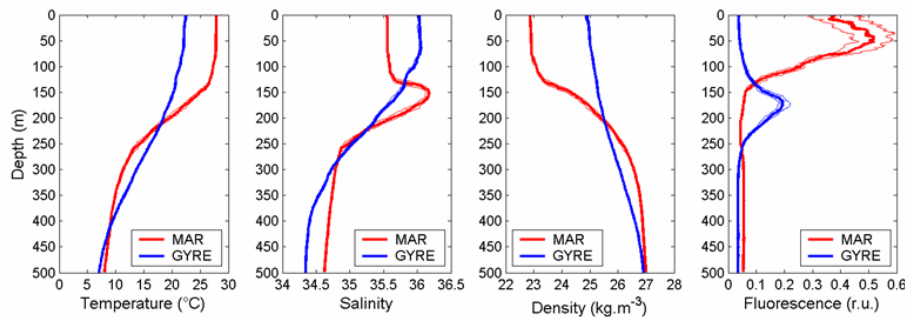


Fig. 2. Median, first quartile and third quartile of all verticals profiles of the CTD data at the MAR ($n=29$) and GYR sites ($n=35$). The hydrological parameters were (from left to right): temperature ($^{\circ}\text{C}$), salinity, density ($\text{kg}\cdot\text{m}^{-3}$) and fluorescence (relative unit).

main vectors of flux are the large settling aggregates. These fractal dimensions are within the range of previous estimates, which range from 1.3 to 2.49 (Jackson et al., 1997; Kilps et al., 1994; Li and Logan, 1995; Logan and Wilkinson, 1990; Xiaoyan and Logan, 1995). The value of 3 is the upper limit and occurs when porosity is constant with diameter. The conserved volume distribution can be calculated from n_c assuming a sphere. The total mass can be calculated knowing the density of the matter in the sphere. At all sites and depth, we use a constant cell density ($\rho=1.027\text{ g cm}^{-3}$) to estimate the total particle mass M .

$$M = \int_0^{\infty} n_c \rho \frac{4\pi}{3} \left(\frac{d_c}{2}\right)^3 dd_c \quad (3)$$

These values of dry weight (DW) can be converted to POC assuming POC=50% DW (Stramski et al., 2008; Alldredge, 1998) and compared to independent POC measurements. The samples for POC analysis were collected on precombusted (450°C) GF/F filters (25 mm in diameter) on board R/V l'Atalante. For each station at all sites, two depth layers were examined in two or three replicated samples. Volume of filtered seawater varied from 0.7 to 8.4 L depending on the station and the concentration of particulate matter in the water (Stramski et al., 2008).

2.4 Size range

The particle size spectra can be calculated by dividing the particle size range into sub-ranges called bins. The HIAC instrument has 50 bins having a log-normal size progression between 1.5 and $100\ \mu\text{m}$ while the UVP data process used for the BIOSOPE cruise has 27 bins having a log-normal size progression between 60 and $5000\ \mu\text{m}$. In the following, the particles ($<30\ \mu\text{m}$) detected by the HIAC instrument will be referred as small particles while the particles ($>100\ \mu\text{m}$) detected by the UVP will be referred as large particles. Number spectra with respect to the reported diameters were calculated by dividing the number concentration of particles in a section by the section width.

Both the HIAC and UVP techniques undersample particles at the lower end of their size ranges, producing anomalous peaks in size spectra. Therefore, we considered only the part of the spectra after the peaks. At the upper limit of the size range for any instrument, there are too few particles are present in a section to allow reliable estimates of particle concentrations, resulting in poor sampling statistics. Assuming that the number of particles within a section is described by a Poisson distribution, there is a counting error estimated as the square root of the mean number of particles in that section (Jackson et al., 2005). We excluded values with 4 or fewer particles within a section from our analysis to exclude counts with too high an uncertainty. As a result, the effective size ranges of both instruments were lower than the nominal size ranges; typically $3.5\text{--}30\ \mu\text{m}$ for the HIAC (instead of $1.7\text{--}100\ \mu\text{m}$) and $100\text{--}2000\ \mu\text{m}$ for the UVP (instead of $60\ \mu\text{m}\text{--}5000\ \mu\text{m}$). Note that the actual upper size limits of both instruments varied slightly as a function of the actual particles abundances. The slopes of the size spectra ($-k$) were calculated independently for the HIAC and UVP with values at either end of their size ranges excluded. In the following, the particles ($<30\ \mu\text{m}$) detected by the HIAC instrument will be referred as small particles while the particles ($>100\ \mu\text{m}$) detected by the UVP will be referred as large particles.

3 Results

3.1 Hydrography and biogeochemistry of the two sites (MAR and GYR)

In the MAR stations, surface waters were warm (up to 27°C) and relatively fresh (~ 35.6) (Fig. 2). The surface layer had a relatively constant temperature to 70–100 m depth. A subsurface fluorescence maximum developed at $\sim 60\ \text{m}$ in the mixed layer and corresponded to a measured maximum of $0.38\ \text{mg Chl-}a\ \text{m}^{-3}$ in the water bottle data (Table 1). There was greater salinity deeper than 100 m signifying the presence of more saline South Tropical Water (the maximum at

Table 1. Properties of the MAR and GYR sites.

	MAR	GYR
0–200 m integrated chlorophyll- <i>a</i> (mg m^{-2})	32.6 ± 2.72	20.56 ± 1.17
Maximum chlorophyll- <i>a</i> (mg m^{-3})	0.38 ± 0.05	0.17 ± 0.008
Maximum chlorophyll- <i>a</i> depth	55 ± 14 m	176 ± 9 m
Euphotic zone depth (<i>Ze</i>)	72 ± 5 m	160 ± 4 m
Mixed layer depth	85 ± 9 m	40 ± 31 m

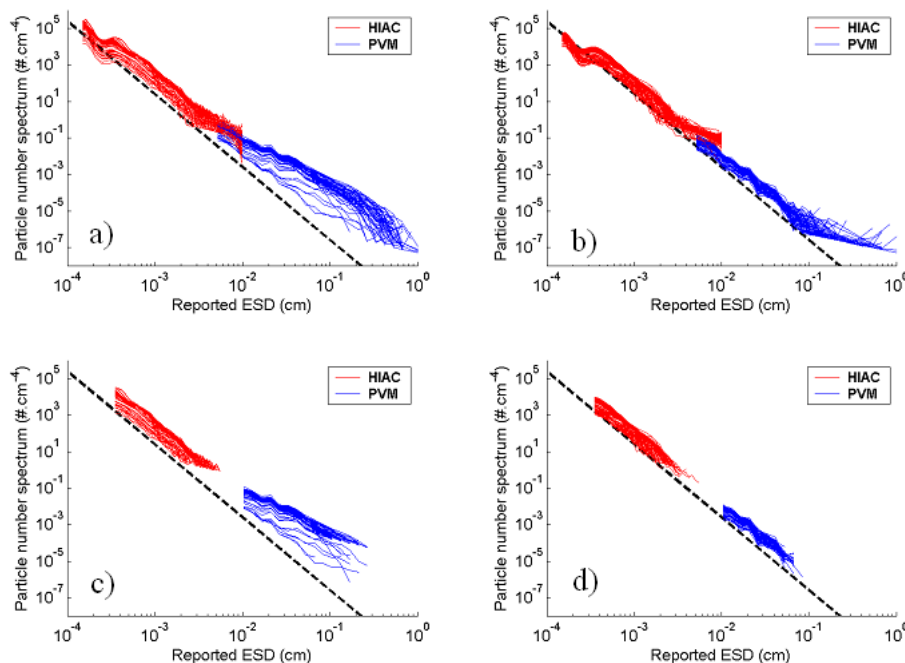


Fig. 3. All number spectra in the upper 200 m depth from the HIAC (red) and the UVP (blue) at the MAR site (a and c) and GYR site (b and d). (a) and (b) are the raw spectra while (c) and (d) are the lower and larger end truncated spectra to account for methodological biases. The slopes of the number spectra have been calculated using (c) and (d). These spectra were calculated using the particle diameters reported by the different instruments. The dashed reference line has a slope of -4 .

160 m). The mean depth of the euphotic zone in this region was 72 m.

The GYR stations differed by having higher surface salinity and lower surface temperature than MAR. The mixed layer was more poorly delimited than at the MAR stations. The GYR stations had extremely low levels of Chl-*a* fluorescence in the surface layer and a Deep Chlorophyll Maxima (DCM), $\sim 0.16 \text{ mg Chl-}a \text{ m}^{-3}$ at around 170 m depth. The mean depth of the euphotic zone in this region was 160 m (Table 1). The TS distributions were relatively constant at both MAR and GYR over the sampling period. The complete description of each site can be found in (Claustre et al., 2008).

3.2 Typical size spectra at GYR and MAR

The number spectra from both instruments at both sites followed the standard pattern of decrease in abundance with increasing reported diameter (Fig. 3). Raw spectra from both instruments show the typical biases at either end of their size ranges. The data follow a nearly straight line at GYR but not at MAR. In this latter site, the slope is not as steep in the size range covered by the UVP.

3.3 Distribution of particle concentrations and spectral slopes at the GYR site

The two instruments showed different vertical patterns for the two populations of particles (Fig. 4). The small particles detected by the HIAC showed higher concentrations in

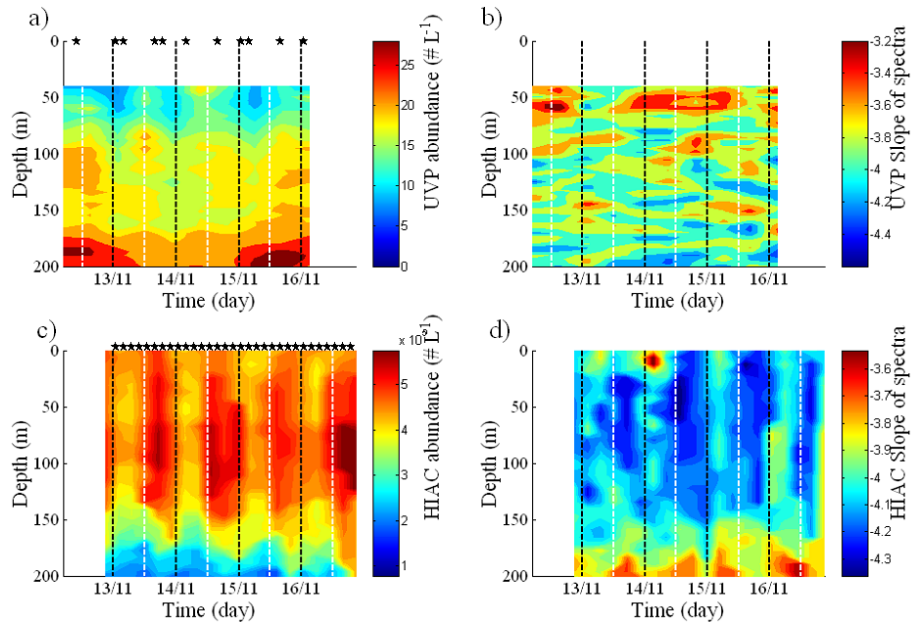


Fig. 4. Temporal distribution of the total particle abundance at the GYR site of the UVP (a) and HIAC (c) and particle slope of size spectra of the UVP (b) and HIAC (d). The black dashed lines indicate local mid-night time while the white dashed lines indicate local mid-day time. The sampling is indicated by the stars.

the upper 150 m with maxima at 100 m. In addition, they showed a strong diel cycle. The maximum of particle abundance occurred in the afternoon, around 4:30 p.m. Note that the attenuation coefficient at 660 nm, a proxy of the carbon concentration, presents exactly the same pattern of diel variation (Claustre et al., 2007a). These diel cycles were coupled with a diel cycle in the slopes of the size spectra. The average slopes over the HIAC size range were steeper during the afternoon around 4:30 p.m. and flatter during the night. The large particle concentrations estimated with the UVP were highest below 100 m depth. The diel variations observed for the small particle slopes were not detectable for the large particles in the UVP data below 40 m.

3.4 Distributions of particle concentrations and spectral slopes at the MAR site

Both large and small particle concentrations were greatest in the upper 80 m at MAR (Fig. 5). Small particles in the upper 75 m had diel cycles for concentration and slope. The pattern of this cycle was identical to that was observed at the GYR station. The large particles detected by the UVP did not show such diel cycles but there was a decrease in abundance and spectral slope after 28 October. The minimum slope was at 100 m depth on 27 October, but was at 140 m depth on 29 October. Note that the temporal decrease of large particles was accompanied by a decrease of the small particles. The spectral slopes of the large particles were lower ($2.3 < k < 2.5$) than those for the small particles ($3.9 < k < 3.7$) in the upper 200 m depth.

3.5 Frequency distributions of spectral slope

The spectral slope values for HIAC particles averaged about 4 during the day and 3.9 during the night at MAR (Fig. 6). At GYR, the small particles showed a double peak for the slope at day (3.95 and 3.7) and one peak at night (3.7). The slopes of 3.7 at day were from deeper than 150 m depth while those with a value of 3.95 were in the upper 100 m (see Fig. 4d). In contrast two distinct slope modes and no diel variation were observed for the large particles detected by the UVP, at values centered on 3.8 and 2.5, respectively for the GYR and MAR sites.

4 Discussion

4.1 Potential origin of particles

Neither the HIAC nor the UVP differentiated between living organisms and detrital material. Additional information collected during the cruise, including WP2 0–200 m vertical net samples (for mesozooplankton counted with the ZOOSCAN system (Grosjean et al., 2004)), microscopic counts of water samples, pigment characterization by HPLC and in situ optical properties, can provide insight to the nature of the particle making up the size spectra.

At GYR, the peak of small particles centered at 100 m was not associated with a peak of fluorescence although it corresponded to a peak of *Prochlorococcus* and a population of non vegetal particles (Grob et al., 2007). According to Grob et al. (2007), the proportion of vegetal particles

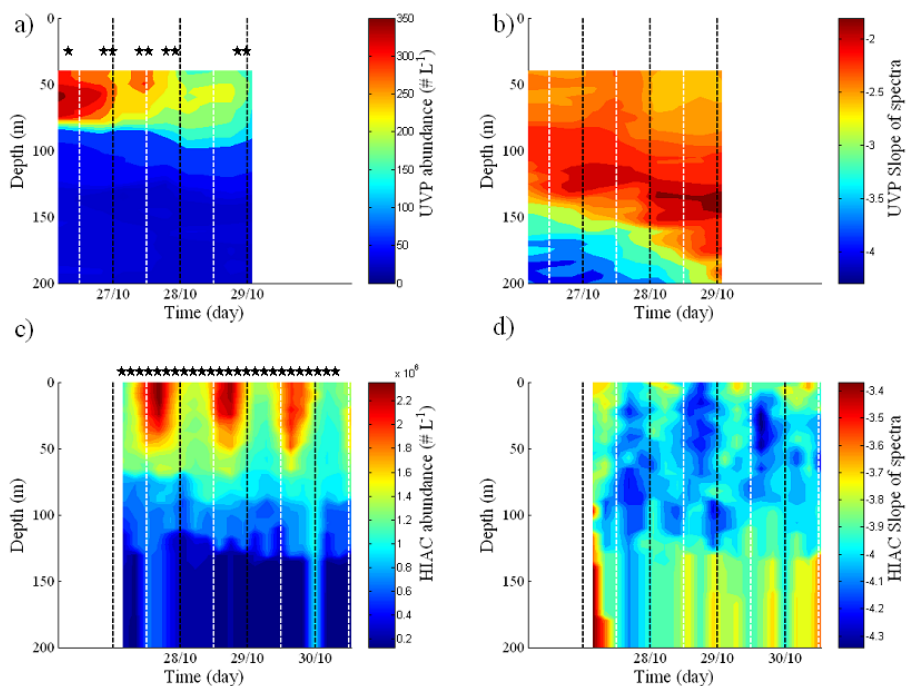


Fig. 5. Temporal distribution of the total particle abundance in the MAR site of the UVP (a) and HIAC (c) and particle slope of size spectra of the UVP (b) and HIAC (d). The black dashed lines indicate local mid-night time while the white dashed lines indicate local mid-day time. The sampling is indicated by the stars.

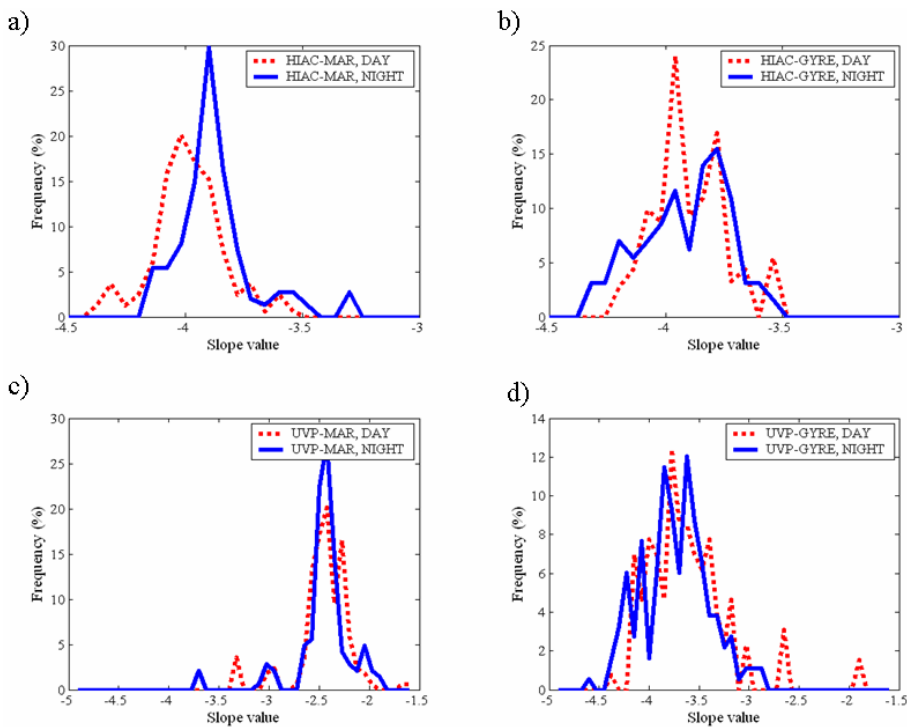


Fig. 6. Day and night frequency distribution of the spectral slopes for particle distributions determined by the HIAC (a) for MAR and (b) for GYR) and the UVP (c) for MAR and d) for GYR).

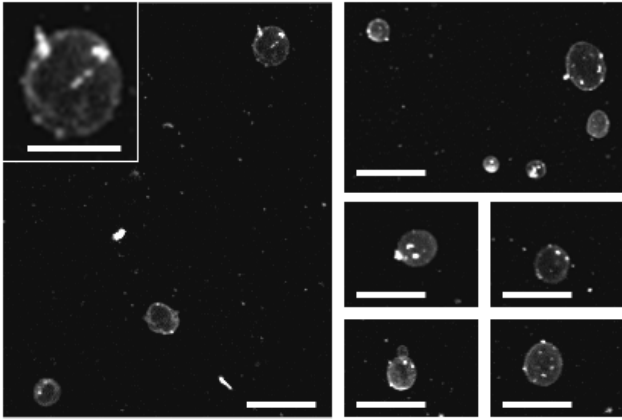


Fig. 7. UVP video images of the unidentified large objects at MAR. All the scale bars are 5 mm but the one in the upper left corner where it is 3 mm.

increased with depth and was the highest in the DCM. Algae in the DCM were mainly picophytoeukaryotes, although some coccolithophorid plates and diatom cells were also present (Beaufort et al., 2007; Gómez et al., 2007; Ras et al., 2007). The small particle did not show any peak in the DCM probably because the minimum size used to calculate the size spectra (3.5 μm) is larger than the dominant phytoplanktonic cells. The large particles had only one maximum in the DCM that was found in all profiles suggesting that the particles at 100 m depth were not a source of aggregates but that the active picophytoeukaryotes, coccolithophorid plates and diatom cells found in the DCM could be. The aggregates that form the material observed by the UVP could also be detritus produced by zooplankton because the Phaeophorbide pigment (a tracer for altered Chl-*a* found in faecal pellets) concentration also had a maximum in this layer (Ras et al., 2007). The large particles could not have been living mesozooplankton ($d > 200 \mu\text{m}$) because animal concentrations in the upper 200 m depth averaged less than 0.1 ind. L^{-1} (personal data) compared to the large particles estimates of 20 part. L^{-1} . In the MAR site, concentration of microphytoplankton ($10 < d < 100 \mu\text{m}$, mostly small pennate diatoms of the genus *Pseudonitzschia*) ranged from 1000 to 32 000 cells L^{-1} (Gómez unpublished data). These concentrations are in the same range as the HIAC counts for particles $d > 10 \mu\text{m}$ (5500 \pm 250 cells L^{-1}). Therefore, many of the particles larger than 10 μm detected by the HIAC in the MAR site were probably diatom cells. Aggregates of *Pseudonitzschia delicatissima* and large *Rhizosolenia bergonii* were observed from 50 to 100 m depth with concentrations of 2 to 20 aggregates L^{-1} and constituted some of the particles larger than $d > 100 \mu\text{m}$. Again, mesozooplankton were not an important fraction of the large particles because their concentrations in the upper 200 m layer were less than 1 ind. L^{-1} (personal data), compared to UVP particle concentrations as great as 100 part L^{-1} .

Most of the large object detected in the UVP images at MAR site were transparent disk-shaped objects with $d = 2\text{--}5 \text{ mm}$ present at concentrations of 1–10 L^{-1} (Fig. 7). They were located throughout the upper 200 m but had a maximum concentration between 120 and 170 m depth. These objects had different shapes than single celled or aggregated large diatoms such as the abundant *Rhizosolenia bergonii* and were not observed in the visual count of samples from Niskin bottles or plankton nets possibly because they had been destroyed during the sample processing. Their shapes are similar to those of large dinoflagellates, such as *Noctiluca*, but these objects are larger. They have not yet been identified but seem to be living organisms. They are mostly responsible for the smaller spectral slopes and the large calculated particle biomass at the MAR site deeper than 100 m. Their role and importance in the ecosystem remain unknown.

4.2 Uncoupled temporal dynamics of small and large particle pools

Small particles showed clear diel cycles in both total abundance and relative size distribution at both MAR and GYR that were not observed in particles detected by the UVP. At a first view, the variations in particle concentration (Figs. 4 and 5) and mean size (data not shown) do not support a phenomenon of autotrophic division where size normally increases during the day due to C fixation, and particle number increases at night due to cell division, although the variation of attenuation coefficient measured at the GYR and MAR stations clearly support diel cycle of C fixation (Claustre et al., 2008). In fact, the variations of particle abundance and size measured within a given size interval are difficult to interpret because they do not necessarily concern the same pools of particles. The unexpected increase of particle concentration observed during the day may correspond to the arrival in the interval of measurement of smaller growing particles, and not only to the division of particles belonging to this size range. This hypothesis is supported by the variations of the slope values which are steeper in the afternoon. The counts acquired with the Coulter counter in the range 0.7–5 μm clearly shows that diel variations of particle number and size obey to a process of cell divisions of picoeucaryotes (Sciandra, personal communication).

These diel variations were not observed in particles detected by the UVP. The fact that this pattern of variability was not observed for the pool of large particles suggests that the dynamics of small and large particles are disconnected at the diel scale. Diel cycles in the large particle spectra do occur (Graham et al., 2000; Lampitt et al., 1993; Stemmann et al., 2000). Explanations that have been proposed to explain them include the disaggregation (Dilling and Alldredge, 2000) or the fecal pellet production (Stemmann et al., 2000) by zooplankton engaged in their daily vertical migration and the periodic coagulation driven by diel cycles in turbulence (Ruiz, 1997). The diel change in the small particle pool is due to

cell division rather than diel biomass growth. The observation that they are uncoupled during the cruise suggests that this life cycle pattern of the phytoplankton cell does not lead to the formation of aggregates because processes in algae are not sufficient to move mass from the primary cells to larger aggregates for these short time scales and low particle concentrations. The diel vertical migration of total zooplankton was not observed in the net data and therefore could not affect the size spectra of the UVP particles.

4.3 Combining the HIAC and UVP size spectra

Care must be taken when comparing results from different instruments because they may not measure the same particle properties. Even the diameter reported by a single instrument can vary depending on the nature of the object (single cell versus aggregate). For example, aperture impedance particle counters, such as the Coulter Counter, measure a particle property that corresponds approximately to the volume of the solid mass composing a porous particle, while imaging instruments frequently measure the cross sectional area of the porous aggregate (Jackson et al., 1997).

The operational size range for the UVP is dominated by porous aggregates ($>60\ \mu\text{m}$). For this reason, it was calibrated with a variety of aggregates whose cross-sectional areas were determined using a stereo microscope. We denote the diameter reported by the UVP as a “fractal diameter”, d_f , because it is not proportional to a mass-equivalent spherical diameter but similar to the outer diameter of a fractal particle. In contrast, the HIAC works in a size range where there are solid single cells ($<20\ \mu\text{m}$) as well as porous aggregates ($>20\ \mu\text{m}$). Laboratory experiments performed on monospecific phytoplankton cultures have shown good agreement between mono-dispersed size distributions measured with HIAC and Coulter particle counters, although the diameters reported by the HIAC can be as much as 10% smaller than those from the Coulter counter. Multiple measurements made on different phytoplankton cultures with the HIAC showed very good agreement between the biovolume calculated assuming that the algae are spheres with the reported diameters and the particulate carbon concentration measured separately, suggesting that the light blockage is proportional to the mass content of the algae. Therefore, we consider the particle diameter reported by the HIAC to be an estimate of the “conserved” diameter, d_c .

However, the assumption that the HIAC reports a conserved diameter may not hold in the case of small aggregates for which the instrument could be respond to the fractal diameter. If we assume that the reported diameter is a fractal diameter and that $D_3=2.3$ then the number spectrum is shifted toward the small particle size compared to the case where d is a conserved diameter (Fig. 8). The explanation is that for a plain sphere, $d_c=d_f$ while for a porous sphere d_f is larger than d_c . As a result, the number spectrum is shifted toward larger size when $d=d_c$. Accordingly, there is

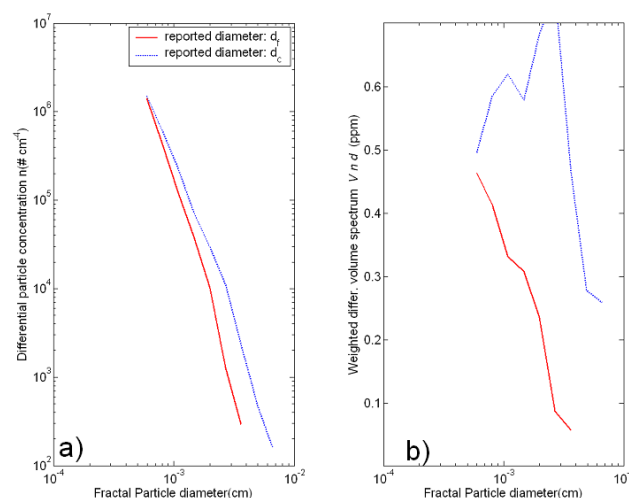


Fig. 8. (a) Number and (b) mass spectra calculated assuming that the HIAC reports a fractal diameter (d_f) and $D_3=2.3$ or a conserved diameter (d_c). The spectrum used in this figure was calculated as the median spectrum of all the samples at the GYR site.

more mass in solid sphere than in porous one of the same diameter and the mass spectrum shows an increase in mass when expressed in terms of d_c . The total HIAC mass is on average 2 times higher if we assume that $d=d_c$. Therefore, this assumption yields a maximum estimate of the total mass contained in the small particles.

We can calculate the mass distribution and a maximum estimate of the total volume of the aggregates using Eq. (3) and assuming that the HIAC reports a conserved diameter and that the UVP reports a fractal diameter. We will assume three fractal dimensions, 1.9, 2.3 and 3. Despite the relative straight nature of the number spectra when plotted using log-log axes, the mass spectra show greater variability because small deviations from the straight line induce large variations in the mass estimates. Therefore, the slope cannot be used to determine the mass distribution of marine particles although it can be a synthetic descriptor of the system. At the GYR site, the volume spectra of particles varied from a dominance of particles smaller than $100\ \mu\text{m}$ ($D_3=1.9$ and 2.3) to a dominance of larger particles ($D_3=3$) (Fig. 9). At the MAR site, the volume of the UVP particle in each bin is always much larger than the HIAC particles volume. The biovolume calculated using the different fractal dimensions varies by a factor of up to 20 showing the sensitivity of estimating the mass using particle size spectra.

The total mass of the HIAC particles should be similar to the total mass obtained from GF/F filtration but not the UVP particles because the sampling volume for the GFF filtration was too low to sample the large particles adequately. The HIAC POC estimates assuming that the HIAC reports a conserved diameter were higher than those measured independently by a factor of two. If we assume that the HIAC

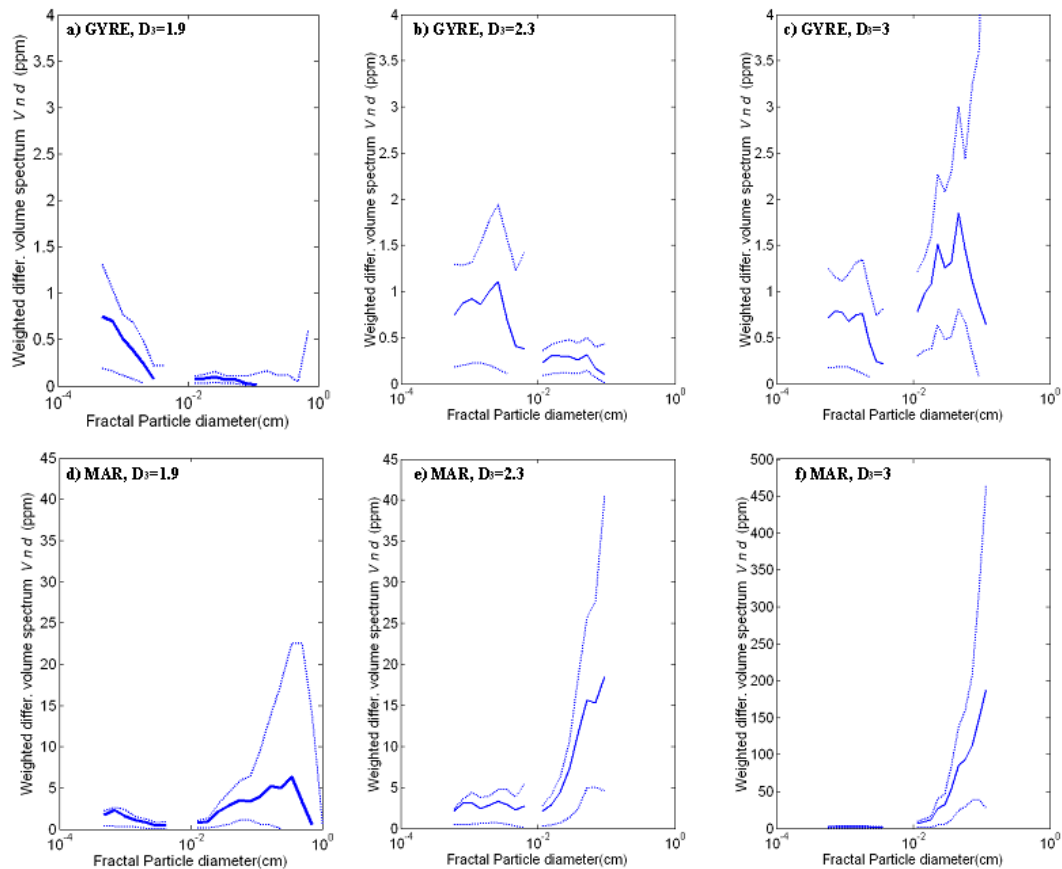


Fig. 9. Percentiles (5%, 50% and 95 %) of each size bin of the particle mass spectra for samples at the GYR site (**a**, **b** and **c** $n=87$) and MAR site (**d**, **e** and **f**, $n=85$). The 5 and 95 percentiles represent the envelope of the observed mass spectra. The area under a curve is the total particle solid volume concentration. The mass of large particles has been calculated using two values for the fractal dimension 1.9 (left column), 2.3 (centre column) and 3 (right column).

reports a fractal diameter, then the POC estimates are of the same range than those measured at 150 m depth with the lowest fractal dimension of 1.9 (Fig. 10). At 5 m, the biomass spectra always exceed the POC estimates. The changes with depth and also sites of the ratio between calculated and measured POC concentrations could also reflect change in the particle properties (higher porosity at surface for instance) that the model does not take into account because of the lack of information on particle properties. The mass dominance of the UVP particles at MAR site may be a methodological artefact because the basic hypothesis of a single relationship between particle mass and diameter is invalid. In that site, we observed a great number of large living objects with probably a lower volume to mass ratio than that of equal-diameter aggregates. This discrepancy highlights the need for a correct estimation of the particle properties when converting the particle size reported by any instrument to the particle mass, particularly if the particles are in fact aggregates for which the fractal and conserved diameter are not the same. Many reports assume that the particles are solid, implying $D_3=3$,

and probably overestimate the importance of the large particles in the mass distribution.

If we extend the mass spectra calculation (with $D_3=1.9$ and 2.3) to all the profiles with combined spectra collected during the cruise then we can estimate the importance of the two populations of particles across the upper 300 m depth of the South Pacific Gyre (Fig. 10). The mass concentrations of both particle populations decreased from the mesotrophic site of the HNLC to the ultraoligotrophic GYR following the trophic trend observed for phytoplankton and c_p (Ras et al., 2007; Grob et al., 2007). We can estimate that the proportion of mass contained in the large particles decreased from the mesotrophic conditions at the border of SPG to the ultraoligotrophy of GYR. However, at GYR site, the disproportion of mass between the two particle pool decreased with depth and using a $D_3=2.3$, the larger fraction equated the mass of the small particles deeper than 200 m depth (data not shown). Therefore, we expect large particles to play an equal or major role in the trophic interaction in the upper waters of the South Pacific Gyre.

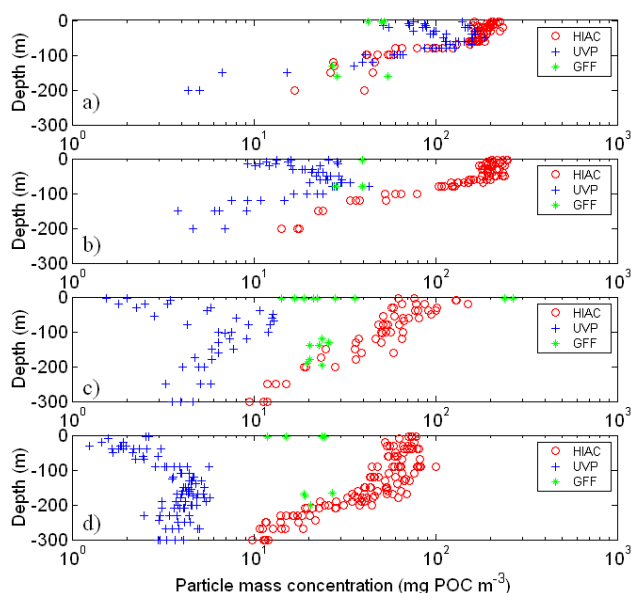


Fig. 10. Vertical profiles of particle mass for the HIAC and the UVP (with $D_3=1.9$ and assuming that both instruments report a fractal diameter) and GF/F POC content in the four sites investigated during the first leg of the BIOSOPE cruise, (a) MAR, (b) HNLC, (c) STA and (d) GYR. The same estimates were made using $D_3=2.3$ but the figures are not shown.

5 Conclusions

The particle size distribution from few μm to few mm cannot always be fit with a unique power relationship. At MAR, the high abundance of large probably living organisms created a shift in the full size spectra of particles. The small ($<30 \mu\text{m}$) and large ($>100 \mu\text{m}$) particle pools have different diel patterns. This implies that the exchange of mass toward the large particles does not take place at daily scale in the SPG area.

Care must be taken when comparing size spectra using different instruments that may not measure the same particle property. Knowing the geometric properties of the particles is crucial to calculate the mass from the particle size spectra because the mass estimates can change by several orders of magnitudes using different parameters to describe aggregates porosity. We show using consistent values to describe particle properties that the number spectra can provide realistic estimates of particle mass for regions where the particle population is composed of particles and aggregates. Using a fractal dimension of 1.9 and 2.3 to describe the porosity of the large aggregates, we calculated the total mass in the different regions of the SPG. Results show that the mass of large particles ($>100 \mu\text{m}$) can equal the mass in the smaller particles. Overall this study highlights the need for measures of particle properties to be able to use the size spectra in biogeochemical applications.

Acknowledgements. This work was supported by the French program PROOF (Processus Biogéochimiques dans l'Océan et Flux), Centre National de la Recherche Scientifique (CNRS), the Institut des Sciences de l'Univers (INSU) and the ZOOPNEC program, part of the French framework of the PNEC project. GJ's contribution was supported by NSF grants OCE-0352127 and OCE-0327644. L. Guidi was financially supported by Ministère de la l'Éducation et de la Recherche and CNRS (France). We also thank the scientific party and the Captain and crew of the RV L'Atalante during the BIOSOPE Expedition and D. Stramski, M. Babin, C. Crob and M. Twardowski who have contributed to the HIAC and POC measurements. We also thank the three reviewers for their useful comments.

Edited by: M. Dai

References

- Allredge, A.: The carbon, nitrogen and mass content of marine snow as a function of aggregate size, *Deep Sea Res. I*, 45, 529–541, 1998.
- Beaufort, L., Couapel, M., Buchet, N., and Claustre, H.: Calcite production by Coccolithophores in the South East Pacific Ocean: from desert to jungle, *Biogeosciences Discuss.*, 4, 3267–3299, 2007, <http://www.biogeosciences-discuss.net/4/3267/2007/>.
- Claustre, H., Huot, Y., Obernosterer, I., Gentili, B., Tailliez, D., and Lewis, M.: Gross community production and metabolic balance in the South Pacific Gyre, using a non intrusive bio-optical method, *Biogeosciences Discuss.*, 4, 3089–3121, 2007, <http://www.biogeosciences-discuss.net/4/3089/2007/>.
- Claustre, H., Sciandra, A., and Vaultot, D.: Introduction to the special section Bio-optical and biogeochemical conditions in the South East Pacific in late 2004: the BIOSOPE program, *Biogeosciences Discuss.*, 5, 605–640, 2008, <http://www.biogeosciences-discuss.net/5/605/2008/>.
- Dilling, L. and Allredge, A. L.: Fragmentation of marine snow by swimming macrozooplankton: A new process impacting carbon cycling in the sea, *Deep Sea Res. I*, 47, 1227–1245, 2000.
- Gómez, F., Claustre, H., Raimbault, P., and Souissi, S.: Two High-Nutrient Low-Chlorophyll phytoplankton assemblages: the tropical central Pacific and the offshore Per-Chile Current, *Biogeosciences*, 4, 1101–1113, 2007, <http://www.biogeosciences.net/4/1101/2007/>.
- Gorsky, G., Picheral, M., and Stemann, L.: Use of the underwater video profiler for the study of aggregate dynamics in the north Mediterranean, *Estuar. Coast. Shelf S.*, 50, 121–128, 2000.
- Graham, W. M., MacIntyre, S., and Allredge, A. L.: Diel variations of marine snow concentration in surface waters and implications for particle flux in the sea, *Deep-Sea Res. I*, 47, 367–395, 2000.
- Grob, C., Ulloa, O., Claustre, H., Huot, Y., Alarcón, G., and Marie, D.: Contribution of picoplankton to the total particulate organic carbon concentration in the eastern South Pacific, *Biogeosciences*, 4, 837–852, 2007, <http://www.biogeosciences.net/4/837/2007/>.
- Grosjean, P., Picheral, M., Warembourg, C., and Gorsky, G.: Enumeration, measurement, and identification of net zooplankton

- samples using the zooscan digital imaging system, *ICES J. Mar. Sci.*, 61, 518–525, 2004.
- Guidi, L., Gorsky, G., Claustre, H., Picheral, M., and Stemmann, L.: Contrasting distribution of aggregates $>100\ \mu\text{m}$ in the upper kilometre of the South-Eastern Pacific, *Biogeosciences Discuss.*, 5, 871–901, 2008, <http://www.biogeosciences-discuss.net/5/871/2008/>.
- Jackson, G. A.: A model for the formation of marine algal flocs by physical coagulation processes, *Deep-Sea Res. I*, 37, 1197–1211, 1990.
- Jackson, G. A., Logan, B. E., Alldredge, A. L., and Dam, H. G.: Combining particle size spectra from a mesocosm experiment measured using photographic and aperture impedence (coulter and elzone) techniques, *Deep-Sea Res. II*, 42, 139–157, 1995.
- Jackson, G. A., Maffione, R., Costello, D. K., Alldredge, A., Logan, B. E., and Dam, H. G.: Particle size spectra between $1\ \mu\text{m}$ and $1\ \text{cm}$ at monterey bay determined using multiple instruments, *Deep Sea Res. I*, 44, 1739–1767, 1997.
- Jackson, G. A., Waite, A. M., and Boyd, P. W.: Role of algal aggregation in vertical carbon export during soiree and in other low biomass environments, *Geophys. Res. Lett.*, 32, L13607, doi:13610.11029/12005GL023180, 2005.
- Kilps, J. R., Logan, B. E., and Alldredge, A. L.: Fractal dimensions of marine snow determined from image analysis of in situ photographs, *Deep Sea Res. I*, 41, 1159–1169, 1994.
- Lampitt, R. S., Hillier, W. R., and Challenor, P. G.: Seasonal and diel variation in the open ocean concentration of marine snow aggregates, *Nature*, 362, 737–739, 1993.
- Li, X. and Logan, B. E.: Size distributions and fractal properties of particles during a simulated phytoplankton bloom in a mesocosm, *Deep-Sea Res. II*, 42, 125–138, 1995.
- Logan, B. E. and Wilkinson, D. B.: Fractal geometry of marine snow and other biological aggregates, *Limnol. Oceanogr.*, 35, 130–136, 1990.
- Mikkelsen, O. A., Milligan, T. G., Hill, P. S., and Moffatt, D.: Insect – an instrumented platform for investigating floc properties close to the seabed, *Limnol. Oceanogr.-Methods*, 2, 226–236, 2004.
- Ras, J., Claustre, H., and Uitz, J.: Spatial variability of phytoplankton pigment distributions in the Subtropical South Pacific Ocean: comparison between in situ and predicted data, *Biogeosciences Discuss.*, 4, 3409–3451, 2007, <http://www.biogeosciences-discuss.net/4/3409/2007/>.
- Ruiz, J.: What generates daily cycles of marine snow?, *Deep-Sea Res. I*, 44, 1105–1126, 1997.
- Sheldon, R. W. and Kerr, S. R.: The population density of monsters in loch ness, *Limnol. Oceanogr.*, 17, 796–798, 1972.
- Sheldon, R. W., Prakash, A., and Sutcliffe Jr., W. H.: The size distribution of particles in the ocean, *Limnol. Oceanogr.*, 17, 327–340, 1972.
- Stemmann, L., Picheral, M., and Gorsky, G.: Diel variation in the vertical distribution of particulate matter ($>0.15\ \text{mm}$) in the nw mediterranean sea investigated with the underwater video profiler, *Deep Sea Res. I*, 47, 505–531, 2000.
- Stramski, D., Reynolds, R. A., Babin, M., Kaczmarek, S., Lewis, M. R., Röttgers, R., Sciandra, A., Stramska, M., Twardowski, M. S., Franz, B. A., and Claustre, H.: Relationships between the surface concentration of particulate organic carbon and optical properties in the eastern South Pacific and eastern Atlantic Oceans, *Biogeosciences*, 5, 171–201, 2008, <http://www.biogeosciences.net/5/171/2008/>.
- Xiaoyan, L. and Logan, B. E.: Size distributions and fractal properties of particles during a simulated phytoplankton bloom in a mesocosm, *Deep-Sea Res. II*, 42, 125–138, 1995.

Distribution of lipid biomarkers and carbon isotope fractionation in contrasting trophic environments of the South East Pacific

I. Tolosa¹, J.-C. Miquel¹, B. Gasser¹, P. Raimbault², C. Goyet³, and H. Claustre⁴

¹International Atomic Energy Agency- Marine Environment Laboratories, 4, quai Antoine 1er, MC 98000, Monaco

²Laboratoire d'Océanographie et de Biogéochimie (UMR 6535 CNRS), Centre d'Océanologie de Marseille, Université de la Méditerranée, Campus de Luminy, 13288 Marseille Cx 09, France

³BDSI, Université de Perpignan, 52 avenue Paul Alduy, 66860 Perpignan, France

⁴Laboratoire d'Océanographie de Villefranche, Observatoire Océanologique, INSU/CNRS/UPMC, UMR 7093, BP 08, F 06230 Villefranche-sur-Mer, France

Received: 28 November 2007 – Published in Biogeosciences Discuss.: 18 December 2007

Revised: 6 May 2008 – Accepted: 27 May 2008 – Published: 30 June 2008

Abstract. The distribution of lipid biomarkers and their stable carbon isotope composition was investigated on suspended particles from different contrasting trophic environments at six sites in the South East Pacific. High algal biomass with diatom-related lipids (24-methylcholesta-5,24(28)-dien-3 β -ol, C₂₅ HBI alkenes, C_{16:4} FA, C_{20:5} FA) was characteristic in the upwelling zone, whereas haptophyte lipids (long-chain (C₃₇-C₃₉) unsaturated ketones) were proportionally most abundant in the nutrient-poor settings of the centre of the South Pacific Gyre and on its easter edge. The dinoflagellate-sterol, 4 α -23,24-trimethylcholest-22(*E*)-en-3 β -ol, was a minor contributor in all of the studied area and the cyanobacteria-hydrocarbon, C₁₇ *n*-alkane, was at maximum in the high nutrient low chlorophyll regime of the subequatorial waters near the Marquesas archipelago.

The taxonomic and spatial variability of the relationships between carbon photosynthetic fractionation and environmental conditions for four specific algal taxa (diatoms, haptophytes, dinoflagellates and cyanobacteria) was also investigated. The carbon isotope fractionation factor (ϵ_p) of the 24-methylcholesta-5,24(28)-dien-3 β -ol diatom marker, varied over a range of 16‰ along the different trophic systems. In contrast, ϵ_p of dinoflagellate, cyanobacteria and alkenone markers varied only by 7–10‰. The low fractionation factors and small variations between the different phytoplankton markers measured in the upwelling area likely reveals uniformly high specific growth rates within the four phyto-

plankton taxa, and/or that transport of inorganic carbon into phytoplankton cells may not only occur by diffusion but also by other carbon concentrating mechanisms (CCM). In contrast, in the oligotrophic zone, i.e. gyre and eastgyre, relatively high ϵ_p values, especially for the diatom marker, indicate diffusive CO₂ uptake by the eukaryotic phytoplankton. At these nutrient-poor sites, the lower ϵ_p values for haptophytes, dinoflagellates and cyanobacteria indicate higher growth rates or major differences on the carbon uptake mechanisms compared to diatoms.

1 Introduction

The sustainability of phytoplankton growth in the world ocean is basically controlled by three factors: nutrient abundance, light availability and the response of phytoplankton to these sources (Falkowski, 1984; Falkowski et al., 1998; Irwin et al., 2006; Litchman et al., 2006). The variability of these factors and their role in biogeochemical processes emerge from the properties of the surface mixed layer. Hence, eutrophic areas, such as upwellings, with continuous nutrient supply to the euphotic zone differ strongly from areas with a permanently nutrient-depleted surface layer. In these areas, e.g. oceanic gyres, a deep pycnocline prevents surface waters from a supply with deeper, more nutrient-rich waters.

Photosynthesis is a major biogeochemical process where carbon dioxide and water are converted into organic carbon with the presence of light. The fate of this organic carbon is therefore intimately linked to the conditions of its synthesis and depends strongly on the composition of the



Correspondence to: I. Tolosa
(i.tolosa@iaea.org)

phytoplankton assemblages. Studying these issues provides essential information for understanding the global marine carbon cycle. In addition to the now widely used chlorophyll and pigment analysis (Barlow et al., 1993; Claustre et al., 2004; Mackey et al., 1996), field data about phytoplankton diversity might also be acquired by the distribution of accessory lipid biomarkers. They provide important information on the phytoplankton composition complementary to that of algal pigments, as well as on the relative importance of carbon sources from heterotrophic bacteria and other zooplankton (Dijkman and Kromkamp, 2006; Pinturier-Geiss et al., 2002; Tolosa et al., 2004).

Isotopic characterization of marine organic matter can provide insight into the conditions under which carbon fixation occurs contributing to the understanding of the global marine carbon cycle. The carbon isotopic composition ($\delta^{13}\text{C}$) of any photosynthetic product and its derived carbon isotope fractionation factor (ϵ_p) reflects the $\delta^{13}\text{C}$ of the carbon source utilized and the modification by the processes and environmental variables involved in its production: growth rate, temperature, dissolved CO_2 , cell geometry, irradiance, etc. (Burkhardt et al., 1999a, b; Eek et al., 1999; Hayes, 1993; Laws et al., 1997; Popp et al., 1998b; Rau et al., 1996). For example, high growth rates of the phytoplankton are linked to high $\delta^{13}\text{C}$ values, i.e. they are enriched in ^{13}C (Bidigare et al., 1999; Laws et al., 1995). However, they become depleted in ^{13}C with increasing concentration of dissolved CO_2 (Burkhardt et al., 1999a; Riebesell et al., 2000). This latter linkage seems to be limited in its extent, and differences of $\delta^{13}\text{C}$ higher than 1–2‰ cannot be explained any more by the change in the CO_2 concentration, but they are rather accounted for by differences in the growth rates of the phytoplankton and in the carbon uptake mechanisms (Bidigare et al., 1997; Burkhardt et al., 1999b; Benthien et al., 2007). Since particulate organic carbon (POC) is a complex mixture of autotrophs, heterotrophs, and detritus, potentially clearer relationships between $\delta^{13}\text{C}$ values and environmental conditions can be obtained using specific biomarkers derived from particular species or taxonomic groups (Bidigare et al., 1999; Pancost et al., 1999; Pancost et al., 1997), compared to the $\delta^{13}\text{C}$ of the bulk POC (Rau et al., 2001; Woodworth et al., 2004). This has become possible with compound-specific isotope-ratio mass spectrometry (Freeman et al., 1990; Hayes et al., 1990).

Our field study uses molecular and stable carbon isotopic ratios of specific lipid biomarkers to evaluate their organic sources and to explore variations in the biogeochemistry of the particulate organic matter in different hydrodynamic and trophic environments from the South East Pacific. These include the eutrophic upwelling area off the Chilean coast, the mesotrophic and HNLC regions south of the equatorial current and the oligotrophic South Pacific Gyre, which was the major focus of this work. The major questions being addressed are:

1. What is the spatial distribution of lipid biomarkers of phyto-, zooplankton and bacteria in the contrasting trophic environments of the South East Pacific?
2. What is the variability of the carbon isotope fractionation (ϵ_p) of different phytoplankton taxa in relation to different environmental conditions characterized by nutrient and dissolved inorganic carbon concentrations, and by productivity regimes? We discuss these results with respect to the processes of carbon uptake and assimilation within the different phytoplankton groups.

2 Materials and methods

2.1 Sampling

Sampling and hydrographic observations were carried on board R/V “L’Atalante” between October and December 2004 and were organized within the framework of the BIOSOPE (Biogeochemistry & Optics South Pacific Experiment) project which is part of the French JGOFS oceanographic programme PROOF. The main hydrodynamical and trophic features for the different zones are described in Claustre et al. (2008).

Samples were taken at six different sites, so called “long stations”, between Tahiti and the Chilean coast (Table 1). The different explored zones exhibited contrasting trophic environments. First, a mesotrophic area downstream of the Marquesas Islands (MAR) and a high nutrient low chlorophyll zone (HNL) upstream of the Islands. Second, an extremely oligotrophic area, very poor in nutrients, located in the centre of the South Pacific Gyre (GYR) and a less oligotrophic site in the east of the gyre (EGY). At the end of the transect, we studied a eutrophic zone highly enriched in nutrients and associated to the upwelling off the Chilean coast (UPW and UPX). UPW station was farther from the coast than UPX and exhibited a more important water stratification.

“Challenger Oceanics” in-situ pumps were used to filter large volumes (400 to 900 liters) of water in the upper 300 m of the water column, to collect suspended particles through a Nitex screen of 70 μm and a precombusted (550 °C) Microquartz filter (QMF, Sartorius) of 1 μm pore size. Only the size fraction collected on the microquartz filter (1–70 μm) was analysed.

2.2 Bulk measurements

Table 2 summarizes the bulk biochemical parameters of the suspended particulate matter along the transect Marquesas Islands-Chilean coast.

Total CO_2 (C_T) and total alkalinity (A_T) of water samples were measured by potentiometry (Azouzi et al., 2007) at all sites except UPW. The dissolved CO_2 concentration was calculated from C_T , alkalinity, temperature, salinity and the

Table 1. Sampling sites.

DATE	Lat.(° S)	Long. (° W)	ACRONYM	Brief description
28/10/2004	8.4	141.3	MAR	Marquesas Islands characterized by high nutrients high chlorophyll
1/11/2004	9.0	136.8	HNL	High nutrient low chlorophyll area east of the Marquesas Islands
12/11/2004	25.6	114.0	GYR	Center of the South Pacific Gyre
28/11/2004	31.8	91.4	EGY	Eastern border of the Gyre
6/12/2004	34.0	73.3	UPW	Upwelling area situated above the abyssal plain
10/12/2004	34.5	72.4	UPX	Upwelling area situated above the continental shelf

Table 2. Selected environmental parameters from the six sites at the sampled depths.

locations-depth (m)	T °C	density Kg m ⁻³	A _T ^a $\mu\text{mol Kg}^{-1}$	C _T ^b $\mu\text{mol Kg}^{-1}$	[CO ₂](aq) $\mu\text{mol Kg}^{-1}$	NO ₃ $\mu\text{mol l}^{-1}$	PO ₄ $\mu\text{mol l}^{-1}$	SiOH ₄ $\mu\text{mol l}^{-1}$	POC $\mu\text{mol l}^{-1}$	Chl a $\mu\text{g l}^{-1}$	t _p ^c hours	PAR ^d (%)
mar3-50 m	27.7	22.9	2363	2024	11.3	1.59	0.28	1.03	1.96	0.41	12.4	2.7
mar3-100 m	26.9	23.2	2356	2052	13.1	3.81	0.39	1.73	0.90	0.21		0.55
mar3-300 m	11.3	26.6	2313	2225	34.7	8.83	0.61	2.66	0.28	0.05		
hnl2-75 m	27.3	23.2	2353	2009	11.0	1.69	0.37	1.18	1.60	0.30	12.4	2.0
hnl1-100 m	26.8	24.5	2382	2097	14.3	1.04	0.50	1.88	0.90	0.26		0.64
hnl2-300 m	11.2	26.6	2319	2238	37.2	31.6	2.39	14.45	0.23	0.05		
gyr2-0 m	22.0	24.6	2364	2048	11.9	0.00	0.12	0.88	0.39	0.03	13.3	100
gyr2-75 m	21.9	25.1	2369	2055	11.8	0.00	0.14	1.04	0.51	0.06		7.5
gyr2-125 m	20.7	25.2	2363	2051	11.7	0.00	0.12	0.96	0.49	0.13		2.5
gyr2-150 m	20.3	25.3	2358	2057	12.1	0.00	0.12	0.71	0.48	0.18		0.97
gyr2-175 m	19.6	25.4	2347	2074	13.3	0.10	0.14	0.71	0.49	0.20		0.32
gyr2-200 m	18.7	25.5	2333	2075	14.1	1.11	0.19	0.79	0.36	0.17		
gyr2-300 m	13.9	26.0	2299	2099	17.2	8.06	0.81	1.93	0.12	0.04		
egy4-70 m	16.5	25.4	2294	2033	12.9	0.53	0.21	1.34	0.95	0.19	13.9	3.6
egy2-200 m	14.5	25.8	2271	2071	16.6	2.96	0.41	1.50	0.25	0.04		
egy4-300 m	10.0	26.4	2267	2119	21.8	15.4	1.07	3.99	0.23	0.03		
upw1-40 m	12.8	25.9				13.0	0.91	8.00	6.92	2.50	14.3	0.15
upw1-100 m	10.8	26.4				28.1	2.6	20.8	1.83	0.07		
upw2-300 m	8.7	26.8				39.0	2.8	33.0	1.03	0.08		
upx3-40 m	12.0	26.0	2274	2197	37.4	22.8	2.02	10.7	3.28	0.79	14.4	0.52
upx2-100 m	10.5	26.4	2294	2258	52.4	23.2	2.32	24.4	1.25	0.11		
upx2-300 m	10.0	26.7	2307	2281	56.0	35.3	3.5	27.9	0.56	0.07		

^a Total alkalinity; ^b Total CO₂; ^c day length; ^d normalised underwater irradiance

concentrations of silicate and phosphate using the CO2SYS program developed for CO₂ system (Lewis and Wallace, 1998). This program is based on equations of the seawater CO₂ system (DOE, 1994) and the dissociation constants of Goyet and Poisson (1989).

Nutrient concentrations (nitrate, phosphate and silicate) were determined onboard using an autoanalyzer (Raimbault et al., 2008). Analysis of organic carbon was done with a "Vario EL" elemental analyser (© elementar Analysensysteme GmbH) after acidification of the filter subsamples fol-

lowing the procedure described in Miquel et al. (1994). The photosynthetically active radiation (PAR) in water was measured using a calibrated hyperspectral profiling radiometer (HyperPro, Satlantic, Inc).

2.3 Lipid extraction

Filters containing the suspended particles were spiked with internal standards (*n*-C₂₄D₅₀, anthracene-*d*₁₀, pyrene-*d*₁₀, perylene-*d*₁₂, friedeline, 5 α -androstane-3 β -ol and cholan-

acid), and extracted by microwave oven with 40 ml of a mixture with $\text{CH}_2\text{Cl}_2/\text{MeOH}$ (3:1) at 70°C for 15 min. Isolation of the neutral and acid lipid fractions were done following the method of Tolosa and de Mora (2004). Extractable lipids were saponified using 1 ml KOH 6% in methanol/water (80:20) plus 1 ml of Milli-Q water (80°C , 1 h). Then the neutral fraction was recovered with *n*-hexane and subject to fractionation by HPLC on a normal phase column (Nucleosil column, $20\text{ cm}\times 0.4\text{ cm}$ i.d. $5\ \mu\text{m}$) to isolate the aliphatic hydrocarbons (F1), polycyclic aromatic hydrocarbons (F2), ketone compounds (F3) and sterol and alcohol fraction (F4). Saponified solutions were acidified with 1 ml HCl 6N to pH 2 and the fatty acids obtained by hydrolysis of wax esters, triacylglycerols, steryl esters and phospholipids were extracted with hexane:ethyl acetate 9:1.

2.4 Gas chromatography

The sterol fraction was treated with *bis*-(trimethylsilyl)-trifluoroacetamide (BSTFA) ($200\ \mu\text{l}$, 70°C , 1 h) to convert the alcohols and sterols to their corresponding trimethylsilyl ethers. The acid fraction was derivatised by transesterifying the lipid extract with $500\ \mu\text{l}$ of 20% BF_3 in methanol at 80°C for 1 h.

Gas chromatography (GC) was performed with a Hewlett Packard HP5890 series II equipped with a flame ionization detector and split/splitless injector. Two fused silica capillary columns were employed: (A) a DB-5 fused silica capillary column ($30\text{ m}\times 0.25\text{ mm}$ i.d.; film thickness $0.25\ \mu\text{m}$) for neutral compounds and fatty acids and (B) a BPX-70 (SGE, $60\text{ m}\times 0.32\text{ mm}\times 0.5\ \mu\text{m}$) for the fatty acids. Helium was the carrier gas (1.2 ml min^{-1}). The oven temperature for the DB-5 was programmed from 60°C (0.5 min hold) to 290°C at 6°C min^{-1} . The GC oven for the BPX-70 column was programmed from 60°C (0.5 min hold) to 250°C at 6°C min^{-1} . Injector and detector temperatures were 270°C and 320°C , respectively.

Aliphatic hydrocarbons, ketones, sterols and fatty acids were quantified by internal standards ($\text{C}_{24}\text{D}_{50}$, friedeline, 5α -androstane- 3β -ol, and cholic acid, respectively). Confirmation of peak identity was obtained using GC with mass spectrometric detection (GC-MS) (Hewlett-Packard 5889B MS "Engine") operated in the electron impact at 70 eV .

2.5 Compound-specific isotope analysis

The lipid biomarkers were analyzed for their stable carbon isotope composition using an HP 5890 GC equipped with a HP 7673 autoinjector and interfaced through a combustion furnace with a FINNIGAN MAT Delta C isotope ratio mass spectrometer (GC/C/IRMS).

The GC/C/IRMS was equipped with a 100% methylpolysiloxane fused silica column (Ultra-1, $50\text{ m}\times 0.32\text{ mm}$ i.d.; $0.5\ \mu\text{m}$ film thickness) pre-connected with a press-fit connector (Supelco, France) to a 0.32 mm

i.d. deactivated fused silica capillary retention gap of 5 m . Injections of $2\ \mu\text{l}$ in iso-octane were made via an on-column injector. The GC oven was programmed from 60 to 100°C at $10^\circ\text{C min}^{-1}$, then to 310°C at 4°C min^{-1} and maintained at 310°C for 40 min. Values reported were determined by at least in triplicate to calculate the average and standard deviation. All $\delta^{13}\text{C}$ values are reported in the delta notation relative to the Pee Dee Belemnite (PDB) standard as follows:

$$\delta^{13}\text{C} = [({}^{13}\text{C}/{}^{12}\text{C})_{\text{sample}}/({}^{13}\text{C}/{}^{12}\text{C})_{\text{PDB}} - 1] \times 10^3 \quad (1)$$

Corrections for the isotopic change introduced in the derivatisation of sterols, fatty alcohols, and fatty acids were determined through derivatisation of standards of known isotopic composition and applying the equation of Jones et al. (1991). Cholesterol, methanol, 18:0 fatty acid and 18:0 FAME of known isotopic carbon composition (measured by elemental analyser coupled to isotope ratio mass spectrometer), were used to calibrate the GC/C/IRMS and correct the isotopic change introduced by the derivatisation. The surrogate standards, 5α -androstane- 3β -ol, cholic acid and the GC internal standard friedelin of known isotopic composition served as internal isotopic standards.

The precision (standard deviation) for most analytes with GC-C-IRMS signals higher than 0.5 V ($m/z\ 44$) was comparable to the instrument specifications (0.5‰). As it is illustrated in Appendix A, the major compound 24-methylcholesta- $5,24(28)$ -dien- 3β -ol ($\text{C}_{28}\Delta^{5,24(28)}$) stanol was integrated together with their minor stanol pair compound (24-methyl- 5α -cholest- $24(28)$ -en- 3β -ol) to yield a single $\delta^{13}\text{C}$ value for both compounds, because of incomplete chromatographic separation.

2.6 Calculations of carbon isotope fractionation (ε_p) and sensitivity study

Molecular ε_p was determined following the general Eq (2) outlined in Freeman and Hayes (1992):

$$\varepsilon_p = [(\delta^{13}\text{CO}_2 + 1000)/(\delta^{13}\text{C}_{\text{pp}} + 1000) - 1] \times 10^3 \quad (2)$$

where CO_2 is its dissolved phase in the water column and C_{pp} the primary photosynthate.

In this study, direct measurement of $\delta^{13}\text{CO}_2$ was not available. Therefore $\delta^{13}\text{CO}_2$ was calculated according to the Eq. (3) of Mook (1974):

$$\varepsilon_b = [(\delta^{13}\text{CO}_2 + 1000)/(\delta^{13}b + 1000) - 1] \times 10^3 = 24.12 - 9866/T \quad (3)$$

where ε_b is the temperature-dependent carbon isotope fractionation of dissolved CO_2 with respect to bicarbonate, T is the absolute temperature in Kelvin, and the reference value of δ^{13} for bicarbonate (b) in sea surface water was taken as +1.5‰ (Quay et al., 2003). We adopt this constant value of δ^{13} bicarbonate for all sites and depths based on (a) the low variability of $\delta^{13}\text{DIC}$ reported for the surface waters of the global ocean, including Pacific (1.55‰), Atlantic (1.56‰)

an Indian Ocean (1.37‰) (Quay et al., 2003), (b) the major contribution of bicarbonate in the total DIC pool (90% of the total) and c) the low variability of $\delta^{13}\text{C}$ DIC in the upper water column (Kroopnick, 1985). Although meridional $\delta^{13}\text{C}$ DIC variability is generally greater than zonal variability, surface $\delta^{13}\text{C}$ DIC in the Pacific ocean varied only by 0.3‰ over the latitudes of the studied area. However, field data of $\delta^{13}\text{C}$ DIC in the Peru upwelling region ranged from -0.65 to 0.81 ‰ (Pancost et al., 1997, Bidigare et al., 1997) whereas in the other areas of the Pacific, it ranged from 1.20 to 1.85 ‰ (Bidigare et al., 1997). Based on the upper and lower bound values of $\delta^{13}\text{C}$ DIC, ε_p might have a maximum range variation of 2‰ whereas a typical variation of ± 0.5 ‰ results in a variation of ± 0.7 ‰ for ε_p . Therefore, $\delta^{13}\text{C}$ DIC do not seem to have major influence on the changing isotopic compositions of organic matter in the upper water column of the ocean, and the likely lower $\delta^{13}\text{C}$ DIC values for the upwelling site would only accentuate the differences between the trophic environments, providing lower ε_p values for the upwelling sites.

$\delta^{13}\text{C}_{\text{pp}}$ (primary photosynthate) for eukaryotic organisms was calculated by using a constant isotopic fractionation of 4.2‰ between photosynthetic lipids and algal biomass. This value has been provided by Popp et al. (1998a) for alkenones and has been used by other authors (Bidigare et al., 1997; Benthien et al., 2002; Harada et al., 2003; Benthien et al., 2005; Popp et al., 2006a). Similarly, we adopted this value for the isoprenoid compounds, e.g. phytol and sterols, used in previous papers (Pancost et al., 1997; Pancost et al., 1999; Bidigare et al., 1999), thus allowing a comparison of ε_p calculated in the present study. However, the offset in $\delta^{13}\text{C}$ values for common lipids relative to the $\delta^{13}\text{C}$ value of biomass might vary considerably between microalgal species, biosynthetic pathways, the site of reactions in the cell (Schouten et al., 1998; Hayes 2001), and by variations in the relative amounts of the major biochemicals in the cell (i.e., proteins, carbohydrates, and lipids) which in addition have different $\delta^{13}\text{C}$ values. Thus, lower isotopic offsets between lipids and total biomass are expected to occur in nutrient limited environments where higher cellular lipid contents relative to proteins and carbohydrates are found (Livne and Sukenik, 1992). This variability might accentuate the range of ε_p between the trophic environments, with higher ε_p values in low-nutrient waters compared to high-nutrient environments. Potential variations of ± 1 ‰ in the isotopic shift between the algal biomass and lipids might result in ε_p variations of ± 1 ‰.

Culture studies of haptophytes have identified an isotopic shift ranging from 3.1 to 5.3‰ between primary photosynthate and alkenone biomarkers (Laws et al., 2001; Riebesell et al., 2000; Jasper and Hayes, 1990; and Popp et al., 1998). In contrast to alkenones, the isotopic offset between algal biomass and other eukaryotic lipid biomarkers is less constrained with reported offsets ranging from -2 to 8 ‰ for different cultures of phytoplankton taxa (Schouten et al., 1998; Hayes, 2001). If we consider the upper and lower

bound values of offsets found for phytol (-0.8 to 4.2 ‰) and diatom sterols (0.6 to 6.4 ‰) in marine diatom cultures, the extreme values of ε_p for phytol and diatom sterols differ by 5 and 6‰ respectively. One reported culture of dinoflagellate exhibited an isotopic fractionation between dinosterol and algal biomass of 4.5‰ (Schouten et al., 1998).

For prokaryote, $\delta^{13}\text{C}_{\text{pp}}$ was estimated from the *n*-heptadecane assuming a constant isotopic fractionation between photosynthetic lipids and algal biomass of 8.4‰ reported by Sakata et al. (1997).

2.7 Estimations of growth rates and intracellular carbon demand in haptophytes assuming purely CO_2 diffusion uptake

Carbon isotopic fractionation for phytoplankton (ε_p) which obtain CO_2 by passive diffusion is summarized by the expression of Popp et al. (1998b):

$$\varepsilon_p = \varepsilon_f - \beta \frac{\mu(V/S)}{[\text{CO}_2]} \quad (4)$$

where ε_f is the fractionation associated with the enzyme-catalyzed carbon fixation step, β is a constant, μ is the specific growth rate, V and S are the volume and surface area of the alga cells and $[\text{CO}_2]$ is the concentration of dissolved CO_2 external to the algal cell. Since β and (V/S) are practically constant for haptophyte taxa, we can transform this constant to the variable *b*-value ($\% \mu\text{mol}$), which serves as a proxy for growth rate and reflects the intracellular carbon demand. This *b*-value was calculated following the Eq. (5) of Bidigare et al. (1997):

$$b = (\varepsilon_f - \varepsilon_p) \times [\text{CO}_2]_{\text{aq}} \quad (5)$$

with ε_f values of 25‰ for eukaryotic algae utilizing Rubisco and β -carboxylase enzymes (Bidigare et al., 1997) and $[\text{CO}_2]_{\text{aq}}$ calculated as described in Sect. 2.2.

Specific growth rates (μ , (d^{-1})) of alkenone producing haptophytes were estimated with the following equation found by Bidigare et al. (1997) in laboratory chemostat culture experiments of *Emiliania huxleyi*:

$$\mu_{cc} = (25 - \varepsilon_p)[\text{CO}_2]/138 \quad (6)$$

and applying the corrections for the effects of day length and respiration on growth rate

$$\mu = [\mu_{cc}/(24/t_p)]0.8 \quad (7)$$

where μ is the 24-h average growth rate, t_p is day length or photoperiod in hours, and the factor 0.8 adjusts the growth rate for dark respiration.

3 Results and discussion

The analytical scheme used in this study identified and quantified ~ 60 individual compounds in the neutral lipid fraction and ~ 40 compounds in the acid fraction. A summary

Table 3. Summary of the lipid biomarkers discussed in this study.

ACRONYM	COMPOUND NAME(S)	Main diagnostic (and minor) sources	References
Phytol	3,7,11,15-tetramethyl-2-hexadecen-1-ol	Phototrophic organisms	(Baker and Louda, 1983)
$\text{C}_{28}\Delta^{5,24(28)}$	24-methylcholesta-5,24(28)-dien-3 β -ol	Diatoms (flagellates)	(Volkman and Hallegraeff, 1988)
C_{25} HBI	Highly branched isoprenoids of C_{25}	Diatoms (flagellates)	(Volkman et al., 1994)
$\text{C}_{16:4}$ FA	6,9,12,15-hexadecatetraenoic acid ($\text{C}_{16:4(n-1)}$)	Diatoms	(Dijkman and Kromkamp, 2006)
$\text{C}_{20:5}$ FA	5,8,11,14,17-eicosopentaenoic acid ($\text{C}_{20:5(n-3)}$)	Diatoms (flagellates)	(Dijkman and Kromkamp, 2006; Volkman et al., 1989)
Total alkenones	Long-chain (C_{37} - C_{39}) unsaturated ketones	Haptophytes/Prymnesiophyceae	(Conte et al., 1995; Volkman et al., 1995)
$\text{C}_{30}\Delta^{22}$, (dinosterol)	4 α -23,24-trimethylcholesta-22(E)-en-3 β -ol	Dinoflagellates	(Robinson et al., 1984)
n - C_{17}	C_{17} n -alkane	Cyanobacteria (green algae)	(Han and Calvin, 1969; Winters et al., 1969)
n -alcohols	n -alkanols, mainly n - C_{14} , n - C_{16} and n - C_{18}	Zooplankton and marine invertebrates (algae)	(Sargent et al., 1977).
$\text{C}_{20:1} + \text{C}_{22:1}$ FA	Long-chain monounsaturated $\text{C}_{20:1}$ and $\text{C}_{22:1}$ FA	Herbivorous mesozooplankton	(Lee et al., 2006)
Branched FA	<i>iso</i> and <i>anteiso</i> branched fatty acids in the carbon number range 15-19.	Heterotrophic bacteria	(Kaneda, 1991)
$\text{C}_{27}\Delta^5$, (cholesterol)	Cholest-5-en-3 β -ol	Zooplankton (algae)	(Volkman, 1986)
Phytosterols	Includes: 27-nor-24-methylcholesta-5,22(E)-dien-3 β -ol; cholesta-5,22(E)-dien-3 β -ol; 24-methylcholesta-5,22(E)-dien-3 β -ol; $\text{C}_{28}\Delta^{5,24(28)}$; 24-ethylcholesta-5,22(E)-dien-3 β -ol; 24-ethylcholest-5-en-3 β -ol and $\text{C}_{30}\Delta^{22}$	Eukaryotic phototrophic organisms	(Muhlebach and Weber, 1998; Tolosa et al., 2003)

of selected lipid biomarkers discussed in this study together with their main sources is shown in Table 3. In particular, we focus on the long-chain unsaturated methylketone ($\text{C}_{37:2}$ alkenone) which is a marker for certain haptophyte algae (Conte et al., 1995, Volkman et al., 1995), the $\text{C}_{28}\Delta^{5,24(28)}$ sterol and HBI which are major components in many diatom (Volkman and Hallegraeff, 1988, Volkman et al., 1994), the dinosterol mainly derived from dinoflagellates (Robinson et al., 1994) and the n - C_{17} alkane derived from cyanobacteria and green algae (Han and Calvin, 1969, Winters et al., 1969). We note, however, that HBIs are not markers for all diatom species since they are mainly synthesized by centric (*Rhizosolenia* species) and pennate diatoms (*Haslea*, *Navicula* and *Pleurosigma*), whereas $\text{C}_{28}\Delta^{5,24(28)}$ sterol has also been found in some dinoflagellates and green algae (Volkman, 1986). Therefore, there might be an offset between the

diatom sterols and the HBIs depending on the diatom species composition. In a similar way, all diatoms do not produce the $\text{C}_{28}\Delta^{5,24(28)}$ sterol, and dinosterol can also be present in certain diatoms (Volkman et al., 1986). Considering that the particle size fraction studied was 1–70 μm , a certain discrimination of bacterial, diatom and zooplankton biomarkers compared to coccolithophorid and dinoflagellate markers might have occurred. Concentrations of the selected lipid biomarkers are summarized in Table 4 and their concentrations normalized to the POC are shown in Appendix B1. The individual carbon isotope ratio for some of the selected lipid biomarkers are shown in Appendix C1. The complete data set of concentrations and $\delta^{13}\text{C}$ values is available on the BIOSOPE Database: <http://www.obs-vlfr.fr/proof/vt/op/ec/biosope/bio.htm>

Table 4. Selected lipid biomarkers concentrations (ng l^{-1}) in suspended particles from the South Pacific Ocean.

locations-depth (m)	phytol	$\text{C}_{28}\Delta^{5,24(28)}$	C_{25} HBI	$\text{C}_{16:4}$ FA	$\text{C}_{20:5}$ FA	Total alkenones	$\text{C}_{30}\Delta^{22}$	$n\text{-C}_{17}$	$n\text{-alcohols}$	$\text{C}_{20:1}+\text{C}_{22:1}$ Branched FA	$\text{C}_{27}\Delta^5$	
mar3-50 m	31	20	2.32	33	98	6.5	4.4	0.13	6.7	2.8	22	13
mar3-100 m	7.0	4.7	0.02	18	36	3.7	0.0	0.04	35	6.7	31	6.7
mar3-300 m	0.60	3.0	0.00	0.0	9.7	0.0	0.0	0.00	9.5	9.3	2.1	1.1
hnl2-75 m	25	30	0.80	29	62	16	5.7	0.25	7.3	2.3	19	13
hnl1-100 m	21	15	0.07	22	54	8.8	4.0	2.3	16	1.7	3.4	24
hnl2-300 m	0.60	1.1	0.00	0.0	5.5	0.0	0.4	0.00	10	0.47	1.2	3.8
gyr2-0 m	1.7	1.9	0.21	1.4	8.2	14	1.6	0.00	12	0.00	4.6	3.7
gyr2-75 m	2.3	1.9	0.02	1.4	7.2	18	1.7	0.13	4.0	0.52	2.5	2.7
gyr2-125 m	5.6	3.2	0.03	2.4	16	23	2.0	0.26	4.2	0.79	3.2	4.5
gyr2-150 m	9.6	3.8	0.15	5.9	25	16	1.1	0.29	7.5	0.46	4.6	5.7
gyr2-175 m	9.9	4.0	0.18	3.8	16	13	0.8	0.32	7.4	0.33	5.2	3.5
gyr2-200 m	12	6.5	0.41	3.9	21	6.9	1.5	0.19	9.8	0.87	5.3	7.0
gyr2-300 m	0.60	0.3	0.00	0.0	2.2	0.0	0.1	0.00	1.6	0.11	0.7	0.9
egy4-70 m	16	20	1.40	17	57	20	2.8	1.2	12	1.7	10	15
egy2-200 m	2.0	2.8	0.00	0.0	13	1.5	0.6	0.67	9.6	0.27	4.7	7.3
egy4-300 m	0.60	1.4	0.00	0.0	9.4	0.5	0.6	0.00	7.0	0.00	3.1	5.6
upw1-40 m	103	55	3.69	139	379	27	9.7	0.23	34	15.8	114	36
upw1-100 m	24	15	0.09	15	106	7.0	3.9	0.28	34	2.5	30	20
upw2-300 m	2.8	2.5	0.00	0.0	24	2.0	0.8	0.08	41	1.1	10	13
upx3-40 m	79	33	2.29	26	143	12	6.1	0.18	90	7.8	57	55
upx2-100 m	26	15	0.75	8.0	101	2.3	3.8	0.16	10	1.4	30	16
upx2-300 m	5.7	5.2	1.73	16	72	1.1	1.0	0.00	215	2.6	9.4	23

3.1 Distribution of phytoplankton, zooplankton and bacterial markers in different trophic environments

Concentrations of phytol, a non-specific marker for phototrophic organisms, if compared at the depth of chlorophyll and POC maxima, were highest at the upwelling sites with 102 ng l^{-1} at UPW and 78 ng l^{-1} at UPX. The mesotrophic sites, MAR and HNL, exhibited intermediate phytol concentrations of 25 to 31 ng l^{-1} . The lowest values were measured at the oligotrophic sites, EGY (16 ng l^{-1}) and in particular at GYR (11 ng l^{-1}), where maximum values of chlorophyll and POC were at 175 m depth. Concentrations of diatom biomarkers, e.g. ($\text{C}_{28}\Delta^{5,24(28)}$ sterol, C_{25} HBI alkenes, $\text{C}_{16:4}$ FA, $\text{C}_{20:5}$ FA), haptophytes biomarkers (total alkenones) and dinoflagellates markers (dinosterol) exhibited a similar distribution as phytol concentrations (Table 4), except in the Gyre where alkenones and dinosterol peaked at shallower depths than phytol and diatom markers.

Highest concentrations of long-chain C_{37} and C_{38} alkenones were measured at the eutrophic UPW site (27 ng l^{-1}) but also at the two gyre sites EGY (20 ng l^{-1}) and GYR (23 ng l^{-1}). These peak values corresponded to the depth of chlorophyll and POC maxima except for the GYR site where the peak was situated at 125 m depth, above the chlorophyll maximum but within maximum POC concentrations. A much lower concentration (6.5 ng l^{-1}) was

recorded at the MAR site. These values are much lower than those reported for suspended particles from the Bering Sea after blooms of *Emiliana huxleyi* and ranging from 0.15 to $3.12 \mu\text{g l}^{-1}$ (Harada et al., 2003), but similar to concentrations observed in suspended particles collected under non-bloom conditions in the surface waters of the North Atlantic and Nordic Sea (Sicre et al., 2002), in the western Sargasso Sea (100 ng l^{-1}) (Conte et al., 2001) and in the oligotrophic North Pacific subtropical gyre ($0.5\text{--}15 \text{ ng l}^{-1}$) (Prahl et al., 2005).

The C_{17} n -alkane, which is produced by aerobic photosynthetic bacteria and green algae (Han and Calvin, 1969; Winters et al., 1969) exhibited a maximum concentration of 2.3 ng l^{-1} , below the chlorophyll and POC maxima at the HNL site and of 1.2 ng l^{-1} at the same depth (70 m) as chlorophyll and POC maxima at the EGY site. The other sites showed concentration levels below 0.5 ng l^{-1} (Table 4). These concentrations were consistent with the abundance distribution of prokaryotic phototrophic organisms, with high abundances at the HNL and EGY sites (Grob et al., 2007).

In all samples, the n -alkanols were dominated by the short-chain fatty alcohols of even carbon number ($n\text{-C}_{14}$, $n\text{-C}_{16}$ and $n\text{-C}_{18}$), which are associated to zooplankton markers (Sargent et al., 1977). With the exception of the two gyre sites (GYR and EGY), maximum concentrations of linear

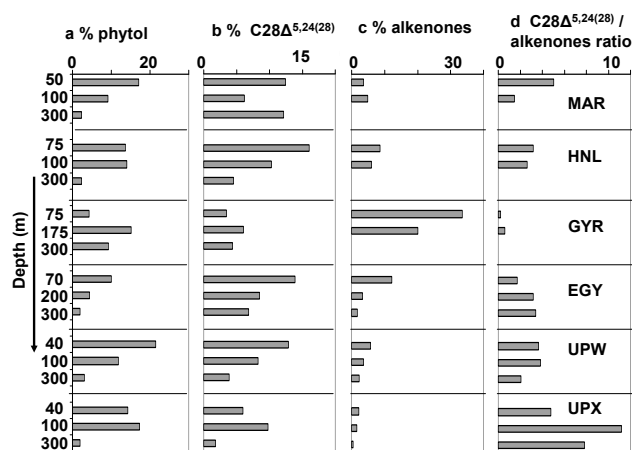


Fig. 1. Percentage contribution of selected lipid biomarkers and biochemical indices: (a) percentage of phytol relative to total neutral lipid concentrations, (b) percentage of 24methylcholesta5,24(28)-dien3 β ol relative to total neutral lipids concentrations; (c) percentage of total alkenones relative to total neutral lipid concentrations; (d) Ratio of 24methylcholesta5,24(28)-dien3 β ol to total alkenones to evaluate the relative contribution of diatoms vs. haptophytes.

alcohols were found below the depth of chlorophyll and POC maxima, at the upwelling sites (UPW, UPX) at 300 m and at the Marquesas sites (MAR, HNL) at 100 m depth. In the Gyre, maximum concentrations of *n*-alcohols coincided with the phytol maximum, though another peak (11.6 ng l⁻¹) was registered at the surface of the GYR site. The fatty acids C_{20:1} and C_{22:1}, typical markers of herbivorous mesozooplankton (Graeve et al., 1994, Dalsgaard et al., 2003, Lee et al., 2006), exhibited the highest concentrations at the upwelling sites (UPW, UPX) at the depth of chlorophyll and POC maxima, but also below the euphotic zone (300 m) at the MAR and UPX sites.

Similar to the phytol distribution, the concentrations of bacterial biomarkers, such as branched fatty acids, were highest at the UPW site (Table 4), whereas the concentrations of zooplankton markers, such as cholesterol and *n*-alcohols exhibited higher abundance at UPX. In general, heterotrophic bacterial populations seemed to be associated to diatom biomass, which is supported by the positive correlation between the $\delta^{13}\text{C}$ of the branched fatty acid (*i*-C₁₅ FA) and the $\delta^{13}\text{C}$ of the C_{20:5} FA ($r=0.81$, $p<0.05$).

Some more insight into the phytoplankton distribution may be gained by comparing the relative contribution of the biomarkers within the total neutral lipids, or normalizing their concentrations to the POC content (Appendix B1). Since both approaches provided similar trends, we used the first approach for our discussion illustrated in Fig. 1. The percentage of phototrophic biomarkers generally followed the chlorophyll and POC distribution except at UPX, where phytol and diatom markers peaked at 100 m depth. Also at HNL, phytol showed relatively high percentages i.e. was enriched

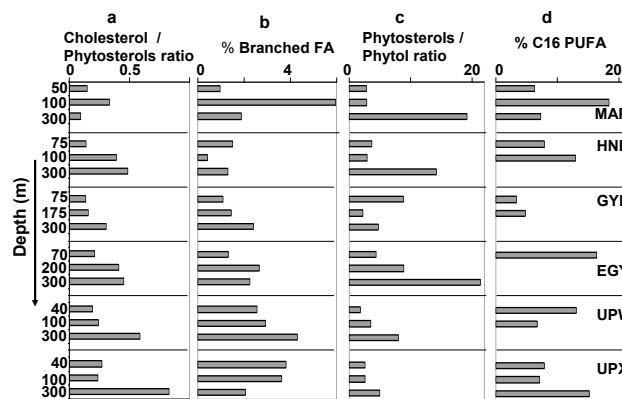


Fig. 2. Values of selected biochemical indices to elucidate the dominant sources in the suspended particles from the different sites. (a) Cholesterol/phytosterols^a ratio to evaluate the relative contribution of zooplankton vs. algal. (b) % Bacterial fatty acid indicator is the sum of all *iso* and *anteiso*- branched chain fatty acids expressed as percent of total fatty acids. (c) Phytosterols/phytol ratio to elucidate the degradation state of the phytoplankton material. (d) % C₁₆ PUFA is the polyunsaturation index of C₁₆ fatty acids to evaluate the ecophysiological state of the marine diatoms.

^a Phytosterols are listed in Table 3.

in the POC, down to 100 m depth. This may be related to the highest relative importance of diatom sterol observed in the euphotic layer (Fig. 1b) and to the presence of diatoms which formed “balls of needles” or clusters (Gómez et al., 2007). In contrast to the diatom biomarkers, the percentage of total alkenones was by far highest in the gyre especially above the chlorophyll maximum (Fig. 1c), where also the concentrations were among the highest of all sites (Table 4). Prymnesiophytes were likely to be the major constituents of eukaryotic phytoplankton in the gyre, suggesting that haptophytes are well adapted to the low nitrate concentrations prevailing in the oligotrophic zone of the Pacific Gyre. Although the lipid content and composition of microalgae can be affected by changes in environmental conditions such as nutrient status, light intensity and temperature (Shifrin and Chrisholm, 1981; Reitan et al., 1994), the C₂₈Δ^{5,24(28)} sterol/alkenones ratio may provide us with an overview on the relative contribution of C₂₈Δ^{5,24(28)} sterol-producing diatoms to alkenone-producing prymnesiophytes. Highest ratios were obtained at the UPX site, and in particular below the euphotic zone. Alkenone-producing haptophytes predominated over diatoms at the GYR site, especially above the chlorophyll maximum whereas the diatom signal showed a deeper maximum at 175 m corresponding to the maximum of both phytol and chlorophyll-*a*. Dinosterol showed overall low percentages (<3%) or concentrations normalized to POC (<0.37 mg g⁻¹C), which indicated a minor contribution of dinoflagellates in the algal mixture of these Pacific waters. The highest dinosterol values were recorded in the HNL as it was also confirmed by pigment

analyses (Ras et al., 2008).

Figure 2 illustrates other diagnostic biomarkers indices to evaluate the relative dominance of zooplankton and bacterial sources within each site as well as the state of the particulate material in the different zones. Although cholesterol is also present in many classes of algae, it is considered a typical marker for zooplankton derived organic matter supply because its concentration becomes enriched after passing the organisms in relation to the algal diet (Harvey et al., 1987). Therefore, the relative abundance of cholesterol over phytosterols has been used as a relative indicator of zooplankton over phytoplankton abundance (Muhleback and Weber, 1998; Tolosa et al., 2003). Here, the cholesterol/phytosterol ratio increased with depth at all sites, and in particular at UPX. This was consistent with the substantial concentrations of *n*-alcohols and zooplanktonic $\text{C}_{20:1}$ and $\text{C}_{22:1}$ fatty acids found at 300 m depth. At most of the sites, the relative importance of bacterial fatty acids was higher below than at the depth of chlorophyll maximum. A contrasting image was observed at UPX where this relative importance was lower. In fact, high bacterial production and a negative net community production were reported from the euphotic zone of UPX (Van Wambeke et al., 2008), which suggests rather “decomposing” conditions compared to “productive” conditions at UPW. At all sites, the ratio of phytosterols/phytol indicated more degraded phytoplankton material at depths below the chlorophyll maximum, but at the gyre site, this was also the case above the maximum. The ratio showed a slightly more degraded material in the euphotic zone of the UPX site as compared to UPW but, at 300 m depth, fresher material was found at UPX.

The polyunsaturation index of C_{16} fatty acids (PUFA % of C_{16}) is an indicator of the ecophysiological state of marine diatom populations because storage lipids, mainly $\text{C}_{16:0}$ and $\text{C}_{16:1}$ FA, are synthesized during senescence, rather than during logarithmic growth (Shin et al., 2000). The high indices observed in the euphotic zone of the UPW site and at 300 m depth of UPX suggest that these PUFA originated from diatoms at logarithmic growth. Moreover, the carbon isotope ratios of lipid biomarkers in the euphotic zone were generally more enriched at UPW compared to UPX (Fig. 3), likely indicating higher growth rates at UPW than at UPX. However, below the euphotic zone of UPX, $\delta^{13}\text{C}$ values identified higher growth rates at depth compared to the surface. All these parameters point out that post-bloom conditions with high concentrations of animal-derived detritus prevailed at the surface of the UPX site, whereas the important signal of zooplankton and diatom markers below the euphotic layer indicated the presence of zooplankton feeding on phytoplankton produced during bloom conditions. These findings are supported by the highest particle flux measured at UPX compared to the UPW site (Miquel et al., 2006) and the high concentration of detritus and senescent colonial diatoms observed by microscope in samples from the euphotic zone at the UPX site (Gómez, personal commu-

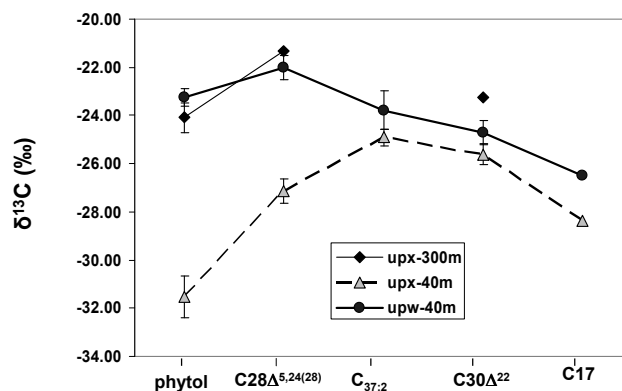


Fig. 3. Carbon isotope ratios ($\delta^{13}\text{C}$) for selected lipid biomarkers in the upwelling zone.

nication). These conclusions contrast, however, with those derived from pigment biomarkers (Ras et al., 2008) where UPW site was characteristic of a typically mature bloom of diatoms and the phytoplankton at site UPX was probably at an early stage of development. Also, much higher nutrient concentrations at the surface of UPX site indicated a recent upwelling of deep water. Overall, these contrasted observations might be accounted for by the different turnover and lability between pigment and lipid compounds which represent different pools of the particulate matter. Pigments are relatively more labile and associated with the living material. In contrast, lipids are included in both the living and detrital particulate pools of the matter.

3.2 Vertical distribution of biomarkers in the center of the gyre

Depth profiles of selected accessory lipid biomarkers in suspended matter from the center of the Gyre are presented in Fig. 4. Phytol concentrations showed very low surface values and they were increasing progressively with depth, with maximum concentration at 150–200 m depth. Relatively high concentrations of *n*-alcohols, cholesterol and branched fatty acids at the surface indicated an important heterotrophic activity in the upper waters. At higher depths (>75 m), both alcohols and cholesterol showed similar profiles as phytol, likely indicating that here, these biomarkers were mainly phytoplanktonic-derived or that zooplankton biomass was strongly associated with the phytoplankton abundance. Branched fatty acids which are derived from heterotrophic bacteria exhibited the maximum concentration between 150 and 200 m depth, following the same trend as planktonic biomass. This feature indicates that the bacterial population is associated with the major planktonic biomass.

Other more specific phototrophic biomarkers, such as sterol markers for diatoms exhibited a similar profile as phytol with two maximum at 150 and 200 m depth. Only few macro diatom species, such as *Nitzschia* and *Dactyliosolen*

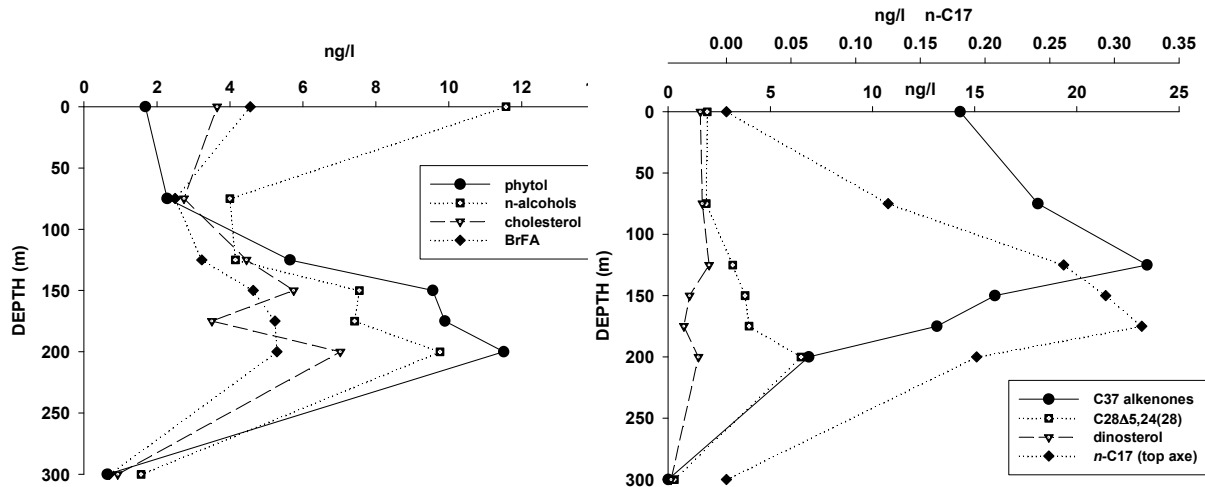


Fig. 4. Depth distribution of selected lipid biomarkers in the suspended particles from the gyre.

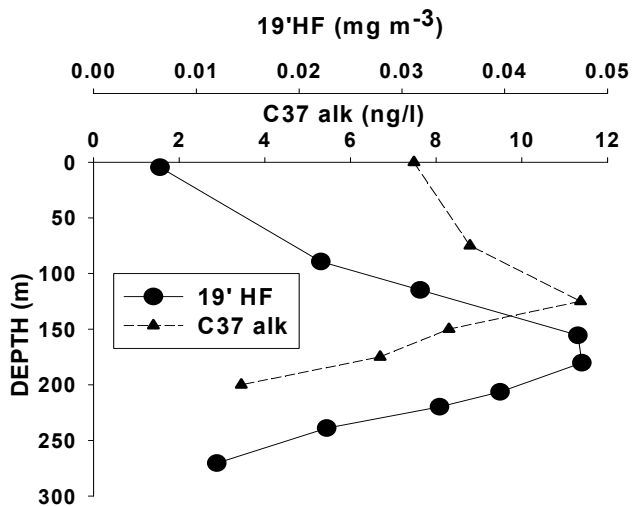


Fig. 5. Profiles for total C_{37} alkenones concentrations (C37 alk) and 19hexanoyloxyfucoxanthin pigment (19'HF) with depth in the suspended particles from the gyre.

were observed between 200 and 300 m depth and a significant number of *Bacteriastrium* associated to a cyanobacteria symbiont was also observed around 140 m depth (Gómez, personal communication). In contrast, the sterol marker for dinoflagellates exhibited a uniform distribution from surface to 125 m depth and a deeper maximum concentration at 200 m depth. Small dinoflagellates were observed in the surface waters of the Gyre center (Gómez, personal communication). The n -alkane C_{17} , which is produced by cyanobacteria and other eukaryotic algae, increased with depth showing a maximum concentration between 125 and 175 m. This coincides with the maximum abundances of *Prochlorococcus* and picoeukaryotes recorded between 100 and 200 m depth (Grob et al., 2007).

The C_{37} alkenones, which are specific markers for some algae of the class *Haptophyceae/Prymnesiophyceae*, including coccolithophorid species such as *Emiliania huxleyi*, exhibited the maximum concentration above the deep chlorophyll maximum, at 125 m depth. Cell densities of different coccolithophorid taxa showed, however, different depth profiles, with a maximum peak between 150–200 m for *Emiliania huxleyi* whereas other taxa peaked at shallower depths (~ 100 m) (Beaufort et al., 2007). These findings indicate that (i) other non-calcifying haptophytes might synthesize alkenones at shallower depths, (ii) that alkenones are not associated with the integrity of coccospheres and/or (iii) that cellular alkenone concentrations varied with the physiological status and species composition of the coccolithophorid assemblage. Furthermore, the concentration of alkenones and the accessory carotenoid 19'Hexanoyloxyfucoxanthin (19'HF) (Ras et al., 2008), characteristics of prymnesiophytes, also exhibited different depth distributions (Fig. 5). Such discrepancy reflects that alkenone-producers in these waters are minor contributors to the 19'HF stock, and that the habitat of alkenone synthesizers diverges from that of the major phytoplankton taxa contributing to the 19'HF distribution. An analogous feature was observed at station ALOHA from the oligotrophic North Pacific Subtropical Gyre (Prahl et al., 2005) and other studies showed that 19'HF abundance was generally not tightly correlated with that of coccolithophorids (Dandonneau et al., 2006). Figure 6 illustrates the carbon isotope composition of the diunsaturated alkenone together with the total concentrations of C_{37} alkenones. More enriched $\delta^{13}\text{C}$ values were obtained for alkenones measured at the depth of the chlorophyll maximum, whereas the higher concentrations of alkenones found at 125 m depth were associated to lower $\delta^{13}\text{C}$ values. Change in irradiance could also partially explain the abrupt change of the carbon isotope composition of the alkenones, since lower photon flux density leads to a lower ^{13}C discrimination

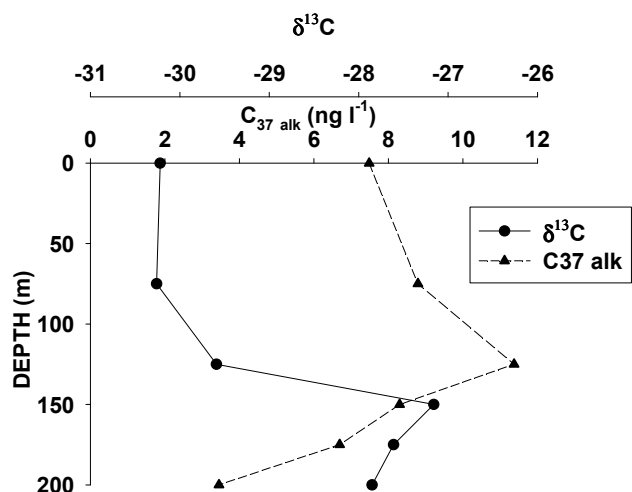


Fig. 6. Profiles for total C_{37} alkenone concentrations and carbon isotope ratio ($\delta^{13}\text{C}$) for the diunsaturated C_{37} alkenone.

increasing the $\delta^{13}\text{C}$ values (Rost et al., 2002; Thompson and Calvert, 1995). As it is shown in Table 2, the % PAR values at depths higher than 125 m were lower than 1%, which would mean that haptophytes were light-limited at these high depths. Consequently, the more enriched $\delta^{13}\text{C}$ values of the alkenone markers at the depth of the chlorophyll maximum might infer that haptophytes are under limited light conditions.

The unsaturation index ($U_{37}^{K'}$) which is widely used as a proxy of sea surface temperature (Prahl and Wakeham, 1987) was calculated as the relative proportion of di- and triunsaturated C_{37} alkenones. This index was converted to a measure of temperature by the commonly used empirical calibration equation $T = (U_{37}^{K'} - 0.039) / 0.034$ (Prahl et al., 1988). The derived temperatures (Fig. 7) were 2 to 3 degrees higher than the measured (CTD) temperatures in surface waters. Discrepancies between the alkenone-calculated and observed temperatures might be caused by stress due to nutrient and light limitation and to differences in the stage of the growth cycle (Conte et al., 1998; Epstein et al., 1998; Yamamoto et al., 2000; Prahl et al., 2003), which result in variable alkenone synthesis. Similar observations were reported in winter at ALOHA station (Prahl et al., 2005). They were explained by simply biogeographical variations observed in the alkenone vs. temperature relationship in natural waters, which may reflect differences in genetic and physiological status of the local alkenone-synthesizing populations. Since haptophytes have a low inorganic phosphorous requirement (critical concentrations of $0.2 \mu\text{mol l}^{-1}$), nitrogen limitation seems likely since inorganic N concentrations at the Gyre stations were well below the half-saturation constant (K_s , the concentration supporting an uptake rate one-half the maximum rate) determined for *E. huxleyi* ($\leq 0.5 \mu\text{mol l}^{-1}$) (Eppley et al., 1969). Overall and according to batch cultures

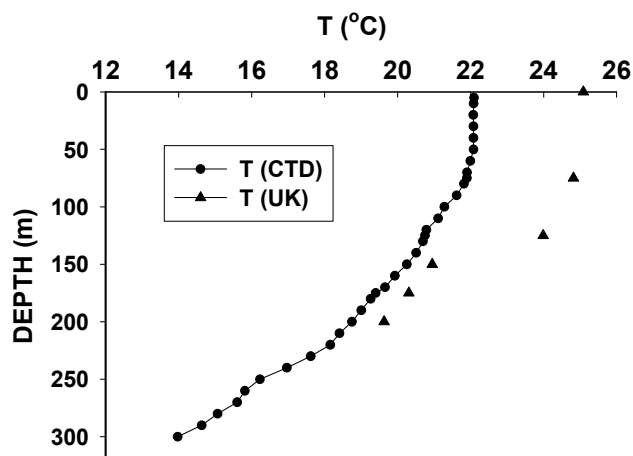


Fig. 7. Profile for CTD temperature and plot for $U_{37}^{K'}$ derived water temperature estimates (see text for details) from suspended particles in the gyre.

of haptophytes (Epstein et al., 1998), the observed increase in the $U_{37}^{K'}$ values with the consequent overestimation of the temperatures, might indicate that this marine phytoplankton taxon is under nutrient-limited “stationary growth” conditions. Although other studies showed an overestimation of temperatures in light-limited cultures (e.g. Prahl et al., 2003), we exclude light limitation as the reason for our overestimation. The light levels measured down to 125 m depth were above light limitation level (Table 2). This overestimation can also be explained by a change in haptophyte ecology towards a dominance of alkenone-producing algae (Prahl et al., 2005; Popp et al., 2006b). Other reasons may be autoxidation of alkenones in these highly irradiated waters (Rontani et al., 2006), and/or degradation of alkenones by aerobic heterotrophic bacteria (Rontani et al., 2008), especially when residence times of particles are long.

3.3 Biogeochemical implications from carbon isotope fractionation

Stable carbon isotope differences between the inorganic carbon source and that of organic carbon synthesized by autotrophic organisms known as photosynthetic carbon fractionation (ϵ_p), can assist in distinguishing between the different CO_2 fixation pathways (Table 5). Maximum carbon isotope fractionation of photoautotrophic organisms using the Calvin cycle, like micro-algae and cyanobacteria is in the range of 20 to 27‰ (Popp et al., 1998b; Sakata et al., 1997). However, the ϵ_p expected for biomarkers derived from eukaryotes can vary between 5 and 25‰ depending basically on $[\text{CO}_2]$, growth rate and the ratio of cellular surface area to volume (Bidigare et al., 1997a; Popp et al., 1998). In contrast, ϵ_p for prokaryotes (cyanobacteria) ranges between 16 and 22‰ because the large surface-to-volume ratio guarantees a large CO_2 supply relative to the cellular demand.

Table 5. Carbon isotope fractionation of CO_2 aq with respect to bicarbonate (ε_b), $\delta^{13}\text{C}\text{CO}_2$ (dissolved in the water column), different carbon isotope fractionation associated with photosynthetic carbon fixation using molecular specific lipid biomarkers (ε_p of biomarkers) and b-value ($\text{‰ } \mu\text{mol kg}^{-1}$) and specific growth rate for alkenone synthesizers.

locations- depth (m)	ε_b (‰)	$\delta^{13}\text{C}\text{CO}_2$ (‰)	ε_p (‰) phytol	ε_p (‰) $\text{C}_{28}\Delta^{5,24(28)}$	ε_p (‰) alkenone	ε_p (‰) $\text{C}_{30}\Delta^{22}$	ε_p (‰) <i>n</i> -C17	b ($\text{‰}\mu\text{mol kg}^{-1}$) alkenone	μ (d^{-1}) alkenone
mar3-50 m	-8.7	-7.2	17.9	21.7	15.6	15.5	16.7	105	0.3
hnl2-75 m	-8.7	-7.2	16.8	23.2	16.0	14.5	18.4	99	0.3
hnl1-100 m	-8.8	-7.3	19.1	23.2		15.7			
gyr2-0 m	-9.3	-7.8			18.7			75	0.2
gyr2-75 m	-9.3	-7.8			18.7	18.2		74	0.2
gyr2-125 m	-9.5	-8.0	18.1	18.6	17.8	17.6		83	0.3
gyr2-150 m	-9.5	-8.0		22.0	15.3	17.4	9.5	117	0.4
gyr2-175 m	-9.6	-8.1	17.9	25.5	15.7			124	0.4
gyr2-200 m	-9.7	-8.2	18.7	23.4	15.8	19.9		129	0.4
egy4-70 m	-10.0	-8.5	20.0	25.4	12.8	18.0	7.6	158	0.5
egy2-200 m	-10.2	-8.7		21.4	12.2	16.9			
egy4-300 m	-10.7	-9.2		19.7					
upw1-40 m	-10.4	-8.9	10.4	9.1	10.4	11.9	9.3		
upw1-100 m	-10.6	-9.1	10.0	7.2	10.7	9.5			
upw2-300 m	-10.9	-9.4		10.0					
upx3-40 m	-10.5	-9.0	18.8	14.2	11.9	12.7	11.2	488 (365) ^a	1.7 (1.2) ^a
upx2-100 m	-10.7	-9.2	18.2	9.3	12.2	9.9			
upx2-300 m	-10.7	-9.3	10.8	8.0		10.0			

^a calculated with the $[\text{CO}_2]$ at the surface

Others pathways, apparently restricted to other bacteria, such as anoxygenic phototrophic bacteria, are the reversed tri-carboxylic acid cycle and the 3-hydroxypropionate pathway, both of which are characterized by significantly smaller isotope effects (ε_p of 2–14 ‰)(van der Meer et al., 2001).

We observed higher taxonomic variations in ε_p for eukaryotic algae growing in the oligotrophic areas (variations of $\sim 10\%$) compared to the eutrophic sites of the upwelling (variations of 3 to 7‰). The variation of the carbon isotope fractionation for the diatom marker covered a range of $\sim 16\%$ along the different trophic systems. In contrast, ε_p of dinoflagellate and alkenone markers varied much less ca. 10 and 7‰, respectively.

Plots of the carbon isotope fractionation of the different eukaryotic markers vs the three major nutrients in the euphotic layer showed similar trends. An example is given in Fig. 8 for the nitrate concentrations, showing a negative logarithmic curve for the diatom biomarker. ε_p values from nutrient-rich waters at eutrophic sites were much lower compared to those in the nitrate limited conditions of the Gyre. However, in oligotrophic waters, the high scatter of ε_p indicates that other factors besides major nutrients are probably affecting the carbon isotope fractionation. This is illustrated

by the small effect of nitrate concentrations on the carbon isotope fractionation of the haptophytes (alkenones).

The carbon isotope fractionation of eukaryotic markers showed also a negative trend with $[\text{CO}_2]_{\text{aq}}$ (Fig. 9). These relationships deviate from the previously reported general oceanic trend (Rau et al., 2001) and culture studies (Burkhardt et al., 1999a) where carbon isotope fractionation increases ($\delta^{13}\text{C}$ decrease) when $[\text{CO}_2]_{\text{aq}}$ increases. However, this apparent deviation has already been observed in Peruvian upwelling waters where it was suggested that a diatom carbon concentrating mechanism (CCM) was likely the cause of the lower ε_p of diatoms in these waters with high $[\text{CO}_2]_{\text{aq}}$. In the present study, we also observed a small effect of $[\text{CO}_2]_{\text{aq}}$ on isotope fractionation of alkenones, which agrees with other studies that privileged potential changes of ε_p due to growth rate and carbon uptake mechanisms in *E. huxleyi* (Benthien et al., 2007; Bidigare et al., 1997). A similar trend was found between $[\text{CO}_2]$ and the ε_p of *n*-C17 (data not shown) which is consistent with a previous work with Popp et al. (1998b) who found for *Synechococcus* that ε_p is independent of the concentration of dissolved CO_2 , likely because its cell geometry guarantees a large CO_2 supply.

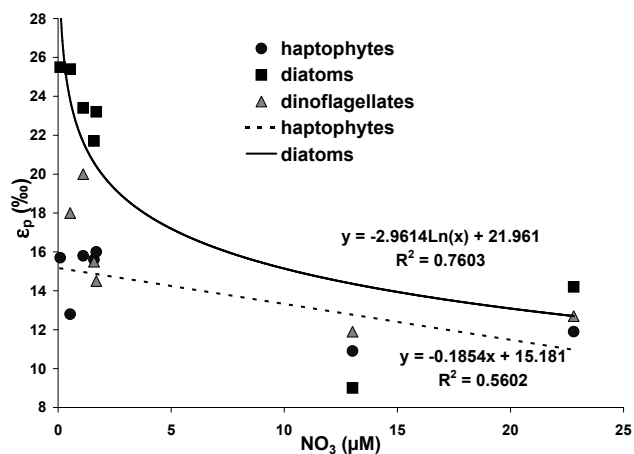


Fig. 8. Carbon isotope fractionation factor of the eukaryotic markers vs. measured nitrate concentrations across the South Pacific Ocean. Logarithmic curve fitting corresponds to diatom marker, linear fitting for haptophytes is shown to illustrate the contrast between diatoms and haptophytes.

Overall, the lower isotope fractionation factors and smaller variations between the different eukaryotic markers measured in the upwelling area might indicate uniformly high growth rates for the three phytoplankton taxa, diatoms, haptophytes and dinoflagellates and/or that phytoplankton may employ carbon concentrating mechanisms (CCM) other than diffusion, which actively transport inorganic carbon into cells. Similar findings were reported by other authors (Pancost et al., 1999; Pancost et al., 1997; Rau et al., 2001; Werne and Hollander, 2004) who invoked that an active transport of bicarbonate into the cell may play a role in the carbon isotope fractionation by phytoplankton in upwelling areas with high concentrations of CO_2 . Light is another factor which may decrease the carbon isotope fractionation under low saturation levels since it has opposite effects on the ε_p compared to nutrient-limited conditions (Rost et al., 2002, Cassar et al., 2006). However, despite light limiting conditions at 40 m, phytoplankton sampled at these depths are not necessarily light limited. In hydrodynamically active zones like the upwelling, it can be reasonably admitted that phytoplankton cells produce under light conditions averaged over the mixed layer and not encountered at the depths they were sampled. Hence, it can be excluded that irradiance affected the isotopic fractionation of the different phytoplankton taxa in the upper mixed layer of the upwelling area.

In contrast, the GYR and EGY sites exhibited the highest carbon isotope fractionation factors for eukaryotic algae and in particular for the diatom marker. Their values reached 25–26‰ which is close to the maximum isotope fractionation of eukaryotic algae utilizing Rubisco and β -carboxylase enzymes (Goericke et al., 1994; Laws et al., 1997). Such high ε_p values cannot be obtained by bicarbonate uptake and are indicative of diffusive CO_2 uptake. Moreover, ac-

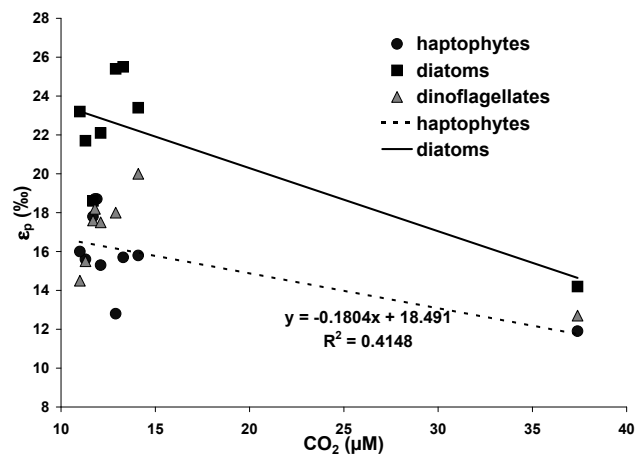


Fig. 9. Carbon isotope fractionation factors of eukaryotic markers vs. CO_2 concentrations.

tive uptake of carbon in oligotrophic sites is rather unlikely because of the higher metabolic energy required and CCM may be inhibited by the low oceanic concentrations of certain trace metals (Morel et al., 1994). In these oligotrophic sites, lowest ε_p values were measured for the haptophytes and dinoflagellates, which might infer higher growth rates for these organisms compared to diatoms.

In the mesotrophic areas of the Marquesas Islands (MAR and HNL sites), ε_p values for alkenone producers and dinosterol were also lower than those for diatoms, but still higher than those estimated in the upwelling area. The similar ε_p values for alkenones measured in the poor-nitrated waters of the Gyre and in the high nutrient waters of the HNL site suggest that nitrogen and phosphate are not the limiting nutrients affecting carbon isotope fractionation by the prymnesiophyte algae. This finding contrasts with a study from the NE Pacific where nitrogen starvation seemed to affect the ε_p values for alkenones (Eek et al., 1999) and adds further support to the “trace-metal-growth-rate” hypothesis (Bidigare et al., 1997), which suggested that micronutrients control growth regardless of the concentrations of PO_4 . Overall, the relatively low ε_p values for alkenones from the oligo- and mesotrophic waters seem to indicate the use of a CCM other than diffusion. However, recent studies provided clear evidence that haptophytes have developed an inefficient but regulated CCM, with a direct uptake of HCO_3^- (Rost et al., 2003). The highest ε_p for dinoflagellates at the GYR and EGY sites are likely associated to lower growth rates and might be explained by the low N:P ratios since optimum dinoflagellate growth occurs at ratios ranging between 6 and 15 (Hodgkiss and Ho, 1997).

The carbon isotope fractionation derived from $n\text{-C}_{17}$ alkane reached the values of 17–19‰ in the mesotrophic waters of the HNL and MAR sites, which are within the range of 16–22‰ reported for cyanobacteria biomass (Sakata et al., 1997). In contrast, the low carbon isotope fractionations

(8 to 12‰) obtained for *n*-C17 in the oligotrophic waters of the GYR and EGY sites as well as in the eutrophic waters of the upwelling area are suggestive of microorganisms which use CO_2 -concentrating mechanisms. Despite substantial advances over the past few years, in the understanding of the mechanism and genes involved in cyanobacterial CCMs (Badger and Price, 2003), the induction of the CCM mechanism remains to be determined (McGinn et al., 2003; Woodger et al., 2005). Also, since similar ε_p values were measured in the upwelling area for biomarkers derived from eukaryotic plankton, it cannot be ruled out that *n*-C17 in the upwelling sites is mainly derived from some eukaryotic source.

The *b*-values and growth rates for alkenone-producing haptophytes measured in the euphotic layer varied almost tenfold, ranging from 75 to 490‰ $\mu\text{mol kg}^{-1}$ and from 0.2 to 1.7 d^{-1} , respectively. The highest growth rates were estimated in the waters of the Chilean upwelling, followed by the EGY (0.5 d^{-1}), the GYR (0.4 d^{-1}) and finally the MAR and HNL (0.3 d^{-1}) sites. The lowest values were found in the surface waters of the Gyre (0.2 d^{-1}). Overall, our *b*-values and growth rates compare to those reported for the Bering Sea, Arabian Sea, Southern Ocean and equatorial Pacific at 140° W (84–136‰ $\mu\text{mol kg}^{-1}$ and 0.2–0.4 d^{-1}) (Bidigare et al., 1997; Harada et al., 2003; Laws et al., 2001) but they are slightly higher than those reported from the Peru upwelling zone (197–397‰ $\mu\text{mol kg}^{-1}$ and 0.5–1 d^{-1}) (Bidigare et al., 1997). This is probably related to the strength of the upwelling as indicated by the higher nutrient and CO_2 concentrations in the sampled area and by the larger photoperiod. It is also noteworthy that the calculated growth rates are maximum estimates and are valid only on the assumption that alkenone producing haptophytes obtain CO_2 (as the only carbon source) solely by passive diffusion, which may not be the case in the nutrient-rich waters of the upwelling zone. Moreover, alkenones may occur well below the euphotic zone (40–100 m) in fecal material produced by herbivorous zooplankton (Grice et al., 1998) and other particles, which have been transported down due to physical mixing and sinking. Through the continuous convective movement in the water column of this dynamic area, the phytoplankton cells are likely to encounter lower average CO_2 concentrations and higher irradiance than at the depths they were sampled. In this sense, if we consider that alkenones found at depths of 40–100 m were produced in the upper layer where CO_2 concentration is lower ($\sim 28 \mu\text{mol kg}^{-1}$) and light is not limited, the estimated growth rate decreases to 1.2 d^{-1} , which is in the range of typical values found in field populations of nutrient rich waters (Bidigare et al., 1997).

The *b*-values for the alkenone synthesizer phytoplankton were well distinguishable between the two contrasting environments: low at the oligotrophic sites and a high value in the upwelling zone. Due to the natural correlation between concentrations of dissolved CO_2 and nutrients, *b*-values obviously co-varied with the concentrations of silicate, ni-

trate and phosphate. However, at the very low phosphate levels ($< 0.4 \mu\text{mol l}^{-1}$) of the oligotrophic sites, *b*-values showed relatively high variation (75–160‰ $\mu\text{mol kg}^{-1}$) and compared very well with the corresponding values reported by Bidigare et al. (1997), but also with those from other oligotrophic areas (Laws et al., 2001; Benthien et al., 2002). This confirms the interpretation given by these authors that growth rates may be controlled by some trace micronutrient (e.g. Zn) (Bidigare et al., 1997; Shaked et al., 2006), and/or that adaptation of the phytoplankton physiology to the low nutrient waters might result in higher variability in the efficiency of the different carbon uptake mechanisms.

4 Summary and conclusions

As a summary, lipid biomarker abundances together with their relative component contribution confirmed the general expectations on the predominance of diatom algae in nutrient-rich waters, and of zooplankton, bacteria and degraded material below the euphotic zone. In contrast, the hyperoligotrophic area of the Gyre was characterized by low concentrations of lipid biomarkers, and especially by unprecedented deep maxima of eukaryotic markers, and rather unexpectedly high heterotrophic activity in surface waters. Among these biomarkers, phytol and the more specific diatom sterols followed the chlorophyll profile. However, highest concentrations were measured for alkenones with maximum values above chlorophyll maximum and above the concentration peak of 19'HF, thus indicating a quite specific community of the alkenone producing prymnesiophytes. Discrepancies between the alkenone-calculated and the in situ temperatures of the surface layer from the gyre seemed to be caused by nutrient limitation and/or degradation of alkenones. Carbon isotope ratios of alkenones markers evidenced that prymnesiophytes inhabiting the depth of the chlorophyll maximum were likely light-limited.

Our results along the different trophic systems in the South East Pacific showed also that source-specific algal biomarkers and compound specific isotope analyses largely responded to the composition of the phytoplankton and to the different processes of carbon acquisition. Within a probably complex pattern of processes that link the ε_p of the different phytoplankton taxa and their environmental factors, our field study illustrates that carbon isotope fractionation values from nutrient-rich waters were much lower compared to those in nitrate limited. However, the high scatter of ε_p in the oligotrophic conditions indicates that other factors besides major nutrients are probably affecting the carbon isotope fractionation. Light not being generally a limiting factor in the euphotic layer, higher growth rates and/or active uptake of HCO_3^- could explain the reduced ε_p values of the nutrient-rich waters. These relatively low and similar ε_p over the different phytoplankton taxa of the nutrient-rich waters implied non-diffusive C transport, whereas the high and

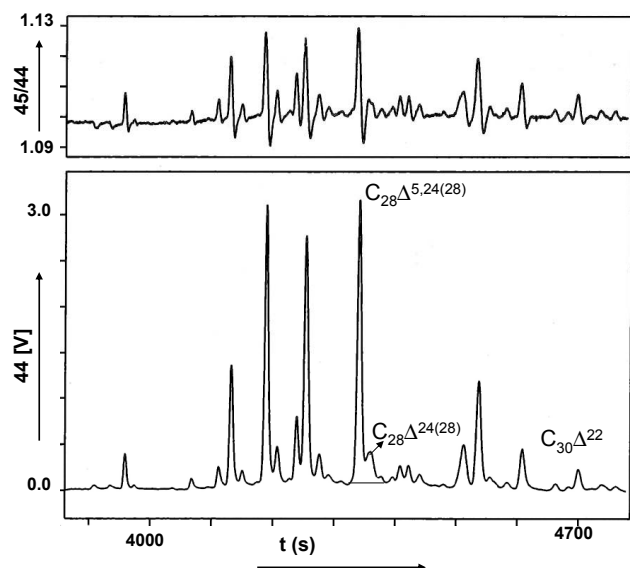


Fig. A1. GC-C-IRMS of the sterol fraction showing the incomplete chromatographic separation of the compound 24-methylcholesta-5,24(28)-dien-3 β -ol ($\text{C}_{28}\Delta^{5,24(28)}$) stenol with their minor stanol pair compound (24-methyl-5 α -cholest-24(28)-en-3 β -ol, $\text{C}_{28}\Delta^{24(28)}$). Both compounds were integrated together to yield a single $\delta^{13}\text{C}$ value.

dispersed ε_p values from the nutrient-poor waters might result from the lower growth rates and from higher variability in the efficiency of the carbon uptake mechanism by diffusion. However, the available data do not allow distinguishing between the two factors.

Acknowledgements. We thank James Orr and Lamia Azouzi for helpful science discussions. Dominique Tailliez and Claudie Bournot are warmly thanked for their efficient help in CTD rosette management and data processing. A. Benthien and two anonymous reviewers are acknowledged by their valuable suggestions and comments on an earlier version of the manuscript.

This is a contribution of the BIOSOPE project of the LEFE-CYBER program. This research was funded by the Centre National de la Recherche Scientifique (CNRS), the Institut des Sciences de l'Univers (INSU), the Centre National d'Etudes Spatiales (CNES), the European Space Agency (ESA), The National Aeronautics and Space Administration (NASA) and the Natural Sciences and Engineering Research Council of Canada (NSERC). The IAEA is grateful for the support provided to its Marine Environment Laboratories by the Government of the Principality of Monaco.

Edited by: J. Middelburg

References

- Azouzi, L., Gonçalves Ito, R., Touratier, F., and Goyet, C.: Anthropogenic carbon in the eastern South Pacific Ocean, *Biogeosciences Discuss.*, 4, 1815–1837, 2007, <http://www.biogeosciences-discuss.net/4/1815/2007/>.
- Badger, M. R. and Price, G. D.: CO_2 concentrating mechanisms in cyanobacteria: molecular components, their diversity and evolution, *J. Exp. Bot.*, 54, 609–622, 2003.
- Baker, E. W. and Louda, J. W.: Thermal aspects in chlorophyll geochemistry. In: *Adv. Org. Geochem.*, 1981, edited by: M. Bjørøy, Wiley, Chichester, 401–421, 1983.
- Barlow, R. G., Mantoura, R. F. C., Gough, M. A., and Fileman, T. W.: Pigment signatures of the phytoplankton composition in the northeastern Atlantic during the 1990 spring bloom. *Deep Sea Res. Pt. II*, 40, 459–477, 1993.
- Beaufort, L., Couapel, M., Buchet, N., and Claustre, H.: Calcite production by Coccolithophores in the South East Pacific Ocean: from desert to jungle, *Biogeosciences Discuss.*, 4, 3267–3299, 2007, <http://www.biogeosciences-discuss.net/4/3267/2007/>.
- Benthien, A., Andersen, N., Schulte, S., Müller, P. J., Schneider R. R., and Wefer, G.: Carbon isotopic composition of the $\text{C}_{37:2}$ alkenone in core-top sediments of the South Atlantic Ocean: effects of CO_2 and nutrient concentrations, *Global Biogeochem. Cy.*, 16, 1012, doi:10.1029/2001GB001433, 2002.
- Benthien, A., Andersen, N., Schulte, S., Muller, P. J., Schneider, R. R. and Wefer, G.: The carbon isotopic record of the $\text{C}_{37:2}$ alkenone in the South Atlantic: Last Glacial Maximum (LGM) vs. Holocene, *Palaeogeography, Palaeoclimatology, Palaeoecology*, 221, 123–140, 2005.
- Benthien, A., Zondervan, I., Engel, A., Hefter, J., Terbruggen, A., and Riebesell, U.: Carbon isotopic fractionation during a mesocosm bloom experiment dominated by *Emiliania huxleyi*: Effects of CO_2 concentration and primary production. *Geochim. Cosmochim. Ac.*, 71, 1528–1541, 2007.
- Bidigare, R. R., Fluegge, A., Freeman, K. H., Hanson, K. L., Hayes, J. M., Hollander, D., Jasper, J. P., King, L. L., Laws, E. A., Milder, J., Millero, F. J., Pancost, R. D., Popp, B. N., Steinberg, P. A., and Wakeham, S. G.: Consistent fractionation of C in nature and in the laboratory: growth-rate effects in some haptophyte algae, *Global Biogeochem. Cy.*, 11, 279–292, 1997.
- Bidigare, R. R., Hanson, K. L., Buesseler, K. O., Wakeham, S. G., Freeman, K. H., Pancost, R. D., Millero, F. J., Steinberg, P. A., Popp, B. N., Latasa, M., Landry, M. R., and Laws, E. A.: Iron-stimulated changes in ^{13}C fractionation and export by equatorial Pacific phytoplankton: Toward a paleogrowth rate proxy, *Paleoceanography*, 14, 589–595, 1999.
- Burkhardt, S., Riebesell, U., and Zondervan, I.: Effects of growth rate, CO_2 concentration, and cell size on the stable carbon isotope fractionation in marine phytoplankton, *Geochim. Cosmochim. Ac.*, 63, 3729–3741, 1999a.
- Burkhardt, S., Riebesell, U., and Zondervan, I.: Stable carbon isotope fractionation by marine phytoplankton in response to daylength, growth rate, and CO_2 availability, *Mar. Ecol.-Progr. Ser.*, 184, 31–41, 1999b.
- Cassar, N., Laws, E. A., and Popp, B. N.: Carbon isotopic fractionation by the marine diatom *Phaeodactylum tricornutum* under nutrient- and light-limited growth conditions, *Geochim. Cosmochim. Ac.*, 70, 5323–5335, 2006.

Table B1. Selected lipid biomarkers concentrations normalized to organic carbon ($\text{mg g}^{-1}\text{C}$) in suspended particles from the South Pacific Ocean.

locations- depth (m)	phytol	$\text{C}_{28}\Delta^{5,24(28)}$	C_{25} HBI	$\text{C}_{16:4}$ FA	$\text{C}_{20:5}$ FA	Total alkenones	$\text{C}_{30}\Delta^{22}$	$n\text{-C}_{17}$	$n\text{-}$ alcohols	$\text{C}_{20:1}$ + $\text{C}_{22:1}$ FA	Branched FA	$\text{C}_{27}\Delta^5$
mar3-50 m	1.3	0.87	0.10	1.4	4.2	0.28	0.19	0.01	0.28	0.12	0.92	0.55
mar3-100 m	0.65	0.44	0.00	1.6	3.3	0.34	0.00	0.00	3.2	0.62	2.9	0.62
mar3-300 m	0.18	0.89	0.00	0.00	2.9	0.00	0.00	0.00	2.8	2.8	0.63	0.33
hnl2-75 m	1.3	1.5	0.04	1.5	3.2	0.83	0.30	0.01	0.38	0.12	1.0	0.68
hnl1-100 m	1.9	1.4	0.01	2.1	5.0	0.81	0.37	0.21	1.5	0.16	0.31	2.2
hnl2-300 m	0.22	0.40	0.00	0.00	2.0	0.00	0.14	0.00	3.6	0.17	0.43	1.4
gyr2-0 m	0.36	0.41	0.04	0.30	1.7	3.1	0.34	0.00	2.5	0.00	0.98	0.79
gyr2-75 m	0.38	0.31	0.00	0.23	1.2	3.0	0.28	0.02	0.65	0.08	0.41	0.44
gyr2-125 m	0.95	0.54	0.01	0.41	2.8	4.0	0.34	0.04	0.71	0.13	0.54	0.77
gyr2-150 m	1.7	0.66	0.03	1.0	4.4	2.8	0.19	0.05	1.3	0.08	0.80	0.99
gyr2-175 m	1.7	0.68	0.03	0.65	2.7	2.2	0.14	0.05	1.3	0.06	0.88	0.60
gyr2-200 m	2.7	1.5	0.09	0.90	4.8	1.6	0.35	0.04	2.3	0.20	1.2	1.6
gyr2-300 m	0.42	0.21	0.00	0.00	1.5	0.00	0.07	0.00	1.1	0.08	0.49	0.63
egy4-70 m	1.4	1.8	0.12	1.5	5.0	1.7	0.25	0.10	1.0	0.15	0.89	1.3
egy2-200 m	0.67	0.93	0.00	0.00	4.3	0.50	0.20	0.22	3.2	0.09	1.6	2.4
egy4-300 m	0.22	0.51	0.00	0.00	3.4	0.18	0.22	0.00	2.5	0.00	1.1	2.0
upw1-40 m	1.2	0.67	0.04	1.7	4.6	0.33	0.12	0.00	0.40	0.19	1.4	0.44
upw1-100 m	1.1	0.69	0.00	0.69	4.8	0.32	0.18	0.01	1.5	0.11	1.3	0.91
upw2-300 m	0.23	0.20	0.00	0.00	2.0	0.16	0.06	0.01	3.3	0.08	0.82	1.0
upx3-40 m	2.0	0.84	0.06	0.65	3.6	0.30	0.15	0.00	2.3	0.20	1.5	1.4
upx2-100 m	1.7	0.99	0.05	0.53	6.7	0.15	0.25	0.01	0.69	0.09	2.0	1.1
upx2-300 m	0.85	0.77	0.26	2.4	11	0.16	0.15	0.00	32	0.39	1.4	3.5

Claustre, H., Hooker, S. B., Van Heukelem, L., Berthon, J.-F., Barlow, R., Ras, J., Sessions, H., Targa, C., Thomas, C. S., van der Linde, D., and Marty, J.-C.: An intercomparison of HPLC phytoplankton pigment methods using in situ samples: application to remote sensing and database activities, *Mar. Chem.*, 85, 41–61, 2004.

Claustre, H., Sciandra, A., and Vaultot, D.: Introduction to the special section bio-optical and biogeochemical conditions in the South East Pacific in late 2004: the BIOSOPE program, *Biogeosciences*, 5, 679–691, 2008, <http://www.biogeosciences.net/5/679/2008/>.

Conte, M. H., Thompson, A., Eglinton, G., and Green, J. C.: Lipid biomarker diversity in the coccolithophorid *Emiliania huxleyi* (*Prymnesiophyceae*) and the related species *Gephyrocapsa oceanica*, *J. Phycol.*, 31, 272–282, 1995.

Conte, M. H., Thompson, A., Lesley, D., and Harris, R. P.: Genetic and physiological influences on the alkenone/alkenoate versus growth temperature relationship in *Emiliania huxleyi* and *Gephyrocapsa Oceanica*. *Geochim. Cosmochim. Ac.*, 62, 51–68, 1998.

Conte, M. H., Weber, J. C., King, L. L., and Wakeham, S. G.: The alkenone temperature signal in western North Atlantic surface waters, *Geochim. Cosmochim. Ac.*, 65, 4275–4287, 2001.

Dalsgaard, J., John, M. S., Kattner, G., Müller-Navarra, D., and Hagen, W.: Fatty acid trophic markers in the pelagic marine environment, *Adv. Mar. Biol.*, 46, 225–340, 2003.

Dandonneau, Y., Montel, Y., Blanchot, J., Giraudeau, J., and

Neveux, J.: Temporal variability in phytoplankton pigments, picoplankton and coccolithophores along a transect through the North Atlantic and tropical southwestern Pacific, *Deep Sea-Res. Pt. I*, 53, 689–712, 2006.

Dijkman, N. A. and Kromkamp, J. C.: Phospholipid-derived fatty acids as chemotaxonomic markers for phytoplankton: application for inferring phytoplankton composition, *Mar. Ecol.-Progr. Ser.*, 324, 113–125, 2006.

DOE: Handbook of Methods for Analysis of the Various Parameters of the Carbon Dioxide System in Seawater; version 2, edited by: Dickson, A. G. and Goyet, C., ORNL/CDIAC-74, 1994.

Eek, M. K., Whiticar, M. J., Bishop, J. K. B., and Wong, C. S.: Influence of nutrients on carbon isotope fractionation by natural populations of *Prymnesiophyte* algae in NE Pacific. *Deep Sea-Res. Pt II*, 46, 2863–2876, 1999.

Eppley, R. W., Rogers, J. N., and McCarthy, J. J.: Half-saturation constants for uptake of nitrate and ammonium by marine phytoplankton, *Limnol. Oceanogr.*, 14, 912–920, 1969.

Epstein, B. L., D'Hondt, S., Quinn, J. G., Zhang J., and Hargraves, P. E.: An effect of dissolved nutrient concentrations on alkenone-based temperature estimates, *Paleoceanography*, 13, 122–126, 1998.

Falkowski, P. G.: Physiological responses of phytoplankton to natural light regimes, *J. Plankton Res.*, 6, 295–307, 1984.

Falkowski, P. G., Barber, R. T., and Smetacek, V.: Biogeochemical controls and feedbacks on ocean primary production. *Science*,

Table C1. Stable carbon isotopic composition ($\delta^{13}\text{C}(\text{‰})\pm\text{s.d.}$ of three replicate injections) of selected lipid biomarkers in suspended particles from the South East Pacific Ocean.

locations-depth (m)	phytol	$\text{C}_{28}\Delta^{5,24(28)\text{a}}$	$\text{C}_{37:2}$ alkenone	$\text{C}_{30}\Delta^{22}$	$n\text{-C}_{17}$	$\text{C}_{20:5}$ FA	$i\text{-C}_{15}^{\text{b}}$ FA
mar3-50 m	-28.8 ± 0.9	-32.4 ± 0.5	-26.7 ± 0.5	-26.6 ± 0.5	-31.7 ± 0.5	-24.0 ± 0.5	-20.7 ± 0.7
hnl2-75m	-27.9 ± 0.5	-34.0 ± 0.5	-27.1 ± 0.5	-25.7 ± 0.5	-33.6 ± 0.5	-24.8 ± 0.7	-21.6 ± 0.5
hnl1-100 m	-30.1 ± 0.5	-34.0 ± 0.5		-26.9 ± 0.6			
gyr2-0 m			-30.2 ± 0.5			-29.3 ± 0.8	-23.3 ± 0.5
gyr2-75 m			-30.3 ± 0.5	-29.7 ± 0.5		-26.5 ± 0.5	-21.6 ± 0.7
gyr2-125 m	-29.9	-30.3	-29.6 ± 0.5	-29.4 ± 0.5		-26.9 ± 0.5	-20.2 ± 0.5
gyr2-150 m		-33.6	-27.2 ± 0.5	-29.3	-25.8 ± 0.5	-26.8 ± 0.5	-23.4 ± 0.6
gyr2-175 m	-29.8	-37.0	-27.6 ± 0.5			-27.6 ± 0.5	-23.5 ± 0.5
gyr2-200 m	-30.6 ± 1.2	-35.1 ± 1.5	-27.8 ± 0.5	-31.8 ± 0.6		-29.5 ± 0.5	-24.8 ± 0.5
egy4-70 m	-32.1 ± 0.5	-37.3 ± 0.6	-25.2 ± 0.6	-30.2 ± 1.2	-24.4 ± 0.5	-28.8 ± 0.8	-25.5 ± 0.5
egy2-200 m		-33.7 ± 0.5	-24.8 ± 0.6	-29.4 ± 0.8		-28.6 ± 1.6	-25.7 ± 0.7
egy4-300 m		-32.6 ± 0.5				-25.8 ± 1.3	-24.2 ± 0.6
upw1-40 m	-23.3 ± 0.5	-22.0 ± 0.5	-23.8 ± 0.5	-24.7 ± 0.8	-26.5 ± 0.5	-24.7 ± 0.6	-19.8 ± 0.5
upw1-100 m	-23.1	-20.5 ± 0.5	-23.8 ± 0.5	-22.7 ± 0.5		-25.0 ± 0.5	-19.7 ± 0.6
upw2-300 m		-23.4 ± 0.7				-26.1 ± 0.5	-22.1 ± 0.5
upx3-40 m	-31.5 ± 0.5	-27.1 ± 0.9	-24.9 ± 0.5	-25.6 ± 0.5	-28.4 ± 0.5	-28.6 ± 0.5	-21.7 ± 0.5
upx2-100 m	-31.1 ± 2.0	-22.5 ± 1.4	-25.4 ± 0.5	-23.2 ± 0.8		-24.2 ± 0.5	-19.3 ± 0.5
upx2-300 m	-24.1 ± 0.7	-21.3 ± 0.6		-23.3		-24.0 ± 0.5	-20.4 ± 0.5

^a the major compound 24-methylenecholesterol ($\text{C}_{28}\Delta^{5,24(28)}$) stanol was integrated together with their minor stanol pair compound ($\text{C}_{28}\Delta^{24(28)}$) to yield a single $\delta^{13}\text{C}$ value for both compounds because of incomplete chromatographic separation.

^b 13-methyl-tetradecanoic acid (iso- C_{15}).

- 281, 200–206, 1998.
- Freeman, K. H. and Hayes, J. M.: Fractionation of carbon isotopes by phytoplankton and estimates of ancient CO_2 levels, *Global Biogeochem. Cy.*, 6, 185–198, 1992.
- Freeman, K. H., Hayes, J. M., Trendel, J. M., and Albrecht, P.: Evidence from carbon isotope measurements for diverse origins of sedimentary hydrocarbons, *Nature*, 343, 254–256, 1990.
- Goericke, R., Montoya, J. P., and Fry, B.: Physiology of isotopic fractionation in algae and cyanobacteria. In: *Stable Isotopes in Ecology and Environmental Science*, Blackwell Science Publishers, 187–221, 1994.
- Gómez, F., Claustre, H., Raimbault, P., and Souissi, S.: Two High-Nutrient Low-Chlorophyll phytoplankton assemblages: the tropical central Pacific and the offshore Perú-Chile Current, *Biogeosciences*, 4, 1101–1113, 2007, <http://www.biogeosciences.net/4/1101/2007/>.
- Goyet, C. and Poisson, A.: New determination of carbonic acid dissociation constants in seawater as a function of temperature and salinity, *Deep Sea-Res.*, 36, 1635–1654, 1989.
- Graeve, M., Hagen, W., and Kattner, G.: Herbivorous or omnivorous? On the significance of lipid compositions as trophic markers in Antarctic copepods, *Deep Sea-Res., Pt I*: 41, 915–924, 1994.
- Grice, K., Klein Breteler, W. C. M., Schouten, S., Grossi, V., de Leeuw, J. W., and Sinninghe Damste, J. S.: Effects of zooplankton herbivory on biomarker proxy records, *Paleoceanography*, 13, 686–693, 1998.
- Grob, C., Ulloa, O., Claustre, H., Huot, Y., Alarcón, G., and Marie, D.: Contribution of picoplankton to the total particulate organic carbon concentration in the eastern South Pacific, *Biogeosciences*, 4, 837–852, 2007, <http://www.biogeosciences.net/4/837/2007/>.
- Han, J. and Calvin, M.: Hydrocarbon distribution of algae and bacteria, and microbiological activity in sediments, *P. Natl. Acad. Sci. USA*, 64, 436–443, 1969.
- Harada, N., Shin, K. H., Murata, A., Uchida, M., and Nakatani, T.: Characteristics of alkenones synthesized by a bloom of *Emiliania huxleyi* in the Bering Sea, *Geochim. Cosmochim. Ac.*, 67, 1507–1519, 2003.
- Hayes, J. M.: Factors controlling ^{13}C contents of sedimentary organic compounds: Principles and evidence, *Mar. Geol.*, 113, 111–125, 1993.
- Hayes, J. M., Freeman, K. H., Popp, B. N., and Hoham, C. H.: Compound-specific isotopic analyses: A novel tool for reconstruction of ancient biogeochemical processes, *Org. Geochem.*, 16, 1115–1128, 1990.
- Hayes, J. M., Fractionation of the isotopes of carbon and hydrogen in biosynthetic processes, edited by: Valley, J. W. and Cole, D.

- R., 2001. *Stable Isotope Geochemistry, Reviews in Mineralogy and Geochemistry* 43, Mineralogical Society of America, 225–278, 2001.
- Harvey, H. R., O'Hara, S. C. M., Eglinton, G. and Corner, E. D. S.: Biotransformation and assimilation of dietary lipids by *Calanus* feeding on a dinoflagellate. *Geochim. Cosmochim. Ac.*, 51, 3031–3040, 1987.
- Hodgkiss, I. J. and Ho, K. C.: Are changes in N:P ratios in coastal waters the key to increased red tide blooms? *Hydrobiologia*, 352, 141–147, 1997.
- Irwin, A. J., Finkel, Z. V., Schofield, O. M. E., and Falkowski, P. G.: Scaling-up from nutrient physiology to the size-structure of phytoplankton communities, *J. Plankton Res.*, 28, 459–471, 2006.
- Jasper, J. and Hayes, J. M.: A carbon isotope record of CO_2 levels during the late Quaternary, *Nature*, 347, 463–465, 1990.
- Jones, D. M., Carter, J. F., Eglinton, G., Jumeau, E. J., and Fenwick, C. S.: Determination of $\delta^{13}\text{C}$ values of sedimentary straight chain and cyclic alcohols by gas chromatography/isotope ratio mass spectrometry. *Biol. Mass Spectrom.*, 20, 641–646, 1991.
- Kaneda, T.: Iso- and anteiso-fatty acids in bacteria: biosynthesis, function, and taxonomic significance, *Microbiol. Rev.*, 55, 288–302, 1991.
- Kroopnick, P. M.: The distribution of ^{13}C of $\sum\text{CO}_2$ in the world oceans, *Deep Sea-Res. Pt I*, 32, 57–84, 1985.
- Laws, E. A., Bidigare, R. R., and Popp, B. N.: Effect of growth rate and CO_2 concentration on carbon isotopic fractionation by the marine diatom *Phaeodactylum tricornutum*. *Limnol. Oceanogr.*, 42, 1552–1560, 1997.
- Laws, E. A., Popp, B. N., Bidigare, R. R., Kennicutt, M. C., and Macko, S. A.: Dependence of phytoplankton carbon isotopic composition on growth rate and $[\text{CO}_2]_{\text{aq}}$: Theoretical considerations and experimental results, *Geochim. Cosmochim. Ac.*, 59, 1131–1138, 1995.
- Laws, E. A., Popp, B. N., Bidigare, R. R., Riebesell, U., Burkhardt, S., and Wakeham, S. G.: Controls on the molecular distribution and carbon isotopic composition of alkenones in certain haptophyte algae. *Geochim. Geophys. Geosci.*, 2, paper number:2000GC000057, 2001.
- Lee, R. F., Hagen, W., and Kattner, G.: Lipid storage in marine zooplankton. *Mar. Ecol.-Progr. Ser.*, 307, 273–306, 2006.
- Lewis, E. and Wallace, D. W. R.: Program Developed for CO_2 System Calculations, ORNL/CDIAC-105. Carbon Dioxide Information Analysis Center, Oak Ridge National Laboratory, U.S. Department of Energy, Oak Ridge, Tennessee, 1998.
- Litchman, E., Klausmeier, C. A., Miller, J. R., Schofield, O. M. and Falkowski, P. G.: Multi-nutrient, multi-group model of present and future oceanic phytoplankton communities, *Biogeosciences*, 3, 585–606, 2006, <http://www.biogeosciences.net/3/585/2006/>.
- Livne, A. and Sukenik, A.: Lipid synthesis and abundance of acetyl CoA carboxylase in *Isochrysis galbana* (Prymnesiophyceae) following nitrogen starvation, *Plant Cell Physiol.* 33, 1175–1181, 1992.
- Mackey, M. D., Mackey, D. J., Higgins, H. W., and Wright, S. W.: CHEMTAX – a program for estimating class abundances from chemical markers: application to HPLC measurements of phytoplankton. *Mar. Ecol.-Progr. Ser.*, 144, 265–283, 1996.
- McGinn, P. J., Price, G. D., Maleszka, R., and Badger, M. R.: Inorganic Carbon Limitation and Light Control the Expression of Transcripts Related to the CO_2 -Concentrating Mechanism in the Cyanobacterium *Synechocystis* sp. Strain PCC6803. *Plant Physiol.*, 132, 218–229, 2003.
- Miquel, J. C., Fowler, S. W., La Rosa, J., and Buat-Menard, P.: Dynamics of the downward flux of particles and carbon in the open northwestern Mediterranean Sea, *Deep Sea-Res.*, 41, 243–261, 1994.
- Miquel, J. C., Gasser B., and Claustre, H.: Export Fluxes in Contrasting Environments of the South-East Pacific Ocean Derived from Drifting Sediment traps (BIOSOPE). *Eos Trans. AGU*. 87(52), Fall Meet. Suppl., Abstract OS13C-1569, 2006.
- Mook, W. G., Bommerson, J. C., and Staverman, W. H.: Carbon isotope fractionation between dissolved bicarbonate and gaseous carbon dioxide. *Earth Planet. Sc. Lett.*, 22, 169–176, 1974.
- Morel, F. M. M., Reinfelder, J. R., Roberts, S. B., Chamberlain, C. P., Lee, J. G. and Yee, D.: Zinc and carbon co-limitation of marine phytoplankton, *Nature*, 369, 740–742, 1994.
- Muhlebach, A. and Weber, K.: Origins and fate of dissolved sterols in the Weddell Sea, Antarctica. *Org. Geochem.*, 29, 1595–1607, 1998.
- Pancost, R. D., Freeman, K. H. and Wakeham, S. G.: Controls on the carbon-isotope compositions of compounds in Peru surface waters, *Org. Geochem.*, 30, 319–340, 1999.
- Pancost, R. D., Freeman, K. H., Wakeham, S. G., and Robertson, C. Y.: Controls on carbon isotope fractionation by diatoms in the Peru upwelling region, *Geochim. Cosmochim. Ac.*, 61, 4983–4991, 1997.
- Parrish, C. C., Wells, J. S., Yang, Z., and Dabinett, P.: Growth and lipid composition of scallop juveniles, *Placoepecten magellanicus*, fed the flagellate *Isochrysis galbana* with varying lipid composition and the diatom *Chaetoceros muelleri*, *Mar. Biol.*, 133, 461–471, 1998.
- Pinturier-Geiss, L., Mejanelle, L., Dale, B., and Karlsen, D. A.: Lipids as indicators of eutrophication in marine coastal sediments, *J. Microbiol. Meth.*, 48, 239–257, 2002.
- Popp, B. N., Kenig, F., Wakeham, S. G., Laws, E. A., and Bidigare, R. R.: Does growth rate affect ketone unsaturation and intracellular carbon isotope variability in *Emiliania huxleyi*? *Paleoceanography*, 13, 35–41, 1998a.
- Popp, B. N., Laws, E. A., Bidigare, R. R., Dore, J. E., Hanson, K. L. and Wakeham, S. G.: Effect of phytoplankton cell geometry on carbon isotopic fractionation. *Geochim. Cosmochim. Ac.*, 62, 69–77, 1998b.
- Popp, B. N., Bidigare, R. R., Deschenes, B., Laws, E. A., Prahl, F. G., Tanimoto, J. K., and Wallsgrave, R. J.: A new method for estimating growth rates of alkenone-producing haptophytes, *Limnol. Oceanogr. Methods*, 4, 114–129, 2006a.
- Popp, B. N., Prahl, F. G., Wallsgrave, R. J., and Tanimoto, J.: Seasonal patterns of alkenone production in the subtropical oligotrophic North Pacific, *Paleoceanography*, 21, PA1004, doi:10.1029/2005PA001165, 2006b.
- Prahl, F.G., Muehlhausen, L.A. and Zahnle, D.L.: Further evaluation of long-chain alkenones as indicators of paleoceanographic conditions. *Geochim. Cosmochim. Ac.*, 52, 2303–2310, 1988.
- Prahl, F. G., Sparrow, M. A., and Wolfe, G. V.: Physiological impacts on alkenone paleothermometry, *Paleoceanography*, 18, 1025, doi:10.1029/2002PA000803, 2003.
- Prahl, F. G., Popp, B. N., Karl, D. M., and Sparrow, M. A.: Ecology and biogeochemistry of alkenone production at Station ALOHA,

- Deep Sea- Res. Pt I, 52, 699–719, 2005.
- Prahl, F. G., and Wakeham, S. G.: Calibration of unsaturation patterns in long-chain ketone compositions for palaeotemperature assessment, *Nature*, 330, 367–369, 1987.
- Quay, P., Sonnerup, R., Westby, T., Sutsman, J. and McNichol, A.: Changes in the $^{13}\text{C}/^{12}\text{C}$ of dissolved inorganic carbon in the ocean as a tracer of anthropogenic CO_2 uptake, *Global Biogeochem. Cy.*, 17(1), 1004, doi:10.1029/2001GB001817, 2003.
- Raimbault, P., Garcia, N., and Cerutti, F.: Distribution of inorganic and organic nutrients in the South Pacific Ocean – evidence for long-term accumulation of organic matter in nitrogen-depleted waters, *Biogeosciences*, 5, 281–298, 2008, <http://www.biogeosciences.net/5/281/2008/>.
- Ras, J., Claustre, H., and Uitz, J.: Spatial variability of phytoplankton pigment distributions in the Subtropical South Pacific Ocean: comparison between in situ and predicted data, *Biogeosciences*, 5, 353–369, 2008, <http://www.biogeosciences.net/5/353/2008/>.
- Rau, G. H., Chavez, F. P., and Friederich, G. E.: Plankton $^{13}\text{C}/^{12}\text{C}$ variations in Monterey Bay, California: evidence of non-diffusive inorganic carbon uptake by phytoplankton in an upwelling environment, *Deep Sea- Res. Pt. I*, 48, 79–94, 2001.
- Rau, G. H., Riebesell, U., and Wolf-Gladrow, D.: A model of photosynthetic C fractionation by marine phytoplankton based on diffusive molecular CO_2 uptake, *Mar. Ecol.-Progr. Ser.*, 133, 275–285, 1996.
- Reitan, K. I., Rainuzzo, J. R., and Olsen, Y.: Effect of nutrient limitation on fatty acid and lipid content of marine microalgae 1, *J. Phycology*, 30, 972–979, 1994.
- Riebesell, U., Revill, A. T., Holdsworth, D. G., and Volkman, J. K.: The effects of varying CO_2 concentration on lipid composition and carbon isotope fractionation in *Emiliania huxleyi*. *Geochim. Cosmochim. Ac.*, 64, 4179–4192, 2000.
- Robinson, N., Eglinton, G., Brassell, S. C., and Cranwell, P. A.: Dinoflagellate origin for sedimentary 4methylsteroids and 5 α (H)-stanols. *Nature*, 308, 419–422, 1984.
- Rontani, J.-F., Marty, J.-C., Miquel, J.-C., and Volkman, J. K.: Free radical oxidation (autoxidation) of alkenones and other microalgal lipids in seawater, *Org. Geochem.*, 37, 354–368, 2006.
- Rontani, J.-F., Harji, R., Guasco, S., Prahl, F. G., Volkman, J. K., Bhosle, N. B., and Bonin, P.: Degradation of alkenones by aerobic heterotrophic bacteria: Selective or not?, *Org. Geochem.*, 39, 34–51, 2008.
- Rost, B., Zondervan, I., and Riebesell, U.: Light-dependent carbon isotope fractionation in the coccolithophorid *Emiliania huxleyi*, *Limnol. Oceanogr.*, 47, 120–128, 2002.
- Rost, B., Riebesell, U., Burkhardt, S., and Sultemeyer, D.: Carbon acquisition of bloom-forming marine phytoplankton, *Limnol. Oceanogr.*, 48, 55–67, 2003.
- Sakata, S., Hayes, J. M., McTaggart, A. R., Evans, R. A., Leckrone, K. J., and Togasaki, R. K.: Carbon isotopic fractionation associated with lipid biosynthesis by a cyanobacterium: Relevance for interpretation of biomarker records, *Geochim. Cosmochim. Ac.*, 61, 5379–5389, 1997.
- Sargent, J. R., Gatten, R. R., and Mcintosh, R.: Wax esters in the marine environment – Their occurrence, formation, transformation and ultimate fates, *Mar. Chem.*, 5, 573–584, 1977.
- Shaked, Y., Xu, Y., Leblanc, K., and Morel, F. M. M.: Zinc availability and alkaline phosphatase activity in *Emiliania huxleyi*: Implications for Zn-P co-limitation in the ocean, *Limnol. Oceanogr.*, 51, 299–309, 2006.
- Shifrin, N. S., and Chisholm, S. W.: Phytoplankton lipids: inter-specific differences and effects of nitrate, silicate and light-dark cycles, *J. Phycology*, 17, 374–384, 1981.
- Shin, K. H., Hama, T., Yoshie, N., Noriki, S., and Tsunogai, S.: Dynamics of fatty acids in newly biosynthesized phytoplankton cells and seston during a spring bloom off the west coast of Hokkaido Island, Japan. *Mar. Chem.*, 70, 243–256, 2000.
- Schouten, S., Klein Breteler, W. C. M., Blokker, P., Schogt, N. C., Rijpstra, W. I., Grice, K., Baas, M., and Sinninghe Damste, J. S.: Biosynthetic effects on the stable carbon isotopic compositions of algal lipids: Implications for deciphering the carbon isotopic biomarker record, *Geochim. Cosmochim. Ac.*, 62, 1397–1406, 1998.
- Sicre, M.-A., Bard, E., Ezat, U., and Rostek, F.: Alkenone distributions in the North Atlantic and Nordic sea surface waters, *Geochem. Geophys. Geosy.*, 3(2), 1013, doi:10.1029/2001GC000159, 2002.
- Thompson, P. A. and Calvert, S. E.: Carbon isotope fractionation by *Emiliania huxleyi*, *Limnol. Oceanogr.*, 40, 673–679, 1995.
- Tolosa, I. and de Mora, S.: Isolation of neutral and acidic lipid biomarker classes for compound-specific-carbon isotope analysis by means of solvent extraction and normal-phase high-performance liquid chromatography, *J. Chromatogr. A*, 1045, 71–84, 2004.
- Tolosa, I., LeBlond, N., Copin-Montegut, C., Marty, J.-C., de Mora, S., and Prieur, L.: Distribution of sterol and fatty alcohol biomarkers in particulate matter from the frontal structure of the Alboran Sea (S. W. Mediterranean Sea), *Mar. Chem.*, 82, 161–183, 2003.
- Tolosa, I., Vescovali, I., LeBlond, N., Marty, J.-C., de Mora, S., and Prieur, L.: Distribution of pigment and fatty acid biomarkers in particulate matter from the frontal structure of the Alboran Sea (S. W. Mediterranean Sea). *Mar. Chem.*, 88, 103–125, 2004.
- van der Meer, M. T. J., Schouten, S., van Dongen, B. E., Rijpstra, W. I. C., Fuchs, G., Damste, J. S. S., de Leeuw, J. W., and Ward, D. M.: Biosynthetic controls on the ^{13}C contents of organic components in the photoautotrophic bacterium *Chloroflexus aurantiacus*, *J. Biol. Chem.*, 276, 10971–10976, 2001.
- Van Wambeke, F., Obernosterer, I., Moutin, T., Duhamel, S., Ulloa, O., and Claustre, H.: Heterotrophic bacterial production in the eastern South Pacific: longitudinal trends and coupling with primary production, *Biogeosciences*, 5, 157–169, 2008, <http://www.biogeosciences.net/5/157/2008/>.
- Volkman, J. K.: A review of sterol markers for marine and terrigenous organic matter, *Org. Geochem.*, 9, 83–99, 1986.
- Volkman, J. K., Barrerr, S. M., Blackburn, S. I., and Sikes, E. L.: Alkenones in *Gephyrocapsa oceanica*: Implications for studies of paleoclimate, *Geochim. Cosmochim. Ac.*, 59, 513–520, 1995.
- Volkman, J. K., Barrett, S. M., and Dunstan, G. A.: C_{25} and C_{30} highly branched isoprenoid alkenes in laboratory cultures of two marine diatoms, *Org. Geochem.*, 21, 407–414, 1994.
- Volkman, J. K. and Hallegraeff, G. M.: Lipids in marine diatoms of the genus *Thalassiosira*: Predominance of 24-methylenecholesterol, *Phytochemistry*, 27, 1389–1394, 1988.
- Volkman, J. K., Jeffrey, S. W., Nichols, P. D., Rogers, G. I., and Garland, C. D.: Fatty acid and lipid composition of 10 species of microalgae used in mariculture, *J. Exp. Mar. Biol. Ecol.*, 128,

- 219–240, 1989.
- Werne, J. P. and Hollander, D. J.: Balancing supply and demand: controls on carbon isotope fractionation in the Cariaco Basin (Venezuela) Younger Dryas to present, *Mar. Chem.*, 92, 275–293, 2004.
- Winters, K., Parker, P. L., and Van Baalen, C.: Hydrocarbons of Blue-Green Algae: Geochemical significance, *Science*, 163, 467–468, 1969.
- Woodger, F. J., Badger, M. R., and Price, G. D.: Sensing of inorganic carbon limitation in *Synechococcus* PCC7942 is correlated with the size of the internal inorganic carbon pool and involves oxygen, *Plant Physiol.*, 139, 1959–1969, 2005.
- Woodworth, M., Goni, M., Tappa, E., Tedesco, K., Thunell, R., Astor, Y., Varela, R., Rafael Diaz-Ramos, J., and Muller-Karger, F.: Oceanographic controls on the carbon isotopic compositions of sinking particles from the Cariaco Basin, *Deep Sea- Res. Pt. I*, 51, 1955–1974, 2004.
- Yamamoto, M., Shiraiwa, Y., and Inouye, I.: Physiological responses of lipids in *Emiliana huxleyi* and *Gephyrocapsa oceanica* (*Haptophyceae*) to growth status and their implications for alkenone paleothermometry, *Org. Geochem.*, 31, 799–811, 2000.

Optical backscattering properties of the “clearest” natural waters

M. S. Twardowski¹, H. Claustre², S. A. Freeman¹, D. Stramski³, and Y. Huot²

¹Department of Research, WET Labs, Inc., Narragansett, RI 02882, USA

²Laboratoire d’Océanographie de Villefranche, UMR-CNRS 7093, Villefranche sur Mer, France

³Marine Physical Laboratory, Scripps Institution of Oceanography, Univ. of California at San Diego, La Jolla, CA 92093-0238, USA

Received: 13 July 2007 – Published in Biogeosciences Discuss.: 30 July 2007

Revised: 24 October 2007 – Accepted: 9 November 2007 – Published: 29 November 2007

Abstract. During the BIOSOPE field campaign October–December 2004, measurements of inherent optical properties from the surface to 500 m depth were made with a ship profiler at stations covering over 8000 km through the Southeast Pacific Ocean. Data from a ~3000 km section containing the very clearest waters in the central gyre are reported here. The total volume scattering function at 117° , $\beta_t(117^\circ)$, was measured with a WET Labs ECO-BB3 sensor at 462, 532, and 650 nm with estimated uncertainties of 2×10^{-5} , 5×10^{-6} , and $2 \times 10^{-6} \text{ m}^{-1} \text{ sr}^{-1}$, respectively. These values were approximately 6%, 3%, and 3% of the volume scattering by pure seawater at their respective wavelengths. From a methodological perspective, there were several results:

- b_{bp} distributions were resolvable even though some of the values from the central gyre were an order of magnitude lower than the lowest previous measurements in the literature;
- Direct in-situ measurements of instrument dark offsets were necessary to accurately resolve backscattering at these low levels;
- accurate pure seawater backscattering values are critical in determining particulate backscattering coefficients in the open ocean (not only in these very clear waters); the pure water scattering values determined by Buiteveld et al. (1994) with a $[1+0.3S/37]$ adjustment for salinity based on Morel (1974) appear to be the most accurate estimates, with aggregate accuracies as low as a few percent; and
- closure was demonstrated with subsurface reflectance measurements reported by Morel et al. (2007) within instrument precisions, a useful factor in validating the backscattering measurements.

This methodology enabled several observations with respect to the hydrography and the use of backscattering as a biogeochemical proxy:

- The clearest waters sampled were found at depths between 300 and 350 m, from 23.5° S , 118° W to 26° S , 114° W , where total backscattering at 650 nm was not distinguishable from pure seawater;
- Distributions of particulate backscattering b_{bp} across the central gyre exhibited a broad particle peak centered ~100 m;
- The particulate backscattering ratio typically ranged between 0.4% and 0.6% at 650 nm through the majority of the central gyre from the surface to ~210 m, indicative of “soft” water-filled particles with low bulk refractive index; and
- b_{bp} showed a distinct secondary deeper layer centered ~230 m that was absent in particulate attenuation c_p data. The particulate backscattering ratio was significantly higher in this layer than in the rest of the water column, reaching 1.2% in some locations. This high relative backscattering, along with the pigment composition and ecological niche of this layer, appear to be consistent with the coccolithophorid *Florisphaera profunda*.

Moreover, results were consistent with several expectations extrapolated from theory and previous work in oceanic and coastal regions, supporting the conclusion that particulate and total backscattering could be resolved in these extremely clear natural waters.

Correspondence to: M. S. Twardowski
(mtwardo@wetlabs2.com)

1 Introduction

Morel et al. (2007) recently reported several optical properties from the South Pacific gyre near Easter Island, generally considered the clearest known naturally occurring waters (with the quotations in the title, after Morel et al. (2007) belying any presumption that there exist no clearer waters). In the Morel et al. (2007) study, a UV-visible radiometer was used to determine downward and upward planar irradiances at discrete depths, from which the diffuse attenuation coefficient and irradiance reflectance could be determined. Furthermore, the inherent optical properties (IOPs) absorption and backscattering were derived through inversion of these parameters with previously published relationships obtained from radiative transfer model simulations. However, particulate backscattering coefficients b_{bp} , obtained by subtracting the backscattering coefficients by seawater b_{bsw} from total backscattering coefficients b_{bt} derived from the inversion, could not be reliably estimated because the noise inherent to the inversion method combined with the uncertainty of the reflectance determinations was on the order of 10^{-3} m^{-1} . Total backscattering values lower than this level in the visible also test our present knowledge of pure seawater scattering coefficients (Morel et al., 2007). The aim of the work described herein is to present measured backscattering and other IOPs from these same waters, in an effort to enhance our understanding of properties that the reflectance inversions of Morel et al. (2007) were not able to fully resolve. By paying careful attention to calibration, measurement, and processing protocols, increasing detector gains for the backscattering sensor, and averaging multiple samples, backscattering uncertainties on the order of 10^{-5} m^{-1} were achieved.

Spectral backscattering is a key parameter influencing the reflectance properties of the ocean (see reviews by Stramski et al., 2004; Twardowski et al., 2005; Zaneveld et al., 2005). It largely controls the Bidirectional Reflectance Distribution Function (BRDF) that describes how a downwelling radiance field is translated into an upwelling radiance field. Backscattering is thus of central importance in the remote sensing of the ocean using passive (i.e. solar source) and active (i.e. artificial source) methods. The specific magnitude of backscattering is particularly important for those algorithms that do not rely on spectral ratios of reflectance or water-leaving radiance, such as the current experimental algorithm for calcite (Balch et al., 2005).

The dominant sources of backscattering in the ocean are scattering by the particle population and the molecular scattering by pure seawater. Dissolved materials besides salts (“truly” dissolved in this case, i.e. not including colloids $<0.2 \mu\text{m}$) are not expected to impart any significant scattering to natural seawater (Shifrin, 1988). Positive correlations have been demonstrated between backscattering by particles, particle concentration and particulate organic carbon (Balch et al., 1999; Stramski et al., 1999), and the particulate

backscattering to scattering ratio (b_{bp}/b_p) has been shown to be an indicator of bulk particle refractive index, a parameter closely related to particle density (Twardowski et al., 2001; Boss et al., 2004; Sullivan et al., 2005; Loisel et al., 2007). Despite progress, however, understanding specific sources of particulate backscattering in the ocean, crucial for interpretation through inversion, is confounded by a rudimentary understanding of the effects of particle nonsphericity and heterogeneous composition (although recent contributions are encouraging; see Clavano et al., 2007 and Gordon, 2006, 2007). The controversial nature of particulate backscattering lends further motivation to our efforts to obtain well-characterized, accurate data with well-defined uncertainties, a requirement before any productive discussion of its origins or a scattering budget may be attempted.

While particulate backscattering typically dominates in coastal waters, molecular backscattering by seawater becomes very significant in oceanic waters (Shifrin, 1988; Morel and Gentili, 1991). Backscattering by seawater is typically considered a “known” in remote sensing and biogeochemical algorithms (Stramski et al., 2004; Twardowski et al., 2005), but a thorough assessment of the accuracy of available values has not been carried out. Considering estimates of pure water and seawater scattering from Morel (1974), Shifrin (1988), and Buiteveld et al. (1994), one could argue that a reasonable uncertainty in scattering by seawater may be greater than 10%. In the extremely clear waters of the South Pacific, this uncertainty has a substantial (50% or more) impact on estimating particulate backscattering because backscattering by the dominant pure seawater component must be subtracted from direct measurements of total backscattering. Such data may thus provide a valuable means to test the current seawater values available in the literature.

Routine field measurement of the backscattering coefficient has been possible with commercially available instrumentation since the late 1990’s (Maffione and Dana, 1997; Moore et al., 2000; Twardowski et al., 2005). Despite employing different calibration methods, different optical configurations, and different processing algorithms, different sensors have previously been found to agree within about 10% (Pegau et al., 2001; Prentice et al., 2002; Boss et al., 2004) and more recently within 3% in data from very clear Crater Lake, Oregon, USA (Boss et al., 2007). The lowest backscattering values reported in the literature, to our knowledge, were measured in Crater Lake by Boss et al. (2007) and Stramska and Stramski (2005) in the Greenland Sea, where b_{bp} in the mid-visible reached values on the order of 10^{-4} m^{-1} .

Distributions of backscattering are presented along a transect through the central South Pacific gyre collected during the Biogeochemistry and Optics South Pacific Experiment (BIOSOPE) cruise aboard the R/V L’Atalante. Our primary objective was to resolve biogeochemical processes occurring in the South Pacific using high sampling rate, profiling optical instrumentation as effective proxies, but a fundamental

first step in this endeavor is determining to what extent the measurements of backscattering and other IOPs are accurate in these extremely clear waters. Future work will delve more thoroughly into analytical and semi-analytical associations between scattering and the underlying particle biogeochemistry.

Study site

The South Pacific anticyclonic gyre is characterized as systematically hyperoligotrophic, with chlorophyll concentrations reaching as low as 0.02 mg m^{-3} at the surface (Morel et al., 2007; Claustre et al., 2007¹). The BIOSOPE cruise occurred in October–December 2004 and consisted of a transect $\sim 8000 \text{ km}$ long from the sub-Equatorial waters near the Marquesas Islands, to Easter Island in the central gyre, to the Chilean upwelling region. Only those measurements collected at stations in the central gyre are considered here (Fig. 1). Deep chlorophyll maxima and euphotic zone depths were typically observed between 160–210 m in this region. For details of the hydrography and the physics of this region, see Claustre et al. (2007)¹.

2 Review of molecular scattering by pure seawater

Past theory and measurements of the volume scattering function and total scattering coefficient by pure seawater, $\beta_{sw}(\theta) \text{ m}^{-1} \text{ sr}^{-1}$ and $b_{sw} \text{ m}^{-1}$, respectively, are reviewed here because of their importance, particularly with respect to backscattering, in clear ocean waters. Pure seawater scattering is typically considered to be small and the common practice is to adopt a certain standard, which is not expected to vary for different environmental conditions of seawater. In terms of total scattering, pure water may contribute up to 10% in the visible for very clear ocean waters, so that this practice is usually not fraught with substantial error. Pure seawater scattering has a much more significant effect in the backward direction, however, owing to the nearly isotropic nature of molecular scattering by water and the strongly forward-peaked characteristic of volume scattering functions of natural particle populations. This results in typically $< 1\%$ of particulate scattering in the open ocean occurring in the backward direction (except for unusual cases such as coccolithophorid blooms), as opposed to 50% of pure seawater scattering. The contributions of seawater and particles to total backscattering are thus comparable in many open ocean waters, and, in the clearest waters, seawater backscattering, $b_{b_{sw}} \text{ m}^{-1}$, readily exceeds an 80% contribution (Shifrin, 1988; Morel and Gentili, 1991). An accurate estimation of $b_{b_{sw}}$ becomes critical when one wishes to isolate particulate

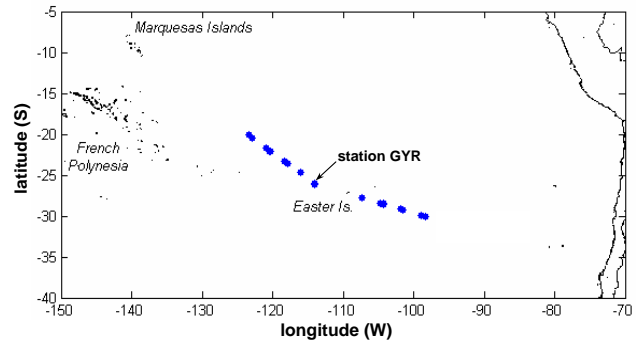


Fig. 1. Map of study region in the Southeast Pacific. Locations are marked in blue for all stations sampled in the very clear central gyre. The station labeled GYR at 114°W longitude was the location of a 4 d time series of measurements.

backscattering from measurements of total backscattering. This is true for any open ocean waters, not only the extremely clear waters addressed in this study.

There are three independent estimates of pure water scattering that may be considered among the most accurate to date; these are found in Morel (1974), Shifrin (1988), and Buiteveld et al. (1994). All three use the same equations from Einstein-Smoluchowski theory, which describes scattering resulting from density and temperature fluctuations in media (Morel, 1974 and Shifrin, 1988 both have excellent reviews). Where the estimates differ is in the physical expressions, mostly derived from empiricism, used as inputs to the equations. For the sake of clarity, the equations are reproduced:

$$\beta_w(90^\circ) = \frac{2\pi^2}{\lambda^4 B_T} k T_a n^2 \left(\frac{\partial n}{\partial P} \right)_T^2 C, \quad (1)$$

where the Cabannes factor $C = \frac{(6+6\delta)}{(6-7\delta)}$, accounts for the anisotropy of water due to fluctuations in molecule orientation. The parameter δ is the depolarization ratio. The volume scattering function is computed from:

$$\beta_w(\theta) = \beta_w(90^\circ) [1 + p(90^\circ) \cos^2(\theta)], \quad (2)$$

where the degree of polarization at 90 degrees, $p(90^\circ)$, is $\frac{(1-\delta)}{(1+\delta)}$. Total scattering is then obtained from:

$$b_w = \frac{16\pi}{3} \beta_w(90^\circ) \left[\frac{1(2+\delta)}{2(1+\delta)} \right]. \quad (3)$$

Removing the effect of anisotropy in Eq. (2), i.e., letting $\delta=0$ so that $p(90^\circ)=1$, results in the classic Rayleigh scattering angular pattern. Notation for the parameters in Eq. (1) is provided in Table 1 along with the expressions adopted by Buiteveld et al. (1994).

The four experimental variable inputs to Eq. (1) are $B_T(T, S)$, $n(\lambda, T, S, P)$, $(\partial n / \partial P)_T(\lambda, T)$, and δ . Where it can be determined, each of the three studies mentioned

¹Claustre, H., Sciandra, A., and Vaultot, D.: Introduction to the special section : bio-optical and biogeochemical conditions in the South East Pacific in late 2004 – the BIOSOPE cruise, Biogeosci. Discuss., in preparation, 2007.

Table 1. Notation

α	amplitude of scattering by unpolarized light, i.e., S_{11} in Bohren and Huffman (1983)
a_x	absorption coefficient, m^{-1} , where subscript $x=t, w, p, ph, g,$ and pg specifies total, water, particulate, phytoplankton, dissolved, and particulate + dissolved, respectively
b_x	scattering coefficient, m^{-1} , where subscript $x=t, w, sw, swB, p, b, bsw, bswB,$ and bp specifies total, water, seawater, seawater values of Buiteveld et al. (1994), particulate, backward, backward seawater, backward seawater values of Buiteveld et al. (1994), and backward particulate, respectively
β_x	volume scattering coefficient, $m^{-1} sr^{-1}$, where subscript $=t, w, swB, swM, swS,$ and p specifies total, water, the seawater values of Buiteveld et al. (1994) the seawater values of Morel, the seawater values of Shifrin, and particulate, respectively (see text)
B_T	isothermal compressibility of water, Pa^{-1} ; Buiteveld et al. (1994) recommend a quadratic fit to the data of Lepple and Millero (1971): $=(5.062271 - 0.03179 T + 0.000407 T^2)10^{-10} a.$
c_x	attenuation coefficient, m^{-1} , where subscript $=t, sw, p, g,$ and pg specifies total, seawater, particulate, dissolved, and particulate+dissolved, respectively
C	Cabannes factor
χ_p	factor in proportionality between particulate backscattering and particulate volume scattering
d	particle diameter, μm
D	sensor calibration dark offset
δ	depolarization ratio (0.051; Farinato and Roswell 1976)
F	size distribution function, m^{-4}
f	sensor calibration scaling factor
f'	factor linking absorption and backscattering to reflectance
k	Boltzmann constant, $1.38054 \cdot 10^{-23} J \text{ } ^\circ K^{-1}$
λ	wavelength, nm
n	refractive index of water; the formulation by McNeil(1977) recommended by Buiteveld et al. (1994), but with the salinity dependent term removed (see text): $=1.3247 + 3.3 \times 10^3 \lambda^{-2} - 3.2 \times 10^7 \lambda^{-4} - 2.5 \times 10^{-6} T^2.$
n_p	particulate refractive index
$\partial n / \partial P$	pressure derivative of n , Pa^{-1} ; Buiteveld et al. (1994) convolve spectral and temperature dependencies as follows: $= \frac{\frac{\partial n}{\partial P}(\lambda, 20) \frac{\partial n}{\partial P}(633, T)}{\frac{\partial n}{\partial P}(633, 20)}$, where $\partial n / \partial P(\lambda, 20)^b = (-0.000156 \lambda + 1.5989)10^{-10} Pa^{-1},$ and $\partial n / \partial P(633, T)^c = (1.61857 - 0.005785 T)10^{-10} Pa^{-1}$
p	degree of polarization
P	pressure, Pa
R	irradiance reflectance
S	salinity
T	temperature, $^\circ C$
T_a	absolute temperature, $^\circ K$
θ	angle (radians or degrees)
W	angular weighting function (rad^{-1})
ψ	spectral response function (nm^{-1})

^a Factor reported as 10^{-11} in Buiteveld et al. (1994).^b O'Conner and Schlupf (1967)^c Evtvushenkov and Kiyachenko (1982)

uses different expressions for these parameters, except both Shifrin (1988) and Morel (1974) use the same δ value of 0.09. Without belaboring the details of the precise differences in the parameters where it is possible to directly compare, a general summarization may be reached that the expressions compiled by Buiteveld et al. (1994) appear to be the most current in the literature (or are at least very close), as might be expected since their work is the most recent. In particular, Buiteveld et al. (1994) use a δ value of 0.051 based on the work of Farinato and Roswell (1976), who claim that the much higher values previously found in the literature were the result of stray light contamination and photometer geometry errors. Their newer values were also closer to a theoretical estimate. The Buiteveld et al. (1994) values were thus adopted here, unless specifically noted otherwise. This decision will be evaluated later.

Because all of the physical expressions entering into Eq. (1) are not provided in Morel (1974) and Shifrin (1988), it is desirable to fit a suitable model to their data to extrapolate results to fine spectral resolution (the values of Buiteveld et al. (1994) may be computed directly for any λ and T). The following relationships are constructed for $T=20^\circ\text{C}$ at atmospheric pressure:

$$\text{Morel : } b_w = 3.50 \left(\frac{\lambda}{450} \right)^{-4.32} 10^{-3} \text{ m}^{-1}, \text{ and} \quad (4)$$

$$\text{Shifrin : } b_w = 1.49 \left(\frac{\lambda}{546} \right)^{-4.17} 10^{-3} \text{ m}^{-1}. \quad (5)$$

In both cases, the amplitude values ($b_w(450)=3.50 \times 10^{-3} \text{ m}^{-1}$ and $b_w(546)=1.49 \times 10^{-3} \text{ m}^{-1}$) were provided in Tables from the original texts. The 4.32 exponent of the model used in Eq. (4) was obtained with a nonlinear hyperbolic fit ($R^2=0.99$) to the 25-nm spaced data provided in Table 4 of Morel using only the data from 350 to 525 nm. This value matches Morel's recommended slope of 4.32. Acceptable accuracies ($<0.5\%$) between the Eq. (4) model and Morel's calculated data are only observed in the 350 to 525 nm spectral range (Table 2). The 4.17 slope used in Eq. (5) was provided on p. 82 of Shifrin (1988). For comparison, the slope for calculations using the Buiteveld et al. (1994) expressions is 4.14. This slope varies negligibly with temperature. The models in Eqs. (4) and (5) are transferable to $\beta_w(\lambda, \theta)$ using Eqs. (2) and (3):

$$\text{Morel : } \beta_w(\lambda, \theta) = 2.18 \left(\frac{\lambda}{450} \right)^{-4.32} [1 + p(90) \cos^2(\theta)] 10^{-4} \text{ m}^{-1} \text{ sr}^{-1}, \text{ and} \quad (6)$$

$$\text{Shifrin : } \beta_w(\lambda, \theta) = 0.93 \left(\frac{\lambda}{546} \right)^{-4.17} [1 + p(90) \cos^2(\theta)] 10^{-4} \text{ m}^{-1} \text{ sr}^{-1} \quad (7)$$

Equation (6) is also only strictly applicable between 350 and 525 nm.

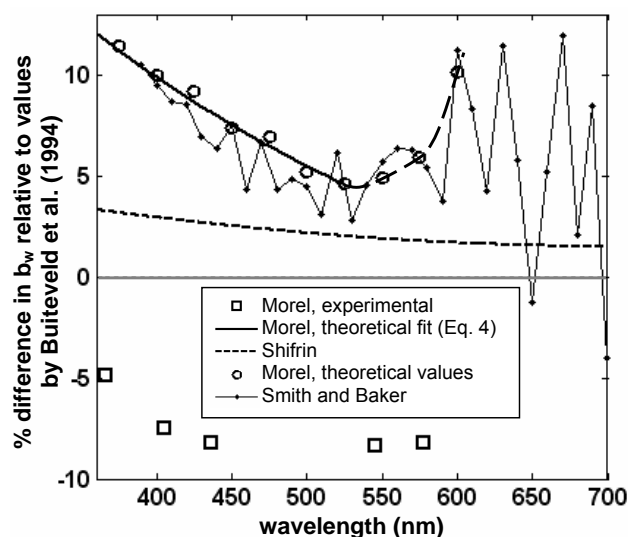


Fig. 2. Comparison of pure water scattering b_w from Buiteveld et al. (1994), Morel (1968, 1974), and Shifrin (1988). Percent differences relative to the values of Buiteveld et al. (1994) are plotted. The gray line demarcates zero. Equation (5) is used for Shifrin's values. Circles represent the theoretical values of Morel (1974). Equation (4) is used to approximate Morel's theoretical values for wavelengths shorter than 525 nm (solid black curve; long dashes approximately extend relationship through Morel's theoretical values at 550, 575, and 600 nm; see Table 2). The experimental values of $\beta_w(90^\circ)$ reported in Morel (1968) are converted to b_w using Eq. (3) and $\delta=0.09$. Note that a δ of 0.051 would increase these experimental values by $\sim 2\%$. The values of Smith and Baker (1981), derived directly from Morel (1974), tend to exhibit more noise because their Table 1 is truncated at 4 decimal places.

Table 2 provides b_w estimates from the various sources with the same wavelength range and resolution of Morel (1974). Shifrin's and Morel's $b_w(\lambda)$ values relative to those of Buiteveld et al. (1994) are plotted in Fig. 2. It can be seen that Shifrin's values are between 1–3% higher throughout the visible and Morel's values range from about 5% higher in the green to $\sim 10\%$ higher in the short blue and near-red. The disagreement between Morel's values and those of Buiteveld et al. (1994) observed in the near-red contradicts statements in Buiteveld et al. (1994). Buiteveld et al. (1994) estimate the accuracy of their pure water scattering values at $\pm 6\%$. Morel (1974) noted that the depolarization ratio has a significant influence on theoretical scattering values. Interestingly, if a δ value of 0.09 is used in the Buiteveld et al. (1994) expressions, their scattering values increase by $\sim 7\%$ (independent of λ). Similarly, the values of Morel (1974) and Shifrin (1988) would decrease by $\sim 7\%$ if a δ value of 0.051 is substituted. Thus, if Morel and Buiteveld et al. (1994) used the same δ , the resulting agreement would improve significantly ($\pm 3\%$ throughout the visible). Since Shifrin's values are already relatively close to Buiteveld's, the effect of the higher δ value used by Shifrin was compensated to a degree in the

Table 2. Pure water scattering parameters.

parameter	λ (nm)										
	350	375	400	425	450	475	500	525	550	575	600
$\beta_w(90^\circ)$ ($10^{-4} \text{ m}^{-1} \text{ sr}^{-1}$) from Morel (1974) ^a	6.47	4.80	3.63	2.80	2.18	1.73	1.38	1.12	0.93	0.78	0.68
b_w ^b (10^{-4} m^{-1}) from Morel (1974) (1)	103.9	77.1	58.3	45.0	35.0	27.8	22.2	18.0	14.9	12.5	10.9
b_w (10^{-4} m^{-1}) modeled from Eq. (4) (2)	103.7	76.9	58.2	44.8	35.0	27.7	22.2	18.0	14.7	12.1	10.1
% difference (1 and 2)	0.25	0.20	0.14	0.37	0.03	0.27	-0.18	0.02	1.52	3.10	7.51
b_w ^c (10^{-4} m^{-1}) from Buiteveld et al. (1994)	92.0	69.2	53.0	41.2	32.6	26.0	21.1	17.2	14.2	11.8	9.9
b_w ^c (10^{-4} m^{-1}) from Shifrin (Eq. 5)	95.2	71.4	54.5	42.4	33.4	26.6	21.5	17.5	14.5	12.0	10.1

^a Line 1 in Table 4 of Morel (1974).

^b Computed from $\beta_w(90^\circ)$ in Line 1 using Eq. (3) and $\delta=0.09$, i.e., $b_{wM}=16.06*\beta_w(90^\circ)$

^c Computed at 20°C.

expressions used for other physical parameters. Incidentally, Shifrin (1988) additionally determined pressure dependencies for pure water scattering, but the maximum effect down to 500 m (the domain of measurements in the work herein) was $1 \times 10^{-5} \text{ m}^{-1}$, negligible with respect to our measurement uncertainties.

In addition to these theoretical estimates, Morel (1966, 1968) also determined $\beta_w(90^\circ)$ experimentally at five wavelengths, from which b_w may be computed via Eq. (3) (Fig. 2). The measurements of Morel (1966) were made relative to optically pure benzene, which were converted to absolute values of $\beta_w(90^\circ)$ in the 1968 study, once a consensus on the absolute values for benzene was reached in the literature. Values of b_w computed from the experimental $\beta_w(90^\circ)$ using a δ of 0.09 range between about 5–8% lower than the values of Buiteveld et al. (1994) (Fig. 2). Using a δ value of 0.051, the values range between 3–6% lower. Thus, we may conclude that if the same δ value of 0.051 that was used in Buiteveld et al. (1994) is used in computing b_w for both Morel's theoretical and experimental data, the results agree with the Buiteveld et al. (1994) theoretical values within their reported accuracy.

The effects of sea salts on pure water scattering are substantial. Sea salts alter the scattering behavior of pure water rather than imparting additional molecular scattering (Shifrin, 1988). Morel (1966, 1968, 1974) determined that dissolving sea salts to a salinity of 35–39 increases scattering by approximately 30%. This relationship was based on measurements in a purified natural seawater sample collected from the Mediterranean, and supported by theoretical extrapolations of results from measurements in artificial seawater and purified NaCl solutions. This is a very valuable data

point because, to our knowledge, there are currently no other measurements of this substantial effect in the literature. In the very clear waters of the central gyre, a 5% uncertainty in this estimate of 30% enhancement can translate into a 50% uncertainty in some b_{bp} estimates. Moreover, efforts to measure b_{bp} in any open ocean environment will be appreciably influenced by the accuracy of this salt effect estimate. This is clearly an area where additional experimentation could be of benefit. Such experiments are extraordinarily difficult to carry out, however, because of the effects of particle contamination in the sample.

We presume linearity with respect to salinity based on theoretical predictions (Shifrin, 1988) and experimental results summarized by Morel (1974) to derive a salinity adjustment of $[1+0.3S/37]$ based on Morel's work. This term is multiplied by b_w and $\beta_w(\lambda, \theta)$ obtained using the expressions of Buiteveld et al. (1994) to obtain b_{swB} and $\beta_{swB}(\lambda, \theta)$, respectively. We consider these values to be the best estimates of pure seawater scattering. MATLAB code to compute these coefficients can be downloaded from: <http://wetlabs.com/appnotes/scatteringcalcstwardo.pdf>. These values, or values very close (<2% difference), have previously been used by Sullivan et al. (2006) and are provided in Morel et al. (2007). Because Morel's ~30% enhancement for seawater was an empirical observation relative to pure water, we do not include the dependency of salinity in the seawater refractive index term (see Table 1). Thus, for seawater, scattering by analogous pure water at a given λ and T is computed, and then the entire salinity effect is assumed accounted for in the adjustment from Morel.

Equation (6) multiplied by the $[1+0.3S/37]$ salinity term results in $\beta_{swM}(\lambda, \theta)$. Similarly, $\beta_{swS}(\lambda, \theta)$ are derived from multiplying Eq. (7) by the salinity adjustment term. It should be noted that in Tables of b_{sw} (546) in Chapt. 3 of Shifrin (1988), the final adjustment for salinity relative to pure water is significantly greater (5–9% higher) than values predicted using the $[1+0.3S/37]$ relationship here, even though Morel's work is cited. Thus, our estimated $\beta_{swS}(\lambda, \theta)$ here would not appear to agree with Shifrin's own seawater values (there are no β_{sw} values provided in Shifrin, but they can be derived from Eqs. (2) and (3) knowing b_{sw}).

For the volume scattering function of pure seawater, the $\beta_{swM}(\lambda, \theta)$ values (or values derived from a very similar model) have typically been adopted as the standard in the literature. For $b_{sw}(\lambda)$, the modeled values of Morel (1974) or the interpolation of these values carried out by Smith and Baker (1981) are typically used.

Pure seawater scattering was halved to obtain pure seawater backscattering. For the computations of pure seawater scattering, in-situ measured temperature (applied in the Buiteveld et al. (1994) expressions, see Table 1) and salinity for each depth bin were applied. It is important to note that the total variations in pure water backscattering as a function of the temperature and salinity ranges sampled were significant with respect to resulting particulate backscattering magnitudes (see below), typically up to $1 \times 10^{-4} \text{ m}^{-1}$ at 532 nm over a 500 m profile.

3 Instrumentation and methods

3.1 Absorption and attenuation coefficients

In-situ measurements of hydrographic and optical parameters were made with a ship deployed profiling package. Conductivity, temperature, and depth parameters were measured with a SeaBird Electronics 9/11+ CTD. Absorption coefficients and beam attenuation coefficients for all the in-water constituents except water, $a_{pg}(\lambda) = a_p(\lambda) + a_g(\lambda)$ and $c_{pg}(\lambda) = c_p(\lambda) + a_g(\lambda)$, were measured with an ac-9 (WET Labs), where a_p and c_p are particulate absorption and attenuation, respectively, and a_g is the absorption coefficient for the dissolved fraction. The ac-9 has dual, 25-cm flow cells in which spectral absorption and attenuation are measured at nine wavelengths in the visible and near-IR with a sampling rate of approximately 6 Hz. The acceptance angle for the attenuation measurement is 0.93° . A second ac-9 was used to measure $a_g(\lambda)$ by fitting a $0.2 \mu\text{m}$ pleated, maxi-capsule filter (Gelman) to the intake of the absorption channel. The parameter $c_p(\lambda)$ was then derived from $c_{pg}(\lambda) - a_g(\lambda)$, and $b_p(\lambda)$, the particulate scattering coefficient, was derived from $c_{pg}(\lambda) - a_{pg}(\lambda)$. Estimates of phytoplankton absorption at 676 nm, $a_{ph}(676)$, were made using the baseline subtraction method (Davis et al., 1997). Total absorption, a_t ,

was computed by adding the pure water absorption values of Pope and Fry (1997).

Details of the method for ac-9 calibration, field use, and the application of corrections for temperature, salinity, scattering error, and time lags are described in Twardowski et al. (1999). Coefficients for correcting the effects of temperature and salinity on pure water absorption and attenuation recently derived by Sullivan et al. (2006) were applied. The ac-9s were calibrated to better than 0.002 m^{-1} replicability at all channels before and after the cruise by passing optically clean, bubble-free water (Barnstead, 4-cartridge Nanopure system) through the flow cells. These calibrations effectively serve as water blanks for the in-situ measurements. Note this method removes the effects of molecular scattering by pure water from the ac-9 measurements, but that the salt enhancement effect remains. This residual salt effect is on the order of 10^{-4} throughout the visible, however, and could be ignored. The Zaneveld et al. (1994) proportional method was used to correct the scattering error in the absorption measurements, where the signal at 715 nm, after temperature and salinity corrections, is assumed to consist entirely of the scattering error, and is then scaled through the visible according to the spectral dependence of measured $c_{pg}(\lambda) - a_{pg}(\lambda)$. After all corrections, ac-9 data were averaged to 1 m bins.

Finer temporal resolution of drifts in the ac-9 used for a_g measurements during the cruise was achieved by cross-calibration to high-sensitivity capillary waveguide spectrophotometric measurements of a_g made on discrete samples from 250 m by Bricaud et al. (2007)². The waveguide pathlength was 2 m with a blank consisting of clean (preashed) salt dissolved in purified water and passed through a $0.2 \mu\text{m}$ filter. Samples from 250 m were chosen because of the excellent consistency in a_g at this depth throughout the cruise (worst case standard deviation of all wavelengths was 0.0036 m^{-1} at $a_g(412)$, $N=9$) and because the temperature profile was relatively homogeneous in this depth range, minimizing variability from ac-9 internal temperature corrections (Twardowski et al., 1999). Drift corrections were obtained by simple subtraction and were linearly extrapolated over the time period of the cruise to obtain corrections for casts without discrete sample a_g measurements. The total deviation in final corrected drifts through the period sampled was typically on the order of 0.001 to 0.002 m^{-1} .

For the ac-9 used primarily for a_{pg} and c_{pg} measurements, drift corrections were anchored at a station in the gyre where consecutive casts were made with and without a $0.2 \mu\text{m}$ pre-filter. Measurements in the dissolved fraction could then be subtracted from successive measurements of the combined dissolved and particulate material, providing a_p and c_p spectra that were the most accurate of any optical measurement that were made with the ac-9s because any uncertainties

²Bricaud, A., Babin, M., Claustre, H., Ras, J., and Tiede, F.: The partitioning of light absorption in South Pacific waters, *Biogeosciences Discuss.*, in preparation, 2007.

in calibration drifts cancel (temperature and salinity relationships verified consistent water types between the consecutive casts). Resulting a_p spectra at 250 m were compared to particulate absorption determined independently on a discrete sample with the filter pad spectrophotometric technique (Bricaud and Stramski, 1990), with agreement better than 0.001 m^{-1} at all wavelengths except 412 nm, where the agreement was 0.0035 m^{-1} . A further evaluation of the filter pad a_p measurements on samples collected at 250 m throughout the central gyre demonstrated excellent consistency (worst case standard deviation of 0.0018 m^{-1} at 412 nm, $N=8$). All a_p and c_p values at 250 m were thus set to the values determined at the central gyre station and the corrected a_g measurements were then added in to obtain the final a_{pg} and c_{pg} values at 250 m, from which final drift corrections were determined and linearly extrapolated to all stations.

Uncertainties in the final ac-9 IOPs are comprised of both random noise error as well as bias error. The former is $<0.001 \text{ m}^{-1}$ at all wavelengths, which was reduced further by depth binning. Based on the above procedures, worst case bias errors for the final a_g , a_{pg} , c_{pg} , and derived a_p , c_p , and b_p are estimated at 0.002 m^{-1} , 0.003 m^{-1} , 0.003 m^{-1} , 0.003 m^{-1} , and 0.004 m^{-1} , respectively. Throughout the cruise, several casts were also collected with either both ac-9s filtered or unfiltered, allowing direct intercomparisons for validation, with agreement at or below these uncertainties.

3.2 Volume scattering and backscattering coefficients

An ECO-BB3 (WET Labs) was used to measure 117° scattering, $\beta_t(117^\circ) \text{ m}^{-1} \text{ sr}^{-1}$, at 462, 532, and 650 nm at a sampling rate of 1 Hz. These measurements are synchronized at 60 Hz to reject ambient light and any inelastic scattering associated with excitation from one of the other sources (however, it is not impossible that inelastic scattering may be excited and detected within a source-detector pair). Before the field deployments, sensor gains were increased in an effort to better resolve very low scattering. The sensor was calibrated at the factory with $2 \mu\text{m}$ microspherical polystyrene beads (Duke Scientific) using established protocols to derive a scaling factor f and dark offset D for each of the three measurements (Moore et al., 2000). Calibrated $\beta_t(117^\circ)$ values are obtained by subtracting D from the raw digital counts and then multiplying by f . Supplied values of f (specific for this instrument) were 2.386×10^{-5} , 1.015×10^{-5} , and $3.781 \times 10^{-6} \text{ m}^{-1} \text{ sr}^{-1} \text{ counts}^{-1}$ for the 462, 532, and 650 nm measurements, respectively. In this work, D values were determined directly in the field by covering the detector only with black electrical tape (using care not to cover any of the source window or leave any of the detector window exposed). This is the most accurate method of D determination since the specific environmental conditions during deployment are taken into account. Vertical pro-

files of dark offsets down to 500 m were constant within the standard deviation of the electronic noise for all three channels. Thus, for each D , the entire profile was averaged and these values (49.9, 53.8, and 59.8 raw counts for measurements at 462, 532, and 650 nm, respectively) were used along with the factory derived f parameters in processing. Drift in the ECO-BB3 calibration parameters over the course of the cruise are assumed negligible. Limited attempts to quantify drifts in ECO sensors in the past have not found any appreciable drift beyond experimental errors over periods of months, although, to our knowledge, a rigorous analysis has not been carried out.

Backscattering coefficients, $b_{bp}(\lambda)$, were derived for each spectral $\beta_t(117^\circ)$ using the method described in Sullivan et al. (2005). Briefly, $\beta_{swB}(\lambda, 117^\circ)$ (see Sect. 2) were subtracted from measured $\beta_t(\lambda, 117^\circ)$ to obtain $\beta_p(\lambda, 117^\circ)$, and then a χ_p factor was used in a proportionality to link b_{bp} and β_p (see Boss and Pegau 2001 and Boss et al., 2004):

$$b_{bp} = 2\pi \chi_p(117^\circ) \beta_p(117^\circ). \quad (8)$$

Based on extensive measurements made in a wide diversity of water types by Sullivan et al. (2005), a value of 0.90 was found for $\chi_p(125^\circ)$. We assumed the $\chi_p(117^\circ)$ would not be significantly different and so the same value was adopted. The $\chi_p(117^\circ)$ parameter was assumed to be spectrally independent after Boss and Pegau (2001). Absorption of the incident and scattered beams (Moore et al., 2000) was corrected using ac-9 measurements, although because of the small effective pathlength ($\sim 3.9 \text{ cm}$) and extreme clarity of the water, these corrections were negligible.

As with the ac-9 IOPs, uncertainties in the final b_{bp} values are comprised of both random noise error as well as possible bias error. Unlike the ac-9, however, some possible bias errors (e.g., errors in determining f) scale with magnitude and are more accurately represented in terms of a % error. Electronic noise errors were 1.7×10^{-5} , 4.4×10^{-6} , and $1.6 \times 10^{-6} \text{ m}^{-1} \text{ sr}^{-1}$ for measurements at 462, 532, and 650 nm, respectively. Depth bin averaging of just a few data points can reduce these errors by more than half. Errors associated with the determination of the D parameters are assumed to be similar. There are two general errors possible with the f parameters: (1) uncertainty in determining the experimental ratio of counts (measured with the ECO sensor) to b_p (measured with an ac-9) during calibration with a series of suspensions of microspheres, and (2) bias errors in the theoretical estimation of the phase function $[\beta_p(\bar{\theta}, \bar{\lambda}) / b_p]$ for these microspheres (note that f is determined by dividing the latter parameter by the former) (Moore et al., 2000). In evaluating the mean square error of experimental data from calibrations, the first source of uncertainty has been determined to be small, typically about 1%.

The second source of uncertainty is more difficult to evaluate. Theoretical $[\beta_p(\bar{\theta}, \bar{\lambda}) / b_p]$ (sr^{-1}) values specific for a given sensor are computed from Mie theory assuming a Gaussian size distribution model with the mean

microsphere size and standard deviation reported by Duke Scientific. The normal dispersion refractive index equation for polystyrene suggested by Duke Scientific is used ($n_p = 1.5663 + 0.00785\lambda^{-2} + 0.000334\lambda^{-4}$, with λ in μm). With full functionality expressed, $[\beta_p(\bar{\theta}, \bar{\lambda})/b_p]$ is obtained as follows:

$$\frac{\beta_p(\bar{\lambda}, \sigma_\lambda, \bar{\theta}, \Delta\theta, \bar{d}, \sigma_d)}{b_p(\bar{\lambda}, \sigma_\lambda, \bar{d}, \sigma_d)} = \frac{\int_0^{\bar{\lambda}+3\sigma_\lambda} \int_{\bar{\lambda}-3\sigma_\lambda}^{\bar{\lambda}+3\sigma_\lambda} \int_{\bar{d}-3\sigma_d}^{\bar{d}+3\sigma_d} W(\theta, \bar{\theta}, \Delta\theta) \Psi(\lambda, \bar{\lambda}, \sigma_\lambda) \alpha(d, \lambda, n_p, \theta) F(d, \bar{d}, \sigma_d) d\lambda d\theta}{2\pi \int_0^{\bar{\lambda}+3\sigma_\lambda} \int_{\bar{\lambda}-3\sigma_\lambda}^{\bar{\lambda}+3\sigma_\lambda} \int_{\bar{d}-3\sigma_d}^{\bar{d}+3\sigma_d} \sin(\theta) \Psi(\lambda, \bar{\lambda}, \sigma_\lambda) \alpha(d, \lambda, n_p, \theta) F(d, \bar{d}, \sigma_d) d\lambda d\theta} \quad (9)$$

Weighting functions W for the scattering measurements, computed numerically from the optical geometry by J. R. V. Zaneveld (WET Labs), are isosceles triangles described by a centroid angle $\bar{\theta}$ and $\Delta\theta$, where the latter parameter is the baseline width of the function (Moore et al., 2000). Each of the ECO-BB3 measurements have identical W defined by $\bar{\theta}=117^\circ$ and $\Delta\theta=36^\circ$. The spectral response of the sensor Ψ is assumed Gaussian, defined by a centroid wavelength $\bar{\lambda}$ and standard deviation σ_λ . The spectral output of the LED source is convolved with the bandwidth of the detector interference filter to obtain Ψ (the relative photodiode detector response within each spectral transmission window is assumed approximately constant). The parameter α is the amplitude of unpolarized light scattering by the microspheres computed from Mie theory and F is the microsphere size distribution defined by a centroid \bar{d} and standard deviation σ_d . Microspheres chosen by WET Labs for calibrations typically have a centroid \bar{d} close to $2 \mu\text{m}$. Reported size distributions have previously been verified in some bead samples using a Coulter Counter device, i.e., newly purchased beads purchased from Duke Scientific have consistently conformed to the reported distributions on the bottle. Volume scattering functions from these beads measured at one degree resolution with a bench top device have closely agreed with associated theoretical phase functions (M. Twardowski, unpubl. data), as other investigators have observed (Volten et al., 1997; Lee and Lewis, 2003; Slade and Boss, 2005). WET Labs calculations of $[\beta_p(\bar{\theta}, \bar{\lambda})/b_p]$ have been independently verified within 1 to 2 percent by E. Boss (University of Maine, personal communication, 2005).

WET Labs normally disregards the spectral response term $\Psi(\lambda)$, as the effect is typically small ($<2\%$). The effect was specifically assessed here for the 462 nm measurement because of concern over a 34 nm spectral separation between the LED source, centered at 436 nm, and the detector interference filter, centered at 470 nm (WET Labs currently employs a ~ 466 nm LED source in this sensor). Convolution of the LED spectral output with the interference filter bandwidth, the resulting spectral response exhibited a $\bar{\lambda}$ of 462 nm, which was adopted for this measurement. The $[\beta_p(\bar{\theta}, \bar{\lambda})/b_p]$ computed with this spectral response included was only 1.6% greater than the value originally used by WET

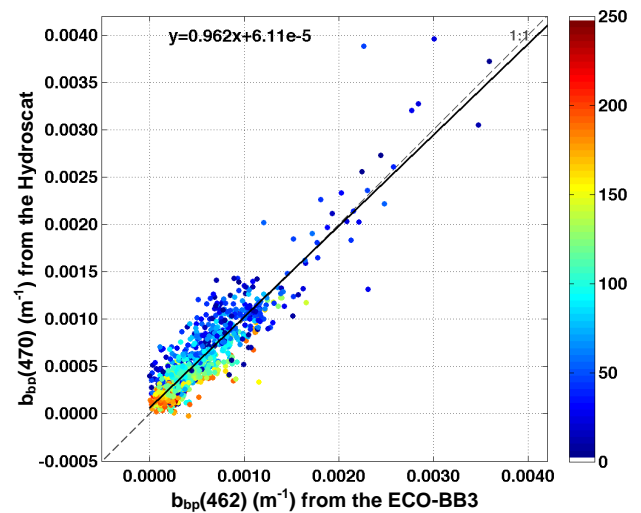


Fig. 3. Comparison of $b_{bp}(470)$ (m^{-1}) data collected with a Hydroscat (HOBI Labs, Inc.) and $b_{bp}(462)$ (m^{-1}) from an ECO-BB3 (WET Labs, Inc.). Dotted line is 1:1 and the solid line is the linear least-squares regression. Data point color and associated colorbar represent sample depth (m). Note that for this comparison, the pure seawater values $\beta_{swM}(117^\circ)$ and $\beta_{swM}(140^\circ)$ from Morel (1974) were used for the ECO-BB3 and Hydroscat, respectively.

Labs, although the 8 nm shift in $\bar{\lambda}$ significantly affects analyses because of the steeply sloped spectrum of pure seawater scattering. For 462, 532, and 650 nm, σ_λ values were 18, 24, and 14 nm, respectively.

In total, the aggregate error from the computation in Eq. (9) is not readily amenable to “bottom up” estimation. An error of several percent may be possible based on indirect evidence of verifying sensor calibration with one bead by making measurements in solutions of other known beads, although errors accumulate from both the calibration and validation aspects in such a comparison. In cross-calibrations of many ECO scattering sensors (Sullivan et al., 2005), agreement has been consistently observed at the $<5\%$ level, which at least demonstrates that if there are bias errors associated with, for example, imprecise size distributions, these errors are very consistent.

Taken as a whole, above mentioned errors in $\beta_t(117^\circ)$ that are independent of magnitude are estimated at 2×10^{-5} , 5×10^{-6} , and $2 \times 10^{-6} \text{ m}^{-1} \text{ sr}^{-1}$ for measurements at 462, 532, and 650 nm, respectively, after 1 m bin averaging. The aggregate error scaling with magnitude, the largest component determining accuracy in waters with higher particle loads, may be anywhere from a few percent to perhaps as large as $\sim 10\%$, within the level of agreement others have previously found between sensors made by different manufacturers (Pegau et al., 2001; Prentice et al., 2002; Boss et al., 2004). Uncertainties in subsequently derived properties such as particulate volume scattering and particulate backscattering will be highly dependent on the accuracy of pure seawater $\beta_{sw}(117^\circ)$ estimates.

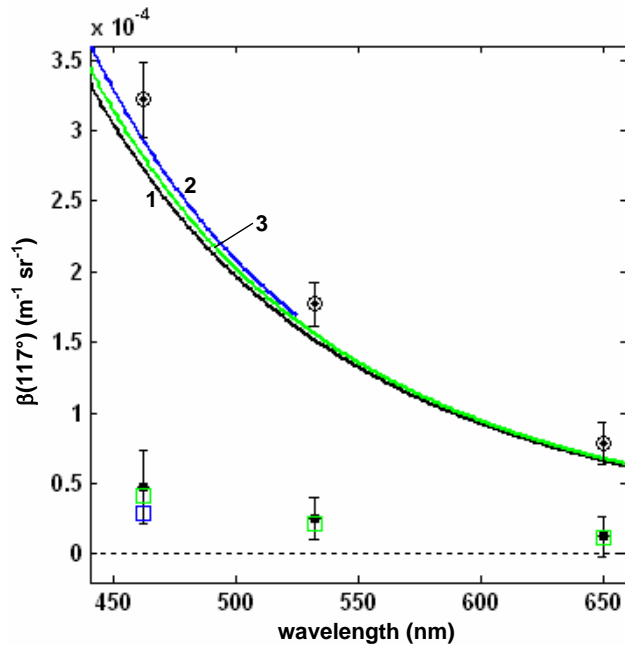


Fig. 4. Means and standard deviations of $\beta_t(\lambda, 117^\circ)$ (black circles with central point) and $\beta_p(\lambda, 117^\circ)$ (filled black circles) from all 1-m binned measurements collected in the central gyre ($N=26\,741$; includes depths from the surface to typically 500 m). The parameters $\beta_p(\lambda, 117^\circ)$ were computed by subtracting pure seawater volume scattering $\beta_{swB}(\lambda, 117^\circ)$ according to Eqs. (1) and (2), based on the expressions of Buiteveld et al. (1994) (black curve labeled 1; see text for details). The $\beta_{swM}(\lambda, 117^\circ)$ values computed from Morel (1974) (blue curve labeled 2) and $\beta_{swS}(\lambda, 117^\circ)$ from Shifrin (1988) (green curve labeled 3) are also plotted, with the spectral range of the former extending only to 525 nm because a satisfactory model for the Morel values at longer wavelengths is lacking (see Table 2). Resulting $\beta_p(\lambda, 117^\circ)$ means computed using these values are plotted as blue (Morel) and green (Shifrin) squares, respectively; the error bars for these points are the same as shown for the black solid circles, but are left out for clarity. All pure seawater volume scattering coefficients were computed for $T=20^\circ\text{C}$ and $S=35$.

A final source of error, also scaling with magnitude, is the $\chi_p(117^\circ)$ used in computing b_{bp} (Eq. 8). Sullivan et al. (2005) found this uncertainty to be approximately 0.01, which translates into a $\sim 1\%$ uncertainty in b_{bp} assuming there were no “sufficiently unusual” particle populations and associated phase functions sampled in this study, i.e., assuming the range in phase function shapes sampled in this study fell within the wide range sampled by Sullivan et al. (2005). Since the χ_p found by Sullivan et al. (2005) was for a different scattering angle, and since their χ_p will also have inherent uncertainties from the b_{bp} derived by multiple angle volume scattering that was used in their regression, uncertainties of a few percent are expected possible.

For details of the methodology for the Hydrosat backscattering sensor data presented here, see Stramski et al. (2007).

Briefly, the Hydrosat measures $\beta_t(140^\circ)$ at 6 wavelengths in the visible. To obtain b_{bp} , $\beta_{sw}(140^\circ)$ was subtracted to obtain $\beta_p(140^\circ)$, and a $\chi_p(140^\circ)$ of 1.13 (Dana and Maffione, 2002) was used to compute b_{bp} from Eq. (8). This sensor was deployed on a profiling package separate from the package containing the ac-9 and ECO-BB3 measurements above. Sampling by both packages typically occurred within a 3 h period.

Data processing and plotting were performed in MATLAB (Mathworks). Interpolation between casts to map distributions in the central gyre was carried out with Transform (Fortner Software). A spherically weighted fill algorithm was used that preserved all original data, where weights drop off according to the square of the inverse of the distance from a missing data value. This algorithm tends to heavily weight known data close to the missing data elements. A simple smoothing algorithm averaging each data point with each of its directly adjacent neighboring data points was then applied.

4 Results

A comparison of ECO-BB3 $b_{bp}(462)$ and Hydrosat $b_{bp}(470)$ data is shown in Fig. 3. These results include data from stations outside the central gyre, extending to the Marquesas Islands and the Chilean upwelling. These were the closest matching wavelengths between the two sensors. Considering that these instruments have different calibration methods, optical configurations (the most obvious being measurement scattering angle), and processing methods, the $\sim 4\%$ agreement is very good. This result is also consistent with the $\sim 3\%$ agreement recently observed by Boss et al. (2007) in Crater Lake. The good agreement, particularly for two sensors with independent calibration methods, is a useful factor in helping to constrain accuracy estimates.

Aggregate mean values of $\beta_t(117^\circ)$ at 462, 532, and 650 nm measured with the ECO-BB3 through the entire central gyre (including 0 to 500 m) were only 18%, 16%, and 20% higher than the corresponding pure seawater values $\beta_{swB}(\lambda, 117^\circ)$ (Fig. 4; Table 3). Standard deviations were also small in absolute and relative terms. For example, the standard deviation of $\beta_t(117^\circ)$ at 532 nm was $1.6 \times 10^{-5} \text{ m}^{-1} \text{ sr}^{-1}$, or 9% of the mean magnitude, for the entire data set across the ~ 3000 km of the central gyre. After subtracting $\beta_{swB}(\lambda, 117^\circ)$ to obtain $\beta_p(\lambda, 117^\circ)$, mean values were approximately factors of 2.5, 5, and 6 greater than estimated uncertainties for measurements at 462, 532 nm, and 650 nm, respectively (Table 3). Subtracting either $\beta_{swM}(\lambda, 117^\circ)$ or $\beta_{swS}(\lambda, 117^\circ)$ resulted in less particulate backscattering, although the means for the entire central gyre data were still positive.

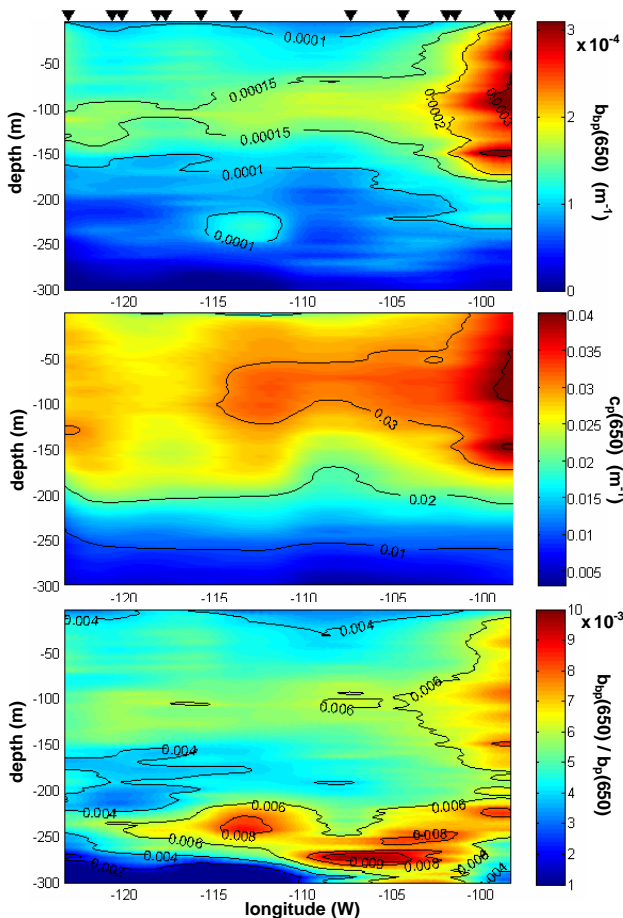


Fig. 5. Distributions of $b_{bp}(650)$, $c_p(650)$, and $b_{bp}(650)/b_p(650)$ in the South Pacific central gyre. For reference, $b_{bswB}(650) = 4.6 \times 10^{-4} \text{ m}^{-1}$ (see text) and $c_{sw}(650) \approx 0.34 \text{ m}^{-1}$ (assumed equivalent to the pure water absorption values of Pope and Fry 1997, within errors). Cast locations marked along the top of the upper graph. Multiple profiles collected at the same station were averaged.

4.1 Distributions in the central gyre

Interpolated distributions of $b_{bp}(650)$, $c_p(650)$, and $b_{bp}(650)/b_p(650)$ in the central gyre are shown in Fig. 5. A particle peak centered at $\sim 100 \text{ m}$ was observed in both b_{bp} and c_p . The increase in magnitude heading east is consistent with an increasing proximity to the frontal transition zone between the gyre and the Chilean upwelling region (see Claustre et al., 2007¹). The parameter b_{bp}/b_p was also elevated in this layer (up to 0.6% and higher east), about 50% greater than values in surrounding waters. Values of b_{bp}/b_p from the surface to 200 m in the central gyre, ranging from about 0.4% to 0.6% west of 104° W , are indicative of “soft” particles with high water content, such as phytoplankton and possibly loosely assembled detrital aggregates (Twardowski et al., 2001).

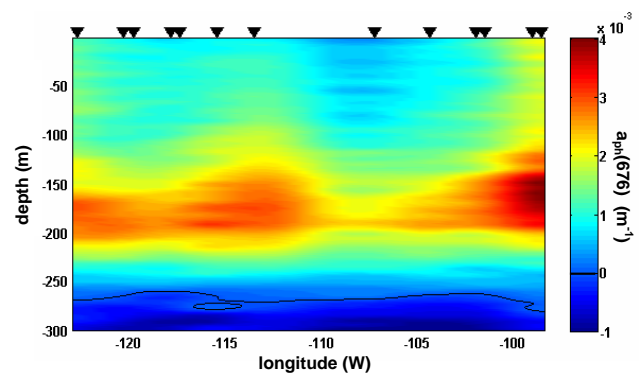


Fig. 6. Distribution of $a_{ph}(676)$ in the central gyre. The contour demarcates zero.

Interestingly, a secondary peak in $b_{bp}(650)$, often observed at depths ranging from 230 m to 270 m, was not distinct in the c_p data. Inspection of b_{bp}/b_p revealed relatively high values, approaching 1%, in this deep layer. This could be an indication that the proportion of “hard” particles had increased in this layer (note, however, that both b_{bp} and c_p indicate that overall particle concentrations are very low relative to the overlying water). It may also be possible that substantial increases in the relative amount of small particles (a few microns and less) could also increase the backscattering ratio in this layer (Twardowski et al., 2001), but the c_p spectral slope, related to mean particle size (Boss et al., 2001), did not support this hypothesis (data not shown). However, b_{bp} and c_p are affected by different portions of the size distribution (Stramski and Kiefer, 1991), with b_{bp} being much more sensitive to small (submicron) particles, thus it is not inconceivable that the two could become decoupled.

Distributions of $a_{ph}(676)$ revealed a deep chlorophyll maximum spanning 160 to 210 m depth (Fig. 6) that was also consistent with ancillary chlorophyll fluorescence measurements (Claustre et al., 2007¹) and HPLC pigment data (Ras et al., 2007). This deep chlorophyll layer corresponded to a minimum in b_{bp}/b_p of $\sim 0.4\%$ (see Fig. 5). Bulk particle refractive indices in this layer estimated from the model of Twardowski et al. (2001) are 1.03, in agreement with previous estimates of refractive indices of phytoplankton (Carder et al., 1972; Aas 1996; Stramski et al., 2001).

An overlay of all the profiles of computed b_{bp} collected at the central gyre stations shows a structure that is typically very consistent for each wavelength (Fig. 7). This consistency lends support to our assumption that the drift in ECO-BB3 calibration parameters was negligible during this period of the cruise. Spectrally, particulate backscattering showed a typical decrease with increasing wavelength. The primary particle maximum centered $\sim 100 \text{ m}$ is identified in backscattering at all three wavelengths. The secondary maximum centered at $\sim 230 \text{ m}$ is distinct in b_{bp} at 532 and 650 nm, but is only weakly present at 462 nm. Furthermore, a clear

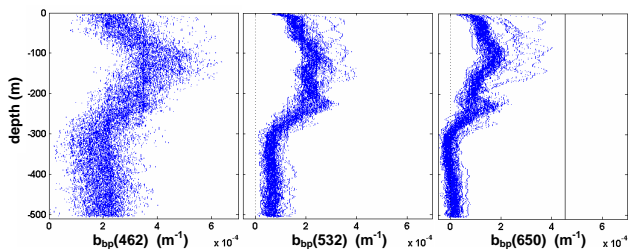


Fig. 7. All profiles ($N=56$) of b_{bp} at 462, 532, and 650 nm from the central gyre, plotted at 1-m depth bins using a 10-point median filter. The lowest values were typically observed at 300–350 m depth. Backscattering by pure seawater falls within the plotted b_{bp} range for 650 nm, and is drawn in as a gray line. Faint vertical banding can be seen, particularly in the $b_{bp}(532)$ data, due to occasions where the raw digital counts included in a depth bin were all the same value.

minimum in $b_{bp}(650)$ is present between 160 and 210 m – the depth of the chlorophyll maximum, see Fig. 6 – that is also apparent in $b_{bp}(532)$, but not obvious in the noisier data at 462 nm.

This spectral variability becomes apparent when viewing spectral ratios (Fig. 8). Both sets of spectral ratio profiles were essentially constant in the surface ~ 140 m, despite substantial changes in b_{bp} magnitude (Fig. 7). This is a reassuring observation, as bias errors in uncertainties can manifest themselves in ratios that are magnitude dependent. Below 140 m, both ratios increased to a peak in the depth range of the chlorophyll maximum, then decreased to a minimum centered at ~ 230 m. Below 230 m, the ratios began increasing in deeper water where uncertainties rapidly made the ratios unresolvable.

The widely assumed $1/\lambda$ spectral model predicts ratios of 1.41 and 1.22 for $b_{bp}(462)/b_{bp}(650)$ and $b_{bp}(532)/b_{bp}(650)$, respectively. The latter ratio was in fact observed from the surface down to ~ 140 m. The spectral shape of particulate attenuation in the clearest waters west of 115°W was also approximately $1/\lambda$ (data not shown). This is the predicted case for particles with minimal absorption that follow a Junge-type hyperbolic size distribution with slope of 4 (volume conserved in all size bins) (Morel 1973; Fournier and Forand 1994; Boss et al., 2001). This distribution was moreover verified in Coulter Counter data from the cruise (see Sciandra et al., 2007³). This slope is often considered to be representative of oceanic particle distributions, and is the predicted “steady state” condition from physical (see Sullivan et al., 2005) and biological (Kiefer and Berwald, 1992) mechanistic processes. For $b_{bp}(462)/b_{bp}(650)$, ratios at the surface to ~ 140 m were about 50% greater than the value expected from the $1/\lambda$ model. The fact that the $1/\lambda$ model did not hold

³Sciandra, A., Stramski, D. and Babin, M.: Variability in particle size distribution in contrasted trophic regions of the South East Pacific, Biogeosci. Discuss., in preparation, 2007.

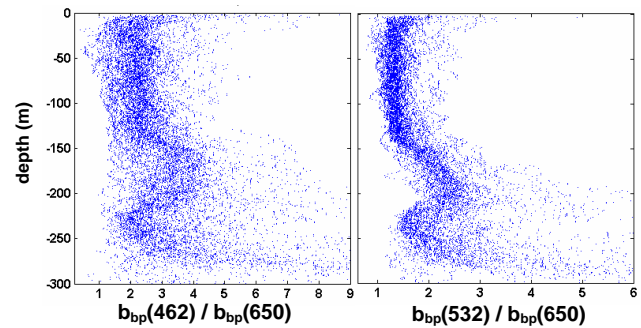


Fig. 8. Profiles ($N=49$) of $b_{bp}(462)/b_{bp}(650)$ and $b_{bp}(532)/b_{bp}(650)$ from the central gyre. Only profiles collected west of 104°W , inclusive, are shown to avoid including the slightly more turbid waters with closer proximity to the frontal zone transition to the Chilean upwelling. A $1/\lambda$ spectral model predicts a ratio of 1.41 for $b_{bp}(462)/b_{bp}(650)$ and 1.22 for $b_{bp}(532)/b_{bp}(650)$.

into the blue is difficult to interpret at this time because our understanding of spectral particulate backscattering in natural waters is unfortunately very limited. Factors such as nonsphericity and anomalous dispersion from particulate absorption structure altering complex index of refraction spectra may play important, but poorly understood, roles. The agreement with independent Hydrosat data (Fig. 3) is a good indication that there are probably no substantial bias errors in the data.

Below 140 m, the ratio $b_{bp}(532)/b_{bp}(650)$ increased to a value of ~ 2.2 in the deep chlorophyll maximum (160 to 210 m depth range), corresponding to a $\sim \lambda^{-4}$ spectral shape. Furthermore, $b_{bp}(462)/b_{bp}(650)$ increased to values up to 3.9 at these depths, also consistent with a $\sim \lambda^{-4}$ spectral shape. This is the spectral shape of Rayleigh scattering, an indication that the particle population in this layer may be dominated by particles much smaller than the wavelengths of light scattered. The $c_p(\lambda)$ spectral slope increased in the chlorophyll maximum as well, but only to a value of ~ 1.5 (data not shown).

Microscope taxonomy (Gomez et al., 2007) and HPLC pigment analyses (Ras et al., 2007) on discrete samples have determined that the phytoplankton assemblage in the deep chlorophyll maximum consisted primarily of cyanobacteria, which have cell diameters of the same order as the wavelengths of light used in the scattering measurements here. Moreover, these cells would not be expected to be Rayleigh scatterers; this is verified in modeled (Morel et al., 1993) and measured (Vallaincourt et al., 2004) backscattering spectra of cyanobacteria. Factors such as nonsphericity and anomalous dispersion that may affect backscattering spectra in ways not predicted by simple Mie theory, are unlikely to have caused the $\sim \lambda^{-4}$ shape because (1) the cells are small (Clavano et al., 2007) and (2) the spectral distribution of pigment absorption, while introducing oscillations in the backscattering

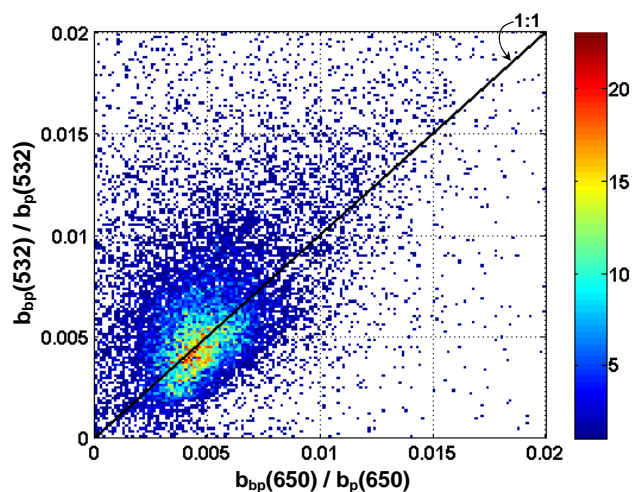


Fig. 9. Relationship between $b_{bp}(532)/b_p(532)$ and $b_{bp}(650)/b_p(650)$ for all 1-m binned measurements from the central gyre. Color denotes frequency.

spectrum over small wavelength ranges, typically tends to impose a broad flattening of the spectrum when the full visible range is considered (Stramski et al., 2001). Thus, to explain the steep spectral slope in backscattering, one would likely need to invoke a large relative population of colloidal particles ($<0.2 \mu\text{m}$) that may include viruses.

The lowest values of b_{bp} were observed at 300 to 350 m depth (Fig. 7; Table 3). For $b_{bp}(650)$, the lowest mean values recorded were negative with a magnitude about our estimated uncertainty for the measurement. These scattering levels are also certainly pushing the limits of our uncertainty in pure seawater values. Overall, however, uncertainties appeared sufficiently good to resolve particulate backscattering in these extremely clear waters.

Previous theoretical analyses have predicted b_{bp}/b_p should exhibit minimal spectral dependence (Ulloa et al., 1994; Twardowski et al., 2001) and this has been supported through a growing body of field work (Boss et al., 2004; Chami et al., 2005; Oubelkier et al., 2006). For the central gyre, the relationship between $b_{bp}(532)/b_p(532)$ and $b_{bp}(650)/b_p(650)$ showed substantial scatter because of propagation of random errors, but a clear peak in the distribution was observed on the 1:1 relationship (Fig. 9), supporting previous findings.

Despite this broad concentration of data around the 1:1 relationship, it is also noteworthy that consistent deviations from this relationship were observed in the deep chlorophyll maximum (data not independently shown). The 1:1 relationship increased up to 1.5:1 [$b_{bp}(532)/b_p(532):b_{bp}(650)/b_p(650)$] within the maximum. This is consistent with the previous observation that the b_{bp} slope increases in this layer were greater in magnitude than c_p slope increases.

Table 3. Parameters from scattering measurements in the South Pacific central gyre. All values expressed in 10^{-4} .

parameter	$\lambda(\text{nm})$		
	462	532	650
$\beta_t(117^\circ)$ ($\text{m}^{-1} \text{sr}^{-1}$)	0.17	0.044	0.016
raw uncertainty ^a			
$\beta_t(117^\circ)$ ($\text{m}^{-1} \text{sr}^{-1}$)	0.2	0.05	0.02
estimated uncertainty ^b			
$\beta_{swB}^c(117^\circ)$ ($\text{m}^{-1} \text{sr}^{-1}$)	2.72	1.52	0.66
b_{bswB}^c (m^{-1})	18.7	10.5	4.6
$\beta_t(117^\circ)$, mean $\pm \sigma$ ($\text{m}^{-1} \text{sr}^{-1}$)	3.2 ± 0.3	1.77 ± 0.16	0.79 ± 0.15
central gyre, 0–500 m			
b_{bp} (m^{-1})	1.4	0.51	0.22
estimated uncertainty ^d			
b_{bp} , mean $\pm \sigma$ (m^{-1})	2.7 ± 1.5	1.42 ± 0.87	0.71 ± 0.81
central gyre, 0–500 m			
b_{bp} , mean $\pm \sigma$ (m^{-1})	2.0 ± 1.2	0.68 ± 0.39	0.04 ± 0.37
central gyre, 300–500 m			
b_{bp} , lowest measured (m^{-1})	0.92	0.37	~ 0

^a i.e., random electronic error

^b Computed over 1-m depth bins; see text.

^c Pure water scattering computed from Buiteveld et al. (1994) at 20°C ; [$+0.3(35)/37$] adjustment for dissolved salts applied after Morel (1974).

^d Assumes the mean central gyre value, a 5% uncertainty in $\beta_{swB}(117^\circ)$, and a 5% uncertainty in $\chi_p(117^\circ)$ (note both uncertainties would be bias errors).

4.2 Time series at the central gyre station, GYR

To resolve diel scale temporal variability in the central gyre, casts were collected every few hours over a 4 d period at station GYR (Fig. 10). The parameter $c_p(650)$ shows a clear diel cycle in the broad particle maximum centered around 90 m depth, reaching maxima around sunset and minima around sunrise. This pattern is consistent with previous observations from the South Pacific (Claustre et al., 1999) and other oceanic locations (e.g. Siegel et al., 1989; Gardner et al., 1995; Walsh et al., 1995), and results from the interaction of several processes, including accumulation of particles through algal growth, synchronized cell division, the removal of particles via loss terms such as grazing, and cellular physiological changes that may affect particle optical properties. This pattern was much less pronounced in the corresponding $b_{bp}(650)$ data, an indication that submicron particles more strongly affecting $b_{bp}(650)$ may not show the same marked cycling observed in $c_p(650)$. The b_{bp}/b_p parameter exhibits a small increase in the ~ 90 m particle maximum, as observed throughout the gyre in Fig. 5.

The secondary peak in b_{bp} at 230–250 m depth was especially pronounced throughout the time series at this station (Fig. 10). Again, the layer was not distinct in the c_p time series data and the b_{bp}/b_p exhibited a strong increase, reaching

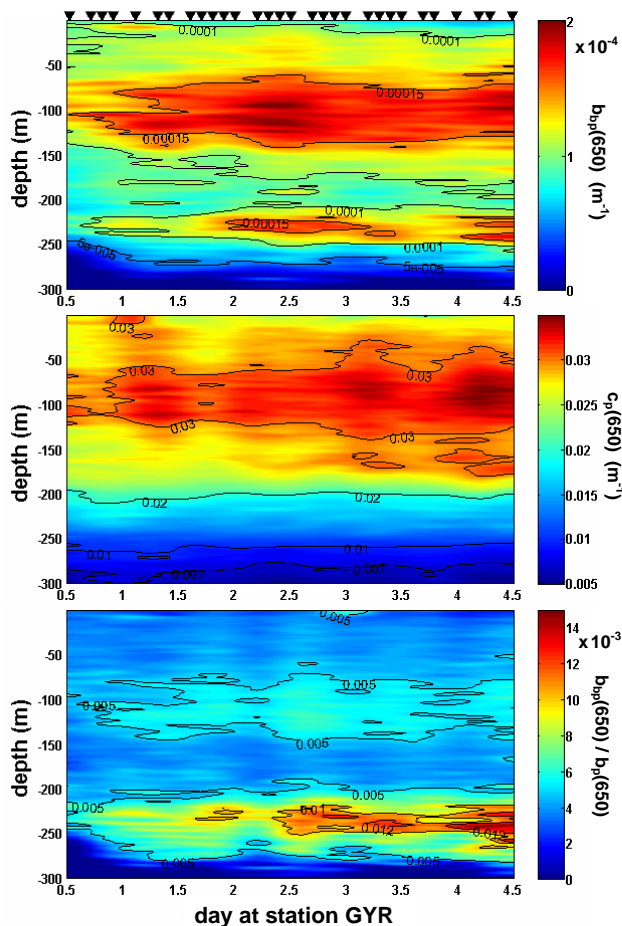


Fig. 10. Time series measurements of $b_{bp}(650)$, $c_p(650)$, and $b_{bp}(650)/b_p(650)$ at station GYR. Day 0 corresponds to 00:00 UTC, 12 November 2004 (subtract 7 h to convert to local time). Cast times marked along the top of the upper graph.

a maximum of greater than 1.2% at some times (note that all of the time series profile data from this station was averaged to obtain the data for the 114°W profile used in the distribution plot in Fig. 6). There may be a very faint diel pattern to the intensity of the deep b_{bp}/b_p layer, but an analysis with the density structure indicates that the layer location and magnitude appear to be primarily modulated by the internal wave field through the sampling period.

4.3 Reflectance estimation, testing closure

At station GYR, surface reflectance R measurements at 532 nm reported in Morel et al. (2007) were 1.15% and 1.08% at depths of 1.49 and 2.1 m, respectively. These measurements were made at approximately noon on 15 November 2004 (labelled station “GYR-5” in Morel et al., 2007) concurrently with IOP measurements (in Fig. 10, cast made at day 3.79). Using the radiative transfer approximation in Eq. (4) of Morel et al. (2007), $R = f' [b_b/(a+b_b)]$, R can

be solved from the IOPs and a suitable f' parameter. Using the f' provided in lookup tables referenced in Morel et al. (2007) and derived previously by Morel and Gentili (2004), surface R was independently estimated at 1.11% with directly measured $b_{bt}(532)$ and $a_t(532)$ (the f' value used was 0.456 and surface a_t and b_{bt} values were 0.047 m^{-1} and $1.18 \times 10^{-3}\text{ m}^{-1}$, respectively). Demonstrating closure with the measurements of Morel et al. (2007) helps to validate the accuracy of our measurements. These results also demonstrate the practical potential of using IOPs to derive remote sensing parameters with good precision.

5 Discussion

Estimated uncertainties in direct measurements of b_b were approximately two orders of magnitude better than uncertainties in results from inverting reflectance measurements (Morel et al., 2007). Better precision in direct measurements of a parameter as opposed to derivation from an inversion may be reasonably expected. Considered together, the two sets of measurements form an excellent complement in characterizing optical properties in the clearest natural waters.

Several aspects of this work were enlightening, and, we believe, significant. Foremost, scattering at 117° was resolved at very low levels. For example, estimated uncertainties were approximately 6%, 3%, and 3% of pure scattering of seawater at 462, 532, and 650 nm, respectively (Table 3). In these clear waters, particulate backscattering could be resolved at better than a few factors of uncertainty except in the very clearest waters deeper than $\sim 300\text{ m}$. Additional depth-bin averaging in the deep water (or collecting time series at depth to average) could help improve uncertainties (but not any bias errors). We believe a key improvement in methodology relative to previous measurements that helped improve uncertainties was the direct in-situ determination of dark off-sets (see Sect. 3.2).

Good agreement was observed between the ECO-BB3 and Hydroscat sensors. The most important difference between these sensors is the calibration method. Calibration of scattering devices requires a “known” scattering medium - this is a Lambertian (isotropic scattering) Spectralon plaque for the Hydroscat (Maffione and Dana, 1997), whereas microspherical bead suspensions are used for the ECO-BB3 (also see Volten et al., 1997; Lee and Lewis, 2003; Slade and Boss, 2005). The $\sim 4\%$ agreement observed is an indication that our estimated accuracies for the ECO-BB3 may be as low as a few percent.

It is interesting to note that a closer look at previous comparisons between ECO scattering sensors and the Hydroscat (e.g., Pegau et al., 2001; Prentice et al., 2002; Boss et al., 2004) reveals that the reported “10% agreement” was not only consistent, but that the Hydroscat was consistently about 10% lower than the ECO-BB3 (E. Boss, University of Maine, personal communication, 2007). Furthermore, a new

correction has been implemented recently for the Hydrosat that accounts for a change in reflectivity of the Spectralon plaque used for calibrations when it is immersed in water versus air (E. Boss, University of Maine, personal communication, 2007). This correction enhances values by about 10%. This may explain both the previous consistent discrepancies as well as the good agreements that are now being observed.

A further result of this work we found significant was the apparent accuracy of both the Buiteveld et al. (1994) pure water scattering values and the $[1+0.3S/37]$ empirical adjustment for salts based on Morel (1974). Useful diagnostics in this analysis are the observed particulate backscattering ratios and spectral ratios (Figs. 5, 8–10). For b_{bp} alone, it is difficult to surmise what a reasonable expectation for absolute magnitude should be in the South Pacific gyre, but previous theoretical and experimental work has determined and verified expected ranges for these ratios (Twardowski et al., 2001; Boss et al., 2004; Sullivan et al., 2005; Twardowski et al., 2006; Loisel et al., 2007). Measured b_{bp}/b_p from the central gyre fall within the range expected, indicative of the “soft,” water-filled organic particles one would expect in the open ocean (Twardowski et al., 2001). In fact, from an analysis of field data (not including the current data) and measurements in culture, Twardowski et al. (2006) concluded that the b_{bp}/b_p of phytoplankton dominated particle assemblages “generally tends to converge on a value around 0.5%,” which closely agrees with the measurements here. Note that the b_p used in this ratio and in the Twardowski et al. (2006) analysis includes volume scattering from $\sim 0.93^\circ$ to $\sim 180^\circ$ based on the acceptance angle of the ac-9 attenuation measurement.

In the surface layer extending to 140 m, the spectral ratio $b_{bp}(532)/b_{bp}(650)$ matched expectations from the $1/\lambda$ model for oceanic backscattering, assuming a Junge-type size distribution of particles (slope ~ -4) with minimal absorption (e.g., Morel 1973, 1988). Furthermore, the relationship between $b_{bp}(532)/b_p(532)$ and $b_{bp}(650)/b_p(650)$ clustered around a 1:1 agreement, also matching expectations. In total, these observations are good evidence that the magnitudes of $b_{bp}(532)$ and $b_{bp}(650)$, which can be considered fully independent measurements, appear accurate at the level of our estimated uncertainties.

These uncertainties for the $b_{bp}(532)$ and $b_{bp}(650)$ values are not only dependent on the uncertainties in the measurement, but also on the uncertainties in the estimates of pure seawater scattering used. These results suggest b_{swB} values are accurate at the $1 \times 10^{-5} \text{ m}^{-1}$ level in the red. Note that Buiteveld et al. (1994) only reported results from their calculations at 20°C to the fourth decimal place. Buiteveld et al. (1994) estimate their accuracy at 6%, which, for $b_{bw}(650) = 3.5 \times 10^{-4} \text{ m}^{-1}$, corresponds to a $2 \times 10^{-5} \text{ m}^{-1}$ uncertainty, consistent with findings here. It was also necessary in these extremely clear waters that the ambient water temperature be used in the computation of b_{bw} to achieve the most accurate results. These results support the use of

$\delta = 0.051$ after Farinato and Roswell (1976). However, since Farinato and Roswell is a single study that lowered a previously accepted constant (Morel, 1974; Shifrin, 1988) by more than 40%, this is certainly a topic that could benefit from additional investigation. In fact, Jonasz and Fournier (2007) have recently recommended the use of $\delta = 0.039$ based on another interpretation of the data of Farinato and Roswell (1976), highlighting the substantial uncertainty that remains in this constant.

Additionally, the $\sim 30\%$ increase relative to pure water scattering recommended by Morel (1974), would also appear accurate at a high level. If we make the cautious assumption based on the b_{bp}/b_p and spectral results that the $b_{bp}(650)$ values were accurate within 20%, this would translate to a $30 \pm 3\%$ range for the effects of salts at a salinity of 37, assuming the values from Buiteveld et al. (1994) were exact. After a close examination, this very good accuracy may actually be quite consistent with the original measurements of Morel (1966). Firstly, Morel’s measurements of $\beta(90^\circ)$ with purified water and with a sample of purified Mediterranean seawater were made relative to benzene, so that the absolute values relied on accurate absolute scattering values for benzene. However, the enhancement in molecular scattering due to seawater was obtained as a ratio of the relative Mediterranean seawater values and the relative pure water values, so that any bias errors associated with calibration cancel. Furthermore, pure water and pure seawater $\beta(90^\circ)$ were resolved at five wavelengths, from 366 to 578 nm, allowing some statistics; the resulting standard deviation around the 1.30 enhancement was 0.01. Morel (1966) could additionally demonstrate through theory that other measurements in artificial seawater and NaCl solutions generally supported the 30% enhancement. As a result, we can conclude that aggregate uncertainties of the best pure seawater estimates, i.e., the values of Buiteveld et al. (1994) with Morel’s salinity enhancement, would appear to be on the order of just a few percent.

The presence of a unique particle layer centered at ~ 230 m was only apparent in backscattering measurements. One explanation for this increased backscattering may be the presence of a layer of coccolithophorids and associated free coccoliths at depth (Honjo and Okada, 1974). An obvious candidate coccolithophorid for this deep layer is *Florisphaera profunda*, known to occupy a niche in the lower photic zone ($< 1\%$ surface irradiance) at the top of the nutricline in subtropical and tropical regions throughout the world’s oceans (Molfin and McIntyre, 1990; Jordan and Chamberlain, 1997; Malinverno et al., 2003). This species was identified in the deepest samples analyzed from the GYR station (depth of 190 m; Luc Beaufort, personal communication, 2007). HPLC pigment analyses additionally identified the coccolithophorid (Prymnesiophyte) pigment 19’-hexanoxyfucoxanthin in samples in the deep layer (Ras et al., 2007). Another clue with respect to the ecological niche was that the depth of the backscattering peak, ~ 230 m,

corresponded to the precise location of the upper boundary of the nutricline (M. Lewis, Dalhousie University, personal communication, 2007). These observations support the presence of a deep coccolithophorid layer with a uniquely identifiable backscattering signature. It is an interesting note that this particular coccolithophorid species, with unique subrectangular plates, is the dominant coccolithophorid in sediment fossil assemblages when nutriclines are found extending only into the lower photic zone, as is the case in the South Pacific gyre (Molfini and McIntyre, 1990; Jordan and Chamberlain, 1997). Thus, the ecology associated with this deep backscattering layer may not simply be a peculiar oddity, but may play a key role in the transfer of carbon to the sediments in these regions.

Another explanation investigated for the deep backscattering peak was possible contamination of the backscattering signals at 532 and 650 nm from *Prochlorococcus* pigments fluorescence. The interference filters used in front of the detectors of the ECO-BB3 have a full-width-half-maximum of 30 and 20 nm at 532 and 650 nm, respectively. It may be possible, if the filter is appropriately located, that fluorescence effects of some pigments with a small Stokes shift may be detectable, particularly in these ultra clear waters. This was deemed unlikely, however, after looking at the pigment distributions obtained from HPLC analyses (Ras et al., 2007). *Prochlorococcus* pigments such as divinyl chl-a (chl-a₂) and divinyl chl-b (chl-b₂) peak in the lower depths of the deep chlorophyll maximum, typically around 200 m at the GYR station, or 30 m shallower in the water column than the apparent peak in backscattering. This trend was consistent throughout the central gyre.

At 462 and 532 nm, the lowest b_{bp} values in the central gyre, 9.2×10^{-5} and $3.7 \times 10^{-5} \text{ m}^{-1}$, respectively, were found between 115° and 118° W longitude in the depth range of 300 to 350 m. At these locations and depths, $b_{bp}(650)$ reached minimums not distinguishable from the pure seawater backscattering values of Buiteveld et al. (1994) multiplied by $[1+0.3S/37]$ from Morel 1974 to account for salts. To our knowledge, these values are about an order of magnitude lower than the lowest previous particulate backscattering measurements made by Boss et al. (2007) in Crater Lake and Stramska and Stramski (2005) in the Greenland Sea.

The ability to resolve total and particulate backscattering structure in the very clear South Pacific central gyre demonstrates the possibility that these optical properties can be effective proxies for biogeochemical parameters in almost any natural waters. Future work will more closely evaluate the relationships between the particle scattering properties and the biogeochemical determinations of particle concentrations and composition.

Acknowledgements. M. Twardowski gratefully acknowledges support for this work from the U.S. Office of Naval Research Optics and Biology and SBIR Programs and the NASA Biology and Biogeochemistry and SBIR Programs. D. Merien was of

valuable assistance in the field and we thank him for his efforts. D. Tailliez and C. Bournot are warmly thanked for their efficient help in CTD rosette management and data processing. Many helpful discussions with R. Zaneveld, C. Moore, J. Sullivan, E. Boss, and A. Morel improved this work. In particular, comments by E. Boss on an earlier version of the manuscript helped to evolve interpretations and improve clarity in a number of sections. This is a contribution of the BIOSOPE project of the LEFE-CYBER program. This project was funded by the Centre National de la Recherche Scientifique (CNRS), the Institut des Sciences de l'Univers (INSU), the Centre National d'Etudes Spatiales (CNES), the European Space Agency (ESA), The National Aeronautics and Space Administration (NASA) and the Natural Sciences and Engineering Research Council of Canada (NSERC).

Edited by: E. Boss

References

- Aas, E.: Refractive index of phytoplankton derived from its metabolite composition, *J. Plankton Res.*, 18(12), 2223–2249, 1996.
- Balch, W. M., Drapeau, D. T., Cucci, T. L., Vaillancourt, R. D., Kilpatrick, K. A., and Fritz, J. J.: Optical backscattering by calcifying algae: separating the contribution by particulate inorganic and organic carbon fractions, *J. Geophys. Res.*, 104, 1541–1558, 1999.
- Balch, W. M., Gordon, H., Bowler, B. C., Drapeau, D. T., and Booth, E. S.: Calcium carbonate measurements in the surface global ocean based on Moderate-Resolution Imaging Spectroradiometer data, *J. Geophys. Res.*, 110, C07001, doi:10.1029/2004JC002560, 2005.
- Bohren, C. J. and Huffman, D. R.: Absorption and scattering of light by small particles, Wiley, New York, 530 pp., 1983.
- Boss, E. and Pegau, W. S.: Relationship of light scattered at an angle in the backward direction to the backscattering coefficient, *Appl. Opt.*, 40, 5503–5507, 2001.
- Boss, E., Twardowski, M. S., and Herring, S.: Shape of the particulate beam attenuation spectrum and its inversion to obtain the shape of the particulate size distribution, *Appl. Opt.*, 40, 4885–4893, 2001.
- Boss, E., Pegau, W. S., Lee, M., Twardowski, M. S., Shybanov, W., Korotaev, G., and Baratange, F.: The particulate backscattering ratio at LEO 15 and its use to study particles composition and distribution, *J. Geophys. Res.*, 109, C01014, doi:10.1029/2002JC001514, 2004.
- Boss, E., Collier, R., Larson, G., Fennel, K., and Pegau, W. S.: Measurements of spectral optical properties and their relation to biogeochemical variables and processes in Crater Lake, Crater Lake National Park, OR, *Hydrobiologia*, 574, 149–159, 2007.
- Bricaud, A. and Stramski, D.: Spectral absorption coefficients of living phytoplankton and nonalgal biogenous matter: A comparison between Peru upwelling area and the Sargasso Sea, *Limnol. Oceanogr.*, 35, 562–582, 1990.
- Buiteveld, H., Hakvoort, J. H. M., and Donze, M.: The optical properties of pure water, *SPIE Ocean Optics XII*, 2258, 174–183, 1994.
- Carder, K. L., Tomlinson, R. D., and Beardsley Jr., G. F.: A technique for the estimation of indices of refraction of marine phytoplankters, *Limnol. Oceanogr.*, 17, 833–839, 1972.

- Chami, M., Shybanov, E. B., Churilova, T. Y., Khomenko, G. A., Lee, M. E.-G., Martynov, O. V., Berseneva, G. A., and Korotaev, G. K.: Optical properties of the particles in the Crimea coastal waters (Black Sea), *J. Geophys. Res.*, 110, C11020, doi:10.1029/2005JC003008, 2005.
- Clavano, W. R., Boss, E., and Karp-Boss, L.: Inherent optical properties of non-spherical marine-like particles – from theory to observation. *Oceanography and Marine Biology, An Annual Review*, 45, 1–38, 2007.
- Claustre, H., Morel, A., Babin, M., Cailliau, C., Marie, D., Marty, J.-C., Tailliez, D., and Vaultot, D.: Variability in particle attenuation and chlorophyll fluorescence in the tropical Pacific: scales, patterns, and biogeochemical implications, *J. Geophys. Res.*, 104(C2), 3401–3422, 1999.
- Dana, D. R. and Maffione, R. A.: Determining the backward scattering coefficient with fixed-angle backscattering sensors – Revisited, *Ocean Optics XVI*, Santa Fe, New Mexico, November, 18–22, 2002.
- Davis, R. F., Moore, C. C., Zaneveld, J. R. V., and Napp, J. M.: Reducing the effects of fouling on chlorophyll estimates derived from long-term deployments of optical instruments, *J. Geophys. Res.*, 102, 5821–5855, 1997.
- Evyushenko, A. M. and Kiyachenko, Y. F.: Determination of the dependence of liquid refractive index on pressure and temperature, *Opt. Spectrosc.*, 52, 56–58, 1982.
- Farinato, R. S. and Roswell, R. L.: New values of the light scattering depolarization and anisotropy of water, *J. Chem. Phys.*, 65, 593–595, 1976.
- Fournier, G. R. and Forand, J. L.: Analytical phase function for ocean water, *Ocean Optics XII*, edited by: Jaffe J. S., *Proc. SPIE*, 2258, 194–201, 1994.
- Gardner, W. D., Chung, S. P., Richardson, M. J., and Walsh, I. D.: The oceanic mixed-layer pump, *Deep Sea Res. Part II*, 42, 757–775, 1995.
- Gordon, H. R.: Backscattering of light from disk-like particles: is fine-scale structure or gross morphology more important?, *Appl. Opt.*, 45, 7166–7173, 2006.
- Gordon, H. R.: Rayleigh-Gans scattering approximation: surprisingly useful for understanding backscattering from disk-like particles, *Opt. Express*, 15(9), 5572–5588, 2007.
- Honjo, S. and Okada, H.: Community structure of coccolithophores in the photic layer of the mid-Pacific, *Micropaleontology*, 20(2), 209–230, 1974.
- Jonasz, M. and Fournier, G.: *Light scattering by particles in water*, Academic Press, Amsterdam, Netherlands, 704 pp., 2007.
- Jordan, R. W. and Chamberlain, A. H. L.: Biodiversity among haptophyte algae, *Biodivers. Conserv.*, 6, 131–152, 1997.
- Kiefer D. A. and Berwald, J.: A random encounter model for the microbial planktonic community, *Limnol. Oceanogr.*, 37(3), 457–467, 1992.
- Lee, M. E. and Lewis, M. R.: A new method for the measurement of the optical volume scattering function in the upper ocean, *J. Atmos. Oceanic Technol.*, 20(4), 563–571, 2003.
- Lepple, F. K. and Millero, F. J.: The isothermal compressibility of seawater near one atmosphere, *Deep-Sea Res.*, 18, 1233–1254, 1971.
- Loisel, H., Meriaux, X., Berthon, J.-F., and Poteau, A.: Investigation of the optical backscattering to scattering ratio of marine particles in relation to their biogeochemical composition in the eastern English Channel and southern North Sea, *Limnol. Oceanogr.*, 52(2), 739–752, 2007.
- Maffione, R. A. and Dana, D. R.: Instruments and methods for measuring the backward-scattering coefficient of ocean waters, *Appl. Opt.*, 36, 6057–6067, 1997.
- Malinverno, E., Ziveri, P., and Corselli, C.: Coccolithophorid distribution in the Ionian Sea and its relationship to eastern Mediterranean circulation during late fall to early winter 1997, *J. Geophys. Res.*, 108(C9), 8115, doi:10.1029/2002JC001346, 2003.
- McNeil, G. T.: Metrical fundamentals of underwater lens systems, *Opt. Eng.*, 16, 128–139, 1977.
- Molfini, B. and McIntyre, A.: Precessional forcing of nutricline dynamics in the Equatorial Atlantic, *Science*, 249, 766–768, 1990.
- Moore, C., Twardowski, M. S., and Zaneveld, J. R. V.: The ECO VSF – A multi-angle scattering sensor for determination of the volume scattering function in the backward direction, *Proc. Ocean Optics XV*, 16–20 October, Monaco, Office Naval Research, USA, CD-ROM, 2000.
- Morel, A.: Etude expérimentale de la diffusion de la lumière par l'eau, les solutions de chlorure de sodium et l'eau de mer optiquement pure, *J. Chim. Phys.*, 10, 1359–1366, 1966.
- Morel, A.: Note au sujet des constants de diffusion de la lumière pour l'eau et l'eau de mer optiquement pures, *Cahiers Oceanographique*, 20, 157–162, 1968.
- Morel, A.: Diffusion de la lumière par les eaux de mer. Résultats expérimentaux et approche théorique, in *Optics of the Sea*, AGARD Lecture Series No. 61, NATO, 3.1.1–3.1.76, 1973.
- Morel, A.: Optical properties of pure water and pure seawater, in: *Optical aspects of Oceanography*, edited by: Jerlov, N. G. and Steemann Nielson, E., Academic, New York, 1–24, 1974.
- Morel, A.: Optical modeling of the upper ocean in relation to its biogenous matter content (Case I waters), *J. Geophys. Res.*, 93, 10 749–10 768, 1988.
- Morel, A. and Gentili, B.: Diffuse reflectance of oceanic waters: its dependence on sun angle as influenced by the molecular scattering contribution, *Appl. Opt.*, 30, 4427–4438, 1991.
- Morel, A. and Gentili, B.: Radiation transport within oceanic (case 1) waters, *J. Geophys. Res.*, 109, C06008, doi:10.1029/2003JC002259, 2004.
- Morel, A., Gentili, B., Claustre, H., Babin, M., Bricaud, A., Ras, J., and Tieche, F.: Optical properties of the “clearest” natural waters, *Limnol. Oceanogr.*, 52, 217–229, 2007.
- O’Conner, C. L. and Schlupf, J. P.: Brillouin scattering in water: the Landau-Paszek ratio, *J. Chem. Phys.*, 47, 31–38, 1967.
- Oubelkheir, K., Clementson, L., Webster, I., Ford, P., Dekker, A., Radke, L., and Daniel, P.: Using inherent optical properties to investigate biogeochemical dynamics in a tropical macro-tidal coastal system, *J. Geophys. Res.*, 111, C07021, doi:10.1029/2005JC003113, 2006.
- Pegau, W. S., Boss, E., Weidemann, A., Korotaev, G., Lee, M., and Shibanov, E.: Measurements of the backscattering coefficient, Abstract from ASLO meeting, Session CS24 – Optics, Albuquerque, NM, 12–16 February, 2001.
- Pope, R. M. and Fry, E. S.: Absorption spectrum (380–700 nm) of pure water. II. Integrating cavity measurements, *Appl. Opt.*, 36, 8710–8723, 1997.
- Prentice, J. E., Weidemann, A. D., Pegau, W. S., Voss, K. J., Lee, M. E., Shybanov, E., Martynov, O., Laux, A. E., Briggs, A., and Chang, G.: Laboratory comparisons of optical scattering instru-

- mentation, *Ocean Optics XVI*, Santa Fe, New Mexico, 2002.
- Ras, J., Claustre, H., and Uitz, J.: Spatial variability of phytoplankton pigment distributions in the Subtropical South Pacific Ocean: comparison between in situ and predicted data, *Biogeosciences Discuss.*, 4, 3409–3451, 2007, <http://www.biogeosciences-discuss.net/4/3409/2007/>.
- Siegel, D. A., Dickey, T. D., Washburn, L., Hamilton, M. K., and Mitchell, B. G.: Optical determination of particulate abundance and production variations in the oligotrophic ocean, *Deep Sea Res. Part A*, 36, 211–222, 1989.
- Shifrin, K.: *Physical optics of ocean water*, American Institute of Physics, New York, 285 pp., 1988.
- Slade, W. H. and Boss, E.: Calibrated near-forward volume scattering function obtained from the LISST particle sizer, *Opt. Express*, 14(8), 3602–3615, 2006.
- Smith, R. C. and Baker, K. S.: Optical properties of the clearest natural waters (200–800 nm), *Appl. Opt.*, 20(2), 177–184, 1981.
- Stramska, M. and Stramski, D.: Variability of particulate organic carbon concentration in the north polar Atlantic based on ocean color observations with Sea-viewing Wide Field-of-view Sensor (SeaWiFS), *J. Geophys. Res.*, 110, C10018, doi:10.1029/2004JC002762, 2005.
- Stramski, D., Reynolds, R., Babin, M., Kaczmarek, S., Lewis, M. R., Rottgers, R., Sciandra, A., Stramska, M., Twardowski, M. S., and Claustre, H.: Relationship between the surface concentration of particulate organic carbon and optical properties in the eastern South Pacific and eastern Atlantic Oceans, *Biogeosciences Discuss.*, 2007.
- Stramski, D. and Kiefer, D. A.: Light scattering by microorganisms in the open ocean, *Prog. Oceanogr.*, 28, 343–383, 1991.
- Stramski, D., Reynolds, R. A., Kahru, M., and Mitchell, B. G.: Estimation of particulate organic carbon in the ocean from satellite remote sensing, *Science*, 285, 239–242, 1999.
- Stramski, D., Bricaud, A., and Morel, A.: Modeling the inherent optical properties of the ocean based on the detailed composition of the planktonic community, *Appl. Opt.*, 40, 2929–2945, 2001.
- Stramski, D., Boss, E., Bogucki, D., and Voss, K.: The role of seawater constituents in light backscattering in the ocean, *Prog. Oceanogr.*, 61, 27–56, 2004.
- Sullivan, J. M., Twardowski, M. S., Donaghay, P. L., and Freeman, S. A.: Using Scattering Characteristics to Discriminate Particle Types in US Coastal Waters, *Appl. Opt.*, 44, 1667–1680, 2005.
- Sullivan, J. M., Twardowski, M. S., Zaneveld, J. R. V., Moore, C., Barnard, A., Donaghay, P., and Rhoades, B.: The hyperspectral temperature and salinity dependencies of absorption by water and heavy water in the 400–750 nm spectral range, *Appl. Opt.*, 45, 5294–5309, 2006.
- Twardowski, M. S., Sullivan, J. M., Donaghay, P. L., and Zaneveld, J. R. V.: Microscale quantification of the absorption by dissolved and particulate material in coastal waters with an ac-9, *J. Atmos. Ocean. Technol.*, 16(12), 691–707, 1999.
- Twardowski, M. S., Boss, E., Macdonald, J. B., Pegau, W. S., Barnard, A. H., and Zaneveld, J. R. V.: A model for estimating bulk refractive index from the optical backscattering ratio and the implications for understanding particle composition in Case I and Case II waters, *J. Geophys. Res.*, 106(C7), 14 129–14 142, 2001.
- Twardowski, M. S., Lewis, M., Barnard, A., and Zaneveld, J. R. V.: In-water instrumentation and platforms for ocean color remote sensing applications, in: *Remote Sensing of Coastal Aquatic Waters*, edited by: Miller, R., Del Castillo, C., and McKee, B., Springer Publishing, Dordrecht, Netherlands, 69–100, 2005.
- Twardowski, M. S., Sullivan, J. S., Dierssen, H., and Zaneveld, J. R. V.: Sources of backscattering in marine waters, *Ocean Sciences Meeting*, Honolulu, HI, February 20–24, Abstract OS32M-02, 2006.
- Ulloa, O., Sathyendranath, S., and Platt, T.: Effect of the particle-size distribution on the backscattering ratio in seawater, *Appl. Opt.*, 33, 7070–7077, 1994.
- Volten, H., de Haan, J. F., Hovenier, J. W., Schreurs, R., and Vassen, W.: Laboratory measurements of angular distributions of light scattered by phytoplankton and silt, *Limnol. Oceanogr.*, 43, 1180–1197, 1998.
- Walsh, I., Chung, S. P., Richardson, M. J., and Gardner, W. D.: The diel cycle in the integrated particle load in the equatorial Pacific: a comparison with primary production, *Deep Sea Res. II*, 42, 465–477, 1995.
- Zaneveld, J. R. V., Kitchen, J. C., and Moore, C. M.: The scattering error correction of reflecting-tube absorption meters, *Ocean Optics XII*, Proc. SPIE 2258, 44–55, 1994.
- Zaneveld, J. R. V., Twardowski, M. S., Lewis, M., and Barnard, A.: Radiative transfer and remote sensing, in: *Remote Sensing of Coastal Aquatic Waters*, edited by: Miller, R. and Del-Castillo, C., Springer-Kluwer Publishing, 1–20, 2005.

Natural variability of bio-optical properties in Case 1 waters: attenuation and reflectance within the visible and near-UV spectral domains, as observed in South Pacific and Mediterranean waters

A. Morel, H. Claustre, D. Antoine, and B. Gentili

Laboratoire d'Océanographie de Villefranche, Université Pierre et Marie Curie (Paris 6) and CNRS/INSU, 06238 Villefranche-sur-mer, CEDEX, France

Received: 18 June 2007 – Published in Biogeosciences Discuss.: 3 July 2007

Revised: 12 October 2007 – Accepted: 14 October 2007 – Published: 26 October 2007

Abstract. The optical properties of Case 1 waters have been empirically related to the chlorophyll concentration, [Chl], historically used as an index of the trophic state and of the abundance of the biological materials. The well-known natural variability around the mean statistical relationships is here examined by comparing the apparent optical properties (spectral downward irradiance attenuation and reflectance) as a function of [Chl] in two Case 1 environments, the Pacific and Mediterranean waters. These oceanic zones apparently represent two extremes of the possible bio-optical variability range around the mean. The systematic deviations, in both directions with respect to the average laws, mainly result from the differing contents in non-algal detrital materials and dissolved colored substance for a given [Chl] level. These contents are higher than the average in the Mediterranean Sea, and lower in the Pacific Ocean, respectively. These divergences between the two water bodies, detectable in the visible spectral domain, are considerably accentuated in the UV domain. The bio-optical properties in this spectral domain (310–400 nm) are systematically explored. They are more varying for a given [Chl] than those in the visible domain. Their prediction based on the sole [Chl] index is thus problematic, although it is probably possible on a regional scale if reliable field data are available. It does not seem, however, that ubiquitous relationships exist for this spectral domain for all Case 1 waters at global scale.

1 Introduction

According to the common use, Case 1 waters are those for which phytoplankton with their accompanying retinue of dissolved and particulate materials of biological origin govern the bulk optical properties. This statement also means that the terrigenous influence (through dissolved or suspended material originating from land) is reduced to its minimum, and actually is supposed to be negligible. Such a definition, based on a biogeochemical criterion, has bio-optical consequences. The apparent and inherent optical properties (AOP, and IOP, sensu Preisendorfer, 1961) of Case 1 waters have been analyzed and it was possible to empirically relate these properties to the chlorophyll concentration (thereafter denoted [Chl]). This concentration, which is routinely, or at least, very often determined at sea, was historically and is still used as a proxy of the whole (algal and non-algal) biological material, or a convenient descriptor of trophic conditions. The choice of this single index was made for obvious practical and methodological reasons. Not less obviously, the inability of such a single parameter to fully describe the whole biological compartment, as soon as there are no strict co-variations between its various components, entails that variability for all Case 1 waters is to be expected. Actually, the dispersion of data (IOP and AOP) around the empirical mean laws mentioned above attested that this variability is considerable (e.g., Gordon and Morel, 1983a; Bricaud et al., 1995; Bricaud et al., 1998; Loisel and Morel, 1998). A hint to the possibility of systematic geographical deviations was dropped by Morel and Maritorena (2001); they compared a restricted number of data from the Mediterranean Sea and from Central South Pacific for the spectral range 400–350 nm. More numerous data, extended down to 310 nm, are now available to examine these differences in detail.

Correspondence to: A. Morel
(morel@obs-vlfr.fr)

During the BIOSOPE cruise (Claustre et al., 2007¹) spectral measurements of the downward and upward planar irradiances, $E_d(\lambda)$ and $E_u(\lambda)$, respectively, were performed along a ~ 8000 km-long transect, from Marquesas islands to the Chilean coast off Concepción. The apparent optical properties, in particular the spectral diffuse attenuation coefficient, $K_d(\lambda)$, for downward irradiance, and the irradiance reflectance, $R(\lambda)$, were derived from the spectroradiometric determinations of $E_d(\lambda)$ and $E_u(\lambda)$, which were made at discrete depths within the water column.

A first study (Morel et al., 2007a) of this dataset was specifically devoted to the exceptional optical properties observed in the center of the South Pacific Gyre, near Easter Island. In this zone we encountered the most oligotrophic waters along the transect, and probably in the whole ocean (satellite Ocean Color imagery has steadily confirmed the extremely low [Chl] values in this zone – see e.g., Fournié (2002), Claustre et al. (2007¹). The exceptional clarity of these waters was in itself a worthwhile topic. This clarity has also allowed an upper limit for the absorption by pure seawater in the UV domain to be inferred. It is worth recalling that the knowledge of this absorption coefficient was highly uncertain, because the scarce published values for the UV domain were questionable and contradictory.

The present paper extends the previous study to the entire South Pacific zone along the transect. Beside the hyper-oligotrophic regime of the central part of the gyre, it also includes the examination of the mesotrophic waters (near Marquesas Islands), the eutrophic waters (Chilean upwelling area), and the transition zones. Along the whole transect, [Chl] in the upper layer ranged from 0.02 to about 2 mg m^{-3} .

The present study also takes advantage of the improved knowledge of the water absorption properties in the UV (namely the 310–400 nm domain) as mentioned above. It thus becomes possible to analyze the optical properties in this spectral domain as a function of the chlorophyll concentration. Such an analysis builds upon a previous study (Morel and Maritorena, 2001), which yet did not examine the 310–350 nm domain, and was only tentative in its conclusions regarding the 350–400 nm domain. This limitation was essentially due to an insufficient amount of field data (and of the lack of reliable values for pure water absorption).

This situation has considerably improved, as the recent $E_d(\lambda)$ and $E_u(\lambda)$ spectral determinations have been systematically extended down to 310 nm. Furthermore, a substantial amount of data for the South Pacific Ocean is now available by pooling together the recent data of the BIOSOPE (2004) cruise with those of the previous (1994) OLIPAC cruise (a S-N transect from Tahiti to 1°N). In addition, the same methodology was employed in other cruises in the Mediter-

ranean Sea (PROSOPE and AOPEX, see Table 1), as well as in South Atlantic (BENCAL cruise). The data of the latter cruise in the eutrophic waters of the Benguela current are used for the sake of completion, as they represent a useful end member in terms of [Chl] in Case 1 waters (values up to 30 mg m^{-3} ; Morel et al., 2006). Therefore, it is presently possible to compare the various oceanic zones (all in Case 1 waters) and to initiate a study of the natural variability of the bio-optical properties in such waters.

1.1 Specific motivations and goals

For many years the $K_d(\lambda)$ coefficients have been empirically studied along with [Chl] (Baker and Smith, 1982; Austin and Petzold, 1981). Actually, the results of these researches were the basis for the development of [Chl]-dependent bio-optical models for Case 1 waters (Gordon and Morel, 1983a; Gordon et al., 1988; Morel, 1988), and of algorithms aiming at assessing [Chl] from the signals recorded by ocean color sensors; more generally, the prediction of the radiation transport within such waters makes use of these results as inputs for a numerical solution of the radiative transfer equation (Morel and Gentili, 2004). The first motivation of the present study is to examine whether the South Pacific waters follow the general trends already observed elsewhere in the global ocean, or in other specific areas (Mediterranean Sea), particularly with regards to the $K_d(\lambda) \leftrightarrow [\text{Chl}]$ relationships. The dependency in shape and magnitude of $R(\lambda)$, upon [Chl] is also to be examined. The complementary objective is to try to explain the departures, if any, from the general trends.

The second aim is to extend the previous studies into the short wavelength region, which is by far less documented with regards to the possible existence of relationships between either $K_d(\lambda)$ or $R(\lambda)$, and [Chl]. The respective influences of the algal populations with their retinue (including organic and inorganic debris, also heterotrophic organisms) and of the colored dissolved material in the UV domain, are still unclear and not quantified.

1.2 Methodology and theoretical background

The $E_u(\lambda, z)$ and $E_d(\lambda, z)$ spectral irradiances were determined at discrete depths (z) by using a calibrated LICOR spectroradiometer (LI-1800 UW) equipped with a cosine collector. The incident radiation on the deck was monitored by using a gimbaled PAR cosine sensor (PNF Biospherical instrument). A detailed description of the equipment, protocols and data processing was provided in recent papers (Morel et al., 2006 and 2007a) and is not repeated. The chlorophyll concentration ([Chl], as mg m^{-3}), was determined for all cruises via High-Performance Liquid Chromatography (HPLC) (Ras et al., 2007). The notation Chl actually represents the sum of the following pigments: chlorophyll-*a* + divinyl chlorophyll-*a* + chlorophyllid-*a* + chlorophyll-*a* alomers and epimers (often referred to as “TChl-*a*”).

¹Claustre, H., Sciandra, A., and Vaultot, D.: Introduction to the special section: Bio-optical and biogeochemical conditions in the South East Pacific in late 2004, the BIOSOPE program, Biogeosciences Discuss., in preparation, 2007.

Table 1. Relevant information regarding the cruises, their geographical areas, and data, used in the present study. The minimal and maximal [Chl] values measured within the upper layer, and the minimal wavelength for the spectral irradiance measurements, are provided for each cruise.

	Min-Max [Chl] (upper layer mg m^{-3})	λ_{min} (nm)	geographical area
"Old Data" N~255			
JGR-88 (1969–1986)	0.025–25.	400	various
MM-01* (1986–1996)	0.035–5.45	(380)-400	various
MM01 includes			
OLIPAC (1994)	0.043–0.293	300	South-central
Pacific MINOS (1996)	0.035–0.089	350	W. and E. Med Sea
"New Data" N~201			
PROSOPE (1999)	0.024–3.75	300	Moroccan upwelling, W. and E. Med Sea
BENCAL (2002)	0.245–29.1	300	Benguela
AOPEX (2004)	0.052–0.162	300	W-Med Sea
BIOSOPE (2004)	0.0195–1.47	300	South-East Pacific

Acronyms : OLIGotrophy in PACific (OLIPAC); Mediterranean InvestigationN of Oligotrophic Systems (MINOS); PROductivity of Oceanic PELagic systems (PROSOPE); BIogeochimistry and Optics South Pacific Experiment (BIO SOPE); Ocean Color Cal/Val in the Benguela upwelling ecosystem (BENCAL); Apparent Optical Properties Experiment (AOPEX).

Information and data available on www.obs-vlfr.fr/proof/index-vt.htm for OLIPAC, PROSOPE, and BIO SOPE cruises on www.Ifremer.fr/sismer for MINOS and AOPEX.

BENCAL Cruise Report, NASA Technical Memorandum 2003-206892, Vol. 27.

A minimal set of definitions is provided below. The spectral attenuation coefficient for downward irradiance, $K_d(\lambda)$, is computed (from null depth, denoted 0^- , to a depth z) as

$$K_d(\lambda) = (1/z) \ln[E_d(\lambda, 0^-)/E_d(\lambda, z)] \quad (1)$$

actually $E_d(\lambda, 0^-)$, just beneath the surface, is not measured but derived from the measurement above the surface, $E_d(\lambda, 0^+)$, (notation 0^+), by applying a spectrally neutral coefficient (0.97) that accounts for the transmission across the air-sea interface. Here the examination is restricted to the upper layer, and z is about or slightly larger than $1/K_d(\text{PAR})$, where PAR represents the polychromatic (400 to 700 nm) photosynthetically available radiation (as used in algal physiology and photosynthesis studies).

The sub-surface irradiance reflectance at a depth z , $R(\lambda, z)$, is defined as

$$R(\lambda, z) = E_u(\lambda, z)/E_d(\lambda, z) \quad (2)$$

The E_d and E_u determinations are separated in time by a few minutes, and both quantities are normalized to a constant incident PAR irradiance at the surface (thanks to the deck reference). The depth, z , is as shallow as possible, and was the minimal depth (about 1 to 2 m) where the $E_u(\lambda, z)$ determination was possible, given the waves and ship's roll. The downward spectral irradiance at the depth z , $E_d(\lambda, z)$, is computed by extrapolating $E_d(\lambda, 0^-)$ from 0^- to z , by using the appropriate $K_d(\lambda)$ coefficients.

Based on the spectral $E_d(\lambda, z)$ determinations, PAR(z) at any depth z is obtained by integrating the $E_d(\lambda, z)$ spectrum

over the 400–700 nm range, according to its definition (Tyler, 1966). By convention, the bottom of the euphotic layer, denoted Z_{eu} , is commonly and (somewhat arbitrarily defined) as that depth where the downward PAR irradiance falls to 1% of its sub-surface value (Ryther, 1956; see also discussion about its significance in Banse, 2006). This 1% level can be determined from the PAR vertical profiles. For some stations and because of technical limitations (actually when Z_{eu} was >135 m), Z_{eu} was determined by using the PNF profiler instrument lowered beyond 135 m. Beside of being crucial information in primary production studies (both for experimental and modeling approaches), Z_{eu} is also a useful index to globally describe the bio-optical state of the entire upper water column; as 99% of the solar visible radiation is absorbed within the 0 - Z_{eu} layer, the knowledge of Z_{eu} is important to predict the solar heat deposition with its consequences on the upper ocean dynamics (Morel et al., 2007b).

2 Results

As said earlier, the data used for the present study are not restricted to the BIO SOPE cruise. All the data used in the present study have been collected with the same instruments and optical and chemical protocols during several recent oceanographic campaigns, as summarized in Table 1. The OLIPAC and BIO SOPE data, both for the South-Eastern Pacific, will be merged. Regarding the Mediterranean Sea, the data from the MINOS, PROSOPE, and AOPEX cruises

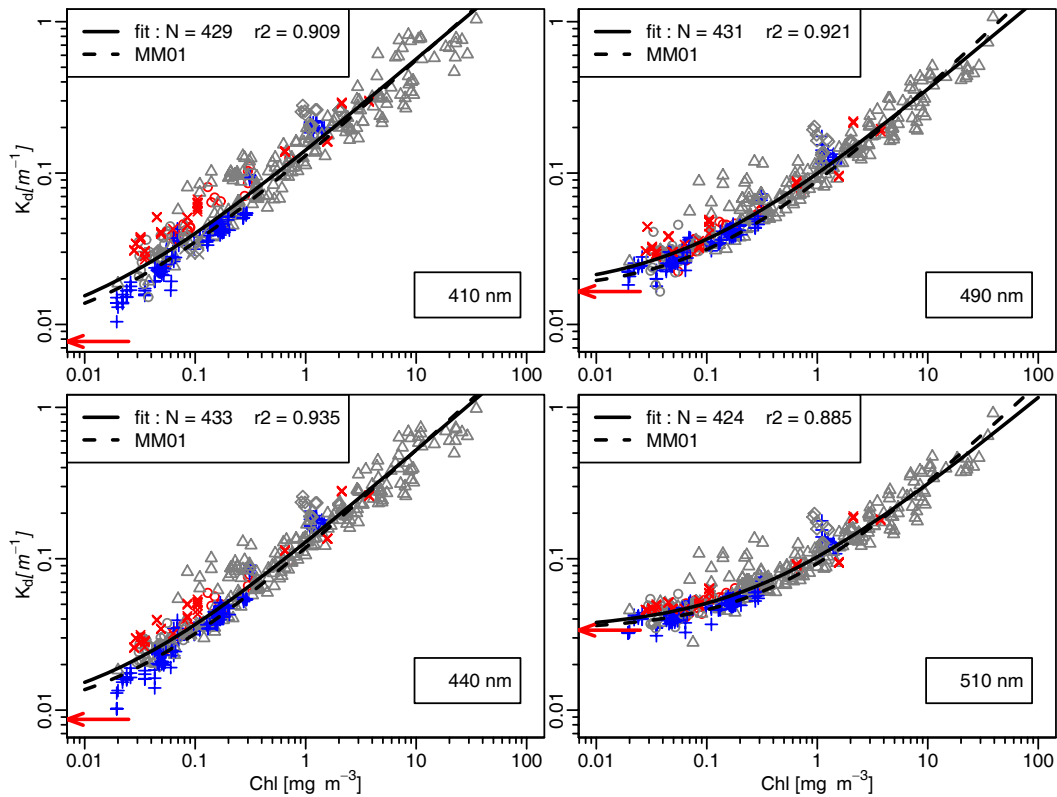


Fig. 1. Plot of the K_d values for the upper layer as a function of [Chl], and for selected wavelengths, as indicated. The red symbols are for the Mediterranean Sea, and the blue symbols for the South Pacific data. The continuous black curve represents the best fit (Eq. 5) for all field data (number of data and r^2 provided in insert); the K_w constant introduced into Eq. (5) is shown as red arrows. The dashed black curve represents the previous (2001) best fit with the χ and e values which were proposed in MM-01.

will also be pooled together. The data of BENCAL, the only cruise in eutrophic Case 1 waters, will be considered to encompass the whole range of [Chl] values. Finally, “old data”, already presented and analyzed in previous studies (Morel, 1988; Morel and Maritorea, 2001, hereafter denoted JGR-88, and MM-01), will be displayed when necessary, especially for the sake of comparison with the “new data”.

2.1 The diffuse attenuation coefficient $K_d(\lambda)$ and its variation with [Chl] in the visible domain

The $K_d(\lambda)$ -[Chl] relationships are displayed in Fig. 1 for some selected wavelengths in the visible part of the spectrum, together with a curve representing the best fit for all data (i.e., “old + new” data). For this statistical analysis, the quantity $K_{\text{bio}}(\lambda)$ is formed as the difference (JGR88)

$$K_{\text{bio}}(\lambda) = K_d(\lambda) - K_w(\lambda), \quad (3)$$

where $K_w(\lambda)$, which represents the contribution by hypothetically pure seawater, is computed (Smith, 1981) as the sum of

the absorption coefficient and the backscattering coefficient for pure seawater (half the scattering coefficient), namely

$$K_w(\lambda) = a_w(\lambda) + \frac{1}{2}b_{sw}(\lambda), \quad (4)$$

Then a linear regression analysis is performed on the log-transforms of the $K_{\text{bio}}(\lambda)$ and [Chl] values for the upper layer, and leads for each wavelength to expressions of the form

$$K(\lambda) = K_w(\lambda) + \chi(\lambda)[\text{Chl}]^{e(\lambda)}, \quad (5)$$

where the coefficient $\chi(\lambda)$ represents the K_{bio} spectrum when [Chl] is 1 mg m^{-3} , and the exponent $e(\lambda)$, which is always below 1, quantifies the non-linear dependency of K_{bio} upon [Chl].

The BIOSOPE and OLIPAC data (blue symbols, Fig. 1) are very similar over their common [Chl] range (0.02 – 0.3 mg m^{-3}). These Pacific waters follow the general trend (black curves) for Case 1 waters. Without being exceptional when considering the overall dispersion, their K_d values lie rather systematically below the curve representing the best fit for all data. In addition, this departure from the mean toward lower values is progressively more accentuated for

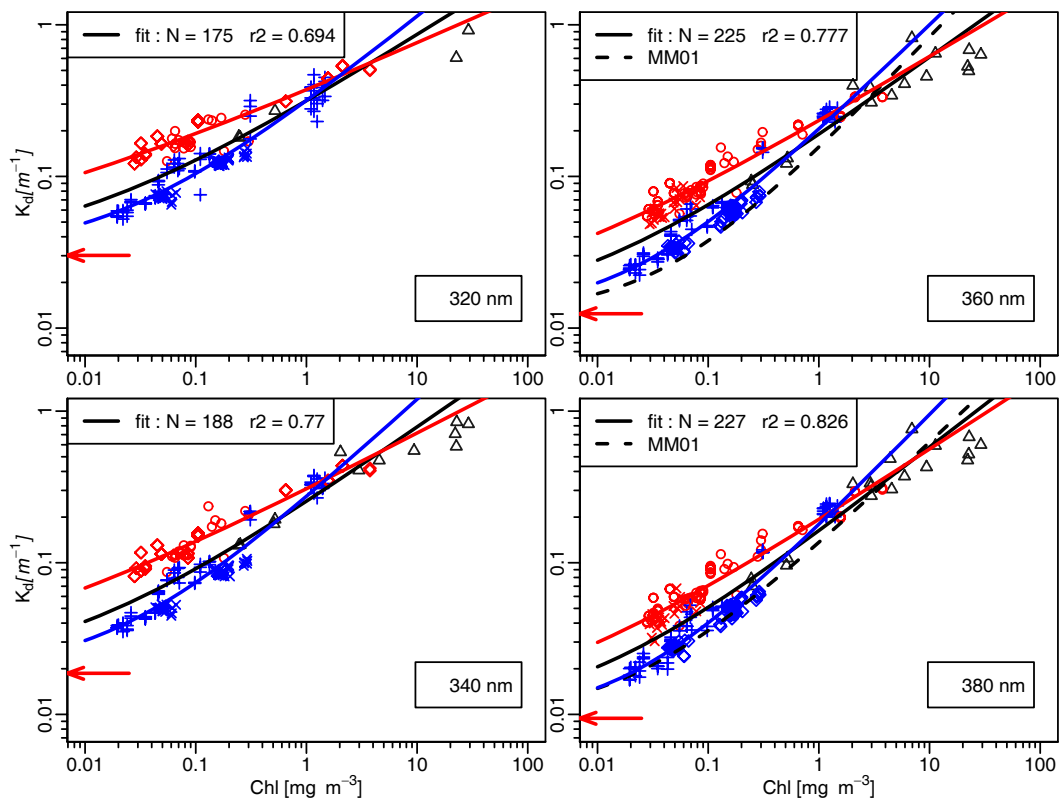


Fig. 2. As in Fig. 1, but for wavelengths in the UV part of the spectrum, as indicated. The meaning of the continuous and dashed black curves is as in Fig. 1; Note that there was no χ and e values below 350 nm in MM-01, therefore no dashed black curve in the panels for 320 and 340 nm. The increased number of data between 340 and 360 nm results from the inclusion of the data from the MINOS cruise in Mediterranean Sea (see Table 1). The blue and red curves represent the separate best fits for the Pacific and Mediterranean data, respectively.

decreasing wavelength (from 510 to 410 nm). In contrast, the Mediterranean K_d values (red symbols), are recurrently above the curve. This opposite distribution of the data from the two oceanic regions explains why, when all data are merged, the best fits and associated parameters, $\chi(\lambda)$ and $e(\lambda)$, remain practically unchanged with respect to those previously presented in the MM-01 study (that already included the OLIPAC data). Separate regressions performed on the Pacific and Mediterranean datasets result in best fit parameters that differ significantly (see below Sect. 3).

2.2 The diffuse attenuation coefficient $K_d(\lambda)$ and its variation with [Chl] in the UV domain

The same analysis as above can be performed within the UV domain by using the revised values of the absorption coefficient by pure seawater recently proposed in Morel et al. (2007a), namely their $a_{w1}(\lambda)$ values. In MM01 such an analysis was attempted for the range 350–400 nm, yet the $a_w(\lambda)$ values used in Eq. (4) were uncertain, and the number of data somewhat insufficient. The backscattering coefficients (Eq. 4) for pure seawater, $b_{sw}(\lambda)$, are derived from Buiteveld (1994) values, and multiplied by 1.30 to account for the effect of salinity (Morel, 1974).

The oligotrophic and mesotrophic waters of the Pacific and Mediterranean behave differently (examples in Fig. 2). For all wavelengths, the Pacific waters are systematically characterized by lower K_d (UV) values, compared to those of Mediterranean waters. This behavior, which was already noted for the shortest wavelengths of the visible spectrum (Fig. 1a), is increasingly confirmed toward the shortest wavelengths in the UV domain. In contrast, there is no longer systematic differences when [Chl] is close to or above 1 mg m^{-3} , i.e., between the K_d values in the Chilean and Moroccan upwelling zones. Interestingly, these values are in continuity with those determined in the Benguela Current, with much higher [Chl] values.

2.3 Separate regression analyses for Pacific and Mediterranean waters

To account for the distinct behaviors of the two water bodies, separate regression analyses are appropriate. They were carried out systematically for all wavelengths from 560 down to 310 nm (increment 5 nm). The two resulting sets of values are graphically compared in Fig. 3a and b, and the regression coefficients in Fig. 3c. The χ and e values differ significantly and increasingly in the UV domain. It is

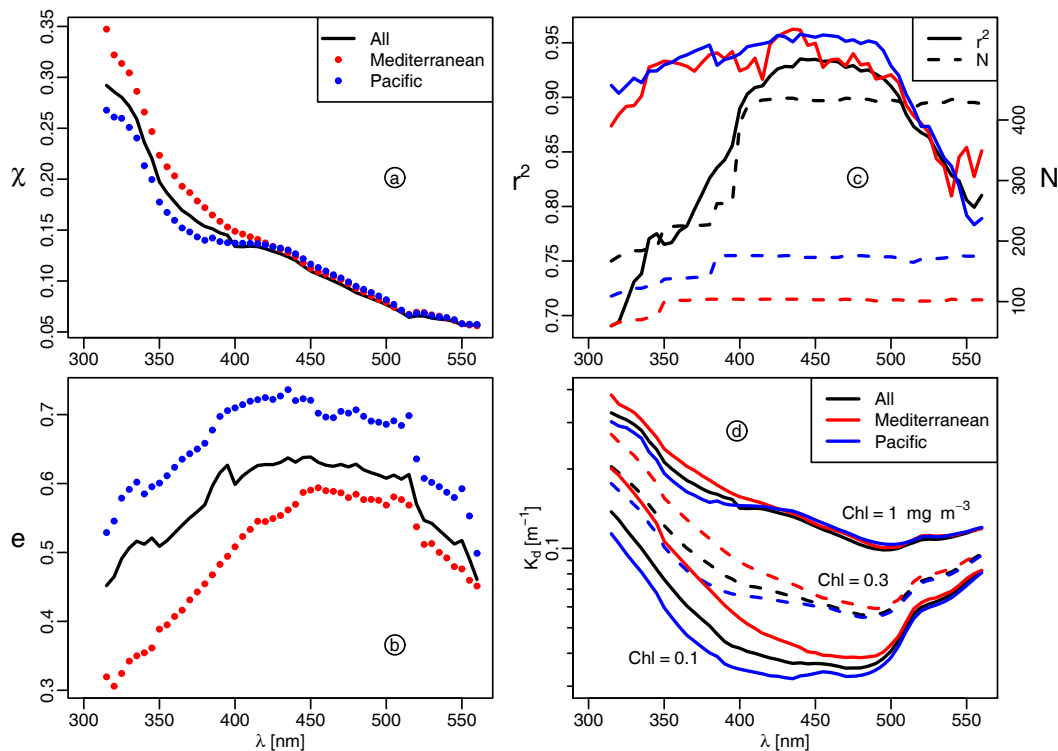


Fig. 3. The $\chi(\lambda)$ (a) and $e(\lambda)$ (b) values corresponding to the best fits (Eq. 5), separately computed for the Pacific (blue) and Mediterranean waters (red); the corresponding coefficient of determination and number of data (r^2 and N) are spectrally displayed in (c). In (d), examples of $K_d(\lambda)$ values computed with the previously shown $\chi(\lambda)$ and $e(\lambda)$ values and for 3 [Chl] values as indicated. In the four panels the black curves show the same quantities when the two datasets are merged.

worth noting that the respective coefficients of determination are high (Fig. 3c) even inside the UV domain. As a consequence, when all data are pooled together, the global correlation logically degrades, particularly in the UV domain. The specific values for the two oceanic provinces are also compared to the adopted χ and e values (limited to 350 nm) resulting from a general merging of all data available (<ftp://oceans.obs-vlfr.fr/pub/morel/2006-e-chi>).

Regarding the $\chi(\lambda)$ parameter (Fig. 3a), the values for the two water bodies are not significantly differing within the 420–560 nm domain. Below 420 nm, the Mediterranean values are ostensibly above the Pacific values (and above the average values, admittedly more influenced by the latter, with about 115 data versus 62 for the former). The spectral shape of the $\chi(\lambda)$ coefficient in the UV domain is characterized for both oceanic areas by a strong increase, with almost a doubling from 410 to 315 nm, and by the presence of a shoulder inside the 330–315 nm region.

Regarding the $e(\lambda)$ exponent (Fig. 3b), large deviations occur between the two sets, with higher values for Pacific waters, and lower ones for the Mediterranean waters. The departure from linearity between K_d and [Chl] is expressed by the $e(\lambda)$ values (always <1); this departure is thus notably larger in the Mediterranean waters within the entire (310–560 nm) spectrum, and especially below 450 nm. Such

a weakening in the dependency upon [Chl] (even with high and significant r^2 values, cf. Fig. 3c) suggests the existence of an optically influential background which would be uncorrelated with the contemporaneous algal stock. On the contrary, the existence of larger $e(\lambda)$ values for Pacific waters globally shows that the dependence upon [Chl] is maintained at a higher degree (lesser non-linearity), which would mean that the interfering effect of a [Chl]-independent background is less marked.

More generally, it is interesting to note the decrease of the $e(\lambda)$ values in the UV compared with those in the visible domain. With various extents this remark holds true in both cases (Mediterranean and Pacific). Accordingly, the UV absorbing material (the dissolved colored organic material, CDOM, and likely some colloidal and particulate material) generally appears to be rather loosely related to the local algal biomass, in contrast to the material responsible for absorption within the visible part of the spectrum, which definitely seems more closely associated with the algae themselves. Therefore, the generic concept of Case 1 waters tends to weaken, or more precisely, to take a more regional sense, as far as the UV domain is concerned.

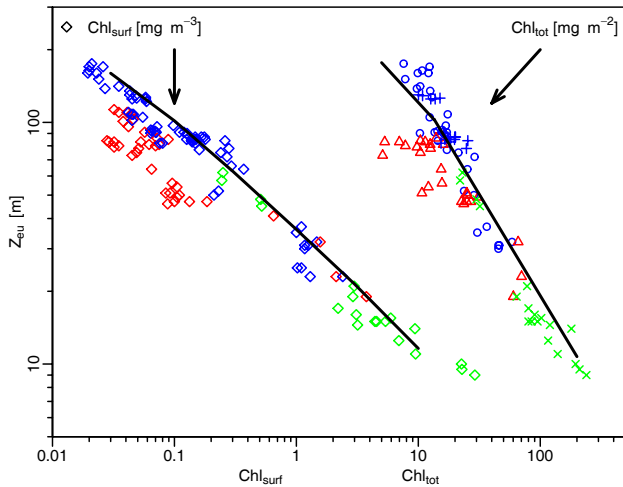


Fig. 4. Left hand side: Z_{eu} as a function of $[\text{Chl}]_{\text{surf}}$, as mg m^{-3} , or, right hand side, as a function of $[\text{Chl}]_{\text{tot}}$, as mg m^{-2} , for the Pacific (blue) and Mediterranean waters (red). The curve for the Z_{eu} - $[\text{Chl}]_{\text{surf}}$ relationship is a modeled one for a sun-zenith angle equal to 30° , and is reproduced from Morel and Gentili, 2004 (their Fig. 1 and Table 1); the curve for the Z_{eu} - $[\text{Chl}]_{\text{tot}}$ relationship is reproduced from MM01 (their Fig. 6). The green symbols are for the eutrophic waters of the Benguela Current (Morel et al., 2006) shown for completion.

2.4 Global visible (PAR) radiation and euphotic depth

Empirical relationships between Z_{eu} and the average chlorophyll concentration within the upper layer $[\text{Chl}]_{\text{surf}}$, or between Z_{eu} and the column integrated concentration, $[\text{Chl}]_{\text{tot}}$ (as mg m^{-2}) have previously been derived for Case 1 waters (JGR88, MM-01). In addition, hyperspectral computations of the radiative transfer were performed (Morel and Gentili, 2004), using the appropriate relationships between the inherent optical properties and $[\text{Chl}]$, and also by accounting for the vertical phytoplankton profiles (as statistically established as a function of $[\text{Chl}]_{\text{surf}}$; see Morel and Berthon, 1989 and also Uitz et al., 2006). This sun angle dependent modeling has explained and validated the mean empirical relationships derived from simultaneous determinations of Z_{eu} and $[\text{Chl}]$ profiles made in the field. Therefore, specific and regional situations can be compared to the “average” relationships.

The experimental Z_{eu} depths are displayed in Fig. 4 as a function of measured $[\text{Chl}]_{\text{surf}}$, or as a function of $[\text{Chl}]_{\text{tot}}$ ($[\text{Chl}]_{\text{tot}}$ is computed by trapezoidal integration over the $[\text{Chl}]$ vertical profiles). The previously published curves (empirical and modeled) depicting the average behavior are also shown. As a first comment, the Pacific waters follow the general pattern; however, in the domain of very low $[\text{Chl}]$ (integrated contents), a distinct departure appears, with observed Z_{eu} values exceeding those corresponding to the average situation. Note that the largest Z_{eu} values, apparently

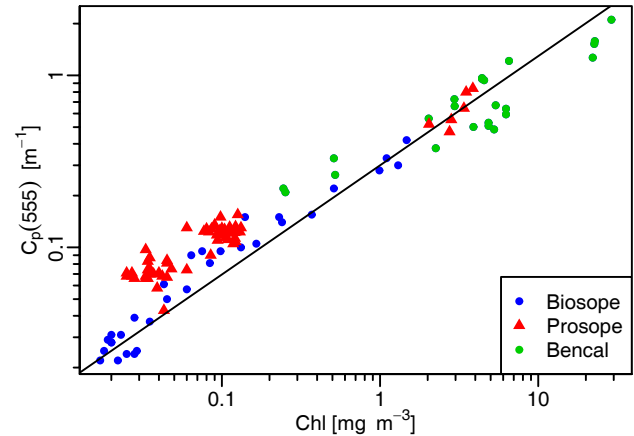


Fig. 5. The particle attenuation coefficient, c_p (as m^{-1}) at the wavelength 555nm, obtained using an ac-9 instrument, and plotted as a function of $[\text{Chl}]$ for the upper layer waters in the Pacific Ocean (blue dots) and in the Mediterranean Sea (red dots). The line represents the relationship $c_p(555) = 0.275 [\text{Chl}]^{0.635}$, derived from $c_p(660)$ in Loisel and Morel (1998; their subsets 2 and 3), and by using a $\lambda^{-0.5}$ dependency for the transfer from 660 to 555 nm.

ever observed (~ 170 m), are located in the central South Pacific gyre (see Fig. 1b in Morel et al., 2007a). Conversely, most of the Mediterranean Z_{eu} values are notably lower than those expected when the average relationship are operated with their $[\text{Chl}]_{\text{surf}}$ values; correlatively, the $[\text{Chl}]_{\text{tot}}$ column contents are considerably reduced compared to the average. The contrast between the two water bodies is such that within similar euphotic layers (e.g. ~ 80 m), the integrated column contents may differ by a factor of about 2, and are notably lower in the Mediterranean waters compared to Pacific. Most likely, such a difference has a potential impact upon the primary production (actual or predicted), to the extent that the first determinant of the primary production is the biomass itself (this topic is out of the scope of the present study).

The above observations about the euphotic layer, show that the global bio-optical state of the entire water columns are markedly different in the two zones. In Mediterranean waters, additional substances efficiently compete with algae in the absorption process inside the PAR spectral domain, whereas in Pacific waters, phytoplankton with their normal retinue seem to be dominant in this process. This interpretation is compatible with the spectral analysis previously made in the visible and UV parts of the spectrum, which have evidenced systematically lower K_d values in Pacific waters than in Mediterranean waters.

2.5 The effect of scattering upon attenuation

Note that in the preceding remarks, the absorption term has been put forward to explain the variations in the diffuse attenuation coefficients. This is justified by the dominance of

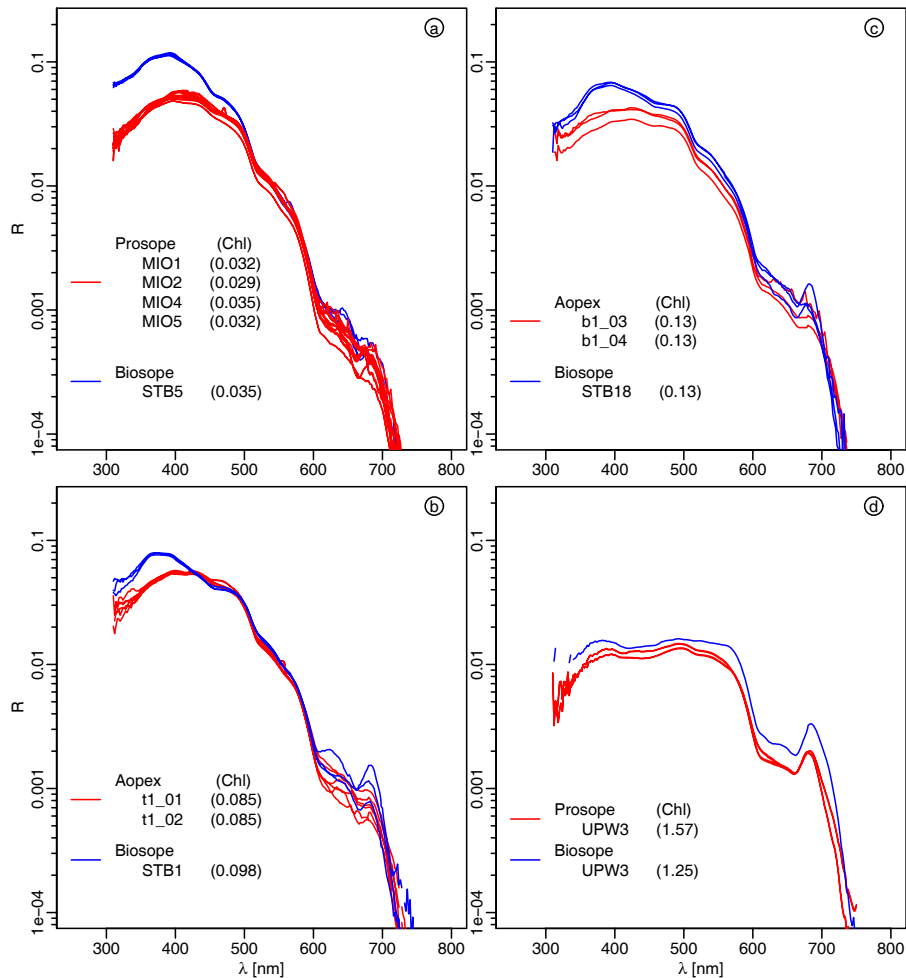


Fig. 6. Reflectance spectra (Eq. 2, as %) for similar [Chl] values as determined in the Pacific Ocean and in the Mediterranean Sea. The panel (d) shows reflectance spectra for the Chilean and Moroccan upwelling zones.

absorption in the diffuse attenuation process. Indeed, K_d can be approximately expressed as (Gordon, 1989)

$$K_d = 1.04(\mu_d)^{-1}(a + b_b), \quad (6)$$

where μ_d is the average cosine for downward irradiance (of the order of 0.6–0.9, depending on solar elevation, wavelength, and [Chl] value), and where a and b_b are the absorption and backscattering coefficients, respectively. The latter is always small when compared to the former; typically it amounts to a few per-cent of the absorption coefficient; it may reach exceptionally 25%, in extremely clear waters and in the blue-violet part of the spectrum (i.e. when the backscattering by water molecule becomes the dominant process). Nevertheless, the influence of the b_b term has to be taken into consideration. If b_b is enhanced in Mediterranean waters (e.g. Claustre et al., 2002), because of the presence of more abundant scattering particles, or because of an increased backscattering efficiency, it may partly contribute to the enhanced K_d values in this zone.

The first argument is supported by Fig. 5, where the particle attenuation coefficients, c_p , are displayed as a function of [Chl] for the Pacific waters and for the Mediterranean waters; also included are some eutrophic waters observed in the South Atlantic (all the c_p values were determined by using AC-9 instruments). At 555 nm, where algal absorption is at its minimum, the attenuation coefficient is a close proxy of the scattering coefficient. Conspicuously, the scattering coefficients in the Mediterranean waters are higher than those in Pacific waters (by almost a factor of 2 for the same [Chl]), whereas the latter follow more closely the empirical mean relationship established by Loisel and Morel (2001). Such rather large deviations in Mediterranean, however, stay within the (wide) range of variability previously observed for other oceanic waters (see Fig. 3 *ibidem*). The presence of submicron Saharan dust in suspension within the upper layer would be a plausible explanation to the enhanced scattering in Mediterranean waters, at least at some seasons (Claustre et al., 2002). More abundant debris than usual or

perhaps coccolithophorids cannot be excluded as other plausible (but not identified) causes.

2.6 The spectral irradiance reflectance

In the hyper oligotrophic situations ($[\text{Chl}] \sim 0.02 \text{ mg m}^{-3}$) found in the South Pacific anticyclonic gyre, the upper layer reflectance spectra exhibit uncommon shapes and exceptionally high values. These spectra have been discussed in Morel et al. (2007a), and presented as being those of the bluest natural waters ever observed in the whole ocean. In brief, the $R(\lambda)$ values for these waters undergo a maximum slightly exceeding 13% in the near UV domain (around 394 nm), and $R(\lambda)$ is still as high as 6% at 310 nm.

This distinct maximum around 394 nm persists when $[\text{Chl}]$ increase (up to 0.13 mg m^{-3}), as shown in Fig. 6a to c; in these figures the reflectance spectra for Pacific and Mediterranean waters with similar $[\text{Chl}]$ are comparatively displayed. The most striking differences between pairs of spectra are observed for the UV domain, and extend toward the violet and blue domain, at least for the lowest $[\text{Chl}]$ values; they tend to diminish for higher $[\text{Chl}]$ values. For the longer wavelengths (say beyond 450–490 nm), the differences in $R(\lambda)$ between the two water bodies are minute, albeit systematic (see discussion below). For the sake of completeness, the last panel of Fig. 6 provides examples of similar eutrophic situations in the Moroccan and Chilean upwelling zones.

At least for Case 1 waters, the ratio of two reflectances at two specific wavelengths (or “band ratio”) is the basis of most of the algorithms (either empirical or semi-analytical) that have been developed for the interpretation of the Ocean Color imagery as captured from space. The semi-analytical algorithm OC4Me (Morel et al., 2007b) by which several and successive band ratios are related to $[\text{Chl}]$ (see legend) is represented by the curve in Fig. 7. The corresponding band ratios derived from the reflectance spectra determined in the Pacific and Mediterranean environments are superimposed on this curve. According to the way it has been built, this semi-analytical algorithm represents an average situation for Case 1 waters. To the extent that these waters experience a natural variability around the statistically averaged values, a scatter of the data is expected; this is clearly demonstrated by Fig. 7. Note that this natural scatter around the average is the main cause of the limitation in the $[\text{Chl}]$ retrieval from space, whatever the algorithm (semi-analytical as here or empirical) that is employed.

The scatter is not completely disorganized, however. Indeed, in the domain of low $[\text{Chl}]$, when the band ratio involved is $R(443)/R(560)$, the Mediterranean waters are often below the modeled curve (actually, most of the data from PROSOPE and AOPEX cruises, but not those from the MINOS cruise, which perhaps indicates a seasonality in this trend). This deviation leads to $[\text{Chl}]$ returns of the algorithm larger than the in situ values. This bias in the Mediterranean waters has already been pointed out and discussed in Claus-

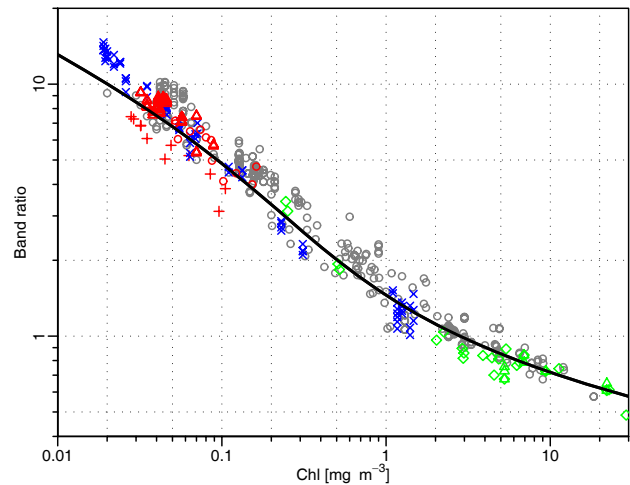


Fig. 7. The curve represents the semi-analytical algorithm (OC4Me) developed for the MERIS sensor to derive $[\text{Chl}]$. It is of the maximum band ratio type; namely, it makes use of the largest ratio of spectral reflectances amongst the three following ones $R(443)/R(560)$, $R(490)/R(560)$, and $R(510)/R(560)$. The switch between the first and second ratio occurs around $[\text{Chl}] \sim 0.54 \text{ mg m}^{-3}$, and between the second and third one around 2.2 mg m^{-3} . The field data are plotted in the same way, so that for most of the Pacific and Mediterranean data (blue and red symbols, respectively), the maximum ratio implied (and plotted) is $R(443)/R(560)$. For the waters of the Moroccan and Chilean upwelling zones, as well as for the Benguela Current data (green symbols) the two other ratios are implied. The grey symbols stand for earlier data already shown in MM01.

tre et al. (2002); actually, specific algorithms for the retrieval of $[\text{Chl}]$ have been proposed and used in the case of this sea (D’Ortenzio et al., 2002; Bricaud et al., 2002).

In contrast, for the Pacific waters, and particularly for very low $[\text{Chl}]$ values ($< 0.03 \text{ mg m}^{-3}$), the measured $R(443)/R(560)$ ratios are slightly higher than the modeled ones, and thus entail a slight underestimate of the actual concentration when applying the nominal algorithm. These departures from the average curve (i.e. from algorithm) are fully coherent with the deviations already noted regarding the spectral attenuation coefficients, a proxy of the absorption coefficients (recall that R is roughly inversely proportional to absorption). In case-1 waters, absorption and backscattering do not tightly co-vary with $[\text{Chl}]$, so that reflectance, or reflectance ratios as above, necessarily show deviations around the values derived from the nominal algorithms. Lee and Hu (2006) defined criteria based on “acceptable” deviations with respect to these algorithms; beyond these thresholds, the waters could not longer be considered as Case 1. These (admittedly arbitrary) criteria appear to be too restrictive compared to the possible deviations as, for instance, those presently observed. Without entering a debate easily of semantic nature, a larger range of waters could be categorized as Case 1

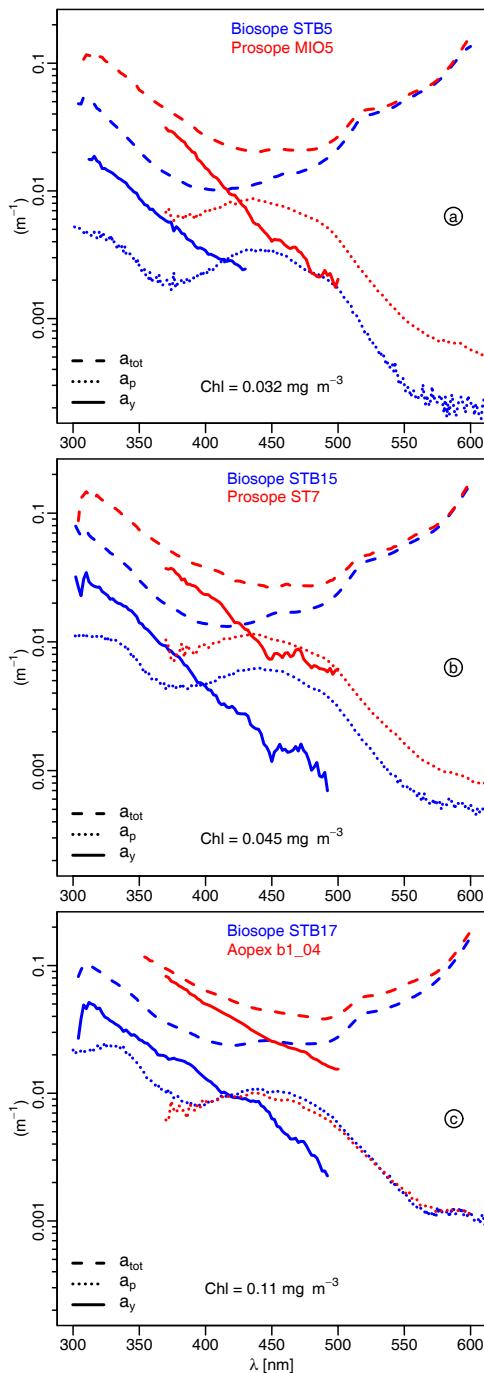


Fig. 8. Spectra of the total absorption coefficient (a_{tot}), derived from the diffuse attenuation coefficient, of the particulate absorption (a_p) determined via the glass fiber filter technique, and of the dissolved colored matter (a_y , see text). (a) For a couple of stations in Pacific and Mediterranean waters (blue and red curves, respectively) with the same chlorophyll concentration, as indicated. (b) and (c) As in (a), but for other [chl] values. Note that during the Mediterranean cruises and because of technical limitations, the a_p determinations were restricted in the UV domain to 370 nm. Consequently, the a_y estimates experience the same spectral limitations. This limitation was removed for the BIOSOPE cruise.

waters, more in conformity with their biogeochemical status and definition, if less stringent criteria were adopted.

3 Discussion

Very likely because the nutricline is extremely deep ($1 \mu\text{MNO}_3^-$ at $\sim 200\text{ m}$; Fig. 5a, Claustre et al., 2007¹), so that the [Chl] values stay minimal over extended water columns (0 to 100 m or more), the oligotrophic waters in the South Pacific gyre are among the clearest natural waters. They are systematically more transparent to solar radiation than “average” Case 1 waters with similar [Chl], and, a fortiori, when compared to Mediterranean waters, that conversely are less transparent than average.

Actually, between individual $K_d(\lambda)$ values in Pacific waters and those resulting from the global $K_d(\lambda) \leftrightarrow [\text{Chl}]$ relationships, the difference is not so large within the visible part of the spectrum. For a merged dataset (all those discussed here plus earlier data), the RMSE for the log-transform $K_d(\lambda)$ and [Chl] data (see Table 4 and Fig. 4, in Morel et al., 2007b) is 0.08 at 510 nm (corresponding to randomly distributed deviations in K_d of about $\pm 20\%$ with respect to the mean). The RMSE progressively increases for decreasing wavelengths; for instance, it reaches 0.12 ($\pm 32\%$ deviations) at 412 nm. Therefore, from this point of view, the Pacific data are not exceptional, as they remain within the expected “normal” dispersion for K_d in Case 1 water (at least $\pm 35\%$). Nevertheless, the important observation is that the observed divergences are “polarized”, i.e., systematically oriented toward the minimal K_d values inside the range of possible dispersion. This orientation, which is not random, undoubtedly reveals differing composition and optical properties of the biogenous material in the oligotrophic Pacific compared with those in average Case 1 waters.

For the Mediterranean Sea, systematic divergences also occur, yet in the opposite direction (K_d systematically above the average). These deviations are observed in the visible domain; into the UV domain, the results of regression analyses show that the divergences between the two water bodies continue to increase. Another striking difference between these waters lies in the degree of dependency of their UV absorbing materials upon the local and contemporaneous chlorophyll concentration. This dependency appears to be much higher in Pacific waters than in Mediterranean waters, as reflected by their respective exponent $e(\lambda)$ values (cf. Fig. 3b).

Consistently, the reflectance spectra of the two bodies also diverge in the violet-blue and UV part of the spectrum in directions which are predictable from their K_d differences. To various degrees, both the violet-blue and UV reflectances are simultaneously affected by the change in bio-optical properties; therefore, some information is present in the visible reflectance about the properties in the UV domain. Actually, ocean color remote sensing in UV has never been routinely attempted; the rationale for providing the presently in flight

sensors with a channel at 412 nm was nevertheless the possibility of discriminating [Chl] from CDOM, and possibly to extrapolate toward the UV domain. Up to now, the atmospheric correction problem at this wavelength has been a serious obstacle to proceed safely in this direction.

Imbedded within the average “laws” for Case 1 waters (for instance, the $K_d(\lambda) \leftrightarrow [\text{Chl}]$ statistical relationships), certain implicit (and non-linear) relationships between the algal and the non-algal compartments are underlying. The algal compartment is presently quantified through [Chl], i.e., the commonly available (albeit imperfect) index. The non-algal compartment includes both dissolved colored material (CDOM) and particulate materials (various debris plus heterotrophic organisms). The optical variability inside Case 1 waters with respect to the average laws (Gordon and Morel, 1983b, 65–67), originates primarily from the fluctuations in the relative proportions of the algal and non-algal compartments. To a second order, the fluctuations inside each compartment (e.g., differing absorbing characteristics from one phytoplankton assemblage to another one, or differing yellow substance or detritus composition) may also induce an additional variability.

Beside the water absorption, the algal pigment absorption with its typical bands is the dominant factor governing the diffuse attenuation in the visible domain. The optical variability around the average laws is lower here than in the UV domain (cf. the r^2 in Fig. 3c). In this UV domain, the optical role of the algal compartment is comparatively diminishing. The various particles (algal, bacterial, heterotrophic communities, and organic debris) are still contributing to absorption in the UV domain (e.g. Stramski and Kiefer, 1998); their UV spectra are characterized by a broad minimum around 360 nm and below this wavelength, a peak of variable amplitude around 320 nm (likely due to mycosporine-like amino acids (see Arrigo et al., 1998; Laurion et al., 2003)). The main source of attenuation, however, is the colored dissolved organic material (CDOM, or “yellow substance”), which is characterized by a regular and steep slope toward the shortest wavelengths. Varying CDOM concentrations, not tightly correlated to the local and contemporaneous algal abundance, are most probably the major cause of the optical variability in the UV.

The dominance of CDOM is illustrated clearly through some comparative examples (Fig. 8). They are based on Figs. 11 and 12 in Morel et al. (2007a), to which are added results from the Mediterranean Sea with identical [Chl]. The additional panel (8c) provides another couple of data for larger values of [Chl]. Beside the total absorption $a_{\text{tot}}(\lambda)$ (obtained by inversion of $K_d(\lambda)$; see *ibid.*), are plotted the experimentally determined particulate absorption spectra, $a_p(\lambda)$, and also the dissolved absorption spectra, $a_y(\lambda)$, obtained by subtracting both $a_p(\lambda)$ and the pure water absorption, $a_w(\lambda)$, from $a_{\text{tot}}(\lambda)$.

In all situations, the yellow substance absorption is preponderant in the UV domain (and even the violet-blue do-

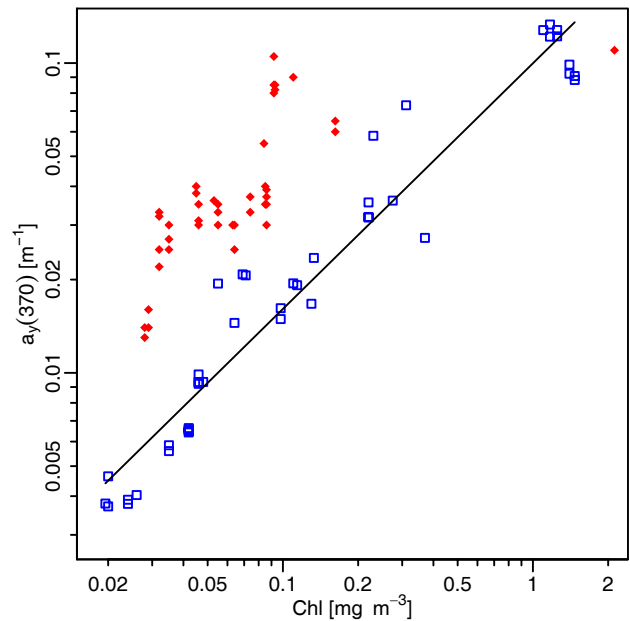


Fig. 9. As a function of [Chl], the CDOM absorption coefficient at 370 nm, for all stations in Pacific (blue symbols, BIOSOPE cruise) and Mediterranean waters (red symbols, PROSOPE and AOPEX cruises). The straight line corresponds to the best fit for the Pacific data only, as already shown in Morel et al. (2007a), which expresses as $a_y(370) = 0.10 [\text{Chl}]^{0.80}$ (with $r^2 = 0.94$ on the log-transform data). Note that the dots beyond 1 mg m^{-3} correspond to waters in the Peruvian (blue) and Moroccan (red) upwelling zones.

main) when compared to the particulate matter absorption. Actually, $a_y(\lambda)$ begins to be smaller than $a_p(\lambda)$ when λ exceeds 425 nm, approximately (and is never smaller at the Mediterranean station AOPEX B1-04). Interestingly, the a_y spectra in the two water bodies are approximately parallel, with an exponential slope around 0.016 nm^{-1} (discussed in Morel et al., 2007a). The difference is in the magnitude of $a_y(\lambda)$; for similar [Chl], the $a_y(\lambda)$ values in the Mediterranean waters are always higher (by a factor 2 or even 3) than in Pacific. Such a systematic difference between the two oceanic zones is clearly seen in Fig. 9 (for $\lambda = 370 \text{ nm}$) which is redrawn from Fig. 13 (*ibid.*), to which the Mediterranean data have been overlaid. A rather loose correlation still exists between the $a_y(370)$ term and [Chl], at least when each zone is considered separately. This is especially true for Pacific waters, maybe because the [Chl] range (2 orders of magnitude) allows a significant trend to be extracted. When all data are pooled together, the covariation almost vanishes (a similar conclusion was drawn by Siegel et al., 2005).

The similarity between this Fig. 9 and the previous Fig. 5 is an interesting feature; compared to the South Pacific waters, the particulate scattering “excess” in Mediterranean waters parallels the “excess” of dissolved absorbing matter. It is tempting to imagine a relation of cause-and-effect, which, however, remains to be demonstrated on the basis of biogeochemical arguments.

4 Conclusions

When examining the natural variability in Case 1 waters, it is necessary to consider separately the visible and the UV domains.

In the visible domain, abundantly documented, it appears that the present data do not exceed the (rather wide) dispersion range already recorded, in particular for the $K_d \leftrightarrow [\text{Chl}]$ relationship. For the two water bodies here studied, the variability is not at random; instead it lies in the systematic character of the observed deviations, either steadily negative (Pacific waters), or positive (Mediterranean waters). Therefore, the generic Case 1 water model is not the most accurate one to describe accurately such local situations. As pointed out by Mobley et al. (2004) “within Case 1 waters, there is a factor-of-two (and sometimes much greater) variability in the values of optical properties for a given chlorophyll value”. The two water bodies examined in this study are demonstrative examples of such situations and of significant departures from the average. This observation does mean that the concept of Case 1 water, or the Chl-based models, fail, but their true significance and their statistically limited validity must be kept in mind. In fact without the use of this concept and in absence of local information, the interpretation of ocean color remote sensing data would have not been possible for about 95% of the oceanic area.

When facing these two rather contrasted situations and geographical zones, the question arises: are we in presence of the end members of the possible variations inside Case 1 waters? This obviously cannot be ascertained, but the consideration of older data may help. These data (the grey dots in Fig. 1, mostly from the Atlantic Ocean) are sometimes superimposed onto or stand between the present Pacific and Mediterranean data. This observation thus suggests a positive answer to the above question, but the consideration of polar waters may lead to another answer (e.g., Reynolds et al., 2001; Stramska et al., 2003).

For the bio-optical state in the UV domain, there is not much information, nor a Case 1 water model. The large differences and variations detected here tend to compromise the reliability of a general model. Actually the notion of Case 1 water, and its usefulness, rest on the dominance of the algal material in shaping the bio-optical properties in the visible part of the spectrum. This dominance no longer exists in the UV; instead, it is replaced by that of the dissolved colored matter, whose origin, life-history, dynamics, and thus resulting concentration, are largely disconnected from the contemporaneous algal presence. According to this argument, comparable environments with respect to [Chl] may largely differ regarding their UV properties. This observation was previously made in the field (Sargasso Sea) regarding the transitional domain of the violet-blue radiation, already affected by this colored matter (Nelson, 1998), and even at global scale via the interpretation of satellite observations (Siegel et al., 2002a and b). In summary, the causes of the natural variability

in Case 1 waters can be identified; as far as the visible domain is concerned, the variability is maintained within limited and already identified bounds. The same causes, however, have an amplified effect in the UV domain and induce more variability, so that the prediction of the optical properties in this spectral domain, if based on the [Chl] index, becomes highly problematic.

Acknowledgements. The HPLC pigment determinations were performed for the PROSOPE cruise by J. Ras, J.-C. Marty, and one of the author (H.C.), and by J. Ras for the BENCAL, AOPEX and BIOSOPE cruises. J. Ras has maintained at a high level the quality control of these pigment determinations throughout this multi-year multi-cruise operation and she is particularly thanked. We acknowledge the help provided at sea by M. Babin, M. Chami, and N. Souaïdia during the radiometric measurements, and E. Leymarie for developing a fast acquisition/processing software dedicated to the spectroradiometers. We are also indebted to Y. Huot for useful comments on a first draft of the present paper.

The crew and officers of the Research Vessels Thalassa, Africana, Le Suroit, and Atalante were instrumental in the success of the successive cruises. The financial supports for these campaigns of the Centre National de la Recherche Scientifique and Institut des Sciences de l'Univers (CNRS and INSU), the Marine Coastal Management (MCM, Cape Town, South Africa), the Centre National d'Etudes Spatiales (CNES), the National Aeronautics and Space Administration (NASA), and the European Space Agency (ESA) were essential and much appreciated.

Edited by: E. Boss

References

- Arrigo, K. R., Robinson, D. H., Worthen, D. L., Schieber, B., and Lizotte, M. P.: Bio-optical properties of the southwestern Ross Sea, *J. Geophys. Res.*, 103, 21 683–21 695, 1998.
- Austin, R. W. and Petzold, T. J.: The determination of the diffuse attenuation coefficient of sea water using the coastal zone color scanner, *Oceanography from Space*, Plenum Press, 239–256, 1981.
- Baker, K. S. and Smith, R. C.: Bio-optical classification and model of natural waters, *Limnol. Oceanogr.*, 27, 500–509, 1982.
- Banse, K.: Should we continue to use the 1% light depth for estimating the compensation depth of phytoplankton for another 70 years?, *Limnol. Oceanogr. Bull.*, 13, 49–51, 2004.
- Bricaud, A., Bosc, E., and Antoine, D.: Algal biomass and sea surface temperature in the Mediterranean basin: Intercomparison of data from various satellite sensors, and implications for primary production estimates, *Remote Sens. Environ.*, 81, 163–178, 2002.
- Bricaud, A., Babin, M., Morel, A., and Claustre, H.: Variability in the chlorophyll-specific absorption coefficients of natural phytoplankton: Analysis and parameterization, *J. Geophys. Res.*, 100, 13 321–13 332, 1995.
- Bricaud, A., Morel, A., Babin, M., Allali, K., and Claustre, H.: Variations of light absorption by suspended particles with chlorophyll a concentration in oceanic (Case 1) waters: Analysis

- and implications for bio-optical models, *J. Geophys. Res.*, 103, 31 033–31 044, 1998.
- Buiteveld, H., Hakvoort, J. H. M., and Donze, M.: The optical properties of pure water, *SPIE Ocean Optics XII*, 2258, 174–183, 1994.
- Claustre, H., Morel, A., Hooker, S. B., Babin, M., Antoine, D., Oubelkheir, K., Bricaud, A., Leblanc, K., Quequiner, B., and Maritorena, S.: Is desert dust making oligotrophic waters greener?, *Geophys. Res. Lett.*, 29, 1469, doi:10.1029/2001GL014056, 2002.
- D’Ortenzio, F., Marullo, S., Ragni, M., Ribera d’Alcala, M., and Santoleri, R.: Validation of empirical SeaWiFS algorithms for chlorophyll a retrieval in the Mediterranean Sea: A case study for oligotrophic seas, *Remote Sens. Environ.*, 82, 79–94, 2002.
- Fougnié, B., Henry, P., Morel, A., Antoine, D., and Montagner, F.: Identification and characterization of stable homogeneous oceanic zones: climatology and impact on in-flight calibration of space sensor over Rayleigh scattering, *Ocean Optics XVI*, Santa Fe, NM, 18–22 November, 2002.
- Gordon, H. R.: Can the Lambert-Beer law be applied to the diffuse attenuation coefficient of ocean water?, *Limnol. Oceanogr.*, 34, 1389–1409, 1989.
- Gordon, H. R. and Morel, A.: Remote sensing of ocean color for interpretation of satellite visible imagery; A review, Springer verlag, 114 pp., 1983
- Gordon, H. R., Brown, O. B., Ewans, R. H., Brown, J. W., Smith, R. C., Baker, K. S., and Clark, D. K.: A semi-analytical radiance model of ocean color, *J. Geophys. Res.*, 93, 10 909–10 924, 1988.
- Laurion, I., Blouin, F., and Roy, S.: The quantitative filter technique for measuring phytoplankton absorption; Interference by MAAs in the UV waveband, *Limnol. Oceanogr. Methods*, 1, 1–9, 2003.
- Lee, Z. P. and Hu, C.: Global distribution of case-1 waters: An analysis from seawifs measurements, *Remote Sens. Environ.*, 101, 270–276, 2006.
- Loisel, H. and Morel, A.: Light scattering and chlorophyll concentration in Case 1 waters: A reexamination, *Limnol. Oceanogr.*, 43, 847–858, 1998.
- Mobley, C. D., Stramski, D., Bissett, W. P., and Boss, E.: Optical modeling of ocean waters: Is the case 1-case 2 classification still useful?, *Oceanography*, 12, 61–67, 2004.
- Morel, A.: Optical properties of pure water and pure seawater, in: *Optical Aspects of Oceanography*, edited by: Steeman-Nielsen, N. G. J. E., Academic, 1–24, 1974.
- Morel, A.: Optical modeling of the upper ocean in relation to its biogenous matter content, *J. Geophys. Res.*, 93, 10 749–10 768, 1988.
- Morel, A. and Berthon, J.-F.: Surface pigments, algal biomass profiles, and potential production of the euphotic layer: Relationships reinvestigated in view of remote sensing applications, *Limnol. Oceanogr.*, 34, 1545–1562, 1989.
- Morel, A., Gentili, B., Chami, M., and J. Ras: Bio-optical properties of high chlorophyll Case 1 waters, and of yellow-substance-dominated Case 2 waters, *Deep-Sea Res. I*, 53, 1439–1559, 2006.
- Morel, A. and Maritorena, S.: Bio-optical properties of oceanic waters: A reappraisal, *J. Geophys. Res.*, 106, 7163–7180, 2001.
- Morel, A. and Gentili, B.: Radiation transport within oceanic (Case 1) water, *J. Geophys. Res.*, 109, C06008, doi:10.1029/2003JC002259, 2004.
- Morel, A., Gentili, B., Claustre, H., Babin, M., Bricaud, A., Ras, J., and Tìèche, F.: Optical properties of the “clearest” waters, *Limnol. Oceanogr.*, 52, 217–229, 2007a.
- Morel, A., Huot, Y., Gentili, B., Werdell, P. J., Hooker, S. B., and Franz, B. A.: Examining the consistency of products derived from various ocean color sensors in open ocean (Case 1) waters in the perspective of a multi-sensor approach, *Remote Sens. Environ.*, 111, 69–88, doi:10.1016/j.rse.2007.03.012, 2007b.
- Nelson, N. B., Siegel, D. A., and Michaels, A. F.: Seasonal dynamics of colored dissolved material in the Sargasso Sea, *Deep-Sea Res. I*, 45, 931–957, 1998.
- Preisendorfer, R. W.: Application of radiative transfer theory to light measurement in the sea, *IUGG Monography*, 10, 11–30, 1961.
- Ras, J., Uitz, J., and Claustre, H.: Spatial variability of phytoplankton pigment distribution in the South East Pacific, *Biogeosciences Discuss.*, 4, 3409–3451, 2007, <http://www.biogeosciences-discuss.net/4/3409/2007/>.
- Reynolds, R. A., Stramski, D., and Mitchell, B. G.: A chlorophyll-dependent semianalytical reflectance model derived from field measurements of absorption and backscattering coefficients within southern ocean, *J. Geophys. Res.*, 106, 7125–7138, 2001.
- Ryther, J. H.: Photosynthesis in the ocean as a function of light intensity, *Limnol. Oceanogr.*, 1, 61–70, 1956.
- Siegel, D. A., Maritorena, S., Nelson, N. B., Hansell, D. A., and Lorenzi-Kayser, M.: Global ocean distribution and dynamics of colored dissolved and detrital organic material, *J. Geophys. Res.*, 107(C12), 3328, doi:10.1029/2001JC000965, 2002.
- Siegel, D. A., Maritorena, S., Nelson, N. B., and Behrenfeld, M. J.: Independence and interdependencies of global ocean color properties: Reassessing the bio-optical assumption, *J. Geophys. Res.*, 110, C07011, doi:10.1029/2004JC002527, 2005a.
- Siegel, D. A., Maritorena, S., Nelson, N. B., Behrenfeld, M. J., and McClain, C. R. Colored dissolved organic matter and its influence on the satellite-based characterization of the ocean biosphere, *Geophys. Res. Lett.*, 32, L20605, doi:10.1029/2005GL024310, 2005b.
- Smith, R. C. and Baker, K. S.: Optical properties of the clearest natural waters (200–800 nm), *Appl. Opt.*, 20, 177–184, 1981.
- Stramska, M., Stramski, D., Hapter, R., Kaczmarek, S., and Ston, J.: Bio-optical relationships and ocean color algorithms for the north polar region of the Atlantic, *J. Geophys. Res.*, 108(C5), 3143, doi:10.1029/2001JC001195, 2003.
- Stramski, D. and Kiefer, D. A.: Can heterotrophic bacteria be important to marine absorption?, *J. Plankton Res.*, 20, 1489–1500, 1998.
- Tyler, J. E.: Report on the the second meeting of the joint group of experts on photosynthetic radiant energy, *UNESCO Technical Papers in Marine Science*, 5, 1–11, 1966.
- Uitz, J., Claustre, H., Morel, A., and Hooker, S. B.: Vertical distribution of phytoplankton communities in open ocean: An assessment based on surface chlorophyll, *J. Geophys. Res.*, 111, C08005, doi:10.1029/2005JC003207, 2006.

Detailed validation of the bidirectional effect in various Case 1 waters for application to ocean color imagery

K. J. Voss¹, A. Morel², and D. Antoine²

¹Department of Physics, University of Miami, Coral Gables, Florida, USA

²Laboratoire d'Océanographie de Villefranche, Université Pierre et Marie Curie et Centre National de la Recherche Scientifique, Villefranche-sur-mer, France

Received: 7 June 2007 – Published in Biogeosciences Discuss.: 27 June 2007

Revised: 17 September 2007 – Accepted: 17 September 2007 – Published: 26 September 2007

Abstract. The radiance viewed from the ocean depends on the illumination and viewing geometry along with the water properties, and this variation is called the bidirectional effect. This bidirectional effect depends on the inherent optical properties of the water, including the volume scattering function, and is important when comparing data from different satellite sensors. The current model of f/Q , which contains the bidirectional effect, by Morel et al. (2002) depends on modeled, not measured, water parameters, thus must be carefully validated. In this paper we combined upwelling radiance distribution data from several cruises, in varied water types and with a wide range of solar zenith angles. We compared modeled and measured $L_{\text{view}}/L_{\text{nadir}}$ and found that the average difference between the model and data was less than 0.01, while the RMS difference between the model and data was on the order of 0.02–0.03. This is well within the statistical noise of the data, which was on the order of 0.04–0.05, due to environmental noise sources such as wave focusing.

1 Introduction

The upwelling radiance distributions, either beneath the interface or emerging from the water, are not isotropic, but vary with illumination and viewing conditions and also with water optical properties. Knowing how to predict this angular variation is important in satellite oceanography, as the analysis of satellite derived upwelling radiances must take into account these variations. This is particularly important when comparing different ocean color sensors as these sensors will view the same spot at different times (hence varied illumination geometry) and under different view angles. One must have a model of this variation of the radiance distribution that is dependent on a small set of parameters, but which can accu-

rately predict the variation. As the available model for Case I waters (Morel et al., 2002) is based on radiation transport computations, it is essentially theoretical in nature. Moreover, it includes assumptions and parameterizations of the inherent optical properties, as a function of the chlorophyll concentration, which presently are not fully verified (this is particularly true for the volume scattering function). Therefore a comparison between field data and model predictions over a wide range of experimental conditions is necessary. This is the objective of the present paper which makes use of recent and numerous observations in the Pacific Ocean and in the Mediterranean Sea.

The shape of the upwelling radiance distribution, $L_u(\theta_o, \theta_v, \phi)$, can be described by the bidirectional function, denoted $Q(\theta_o, \theta_v, \phi_v)$, which is defined as:

$$Q(\theta_o, \theta_v, \phi_v) = E_u/L_u(\theta_o, \theta_v, \phi_v) \quad (1)$$

where θ_o is the solar zenith angle, θ_v is the view nadir angle, ϕ is the azimuth between these two directions, and E_u is the planar upward irradiance, i.e., the integral of the upward radiance field over the half space (2π sr). The Morel et al. (2002) model, which is commonly used in satellite oceanography, characterizes the variations in Q as a function of the three angles and of the chlorophyll concentration, [Chl]. [Chl] is a convenient index for Case I waters as it characterizes the bio-optical state of the water bodies. This model incorporates both a correction for this varying Q factor, and also a correction for the f factor. The f factor relates the irradiance reflectance to the absorption coefficient and the backscattering coefficient, a and b_b , respectively, through

$$R(\lambda) = f(\lambda)[b_b(\lambda)/a(\lambda)]. \quad (2)$$

where $f(\lambda)$ for a given water is also dependent on the solar zenith angle.

This paper will describe our results in validating the Q factor. The problem of validating f could be addressed with irradiance reflectance measurements combined with b_b and

Correspondence to: K. J. Voss
(voss@physics.miami.edu)

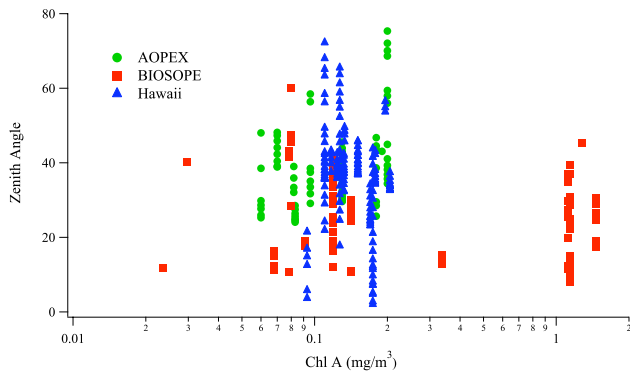


Fig. 1. Data distribution in terms of [Chl] and solar zenith angle.

a measurements, but we do not have a large database of contemporaneous b_b and a coefficients for such a validation.

In the past we have had two investigations looking at the accuracy of the series of Q values as predicted by models (Morel et al., 1995; Voss and Morel, 2005). Each of these was done with a different version of our radiance distribution camera systems (RADS: Voss, 1989; RADS-II, Voss and Chapin, 1992). These early instruments were large and slow and provided a limited data set. Recently we have developed a new generation of radiance distribution camera systems specifically aimed at looking at the upwelling radiance distribution (NuRADS: Voss and Chapin, 2005). With this new instrument we have an extensive set of upwelling radiance distribution data in both Case I and Case II waters. This paper will concentrate on the Case I waters, as this is where the 2002- model was designed to work. The Case II situation is much more complicated, less predictable (e.g. Loisel and Morel, 2001), and will be separately addressed in later work.

The first investigation (1995) was carried out off of California with a stable [Chl] value (0.3 mg m^{-3}), and widely varying sun zenith angle (32° to 80°). In contrast, the second investigation (2005), with measurements around the Baja Peninsula, encompassed a large range of chlorophyll concentrations ([Chl] from 0.14 to 11 mg m^{-3}), whereas the sun angle remained in a rather restricted range (28° to 40°). Although these validations were successful, it is still highly desirable to test the quality of the predictions over a larger variety of situations, regarding both the trophic state of the waters and the illumination conditions. In the present study, we will specifically concentrate on two cruises, in the South Pacific and Mediterranean Sea, and several short cruises near Hawaii, which together offer such a variety of situations.

During the BIOSOPE cruise in the South Pacific, extremely clear oligotrophic waters ([Chl] $< 0.03 \text{ mg m}^{-3}$), as well as moderately eutrophic waters inside the Chilean upwelling zone ([Chl] $> 1.4 \text{ mg m}^{-3}$) were encountered. The AOPEX cruise took place in the Mediterranean, and while the water types were not as varied ([Chl] ~ 0.07 to 0.15 mg m^{-3}), we had the opportunity to sample the radiance

distribution for a variety of solar zenith angles. In addition to these two cruises, we have an extensive set of radiance distribution measurements in clear waters around Hawaii ([Chl] approximately 0.1 mg m^{-3}). All of the radiance distribution measurements were done with the camera just below the surface (at approximately 0.75 m).

2 Data set description

The distribution of the data set is best described by Fig. 1 that illustrates the range of [Chl] and solar zenith angle for the radiance distribution data presented in this paper. The Hawaii data set has points in the [Chl] range below 0.2 mg m^{-3} , but has a large range of solar zenith angles, from almost 0° to over 70° . The AOPEX data is over a similar [Chl] range ($< 0.2 \text{ mg m}^{-3}$) but a slightly more limited solar zenith angle range ($20^\circ < \theta_o < 75^\circ$). The BIOSOPE data from the South Pacific has the wider [Chl] range, from < 0.05 to $> 1.4 \text{ mg m}^{-3}$, and θ_o from 10° to 60° . The entire data set, however, does have a large hole in the 0.4 to 1.0 mg m^{-3} range.

For the AOPEX and BIOSOPE cruises, the chlorophyll concentration was determined via High-Performance Liquid Chromatography (HPLC), according to a slightly modified version (see Ras et al., 2007) of the method initiated by Van Heukelen and Thomas (2001). The simplified notation [Chl] actually represents the sum of the concentrations of the following suite of pigments: chlorophyll a, divinyl chlorophyll a, chlorophyllid a, and chlorophyll a allomers and epimers.

The upward radiance data set was obtained using the NuRADS camera system, that has been described in detail previously (Voss and Chapin, 2005). The important details are that it has an automatic filter changer, with positions for 6 spectral filters, a cooled CCD camera, and a fisheye lens to capture the complete upwelling hemisphere of data. In this paper we will use only 4 of these filters: 412, 436, 486, 526 nm. The other 2 filters are at longer wavelengths, and there is appreciable instrument self-shadowing even in clear water. In the configuration used in most of these cruises, floatation is attached to the back of the camera, and the instrument can be floated away from the ship at a distance exceeding 50 m , to avoid ship shadow, and tethered to the ship using a neutrally buoyant cable which combines power and communication. A portion of the data set was obtained with this system, while another portion was obtained while the instrument was in the configuration shown in Fig. 2. The system can automatically cycle through the spectral filters and collect data that are stored on the internal hard drive. It takes approximately 2 min to obtain a complete set of spectral data, and the instrument typically is set to continually cycle and collect multiple sets of radiance distribution data at each wavelength.

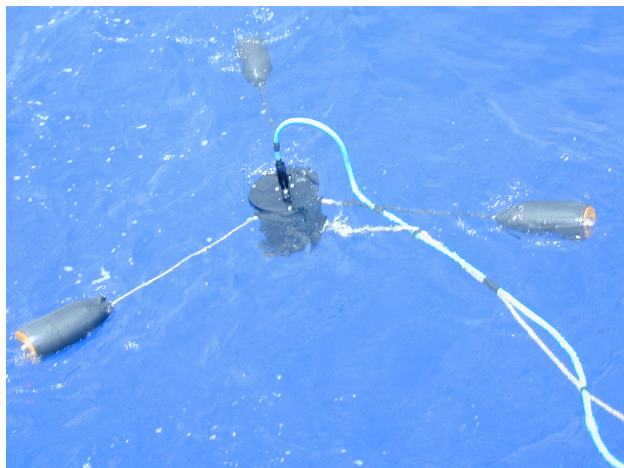


Fig. 2. Illustrating NuRads in its deployment configuration. The instrument can be floated away from the ship, suspended on the floats just below the surface.

3 Data reduction

Pre- and post-calibrations were done on the instruments for each cruise. The overall process to calibrate these systems is described in Voss and Zibordi (1989). An additional calibration step has been found to be required which accounts for the immersion of the dome window used in the system and its affect on the throughput of the optical system (immersion factor). This calibration step is briefly described in Voss and Chapin (2005). Images from the system have the calibration applied and result in a fisheye projection image of the upwelling radiance distribution. An example image is shown in Fig. 3.

The NuRADS instrument obtains a complete spectral set of data every 2 min. However, since the whole upwelling radiance distribution is obtained very quickly (less than 1 s), individual images often have strong features, such as wave focusing (seen in Fig. 3), which need to be averaged out. During the data reduction process we look at each image and determine, manually, where the anti-solar point is located. This point is obvious as it is the point where the wave focused light rays converge. Once this point has been determined, a computer program determines where the nadir point should be. This process uses the known angular distance between the anti-solar point and nadir, and looks for symmetry around the principal plane (plane containing the nadir and anti-solar point). When the geometry (nadir and anti-solar point in each image) has been determined, we average images taken within 10 min. Since the image should be symmetric around the principal plane, we average each half of the image together. For the data presented in this paper, we exclude data for which only one image (both halves) are averaged, so each data point effectively represents the average of between 4 and 10 separate image halves. Images are

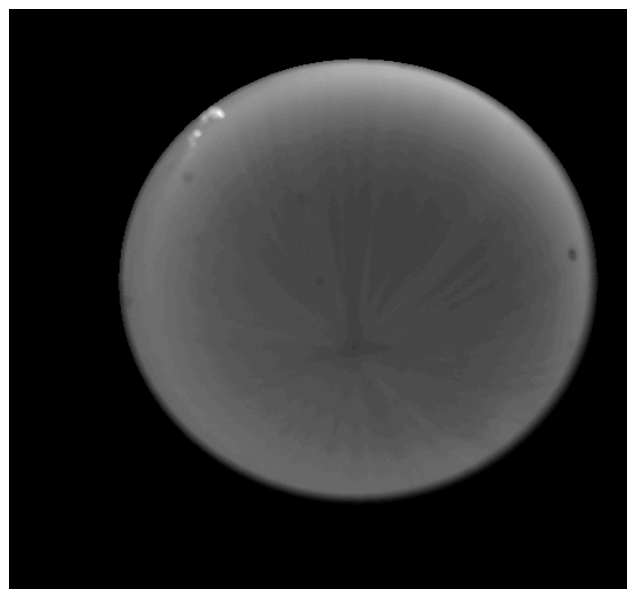


Fig. 3. Example upwelling radiance distribution image. This example is from the AOPEX cruise, on 11/8/2004. Solar zenith angle is 35° , $[\text{Chl}] = 0.1 \text{ mg m}^{-3}$, wavelength is 526 nm. The geometry of this image is such that the nadir point is the center of the circle, the projection places nadir angle as directly related to the radius from the center. The edge of the circle is a nadir angle of 90° . The anti-solar point is visible in the lower portion of the circle, defined as where the sun rays (the star pattern) converge. The azimuthal direction towards the sun is at the top of the image. The dark circles in the image are artifacts of the optical system and are masked out during the averaging process, while the bright part at the top left is probably a small portion of cable.

excluded if there is contamination in anyway (cables floating into view for example) or the anti-solar point can not be determined (most often because of clouds). In addition, to further reduce noise, each data point from each image is an average of a 3×3 pixel area (each pixel represents an angular change of approximately 0.4 degrees). An example after this data processing, for the image set containing the image shown in Fig. 3, is shown in Fig. 4.

It is important to understand that there is still environmental noise left in these images. A portion of this noise may be from our instrument system, however this is dominated by effects due to wave focusing, small scale inhomogeneities in the water column, and other natural sources. To illustrate how large these variations can be we collect the σ of each data point averaged, i.e.

$$\sigma = \sqrt{\sum (x - \bar{x})^2 / N} / \bar{x}, \quad (3)$$

where x is a specific pixel value in radiance units (not normalized), and \bar{x} is the average radiance for that view geometry. N is the number of pixels averaged, which is 9 pixels/image half times the number of image halves, thus between 36 and 90 pixels. Figure 5 shows σ of the average

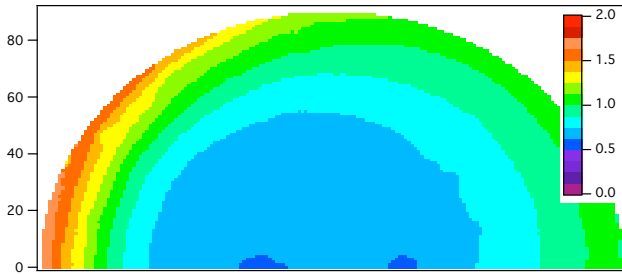


Fig. 4. AOPEX data set, solar zenith angle approximately 35° , data shown in $\mu\text{W cm}^{-2} \text{sr}^{-1} \text{nm}^{-1}$. This is an average of 4 images, so each point represents 8 realizations of the radiance distribution. Here L_{nadir} is $0.64 \mu\text{W cm}^{-2} \text{sr}^{-1} \text{nm}^{-1}$, Q_n is 3.72 sr and μ_u , the upwelling average cosine, is 0.44. One can see that the wave focusing has been averaged out through this process. In this projection the anti-solar point is towards the right of the image along the x-axis. The direction towards the sun is on the left side of the image. Nadir is represented along the x-axis in the center of the semicircle. The nadir angle is proportional to the radial distance from the center; data exists out to 90 degrees, or the horizon.

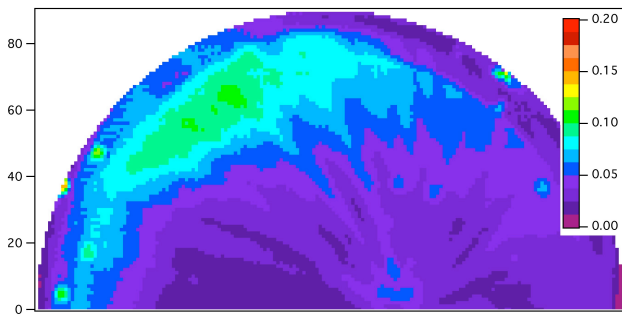


Fig. 5. σ for each data point, in the same projection as Fig. 4. As can be seen σ can range >0.1 in some areas.

shown in Fig. 4. As can be seen σ shows the effect of wave focusing directly through the apparent sun-rays in this image. However the area with the largest σ is towards the horizon. Figure 6 shows a histogram of σ for one of these averages. As can be seen the peak in the histogram is on the order of 0.03, which limits how well the data could agree with even the best model for individual points.

Any instrument, placed in the water, will have systematic measurement errors due to instrument self-shadowing. For this paper we estimated the effect of self-shadowing following a variation of the algorithm of Gordon and Ding (1992). This algorithm assumes that the shadowing is only proportional to the absorption coefficient of the water and the viewing pathlength that is directly shadowed by the instrument. The original Gordon and Ding (1992) algorithm had a simple disk casting the shadow, we extended this to a three dimensional object, with the dimensions of NuRADS, and calculated the shadowlength taking into account the refracted so-

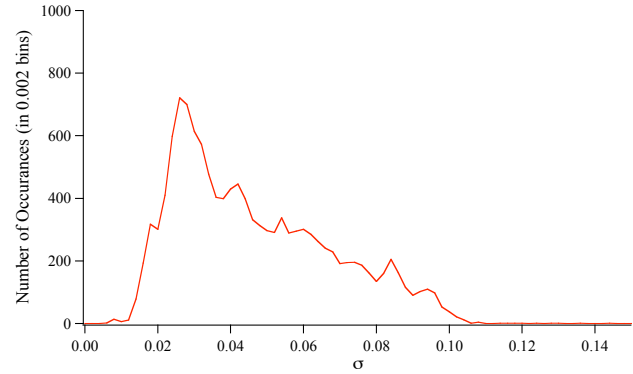


Fig. 6. Histogram of σ of the individual μ data points used in above comparison with the model.

lar zenith angle, view angle, and absorption coefficient. The absorption coefficient was derived from the measured [Chl] using the model of Morel and Maritorena (2001). Because this model is a simple approximation, we only used data for which the shadowing correction was less than 5%. It is possible to derive a more complete correction for shadowing (e.g. Helliwell et al. (1990) and Leathers et al. (2001)), however for radiance distribution measurements, such as these, complete knowledge of the seawater volume scattering function (VSF) is required. While we could use the VSF used in the model, this would influence the independence of our comparison with the data.

Our comparison will be between $L_{\text{view}}/L_{\text{nadir}}$ for the data and those predicted by the Morel et al. (2002) model and associated tables. According to Eq. (1), the ratio of a slant upward radiance to the nadir radiance is the inverse ratio of the corresponding Q -quantities, so

$$L_u(\theta_o, \theta_v, \phi_v)/L_u(\theta_o, \theta_v=0, \phi_v=0) = Q_n/Q(\theta_o, \theta_v, \phi_v) \quad (4)$$

here the quantity Q_n represents the particular value for the nadir direction, i.e., $Q(\theta_o, \theta_v=0, \phi_v=0)$, which still depends on the sun position.

We use the quasi-contemporaneous [Chl] determinations, together with the specific illumination geometry, as determined by the instant of measurement, to enter into the Q -tables.

4 Results

Typical results are shown in Fig. 7 for one day during the BIOSOPE cruise (Station 17, 1/12/2004). $L_{\text{view}}/L_{\text{nadir}}$ for the data and model are displayed, and each data point represents a different direction or data set in that day. The resolution of direction is every 5 degrees in nadir and 15 degrees in Azimuth, thus there can be approximately 8 (5–40 degrees in nadir angle) \times 12 (0–180 degrees in azimuth angle) = 96 points from each radiance distribution data set. Note that the

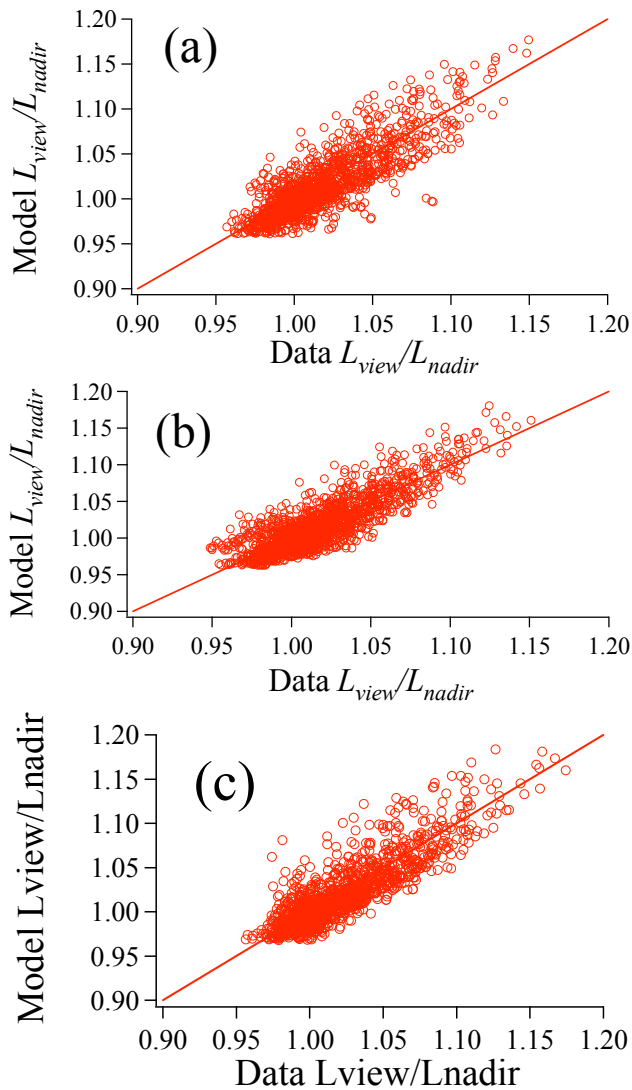


Fig. 7. Graph of model vs data of the ratio L_{view}/L_{nadir} for the BIOSOPE Station # 17; [Chl] was 0.11 mg m^{-3} in the upper layer. (a) 412 nm, (b) 436 nm, and (c) 486 nm. The 1:1 line is also shown.

nadir angle is limited to upward radiances inside the Snell cone, able to emerge from the sea after refraction. For each day we calculated the deviation between the model and data in two ways, first the average difference was determined by:

$$\text{Difference} = \sum (\text{data} - \text{model}) / N, \tag{5}$$

and the RMS was determined by:

$$\text{RMS} = \sqrt{\sum (\text{data} - \text{model})^2 / N}. \tag{6}$$

Through our data set we can look at these factors as a function of [Chl] and solar zenith angle to see if there are any biases in the model. Figures 8a–d shows this for the 4 wavelengths. In these figures the red dots correspond to the average difference (Eq. 5) while the bars correspond to 1 std

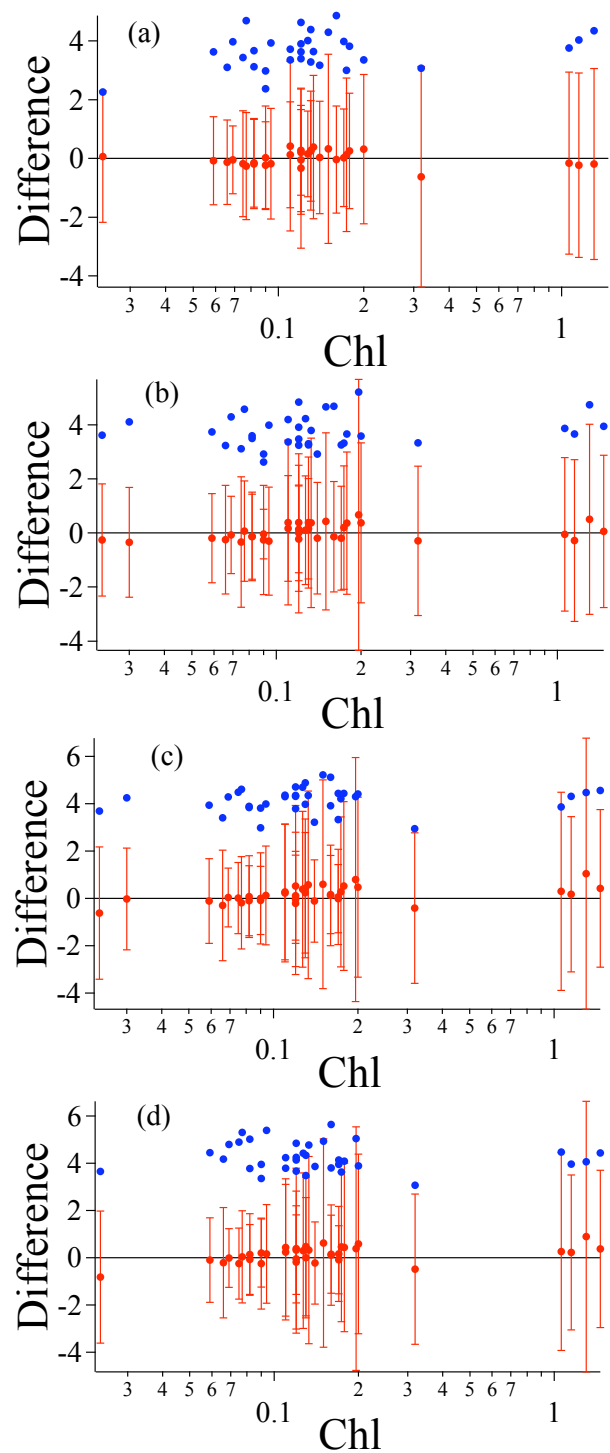


Fig. 8. Comparison for the entire data set between L_{view}/L_{nadir} the model and the data. (a) 412 nm, (b) 436 nm, (c) 486 nm, and (d) 526 nm. The red dots are the average difference in agreement between the model and the data. The bars on each data point are ± 1 std. The blue dots are σ obtained in the image averaging process and represents the environmental noise in the images.

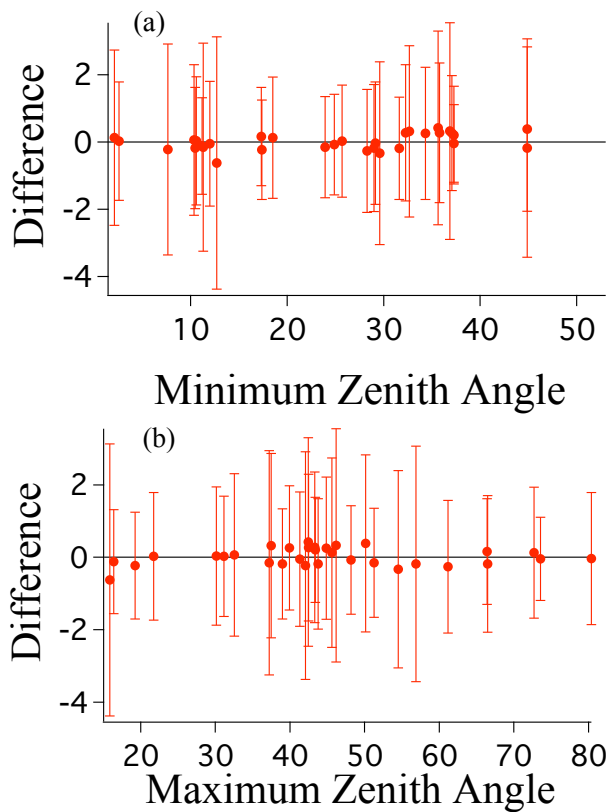


Fig. 9. Difference between the model and data $L_{\text{view}}/L_{\text{nadir}}$, shown as a function of solar zenith angle. Average difference is shown as red dots, bars are ± 1 standard deviation. **(a)** Maximum solar zenith angle during that data collection, **(b)** Minimum solar zenith angle during that data collection. As can be seen there is no systematic trend in this difference as a function of solar zenith angle. This example shows the data at 412 nm; there is no significant trend at any of the other wavelengths.

(Eq. 6). While collecting the difference and RMS, we also find the average σ for the data (effectively the average of Fig. 5, for each data point). This gives a measure of the environmental noise for that point, and is shown as the blue squares.

We can also look to see if there is any bias with respect to solar zenith angle. For each day of data we collected the minimum and maximum solar zenith angle, during the data acquisition. These results are shown in Fig. 9. Figures 8 and 9, taken together, show that in this data set there is no systematic difference with either [Chl] or solar zenith angle. In both cases the average difference is much less than 0.01. This is well within both the standard deviation of the difference between the model and measurement and the σ in the measurement alone. In general the RMS difference between the model and data ranged from 0.01 to 0.04, but was mostly on the order of 0.02–0.03. The largest difference tends to be towards the longer wavelengths where increased shadowing

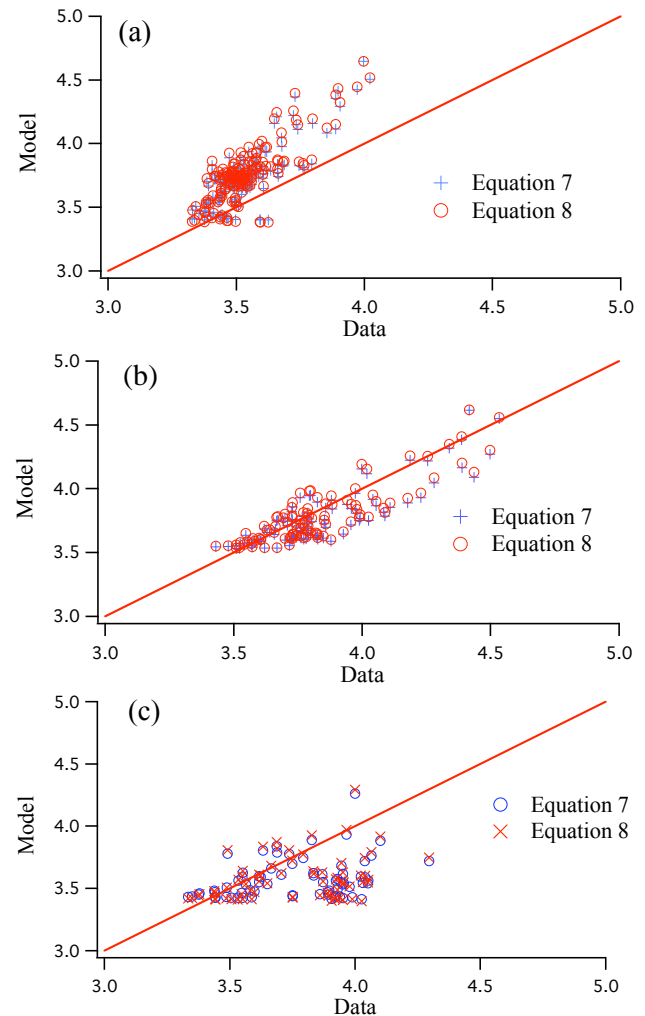


Fig. 10. Aas and Hojerslev (1999) Q_{nadir} (sr) fit to data set (486 nm). **(a)** Hawaii data, **(b)** AOPLEX (Mediterranean), **(c)** BIOSOPE (South Pacific). As can be seen, the best fit is with the AOPLEX data. The 1:1 line is also shown.

may be causing problems in the data.

We can also use this data set to investigate the available models of $Q_{\text{nadir}}=Q(\theta_o, \theta_v=0, \phi_v=0)$. Aas and Hojerslev (1999), using a parameterization based on a dataset from relatively clear Mediterranean waters, predicted that Q_{nadir} , at blue (465–475 nm) wavelengths, should follow either:

$$Q_{\text{nadir}} = 5.33 \exp(-0.45 \cos(\theta_o)) \text{ sr, or} \quad (7)$$

$$Q_{\text{nadir}} = 5.20 - 1.82 \cos(\theta_o) \text{ sr.} \quad (8)$$

Morel et al. (2002) provided an alternate model, which includes a parameter for varying water types given by:

$$Q_{\text{nadir}}(\theta_o, \lambda, [\text{Chl}]) = Q_o(0, \lambda, [\text{Chl}]) + S_{Q_n}(\lambda, [\text{Chl}])[1 - \cos(\theta_o)] \quad (9)$$

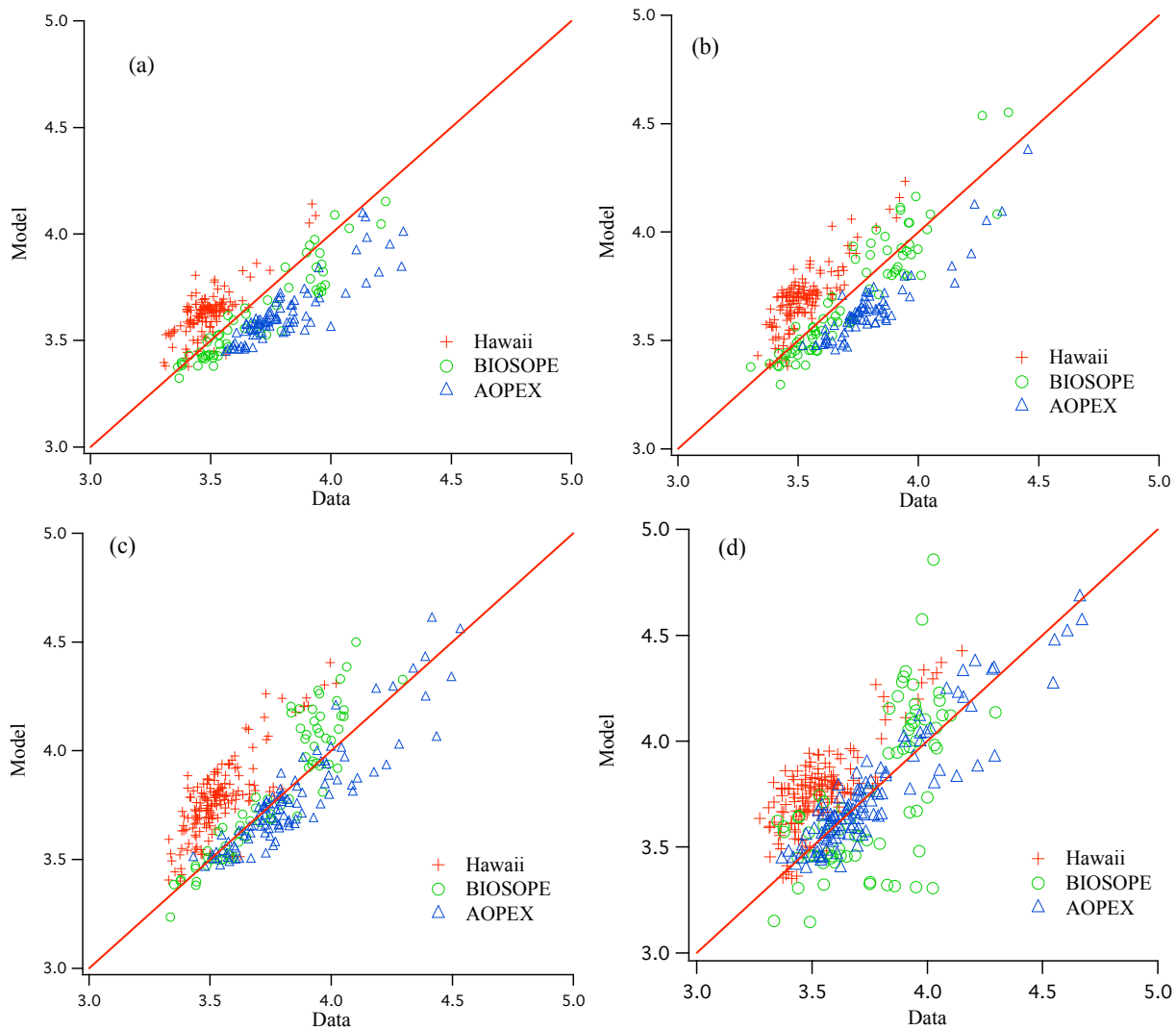


Fig. 11. Comparison of Morel et al. (2002) Q_n (sr) model with data set. (a) 412 nm, (b) 436 nm, (c) 486 nm, and (d) 526 nm. The 1:1 line is also shown.

where $Q_0(0, \lambda, [\text{Chl}])$ and $S_{Q_n}(\lambda, [\text{Chl}])$ can be interpolated from Table 2 in Morel et al. (2002).

The variations in both the initial term, Q_0 , and the slope, S_{Q_n} , with the chlorophyll concentration (used as bio-optical index) are by far not negligible, and are important when comparing predictions to actual data obtained in Case 1 waters with various trophic levels.

Figure 10 illustrates how well Eqs. (7) and (8) fit this data set. As can be seen, the best agreement is for the AOPEX data set, which is not surprising as this data set was obtained in the Western Mediterranean Sea, which was where the empirical factors in Eqs. (7) and (8) were determined, probably with similar [Chl] values. To quantitatively characterize this fit we calculate the RMS difference between the model and data. The RMS for these fits are 0.24 sr (Hawaii), 0.14 sr

(AOPEX), 0.30 sr (BIOSOPE), and 0.24 sr for the combined data set. This also shows that Eqs. (7) and (8) are very good at fitting the AOPEX data set, and not as good at the other sites. It is obvious that a line fitted between the model and data would be significantly different than 1 for both the Biosope and Hawaii data.

Figure 11 illustrates the fit of Eq. (9) to the data set for the 4 wavelengths. The RMS differences are shown in Table 1. The model fits the data a little better than the earlier model, but there are differences in the individual data sets. Interestingly, for most wavelengths, there is a good fit of the model to the BIOSOPE data, that extend over a rather wide range of Q_{nadir} values, in correspondence with the wider [Chl] range encountered during this campaign. However, we did not have [Chl] values approaching 10 mg m^{-3} , thus did not see the

Table 1. RMS difference between Q_n (sr) model (Morel et al., 2002) and data set.

	Wavelength			
	412	436	486	526
Cruise	0.11	0.10	0.14	0.17
BIOSOPE	0.20	0.18	0.12	0.11
AOPEX	0.16	0.19	0.26	0.26
Combined	0.16	0.17	0.21	0.20

predicted maximal Q_{nadir} values (close to 5 steradians) as observed in the Gulf of California (Voss and Morel, 2005).

Zibordi and Berthon (2001) have described an additional model for Q_{nadir} based on data obtained in the Adriatic Sea, however this water type was significantly different than our data base, hence did not agree very well with our data and is not shown.

5 Conclusions

The comparison between model predictions and field data has been carried out over a wide range of environmental conditions with respect to the trophic state of the water and the sun position in clear skies. The bidirectional variation (polar and azimuthal angles) of the upward radiance distribution compared to the radiance from nadir direction, as well as the variation of this particular radiance with the sun angle have been successfully tested. The model (Morel et al., 2002) proves to be a very good tool in reproducing the various radiance distributions that we observed in our extensive data set for Case I waters. However each real, measured, radiance distribution has many features in it due to wave focusing and downwelling illumination variations. As such, while the model is able to accurately predict the average, it will never exactly fit a measured radiance distribution (nor should it be expected to do this). Much more work needs to be done to move this Case I model into the Case II regime. We currently are looking at this Case II situation with 2 data sets collected in the Chesapeake Bay, and are also looking into issues of the polarization of the upwelling light field.

As a practical conclusion, it can be added that the bidirectional corrections based on the lookup tables generated from the model, and presently applied to ocean color imagery, is sound and amply validated for Case I waters, i.e., for most parts of the global ocean. The application of such a correction is needed for a meaningful comparison of the normalized water-leaving radiances inside and between various scenes, as well as for a merging of products derived from various sensors.

Acknowledgements. This work was supported by NASA (#NNG04HZ21C to KV). N. Souaidia and A. Chapin were, respectively, instrumental to collecting the BIOSOPE and AOPEX radiance distribution data; J. Ras who made the pigment analyses for both cruises is warmly thanked. The Hawaii data was collected in collaboration with D. Clark's group at NOAA/NESDIS, specifically M. Ondrusek and Yong Sung Kim.

The BIOSOPE and AOPEX projects and cruises were funded by CNRS and INSU (Centre National pour la Recherche Scientifique and Institut des Sciences de l'Univers), by the Centre National d'Etudes Spatiales (CNES), by the European Space Agency (ESA), and by the National Aeronautics and Space Administration (NASA), and, for BIOSOPE (a project of the LEFE-CYBER program), by the Engineering Research Council of Canada (NSERC).

The expertise of the captains, officers and crews of the research vessels Atalante (BIO SOPE) and Suroit (AOPEX) were essential for the success of these campaigns. We thank H. Claustre and A. Sciandra, the chief scientists of the BIOSOPE campaign.

This paper is dedicated to the memory of A. Chapin, a colleague and friend for over 20 years. He was instrumental in the development of the series of electro-optic radiance distribution cameras, along with many other instruments, and contributed to many experiments at sea during this long period.

Edited by: E. Boss

References

- Aas, E. and Hojerslev, N. K.: Analysis of underwater radiance distribution observations: Apparent optical properties and analytical functions describing the angular radiance distributions, *J. Geophys. Res.*, 104, 8015–8024, 1999.
- Gordon, H. R. and Ding, K.: Self-shading of in-water optical measurements, *Limnol. Oceanogr.*, 37, 491–500, 1992.
- Helliwell, W. S., Sullivan, G. N., Macdonald, B., and Voss, K. J.: A finite-difference discrete-ordinate solution to the three dimensional radiative transfer equation, *Transport Theor. Stat.*, 19, 333–356, 1990.
- Leathers, R., Downes, T. V., and Mobley, C. Self-shading correction for upwelling sea-surface radiance measurements made with buoyed instruments, *Opt. Express*, 8, 561–570, 2001.
- Loisel, H. and Morel, A.: Non-isotropy of the upward radiance field in typical coastal (Case-2) waters, *Int. J. Remote Sens.*, 22, 275–295, 2001.
- Morel, A., Antoine, D., and Gentili, B.: Bidirectional reflectance of oceanic waters: Accounting for Raman emission and varying particle scattering phase function, *Appl. Opt.* 41, 6289–6306, 2002.
- Morel, A., and Maritorena, S. Bio-optical properties of oceanic waters: a reappraisal. *J. Geophys. Res.*, 106, 7163–7180, 2001.
- Morel, A., Voss, K. J., and Gentili, B.: Bi-directional reflectance of oceanic waters: A comparison of model and experimental results, *J. Geophys. Res.*, 100, 13 143–13 150, 1995.
- Ras, J., Uitz, J., and Claustre, H.: Spatial variability of phytoplankton pigments distribution in the South East Pacific, *Biogeosciences Discuss.*, accepted, 2007.
- Van Heukelen, L. and Thomas, C. S.: Computer-assisted high-performance liquid chromatography method development with

- application to the isolation and analysis of phytoplankton pigments, *J. Chromatogr.*, 910, 31–49, 2001.
- Voss, K. J.: Electro-optic camera system for measurement of the underwater radiance distribution, *Opt. Eng.*, 28, 241–247, 1989.
- Voss, K. J. and Chapin, A. L.: Next generation in-water radiance distribution camera system, *Proc. Soc. Photo-Optical Instrumentation Engineers*, 1750, 384–387, 1992.
- Voss, K. J. and Chapin, A. L.: Upwelling radiance distribution camera system, *NURADS, Opt. Express*, 13, 4250–4262, 2005.
- Voss, K. J. and Morel, A.: Bidirectional reflectance function for oceanic waters with varying chlorophyll concentrations: Measurements versus predictions, *Limnol. Oceanogr.*, 50, 698–705, 2005.
- Voss, K. J. and Zibordi, G.: Radiometric and geometric calibration of a spectral electro-optic “fisheye” camera radiance distribution system, *J. Atmos. Ocean. Techn.*, 6, 652–662, 1989.
- Zibordi, G. and Berthon, J.-F.: Relationships between Q- factor and seawater optical properties in a coastal region, *Limnol. Oceanogr.*, 46, 1130–1140, 2001.

Relationships between the surface concentration of particulate organic carbon and optical properties in the eastern South Pacific and eastern Atlantic Oceans

D. Stramski¹, R. A. Reynolds¹, M. Babin^{2,3}, S. Kaczmarek⁴, M. R. Lewis⁵, R. Röttgers⁶, A. Sciandra^{2,3}, M. Stramska⁷, M. S. Twardowski⁸, B. A. Franz⁹, and H. Claustre^{2,3}

¹Marine Physical Lab., Scripps Institution of Oceanography, Univ. of California at San Diego, La Jolla, CA 92093-0238, USA

²CNRS, UMR 7093, Laboratoire d'Océanographie de Villefranche (LOV), 06230 Villefranche-sur-mer, France

³Université Pierre et Marie Curie-Paris6, UMR 7093, LOV, 06230 Villefranche-sur-mer, France

⁴Institute of Oceanology, Polish Academy of Sciences, Powstanców Warszawy 55, 81-712 Sopot, Poland

⁵Department of Oceanography, Dalhousie University, Halifax, NS, BH3 4J1, Canada

⁶Institute for Coastal Research, GKSS Research Center, Geesthacht, Max-Planck-Str., 21502 Geesthacht, Germany

⁷Center for Hydro-Optics & Remote Sensing, San Diego State Univ., 6505 Alvarado Rd., San Diego, CA 92120, USA

⁸Department of Research, WET Labs, Inc., 165 Dean Knauss Dr., Narragansett, RI 02882, USA

⁹Science Applications International Corporation, NASA Goddard Space Flight Center, Greenbelt, MD 20771, USA

Received: 12 September 2007 – Published in Biogeosciences Discuss.: 2 October 2007

Revised: 7 January 2008 – Accepted: 11 January 2008 – Published: 14 February 2008

Abstract. We have examined several approaches for estimating the surface concentration of particulate organic carbon, POC, from optical measurements of spectral remote-sensing reflectance, $R_{rs}(\lambda)$, using field data collected in tropical and subtropical waters of the eastern South Pacific and eastern Atlantic Oceans. These approaches include a direct empirical relationship between POC and the blue-to-green band ratio of reflectance, $R_{rs}(\lambda_B)/R_{rs}(555)$, and two-step algorithms that consist of relationships linking reflectance to an inherent optical property IOP (beam attenuation or backscattering coefficient) and POC to the IOP. We considered two-step empirical algorithms that exclusively include pairs of empirical relationships and two-step hybrid algorithms that consist of semianalytical models and empirical relationships. The surface POC in our data set ranges from about 10 mg m^{-3} within the South Pacific Subtropical Gyre to 270 mg m^{-3} in the Chilean upwelling area, and ancillary data suggest a considerable variation in the characteristics of particulate assemblages in the investigated waters. The POC algorithm based on the direct relationship between POC and $R_{rs}(\lambda_B)/R_{rs}(555)$ promises reasonably good performance in the vast areas of the open ocean covering different provinces

from hyperoligotrophic and oligotrophic waters within subtropical gyres to eutrophic coastal upwelling regimes characteristic of eastern ocean boundaries. The best error statistics were found for power function fits to the data of POC vs. $R_{rs}(443)/R_{rs}(555)$ and POC vs. $R_{rs}(490)/R_{rs}(555)$. For our data set that includes over 50 data pairs, these relationships are characterized by the mean normalized bias of about 2% and the normalized root mean square error of about 20%. We recommend that these algorithms be implemented for routine processing of ocean color satellite data to produce maps of surface POC with the status of an evaluation data product for continued work on algorithm development and refinements. The two-step algorithms also deserve further attention because they can utilize various models for estimating IOPs from reflectance, offer advantages for developing an understanding of bio-optical variability underlying the algorithms, and provide flexibility for regional or seasonal parameterizations of the algorithms.

1 Introduction

Optical measurements performed from various in situ and remote sensing platforms provide an effective tool for studying biogeochemically significant constituents of ocean waters. In comparison with traditional methods that require analysis of



Correspondence to: D. Stramski
(dstramski@ucsd.edu)

discrete water samples, optical measurements allow significant extension of observational time and space scales through the use of instruments deployed on in-water vertical profiling systems, moorings, drifters, autonomous vehicles, as well as air-borne and space-borne platforms (Robinson, 2004; Myers and Miller, 2005; Twardowski et al., 2005).

In situ measurements of the beam attenuation coefficient have long been used to characterize bulk particulate properties, most notably the dry mass concentration of suspended particulate matter, SPM (Zaneveld, 1973; Baker and Lavelle, 1984; Gardner et al., 1985; Bishop, 1986, 1999; Spinrad, 1986). Relationships between ocean reflectance and SPM have also been investigated for the purpose of estimating SPM from remote sensing (Gordon and Morel, 1983; Stumpf and Pennock, 1989; Doxaran et al., 2002).

Similarly, it has long been recognized that optical measurements provide a useful proxy for the concentration of the primary pigment in phytoplankton, chlorophyll-*a* (Chl-*a*). The development of bio-optical algorithms linking measurable optical properties to Chl-*a* has been the focus of numerous studies over the last three decades. Field data have been used to examine empirical relationships between Chl-*a* and inherent optical properties (IOPs) such as the absorption coefficient (e.g., Garver et al., 1994; Bricaud et al., 1995, 1998), the beam attenuation coefficient (e.g., Voss, 1992; Loisel and Morel, 1998), the scattering coefficient (e.g., Gordon and Morel, 1983; Loisel and Morel, 1998), and the backscattering coefficient (e.g., Reynolds et al., 2001; Stramska et al., 2006). Field measurements of Chl-*a* and apparent optical properties (AOPs) such as ocean reflectance and the diffuse attenuation coefficient for downward irradiance have been also analyzed extensively for establishing bio-optical models and algorithms (e.g., Smith and Baker, 1978; Gordon and Morel, 1983; Morel, 1988; O'Reilly et al., 1998; Morel and Maritorena, 2001). Probably the single most studied bio-optical relationship in recent decades has been that linking surface Chl-*a* to remote-sensing reflectance of the ocean. This has been driven by interest in the study of phytoplankton biomass and primary productivity from satellite remote sensing (e.g., Platt and Sathyendranath, 1988; Yoder et al., 1993; Antoine et al., 2005). Empirical relationships for estimating Chl-*a* from reflectance are currently used for routine processing of global satellite imagery of ocean color (O'Reilly et al., 2000).

For studies of ocean biogeochemistry and its potential role in climate it is carbon, not chlorophyll, which is usually of most direct interest. The particulate organic carbon (POC) pool in the surface ocean, which includes autotrophic and heterotrophic organisms and biogenic detrital particles, represents one carbon reservoir of substantial interest. POC is a highly dynamic carbon pool and its variability is poorly characterized. Sinking of POC from surface waters is part of the biological pump that provides a mechanism for storing carbon in the deep ocean, a long-term sink for atmospheric CO₂ (Volk and Hoffert, 1985; Longhurst and Har-

risson, 1989). The knowledge of total POC and subsequent inference of the phytoplankton portion of POC is essential to the development of methods for estimating phytoplankton growth rates and carbon-based net primary production from satellite observations (Behrenfeld et al., 2005). Because the turnover time of carbon biomass is relatively short (1–2 weeks), satellite capabilities to monitor changes in particulate carbon pools can effectively aid in studies related to the biological pump.

Relationships between ocean optical properties and POC first appeared in the late 1980s. Morel (1988) demonstrated a relationship between the scattering coefficient at a light wavelength (in vacuo) $\lambda=550$ nm, $b(550)$, with Chl-*a* and a relationship between POC and Chl-*a*, both obtained from a large data set collected in different oceanic regions. These two relationships suggested the existence of a nearly linear relationship between $b(550)$ and POC. Morel's data showed a general trend of covariation of POC with Chl-*a* over 3 orders of magnitude range in Chl-*a*, but also at any given Chl-*a* there existed a significant several-fold variation in the POC:Chl-*a* ratio. Because this variability is difficult to predict, POC cannot be estimated directly from Chl-*a* with consistently good accuracy. Linking POC to optics by converting SPM to POC through the use of SPM-specific optical coefficients such as the beam attenuation (Siegel et al., 1989) is also limited by large and difficult to predict variations in the conversion factors. Therefore, concurrent measurements of POC and optical parameters appear naturally as the most desirable approach for linking these variables.

Laboratory experiments with marine phytoplankton cultures suggest that the POC-specific scattering coefficient and the POC-specific beam attenuation coefficient (which is dominated by scattering) exhibit relatively small variations for a wide range of growth conditions (Stramski and Morel, 1990; Stramski and Reynolds, 1993). At the level of individual particles, the mechanism responsible for the relatively robust relationship between scattering and POC can be attributed to both a relation between the cellular carbon content and cell size (Verity et al., 1992; Montagnes et al., 1994) and a relation between the intracellular carbon concentration and refractive index of cells (Stramski, 1999; DuRand et al., 2002).

Measurements of the particulate beam attenuation coefficient at 660 nm, $c_p(660)$, and POC constitute the largest amount of field data presently available for examining relationships between POC and ocean optical properties. Early reports on the relationship between POC and $c_p(660)$ based on data from the North Atlantic and Southern Ocean (Gardner et al., 1993; Villafane et al., 1993) were soon followed by similar studies in different regions of the world's ocean (Marra, 1995; Gundersen et al., 1998; Loisel and Morel, 1998; Bishop, 1999; Claustre et al., 1999; Gardner et al., 2000; Stramska and Stramski, 2005). Most recently, Gardner et al. (2006) made a synthesis of the POC vs. $c_p(660)$ relationships for nine different regions comprising a total of

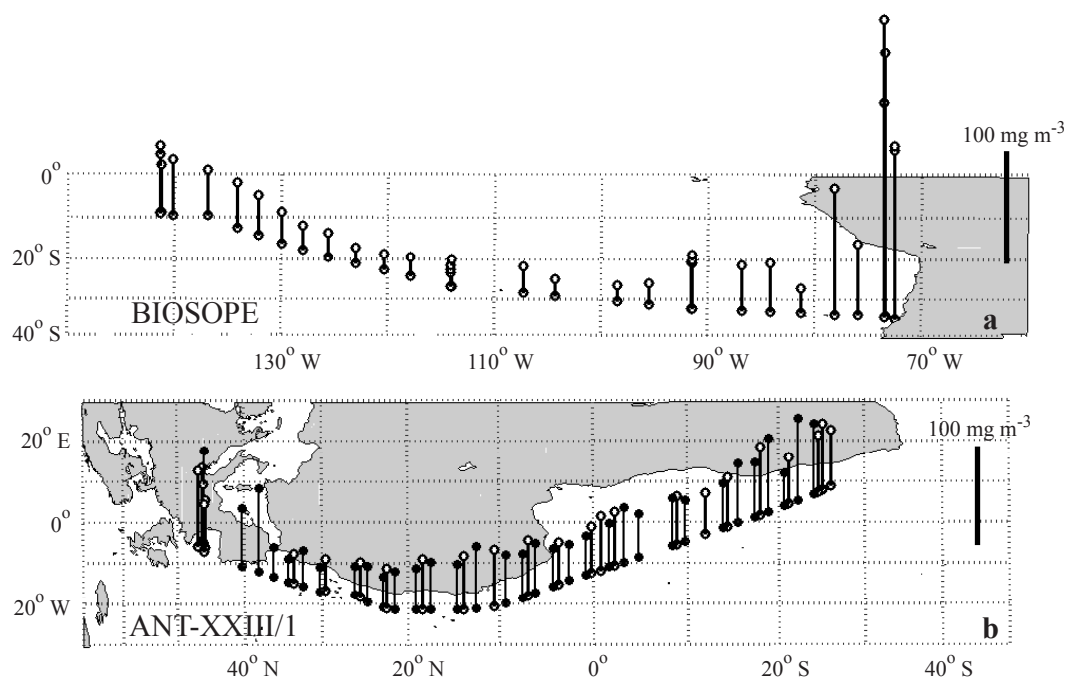


Fig. 1. Locations of stations along (a) the west-to-east BIOSOPE cruise track in the eastern South Pacific and (b) the north-to-south ANT-XXIII/1 cruise track in the eastern Atlantic. The values of surface concentration of POC are illustrated with vertical bars. Lower open circles on the bars indicate locations of stations at which POC determinations were accompanied with in situ optical measurements (all stations in the case of the BIOSOPE cruise). For the ANT-XXIII/1 cruise, we additionally show a significant number of underway sampling stations at which no in situ optical measurements were taken (denoted by filled circles). The POC data from these underway stations are not included in the correlational analysis presented in this study. The scale bars at the right of each figure correspond to a POC concentration of 100 mg m^{-3} .

nearly 4500 data pairs. While indicating that a linear function provides a reasonably good fit to the data, their analysis also revealed a considerable variation in the slope of the relationship (~ 2 -fold) and in the squared correlation coefficient (from ~ 0.5 to 0.9) among the regional data sets.

Development of a remote sensing capability for estimating POC has led to an increased interest in the relationships between POC and the spectral remote-sensing reflectance, $R_{rs}(\lambda)$. Few studies exist in which simultaneously collected in situ data were used for the development of empirical algorithms for estimating POC directly from R_{rs} or from a combination of R_{rs} and IOP data (Stramski et al., 1999; Stramska and Stramski, 2005; Pabi and Arrigo, 2006). Alternative approaches for remote sensing of POC have also been attempted but the algorithms were parameterized from field measurements of POC and optical data that were not all collected in situ (because satellite data products were included), or were not collected during the same field experiments (Loisel et al., 2001; Loisel et al., 2002; Mishonov et al., 2003; Gardner et al., 2006). These approaches thus have significant limitations that are related primarily to mismatches between the temporal and/or spatial scales for the determinations of variables involved in the algorithms.

In this study, we collected contemporaneous POC and optical data, including the spectral remote-sensing reflectance, backscattering coefficient, and beam attenuation coefficient, along a west-to-east transect in the eastern South Pacific Ocean and along a north-to-south transect in the eastern Atlantic Ocean. We examine empirical relationships between the surface POC concentration and optical properties with emphasis on algorithms for estimating POC from remote-sensing reflectance. Our primary objective is to provide candidate POC algorithms for the application of satellite ocean color imagery within the subtropical and tropical provinces of the Pacific and Atlantic Oceans.

2 Data and methods

2.1 Study areas

Field measurements in the eastern South Pacific Ocean were conducted during the French expedition BIOSOPE (Biogeochemistry & Optics South Pacific Experiment) on R/V l'Atalante, which took place from 17 October through 15 December, 2004. Measurements were taken on a west-to-east transect between the Marquesas Islands and the coast of Chile. Figure 1a shows the locations of stations at which

data for this study were collected, and illustrates the surface concentration of POC at each station. This study area spans different ecological provinces and trophic conditions, including mesotrophic subequatorial waters near the Marquesas Islands, oligotrophic and hyperoligotrophic waters within the South Pacific Subtropical Gyre (SPSG) Province, as well as highly productive upwelling waters off Chile which comprise part of the Humboldt Current Coastal Province (Longhurst, 1998). The upwelling data were collected at both off-shelf and shelf stations. The general oceanographic conditions and variability in the bio-optical and biogeochemical characteristics for the BIOSOPE study area are summarized in Claustre et al. (2008), and the optical properties of the extremely clear waters within the SPSG are discussed in Morel et al. (2007) and Twardowski et al. (2007).

Data in the Atlantic Ocean were collected during the German expedition ANT-XXIII/1 on R/V *Polarstern*, which covered the period from 13 October to 17 November, 2005. Measurements were taken along a north-to-south transect in the eastern Atlantic between the Bay of Biscay and the African coast of Namibia (Fig. 1b). The stations were situated within open ocean waters that cover various ecological provinces such as North Atlantic Subtropical Gyre, North Atlantic Tropical Gyre, Eastern Tropical Atlantic, and South Atlantic Gyral Province (Longhurst, 1998). Note that the range in surface POC observed within the Atlantic study area is not as large as that encountered on the BIOSOPE cruise (Fig. 1).

As our present interest lies in determining relationships for satellite remote sensing applications, we restrict our data set to measurements obtained in the surface waters. The three main optical properties that are used in this study for correlating with POC are the remote-sensing reflectance, the beam attenuation coefficient, and the backscattering coefficient.

2.2 POC determinations

The POC data were obtained using a method generally consistent with JGOFS protocols (Knap et al., 1996). Surface water samples were collected from Niskin bottles triggered at a depth of ~ 5 m during the CTD/rosette cast, then filtered through precombusted 25 mm Whatman GF/F filters (450°C for 5 h) under low vacuum (pressure differential across the filters < 150 mm Hg). Filtered volumes were adjusted according to expected POC concentration (~ 1 to 8.4 L on BIOSOPE with the largest volumes in the gyre and smallest volumes in the Chilean upwelling, and 2–4 L on ANT-XXIII/1). Following filtration, filters were transferred to clean glass scintillation vials, dried at 55°C, and stored until post cruise analysis. A number of unused filters from each lot of precombusted filters were selected as blanks during the cruises. The blank filters were used to quantify background amount of organic carbon on filters and were processed identically to regular sample filters with the exception that the filtration step was not applied.

The determination of POC was made with a standard CHN analysis involving high temperature combustion of sample filters (Parsons et al., 1984). A CEC 440HA Elemental Analyzer (Control Equipment Corp., now Exeter Analytical) was used. Prior to combustion, 0.25 mL of 10% HCl was applied to each filter for removal of inorganic carbon and the acid-treated filters were re-dried at 55°C. The final values of POC concentration were calculated by subtracting the average mass of organic carbon determined on blank filters from the mass of carbon determined on sample filters, and then dividing this result by the measured volume of filtered sample. Triplicate (nearly all BIOSOPE stations) or duplicate (few BIOSOPE and all ANT-XXIII/1 stations) POC samples were taken for each station and averaged to produce the final result of POC concentration. The average coefficient of variation for replicate samples was 6% for BIOSOPE and 5% for ANT-XXIII/1.

POC determinations are subject to several potential sources of errors and there is continued need for further research to improve the methodology. Recently, Gardner et al. (2003) reviewed these issues. In brief summary, the causes for potential positive bias (overestimation) of POC include adsorption of dissolved organic carbon (DOC) onto filters during filtration and contamination of samples due to, for example, exposure to air during handling. There are, however, other causes which can produce a negative bias (underestimation) of POC, such as undersampling of the rare large particles, incomplete retention of particles on filters, and the loss of POC due to the impact of pressure differential on particles across the filters (e.g., breakage of fragile plankton cells). The quantification of all these effects is impossible from a practical standpoint, and therefore the accuracy of POC determinations remains unspecified.

Although we attempted to minimize some of these problems as much as possible in our study (e.g., minimal sample exposure to air during handling and low vacuum during filtration), other potential problems could not be directly addressed. It was previously recommended that determining proper blanks accounting for DOC adsorption is important, especially in waters with low POC (Menzel, 1966; Moran et al., 1999; Gardner et al., 2003). The methods that were used to estimate DOC adsorption involved either exposure of blank filters to filtered seawater or filtration of several different volumes of sample, plotting organic carbon mass on a filter as a function of volume filtered, and accepting the intercept on the carbon axis as a blank. We have not tested these methods in our study primarily because such special effort towards minimizing just one source of positive bias in POC determinations does not guarantee better estimates of POC, as the sources of negative bias cannot be eliminated from the applied method (e.g., incomplete retention of particles on GF/F filters). Our approach was focused on minimizing statistical uncertainties in POC estimates through the preparation of replicate samples with sufficient filtration volumes to maximize the ratio of the mass of organic carbon

on the sample filter to that on the blank filter. This approach appeared to be especially important in hyperoligotrophic waters with surface POC below 20 mg m^{-3} , where volumes exceeding 8 L for each replicate sample were filtered. In addition, our blank determinations are based on a relatively large number of blank filters (~ 20 per cruise). For the BIOSOPE cruise, our average blank determinations were $16.7 \mu\text{g C}$ per filter for the stations west of Easter Island and $37.6 \mu\text{g C}$ per filter for the stations east of Easter Island (as two different lots of filters were used on the cruise). The ratio of the blank values to the mass of organic carbon on sample filters was, on average, 14% (3.7–48% range with generally higher percentages at gyre stations). For the ANT-XXIII/1 cruise this ratio was lower, on average 4.5% and never more than 8%, as the blank values were also lower (typically less than $10 \mu\text{g C}$ per filter). The methodological issues discussed above underscore the difficulty in accurate determinations of POC, especially at very low concentrations. Although the accuracy of POC is unknown and is likely variable, one can expect that samples differing from one another by less than about 5 mg m^{-3} cannot be resolved within current measurement uncertainties, which has particular ramifications for hyperoligotrophic waters where POC is less than 20 mg m^{-3} .

2.3 Optical measurements and data processing

2.3.1 Radiometric measurements and remote-sensing reflectance

The spectral remote-sensing reflectance, $R_{rs}(\lambda)$ in sr^{-1} , is defined as the ratio of nadir water-leaving radiance, $L_w(\lambda)$, to the downwelling plane irradiance, $E_d(\lambda)$, where both quantities are measured just above the sea surface ($z=0^+$). On the BIOSOPE cruise, $R_{rs}(\lambda)$ was determined from direct shipboard above-water measurements of $E_d(\lambda, z=0^+)$ in $\text{W m}^{-2} \text{ nm}^{-1}$, and subsurface measurements of nadir upwelling radiance, $L_u(\lambda, z=0.2 \text{ m})$ in $\text{W m}^{-2} \text{ nm}^{-1} \text{ sr}^{-1}$, made at a depth z of 0.2 m below the ocean surface. The underwater measurements were made with a calibrated hyperspectral profiling radiometer (HyperPro, Satlantic, Inc.) adapted to float at the sea surface and tethered such that the instrument operated at a distance of $\sim 100 \text{ m}$ from the vessel. Instrument tilt was measured directly and radiometric measurements were rejected if tilt exceeded 5° . Measurements were made over the spectral region 380–800 nm with a spectral resolution of 3.3 nm and with each band having a full-width-half-maximum (FWHM) bandpass of 10 nm. Dark current values were taken every 5 samples by use of an internal shutter and linearly interpolated as a function of time for each light value, and subtracted from the observations. Calibration coefficients and corrections for immersion effects were obtained following standard protocols (Mueller et al., 2003) and applied to the measurements. Irradiance and radiance data were taken for 3 minutes at each deployment, with each observation within the deployment time series rep-

resenting integration times of 0.03 to 0.5 s, depending on the intensity of the incident (ir)radiance. These measurements were then interpolated to a common time frame at an interval of 2 s and to a common spectral resolution every 2 nm.

Upwelling radiance measurements taken at a depth of 0.2 m were propagated to the sea surface using an iterative approach that estimates the spectral diffuse attenuation coefficient from spectral ratios of measured radiance. From the computed upwelling radiance just below the surface, $L_u(\lambda, z=0^-)$, the nadir water-leaving radiance above the sea surface, $L_w(\lambda)$, was then determined based on the transmittance coefficient for nadir radiance across the water-air interface (Mueller et al., 2003). This transmittance coefficient includes the effects of Fresnel reflectance and a change in solid angle, so $L_w(\lambda)/L_u(\lambda, z=0^-)=[1-(1-n_w)^2/(1+n_w)^2]n_w^{-2}$, where n_w is the refractive index of water. The values of n_w in the visible spectral region can vary slightly near 1.34 (e.g., Mobley, 1994), so the values of $L_w(\lambda)/L_u(\lambda, z=0^-)$ assumed in the literature vary slightly as well. For the BIOSOPE data, $L_w(\lambda)/L_u(\lambda, z=0^-)=0.54$ was used. Finally, a three-minute time series of R_{rs} was made by dividing the computed water-leaving radiance by the measured downward irradiance for each time interval, and an average value of $R_{rs}(\lambda)$ was computed for each deployment.

On the ANT-XXIII/1 cruise, $R_{rs}(\lambda)$ was determined from measurements of underwater vertical profiles of $L_u(\lambda, z)$ and $E_d(\lambda, z)$ with a freefall spectroradiometer, SeaWiFS Profiling Multichannel Radiometer (SPMR, Satlantic, Inc.), following standard protocols (Mueller et al., 2003). Measurements were made at 13 spectral wavebands (centered at 339, 380, 412, 442, 470, 490, 510, 532, 555, 590, 620, 666, and 682 nm with a FWHM bandwidth of 10 nm each) away from ship perturbations. Three to four replicate vertical casts were taken at each station. Initial data processing was done using ProSoft ver. 7.7 (Satlantic, Inc.), which included the application of dark offsets and manufacturer's radiometric calibration, binning data to 0.1 m depth interval, and rejecting data with tilt $>5^\circ$ (typically near the surface within the first 5 m). Profiles with questionable data quality, such as profiles that did not agree with other replicate casts or profiles during variable sky conditions (for example, a heterogeneous cloud over the Sun's disk) were rejected from subsequent analysis.

For each profile accepted, a depth interval within the upper mixed layer (typically 5 to 15 or 20 m, but variable on a cast-by-cast basis depending upon visual inspection of profiles) was defined for calculation of the vertical attenuation coefficients for downwelling irradiance (K_d) and upwelling radiance (K_{Lu}). Using these K_d and K_{Lu} values, the profiles of $E_d(\lambda, z)$ and $L_u(\lambda, z)$ were extrapolated from $\sim 5 \text{ m}$ to immediately beneath the sea surface. The subsurface estimates of $E_d(\lambda, z=0^-)$ and $L_u(\lambda, z=0^-)$ were propagated through the surface to yield the above-water estimates of downwelling irradiance, $E_d(\lambda, z=0^+)$, and water-leaving radiance, $L_w(\lambda)$, which

are required for the final calculation of $R_{rs}(\lambda)$. The coefficients for propagating E_d and L_u through the water-air interface were: $E_d(\lambda, z=0^+)/E_d(\lambda, z=0^-)=1/0.957$ and $L_w(\lambda)/L_u(\lambda, z=0^-)=0.5425$. The value of 0.5425 is nearly the same ($\sim 0.5\%$ difference) as that used for the BIOSOPE data processing. Note that with our assumptions for the transmittance of irradiance and radiance, the relationship between $R_{rs}(\lambda)$ and its counterpart reflectance just below the surface is: $R_{rs}(\lambda)=0.519 L_u(\lambda, z=0^-)/E_d(\lambda, z=0^-)$. The final estimate of $R_{rs}(\lambda)$ for each ANT-XXIII/1 station was obtained by averaging the results from replicate casts.

We also note that in this study of clear ocean waters with chlorophyll-*a* typically less than 0.5 mg m^{-3} , no correction for instrument self-shading was deemed necessary, as the calculated effect on the upwelling radiance is less than 1–2% for the blue-green bands that are of primary interest to our POC algorithm development.

2.3.2 Inherent optical properties

The beam attenuation coefficient at 660 nm, $c(660)$, was measured on both cruises with a C-Star transmissometer (WET Labs, Inc.) along a 25-cm pathlength within seawater. On the BIOSOPE cruise, the transmissometer was interfaced to a CTD-rosette and the raw transmissometer voltages were acquired during down- and upcasts. On ANT-XXIII/1, the transmissometer data were also acquired during the down- and upcasts but the instrument was part of a profiling package that included backscattering sensors and an additional C-Star transmissometer for measuring c at 488 nm. The beam attenuation coefficient can be considered as the sum of contributions due to particles (c_p), colored dissolved organic matter CDOM (c_{CDOM}), and pure seawater (c_w). At 660 nm, c_{CDOM} in surface open ocean waters is so small that it can be safely ignored (Bricaud et al., 1981); this assumption is also supported by a_{CDOM} data from the BIOSOPE (A. Bricaud, personal communication) and ANT-XXIII/1 cruises (Röttgers and Doerffer, 2007). Thus, the measurements of $c(660)$ allow the determination of the particle beam attenuation as $c_p(660)\approx c(660)-c_w(660)$.

Processing of raw transmissometer data included quality checking of down- and uptraces, rejecting doubtful and excessively noisy data, and averaging into 1-m depth bins. An important step of processing required for converting the raw transmissometer data to calibrated beam attenuation values was the determination of the highest raw transmittance voltages during each cruise, which correspond to the lowest beam attenuation values. This minimum attenuation is assumed in our data processing to represent the pure seawater coefficient, $c_w(660)$. This approach for determining $c_w(660)$ is preferred over the use of imperfect pure water calibrations of the instrument in the laboratory, and it can also account for variations in the cleanliness of optical windows or other instrumental drifts during the cruise (Loisel and Morel, 1998; Gardner et al., 2006). On BIOSOPE, the $c_w(660)$ values

were determined on a cast-by-cast basis from transmissometer data at depths of 470–500 m. On ANT-XXIII/1, routine deployments of our transmissometers were made to depths of 250–300 m, which precluded such an approach. At 5 stations, however, deep casts (2000–3000 m) were made with the ship's CTD-rosette which also included a transmissometer. The observed increase in transmissometer voltage between 300 m and the stable clear deep-water value at these stations was determined, and the average increase was subsequently used to calculate the appropriate reference voltage of $c_w(660)$ for transmissometers deployed on our instrument package. The $c_p(660)$ data averaged over the depth range of 4–6 m for BIOSOPE and 6–8 m for ANT-XXIII/1 were assumed to represent the surface beam attenuation values. The data from shallower depths were rejected because the signal measured near the sea surface often exhibited significant fluctuations. One possible cause of these fluctuations is the intermittent nature of bubble clouds entrained into water by breaking waves (Stramski and Tęgowski, 2001; Terrill et al., 2001).

The spectral backscattering coefficient, $b_b(\lambda)$, was also measured with in situ instruments deployed in a vertical profiling mode. On both cruises, the determinations of $b_b(\lambda)$ were made from measurements with a Hydrosat-6 and two α - β sensors (HOBI Labs, Inc.). These instruments are equipped with light-emitting diodes (LEDs) and photodiode detectors arranged in a geometry that provides a measurement of the spectral volume scattering function, $\beta(\psi, \lambda)$, at an effective scattering angle of $\psi=140^\circ$ (Maffione and Dana, 1997). The Hydrosat-6 provided measurements at six wavebands (nominal wavelengths of 442, 470, 550, 589, 620, and 671 nm) and the α - β sensors at one waveband each (420 and 510 nm). The 620-nm band failed to operate correctly on the BIOSOPE cruise. The nominal wavelengths correspond to nominal center wavelengths of interference filters placed in front of the detectors. The FWHM bandwidth of filters was 10 nm and the filters have ± 2 nm tolerances on their nominal bandwidth and center wavelength. The LED bandwidths are substantially wider (20 to 30 nm) than the filters and the LED peak does not necessarily match the filter peak for a given waveband. Therefore, the actual centroid wavelength does not necessarily match the nominal wavelength of the waveband. It is difficult to determine the exact spectral characteristics of the wavebands because the unique spectral data of the LEDs and filters used in individual instrument channels are not available. It is estimated, however, that the maximal difference between the actual centroid and nominal wavelengths would typically be 2 to 3 nanometers and perhaps 4 to 5 nm under worst-case assumptions (D. Dana, personal communication). These worst-case assumptions imply that the peak of the LED is outside the filter's 10 nm passband and the LED spectrum goes all the way to zero at one side of a 10 nm passband (which is very unlikely). A small spectral shift (up to 0.5–1 nm) resulting from the fact that light that goes through the filters is not perfectly collimated was also

taken into account in that estimation.

Backscattering data were calculated with a method described originally by Maffione and Dana (1997) with refinements presented in Boss and Pegau (2001). Initial data processing was done with HOBI Labs HydroSoft software version 2.71 utilizing manufacturer's calibrations, with subsequent processing carried out using custom-written software. The spectral backscattering coefficient was calculated from the measured $\beta(140^\circ, \lambda)$ using the relation: $b_b(\lambda) = b_{bp}(\lambda) + b_{bw}(\lambda) = 2\pi\chi[\beta(140^\circ, \lambda) - \beta_w(140^\circ, \lambda)] + b_{bw}(\lambda)$. The coefficient $b_b(\lambda)$ is considered to be the sum of contributions from particle backscattering, $b_{bp}(\lambda)$, and pure seawater backscattering, $b_{bw}(\lambda)$. For each wavelength, we used a value of 1.13 for the χ parameter that is involved in the conversion of the particle volume scattering function, $\beta_p(140^\circ, \lambda)$, to $b_{bp}(\lambda)$ (Dana and Maffione, 2002). The values of $\beta_p(140^\circ, \lambda)$ were calculated as a difference between measured $\beta(140^\circ, \lambda)$ and the pure seawater values of $\beta_w(140^\circ, \lambda)$.

Theoretical estimates of pure water scattering available in the literature show some differences (Morel, 1974; Shifrin, 1988; Buiteveld et al., 1994). The main cause of the differences is the assumed value of the depolarization ratio δ for water molecules. For example, the estimates by Morel (1974) were obtained with $\delta=0.09$ and those of Buiteveld et al. (1994) with $\delta=0.051$. The lower values of δ result in lower estimates of scattering (e.g., Jonasz and Fournier, 2007; Twardowski et al., 2007). On the basis of the study by Farinato and Roswell (1975), Jonasz and Fournier (2007) suggested that an adequate value of δ may be as low as 0.039. The theoretical estimates for lower values of δ were also shown to be closer to the experimental estimates of pure water scattering reported in Morel (1974). However, considering all the factors involved in the theoretical or experimental determinations, one may deduce that any particular approach or data set of pure water and pure seawater scattering available in the literature can involve uncertainties up to several percent. This level of uncertainty has particularly large impact on estimating particle backscattering from measurements of total backscattering in clear ocean waters where pure seawater contribution usually dominates the total backscattering signal. These issues are discussed in Morel (2007) and in greater detail in Twardowski et al. (2007).

In this study, we applied two sets of pure seawater scattering values, one representing the theoretical estimates from Morel (1974), and the other based on the procedure described in Buiteveld et al. (1994). The Morel (1974) values have commonly been used in the past, including the processing of backscattering measurements, and these values are also built-in the HOBI Labs Hydrosoft software as one standard option. The Morel (1974) spectral values of $\beta_w(140^\circ, \lambda)$ were calculated as $\beta_w(140^\circ, \lambda_o) \times (\lambda_o/\lambda)^{4.32}$ using $\beta_w(140^\circ, \lambda_o) = 2.18 \times 10^{-4} \text{ m}^{-1} \text{ sr}^{-1}$ at a reference wavelength $\lambda_o = 525 \text{ nm}$. $\beta_w(140^\circ, 525)$ was determined from scattering at 90° using the value of

$\beta_w(90^\circ, 525) = 1.46 \times 10^{-4} \text{ m}^{-1} \text{ sr}^{-1}$ (from Table 4 in Morel, 1974) and the depolarization ratio $\delta = 0.09$ (see Eq. (10) in Morel, 1974). We note that these determinations represent water temperature $T = 20^\circ\text{C}$ and salinity $S = 35\text{--}39\text{‰}$. In this study, the application of backscattering data to the POC algorithm development is focused on the use of surface values of b_b and b_{bp} at 555 nm, which is a nominal wavelength of the green band on the Sea-viewing Wide Field-of-view Sensor (SeaWiFS) that provides satellite imagery of ocean color. At this wavelength, Morel's estimate of b_{bw} is $9.22 \times 10^{-4} \text{ m}^{-1}$.

The original formulas for pure water scattering given in Buiteveld et al. (1994) assume $\delta = 0.051$ and allow the calculations as a function of water temperature at salinity $S = 0$. The pure seawater scattering can then be calculated for any salinity using the multiplicative adjustment factor of $[1 + 0.3S/37]$ (Twardowski et al., 2007). We made such calculations for surface waters at each station where our backscattering measurements were taken, using measured values of T and S (see Buiteveld et al., 1994 and Twardowski et al., 2007 for a complete set of equations). For $\lambda = 555 \text{ nm}$, the resulting Buiteveld et al. values of pure seawater backscattering coefficient b_{bw} are, on average, $8.748 \times 10^{-4} \text{ m}^{-1}$ (standard deviation, $\text{SD} = 6.1 \times 10^{-6}$, $N = 59$). The small variation about the average value is associated mainly with the encountered range of surface water temperature from about 13.3°C to 29.2°C , and to a lesser extent with the range of salinity from about 33.9 to 37.1‰. Note that the average value of $b_{bw}(555)$ based on Buiteveld et al. (1994) procedure with the salinity adjustment is about 5% lower than the $b_{bw}(555)$ estimate from Morel (1974). The use of the Buiteveld et al. values increases our estimates of $b_{bp}(555)$ by over 20% for the clearest waters within the South Pacific Subtropical Gyre and by about 2% for the Chilean upwelling stations. For other stations with intermediate levels of particle load in water, this increase ranges generally from about 3% to 10%. One of the POC algorithms analyzed in this study utilizes backscattering measurements at 555 nm (Sect. 3.3.2). For this algorithm, we report results based on both the Buiteveld et al. and Morel estimates of b_{bw} . Otherwise, the reported backscattering results are based on the use of Buiteveld et al. values of b_{bw} unless specifically noted.

For each waveband, backscattering data also require a correction for attenuation of light (so-called " σ -correction"). This correction was made with the parameter K_{bb} estimated from the relation $K_{bb} = a_p + a_{\text{CDOM}} + 0.4b_p$ (HydroSoft software ver. 2.71) employing independent determinations of the spectral absorption coefficient by particles, $a_p(\lambda)$, spectral absorption coefficient by CDOM, $a_{\text{CDOM}}(\lambda)$, and spectral scattering coefficient by particles, $b_p(\lambda)$. For BIOSOPE, these absorption and scattering estimates were obtained from measurements with ac-9 instruments (Twardowski et al., 1999; 2007). The spectral absorption measurements were corrected for the scattering error by subtracting the signal measured at 715 nm from the measurements at all other ac-9 wavelengths. In cases where backscattering spectral

bands did not match those of the ac-9, ac-9 data were linearly interpolated with respect to wavelength to enable the σ -correction. For the ANT-XXIII/1 cruise, the estimates of $a_{\text{CDOM}}(\lambda)$ and $a_p(\lambda)$ were obtained from high spectral resolution measurements on discrete water samples with a point-source integrating cavity absorption meter, PSICAM (Röttgers et al., 2005; Röttgers and Doerffer, 2007). The PSICAM absorption measurements and in situ beam attenuation measurements with C-Stars at 488 and 660 nm were used to obtain b_p values. Accurate measurements of beam attenuation at as little as two wavelengths were shown to provide a good basis for determinations at other wavelengths in the visible spectral region (Boss et al., 2001). The power function fit was applied to our measurements at 488 and 660 nm to produce the spectral data of $c(\lambda) - c_w(\lambda)$, and hence $b_p(\lambda) = c(\lambda) - c_w(\lambda) - a_p(\lambda) - a_{\text{CDOM}}(\lambda)$. The magnitude of σ -correction of backscattering for both cruises was small, generally $<0.5\%$ (maximum of 4.5–5% for the blue wavelengths at upwelling stations off Chile).

After calculation of σ -corrected $b_b(\lambda, z)$, the profile data were split into down- and upcasts, inspected for quality, smoothed, and averaged into depth bins (0.5 or 1 m). Because significant fluctuations in the measured signal were often observed at the shallowest depths, data in the near surface were not used in subsequent analyses. Surface values of backscattering were determined for each cruise by averaging over the same depth range as used for determining surface beam attenuation coefficient (4–6 m for BIOSOPE, 6–8 m for ANT-XXIII/1). After additional quality control, the surface data were typically calculated by averaging the down- and upcast values.

As we have not measured $b_b(555)$ (note that our closest measured nominal wavelength is 550 nm), our final estimates of $b_b(555)$ were obtained from the power function fit applied to our spectral data of $b_b(\lambda)$. Because $b_b(\lambda)$ is expected to be generally a smooth monotonic function of λ , especially in the absence of intense phytoplankton blooms, the use of final backscattering values from the spectral power fit has an advantage of smoothing out potential positive and negative uncertainties that may be present in the measured data at individual spectral channels (for example, calibration uncertainties or the influence of a large particle on a single sensor channel). In the calculations of spectral fits b_b vs. λ , we excluded data measured at 671 nm to avoid the potential effect of contamination of the backscattering signal within this waveband by chlorophyll-*a* fluorescence. For $\lambda=550$ nm, the values from the power fit were higher, on average, by $\sim 3\%$ than the measured values for the BIOSOPE data set. For ANT-XXIII/1 the agreement between these values was within 0.5%.

The final backscattering results for the BIOSOPE cruise were obtained by averaging results from separate pre-cruise and post-cruise calibrations, which minimized the effect of the differences between these calibrations. These differences were fairly significant. For example, the final $b_b(555)$ based

on averaging results from both calibrations are higher, on average, by $\sim 4\%$ than the pre-cruise calibration-based estimates. For $b_{bp}(555)$ these differences are larger (average $\sim 10\%$ and maximum $\sim 25\%$ within the SPSG waters). For the ANT-XXIII/1 cruise, a post-cruise calibration was used.

2.4 Ancillary analysis of discrete water samples

The supplementary data on the bulk particulate properties used in this study include the dry mass concentration of suspended particulate matter, SPM, and the chlorophyll-*a* concentration. During ANT-XXIII/1, SPM samples were obtained from Niskin bottles and the particulate matter was collected by filtration of 6 to 11 L of seawater on precombusted (450°C for 4 h), prewashed (purified water), and pre-weighed glass-fiber filters (Whatman GF/F, diameter 47 mm) using a protocol described in Van der Linde (1998). This protocol includes careful rinsing of filters with distilled water after filtration to remove salts. The particle mass determinations were made after the cruise with a microbalance (Sartorius Type BP210 D, resolution 0.01 mg). During BIOSOPE, a similar method was employed with the exception that 25 mm GF/F filters were used and the filters were not prewashed. The lack of prewashing could have led to underestimation of SPM because of possible loss of filter fibers during filtration (as discussed in Sect. 3.1). At BIOSOPE stations triplicate samples were prepared for SPM determinations by filtering 1.5 to 8.4 L of seawater. The filters were frozen until later gravimetric analysis in laboratory. This analysis was made with a Metler-Toledo MT5 microbalance (resolution 0.001 mg). The average coefficient of variation for triplicate samples was 13%.

In addition, at several BIOSOPE stations east of Easter Island replicate samples for SPM were collected from Niskin bottles, including the “dregs” (i.e., sample below spigot), by opening the bottom stopcock and passing the water through a screen with a pore size of $153\ \mu\text{m}$. The particulate samples were then collected on pre-weighed $0.4\ \mu\text{m}$ polycarbonate filters of 47 mm diameter (Poretics). After filtration, the Poretics filters were also rinsed with distilled water to remove salts, and frozen until gravimetric analysis in laboratory (Fisher Scientific accu-124D balance, 0.01 mg resolution). The SPM determinations on Poretics filters represents the only analysis of discrete water samples in which the dregs were included. For other analyses, samples were drawn from the spigot. For several stations where SPM samples were collected on both GF/F filters and Poretics filters that included the dregs, no systematic differences between the two determinations were observed.

The BIOSOPE samples for phytoplankton pigments were analyzed by HPLC (High Performance Liquid Chromatography) with a modified version of the method of Van Heukelem and Thomas (2001) as described in Ras et al. (2007). From this analysis we here use the surface concentrations of total chlorophyll-*a* (TChl-*a*), which represents the summed

contributions of monovinyl chlorophyll-*a* (MVChl-*a*), divinyl chlorophyll-*a* (DVChl-*a*), chlorophyllide-*a* (Chlide), and the allomeric and epimeric forms of chlorophyll-*a*. For the ANT-XXIII/1 cruise, surface concentration of chlorophyll-*a* was measured with both HPLC (Van Heukelem and Thomas, 2001) and fluorometric methods (Holm-Hansen et al., 1965; Trees et al., 2002) in the Center for Hydro-Optics & Remote Sensing (CHORS) laboratory at San Diego State University. Later analysis revealed that the CHORS HPLC system resulted in an overestimation of TChl-*a* (C. Trees, personal communication). To obtain the corrected estimate of TChl-*a* we applied the following equations to the original (uncorrected) estimates of major components of TChl-*a*: MVChl-*a*(corrected) = 0.598 MVChl-*a*(uncorrected) + 0.0073 and DVChl-*a*(corrected) = 0.655 DVChl-*a*(uncorrected) + 0.0003. The corrections for MVChl-*a* and DVChl-*a* were developed with field data used in the SeaHARRE-3 intercalibration experiment (C. Trees, personal communication). The surface data from ANT-XXIII/1 show the relationship between the corrected HPLC-derived TChl-*a* and the fluorometric Chl-*a*: TChl-*a* = 0.6738 Chl-*a*(fluorometric) + 0.00633 (determination coefficient $R^2=0.981$, 59 data pairs for surface samples). Such difference between the HPLC and fluorometric determinations is within the range of previous observations (Bianchi et al., 1995; Reynolds et al., 2001). In this study we present the HPLC-derived TChl-*a* data.

2.5 Temporal correspondence of various measurements

On the ANT-XXIII/1 cruise, the deployments of SPMR, IOP instrument package, and CTD-rosette for water sampling usually took less than 1 h. The SPMR and CTD-rosette were usually deployed simultaneously and the IOPs were measured either just before or after the CTD-rosette. Throughout the cruise these deployments were made between noon and 2 p.m. local time. Time differences between the acquisition of relevant data on the BIOSOPE cruise are larger than on ANT-XXIII/1 because of specific logistics and research program of BIOSOPE. During BIOSOPE the reflectance measurements with HyperPro instrument were taken, on average, at about 12:30 p.m. local time (SD=1.5 h), the backscattering measurements at 1:40 p.m. (SD=2 h 15 min), and the CTD-rosette casts (sampling for surface POC and measurements of beam attenuation) at 2:10 p.m. (SD=2 h 15 min). While recognizing the practical limitations for making perfectly concurrent and co-located measurements of various variables on oceanographic cruises, we assume that our data were collected simultaneously or nearly-simultaneously for the purposes of our correlational analysis. All data were collected at relatively high solar elevation but sky conditions covered a broad range from overcast to clear skies.

3 Results and discussion

3.1 Bulk characteristics of particle assemblages

Figure 2 shows the range of variability for several bulk properties of suspended particulate matter in surface waters along the cruise tracks in the Pacific and Atlantic Oceans. For most parameters the overall range of variability in our data set is determined by the BIOSOPE data. For example, we observed over 20-fold range in POC from about 12 to 270 mg m⁻³ and nearly 100-fold range in TChl-*a* from 0.016 to 1.5 mg m⁻³. The lowest values were measured within the South Pacific Subtropical Gyre (SPSG) and the highest values in the upwelling area off Chile. The POC:TChl-*a* ratio ranged from about 100 at the upwelling stations to over 1000 at the SPSG stations. The Atlantic data fall within the range of BIOSOPE data. During ANT-XXIII/1, POC ranged from 24 to 95 mg m⁻³, TChl-*a* from 0.09 to 0.5 mg m⁻³, and POC:TChl-*a* from 150 to 600.

The characteristic longitudinal variability observed in the BIOSOPE data may be partially attributed to relatively smooth variations in environmental forcing factors such as nutrients, temperature, and mixed layer light levels. These variations result in the trends in plankton biomass indicators (TChl-*a*, POC) and most likely also in phytoplankton physiological responses such as changes in cellular carbon to chlorophyll-*a* ratio. In addition to possible physiological changes in phytoplankton, part of the observed variability in the POC:TChl-*a* ratio can also be attributed to considerable variation in the detailed composition of particulate assemblages, which normally occurs at significant spatial scales across oceanic basins. This variation in particulate assemblages manifests itself, for example, through changes in the species composition of the plankton community, changes in the contributions of phytoplankton and non-phytoplankton particles to total POC, or changes in particle size distribution. All of these changes were observed along the BIOSOPE cruise track (Grob et al., 2007; Ras et al., 2007; Loisel et al., 2006; Stemmann et al., 2007). The HPLC analysis of accessory pigments for the ANT-XXIII/1 cruise (data not shown here) also indicated variation in phytoplankton composition along the latitudinal transect within the eastern Atlantic. We also note that the interplay of all the factors that contribute to the variability in the POC:TChl-*a* ratio underscores the difficulty in directly estimating POC from chlorophyll-*a*.

Our analysis of SPM data from BIOSOPE revealed a possibility of underestimation because these determinations were made on non-pretreated GF/F filters which could have lost some mass during filtration of usually large sample volumes (due to loss of filter fibers). This hypothesis appears to be supported by the regression analysis of SPM vs. POC which shows a significant negative intercept. Specifically, for the entire BIOSOPE data set of surface samples we found that the best fit obtained with a Model II regression is: SPM=2.132 POC−9.839 ($R^2=0.928$, $N=34$). Nearly

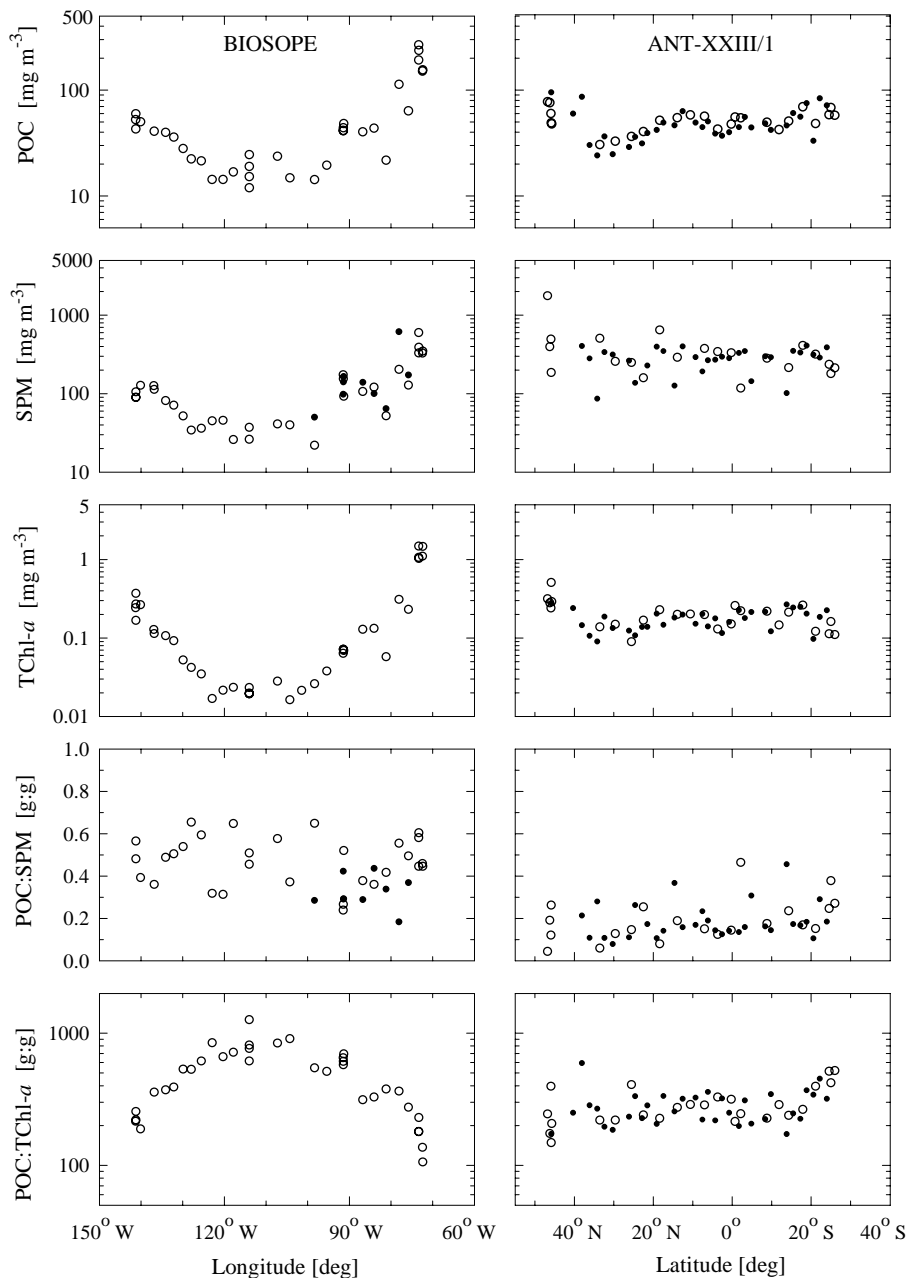


Fig. 2. Bulk characteristics of suspended particulate matter measured on surface samples along the BIOSOPE (left-hand panels) and ANT-XXIII/1 (right-hand panels) cruise tracks. From top to the bottom, the graphs show the concentration of particulate organic carbon (POC), the dry mass concentration of suspended particulate matter (SPM), the total concentration of chlorophyll-*a* derived from HPLC analysis (TChl-*a*), the ratio of POC to SPM, and the ratio of POC to TChl-*a*. For SPM and POC:SPM data from BIOSOPE, the open circles indicate the SPM determinations on GF/F filters and the solid circles on Poretics filters. For ANT-XXIII/1 the open circles indicate data from stations where in situ optical measurements were made, and solid circles indicate data from underway stations which are not included in the correlational analysis presented in this study.

identical fit was obtained when we included additional 15 data pairs from depths between 25 and 195 m. This analysis suggests that SPM could be underestimated, on average, at least by approximately 10 mg m^{-3} . Therefore, our surface

SPM data for BIOSOPE presented in Fig. 2 were corrected by adding a value of 9.839 mg m^{-3} to the original determinations of SPM.

Although accurate measurements of SPM in clear waters such as those within the SPSG are very difficult, we can assume that the final data of SPM and POC:SPM ratio in Fig. 2 reveal the main features of variability during the BIOSOPE cruise as well as between the BIOSOPE and ANT-XXIII/1 cruises. The range of SPM on BIOSOPE was from about 20 to 600 mg m⁻³ and that for ANT-XXIII/1 from about 100 to 650 mg m⁻³. The exception was one measurement in the Bay of Biscay with a much higher particle load (SPM≈1770 mg m⁻³). It is noteworthy that the POC:SPM ratio is generally higher for BIOSOPE than ANT-XXIII/1. The POC:SPM ratio varies from about 0.24 to 0.65 for BIOSOPE (based on the corrected SPM determinations on GF/F filters) and from 0.044 to 0.46 for ANT-XXIII/1. Whereas the average value for this ratio is 0.47 (SD=0.11) for the BIOSOPE cruise, it is only 0.19 (SD=0.09) for ANT-XXIII/1.

The variability in POC:SPM indicates that there was variation in the composition of particulate matter in terms of relative contributions of organic and inorganic particles to SPM. Under the assumption that POC comprises 40–50% of the total mass of particulate organic matter POM (e.g., Copin-Montégut, 1980; Honjo et al., 1995), the contribution of organic material to SPM can be roughly estimated. The relatively high values of POC:SPM data on BIOSOPE suggest the general dominance of POM in total particulate mass (from over 50% to more than 90%). Even if the POC:SPM ratios for BIOSOPE are still overestimated to some degree due to incomplete correction for SPM underestimation, the notion about the dominance of organic matter appears to be robust. The POC:SPM data on ANT-XXIII/1 indicate more variable scenarios. At the northernmost station located in the Bay of Biscay, the estimate of POM contribution to SPM is as low as 9–11%. The ANT-XXIII/1 samples from nine other stations with locations extending southward as far as about 18° N suggest a relatively small role of organic matter in particulate mass concentration. The POC:SPM ratios of 0.06–0.128 correspond to the contributions of POM to SPM of ≤33% at these stations. These results are consistent with observations indicating that these oceanic waters may be affected by atmospheric deposition of mineral dust transported from Africa, especially from the Sahara desert (Sarhou et al., 2003). The other extreme cases on ANT-XXIII/1 are found at a few stations south of equator which show high values of POC:SPM (~0.46), thus indicating that POM likely accounts for >90% of SPM. It is also important to note that biogenic calcite particles, which include mainly coccolithophores and associated detached coccoliths (e.g., Milliman, 1993; Balch et al., 1999), could affect the above considerations in a sense that these particles contribute to SPM, but not to POM estimated from POC.

Summarizing the POC:SPM data set, we note that particulate organic matter was not always a dominant component of the total particulate matter in terms of mass. As our data include several open ocean stations in the Atlantic with the pos-

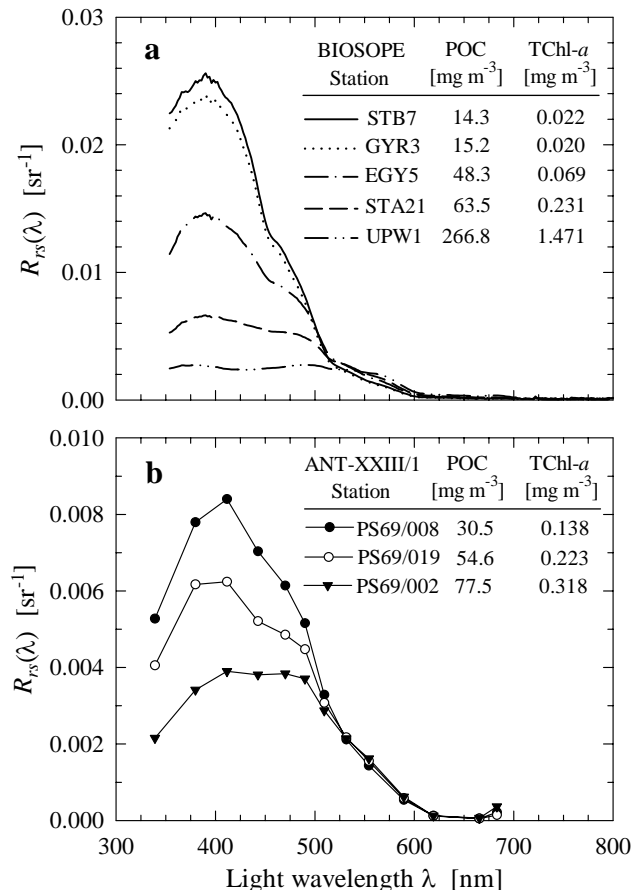


Fig. 3. Example spectra of remote-sensing reflectance, $R_{rs}(\lambda)$, measured on the BIOSOPE (a) and ANT-XXIII/1 (b) cruises at stations with different levels of surface particulate organic carbon (POC) and chlorophyll-*a* (TChl-*a*) concentrations. The name of the station and the POC and TChl-*a* concentrations are indicated.

sibility of significant contribution of non-biogenic inorganic particles to SPM, we cannot assume that all the data considered in this study satisfy the traditional bio-optical definition of the so-called Case 1 waters (Morel and Prieur, 1977; Gordon and Morel, 1983). Another point to be emphasized from the considerations presented in this section is that although our present data set for developing POC algorithms is restricted in terms of number of data points and geographic coverage, it does represent a range of variability associated with changes in both the detailed composition of particulate assemblages and the physiological status of phytoplankton communities, which occur typically in surface waters across oceanic basins.

3.2 Reflectance band ratio algorithm for POC

Figure 3 illustrates characteristic variations in remote-sensing reflectance, $R_{rs}(\lambda)$, associated with differences in

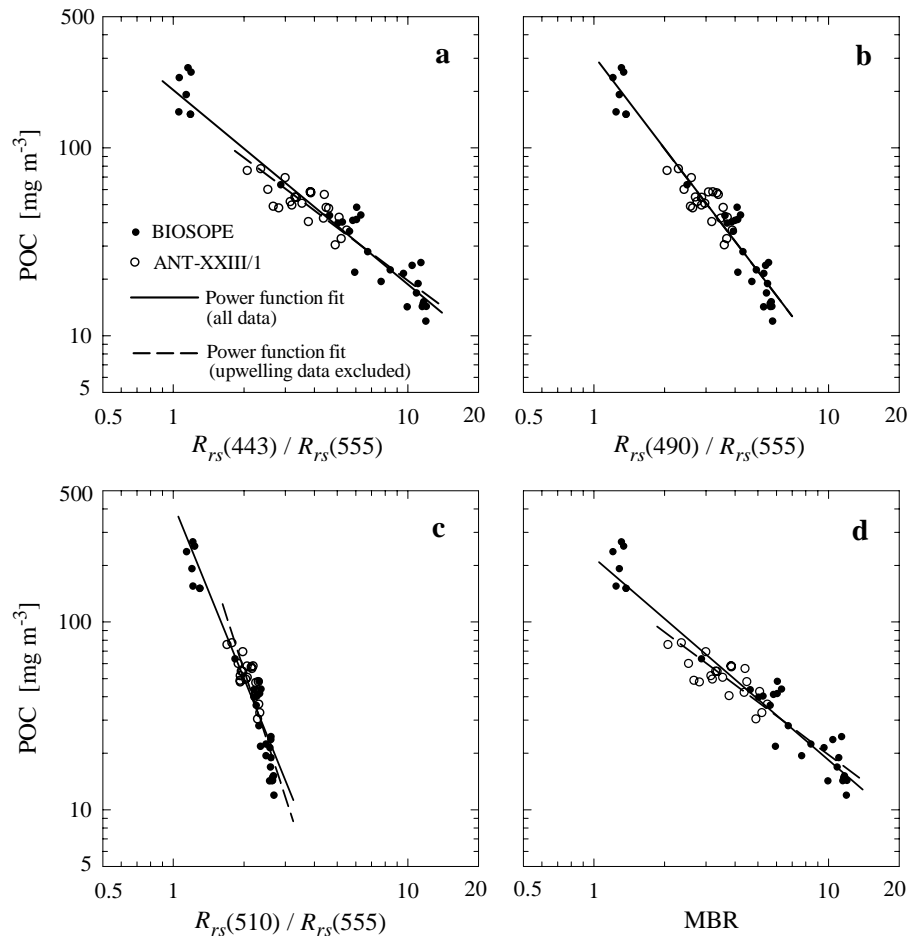


Fig. 4. Relationships between surface concentration of particulate organic carbon, POC, and the blue-to-green band ratio of remote-sensing reflectance, $R_{rs}(\lambda_B)/R_{rs}(555)$. The light wavelength λ_B is either 443 nm (a), 490 nm (b), or 510 nm (c), and MBR (d) is the maximum band ratio which refers to the maximum value of the three band ratios considered. The data points for the BIOSOPE and ANT-XXIII/1 cruises and the power function fits to all data (solid lines) and the limited data sets with Chilean upwelling stations excluded (dashed lines) are shown in all panels. Note that the solid and dashed lines are indistinguishable from one another in (b) (see Table 2 for regression coefficients and error statistics).

POC and TChl-*a* concentrations. The most pronounced variation in $R_{rs}(\lambda)$ occurs in the blue spectral region, whilst variation in the green wavebands is relatively small. For the selected BIOSOPE stations shown in Fig. 3a, we observe about 7-fold decrease in $R_{rs}(\lambda)$ at 443 nm and 1.5-fold increase at 555 nm, which is accompanied by nearly 20-fold increase in POC and 70-fold increase in TChl-*a*. The $R_{rs}(\lambda)$ spectra corresponding to low POC or low TChl-*a* show higher blue-to-green (B-G) band ratios of $R_{rs}(\lambda)$ than those corresponding to higher POC and TChl-*a*. Similar observations have long been recognized as a basis for the development of empirical algorithms for estimating chlorophyll-*a* concentration from ocean color observations (Clarke et al., 1970; O'Reilly et al., 1998). Such algorithms rely primarily on the fact that variations in $R_{rs}(\lambda)$ at blue wavelengths are driven largely by

changes in the absorption coefficient of seawater due to varying concentration of pigment-containing phytoplankton and covarying biogenous matter, especially in the open ocean or Case 1 waters.

A similar reasoning can be applied to the estimation of POC from the B-G reflectance ratio by assuming that this ratio is driven largely by absorption associated with all POC-containing particles. Although the spectral absorption properties differ among various types of organic particles such as detritus, heterotrophic organisms, and phytoplankton, it is notable that they all exhibit a common feature of increased absorption from the green toward the blue spectral region. Thus, a sizable increase in the concentration of any type of particles containing organic carbon is expected to exert a qualitatively similar effect in a sense that an increase in

Table 1. Equations used for calculating error statistics. P_i is the variable predicted from the regression fit, for example the predicted POC concentration (in mg m^{-3}), O_i the measured variable, for example the measured POC concentration (in mg m^{-3}), \bar{O} the mean value of measured variable, R^2 the determination coefficient, RMSE the root mean square error (in units of the measured and predicted variable), MNB the mean normalized bias (in percent), NRMS the normalized root mean square error (in percent), N the number of observations, and m the number of coefficients in the fit.

Determination coefficient	$R^2 = 1 - \frac{\sum_{i=1}^N (P_i - O_i)^2}{\sum_{i=1}^N (O_i - \bar{O})^2}$
Root mean square error	$\text{RMSE} = \left[\frac{1}{N-m} \sum_{i=1}^N (P_i - O_i)^2 \right]^{\frac{1}{2}}$
Mean normalized bias	$\text{MNB} = \frac{1}{N} \sum_{i=1}^N \left(\frac{P_i - O_i}{O_i} \right) 100$
Normalized root mean square error	$\text{NRMS} = \left[\frac{1}{N-1} \sum_{i=1}^N \left(\frac{P_i - O_i}{O_i} - \frac{\text{MNB}}{100} \right)^2 \right]^{\frac{1}{2}} 100$

POC will be accompanied with a decrease in the B-G reflectance band ratio. In addition to this first order effect due to concentrations of organic particles and their general absorption features in the blue-green spectral region, there will be variations in the optical properties between particle types and variations in the detailed composition of particle assemblages, which are expected to introduce some variability in the relationship between POC and the B-G ratio. Earlier tests of such empirical relationship were, however, highly encouraging (Stramska and Stramski, 2005).

Figure 4 shows the relationships between POC and the B-G band ratios of remote-sensing reflectance, $R_{rs}(\lambda_B)/R_{rs}(555)$, where $\lambda_B=443, 490, \text{ or } 510 \text{ nm}$, and MBR is the maximum band ratio of the three band ratios considered. Here the wavelengths of 443, 490, 510, and 555 nm are used for consistency with SeaWiFS wavebands. However, these relationships may be applicable to other satellite sensors with similar bands, for example Moderate-Resolution Imaging Spectroradiometer (MODIS) bands 9, 10, and 12 that are centered approximately at 442, 487, and 547 nm. The formulas used for calculating the error statistics for the various relationships examined in this study are provided in Table 1. All regression analyses presented in the figures and tables represent Model I regression, as this type of regression model is suitable for the analysis of experimental data whose aim is to provide predictive relationships between two variables (Sokal and Rohlf, 1995). The summary of regression parameters and the resulting error statistics for the relationships from Fig. 4 are given in Table 2.

A power function provides a good fit to our data of POC vs. reflectance band ratios with the determination coefficient, R^2 , close to 0.9 for $R_{rs}(443)/R_{rs}(555)$, $R_{rs}(490)/R_{rs}(555)$, and MBR. The error statistics also indicate a capability for achieving relatively good estima-

tion of POC from these band ratios. For example, the empirical algorithm POC vs. $R_{rs}(443)/R_{rs}(555)$ is characterized by a mean normalized bias (MNB) of 2.26% and the normalized root mean square error (NRMS) of 21.68%. These errors are similar if $R_{rs}(490)/R_{rs}(555)$ or MBR are used instead of $R_{rs}(443)/R_{rs}(555)$, but noticeably higher if $R_{rs}(510)/R_{rs}(555)$ is used. The relationship POC vs. $R_{rs}(510)/R_{rs}(555)$ has the additional shortcoming of a small dynamic range of the band ratio.

We suggest that the best POC algorithms based on our data set are the power functions relating POC to $R_{rs}(443)/R_{rs}(555)$ or $R_{rs}(490)/R_{rs}(555)$. The $R_{rs}(443)/R_{rs}(555)$ data exhibit a broader dynamic range than $R_{rs}(490)/R_{rs}(555)$ and the slope of POC vs. $R_{rs}(443)/R_{rs}(555)$ is less steep than that for POC vs. $R_{rs}(490)/R_{rs}(555)$, that is -1.034 for the former relationship and -1.639 for the latter relationship. These two relationships are reasonably consistent with previous determinations based on the use of historical POC and $R_{rs}(\lambda)$ from several oceanic regions (Stramska and Stramski, 2005). For example, in that earlier study the A and B coefficients of the power function POC vs. $R_{rs}(443)/R_{rs}(555)$ were 196.16 and -1.114 , respectively. These values are close to 203.2 and -1.034 obtained in this study (see Table 2). Because our field data imply that the algorithms utilizing $R_{rs}(443)/R_{rs}(555)$ or $R_{rs}(490)/R_{rs}(555)$ have similar performance, we recommend that the choice of particular reflectance band ratio for the use in satellite applications should be based on the expected accuracy of the satellite-derived reflectances and band ratios (see Bailey and Werdell, 2006).

The majority of POC measurements in the present data set are lower than 100 mg m^{-3} , with only six higher values obtained in the Chilean upwelling waters (BIOSCOPE stations UPW and UPX). We examined the influence of these stations

Table 2. Summary of fitted equations and error statistics for the POC band ratio algorithms depicted in Fig. 4. Power functions $POC=A_i [R_{rs}(\lambda_B)/R_{rs}(555)]^{B_i}$ (where $R_{rs}(\lambda_B)/R_{rs}(555)$ is the blue-to-green band ratio of remote-sensing reflectance, POC is in mg m^{-3} , and A_i and B_i are regression coefficients) were fitted by least squares linear regression analysis using \log_{10} -transformed data of POC and $R_{rs}(\lambda_B)/R_{rs}(555)$. All regression coefficients and statistical parameters have been recalculated to represent the non-transformed data. The light wavelength λ_B is either 443, 490, or 510 nm and MBR is the maximum band ratio which refers to the maximum value of the three band ratios considered. R^2 is the determination coefficient, RMSE the root mean square error, MNB the mean normalized bias, NRMS the normalized root mean square error, and N the number of observations (see Table 1 for statistical formulas).

POC= $A_1 [R_{rs}(\lambda_B)/R_{rs}(555)]^{B_1}$ for all data:							
$R_{rs}(\lambda_B)/R_{rs}(555)$	A_1	B_1	R^2	RMSE [mg m^{-3}]	MNB [%]	NRMS [%]	N
$R_{rs}(443)/R_{rs}(555)$	203.2	-1.034	0.871	21.29	2.26	21.68	53
$R_{rs}(490)/R_{rs}(555)$	308.3	-1.639	0.906	18.38	2.28	21.71	52
$R_{rs}(510)/R_{rs}(555)$	423.0	-3.075	0.900	18.75	3.22	26.72	53
MBR	219.7	-1.076	0.845	23.54	2.51	22.84	52

POC= $A_2 [R_{rs}(\lambda_B)/R_{rs}(555)]^{B_2}$; same as above but with Chilean upwelling stations removed from the regression analysis (i.e., BIOSOPE stations UPW and UPX excluded):							
$R_{rs}(\lambda_B)/R_{rs}(555)$	A_2	B_2	R^2	RMSE [mg m^{-3}]	MNB [%]	NRMS [%]	N
$R_{rs}(443)/R_{rs}(555)$	169.7	-0.936	0.804	7.85	1.96	20.31	47
$R_{rs}(490)/R_{rs}(555)$	307.5	-1.637	0.771	8.55	2.23	21.44	46
$R_{rs}(510)/R_{rs}(555)$	792.6	-3.828	0.671	10.17	2.76	24.06	47
MBR	168.6	-0.934	0.807	7.85	1.97	20.32	46

on the regression analysis. The regression lines obtained with upwelling stations excluded are similar to those obtained for all data (Fig. 4). For POC vs. $R_{rs}(490)/R_{rs}(555)$, the regression line without upwelling stations is actually indistinguishable from the line based on all data as the A and B coefficients are very similar (see Table 2). Whereas the R^2 values decreased, the MNB and NRMS errors improved slightly after removal of upwelling data points. In conclusion, this analysis suggests that our algorithms based on all BIOSOPE and ANT-XXIII/1 data can be, to first approximation, applicable to vast areas of subtropical and tropical Pacific and Atlantic Oceans ranging from hyperoligotrophic waters where surface POC is less than 20 mg m^{-3} to upwelling waters where POC is on the order of a few hundred milligrams per m^3 . Additional tests (not shown here) indicated that the power function algorithms shown in Fig. 4 and Table 2 provide better fits to our data than other formulations, such as the fourth order polynomial function currently used in the Ocean Chlorophyll (OC4) algorithm (O'Reilly et al., 2000).

It is important to note that the error statistics for the POC algorithms compare favorably with the error statistics for the band ratio chlorophyll algorithms that have been routinely used for many years (Tables 2 and 3). While the modified OC4 fit tuned to our data of TChl- a vs. MBR leads to small improvements of the error statistics compared with the standard OC4, still better fit to our data is provided by a power function. The MNB and NRMS errors for this power func-

tion are very similar to the errors of our best power function algorithms for POC. This result contributes additional support for the use of POC algorithms with the expectation that their performance will be similar to that of chlorophyll algorithms.

Figure 5 illustrates example results obtained with the application of our POC band ratio algorithms to the satellite imagery from SeaWiFS. Global SeaWiFS data spanning the months of January and July 2005 (900 orbits) were processed from observed top-of-atmosphere radiance to remote-sensing reflectance at the native sensor resolution using the standard calibration and atmospheric correction algorithms associated with SeaWiFS Reprocessing 5.1 (Franz et al., 2005). POC was derived from the retrieved satellite R_{rs} using the POC algorithms based on $R_{rs}(443)/R_{rs}(555)$ and $R_{rs}(490)/R_{rs}(555)$ (see the upper part of Table 2, all data). Satellite-derived chlorophyll- a concentration (Chl) was obtained using the OC4 version 4 chlorophyll algorithm of O'Reilly et al. (1998). After screening for clouds, cloud shadows, stray light, high sun glint, atmospheric correction failure, and algorithm failure conditions (e.g., negative R_{rs}), the derived POC and Chl concentrations were spatially and temporally composited into global monthly products at $9.2 \times 9.2 \text{ km}$ equal area bins (Campbell et al., 1995), and then mapped to a 0.083-deg equirectangular projection. Global images of POC obtained with the algorithm utilizing the band ratio $R_{rs}(443)/R_{rs}(555)$ are shown in Fig. 5. These images

are accompanied by histogram distributions that compare the number of occurrences of POC values for both the $R_{rs}(443)/R_{rs}(555)$ algorithm and the $R_{rs}(490)/R_{rs}(555)$ algorithm. The similarity of the distributions for a given month indicate that both algorithms provide similar estimates of POC. The most frequently observed values of POC range from about 30 to 60 mg m^{-3} , but it is notable that the distribution for January 2005 shows a bimodal feature. The POC algorithms provide the added value to satellite observations in terms of the capability for monitoring not only the surface POC reservoir but also the POC:Chl ratio that represents a useful index of oceanic ecosystems. Figure 5 also shows the images of the POC:Chl ratio, which were determined as a ratio of the POC and Chl mapped images. The histogram distributions show that the most frequently observed values of POC:Chl are between 300 and 400 g:g, and that values below 100 or above 1000 are rare. One of the noteworthy features seen in the presented satellite images are the lowest POC and the highest POC:Chl values within the South Pacific Subtropical Gyre, which is especially well-pronounced in January 2005. These satellite-derived results for SPSG are generally consistent with our BIOSOPE measurements that were taken just a few months earlier, as shown in Fig. 2.

3.3 Two-step algorithms for POC

Our two-step algorithm approach consists of combining two relationships or two algorithm components, generally referred to as steps. The first step connects the apparent optical property (AOP) of the ocean with an inherent optical property (IOP) of seawater. The second step connects the seawater constituent concentration with the IOP. In the application of the two-step algorithm, the first step provides a means for estimating IOP from remote-sensing reflectance, and the second step for estimating POC from the IOP. This two-step feature may be particularly useful for developing an understanding of bio-optical variability underlying the algorithms and also offers flexibility in the development of regional or seasonal parameterizations of the algorithms. For example, while the first step can possibly be developed in such a way that it is fairly robust over large oceanic regions or generally weakly dependent on environmental conditions, the second step may require significant tuning to regional or seasonal variability within the ocean.

We examined three different versions of the two-step algorithm. In the first two versions, which can be referred to as two-step empirical approaches, both steps of the algorithm utilize empirical relationships. In the third version, referred to as two-step hybrid approach, a semianalytical model for estimating IOPs from reflectance is used in the first step of the algorithm, and then the empirical relationship is used in the second step of the algorithm.

Specifically, in the first version of our two-step empirical algorithm, the AOP is the blue-to-green reflectance band ratio, $R_{rs}(\lambda_B)/R_{rs}(555)$, which is linked to the particulate

Table 3. Summary of error statistics for the Ocean Chlorophyll 4 (OC4) algorithm tested with the BIOSOPE and ANT-XXIII/1 data. The OC4 algorithm estimates the surface chlorophyll-*a* concentration as $10^{p_1+p_2X+p_3X^2+p_4X^3+p_5X^4}$, where $X=\log_{10}(\text{MBR})$ and MBR is the maximum band ratio of remote-sensing reflectance. The error statistics are shown for the standard OC4v4 algorithm (where v4 stands for version 4) whose regression coefficients are: $p_1=0.366$; $p_2=-3.067$; $p_3=1.93$; $p_4=0.649$; and $p_5=-1.532$ (O'Reilly et al., 2000). For comparison, included are the error statistics for a modified OC4 fit and for the power function fit obtained from the regression analysis applied to the BIOSOPE and ANT-XXIII/1 data. The modified OC4 fit was obtained by fitting the OC4 formula to the data while constraining the regression coefficients to within 50% of the standard OC4v4 coefficients. The modified OC4 coefficients are: $p_1=0.472$; $p_2=-3.549$; $p_3=2.843$; $p_4=0.3245$; and $p_5=-1.768$. The power function fit to our data is $\text{TChl-}a=1.8814 \text{ MBR}^{-1.8233}$. R^2 is the determination coefficient, RMSE the root mean square error, MNB the mean normalized bias, NRMS the normalized root mean square error, and N the number of observations (see Table 1 for statistical formulas).

	R^2	RMSE [mg m^{-3}]	MNB [%]	NRMS [%]	N
Standard OC4	0.930	0.094	2.85	35.78	51
Modified OC4	0.912	0.105	-2.64	28.96	51
Power function	0.937	0.089	2.35	22.60	51

beam attenuation coefficient, $c_p(660)$. In the second step of the algorithm, POC is linked to $c_p(660)$. This approach has been previously examined with data from the north polar Atlantic and it was used to study surface POC in that region with satellite observations (Stramska and Stramski, 2005).

In the second version of our two-step empirical algorithm, the AOP and IOP quantities are both at a single waveband in the green spectral region. In the first step, the remote-sensing reflectance, $R_{rs}(555)$, is linked to the backscattering coefficient, $b_b(555)$, and in the second step POC is linked to particulate backscattering, $b_{bp}(555)$. This type of two-step algorithm to estimate POC from ocean reflectance has been previously proposed and tested with satellite data in the Southern Ocean (Stramski et al., 1999).

Finally, in the hybrid version of our two-step algorithm, we tested two semianalytical models for estimating the backscattering coefficient, $b_b(555)$, from remote-sensing reflectance. The semianalytical models are thus used as a first step of the hybrid algorithm. The second step of the algorithm is simply represented by the empirical relationship between POC and $b_{bp}(555)$. We note that the hybrid approach may, in principle, be also applicable to the two-step algorithm involving the beam attenuation coefficient as an IOP. Attempts to develop reflectance inversion models for estimating particle beam attenuation have been undertaken (Roesler and Boss, 2003), but this approach is not tested in our study.

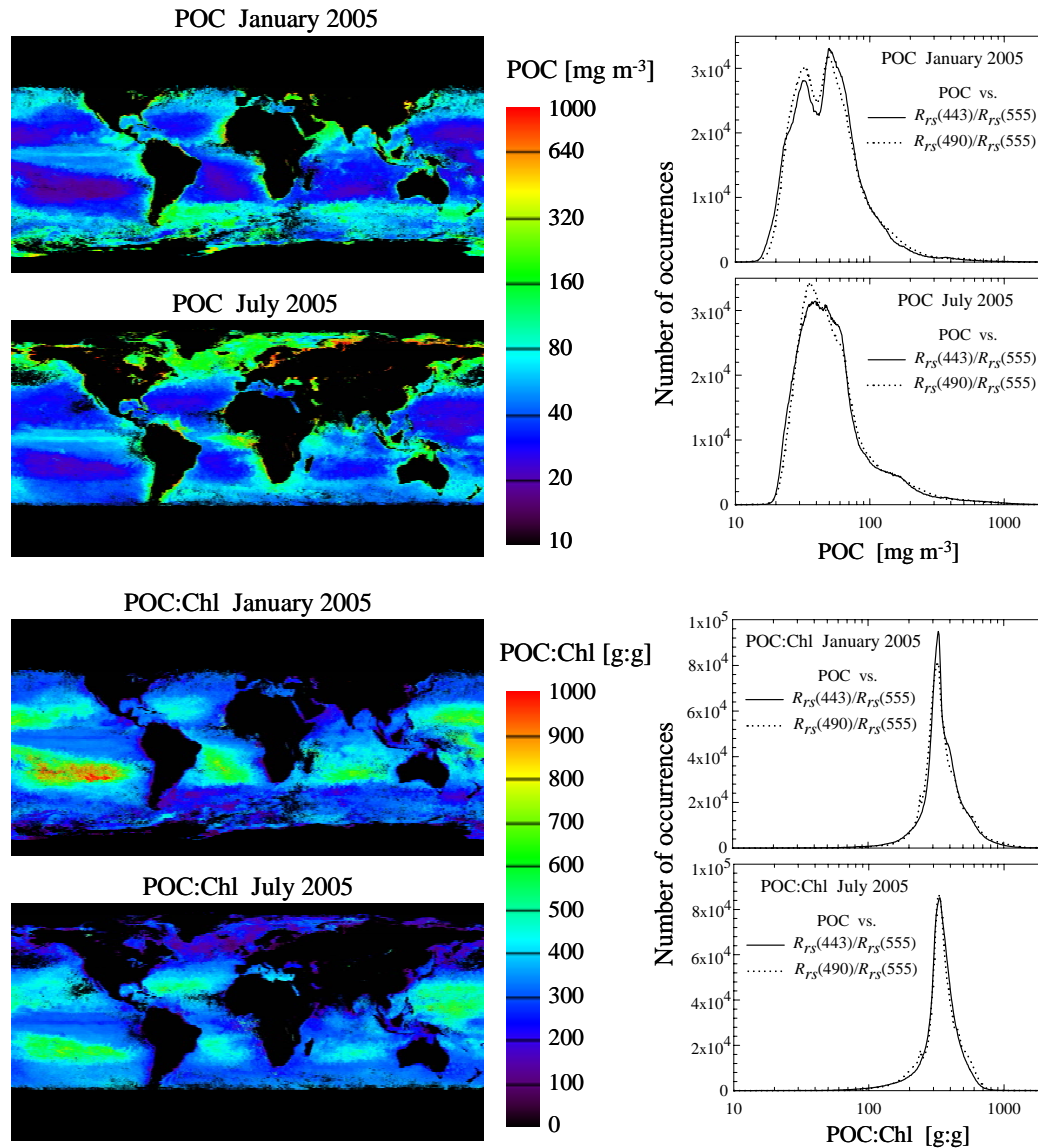


Fig. 5. Monthly composite images (left-hand panels) of surface concentration of particulate organic carbon (POC) and the POC-to-chlorophyll-*a* ratio (POC:Chl). The images were derived from satellite observations with SeaWiFS in January 2005 and July 2005 (see text for details). POC images are presented in a logarithmic scale from 10 to 1000 mg m⁻³ and the POC:Chl images are linearly scaled from 0 to 1000 (g:g). The images were derived using the POC algorithm based on $R_{rs}(443)/R_{rs}(555)$. The histogram distributions corresponding to each image are presented in right-hand panels. For comparison, additional histograms obtained using the POC algorithm based on $R_{rs}(490)/R_{rs}(555)$ are shown. All histograms were created using bins of constant width (0.005) for the log-transformed variables of POC and POC:Chl.

3.3.1 Reflectance band ratio vs. beam attenuation approach

Figures 6 and 7 illustrate a two-step empirical approach to the POC algorithm development, which involves $R_{rs}(\lambda_B)/R_{rs}(555)$ as an AOP and $c_p(660)$ as an IOP. Our data show that $c_p(660)$ can be estimated from $R_{rs}(\lambda_B)/R_{rs}(555)$ (Fig. 6). As indicated by the error statistics in Table 4, the best results are obtained when

$R_{rs}(443)/R_{rs}(555)$ or maximum-band ratio (MBR) are used. In these cases the MNB values are below 3% and the NRMS below 25%. We point out that $c_p(660)$ can be reasonably well estimated from $R_{rs}(\lambda_B)/R_{rs}(555)$ using a single relationship derived from our entire data set covering waters from hyperoligotrophic to upwelling areas. This is noteworthy as it suggests that the relationship between $c_p(660)$ and $R_{rs}(\lambda_B)/R_{rs}(555)$ can represent a fairly robust component

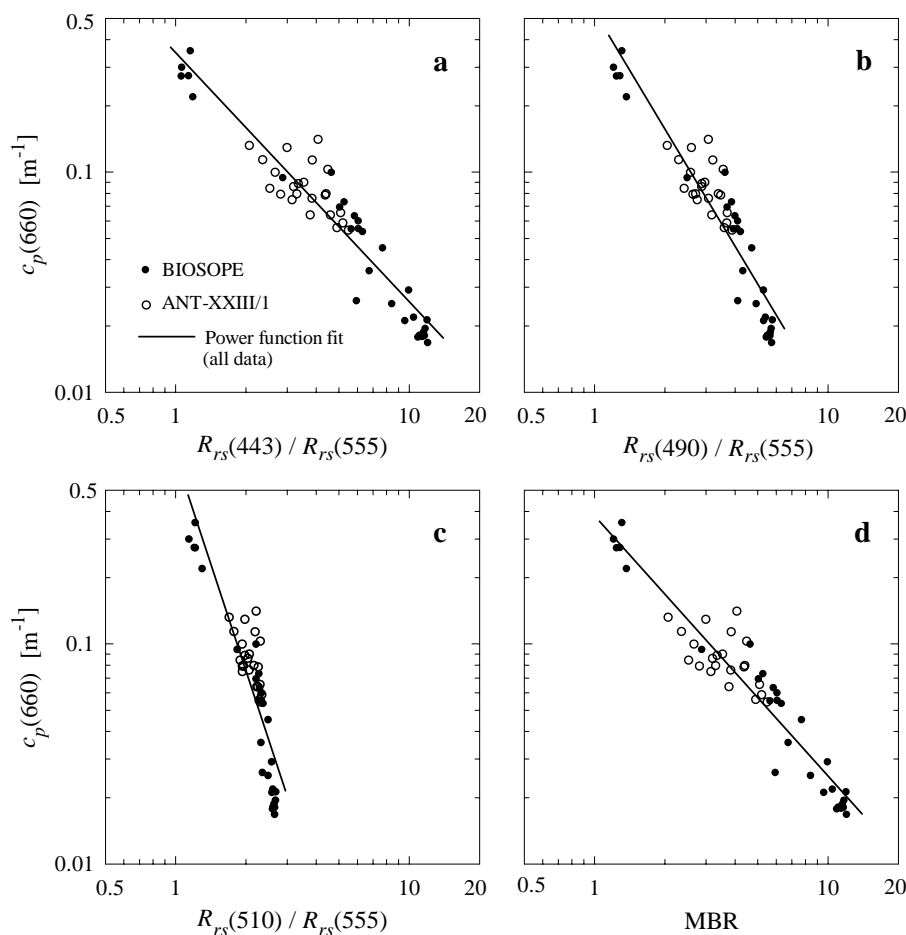


Fig. 6. Relationships between surface values of the particulate beam attenuation coefficient, $c_p(660)$, and the blue-to-green band ratio of remote-sensing reflectance, $R_{rs}(\lambda_B)/R_{rs}(555)$. The light wavelength λ_B is either 443 nm (a), 490 nm (b), or 510 nm (c), and MBR (d) is the maximum band ratio which refers to the maximum value of the three band ratios considered. The data points for the BIOSOPE and ANT-XXIII/1 cruises and the power function fits to all data are shown in all panels (see Table 4 for regression coefficients and error statistics).

of the two-step POC algorithm. Such robustness may appear somewhat surprising because variations in $c_p(660)$ are driven primarily by particle scattering in the red part of the spectrum and variations in $R_{rs}(\lambda_B)/R_{rs}(555)$ by particle and CDOM absorption in the blue part of the spectrum. It is apparently a high degree of covariation of these processes within our data set that explains this result. We also note that previous analysis of data from the north polar Atlantic suggested that this relationship can show little sensitivity to regional and seasonal bio-optical variability (Stramska and Stramski, 2005; Stramska et al., 2006). Both the previous and present results indicate that the $c_p(660)$ vs. $R_{rs}(\lambda_B)/R_{rs}(555)$ relationship represents a promising component of the two-step POC algorithm, which requires attention in future research.

The data for the second relationship of the two-step algorithm, POC vs. $c_p(660)$, show that a linear function provides a reasonably good fit to our entire data set (Fig. 7). This

fit has MNB of about -3% and NRMS of about 25% (Table 4). We also examined the regression POC vs. $c_p(660)$ with the five upwelling data pairs excluded. This resulted in a decrease in the slope and an increase of the intercept of the linear fit. The slope of ~ 460 (units are mg C m^{-2}) for our fit with no upwelling data is within the range reported for different regions of the world's oceans (Gardner et al., 2006). The slope of ~ 660 based on all our data including the five upwelling data pairs is similar to the steepest slope in the data set of Gardner et al. (2006), which was observed by those investigators in the Ross Sea. The relatively steep slopes ($\sim 500\text{--}585$) were also previously observed in tropical and equatorial Pacific waters (Claustre et al., 1999; Behrenfeld and Boss, 2006; Gardner et al., 2006). On the basis of 3462 data pairs from eight regions (not including the Ross Sea), Gardner et al. (2006) determined the average slope of ~ 380 , which is smaller than the estimates in the present study. Unlike our analysis, however, the Gardner et al. database is not

Table 4. Summary of fitted equations and error statistics for the two-step empirical POC algorithm depicted in Figs. 6 and 7. The coefficients C_1 and C_2 of power function (i.e., step 1 equation) were obtained from least squares linear regression analysis using \log_{10} -transformed data of $c_p(660)$ and $R_{rs}(\lambda_B)/R_{rs}(555)$. The regression coefficients and statistical parameters have been recalculated to represent the non-transformed data. The ordinary least squares linear regression was applied to calculate the coefficients D_1 and D_2 of the step 2 equation. $c_p(660)$ is in m^{-1} and POC is in mg m^{-3} . R^2 is the determination coefficient, RMSE the root mean square error, MNB the mean normalized bias, NRMS the normalized root mean square error, and N the number of observations (see Table 1 for statistical formulas).

Step 1 equation: $c_p(660) = C_1 [R_{rs}(\lambda_B)/R_{rs}(555)]^{C_2}$							
$R_{rs}(\lambda_B)/R_{rs}(555)$	C_1	C_2	R^2	RMSE [m^{-1}]	MNB [%]	NRMS [%]	N
$R_{rs}(443)/R_{rs}(555)$	0.349	-1.131	0.896	0.0243	2.93	24.45	52
$R_{rs}(490)/R_{rs}(555)$	0.536	-1.771	0.836	0.0308	3.99	28.38	51
$R_{rs}(510)/R_{rs}(555)$	0.704	-3.224	0.702	0.0412	7.12	39.56	52
MBR	0.382	-1.182	0.906	0.0233	2.91	24.55	51

Step 2 equation: $\text{POC} = D_1 c_p(660) + D_2$							
	D_1	D_2	R^2	RMSE [mg m^{-3}]	MNB [%]	NRMS [%]	N
All data	661.9	-2.168	0.934	12.95	-2.98	24.98	59
Upwelling data excluded	458.3	10.713	0.888	6.68	4.63	21.29	54

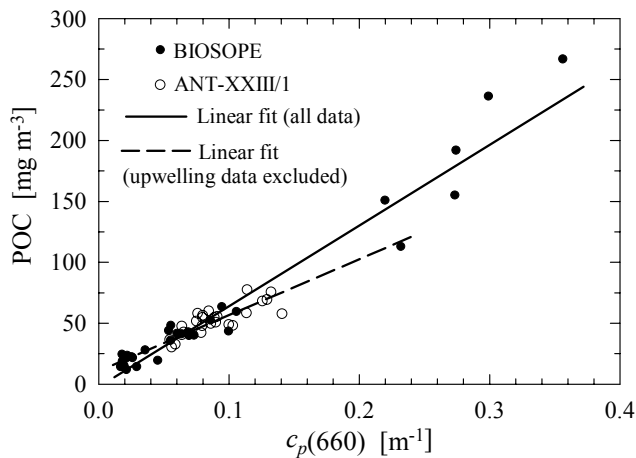


Fig. 7. Relationship between surface concentration of particulate organic carbon, POC, and particulate beam attenuation coefficient, $c_p(660)$. The data points for the BIOSOPE and ANT-XXIII/1 cruises and the linear function fits to all data (solid line) and the limited data sets with Chilean upwelling stations excluded (dashed line) are shown (see Table 4 for regression coefficients and error statistics).

limited to surface data but includes the upper ocean layer to a depth of about 250 m. It is possible that the variability observed in that large data set is associated not only with regional differentiation but also partly with vertical variations (see also Loisel and Morel, 1998).

Another factor that deserves attention in such comparative analysis is the potential difference in the estimates of the measured beam attenuation coefficient obtained with various types of commercial or custom-built beam transmissometers that have different acceptance angle for the detector. This is a critical technical parameter for measuring beam attenuation. Although the effective acceptance angle should be as small as practically possible, differences exist between instrument models. Instruments with larger acceptance angles are expected to provide lower estimates of beam attenuation, i.e., larger underestimation of true beam attenuation, compared with instruments with smaller acceptance angles. Unfortunately, manufacturers often do not provide information on the effective acceptance angle in the specifications of commercial beam transmissometers.

The aggregate error statistics for the two-step algorithm depicted in Figs. 6 and 7 are reasonably good regardless of whether or not the Chilean upwelling data are included in the analysis (Table 5). The differences in carbon-specific beam attenuation coefficient, $c_{p,\text{POC}}^*(660)$, within our data set are generally small. For BIOSOPE the average $c_{p,\text{POC}}^*(660)$ is $1.46 \times 10^{-3} \text{ m}^2 (\text{mg C})^{-1}$ ($\text{SD}=3.9 \times 10^{-4}$, $N=34$). Nearly identical average is obtained for that cruise with five upwelling data excluded. For ANT-XXIII/1, the average $c_{p,\text{POC}}^*(660)$ is $1.69 \times 10^{-3} \text{ m}^2 (\text{mg C})^{-1}$ ($\text{SD}=2.7 \times 10^{-4}$, $N=25$). We note, however, that the potential differentiation of the POC vs. $c_p(660)$ relationship in surface oceanic waters could be used as a basis for developing region- or season-specific parameterizations of the two-step algorithm.

Table 5. Summary of aggregate error statistics for the composite representation of the two-step empirical POC algorithm depicted in Figs. 6 and 7. The composite formulation of the algorithm is: $POC = D_1 \{C_1 [R_{rs}(\lambda_B)/R_{rs}(555)]^{C_2}\} + D_2$. The coefficients C_1 and C_2 of the step 1 equation and the coefficients D_1 and D_2 of the step 2 equation are given in Table 4. POC is in mg m^{-3} , R^2 is the determination coefficient, RMSE the root mean square error, MNB the mean normalized bias, NRMS the normalized root mean square error, and N the number of observations (see Table 1 for statistical formulas).

All data:					
$R_{rs}(\lambda_B)/R_{rs}(555)$	R^2	RMSE [mg m^{-3}]	MNB [%]	NRMS [%]	N
$R_{rs}(443)/R_{rs}(555)$	0.889	18.07	-5.43	23.28	52
$R_{rs}(490)/R_{rs}(555)$	0.875	19.31	-5.36	21.84	51
$R_{rs}(510)/R_{rs}(555)$	0.823	22.79	-4.56	24.84	52
MBR	0.885	18.54	-5.01	24.74	51
BIO SOPE upwelling data excluded:					
$R_{rs}(\lambda_B)/R_{rs}(555)$	R^2	RMSE [mg m^{-3}]	MNB [%]	NRMS [%]	N
$R_{rs}(443)/R_{rs}(555)$	0.793	8.26	4.25	25.20	47
$R_{rs}(490)/R_{rs}(555)$	0.777	8.64	3.62	28.23	46
$R_{rs}(510)/R_{rs}(555)$	0.638	10.91	3.17	35.73	47
MBR	0.794	8.32	5.46	24.65	46

3.3.2 Single-wavelength reflectance vs. backscattering approach

The relationships of the two-step empirical algorithm utilizing a single wavelength of 555 nm are shown in Fig. 8. In this green spectral region absorption by most particle types is weak. Therefore, one may expect that the variation in $R_{rs}(555)$ will be often driven largely by changes in the backscattering coefficient $b_b(555)$, and to a lesser degree by absorption, especially in clear oceanic waters. Overall, however, as a result of interplay of absorption and backscattering we observe relatively small changes in $R_{rs}(555)$ with an increase in POC compared to changes in R_{rs} at the blue wavelengths (see Fig. 3). This type of POC algorithm based on single-wavelength reflectance offers the potential benefit of decoupling the estimation of POC from the estimation of chlorophyll-*a* that is based on the B-G band ratio of reflectance. There are, however, limitations of the single-wavelength algorithm, especially for satellite applications. Specifically, this algorithm will be highly sensitive to the accuracy of the magnitude of satellite-derived reflectance, and the required accuracy may not be easily achieved on a routine basis. This requirement is generally not as critical when reflectance band ratios are used. Also, whereas the single-wavelength two-step algorithm is characterized by a relatively small dynamic range of R_{rs} in the green spectral region, the B-G band ratio algorithm is characterized by a

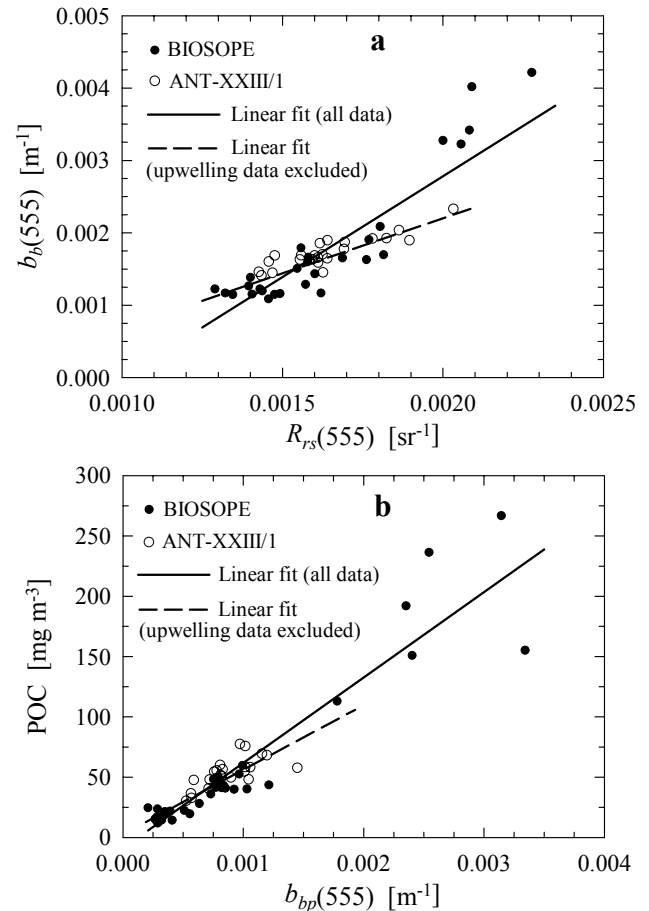


Fig. 8. (a) Relationship between surface values of the backscattering coefficient, $b_b(555)$, and remote-sensing reflectance, $R_{rs}(555)$. (b) Relationship between surface concentration of particulate organic carbon, POC, and particulate backscattering coefficient, $b_{bp}(555)$. The data points for the BIOSOPE and ANT-XXIII/1 cruises and the linear function fits to all data (solid lines) and the limited data sets with Chilean upwelling stations excluded (dashed lines) are shown in both panels (see Table 6 for regression coefficients and error statistics).

larger dynamic range due to large variations in R_{rs} at blue wavelengths in response to variations in POC (see Fig. 3).

In the application of the single-wavelength empirical algorithm, the backscattering coefficient $b_b(555)$ is first determined from $R_{rs}(555)$ (Fig. 8a), and then POC is estimated from $b_{bp}(555)$, where $b_{bp}(555) = b_b(555) - b_{bw}(555)$ (Fig. 8b). The regression coefficients and error statistics for these relationships are presented in Table 6, which includes results for two estimates of pure seawater backscattering coefficient, $b_{bw}(555)$, one based on Buiteveld et al. (1994) with the salinity adjustment and the other based on Morel (1974). The step 1 relationship is nearly the same for both versions of $b_{bw}(555)$, because the final estimates of $b_b(555)$ show very

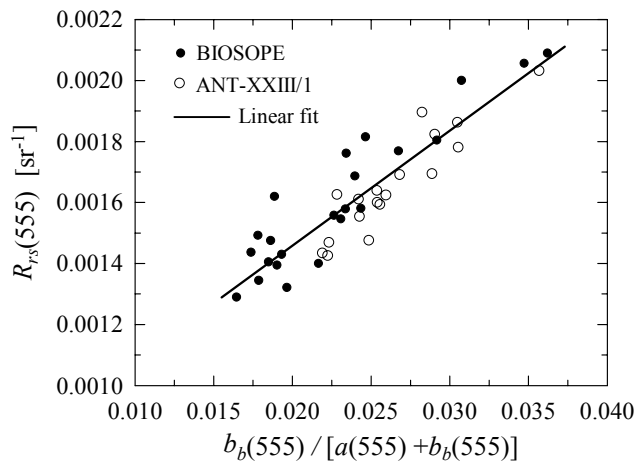


Fig. 9. Relationship between remote-sensing reflectance, $R_{rs}(555)$, and the ratio of absorption to the sum of absorption and backscattering coefficients, $b_b(555)/[a(555)+b_b(555)]$. The data points for the BIOSOPE and ANT-XXIII/1 cruises and the linear function fit to all data are shown. The equation of the fit is: $R_{rs}(555)=0.03771 b_b(555)/[a(555)+b_b(555)]+7.04\times 10^{-4}$ (coefficient of determination $R^2=0.822$, number of observations $N=41$). At the limit of pure seawater, the results of this regression analysis within 95% confidence interval are consistent with radiative transfer simulations.

small changes due to the variation in the assumed values of $b_{bw}(555)$. The effect of $b_{bw}(555)$ on the step 2 relationship involving $b_{bp}(555)$ is noticeable, especially for the intercept coefficient, albeit still small. The aggregate error statistics calculated from the composite formula of the two-step algorithm are nearly the same for both estimates of $b_{bw}(555)$ but show relatively large errors which caution against indiscriminate use of this algorithm (Table 6). The separate relationships of the two-step algorithm are examined in greater detail below to address this problem. In this analysis, we discuss the results obtained using the $b_{bw}(555)$ values based on Buiteveld et al. (1994) with the salinity adjustment.

The relationship $b_b(555)$ vs. $R_{rs}(555)$ is significantly influenced by five data points collected in the Chilean upwelling waters, where $b_b(555)$ exceeded 0.003 m^{-1} (Fig. 8a). As a result, the regression line calculated from all data points provides an inadequate representation of the patterns present in the entire data set. This is clear even though the statistical characteristics of this fit have reasonably good values (Table 6). The relevant observation is that upwelling waters show reduced reflectance compared with the expectation from the general trend line for all non-upwelling data points. This effect can be further examined by noting that the upwelling values of $R_{rs}(555)$, which are close to or slightly above the value of 0.002 sr^{-1} , are associated with higher values of $b_b(555)$ compared to a station from the ANT-XXIII/1 cruise (PS69/027) with a similar value of $R_{rs}(555)$. This

suggests that, in addition to differences in $b_b(555)$, there were also significant differences in the absorption coefficient $a(555)$ between the Chilean upwelling stations and the station PS69/027 (which is the southernmost station on the ANT-XXIII/1 cruise, located at 25.97° S , 9.37° E). The absorption data confirm this expectation. Whereas $a(555)$ at PS69/027 was 0.063 m^{-1} , the values at the upwelling stations ranged from about 0.09 to 0.107 m^{-1} ; higher by a factor of 1.4–1.7 compared with PS69/027. Importantly, very similar factors are found for $b_b(555)$ that was about 0.0023 m^{-1} at PS69/027 and 0.0033 – 0.0042 m^{-1} at the upwelling stations. Because $R_{rs}(\lambda)$ is driven primarily by the ratio $b_b(\lambda)/[a(\lambda)+b_b(\lambda)]$, and because $b_b(\lambda)$ is typically much smaller than $a(\lambda)$, similar parallel changes in $b_b(555)$ and $a(555)$ lead to the similar values of $R_{rs}(555)$ for the upwelling stations and the PS69/027 station seen in Fig. 8a. These results are further supported in Fig. 9, where $R_{rs}(555)$ plotted against $b_b(555)/[a(555)+b_b(555)]$ follow approximately one linear relationship, albeit some scatter in the data exists. Importantly, the three rightmost data points in Fig. 9 (two of which are BIOSOPE upwelling stations and one is PS69/027) are close to one another. We also note that $b_b(555)$ was never more than 3.8% of $a(555)$ in our data set, and that the highest $b_b(555)/a(555)$ was observed at the BIOSOPE upwelling station (UPW1).

The main conclusion from Fig. 8a is that the determination of a single empirical relationship of $b_b(555)$ vs. $R_{rs}(555)$ over a range of oceanic conditions is impossible. Similar $R_{rs}(555)$ values can be observed when large differences in $b_b(555)$ and POC occur. For the selected stations with similar $R_{rs}(555)$ in our data set, POC was 58 mg m^{-3} at the PS69/027 station and 150 – 270 mg m^{-3} at the upwelling stations (TChl-*a* was also significantly different; 0.11 mg m^{-3} and 1 – 1.5 mg m^{-3} , respectively). Comparable limitation for the direct empirical estimation of b_b from R_{rs} has been observed previously in the Southern Ocean (Stramski et al., 1999), where data collected within a bloom of *Phaeocystis antarctica* ($\text{POC}>800\text{ mg m}^{-3}$) were characterized by significantly higher backscattering coefficient compared to other data at similar $R_{rs}(555)$ values of 0.002 – 0.003 sr^{-1} . Such limitation is due to possible considerable effect of variation in $a(555)$ on $R_{rs}(555)$. This is seen for the entire data set presented in Fig. 8a, where the maximum-to-minimum ratio of $b_b(555)$ is about 3.9, and the analogous ratio for $a(555)$ is 1.8, which implies a significant effect of variation in $a(555)$ on $R_{rs}(555)$. With the upwelling stations excluded, however, these ratios are 2.4 for backscattering and 1.3 for absorption (or 1.7 and 1.08, respectively, if only the ANT-XXIII/1 data are considered). Because the data with upwelling stations excluded show smaller effect of $a(555)$, the estimation of $b_b(555)$ from $R_{rs}(555)$ is improved (see the statistics for Step 1 equation in Table 6). Therefore, the use of a single empirical relationship $b_b(555)$ vs. $R_{rs}(555)$ may perhaps be justifiable over a limited range of oceanic conditions in relatively clear waters where $\text{POC}\leq 100\text{ mg m}^{-3}$.

Table 6. Summary of fitted equations and error statistics for the two-step empirical POC algorithm depicted in Fig. 8. Least squares linear regression analysis was applied to calculate the coefficients E_1 , E_2 , F_1 , and F_2 . R^2 is the determination coefficient, RMSE the root mean square error, MNB the mean normalized bias, NRMS the normalized root mean square error, and N the number of observations (see Table 1 for statistical formulas). $b_b(555)$, $b_{bp}(555)$, and $b_{bw}(555)$ are in m^{-1} , POC is in mg m^{-3} , and $R_{rs}(555)$ in sr^{-1} . The results were obtained with pure seawater backscattering values, $b_{bw}(555)$, calculated according to Buiteveld et al. (1994) with the salinity adjustment (see text for details). These values vary slightly in our data set with water temperature and salinity, but the average $b_{bw}(555)=8.748 \times 10^{-4} \text{ m}^{-1}$ can be used in the application of this two-step algorithm with no significant impact on its performance. For comparison, the results obtained with $b_{bw}(555)=9.22 \times 10^{-4} \text{ m}^{-1}$ from Morel (1974) are also shown.

Step 1 equation: $b_b(555) = E_1 R_{rs}(555) + E_2$								
	b_{bw}	E_1	E_2	R^2	RMSE [m^{-1}]	MNB [%]	NRMS [%]	N
All data	Buiteveld	2.787	-0.002792	0.783	0.0003254	1.48	17.38	51
All data	Morel	2.785	-0.002794	0.783	0.0003251	1.48	17.41	51
Upwelling data excluded	Buiteveld	1.521	-0.000843	0.689	0.0001671	1.24	11.89	46
Upwelling data excluded	Morel	1.520	-0.000846	0.690	0.0001665	1.24	11.88	46

Step 2 equation: $\text{POC} = F_1 b_{bp}(555) + F_2$, where $b_{bp}(555) = b_b(555) - b_{bw}(555)$								
	b_{bw}	F_1	F_2	R^2	RMSE [mg m^{-3}]	MNB [%]	NRMS [%]	N
All data	Buiteveld	70850.7	-9.088	0.863	18.66	1.02	28.28	59
All data	Morel	71002.0	-5.500	0.863	18.62	1.16	27.99	59
Upwelling data excluded	Buiteveld	53606.7	2.468	0.777	9.32	5.28	24.29	54
Upwelling data excluded	Morel	53932.4	5.049	0.778	9.30	5.33	24.34	54

Composite equation of the two-step algorithm: $\text{POC} = F_1 [E_1 R_{rs}(555) + E_2 - b_{bw}(555)] + F_2$							
	b_{bw}	R^2	RMSE [mg m^{-3}]	MNB [%]	NRMS [%]	N	
All data	Buiteveld	0.587	35.14	6.90	72.87	51	
All data	Morel	0.586	35.19	7.19	73.04	51	
Upwelling data excluded	Buiteveld	0.655	14.34	15.54	46.43	46	
Upwelling data excluded	Morel	0.653	14.38	15.73	46.71	46	

The second relationship of the two-step algorithm, POC vs. $b_{bp}(555)$, is depicted in Fig. 8b. In this case, several data points collected at upwelling stations with $\text{POC} \geq 150 \text{ mg m}^{-3}$ show significant scatter but do not suggest a clearly different pattern compared with the remaining data. The relationship for the entire data set has acceptable error statistics with MNB of about 1% and NRMS of about 28% (Table 6). The removal of upwelling data from the analysis results in less steep slope; the effect similar to that seen in the POC vs. $c_p(660)$ relationship in Fig. 7. Although the fitted regression coefficients for POC vs. $b_{bp}(555)$ differ between the entire data set and the limited data set with upwelling stations excluded (Table 6), the adoption of a relationship based on all data would at this point appear reasonable, especially considering the limited number of our observations and their distribution with few data collected at inter-

mediate and higher POC. However, one can generally expect that the POC vs. $b_{bp}(555)$, like any POC vs. IOP relationship, may undergo significant variations due to temporal and spatial variability in particulate assemblages of different oceanic regions. Such expectation is supported by earlier observations in the Southern Ocean where $b_{bp}(555)$ was typically higher in the Antarctic Polar Front Zone than in the Ross Sea at similar levels of POC (Stramski et al., 1999), indicating differences in the carbon-specific backscattering coefficient. A definitive judgment of whether the carbon-specific backscattering was different in the water bodies examined during BIOSOPE and ANT-XXIII/1 is difficult with our data but the discussion in Sect. 3.4 provides some insights into this question.

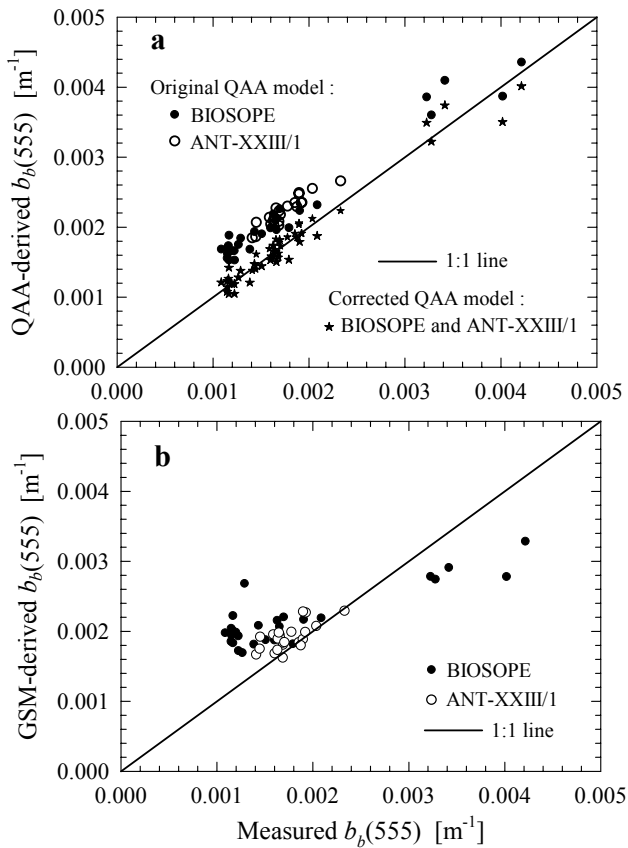


Fig. 10. Particulate backscattering coefficient, $b_b(555)$, derived from a semianalytical model as a function of measured $b_b(555)$ for (a) a semianalytical model of Lee et al. (2002) referred to as QAA, and (b) a semianalytical model of Garver and Siegel (1997) updated by Maritorena et al. (2002), referred to as GSM. Panel (a) shows the results for both the original QAA model and the corrected QAA model (see text and Table 7 for details). The results in panel (b) are for the GSM model.

3.3.3 Two-step hybrid approach

In addition to approaches based exclusively on empirical relationships, we have also examined a two-step approach referred to as a hybrid approach. In the hybrid approach we use a semianalytical model as a means for retrieving $b_b(555)$ from $R_{rs}(\lambda)$ in the first step of the algorithm. The second step of the hybrid algorithm is the same as described above, that is POC is derived from $b_{bp}(555)$ using our empirical relationship from Fig. 8b (see also Table 6).

We examined two semianalytical models that are currently used quite commonly in the area of ocean color research. The first model, referred to as the Quasi-Analytical Algorithm (QAA), was developed by Lee et al. (2002). The second model, referred to as the GSM model (for Garver-Siegel-Maritorena), was initially developed by Garver and Siegel (1997) and later updated by Maritorena et al. (2002). For

examining the QAA model we followed the procedure described in Lee et al. (2006) (Eqs. 10.2, 10.3, 10.6, and 10.7 in that reference). In brief, the diffuse attenuation coefficient for downwelling irradiance, $K_d(555)$, was first estimated from the measured MBR. Then, the absorption coefficient, $a(555)$, was obtained from the measured $R_{rs}(555)$ and the derived $K_d(555)$. Finally, the backscattering coefficient, $b_b(555)$, was obtained from the relationship between $R_{rs}(555)$ and the ratio $b_b(555)/[a(555) + b_b(555)]$. In the evaluation of the GSM model we utilized an IDL code (available at <http://www.icess.ucsb.edu/OCisD/>) with a standard set of parameters optimized for applications to offshore oceanic waters (see Table 2 in Maritorena et al., 2002). In particular, we first retrieved $b_{bp}(443)$ from $R_{rs}(\lambda)$ measured at five wavelengths: 412, 443, 490, 510, and 555 nm. We then calculated $b_{bp}(555)$ using the spectral slope of $\eta=1.0337$ for the particulate backscattering (see Eq. 3c in Maritorena et al., 2002). The sum of $b_{bp}(555)$ and $b_{bw}(555)=0.000922 \text{ m}^{-1}$ yielded the GSM-derived $b_b(555)$. In this case we used $b_{bw}(555)$ from Morel (1974) because Morel's pure seawater backscattering values were used in the development of the GSM model.

Figure 10a compares the QAA-derived $b_b(555)$ with the measured $b_b(555)$. For our entire data set, the QAA provides a systematic overestimation of measured $b_b(555)$. This overestimation is characterized by a nearly constant offset over the examined range of conditions from the gyre to upwelling stations. The linear regression between the measured and QAA-derived $b_b(555)$ (not shown here) has a slope of about 1.05 (which is notably close to 1) and an intercept of $-0.0005541 \text{ m}^{-1}$ ($R^2=0.957$, $N=50$). Using the original QAA-derived backscattering coefficient, $b_{b,\text{original}}(555)$, as inputs to this regression function, we obtained new values of $b_b(555)$ referred to as the corrected QAA-derived backscattering coefficient, $b_{b,\text{corrected}}(555)$. These corrected values are in good agreement with the measurements (Fig. 10a). The error statistics for the derivation of $b_{b,\text{corrected}}(555)$ is very good as MNB is only about 0.4% and NRMS is 7.6% (Table 7). The errors, especially MNB, are obviously much higher for $b_{b,\text{original}}(555)$. Table 7 also demonstrates that the aggregate error statistics is quite satisfactory for the hybrid two-step POC algorithm, in which $b_{b,\text{corrected}}(555)$ is used. On the basis of our data set such POC algorithm has a small MNB of about 0.7%. The NRMS of 33% is significant but still acceptable. Therefore, this type of algorithm has the potential for good performance. However, because the relatively good results were here obtained only after the application of considerable empirical correction (based on our field data) to the original QAA model, further improvements in semianalytical modeling are desirable. We verified, for example, that the estimates of absorption coefficient, $a(555)$, obtained with the QAA model were, on average, lower by about 8% than the measured $a(555)$ in our data set. These tests of absorption retrievals suggest that it was not the absorption component of the QAA model which caused the

Table 7. Summary of error statistics for the two-step hybrid POC algorithm. In step 1, $b_b(555)$ is derived from the Quasi-Analytical Algorithm (QAA) of Lee et al. (2002). Statistics for the original QAA model and for the corrected QAA model are shown. The corrected $b_b(555)$ was obtained from the original QAA-derived $b_b(555)$ using a linear relationship: $b_{b,\text{corrected}}(555) = 1.049 b_{b,\text{original}}(555) - 0.0005541$. Aggregate statistics for the hybrid two-step POC algorithm are also shown, where $b_b(555)$ is obtained in step 1 using the corrected QAA model, and the coefficients F_1 and F_2 are from the step 2 equation given in Table 6. R^2 is the determination coefficient, RMSE the root mean square error, MNB the mean normalized bias, NRMS the normalized root mean square error, and N the number of observations (see Table 1 for statistical formulas). $b_b(555)$ is in m^{-1} , POC is in mg m^{-3} , and the pure seawater backscattering, $b_{bw}(555)$, was calculated according to Buiteveld et al. (1994) with the salinity adjustment (see text for details).

Step 1: $b_b(555)$ calculated from QAA model					
	R^2	RMSE [m^{-1}]	MNB [%]	NRMS [%]	N
Original QAA	0.537	0.0004787	28.47	12.19	50
Corrected QAA	0.957	0.0001467	0.36	7.59	50

Aggregate statistics for the two-step hybrid algorithm: $\text{POC} = F_1[b_{b,\text{corrected}}(555) - b_{bw}(555)] + F_2$					
	R^2	RMSE [mg m^{-3}]	MNB [%]	NRMS [%]	N
	0.871	19.47	0.73	33.02	50

retrievals of $b_b(555)$ to be systematically higher than the backscattering measurements.

The need for further improvements in semianalytical models is also supported by a comparison of GSM-derived $b_b(555)$ with measured $b_b(555)$ in Fig. 10b. Again we see that the semianalytical model does not provide consistently good agreement with the measurements. For our data set, the GSM model shows a tendency to overestimate the measured $b_b(555)$ at low values (especially at the gyre stations) and underestimate the measurements at higher values at the upwelling stations. Such biases that appear to depend on environmental conditions limit the usefulness of the GSM model in its present form in the development of POC algorithms. We note, however, that the GSM model showed significantly better performance for retrieving TChl- a with our data set. In this case, the bias was small (MNB = -3%) although NRMS remained significant at about 35%.

3.4 Variability in particulate backscattering ratio

The relationships between POC and IOPs, such as those presented in Figs. 7 and 8b, are variable in the ocean. The variability in these relationships can be attributed to two causes;

first, variations in the characteristics of particulate assemblage which affect IOPs, such as the particle concentrations and distributions of particle size and refractive index within the assemblage, and second, variations in the distribution of organic carbon among the various particle types and particle size classes within an assemblage. Both Fig. 7 and 8b show that the removal of the upwelling data from the analysis leads to a smaller slope of the POC vs. IOP relationships in our data set. A closer inspection of Fig. 8b also suggests that many non-upwelling BIOSOPE measurements are characterized by higher carbon-specific backscattering of particles than the ANT-XXIII/1 measurements. This is seen in that many BIOSOPE data are below and the ANT-XXIII/1 data are above the regression fit (see the dashed line in Fig. 8b). For the non-upwelling data from BIOSOPE, the average value of the carbon-specific particulate backscattering coefficient, $b_{pp,\text{POC}}^*(555)$, is $1.97 \times 10^{-5} \text{ m}^2 (\text{mg C})^{-1}$ ($\text{SD} = 4.6 \times 10^{-6}$, $N = 29$). For ANT-XXIII/1 the average $b_{pp,\text{POC}}^*(555)$ is $1.66 \times 10^{-5} \text{ m}^2 (\text{mg C})^{-1}$ ($\text{SD} = 2.8 \times 10^{-6}$, $N = 25$).

Although these observations are subject to inevitable uncertainties in the determinations of POC and b_{pp} in clear ocean waters, it is useful to tentatively test the possible differentiation in the carbon-specific backscattering between the two cruises by examining the particulate backscattering ratio, $\tilde{b}_{bp} = b_{pp}(555)/b_p(555)$. The parameter \tilde{b}_{bp} describes the fraction of light scattered by particles in backward directions, and hence it is independent of particle concentration but is sensitive to physicochemical particle properties such as size and refractive index (e.g., Morel and Bricaud, 1986). The potential usefulness of \tilde{b}_{bp} to study composition of marine particulate matter has been examined recently (Twardowski et al., 2001; Boss et al., 2004; Sullivan et al., 2005; Whitmire et al., 2007). Figure 11 compares the surface data of \tilde{b}_{bp} plotted against POC from the BIOSOPE and ANT-XXIII/1 cruises. It is remarkable that the BIOSOPE values of \tilde{b}_{bp} are higher than the ANT-XXIII/1 values. For the BIOSOPE data set the average \tilde{b}_{bp} is 0.0104, whereas for the ANT-XXIII/1 data set it is 0.0054. The higher \tilde{b}_{bp} can generally be associated with an increased role of small-sized particles contributing to b_b (especially those $\leq 1-2 \mu\text{m}$), an increase in the bulk refractive index of particles, or both. Unfortunately, detailed characterization of particle properties required for rigorous analysis of their effects on \tilde{b}_{bp} are not easily or routinely acquired on oceanographic cruises.

Despite these limitations, we can explore the results in Fig. 11 in terms of available information about particle properties in the investigated waters. The data of POC:SPM collected on the BIOSOPE cruise (Fig. 2), the location of the BIOSOPE study area away from terrestrial sources, and low deposition of atmospheric particles suggest the dominance of organic particles. In contrast, some measurements in the Atlantic were likely made on water samples with significant contribution of terrigenous inorganic particles, which is

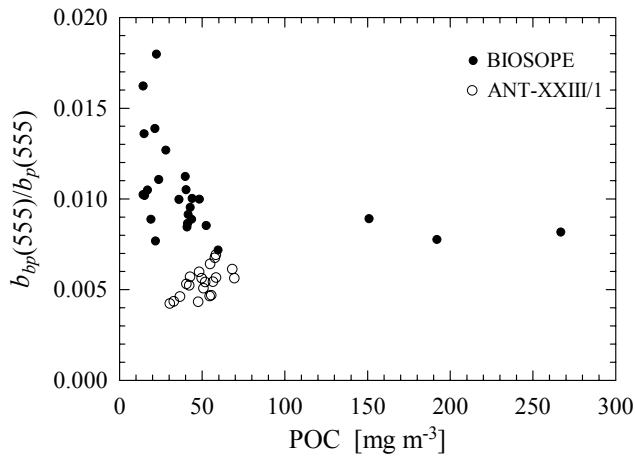


Fig. 11. Particulate backscattering ratio, $b_{bp}(555)/b_p(555)$, plotted as a function of surface concentration of particulate organic carbon, POC, for the BIOSOPE and ANT-XXIII/1 cruises.

indicated by larger range in POC:SPM including low values of this ratio on the ANT-XXIII/1 cruise (Fig. 2). A common assumption is that marine organic particles have generally lower refractive index (relative to water) than inorganic particles (Kerr, 1977; Aas, 1996). We must stress, however, the limitation of this common assumption, which is that the relatively low refractive index of organic particles can be assigned with certainty only to living biological cells that contain significant amount of water (i.e., the so-called “soft” particles). The calcifying algae are the noteworthy exception with higher refractive index because they produce calcite (CaCO_3) scales. The refractive index of non-living organic particles suspended in seawater is poorly understood, mainly because the water content of such particles remains poorly characterized. Nonetheless, if any differences in the bulk refractive index of particulate matter between the BIOSOPE and ANT-XXIII/1 data were to be hypothesized, one could speculate that at least some ANT-XXIII/1 data corresponding to presumably high inorganic contribution (i.e., the stations with the lowest POC:SPM in Fig. 2) would have the highest refractive index. However, the \tilde{b}_{bp} values from ANT-XXIII/1 show relatively small range and are lower than BIOSOPE data, which would suggest that the potential variability in particle refractive index is not the major factor responsible for the differences in \tilde{b}_{bp} between the cruises shown in Fig. 11.

From a refractive index perspective, it is also of interest to consider possible variability in biogenic calcite particles, mainly coccolithophore phytoplankton species and detached coccoliths, which have high refractive index. Balch et al. (1999) estimated that in typical nonbloom conditions suspended coccoliths may account for 10–20% of light backscattering, which indicates that calcite particles are generally an important scattering component in the ocean. The

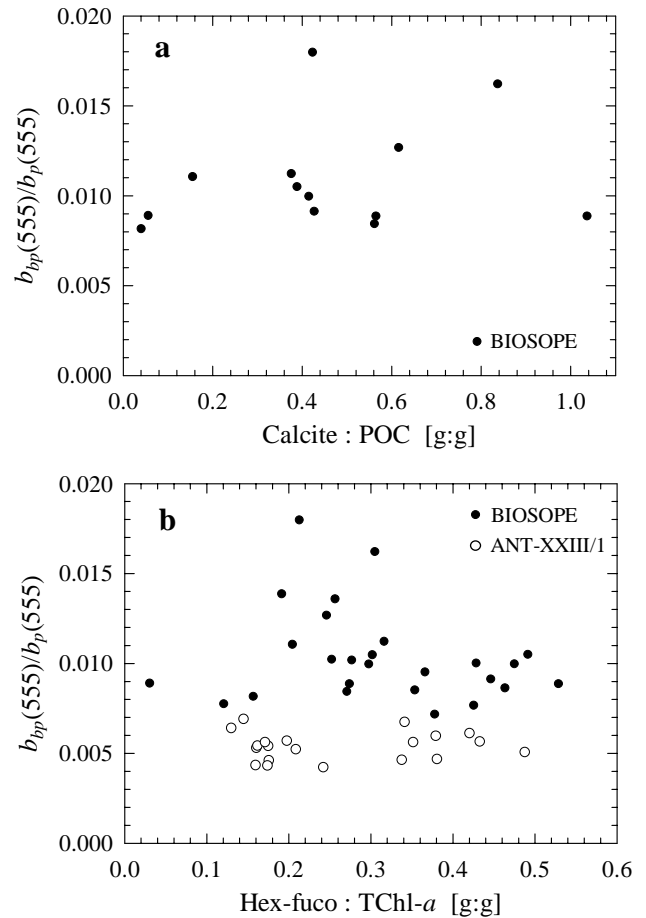


Fig. 12. Particulate backscattering ratio, $b_{bp}(555)/b_p(555)$, plotted as a function of (a) ratio of surface concentration of particulate calcite to POC for the BIOSOPE cruise, and (b) pigment ratio Hex-fuco:TChl-*a* in surface waters for the BIOSOPE and ANT-XXIII/1 cruises. The calcite and pigment data for BIOSOPE are taken from Beaufort et al. (2007) and Ras et al. (2007), respectively.

surface concentration of suspended calcite particles on the BIOSOPE cruise ranged from about 3 to 25 $\text{mg CaCO}_3 \text{ m}^{-3}$ (Beaufort et al., 2007). The lowest values were observed in the gyre and the highest values in the transition zone between the eastern boundary of the gyre and the upwelling stations. These concentrations and the calcite-specific backscattering coefficient that was previously determined to be about $1.37 \times 10^{-5} \text{ m}^2 (\text{mg CaCO}_3)^{-1}$ (Balch et al., 1999, 2001) can be used to obtain estimates of the backscattering coefficient due to calcite particles. These estimates range from about $4 \times 10^{-5} \text{ m}^{-1}$ in the gyre to $3.4 \times 10^{-4} \text{ m}^{-1}$ in the transition zone between the gyre and upwelling area. The values of $b_{bp}(555)$ from measurements in the gyre were between 2.1×10^{-4} and $3.4 \times 10^{-4} \text{ m}^{-1}$ and the higher values in the transition zone were between 1×10^{-3} and $1.8 \times 10^{-3} \text{ m}^{-1}$. These calculations suggest that calcite particles could have

made a significant contribution to particulate backscattering from about 10% to over 30% at some BIOSOPE stations. Such contributions can, in turn, suggest an enhancement of the backscattering ratio due to highly refractive calcite particles. A tendency for $\tilde{b}_{bp}(555)$ to increase with the ratio of calcite concentration to POC concentration in surface waters is unclear for the 13 data pairs available from BIOSOPE, albeit cannot be completely ruled out (Fig. 12a). In this figure, the calcite:POC ratio may be considered as an approximate index for the contribution of calcite particles with high refractive index to the total pool of organic particles, which are characterized by a lower value of the bulk refractive index than that of calcite.

Similar estimation is not possible for ANT-XXIII/1 because no determinations of calcite concentration were made. We can, however, compare BIOSOPE and ANT-XXIII/1 in terms of the 19'-Hexanoyloxyfucoxanthin (Hex-fuco) pigment, which is often used as a diagnostic index for the presence of phytoplankton species from the group of Prymnesiophytes, to which coccolithophores belong (e.g., Vidussi et al., 2001; Ras et al., 2007). Although Hex-fuco is not a unique index of coccolithophores, the concentration of this pigment showed a similar pattern to calcite concentration along the BIOSOPE cruise track (Beaufort et al., 2007; Ras et al., 2007). The range of the pigment ratio Hex-fuco:TChl-*a* is similar for both cruises (with the exception of one data point from the Chilean shelf that has the lowest pigment ratio of 0.03) and \tilde{b}_{bp} shows no tendency to increase with Hex-fuco:TChl-*a* (Fig. 12b). The lack of such tendency is also observed when b_{bp} is plotted vs. Hex-fuco concentration (not shown). Thus these data provide no evidence that coccolithophores could have been responsible for enhanced \tilde{b}_{bp} on BIOSOPE compared with ANT-XXIII/1.

Another factor that can contribute to the differences in \tilde{b}_{bp} between BIOSOPE and ANT-XXIII/1 is the variation in particle size distribution (PSD). PSD data were acquired on BIOSOPE with a Beckman-Coulter Multisizer III equipped with a 30 μm aperture tube and occasionally with a 20 μm tube (Loisel et al., 2006). This instrument setup allowed us to size particles as small as 0.5–0.7 μm . One of the most important results obtained with the particle analysis was a steep slope of PSD, which was observed consistently in the submicrometer size range at oligotrophic and hyperoligotrophic BIOSOPE stations. The slope (ξ) of the power function fit to the PSD data, or more specifically, the slope of the density function of the so-called Junge-type differential size distribution $F(D) \sim D^{-\xi}$, varied typically from 5 to 7 in the submicrometer range for surface samples (Loisel et al., 2006). For particles larger than 1 μm , ξ was usually close to 4 (Stemmann et al., 2007), which is generally consistent with previous PSD data for marine particles (e.g., Bader, 1970).

The steep slopes in the submicrometer range suggest a very large contribution of small particles from colloidal size range to the overall concentration of particles. These small-sized particles are expected to make higher percent contri-

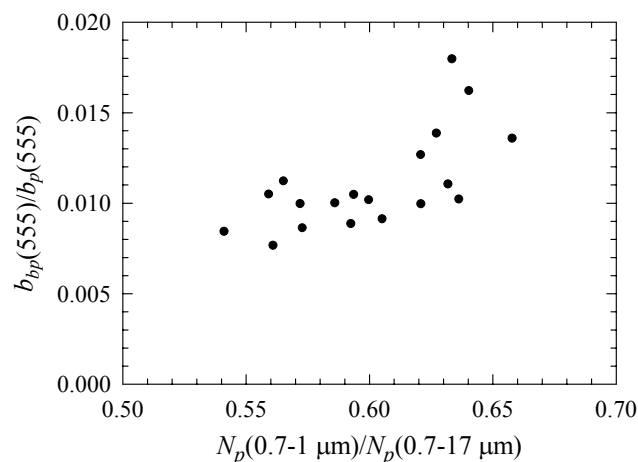


Fig. 13. Particulate backscattering ratio, $b_{bp}(555)/b_p(555)$, plotted as a function of the contribution of submicrometer particles to the total concentration of particles measured on the BIOSOPE cruise with a Beckman Coulter Multisizer III equipped with a 30- μm aperture tube. The submicrometer particles are here represented by the concentration of particles, $N_p(0.7-1 \mu\text{m})$, with equivalent diameter between 0.7 and 1 μm , and the total particle concentration, $N_p(0.7-17 \mu\text{m})$, refers to particles in the size range from 0.7 to 17 μm .

bution to particulate backscattering than to total particulate scattering, so the particulate backscattering ratio \tilde{b}_{bp} is expected to increase with an increased contribution of small particles to total particle concentration (e.g., Stramski and Kiefer, 1991). The effect of an increase in \tilde{b}_{bp} with increasing slope of PSD has been demonstrated explicitly with modeling results based on Mie scattering theory (Twardowski et al., 2001). According to those results, a particle assemblage that covers a broad range of sizes with a single slope ξ somewhat steeper than 4, can easily achieve the backscattering ratio \tilde{b}_{bp} of about 0.01 or higher, even if the relative refractive index of particles is as low as 1.02. Therefore, it is conceivable that the PSDs with particularly steep slopes in the submicrometer range were at least partly responsible for the \tilde{b}_{bp} values close to or above 0.01 in the BIOSOPE data set. For this data set, we observe a tendency for \tilde{b}_{bp} to increase with increasing contribution of submicrometer particles to the total concentration of particles measured with Beckman-Coulter instrument, which is consistent with theoretical predictions (Fig. 13). Unfortunately, no PSD data are available from ANT-XXIII/1 so we cannot ascertain that less steep size distributions, especially in the small-size range, could be one of the main reasons for lower \tilde{b}_{bp} on that cruise.

The question of whether potential errors in the determinations of \tilde{b}_{bp} on the BIOSOPE and ANT-XXIII/1 cruises could lead to the differences shown in Fig. 11 also deserves consideration. We recall that the determinations of $b_{bp}(555)$ were made on both cruises with the same instrumentation, deployment methods, and procedures for data processing.

Therefore, the possibility of significant bias in the $b_{bp}(555)$ estimates for one cruise relative to the other cruise is unlikely, albeit it cannot be excluded. Twardowski et al. (2007) indicated, for example, that measuring dark signal of the backscattering instruments under actual environmental conditions can be critical to ensure high accuracy, especially in very clear waters. We have not measured dark signals in situ; however, for the BIOSOPE cruise we have had available pre-cruise and post-cruise manufacturer's calibrations, which include measurements of dark signals. We verified that the \tilde{b}_{bp} values based on averaging pre-cruise and post-cruise calibrations (shown in Fig. 11) are higher, on average, by about 10% ($\sim 20\%$ at the most) than the values based on pre-cruise calibration. The lower pre-cruise calibration-based values of \tilde{b}_{bp} on the BIOSOPE cruise would still be generally higher than \tilde{b}_{bp} from ANT-XXIII/1.

The estimates of particulate scattering, $b_p(555)$, which also enter the calculations of \tilde{b}_{bp} , were obtained with different methods on the two cruises but again no particular source for bias significant enough to explain differences in Fig. 11 was identified in these determinations. We verified potential differences in the determinations of $b_p(555)$ from ac-9 measurements on BIOSOPE, which can arise from the application of different methods for correcting the absorption measurements for scattering error. For the surface data considered, the use of the proportional method, in which the scattering error is allowed to vary with wavelength (Zaneveld et al., 1994), would result in $b_p(555)$ values higher, on average, by only 3% compared with the values obtained with the simple wavelength-independent scattering correction based on the subtraction of absorption signal measured at 715 nm. We recall that the latter method was used to generate the BIOSOPE data of \tilde{b}_{bp} in Fig. 11. The \tilde{b}_{bp} values calculated with the proportional scattering correction method would be lower, on average, by about 2% (6% at the most) than the data shown in Fig. 11. For the surface data from the BIOSOPE cruise, we have also verified that the estimates of $c-c_w$ from ac-9 tend to be higher than the estimates from C-Star transmissometer, which may result, at least partly, from a smaller acceptance angle of the ac-9 detector compared with that of the C-Star. The possible tendency for higher estimates of $b_p(555)$ from ac-9 compared with C-Star cannot explain the observed differences in \tilde{b}_{bp} between the cruises as ac-9 was used on BIOSOPE and C-Star on ANT-XXIII/1.

Whereas the differences in the backscattering ratio are generally consistent with differences in the carbon-specific backscattering coefficient between the Pacific and Atlantic data sets, the above discussion revealed difficulties in achieving an unambiguous interpretation of these results in terms of available data on particle characteristics and methodological issues. We were unable to identify any obvious methodological issues, but they cannot be ruled out as a possible source of the observed differences in \tilde{b}_{bp} between the cruises. We note that our BIOSOPE estimates of surface \tilde{b}_{bp} tend to

be higher than average estimates of \tilde{b}_{bp} presented in Twardowski et al. (2007) which were determined with a different methodology, namely from measurements with an ECO-BB3 instrument (WET Labs, Inc.). These discrepancies underscore the considerable difficulties in accurate estimation of b_{bp} in clear ocean waters. Nevertheless, the results from Fig. 11 are intriguing and require verification in future experiments. These results suggest differences in the physico-chemical properties of particulate assemblages between the investigated Pacific and Atlantic waters. Such differences could have consequences to the relationships between POC and optical properties, which are seen to some extent in the present data set of POC vs. b_{bp} . These results thus emphasize the need for increased efforts in detailed characterization of particle properties in tandem with optical measurements taken during oceanographic cruises or experiments.

4 Conclusions

We have examined several approaches for estimating surface concentration of POC from optical measurements of remote-sensing reflectance, $R_{rs}(\lambda)$, using field data collected in tropical and subtropical surface waters of the eastern South Pacific and eastern Atlantic Oceans. The approach based on the direct empirical relationship between POC and the blue-to-green band ratio of reflectance, $R_{rs}(\lambda_B)/R_{rs}(555)$, promises reasonably good performance in the vast areas of the open ocean covering different provinces from hyperoligotrophic and oligotrophic waters within subtropical gyres to eutrophic coastal upwelling regimes characteristic of eastern ocean boundaries. The surface POC in our data set ranged from about 10 mg m^{-3} within the South Pacific Subtropical Gyre to 270 mg m^{-3} in Chilean upwelling waters. The measurements of POC:SPM, POC:TChl-*a*, phytoplankton pigments, and the backscattering ratio exhibit a significant range of variation, which indicates that our data set encompasses considerable variation in characteristics of oceanic particulate assemblages. Among the four band ratio algorithms examined, the best error statistics were found for power function fits to the data of POC vs. $R_{rs}(443)/R_{rs}(555)$ and POC vs. $R_{rs}(490)/R_{rs}(555)$ and these algorithms showed little sensitivity to whether or not the Chilean upwelling data were included in the analysis (Fig. 4 and Table 2).

We recommend that these algorithms can now be implemented for routine processing of ocean color satellite data to produce maps of surface POC within the global ocean. The judgment of whether to begin this processing with $R_{rs}(443)/R_{rs}(555)$ or $R_{rs}(490)/R_{rs}(555)$ (or perhaps both algorithms) should probably depend on current understanding of which of these band ratios is retrieved from satellite imagery with consistently better accuracy. Like many ocean bio-optical data products currently derived from satellite ocean color imagery, we expect that the surface POC from our proposed algorithms can have the status of an

evaluation data product for continued work on algorithm development and refinements. There remain significant challenges to ensure consistent accuracy in POC retrievals from reflectance, for example the accurate field determinations of low levels of POC in very clear oligotrophic waters necessary for the algorithm development are themselves very difficult to achieve. We expect, however, that the accuracy of satellite retrievals of POC will be adequate for many applications such as the estimation of large scale or global budgets of surface POC. We also note that our proposed band ratio algorithms have similar regression coefficients to those previously determined from selected historical data sets that included 205 data pairs of POC and reflectance measured in several oceanic regions (Stramska and Stramski, 2005). This good comparison further supports our recommendation to begin processing of satellite ocean color imagery for estimating POC. At this time the use of our algorithms based on the BIOSOPE and ANT-XXIII/1 data appears preferable over additional consideration of historical data because our two data sets ensure a higher degree of consistency of methods used to collect field data for the algorithm development. Nevertheless, because the present amount and geographic coverage of simultaneously collected POC and reflectance data in the field is rather small, the exploration of historical data in the context of POC algorithm development is still worthwhile to pursue.

Other approaches for estimating POC from ocean reflectance that were examined in this study can be referred to as the two-step POC algorithms. In these approaches an IOP is first derived from an AOP (i.e., reflectance measurements) and then POC is derived from an IOP. The potential benefits of this two-step concept include flexibility for developing regionally and/or seasonally parameterized algorithms and insights into bio-optical variability that affects the algorithm relationships. One of our two-step empirical algorithms utilizes the particle beam attenuation coefficient, $c_p(660)$, as an IOP and the blue-to-green reflectance ratio, $R_{rs}(\lambda_B)/R_{rs}(555)$, as an AOP (Figs. 6 and 7, Tables 4 and 5). This algorithm may become particularly attractive if further research supports the robustness of the relationship $c_p(660)$ vs. $R_{rs}(\lambda_B)/R_{rs}(555)$ under various oceanic conditions. The second relationship of the algorithm, POC vs. $c_p(660)$, is generally expected to exhibit regional/seasonal variations due to varying properties of marine particulate assemblages, so it could be utilized as an algorithm component in regional/seasonal parameterizations. In our BIOSOPE and ANT-XXIII/1 data sets, however, such differentiation effects within the POC vs. $c_p(660)$ data were relatively small.

In the other two-step empirical algorithm, we utilized a single wavelength approach with the backscattering coefficients, $b_b(555)$ and $b_{bp}(555)$, as IOPs and remote-sensing reflectance, $R_{rs}(555)$, as an AOP (Fig. 8, Table 6). This algorithm showed less satisfactory error statistics than other algorithms examined in this study, particularly because of characteristically different patterns of upwelling and other

(non-upwelling) data in the $b_b(555)$ vs. $R_{rs}(555)$ relationship. The variability in this relationship indicates a limitation for the use of this algorithm over a broad range of conditions. The potential variability in the step 2 relationship between POC and $b_{bp}(555)$ due to variations in the carbon-specific backscattering also cautions against indiscriminate use of this algorithm and highlights the need for further research to improve an understanding of IOPs in terms of physicochemical characteristics of particulate assemblages. Another limitation of the single-wavelength algorithm for satellite applications arises from the requirement for accurate satellite estimates of the absolute magnitude of $R_{rs}(555)$. This problem may not be as severe when reflectance band ratios are used as input to the algorithms. However, the two-step single-wavelength POC algorithm based on input $R_{rs}(555)$ has potential for decoupling the estimation of POC from chlorophyll-*a* estimates that are obtained from empirical band ratio algorithms. Naturally, if the same reflectance band ratios are used as input to POC and chlorophyll algorithms, then both estimated variables are unrealistically forced to always covary. Thus, additional work on approaches such as that based on $R_{rs}(555)$ appears to be warranted as part of further research on POC algorithm development and refinements.

We anticipate that further research will address not only empirical correlational algorithms but also other approaches that may involve semianalytical and radiative transfer-based modeling. In this study, we examined two semianalytical algorithms for estimating IOPs from ocean reflectance; one referred to as QAA (Lee et al., 2002) and the other as GSM (Garver and Siegel, 1997; Maritorena et al., 2002). We tested the potential usefulness of QAA and GSM for deriving $b_b(555)$ from $R_{rs}(\lambda)$ as a first step of the two-step POC algorithm. When applied to our data set, both QAA- and GSM-derived $b_b(555)$ showed significant disagreement with the measured $b_b(555)$. Such results highlight general difficulties in the development of semianalytical models that perform consistently well in a variety of marine optical environments. Further improvements in these types of models will aid in efforts to refine POC algorithms.

Acknowledgements. This is a contribution of the BIOSOPE project in the eastern South Pacific as part of the LEFE-CYBER program, which was funded by the Centre National de la Recherche Scientifique (CNRS), the Institut des Sciences de l'Univers (INSU), the Centre National d'Etudes Spatiales (CNES) in France, the European Space Agency (ESA), the National Aeronautics and Space Administration (NASA) in USA, and the Natural Sciences and Engineering Research Council (NSERC) in Canada. The Alfred-Wegener Institute for Polar and Marine Research (Bremerhaven, Germany) kindly made it possible for us (D. S., R. A. R., S. K., M. S., and R. R.) to participate in the ANT-XXIII/1 cruise in the eastern Atlantic. This study was supported by NASA Ocean Biology and Biogeochemistry Program (NNG04GO02G awarded to D. S.) and NSF Chemical Oceanography Program (OCE-0324680 to D. S. and OCE-0324346 to M. S.). We thank D. Tailliez and

C. Marec for assistance in CTD-rosette deployments and data processing on the BIOSOPE cruise, J. Ras for providing HPLC data, and L. Beaufort for calcite data from BIOSOPE. We also thank M. R. van der Loeff, the chief scientist of ANT-XXIII/1, for accommodating our research program on the cruise, K. Heymann for SPM determinations on ANT-XXIII/1, and G. Dieckmann and J. Schwarz for their assistance and for providing filtration equipment. The scientists, officers, and crews of R/V l'Atalante and R/V Polarstern are acknowledged for providing logistical support and their help onboard during the field work. The IDL code of the GSM semianalytical model was provided by S. Maritorena and D. Siegel, and M. Behrenfeld and W. Gardner provided valuable comments on the manuscript. The analysis of samples for particulate organic carbon was made at Marine Science Institute Analytical Laboratory, University of California at Santa Barbara. The HPLC analysis of pigment samples from the ANT-XXIII/1 cruise was made at Center for Hydro-Optics and Remote Sensing, San Diego State University. We dedicate this work to the memory of our friend and colleague S. Kaczmarek, who tragically passed away shortly after his participation in the ANT-XXIII/1 cruise.

Edited by: E. Boss

References

- Aas, E.: Refractive index of phytoplankton derived from its metabolite composition, *J. Plankton Res.*, 18, 2223–2249, 1996.
- Antoine, D., Morel, A., Gordon, H. R., Banzon, V. F., and Evans, R. H.: Bridging ocean color observations of the 1980s and 2000s in search of long-term trends, *J. Geophys. Res.*, 110, C06009, doi:10.1029/2004JC002620, 2005.
- Bailey, S. W. and Werdell, P. J.: A multi-sensor approach for the on-orbit validation of ocean color satellite data, *Remote Sens. Environ.*, 102, 12–23, 2006.
- Bader, H.: The hyperbolic distribution of particle sizes, *J. Geophys. Res.*, 75, 2822–2830, 1970.
- Baker, E. T. and Lavelle, J. W.: The effect of particle size on the light attenuation coefficient of natural suspensions, *J. Geophys. Res.*, 89, 8179–8203, 1984.
- Balch, W. M., Drapeau, D. T., Cucci, T. L., Vaillancourt, R. D., Kilpatrick, K. A., and Fritz, J. J.: Optical backscattering by calcifying algae: Separating the contribution of particulate inorganic and organic carbon fractions, *J. Geophys. Res.*, 104, 1541–1558, 1999.
- Balch, W. M., Drapeau, D. T., Fritz, J. J., Bowler, B. C., and Nolan, J.: Optical backscattering in the Arabian Sea – continuous underway measurements of particulate inorganic and organic carbon, *Deep-Sea Res. I*, 48, 2423–2452, 2001.
- Beaufort, L., Couapel, M., Buchet, N., and Claustre, H.: Calcite production by coccolithophores in the South East Pacific Ocean: from desert to jungle, *Biogeosciences Discuss.*, 4, 3267–3299, 2007, <http://www.biogeosciences-discuss.net/4/3267/2007/>.
- Behrenfeld, M. and Boss, E.: Beam attenuation and chlorophyll concentrations as alternative optical indices of phytoplankton biomass, *J. Mar. Res.*, 64, 431–451, 2006.
- Behrenfeld, M. J., Boss, E., Siegel, D. A., and Shea, D. M.: Carbon-based ocean productivity and phytoplankton physiology from space, *Global Biogeochem. Cy.*, 19, GB1006, doi:10.1029/2004GB002299, 2005.
- Bianchi, T. S., Lambert, C., and Biggs, D. C.: Distribution of chlorophyll a and phaeopigments in the northwestern Gulf of Mexico: A comparison between fluorometric and high-performance liquid chromatography measurements, *Bull. Mar. Sci.*, 51, 25–32, 1995.
- Bishop, J. K. B.: The correction and suspended matter calibration of Sea Tech transmissometer data, *Deep-Sea Res.*, 33, 121–134, 1986.
- Bishop, J. K. B.: Transmissometer measurement of POC, *Deep-Sea Res. I*, 46, 353–369, 1999.
- Boss, E. and Pegau, W. S.: The relationship of light scattering at an angle in the backward direction to the backscattering coefficient, *Appl. Opt.*, 40, 5503–5507, 2001.
- Boss, E., Pegau, W. S., Lee, M., Twardowski, M. S., Shybanov, E., Korotaev, G. and Baratange, F.: Particulate backscattering ratio at LEO 15 and its use to study particle composition and distribution, *J. Geophys. Res.*, 109, C01014, doi:10.1029/2002JC001514, 2004.
- Boss, E., Twardowski, M. S., and Herring, S.: Shape of the particulate beam attenuation spectrum and its inversion to obtain the shape of the particulate size distribution, *Appl. Opt.*, 40, 4885–4893, 2001.
- Bricaud, A., Babin, M., Morel, A. and Claustre, H.: Variability in the chlorophyll-specific absorption coefficients of natural phytoplankton: Analysis and parameterization, *J. Geophys. Res.*, 100, 13 321–13 332, 1995.
- Bricaud, A., Morel, A., Babin, M., Allali, K., and Claustre, H.: Variations of light absorption by suspended particles with chlorophyll a concentration in oceanic (case 1) waters: Analysis and implications for bio-optical models, *J. Geophys. Res.*, 103, 31 033–31 044, 1998.
- Bricaud, A., Morel, A., and Prieur, L.: Absorption by dissolved matter of the sea (yellow substance) in the UV and visible domains, *Limnol. Oceanogr.*, 26, 43–53, 1981.
- Buiteveld, H., Hakvoort, J. H. M., and Donze, M.: The optical properties of pure water, in: *Ocean Optics XII*, Proc. SPIE, Vol. 2258, edited by: Jaffe, J. S., SPIE, Bellingham, Washington, 174–183, 1994.
- Campbell, J.W., Blaisdell, J. M., and Darzi, M.: Level-3 SeaWiFS Data Products: Spatial and Temporal Binning Algorithms, in: *NASA Tech. Memo. 104566*, Vol. 32, edited by: Hooker, S. B., Firestone, E. R., and Acker, J. G., NASA Goddard Space Flight Center, Greenbelt, Maryland, 73 pp., 1995.
- Clarke, G. L., Ewing, G. C., and Lorenzen, C. J.: Spectra of backscattered light from the sea obtained from aircraft as a measure of chlorophyll concentration, *Science*, 167, 1119–1121, 1970.
- Claustre, H., Morel, A., Babin, M., Cailliau, C., Marie, D., Marty, J.-C., Taillez, D., and Vaulot, D.: Variability in particle attenuation and chlorophyll fluorescence in the tropical Pacific: Scales, patterns, and biogeochemical implications, *J. Geophys. Res.*, 104, 3401–3422, 1999.
- Claustre, H., Sciandra, A., and Vaulot, D.: Introduction to the special section Bio-optical and biogeochemical conditions in the South East Pacific in late 2004: the BIOSOPE program, *Biogeosciences Discuss.*, 5, 605–640, 2008, <http://www.biogeosciences-discuss.net/5/605/2008/>.

- Copin-Montégut, G.: Matière en suspension dans les eaux de mer: répartition, composition chimique, origine et évolution. Ph.D. thesis. Laboratoire de Physique et Chimie Marines, Université Pierre et Marie Curie, 173 pp., 1980.
- Dana, D. R. and Maffione, R. A.: Determining the backward scattering coefficient with fixed-angle backscattering sensors – Revisited, *Ocean Optics XVI*, Santa Fe, New Mexico, November 18–22, 2002.
- Doxaran, D., Froidefond, J.-M., and Castaing, P.: A reflectance band ratio used to estimate suspended matter concentrations in sediment-dominated coastal waters, *Int. J. Remote Sens.*, 23, 5079–5085, 2002.
- DuRand, M. D., Green, R. E., Sosik, H. M., and Olson, R. J.: Diel variations in optical properties of *Micromonas pusillas* (Prasinophyceae), *J. Phycol.*, 38, 1132–1142, 2002.
- Farinato, R. S. and Roswell, R. L.: New values of the light scattering depolarization and anisotropy of water, *J. Chem. Phys.*, 65, 593–595, 1975.
- Franz, B. A., Werdell, P. J., Meister, G., Bailey, S. W., Eplee Jr., R. E., Feldman, G. C., Kwiatkowska, E., McClain, C. R., Patt, F. S., and Thomas, D.: The continuity of ocean color measurements from SeaWiFS to MODIS, in: *Earth Observing Systems X*, Proc. SPIE, 5882, edited by: Butler, J. J., SPIE, Bellingham, Washington, 13 pp., 2005.
- Gardner, W. D., Biscaye, P. E., Zaneveld, J. R. V., and Richardson, M. J.: Calibration and comparison of the LDGO nephelometer and the OSU transmissometer on the Nova Scotian Rise, *Mar. Geol.*, 66, 323–344, 1985.
- Gardner, W. D., Mishonov, A. V., and Richardson, M. J.: Global POC concentrations from in-situ and satellite data, *Deep-Sea Res. II*, 53, 718–740, 2006.
- Gardner, W. D., Richardson, M. J., Carlson, C. A., Hansell, D., and Mishonov, A. V.: Determining true particulate organic carbon: bottles, pumps and methodologies, *Deep-Sea Res. II*, 50, 655–674, 2003.
- Gardner, W. D., Richardson, M. J., and Smith, W. O.: Seasonal patterns of water column particulate organic carbon and fluxes in the Ross Sea, Antarctica, *Deep-Sea Res. II*, 47, 3423–3449, 2000.
- Gardner, W. D., Walsh, I. D., and Richardson, M. J.: Biophysical forcing of particle production and distribution during a spring bloom in the North Atlantic, *Deep Sea Res. II*, 40, 171–195, 1993.
- Garver, S. and Siegel, D. A.: Inherent optical property inversion of ocean color spectra and its biogeochemical interpretation. I. Time series from the Sargasso Sea, *J. Geophys. Res.*, 102, 18 607–18 625, 1997.
- Garver, S., Siegel, D. A., and Mitchell, B. G.: Variability in near-surface particulate absorption spectra: What can a satellite ocean color imager see?, *Limnol. Oceanogr.*, 39, 1349–1367, 1994.
- Gordon, H. R. and Morel, A.: Remote assessment of ocean color for interpretation of satellite visible imagery – A review, *Lecture notes on coastal and estuarine studies*, Springer-Verlag, New York, 1983.
- Grob, C., Ulloa, O., Claustre, H., Huot, Y., Alarcon, G., and Marie, D.: Contribution of picoplankton to the total particulate organic carbon concentration in the eastern South Pacific, *Biogeosciences*, 4, 837–852, 2007, <http://www.biogeosciences.net/4/837/2007/>.
- Gundersen, J. S., Gardner, W. D., Richardson, M. J., and Walsh, I. D.: Effects of monsoons on the seasonal and spatial distribution of POC and chlorophyll in the Arabian Sea, *Deep-Sea Res. II*, 45, 2103–2132, 1998.
- Holm-Hansen, O., Lorenzen, C. J., Holmes, R. W., and Strickland, J. D. H.: Fluorometric determination of chlorophyll, *J. Cons. Int. Expl. Mer*, 30, 3–15, 1965.
- Honjo, S., Dymond, J., Collier, R., and Manganini, S. J.: Export production of particles to the interior of the equatorial Pacific Ocean during the 1992 EqPac experiment, *Deep-Sea Res. II*, 42, 831–870, 1995.
- Jonasz, M. and Fournier, G. R.: *Light Scattering by Particles in Water*, Theoretical and Experimental Foundations, Elsevier, Amsterdam, 2007.
- Kerr, P. F.: *Optical Mineralogy*, Fourth Edition, McGraw-Hill, New York, 1977.
- Knap, A., Michaels, A., Close, A., Ducklow, H., and Dickson, A. (Eds.): *Protocols for the Joint Global Ocean Flux Study (JGOFS) Core Measurements*, JGOFS Report Nr. 19 (Reprint of the IOC Manuals and Guides No. 29, UNESCO, Paris, 1994), 170 pp., 1996.
- Lee, Z. P., Carder, K. L., and Arnone, R. A.: Deriving inherent optical properties from water color: a multiband quasi-analytical algorithm for optically deep waters, *Appl. Opt.*, 41, 5755–5772, 2002.
- Lee, Z. P., Carder, K. L., and Arnone, R. A.: The quasi-analytical algorithm, in: *Remote Sensing of Inherent Optical Properties: Fundamentals, Tests of Algorithms, and Applications*, IOCCG Report Number 5, edited by: Lee, Z. P., International Ocean-Colour Coordinating Group, Dartmouth, Canada, 73–79, 2006.
- Loisel, H., Bosc, E., Stramski, D., Qubelkheir, K., and Deschamps, P.-Y.: Seasonal variability of the backscattering coefficient in the Mediterranean Sea based on satellite SeaWiFS imagery, *Geophys. Res. Lett.*, 28, 4203–4206, 2001.
- Loisel, H. and Morel, A.: Light scattering and chlorophyll concentration in case 1 waters: A reexamination, *Limnol. Oceanogr.*, 43, 847–858, 1998.
- Loisel, H., Nicolas, J.-M., Deschamps, P.-Y., and Frouin, R.: Seasonal and inter-annual variability of particulate organic matter in the global ocean, *Geophys. Res. Lett.*, 29(24), 2196, doi:10.1029/2002GL015948, 2002.
- Loisel, H., Nicolas, J.-M., Sciandra, A., Stramski, D., and A. Poteau, A.: Spectral dependency of optical backscattering by marine particles from satellite remote sensing of the global ocean, *J. Geophys. Res.*, 111, C09024, doi:10.1029/2005JC003367, 2006.
- Longhurst, A. R.: *Ecological Geography of the Sea*, Academic Press, San Diego, California, 1998.
- Longhurst, A. R. and Harrison, W. G.: The biological pump: Profiles of plankton production and consumption in the upper ocean, *Prog. Oceanogr.*, 22, 47–123, 1989.
- Maffione, R. A. and Dana, D. R.: Instruments and methods for measuring the backward-scattering coefficient of ocean waters, *Appl. Opt.*, 36, 6057–6067, 1997.
- Maritorena, S., Siegel, D. A., and Peterson, A. R.: Optimization of a semianalytical ocean color model for global-scale applications, *Appl. Opt.*, 41, 2705–2714, 2002.
- Marra, J., Langdon, C., and Knudson, C. A.: Primary production, water column changes, and the demise of a *Phaeocystis* bloom at

- the Marine Light-Mixed Layer site (59° N, 21° W) in the north-east Atlantic Ocean, *J. Geophys. Res.*, 100, 6633–6067, 1995.
- Menzel, D. W.: Particulate organic carbon in the deep sea, *Deep-Sea Res. I*, 14, 229–238, 1966.
- Milliman, J. D.: Production and accumulation of calcium carbonate in the ocean: budget of a nonsteady state, *Global Biogeochem. Cy.*, 7, 927–957, 1993.
- Mishonov, A. V., Gardner, W. D., and Richardson, M. J.: Remote sensing and surface POC concentration in the South Atlantic, *Deep Sea Res. II*, 50, 2997–3015, 2003.
- Mobley, C. D.: *Light and Water. Radiative Transfer in Natural Waters*, Academic Press, San Diego, California, 1994.
- Montagnes, D. J., Berges, J. A., Harrison, P. J., and Taylor, F. J. R.: Estimation of carbon, nitrogen, protein, and chlorophyll a from volume in marine phytoplankton, *Limnol. Oceanogr.* 39, 1044–1060, 1994.
- Moran, S. B., Charette, M. A., Pike, S. M., and Wicklund, C. A.: Differences in seawater particulate organic carbon concentration in samples collected using small- and large-volume methods: the importance of DOC adsorption to the filter blank, *Mar. Chem.*, 67, 33–42, 1999.
- Morel, A.: Optical properties of pure water and pure sea water, in: *Optical Aspects of Oceanography*, edited by: Jerlov, N. G. and Steeman-Nielsen, E., Academic Press, New York, 1–24, 1974.
- Morel, A.: Optical modeling of the upper ocean in relation to its biogenous matter content (case I waters), *J. Geophys. Res.*, 93, 10 749–10 768, 1988.
- Morel, A. and Bricaud, A.: Inherent optical properties of algal cells including picoplankton: theoretical and experimental results, in: *Photosynthetic Picoplankton*, *Can. Bull. Fish. Aquat. Sci.*, 214, edited by: Platt, T. and Li, W. K. W., Dept. Fish. Oceans, Ottawa, Canada, 521–559, 1986.
- Morel, A., Gentili, B., Claustre, H., Babin, M., Bricaud, A., Ras, J., and Tièche, F.: Optical properties of the “clearest” natural waters, *Limnol. Oceanogr.*, 52, 217–229, 2007.
- Morel, A. and Maritorena, S.: Bio-optical properties of oceanic waters: A reappraisal, *J. Geophys. Res.*, 106, 7163–7180, 2001.
- Morel, A., and Prieur, L.: Analysis of variations in ocean color, *Limnol. Oceanogr.*, 22, 709–722, 1977.
- Mueller, J. L., Fargion, G. S., and McClain, C. R. (Eds.): *Ocean Optics Protocols for Satellite Ocean Color Sensor Validation, Revision 4, Volume III: Radiometric Measurements and Data Analysis Protocols*, NASA/TM-2003-211621/Rev4-Vol. III, NASA Goddard Space Flight Center, Greenbelt, Maryland, 78 pp., 2003.
- Myers, J. S. and Miller, R. L.: Optical airborne remote sensing, in: *Remote Sensing of Coastal Aquatic Waters*, edited by: Miller, R. L., Del Castillo, C. E., and McKee, B. A., Springer, Dordrecht, Netherlands, 51–67, 2005.
- O’Reilly, J. E., Maritorena, S., Mitchell, B. G., Siegel, D. A., Carder, K. L., Garver, S. A., Kahru, M., and McClain, C. R.: Ocean color chlorophyll algorithms for SeaWiFS, *J. Geophys. Res.*, 103, 24 937–24 953, 1998.
- O’Reilly, J. E., Maritorena, S., Siegel, D. A., et al: Ocean Color Chlorophyll a Algorithms for SeaWiFS, OC2, and OC4: Version 4, in: *SeaWiFS Postlaunch Technical Report Series, Vol. 11, SeaWiFS Postlaunch Calibration and Validation Analyses, Part 3*, NASA/TM-2000-206892, Vol. 11, edited by: Hooker, S. B. and Firestone, E. R., NASA, Greenbelt, Maryland, 9–27, 2000.
- Pabi, S. and Arrigo, K. R.: Satellite estimation of marine particulate carbon in waters dominated by different phytoplankton taxa, *J. Geophys. Res.*, 110, C10018, doi:10.1029/2005JC003137, 2006.
- Parsons, T. R., Maita, Y., and Lalli, C. M.: *A Manual of Chemical and Biological Methods for Seawater Analysis*, Elsevier, New York, 1984.
- Platt, T. and Sathyendranath, S.: Oceanic primary production: Estimation by remote sensing at local and regional scales, *Science*, 241, 1613–1620, 1988.
- Ras, J., Claustre, H., and Uitz, J.: Spatial variability of phytoplankton pigment distributions in the Subtropical South Pacific Ocean: comparison between in situ and predicted data, *Biogeosciences Discuss.*, 4, 3409–3451, 2007, <http://www.biogeosciences-discuss.net/4/3409/2007/>.
- Reynolds R. A., Stramski D., and Mitchell, B. G.: A chlorophyll-dependent semianalytical model derived from field measurements of absorption and backscattering coefficients within the Southern Ocean, *J. Geophys. Res.*, 106, 7125–7138, 2001.
- Robinson, I. S.: *Measuring Oceans from Space: The Principles and Methods of Satellite Oceanography*, Springer-Praxis, Chichester, UK, 2004.
- Roesler, C. S. and Boss, E.: Spectral beam attenuation coefficient retrieved from ocean color inversion, *Geophys. Res. Lett.*, 30(9), 1468, doi:10.1029/2002GL016185, 2003.
- Röttgers, R. and Doerffer, R.: Measurements of optical absorption by chromophoric dissolved organic matter using a point-source integrating-cavity absorption meter, *Limnol. Oceanogr. Methods*, 5, 126–135, 2007.
- Röttgers, R., Schönfeld, W., Kipp, P.-R., and Doerffer, R.: Practical test of a point-source integrating-cavity absorption meter: the performance of different collector assemblies, *Appl. Opt.*, 44, 5549–5560, 2005.
- Sarthou, G., Baker, A. R., Blain, S., Achterberg, E. P., Boye, M., Bowie, A. R., Croot, P., Laan, P., de Baar, H. J. W., Jickells, T. D., and Worsfold, P. J.: Atmospheric iron deposition and sea-surface dissolved iron concentrations in the eastern Atlantic Ocean, *Deep-Sea Res. I*, 50, 1339–1352, 2003.
- Shifrin, K. S.: *Physical Optics of Ocean Water*, American Institute of Physics, New York, 1988.
- Siegel, D. A., Dickey, T. D., Washburn, L., Hamilton, M. K., and Mitchell, B. G.: Optical determination of particulate abundance and production variations in the oligotrophic ocean, *Deep-Sea Res.*, 36, 211–222, 1989.
- Smith, R. C. and Baker, K. S.: The bio-optical state of ocean waters and remote sensing, *Limnol. Oceanogr.*, 23, 247–259, 1978.
- Sokal, R. R. and Rohlf, F. J.: *Biometry: The Principals and Practice of Statistics in Biological Research*, Third Edition, W. H. Freeman and Company, New York, 1995.
- Spinrad, R. W.: A calibration diagram of specific beam attenuation, *J. Geophys. Res.*, 91, 7761–7764, 1986.
- Stemann, L., Eloire, D., Sciandra, A., Jackson, G. A., Guidi, L., Picheral, M., and Gorsky, G.: Volume distribution for particles between 3.5 μm and 2000 μm in the upper 200 m region of the South Pacific Gyre, *Biogeosciences Discuss.*, 3377–3407, 2007.
- Stramska, M. and Stramski, D.: Variability of particulate organic carbon concentration in the north polar Atlantic based on ocean color observations with Sea-viewing Wide Field-of-View Sensor (SeaWiFS), *J. Geophys. Res.*, 111, C09003, doi:10.1029/2004JC002762, 2005.

- Stramska, M., Stramski, D., Kaczmarek, S., Allison, D. B., and Schwarz, J.: Seasonal and regional differentiation of bio-optical properties within the north polar Atlantic, *J. Geophys. Res.*, 111, C08003, doi:10.1029/2005JC003293, 2006.
- Stramski, D.: Refractive index of planktonic cells as a measure of cellular carbon and chlorophyll a content, *Deep-Sea Res. I*, 46, 335–351, 1999.
- Stramski, D. and Kiefer, D. A.: Light scattering by microorganisms in the open ocean, *Prog. Oceanogr.*, 28, 343–383, 1991.
- Stramski, D. and Morel, A.: Optical properties of photosynthetic picoplankton in different physiological states as affected by growth irradiance, *Deep-Sea Res.*, 37, 245–266, 1990.
- Stramski, D. and Reynolds, R. A.: Diel variations in the optical properties of a marine diatom, *Limnol. Oceanogr.*, 38, 1347–1364, 1993.
- Stramski, D., Reynolds, R. A., Kahru, M., and Mitchell, B. G.: Estimation of particulate organic carbon in the ocean from satellite remote sensing, *Science*, 285, 239–242, 1999.
- Stramski, D. and Tęgowski, J.: Effects of intermittent entrainment of air bubbles by breaking wind waves on ocean reflectance and underwater light field, *J. Geophys. Res.*, 106, 31 345–31 360, 2001.
- Stumpf, R. P. and Pennock, J. R.: Calibration of a general optical equation for remote sensing of suspended sediments in a moderately turbid estuary, *J. Geophys. Res.*, 94, 14 363–14 371, 1989.
- Sullivan, J. M., Twardowski, M. S., Donaghay, P. L., and Freeman, S. A.: Use of optical scattering to discriminate particle types in coastal waters, *Appl. Opt.*, 44, 1667–1680, 2005.
- Terrill, E. J., Melville, W. K., and Stramski, D.: Bubble entrainment by breaking waves and their influence on optical scattering in the upper ocean, *J. Geophys. Res.*, 106, 16 815–16 823, 2001.
- Trees, C. C., Bidigare, R. R., Karl, D. M., Van Heukelem, L., and Dore, J.: Fluorometric chlorophyll a: Sampling, laboratory methods, and data analysis protocols, in: *Ocean Optics Protocols for Satellite Ocean Color Sensor Validation*, NASA/TM-2002-210004/Rev3-Vol2, edited by: Mueller, J. L. and Fargion, G. S., NASA Goddard Space Flight Center, Greenbelt, Maryland, 269–283, 2002.
- Twardowski, M. S., Boss, E., Macdonald, J. B., Pegau, W. S., Barnard, A. H., and Zaneveld, J. R. V.: A model for estimating bulk refractive index from the optical backscattering ratio and the implications for understanding particle composition in case I and case II waters, *J. Geophys. Res.*, 106, 14 129–14 142, 2001.
- Twardowski, M. S., Claustre, H., Freeman, S. A., Stramski, D., and Huot, Y.: Optical backscattering properties of the “clearest” natural waters, *Biogeosciences*, 4, 1041–1058, 2007, <http://www.biogeosciences.net/4/1041/2007/>.
- Twardowski, M. S., Lewis, M., Barnard, A., and Zaneveld, J. R. V.: In-water instrumentation and platforms for ocean color remote sensing applications, in: *Remote Sensing of Coastal Aquatic Waters*, edited by: Miller, R. L., Del Castillo, C. E., and McKee, B. A., Springer, Dordrecht, Netherlands, 69–100, 2005.
- Twardowski, M. S., Sullivan, J. M., Donaghay, P. L., and Zaneveld, J. R. V.: Microscale quantification of the absorption by dissolved and particulate material in coastal waters with an ac-9, *Atmos. Ocean. Technol.*, 16, 691–707, 1999.
- Van der Linde, D. W.: Protocol for determination of total suspended matter in oceans and coastal zones, Technical Note No. 1.98.182, CEC-JRC, Ispra, Italy, 8 pp., 1998.
- Van Heukelem L. and Thomas, C. S.: Computer-assisted high-performance liquid chromatography method development with applications to the isolation and analysis of phytoplankton pigments, *J. Chromatogr. A*, 910, 31–49, 2001.
- Verity, P. G., Robertson, C. Y., Tronzo, C. R., Andrews, M. G., Nelson, J. R., and M. E. Sieracki, M. E.: Relationships between cell volume and the carbon and nitrogen content of marine photosynthetic nanoplankton, *Limnol. Oceanogr.*, 37, 1434–1446, 1992.
- Vidussi, F., Claustre, H., Manca, B. B., Luchetta, A., and Marty, J. C.: Phytoplankton pigment distribution in relation to upper thermocline circulation in the eastern Mediterranean Sea during winter, *J. Geophys. Res.*, 106, 19 939–19 956, 2001.
- Villafane, V., Helbling, W., and Holm-Hansen, O.: Phytoplankton around Elephant Island, Antarctica, *Polar Biol.*, 13, 183–191, 1993.
- Volk, T. and Hoffert, M. I.: Ocean carbon pumps: Analysis of relative strengths and efficiencies in ocean-driven atmospheric CO₂ changes, in: *The Carbon Cycle and Atmospheric CO₂: Natural Variations Archean to Present*, Geophys. Monogr. Ser., Vol. 32, edited by: Sundquist, E. T. and Broecker, W. S., AGU, Washington, D.C., 99–110, 1985.
- Voss, K. J.: A spectral model of the beam attenuation coefficient in the ocean and coastal areas, *Limnol. Oceanogr.*, 37, 501–509, 1992.
- Whitmire, A. L., Boss, E., Cowles, T. J., and Pegau, W. S.: Spectral variability of the particulate backscattering ratio, *Opt. Exp.*, 15, 7019–7031, 2007.
- Yoder, A. Y., McClain, C. R., Feldman, G. C., and Esaias, W. E.: Annual cycles of phytoplankton chlorophyll concentrations in the global ocean: A satellite view, *Global Biogeochem. Cy.*, 7, 181–193, 1993.
- Zaneveld, J. R. V.: Variation of optical sea parameters with depth, in: *Optics of the Sea (Interface and In-water Transmission and Imagery)*, Lecture Series, Vol. 61, NATO, 2.3-1–2.3-22, 1973.
- Zaneveld, J. R. V., Kitchen, J. C., and Moore, C. M.: The scattering error correction of reflecting-tube absorption meters, in: *Ocean Optics XII*, Proc. SPIE, Vol. 2258, edited by: Jaffe, J. S., Bellingham, Washington, 44–55, 1994.

Corrigendum to

“Relationships between the surface concentration of particulate organic carbon and optical properties in the eastern South Pacific and eastern Atlantic Oceans” published in *Biogeosciences*, 5, 171–201, 2008

D. Stramski

Marine Physical Lab., Scripps Institution of Oceanography, Univ. of California at San Diego, La Jolla, CA 92093-0238, USA

The paper “Relationships between the surface concentration of particulate organic carbon and optical properties in the eastern South Pacific and eastern Atlantic Oceans” by Stramski et al. (*Biogeosciences*, 5, 171–201, 2008) contains an error in the values of the particulate backscattering ratio at 555 nm, $\tilde{b}_{bp} = b_{bp}(555)/b_p(555)$, depicted for the ANT-XXIII/1 cruise in Figs. 11 and 12b. The reported values were too low due to an inadvertent mistake in which incorrect values of the particulate scattering coefficient, $b_p(555)$, were used in the calculation of \tilde{b}_{bp} . I offer my apologies to the co-authors, reviewers, and readers of the paper.

Here the corrected Figs. 11 and 12b are presented. In contrast to the original figures contained in the paper, the corrected values of the particulate backscattering ratio, $b_{bp}(555)/b_p(555)$, are seen to be generally similar for the two cruises compared, BIOSOPE and ANT-XXIII/1. For the BIOSOPE data set the average value is 0.0104 (standard deviation $SD=0.0026$), whereas for the ANT-XXIII/1 data set it is 0.0090 ($SD=0.0010$). The erroneous average value reported in the original paper for ANT-XXIII/1 was 0.0054, which incorrectly suggested significant systematic difference between the two cruises. In actuality, no significant differences are observed, with the exception of a few BIOSOPE stations that show a somewhat higher backscattering ratio compared to the rest of the data set. In consequence, the discussion focusing on the differences between the cruises presented in Sect. 3.4 (p. 193–196) of the original paper is largely irrelevant. However, all other results and conclusions including the POC algorithms are unaffected by this error.

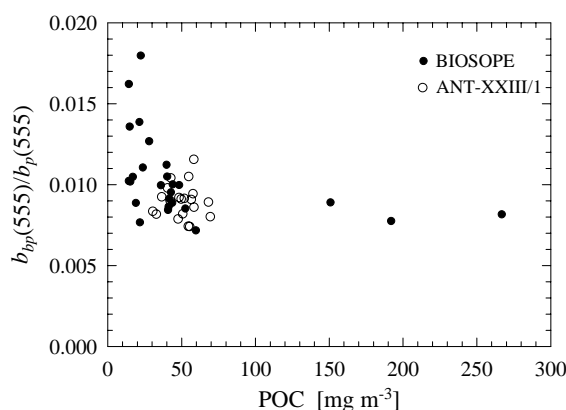


Fig. 11. Particulate backscattering ratio, $b_{bp}(555)/b_p(555)$, plotted as a function of surface concentration of particulate organic carbon, POC, for the BIOSOPE and ANT-XXIII/1 cruises.

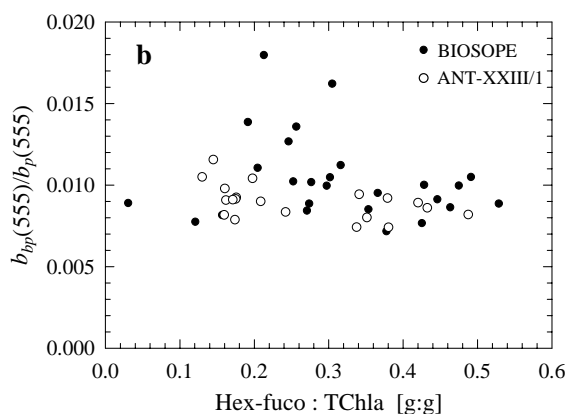


Fig. 12. (b) Particulate backscattering ratio, $b_{bp}(555)/b_p(555)$, plotted as a function of pigment ratio Hex-fuco:TChla in surface waters for the BIOSOPE and ANT-XXIII/1 cruises.



Correspondence to: D. Stramski
(dstramski@ucsd.edu)

Particle optical backscattering along a chlorophyll gradient in the upper layer of the eastern South Pacific Ocean

Y. Huot¹, A. Morel¹, M. S. Twardowski², D. Stramski³, and R. A. Reynolds³

¹CNRS, Laboratoire d'Océanographie de Villefranche, 06230 Villefranche-sur-mer, France; Université Pierre et Marie Curie-Paris 6, Laboratoire d'Océanographie de Villefranche, 06230 Villefranche-sur-mer, France

²Department of Research, WET Labs, Inc., 165 Dean Knauss Dr., Narragansett, RI 02882, USA

³Marine Physical Laboratory, Scripps Institution of Oceanography, University of California at San Diego, La Jolla, CA 92093-0238, USA

Received: 13 November 2007 – Published in Biogeosciences Discuss.: 3 December 2007

Revised: 12 March 2008 – Accepted: 13 March 2008 – Published: 7 April 2008

Abstract. The particulate scattering, b_p , and backscattering, b_{bp} , coefficients are determined by the concentration and physical properties of suspended particles in the ocean. They provide a simple description of the influence of these particles on the scattering of light within the water column. For the remote observation of ocean color, b_{bp} along with the total absorption coefficient govern the amount and spectral qualities of light leaving the sea surface. However, for the construction and validation of ocean color models measurements of b_{bp} are still lacking, especially at low chlorophyll a concentrations ([Chl]). Here, we examine the relationships between spectral b_{bp} and b_p vs. [Chl] along an 8000 km transect crossing the Case 1 waters of the eastern South Pacific Gyre. In these waters, over the entire range of [Chl] encountered (~ 0.02 – 2 mg m^{-3}), both b_{bp} and b_p can be related to [Chl] by power functions (i.e. b_p or $b_{bp} = \alpha [\text{Chl}]^\beta$). Regression analyses are carried out to provide the parameters α and β for several wavelengths throughout the visible for both b_{bp} and b_p . When applied to the data, these functions retrieve the same fraction of variability in b_{bp} and b_p (coefficients of determination between 0.82 and 0.88). The b_{bp} coefficient fall within the bounds of previous measurements at intermediate and high [Chl] recently published. Its dependence on [Chl] below $\sim 0.1 \text{ mg m}^{-3}$ is described for the first time with in situ data. The backscattering ratio (i.e. b_{bp}/b_p) with values near 0.01 for all stations appears to be spectrally neutral and not significantly dependent on [Chl]. These results should foster the development of improved forward models of the mean optical properties for oceanic Case 1 waters as well as inverse models based upon them.

1 Introduction

The phenomenon of light scattering within a water body is due to water molecules (plus ions) and different types of particles in suspension. Forward scattering corresponds to the fraction of scattering occurring in the forward hemisphere centred on the direction of propagation of the incident radiation. Backscattering occurs in the symmetrical hemisphere centred on the reverse direction. The total scattering coefficient at wavelength λ (units are nm), represented by $b(\lambda)$ (m^{-1}), is the sum of the coefficients for forward, $b_f(\lambda)$, and backward, $b_b(\lambda)$, scattering.

There are many reasons for studying the light scattering properties of natural waters. To the extent that the contribution from water molecules is known, scattering properties contain both qualitative and quantitative information about the particles present in the water body. Regarding the backscattering coefficient of marine particles, $b_{bp}(\lambda)$, the two main motivations for studying its magnitude and spectral properties are that: (i) they depend upon, and thus may provide useful information about, the size distribution function and bulk refractive index of the particle population (Ulloa et al., 1994; Morel and Maritorena, 2001; Twardowski et al., 2001), and (ii) the sum of $b_{bp}(\lambda)$ and the backscattering coefficient of pure water, $b_{bw}(\lambda)$, governs the reflectance of the upper layer (Gordon et al., 1975; Morel and Prieur, 1977). The spectral reflectance, $R(\lambda)$ (dimensionless), defined as the ratio of the spectral upward to the downward irradiance just beneath the surface, is essentially related to the ratio $b_b(\lambda)/a(\lambda)$, where $a(\lambda)$ (m^{-1}) is the spectral absorption coefficient, and $b_b(\lambda) = b_{bp}(\lambda) + b_{bw}(\lambda)$ is the total backscattering coefficient of the water body. The changes in the spectral shape of $R(\lambda)$ form the basis of ocean color radiometry



Correspondence to: Y. Huot
(huot@obs-vlfr.fr)

and its applications. In particular, these changes are used to estimate from space the chlorophyll concentration, [Chl] (mg m^{-3}), within the upper layer of oceanic waters (e.g. Clark and Ewing, 1974; O'Reilly et al., 1998).

When building forward models of $R(\lambda)$ as a function of [Chl] (Gordon and Morel, 1983; Gordon et al., 1988; Morel, 1988), empirical relationships derived from field observations were available to describe the mean trend in $a(\lambda)$ as a function of [Chl]. By contrast, analogous relationships have not been established for the quantity $b_{bp}(\lambda)$ and its variation over the full [Chl] range encountered in the open ocean ($\sim 0.02\text{--}30 \text{ mg m}^{-3}$). This is particularly true of low [Chl] waters as only a very limited amount of $b_{bp}(\lambda)$ data have been published below 0.1 mg m^{-3} . Therefore, modeling studies are necessarily based on assumptions regarding this term (e.g., IOCCG, 2006). Only recently have coincident field data become available for relating [Chl] to $b_{bp}(\lambda)$ (Balch et al., 2001; Reynolds et al., 2001; Twardowski et al., 2001; Stramska et al., 2003; Sullivan et al., 2005; Stramska et al., 2006; Whitmire et al., 2007). A large amount of scatter is present in most of these datasets, which may reflect true natural variability in oceanic waters. However, in some more coastal datasets, terrigenous particles or sediments probably play a sizeable role in the light backscattering process, which produces larger potential variability in these data (e.g., Fig. 9 in Twardowski et al., 2001). The variability in the b_{bp} vs. [Chl] relationship may also result from experimental uncertainties, which are inevitably attached to the rather difficult measurement of backscattering.

Along the BIOSOPE (Biogeochemistry and Optics South Pacific Experiment) 8000 km-long transect in the eastern South Pacific Ocean (Claustre et al., 2007¹), $b_{bp}(\lambda)$ measurements were performed with great care and under favorable conditions (Twardowski et al., 2007; Stramski et al., 2008). Moreover, these data were obtained unquestionably in a Case 1 water environment, distant from terrigenous influences, which encompassed a wide [Chl] range from 0.02 to 2 mg m^{-3} . Note that roughly 99% of the world's ocean has a near-surface [Chl] value within this range (Antoine et al., 2005). Therefore, if a relationship between the magnitudes of b_{bp} and [Chl] actually exists, these contemporaneous measurements in such an environment should reveal it. This is the first aim of the present paper.

Our emphasis will be on the $b_{bp}(\lambda)$ and [Chl] data from the upper layer of the water column, which contributes to the optical signal leaving the ocean detected by ocean color remote sensors. The $b_{bp}(\lambda)$ data from deeper layers are beyond the scope of the present paper. In general, such analyses of backscattering could potentially provide information about the nature of scattering material and its modification along

the vertical (e.g. changes in the proportions of living vs. non-living particles, size distribution of particles and their chemical composition via the refractive index, pigment changes resulting from photoacclimation of algae, and so on).

The second aim of our study is to examine the spectral shape of $b_{bp}(\lambda)$ and to compare it with the spectral behavior of $b_p(\lambda)$. In modeling approaches, it is generally postulated that both coefficients follow the same spectral trend, which means that their ratio,

$$\tilde{b}_{bp}(\lambda) = b_{bp}(\lambda) / b_p(\lambda) \quad (1)$$

referred to as the particle backscattering ratio or backscattering probability, $\tilde{b}_{bp}(\lambda)$ (unitless), is spectrally neutral. Actually, this assumption is not supported by theory (Morel and Bricaud, 1981), at least for heavily pigmented particles such as phytoplankton cells, nor by experiments made with pure algae grown in culture (Ahn et al., 1992). This assumption could possibly be an acceptable approximation when dealing with natural particle assemblages because they include a considerable amount of rather colorless debris and tiny heterotrophic organisms (mostly bacteria), viruses, and other numerous small-sized particles which largely contribute to $b_{bp}(\lambda)$ (Morel and Ahn, 1991; Stramski and Kiefer, 1991). A detailed understanding of the contribution of various particle types to $b_{bp}(\lambda)$ remains limited (Stramski et al., 2004). Both the magnitude and spectral behavior of $\tilde{b}_{bp}(\lambda)$ will be examined here on the basis of measurements made in the Pacific Ocean. Comparisons with other data sources will also be presented.

2 Instrumentation and methods

The particle beam attenuation coefficient, $c_p(\lambda)$ (m^{-1}), and the sum of absorption coefficients of particulate and dissolved components, $a_{nw}(\lambda)$ (m^{-1}), were measured at nine wavelengths with an ac-9 instrument (WET Labs). From these measurements, the $b_p(\lambda)$ coefficient is straightforwardly derived from $b_p(\lambda) = c_p(\lambda) - a_{nw}(\lambda)$. The backscattering measurements were made at three wavelengths (462, 532, and 650 nm) by deploying an ECO-BB3 (WET Labs; hereafter referred to as the BB3) profiling instrument. The operation and calibration of these instruments, as well as the methods for processing the raw data to derive $b_{bp}(\lambda)$, are described in detail by Twardowski et al. (2007). Dark offset calibration parameters for the BB3 were measured directly in situ during BIOSOPE for optimal accuracy.

The backscattering coefficient was also determined at eight other wavelengths using a Hydrosat-6 (HOBI Labs, wavebands 442, 470, 550, 589, 620 and 671 nm) and two α - β instruments (HOBI Labs, wavebands 420 and 510 nm). Note that the Hydrosat band at 620 nm did not function during the BIOSOPE cruise and that we have removed the band at 671 nm from the analysis to avoid the potential influence of chlorophyll fluorescence. Because the configuration for

¹Claustre, H., Sciandra, A., and Vaultot, D.: Introduction to the special section Bio-optical and biogeochemical conditions in the South East Pacific in late 2004: the BIOSOPE program, Biogeosciences Discuss., 5, 605–640, 2008

backscattering measurements is identical for the Hydrosat-6 and α -beta instruments, for brevity this dataset is hereafter referred to as the Hydrosat dataset. As in Stramski et al. (2008), the Hydrosat data reported here are derived from fitting a spectral power law model to the measured total backscattering spectra. The processing of these data is described in detail in Stramski et al. (2008), to which the reader is referred. An evaluation of the effect of using different published values for pure water scattering is made in Twardowski et al. (2007; see also Stramski et al., 2008). It was found that this effect upon the derived $b_{bp}(\lambda)$ values can be very significant, especially in oligotrophic and hyper-oligotrophic waters.

The $b_p(\lambda)$ and $b_{bp}(\lambda)$ data selected from the quasi-continuous vertical profiles are those within the upper layer which coincide with the sampling depths for pigment determinations (made by high performance liquid chromatography, Ras et al., 2007). The total chlorophyll-*a* concentration, simply denoted [Chl], is defined as the sum of monovinyl chlorophyll-*a* (including epimeric and allomeric forms), divinyl chlorophyll-*a*, and chlorophyllide-*a*. The upper layer is operationally defined as the layer between the surface and $z \approx 2/K_d(490)$, where $K_d(490)$ (m^{-1}) is the attenuation coefficient for downward irradiance at 490 nm. This attenuation coefficient was determined from spectroradiometric measurements of downward irradiance (Morel et al., 2007). The depth z of this layer varied along the whole transect between approximately 20 m (Chilean upwelling zone) and 85 m (in the central part of the hyper-oligotrophic gyre).

3 Theoretical aspects, existing parameterizations and observations

In contrast to $b_{bp}(\lambda)$, the $b_p(\lambda)$ coefficient has been well documented for several decades. A statistical analysis of field data provided a non-linear dependency between $b_p(550)$ and [Chl] (Gordon and Morel, 1983, their Fig. 5a)

$$b_p(550) = 0.3[\text{Chl}]^{0.62} \quad (2)$$

This initial expression was then revisited by Loisel and Morel (1998) who proposed that particle scattering (at 660 nm) for the upper homogeneous layer of the ocean can be empirically related to [Chl] alternatively through one of two relationships. The first general relationship

$$b_p(660) = 0.347[\text{Chl}]^{0.766} \quad (2a)$$

was obtained when all pairs of available data (number of observations, $N=850$) were considered (data subsets 1, 2 and 3 in reference above). The second relationship

$$b_p(660) = 0.252[\text{Chl}]^{0.635} \quad (2b)$$

was obtained when considering only subsets 2 and 3 from the tropical Atlantic and Pacific and the Mediterranean Sea

($N=614$). Data collected in North Atlantic waters (subset 1) showed enhanced $b_p(660)$ values, likely due to the presence of coccolithophores or detached liths. For this reason, as discussed in Loisel and Morel (1998), two separate regression analyses were performed leading to Eq. 2a and b.

The spectral dependency of $b_p(\lambda)$ can be explored theoretically (i.e. via Mie theory or van de Hulst's anomalous diffraction approximation) for spherical particles that are assumed to be weakly or non-absorbing, and when their size distribution (in principle with sizes extending from 0 to ∞) obeys a Junge power function law with an exponent $-j$. In this case, $b_p(\lambda)$ strictly varies as λ^{ν} , where the exponent $\nu=3-j$ (Morel, 1973). Bader (1970) showed that the Junge law applies generally for marine particles and that a central value for j is approximately 4. Given this average value for j , which has been repeatedly observed, the exponent ν would be around -1 and thus the λ^{-1} spectral model for scattering is often adopted. Departures from $j=4$ are observed and were indeed found during the BIOSOPE cruise².

As mentioned, the true limitation of the maximal size of natural particles (Boss et al., 2001), and more importantly, the lack of knowledge of the particle size distribution in the sub-micron range (as well as their non-zero absorption), disturbs the rigor of the above relationship between the ν and j exponents. In Morel and Maritorena (2001, their Eq. 14), the λ^{-1} dependency was kept at the lower limit of the [Chl] range (0.02 mg m^{-3}), and was then progressively reduced toward λ^0 with increasing [Chl] to account for the fact that the bulk particulate matter becomes generally more absorbing (and less scattering) in the blue-green spectral region with increasing [Chl] over its oceanic range. Based on these assumptions, Eq. 2a and b can be extended to other wavelengths according to

$$b_p(\lambda) = b_p(660) \left[\frac{\lambda}{660} \right]^{\nu} \quad (3)$$

where the exponent ν is allowed to vary (from -1 to 0) as a function of [Chl]

$$\begin{aligned} \nu([\text{Chl}]) &= 0.5(\log_{10}[\text{Chl}] - 0.3) \text{ when } 0.02 < [\text{Chl}] < 2 \text{ mg m}^{-3} \\ \text{and} & \\ \nu &= 0 \text{ when } [\text{Chl}] > 2 \text{ mg m}^{-3}. \end{aligned} \quad (4)$$

In the absence of backscattering measurements, apart from a few studies such as those of Petzold (1972), theoretical computations were necessary (Morel and Bricaud, 1981, 1986). They were made again with Mie theory assuming Junge-type size distributions and reasonable values for the relative refractive index of suspended material (Ulloa et al., 1994; Morel and Maritorena, 2001; Twardowski et al., 2001). Such computations provided the backscattering ratio $\hat{b}_{bp}(\lambda)$

² Sciandra, A. Stramski, D., Babin, M. Twardowski, M. S., Grob, C. Diel and spatial variability of the particle size distributions, notably of submicron particles, in the South Pacific Ocean, in preparation, 2007.

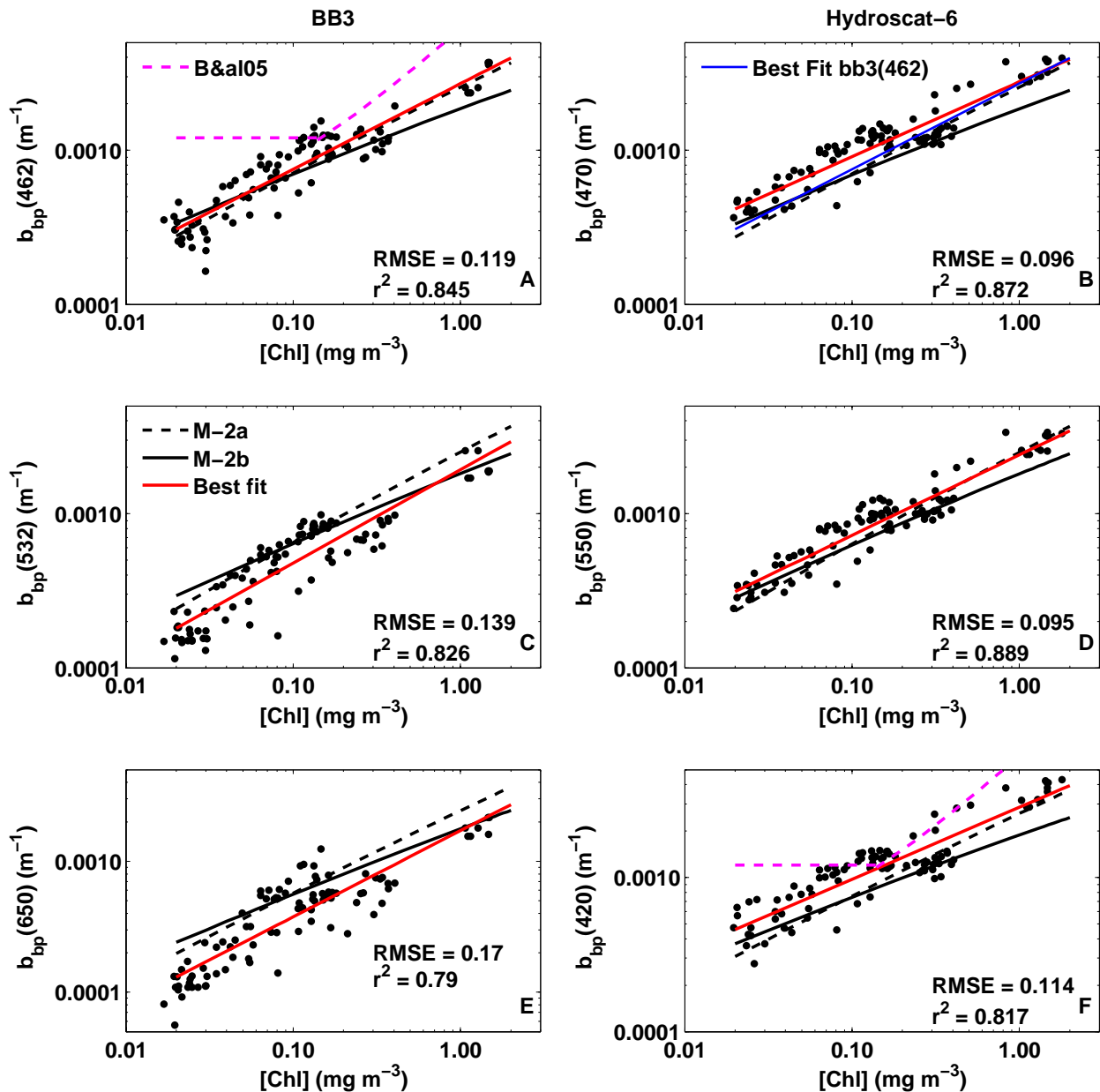


Fig. 1. Particulate backscattering coefficients measured at different wavelengths with two instruments as a function of chlorophyll-*a* concentration: left column with BB3 (Twardowski et al., 2007) and right column with Hydroscat instruments (Stramski et al., 2008). Twardowski (2007) presents a comparison of these two sensors at 470 nm. In each panel (see the common legend for all panels in panel C) the line of best fit is represented in red; the dashed black curve results from the algorithm of Morel and Maritorena (2001), and the continuous black curve is a modification of the former when Eq. 2b replaces Eq. 2a (see text). (A) For $\lambda=462\ nm$, the magenta dashed line is the bilinear relationship obtained by Behrenfeld et al. (2005) to represent the b_{bp} vs. $[Chl]$ relationship. (B) For $\lambda=470\ nm$, the blue line represents the best fit to the BB3 data from panel A (at 462 nm). (C) For $\lambda=532\ nm$, (D) For $\lambda=550\ nm$. (E) For $\lambda=650\ nm$. (F) For $\lambda=420\ nm$, the magenta line is the same as in panel A. Equations for the best fit lines are provided in Table 1 along with the other wavebands measured with the Hydroscat. All the RMSE and r^2 values provided herein were obtained for \log_{10} -transformed data.

(Eq. 1). Under the adopted assumptions, the computed values of $\tilde{b}_{bp}(\lambda)$ were rather low, around or below 0.01 for the biogenous material (with low refractive index) typically present in Case 1 waters. Similar computations to simulate

pure phytoplankton cultures with their log-normal size distributions provided even lower values ($\sim 10^{-3}$ – 10^{-4}), which were confirmed by experiments (Ahn et al., 1992). In addition, the $b_{bp}(\lambda)$ spectra for algae exhibit features within the

Table 1. Regression coefficients and statistics of the fits for the particulate backscattering (number of observations $N=97$ for the Hydroscat and $N=92$ for the BB3) and particulate scattering coefficients ($N=77$) as a function of the chlorophyll concentration.

λ	$b_{bp} = \alpha_1[\text{Chl}]^{\beta_1}$				$b_p = \alpha_2[\text{Chl}]^{\beta_2}$			
	α_1 (CI ♣)	β_1 (CI ♣)	r^{2*}	RMSE* (MAPE [⊗])	α_2 (CI ♣)	β_2 (CI ♣)	r^{2*}	RMSE* (MAPE [⊗])
412	-	-	-	-	0.38(0.06)	0.63(0.06)	0.87	0.11 (22)
420 ^{1,3}	0.0029(0.0003)	0.47(0.05)	0.82	0.11 (23)	0.36(0.05)	0.61(0.05)	0.87	0.11 (21)
440	-	-	-	-	0.33(0.04)	0.57(0.05)	0.88	0.10 (19)
442 ^{1,3}	0.0029(0.0003)	0.47(0.04)	0.85	0.10 (21)	0.33(0.04)	0.57(0.05)	0.88	0.10 (19)
462 ^{2,3}	0.0027(0.0003)	0.56(0.05)	0.85	0.12 (23)	0.33(0.04)	0.58(0.05)	0.88	0.10 (19)
470 ^{1,3}	0.0028(0.0002)	0.49(0.04)	0.87	0.10 (19)	0.33(0.04)	0.59(0.05)	0.88	0.10 (19)
488	-	-	-	-	0.33(0.04)	0.60(0.05)	0.88	0.11 (20)
510 ^{1,3}	0.0026(0.0002)	0.50(0.04)	0.89	0.09 (19)	0.33(0.04)	0.60(0.05)	0.88	0.11 (20)
532 ^{2,3}	0.0019(0.0003)	0.61(0.06)	0.83	0.14 (29)	0.32(0.04)	0.61(0.05)	0.88	0.11 (20)
550 ^{1,3}	0.0024(0.0002)	0.52(0.04)	0.89	0.10 (18)	0.32(0.04)	0.62(0.05)	0.88	0.11 (21)
555	-	-	-	-	0.32(0.04)	0.62(0.05)	0.88	0.11 (21)
589 ^{1,3}	0.0022(0.0002)	0.54(0.04)	0.89	0.10 (19)	0.29(0.04)	0.61(0.05)	0.88	0.11 (21)
650 ²	0.0017(0.0003)	0.66(0.07)	0.79	0.17 (31)	0.26(0.04)	0.58(0.05)	0.87	0.11 (21)
676	-	-	-	-	0.24(0.03)	0.59(0.05)	0.87	0.11 (21)
715	-	-	-	-	0.27(0.04)	0.60(0.05)	0.88	0.11 (20)

¹ Hydroscat backscattering data.

² BB3 backscattering data.

³ Scattering data interpolated to the BB3 and Hydroscat wavebands.

♣ 95% confidence interval on the parameters.

* On the decimal log transformed data (unitless).

⊗ Mean absolute percent error = $\frac{100}{N} \sum_i |(\hat{y}_i - y_i)/y_i|$ where N is the number of samples, \hat{y}_i is the estimated value and y_i is the measured value of the i th sample.

pigment absorption bands. Such a spectral dependency, however, is not expected for most natural particle assemblages. In the open ocean, except in bloom conditions, phytoplankton cells are postulated to contribute only a small amount to $b_{bp}(\lambda)$ while other smaller particles have a dominant influence. In particular, these other particles include small-sized non-living particles with perhaps sizable contributions of heterotrophic microbes (Morel and Ahn, 1991; Stramski and Kiefer, 1991) and of coccoliths if present in sufficient concentrations (Balch et al., 2001). The quasi-neutral character of $\tilde{b}_{bp}(\lambda)$ within the visible spectrum has been recently observed in field experiments (Whitmire et al., 2007).

In Morel and Maritorena (2001, see their Eq. 13), \tilde{b}_{bp} is spectrally flat. Under this assumption the spectral dependency of $b_{bp}(\lambda)$ follows that of $b_p(\lambda)$ as expressed by Eqs. 3 and 4. The \tilde{b}_{bp} is also posited to depend on [Chl] according to

$$\tilde{b}_{bp} = 0.002 + 0.01(0.50 - 0.25\log_{10}[\text{Chl}]) \quad (5)$$

A model representing the spectral backscattering coefficient is thus obtained as follows. Upon rearranging Eq. 1, $b_{bp}(\lambda)$ is expressed as $b_{bp}(\lambda) = \tilde{b}_{bp} b_p(\lambda)$ and $\tilde{b}_{bp}(\lambda)$ is obtained from Eq. 5 so that \tilde{b}_{bp} decreases from 0.012 to 0.007 when [Chl] increases from 0.01 to 1 g m⁻³. The $b_p(660)$ val-

ues utilized here are those computed as a function of [Chl] by using Eq. 2a, or Eq. 2b thus providing two expressions for $b_{bp}(\lambda)$ referred to respectively as M-2a, and M-2b. Equations 3 and 4 are then applied to obtain the $b_p(\lambda)$ values at appropriate wavelengths.

Recent field measurements have provided the first empirical expressions of the backscattering ratio as a function of [Chl]. For all their data from Case 1 waters, Twardowski et al. (2001) arrived at

$$\tilde{b}_{bp}(532) = 0.0096[\text{Chl}]^{-0.253} \quad (6)$$

whereas Whitmire et al. (2007), considering only the data determined within the upper layer, obtained the following relationship

$$\tilde{b}_{bp}(555) = 0.0074[\text{Chl}]^{-0.042} \quad (7)$$

Although these relationships are statistically significant, there is a large amount of scatter around the fits and both studies covered only restricted [Chl] ranges. From these two datasets and according to Eqs. 6 and 7, \tilde{b}_{bp} thus appears to have a weak or no dependency on [Chl]. The study of Stramska et al. (2006) in the north polar Atlantic observed a slightly increasing \tilde{b}_{bp} with decreasing [Chl] and showed

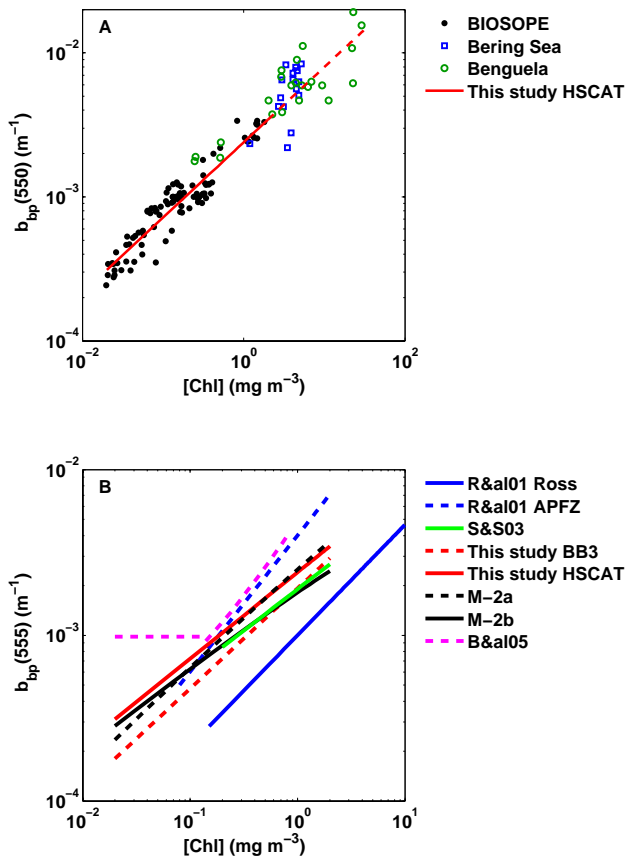


Fig. 2. Extension beyond 2 mg chl m^{-3} of the relationship between particulate backscattering coefficient at 555 nm and the concentration of chlorophyll-*a* and comparison with previously published relationships. **(A)** Superimposed onto the BIOSOPE data from Fig. 1d are two datasets with higher chlorophyll concentration. The first was obtained in the Bering Sea with a Hydroscat-6 instrument and the second obtained in the Benguela upwelling system by simultaneous inversion of the diffuse attenuation coefficient and the irradiance reflectance (Morel et al., 2006). The red line is the best fit obtained in Fig. 1d for the range of [Chl] encountered during BIOSOPE, the dashed part is the extension of this fit up to [Chl] of 30 mg chl m^{-3} . **(B)** The top five curves (see legend) were obtained using in situ data from the studies of Reynolds et al. (R&al01, 2001) in (i) the Ross Sea and (ii) the Antarctic Polar Front Zone, (APFZ), (iii) Stramska and Stramski (S&S03, 2003) in the North Polar Atlantic and from our studies using (iv) the BB3 at 532 nm (this study BB3), and (v) the Hydroscat at 550 nm (this study HSCAT). The following two curves, M-2a and M-2b, were obtained from Eq. 2a and b respectively, and Eqs. 3, 4 and 5 (see text for details). The last curve was obtained by Behrenfeld et al. (B&al05, 2005) from remote sensing data (MODIS AQUA sensor) using the model described in Maritorena et al. (2002). We have applied a spectral dependence of $\lambda^{-1.03}$ to transfer the curve reported at 440 nm to 555 nm consistent with the slope used by the GSM model (Maritorena et al., 2002).

that \tilde{b}_{bp} varied roughly by a factor of two to three for a given [Chl] depending on season for the same oceanic region. They did not, however, provide a functional fit to their data, which showed significant scatter. The relationship obtained by Sullivan et al. (2005), shows even more scatter and deals exclusively with coastal waters around the United States, where the influence of mineral particles is likely frequent and important. Again in US coastal waters, Snyder et al. (2008) found highly variable backscattering ratios (between 0.005 to 0.06) but did not relate their results to [Chl].

4 Results

In what follows we will first examine the dependence of the spectral backscattering coefficient on [Chl]. Then, we will carry out a similar analysis for the spectral scattering coefficient. Finally, we will focus on the backscattering ratio.

The particle backscattering coefficients as obtained with the BB3 and Hydroscat instruments are displayed for several wavelengths as a function of [Chl] for all stations of the BIOSOPE cruise in Fig. 1. Note that Twardowski et al. (2007) also present a comparison of BIOSOPE data between these two sensors at 470 nm (see also Stramski et al., 2008 for an analysis of Hydroscat data). Regardless of the wavelength, the $b_{bp}(\lambda)$ values increase rather regularly with increasing [Chl] for both instruments. Such increases of $b_{bp}(\lambda)$ are not unexpected because $b_p(\lambda)$ is known to show a steadily increasing trend with increasing [Chl] (e.g. Gordon and Morel, 1983) and, to the extent that $b_{bp}(\lambda)$ is expected to be sufficiently stable, the variations in $b_{bp}(\lambda)$ must roughly follow those of $b_p(\lambda)$.

A high correlation between $b_{bp}(\lambda)$ and [Chl] is observed on log-transformed data in Fig. 1 (see r^2 in each panel and in Table 1; r^2 and RMSE are provided for the decimal log-transformed data). The straight red line representing the best fit is plotted in Fig. 1, and it can be compared to the two models (M-2a and M-2b) for $b_{bp}(\lambda)$. While the fit and models do not coincide, the models provides a reasonably accurate description of the slope and amplitude within their respective uncertainties. For M-2a, which is apparently the best model for this dataset, the largest differences occur at 650 nm where the model overestimates the data by a factor of ~ 2 . Ostensibly, the regular linear increase in log space extends beyond the [Chl] domain encountered during the BIOSOPE cruise as demonstrated by Fig. 2a. In this figure, in addition to the results from the BIOSOPE cruise, are displayed $b_{bp}(550)$ values measured in the Bering Sea (with [Chl] near 5 mg m^{-3}) and data obtained by the simultaneous inversion of the diffuse attenuation coefficient and irradiance reflectance in the eutrophic waters ([Chl] between 0.2 and 30 mg chl m^{-3}) of the Benguela upwelling system (Morel et al., 2006).

The measurements made during the BIOSOPE cruise in low [Chl] waters agree with to those obtained during other cruise in case 1 waters with moderate to high [Chl]. Indeed,

apart from measurements in the Ross Sea, a comparison of the regression lines obtained in this study with previously described relationships of $b_{bp}(\lambda)$ vs. [Chl] for Case 1 waters measured *in situ* show a good consistency (Fig. 2b).

Prior to the present analysis, only the study of Behrenfeld et al. (2005) provided a functional relationship for [Chl] below 0.10 mg m^{-3} (shown in Fig. 1 panels A and F and Fig. 2b), but it was derived from remote sensing data not from *in situ* data. That relationship shows a levelling off of $b_{bp}(440)$ near a value of 0.0012 m^{-1} for [Chl] below 0.14 mg m^{-3} . In contrast, the models of $b_{bp}(\lambda)$ based on measurements of $b_p(\lambda)$ combined with hypotheses on the dependence of $\tilde{b}_{bp}(\lambda)$ on [Chl] (Eqs. 2a, 2b, 3, 4, and 5) suggest a continuous decrease of $b_{bp}(\lambda)$ with decreasing [Chl] at all wavelengths. The present measurements agree better with these models compared to the proposition of Behrenfeld et al. (2005) especially at low [Chl].

For describing the dependence of $b_{bp}(\lambda)$ on [Chl] using the direct measurements of $b_{bp}(\lambda)$, a model such as the one provided by the set of equations 2 through 5 can be simplified to a single equation, as there is no need for the parameterization of the intermediate term $\tilde{b}_{bp}(\lambda)$. A spectrally resolved empirical model of $b_{bp}(\lambda)$ (between 420 and 650 nm) can be written as:

$$b_{bp}(\lambda) = \alpha_1(\lambda) [\text{Chl}]^{\beta_1(\lambda)} \quad (8)$$

where $\alpha_1(\lambda)$ and $\beta_1(\lambda)$ are the multiplicative coefficient and an exponent obtained from fitting a power function to the data, respectively (Table 1 and Fig. 3). It is also found that the parameter $\alpha_1(\lambda)$ decreases linearly with wavelength

$$\alpha_1(\lambda) = 2.267 \times 10^{-3} - 5.058 \times 10^{-6} (\lambda - 550) \quad (8a)$$

for both the Hydrosat and BB3 datasets, although the Hydrosat dataset shows concave residuals while the BB3 dataset shows convex residuals. The slope parameter, $\beta_1(\lambda)$, also depends linearly on wavelength for both instruments, but the relationships differ slightly (see caption Fig. 3). Because there is no clear reason to assume that the data from one of the instruments are better compared to those of the other instrument, a mean relationship for $\beta_1(\lambda)$ can be adopted as follows (“proposed” curve in Fig. 3)

$$\beta_1(\lambda) = 0.565 + 0.000486(\lambda - 550) \quad (8b)$$

This relationship when applied to the whole dataset ($n=858$) provides an mean absolute percent error (see Table 1 for definition) of 25.2%, an RMSE on the decimal log transformed data of 0.134 and a coefficient of determination of $r^2=0.87$. The slight deviation from the general trend of the BB3 data at 532 nm shown in Fig. 3a and the relatively small discrepancy in the measured $\beta_1(\lambda)$ between the two instruments likely originate, at least partly, from differences in calibration and processing methods between them (described in details in Twardowski et al., 2007; Stramski et al., 2008).

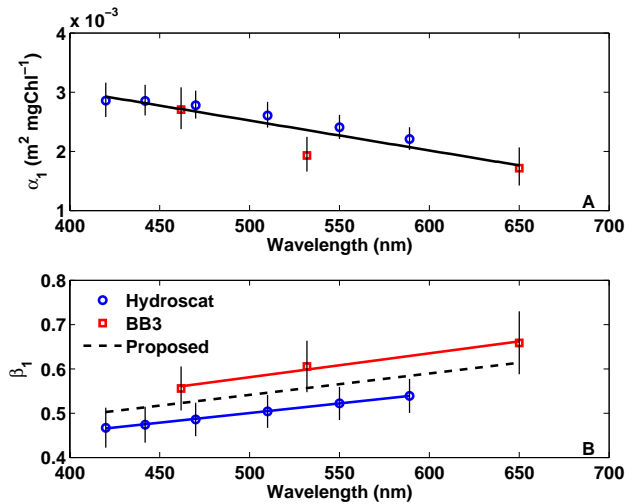


Fig. 3. Spectral dependencies of the parameters for the equation $b_{bp}(\lambda) = \alpha_1(\lambda) [\text{Chl}]^{\beta_1(\lambda)}$ that describes the relationship between the particulate backscattering coefficients $b_{bp}(\lambda)$ and [Chl]. **(A)** $\alpha_1(\lambda)$ vs. λ . The black line is the best fit represented by a linear model. Note that this departs from the power law often adopted; given the uncertainty in the data we adopted the simplest representation. A power law fit gives a value of -1.14 for the “spectral slope” (i.e. ν in Eq. 3 assuming a spectrally flat $\tilde{b}_{bp}(\lambda)$). **(B)** $\beta_1(\lambda)$ vs. λ . The continuous red and blue lines are best fits of linear models to the data points from the BB3, $\beta_1^{\text{BB3}}(\lambda) = 0.608 + 0.000538(\lambda - 550)$, and Hydrosat, $\beta_1^{\text{Hydrosat}}(\lambda) = 0.522 + 0.000434(\lambda - 550)$, instruments respectively. The dashed black line is the proposed model (see Eq. 8b), which is intermediate between the data from the two instruments. For both panels, the vertical lines represent the 95% confidence interval on the parameters.

Nevertheless, the differences between the Hydrosat and the BB3 within the present dataset remain small, especially when compared with the natural variability observed in the $b_{bp}(\lambda)$ vs. [Chl] in the ocean (see Fig. 2).

Figure 4 shows the $b_p(\lambda)$ data as a function of [Chl] for the same stations and depths as presented for the backscattering coefficient. The best fit to the data and the modelled curves are derived similarly to those in Fig. 1 (except that Eq. 5 is not used) and are also displayed in Fig. 4. The distribution of the data and the fits (r^2 and RMSE in Table 1) demonstrate that scattering by particulate material is highly correlated with [Chl], (an already established fact in case 1 waters) and that the previous formulations of these relationships (i.e. Eq. 2a and b) remain generally applicable to the eastern South Pacific waters. The empirical relationship of $b_p(\lambda)$ vs. [Chl], analogous to the one developed above for $b_{bp}(\lambda)$, is thus expressed as

$$b_p(\lambda) = \alpha_2(\lambda) [\text{Chl}]^{\beta_2(\lambda)} \quad (9)$$

The spectral dependencies of the regression parameters (see Table 1 for $\alpha_2(\lambda)$ and $\beta_2(\lambda)$ values) shows a linearly

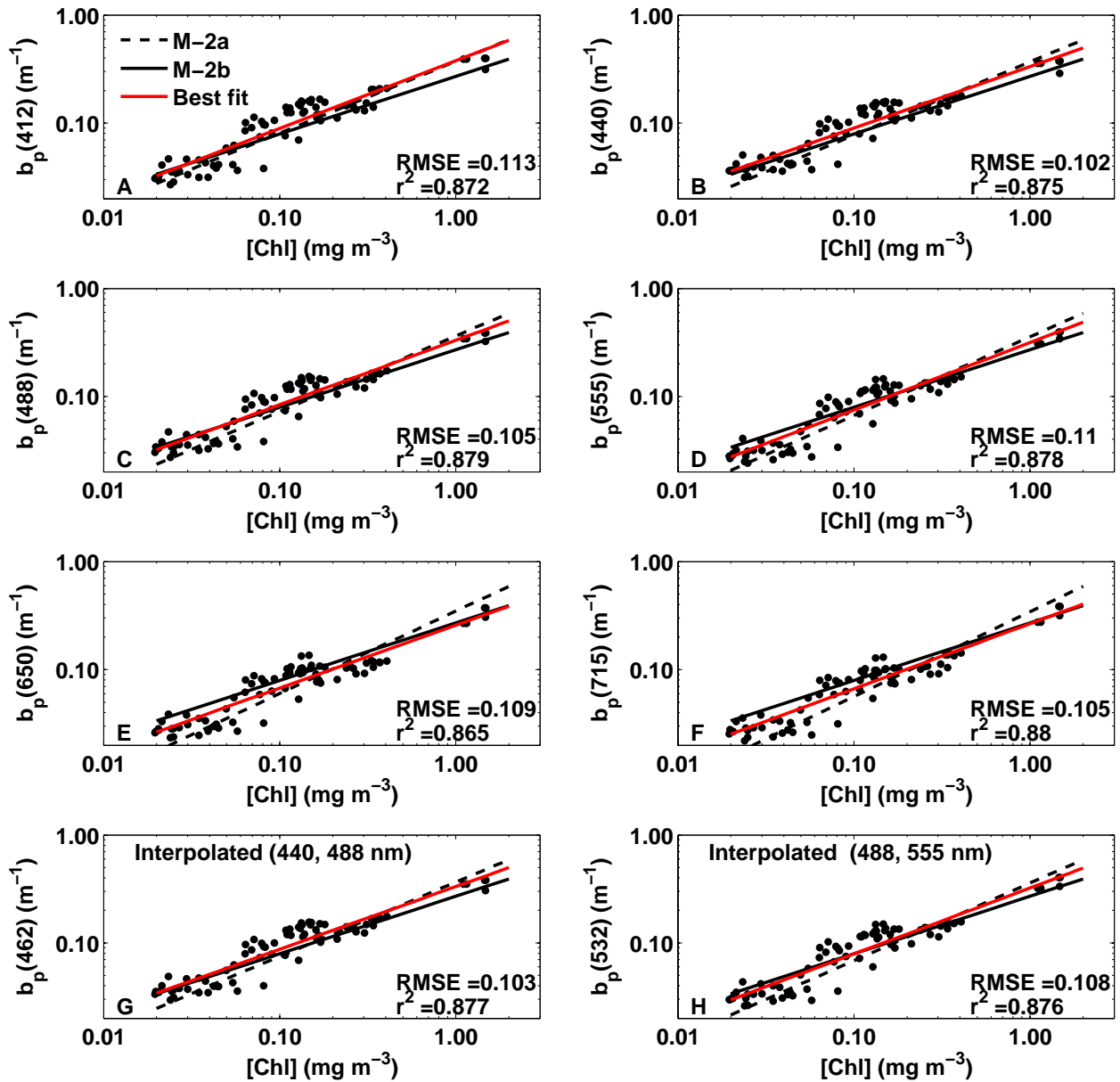


Fig. 4. As in Fig. 1, but for the particle scattering coefficient derived from measurements with the ac-9 instrument. For the two lower panels, the data have been interpolated between the wavelengths available on the ac-9 to match the wavelengths of the BB3 instrument.

decreasing trend for $\alpha_2(\lambda)$ and a rather constant value for $\beta_2(\lambda)$ (Fig. 5)

$$\alpha_2(\lambda) = 0.309 - 0.000384(\lambda - 550) \quad (9a)$$

and

$$\beta_2(\lambda) = 0.60. \quad (9b)$$

This relationship when applied to the whole dataset ($n=616$) provides an mean absolute percent error (see Table 1 for definition) of 25.2%, an RMSE on the decimal log transformed data of 0.125 and a coefficient of determination of

$r^2=0.88$. Given the spectral shape of $\alpha_2(\lambda)$ (Fig. 5a) it is tempting to interpret the faint spectral features in terms of phytoplankton absorption effects. However, the magnitude of the confidence interval for the estimates of $\alpha_2(\lambda)$ hardly allow such an interpretation. These results are very similar and certainly not significantly different from those presented by Gordon and Morel (1983) at 550 nm (Eq. 2) and Loisel and Morel (1998) at 660 nm (though closer to Eq. 2b at this waveband).

Additional useful information can be obtained from Figs. 1 and 4, and associated statistical analyses. Firstly and

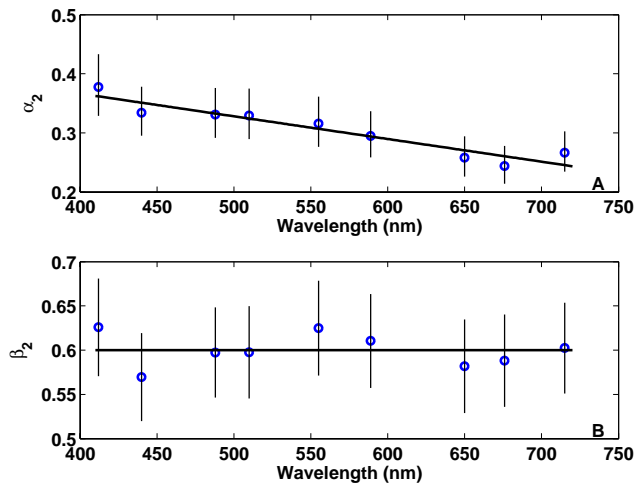


Fig. 5. Spectral dependencies of the parameters in the equation $b_p(\lambda) = \alpha_2(\lambda) [\text{Chl}]^{\beta_2(\lambda)}$ that describe the relationship between $b_p(\lambda)$ and $[\text{Chl}]$. (A) The black line represents a linear model fitted to the data. A power law fit to α_2 give a value of -0.70 for the “spectral slope” (i.e. ν in Eq. 3). B) The black line represents the average of all data. See Fig. 3 for other relevant details and Eq. 9a and 9b for values of the fitted parameters.

somewhat surprisingly, the fits for $b_{bp}(\lambda)$ vs. $[\text{Chl}]$ are as good as those for $b_p(\lambda)$ (see Table 1) and secondly, the best fit regression formulas for $b_{bp}(\lambda)$ and $b_p(\lambda)$ vs. $[\text{Chl}]$ are both of the same form, i.e., $b_{bp}(\lambda)$ or $b_p(\lambda)$. Under the condition that phytoplankton are not the particles responsible for most of the particulate backscattering but contribute more efficiently to particulate scattering, these results imply a conspicuously tight link between phytoplankton biomass and other, mostly biogeochemical, tiny particles.

Therefore, the ratios of spectrally matched $b_{bp}(\lambda)$ and $b_p(\lambda)$ from power function fits result in the particulate backscattering ratio

$$\tilde{b}_{bp}(\lambda) = \frac{b_{bp}(\lambda)}{b_p(\lambda)} = \frac{\alpha_1(\lambda) [\text{Chl}]^{\beta_1(\lambda)}}{\alpha_2(\lambda) [\text{Chl}]^{\beta_2(\lambda)}}. \quad (10)$$

For any given wavelength, the average value of $\tilde{b}_{bp}(\lambda)$ when $[\text{Chl}] = 1 \text{ mg m}^{-3}$ is provided by the ratio $\alpha_1(\lambda)/\alpha_2(\lambda)$ while its variation with $[\text{Chl}]$ is expressed through an exponent which amounts to the difference $\beta_1(\lambda) - \beta_2(\lambda)$.

The results of these computations are presented in Table 2. They differ slightly depending on whether the BB3 or the Hydrosicat datasets are used. Using the BB3 data, the \tilde{b}_{bp} values at the three wavelengths are similar and the mean value is 0.0069. The mean value of the exponent is -0.02, when we disregard the wavelength 650 nm where the RMSE for b_{bp} is higher. On average within the spectrum, \tilde{b}_{bp} can thus be expressed as

$$\tilde{b}_{bp} = 0.0069 [\text{Chl}]^{-0.02} \quad (11a)$$

Table 2. Parameters describing the relationship between the backscattering ratio and chlorophyll ($\tilde{b}_b = A[\text{Chl}]^B$).

Wavelength	A ($\text{m}^2 \text{ mg Chl}^{-1}$)	B (unitless)
420 ¹	0.0078	-0.14
442 ¹	0.0085	-0.10
462 ²	0.0081	-0.03
470 ¹	0.0084	-0.10
510 ¹	0.0080	-0.10
532 ²	0.0060	-0.01
550 ¹	0.0076	-0.10
589 ¹	0.0075	-0.07
(650) ²	0.0067	0.08
Average BB3	0.0069	-0.02*
Average Hydrosicat	0.0080	-0.10
Average Hydrosicat and BB3	0.0077	0.081*

¹ Hydrosicat backscattering data.

² BB3 backscattering data.

* Without 650 nm, which shows a higher RMSE for b_{bp} .

For the whole BB3 dataset, including 650 nm, the expression has a mean absolute percent error of 28.4%, and a coefficient of determination of $r^2 = 0.05$, the latter reflecting the absence of variability with $[\text{Chl}]$. This expression is close to that of Whitmire et al. (2007) (see Eq. 7 above) and means that the \tilde{b}_{bp} tends to be independent from $[\text{Chl}]$ (the exponent is not significantly different from 0), at least for the range of concentrations observed in the investigated region. Using the Hydrosicat data and averaging over the six wavebands, we find

$$\tilde{b}_{bp} = 0.0080 [\text{Chl}]^{-0.10} \quad (11b)$$

As the exponent is significantly different from zero, this would suggest a weak dependence of on $[\text{Chl}]$, numerically similar to that expressed by Eq. (5). For the whole Hydrosicat dataset, the expression has a mean absolute percent error of 16.5%, and a coefficient of determination of $r^2 = 0.28$.

The backscattering ratio can also be analyzed on a measurement-by-measurement basis, i.e. by considering the \tilde{b}_{bp} values produced by the pairs of particle backscattering and particle scattering values obtained directly from measurements for each wavelength. These data are shown in Fig. 6a for the BB3 and Fig. 6b for the Hydrosicat. Also are displayed on this figure several proposed relationships namely (i) Eq. 6, and (ii) Eq. 7, (iii) the relationship proposed by Sullivan et al. (2005) for coastal waters, (iv) the “theoretical” expression corresponding to Eq. 5, (v) a similar relationship proposed by Ulloa et al. (1994), and (vi) the curves from Eq. 11a (for Fig 6a) and Eq. 11b (for Fig. 6b). The actual BB3 data are generally below the various curves for low chlorophyll concentrations, except for the relationship of Whitmire et al. (2007). There is also a considerable

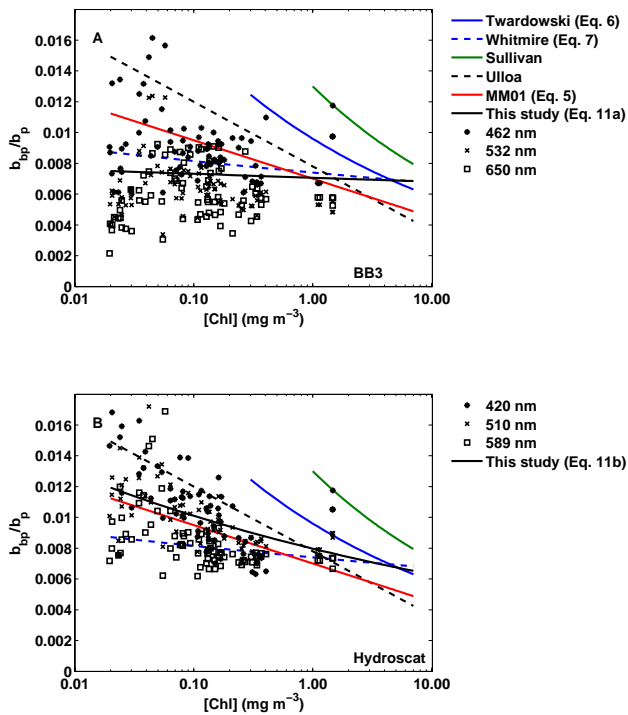


Fig. 6. Data points represent the particulate backscattering ratio, \tilde{b}_{bp} , computed from paired values of b_{bp} and b_p obtained from the BB3 (panel A), Hydroscat (panel B), and ac-9 measurements, plotted as a function of chlorophyll *a* concentration, [Chl]. Also included are several curves as follows. The empirical curves are those proposed by Twardowski et al. (2006) (i.e. Eq. 6); Whitmire et al. (2007) (i.e. Eq. 7); and Sullivan et al. (2005) for coastal waters (i.e. $\tilde{b}_{bp}=0.013 [\text{Chl}]^{-0.216}$). The empirical curves are limited to the range of [Chl] in the respective datasets. The curve from a semi-empirical model is that proposed by Ulloa et al. (1994), namely $\tilde{b}_{bp}=0.0078-0.0042 \log_{10} [\text{Chl}]$. The curve denoted as “MM01” is obtained according to Morel and Maritorena (2001) (see Eq. 5 in this study). Finally, the curve “This study” represents the spectrally averaged curve obtained in this work (see Eq. 11a for panel A and Eq. 11b for panel B).

amount of scatter in the data points regardless of the wavelength. For the Hydroscat, the data points are rather well represented by the Morel-Maritorena (2001) model. A condensed representation of the data points from Fig. 6 in terms of a box-and-whiskers plot is provided in Fig. 7. The median value of \tilde{b}_{bp} for each wavelength is shown with the range of variation (outliers excluded) as well as the corresponding quartiles. Pairs of $b_{bp}(\lambda)$ and $b_p(\lambda)$ were also determined within the Benguela upwelling system characterized by moderate to very high [Chl]. From these pairs, the spectral

$\tilde{b}_{bp}(\lambda)$ values have been derived. In Fig. 7 are plotted the average of all $\tilde{b}_{bp}(\lambda)$ values (± 1 sd, pink area) so obtained (see also Fig. 15c in Morel et al., 2006). These $\tilde{b}_{bp}(\lambda)$ ratios superimpose onto, and nicely coincide with those of the South Pacific.

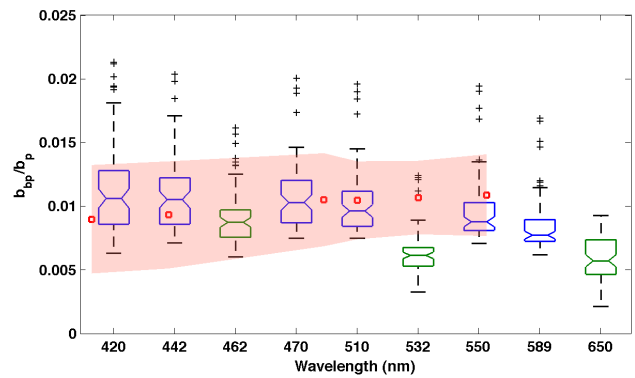


Fig. 7. Box and whiskers plot of $\tilde{b}_{bp}(\lambda)$ for each wavelength, which illustrates the relative distribution of data around the median. The height of the boxes represents the two central quartiles (25% to 50% and 50% to 75%). The horizontal bars (whiskers) show the extreme deviations (1.5 times the interquartile range), and the points outside these values are considered outliers and are individually displayed as black “+”. Boxes for which the width of the notch areas (waist) overlap have median values that are not statistically different at the 5% significance level. The boxes with green and blue lines represent data from the BB3 and Hydroscat instruments, respectively. The red circles represent the average values of all the $\tilde{b}_{bp}(\lambda)$ (i.e. Case 1 and Case 2-Y waters, see figure 15 in Morel et al., 2006) obtained by inversion of K_d and reflectance for the BENCAL cruise, the colored area represent plus and minus one standard deviation from these values.

Both approaches, namely the indirect one based on the use of the best fits to $b_{bp}(\lambda)$ vs. [Chl] and $b_p(\lambda)$ vs. [Chl], and the direct one based on the use of paired measured data of $b_{bp}(\lambda)$ and $b_p(\lambda)$, are consistent within the limits of confidence and support the parameterization provided by Eq. 11a and b. Equations 11a and b do not account for the spectral effects. We could derive the spectral behavior of $\tilde{b}_{bp}(\lambda)$ as well as its change with [Chl] using Eq. 10 by replacing its numerator by the results of Eq. 8 and its denominator by those of Eq. 9. However, the scatter of the points (seen in Fig. 6) underlying these relationships would make any conclusions regarding the results very speculative.

5 Discussion and Conclusion

The first aim of the present study was to examine the potential existence and the functional dependence of the relationship between $b_{bp}(\lambda)$ and [Chl]. In particular, we were interested in the low [Chl] waters below $\sim 0.15 \text{ mg m}^{-3}$, which are encountered in approximately 90% of the ocean surface (Antoine et al., 2005) and where relatively few in situ measurements have been made. The important result presented here is that such empirical relationships exist in Case 1 waters over the full [Chl] range investigated ($0.02\text{--}2 \text{ mg m}^{-3}$) and can be represented using simple power function of [Chl]. These relationships were also found to be applicable

to regions with much higher [Chl] (Bering Sea and Benguela upwelling). Furthermore, these relationships are as significant (similar RMSE) as those already established for the particle scattering coefficient, b_p , and they are wavelength dependent. These results should be helpful in further development and refinement of forward models of ocean color and in the construction of synthetic datasets for inverse modeling purposes (e.g. IOCCG, 2006), particularly at low chlorophyll concentrations.

From a remote sensing perspective, such a description of $b_{bp}(\lambda)$ is particularly important when developing forward models. Indeed, bio-optical and reflectance models require detailed knowledge and parameterization of the average trends in the inherent optical properties, at least within Case 1 waters where these trends can be related to [Chl]. Up until now and in the absence of data, models have relied on assumptions about $b_{bp}(\lambda)$. A common belief was that the light backscattering process is perhaps less predictable than other processes such as total scattering and absorption, and would thus form the weak link in the modelling approaches. According to the present analysis, it seems that this is not the case, since the prediction of $b_{bp}(\lambda)$ from [Chl] would not be worse (nor better, i.e., roughly within a factor of 2 or 3) than those for other inherent optical properties.

Prior to this study, two main propositions existed that included [Chl] below 0.1 mg m^{-3} , one formulated by Morel and Maritorena (2001) and the other by Behrenfeld et al. (2005). The latter is based on simultaneous retrievals of [Chl] and $b_{bp}(\lambda)$ from remotely sensed ocean color radiometric data. Our present experimental findings, which are based on coincident in situ measurements of $b_p(\lambda)$, $b_{bp}(\lambda)$, and [Chl] are more consistent with the formulation of Morel and Maritorena (2001) that accounts for a continuously decreasing $b_{bp}(\lambda)$ with decreasing [Chl]. These concomitant decreases contrast with the flat relationship adopted by Behrenfeld et al. (2005) for the low chlorophyll concentrations that predicts an invariant $b_{bp}(440)$ value (near 0.0012 m^{-1}) when [Chl] is below 0.14 mg m^{-3} . Actually, Behrenfeld et al. (2005) used the Garver-Siegel-Maritorena inversion model (Maritorena et al., 2002), and a bias in the satellite-derived backscattering coefficient probably occurs when this model is used at low [Chl] (see Appendix). This bias may explain the bilinear relationship adopted by Behrenfeld et al. (2005).

Our second aim was to examine if any difference in the spectral behavior of the backscattering and scattering coefficient existed. To this end, we analyzed the particulate backscattering ratio. This analysis shows that $\tilde{b}_{bp}(\lambda)$ is essentially spectrally neutral and its value (around 0.01) does not depend on the trophic state of case 1 waters.

The unquestionably case 1 nature of the environment sampled allowed us to obtain the clear trends described herein with limited variability due to external influences. It must, however, be kept in mind that in this region, the influence of aerosol deposition onto the ocean is amongst the lowest in

the world's ocean (Gao et al., 2003) and hence extrapolation of these results to other oceanic regions must be made with care. In particular, the relationship for regions in which a greater abundance of mineral particles could play an important role might depart from the relationships derived here.

It is clear that within this paper we present field observations but we do not provide an explanation for the origin of the backscattering in the ocean. Indeed, the backscattering process is associated with tiny particles (Morel and Ahn, 1991; Stramski and Kiefer, 1991), while the scattering process results from the presence of particles of much larger size (by a factor of ~ 10) such as that of most algal cells. Therefore, the fact that b_p is related to [Chl] is naturally expected in case 1 waters, and actually observed. More intriguing is the fact that b_{bp} is also tightly linked to [Chl], which implies that the abundance of tiny, a priori non-algal, particles is, nonetheless, proportional to the abundance of algae. Heterotrophic bacteria and viruses concentration are very likely tightly linked to algal concentration. Their contribution to total backscattering, however, remains limited (Morel and Ahn, 1991; Stramski and Kiefer, 1991). Therefore, the unidentified "missing backscattering term" (probably debris of all kinds?) would also be proportional to the algal concentration, which remains to be explained on a biogeochemical basis.

Appendix

Examination of the remotely sensed backscattering coefficient in the BIOSOPE zone

Due to the generally cloudy conditions, a very limited number of satellite and in situ match-up observations were obtained during the BIOSOPE cruise. This unfavorable situation does not provide a sufficient number of data points over a wide [Chl] range to test directly the performance of remote sensing models for backscattering such as those presented by IOCCG (2006). Instead, here we use an indirect approach based on the comparison of satellite-derived [Chl] with satellite-derived backscattering coefficients.

For all scenes acquired by the MODIS AQUA sensor in the BIOSOPE zone during the month of November 2004, we applied two semi-analytical inverse models of ocean color to obtain $b_{bp}(443)$ and extracted the results along the transect (independently of the date). The two models used are the SEADAS 5.1.3 implementations of 1) the Quasi-Analytical Algorithm (QAA, Lee et al., 2002) and 2) the Garver-Siegel-Maritorena model (GSM, Maritorena et al., 2002). The backscattering coefficient retrieved from these models is then plotted against [Chl] retrieved with the OC3M algorithm (Fig. A1).

This analysis shows that within the South Pacific Gyre, the GSM model returns nearly constant b_{bp} values below $[\text{Chl}] = 0.1 \text{ mg m}^{-3}$. The magnitude of this constant value corresponds roughly to the horizontal portion of the relationship

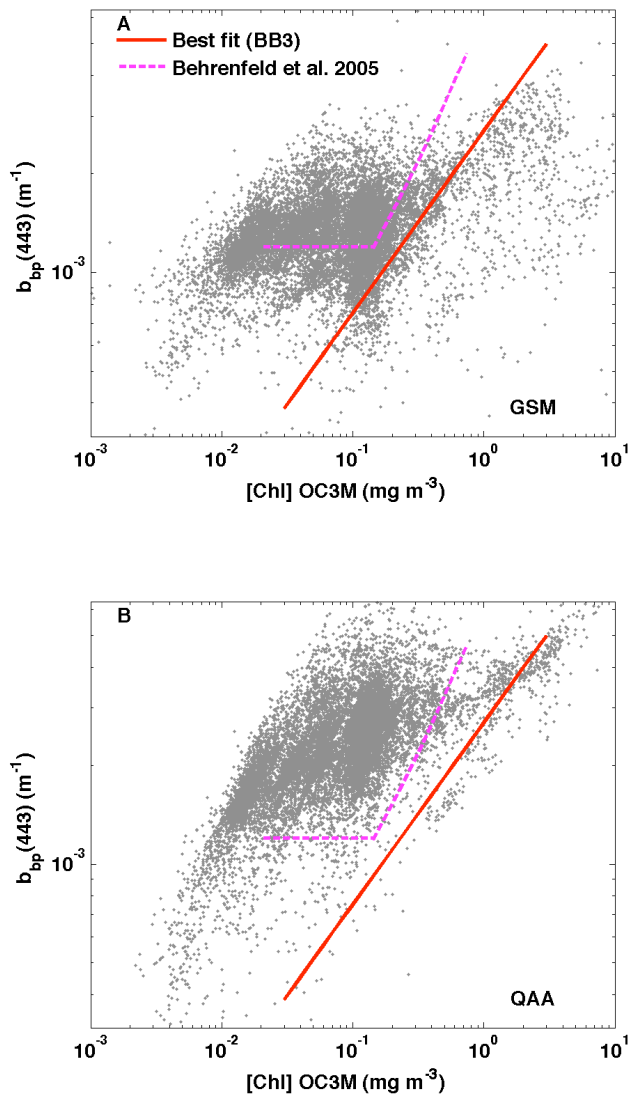


Fig. A1. The particulate backscattering coefficient at 443 nm retrieved using two ocean color semi-analytical inverse models as a function of the chlorophyll concentration obtained using the OC3M algorithm along the BIOSOPE transect. **(A)** The GSM model, **(B)** the QAA model. On both panels the relationships fitted to the BB3 data at 462 nm as well as the bilinear relationship obtained by Behrenfeld et al. (2005) (at 440 nm) are overlaid.

proposed by Behrenfeld et al. (2005). In contrast, the in situ data show continuously decreasing values, which suggest that the horizontal segment in the Behrenfeld et al. (2005) curve originates from biases in the remotely sensed backscattering coefficient, and not from physiological adjustments in phytoplankton. The results obtained using the QAA model show an irregular decrease in the backscattering coefficients, more similar to those measured in the Gyre, except that the slope is less steep leading to an overestimate of the backscattering coefficient by $\sim 270\%$ relative to the in situ data at $[\text{Chl}] = 0.02 \text{ mg m}^{-3}$.

Acknowledgements. D. Tailliez and C. Marec are warmly thanked for their efficient help in CTD rosette management and data processing. Data from the Bering Sea were provided by J. J. Cullen from a research program supported by NOAA/PMEL, NSERC Research Partnerships and the US Office of Naval Research. This is a contribution of the BIOSOPE project of the LEFE-CYBER French program. This research was funded by the Centre National de la Recherche Scientifique (CNRS), the Institut des Sciences de l'Univers (INSU), the Centre National d'Études Spatiales (CNES), the European Space Agency (ESA), the National Aeronautics and Space Administration (NASA) and the Natural Sciences and Engineering Research Council of Canada (NSERC). Y. H. was funded by a postdoctoral scholarship from CNES (France).

Edited by: E. Boss

References

- Ahn, Y. H., Bricaud, A., and Morel, A.: Light backscattering efficiency and related properties of some phytoplankters, *Deep-Sea Res. Pt.*, 39, 1835–1855, 1992.
- Antoine, D., Morel, A., Gordon, H. R., Banzon, V. F., and Evans, R. H.: Bridging ocean color observations of the 1980s and 2000s in search of long-term trends, *J. Geophys. Res.*, 110, C06009, doi:10.1029/2004JC002620, 2005.
- Bader, H.: The hyperbolic distribution of particle sizes, *J. Geophys. Res.*, 75, 2822–2830, 1970.
- Balch, W. M., Drapeau, D. T., Fritz, J. J., Bowler, B. C., and Nolan, J.: Optical backscattering in the arabian sea - continuous underway measurements of particulate inorganic and organic carbon, *Deep-Sea Res. Pt. I*, 48, 2423–2452, 2001.
- Behrenfeld, M. J., Boss, E., Siegel, D. A., and Shea, D. M.: Carbon-based ocean productivity and phytoplankton physiology from space, *Global Biogeochem. Cy.*, 19, GB1006, doi:10.1029/2004GB002299, 2005.
- Boss, E., Twardowski, M. S., and Herring, S.: Shape of the particulate beam attenuation spectrum and its inversion to obtain the shape of the particulate size distribution, *Appl. Opt.*, 40, 4885–4893, 2001.
- Clark, G. L., and Ewing, G. C.: Remote spectroscopy of the sea for biological production studies, in: *Optical aspect of oceanography*, edited by: Jerlov, N. G., and Nielsen, E. S., Academic, New York, 494, 1974.
- Gao, Y., Fan, S.-M., and Sarmiento, J. L.: Aeolian input to the ocean through precipitation scavenging: A modeling perspective and its implication for natural iron fertilization in the ocean, *J. Geophys. Res.*, 108, 4221, doi:10.1029/2002JD002420, 2003.
- Gordon, H. R., Brown, O. B., and Jacobs, M. M.: Computed relationships between inherent and apparent optical properties of a flat homogeneous ocean, *Appl. Opt.*, 14, 417–427, 1975.
- Gordon, H. R. and Morel, A.: Remote assessment of ocean color for interpretation of satellite visible imagery: A review, *Lecture notes on coastal and estuarine studies*, Springer Verlag, Heidelberg, Germany, 114 pp., 1983.
- Gordon, H. R., Brown, O. B., Evans, R. H., Brown, J. W., Smith, R. C., Baker, K. S., and Clark, D. K.: A semianalytic radiance model of ocean color, *J. Geophys. Res.*, 93, 10 909–10 924, 1988.

- IOCCG: Remote sensing of inherent optical properties: Fundamentals, tests of algorithms, and applications, in: Reports of the International Ocean-Colour Coordinating Group, edited by: Lee, Z.-P., No. 5, IOCCG, Dartmouth, Canada, 126, 2006.
- Lee, Z. P., Carder, K. L., and Arnone, R. A.: Deriving inherent optical properties from water color: A multiband quasi-analytical algorithm for optically deep waters, *Appl. Opt.*, 41, 5755–5772, 2002.
- Loisel, H. and Morel, A.: Light scattering and chlorophyll concentration in case 1 waters: A reexamination, *Limnol. Oceanogr.*, 43, 847–858, 1998.
- Maritorena, S., Siegel, D. A., and Peterson, A. R.: Optimization of a semianalytical ocean color model for global-scale applications, *Appl. Opt.*, 41, 2705–2714, 2002.
- Morel, A.: Diffusion de la lumière par les eaux de mer. Resultats expérimentaux et approche théorique., AGARD lectures series, 3.1.1–3.1.76, 1973.
- Morel, A. and Prieur, L.: Analysis of variations in ocean color, *Limnol. Oceanogr.*, 22, 709–722, 1977.
- Morel, A. and Bricaud, A.: Theoretical results concerning the optics of phytoplankton, with special references to remote sensing applications, in: *Oceanography from space*, edited by: Gower, J. F. R., Plenum, New York, 313–327, 1981.
- Morel, A. and Bricaud, A.: Inherent properties of algal cells including picoplankton: Theoretical and experimental results., in: *Photosynthetic picoplankton*, edited by: Platt, T. and Li, W. K. W., Canadian bulletin of fisheries and aquatic sciences, 521–559, 1986.
- Morel, A.: Optical modeling of the upper ocean in relation to its biogenous matter content (case 1 waters), *J. Geophys. Res.*, 93, 10 749–10 768, 1988.
- Morel, A. and Ahn, Y.-H.: Optics of heterotrophic nanoflagellates and ciliates: A tentative assessment of their scattering role in oceanic waters compared to those of bacterial and algal cells, *J. Mar. Res.*, 49, 177–202, 1991.
- Morel, A. and Maritorena, S.: Bio-optical properties of oceanic waters: A reappraisal, *J. Geophys. Res.*, 106, 7163–7180, 2001.
- Morel, A., Gentili, B., Chami, M., and Ras, J.: Bio-optical properties of high chlorophyll case 1 waters and of yellow-substance-dominated case 2 waters, *Deep-Sea Res. Pt. I*, 53, 1439–1459, 2006.
- Morel, A., Gentili, B., Claustre, H., Babin, M., Bricaud, A., Ras, J., and Tièche, F.: Optical properties of the “Clearest” Natural waters, *Limnol. Oceanogr.*, 52, 217–229, 2007.
- O’Reilly, J. E., Maritorena, S., Mitchell, B. G., Siegel, D. A., Carder, K. L., Garver, S. A., Kahru, M., and McClain, C. R.: Ocean color chlorophyll algorithms for SeaWiFS, *J. Geophys. Res.*, 103, 24 937–24 953, 1998.
- Petzold, T. J.: Volume scattering functions for selected ocean waters, Scripps Institution of Oceanography, Visibility Lab, San Diego, 85, 1972.
- Ras, J., Claustre, H., and Uitz, J.: Spatial variability of phytoplankton pigment distributions in the subtropical South Pacific ocean: Comparison between in situ and predicted data, *Biogeosciences*, 5, 353–369, 2007, <http://www.biogeosciences.net/5/353/2007/>.
- Reynolds, R. A., Stramski, D., and Mitchell, B. G.: A chlorophyll-dependent semianalytical reflectance model derived from field measurements of absorption and backscattering coefficients within the southern ocean, *J. Geophys. Res.*, 106, 7125–7138, 2001.
- Snyder, W. A., Arnone, R. A., Davis, C. O., Goode, W., Gould, R. W., Ladner, S., Lamela, G., Rhea, W. J., Stavn, R., Sydor, M., and Weidemann, A.: Optical scattering and backscattering by organic and inorganic particulates in U.S. Coastal waters, *Appl. Opt.*, 47, 666–677, 2008.
- Stramska, M., Stramski, D., Hapter, R., Kaczmarek, S., and Ston, J.: Bio-optical relationships and ocean color algorithms for the north polar region of the Atlantic, *J. Geophys. Res.*, 108, 3143, doi:10.1029/2001JC001195, 2003.
- Stramska, M., Stramski, D., Kaczmarek, S., Allison, D. B., and Schwarz, J.: Seasonal and regional differentiation of bio-optical properties within the north polar Atlantic, *J. Geophys. Res.*, 111, C08003, doi:10.1029/2005JC003293, 2006.
- Stramski, D. and Kiefer, D. A.: Light scattering by microorganisms in the open ocean, *Prog. Oceanogr.*, 28, 343–383, 1991.
- Stramski, D., Boss, E., Bogucki, D., and Voss, K. J.: The role of seawater constituents in light backscattering in the ocean, *Prog. Oceanogr.*, 61, 27–56, 2004.
- Stramski, D., Reynolds, R. A., Babin, M., Kaczmarek, S., Lewis, M. R., Röttgers, M., Sciandra, A., Stramska, M., Twardowski, M. S., Franz, B. A., and Claustre, H.: Relationships between the surface concentration of particulate organic carbon and optical properties in the eastern South Pacific and eastern Atlantic oceans., *Biogeosciences*, 5, 171–201, 2008, <http://www.biogeosciences.net/5/171/2008/>.
- Sullivan, J. M., Twardowski, M. S., Donaghay, P. L., and Freeman, S. A.: Use of optical scattering to discriminate particle types in coastal waters, *Appl. Opt.*, 44, 1667–1680, 2005.
- Twardowski, M. S., Boss, E., Macdonald, J. B., Pegau, W. S., Barnard, A. H., and Zaneveld, J. R. V.: A model for estimating bulk refractive index from the optical backscattering ratio and the implications for understanding particle composition in case i and case ii waters, *J. Geophys. Res.*, 106, 14 129–14 142, 2001.
- Twardowski, M. S., Claustre, H., Freeman, S. A., Stramski, D., and Huot, Y.: Optical backscattering properties of the “clearest” natural waters, *Biogeosciences*, 4, 1041–1058, 2007, <http://www.biogeosciences.net/4/1041/2007/>.
- Ulloa, O., Sathyendranath, S., and Platt, T.: Effect of the particle-size distribution on the backscattering ratio in seawater, *Appl. Opt.*, 33, 7070–7077, 1994.
- Whitmire, A. L., Boss, E., Cowles, T. J., and Pegau, W. S.: Spectral variability of the particulate backscattering ratio, *Opt. Express.*, 15, 7019–7031, 2007.

Relationship between photosynthetic parameters and different proxies of phytoplankton biomass in the subtropical ocean

Y. Huot¹, M. Babin¹, F. Bruyant², C. Grob⁴, M. S. Twardowski³, and H. Claustre¹

¹CNRS, Laboratoire d'Océanographie de Villefranche, 06230 Villefranche-sur-Mer, France; Université Pierre et Marie Curie-Paris 6, Laboratoire d'Océanographie de Villefranche, 06230 Villefranche-sur-Mer, France

²Dalhousie University, Department of Oceanography, 1355 Oxford Street, Halifax N.S. B3H 4J1, Canada

³WET Labs, Inc., Department of Research, 165 Dean Knauss Dr., Narragansett, RI 02882, USA

⁴Graduate Program in Oceanography, Department of Oceanography and Center for Oceanographic Research in the eastern South Pacific, University of Concepción, Casilla 160-C, Concepción, Chile

Received: 20 February 2007 – Published in Biogeosciences Discuss.: 1 March 2007

Revised: 7 September 2007 – Accepted: 22 September 2007 – Published: 16 October 2007

Abstract. Probably because it is a readily available ocean color product, almost all models of primary productivity use chlorophyll as their index of phytoplankton biomass. As other variables become more readily available, both from remote sensing and in situ autonomous platforms, we should ask if other indices of biomass might be preferable. Herein, we compare the accuracy of different proxies of phytoplankton biomass for estimating the maximum photosynthetic rate (P_{\max}) and the initial slope of the production versus irradiance (P vs. E) curve (α). The proxies compared are: the total chlorophyll *a* concentration (Tchl*a*, the sum of chlorophyll *a* and divinyl chlorophyll), the phytoplankton absorption coefficient, the phytoplankton photosynthetic absorption coefficient, the active fluorescence in situ, the particulate scattering coefficient at 650 nm ($b_p(650)$), and the particulate backscattering coefficient at 650 nm ($b_{bp}(650)$). All of the data (about 170 P vs. E curves) were collected in the South Pacific Ocean. We find that when only the phytoplanktonic biomass proxies are available, $b_p(650)$ and Tchl*a* are respectively the best estimators of P_{\max} and α . When additional variables are available, such as the depth of sampling, the irradiance at depth, or the temperature, Tchl*a* is the best estimator of both P_{\max} and α .

1 Introduction

Photosynthesis (P) in the ocean can be conveniently described using two basic quantities: the phytoplankton biomass (B), and the photosynthetic rates per unit biomass P^B ; $P = B P^B$. Both quantities can be measured in situ and are highly variable. To obtain global estimates of productivity, however, these quantities must be estimated for all oceans and with sufficient temporal resolution and this cannot be achieved by shipboard sampling. Because phytoplankton absorption changes the color of the light leaving the ocean, B can be obtained accurately using satellite imagery (using chlorophyll *a* as a proxy). Since P^B cannot be measured on large scales continuously, an alternative method must be used to estimate it. Finding an appropriate method has proven difficult. Indeed, despite years of research, its estimate remains the largest uncertainty in our models of oceanic primary production.

The main variable influencing P^B is the incident irradiance. Describing this influence is relatively simple as it can be mathematically represented by a saturating function (Falkowski and Raven, 1997): the so-called PvsE curve. This function can be parameterized using two parameters: α^B [usually $\text{mgC}(\text{mgChl})^{-1} \text{h}^{-1} (\mu\text{mol photon m}^{-2} \text{s}^{-1})^{-1}$] which describes the initial slope; and P_{\max}^B [usually $\text{mgC}(\text{mgChl})^{-1} \text{h}^{-1}$] which describes the amplitude of the light-saturated plateau. If P_{\max}^B and α^B are known, the influence of incident light on P^B is known. The most difficult aspect is the prediction of variability in P_{\max}^B and α^B that originates from changes in the physiological state (i.e.

Correspondence to: Y. Huot
(huot@obs-vlfr.fr)

photoacclimation and nutritional status) of phytoplankton or in the species composition of the community.

On the one hand, it has long been observed that if P_{\max}^B is normalized to carbon (B =carbon), P_{\max}^B is almost independent of the growth irradiance, reflecting a parallel physiological adjustment of the maximal capacity to fix carbon and the cellular carbon quota. On the other hand, normalization by chlorophyll a shows lower values at low growth irradiance reflecting photoacclimation processes. In an opposite fashion, the light limited portion of the curve, when normalized to chlorophyll a , is largely independent of growth irradiance, but varies due to photoacclimation when normalized to carbon. The ubiquitous nature of these relationships for most algal groups has been reviewed by MacIntyre et al. (2002), and several growth and photoacclimation models have been built to match these observations. It results that, to remove an important source of physiological variability, that due to photoacclimation, and to obtain photosynthetic parameters that are independent of growth irradiance, carbon is a better quantity to normalize the light saturated rates and chlorophyll a is better to normalize the light limited part of the curve.

Unfortunately, a direct measure of phytoplankton carbon in situ or from remote sensing does not exist, such that all models of primary productivity published to date use chlorophyll a to normalize both α^B and P_{\max}^B . Since variability in the biomass-normalized depth-integrated primary production is thought to be mostly driven by the light-saturated rate of photosynthesis (Behrenfeld and Falkowski, 1997), progress in predicting P_{\max}^B is central to estimating oceanic primary production more accurately.

Therefore, if carbon could be measured or estimated accurately, phytoplankton carbon might provide a good alternative for these models. Recently, Behrenfeld and colleagues (Behrenfeld et al., 2005; Behrenfeld and Boss, 2003, 2006) suggested that light scattering could provide an accurate proxy of phytoplankton carbon. These suggestions have brought to the forefront questions regarding the interpretation of these optical parameters. Though it has long been known that the beam attenuation coefficient (c_p , m^{-1}) is a good proxy of the total particulate organic carbon (POC) in case 1 waters (Morel, 1988; Gardner et al., 2006, and references therein), the suggestion of Behrenfeld and Boss (2003) that it represents an accurate proxy of phytoplankton carbon merits further research. In a similar way, the particulate backscattering coefficient (b_{bp} , m^{-1}), which can be obtained from satellite remote sensing, has been used to estimate the concentration of POC (Stramski et al., 1999). More recently, Behrenfeld et al. (2005) based on a good correlation between b_{bp} and chlorophyll a proposed the utilization of the backscattering coefficient to estimate the phytoplankton carbon over large space and time scales. Aware that the sources of backscattered light in the ocean remain unknown (Stramski et al., 2004), we will examine here both b_{bp} and c_p as potential alternatives to *Tchl*a for constraining the variability of photosynthetic parameters. In this analysis, because mea-

surements of the scattering coefficient (b_p , m^{-1}), are available, we will use them instead of c_p , since c_p is generally used as a surrogate for b_p .

Another proxy of biomass examined herein is phytoplankton absorption (\bar{a}_{phy} , m^{-1}). Indeed it has sometimes been argued that \bar{a}_{phy} is preferable to *Tchl*a for studies of primary productivity (Perry, 1994; Lee et al., 1996; Marra et al., 2007). The basis for this proposition is that \bar{a}_{phy} is more directly linked both to the remote sensing signal and photosynthetic processes than *Tchl*a (Perry, 1994). The evidence for this suggestion is, however, still lacking on large oceanic scales. Other potentially useful measures examined in this paper are the: photosynthetic absorption (\bar{a}_{ps} , m^{-1}) which encompasses all and only the photosynthetic pigments; chlorophyll a fluorescence, which is due to the absorption by all photosynthetic pigments and has the advantage of being readily measured in the ocean with high temporal and spatial resolution but is strongly affected by the physiological state of the algae; and, finally, picophytoplankton biovolume obtained by flow cytometry.

After providing some background to give a mechanistic basis for the interpretation of the photosynthetic parameters, we will use straightforward analyses to verify if any of these biomass proxies can be substituted for *Tchl*a to obtain better predictions of the phytoplankton photosynthetic parameters. Our study will use a dataset obtained during the BIOSOPE cruise. This cruise encompassed a large range of trophic conditions from the hyperoligotrophic waters of the South Pacific Gyre to the eutrophic conditions associated with the Chile upwelling region, also investigating the mesotrophic HNLC (high nutrient low chlorophyll) waters of the sub-equatorial region and in the vicinity of the Marquesas Islands. We verify that the relationships obtained are applicable to other regions by comparing our results with those obtained during the PROSOPE cruise which sampled the Moroccan upwelling and the Mediterranean sea.

2 Background

To quantitatively evaluate potential alternatives to *Tchl*a and interpret them within a more general and fundamental frame, we use the knowledge from theory and laboratory experiments that allows us to describe the photosynthetic parameters before normalization to biomass, that is P_{\max} and not P_{\max}^B and α not α^B .

The P_{\max} depends on the concentration (n_{slowest} , m^{-3}) and the average maximum turnover time ($\bar{\tau}_{\text{slowest}}$, s atoms $^{-1}$) of the slowest constituent pool in the photosynthetic reaction chain,

$$P_{\max} = 7.174 \times 10^{-17} \frac{n_{\text{slowest}}}{\bar{\tau}_{\text{slowest}}}, \quad (1)$$

where 7.174×10^{-17} mg C atoms $^{-1}$ s h $^{-1}$ is the conversion factor from seconds to hours and mg of carbon to atoms.

Alternatively, P_{\max} can also be related to an instantaneous maximum carbon specific growth rate (μ_{\max} , d^{-1}) realized under saturating irradiance (neglecting respiration and other losses) as $P_{\max} = C_{\text{phy}} \mu_{\max} / DD$, where D is the daylength (hours per day) and C_{phy} the phytoplankton carbon (mg C m^{-3}). This growth rate is an overestimate of the 24-h growth rate since it is valid only under saturating conditions that are not present throughout the day. To analyze our results we will mostly use the representation given in Eq. (1) as it provides a mechanistic explanation of the processes influencing P_{\max} .

The two formulations are equivalent since $C_{\text{phy}} \mu_{\max} = cte (n_{\text{slowest}} / \bar{\tau}_{\text{slowest}})$, where cte is a proportionality constant.

The initial slope of the photosynthesis irradiance curve is given by the product of the spectrally weighted photosynthetic absorption (m^{-1}),

$$\bar{a}_{ps} = \frac{\int_{400}^{700} a_{ps}(\lambda) \overset{\circ}{E}(\lambda) d\lambda}{\int_{400}^{700} \overset{\circ}{E}(\lambda) d\lambda}, \quad (2)$$

and the maximum quantum yield of carbon fixation for photons absorbed by photosynthetic pigments ($\varphi_{C_{\max}}^{ps}$, $\text{mol C} [\text{mol photons absorbed}]^{-1}$) as follows:

$$\alpha = 43.2 \bar{a}_{ps} \varphi_{C_{\max}}^{ps}. \quad (3)$$

In Eq. (3), the factor $43.2 \text{ mg C mol C}^{-1} \text{ mol photons}^{-1} \text{ s h}^{-1}$ accounts for the conversion from seconds to hours, $\mu\text{mol photons}$ to mol photons , and mg C to mol C .

Thus n_{slowest} and \bar{a}_{ps} are measures of biomass (both scale with the number of cells), the first representing the concentration of slowest molecule in water and the second providing a good proxy of the concentration of pigmented molecule. Therefore, both P_{\max} and α are described by a different ‘‘amount’’ or ‘‘biomass’’ term (n_{slowest} and \bar{a}_{ps}), and a term that encompasses variability in the physiological or photosynthetic efficiency ($\bar{\tau}_{\text{slowest}}$ and $\varphi_{C_{\max}}^{ps}$). It follows that, in theory, the best index of phytoplankton biomass for the sake of estimating primary production are n_{slowest} for the light-saturated region of the curve, and \bar{a}_{ps} for the light-limited region of the curve. The exact nature of n_{slowest} , however, remains largely unknown in the ocean (though the RUBISCO enzyme is often considered the slowest pool; Sukenic et al., 1987).

To assess the accuracy with which different proxies of phytoplankton biomass allow us to retrieve the photosynthetic parameters, we will use non-linear regression analyses where we will compare directly P_{\max} and α to proxies of biomass measured in situ. The trend line will provide the average relationship while the variability around the trend line will provide an estimate of the accuracy with which each proxy of biomass retrieves the ‘‘biomass component’’ of P_{\max} and α , namely n_{slowest} and \bar{a}_{ps} . The non-linearity of the relationships will allow us to account for second order effects,

which would be not easy using normalized values without encountering potential statistical biases (Berges, 1997).

To understand the source of variability around our regression line, it is useful to represent equations 1 and 3 above in terms of normalized quantities. Essentially, the variability around the mean normalized value will be similar to the variability around our regression (because we use non-linear regression with an intercept they are not exactly equivalent). Normalization of P_{\max} to different proxies of phytoplankton biomass (B) leads to $P_{\max}^B = 7.174 \times 10^{-17} \left[\frac{n_{\text{slowest}}}{B} \right] \frac{1}{\bar{\tau}_{\text{slowest}}}$, and the same normalization for α leads to $\alpha^B = 43.2 \left[\frac{\bar{a}_{ps}}{B} \right] \varphi_{C_{\max}}^{ps}$. Since the variability in $\varphi_{C_{\max}}^{ps}$ and $\bar{\tau}_{\text{slowest}}$ should not be related to B , normalization by B removes most of the variability in P_{\max} and α originating from changes in biomass (i.e. making the term in the square brackets nearly constant). Any proxy of biomass that covaries with \bar{a}_{ps} and n_{slowest} will remove some of the variability, but proxies that account for a greater fraction of the variability will perform best. For example, normalizing α by \bar{a}_{phy} does not account for the variability in the ratio of photosynthetic absorption to total phytoplankton absorption, while normalizing by $Tchl a$ leaves the variability in the photosynthetic absorption to $Tchl a$. Table 1 describes the different sources of variability that are not accounted for when a given biomass proxy is used to normalize the photosynthetic parameters. To aid in the interpretation of our results, and to elaborate on Table 1, we address in more detail here the case of the scattering and backscattering coefficients.

The interest of using b_p and b_{bp} as mentioned before lies in their potential for providing information about the phytoplankton carbon biomass. The particulate scattering coefficient is, however, the sum of scattering by all particles. The relative contribution of each particle type depends on their scattering efficiency (which depends on their size, shape, structure, and index of refraction) and on their concentration (Morel and Bricaud, 1986; Morel, 1973). Given a Junge particle distribution of homogenous spherical particles, those in the size range of 0.5 to 20 μm (Morel, 1973) will be the most effective at scattering. In the ocean, we can express the particulate scattering coefficient as $b_p = b_{\text{phy}} + b_{\text{bact}} + b_{\text{het}} + b_{\text{vir}} + b_{\text{min}} + b_{\text{bub}} + b_{\text{org}}$, where b_{phy} , b_{bact} , b_{het} , b_{vir} , b_{min} , b_{bub} , and b_{org} are the contributions from phytoplankton, bacteria, small non-bacterial heterotrophs, viruses, mineral particles, bubbles, and non-living organic matter, respectively. We can thus express the scattering normalized P_{\max} as:

$$P_{\max}^b = 7.174 \times 10^{-17} \left(\frac{n_{\text{slowest}}}{b_{\text{phy}}} \right) \left(\frac{b_{\text{phy}}}{b_p} \right) \frac{1}{\bar{\tau}_{\text{slowest}}}$$

a similar equation is obtained for α :

$$\alpha^b = 43.2 \left(\frac{\bar{a}_{ps}}{b_{\text{phy}}} \right) \left(\frac{b_{\text{phy}}}{b_p} \right) \varphi_{C_{\max}}^{ps}$$

Table 1. Summary of sources of variability in the photosynthetic parameters that are not accounted for by the normalization to different biomass proxies (always listed as point #1 below), and the principal origin of this variability (presented below as point #2). See Falkowski and Raven (1997) for details regarding the absorption based proxies; further explanation of the scattering based proxies are developed in the text.

		Absorption-related biomass proxies		
	Tchl _a	\bar{a}_{ps}	\bar{a}_{phy}	Fluorescence
	1) ratio: $n_{slowest}/Tchl_a$. 2) Photoacclimation and nutritional status. Expected to increase with increasing growth irradiance and nutrient availability. Also influenced by species composition.	1) ratio: $n_{slowest}/\bar{a}_{ps}$. 2) The same sources as Tchl _a , plus packaging effects and pigment composition. Expected to increase with increasing growth irradiance	1) ratio: $n_{slowest}/\bar{a}_{phy}$. 2) The same sources as \bar{a}_{ps} .	1) ratio: $n_{slowest}/(\bar{a}_{ps}\varphi_f^{ps})$ where φ_f^{ps} is the quantum yield of fluorescence. 2) Same sources as for \bar{a}_{ps} plus variability due to the quantum yield of fluorescence.
	1) Chlorophyll specific absorption coefficient ($\bar{a}_{ps}^* = \bar{a}_{ps} Tchl_a$). 2) Pigment composition and packaging, and thus the physiological status and species composition.	1) Physiologically none. 2) Methodologically, it may be susceptible to larger variability than expected due to significant errors in the estimation of \bar{a}_{ps} .	1) ratio: $\bar{a}_{ps}/\bar{a}_{phy}$ 2) Photoacclimation, nutritional status and species composition. Also affected by errors in the determination of phytoplankton absorption.	1) ratio: $\bar{a}_{ps}/\bar{a}_{ps}\varphi_f^{ps}$ 2) Additional variability in φ_f^{ps} and different measuring irradiance used to “weight” \bar{a}_{ps} , and, hence, on the pigment composition.
		Scattering-related biomass proxies		
	b_p (or c_p)	b_{bp}	biovolumes	
	1) $\left(\frac{n_{slowest}}{b_{phy}}\right) \left(\frac{b_{phy}}{b_{phy}+b_{bact}+b_{het}+b_{vir}+b_{min}+b_{bub}+b_{org}}\right)$ 2) See text for further details.	1) Same equation as for b_p (replacing b_p by b_{bp}). 2) See text for further details.	1) The intracellular $n_{slowest}$ concentration. 2) Physiological status and species composition. Methodologically limited by the accuracy in volume determination and cellular volumes observed by flow cytometry.	
	1) $\left(\frac{\bar{a}_{ps}}{b_{phy}}\right) \left(\frac{b_{phy}}{b_{phy}+b_{bact}+b_{het}+b_{vir}+b_{min}+b_{bub}+b_{org}}\right)$ 2) See text for further details.	1) Same equation as for b_p (replacing b_p by b_{bp}). 2) See text for further details.	The volume specific absorption coefficient. Dependent on physiological status. Same methodological problems as above.	

Therefore, b_p provides a good proxy of phytoplankton biomass for normalizing the photosynthetic parameters if b_{phy} is a good proxy for $n_{slowest}$ or \bar{a}_{ps} (i.e. low natural variability within the first parentheses of the equations above) and if, in addition, it meets one of three requirements (low variability in the second parentheses of above equations): 1) b_p must be mostly influenced by b_{phy} and all other constituents must represent small or negligible contributions to scattering; 2) all other constituents scattering coefficients

must covary tightly with b_{phy} ; or 3) a combination of the first two conditions leading to a reduced variability in the b_{phy} to b_p ratio.

From monoculture of phytoplankton, we know that b_{phy} is a good measure of phytoplankton carbon; while the carbon per cell shows large variability during the day, the carbon specific attenuation and scattering coefficient remain nearly constant (Stramski et al., 1995; Stramski and Reynolds, 1993; Claustre et al., 2002). The interspecific variability

seems to remain within a factor of ~ 5 . If b_p is found to be a good estimator of P_{\max} , it is however unlikely that it would be affected mainly by the carbon in n_{slowest} , more likely the covariation of n_{slowest} with total phytoplankton carbon would be the cause.

To be a good proxy of phytoplankton biomass, the particulate backscattering coefficient must meet the same three conditions mentioned above for b_p . However, based on Mie theory, particulate backscattering is due to the same constituents as scattering, but the efficiency of backscattering is more strongly weighted towards smaller-size particles (~ 0.1 to $1 \mu\text{m}$ cf., Morel and Ahn, 1991).

3 Materials and methods

All of the data presented herein were collected during the BIOSOPE and PROSOPE cruises. BIOSOPE sampled 2 transects from the Marquesas Islands to Easter Island, and from Easter Island to Concepcion Chile, through the South Pacific Gyre from 26 October to 10 December 2004. PROSOPE sampled the Morocco upwelling and the Mediterranean Sea from 4 September to 4 October 1999 (see Oubelkheir et al., 2005, for cruise track). Because the dataset for the BIOSOPE cruise is more complete and allows consistent analyses between the parameters studied, we carried out the statistical analysis on that dataset only, and used the PROSOPE dataset for comparison purposes only. While we will not discuss the comparison with the PROSOPE dataset further, we will mention here that trends and absolute values compare well with the BIOSOPE dataset for all variables. All the data shown here are obtained from CTD and rosette casts made near solar noon. Nine depths were usually sampled for the PvsE experiments and all data are matched to these depths. For discrete samples obtained from Niskin bottles (e.g. *Tchl**a*, PvsE parameters and absorption), we compare data from the same bottle or from duplicate bottles from the same depth as the PvsE curve data. The data obtained from profiling instruments (e.g. CTD, fluorescence, b_p and b_{bp}), are from the same cast as that of the PvsE sample, and represent the average over 2 m centered on the depth of the PvsE bottle.

3.1 Photosynthesis vs. irradiance curves

The PvsE curves of the particulate fraction were determined by closely following the protocol of Babin et al. (1994). One modification was made for the BIOSOPE cruise (but not PROSOPE): we replaced the GFF filters with $0.2 \mu\text{m}$ pore size polycarbonate membrane filters. This modification reduced the dispersion observed in surface samples (M. Babin, personal observation). Incubations lasted between 2 and

3.5 h. The data were fit to the following equation (Platt et al., 1980; MacIntyre and Cullen, 2005):

$$P = P_s \left[1 - \exp\left(-\frac{E}{P_s} \alpha\right) \right] \left[\exp\left(-\beta \frac{E}{P_s}\right) \right] + P_o$$

where P_s ($\text{mgC m}^{-3} \text{h}^{-1}$) is an hypothetical maximum photosynthetic rate without photoinhibition and an analytic function of β , α and P_{\max} ; β ($\text{mg C m}^{-3} \text{h}^{-1} [\mu\text{mol photons m}^{-2} \text{s}^{-1}]^{-1}$) is a parameter describing the reduction of the photosynthetic rates due to photoinhibition at high irradiance; and P_o an intercept term. The P_{\max} reported herein are equal to $P_{\max} + P_o$ where $P_{\max} = P_s (\alpha / (\alpha + \beta)) (\beta / (\alpha + \beta))^{\alpha / \beta}$. The 95% confidence interval (CI) on the parameters was estimated using the standard MATLAB routine *nlpredci.m*. Estimated parameters for which the CI was greater than 50% of the parameter value were discarded. To have a uniform dataset, we also discarded the points for which there were no concurrent values for all of the following: *Tchl**a*, b_p , b_{bp} , a_{phy} , a_{ps} , and nitrate. This left 159 points for P_{\max} and 153 points for α from an original dataset of 338 PvsE curves. Roughly half of the points (77 for P_{\max} and 75 for α) were excluded because of the criteria we chose for the CI. Since the number of phytoplankton biovolume estimates was significantly smaller, data for missing biovolume estimates were not excluded.

3.2 Pigments

The concentration of phytoplankton pigments was measured by HPLC, using a method modified from the protocol of Van Heukelem and Thomas (2001) for the BIOSOPE cruise (Ras et al., 2007), and Vidussi et al. (1996) for the PROSOPE cruise.

3.3 Phytoplankton and photosynthetic absorption

The method used for phytoplankton absorption spectra measurements is detailed in the works of Bricaud et al. (1998) and Bricaud et al. (2004). Photosynthetic absorption was obtained following the procedure of Babin et al. (1996) using the individual pigment spectra in solution given by Bricaud et al. (2004). Both were weighted according to the irradiance inside the photosynthetron (see Eq. 4; the same equation was used for \bar{a}_{phy} by replacing a_{ps} by a_{phy}) to provide an average value for the spectra.

3.4 Fluorescence

Fluorescence was measured in situ using an Aquatracka III fluorometer (Chelsea Technology Group) placed on the same rosette as the Niskin bottle for the discrete samples. No correction for the decrease of fluorescence due to non-photochemical quenching was attempted and this is expected to increase the variability in the comparison with other biomass proxies.

3.5 Scattering and backscattering coefficient

The particulate scattering (b_p) and backscattering coefficients (b_{bp}) were measured using an AC-9 (WET Labs) and an ECO-BB3 sensor (WET Labs), respectively. AC-9 data were acquired and processed according to the method of Twardowski et al. (1999), using the temperature and salinity correction coefficients obtained by Sullivan et al. (2006). Scattering errors in the reflective tube absorption measurement were corrected using the spectral proportional method of Zaneveld et al. (1994). Between field calibrations with purified water during the cruise, instrument drift was fine-tuned to independent measurements of absorption in the dissolved fraction made on discretely collected samples by (Bricaud et al., 2007)¹. The ECO-BB3 data were processed according to Sullivan et al. (2005), using the chi-factors obtained therein to convert volume scattering measurements at 117° to backscattering coefficients. For optimal accuracy, direct measurements of in situ dark counts were periodically collected by placing black tape over the detectors for an entire cast. More details on the processing in Twardowski et al. (2007).

3.6 Diffuse attenuation coefficient

The diffuse attenuation coefficient (K_d , m^{-1}) in the visible bands was obtained as described in Morel et al. (2007).

3.7 Phytoplankton biovolumes

Prochlorococcus, *Synechococcus* and picophytoeukaryote biovolumes were estimated from mean cell size and abundance by assuming a spherical shape. See Grob et al. (2007) for details. Cell abundances were directly determined using flow cytometry, except for the weakly fluorescent surface *Prochlorococcus* populations whose abundance was estimated from divinyl chlorophyll *a* concentrations. Mean cell sizes were obtained by establishing a direct relationship between the cytometric forward scatter signal (FSC) normalized to reference beads and cell size measured with a Coulter Counter for picophytoplanktonic populations isolated in situ and cells from culture (see Sect. 2.1 and Fig. 3a in Grob et al., 2007). Mean cell sizes were then used to calculate cell volumes assuming a spherical shape. Finally, biovolumes ($\mu m^3 ml^{-1}$) were obtained by multiplying cell volume and abundance. Because, as noted above, in surfaces water at some stations, the *Prochlorococcus* population fluorescence was undetectable, we discarded all *Prochlorococcus* measurements for this study. The biovolumes thus include only the *Synechococcus* and picophytoeukaryotes. The maximum cell diameter observed with the instrument settings used during the cruise was 3 μm . This included most of the

phytoplankton cells in oligotrophic waters but missed a significant fraction in more eutrophic waters. Similarly, the absence of *Prochlorococcus* may miss a significant fraction of the biomass in oligotrophic waters.

3.8 Stepwise regression and determining the quality of fits

We use three quantities to assess the quality of fits: the correlation coefficient (r), the root mean square error (RMSE), and the mean absolute percent error (MAPE). While the first two are more commonly used statistical measures of fits, the third provides an estimate of variability that is independent of range or absolute values (relative measure, without units) of the data and hence is more easily comparable between different estimated variables. The MAPE is expressed as a fraction (instead of a percentage, sometimes abbreviated as MAE in the literature) and is calculated as $MAPE = \frac{1}{n} \sum_{i=1}^n \left(Y_i - \hat{Y}_i \right) / Y_i$, where Y is the measured data, \hat{Y} is the estimated value and n the total number of points.

All stepwise regressions will be conducted with the following constraints: a variable is added if the maximum p-value is 0.05 and removed if the minimum p-value is 0.10. The p-values provided in the text regarding the stepwise regression are the probability that the regression coefficient is equal to 0.

4 Results and discussion

4.1 Overview of the dataset

This dataset was collected in case 1 waters. In these waters, away from land influences, all the optical properties covary with the phytoplanktonic biomass (which spanned roughly 3 orders of magnitude) as it underlies the functioning of the whole ecosystem. Indeed, an overview of the biomass data collected during the BIOSOPE cruise shows that most variables follow the trends expected as a function of chlorophyll *a* for case 1 waters (Fig. 1); the relationships between surface measurements of b_p , b_{bp} , and a_{phy} , and *Tchl a* concentration are consistent with statistical relationships previously established (Bricaud et al., 2004; Loisel and Morel, 1998; Morel and Maritorena, 2001). It is interesting to note the resemblance between panels A and H showing respectively b_p and the phytoplankton biovolume obtained from the flow cytometry measurements as a function of the *Tchl a* concentration. Despite (or because of) the lack of *Prochlorococcus* in the biovolumes dataset and the upper limit of 3 μm , and unless strongly covarying particles are present, this suggests that variability in b_p is in large part influenced by the biovolume (similar to carbon concentration) of phytoplankton. A similar observation can be made with respect to P_{max} and biovolumes which both shows patterns that reassembles strongly those of b_p and suggest that they are good proxy

¹Bricaud, A., Babin, M., Claustre, H., Ras, J., and Tieche, F.: The par titoning of light absorption in South Pacific Waters, in preparation, 2007.

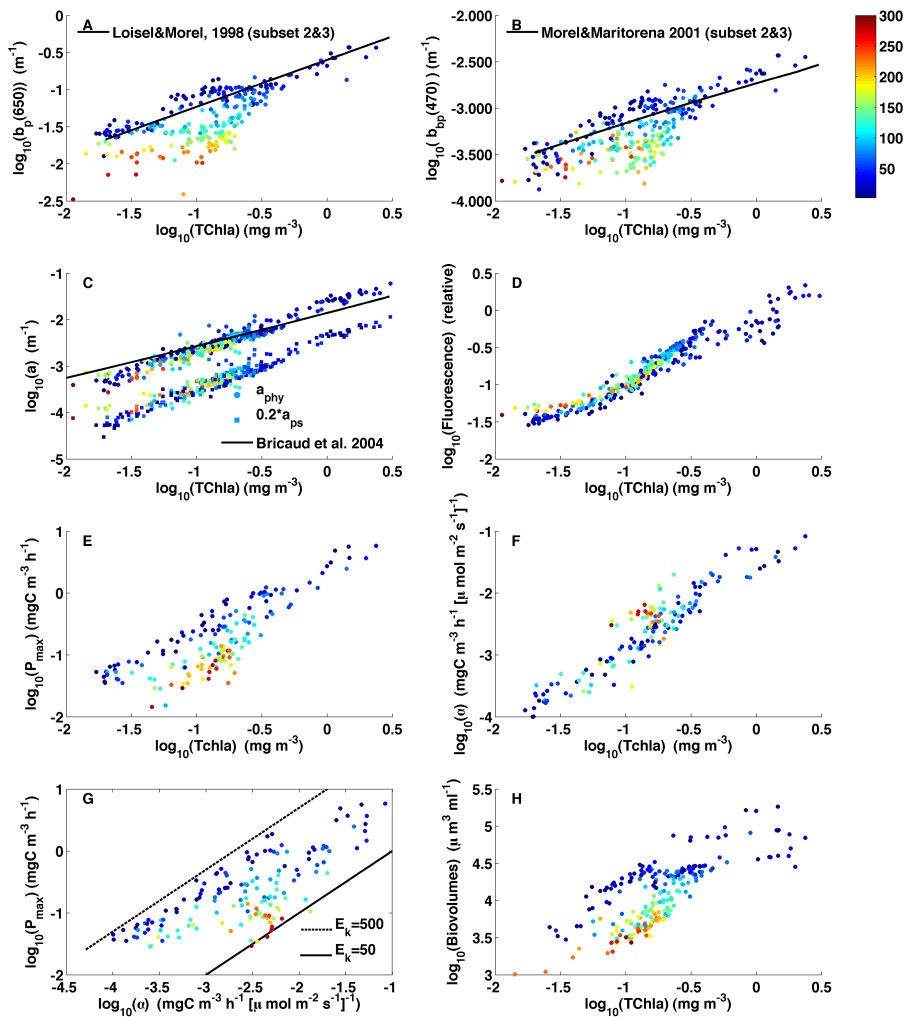


Fig. 1. Comparison of different estimators of phytoplankton biomass obtained during the BIOSOPE cruise with published statistics for case 1 waters. (A) Particulate scattering coefficient at 650 nm vs. Tchl_a (sum of chlorophyll *a* and divinyl chlorophyll (A), (B) Backscattering coefficient at 470 nm vs. Tchl_a, (C) Phytoplankton and photosynthetic absorption multiplied by 0.2 (allows it to be discerned from the former) weighted by the photosynthetron irradiance spectra vs. Tchl_a, (D) In situ fluorescence vs. Tchl_a, (E) P_{\max} vs. Tchl_a, (F) α vs. Tchl_a, (G) P_{\max} vs. α , lines are for two extreme saturation irradiances (E_k) for photosynthesis, (H) Biovolume obtained from a calibrated flow cytometer vs. Tchl_a. Colorscale represents depth.

of the slowest pool. The decrease of b_p with depth for a given Tchl_a concentration (Fig. 1a) is consistent with the oft-reported trends attributed to a “photoacclimation-like” behavior (i.e. an increase in the Tchl_a per scattering particle, cf. Kitchen et al., 1990). A similar trend is observed in b_{bp} (Fig. 1b). The phytoplankton absorption coefficient (Fig. 1c) generally follows the statistical relationship established for case 1 waters by Bricaud et al. (2004) but shows a slightly higher slope and lower intercept. A sigmoidal shape is observed in log space for the fluorescence vs. Tchl_a relationship (Fig. 1d). A clear depth dependence is observed in the P_{\max} vs. Tchl_a relationship, while this dependence is reversed and much less accentuated for α (Figs. 1e and f; see Methods section). The relationship between α and P_{\max} (Fig. 1g) also shows a depth dependence which rep-

resents changes in E_k with depth (i.e. higher values at the surface; lower values at depth) consistent with photoadaptation (or less-likely photoacclimation). The predominant factor in these changes of E_k are likely photoadaptation rather than photoacclimation as there is a layering of species with depth in these stratified environments (see Ras et al., 2007).

So while all properties covary with one another, there remains some variability. This remaining variability, however, is not all random (e.g. depth dependence of the b_p vs. Tchl_a relationship) and thus contains information about the system. If this information is pertinent to the retrieval of photosynthetic parameters some of the measures should provide less variability when compared with the photosynthetic parameters than other.

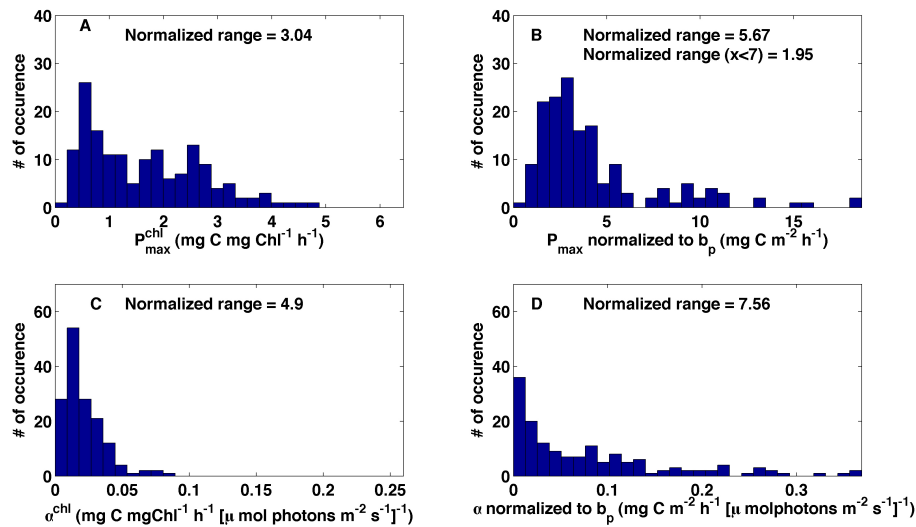


Fig. 2. Histograms of the photosynthetic parameters measured during the BIOSOPE cruise. (A) P_{\max}^{chl} , (B) P_{\max} normalized to b_p , (C) α^{chl} , (D) α normalized to b_p . The normalized range was calculated as $(\min(x) - \max(x)) / \text{median}(x)$, where x is the normalized photosynthetic parameter. It provides a rough guide to compare the variability between the different panels. For panel (B), two ranges are given, one for the whole dataset, as in the other panels, and one for normalized P_{\max} smaller than $7 \text{ mg C m}^{-2} \text{ h}^{-1}$ for (focusing on the “normal” region of the distribution). The abscissas are scaled such that the ratio of the maximum of the axis to the minimum value of the data are equal (for each row independently).

Table 2. Statistical difference between the different index of biomass used for predicting P_{\max} and α (in Figs. 3 to 6). The estimator for which the correlation coefficient is not different at the 95% confidence level share the same letter. Letters are ordered alphabetically to the quality of the fits (Figs. 3, 4, 5 and 6), the best correlation have an “a” and the worst a “c”.

	b_p	Biovolume	Tchl a	b_{bp}	a_{phy}	fluorescence	a_{ps}
P_{\max}	a	a, b	b	b	b	b	b
α	c	c	a	c	b	a, b	a, b

A comparison of the distributions of the photosynthetic parameters when they are normalized to Tchl a or to the particulate scattering coefficient is provided in Fig. 2. The values obtained for P_{\max}^{chl} [0.26 to $7.2 \text{ mg C (mg chl)}^{-1} \text{ h}^{-1}$] and α^{chl} [0.0028 to $0.086 \text{ mg C (mg chl)}^{-1} \text{ h}^{-1} (\mu\text{mol photons m}^{-2} \text{ s}^{-1})^{-1}$] are consistent with values from the literature, but clearly do not cover the full range of variability reported. A review of several datasets of photosynthetic parameters by Behrenfeld et al. (2004) gives a range of 0.04 to 24.3 (mostly between ~ 0.5 and ~ 10) $\text{mg C (mg chl)}^{-1} \text{ h}^{-1}$ for P_{\max}^{chl} , and of 0.0004 to ~ 0.7 (mostly between ~ 0.005 and ~ 0.2) $\text{mg C (mg chl)}^{-1} \text{ h}^{-1} (\mu\text{mol photons m}^{-2} \text{ s}^{-1})^{-1}$ for α^{chl} though some variability in α^{chl} originates from the different spectra used for the measurement irradiance. Using a crude index of dispersion, the normalized range (see Fig. 2 caption for details and the values reported on the graphs), shows that normalization of both P_{\max} and α by Tchl a reduces the variability in the data relative to normalization by

b_p (but only slightly in the case of P_{\max}). The distribution for P_{\max} normalized to b_p , however, shows a normal distribution of points below values of $7 \text{ mg C m}^{-2} \text{ h}^{-1}$ with a long tail above. If we consider only the points below that threshold, the variability is much reduced and becomes lower than when Tchl a is used as the normalization factor. The higher P_{\max} normalized to b_p values occur mostly in regions with higher chlorophyll concentrations (coastal upwelling regions, deep chlorophyll maxima, and Marquesas Islands). This could be the result of real physiological variability or indicate a bias in the normalization by b_p with trophic status (e.g. ratio of b_{phy}/b_p increasing with increasing chlorophyll concentration, see Table 1 and Background section).

4.2 Determining the best proxy of phytoplankton biomass to predict photosynthetic parameters

Figures 3 and 4 show the comparison between P_{\max} and different measures of biomass. On both figures, the left panels show the scatter plots of P_{\max} against the different biomass indices measured, and a 2nd order polynomial obtained on the log-transformed data. The right-hand-side panels show the values of P_{\max} predicted by using the polynomial fit against the measured values (the statistics of the fits are also provided). As previously mentioned, all fits and statistics refer only to the BIOSOPE dataset as it is more complete and allows a consistent comparison of all proxies of biomass from an equal number of points taken simultaneously, or near simultaneously, while the PROSOPE dataset is superposed for comparative purposes only. While P_{\max} is expected to

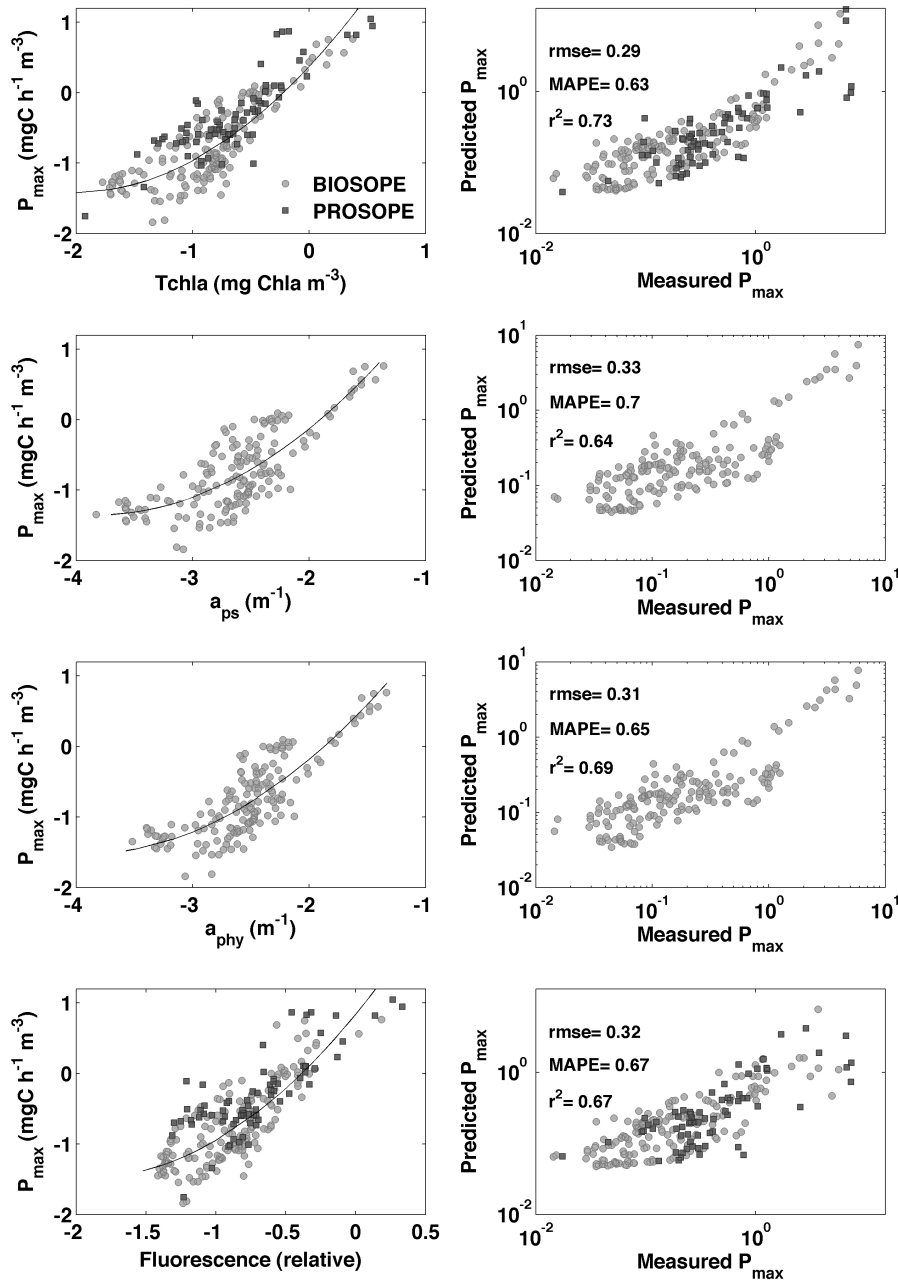


Fig. 3. Relationships between four estimators of biomass and P_{\max} . Left Column: P_{\max} vs. the different estimators. The black line represents the best-fit second order polynomial. Right column: Measured and estimated P_{\max} using the best-fit line in the left column. Also shown are the statistics of the predictions.

covary strongly with all proxies of biomass, what interests us here is the remaining variability, which should be lower for the better proxies. Several points can be made about these figures. Firstly, the $b_p(650)$ and biovolumes estimated from flow cytometry measurements provide the best estimates of P_{\max} (Fig. 4). Since the variability in $\bar{\tau}_{\text{slowest}}$ and the measurement errors on P_{\max} are equal for all panels, this suggests that $b_p(650)$ is the best single measure of n_{slowest} . Secondly,

the backscattering coefficient provides estimates of P_{\max} that are equivalent to those using $Tchl a$. However, at low values of P_{\max} the predictability is reduced as the slope between P_{\max} and b_{bp} is much smaller (as two become essentially independent). Indeed, for values of $P_{\max} < \sim 0.1$, b_{bp} continues to decrease while P_{\max} remains constant. Thirdly, a_{ps} , a_{phy} and chlorophyll fluorescence all perform similarly in estimating P_{\max} but slightly worse than $Tchl a$. We can summarize

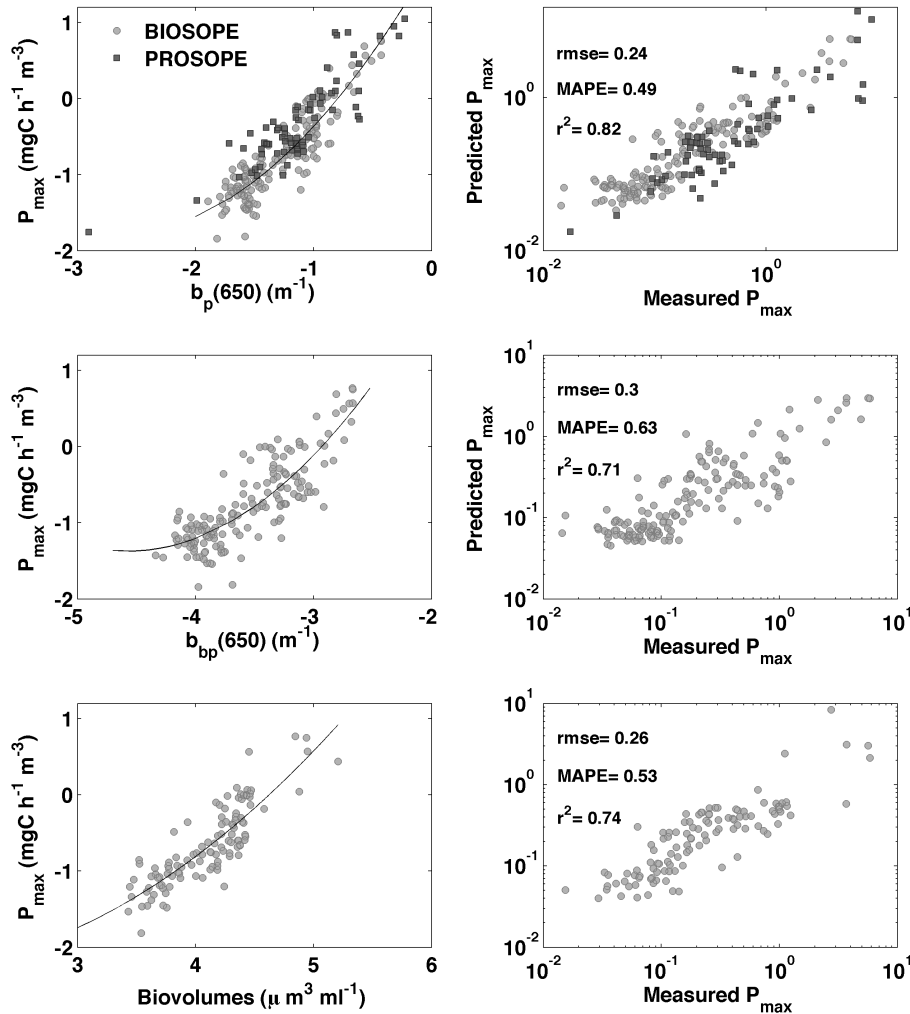


Fig. 4. Relationships between three estimators of biomass and P_{\max} . See Fig. 3 for details.

these results in terms of decreasing accuracy of estimates (using MAPE as the index) as follows: $b_p \approx \text{biovolume} > \text{Tchl}a \approx b_{bp} \approx \text{fluo} \approx a_{\text{phy}} \approx a_{ps}$. Statistically (see Table 2 for a complete comparison), the correlation coefficient (r) on b_p is significantly greater ($p < 0.05$, t-test on the z-transform of the correlation coefficient, Sokal and Rohlf, 1995) than the parameters with values of r equal to or lower than that of Tchl*a* (i.e. Tchl*a*, b_{bp} , fluorescence, a_{phy} , a_{ps}). There is no significant difference between the correlation coefficients on the other parameters.

Figure 5 shows the comparison between α and different measures of biomass. In contrast with the P_{\max} measurements, both measures of scattering as well as the biovolume estimates perform very poorly, while Tchl*a* and \bar{a}_{ps} show the best estimates, with Tchl*a* not significantly better than \bar{a}_{ps} . Finally, fluorescence is followed by \bar{a}_{phy} . In summary, estimators order as follows (from the most to the least accurate): Tchl*a* \approx \bar{a}_{ps} \approx fluo $>$ \bar{a}_{phy} \gg $b_p >$ biovolumes $>$ b_{bp} . Statistically (see Table 2 for a complete comparison), the cor-

relation coefficient of Tchl*a* is significantly greater than the other proxies with values of r equal or lower to that of a_{phy} ($p < 0.05$; t-test on z-transform). The correlation coefficient on \bar{a}_{phy} is significantly different from b_p , b_{bp} or biovolumes ($p < 0.001$; t-test on the z-transform).

To summarize these results, it can be said that we obtained very intuitive results for the relationships between α and the different proxies of biomass. Indeed, that Tchl*a*, \bar{a}_{ps} , and \bar{a}_{phy} provide the best measures of α is what we expected as they represent a measure closely related to the absorption of photosynthetic pigments. On the other hand, the results concerning P_{\max} are more noteworthy: b_p , despite not being specific to phytoplankton, provides a better estimate of P_{\max} than the traditional measure of Tchl*a*. These results are consistent with those of Behrenfeld et al. (2005); Behrenfeld and Boss (2006) where they showed that the ratio $c_p/\text{Tchl}a$ provided good estimates of $P_{\max}/\text{Tchl}a$. Hence, for the waters studied here, which are representative of many oceanic waters, b_p is the best proxy for estimating P_{\max} when no other

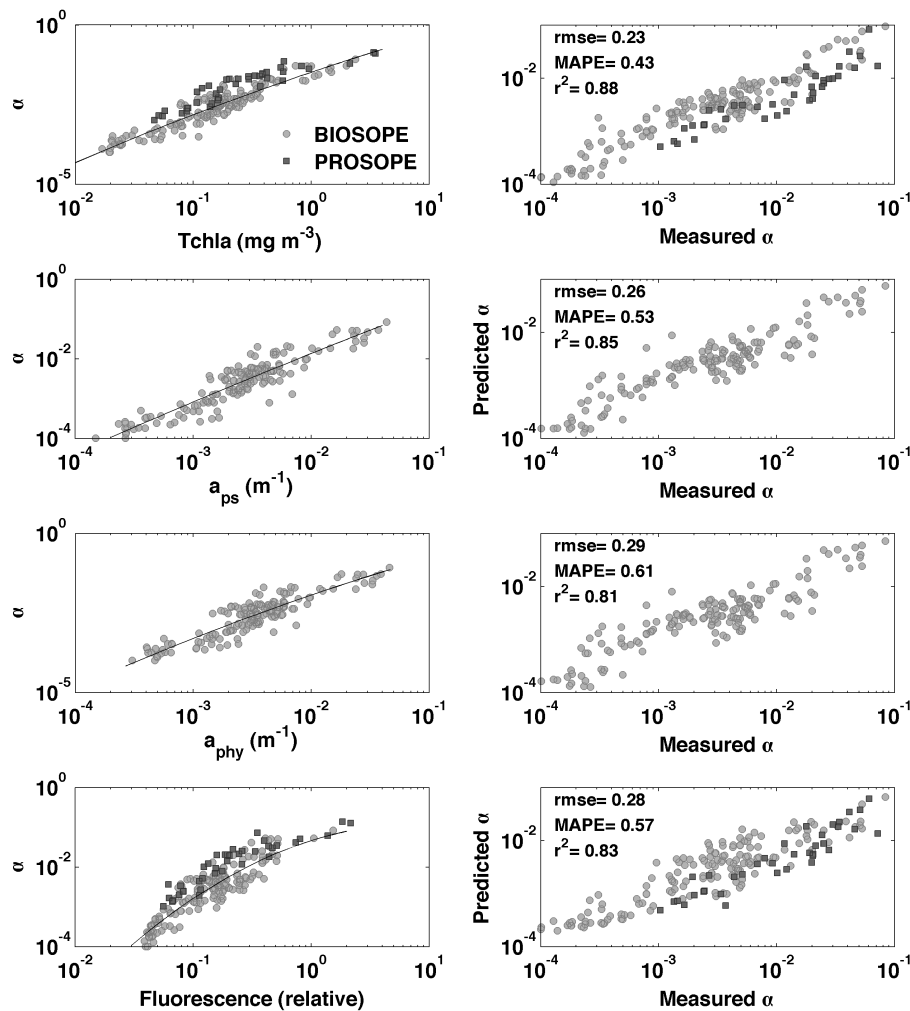


Fig. 5. Relationships between four estimators of biomass and α (in $\text{mgC m}^{-3} \text{h}^{-1} [\mu\text{mol photon m}^{-2} \text{s}^{-1}]^{-1}$). Left Column: α versus the different biomass estimators. The black line represents the best-fit second order polynomial. Right column: Measured and estimated α using the best-fit line in the left column. Also shown are the statistics of the predictions.

measurements are available. This means that b_p is strongly influenced by phytoplankton scattering or that the scattering coefficients of all other particulate matter show tight relationships with the phytoplankton scattering coefficient. Furthermore, since it is better correlated to P_{max} than $\text{Tchl}a$, which is present only in phytoplankton, it implies that b_p provides a measure that covaries better with n_{slowest} than $\text{Tchl}a$. Consequently, it implies that there is considerable variability in the ratio $n_{\text{slowest}}/\text{Tchl}a$ (not correlated with $\text{Tchl}a$). Even more interesting is the good retrieval of P_{max} using $b_{bp}(650)$ which is equivalent to estimates using $\text{Tchl}a$. Because the size fractions that are expected to influence b_{bp} the most are smaller than the smallest phytoplankton (assuming a Junge distribution, generally observed during BIOSOPE, Sciandra et al., 2007)², it implies that either backscattering from that fraction

²Sciandra, A., Stramski, D., and Babin, M.: Variability in particle size distribution in contrasted trophic regions of the South East Pacific, in preparation, 2007.

is very well correlated with phytoplankton backscattering, or phytoplankton cells are affecting b_{bp} more than expected.

We now want to examine the possibility of predicting the large variability in the ratio of $n_{\text{slowest}}/\text{Tchl}a$ using other environmental variables and examine if the relationship with b_p can be further improved with these same variables.

4.3 Using environmental variables in addition to proxies of phytoplankton biomass

While the results of the previous analysis are interesting, it remains a somewhat academic exercise because biomass proxies are rarely obtained without at least some information about the sampled location and environment. We thus, now turn to our second question. Can we improve the estimates of α and P_{max} by using additional measurable quantities? In other words, what is the origin of the remaining variability?

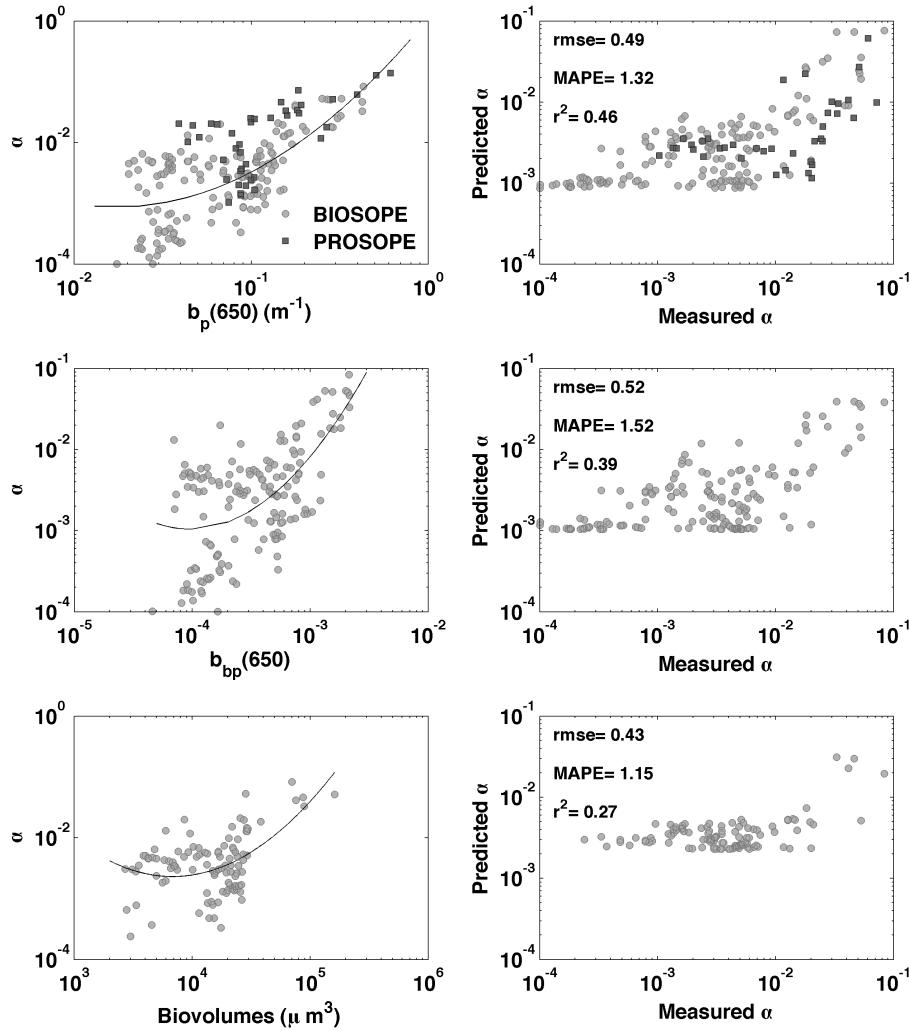


Fig. 6. Relationships between three estimators of biomass and α (in $\text{mgC m}^{-3} \text{h}^{-1} [\mu\text{mol photon m}^{-2} \text{s}^{-1}]^{-1}$). See Fig. 5 for details.

To address this question we used a stepwise regression analysis with the log transform of α and P_{max} as our dependent variable and a series of potentially relevant independent variables. For each fit, we used only one log-transformed “biomass proxy” (i.e. whether $\log(\text{Tchl}a)$, $\log(b_p)$, $\log(b_{bp})$...). The analysis was conducted for all depths. Table 3 provides all the independent variables tested and a summary of the results. A succinct rationale is given for the different variables used (the variables squared allow non-linear relationships to be present). Depth is a general proxy for growth irradiance (including UV), nutrient availability, and mixing regime (while different types of waters were encountered, light, UV and diffusivity coefficient always decrease with depth while nutrient always increase). Temperature is expected to have an effect on enzymatic rates and species composition. The log of the mean PAR irradiance at depth over the last three days provides a measure of irradiance experienced by the cells in their recent past (often

referred to as light history), potentially affecting their photoacclimation status. The log of the theoretical PAR irradiance at depth provides a measure essentially similar to the optical depth (except that the surface irradiance is accounted for) and provides a longer term (\sim weeks) proxy of the mean irradiance value at depth; relevant to processes of competitive exclusion (by species that have different photoadaptation). The nitrate concentration is used as a proxy of nutrient availability. Figure 7 compares graphically the results for P_{max} using $b_p(650)$ and $\text{Tchl}a$ as the independent biomass variable.

The results are clear (see Table 3, e.g. MAPE row). Using other independent variables beyond biomass, it is possible to significantly improve the relationship between P_{max} and $\text{Tchl}a$ (as well as a_{phy} , a_{ps} , and fluorescence). However, the same does not occur for b_p or b_{bp} , for which the relationships improve only marginally by using several new variables. Most of the improvements using $\text{Tchl}a$ arise from

Table 3. Stepwise fit results for P_{\max} vs. different indices of biomass. Values represent the fitted coefficients for each variable. NU is used for “Not Used in the fit” (e.g. $P_{\max}(\text{Tchl}a)=0.236+1.07\log_{10}(\text{Tchl}a)-6.18\text{E}-3z+1.35\text{E}-5z^2+1.55\text{E}-2T$).

	Tchl a	a_{ps}	a_{phy}	fluo	$b_p(650)$	$b_{bp}(650)$
Intercept	0.236	2.42	2.71	0.509	2.05	14.5
Log $_{10}$ (Biomass)	1.07	-4.42E-03	-5.39E-3	-6.84E-3	3.21	6.83
Log $_{10}$ (Biomass) ²	NU	8.32E-06	1.16E-5	1.61E-5	0.677	0.834
Depth	-6.81E-3	3.34E-2	3.18E-2	NU	NU	NU
Depth ²	1.35E-5	NU	NU	NU	NU	NU
T	1.55E-2	-9.52E-2	NU	NU	NU	-1.95E-1
T ²	NU	1.34E-02	NU	NU	5.36E-3	5.37E-3
Log $_{10}$ (E $_{\text{growth}}$) [†]	NU	NU	NU	5.18E-3	NU	NU
Log $_{10}$ (PAR $_{\text{theo}}$) [§]	NU	NU	NU	NU	NU	NU
Log $_{10}$ (PAR $_{\text{theo}}$) ²	NU	1.82	1.93	1.21	-5.55E-3	NU
Log $_{10}$ (NO $_3$)	NU	0.143	0.161	NU	NU	NU
RMSE	0.15	0.16	0.16	0.18	0.21	0.25
MAPE	0.29	0.31	0.30	0.36	0.43	0.54
R ²	0.93	0.92	0.90	0.90	0.86	0.80

[†] E $_{\text{growth}}$ is the mean PAR irradiance during daylight ($\mu\text{mol photon m}^{-2} \text{s}^{-1}$) at the sampling depth over the three days previous to the sampling day. It is calculated using the incident irradiance measured on the ship and the attenuation coefficient measured at the station.

[§] PAR $_{\text{theo}}$ is the mean PAR irradiance calculated using the Gregg and Carder (1990) model at the sampling depth using the attenuation coefficient measured at the station for the sampling day. Therefore it does not account for cloudiness.

Table 4. Stepwise fit results for α vs. different indices of biomass. Values represent the fitted coefficients for each variable. NU is used for “Not Used in the fit”.

	Tchl a	$b_p(650)$	$b_{bp}(650)$	a_{ps}	a_{phy}	fluo
Intercept	-1.39	0.63	19.0	1.28	1.36	-1.18
Log $_{10}$ (Biomass)	1.36	3.40	767	1.91	1.29	1.47
Log $_{10}$ (Biomass) ²	NU	0.652	0.96	0.114	NU	NU
Depth	NU	NU	7.66E-3	NU	-1.12E-2	-3.43E-3
Depth ²	4.81E-6	2.33E-5	5.48E-5	1.22E-5	4.77E-5	2.71E-5
T	NU	NU	-0.642	NU	NU	-1.24E-2
T ²	NU	3.00E-4	1.52E-2	4.64E-4	2.94E-4	NU
Log $_{10}$ (E $_{\text{growth}}$) [†]	-3.07E-2	NU	NU	NU	NU	NU
Log $_{10}$ (PAR $_{\text{theo}}$) [§]	NU	NU	0.155	NU	NU	NU
Log $_{10}$ (PAR $_{\text{theo}}$) ²	NU	-1.99E-2	-4.09E-2	NU	-2.29E-2	NU
Log $_{10}$ (NO $_3$)	NU	NU	-4.01E-2	NU	-1.167E-2	1.43E-2
RMSE	0.21	0.30	0.31	0.22	0.23	0.21
MAPE	0.40	0.65	0.66	0.44	0.44	0.41
R ²	0.90	0.80	0.78	0.89	0.88	0.90

[†] See Table 3

[§] See Table 3

accounting for the depth effects. This is not unexpected given the clear depth dependence of P_{\max} for a given Tchl a concentration observed in Fig. 1e. The relationships retrieved or the parameters used are not discussed further here, but the result that interests us is that the pigment or absorption based estimates of P_{\max} can be relatively easily improved beyond a simple biomass relationship whereas the same is not true for the scattering based methods. The latter hence

have lower predictive skill when other sources of variability are accounted for. We also note that the errors on the prediction of P_{\max} using this simple regression approach with Tchl a are very reasonable; the average error (MAPE) is 25% for the BIOSOPE dataset (see Table 3) and 33% for the independent PROSOPE dataset.

We carried out a similar analysis for α (Table 4 and Fig. 8). In this case, all estimates improved by important margins

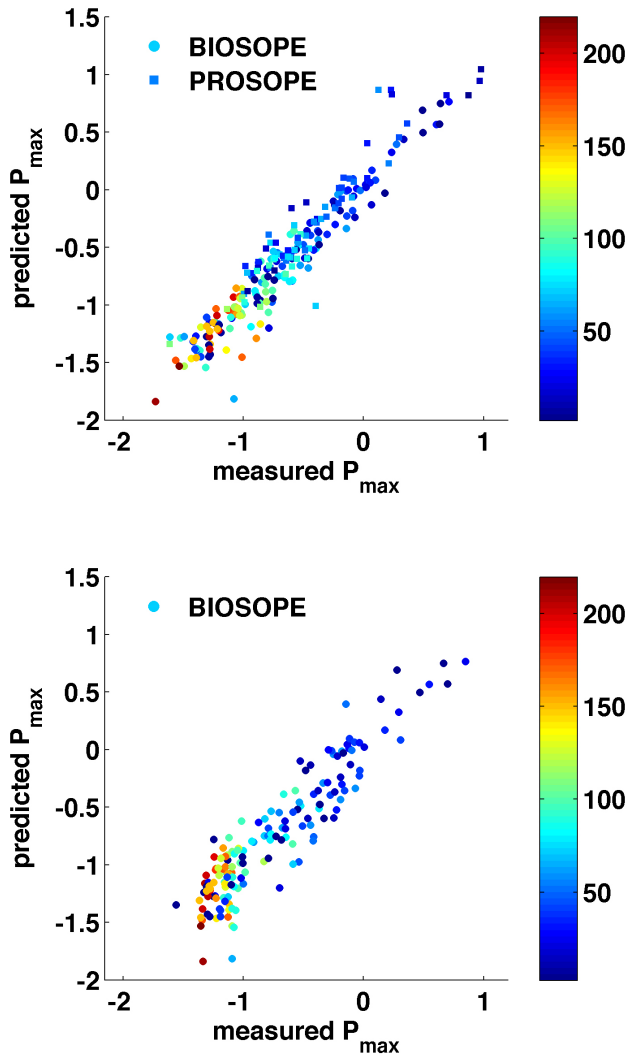


Fig. 7. Prediction of P_{\max} using several variables. (a) Using *Tchl_a* as the biomass index and other variables as given in Table 3. (b) Same as (a) except using b_p as the biomass proxy.

relative to the relationship using only the biomass index. However, the *Tchl_a* and absorption based measures remained significantly better than the scattering based methods (Table 4). In fact, the improvements in the scattering based methods are due to the fact that they started off so poorly, and any variable that is somewhat correlated with α or *Tchl_a* will improve the relationships.

4.4 Additional information in scattering beyond *Tchl_a*

An important question remains: given the regression using *Tchl_a* and environmental variables, can scattering based variables allow us to improve estimates of P_{\max} and α ? In other words, is there supplementary information in the scattering based proxies? This question can also be addressed by a stepwise regression analysis, by verifying if adding scatter-

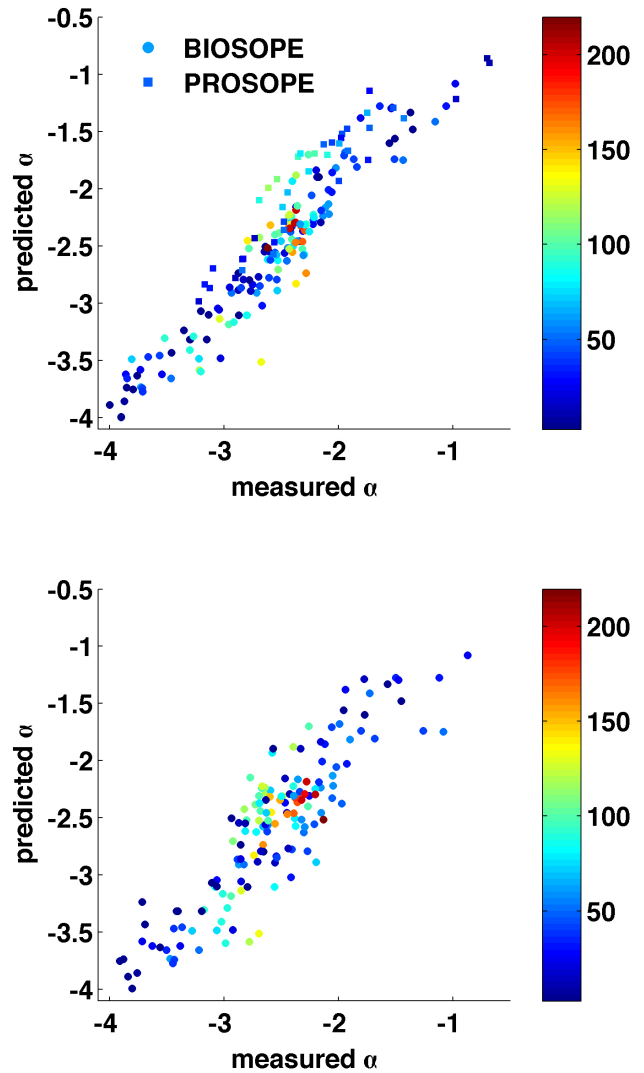


Fig. 8. Prediction of α (in $\text{mgC m}^{-3} \text{h}^{-1} [\mu\text{mol photon}^{-2} \text{s}^{-1}]^{-1}$) using several variables. (a) Using *Tchl_a* as the biomass index and other variables as given in Table 4. (b) Same as (a) except using b_p as the biomass proxy.

ing based measures improves the fit significantly. We tested the addition of the following variables: $b_p(650)$, $b_p(650)^2$, and $\text{Tchl}_a/b_p(650)$. Only the $b_p(650)$ provided a very small but significant improvement to the fits for P_{\max} (RMSE decreased from 0.1488 to 0.1441). None provided significant improvements in the regression of α (all had values of $p > 0.14$). We therefore conclude that, for the waters studied, the bulk scattering measurements adds very little to the estimates of photosynthetic parameters, once basic information regarding chlorophyll concentration and irradiance at depth is available (see Tables 3 and 4).

This conclusion is of course only valid for the environments and the space and time scales that we studied. Scattering based measurements have been proposed to help in the estimation of primary production based on diurnal changes in the c_p (e.g. Siegel et al., 1989; Claustre et al., 2007) or of phytoplankton carbon concentration and growth rate from space on large spatial scales (Behrenfeld et al., 2005). These applications are beyond the scope of our analysis and our results are difficult to extrapolate to them.

4.5 Estimation of primary productivity using empirical relationships

Primary productivity models are generally expressed with the production (P)-irradiance relationship normalized to biomass (e.g. P^B). This relationship is depth integrated and then multiplied by biomass, $P = B P^B$ (the depth integration can occur after the multiplication by biomass if depth photosynthetic parameters vary with depth). In order to reduce the variability in P^B , some authors relate it to its location and time (Platt and Sathyendranath, 1999; Longhurst, 1998), while others describe it in terms of environmental variables (e.g. P^B (T , Salinity, E_d)) (Behrenfeld and Falkowski, 1997). The aim of our study is to identify the normalization factor (“ B ”) that reduces as much as possible the variability in the photosynthetic parameters. In doing so, we obtain regressions that predict P_{\max} and α from different biomass proxies and environmental variables (Table 3 and Table 4). Our relationships can thus be written as $P = f(B, T, \text{Salinity}, E_d, z, \dots)$. Therefore, these relationships, or extensions of them, could be used in primary production models using remote sensing data, but without the need to multiply the resulting primary production by an estimate of the phytoplankton biomass. Here, the phytoplankton biomass serves directly as a predictive variable.

5 Conclusions

Within the context of evolving ocean observation technology, our analysis consolidates a rationale for the direction taken over the past 50 years or so for estimating primary productivity. Indeed, we find that chlorophyll a remains the best proxy of phytoplankton biomass for studies of primary productivity. In particular, we find that the scattering coefficient (and other scattering-based variables) did not provide information about the photosynthetic parameters that could not be more accurately estimated by a measure of chlorophyll a (or fluorescence) and incident irradiance at depth. This is probably due as much to the superior accuracy of the estimation of *Tchl* a compared to other measurements as to its specificity to phytoplankton. There is one main limitation in our present study: most of our dataset originates from subtropical stratified waters (BIOSOPE) and warm temperate waters (PROSOPE). Photosynthetic parameters depend on environ-

mental variables and thus on the regions sampled. While our measurements are representative of a wide range of chlorophyll concentrations (from ~ 0.02 to $\sim 3 \text{ mg m}^{-3}$), they are not representative, for example, of polar or cold temperate water columns. It is possible that in these waters scattering-based measurement prove to be more robust for the determination of phytoplankton photosynthetic parameters.

Acknowledgements. D. Tailliez and C. Marec are warmly thanked for their efficient help in CTD rosette management and data processing. We also want to thank F. Tièche for processing the phytoplankton absorption data, P. Raimbault, J. Ras and A. Morel for providing the nutrient, HPLC and irradiance data. This is a contribution of the BIOSOPE project of the LEFE-CYBER French program. This research was funded by the Centre National de la Recherche Scientifique (CNRS), the Institut des Sciences de l’Univers (INSU), the Centre National d’Etudes Spatiales (CNES), the European Space Agency (ESA), the National Aeronautics and Space Administration (NASA) and the Natural Sciences and Engineering Research Council of Canada (NSERC). Y. Huot was funded by postdoctoral scholarships from NSERC (Canada) and CNES (France). C. Grob was supported by CONICYT (Chili) through the FONDAP Program and a graduate fellowship, and by the ECOS-CONICYT Program.

Edited by: E. Boss

References

- Babin, M. and Morel, A.: An incubator designed for extensive and sensitive measurements of phytoplankton photosynthetic parameters, *Limnol. Oceanogr.*, 39, 694–702, 1994.
- Babin, M., Morel, A., Claustre, H., Bricaud, A., Kolber, Z., and Falkowski, P. G.: Nitrogen- and irradiance-dependent variations of the maximum quantum yield of carbon fixation in eutrophic, mesotrophic and oligotrophic marine systems, *Deep-Sea Res. Pt I*, 43, 1241–1272, 1996.
- Behrenfeld, M. J. and Falkowski, P. G.: A consumer’s guide to phytoplankton primary productivity models, *Limnol. Oceanogr.*, 42, 1479–1491, 1997.
- Behrenfeld, M. J. and Boss, E.: The beam attenuation to chlorophyll ratio: An optical index of phytoplankton physiology in the surface ocean?, *Deep-Sea Res. Pt I*, 50, 1537–1549, 2003.
- Behrenfeld, M. J., Prasil, O., Babin, M., and Bruyant, F.: In search of a physiological basis for covariations in light-limited and light-saturated photosynthesis, *J. Phycol.*, 40, 4–25, 2004.
- Behrenfeld, M. J., Boss, E., Siegel, D. A., and Shea, D. M.: Carbon-based ocean productivity and phytoplankton physiology from space, *Global Biogeochem. Cy.*, 19, GB1006, doi:10.1029/2004GB002299, 2005.
- Behrenfeld, M. J. and Boss, E.: Beam attenuation and chlorophyll concentration as alternative optical indices of phytoplankton biomass, *J. Mar. Res.*, 64, 431–451, 2006.
- Berges, J. A.: Ratios, regression statistics, and “Spurious” Correlation, *Limnol. Oceanogr.*, 42, 1006–1007, 1997.
- Bricaud, A., Claustre, H., Ras, J., and Oubelkheir, K.: Natural variability of phytoplankton absorption in oceanic waters: Influence of the size structure of algal populations, *J. Geophys. Res.-Oceans*, 109, C11010, doi:10.1029/12004JC002419, 2004.
- Claustre, H., Bricaud, A., Babin, M., Bruyant, F., Guillou, L., Le Gall, F., Marie, D., and Partensky, F.: Diel variations

- in prochlorococcus optical properties, *Limnol. Oceanogr.*, 47, 1637–1647, 2002.
- Claustre, H., Huot, Y., Obernosterer, I., Gentili, B., Tailliez, D., Lewis, M.: Gross community production and metabolic balance in the South Pacific Gyre, using a non intrusive bio-optical method, *Biogeosciences Discuss.*, 4, 3089–3121, 2007, <http://www.biogeosciences-discuss.net/4/3089/2007/>.
- Falkowski, P. G. and Raven, J. A.: *Aquatic photosynthesis*, First ed., Blackwell Science, Malden, 375 pp., 1997.
- Gardner, W. D., Mishonov, A., and Richardson, M. J.: Global poc concentrations from in-situ and satellite data, *Deep-Sea Res. Part II*, 53, 718–740, 2006.
- Gregg, W. W. and Carder, K. L.: A simple spectral solar irradiance model for cloudless maritime atmosphere, *Limnol. Oceanogr.*, 35, 1657–1675, 1990.
- Grob, C., Ulloa, O., Claustre, H., Huot, Y., Alarcon, G., and Marie, D.: Contribution of picoplankton to the total particulate organic carbon concentration in the eastern South Pacific, *Biogeosciences*, 4, 837–852, 2007, <http://www.biogeosciences.net/4/837/2007/>.
- Kitchen, J. C., Ronald, J., and Zaneveld, V.: On the noncorrelation of the vertical structure of light scattering and chlorophyll a in case I waters, *J. Geophys. Res.-Oceans*, 95, 20 237–20 246, 1990.
- Lee, Z. P., Carder, K. L., Marra, J., Steward, R. G., and Perry, M. J.: Estimating primary production at depth from remote sensing, *Appl. Optics*, 35, 463–474, 1996.
- Loisel, H. and Morel, A.: Light scattering and chlorophyll concentration in case I waters: A reexamination, *Limnol. Oceanogr.*, 43, 847–858, 1998.
- Longhurst, A. R.: *Ecological geography of the sea*, Academic Press, San Diego, 398 pp., 1998.
- MacIntyre, H. L. and Cullen, J. J.: Using cultures to investigate the physiological ecology of microalgae, in: *Algal culturing techniques*, edited by: Anderson, R. M., Academic Press, 2005.
- Marra, J., Trees, C. C., and O'Reilly, J. E.: Phytoplankton pigment absorption: A strong predictor of primary productivity in the surface ocean, *Deep-Sea Res. Pt I*, 54, 155–163, 2007.
- Morel, A.: Diffusion de la lumière par les eaux de mer. Resultats expérimentaux et approche théorique., AGARD lectures series, 3.1.1–3.1.76, 1973.
- Morel, A. and Bricaud, A.: Inherent properties of algal cells including picoplankton: Theoretical and experimental results, in: *Photosynthetic picoplankton*, edited by: Platt, T. and Li, W. K. W., Canadian bulletin of fisheries and aquatic sciences, 521–559, 1986.
- Morel, A.: Optical modeling of the upper ocean in relation to its biogenous matter content (case I waters), *J. Geophys. Res.-Oceans*, 93, 10 749–10 768, 1988.
- Morel, A. and Ahn, Y.-H.: Optics of heterotrophic nanoflagellates and ciliates: A tentative assessment of their scattering role in oceanic waters compared to those of bacterial and algal cells, *J. Mar. Res.*, 49, 177–202, 1991.
- Morel, A. and Maritorena, S.: Bio-optical properties of oceanic waters: A reappraisal, *J. Geophys. Res.-Oceans*, 106, 7163–7180, 2001.
- Morel, A., Gentili, B., Claustre, H., Babin, M., Bricaud, A., Ras, J., and Tieche, F.: Optical properties of the “Clearest” Natural waters, *Limnol. Oceanogr.*, 52, 217–229, 2007.
- Oubelkheir, K., Claustre, H., Sciandra, A., and Babin, M.: Bio-optical and biogeochemical properties of different trophic regimes in oceanic waters, *Limnol. Oceanogr.*, 50, 1795–1809, 2005.
- Perry, M. J.: Measurements of phytoplankton absorption other than per unit of chlorophyll a, in: *Ocean optics*, edited by: Spinrad, R. W., Carder, K. L., and Perry, M. J., Oxford monographs on geology and geophysics, Oxford University Press, New York, 107–116, 1994.
- Platt, T., Gallegos, C. L., and Harrison, W. G.: Photoinhibition of photosynthesis in natural assemblages of marine phytoplankton, *J. Mar. Res.*, 38, 687–701, 1980.
- Platt, T. and Sathyendranath, S.: Spatial structure of pelagic ecosystem processes in the global ocean, *Ecosystems*, 2, 384–394, 1999.
- Ras, J., Claustre, H., and Uitz, J.: Spatial variability of phytoplankton pigment distributions in the Subtropical South Pacific Ocean: comparison between in situ and predicted data, *Biogeosciences Discuss.*, 4, 3409–3451, 2007, <http://www.biogeosciences-discuss.net/4/3409/2007/>.
- Siegel, D. A., Dickey, T. D., Washburn, L., Hamilton, M. K., and Mitchell, B. G.: Optical determination of particulate abundance and production variations in the oligotrophic ocean, *Deep-Sea Res.*, 36, 211–222, 1989.
- Sokal, R. R. and Rohlf, F. J.: *Biometry the principles and practice of statistics in biological research*, 3 ed., W.H. Freeman and Company, New York, 887 pp., 1995.
- Stramski, D. and Reynolds, R. A.: Diel variations in the optical properties of a marine diatom, *Limnol. Oceanogr.*, 38, 1347–1364, 1993.
- Stramski, D., Shalapyonok, A., and Reynolds, C. S.: Optical characterization of the marine oceanic unicellular cyanobacterium *synechococcus* grown under a day-night cycle in natural irradiance, *J. Geophys. Res.-Oceans*, 100, 13 295–13 307, 1995.
- Stramski, D., Reynolds, C. S., Kahru, M., and Mitchell, B. G.: Estimation of particulate organic carbon in the ocean from remote sensing, *Science*, 285, 239–242, 1999.
- Stramski, D., Boss, E., Bogucki, D., and Voss, K. J.: The role of seawater constituents in light backscattering in the ocean, *Prog. Oceanogr.*, 61, 27–56, 2004.
- Sukenic, A., Bennett, J., and Falkowski, P. G.: Light-saturated photosynthesis – limitation by electron transport or carbon fixation, *Biochim. Biophys. Acta*, 891, 205–215, 1987.
- Sullivan, J. M., Twardowski, M. S., Zaneveld, J. R., Moore, C., Barnard, A., Donaghay, P. L., and Rhoades, B.: The hyperspectral temperature and salinity dependencies of absorption by water and heavy water in the 400–750 nm spectral range, *Appl. Optics*, 45, 5294–5309, 2006.
- Twardowski, M. S., Sullivan, J. M., Donaghay, P. L., and Zaneveld, J. R.: Microscale quantification of the absorption by dissolved and particulate material in coastal waters with an ac-9, *J. Atmos. Ocean. Tech.*, 16, 691–707, 1999.
- Twardowski, M. S., Claustre, H., Freeman, A., Stramski, D., and Huot, Y.: Optical backscattering properties of the “clearest” natural waters, *Biogeosciences Discuss.*, 4, 2441–2491, 2007, <http://www.biogeosciences-discuss.net/4/2441/2007/>.
- Zaneveld, J. R. V., Kitchen, J. C., and Moore, C. C.: The scattering error correction of reflecting tube absorption meters, *Ocean Optics XII*, 44–55, 1994.